AD-A286 216



AGARD-AR-303 Vol. II

# AGARD

ADVISORY GROUP FOR AEROSPACE RESEARCH & DEVELOPMENT
7 RUE ANCELLE, 92200 NEUILLY-SUR-SEINE, FRANCE

DTIC ELECTE NOV 1 0 1994 S

94-34820

AGARD ADVISORY REPORT NO 303

# A Selection of Experimental Test Cases for the Validation of CFD Codes

(Recueil de cas d'essai expérimentaux pour la validation des codes de l'aérodynamique numérique)

## Volume II

This document has been approved for public release and sale; its distribution is unlimited.

*This Advisory Report was prepared at the request of the Fluid Dynamics Panel.*

NORTH ATLANTIC TREATY ORGANIZATION

Published August 1994

*Distribution and Availability on Back Cover*

AGARD

ADVISORY GROUP FOR AEROSPACE RESEARCH & DEVELOPMENT

7 RUE ANCELLE, 92200 NEUILLY-SUR-SEINE, FRANCE

AGARD ADVISORY REPORT NO 303

# A Selection of Experimental Test Cases for the Validation of CFD Codes

(Recueil de cas d'essai expérimentaux pour la validation des codes de l'aérodynamique numérique)

## Volume II

Accesion For
NTIS
DTIC
Unannounced
Justification
By
Distribution
Availability Codes
Dist
A-1

This Advisory Report was prepared at the request of the Fluid Dynamics Panel.



North Atlantic Treaty Organization
*Organisation du traité de l'Atlantique Nord*

DTIC QUALITY INSPECTED 5

94 11 8 030

# The Mission of AGARD

According to its Charter, the mission of AGARD is to bring together the leading personalities of the NATO nations in the fields of science and technology relating to aerospace for the following purposes:

- Recommending effective ways for the member nations to use their research and development capabilities for the common benefit of the NATO community;
- Providing scientific and technical advice and assistance to the Military Committee in the field of aerospace research and development (with particular regard to its military application);
- Continuously stimulating advances in the aerospace sciences relevant to strengthening the common defence posture;
- Improving the co-operation among member nations in aerospace research and development;
- Exchange of scientific and technical information;
- Providing assistance to member nations for the purpose of increasing their scientific and technical potential;
- Rendering scientific and technical assistance, as requested, to other NATO bodies and to member nations in connection with research and development problems in the aerospace field.

The highest authority within AGARD is the National Delegates Board consisting of officially appointed senior representatives from each member nation. The mission of AGARD is carried out through the Panels which are composed of experts appointed by the National Delegates, the Consultant and Exchange Programme and the Aerospace Applications Studies Programme. The results of AGARD work are reported to the member nations and the NATO Authorities through the AGARD series of publications of which this is one.

Participation in AGARD activities is by invitation only and is normally limited to citizens of the NATO nations.

The content of this publication has been reproduced
directly from material supplied by AGARD or the authors.

Published August 1994

Copyright © AGARD 1994
All Rights Reserved

ISBN 92-836-1003-2



*Printed by Canada Communication Group*
*45 Sacré-Cœur Blvd., Hull (Québec), Canada K1A 0S7*

# Introduction

Computational Fluid Dynamics (CFD) has developed to the point where the flow field around practical aircraft and missile configurations can be described fairly realistically. Although problems related to the numerical accuracy (grid refinement) and turbulence modeling still limit the application of these codes, their use today is an integral part of aircraft development and design. Before a specific code can be used with confidence, it is essential to validate the code (to test the capability of the code to describe the physics of the flow correctly) or to calibrate the code (to establish the usefulness and reliability of the code for practical design applications). An essential part of the validation process is a comparison of the CFD code with the experiment.

In 1979 AGARD's Fluid Dynamics Panel established Working Group 4 to compile a number of suitable experiments for such a comparison. This has resulted in AGARD AR-138 (together with an Appendix published in 1984). The working group limited its scope at that time to two-dimensional airfoils, slender bodies and wing/body configurations. Some of the test cases have been used extensively in the past and are still used today. Since the publication of AR-138, CFD methods have improved considerably. More complex geometrical configurations with much more complex flow fields can now be calculated in fine detail. As a result of this, detailed experiments that cover a wider range of flow types and geometries are required for CFD validation. Many experiments that suit these needs have been made, but the results are not always easily accessible. For that reason AGARD FDP decided in 1990 to establish another Working Group on "The Selection of Experimental Test Cases for CFD Validation". The first meeting of the Working Group took place in Amsterdam in the fall of 1990 and 7 meetings later the working group members returned to Amsterdam for their final meeting.

In the very beginning of the Working Group, it was decided to concentrate mainly on "validation" rather than "building block" or "calibration" experiments. Hence, the Working Group limited its scope of interest to the flow around generic configurations of practical interest. A questionnaire was sent out to request test cases. In total, over 100 questionnaires were returned. Out of these, 65 were objectively selected for a more detailed written report and subsequent evaluation by the working group members. As a result of this evaluation, 39 test cases were selected for inclusion in this report.

The report has been split up in two volumes. Volume I provides a review of the theoretical (chapter 2) and experimental (chapter 3) requirements, followed by a general introduction to the test cases (chapter 4), a two-page summary of all test cases (chapter 5) and finally a discussion and some recommendations for the future (chapter 6). The detailed information on the 39 test cases can be found in Volume II. Accompanying this is a set of floppy disk's where the relevant data of all test cases have been compiled. This set of floppy disks can be obtained upon request through AGARD's National Distribution Centers.

The Working Group found it difficult to select reliable test cases. The inclusion of a test case within the data base does not automatically guarantee good quality. The Working Group takes no responsibility for the fitness or otherwise of the data base information or for any decisions made thereafter on the basis of that information. In fact, it is felt that the usefulness and reliability of a particular test case can only be judged after a comparison of theory and experiment. For that reason, AGARD FDP would appreciate it very much if the experience with the particular test cases could be reported to the Chairman of AGARD's FDP TES Committee on "Wind Tunnel Testing Techniques". A standard form for this can be found at the back of this report.

In the Working Group, chaired by A. Elsenaar, both theoreticians and experimentalists were represented. Two subcommittees headed by E.G. Waggoner and P.R. Ashill formulated the requirements from the point of view of CFD development and experiment respectively. Other active members of the group were J. Muylaert, D. Jones, V. Schmitt, H. Körner, E. Stanewsky, M. Onorato, U. Kaynak, M. Burt, S. Lekoudis, E. H. Hirschel and D. Brown. C. Hirsch followed the activities of the Working Group on behalf of the Propulsion and Energetic Panel (PEP).

**This page has been deliberately left blank.**

# Introduction

L'aérodynamique numérique (CFD) a évolué au point où les champs d'écoulement autour de configurations réelles d'aéronefs et de missiles peuvent être représentés de façon assez fidèle. Bien que l'application des codes soit toujours limitée par certains problèmes liés à la précision numérique (finesse des maillages) et à la modélisation des tourbillons, leur emploi aujourd'hui fait partie intégrante du processus de conception et de développement des aéronefs. Avant de pouvoir utiliser un code donné avec confiance, il est indispensable soit de le valider (tester la capacité du code à décrire correctement la physique de l'écoulement), soit de le vérifier (établir l'utilité et la fiabilité du code en vue d'applications concrètes). L'un des éléments essentiels de processus de validation est la comparaison du code CFD avec des résultats expérimentaux.

En 1979, le Panel AGARD de la dynamique des fluides a créé le groupe de travail No. 4, qui avait pour mandat de dresser une liste d'expériences permettant de faire une telle comparaison. Ce travail a débouché sur la rédaction du document AGARD AR-138 (et d'une annexe publiée en 1984). Le groupe a volontairement limité le domaine de ses recherches aux profils aérodynamiques bidimensionnels, aux corps effilés et aux configurations voilure/fuselage. Certains des cas d'essai ont été très largement utilisés dans le passé et le sont toujours. Les méthodes CFD se sont considérablement améliorées depuis la publication du AR-138. Aujourd'hui, le calcul détaillé de configurations géométriques beaucoup plus complexes, aux champs d'écoulement plus complexes, est tout à fait faisable. Par conséquent, des expériences couvrant une gamme plus large de types d'écoulement et de géométries sont demandées pour la validation CFD. Bon nombre d'expériences répondant à ces critères ont été réalisées, mais l'accès aux résultats pose souvent des problèmes. Pour ces raisons, en 1990, le Panel AGARD de la dynamique des fluides a décidé de créer un autre groupe de travail, sur —le choix de cas d'essai expérimentaux pour la validation CFD". Le groupe s'est réuni pour la première fois à Amsterdam en automne 1990. Sept réunions plus tard, les membres sont retournés à Amsterdam pour la réunion finale.

Au tout début des travaux de ce groupe de travail, il a été décidé de porter l'effort principal sur —la validation" plutôt que sur des expériencesdutype—modulaire"ou—étalonnage". Par conséquent, le groupe de travail a limité son domaine d'intérêt aux écoulements autour de configurations génériques d'intérêt pratique. Un questionnaire a été diffusé afin de recueillir des cas d'essai. En tout, plus de 100 questionnaires ont été retournés, dont 65 ont été sélectionnés objectivement en vue de l'établissement d'un rapport écrit plus détaillé pour évaluation ultérieure par les membres du groupe. Suite à cette évaluation, 39 cas d'essai ont été choisis pour incorporation dans le présent rapport.

Le rapport est en deux volumes : le volume I donne un aperçu des besoins théoriques (chapitre 2) et expérimentaux (chapitre 3), suivi d'une introduction générale aux cas d'essai (chapitre 4), un résumé de l'ensemble des cas d'essai de deux pages (chapitre 5) et finalement d'un débat qui débouche sur des recommandations pour l'avenir (chapitre 6). Le détail des 39 cas d'essai est donné au volume II. Le rapport est accompagné d'un jeu de disquettes contenant les données appropriées à tous les cas d'essai. Ces disquettes sont disponibles à la demande auprès des Centres de distribution nationaux de l'AGARD.

Le groupe de travail a éprouvé des difficultés pour choisir des cas d'essai fiables. La présence d'un cas d'essai dans la base de données ne représente pas la garantie systématique de sa qualité. Le groupe de travail n'accepte aucune responsabilité ni de la justesse, ni de tout autre qualité des informations contenues dans la base de données, ni de toute décision prise ultérieurement sur la base de ces informations. En effet, les auteurs sont de l'avis que l'applicabilité et la fiabilité d'un cas d'essai donné ne peuvent être appréciées qu'après avoir confronté la théorie et l'expérience. Pour ces raisons, le Panel FDP de l'AGARD aimerait que des retours d'information concernant des cas d'essai particuliers soient adressés au Président du comité AGARD FDP TES sur —les techniques d'essais en soufflerie". Un formulaire à cet effet est joint à ce rapport.

Dans ce groupe de travail, qui était présidé par A. Elsenaar, les théoriciens ont été représentés, aussi bien que les expérimentalistes. Les objectifs du point de vue du développement CFD et des expériences ont été définis par deux comités, présidés par E. G. Waggoner et P. R. Ashill respectivement. Parmi les autres membres actifs du groupe on distingue J. Muylaert, D. Jones, V. Schmitt, H. Körner, E. Stanewsky, M. Onorato, U. Kaynak, M. Burt, S. Lekoudis, E. H. Hirschel et D. Brown. C. Hirsch a suivi les activités du groupe pour le compte du Panel AGARD de Propulsion et d'énergétique (PEP).

**This page has been deliberately left blank.**

# Contents


| Test Case Number | | Page |
|---|---|---|
| A1 | **2-D airfoil tests including side wall boundary layer measurements**<br>by W. Bartelheimer, K.H. Horstmann, W. Puffert-Meissner (DLR, Braunschweig) | A1-1 |
| A2 | **Measurements on a two-dimensional aerofoil with high-lift devices**<br>by I.R.M. Moir (DRA, Farnborough) | A2-1 |
| A3 | **Investigation of the flow over a series of 14%-thick supercritical aerofoils with significant rear camber**<br>by P.R. Ashill (DRA, Bedford) | A3-1 |
| A4 | **Surface pressure and wake drag measurements on the Boeing A4 airfoil in the IAR 1.5 × 1.5 m wind tunnel facility**<br>by D.J. Jones and Y. Nishimura (IAR/NRC, Canada) | A4-1 |
| A5 | **2-D aileron effectiveness study**<br>by C.D. Chin, C.J. Dominik, F.T. Lynch, D.L. Rodriguez (McDonnell Douglas, Long Beach) | A5-1 |
| A6 | **Investigation of an NLF(1)-0416 airfoil in compressible subsonic flow**<br>by P. Guntermann and G. Dietz (RWTH-Aachen) | A6-1 |
| A7 | **Experiments in the trailing edge flow of an NLR 7702 airfoil**<br>by L.H.J. Absil and D.M. Passchier (Delft Univ. of Technology) | A7-1 |
| A8 | **Two-dimensional 16.5% thick supercritical airfoil NLR 7301**<br>by S.O.T.H. Han (NLR) | A8-1 |
| A9 | **Low-speed surface pressure and boundary layer measurement data for the NLR 7301 airfoil section with trailing edge flap**<br>by B. van den Berg and J.H.M. Gooden (NLR) | A9-1 |
| A10 | **Data from the GARTEUR (AD) Action Group 02 Airfoil CAST7/DO A4 experiments**<br>by A. Mignosi and J.P. Archambaud (ONERA) and E. Stanewsky (DLR, Göttingen) | A10-1 |
| A11 | **OAT15A Airfoil Data**<br>by A.M. Rodde and J.P. Archambaud (ONERA) | A11-1 |
| A12 | **A supercritical airfoil experiment**<br>by G.G. Mateer, H.L. Seegmiller (NASA-Ames) and J. Szodruch (MBB-Bremen) | A12-1 |
| A13 | **Two-dimensional high-lift airfoil data for CFD code validation**<br>by G.W. Brune (Boeing) | A13-1 |
| B1 | **Measurements of the flow over a low aspect-ratio wing in the Mach number range 0.6 to 0.87 for the purpose of validation of computational methods**<br>by M.C.P. Firmin and M.A. McDonald (DRA, Farnborough) | B1-1 |
| B2 | **Detailed study at supersonic speeds of the flow around delta wings**<br>by M.J. Simmons (DRA, Bedford) | B2-1 |
| B3 | **Pressure distributions on research wing W4 mounted on an axisymmetric body**<br>by J.L. Fulker (DRA, Bedford) | B3-1 |
| B4 | **DLR-F4 wing body configuration**<br>by G. Redeker (DLR/DRA/ONERA/NLR) | B4-1 |

| | | |
|---|---|---|
| **B5** | **DLR-F5: test wing for CFD and applied aerodynamics**<br>by H. Sobieczky (DLR, Göttingen) | **B5-1** |
| **B6** | **Low aspect ratio wing experiment**<br>by M. Olsen and H.L. Seegmiller (NASA-Ames) | **B6-1** |
| **C1** | **Wind tunnel investigations of the appearance of shocks in the windward region of bodies with circular cross section at angle of attack**<br>by H. Esch (DLR, Cologne) | **C1-1** |
| **C2** | **Three-dimensional boundary layer and flow field data of an inclined prolate spheroid**<br>by H.-P. Kreplin (DLR, Göttingen) | **C2-1** |
| **C3** | **Force and pressure data of an ogive-nosed slender body at high angles of attack and different Reynolds numbers**<br>by K. Hartman (DLR, Göttingen) | **C3-1** |
| **C4** | **Ellipsoid-cylinder model**<br>by D. Barberis (ONERA, Châtillon) | **C4-1** |
| **C5** | **Supersonic vortex flow around a missile body**<br>by D. Barberis (ONERA, Châtillon) | **C5-1** |
| **C6** | **Test data on a non-circular body for subsonic, transonic and supersonic Mach numbers**<br>by P. Champigny (ONERA, Châtillon) | **C6-1** |
| **D1** | **Wind tunnel test on a 65° delta wing with a sharp or rounded leading edge — The International Vortex Flow Experiment**<br>by A. Elsenaar (NLR) | **D1-1** |
| **D2** | **Delta-wing model**<br>by D. Barberis (ONERA, Châtillon) | **D2-1** |
| **D3** | **Experimental investigation of the vortex flow over a 76/60-deg double delta wing**<br>by N.G. Verhaagen and J.E.J. Maseland (Delft Univ. of Technology) | **D3-1** |
| **D4** | **Wind tunnel tests on a 65° delta wing with rounded leading edges — The International Vortex Flow Experiment**<br>by K. Hartmann, K.A. Bütefisch and H. Pszolla (DLR, Göttingen) | **D4-1** |
| **D5** | **Investigation of the flow development on a highly swept canard/wing research model with segmented leading- and trailing edge flaps**<br>by D. Stanniland (ARA) | **D5-1** |
| **E1** | **Subsonic flow around US-Orbiter model FALKE in the DNW**<br>by R. Radespiel and A. Quast (DLR, Braunschweig) and<br>D. Eckert (DNW, Netherlands) | **E1-1** |
| **E2** | **Pressure distribution measurements on an isolated TPS 441 nacelle**<br>by R. Kiock (DLR, Braunschweig) and W. Baumert (DLR, Göttingen) | **E2-1** |
| **E3** | **Single-engine tail interference model**<br>by B.L. Berrier (NASA, Langley) | **E3-1** |
| **E4** | **Twin engine afterbody model**<br>by D.J. Wing (NASA, Langley) | **E4-1** |
| **E5** | **STOVL CFD model test case**<br>by K.R. Roth (NASA, Ames) | **E5-1** |
| **E6** | **Low speed propeller slipstream aerodynamic effects**<br>by I. Samuelsson (FFA) | **E6-1** |

| | | |
|---|---|---|
| **E7** | **Experimental data on the aerodynamic interactions between a helicopter rotor and an airframe**<br>by J.G. Leishman and Nai-pei Bi (Centre for Rotorcraft Education and Research) | **E7-1** |
| **E8** | **Investigation into the aerodymamic characteristics of a combat aircraft research model fitted with a forward swept wing**<br>by D. Stanniland (ARA) | **E8-1** |
| **E9** | **Investigation of the influence of pylons and stores on the wing lower surface flow**<br>by D. Stanniland (ARA) | **E9-1** |
| **Annex A** | **Procedure for obtaining and using floppy disks** | **A-1** |

# 2-D AIRFOIL TESTS INCLUDING SIDE WALL BOUNDARY LAYER MEASUREMENTS

BY

W. BARTELHEIMER, K.H. HORSTMANN
INSTITUT FÜR ENTWURFSAERODYNAMIK
W. PUFFERT-MEIßNER
HAUPTABTEILUNG WINDKANÄLE

DEUTSCHE FORSCHUNGSANSTALT FÜR LUFT- UND RAUMFAHRT
FLUGHAFEN
D-3300 BRAUNSCHWEIG

## 0. INTRODUCTION

The data presented in this contribution were obtained in the DLR Transonic Wind Tunnel Braunschweig. The intent of the experiment was to provide data giving information on the developpment of the TWB-side wall boundary layer in the presence of a typical transonic airfoil model for further investigation of the influence of the side wall boundary layer on 2-D airfoil measurements. For this purpose boundary layer pitot pressures were measured in 13 different side wall positions around the airfoil. Airfoil pressure distributions were obtained in several spanwise positions by sliding the airfoil model in spanwise direction.

The test cases investigated correspond to the design flow conditions of the airfoil (Ma = 0.73, $\alpha$ = 1.5°) and to a low ($\alpha$ = 0°) and a high ($\alpha$ = 3.0°) lift value at the same Mach number. For these cases wall pressure distributions were measured on the centre slat of the top and bottom walls. Additionally to the pressure measurements some oil flow pictures were made on the upper airfoil surface and the adjacent wind tunnel side wall to get more insight in the structure of the flow.

In order to have well defined wind tunnel boundary conditions for the evaluation by computational methods, the slotted top and bottom walls of the test section were closed for these specific tests. This means, of course, that the presented airfoil pressure distributions do not correspond to free flight conditions and are not comparable to wind tunnel results obtained in slotted or perforated transonic test sections.

## 1. GENERAL DESCRIPTION

| | |
|---|---|
| 1.1 Model designation | VA2-1 |
| 1.2 Model type | 2-Dimensional airfoil |
| 1.3 Purpose of tests | Investigation of influence of wind tunnel side wall boundary layer on 2-D airfoil measurements at transonic speeds. |
| 1.4 Dominant flow physics | Change of wall boundary layer parameters under influence of airfoil flow field. An example is shown in Figure 2. |
| 1.5 Additional remarks | The top and bottom walls of the test section, which are normally slotted for airfoil tests, were closed for this investigation. |

## 2. DETAILS OF MODEL

| | |
|---|---|
| 2.1 Airfoil data | Supercritical airfoil designed by VFW with a thickness/chord ratio of 13%, Figure 1. The dimensions of the model are 200 mm chord length and 1 m span width. |
| 2.1.1 Aspect ratio | 5 |
| 2.2 Geometric definition | Measured airfoil coordinates see Table 1. The model surface was painted and finished to a surface roughness of about 3 microns. |

| | |
|---|---|
| 2.3 Model Support | The model was mounted through the tunnel side wall turntables by means of aluminium jaws and plastic inserts shaped to fit the airfoil contour, allowing the spanwise variation of the pressure measurement orifice plane of the airfoil. |

## 3. GENERAL TUNNEL INFORMATION

| | |
|---|---|
| 3.1 Tunnel designation | Transonic Wind Tunnel Braunschweig (TWB) |
| 3.2 Organization | Deutsche Forschungsanstalt für Luft- und Raumfahrt e.V., Hauptabteilung Windkanäle, Abteilung Braunschweig. |
| 3.3 Tunnel characteristics | |
| - Type | Blowdown |
| - Operating envelope | Mach number range: 0.3 to 0.95<br>Reynolds number range: 3 to 12 million at Ma = 0.7, based on 150mm chord length, (see Figure 3). |
| - Minimum run time | 7 seconds |
| 3.4 Test section | |
| 3.4.1 Model installation | Figure 4 shows the TWB-test section and Figure 5 shows schematically the model installation in reference to the locations, where boundary layer values were measured. |
| 3.4.2 Test section dimensions | 0.34m x 0.6m x 2.8m |
| 3.4.3 Wall geometry details | - Solid side walls<br>- Solid top and bottom walls, divergence 0.25° each.<br>Top and bottom walls are normally slotted with 2.35% open area ratio. |
| 3.5 Freestream conditions | |
| 3.5.1 Determination of reference flow conditions | |
| Total pressure | Measured at end of settling chamber by four connected total probes. |
| Static pressure | Measured by wall pressure orifices in the top and bottom walls 1.15m ahead of model pitch axis. |
| Total temperature | Measured at end of settling chamber (same location as total pressure). |
| Static temperature | Calculated using isentropic flow equations |
| 3.5.2 Tunnel calibration | - Empty tunnel calibration by longitudinal static pressure measurements on centre of top and bottom walls and static/total pressure probe measurements at location of model pitch axis.<br>- Flow angularity determined with airfoil model installed in both normal and inverted attitude.<br>- Date of last calibration 1987 |

3.6 Flow quality

| | |
|---|---|
| 3.6.1 Flow uniformity | - Pressure coefficient variation over model chord length : ± 0.0023<br>- Mach number variation over model chord length : ± 0.0009<br>- Mach number variation during a run : ± 0.0015<br>- Variation of flow angularity not measured |
| 3.6.2 Temperature variation | - No temperature control during a run<br>- Variation during a run : 2°/sec after establishment of constant flow conditions. |
| 3.6.3 Flow unsteadiness | - Results of turbulence level measurements will be available in August 1993. |

## 4. INSTRUMENTATION

4.1 Model position

| | |
|---|---|
| 4.1.1 Geometrical incidence | The model is mounted in tunnel side wall turntables, which are connected mechanically and driven hydraulically. Model geometrical incidence is measured with an incremental angle encoder on the left turntable and a bidirectional counter. |
| 4.1.2 Accuracy of geometrical incidence | Model incidence setting : ± 0.02° |

4.2 Model pressure measurements

| | |
|---|---|
| 4.2.1 Number and disposition of pressure holes | 53 pressure orifices located in one cross section plane, hole diameter 0.5mm.<br>Chordwise distribution of pressure orifices see Figure 1 and Table 2.<br>Measured spanwise stations for $\alpha$ = 1.5°:<br>2,10,20,40,80,140,170,200mm from side wall.<br>Closest position to the wall (2 mm) was well within the side wall boundary layer.<br>Spanwise stations for $\alpha$ = 0° and 3°:<br>10,20,40,200mm from side wall.<br>Figure 6 shows an example for the change in pressure distribution in spanwise direction. |
| 4.2.2 Range and accuracy of pressure transducers | Model surface pressures and total pressures of boundary layer :<br>Range ± 310kPa (± 45psi)<br>Accuracy ± 0.3kPa<br><br>Wall pressures :<br>Range ± 35kPa (± 5psi)<br>Accuracy ± 0.035kPa |
| 4.2.3 Dynamic pressures | Not measured |

4.4 Boundary layer and flow field measurements

| | |
|---|---|
| 4.4.1 Measurement technique | Boundary layer measurements were made with three different rakes consisting each of 22 total pressure probes and one static probe. |

| | |
|---|---|
| 4.4.2 Flow region investigated | All boundary layer measurements were made on the left test section side wall at 13 different positions, see Figure 5. |
| 4.4.3 Probe details | Figure 8 shows the 3 boundary layer rakes used for the measurements :<br>Rake 1 for positions 1 and 2 (see Fig. 5)<br>Rake 2 for positions 3,4 and 6<br>Rake 3 for positions 5 and 7 to 13 |
| 4.5 Surface flow visualisation | |
| 4.5.1 Measurement technique | Oil flow technique |
| 4.5.2 Surfaces were flow is visualized | Upper airfoil surface and wind tunnel side wall around airfoil model. |
| 4.5.3 Form of data | Photograph |
| 4.7 Tunnel wall measurements | Static pressure measurements in longitudinal direction on the centre lines of top and bottom wall, covering a range of 1.6m. |

## 5. TEST MATRIX AND CONDITIONS

| | |
|---|---|
| 5.1 Detailed test matrix | |
| 5.1.1 Number of test cases | 3<br>- Mach number : Ma = 0.73<br>- Reynolds number : Re = 6 million<br>- Model incidences : $\alpha$ = 0°,1.5°,3° |
| 5.1.2 Number of configurations | 1 |
| 5.2 Model/tunnel relations | |
| 5.2.1 Blockage (frontal area) | 4.2% |
| 5.2.2 Model span/tunnel width | 1.0 |
| 5.2.3 Wing area/tunnel cross section | 0.324 |
| 5.2.4 Height/chord ratio | 3.0 |
| 5.2.5 Width/chord ratio | 1.7 |
| 5.2.6 Adiabatic wall temperatures | Not reached due to temperature drop during tunnel starting up procedure and short running time. Deviation from adiabatic wall temperatures is in the range of 15° to 25°, depending on test run frequency.<br>The variation of model temperature during the measurements itself is about 3° and does not have a significant effect for airfoil tests with fixed transition. |
| 5.3 Transition details | |
| 5.3.1 Form of transition | Fixed transition for all test cases |
| 5.3.2 Details of fixed transition | - Transition trip strip 3mm wide at 5% chord location on upper and lower surface, formed with a row of 7 layers of Letraset triangles (total hight 0.032mm).<br>- Effectivness was verified by infrared image technique for same configuration and same flow conditions in earlier tests, which showed that transition occured at 6% chord (Ref. 8.2). |

## 6. DATA

### 6.1 Availability of data

| | |
|---|---|
| 6.1.1 Organization owning the data | DLR |
| 6.1.2 Person responsible for data | W. Puffert-Meißner<br>Hauptabteilung Windkanäle<br>Deutsche Forschungsanstalt für Luft- und Raumfahrt<br>Flughafen<br>3300 Braunschweig<br><br>Tel 0531 3952422<br>Fax 0531 3952829 |
| 6.1.3 | Data are freely available |

### 6.2 Suitability of data for CFD validation

| | |
|---|---|
| 6.2.1 | Data are suitable for "in-tunnel" calculation. |
| 6.2.2 | Data not corrected to simulate "free-air" conditions. Computed magnitude of blockage is $\Delta Ma = 0.024$ for this test case (closed top and bottom walls). |

### 6.3 Type and form in which data are available

| | |
|---|---|
| 6.3.1 Type and form of data | - Airfoil pressure distributions (pressure coeficients).<br>- Normal lift and pitching moment coefficients.<br>- Side wall boundary layer pressure distributions (ratio of boundary layer total pressure to tunnel reference total pressure).<br>- Calculated boundary layer displacement and momentum thickness.<br>- Test section wall pressure distributions (pressure coefficients) .<br>- Flow visualisation data (photographs) |
| 6.3.2 Data carrier | - Printed form<br>- Floppy disk (ASCII file) |

### 6.4 Corrections applied to data

No corrections applied to airfoil data and side wall boundary layer total pressures.
- Correction of static pressures measured with boundary layer rakes (calibrated against empty tunnel side wall pressure).
- Correction of tunnel wall pressures with empty test section pressure distribution.

## 7. DATA ACCURACY

### 7.1 Estimate of accuracy

| | |
|---|---|
| 7.1.1 Free stream conditions | - Mach number : ± 0.001<br>- Model incidence : ± 0.02° |
| 7.1.2 Measured data | - Lift coefficient : ± 0.3%<br>- Moment coefficient : ± 0.5%<br>- Pressure coefficient : ± 0.5%<br>- total pressure ratio : ± 0.8% (boundary layer) |

| | |
|---|---|
| 7.2 Repeat measurements | During each wind tunnel run (corresponding to one particular angle of incidence) three complete data sets were measured, from which one was selected. An example is shown in Figure 7. |
| 7.3 Redundant measurements | No redundant measurements were made |

## 8. REFERENCES


| | |
|---|---|
| 8.1 On the wind tunnel | Puffert-Meißner,W.<br>The Transsonic Windtunnel (TWB) at DFVLR in Braunschweig (Status 1987).<br>ESA-TT-1114, 1988 |
| 8.2 On the model | Müller, R.<br>Meßergebnisse am Profil VA2 bei zwei verschiedenen Meßstreckenkonfigurationen.<br>DLR-IB 129-90/11, 1990 |
| 8.3 On the particular test and test results | Bartelheimer, W.<br>Experimentelle Untersuchung der Seitenwandgrenzschichten im Transsonischen Windkanal Braunschweig (TWB).<br>DLR Studienarbeit Nr. 91/2, 1991 |


## 9. LIST OF SYMBOLS

| | | | |
|---|---|---|---|
| Ma | Mach number | H | Test section height |
| Re | Reynolds number | x | Coordinate in londitudinal direction of test section from model pitch axis |
| Po | Total pressure | y | Coordinate in airfoil spanwise direction from left test section side wall |
| Pstat | Static pressure | x/l | Airfoil chord position as fraction of chord rom airfoil leading edge |
| Cp | Pressure coefficient | z/l | Airfoil vertical profile coordinates as fraction of chord from chordline |
| Cn | Normal force coefficient | $\alpha$ | Angle of incidence of airfoil |
| Cm | Pitching moment coefficient | l | airfoil chord length |
| $\delta 1$, delta-1 | Boundary layer displacement thickness | XGR | location of boundary layer rake on test section side wall in longitudinal direction from model pitch axis |
| $\delta 2$, delta-2 | Boundary layer momentum thickness | HGR | location of boundary layer rake on test section side wall in horizontal direction from side wall centre line |

| | Oberseite | | Unterseite | |
|---|---|---|---|---|
| Pkt. | x/l | z/l | x/l | z/l |
| 1 | 0.00000 | 0.00000 | 0.00007 | -0.00142 |
| 2 | 0.00054 | 0.00442 | 0.00065 | -0.00716 |
| 3 | 0.00338 | 0.01093 | 0.00045 | -0.01157 |
| 4 | 0.00954 | 0.01706 | 0.01086 | -0.01698 |
| 5 | 0.01754 | 0.02334 | 0.01867 | -0.02258 |
| 6 | 0.02699 | 0.02759 | 0.02783 | -0.02710 |
| 7 | 0.03815 | 0.03097 | 0.03737 | -0.03091 |
| 8 | 0.04651 | 0.03409 | 0.04682 | -0.03414 |
| 9 | 0.05397 | 0.03673 | 0.05645 | -0.03692 |
| 10 | 0.06354 | 0.03911 | 0.06635 | -0.03951 |
| 11 | 0.07324 | 0.04126 | 0.07597 | -0.04163 |
| 12 | 0.08294 | 0.04316 | 0.08586 | -0.04366 |
| 13 | 0.09265 | 0.04489 | 0.09577 | -0.04554 |
| 14 | 0.10242 | 0.04648 | 0.10567 | -0.04729 |
| 15 | 0.11234 | 0.04795 | 0.11538 | -0.04891 |
| 16 | 0.12238 | 0.04931 | 0.12556 | -0.05043 |
| 17 | 0.13295 | 0.05062 | 0.13545 | -0.05184 |
| 18 | 0.14383 | 0.05184 | 0.14539 | -0.05314 |
| 19 | 0.15470 | 0.05300 | 0.15532 | -0.05434 |
| 20 | 0.16461 | 0.05409 | 0.16524 | -0.05546 |
| 21 | 0.17536 | 0.05513 | 0.17517 | -0.05646 |
| 22 | 0.18542 | 0.05612 | 0.18509 | -0.05739 |
| 23 | 0.19533 | 0.05706 | 0.19502 | -0.05825 |
| 24 | 0.20524 | 0.05795 | 0.20498 | -0.05900 |
| 25 | 0.21515 | 0.05879 | 0.21477 | -0.05966 |
| 26 | 0.22507 | 0.05958 | 0.22480 | -0.06025 |
| 27 | 0.23498 | 0.06033 | 0.23479 | -0.06077 |
| 28 | 0.24493 | 0.06103 | 0.24482 | -0.06123 |
| 29 | 0.25484 | 0.06169 | 0.25481 | -0.06158 |
| 30 | 0.26476 | 0.06230 | 0.26452 | -0.06187 |
| 31 | 0.27471 | 0.06288 | 0.27444 | -0.06210 |
| 32 | 0.28466 | 0.06340 | 0.28439 | -0.06225 |
| 33 | 0.29460 | 0.06390 | 0.29430 | -0.06235 |
| 34 | 0.30454 | 0.06433 | 0.30424 | -0.06238 |
| 35 | 0.31448 | 0.06476 | 0.31416 | -0.06233 |
| 36 | 0.32444 | 0.06514 | 0.32407 | -0.06222 |
| 37 | 0.33438 | 0.06549 | 0.33400 | -0.06205 |
| 38 | 0.34434 | 0.06579 | 0.34388 | -0.06180 |
| 39 | 0.35429 | 0.06606 | 0.35381 | -0.06149 |
| 40 | 0.36422 | 0.06630 | 0.36372 | -0.06111 |
| 41 | 0.37418 | 0.06650 | 0.37363 | -0.06066 |
| 42 | 0.38413 | 0.06667 | 0.38352 | -0.06015 |
| 43 | 0.39408 | 0.06680 | 0.39341 | -0.05957 |
| 44 | 0.40404 | 0.06691 | 0.40334 | -0.05893 |
| 45 | 0.41403 | 0.06697 | 0.41322 | -0.05821 |
| 46 | 0.41999 | 0.06700 | 0.42317 | -0.05745 |
| 47 | 0.42994 | 0.06700 | 0.43303 | -0.05662 |
| 48 | 0.43991 | 0.06695 | 0.44291 | -0.05572 |
| 49 | 0.44987 | 0.06688 | 0.45288 | -0.05476 |
| 50 | 0.45984 | 0.06676 | 0.46280 | -0.05369 |
| 51 | 0.46979 | 0.06662 | 0.47255 | -0.05257 |
| 52 | 0.47978 | 0.06644 | 0.48245 | -0.05137 |
| 53 | 0.48975 | 0.06623 | 0.49235 | -0.05011 |
| 54 | 0.49969 | 0.06599 | 0.50217 | -0.04877 |
| 55 | 0.50968 | 0.06569 | 0.51207 | -0.04736 |
| 56 | 0.51965 | 0.06535 | 0.52194 | 0.04590 |

| | Oberseite | | Unterseite | |
|---|---|---|---|---|
| Pkt. | x/l | z/l | x/l | z/l |
| 57 | 0.52961 | 0.06499 | 0.53181 | -0.04436 |
| 58 | 0.53961 | 0.06458 | 0.54170 | -0.04276 |
| 59 | 0.54957 | 0.06414 | 0.55157 | -0.04110 |
| 60 | 0.55956 | 0.06367 | 0.56146 | -0.03939 |
| 61 | 0.56953 | 0.06315 | 0.57134 | -0.03763 |
| 62 | 0.57950 | 0.06260 | 0.58121 | -0.03584 |
| 63 | 0.58949 | 0.06201 | 0.59107 | -0.03393 |
| 64 | 0.59946 | 0.06138 | 0.60096 | -0.03199 |
| 65 | 0.60945 | 0.06070 | 0.61086 | -0.03002 |
| 66 | 0.61942 | 0.05999 | 0.62072 | -0.02799 |
| 67 | 0.62941 | 0.05923 | 0.63067 | -0.02593 |
| 68 | 0.63939 | 0.05844 | 0.64061 | -0.02389 |
| 69 | 0.64937 | 0.05760 | 0.65060 | -0.02185 |
| 70 | 0.65936 | 0.05673 | 0.66058 | -0.01986 |
| 71 | 0.66936 | 0.05581 | 0.67058 | -0.01790 |
| 72 | 0.67934 | 0.05486 | 0.68057 | -0.01599 |
| 73 | 0.68934 | 0.05386 | 0.69052 | -0.01411 |
| 74 | 0.69933 | 0.05284 | 0.70051 | -0.01227 |
| 75 | 0.70933 | 0.05177 | 0.71052 | -0.01047 |
| 76 | 0.71932 | 0.05066 | 0.72054 | -0.00873 |
| 77 | 0.72933 | 0.04951 | 0.73057 | -0.00704 |
| 78 | 0.73932 | 0.04833 | 0.74075 | -0.00541 |
| 79 | 0.74932 | 0.04710 | 0.75073 | -0.00390 |
| 80 | 0.75934 | 0.04584 | 0.76081 | -0.00249 |
| 81 | 0.76935 | 0.04454 | 0.77092 | -0.00120 |
| 82 | 0.77933 | 0.04321 | 0.78102 | -0.00003 |
| 83 | 0.78936 | 0.04183 | 0.79117 | 0.00102 |
| 84 | 0.79939 | 0.04042 | 0.79876 | 0.00172 |
| 85 | 0.80940 | 0.03898 | 0.80884 | 0.00256 |
| 86 | 0.81941 | 0.03752 | 0.81897 | 0.00329 |
| 87 | 0.82944 | 0.03601 | 0.82911 | 0.00392 |
| 88 | 0.83945 | 0.03448 | 0.83925 | 0.00440 |
| 89 | 0.84947 | 0.03291 | 0.84938 | 0.00479 |
| 90 | 0.85950 | 0.03131 | 0.85701 | 0.00499 |
| 91 | 0.86954 | 0.02969 | 0.86714 | 0.00514 |
| 92 | 0.87955 | 0.02804 | 0.87727 | 0.00521 |
| 93 | 0.88958 | 0.02635 | 0.88742 | 0.00516 |
| 94 | 0.89961 | 0.02462 | 0.89757 | 0.00498 |
| 95 | 0.90963 | 0.02288 | 0.90770 | 0.00471 |
| 96 | 0.91967 | 0.02109 | 0.91785 | 0.00431 |
| 97 | 0.92968 | 0.01927 | 0.92800 | 0.00385 |
| 98 | 0.93972 | 0.01740 | 0.93813 | 0.00328 |
| 99 | 0.94972 | 0.01550 | 0.94829 | 0.00260 |
| 100 | 0.95975 | 0.01355 | 0.95843 | 0.00185 |
| 101 | 0.96972 | 0.01154 | 0.96855 | 0.00098 |
| 102 | 0.97970 | 0.00946 | 0.97867 | 0.00004 |
| 103 | 0.98968 | 0.00727 | 0.98871 | 0.00090 |
| 104 | 0.99389 | 0.00649 | 0.99852 | 0.00172 |
| 105 | 1.00000 | 0.00486 | 1.00000 | -0.00185 |

TABLE 1

MEASURED SECTION COORDINATES

| OBERSEITE | | | | UNTERSEITE | | | |
|---|---|---|---|---|---|---|---|
| NR. | X/L | NR. | X/L | NR. | X/L | NR. | X/L |
| 1 | .0000 | 16 | .3798 | 32 | .0032 | 47 | .6501 |
| 2 | .0040 | 17 | .4197 | 33 | .0069 | 48 | .7001 |
| 3 | .0079 | 18 | .4597 | 34 | .0188 | 49 | .7501 |
| 4 | .0137 | 19 | .5000 | 35 | .0495 | 50 | .8003 |
| 5 | .0244 | 20 | .5399 | 36 | .0996 | 51 | .8525 |
| 6 | .0391 | 21 | .5798 | 37 | .1495 | 52 | .9001 |
| 7 | .0599 | 22 | .6198 | 38 | .1996 | 53 | .9500 |
| 8 | .0796 | 23 | .6598 | 39 | .2596 | | |
| 9 | .0996 | 24 | .6998 | 40 | .2997 | | |
| 10 | .1396 | 25 | .7500 | 41 | .3499 | | |
| 11 | .1796 | 26 | .7997 | 42 | .3997 | | |
| 12 | .2197 | 27 | .8491 | 43 | .4500 | | |
| 13 | .2597 | 28 | .8997 | 44 | .5000 | | |
| 14 | . 98 | 29 | .9498 | 45 | .5500 | | |
| 15 | .3398 | 30 | .9748 | 46 | .5999 | | |
| | | 31 | 1.0000 | | | | |

TABLE 2

LOCATIONS OF PRESSURE MEASUREMENT ORIFICES

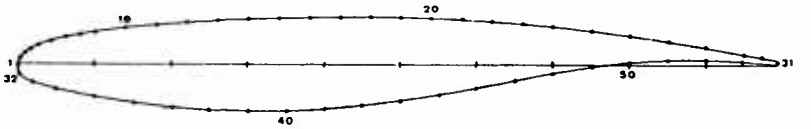



FIGURE 1

SECTION PROFILE OF VA2 AIRFOIL

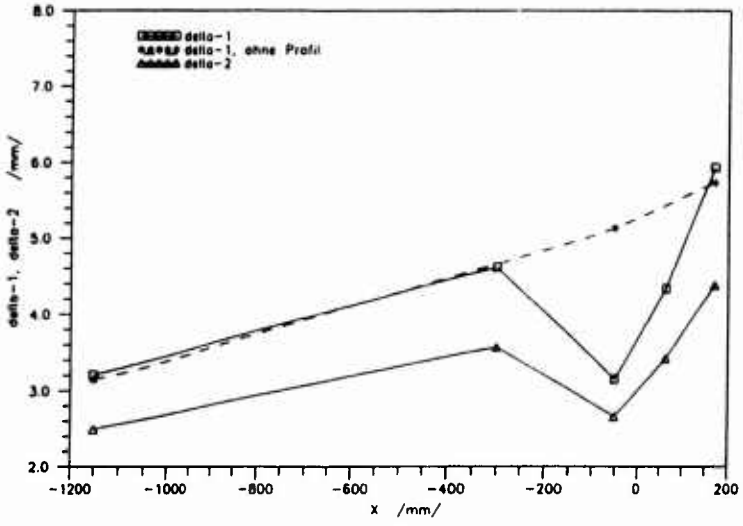



FIGURE 2

CHANGE OF WALL BOUNDARY LAYER PARAMETERS IN LONGITUDINAL DIRECTION UNDER INFLUENCE OF AIRFOIL FLOW FIELD ($\alpha$ = 0°)

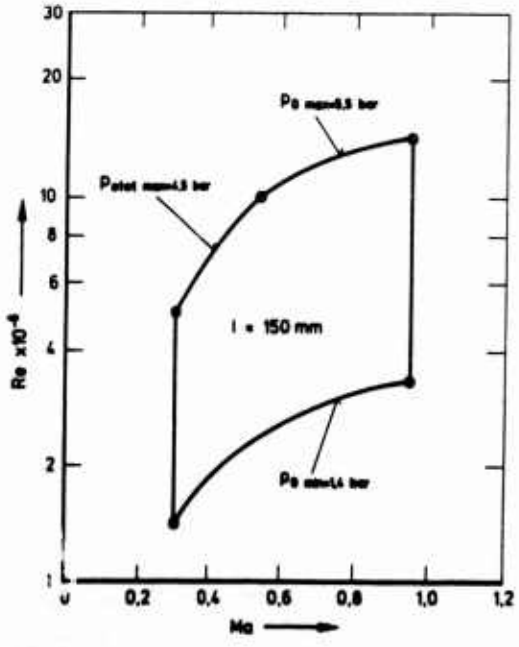



FIGURE 3

OPERATING RANGE OF TWB

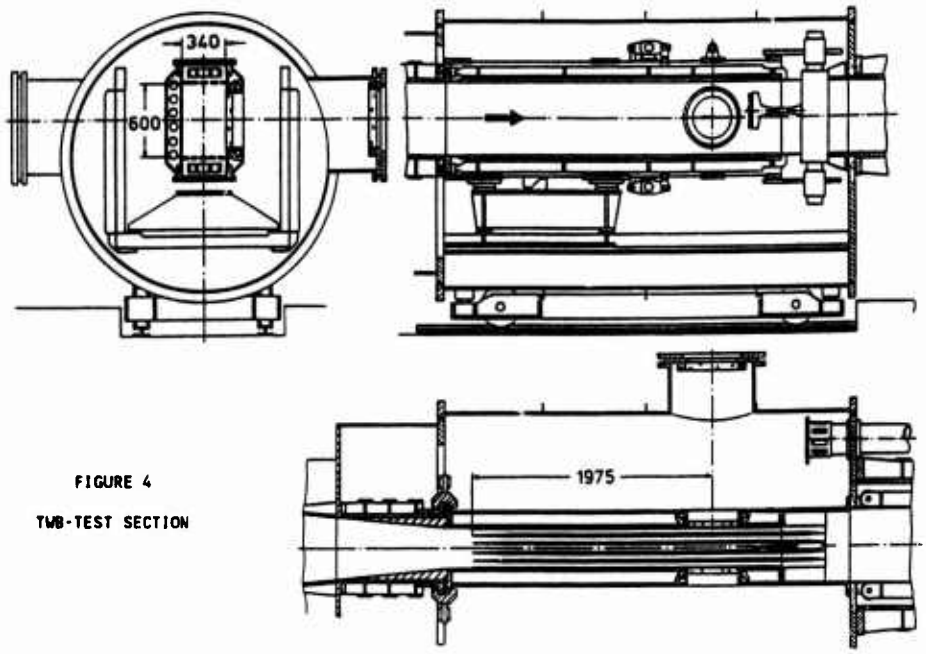



FIGURE 4

TWB-TEST SECTION

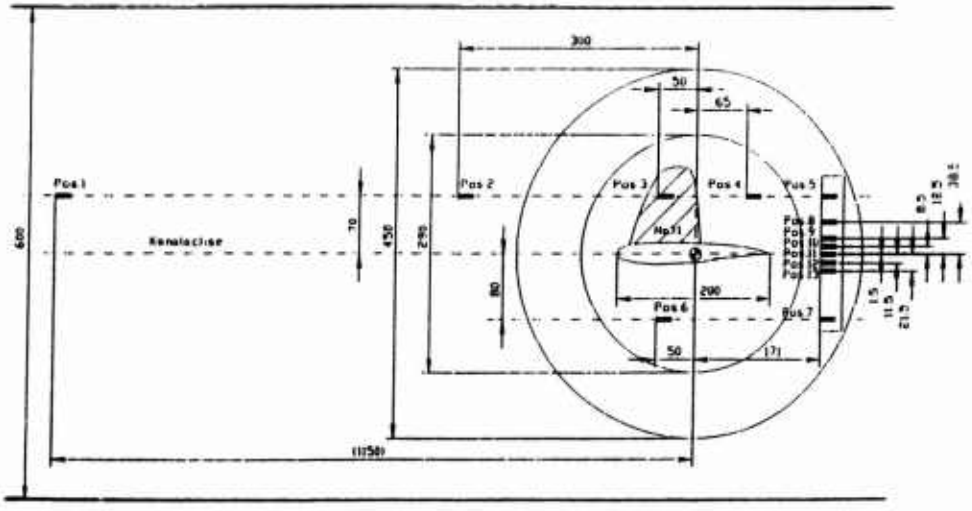



FIGURE 5

LOCATION OF BOUNDARY LAYER MEASUREMENTS ON SIDE WALL

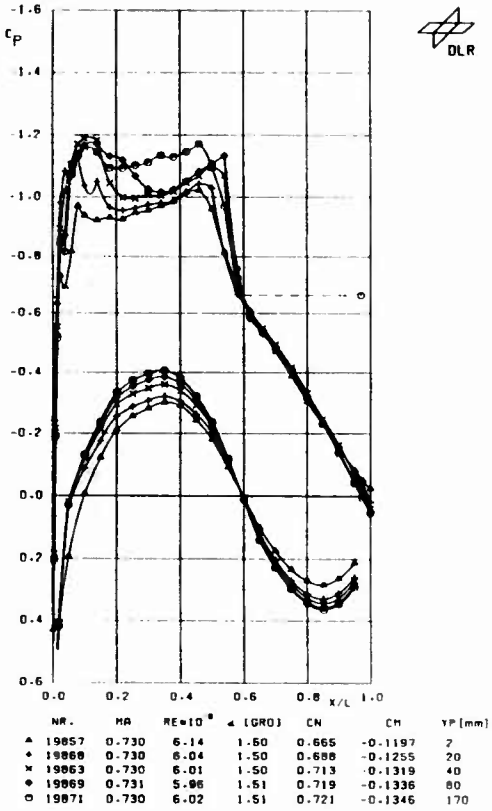
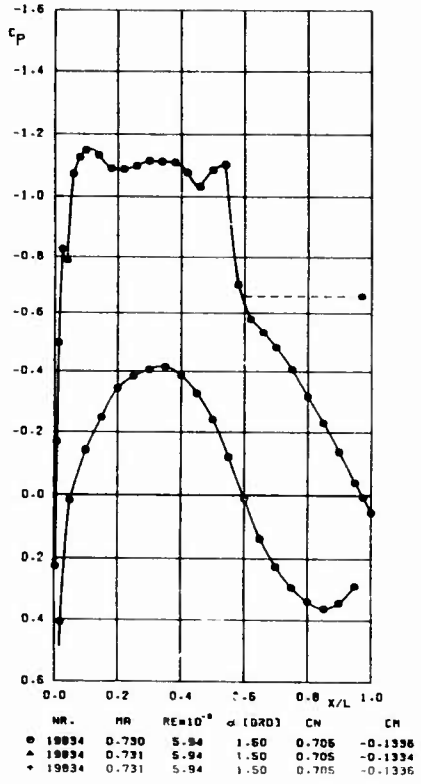



FIGURE 6

CHANGE OF PRESSURE DISTRIBUTION IN SPANWISE DIRECTION



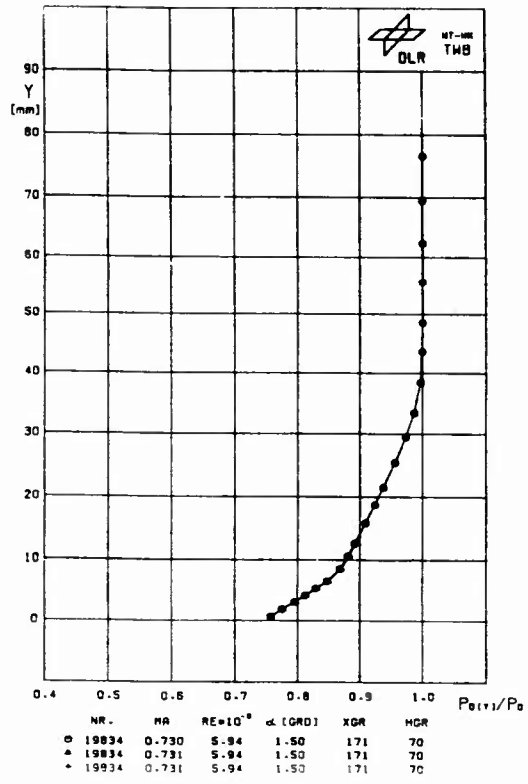




FIGURE 7

REPEAT MEASUREMENTS OF AIRFOIL PRESSURE DISTRIBUTION AND SIDE WALL BOUNDARY LAYER

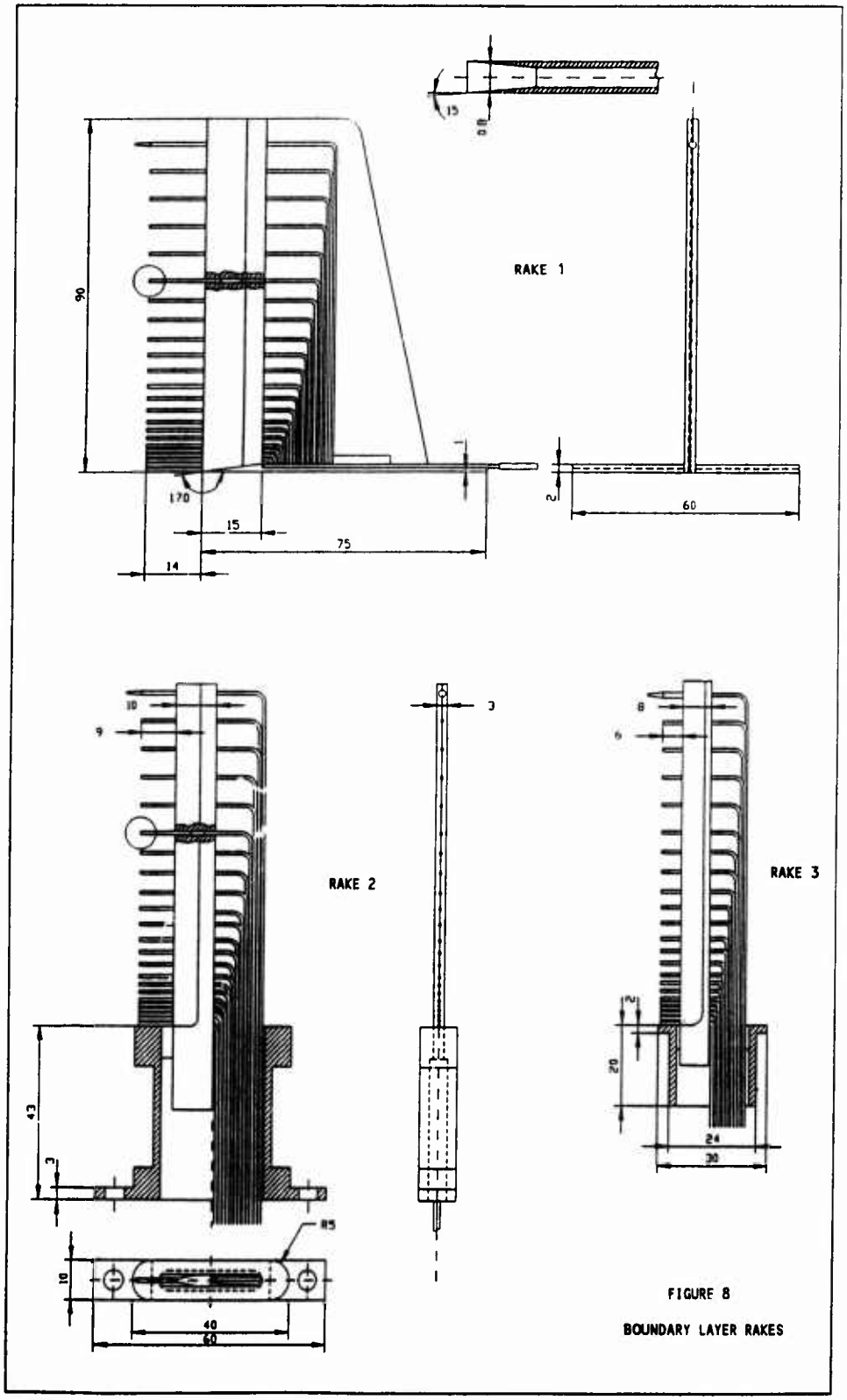



FIGURE 8

BOUNDARY LAYER RAKES

# MEASUREMENTS ON A TWO-DIMENSIONAL AEROFOIL WITH HIGH-LIFT DEVICES

by

I.R.M.Moir
DRA Farnborough

## 0 INTRODUCTION

The tests detailed in this submission were carried out by the former British Aircraft Corporation in support of the National High Lift Programme. This Programme was a collaborative project between the Royal Aerospace Establishment Farnborough (now part of the DRA) and the aircraft industry with the aim of increasing the understanding and knowledge of all aspects of high-lift systems, and to provide a fund of data which would benefit the design of future transport aircraft.

Wind-tunnel tests were carried out on four models:

(i) A 3-D half model (RAE)
(ii) a swept panel wing (HSA Hatfield)
(iii) a quasi-2D (end-plate) model (BAC Weybridge)
(iv) a 2D model (BAC Weybridge)

BAC Warton also carried out structural analyses on various leading-edge and trailing-edge devices.

The present cases are results from the 2D tests which covered investigations into two leading-edge and two trailing-edge devices. The model had a supercritical aerofoil section, a chord of 0.7635m, and was mounted between turntables in the floor and roof of the BAC 3.96m x 2.74m low-speed wind-tunnel. Two-dimensional conditions were maintained by local suction around the wing/wall junctions. Surface pressures were measured on all the components of the wing, at two spanwise stations, one near the tunnel centreline and one near the roof. These pressures were integrated to give overall lift, drag and pitching moment coefficients. A pitot/static traverse through the wake provided the total momentum deficit. Traverses perpendicular to the wing surface at various chordwise locations provided information on wake and boundary layer development and interaction. Flow visualisation was provided by tufting of the wing surfaces.

## 1 GENERAL DESCRIPTION

### 1.1 Model name or designation

The model will be referred to as NHLP 2D.

### 1.2 Model type and flow conditions

The model consisted of a two-dimensional wing with high-lift devices, designed for testing at low subsonic speeds.

### 1.3 Design requirements and purpose of tests

The model was designed for tests on a wide range of high-lift devices. The position and deflection angle of these could be varied. Two-dimensional flow conditions were maintained during tests by the use of local suction at the wing/wall junctions.

### 1.4 Dominant flow physics

The performance of a high-lift wing is dependent upon a strong interaction between the wakes and boundary layers associated with each element (e.g. slat/wing/flap etc.). Each downstream element enables the element ahead of it to carry a higher load than it would in isolation, due to the fact that its trailing-edge is situated in the suction field of the downstream element; this makes the pressure at the trailing-edge significantly negative, so that, for a given pressure recovery, higher peak suctions can be sustained. At the same time, the wake from the upstream element can interact with the boundary layer on the downstream element, thickening the latter and producing earlier separation. The former effect demands that the two elements be moved closer together, while the latter requires the two to be separated. This leads to the concept of optimum relative positions of the elements of a high-lift aerofoil. These mechanisms are illustrated in Fig 1 which shows typical pressure distributions on a three element aerofoil, together with wake/boundary layer profiles and development, derived from these profiles. Also shown is a typical plot of lift coefficient against angle of incidence which illustrates the variation of $C_L$ with slat position.

### 1.5 Additional remarks

The data offered here were gathered in the early 1970's, before CFD methods attained accuracy sufficient to make the comparison between theory and experiment of significance throughout the whole flow-field. Unfortunately the data presented here consist only of

surface pressures on the model and measurements of static and total head variation through the wake and boundary layers at selected chordwise positions. Despite this, the data form an unusually wide coverage of different slotted high-lift systems at moderately high Reynolds Number in a flow with an exceptionally high degree of 2-dimensionality.

The technique of using wall suction, not only to prevent the separation of side-wall boundary layers, but also to reduce their growth substantially, has been proved in a number of previous experiments[1,2,3], and leads to a flow which is closely 2-dimensional. Since accurate data of this type, with highly deflected flaps, are difficult and expensive to obtain, this set should afford a valuable addition to the library of test cases available to AGARD countries.

## 2 DETAILS OF MODEL

### 2.1 General geometric arrangement

Fig 2a shows the NHLP 2D model planform, and a typical aerofoil cross-section.

### 2.2 Configurations

Fig 2b shows the alternative high-lift devices tested.

### 2.3 Wing and aerofoil data.

#### 2.3.1 Planform

| | |
|---|---|
| Span | = 2.743m |
| Aspect ratio | = 3.593 |
| Area | = 2.094m |

#### 2.3.2 Basic aerofoil section

Wing section: BAC 3-11/RES/30/21
Thickness/chord = 11%
Nose radius r/c = 0.0137

### 2.7 Geometric definition

The aerofoil profile was numerically defined, and the design ordinates are provided. Tolerance on the profile is ±0.13mm. Roughness data are not available.

### 2.8 Model support details

The model was mounted between turntables in the floor and roof of the tunnel, as shown in Fig 2a.

#### 2.8.2 Special features of mounting

Local suction was applied around the wing roots as shown in Fig 2c.

## 3 GENERAL TUNNEL INFORMATION

### 3.1 Tunnel designation

BAC Weybridge 3.96m x 2.74m

### 3.2 Organisation running tunnel:

British Aircraft Corporation(BAC)

### 3.3 Type of tunnel

Low-Speed, closed circuit.
Operating envelope: 12.2m/sec → 97.5m/sec
Maximum Re/m = 6.6 x $10^6$

### 3.4 Test Section

#### 3.4.1 Test section details

Fig 3 shows the model in the tunnel working section.

#### 3.4.2 Test section dimensions

3.96m x 2.74m x 6.35m
Corner fillet size: 0.762m x 0.762m approx.

#### 3.4.3 Wall geometry details

Walls of working section were solid.
No wall static pressures were measured.
Boundary layer control was applied in the region of the wing roots only.
Wall boundary layer total thickness was 88mm and displacement thickness was 10.5mm approximately.

### 3.5 Freestream conditions

#### 3.5.1 Reference pressure measurement

Total pressure was measured by a tapping in the maximum section.
Static pressure was measured by a tapping at the position shown in Fig 3. Positional corrections were applied to these readings.
Static temperature was not measured.

#### 3.5.2 Tunnel calibration

The tunnel was calibrated over three transverse planes within the working section in the region of the model, at a wind velocity of 30.5m/sec. A pitot-static tube with an ellipsoidal head was traversed over a grid with intervals 0.304m horizontally and 0.152m vertically.
The tunnel was last calibrated in about 1969.

### 3.6 Flow Quality of empty tunnel

#### 3.6.1 Flow uniformity

The static pressure varied approximately 0.4% over the model chord, and insignificantly across the span.
The Mach number was held constant during a run.
The flow angularity was measured by a pitch meter.
The upwash at the model station was 0.23°.
Sidewash is not available.

#### 3.6.2 Temperature variation

The tunnel temperature could not be controlled and varied approximately 5°C during a run. The variation within the tunnel is not available.

#### 3.6.3 Flow unsteadiness

The tunnel turbulence factor was 1.068.
The noise level is not available.

## 4 INSTRUMENTATION

### 4.1 Model position

#### 4.1.1 Measurement of geometrical incidence

The geometrical incidence was derived from the rotation angle of the turntables.

#### 4.1.2 Accuracy of incidence measurement = ±0.05°.

### 4.2 Model pressure measurement

#### 4.2.1 Number and disposition of pressure tappings

Fig 4a indicates the position of the pressure tappings on the components of the model. Tappings are located at two spanwise stations as shown in Fig 2a.

#### 4.2.2 Range of pressure transducers

Statham unbonded strain-gauge type pressure transducers were used with ranges matched to the expected pressures on the wing. 34.5kPa,17.2kPa,6.9kPa and 3.4kPa ranges were used.

#### 4.2.3 Dynamic pressures were not measured.

### 4.3 Force and moment measurement

#### 4.3.1 Type of balance

No balance was used as sectional force and moment coefficients were obtained from integration of the pressure coefficients.

### 4.4 Boundary layer and flow field measurements

**4.4.1/2/3** Boundary layer measurements were made by traversing a pitot/static probe normal to the wing surface. Wake momentum deficit was measured by a pitot/static rake mounted downstream of the model on a traversing rig which enabled it to be aligned with the model wake, as shown in Fig 4b.

### 4.5 Surface flow visualisation.

**4.5.1/2** Surface flow visualisation was carried out by means of wool tufts attached to the surface at various locations on the wing and leading and trailing edges.

#### 4.5.3 Results of flow visualisation

These are in the form of photographs, but cannot be made available.

## 5 TEST MATRIX AND CONDITIONS

### 5.1 Detailed test matrix

#### 5.1.1 Number of selected test cases

Eight test cases are offered, consisting of surface pressure measurements and boundary layer traverses at two angles of incidence for one configuration, and at three angles of incidence for two other configurations. Note that not all boundary layer traverse positions are covered at each angle of incidence. The configurations offered are listed in 5.1.2.

#### 5.1.2 Configurations tested

The configurations tested were:

(i) L1 slat (12.5%) at 25° + T2 single-slotted flap at 20°
(ii) L1 slat + T7 double-slotted flap at 40°
(iii) L1 slat + T8 triple-slotted flap(7.5°,40°,20°)

#### 5.1.3 Test matrix

A full test matrix is given in Table 1.

### 5.2 Model/tunnel relations

#### 5.2.1 Maximum blockage

Maximum solid blockage = $\Delta U/U_0$ = 0.00169

#### 5.2.2 Model span/tunnel width = 1

#### 5.2.3 Wing area/tunnel cross section

S/C = 0.215 approx (area of fillets has been estimated)

**5.2.4 Tunnel height/chord ratio** = 3.593

**5.2.5 Tunnel width/chord ratio** = 5.190

**5.3 Transition details**

**5.3.1** Transition was fixed on the wing upper and lower surfaces.

**5.3.2** At high-lift the upper surface transition was forward of the transition fix due to a short laminar bubble near the leading-edge.

**5.3.3** Details of the transition fixing is shown in Fig 5. No data are available on the effectiveness of the fixing, apart from as stated in 5.3.2.

**6 DATA**

**6.1 Availability of data**

**6.1.1 Organisation owning the data**

Defence Research Agency, Farnborough

**6.1.2 Person responsible for the data**

Dr D.S.Woodward,
Superintendant AP3 Division,
Aerodynamics & Propulsion Dept.,
X80 Building,
Defence Research Agency,
Farnborough,
Hampshire GU14 6TD
United Kingdom
Tel: 0252-395377
Fax: 0252-377783

**6.1.3 Availability of data**

The data specified in this document are freely available.

**6.2 Suitability of data for CFD validation.**

**6.2.1** Data are suitable for 'in tunnel' calculation, although no wall pressure data are available. Data are corrected for solid blockage, and by a simple correction to incidence to represent the effect of wall constraint as follows:

$$\Delta\alpha = 0.0693(C_L + 4C_m)^\circ$$

No camber or wake blockage corrections have been applied, but full incidence polars will be supplied for the calculation of these quantities.

**6.2.2** Data are corrected to simulate 'free-air' conditions.

**6.3 Type and form in which data are available.**

**6.3.1** Details are given in Table 2 of the form in which the various components of the data exist.

Freestream velocity is corrected for solid blockage.

Pressure coefficients are based of freestream dynamic pressure, corrected for solid blockage.

Force and moment coefficients are based on corrected freestream dynamic pressure, and are also corrected for wall constraint, as detailed in 6.2.1.

**6.3.2** At the time of the preparation of this document the data were only available in printed form, but were being prepared for availability on floppy disk.

**6.3.3/4 Extent of data**

This was not available at the time of preparation of this document.

**6.4 Corrections applied to data.**

**6.4.1 Lift interference and blockage correction**

The data are considered to be globally correctable. Classical correction methods are applied according to Ref 4.
Dynamic pressure, angle of incidence, and pressure coefficients are corrected. Some uncorrected data may be available.

**6.4.2 Side wall interference corrections**

The wall boundary layer was removed by suction in the region of the model.

**6.4.5 Aeroelastic deformation**

This was not measured as the model itself was rigidly mounted and the high-lift devices were mounted on 10 brackets which minimised deformation.

**6.4.6** It is not known if corrections were made for effect of wake traverse, etc. No measurements were made to determine the effect of bracket wake on the flow.

**7 DATA ACCURACY AND REPEATABILITY ASSESSMENT**

**7.1 Accuracy estimates**

**7.1.1 Free-stream conditions**

Mach number - ±0.5%
Flow velocity - as Mach No

Angle of incidence - ±0.05°

**7.1.2 Measured data**

Forces and moments -
$C_N$ ±0.12%
$C_A$ ±0.2%
$C_m$ ±0.15%

Pressure coefficients - ±0.1%

**7.2 Repeat measurements.**

**7.2.1 Type and number of repeats during one test series**

Unknown

**7.2.2 Type and number of repeats in successive tests**

Unknown

**7.4 Other tests on the same nominal geometry.**

**7.4.1** The model was not tested in any other tunnel.

**7.4.2** Related models have been tested in other tunnels - see Introduction.

## 8 REFERENCES


1. D.N.Foster, H.P.A.H.Irwin, B.R.Williams — The Two-Dimensional Flow around a Slotted Flap. R&M 3681 1971

2. I.R.M.Maar, D.N.Foster, D.R.Holt — The Measurement and Analysis of the Profile Drag of a Wing with Slotted Flap. RAE TR 71158 1971

3. D.N.Foster, P.R.Ashill, B.R.Williams — The nature, development, and effect of the Viscous Flow around an Aerofoil with High Lift Devices. RAE TR 72227 1972

4. H.C.Garner, E.W.E.Rogers, W.E.A.Acum, E.C.Maskell — Subsonic Wind Tunnel Corrections AGARDOGRAPH 109 October 1966

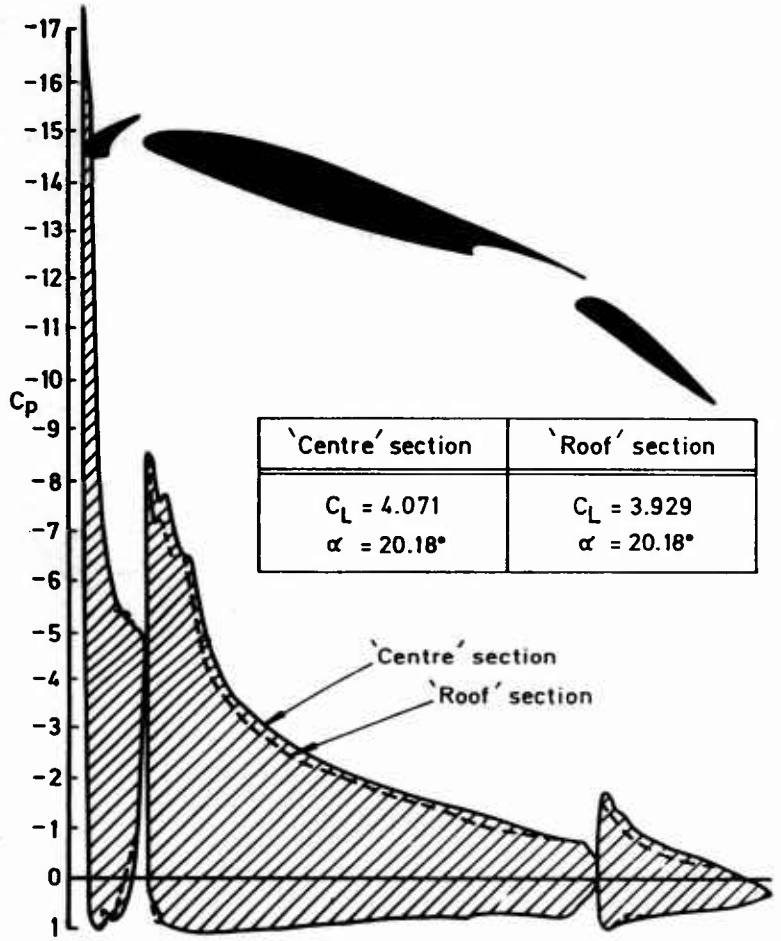
**TABLE 1**

| Case No. | Slat | Flap | $U_0$ m/s | q kPa | Re $x10^{-6}$ | Notes |
|---|---|---|---|---|---|---|
| 1 | L1 | T2 | 67.0 | 2.75 | 3.52 | Optimum slat position. Boundary layer traverse at $\alpha$ = 4°, at 25% wing chord,shroud t/e,50% flap chord,flap t/e. |
| 2 | L1 | T2 | 67.0 | 2.75 | 3.52 | Optimum slat position. Boundary layer traverse at $\alpha$ = 20°, at 25% wing chord,shroud t/e,50% flap chord,flap t/e. |
| 3 | L1 | T7 | 54.9 | 1.85 | 2.88 | Boundary layer traverses at $\alpha$ = 3°, at 37.2% wing chord, aft of flap trailing edge. |
| 4 | L1 | T7 | 54.9 | 1.85 | 2.88 | Boundary layer traverses at $\alpha$ = 17°, at 37.2%,80%,91% wing chord, 50% vane chord, 50%,75% flap,aft of flap trailing edge. |
| 5 | L1 | T7 | 54.9 | 1.85 | 2.88 | Boundary layer traverses at $\alpha$ = 19°, at 37.2%,80%,91% wing chord, 50% vane chord, 50%,75% flap,aft of flap trailing edge. |
| 6 | L1 | T8 | 54.9 | 1.85 | 2.88 | Boundary layer traverse at $\alpha$ = 3°, aft of flap trailing edge. |
| 7 | L1 | T8 | 54.9 | 1.85 | 2.88 | Boundary layer traverse at $\alpha$ = 15°, aft of wing shroud t/e, flap shroud t/e, flap t/e. |
| 8 | L1 | T8 | 54.9 | 1.85 | 2.88 | Boundary layer traverse at $\alpha$ = 17°, aft of wing shroud t/e, flap shroud t/e, flap t/e. |

Notes: Surface pressures measured and wake traverse for all cases.
Re is based on retracted chord of 0.7635m.

**TABLE 2**

| Data | Engineering Units | Coefficients | Normalised | Uncorrected | Corrected |
|---|---|---|---|---|---|
| Freestream Conditions | Yes | - | - | - | Yes |
| Surface Pressures | No | Yes | No | No | Yes |
| Forces | No | Yes | No | Yes | Yes |
| b/l Data | Yes | Yes | No | No | Yes |
| Wake Data | Yes | Yes | No | No | Yes |




| 'Centre' section | 'Roof' section |
|---|---|
| $C_L$ = 4.071<br>$\alpha$ = 20.18° | $C_L$ = 3.929<br>$\alpha$ = 20.18° |

Fig 1a Typical pressure distribution on three element high-lift aerofoil

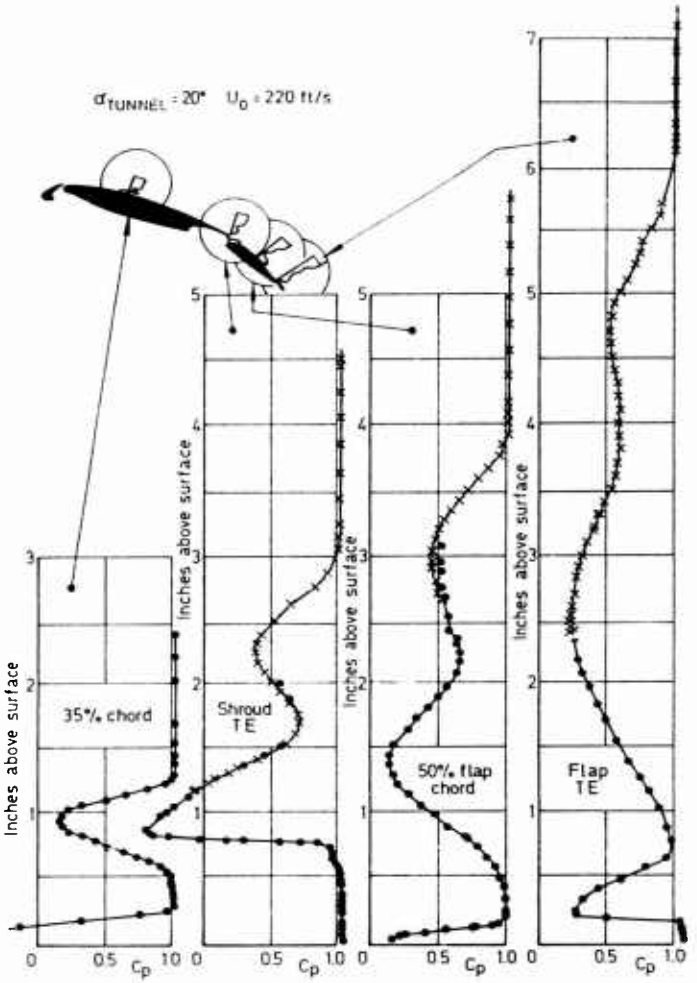



Fig 1b Typical wake/boundary layer velocity profiles

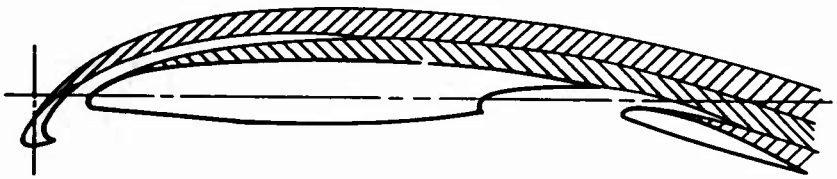


Fig 1c Wake/boundary layer interaction on three element high-lift aerofoil

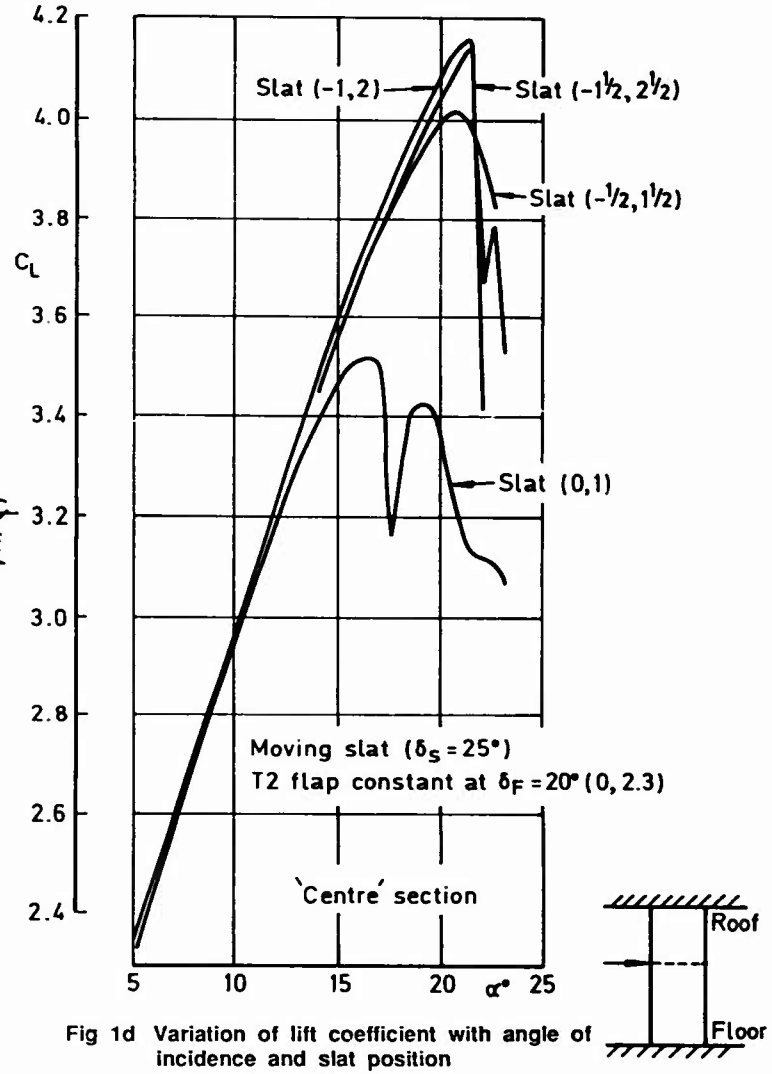



Fig 1d Variation of lift coefficient with angle of incidence and slat position

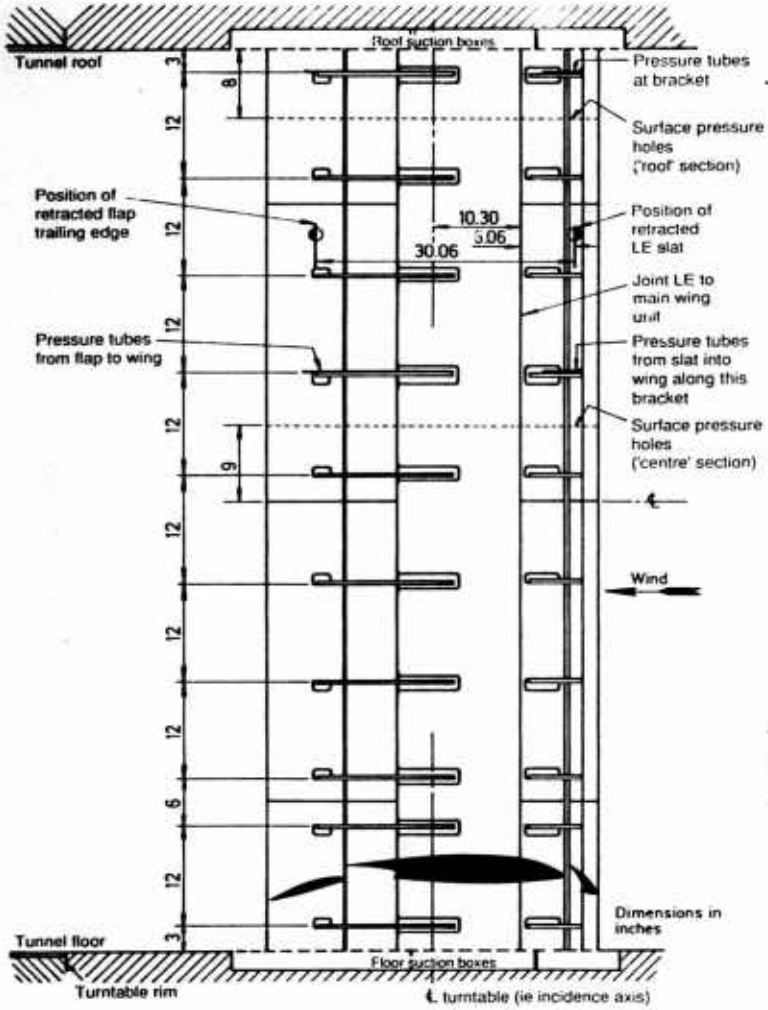



Fig 2a NHLP 2D model planform

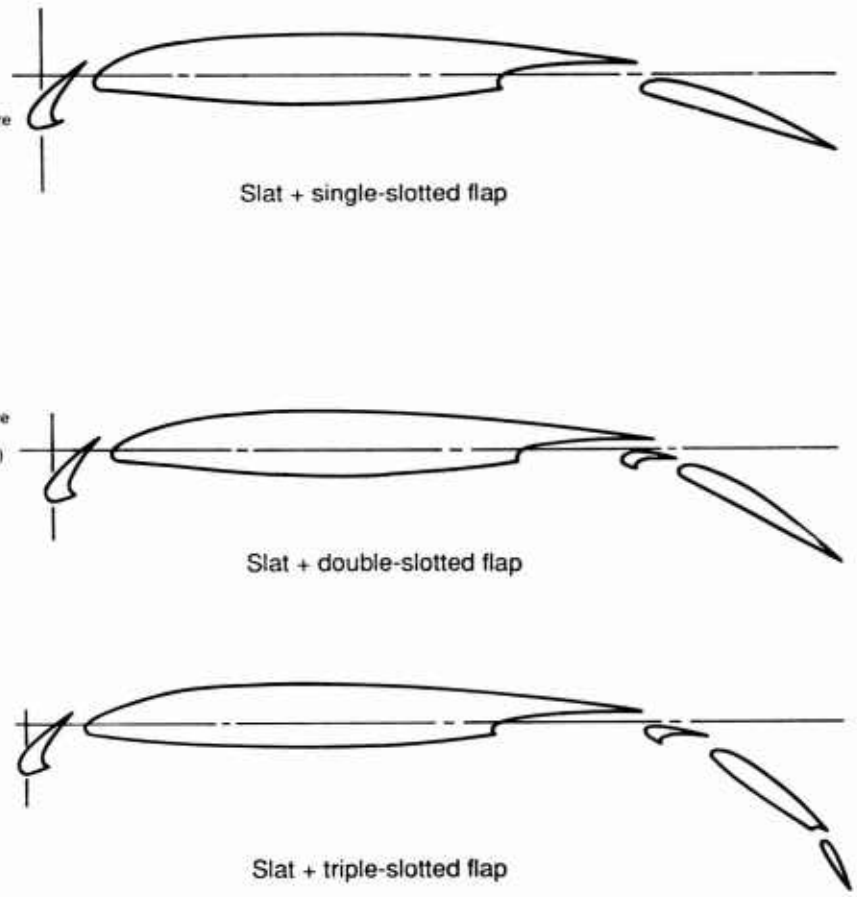
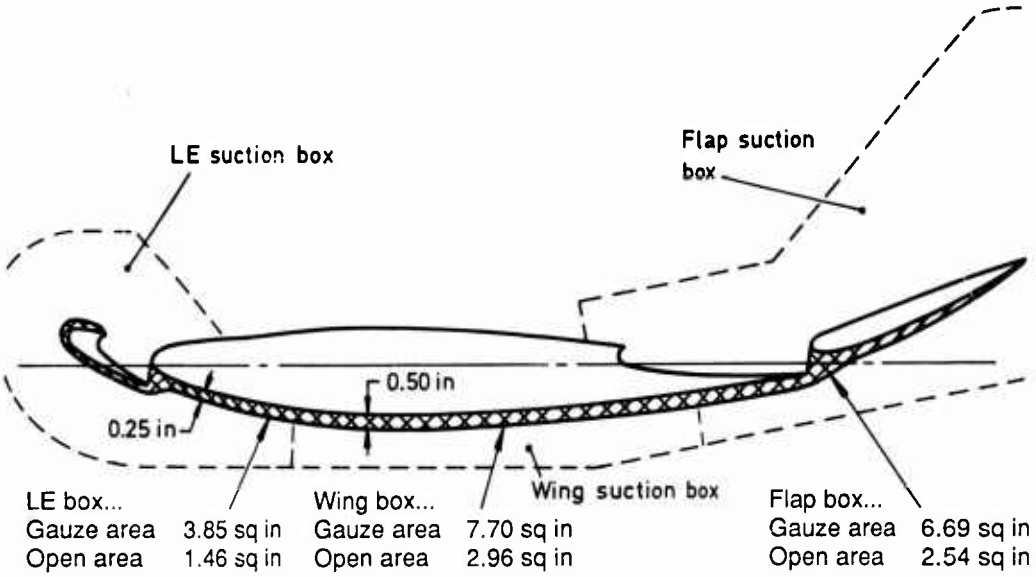



Fig 2b Alternative configurations




The porous area of each box is sealed by cover plates and tape to leave only the open strip along profile upper surface as shown in sketch

**Fig 2c Distribution of suction areas around wing at roof and floor of tunnel**

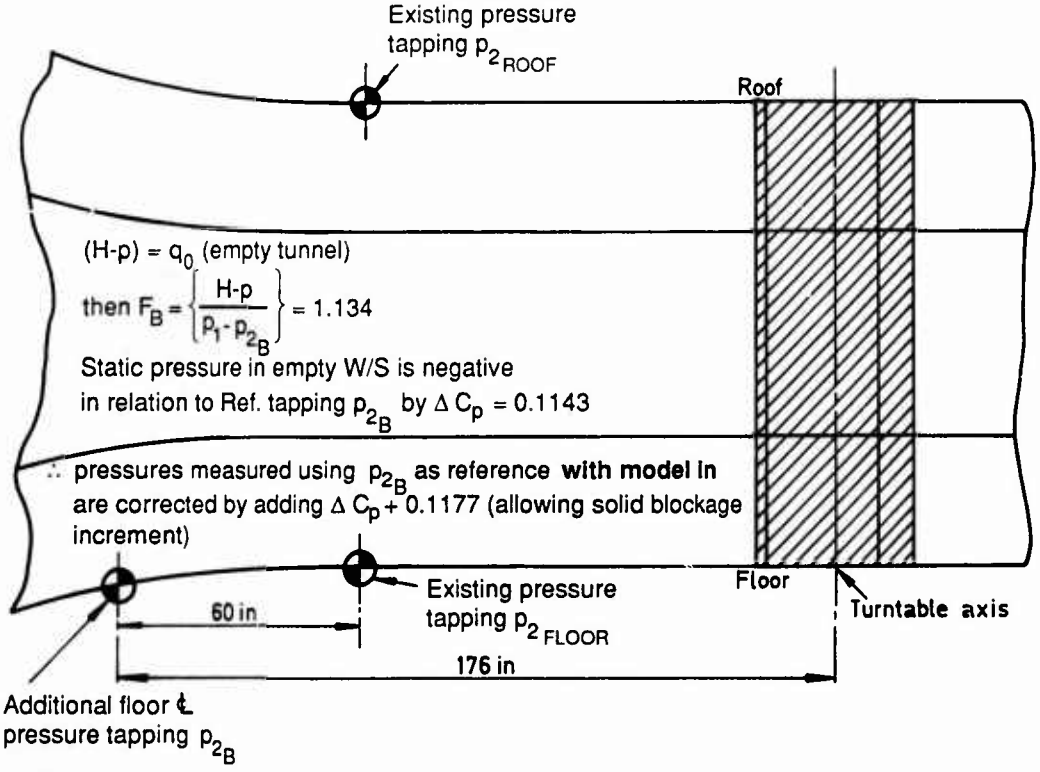



**Fig 3 NHLP 2D model in tunnel, showing reference pressure tappings**

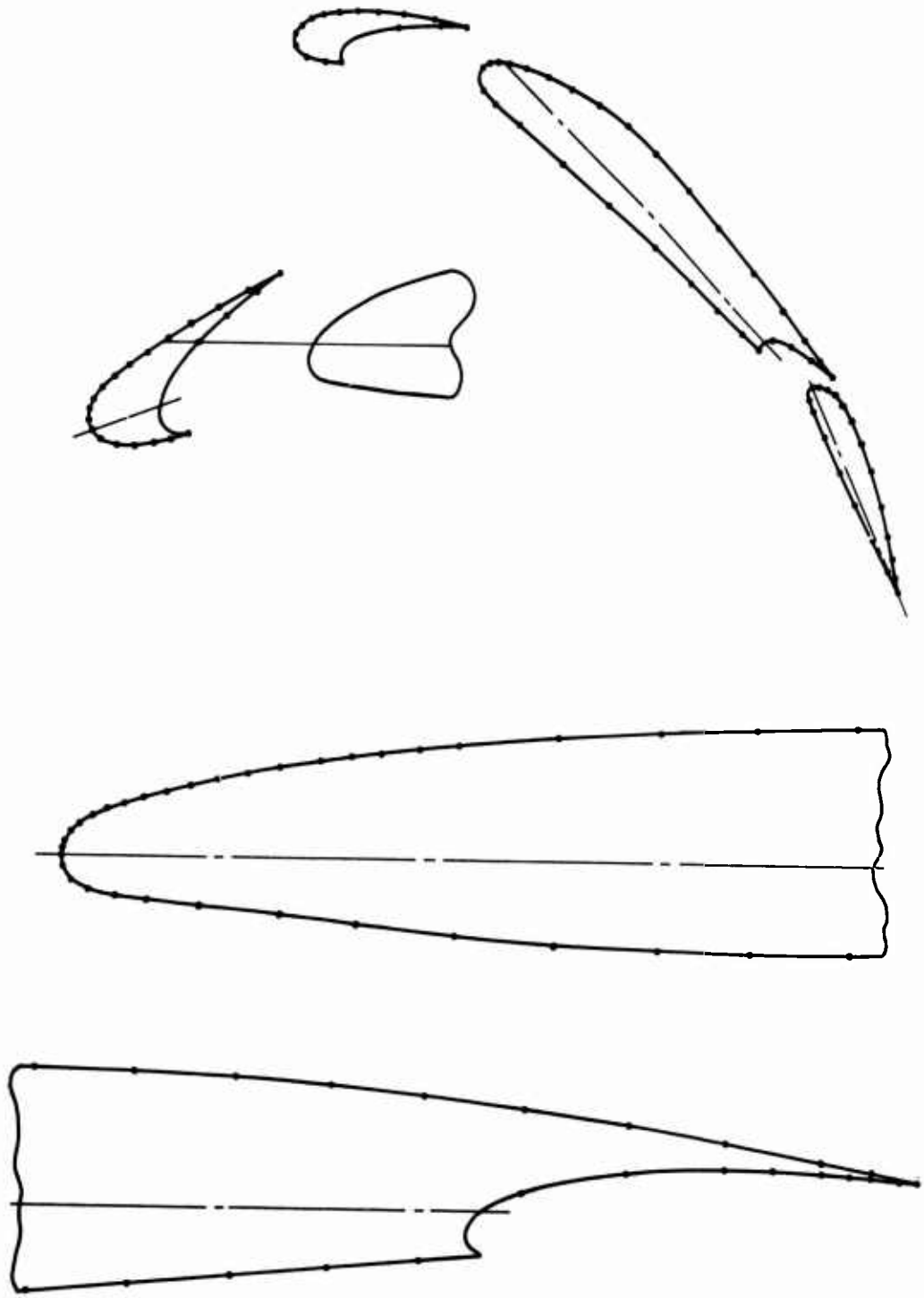
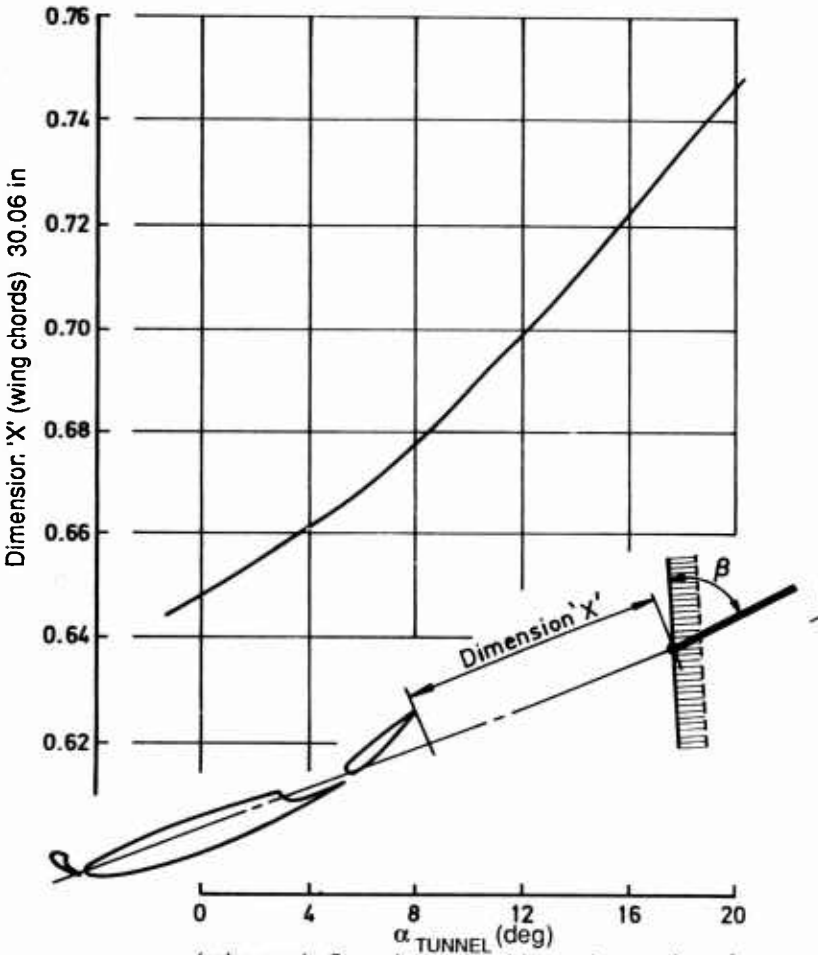


Fig 4a Positions of pressure tappings on wing surface




(rake angle β predetermined from observation of cotton streamer attached to rake)

**Fig 4b Position of wake rake relative to model**

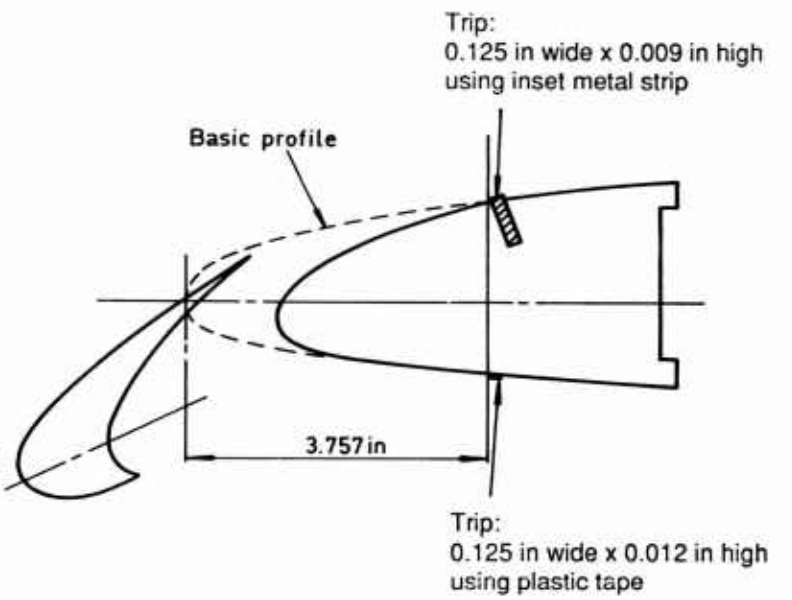



**Fig 5 Details of transition fix**

# INVESTIGATION OF THE FLOW OVER A SERIES OF 14%-THICK SUPERCRITICAL AEROFOILS WITH SIGNIFICANT REAR CAMBER

by

P.R. Ashill
Defence Research Agency
Bedford, MK41 6AE, UK

## 0 INTRODUCTION

The experiments described in this submission were performed on various aerofoil sections, all of 14% thickness/chord ratio and with significant rear camber. The main aim was to obtain an improved understanding of viscous effects on flows over aerofoils with severe adverse pressure gradients. Such gradients can be found at the rear of aerofoils with significant rear camber and at the foot of shock waves.

The tests were performed in the 8ft x 8ft Pressurised, Subsonic/Supersonic Wind Tunnel at the Defence Research Agency (DRA, formerly the Royal Aerospace Establishment) Bedford between November 1976 and February 1982. This wind tunnel has solid walls and, since the aerofoil chord to tunnel height is relatively large (0.26), the data are strictly not correctable. This was recognised from the outset, the main concern of the investigation being with studying flows rather than performing tests on a prescribed shape. However, the wall boundary conditions are well defined and so the data may be useful for validating CFD codes which include allowance for the wind-tunnel walls. In addition, measurements were made of the static pressures on the roof and floor of the working section, providing an independent check on the accuracy of the representation of the walls in any CFD method. Despite the caveat above about correctability, it is believed that the cases presented having weak shock waves may be used to assess free-air calculation methods provided that allowance is made in the calculation for wall-induced camber. Cases suitable for such work are highlighted in Section 6.2 where details are also given of the camber correction.

## 1 GENERAL DESCRIPTION

### 1.1 Model name or designation

Model 2058, 2D aerofoil model with various trailing-edge shapes aft of 65% chord.

### 1.2 Model type and flow conditions

2D aerofoil. Subsonic free stream. The tests include examples with shock waves and with separations near the trailing edge.

### 1.3 Design requirements, purpose of test

The model had aerofoil sections of 14% thickness chord ratio and was designed so that the section aft of 65% chord could be changed. This allowed flows with rear pressure distributions of differing form and with gradients of varying degrees of severity to be studied. Three classes of pressure distribution on the rear 40% to 50% chord were investigated, as illustrated schematically in Fig 1. As shown in Fig 1, six aerofoils with pressure distributions on the rear of the upper surface of the 'convex' type were studied. For this type of pressure distribution, the pressure gradient becomes increasingly adverse towards the trailing edge. Of these six aerofoils, three had aerodynamically-sharp trailing edges and the remaining three had blunt bases. The solitary section with a 'two-part' rear pressure distribution (ie with the pressure rising towards the trailing edge in two stages or parts) had a blunt base of ½% thickness. Two sections were tested with 'relaxing' pressure distributions (ie with pressure gradients decreasing towards the trailing edge). All the aerofoil sections were designed to have similar boundary-layer characteristics on the lower surface.

### 1.4 Dominant flow physics

The dominant flow physics are a) turbulent boundary layers in large adverse pressure gradients (Fig 1), b) the interactions between these boundary layers and the inviscid flow and c) shock waves on the upper surface with, in some cases, associated separations.

## 2 DETAILS OF MODEL(S)

### 2.1 General geometric arrangement

A general arrangement of the model with a typical aerofoil section (RAE5225) is shown in Fig 2. This

figure illustrates the detachable trailing edge, noted above, and the air-injection technique[1] used to 'fix' boundary-layer transition on both surfaces. The layout of the model in the working section, showing the relative streamwise positions of the model, the wake rake, used to determine drag, and the static pressure tappings in the roof and floor of the test section are shown in Fig 3.

**2.2 Configurations** See Fig 1.

**2.3 Aerofoil section data**

**2.3.1 Planform**

| | |
|---|---|
| Model chord | = 0.635m |
| Model span | = 2.438m |
| Model aspect ratio | = 3.84 |

**2.3.2 Basic aerofoil sections**

See Fig 1. All the sections had a thickness/chord ratio of 14% and a nose radius to chord ratio r/c = 0.0144.

**2.7 Geometric**

The shape of each section is defined numerically. Both design and measured ordinates are given. The errors in shape are in the region of 0.1mm (0.00015 x chord). Surface finish is within the range 0.1 - 0.2$\mu$m.

**2.8 Model support details**

The model was mounted in a rotating mechanism on one side of the working section and was free to rotate in a bearing on the other side.

## 3 GENERAL TUNNEL INFORMATION

**3.1 Tunnel designation**

8ft x 8ft Pressurised, Subsonic/Supersonic Wind Tunnel.

**3.2 Organisation running the tunnel**

Defence Research Agency
(formerly Royal Aerospace Establishment),
Aerodynamics and Propulsion Department,
Bedford,
MK41 6AE, England

**3.3 Tunnel characteristics**

Type of tunnel: continuous flow, closed circuit.
Operating envelope: See Fig 4

**3.4 Test section**

**3.4.1 Test section details** See Fig 3

**3.4.2 Test section dimensions**

2.44m x 2.44m x 14m.

**3.4.3 Wall geometry details**

Type of walls: solid, flexible upper and lower walls for supersonic operation. Shapes of upper and lower walls are set for subsonic tests in such a way as to minimise the pressure gradient on the centre line when the test section is empty[2]. Wall pressures are measured along the centre lines of the roof and floor (Fig 3). Typical wall boundary-layer displacement thickness: 19mm. For further details see Ref 3.

**3.5 Free-stream conditions**

**3.5.1 Reference conditions**

Total pressure: Determined using a pitot in the settling chamber and a 'Midwood' self-balancing capsule manometer of range 400kPa and accuracy $\pm$0.03% full scale. Static pressure: The reference static pressure tapping is on the centre-line of the sidewall at x = -4.58m, where x is distance along the tunnel axis downstream from the model leading edge (Fig 3). The differential 'Midwood' manometer used for this measurement was of range 100kPa and accuracy 0.03% full scale. Static temperature: This is inferred from total temperature measured to an accuracy of $\pm$0.1K by a probe in the settling chamber.

**3.5.2 Tunnel calibration**

Measurements were made of static pressures on the centre-line of the roof and floor of the test section (Ref 2) using differential 'Midwood' manometers of range $\pm$100kPa and accuracy $\pm$0.03% full scale. The last calibration was performed (using electronic scanning of pressure transducers) in October 1991, calibrations being performed annually.

**3.6 Flow quality**

**3.6.1 Flow uniformity**

For static pressure variations along the model axis see Ref 2, but typically $\Delta Cp$ = O(0.0001) with the diffuser choked, as in the present tests. The variation of (uncorrected) Mach number during a run is within 0.001.

Average flow angularity has not been determined for the present tests. However, it is routinely determined for

sting-mounted complete models by comparing force measurements made with the model erect and inverted. Some data on flow angularity has also been obtained for typical swept-wing half models (mounted in the same way as in the present case) by testing a model with a horizontal plane of symmetry. In both cases, the implied average downwash angle has been found to be up to about 0.03°.

### 3.6.2 Temperature variation

The temperature is controlled during the run by altering the flow of water through the cooler in the settling chamber. Temperature can be controlled to within 0.5°. Temperature variation within the tunnel is not known.

### 3.6.3 Flow unsteadiness

Overall turbulence level is not known but overall noise level is typically $C_{prms}$ = 0.004. For further information on the noise characteristics of the wind tunnel see Ref 3.

## 4 INSTRUMENTATION

### 4.1 Model position

Geometrical incidence is measured by a digital encoder attached to the mechanism for rotating the model. The datum for these measurements is determined using an accurate electro-level meter. The accuracy of the setting is estimated to be ±0.005°.

### 4.2 Model pressure measurements

There are 50 static-pressure measurement holes on the centre line of the model and 11 holes at stations about one chord either side of the model centre line. The differential pressure transducers used for these measurements were of range ±100 kPa with an accuracy of ±0.05% full scale.

No dynamic pressure measurements were made.

### 4.4 Boundary layer and flowfield measurements

Mean-flow boundary-layer profiles were measured at four chordwise locations on the lower surface of the RAE 5225 aerofoil (57%, 65%, 72.5% and 80% chord). Static and total pressure probes were mounted off the centre-line of the model with the two types of probe displaced spanwise relative to each other as shown in Fig 5. This permitted the simultaneous operation of four probes during a given tunnel run. Each of the probes was circular in cross section, the pitot tubes having an outside diameter of 0.5mm and an inside diameter of 0.3mm, while the static tubes were of 1mm diameter. The traversing gear used for these probes is shown in Fig 5.

Static and total pressures were also measured in the boundary layers at 99% chord above the upper surface and below the lower surface of the aerofoil RAE 5225 using the probe installation shown in Fig 6. The installation comprised two pitot tubes of circular cross section and of inside and outside diameters 0.3mm and 0.5mm. The static tubes were of 1mm diameter.

Skin friction measurements were made on the RAE 5225 aerofoil using the razor-blade technique[5]. In this method, razor blades, cut to an appropriate shape, were glued to the model surface over selected static pressure holes and 'surface' pitot pressures were measured during a dedicated tunnel run. These were then used, in conjunction with static pressures measured in a normal run (ie without razor blades), to evaluate skin-friction coefficients, using the calibration of Gaudet given in Ref 5. Measurements were made at 13 positions on the upper surface and 11 positions on the lower surface. Details of the positions of these measurements are given, along with the data, on floppy disk.

Pitot and static pressures were measured in the wake at the vertical plane of symmetry at about two chords downstream of the model. The rake of tubes used for this purpose comprised 91 pitot tubes; the central 81 tubes were at 6.35mm pitch and the remaining 10 at intervals of 12.7mm. Two static tubes were used, with one at each extremity of the rake.

As with the model pressure measurements, all the pressures for boundary layer and flowfield surveys were measured with differential pressure transducers of range ±102kPa with an accuracy of ±0.2% full scale.

### 4.5 Surface flow visualisation

Surface oil flows were performed by ejecting oil through static holes aft of 65% chord on the lower surface of the aerofoil RAE 5225. These visualisations were photographed using cameras in the tunnel roof.

### 4.7 Tunnel wall measurements

#### 4.7.1 Types of Measurements

Measurements were made of static pressures on the centre line of the roof and floor of the test section at the positions shown in Fig 3.

## 5 TEST MATRIX AND CONDITIONS

### 5.1 Detailed test matrix

Results for a total of nine test cases are available,

including examples of all three types of rear pressure distribution on the upper surface. These are summarised below Table I which presents the details of the various test cases.

### 5.2 Model/tunnel relations

#### 5.2.1 Maximum blockage

$\Delta M = 0.015$ for the selected test cases.

#### 5.2.2 Model span/tunnel width

The model spans the tunnel.

#### 5.2.3 Wing area/tunnel cross section area

0.260

#### 5.2.4 Height/chord ratio 3.84

#### 5.2.5 Width/chord ratio 3.84

#### 5.2.6 Wall temperatures

Model temperature was not measured but tunnel temperature was controlled so that excursions of model recovery temperature were minimised.

### 5.3 Transition details

The tests were made with transition 'fixed' at 5% chord on both surfaces using the air-injection technique[1]. For details of the size and spacing of the holes through which the air was emitted see Fig 2. The technique was verified by varying the amount of air supplied to each surface and noting the variation of drag with air mass flow[1].

## 6 DATA

### 6.1 Availability of data

#### 6.1.1 Organization owning data

Defence Research Agency, Bedford.

#### 6.1.2 Person responsible for data

Dr P R Ashill
Aerodynamics & Propulsion Department
Building 17
Defence Research Agency
Bedford, MK41 6AE
England
Tel. 44 234 225804
Fax. 44 234 225848

#### 6.1.3 Availability of data

Data specified in questionnaire are available.

### 6.2 Suitability of data for CFD validation

The data are suitable for validating 'in tunnel' calculations methods. The data are, however, corrected to 'free-air' conditions. Details are provided of the corrections made for blockage and wall-induced angle of incidence. Some of the cases given in Table I are believed to be suitable for assessing 'free-air' codes. These cases (A, B1, C1, D and E) either have essentially subcritical flows, or weak shock waves, for which chordwise variation of wall-induced upwash that is characteristic of solid-wall tunnels can be catered for by changing the camber of the aerofoil in the CFD calculation[7]. The non-dimensional increment applied to the aerofoil camber ordinate is written as:

$$\delta Z = \frac{C_N}{\beta}\,\frac{\pi}{48}\left(\frac{c}{h}\right)^2 X(1-X)$$

where c/h is aerofoil chord to tunnel height ratio.
$C_N$ is normal force coefficient.
X is distance along aerofoil chord from leading edge, made non dimensional by aerofoil chord.
$\beta$ $\sqrt{(1 - M^2)}$ and M is free-stream Mach number.

### 6.3 Type and form in which data are available

#### 6.3.1 a) Free stream

Mach number corrected for tunnel wall (roof and floor) interference.

#### b) Pressure

Coefficients based on free-stream dynamic pressure, corrected for tunnel wall (roof and floor) interference, and model chord.

#### c) Forces

Coefficients based on free-stream dynamic pressure, corrected for tunnel-wall (roof and floor) interference.

#### d) Boundary Layers

Thickness: Displacement and momentum thickness are determined using the alternative definitions given in Ref 6 which allow for the variation in static pressure across the boundary

layer normal to the surface of the model. The method used to extrapolate the measured profiles, to facilitate accurate determination of the boundary layer thickness, is as described in Ref 6. In the data presented the boundary-layer thicknesses are made non-dimensional by aerofoil chord.

Profiles: The local velocity is referred to the velocity of a hypothetical flow having the same static pressure as that measured at the wall, but with a total pressure equal to that at the edge of the boundary layer. In determining this velocity ratio, it is assumed that total temperature is constant through the flow measured. Velocity ratio and static-pressure coefficient are determined at approximately 30 points at roughly even intervals of $\log_{10}$ (y), where y is distance from and normal to model surface.

### 6.3.2 Data Carrier

Available on floppy disc.

### 6.4 Corrections applied to data

### 6.4.1 Lift interference and blockage correction

Two methods were used to determine blockage, one using a model representation (due originally to Goethert[7]) and the other a two-component method[8]. The results obtained by these independent methods have been found to be in good agreement. In the two-component method the effect of the wall boundary layer on the normal component of velocity is ignored but a limited number of checks indicated that this contribution is negligible. The corrections for blockage have been obtained by the model representation method.

The correction to angle of incidence is obtained using linear theory; these corrections have been shown to be in good agreement with corresponding values given by the two-component method.

### 6.4.2 Side wall interference corrections

No corrections have been applied to either Mach number or angle of incidence for this effect. However, calculations made using a modified version[9] of the Barnwell/Sewall method[10,11] suggest that the correction to Mach number is probably less than 0.001.

### 6.4.5 Aeroelastic deformation

Owing to the fact that the model was free to rotate at one end, it was able to twist under load. The amount of twist was determined from a prior static loading and by inferring the loads acting on the model during the test from the pressure measurements. The calculated reduction in angle of incidence at the centre-line of the model is between 0.01° and 0.08° for the cases considered (Table I). This change in angle is applied as a correction to model angle of incidence. The twist over the central 50% span of the model is about half the value of the change in incidence at the centre-line.

## 7 DATA ACCURACY AND REPEATABILITY ASSESSMENT

### 7.1 Estimated accuracies

$R_c = 20 \times 10^6$

**Free stream conditions**

| | |
|---|---|
| Mach number | $= \pm 0.001$ |
| Incidence | $= \pm 0.03°$ |

**Pressure and Forces**

| | |
|---|---|
| Cp | $= \pm 0.002$ |
| Lift coefficient | $= \pm 0.002$ |
| Drag coefficient | $= \pm 0.0001$ |
| Pitching moment coefficient | $= \pm 0.002$ |

### 7.2 Repeat measurements

Good repeatability has been obtained both within and between test campaigns. For example, drag coefficient has been shown to repeat to within about $\pm 0.0001$ (Fig 7) and pressure coefficient to within about $\pm 0.001$ between campaigns performed a number of years apart.

## 8 REFERENCES

1 P R Ashill, J L Fulker, D J Weeks
The air-injection method of fixing boundary-layer transition and investigating scale effects.
The Aeronautical Journal, May 1987, pp 214-224.

2 D Isaacs
Calibration of the RAE Bedford 8ft x 8ft Wind Tunnel at Subsonic Speeds, Including a Discussion of the Correction to the Measured Pressure Distribution to Allow for the Direct and Blockage Effects due to the Calibration Probe.
ARC R&M 3583. 1967.

3 K G Winter, L Gaudet
Turbulent boundary-layer studies at high Reynolds numbers at Mach numbers between 0.2 and 2.8.
ARC R&M 3712, 1970

4 J D Whitfield, N S Dougherty Jr
A Survey of Transition Research at AEDC.
AGARD-CP-224, "Laminar-Turbulent Transition", 1977, Paper 25.

5 K G Winter
An outline of the techniques available for the measurement of skin friction in turbulent boundary layers.
VKI Lecture Series 'Compressible Turbulent Boundary Layers' March 1-5, 1976.

6 P H Cook, M A McDonald, M C P Firmin
Aerofoil RAE 2822 - Pressure Distributions, and Boundary Layer and Wake Measurements.
AGARD AR-138, 1979, Paper A6.

7 B Goethert
Windkanalkorrekturen bei hohen Unterschallgeschwindigkeiten unter besonderer Berucksichtigung des geschlossenen Kreiskanals.
Deutsche Luftfahrtforschung Forschungsbericht 1216, 1940 (translated as NACA Tech Memo 1300)

8 P R Ashill, D J Weeks
A Method for Determining Wall-Interference Corrections in Solid Wall Tunnels from Measurements of Static Pressure at the Walls.
AGARD-CP-335, 1982, Paper 1.

9 P R Ashill
Effects of Sidewall Boundary Layers on Aerofoils Mounted from Sidewalls of Wind Tunnels - Experimental Evidence and Developments of Theory.
RAE TR 83065, 1983.

10 R W Barnwell
Similarity Rule for Sidewall Boundary-Layer Effect in Two-Dimensional Wind Tunnels.
AIAA Journal, Vol.18, No.9, Sept.1980, pp. 1149-1151.

11 W G Sewall
Effects of Sidewall Boundary-Layer Effect in Two-Dimensional Subsonic and Transonic Wind Tunnels.
AIAA Journal, Vol.20, No.9, Sept. 1982, pp. 1253-1256.

12 P R Ashill, D J Weeks, J L Fulker
Wind Tunnel Experiments on Aerofoil Models for the Assessment of computational flow Methods.
AGARD-CP-437 Vol 1 Paper 4, 1988.

13 P R Ashill
Calculation and Measurement of Transonic Flows Over Aerofoils with Novel Rear Section.
ICAS-88-3.10.2, 1988

| IDENTIFICATION | | CONDITIONS | | | POSITION | | OTHER INFORMATION | |
|---|---|---|---|---|---|---|---|---|
| CASE NO. | CONF/RUN/ DP | Mach No. | q kPa | Rc x $10^{-6}$ | $\alpha°$ | $C_L$ | Types of measurements | Remarks |
| A | 25/1/1402 | 0.598 | 55.9 | 19.99 | 1.38 | 0.433 | a,b | RAE 5225 |
| B1 | 25/1/1426 | 0.735 | 19.4 | 6.03 | 1.16 | 0.403 | a,b,c | RAE 5225 |
| B2 | 25/1/1436 | 0.737 | 19.5 | 6.04 | 2.33 | 0.659 | a,b | RAE 5225 |
| B3 | 25/1/1378 | 0.734 | 65.87 | 19.97 | 0.85 | 0.407 | a,b | RAE 5225 |
| B4 | 25/1/1389 | 0.736 | 66.10 | 20.03 | 1.97 | 0.640 | a,b | RAE 5225 |
| C1 | 330/2/2210 | 0.735 | 18.9 | 6.02 | 1.16 | 0.443 | a,b | RAE 5230 |
| C2 | 330/2/2221 | 0.736 | 18.9 | 6.02 | 2.34 | 0.706 | a,b | RAE 5230 |
| D | 536/1/19 | 0.734 | 18.5 | 6.04 | 1.28 | 0.410 | a,b | RAE 5236 |
| E | 534/2/766 | 0.734 | 19.3 | 6.04 | 0.90 | 0.434 | a,b | RAE 5234 |

Notes:

1 Types of measurements: a) Pressure measurements on model and wind-tunnel walls, b) Measurements of total and static pressure in the wake, and c) Mean-flow measurements in the boundary layer on the model.

2 The flows may be defined as follows:

A: A case with uniformly subcritical flow and a suction peak on the upper surface near the leading edge, RAE 5225 (Fig 8).

B1: A flow with a weak shock wave on the upper surface, subcritical flow on the lower surface. A limited region of separation is expected upstream of the trailing edge on the upper surface, RAE 5225 (Fig 9).

B2: A flow with a shock wave of moderate strength on the upper surface and a limited region of separation is expected just upstream of the training edge on the upper surface, RAE 5225 (Fig 10).

B3: Similar to Flow B1 but with attached flow on the upper surface, RAE 5225.

B4: Similar to Flow B2 but with attached flow on the upper surface, RAE 5225.

C1: Similar to Flow B1 but with more extreme tendencies towards separation on the upper surface, RAE 5230 (Fig 11).

C2: Similar to Flow B2 but with more extreme tendencies towards separation on the upper surface, RAE 5230 (Fig 12).

D: Similar to Flows B1 and C1 but with a different form of rear pressure distribution on the upper surface, RAE 5236 (Fig 13).

E: Similar to Flows B1, C1 and D but with a different form of rear pressure distribution on the uppaer surface, RAE 5234 (Fig 14).

3 The figures illustrating pressure distributions for these flows also contain predicted pressure distributions by the BVGK transonic aerofoil theory and by the VGK or 'standard theory [12,13].

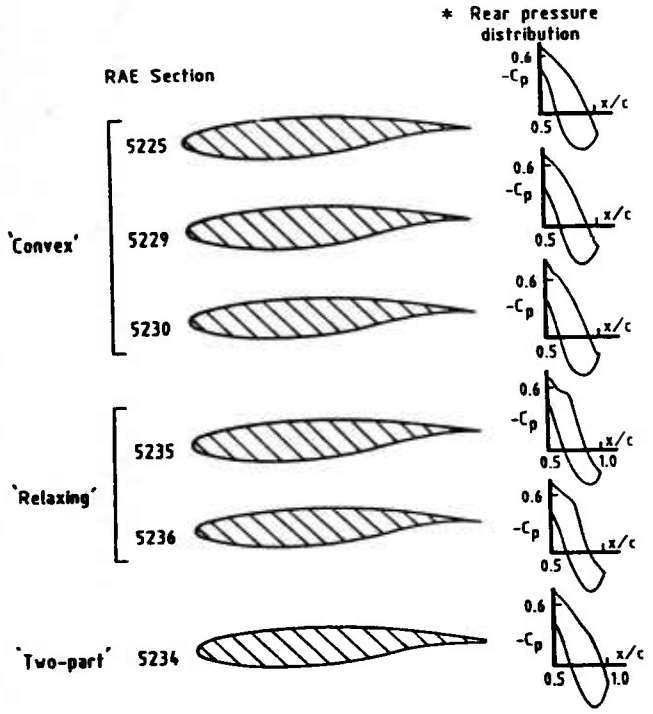



**Fig 1** **Families of aerofoils studied**

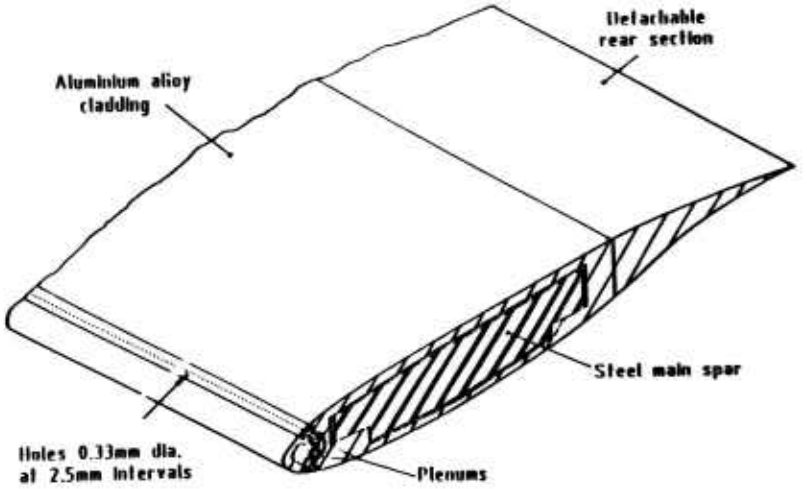



**Fig 2** **Isometric view of model showing air-injection system**

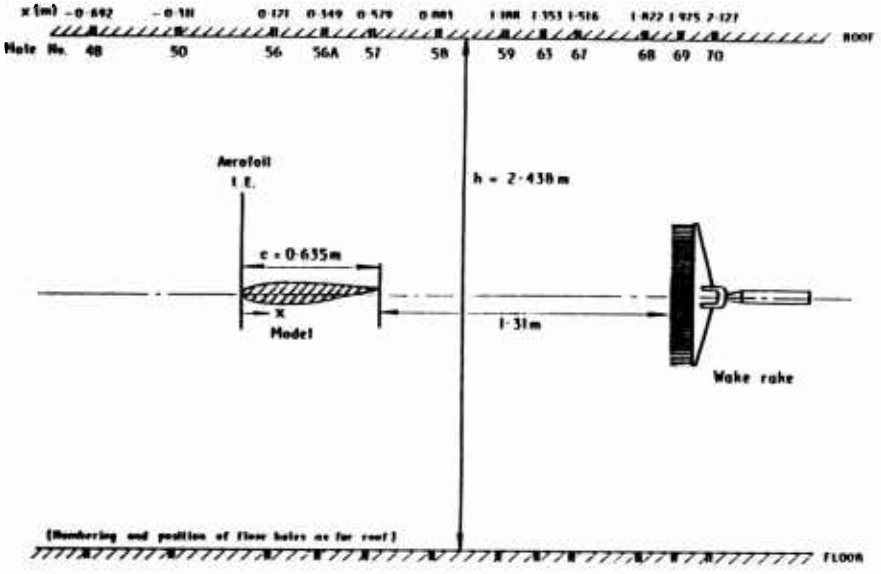



**Fig 3** **Numbering and positions of wall static pressure holes in roof and floor of working section.**

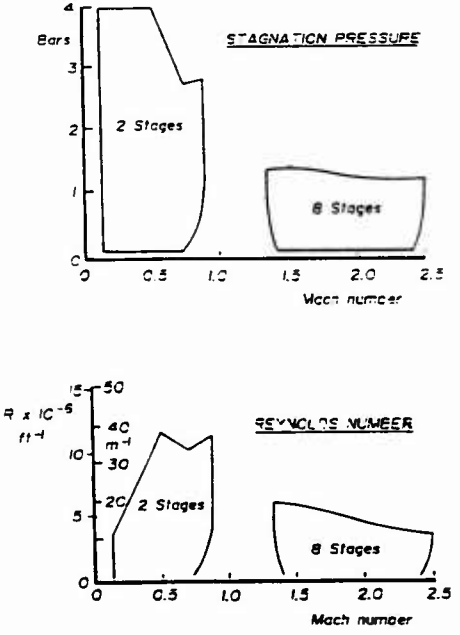



**Fig 4** **8ft x 8ft Tunnel operating envelopes**

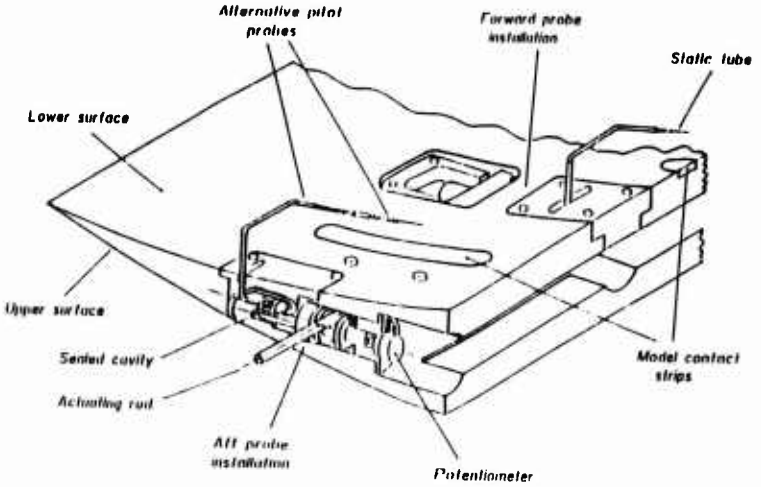



**Fig 5** Traverse mechanism for lower surface boundary layer probes

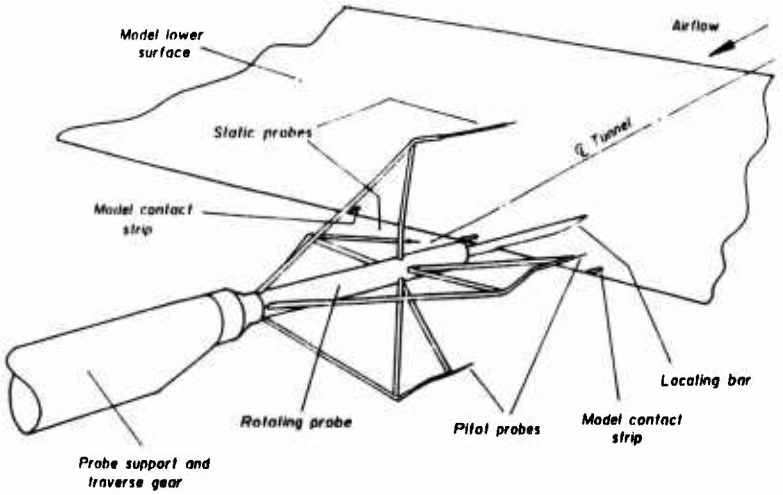



**Fig 6** Trailing edge boundary layer traverse equipment

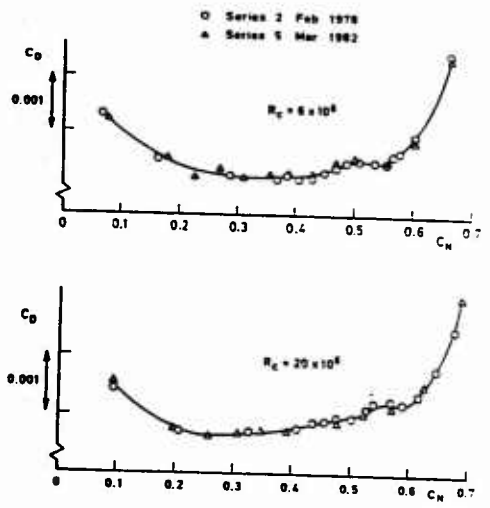



**Fig 7** **Evidence of repeatability of drag data between test series - RAE5225, M = 0.734, transition fixed**

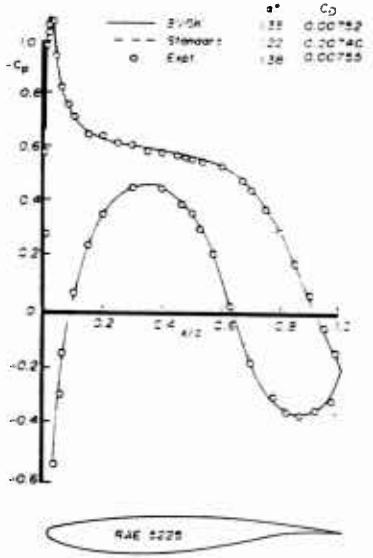



**Fig 8** **Case A1, $C_L$ = 0.433, M = 0.598, R = 19.99 x $10^6$**

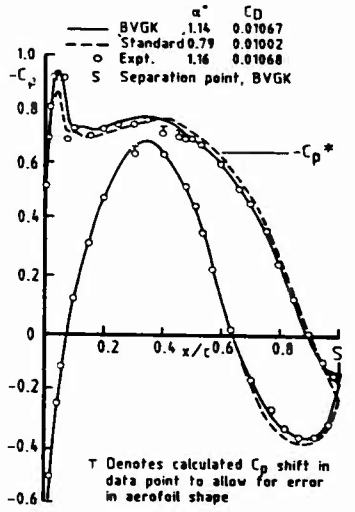



**Fig 9** **Case B1, $C_L$ = 0.403, M = 0.735, R = 6.03 x $10^6$**

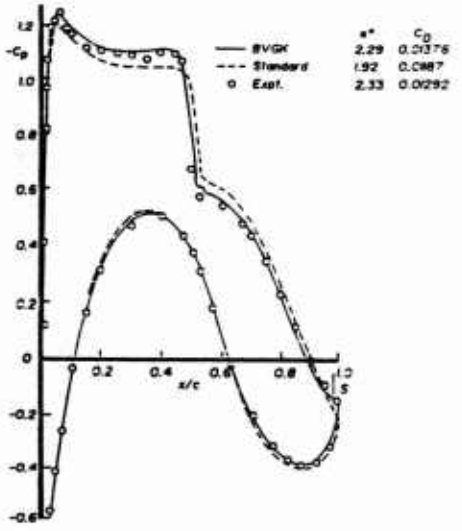



Fig 10 Case B2, $C_L$ = 0.659, M = 0.737, R = 6.04 x $10^6$

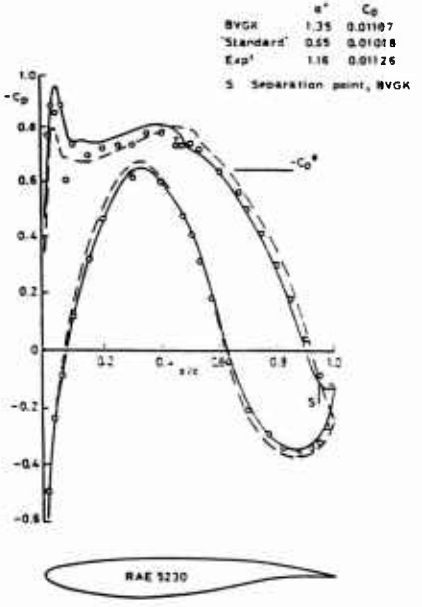



Fig 11 Case C1, $C_L$ = 0.443, M = 0.735, R = 6.02 x $10^6$

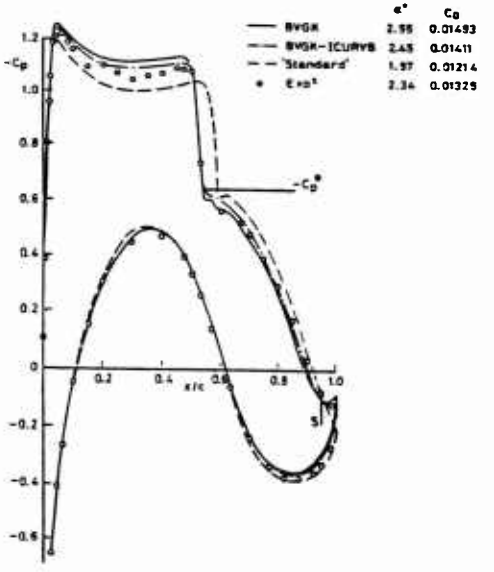



Fig 12 Case C2, $C_L$ = 0.706, M = 0.736, R = 6.02 x $10^6$

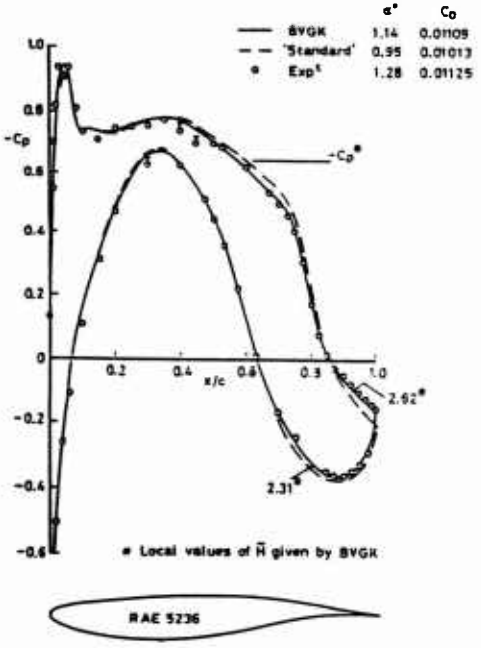



Fig 13 Case D, $C_L$ = 0.410, M = 0.734, R = 6.04 x $10^6$

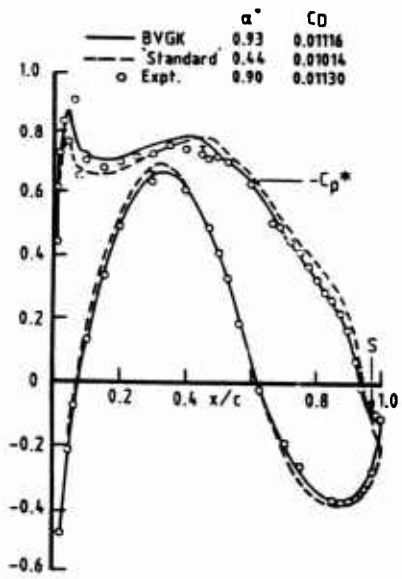



Fig 14 Case E, $C_L$ = 0.434, M = 0.734, R = 6.04 x $10^6$

# Surface Pressure and Wake Drag Measurements on the Boeing A4 Airfoil in the IAR 1.5X1.5m Wind Tunnel Facility.

by

D.J.Jones and Y.Nishimura
IAR/NRC, Ottawa, CANADA

## 0 Introduction.

This 10.2% maximum thickness to chord airfoil has become a standard airfoil for Boeing wind tunnel tests in the IAR 1.5X1.5m facility. In order to study wall constraint effects, several different chord lengths have been used in the narrow span (38.1cm) IAR facility and a 30.5 cm chord model was tested in the 1.5m wide facility. The latter data from the wide span facility are presented here. This data has a small sidewall correction while the upper and lower walls are accounted for using Mokry's wall correction procedures. Transition was fixed at 10% and all runs were made at a chord Reynolds number of 14 million. The tests were carried out in June-July, 1991.

## 1. GENERAL DESCRIPTION.

### 1.1 Model name

Boeing A4 airfoil

### 1.2 Model type and flow conditions

2-D airfoil. Subsonic free stream usually with supercritical flow.

### 1.3 Design requirements, purpose of test

The design philosophy, at the supercritical design condition, was to accelerate the flow rapidly on the upper surface and gradually lower the speed so that the shock is quite weak. High aft loading was also an aim. The test was conducted specifically to obtain accurate data for validation purposes, both for CFD and for comparing to results in the narrow span (38.1cm) facility at IAR.

## 2. DETAILS OF MODEL

### 2.1 General geometric arrangement

Fig 1 shows the IAR 1.5mX1.5m tunnel and the airfoil model as installed is shown in Fig 2. The end plates (or flow splitter plates) between which the airfoil was mounted are shown as is the yoke system to pitch the airfoil. These end plates were installed to limit the size of the sidewall boundary layer. The wake rake to measure wake drag (if mounted vertically) and to check for two dimensionality of the flow (if horizontal) is also shown. Fig 3 shows the airfoil cross-section.

### 2.2 Configurations

Only one configuration

### 2.3 Airfoil section data

#### 2.3.1 Planform

1.358m span with 0.305m chord gives aspect ratio of 4.452

#### 2.3.2 Basic airfoil section

Fig 3 shows the airfoil cross section
- 10.2% maximum thickness/chord
- Nose radius/chord approximately 0.0167

### 2.7 Geometry

Airfoil defined numerically.
Design coordinates shown in Table 1
Tolerances ±0.007cms
Surface roughness 0.41 microns

### 2.8 Model support details

Model supported by spuds housed in bearings at both ends of the model

## 3 GENERAL TUNNEL INFORMATION

### 3.1 Tunnel designation

IAR 1.5X1.5m pressurised trisonic wind tunnel

### 3.2 Organisation running the tunnel

Test conducted by the High Speed Aerodynamics Laboratory of IAR

### 3.3 Tunnel characteristics

Blowdown tunnel. Trisonic (0.15<M<4.25), high Reynolds number (up to 70 million per metre) facility. Run time 7 to 170 secs.

### 3.4.1 Test section details

Fig 2 shows the mounting of the model and relevant features.

### 3.4.2 Test section dimensions

1.5X1.5 metre test section

### 3.4.3 Wall geometry details

Slanted porous upper and lower walls with 2% porosity, wall pressures are measured and are available on the floppy disk.
Sidewall boundary layer is not controlled but grows along the solid endplates. Typical sidewall boundary layer thickness is 3.0mm at the model location.

**3.5 Freestream conditions**

**3.5.1 Reference conditions**
Total pressure was measured at inlet to test section. Static reference pressure was measured at a wall orifice located 1.638m upstream of the airfoil pitch axis (which is 11.76 cms from the airfoil leading edge) near the tunnel ceiling's centreline. Stagnation temperature was measured by a thermometer in the settling chamber. Static temperature was obtained by calculation, assuming isentropic flow.

**3.5.2 Tunnel calibration**
Empty tunnel pressure surveys on ceiling, floor, sidewall (splitter plates). Sidewall boundary layer thickness measured by a 24 probe rake.

**3.6 Flow quality**

**3.6.1 Flow uniformity (empty tunnel)**
Static pressure variation ±0.02psi over model length.
Mach number variation negligible over model length.
Mach number variation during a run ±0.001.
Flow angularity not measured although the normal 1.5m transonic test section has a downwash of 0.25°; this may not be true with the splitter plates installed. It is suggested that fixed lift be used for CFD validation.

**3.6.2 Temperature Variation**
2 deg K

**3.6.3 Flow unsteadiness**
Turbulence level about 0.5 to 0.6% for the transonic range. The limited flow viz indicated that transition in these cases was at the 10% x/c distance from the leading edge i.e. at the fixed transition location.
Noise level $(\Delta p/q)$rms=0.01 at M=0.4 to C.8

**4. INSTRUMENTATION**

**4.1 Model Position**

**4.1.1** Geometrical incidence measured using potentiometers and accelerometer (average taken).

**4.1.2** Accuracy of geometrical incidence from potentiometers ±0.03° but note empty tunnel upwash/downwash not measured.

**4.2 Model pressure measurements**
**4.2.1** 80 pressure holes (see fig 3) at each of 3 spanwise locations; one near centreline (5 cms to port side), one 38 cms to port and the last 51 cms to starboard. Only the first of these is on the floppy disk and some bad pressures were eliminated leaving 70 surface pressures for each scan.

**4.2.2** Kulite 1379 kPa (200psia) transducers (range 1138 kPa (165psia)), accuracy ±0.69kPa (±0.1psia)
**4.2.3** No dynamic pressure measurements were taken.

**4.5 Surface flow visualisation**
Fluorescent oil photographs of the top surface were taken.

**4.7 Tunnel wall measurements**

**4.7.1 Types of measurements**
Pressures and wake rake drag.

**4.7.2** Upper and lower wall pressures recorded at 32 stations stretching from about 1.8m forward to 0.96m aft of model pitch axis which is 11.76 cms from the airfoil leading edge. Note that the pitch axis is the origin for the rail pressures.

**5. TEST MATRIX AND CONDITIONS**

**5.1.1** 96 test cases, see Table 2, are on the floppy disk. IAR suggests computing the 13 cases as marked in Table 2 for CFD validation. The bulk of these cases are at the highest lift for each Mach number. The 2 cases showing trailing edge divergence (indicating separation) will be particularly challenging.

**5.1.2** One configuration only

**5.1.3** All runs at chord Reynolds number of 14 million with Mach numbers of 0.6, 0.7, 0.72, 0.74, 0.76, 0.77, 0.78, 0.79, 0.80, 0.81. Normally nine scans for each Mach number from $C_L$=0 to about $C_L$=0.7. All with transition fixed at 10% chord on the upper and lower surfaces.

**5.2 Model/tunnel relations**
**5.2.1** Maximum blockage 2% based on 10.2% thick airfoil with 30.5 cm chord
**5.2.2** Span/width = 0.905 (endplates mounted off the tunnel wall)
**5.2.3** Wing area/tunnel cross section area=0.18
**5.2.4** Height/chord ratio=5
**5.2.5** Width/chord ratio=4.454
**5.2.6** Wall temperatures not investigated

**5.3 Transition details**

For all the data, transition fixed at 10% chord on upper and lower surfaces. A series of circular disks

nominally 1.27mm in diameter, 0.05mm in height and spaced 2.54mm apart. The effectiveness and the effect on drag has been investigated in previous studies but the drag quoted here (from wake rake data) has not been corrected for the transition trip. Best estimates are that drag is 0.0002 high due to the disks.

## 6. DATA

### 6.1 Availability of data

**6.1.1 Organisations owning the data**
IAR and Boeing Commercial Airplane Company (Seattle, WA)

**6.1.2 Persons responsible for the data**
D.J.Jones or Y.Nishimura
High Speed Aerodynamics Laboratory
Institute for Aerospace Research
National Research Council
Montreal Rd.,
Ottawa K1A OR6
CANADA

**6.1.3 Availability of the data**
Data specified in Table 2 is on the floppy disk.

### 6.2 Suitability of the data for CFD validation

The data on floppy disk have been corrected for upper/lower walls using only the linear correction of Mokry and Ohman (Ref 8.4.1). Table 4 gives the Mach number fully corrected for nonlinearity and for sidewall interference and so is suitable for 'free-air' validation. It is suggested to compare $p/p_0$ (stagnation reference pressure) as these quantities are invariant (they are measured directly) with free stream Mach number. If comparing Cp values then they must be reevaluated, using new values for $p_\infty$ as given below using the 'fully corrected' Mach numbers quoted in Table 4. The lift coefficients also must be corrected using the formulae:

$$p_{\infty,1} = (1+0.2*M_1^2)^{3.5}$$

$$p_{\infty,2} = (1+0.2*M_2^2)^{3.5}$$

$$C_{L,2} = C_{L,1}\frac{p_{\infty,2}}{p_{\infty,1}}\frac{M_1^2}{M_2^2}$$

where $p_\infty$ is the freestream pressure, M is the freestream Mach number (with appropriate corrections) and subscripts 1 and 2 refer to old and new values of the variables.
Note that the data point at about x/c=0.44 on the upper surface (see Fig.4) is usually in error and should be ignored. Also the pressure reading at x/c about 0.1 in the floppy file should be ignored as it is affected by the transition disks (it has already been removed from Fig 4).

**6.2.1** Data are not suitable for in-tunnel computations since only pressure is available as a boundary condition and the porous wall (slanted holes) boundary condition is not known. Careful evaluation of the wall corrections make the data suitable for 'free air' calculations.

**6.2.2** Data are corrected for top and bottom walls using Mokry's linear methods (Ref 8.4.1) together with a further correction, again due to Mokry, which accounts for the nonlinearity of the flow field (Ref 8.4.2). Sidewall corrections using Jones and Chan's full transonic method are also applied (Ref 8.4.3).

### 6.3 Type and form in which data are available

**6.3.1** Cp versus x/c, force data (integrated from the pressures) and wake drags as well as upper and lower rail pressures are available.

**6.3.2 Data Carrier** Floppy disk

### 6.4 Corrections applied to data

**6.4.1 Lift interference and blockage correction**
Upper and lower wall constraints are corrected for by using Mokry and Ohman's theory which is a linear technique using rail pressures on those walls. The model is represented by a source, a vortex and a doublet, Ref 8.4.1. A new method due to Mokry (Ref 8.4.2), which accounts for the nonlinearity of the flowfield, is also used to improve the doublet's magnitude by relating it to the value obtained by comparison with an 'Euler' flowfield obtained from a FLO52 computation. The values for $\Delta M$ obtained from this analysis are itemised in Table 4, the values are additive to those obtained from the linear theory.
The $\alpha$ correction using linear theory is applied to the quoted data; this method assumes that the upstream $\alpha$ is 0° and so there is an error in $\alpha$(corrected) since the empty tunnel flow angularity was not measured (see 3.6.1). IAR recommend fixing the lift to obtain comparison with CFD.

**6.4.2 Sidewall interference corrections**
A sidewall correction to Mach number is computed based on the theory of Jones and Chan (Ref 8.4.3). This is based on computing the sidewall boundary layer and simulating this by a transpiration velocity applied at the sidewalls. A comparison of the wing flow with and without the boundary layer growth then indicates the size of the correction. Results using this method which are applicable to the data presented here are given in Ref 8.4.4. Table 4 gives the sidewall $\Delta M$ corrections computed for the present cases; they are additive to the upper/lower wall corrections.

**6.4.5 Aeroelastic deformation**
Torsional twisting of the model results in an incidence different from the measured incidence. Torsional deflection was derived from static calibration data on the model. This correction has not been applied to the quoted $\alpha$. It is typically about -0.37° at zero lift and is close to zero at a lift coefficient of 0.75 with a linear variation in between.

## 7. DATA ACCURACY AND REPEATABILITY ASSESSMENT

### 7.1 Estimated accuracies

7.1.1 $\Delta M$ as measured ±0.001. The accuracy of the correction methods (top, bottom and sidewall) is expected to give a total error of about ±0.002.
$\Delta\alpha$ ±0.03° as measured (but corrected $\alpha$ will not be this accurate - see 3.6.1 and 6.4.1)

7.1.2 Pressure coefficients $\Delta Cp$=±0.01
Wake pressure $\Delta p$(wake)=±0.069 kPa (±0.01 psi)

### 7.2 Repeat Measurements

7.2.1 Free stream conditions were repeated to test repeatability at M=0.7 and M=0.79. Repeatability was very good as seen from Fig 4.

## 8 REFERENCES

**8.1 On the wind tunnel**
**8.1.1** L.H.Ohman et al. 'New Transonic Test Sections for the NAE 5ftX5ft Trisonic Wind Tunnel'. NRC Report NAE-AN-62, Jan 1990.
**8.1.2** D.Brown 'Information for Users of the National Research Council's 5ftX5ft Blowdown Wind Tunnel at the National Aeronautical Establishment: Second Edition'. NRC Report LTR-HA-6, Sept 1970.

**8.3 Particular Test and Test results**
**8.3.1** Y.Nishimura 'Wind Tunnel Investigations on a Full Span 2-D Airfoil Model in the IAR 1.5m Wind Tunnel - BCAC and IAR Collaborative Work Program'. NRC Report LTR-HA-5X5/0205, May 1992 (restricted distribution)

**8.4 Correction Methods**
**8.4.1** Mokry M and Ohman L.H. "Application of Fast Fourier Transform to Two-Dimensional Wind Tunnel Wall Interference". Journal of Aircraft, Vol 17, No 16, June 1980.
**8.4.2** Mokry M. "Influence of the Transonic Doublet in the Far- and Mid-Field of a Lifting Airfoil". NRC/IAR Report to be published.
**8.4.3** Jones D.J. and Chan Y.Y. "A Numerical and Experimental Evaluation of the Sidewall Boundary Layer Effects on Aerofoils Tested in Wind Tunnel Facilities". Proceedings of the RAeS Conference: Wind Tunnels and Wind Tunnel Test Techniques, Southampton U.K., 14-17 Sept 1992.
**8.4.4** Jones D.J. and Chan Y.Y. "Results of Wind Tunnel Sidewall Interference Computations using a Transpiration Method to Represent the Sidewall Boundary Layer". NRC/IAR Report to be published.

UPPER SURFACE 54 POINTS:

| X/C | Y/C |
|---|---|
| 0.00000 | 0.00035 |
| 0.00500 | 0.01116 |
| 0.01000 | 0.01497 |
| 0.02000 | 0.01934 |
| 0.03000 | 0.02233 |
| 0.04000 | 0.02478 |
| 0.05000 | 0.02689 |
| 0.06000 | 0.02874 |
| 0.07000 | 0.03040 |
| 0.08000 | 0.03190 |
| 0.09000 | 0.03327 |
| 0.10000 | 0.03454 |
| 0.12500 | 0.03733 |
| 0.15000 | 0.03972 |
| 0.17500 | 0.04180 |
| 0.20000 | 0.04361 |
| 0.22500 | 0.04520 |
| 0.25000 | 0.04660 |
| 0.27500 | 0.04784 |
| 0.30000 | 0.04893 |
| 0.32500 | 0.04988 |
| 0.35000 | 0.05070 |
| 0.37500 | 0.05138 |
| 0.40000 | 0.05194 |
| 0.42000 | 0.05230 |
| 0.44000 | 0.05258 |
| 0.46000 | 0.05276 |
| 0.48000 | 0.05284 |
| 0.50000 | 0.05282 |
| 0.52000 | 0.05271 |
| 0.54000 | 0.05249 |
| 0.56000 | 0.05215 |
| 0.58000 | 0.05171 |
| 0.60000 | 0.05115 |
| 0.62000 | 0.05046 |
| 0.64000 | 0.04963 |
| 0.66000 | 0.04865 |
| 0.68000 | 0.04750 |
| 0.70000 | 0.04615 |
| 0.72500 | 0.04415 |
| 0.75000 | 0.04177 |
| 0.78000 | 0.03842 |
| 0.81000 | 0.03457 |
| 0.84000 | 0.03024 |
| 0.87000 | 0.02549 |
| 0.90000 | 0.02037 |
| 0.92000 | 0.01677 |
| 0.94000 | 0.01303 |
| 0.95000 | 0 01110 |
| 0.96000 | 0.00911 |
| 0.97000 | 0.00705 |
| 0.98000 | 0.00492 |
| 0.99000 | 0.00274 |
| 1.00000 | 0.00056 |

LOWER SURFACE 27 POINTS:

| X/C | Y/C |
|---|---|
| 0.00000 | 0.00035 |
| 0.00500 | -0.01164 |
| 0.01000 | -0.01551 |
| 0.02000 | -0.02118 |
| 0.04000 | -0.02858 |
| 0.06000 | -0.03330 |
| 0.08000 | -0.03669 |
| 0.10000 | -0.03932 |
| 0.15000 | -0.04402 |
| 0.20000 | -0.04699 |
| 0.25000 | -0.04875 |
| 0.30000 | -0.04948 |
| 0.35000 | -0.04931 |
| 0.40000 | -0.04840 |
| 0.45000 | -0.04682 |
| 0.50000 | -0.04454 |
| 0.55000 | -0.04130 |
| 0.60000 | -0.03676 |
| 0.65000 | -0.03062 |
| 0.70000 | -0.02289 |
| 0.75000 | -0.01411 |
| 0.81000 | -0.00384 |
| 0.87000 | 0.00261 |
| 0.92000 | 0.00331 |
| 0.96000 | 0.00191 |
| 0.99000 | 0.00010 |
| 1.00000 | -0.00056 |

**Table 1. A4 Airfoil Coordinates**

**Table 2. Test Data Available. Three scans per wind tunnel run**

| Run | M (nominal) | $C_L$ values[1] SCAN 1 | 2 | 3 | Suggested for CFD Validation | Comments for validation |
|---|---|---|---|---|---|---|
| 37893 | 0.60 | -0.024, | 0.165, | 0.364 | Scan 1 | Low M; zero lift |
| 37894 | 0.60 | 0.463, | 0.521, | 0.574 | | |
| 37895 | 0.60 | 0.566, | 0.631, | 0.690 | | |
| 37896 | 0.70 | -0.026, | 0.152, | 0.330 | Scan 3 | 'Subcritical case' |
| 37897 | 0.70 | 0.415, | 0.466, | 0.507 | | |
| 37898 | 0.70 | 0.503, | 0.554, | 0.610 | | |
| 37929 | 0.70 | 0.595, | 0.649, | 0.709 | Scan 3** | High lift; increasing Mach number trends in succeeding cases |
| 37899 | 0.72 | -0.026, | 0.174, | 0.381 | | |
| 37900 | 0.72 | 0.452, | 0.540, | 0.582 | | |
| 37901 | 0.72 | 0.590, | 0.657, | 0.724 | Scan 3 | |
| 37902 | 0.74 | -0.023, | 0.171, | 0.383 | | |
| 37903 | 0.74 | 0.488, | 0.537, | 0.579 | | |
| 37904 | 0.74 | 0.604, | 0.659, | 0.736 | Scan 3 | |
| 37905 | 0.76 | -0.040, | 0.172, | 0.385 | | |
| 37906 | 0.76 | 0.493, | 0.552, | 0.581 | | |
| 37907 | 0.76 | 0.617, | 0.681, | 0.734 | Scan 3 | |
| 37908 | 0.77 | -0.031, | 0.184, | 0.378 | | |
| 37909 | 0.77 | 0.488, | 0.543, | 0.580 | | |
| 37910 | 0.77 | 0.608, | 0.666, | 0.733 | Scan 3 | |
| 37911 | 0.78 | -0.038, | 0.176, | 0.376 | | |
| 37912 | 0.78 | 0.483, | 0.541, | 0.573 | | |
| 37913 | 0.78 | 0.600, | 0.661, | 0.717 | Scan 3 | |
| 37914 | 0.79 | -0.035, | 0.176, | 0.382 | | |
| 37915 | 0.79 | 0.442, | 0.497, | 0.555 | | |
| 37917 | 0.79 | 0.616, | 0.660, | 0.717 | Scan 3 | |
| 37918 | 0.80 | -0.049, | 0.169, | 0.377 | | |
| 37919 | 0.80 | 0.431, | 0.494, | 0.549 | | |
| 37920 | 0.80 | 0.607, | 0.661, | 0.696 | Scans 2,3 | Scan 3 shows trailing edge divergence indicating flow separation |
| 37921 | 0.81 | -0.049, | 0.161, | 0.269 | | |
| 37922 | 0.81 | 0.366, | 0.421, | 0.475 | | |
| 37923 | 0.81 | 0.473, | 0.524, | 0.588 | Scans 2,3 | Scan 3 shows trailing edge divergence indicating flow separation |
| 37926 | 0.79 | 0.659* | 0.713* | 0.759 | | |

* Repeat of two scans in Run 37917

** The drag for this scan is not correct (out of air) but Cp model is good. The user may prefer to use scan 2.

**Note**

1. Corrected only for Mokry's linear theory Ref 8.4.1. $C_L$ should be corrected according to Section 6.2. Use lift rather than $\alpha$ for computations.

**Table 3. Form of Data**

| Data | Eng. Units | Coeff | Normalized | Uncorrected | Corrected[1] |
|---|---|---|---|---|---|
| Freestream Conditions | X | / | / | / | X |
| Surface pressures | / | X | X | / | X |
| Forces integrated from pressure | / | X | / | / | X |
| Wake data | / | X | / | / | X |

**Note**
1. Corrected only for Mokry's linear theory Ref 8.4.1. $p/p_0$ does not need correction and $C_l$ should be corrected according to Section 6.2. Use lift rather than $\alpha$ for comparison.

**Table 4. Mach number corrections for each run on floppy. 3 scans per run.**

| | SCAN | | | SCAN | | | SCAN | | | SCAN | | |
|---|---|---|---|---|---|---|---|---|---|---|---|---|
| | 1 | 2 | 3 | 1 | 2 | 3 | 1 | 2 | 3 | 1 | 2 | 3 |
| RUN | M(linear corrn.)[1] | | | -ΔM(nonlinear)[2] | | | -ΔM(sidewall)[3] | | | M(fully corrected) | | |
| 37893 | 0.600 | 0.600 | 0.600 | 0.000 | 0.000 | 0.000 | 0.000 | 0.000 | 0.000 | 0.600 | 0.600 | 0.600 |
| 37894 | 0.599 | 0.599 | 0.598 | 0.000 | 0.000 | 0.001 | 0.000 | 0.000 | 0.000 | 0.599 | 0.599 | 0.597 |
| 37895 | 0.598 | 0.598 | 0.598 | 0.001 | 0.001 | 0.001 | 0.000 | 0.000 | 0.000 | 0.597 | 0.597 | 0.597 |
| 37896 | 0.703 | 0.703 | 0.701 | 0.001 | 0.001 | 0.001 | 0.000 | 0.000 | 0.001 | 0.702 | 0.702 | 0.699 |
| 37897 | 0.700 | 0.700 | 0.698 | 0.001 | 0.001 | 0.001 | 0.001 | 0.001 | 0.002 | 0.698 | 0.698 | 0.695 |
| 37898 | 0.699 | 0.698 | 0.698 | 0.001 | 0.001 | 0.001 | 0.002 | 0.002 | 0.002 | 0.696 | 0.695 | 0.695 |
| 37929 | 0.702 | 0.702 | 0.701 | 0.001 | 0.001 | 0.001 | 0.002 | 0.002 | 0.002 | 0.699 | 0.699 | 0.698 |
| 37899 | 0.723 | 0.724 | 0.719 | 0.001 | 0.001 | 0.001 | 0.000 | 0.001 | 0.001 | 0.722 | 0.722 | 0.717 |
| 37900 | 0.720 | 0.719 | 0.719 | 0.001 | 0.001 | 0.001 | 0.001 | 0.002 | 0.002 | 0.718 | 0.716 | 0.716 |
| 37901 | 0.722 | 0.722 | 0.722 | 0.001 | 0.001 | 0.002 | 0.002 | 0.002 | 0.002 | 0.719 | 0.719 | 0.718 |
| 37902 | 0.744 | 0.745 | 0.744 | 0.001 | 0.001 | 0.001 | 0.000 | 0.001 | 0.001 | 0.743 | 0.743 | 0.742 |
| 37903 | 0.742 | 0.742 | 0.742 | 0.001 | 0.001 | 0.002 | 0.001 | 0.002 | 0.002 | 0.740 | 0.739 | 0.738 |
| 37904 | 0.742 | 0.742 | 0.742 | 0.002 | 0.002 | 0.002 | 0.002 | 0.002 | 0.002 | 0.738 | 0.738 | 0.738 |
| 37905 | 0.764 | 0.765 | 0.763 | 0.001 | 0.001 | 0.001 | 0.000 | 0.001 | 0.001 | 0.763 | 0.763 | 0.761 |
| 37906 | 0.763 | 0.762 | 0.762 | 0.002 | 0.002 | 0.002 | 0.001 | 0.002 | 0.002 | 0.760 | 0.758 | 0.758 |
| 37907 | 0.762 | 0.762 | 0.762 | 0.002 | 0.002 | 0.003 | 0.002 | 0.002 | 0.002 | 0.758 | 0.758 | 0.757 |
| 37908 | 0.770 | 0.771 | 0.769 | 0.002 | 0.001 | 0.001 | 0.000 | 0.001 | 0.001 | 0.768 | 0.769 | 0.767 |
| 37909 | 0.768 | 0.768 | 0.768 | 0.002 | 0.002 | 0.002 | 0.001 | 0.002 | 0.002 | 0.765 | 0.764 | 0.764 |
| 37910 | 0.768 | 0.767 | 0.768 | 0.002 | 0.003 | 0.003 | 0.002 | 0.002 | 0.002 | 0.764 | 0.762 | 0.763 |
| 37911 | 0.779 | 0.780 | 0.779 | 0.002 | 0.001 | 0.002 | 0.000 | 0.001 | 0.001 | 0.777 | 0.778 | 0.776 |
| 37912 | 0.778 | 0.777 | 0.776 | 0.002 | 0.002 | 0.002 | 0.001 | 0.002 | 0.002 | 0.775 | 0.773 | 0.772 |
| 37913 | 0.777 | 0.776 | 0.776 | 0.003 | 0.003 | 0.003 | 0.002 | 0.002 | 0.002 | 0.772 | 0.771 | 0.771 |
| 37914 | 0.789 | 0.790 | 0.788 | 0.002 | 0.002 | 0.002 | 0.000 | 0.001 | 0.001 | 0.787 | 0.787 | 0.785 |
| 37915 | 0.791 | 0.790 | 0.790 | 0.002 | 0.002 | 0.003 | 0.001 | 0.001 | 0.002 | 0.788 | 0.787 | 0.785 |
| 37917 | 0.789 | 0.788 | 0.788 | 0.003 | 0.003 | 0.004 | 0.002 | 0.002 | 0.002 | 0.784 | 0.783 | 0.782 |
| 37918 | 0.803 | 0.803 | 0.802 | 0.003 | 0.002 | 0.002 | 0.000 | 0.001 | 0.001 | 0.800 | 0.800 | 0.799 |
| 37919 | 0.801 | 0.800 | 0.800 | 0.003 | 0.003 | 0.003 | 0.001 | 0.001 | 0.002 | 0.797 | 0.796 | 0.795 |
| 37920 | 0.799 | 0.799 | 0.798 | 0.004 | 0.004 | 0.004 | 0.002 | 0.002 | 0.002 | 0.793 | 0.793 | 0.792 |
| 37921 | 0.813 | 0.813 | 0.813 | 0.004 | 0.003 | 0.003 | 0.000 | 0.000 | 0.001 | 0.809 | 0.810 | 0.809 |
| 37922 | 0.811 | 0.811 | 0.810 | 0.003 | 0.003 | 0.003 | 0.001 | 0.001 | 0.001 | 0.807 | 0.807 | 0.806 |
| 37923 | 0.810 | 0.809 | 0.809 | 0.003 | 0.003 | 0.004 | 0.001 | 0.002 | 0.002 | 0.806 | 0.804 | 0.803 |
| 37926 | 0.789 | 0.789 | 0.788 | 0.003 | 0.004 | 0.004 | 0.002 | 0.002 | 0.002 | 0.784 | 0.783 | 0.782 |

**Notes:**
1. **Mach number as printed on floppy applying Mokry's linear correction; Ref 8.4.1**
2. **Correction to Mokry's linear theory for nonlinear effects; Ref 8.4.2**
3. **Correction for sidewall boundary layer; Ref 8.4.3**

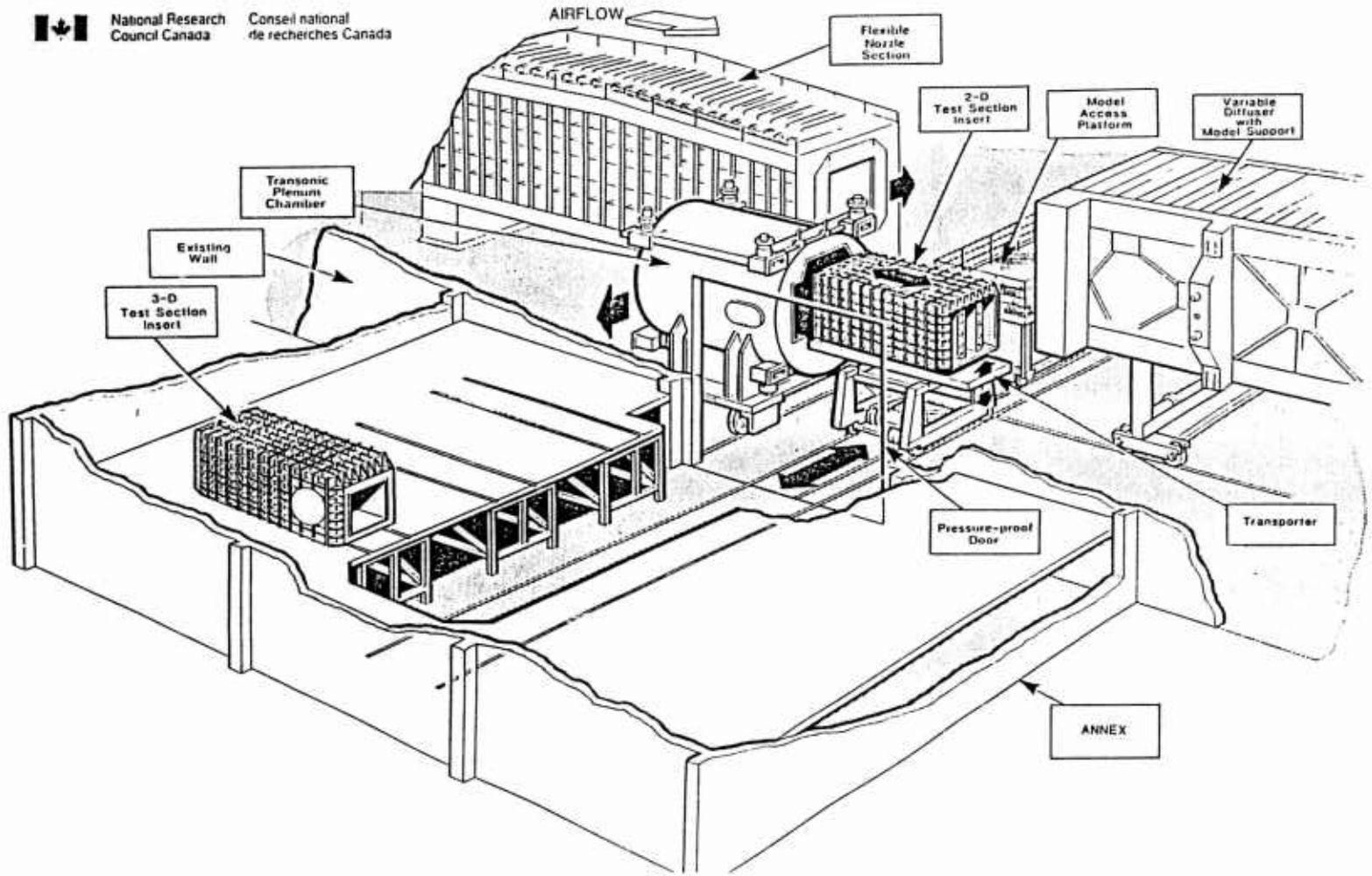



**Fig 1. The IAR 1.5X1.5m Wind Tunnel and the Roll-In Roll-out Test Sections**

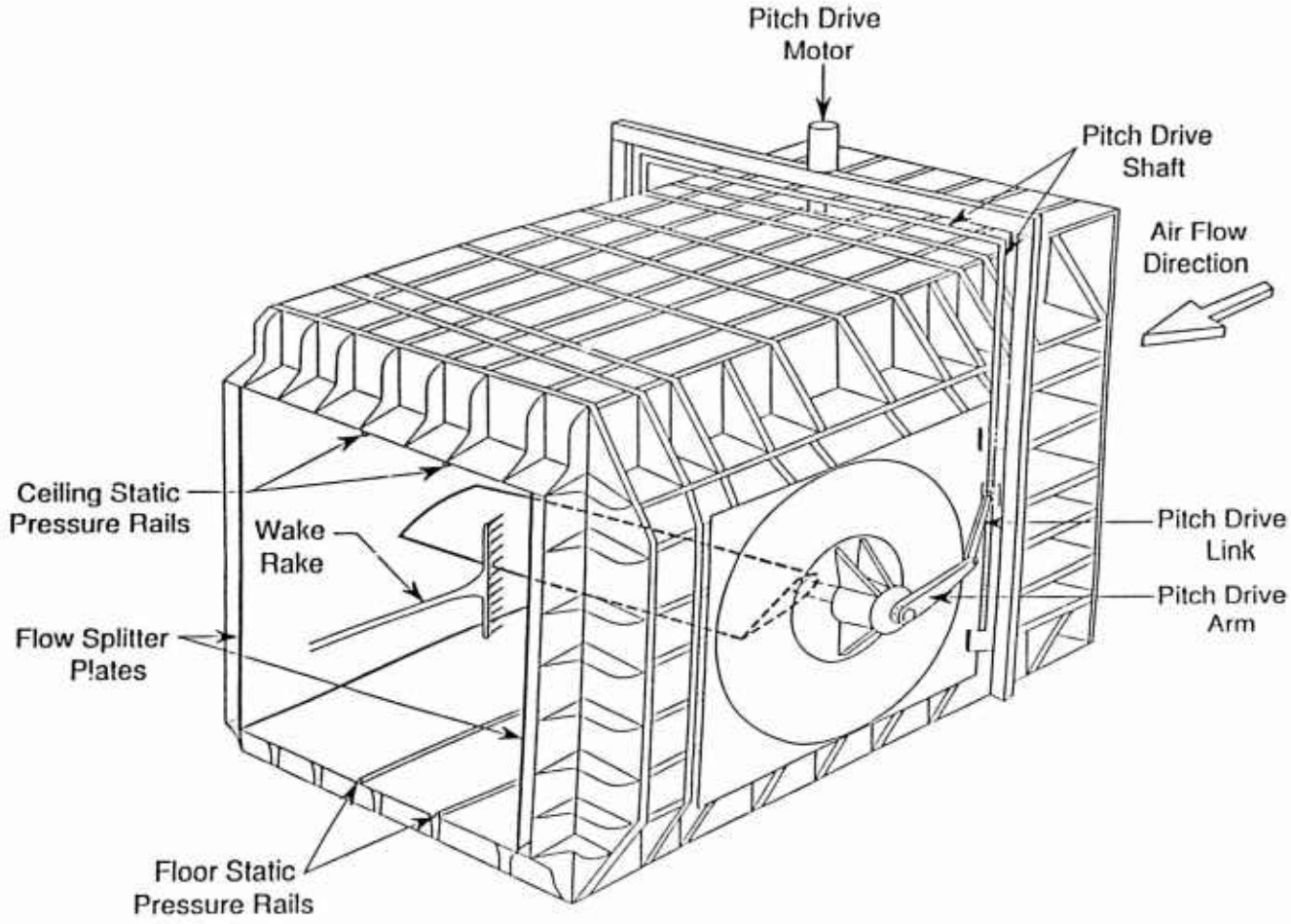



Fig 2. The 3-D Test Section Insert used for the Boeing A4 Airfoil Tests

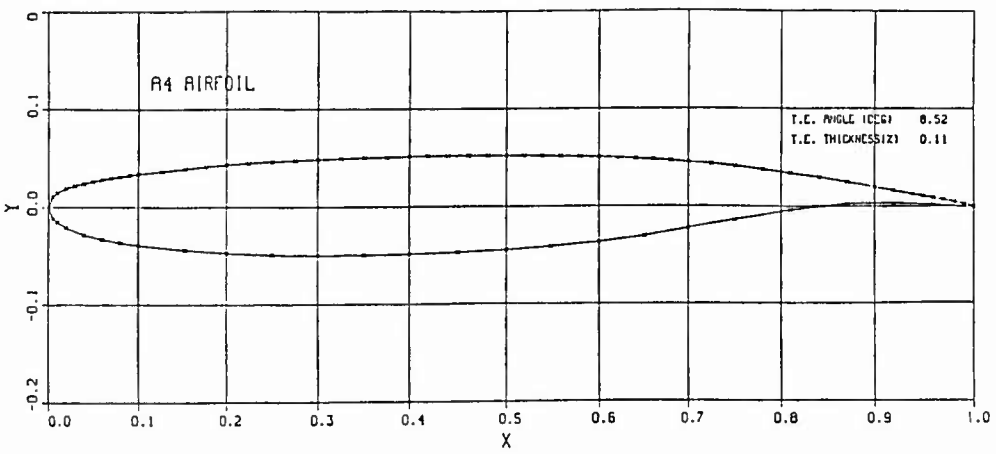



Fig 3. The Boeing A4 Airfoil Showing the Planned Pressure Orifice Locations

EXPERIMENT, RUN 37926

| ALPHA | M | CL | CM | CDW |
|---|---|---|---|---|
| 1.46 | 0.789 | 0.659 | -0.124 | 0.0120 |

EXPERIMENT, RUN 37917

| ALPHA | M | CL | CM | CDW |
|---|---|---|---|---|
| 1.43 | 0.788 | 0.660 | -0.123 | 0.0119 |

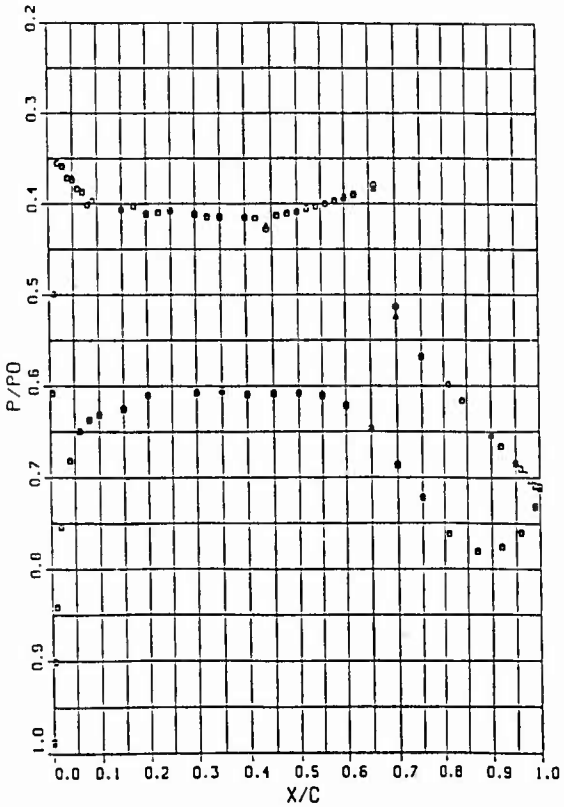



Fig 4. Data from Two Separate Runs Shows the Repeatability

# 2-D AILERON EFFECTIVENESS STUDY

by

**V.D. Chin, C.J. Dominik, F.T. Lynch, D.L. Rodriguez**
**McDonnell Douglas Corporation**
**Long Beach, California**

## 0. Introduction

The experimental data described in this contribution were obtained in the IAR High Reynolds Number 60" x 15" (1.5m x 0.38m) Two-Dimensional Test Facility. The purpose of the experiment was to investigate the effects of Reynolds number and Mach number on aileron effectiveness and to evaluate effectiveness of viscous scaling techniques that attempt to simulate flow at higher Reynolds numbers.

The advent of the modern transport wing has prompted a renewed interest in the transonic characteristics of ailerons. In addition to their traditional role of lateral (roll) control, ailerons are used for wing load alleviation and to improve cruise performance through the "drooped aileron" concept. An understanding of the prevailing flow physics which limit the transonic performance of ailerons is necessary for the successful design of a control system that satisfies the multi-role requirements of the aileron.

Figure 1 illustrates some typical results that were obtained from this test. These results showed a linear variation of lift for upward trailing edge deflections but a highly nonlinear variation for downward deflections. This nonlinear behavior, equivalent to a loss in aileron effectiveness, became worse at higher angles of attack and higher Mach numbers. In addition, the viscous scaling technique that was used at lower Reynolds numbers was found to be inadequate for modeling flow at higher Reynolds numbers.

The data acquired from this test were for a series of aileron deflections varying from -5° to +5° at Mach numbers of 0.717 and 0.746 and chord Reynolds numbers of 5, 15, and 25 million. The following types of data were obtained: airfoil surface pressure distributions; wake drag, which was determined by wake transversing probes; lift and drag forces and pitching moment, which were determined by force balance readings and surface pressure integrations; and floor and ceiling pressure distributions, which were used to compute wall interference effects.

One of the difficulties in wind tunnel testing is accounting for the effects of wall interference to reinterpret the data for "free air "conditions. Corrections for interference effects of the floor and ceiling and for the sidewall boundary layer effects were applied to the data. The data are available corrected for floor and ceiling effects, and corrected for both floor and ceiling interference and sidewall boundary layer effects.

## 1. General Description

| | | |
|---|---|---|
| 1.1 | Model name or designation | McDonnell Douglas DLBA032 airfoil |
| 1.2 | Model type/flow conditions | 2D supercritical airfoil; transonic |
| 1.3 | Purpose | To determine the effects of Reynolds number and Mach number on aileron effectiveness. |
| 1.4 | Dominant flow physics | Shock development, trailing edge separation. See Figure 1. |

## 2. Details of Model (Ref. 4)

| | | |
|---|---|---|
| 2.1 | Geometric arrangement | Unswept wing with 10.0" (0.254 m) chord spanning width of wind tunnel test section (15" (0.38m)) to simulate 2D flow. |
| 2.2 | Configurations tested | Aileron deflections of -5°, -2°, 0°, 1°, 2°, 3°, 4°, 5°. |
| 2.3 | Airfoil data | |
| 2.3.1 | Airfoil shape | Supercritical aft-loaded airfoil with 2.25% aft camber. See Figure 2. |
| 2.3.2 | Thickness/chord | 0.1228 |
| 2.3.3 | Nose radius/chord | 0.0179 |
| 2.3.4 | Trailing edge thickness | 0.50% chord |
| 2.3.5 | Aileron data | Aileron hinge line is at 75.0% chord. Deflection are set by replacing the interchangeable bracket shown in Figure 2. A 0.01" (.25mm) gap is modeled between the main airfoil and the aileron. A typical deflection is shown in Figure 3. |
| 2.4 | Geometric Definition | |
| 2.4.1 | Analytical/numerical | Numerical |
| 2.4.2 | Design/measured | Measured |
| 2.4.3 | Tolerances | ±0.002" (±0.005 cm) for leading edge 5% chord.<br>±0.005" (±0.013 cm) from 5% to 75% chord.<br>±0.0015" (±0.0038 cm) for aileron. |
| 2.4.4 | Surface roughness | 16 min (400 nm) |
| 2.5 | Model support details | |
| 2.5.1 | Support geometry | Side wall balances connected to airfoil by two pins at each end. See Figure 4. |
| 2.5.2 | Special feature | The balance can rotate to allow for angle of incidence control along with the measurement of chord and normal forces and pitching moment. |

## 3. General Tunnel Information

| | | |
|---|---|---|
| 3.1 | Tunnel designation | 2-D High Reynolds Number Test Facility of the IAR 1.5m x 1.5m Trisonic Blowdown Wind Tunnel. |
| 3.2 | Organization | High Speed Aerodynamics Laboratory<br>Institute for Aerospace Research<br>National Research Council of Canada<br>Montreal Road<br>Ottawa, Ontario<br>K1A OR6<br>Canada |

| | | |
|---|---|---|
| 3.3 | Tunnel characteristics | |
| | 3.3.1 Type of tunnel | Blowdown tunnel with interchangeable test sections. |
| | 3.3.2 Operating envelope | Mach numbers from 0.1 to 1.1. Reynolds numbers from 4 to 50 million/ft (13 to 164 million/m). Total pressures from 60 to 180 psia (0.41 to 1.24 MPa). |
| 3.4 | Test section | |
| | 3.4.1 Test section and mount details | See Figure 5. |
| | 3.4.2 Test section dimensions | 60" (0.38m) in height and 15" (1.5m) in width. Test section length with parallel walls is 141" (3.56m). |
| | 3.4.3 Wall geometry details | |
| | 3.4.3.1 Wall type | Ceiling and floor have adjustable porosity (0.5% - 6%) to reduce boundary layer effects. Sidewalls are solid except for 18"x24" (46cm x 61cm) boundary layer suction panels located at the model mount. |
| | 3.4.3.2 Open area ratio | Adjustable; 0.005 to 0.060. |
| | 3.4.3.3 Wall pressures | Measured along floor and ceiling with 1.0" (25.4mm) rails located midway between the sidewalls extending 83" (2.1m) upstream and 47" (1.2m) downstream of the model pitch axis. Sidewall pressures not measured. |
| | 3.4.3.4 Boundary layer control | The sidewall boundary layer is removed at the test section inlet by bleed slots. The new sidewall boundary layer which develops as the flow reaches the model is then thinned or removed through the 18"x 24" (45cm x 61cm) porous panel and mount disk which surround the model end using suction. The floor and ceiling were porous throughout the length of the test section. |
| | 3.3.4.5 Typical boundary layer displacement thickness at balance centerline. | 0.15" (.38 cm) for Re = 15 x $10^6$ /ft (49 x $10^6$/m) and a suction velocity ratio ($v/U_\infty$) of 0.0078 (Ref. 1, Fig. 11). |
| 3.5 | Free stream conditions | |
| | 3.5.1 Ref. conditions determined by | |
| | 3.5.1.1 Total pressure | Parascientific Digiquartz 200 psia (1.38 MPa) pressure transducer on pitot probe at inlet of test section. |

| | |
|---|---|
| 3.5.1.2 Static pressure | Digiquartz 200 psia (1.38 MPa) pressure transducer in pressure tap located 81" (206cm) upstream of balance centerline. |
| 3.5.1.3 Total temperature | Resistance thermometer (RdF probe) in tunnel settling chamber. |
| 3.5.1.4 Static temperature | Not determined. Calculated from conditions determined above. |

3.5.2 Tunnel calibration

| | |
|---|---|
| 3.5.2.1 Method | Static pressure tubes were mounted at the centerline and along the floor and ceiling. Pressure taps were also installed along the floor, ceiling, and one sidewall. The reference pressure tap was located 81" (2.1 m) upstream of the balance. These were used to determine the flow uniformity over vertical planes in the test section. The wake rake was also used to determine the total pressure uniformity across the test section. Flow quality (turbulence and noise levels) was determined using hot wire probes spanning half of the width of the test section along the centerline of the balance. A microphone probe mounted at the center of the test section was used to compliment the hot wire measurements. Sidewall boundary layer measurements were made using boundary layer rakes. |
| 3.5.2.2 Date of last calibration | 1989 |

3.6 Flow quality (empty tunnel)

3.6.1 Flow uniformity

| | |
|---|---|
| 3.6.1.1 Pressure variations from reference value over model length | $\Delta P/P_o \approx$ -0.0012 to -0.0024 with $(P/P_o)_{nom}$= 1.1166 and 2% porosity (floor & ceiling), Re = 15 x $10^6$/ft (49 x $10^6$/m) (Ref. 1, Fig. 9a). |
| 3.6.1.2 Mach no. variations from reference value over model length | $\Delta M \approx$ -0.002 to -0.004 with $M_{nom}$ = 0.400 and 2% porosity (floor & ceiling), Re = 15 x $10^6$/ft (49 x $10^6$/m) (Ref. 1, Fig. 9a). |
| 3.6.1.3 Mach no. variations during a run | 0.0006 standard deviation (Ref. 2, p. 9). |
| 3.6.1.4 Average flow angularity | Using a 9" (23 cm) chord model, the balance forces were measured over small incidence ranges with the model in the upright and inverted configurations. The average flow angularity was determined by comparing the forces measured in these two orientations. For a Mach no. of 0.70, the average flow angularity was found to be a downwash of 0.14° (Ref. 2, Fig. 16). |

| | |
|---|---|
| 3.3.1.5 Flow angularity variations from reference value over model length | Not measured. |
| 3.6.2 Temperature variation | Not measured. |
| 3.6.3 Flow steadiness | |
| 3.6.3.1 Overall turbulence level | For Re = 15 x $10^6$/ft (49 x $10^6$/m), turbulence intensity, $(\tilde{u}/\bar{u})_{rms}$, varies from 0.23% at M=0.5 to 0.35% at M=0.8 (Ref. 1, p.16). |
| 3.6.3.2 Overall noise level | For Re = 15 x $10^6$/ft (49 x $10^6$/m), pressure fluctuation, $Cp_{rms}$, varies from 0.55% at M=0.4 to 0.80% at M=0.8 (Ref. 1, p. 16). |

## 4. Instrumentation

| | |
|---|---|
| 4.1 Model position | |
| 4.1.1 Incidence measurement method | The incidence angle is measured by a potentiometer mounted on the pitch drive system (Ref. 3, p. 9). |
| 4.1.2 Model incidence accuracy | ±0.03° (Ref. 2, p. 9) |
| 4.2 Model pressure measurements | |
| 4.2.1 Pressure holes, no. & position | 80 pressure taps. See Figure 2 for location. |
| 4.2.2 Transducer range & accuracy | Maximum pressure of 200 psia (1400 kPa) with an accuracy of ±0.10 psi (0.7 kPa) (Ref. 2, p. 9). |
| 4.2.3 Dynamic pressures measured | No. |
| 4.3 Force and moment measurements | |
| 4.3.1 Type and location of balance | Three component (normal force, axial force, and pitching moment) strain gage balance mounted in each sidewall. See Figure 6. |
| 4.3.2 Maximum range and accuracy | Maximum allowable loads are 20,000 $lb_f$ (89 kN) for normal force, 2000 $lb_f$ (8.9 kN) for axial force, and 45,000 lb-in (7.9 MN-m) for pitching moment (Ref. 2, Fig. 6). Accuracies are ±20 lb (±8.9 N) for normal, ±2 lb (±.89 N) for axial, and ±65 lb-in (±730 N-cm) for pitching moment (Ref. 2, p. 9) |
| 4.4 Flow field measurements | |
| 4.4.1 Technique | Pitot tube rake transversing the wake region 21" (53 cm) downstream of balance center of rotation (approximately one chord length downstream from trailing edge of a 12" (30 cm) chord model). |
| 4.4.2 Region investigated | Airfoil wake region is probed by the transversing wake rake. The rake averages about 240 measurements across the usual range of 18" (46 |

| | | |
|---|---|---|
| | | cm) above to 8" (20 cm) below the centerline of the balance. The rake system is capable of detecting pressure gradients and is able to automatically increase measurements in the actual wake of the model where large pressure gradients exist. See Figure 7. |
| | 4.4.3 Wake rake details | See Figure 7. |
| 4.5 | Tunnel wall measurements | |
| | 4.5.1 Type | Static wall pressures were measured on floor and ceiling. |
| | 4.5.2 Press. hole location & number | Pressure holes are located between 77.1" (196 cm) upstream and 44.9" (114 cm) downstream of the of the balance. They are non-uniformly spaced with a higher concentration around the model region. The average spacing between holes is approximately 6" (15 cm). |

## 5. Test Matrix and Conditions

| | | |
|---|---|---|
| 5.1 | Detailed test matrix | |
| | 5.1.1 No. of selected test cases | 25 |
| | 5.1.2 No. of configurations tested | 1 model with different aileron deflections. |
| | 5.1.3 Test matrix details | See Table (I). |
| 5.2 | Model/tunnel relations | |
| | 5.2.1 Maximum blockage | 0.020 (airfoil frontal area / test section area) |
| | 5.2.2 Model span/tunnel width | 1.0 |
| | 5.2.3 Wing area/test section area | 0.167 |
| | 5.2.4 Height/chord ratio | 6 |
| | 5.2.5 Width/chord ratio | 1.5 |
| 5.3 | Transition details | |
| | 5.3.1 Free or fixed transition | Fixed for Re = 5 & 15 x $10^6$<br>Free for Re = 25 x $10^6$ |
| | 5.3.2 Free transition details | |
| | 5.3.2.1 Transition location | For Re = 25 x $10^6$, transition location (x/c)<br>Upper surface - L.E. Lower surface - L.E. |
| | 5.3.2.2 Transition verification | No experimental verification of the transition location was performed during this wind tunnel test. However, previous work (Ref. 5) on the same airfoil using vacuum deposited hot film gages showed natural transition to occur at the leading edge for Reynolds number =25x$10^6$. |

5.3.3 Fixed transition details

| | |
|---|---|
| 5.3.3.1 Transition location | For Re = 5 x $10^6$, transition location (x/c):<br>Upper surface - 0.15 Lower surface - 0.28<br>For Re = 15 x $10^6$, transition location (x/c):<br>Upper surface - 0.10 Lower surface - 0.15 |
| 5.3.3.2 Type and size of strip | For Re = 5 x $10^6$, transition strip consisted of 0.0032" (0.081 mm) high, 0.045" (1.1 mm) dia.disks spaced 0.10" (2.5 mm) apart<br><br>For Re = 15 x $10^6$, transition strip consisted of 0.0016" (0.041 mm) high, 0.045" (1.1 mm) dia.disks spaced 0.10" (2.5 mm) apart<br><br>No estimate of the drag associated with the transition strips was performed. |
| 5.3.3.3 Trip verification | Trip locations for Re = 5 x $10^6$ and Re = 15 x $10^6$ were established using a CFD method to match boundary layer thickness at the trailing edge of the airfoil to that of Re = 25 x $10^6$. No experimental verification of the natural transition location was performed during this wind tunnel test. However, previous work (Ref. 5) on the same airfoil using vacuum deposited hot film gages showed natural transition to occur at the following locations:<br><br>For Re = 5 x $10^6$, natural transition location (x/c):<br>Upper surface - 0.40 Lower surface - 0.50<br>For Re = 15 x $10^6$,natural transition location (x/c):<br>Upper surface - 0.33 Lower surface - 0.50 |

## 6. Data

6.1 Availability of data

| | |
|---|---|
| 6.1.1 Organization of ownership | McDonnell Douglas Corporation |
| 6.1.2 Responsible party | Frank T. Lynch, Group Leader<br>Aerodynamics Technology, Flight Performance<br>Mail Code 36-41<br>3855 Lakewood Blvd.<br>Long Beach, CA 90846-0001<br>USA<br>Phone Number: (310) 593-2947<br>Fax number: (310) 593-7593 |
| 6.1.3 Are data freely available? | Yes. |
| 6.1.4 Contact | Frank T. Lynch (address above) |

6.2 Suitability of data for CFD validation

| | |
|---|---|
| 6.2.1 For "in-tunnel" calculation? | No. |

| | | |
|---|---|---|
| 6.2.2 | Corrected for "free air" conditions? | The data would be suitable for 2D "free air" calculations since it was corrected for sidewall boundary layer effects and ceiling and floor interference effects. |
| 6.3 | Type and form of data available | |
| 6.3.1 | Type and form | See Table (II). |
| 6.3.2 | Data carrier | Floppy Disks |
| 6.4 | Corrections applied to data | |
| 6.4.1 | Floor and ceiling interference | Mach number and angle of attack were corrected for floor and ceiling wall interference using the "Mokry" correction. All other flow variables were corrected using these corrected quantities. The tunnel wall pressure measurements were used to determine the corrections for Mach number and angle of attack necessitated by the flow constraints of the tunnel walls. See (Ref. 6) for more details. |
| 6.4.2 | Sidewall boundary layer | Mach number and pressure coefficient were corrected for sidewall boundary layer effects using the "Murthy" correction. The "Murthy" correction accounts for the change in effective test section area due to the sidewall boundary layer. The "Murthy" corrections are applied to "Mokry" corrected data in a sequential manner. The "Murthy" corrections are as follows: |

$$M_{murthy} = M_{mokry} / (1+k)^{0.5}$$

$$C_{pmurthy} = C_{pmokry} (1+k)^{0.5}$$

where;

$$k = (2 + 1/H - M^2_{mokry})(2\delta^* /b)$$

$$H \approx 1.4$$

$$\delta^* \approx 0.15" \quad (Re = 15x10^6 /ft)$$

See (Ref. 7) for more details.

## 7. Data Accuracy and Repeatability Assessment

| | | |
|---|---|---|
| 7.1 | Estimated accuracy of: | |
| 7.1.1 | Free stream conditions | |
| 7.1.1.1 | Mach number | ±0.0004 |
| 7.1.1.2 | Flow velocity | ±1 ft/sec (±.3 m/s) |
| 7.1.1.3 | Model incidence | ±0.03° |

| | | |
|---|---|---|
| 7.1.2 | Measured data | |
| 7.1.2.1 | Balance forces and moments | Accuracies are ±20 lb (±89 N) for normal, ±2 lb (±8.9 N) for axial, and ±65 lb-in (±730 N-cm) for pitching moment (Ref. 2, p. 9) |
| 7.1.2.2 | Pressures | Wall: ±0.005 psi (±30 Pa), model: ±0.10 psi (±700 Pa) (Ref. 2, p. 9) |
| 7.1.2.3 | Wake pressure | ±0.01 psi (±70 Pa) (Ref. 2, p. 9) |
| 7.2 | Repeat measurements, type & number | Repeat measurements were made for selected configurations as noted in Table (I). Figure 8 shows typical examples of data repeatability. |
| 7.3 | Redundant flow quantities measured | Lift force was measured using both the balance and the integrated pressure readings. Pitching moment was measured using the balance and the integrated pressures. Typical examples of the agreement between these measurements are shown in Figure 9. |

## 8. References


8.1 Wind tunnel

1. Ohman, L.H., Brown,D., Chan, Y.Y., Galway, R.D., Hashim, S.M., Khalid, M., Malek, A., Mokry, M.,Tang, N., & Thain, J., "New Transonic Test Sections for the NAE 5ftx5ft Trisonic Wind Tunnel," NAE-AN-62, January 1990.
2. Galway, R.D., "The IAR High Reynolds Number Two-Dimensional Test Facility - A Description of Equipment and Procedures Common to Most 2-D Airfoil Tests," IAR-AN-66, June 1990.
3. Ohman, L.H., "The NAE High Reynolds Number 15 in. x 60 in. Two-Dimensional Test Facility; Part 1," LTR-HA-4, April 1970.

8.2 Model

4. Dolfinger, D.F., "Wind Tunnel Model LB-350M Operating Report for Test of an Advanced Design Two-Dimensional Airfoil, NAE 15x60-inch Wind Tunnel," MDC k4752, January 1990.
5. Fancher, M.F., "Aspects of Cryogenic Wind Tunnel Testing Technology at Douglas," AIAA-82-0606, March 22-24, 1982.

8.3 Correction methods

6. Mokry, M., "Subsonic Wall Interference Corrections for Finite-Length Test Sections Using Boundary Pressure Measurements," *in* "Wall Interference in Wind Tunnels," AGARD-CP-335, September 1982.

7. Murthy, A.V., "Corrections for Attached Sidewall Boundary-Layer Effects in Two-Dimensional Airfoil Testing," NASA Contractor Report 3873, February 1985.

## 9. List of Symbols

| | |
|---|---|
| $\alpha$ | angle of attack |
| $\delta_a$ | aileron deflection from reference chord |
| $\delta^*$ | displacement thickness |
| b | tunnel width |
| $C_l$ | Lift Coefficient |
| $C_d$ | Drag Coefficient |
| $C_m$ | Pitching moment coefficient |
| Cp | pressure coefficient |
| $Cp_{mokry}$ | pressure coefficient with Mokry correction applied |
| $Cp_{murthy}$ | pressure coefficient with Murthy correction applied |
| $Cp_{rms}$ | static pressure fluctuations (noise levels) |
| H | shape factor |
| M | Mach number |
| $M_{murthy}$ | Mach number with Murthy correction applied |
| $M_{mokry}$ | Mach number with Mokry correction applied |
| TEU | Trailing edge deflection is upwards |
| TED | Trailing edge deflection is downwards |
| RN | Reynolds number |
| $\tilde{u}/\tilde{u}$ | fractional disturbance from average local velocity |
| $(\tilde{u}/\tilde{u})_{rms}$ | turbulence intensity |

# Table I. Test Matrix

| IDENT. | FLOW CONDITION | | POSITION TESTED | | OTHER INFO | |
|---|---|---|---|---|---|---|
| CASE NO. | Mach No. (corrected) | Reynolds No. | $\alpha$ | $\delta_{aileron}$ | measurement type | repeat measurements |
| 1.01 - 1.12 | .717 | $5 \times 10^6$ | -0.02° : 2.77°. | 0° | all | no |
| 2.01 - 2.12 | .717 | $5 \times 10^6$ | -0.11° : 2.68° | 2° | all | no |
| 3.01 - 3.12 | .717 | $5 \times 10^6$ | -0.16° : 2.64° | 3° | all | no |
| 4.01 - 4.12 | .717 | $5 \times 10^6$ | -0.18° : 2.62° | 4° | all | no |
| 5.01 - 5.11 | .717 | $15 \times 10^6$ | 0.30° : 2.65° | -5° | all | yes |
| 6.01 - 6.11 | .717 | $15 \times 10^6$ | 0.02° : 2.44° | -2° | all | yes |
| 7.01 - 7.11 | .717 | $15 \times 10^6$ | -0.13° : 2.28° | 0° | all | yes |
| 8.01 - 8.11 | .717 | $15 \times 10^6$ | -0.17° : 2.22° | 1° | all | yes |
| 9.01 - 9.11 | .717 | $15 \times 10^6$ | -0.23° : 2.15° | 2° | all | yes |
| 10.01 - 10.11 | .717 | $15 \times 10^6$ | -0.28° : 2.11° | 3° | all | yes |
| 11.01 - 11.11 | .717 | $15 \times 10^6$ | -0.30° : 2.08° | 4° | all | yes |
| 12.01 - 12.11 | .717 | $15 \times 10^6$ | -0.33° : 2.08° | 5° | all | yes |
| 13.01 - 13.11 | .747 | $15 \times 10^6$ | 0.30° : 2.47° | -5° | all | no |
| 14.01 - 14.11 | .747 | $15 \times 10^6$ | 0.02° : 2.20° | -2° | all | no |
| 15.01 - 15.11 | .747 | $15 \times 10^6$ | -0.18° : 2.08° | 0° | all | no |
| 16.01 - 16.11 | .747 | $15 \times 10^6$ | -0.23° : 2.05° | 1° | all | no |
| 17.01 - 17.11 | .747 | $15 \times 10^6$ | -0.26° : 2.02° | 2° | all | no |
| 18.01 - 18.11 | .747 | $15 \times 10^6$ | -0.30° : 2.03° | 3° | all | no |
| 19.01 - 19.11 | .747 | $15 \times 10^6$ | -0.32° : 2.04° | 4° | all | no |
| 20.01 - 20.11 | .747 | $15 \times 10^6$ | -0.33° : 2.05° | 5° | all | no |
| 21.01 - 21.11 | .717 | $25 \times 10^6$ | 0.68° : 1.98° | 0° | all | no |
| 22.01 - 22.07 | .717 | $25 \times 10^6$ | 0.56° : 1.38° | 2° | all | no |
| 23.01 - 23.11 | .717 | $25 \times 10^6$ | 0.56° : 2.31° | 3° | all | no |
| 24.01 - 24.10 | .717 | $25 \times 10^6$ | 0.50° : 2.39° | 4° | all | no |
| 25.01 - 25.06 | .717 | $25 \times 10^6$ | 0.99° : 2.37° | 5° | all | no |

all - surface pressures, force & moment coefficients (balance & integrated pressures), and wake rake data (drag)

Note: Angle of attack ranges are available in nonuniform increments of approximately 0.25°.

## Table II. Data Availablitity

| DATA | ENG. UNITS | COEFFICIENTS | CORRECTED (floor & ceiling) | CORRECTED (floor, ceiling, sidewall B. L.) |
|---|---|---|---|---|
| FREESTREAM CONDITIONS | X | | X | X |
| SURFACE PRESSURES | | X | X | X |
| FORCES & PITCHING MOMENT | | X | X | X |
| WAKE DATA | | X | X | X |

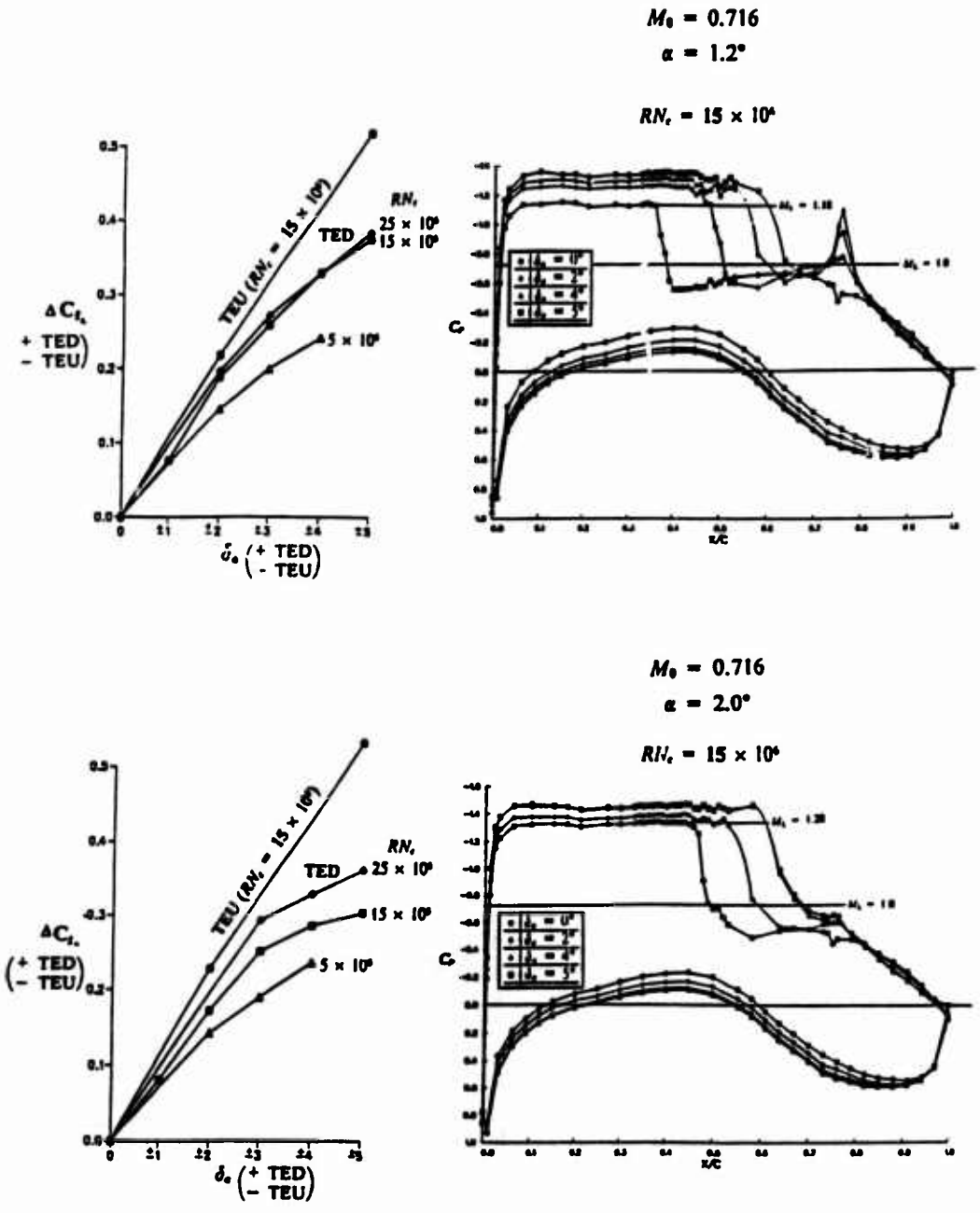


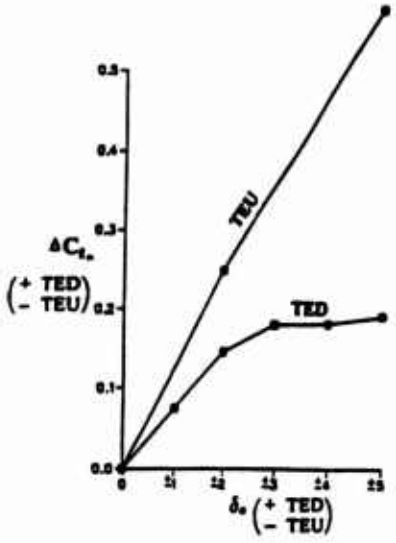

**Figure 1a**

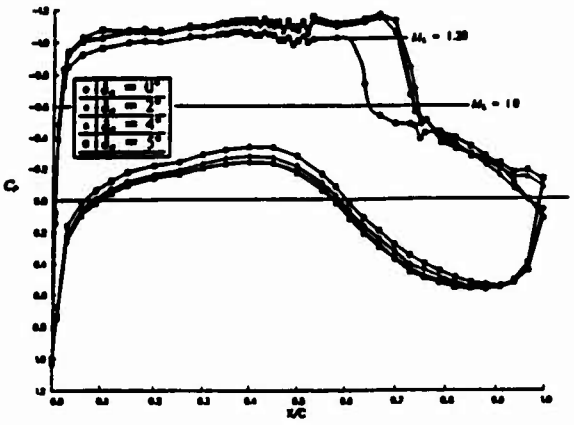
**2-D Aileron Effectiveness Test Results**

$M_0 = 0.746$

$\alpha = 0.9°$

$RN_c = 15 \times 10^6$

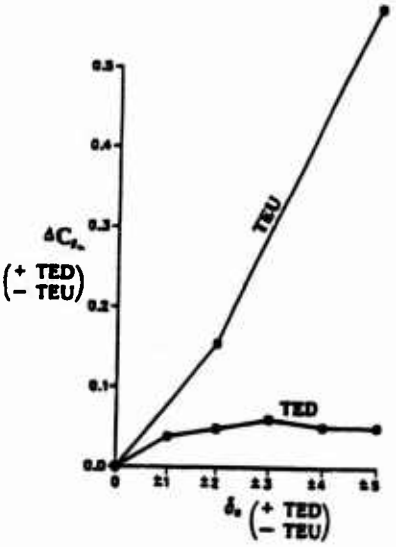



$M_0 = 0.746$

$\alpha = 2.1°$

$RN_c = 15 \times 10^6$



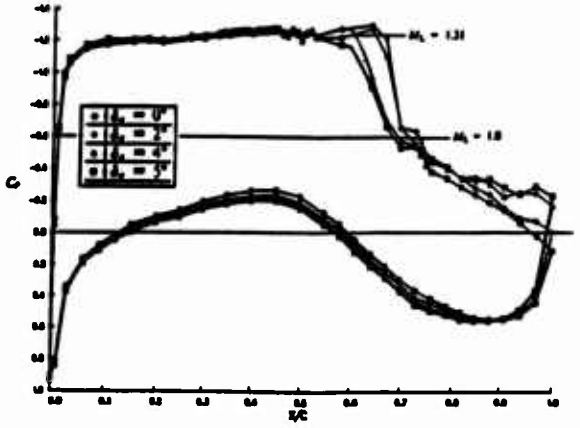




**Figure 1b**

**2-D Aileron Effectiveness Test Results**

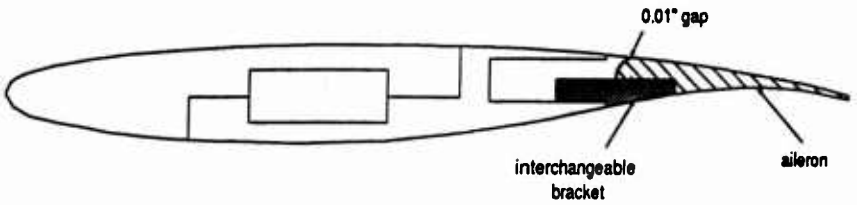
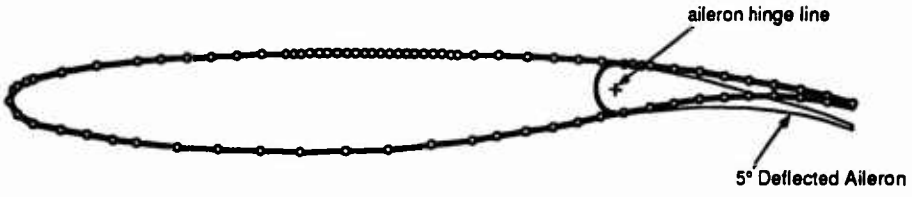



**Figure 2**

**DLBA032 Airfoil Model Structure**




• Pressure Orifice

**Figure 3**

**DLBA032 Airfoil with Pressure Orifices**

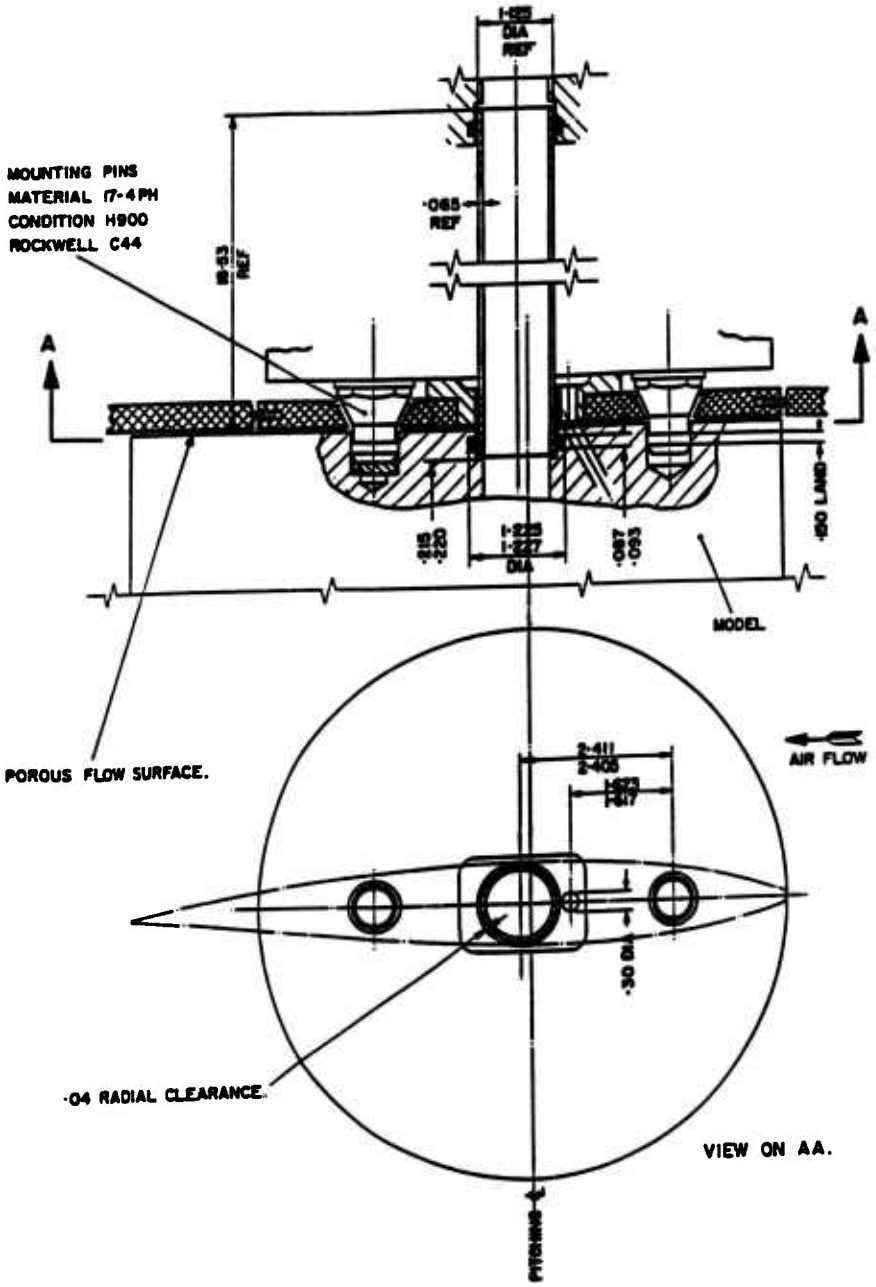



**Figure 4**

**Model Support Geometry**

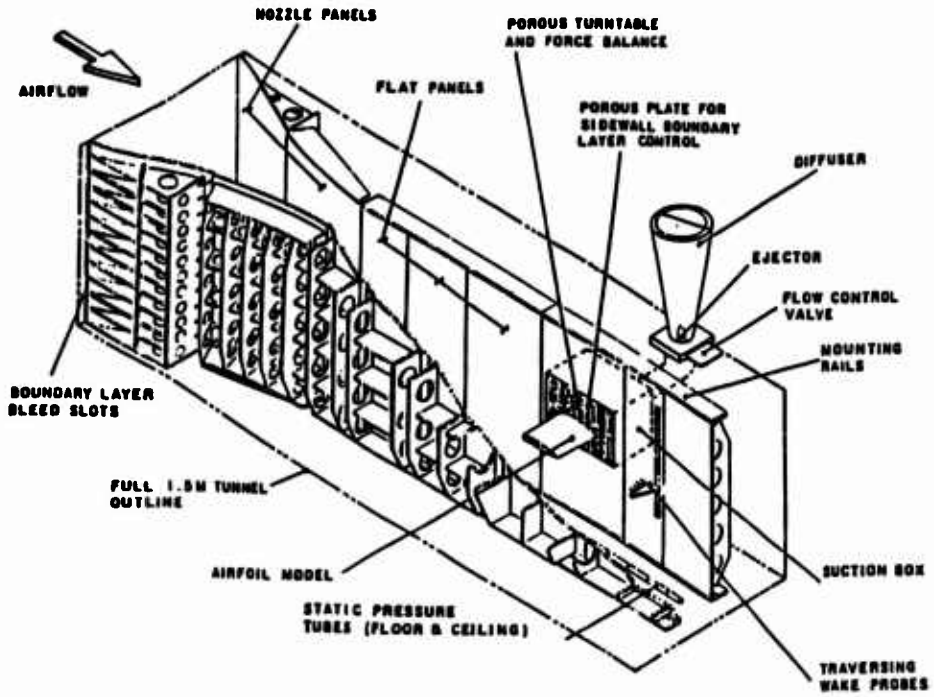



Figure 5

Test Section and Mount Details

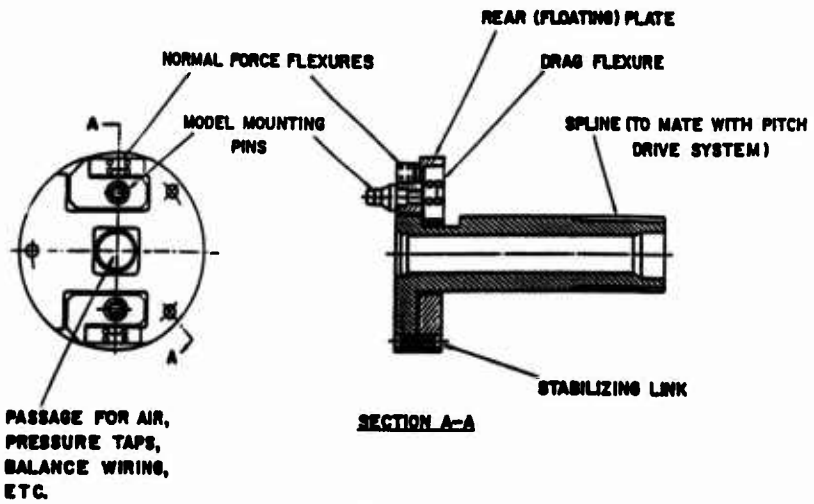
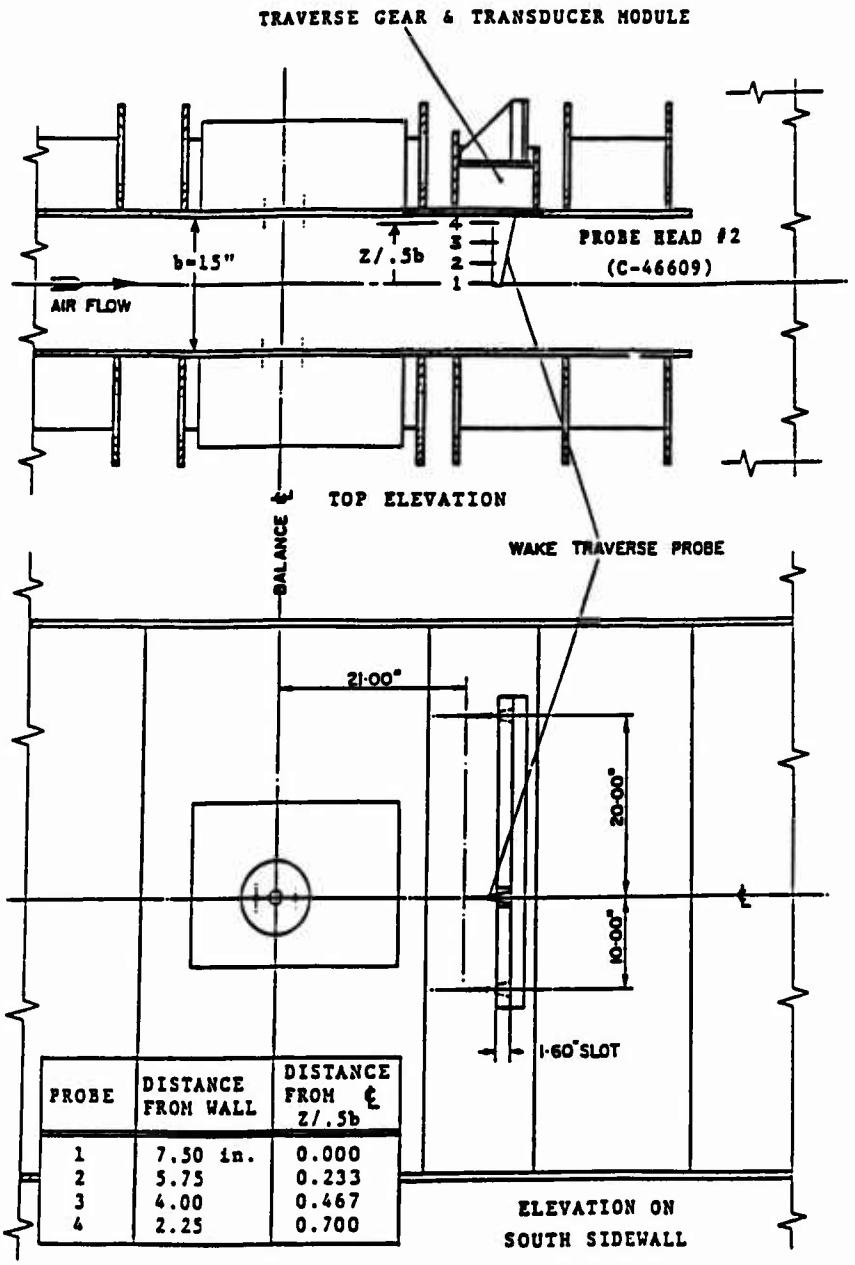



Figure 6

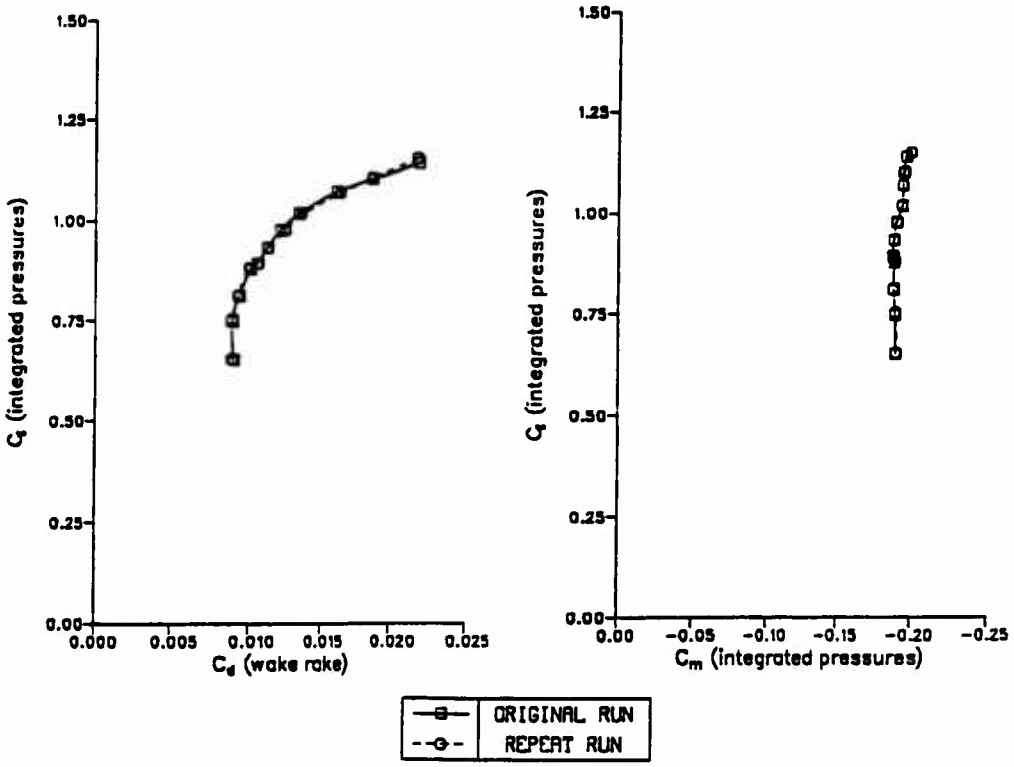
Strain Gage Balance Details




| PROBE | DISTANCE FROM WALL | DISTANCE FROM ℄ Z/.5b |
|---|---|---|
| 1 | 7.50 in. | 0.000 |
| 2 | 5.75 | 0.233 |
| 3 | 4.00 | 0.467 |
| 4 | 2.25 | 0.700 |

**Figure 7**

**Wake Rake Details**



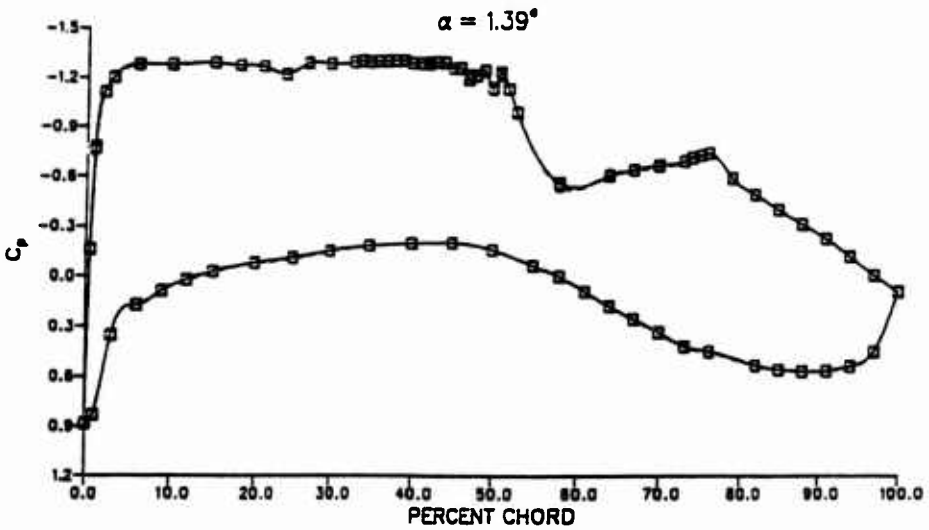




**Figure 8**

**Typical Data Repeatability**

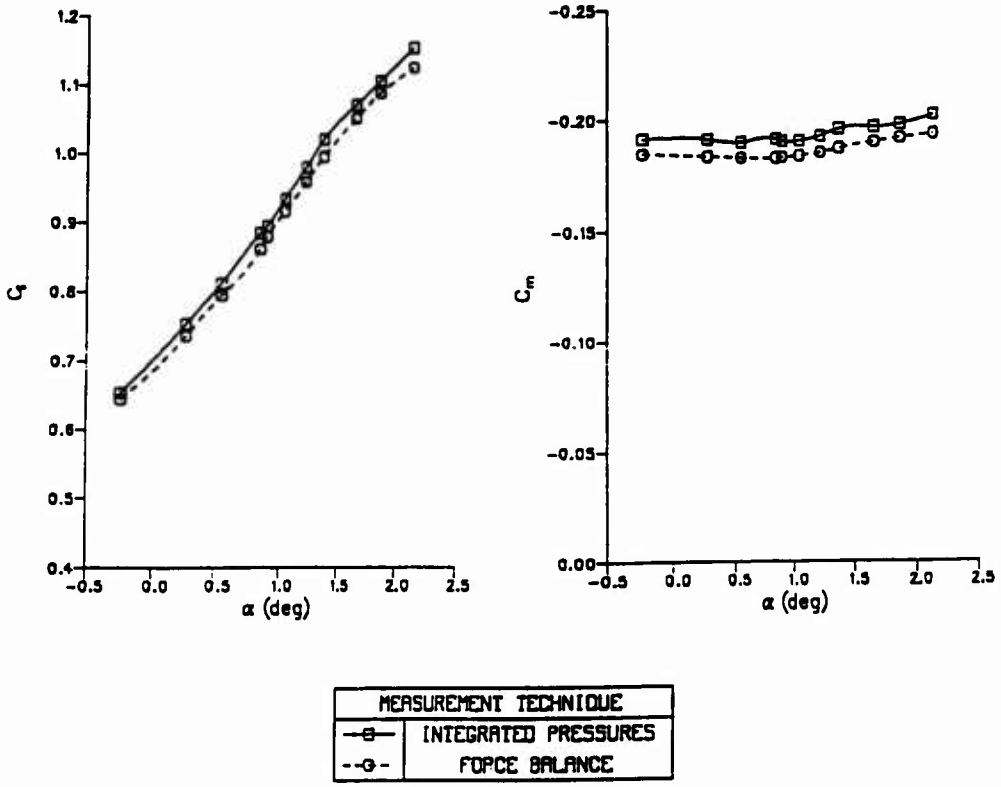



**Figure 9**

**Comparison of Force and Moment Measurements Obtained from Integrated Pressures and Balance Readings**

# GE-10. INVESTIGATION OF AN NLF(1)-0416 AIRFOIL IN COMPRESSIBLE SUBSONIC FLOW

BY

**P. Guntermann and G. Dietz**
Aerodynamisches Institut of the RWTH-Aachen
Director: E. Krause Ph. D.
Wüllnerstr. zw. 5 u. 7
W-5100 Aachen, Germany

## 0 INTRODUCTION

The data presented in this contribution were obtained in the 40 × 40 $cm^2$ Transonic Wind Tunnel at the Aerodynamisches Institut of the RWTH Aachen within the research program "Entwicklung von Berechnungsverfahren für Probleme der Strömungsmechanik" sponsored by the Stiftung Volkswagenwerk. The aim of the experimental part of the research program was to investigate the influence of compressibility on the location of transition. For this purpose a natural-laminar-flow airfoil NLF(1)-0416, designed for incompressible flow, was investigated. Starting with incompressible free stream conditions the Mach number was increased until transonic flow was obtained. The experiments on the NLF(1)-0416 should provide aerodynamical forces such as lift and drag and data concerning the location and the underlying physical mechanism of transition. Therefore different measuring techniques, e. g. liquid chrystal coating and multi-sensor hot-film technique, were tested. To verify the existence of a laminar separation bubble the topology of the boundary layer was visualized. Regarding the different turbulence levels there is a good agreement of the experimental results with those obtained at NASA-Langley, which are available up to Mach numbers of 0.4. Numerical results correspond to the experiments at higher Mach numbers too. Experiments were carried out to get information about the influence of small disturbances of the profile surface on the pressure distribution, the drag, and the location of transition. In continuation of this research a wind tunnel model with adjustable geometry of its upper surface was developed and manufactured. The influence of small surface variations on the location of transition or separation will be investigated experimentally, but these tests are not part of the presented data set.

## 1 GENERAL DESCRIPTION

| | |
|---|---|
| 1.1 Model name or designation | NLF(1)-0416 |
| 1.2 Model type | 2-D airfoil (Airfoil data see GE-10.8.2) |
| 1.3 Design requirements, purpose of test | This natural-laminar-flow airfoil was designed for general aviation applications in incompressible flow. Measurement techniques for detection of transition have been validated. Investigation of Ma- and Re-effects on natural-laminar-flow airfoils and effects of small variation of geometry will be used for a data base to validate CFD. |
| 1.4 Dominant flow physics | Transition at laminar airfoils in low Reynolds number flow is often forced by a laminar separation. The boundary layer becomes turbulent and the flow reattaches. This phenomenon is called a laminar separation bubble. Typical pressure distributions are shown in FIGS. GE-10.4/5. The measured and computed separation and transition locations are marked. The location of transition can be determined by multi-sensor hot-film measurements. A sudden increase of fluctuations indicates the transition process (See FIG. GE-10.8). The existence of a laminar separation bubble can be recognized by phase reversal phenomena. FIG. GE-10.9 shows a differential interferogram of a laminar separation bubble. The transition line on the surface of the airfoil can be visualized by surface coating with liquid chrystals (See FIG. GE-10.10). At some locations transition is caused by disturbances, e. g. by pressure taps. |

## 2 DETAILS OF MODEL

| | |
|---|---|
| 2.3 Airfoil data | |
| 2.3.2 Basic airfoil | |
| • Thickness/chord ration | 16 % |
| • Nose radius/chord | 1.55 % |
| 2.4 Body data | |
| 2.4.1 Shape | |
| • Chord length | 200 mm |
| 2.7 Geometric definition of all components | |
| • Shape specification | Numerical |
| • Co-ordinates | Measured |
| • Tolerances | ±0.05 mm (i.e. ±0.025 % c), no short wave deviations |
| • Surface roughness | Finished with grinding-paper 1000 |
| 2.8 Model support details | |
| 2.8.2 Special features of mounting | Mounted by bolts through the panes of the wind tunnel (no influences on flow by support) |

## 3 GENERAL TUNNEL INFORMATION

| | |
|---|---|
| 3.1 Tunnel designation | 40 × 40 cm$^2$ Transonic Wind Tunnel at the Aerodynamisches Institut of the RWTH Aachen |
| 3.2 Organization running the tunnel | Aerodynamisches Institut of the RWTH Aachen |
| 3.3 Tunnel characteristics | |
| • Type of tunnel | Intermittent suction tunnel |
| • Indicate operating envelope | Ma 0.18 to 3.6, $Re_{\sqrt{A_{MK}}}$ 1.6 $10^6$ to 6 $10^6$ |
| • Minimum run time | 3 to 10 sec |
| 3.4 Test section | |
| 3.4.2 Test section dimensions | 400 × 400 × 1414 mm$^3$ |
| 3.4.3 Wall geometry details | |
| • Type of walls | Adaptive top and bottom walls (See GE-10.8.1) |
| • Boundary layer control on walls | Numericaly integrated in adaption control process |
| • Typical wall boundary layer displacement thickness | 20 mm |
| 3.6 Flow quality (empty tunnel) | |
| 3.6.1 Flow uniformity | |
| • Mach number variation over model length and span | lower 1 % |
| • Mach number variation during a run | lower 1 % |
| 3.6.3 Flow unsteadiness | |
| • Overall turbulence level | 0.2 % to 0.7 % (Dependent on Mach number, see FIG. GE-10.3) The fairly high turbulence level is given by the wind tunnel. Further investigations on its spectra, its effect on transition, and on the development of the turbulent boundary layer are still expected. |

## 4 INSTRUMENTATION

| | |
|---|---|
| 4.1 Model position | |
| 4.1.1 Geometrical incidence measurement | Nonius |
| 4.1.2 Accuracy of geometrical incidence | ±0.1$^0$ |

4.2 Model pressure measurements

| | |
|---|---|
| 4.2.1 Total number and disposition of pressure holes | 50 (See FIG. GE-10.1) |
| 4.2.2 Range and accuracy of pressure transducers | 0 hPa to 1000 hPa ± 0.05 hPa |
| 4.2.3 Dynamic pressures | Measured in some cases, dissolvable frequency about 100 Hz |

4.3 Force measurements

| | |
|---|---|
| 4.3.1 Type of measurement | Lift coefficient by integrating pressure coefficients upon airfoil surface, drag coefficient by wake measurement (See FIG. GE-10.7 |
| 4.3.2 Accuracy of all components | The uncertainty in determining the lift coefficient is estimated to be less than ±0.5 %, of the drag coefficient less than ±2.5 %. |

4.4 Boundary layer and flow field measurements

| | |
|---|---|
| 4.4.1 Measurement technique applied | Model: Pressure probes, multi-sensor hot-film (See FIG. GE-10.6/8; n-factors cannot be determined because of the measurement system noise threshold); Flowfield: Hot wires, LDA |
| 4.4.2 Flow regions investigated | Boundary layer, wake, flow field around the upper surface of the airfoil |

4.5 Surface flow visualization

| | |
|---|---|
| 4.5.1 Measurement technique applied | Liquid chrystals (See FIG. GE-10.10), oil |
| 4.5.2 Surfaces with flow visualization | Upper surface of the airfoil |
| 4.5.3 Form of data | Photography |

4.6 Flow field visualization

| | |
|---|---|
| 4.6.1 Technique applied | Colour-schlieren, differential interferometry |
| 4.6.2 Plane with flow visualization | Region above airfoil, surroundings of transition or laminar separation bubble (See FIG. GE-10.9) |
| 4.6.3 Form of data | Photography |

4.7 Tunnel wall measurements

| | |
|---|---|
| 4.7.1 Type of measurements | Pressures |
| 4.7.2 Location and number of pressure holes | 48 (See FIG. GE-10.2) |

5 TEST MATRIX AND CONDITIONS

5.1 Detailed test matrix

| | |
|---|---|
| 5.1.1 Number of selected test cases | 34 |
| 5.1.2 Number of configurations tested | 1 |

5.1.3 Test matrix table

| Identification | Flow condition | | | Position | Other information | |
|---|---|---|---|---|---|---|
| Case No. | Ma | q[kPa] | Re[$10^6$] | $\alpha$[$^0$] | type of measurements | remarks |
| 1.01-1.05 | 0.18, 0.3(0.1)0.6 | 2.2-21.7 | 0.8-2.3 | 0 | a, c | 2 |
| 2.01-2.09 | 0.4 | 10.0 | 1.7 | -3(1)5 | a, b | 2 |
| 3.01-3.02 | 0.5 | 14.8 | 2.0 | 0 | a, b, c, d, e | 1, 2, 3 |
| 4.01-4.18 | 0.3, 0.5 | 5.9, 14.8 | 1.3, 2.0 | -3(1)5 | a, d, e | 2 |

**Legend:**
**Type of measurements: (a) pressures, (b) wake, (c) flow visualization, (d) multi-sensor hot-film, (e) liquid chrystals/oil**
**Remarks: (1) detailed visualization of separation bubble, (2) transition free, (3) transition fixed**
**Note: Due to wind tunnel facilities the Reynolds number depends on Mach number.**

| | |
|---|---|
| 5.2 Model/tunnel relations | |
| 5.2.1 Model span/tunnel width | 1.0 |
| 5.2.2 Tunnel cross section | 400 × 400 mm$^2$ |
| 5.2.3 Height/chord ratio | h/c = 2.0 |
| 5.2.4 Width/chord ratio | b/c = 2.0 |
| 5.2.5 Adiabatic wall temperatures | Not reached |
| 5.3 Transitional details | |
| 5.3.1 Transition | Free and fixed |
| 5.3.2 Details of free transition | |
| • Natural transition verification | Comparison of the results by different applicated measurement techniques and numerical flow simulation (See FIGS. GE-10.8/10). The locations of transition are detected by analysing the multi-sensor hot-film data by statistical methods. The location where the skewness of the voltage data is equal to zero corresponds nearly to the location of 50% intermittence (See GE-10.8.3). The hot-film sensors are located at 10.5(2.5)68.0 % c. (See FIG. GE-10.1) |
| • Verified test cases | All test cases with free transition |
| 5.3.3 Details of fixed transition | |
| • Transition location | 7.5 % c |
| • type and size of trip | Letraset, Letraline(TM) 119 1/16 × 650 flex 1.59mm |
| • Verification of effectiveness of trip | By disappearance of laminar separation bubble downstream of the trip |
| • Verified test cases | All test cases with fixed transition |
| 6 DATA | |
| 6.1 Availability of data | |
| 6.1.1 Organization owning the data | Aerodynamische Institut of the RWTH Aachen |
| 6.1.2 Responsible person for the data | Dipl.-Ing. P. Guntermann<br>Aerodynamisches Institut of the RWTH-Aachen<br>Wüllnerstr. zw. 5 u. 7<br>W-5100 Aachen, Germany<br>Tel.: 02 41 / 80 - 54 26<br>Fax.: 02 41 / 40 - 38 33<br>E-Mail: peter@aia004.aia.rwth-aachen.de |
| 6.1.3 Availability of data | Free |
| 6.2 Suitability of data for CFD validation | |
| 6.2.1 Suitability for "in-tunnel" calculation | Yes |
| 6.2.2 Corrected data to simulate "free-air" conditions | Yes |
| 6.3 Type and form in which data are available | |
| 6.3.1 Type and form | Stored in ASCII format on floppy disk |
| 6.3.2 Data carrier | Floppy disk |
| 6.3.3 Extent of geometry data | about 2 kBytes |
| 6.3.4 Extent of aerodynamic test data | about 120 MByte |
| 6.4 Corrections applied to data | |
| 6.4.1 Side wall interference corrections | Included in adaption process (For details see GE-10.3.4.3). The top and bottom walls are adapted with a geometry obtained from experiments with an empty test section and a geometry determined by a perturbation potential calculation coupled to a boundary layer calculation. The errors due to the remaining side wall interference are expected to be small. |

| | |
|---|---|
| 6.4.4 Sting and support corrections | Not necessary |

## 7 DATA ACCURACY AND REPEATABILITY ASSESSMENT

| | |
|---|---|
| 7.1 Estimate accuracy of | |
| 7.1.1 Free stream conditions | |
| • Mach number | about ±1 % (The accuracy is given by the applied Scanivalve system for velocity measurement) |
| • flow velocity | about ±1 % |
| • Model incidence | $\pm 0.1^0$ |
| 7.1.2 Measured data | |
| • Forces | The uncertainty in determining the lift coefficient is estimated to be less than ±0.5 %, of the drag coefficient less than ±2.5 %. |
| • Pressure coefficients | The uncertainty in measuring is less than ±0.5 %. |
| 7.1.3 Repeated measurement | |
| A. Type and number of repeat measurements within one test campaign | All types at least 2 times |
| B. Type and number of repeat measurements in successive campaigns | All types at least 3 times |
| 7.1.4 Redundant measurements | |
| A. Indicate flow quantities that have been measured independently by different techniques | Transition and laminar separation bubble locations |
| B. Checks made on internal consistency of the data | See GE-10.5.3.2 |
| 7.1.5 Other tests on same geometry | |
| A. Investigation of a different model (same geometry) in another wind tunnel | NASA-Langley (See GE-10.8.2) |

## 8 REFERENCES

| | |
|---|---|
| 8.1 On the wind tunnel | Romberg, H. J., "Experimentelle Untersuchung der schallnahen Umströmung eines superkritischen Tragflügelprofils unter besonderer Berücksichtigung von Windkanalinterferenzen", Dissertation, RWTH-Aachen, 1990. |
| 8.2 On the model | Somers D. M., "Design and Experimental Results for a Natural-Laminar-Flow Airfoil for General Aviation Applications", NASA TP 1861, Hampton, 1981. |
| 8.3 On applied measurement techniques | Kornberger, M., "Transitionsbestimmung mit Multisensor-Heißfilmtechnik im Windkanal und im Freiflug", Dissertation, RWTH Aachen, 1992. |
| 8.4 On wind tunnel, model and tests | Guntermann, P., "Entwicklung eines Profilmodells mit variabler Geometrie zur Untersuchung des Transitionsverhaltens in kompressibler Unterschallströmung", Dissertation, RWTH Aachen, 1992. |

## 9 LIST OF SYMBOLS

| | |
|---|---|
| $A_{MK}$ | Cross section area of the test section |
| b | Tunnel width |
| c | Chord length |
| $c_a$ | Lift coefficient |
| $c_p$ | Pressure coefficient |
| $c_w$ | Drag coefficient |

| | |
|---|---|
| h | Tunnel hight |
| Ma | Mach number |
| Re | Reynolds number |
| Tu | Turbulence level |
| q | Dynamic pressure |
| U', $\bar{U}$ | Sensor voltage (RMS, mean value) |
| x | Chordwise coordinate |
| $x_{Tr}$ | Chordwise transition location |

## 10 FIGURES

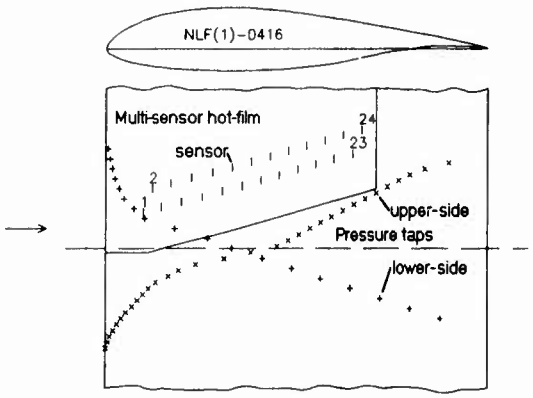



FIG. 1 Above: Cross-section of the NLF(1)-0416
Below: Part of the ground-plan of the model with the positions of the hot-film sensors and pressure taps (From GE-10.8.4)

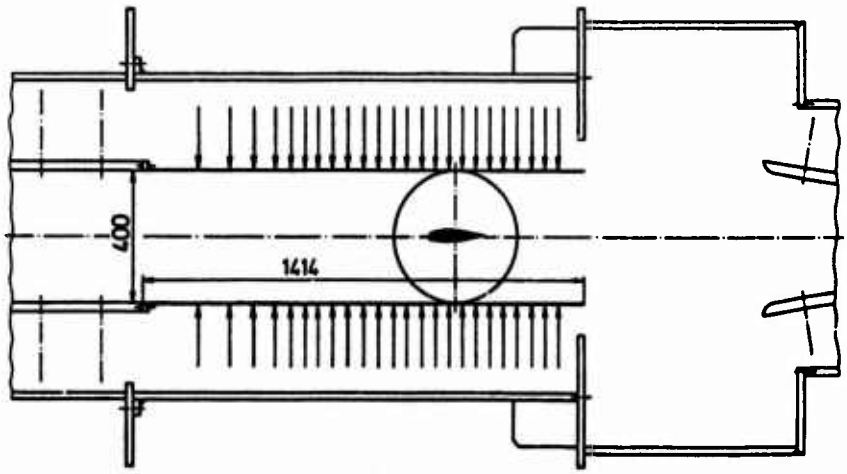



FIG. 2 Test section with adaptive top and bottom wall

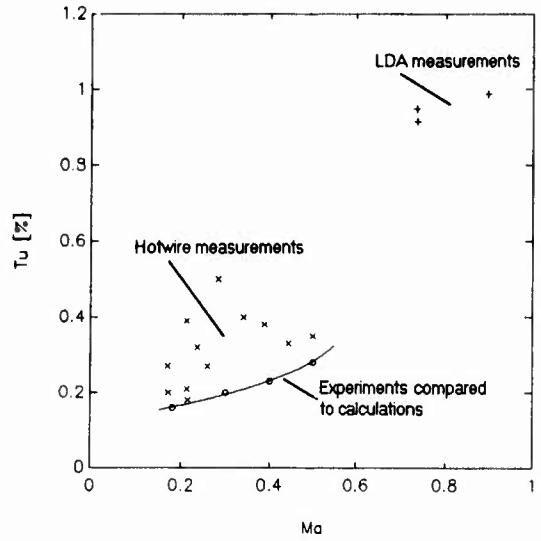



FIG. 3 Dependence of the turbulence level on Mach number. The hot-wire (×) and LDA (+) results are obtained by experiments with an empty test section. Amplification factors n at the transition location are determined by comparing experimentally obtained transition locations to locations resulting from boundary-layer calculations with an $e^n$ transition prediction. These amplification factors correspond to turbulence levels after Mack [1] and the results are visualized by the line (—) (From GE-10.8.4).

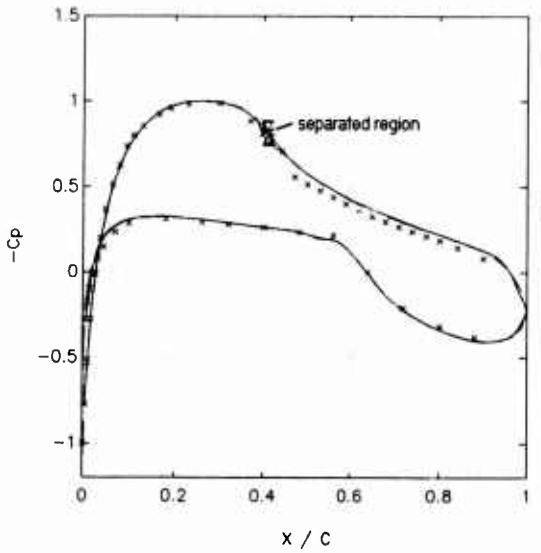



FIG. 4 Measured $c_p$-distribution (×) compared to Navier-Stokes (– · –) and potential-boundary layer (—) calculations (Case No. 3.01; Λ measured, ∇ calculated transition location, ≻≺ separated region; from GE-10.8.4)

[1] Mack, L. M., "Transition Prediction and Linear Stability Theory", AGARD CP No. 224, 1977.

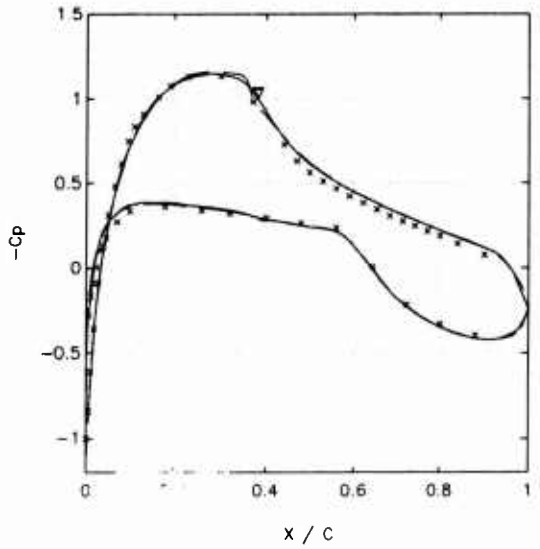



FIG. 5 Measured $c_p$-distribution (×) compared to Navier-Stokes (– · –) and potential-boundary layer (—) calculations (Case No. 1.05; ∇ calculated transition location; from GE-10.8.4)

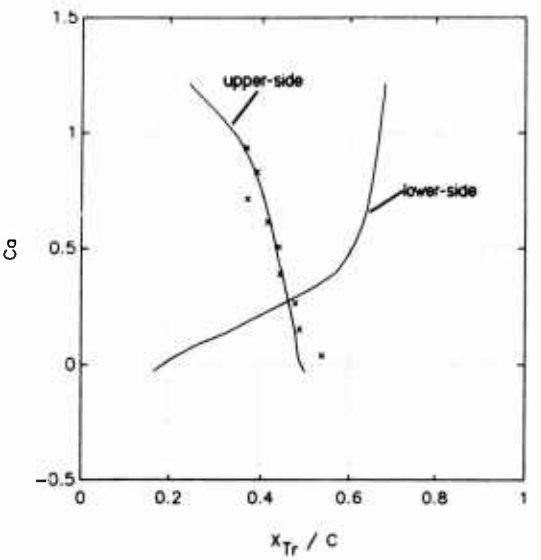



FIG. 6 Measured transition locations (×) compared to potential-boundary layer (—) calculations (Case No. 2; from GE-10.8.4)

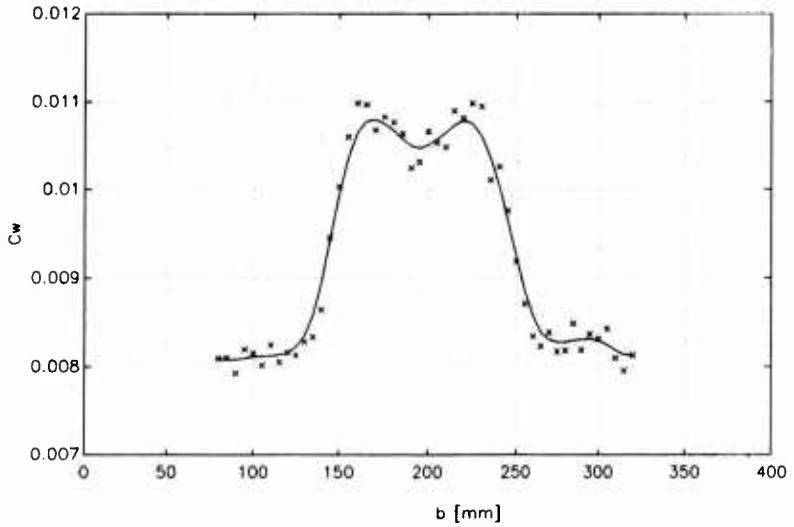



FIG. 7 Measured $c_w$ to spanwidth b distribution (×) (Case No. 3.01). The wake in the middle of the model is disturbed by pressure taps. (From GE-10.8.4)

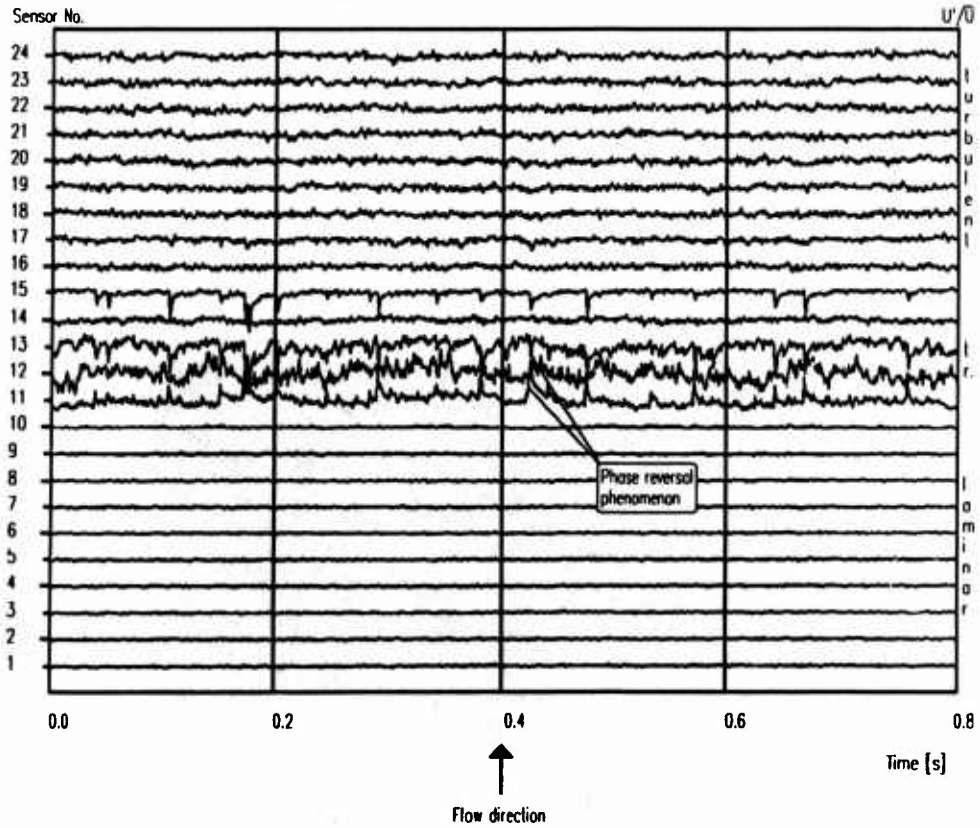



FIG. 8 Example of multi-sensor hot-film signals

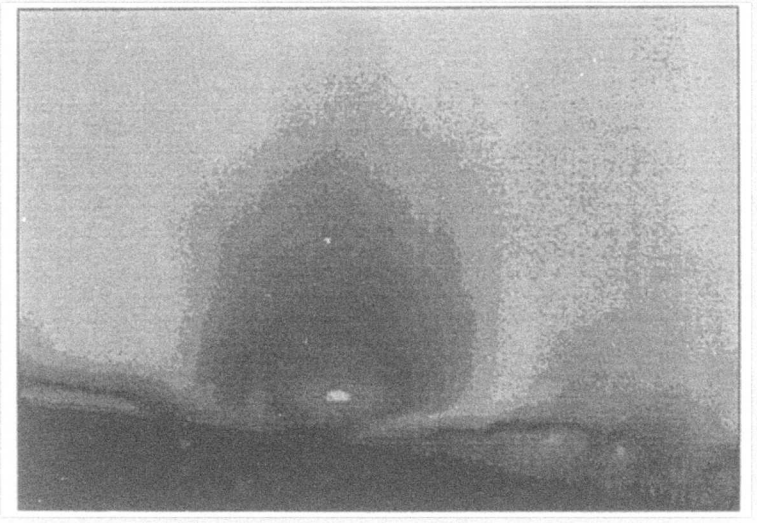


FIG. 9 Differential interferogram of a laminar separation bubble (Case No. 3.01, width of section about 15 mm; from GE-10.8.4)

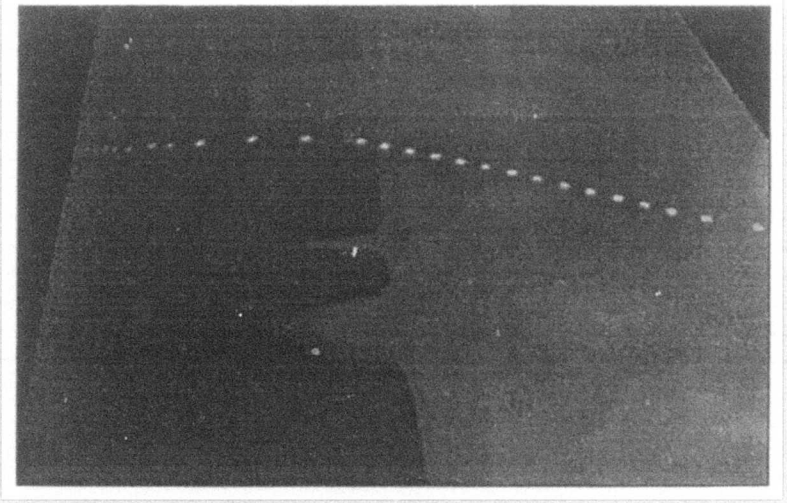


FIG. 10 Detection of the location of transition by liquid chrystals (Case No. 3.01; from GE-10.8.4)

# EXPERIMENTS IN THE TRAILING EDGE FLOW OF AN NLR 7702 AIRFOIL

BY

L.H.J. ABSIL AND D.M. PASSCHIER
LOW SPEED AERODYNAMICS LABORATORY
FACULTY OF AEROSPACE ENGINEERING
DELFT UNIVERSITY OF TECHNOLOGY
P.O. BOX 5058, 2600 GB DELFT
THE NETHERLANDS

## INTRODUCTION

Detailed mean flow and turbulence properties are presented of the flow in the vicinity of an airfoil trailing edge, to provide data for the development of turbulence models and the validation of computational methods.

## 1. GENERAL DESCRIPTION

| | |
|---|---|
| 1.1. Model | NLR 7702 airfoil |
| 1.2. Model type | 2-D airfoil |
| 1.3. Purpose of test | to provide reliable and detailed data of the complicated flow near the trailing edge of a modern airfoil |
| 1.4. Dominant flow physics | The upper surface boundary layer is near separation, while the lower surface boundary layer is developing in a negative pressure gradient. The two boundary layers merge into a highly asymmetric near wake (see fig. 1). |

1.5. The available data are limited to a region close to the trailing edge.
Recently a number of upstream boundary layer stations (from 50% chord on both sides) have been measured; these data will become available in the future.

## 2. DETAILS OF MODEL

2.1. General geometric arrangement (see fig. 2)
2-d airfoil model

2.3.2. Wing section NLR 7702 (see fig. 3)
. chord 600 mm
. thickness 14% chord
. angle of attack $4^{o}$
. 0.3 mm wire trip at 30% chord on lower surface

## 3. GENERAL TUNNEL INFORMATION

3.1. Tunnel Designation LST, Low Speed, Low Turbulence Tunnel

| | |
|---|---|
| 3.2. Organisation | Low Speed Aerodynamics Lab., Faculty of Aerospace Engineering, Delft University of Technology, the Netherlands. |
| 3.3. Tunnel Characteristics | Closed return type (see fig. 4). Maximum speed 120 m/s. |
| 3.4. Test Section | |
| 3.4.1. Set Up | see fig. 2 |
| 3.4.2. Dimensions | 1.80 x 1.25 x 2.60 m. |
| 3.5. Free stream conditions | |
| 3.5 1. Reference conditions | Total pressure measured in settling chamber. Static pressure measured halfway contraction. Calibration provides dynamic pressure in empty test section. Temperature measured in settling chamber. $U_{ref}$ is based on this dynamic pressure. |
| 3.6. Flow quality | Turbulence level at tunnel speed of 35 m/s (during present tests): 0.03%. |
| | During a run a slight temperature rise occurs. Tunnel speed is adjusted to keep Reynolds number constant at $1.47 \times 10^6$. |

4. INSTRUMENTATION

4.1. Model incidence is fixed at $\alpha = 4^o$.

4.2. Pressure measurements

4.2.1. Disposition of pressure hole, see table 1.

4.2.2. Overall pressure distributions measured with multitube liquid manometer (accuracy 1 to 2 Pa).
Detailed pressure distribution measured with 'Barocel' pressure transducer, (accuracy 0.1 Pa).

4.4. Boundary layer and wake measurements.

4.4.1. Measurement techniques

| | |
|---|---|
| . Preston tubes | Upper surface: 0.6, 0.9, 1.5, 2.0 mm. |
| . Lower surface | 0.5, 0.7, 1.1, 1.6 mm. |
| (. Pressure probes | In the wake static/total pressures were measured at an earlier stage, under slightly different conditions for the lower surface boundary layer trip). |

| | |
|---|---|
| . LDV (main body of measurements) | |
| . Laser | 5W |
| . Optics | 2 component dual-beam TSI modular optics, operated in $20^{o}$ off-axis forward scatter. Bragg cells present in both components. |
| . Three optical set-ups were used: | During the boundary layer traverses the optics were aligned such that the components measured were at about $\pm 45^{o}$ with respect to the surface. During the wake traverses components at $45^{o}$ to the tunnel axis were measured. |
| . Hot wire | Single and crosswire probes with DANTEC model C constant current anemometers were used at a few stations to provide additional information about LDV reliability. Probes were supported by a strut spanning the width of the tunnel. |
| 4.4.2. Flow regions investigated | Last 6% chord of upper and lower surface boundary layers, and first 6% of the wake. The measurement grid is shown in fig. 5. (Actually during measurements, the grid was refined at some position, if necessary). |

## 5. TEST MATRIX AND CONDITIONS

5.1. See table 2.

5.3. Transition details

| | |
|---|---|
| Upper surface | free transition with laminar separation bubble (see surface pressure distribution, fig. 6). |
| Lower surface | fixed transition (0.3 mm dia wire at 30% chord). |

## 6. DATA

6.1. Availability of data

| | |
|---|---|
| 6.1.1. Organization owning the data | Low Speed Aerodynamics Laboratory<br>Faculty of Aerospace Engineering<br>Delft University of Technology. |
| 6.1.2. Responsible for data | D.M. Passchier<br>Kluyverweg 1<br>2629 HS Delft<br>tel. 015-786386<br>fax: 015-783533 |

6.1.3. The data are freely available.

6.2.1. The data may be suitable for "in tunnel" calculation, although no information on tunnel wall boundary layers is available.

6.3.1. (see table 3). Data are available with
. all velocities non-dimensionalized with a (given) reference velocity (see 3.5.1).
. all pressures as pressure coefficients
. Preston tube measurements as $c_f$.

6.3.2. Data carrier — floppy disk (Lotus worksheet format, or ASCII format).

6.3.4. All averages of LDV data take an extent of several Mbytes. Arithmic averages are distributed in floppy disk.

6.4. Corrections applied to data.

6.4.6. Small corrections (order 0.2 mm) for wall distance are applied, based on wall law fitting of near wall data.

## 7. DATA ACCURACY AND REPEATABILITY ASSESSMENT

7.1. Accuracy

7.1.1. Free stream conditions — Reynolds number constant within 1% (nominal value $R_c = 1.47 \times 10^6$). $M_\infty = 0.1$.

7.1.2. Measured data

Typical overall accuracy — Mean velocity < 1%
Reynolds shear stress < 5%.

7.2. Repeat measurements

7.2.1. In different campaigns — see fig. 7.

7.2.2. In different compaigns — Overlap data of wake and boundary layer traverses, all different with optical set ups); fig. 8.

7.3. Redundant measurements

7.3.1. Additional hotwire measurement.

Typical example: fig. 9, 10.

7.3.2. Internal consistency (see also 7.2.2).

2-d checks:
- spanwise traverses, indicating no significant variations
- continuity check from measured data

example, fig. 11.
- complete Navier Stokes momentum check of measured data
example, fig. 12.

7.5. Examples of flow development — figs 13 to 20.

8. REFERENCES


. L.H.J. Absil
. D.M. Passchier
LDA Measurements in the highly asymmetric trailing edge flow of an NLR 7702 airfoil. In: Proceedings of the 5th international symposium on the application of laser Techniques to fluid mechanics, Lisbon 1990.

. L.H.J. Absil
. D.M. Passchier
LDA Measurements in the highly asymmetric trailing edge flow of an NLR 7702 airfoil. Delft University of Technology, Faculty of Aerospace Engineering, report LR 446, 1990. (Also published as National Aerospace Laboratory NLR TP 90353L, 1990).

. L.H.J. Absil
. D.M. Passchier
An Experimental Study of the Trailing Edge Flow of an NLR 7702 Airfoil, using LDA. In: Engineering Turbulence Modelling and Experiments 2. Proceedings of the second International Symposium on Engineering Turbulence Modelling and Measurements, Florence, 1993.
Ed. W. Rodi, F. Martinelli, Elsevier, 1993.

Table 1: Coordinates of pressure holes

| i | Upper side | | Lower side | |
|---|---|---|---|---|
| | x | y | x | y |
| 1 | .000 | -.080 | .000 | -.080 |
| 2 | .170 | .810 | .370 | -1.410 |
| 3 | .450 | 1.345 | .650 | -1.770 |
| 4 | .700 | 1.710 | .870 | -2.150 |
| 5 | .930 | 1.980 | 1.100 | -2.410 |
| 6 | 1.370 | 2.420 | 1.470 | -2.740 |
| 7 | 2.420 | 3.260 | 2.530 | -3.400 |
| 8 | 3.020 | 3.670 | 3.100 | -3.640 |
| 9 | 3.970 | 4.220 | 4.120 | -4.000 |
| 10 | 4.980 | 4.730 | 5.130 | -4.280 |
| 11 | 6.000 | 5.160 | 6.000 | -4.480 |
| 12 | 7.020 | 5.520 | 7.020 | -4.680 |
| 13 | 8.050 | 5.820 | 8.130 | -4.860 |
| 14 | 8.980 | 6.040 | 9.070 | -5.020 |
| 15 | 10.050 | 6.320 | 10.070 | -5.170 |
| 16 | 11.080 | 6.410 | 11.120 | -5.300 |
| 17 | 12.070 | 6.550 | 12.120 | -5.410 |
| 18 | 13.130 | 6.690 | 13.080 | -5.510 |
| 19 | 14.100 | 6.810 | 14.050 | -5.600 |
| 20 | 15.050 | 6.930 | 15.030 | -5.680 |
| 21 | 16.050 | 7.050 | 16.120 | -5.760 |
| 22 | 17.050 | 7.150 | 17.070 | -5.820 |
| 23 | 18.120 | 7.260 | 18.100 | -5.880 |
| 24 | 19.030 | 7.350 | 19.030 | -5.930 |
| 25 | 20.080 | 7.440 | 20.070 | -5.980 |
| 26 | 22.080 | 7.590 | 22.050 | -6.040 |
| 27 | 24.080 | 7.720 | 24.030 | -6.095 |
| 28 | 26.000 | 7.820 | 26.070 | -6.110 |
| 29 | 28.030 | 7.910 | 28.070 | -6.110 |
| 30 | 30.120 | 7.990 | 30.070 | -6.081 |
| 31 | 32.050 | 8.030 | 32.080 | -6.050 |
| 32 | 34.100 | 8.070 | 34.100 | -5.990 |
| 33 | 36.130 | 8.080 | 36.080 | -5.920 |
| 34 | 38.070 | 8.085 | 38.050 | -5.830 |
| 35 | 40.080 | 8.060 | 40.020 | -5.710 |
| 36 | 42.030 | 8.040 | 42.100 | -5.580 |
| 37 | 44.050 | 7.990 | 44.080 | -5.440 |
| 38 | 46.030 | 7.920 | 46.080 | -5.270 |
| 39 | 48.020 | 7.840 | 47.980 | -5.090 |
| 40 | 50.080 | 7.740 | 49.980 | -4.900 |
| 41 | 52.030 | 7.620 | 52.030 | -4.680 |
| 42 | 54.080 | 7.490 | 53.980 | -4.440 |
| 43 | 56.030 | 7.330 | 56.020 | -4.180 |
| 44 | 58.050 | 7.160 | 58.020 | -3.900 |
| 45 | 60.050 | 7.020 | 60.000 | -3.610 |
| 46 | 62.030 | 6.780 | 62.030 | -3.290 |
| 47 | 64.020 | 6.560 | 64.080 | -2.950 |
| 48 | 65.980 | 6.330 | 66.020 | -2.600 |
| 49 | 68.050 | 6.080 | 68.000 | -2.230 |
| 50 | 70.070 | 5.810 | 69.970 | -1.860 |
| 51 | 72.030 | 5.550 | 71.950 | -1.490 |
| 52 | 74.150 | 5.250 | 74.030 | -1.110 |
| 53 | 76.000 | 4.990 | 76.000 | -.790 |
| 54 | 78.020 | 4.700 | 78.030 | -.510 |
| 55 | 80.080 | 4.190 | 79.950 | -.280 |
| 56 | 81.050 | 4.190 | 81.030 | -.180 |
| 57 | 82.120 | 4.040 | 81.620 | -.130 |
| 58 | 83.030 | 3.890 | 83.020 | -.020 |
| 59 | 84.050 | 3.690 | 84.000 | .030 |
| 60 | 85.070 | 3.510 | 85.070 | .080 |
| 61 | 86.150 | 3.310 | 85.970 | .110 |
| 62 | 87.120 | 2.930 | 87.150 | .126 |
| 63 | 88.080 | 2.930 | 87.930 | .135 |
| 64 | 89.100 | 2.710 | 88.980 | .144 |
| 65 | 90.080 | 2.510 | 90.020 | .138 |
| 66 | 91.070 | 2.280 | 91.200 | .120 |
| 67 | 92.150 | 2.040 | 92.070 | .110 |
| 68 | 93.150 | 1.800 | 92.070 | .090 |
| 69 | 94.130 | 1.560 | 93.800 | .070 |
| 70 | 95.000 | 1.340 | 94.980 | .050 |
| 71 | 96.020 | 1.080 | 95.900 | .030 |
| 72 | 96.930 | .850 | 96.950 | .000 |
| 73 | 97.620 | .670 | 97.920 | -.020 |
| 74 | 98.430 | .470 | 98.820 | -.050 |
| 75 | 99.300 | .260 | 99.550 | -.070 |

Table 2: Test Matrix

| position (s/c %) | LDA | HW cross | HW single | Preston |
|---|---|---|---|---|
| | | Upper surface boundary layer | | |
| 94.72 | x | x | | x |
| 95.79 | x | x | | x |
| 97.48 | x | x | | x |
| 98.40 | x | x | | x |
| 98.72 | x | x | | x |
| 99.04 | x | x | | x |
| 99.39 | x | x | | x |
| 99.68 | x | x | | x |
| 100.00 | x | x | | x |
| | | Lower surface | | |
| 93.78 | x | | x | x |
| 95.58 | x | | | x |
| 97.91 | x | | | x |
| 98.50 | x | | | x |
| 99.00 | x | | | x |
| 99.55 | x | | | x |
| 100.00 | x | | x | x |
| | | Wake | | |
| 100.00 | x | | | |
| 100.25 | x | | | |
| 100.50 | x | x | | |
| 101.0 | x | | | |
| 101.5 | x | | | |
| 102 | x | | | |
| 104 | x | | | |
| 106 | x | | | |

Table 3: LDV data available for all station

- U, V, $u^2$, $v^2$, uv, $uv^2$, $u^2v$, $v^3$, $u^3$, $S_u$, $S_v$, $K_u$, $K_v$

(Skewness and Kurtosis are defined as

$$S_u = \frac{\overline{u^3}}{(\overline{u^2})^{3/2}}$$

$$K_u = \frac{\overline{u^4}}{(\overline{u^2})^2}$$

all non-dimensionalized with $U_{ref}$

available: arithmetic averages - on floppy disk
( : weighted averages - with total velocity
- with interarrival time (not included on floppy disk)

- integral parameters ($\delta^*$, $\theta$)
- eddy viscosities

All raw data are still available; on request other statistics may be obtained. (e.g. velocity histograms (probability density functions)).

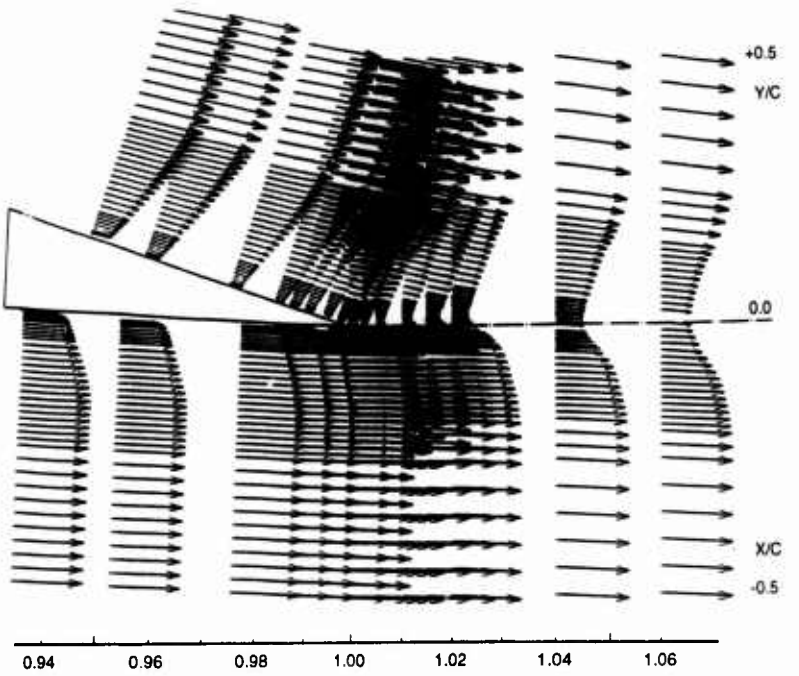



Fig. 1 Overview of flow; Mean Velocity vectors

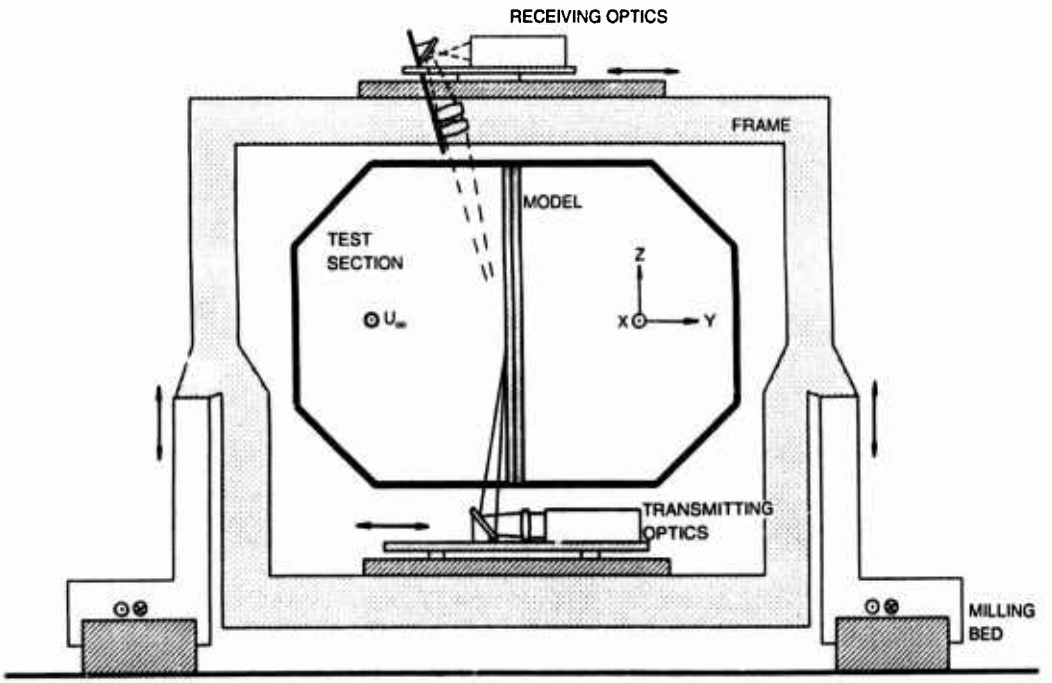



Fig. 2 Test set up

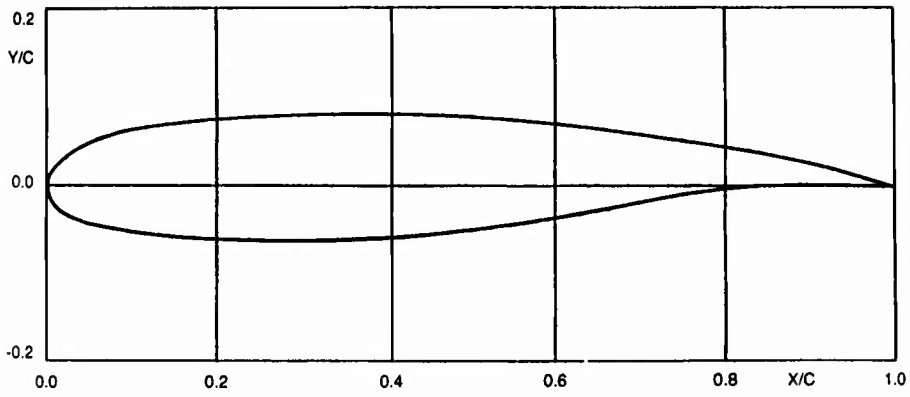



Fig. 3 The NLR 7702 airfoil

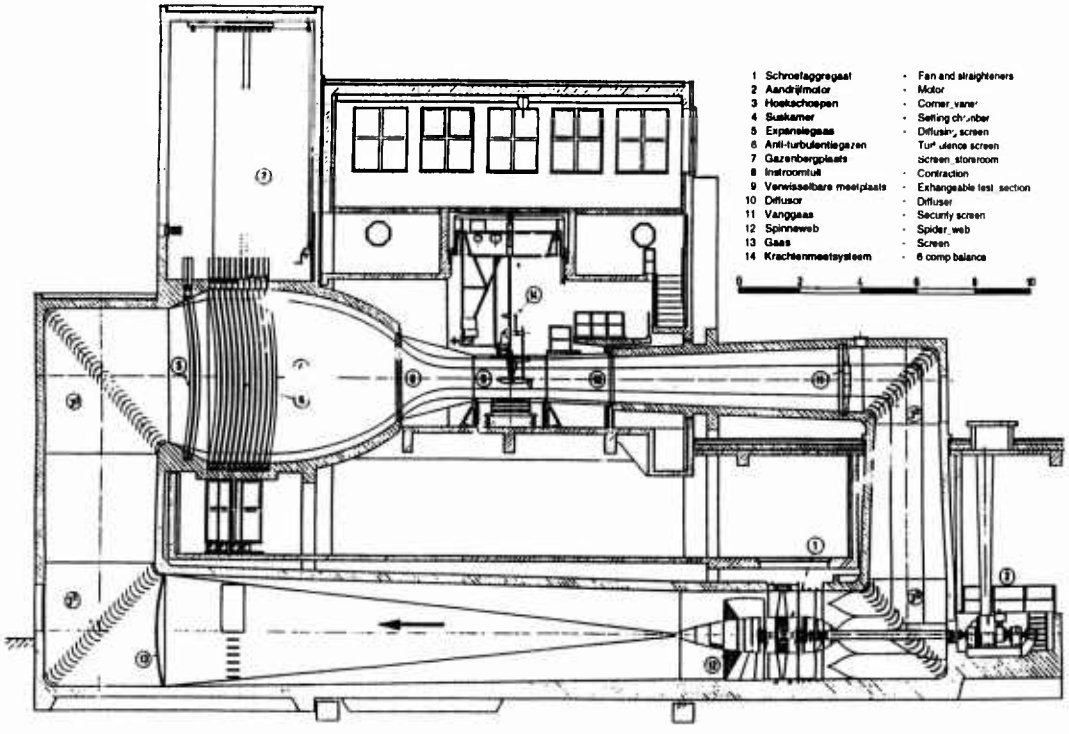



Fig. 4 The Low Speed Wind Tunnel

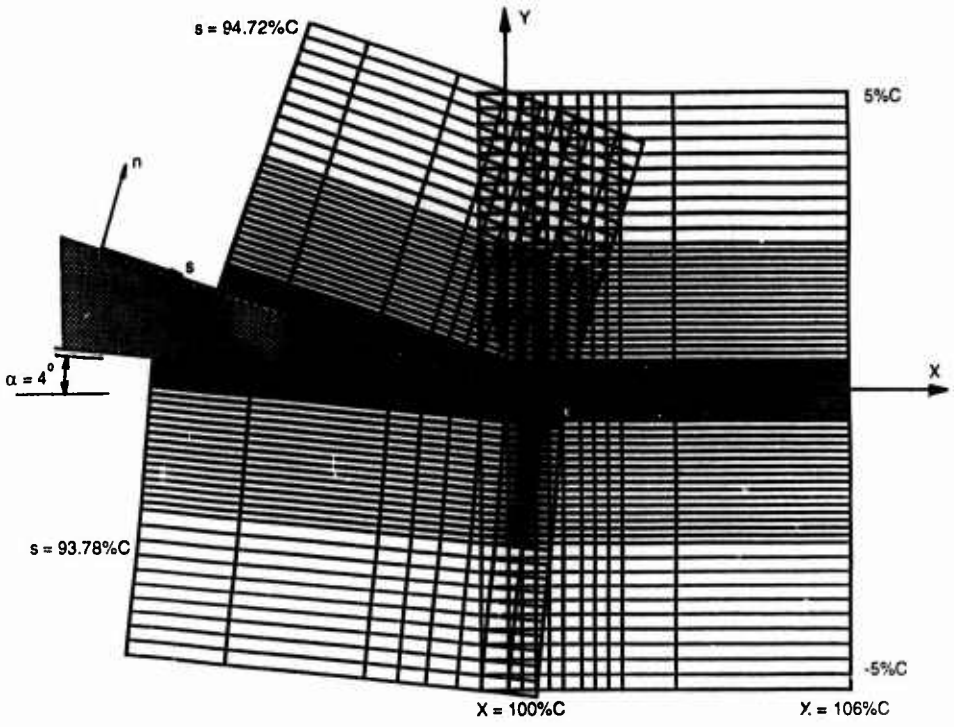



Fig. 5 The measurement grid

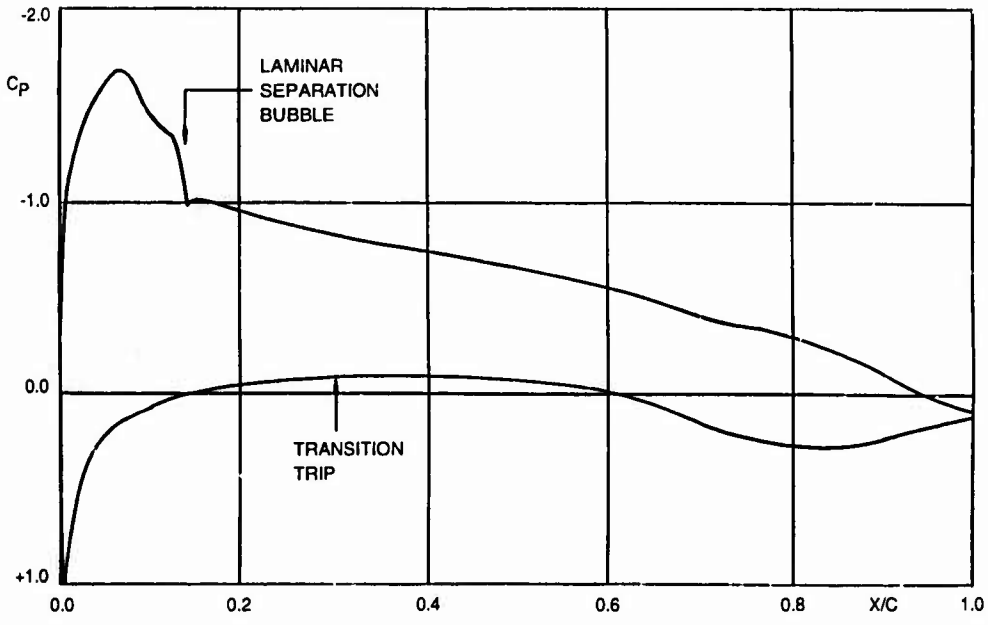



Fig. 6 Pressure distribution NLR 7702
$\alpha = 4^{\circ}$

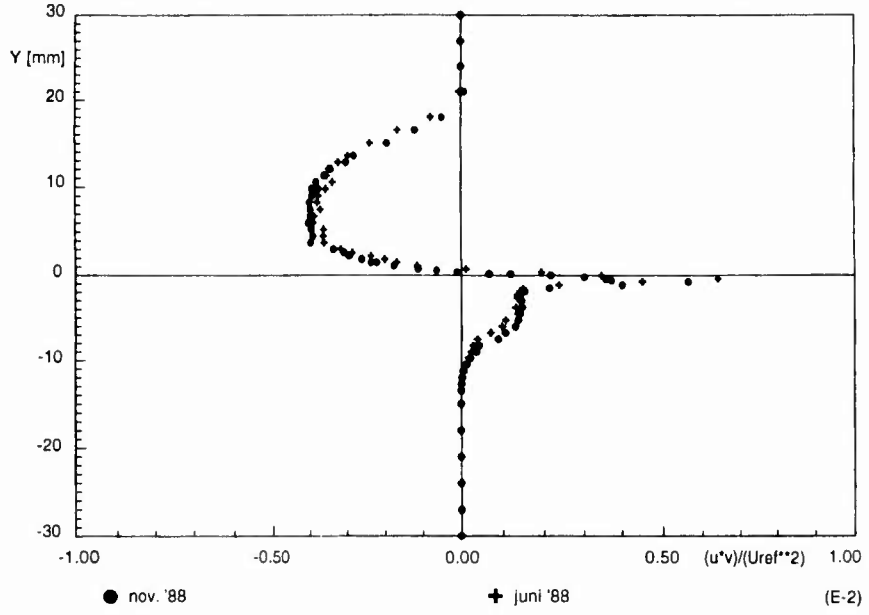



Fig. 7 Reproduction; turbulent shear stress

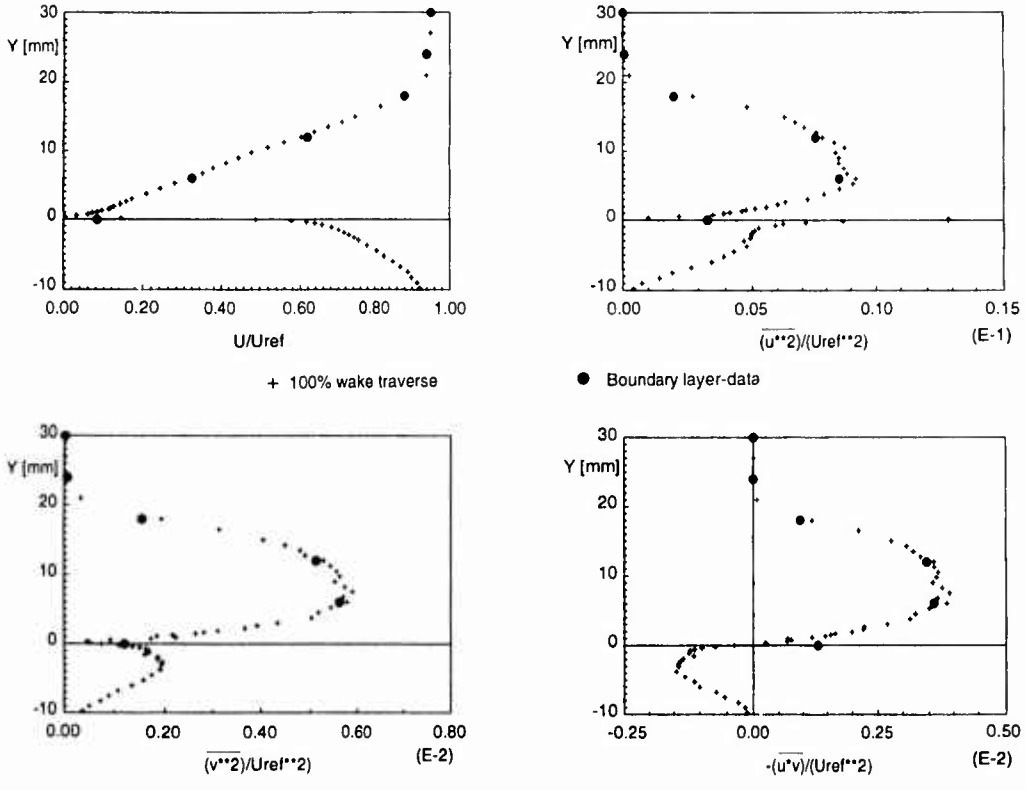



Fig. 8 Comparison of wake- and boundary layer data at overlap stations

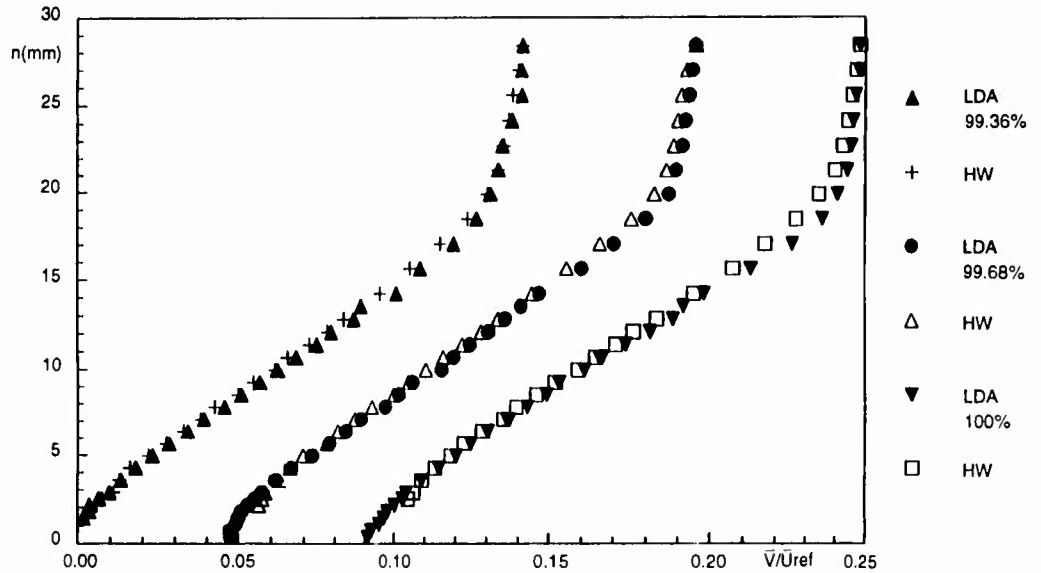



Fig. 9 Comparison of cross hotwire and LDA data: mean velocity $\bar{V}$

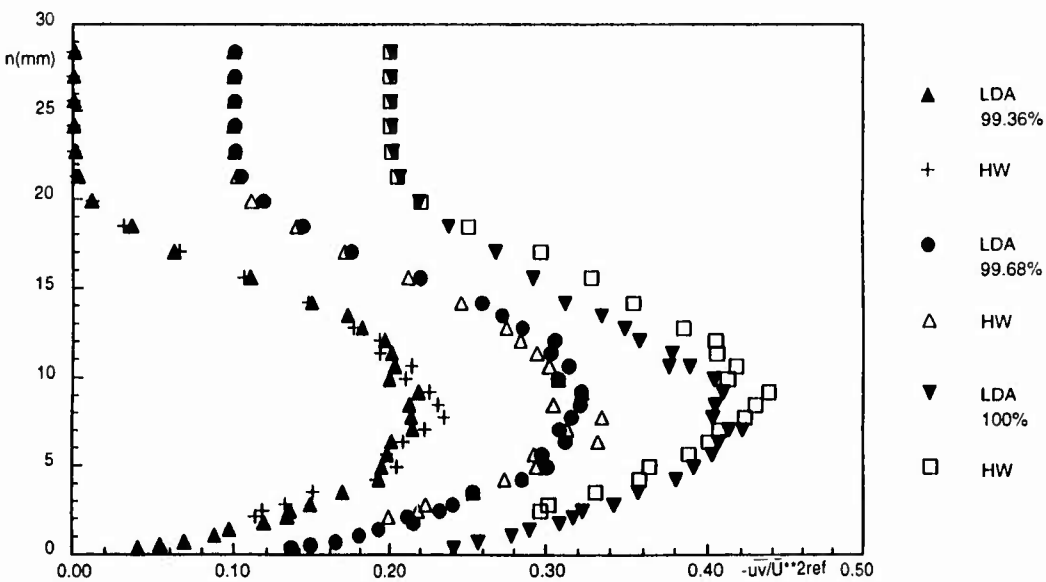



Fig. 10 Comparison of cross hotwire and LDA data: Reynold shear stress

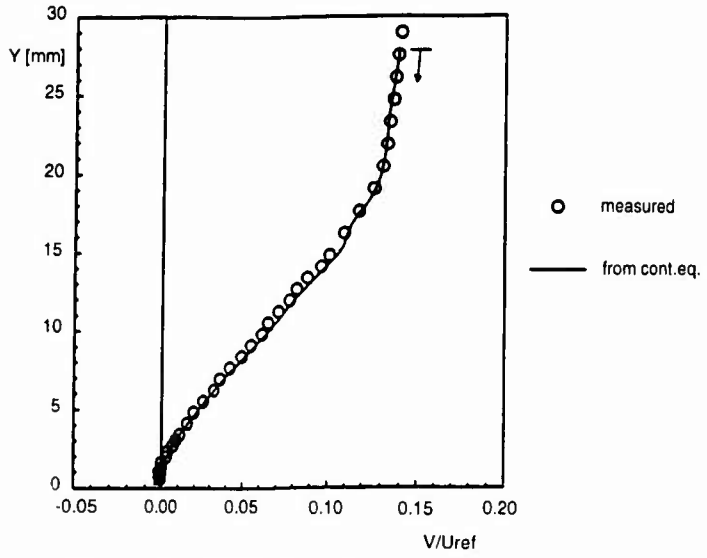



Fig. 11 Continuity check upper surface, X/C = 98.4%

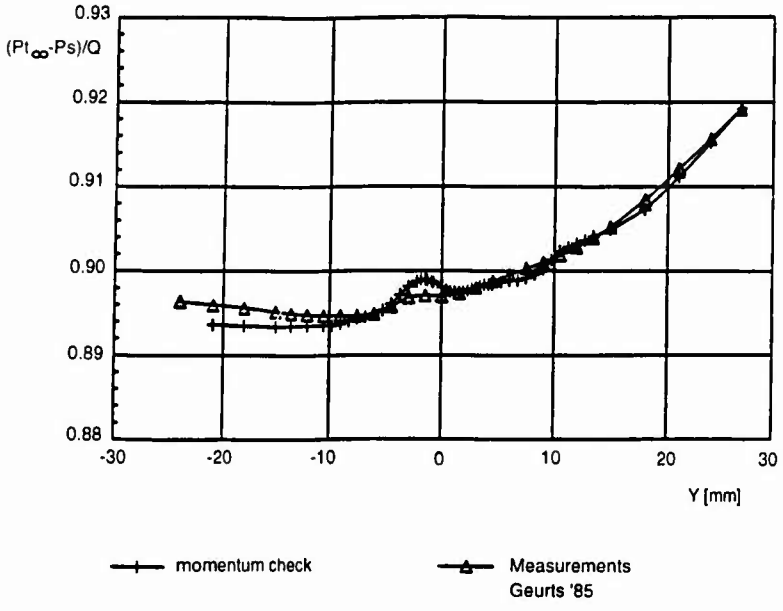



Fig. 12 Momentum check wake X/C = 104%

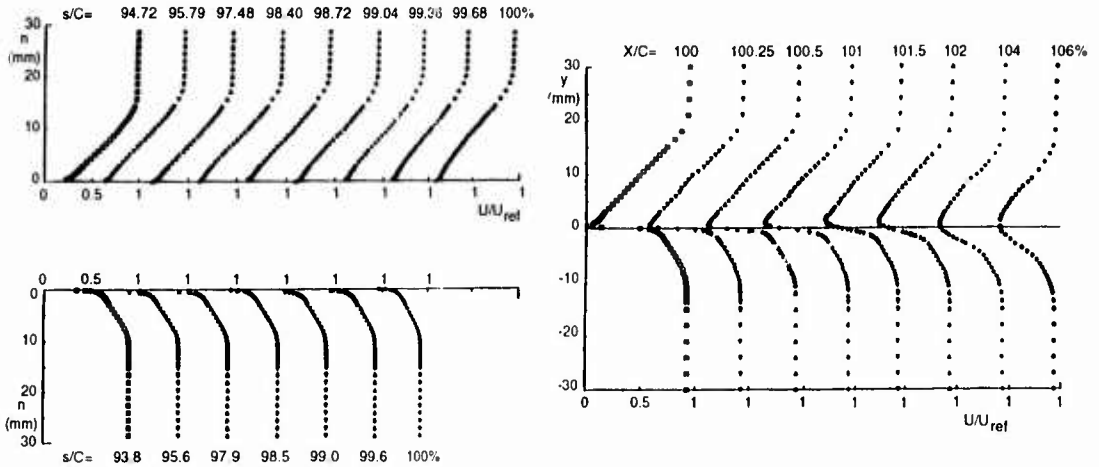



Fig. 13 Distribution of streamwise mean velocity: upper left, upper-surface boundary layer; lower left, lower-surface boundary layer; right, wake

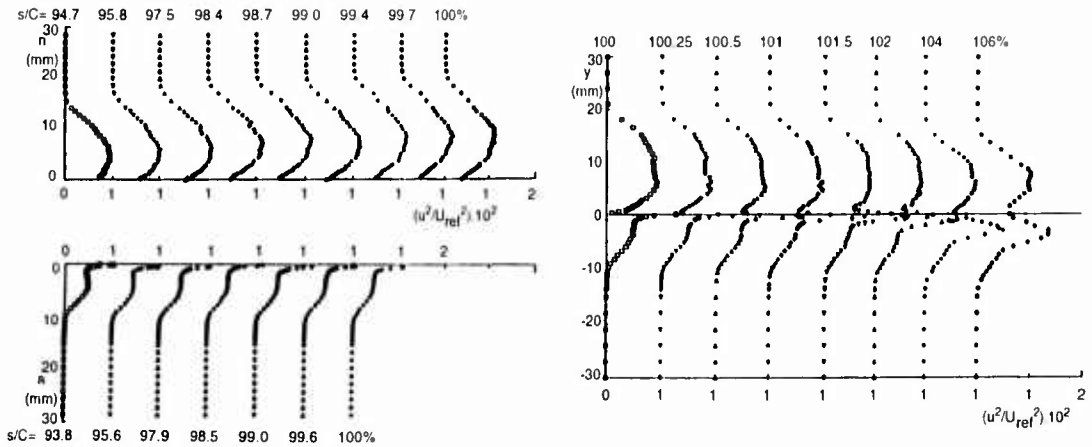



Fig. 14 Distribution of Reynolds normal stress $\overline{u^2}$

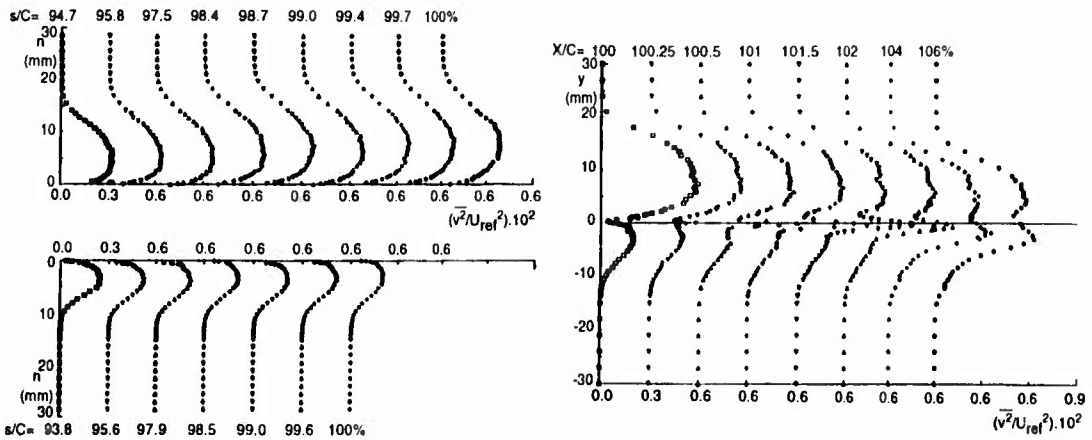



Fig. 15 Distribution of Reynolds normal stress $\overline{v^2}$

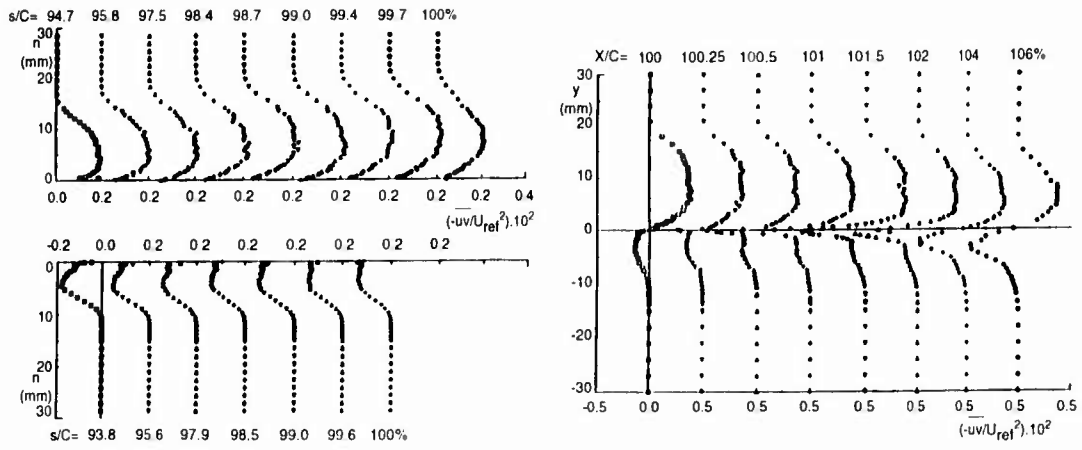



Fig. 16 Distribution of Reynolds normal stress $-\overline{uv}$

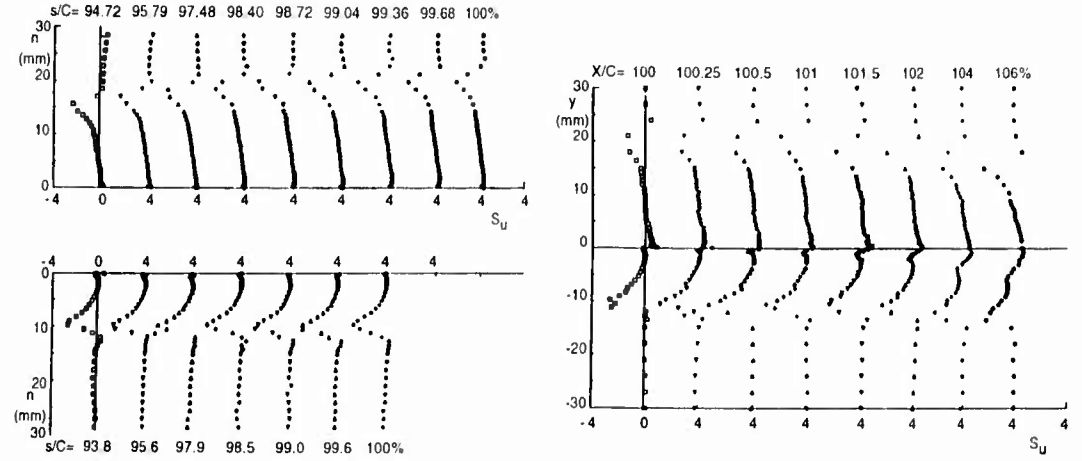



Fig. 17 Distribution of Skewness factors $S_u$

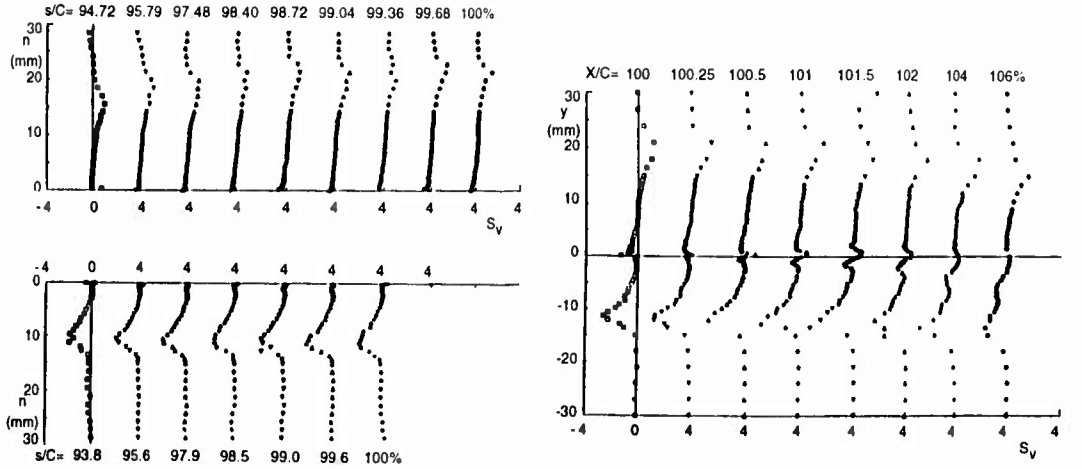



Fig. 18 Distribution of Skewness factors $S_v$

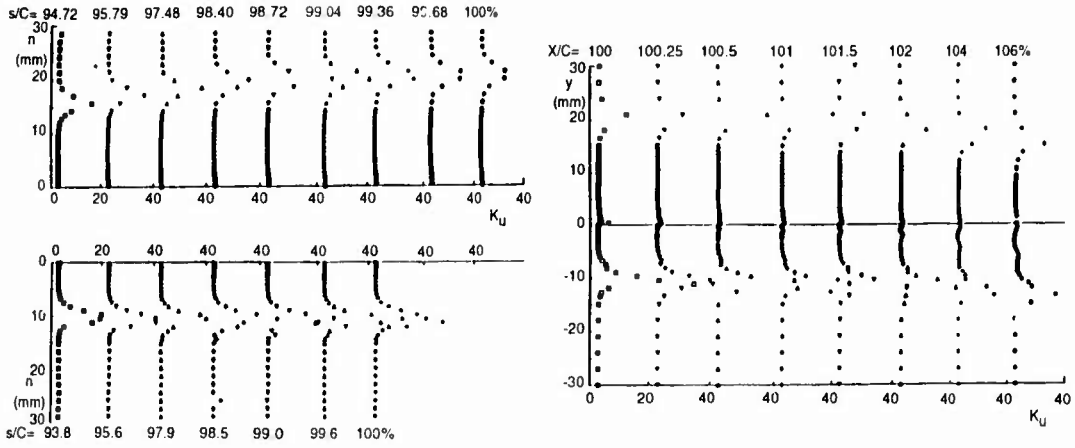



Fig. 19 Distribution of Kurtosis factors $K_u$

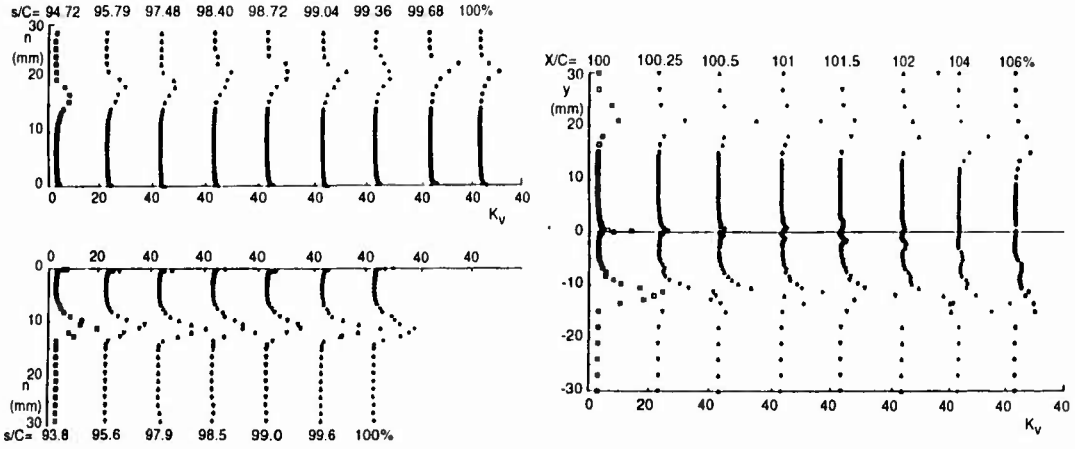



Fig. 20 Distribution of Kurtosis factors $K_v$

# TWO-DIMENSIONAL 16.5% THICK SUPERCRITICAL AIRFOIL NLR 7301

S.O.T.H. HAN
NATIONAL AEROSPACE LABORATORY NLR
ANTHONY FOKKERWEG 2
1059 CM AMSTERDAM
THE NETHERLANDS

## 0. INTRODUCTION

This thick supercritical airfoil designed for a lift-coefficient of 0.595 at a Mach number of 0.721 (potential flow conditions) was an early NLR design of a supercritical airfoil made in 1973. The airfoil was designed with the hodograph method and has a rather blunt nose with a roof-top type pressure distribution. A typical other feature of this airfoil is that it is highly rear loaded, both on the upper surface and on the lower surface. Because of this rear loading, the airfoil is close to trailing edge separation on the upper surface and separation in the cove region around 70% chord at the lower surface. Tests have been made originally in the NLR (Transonic) Pilot Tunnel at a Reynolds number of 2.2 million (the design condition). The results of these tests have been included in AGARDograph AR-138. At about the same time test were made in the Compressible Flow Facility (CFF) of Lockheed (Georgia, USA) for the Reynolds number of 10, 20 and 30 million.

In the eighties, when more advanced computer codes became available that could cope with airfoils that experienced a limited extent of separation, there was an urgent need for reliable data to validate the computer codes for these conditions. Also, the problem of scaling (low Reynolds number) wind tunnel tests to (the much higher) flight Reynolds numbers raised (again) considerably interest. For both reasons it was decided to repeat the original NLR 7301 experiments on a larger two-dimensional model in the large transonic windtunnel HST of NLR. The tests covered the low speed and transonic speed regimes whereas part of the measurements was performed at constant lift for a range of Reynolds numbers to study the indirect Reynolds number effects in more detail.

## 1. GENERAL DESCRIPTION

### 1.1 Model name or designation

Airfoil NLR 7301

### 1.2 Model type and flow conditions

Two-Dimensional Airfoil; sub- and transonic flow conditions

### 1.3 Design requirements

Supercritical shock-free flow at Mach=0.721 and $C_L$=0.595 (potential flow!)

### 1.4 Dominant flow physics

a) Reynolds number effects on pressure distributions, drag (including drag creep) and maximum lift;
b) upper surface trailing edge separation and (close to) lower surface separation in the cove region;
See e.g. fig. 1 to 5.

### 1.5 Additional remarks

Test case designed to study Reynolds number effects at constant lift

## 2 DETAILS OF MODEL

### 2.1 General geometric arrangement

.5 m chord, 2 m span; see fig.6

### 2.2 Aspect ratio

4

### 2.3 Basic wing section

See fig.7

### 2.4 Thickness to chord ratio

0.165

### 2.5 Geometric definition of components

- how is shape defined
  numerically
- design or measured coordinates
  designed
- tolerances
  0.01% of chord over first 20% of chord
  0.10 mm over the remaining part
  slope tolerance 1:300
- surface roughness
  < 0.4 $\mu$m(rma)

### 2.6 Model support details

The model spanned the windtunnel, mounted in two co-rotating windows in the tunnel side walls; to prevent excessive bending of the model two additional thin and streamline shaped support struts were

attached to the lower surface at 20% and 80% span (see fig.8)
It is believed that these struts are located sufficiently far away to not efffect the flow over the airfoil at the pressure section; moreover the lower side of the airfoil is subsonic at nearly all flow conditions.

## 3. GENERAL TUNNEL INFORMATION

### 3.1 Tunnel designation
High Speed Wind Tunnel HST

### 3.2 Organisation running the tunnel
National Aerospace Laboratory NLR,
Amsterdam, The Netherlands

### 3.3 Tunnel characteristics
closed circuit; see fig. 9 for operating conditions

### 3.4 Test section

#### 3.4.1 Model mounting and instrumentation
see fig.6

#### 3.4.2 Test section dimensions
2.00x1.60x2.70 (widthxheightxlength)

#### 3.4.3 Wall geometry
- slotted top and bottom walls; closed side walls
- open area ratio 12% per wall
- top and bottom wall pressures measured on slat at tunnel center line (see fig.10)
- no boundary layer control on side walls; typical side wall boundary layer displacement thickness ≈ 7 mm

### 3.5 Freestream conditions

#### 3.5.1 Reference flow conditions
- total pressure: settling chamber
- static pressure: upstream pressure hole (No.18;fig. 10) [Note that this provides the reference pressure during the tests; subsequently a wall correction procedure is applied based on measured wall pressures; see 6.4]
- static temperature: from total temperature in settling chamber and (tunnel wall corrected) Mach number

#### 3.5.2 Tunnel calibration
- "long static tube" at tunnel centre line and side wall pressures;
- last "long static tube" calibration:1980; regular checks on possible changes from side wall pressures

### 3.6 Flow quality (empty tunnel)

#### 3.6.1 Flow uniformity
- Mach number variation over model chord: < .002 (at Mach=.75)
- Mach number variation during a run: < ± .001
- tunnel flow assumed to be parallel with tunnel centre line; estimated uncertainty in incidence +.1 to .2° (an average value of ≈.15° is found from model upright and inverted tests with 3-D models)
- variation of flow angularity over model span: not measured; estimated to be less then .2 °

#### 3.6.2 Temperature variation
- temperature can be controlled during a run;
- variation during a run less then 1° to 3° depending on Mach and Reynolds number

#### 3.6.3 Flow unsteadiness
- turbulence level not measured but assumed to be very low in view of the high contraction ratio (1:25);
- overall noise level:

$$.5\% < C_p\text{-RMS} < 1\%$$

## 4 INSTRUMENTATION

### 4.1 Model position
- model incidence calculated from rotational position of port supporting window applying a correction for model deformation (torsion and bending) under aerodynamic load as derived from Q-flex inclinometer readings in centre section (see fig. 6);
- accuracy: ± .02° (excluding mean flow direction; see 3.6.1)

#### 4.2.1 Number and disposition of pressure holes
- 67 steady pressure holes (fig. 7)

#### 4.2.2 Range and accuracy of pressure transducers
- near the nose: 25 psi range
- others: 8 psi range
- accuracy: ± .2% Full Scale

### 4.3 Boundary layer and flow field measurements
- hot films (see fig. 6) only used for transition detection during free transition tests
- wake rake measurements (see fig.8 and fig.11 for details)

### 4.4 Surface flow visu
Acenaphtene to optimize transition strips

### 4.5 Tunnel wall measurements
upper and lower wall 25 pressures each on slat at tunnel centre line; see fig.10

## 5. TEST MATRIX AND CONDITIONS

### 5.1 Detailed test matrix
see TABLE I to III

**5.2 Model/tunnel relations**
- maximum blockage: 5.2 %
- wing area: 1 $m^2$
- tunnel cross section: 3.2 $m^2$
- height/chord ratio: 3.2
- width/chord ratio: 4.0
- adiabatic wall temperatures reached

**5.3 Transition details**

**5.3.1 Free or fixed transition**
low speed: free transition
high speed: fixed transition

**5.3.2 Details of free transition**
- natural transition measured with hot films; test results available as RMS-values (mV)/dynamic pressure

**5.3.3 Details of fixed transition**
- see fig.12
- trip verification with acenaphtene

**6. DATA**

**6.1 Availability of data**

**6.1.1 Organisation owing data**
NLR/NIVR

**6.1.2 Who is responsible for the data**
- P.B. Rohne
- tel (020) 5113360
- fax (020) 5113210

**6.1.3 Are data freely available**
Yes

**6.2 Suitability of data for CFD validation**
- data are corrected to "free-air" conditions

**6.3 Type and form in which data are available**

**6.3.1 Type and form**
tables

**6.3.2 Data carrier**
floppy disk (340 Kbyte)

**6.4 Corrections applied to data**

**6.4.1 Lift interference and blockage corrections**
- data are considered globally correctable;
- a one component (Schwarz-type) measured boundary condition method was applied using a model representation with higher order point singularities including a transonic doublet; see ref.7
- the in- and outflow planes were determined by interpolation between top and bottom wall pressures

**6.4.2 Corrections and order of magnitude**
- Mach ($p_{static}$,q,$c_l$,$c_d$,$c_m$):
  $\Delta Ma/Ma < .01$
- $\alpha$ : $-2 < \Delta\alpha/c_l < 0$

**6.4.3 Side wall interference corrections**
not significant in view of the high aspect ratio (4!)

**7. DATA ACCURACY AND REPEATABILITY ASSESSMENT**

**7.1 Accuracy estimates**

**7.1.1 Free stream conditions**
$\Delta$ Mach < .002
$\Delta\alpha < .2$ °

**7.1.2 Measured data**
$\Delta c_l < \pm .0035$
$\Delta c_d < \pm .0005$ from wake measurements (absolute level; trends will be better then $\pm$ .0002)
$\Delta c_m < \pm .0080$
$\Delta c_p < \pm .005$ or $\pm .01$ in LE pressure peaks

**7.2 Repeat measurements**
not reported

**7.3 Redundant measurements**
- pressure taps (even/uneven) have been connected to different pressure transducers in an alternating way (applies for model surface pressures, wall pressures and wake rake pressures)

**7.4 Other tests made**
The following test have been made on the same geometry but at different scale:
- on a .18 m chord model in the NLR Pilot Tunnel and the Lockheed Compressible Flow Facility (CFF)
- on a .57 m model in the low speed windtunnel LST

Typical comparisons are presented in ref.5 and 6; see also fig.13 to 16

Comments on the comparisons shown in the figures 13 to 16
- the low speed comparison (fig. 13, 14) is fair apart from significant differences near maximum lift, notably at the higher Mach numbers; this is believed to be due to tunnel side wall effects (that will effect the flow particularly at separated flow conditions) and tunnel wall interference (the LST results are corrected in a classical way)
- the high speed results show a fair agreement at Mach = .6, except close to maximum lift (fig. 15b); at Mach = .675 the agreement in pressure distribution is reasonable in view of the apparent differences in lift; at Mach = .75 differences appear to be much more pronounced but they can partly be understood from differences in test conditions: the shock moves rapidly downstream

with increasing incidence (fig. 16c) whereas separated flow (fig. 16d) is considered to be especially sensitive, also for side wall effects. In view of the observed differences and sensitivities it is suggested to make comparisons with CFD at constant lift.

## 8. REFERENCES


1. User's guide to the 1.60x2.0 $m^2$ High Speed Wind Tunnel HST of the National Aerospace laboratory NLR
2. Boerstoel, J.W., "Design of shock-free basic aerofoils for a van Egmond, J.A. supercritical wing" (aerofoils NLR HT 730810, HT 7310815, HT 7310818), NLR TR 75077 C
3. AGARDograph AR 138
4. Rohne, P.B. and Stalpers, J.M.V. "Data report of an investigation on 2-D model 7301 in the high speed wind tunnel HST, NLR TR 87001L
5. Han, S.O.T.H., "The low speed maximum lift coefficient of airfoil 7301; a selection of HST results", Memorandum AC-86-014L
6. Han, S.O.T.H., Analysis of the high speed HST test results of airfoil 7301, NLR TR 87168 C
7. Smith, J., "Measured boundary condition methods for 2D flow", NLR MP 82022U.


| MEASUREMENTS | DPN's | Mach | $C_L$ | $Re_c*10^{-6}$ | TRANSITION | REMARKS |
|---|---|---|---|---|---|---|
| Low speed $\alpha$ runs | 1293 - 1352 | 0.12 | $1 \leq C_L \leq C_{Lmax}$ | 4.50 | Natural | |
| | 1458 - 1475 | 0.20 | | 2.85 | | |
| | 1375 - 1395 | | | 4.50 | | |
| | 1355 - 1374 | | | 6.00 | | |
| | 1396 - 1417 | 0.30 | $-0.1 \leq C_L \leq C_{Lmax}$ | 4.50 | | |

Table I Test matrix of main program

| MEASUREMENTS | DPN's | Mach | $C_L$ | ALPHA | $Re_c*10^{-6}$ | TRANSITION | REMARKS |
|---|---|---|---|---|---|---|---|
| High speed α runs | 4180 - 4183, 4252, 4184 - 4186, 4254, 4187 - 4192 | 0.60 | 0.0133 - 0.9060, | -1.47 - 5.78 | 3.60 | Carborundum 80 at 7% on u.s. and l.s. | |
| | 4208 - 4210, 4237 , 4238, 4212 , 4222, 4214 , 4215 | 0.745 | -0.0361 - 0.5999, | -1.39 - 2,97 | | | |
| | 4026 , 4027, 4087 , 4029, 4088 , 4030, 4089 , 4032 - 4038 | 0.60 | 0.0462 - 0.9693, | -1.62 - 6.26 | 12.50 | Carborundum 220 at 7% on u.s. and l.s. | |
| | 4053 , 4054, 4104 , 4056, 4106 , 4057, 4058 | 0.745 | 0.0208 - 0.6783 | -1.60 - 1.72 | | | |

Table II High speed test cases for code evaluation ($\alpha$ variable)

| MEASUREMENTS | DPN's | Mach | $C_L$ | ALPHA | $Re_c*10^{-6}$ | TRANSITION | REMARKS |
|---|---|---|---|---|---|---|---|
| High speed α runs | 4252 , 4249, 4246 , 4242, 4239 , 4237, 4235 , 4234 | 0.5985 - 0.773 | ≈ 0.30 | 0.60 , 0.68, 0.71 , 0.70, 0.70 , 0.69, 0.67 , 0.93 | 3.60 | Carborundum 80 at 7% on u.s. and l.s. | |
| | 4185 , 4199, 4247 , 4243, 4240 , 4238, 4236 | 0.6001 - 0.754 | ≈ 0.46 | 1.71 , 1.69, 1.54 , 1.45, 1.35 , 1.28, 1.34 | | | |
| | 4087 , 4090, 4096 , 4097, 4101 , 4104, 4080 , 4074 | 0.5984 - 0.773 | ≈ 0.30 | 0.06 , -0.01, 0.03 , -0.02, -0.06 , -0.15, -0.20 , -0.20 | 12.50 | Carborundum 220 at 7% on u.s. and l.s. | |
| | 4088 , 4091, 4094 , 4100, 4102 , 4056, 4108 | 0.5993 - 0.753 | ≈ 0.45 | 1.11 , 0.94, 0.90 , 0.69, 0.62 , 0.54, 0.49 | | | |

Table III High speed test cases for code validation (Mach variable)

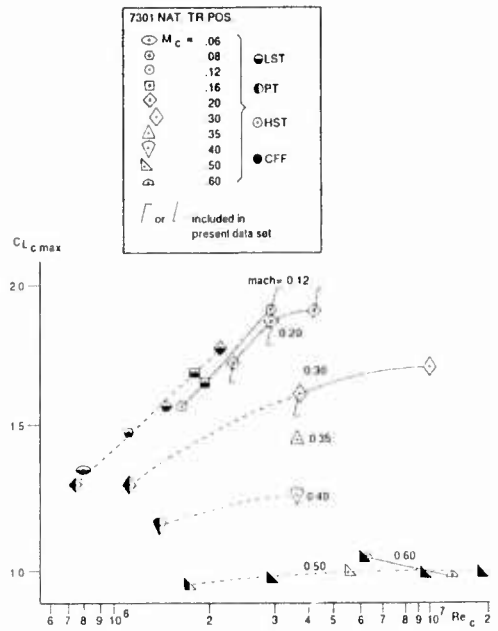



*Fig. 1 $C\ell_{max}$ vs. $Re_c$*

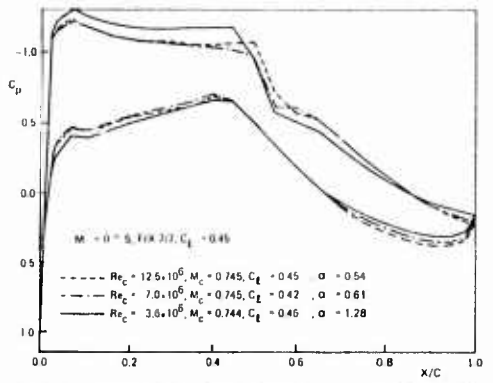



*Fig. 2 Reynolds number effect on pressure distribution, $C_\ell \approx$ constant*

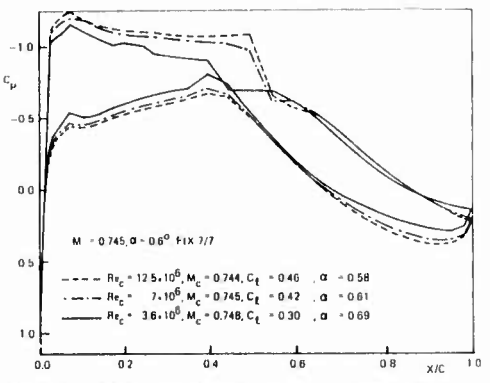



*Fig. 3 Reynolds number effect on pressure distribution, $\alpha \approx$ constant*

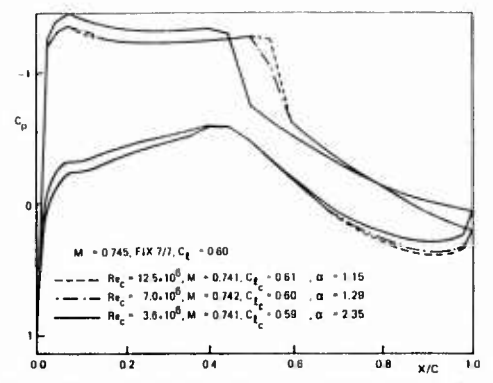



*Fig. 4 Reynolds number effect on pressure distribution, $C_\ell \approx$ constant*

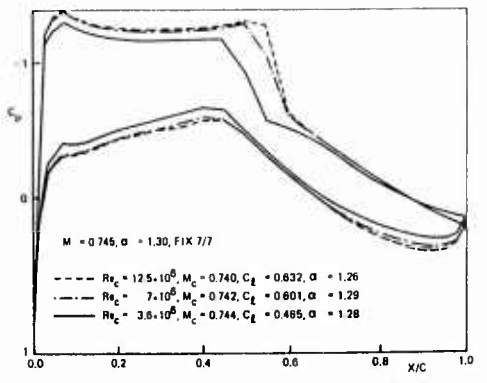



*Fig. 5 Reynolds number effect on pressure distribution, $\alpha \approx$ constant*

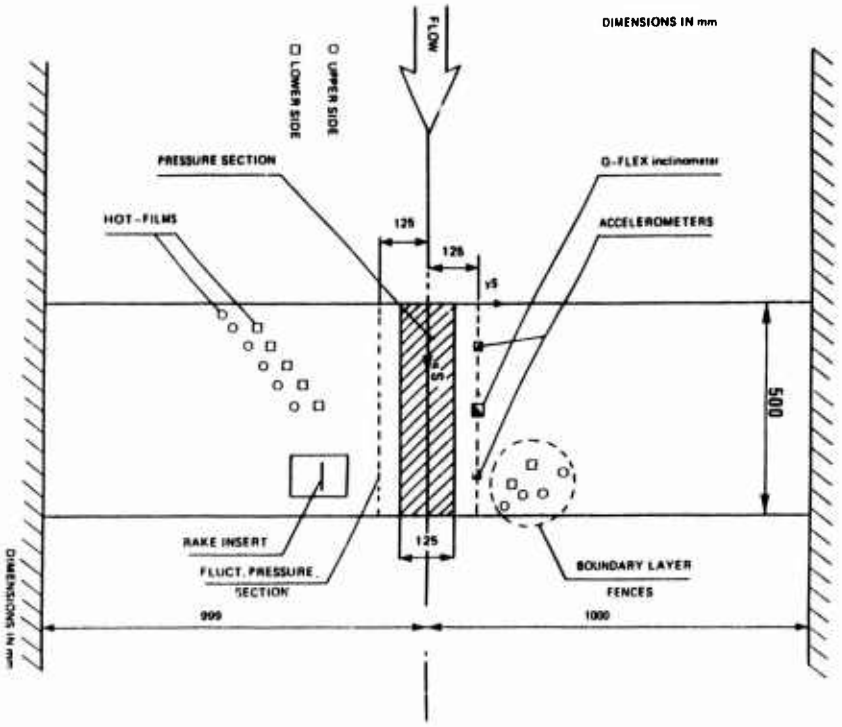



*Fig. 6 Model with instrumentation*

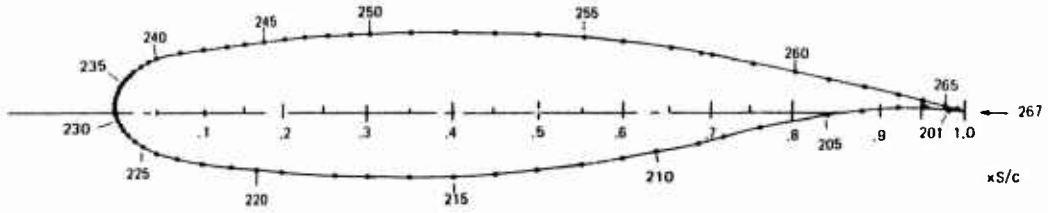



*Fig. 7 Main pressure section*

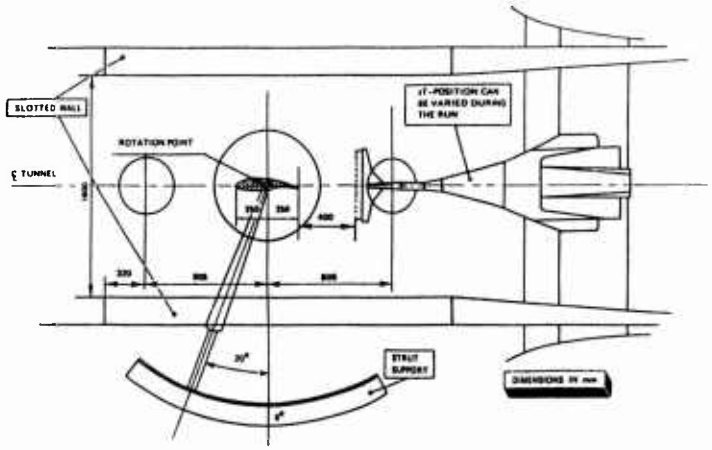



*Fig. 8 Model position in test section*

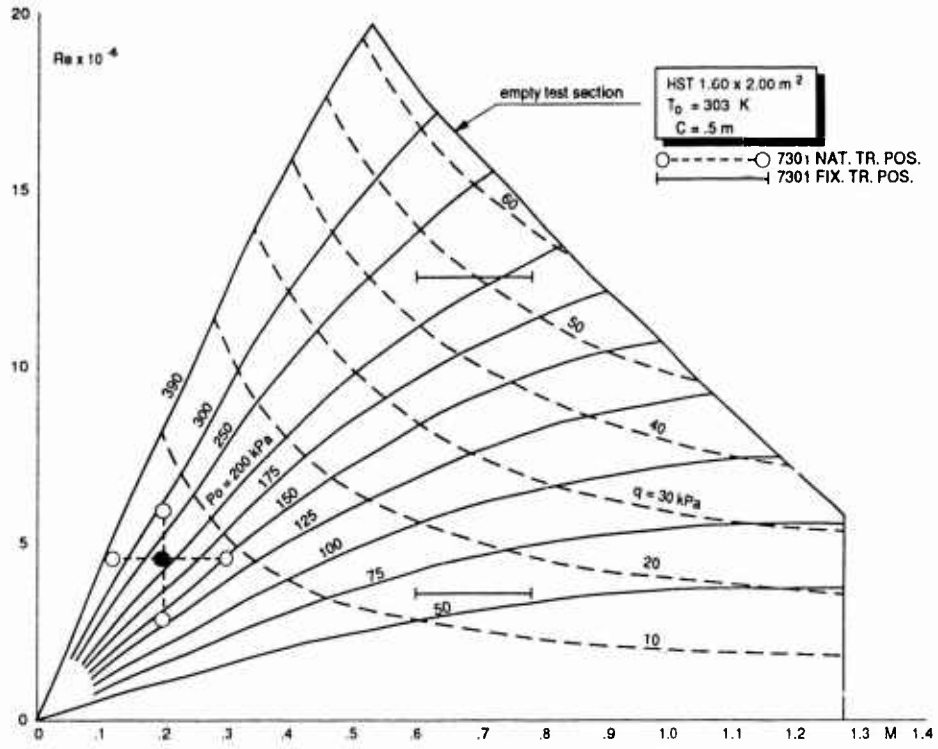



*Fig. 9 The Reynolds number as a funtion of Mach number based on a model chord of.5m (2-D model 7301)*

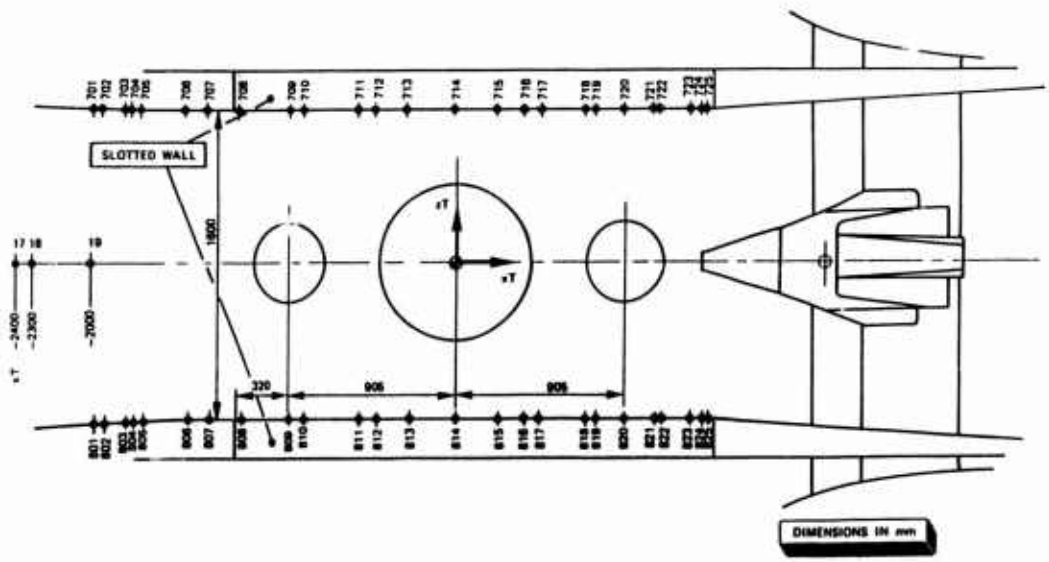



*Fig. 10 Position and numbering of the tunnel wall pressure holes*

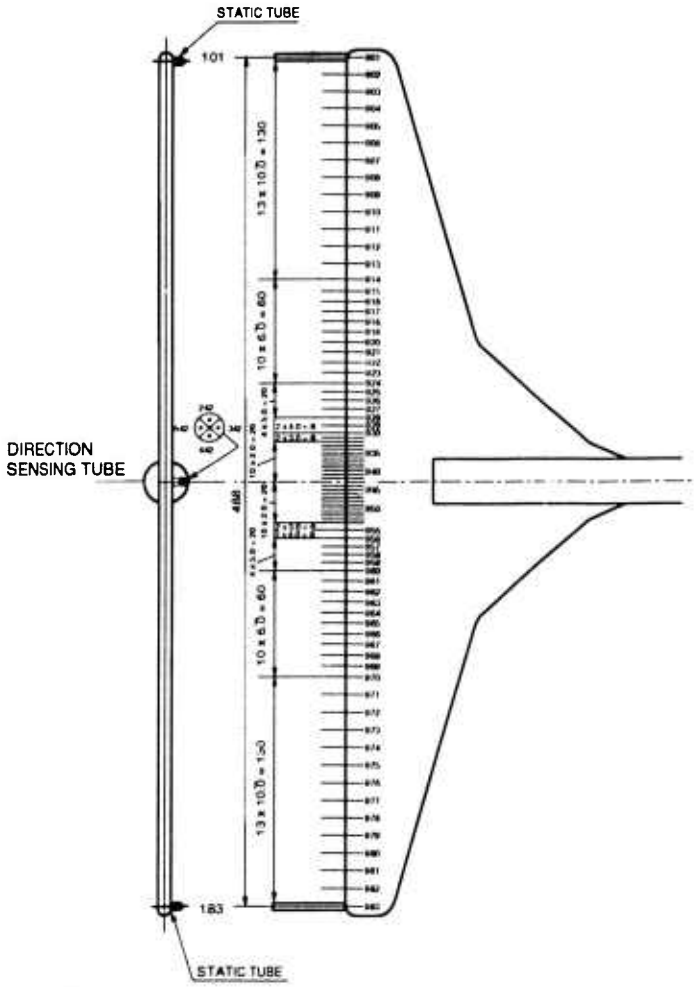
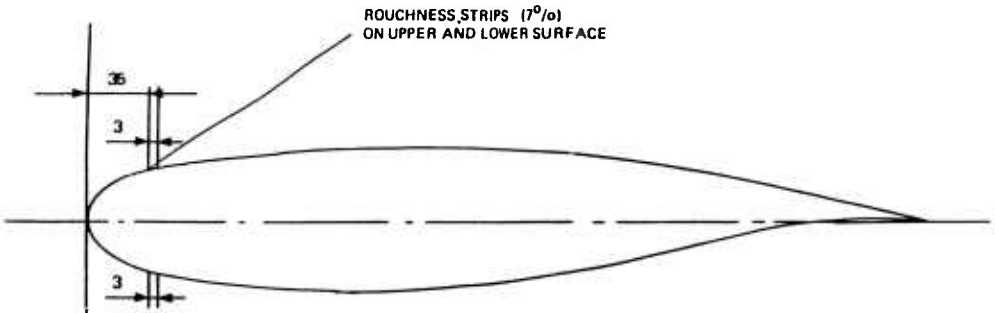



*Fig. 11 Position and numbering of the wake rake pressure tubes*




| RE | CARBORUNDUM GRIT SIZE | | STRIP POSITION |
|---|---|---|---|
| | UPPER | LOWER | |
| 3.6 | 80 | 80 | 7 °/o |
| 12.5 | 220 | 220 | 7 °/o |

COVERING OF THE CARBORUDUM ≤ 20 °/o

DIMENSIONS IN mm

*Fig. 12 Position and grit size of the carborundum roughness strips*

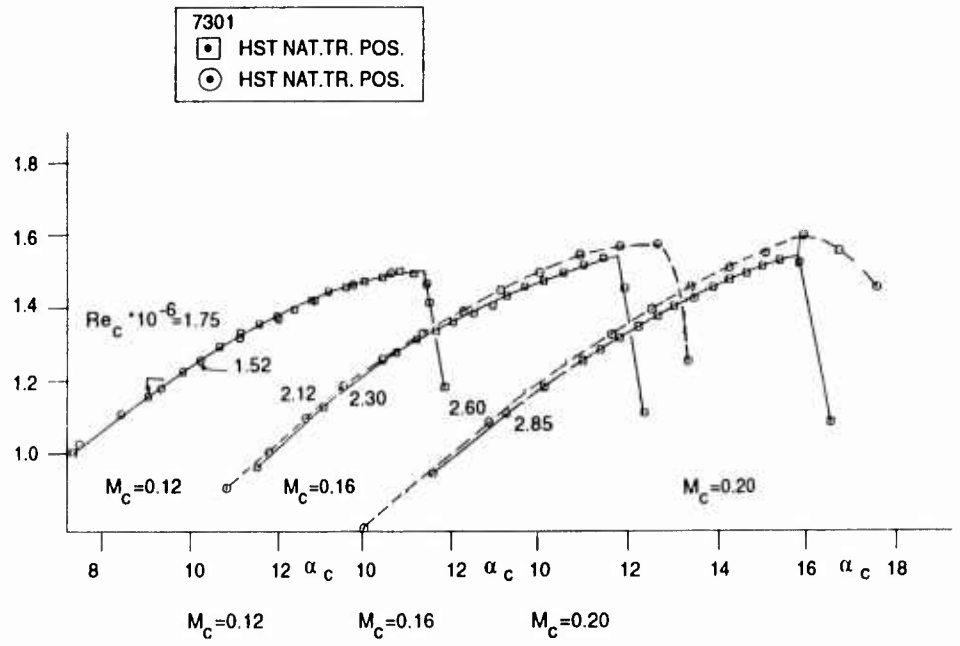



*Fig. 13 HST vs LST Comparison; $C_l$ vs $\alpha$*

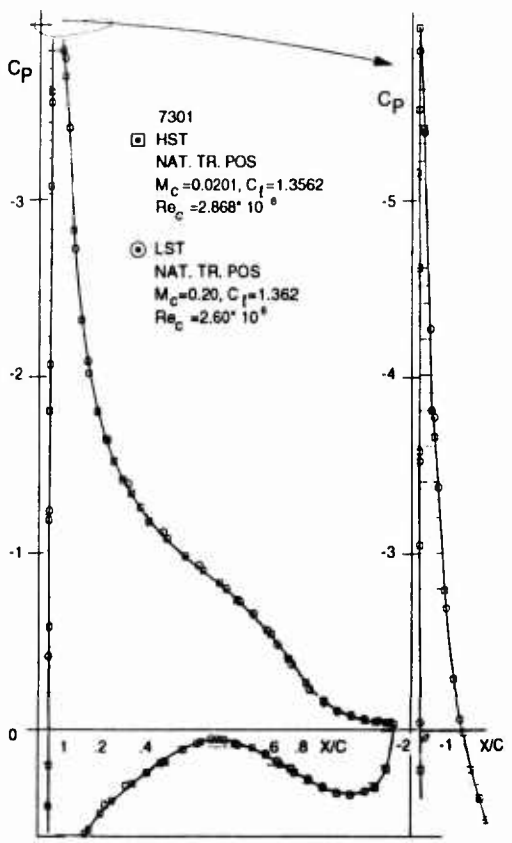



*Fig. 14 HST vs LST comparison $C_p$ vs x/c; M= 0.20*

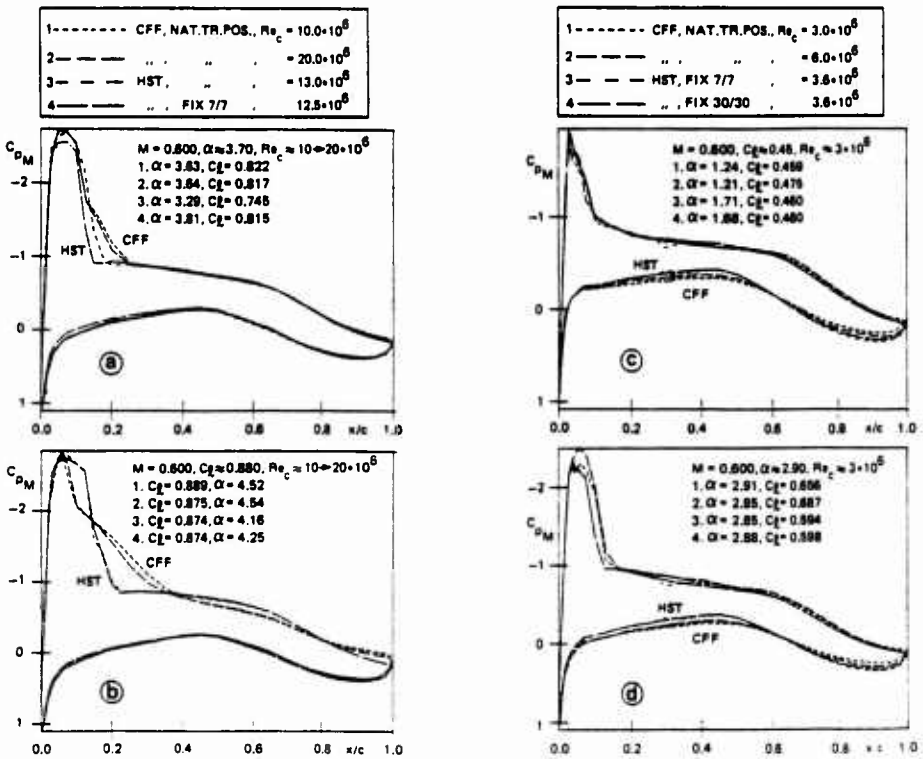



*Fig. 15 HST vs CFF comparison $C_p$ vs $x/c$; M= 0.600*

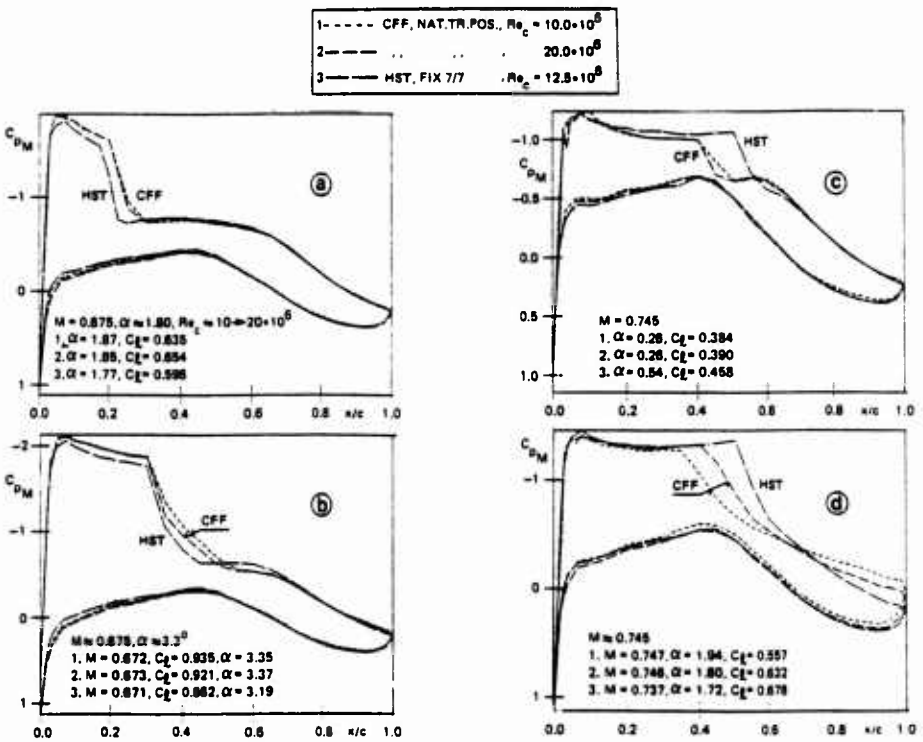



*Fig. 16 HST vs CFF comparison $C_p$ vs $x/c$; M= 0.675 and 0.745*

# LOW-SPEED SURFACE PRESSURE AND BOUNDARY LAYER MEASUREMENT DATA FOR THE NLR 7301 AIRFOIL SECTION WITH TRAILING EDGE FLAP

by B. van den Berg and J.H.M. Gooden

## 0. INTRODUCTION

Test data are given for a two-dimensional wing flap configuration, which has been so designed that nowhere flow separations occur, apart from a small laminar separation bubble on the wing nose. The 32% chord trailing edge flap is deflected 20°. Two widths of the gap between wing and flap have been applied, with mixing of the wing wake and flap boundary layer occurring with the smaller gap. The experiment has been carried out at a Reynolds number Re,c = 2.51 * E6 and a Mach number of about Ma = 0.185.

The measurements comprise surface pressure data, from which lift and pitching moment coefficients were calculated, at various angles of attack from zero up to beyond stall. At three angles of attack the drag has been determined from wake traverses. At these angles mean flow measurements in the boundary layer and wake have been executed at 16 stations. In addition turbulence data were obtained at 5 stations in the wing wake above the flap. Surface flow visualization data are also available.

## 1 GENERAL DESCRIPTION

| | | |
|---|---|---|
| 1.1 | Model designation | NLR 7301 with flap. |
| 1.2 | Model type | Two-dimensional. |
| 1.3 | Design requirement | Model was designed to provide an as simple as possible test case for low-speed multi-element airfoil calculation methods. |
| 1.4 | Dominant flow physics | Interaction between the two airfoil elements, both inviscid and viscous. |

## 2 DETAILS OF MODEL

| | | |
|---|---|---|
| 2.1 | General geometry | Cylindrical model of wing with trailing edge flap (see fig. 1). Basic-airfoil chord = 0.57 m. |
| 2.2 | Configurations | Test have been done at one flap angle, 20°, and two flap gap widths, 2.6% and 1.3% chord. |
| 2.3 | Airfoil data | Basic airfoil section is NLR 7301. |
| 2.4 | Model support details | Model was mounted vertically from wall to wall, spanning the tunnel test section. |

| | | |
|---|---|---|
| 2.5 | Model deformation | The position of the flap relative to the main wing is affected slightly by airloads, due to the limited stiffness of the flap brackets. Measurements showed that the flap gap decreases with wind-on by approximately 0.2% chord and the flap angle by about 0.2 or 0.3 degrees. |
| 3 | GENERAL TUNNEL INFORMATION | |
| 3.1 | Tunnel designation | Most of the tests have been carried out in the NLR LST 3*2m in Amsterdam; some additional data were obtained later in the new NLR LST 3*2.25m in the North-East Polder. |
| 3.2 | Organization running tunnel | NLR, The Netherlands. |
| 3.3 | Tunnel characteristics | Low-speed wind tunnel of conventional design. |
| 3.4 | Test section | Closed-wall test section. Width: 3m; height: 2.1m/2.25m; length: 4m/8.75m for old/new tunnel, respectively. Blowing boundary layer control was applied on tunnel walls to avoid premature stall at model tunnel wall junctions. |
| 3.5 | Flow quality | NLR LST 3*2m wind tunnel in Amsterdam (used for most of the measurements): variation of mean velocity across test section: 0.5%. Free-stream turbulence level: < 0.2%.<br>NLR LST 3*2.25m wind tunnel in the North-East Polder (used for the turbulence measurements in the wing wake above the flap): variation of mean velocity across test section: < 0.2%. Free-stream turbulence level: < 0.04%. |
| 4 | INSTRUMENTATION | |
| 4.1 | Model position | Accuracy of geometrical angle of attack of main wing: ± .05°. |
| 4.2 | Model pressures | Surface pressure hole positions are indicated in fig. 1. Typical measured surface pressure distributions are shown in fig. 2. Estimated accuracy of pressure coefficients: ± 0.01 or ± 0.5%. |

4.3 Forces and moments

Lift and pitching moment have been obtained from integration of the model surface pressures. Drag has been determined from wake traverses at several spanwise positions at one chord distance behind the model trailing edge. Estimated accuracy: lift coefficient: ± 0.01. Pitching moment coefficient: ± 0.005. Drag coefficient: ± 2%. (Spanwise variation in local wake drag traverse data: < 5%.)

4.4 Skin friction

Skin friction coefficients, determined with various indirect methods, are plotted in fig. 3 for the wing upper surface. Accuracy estimate: ± 10%.

4.5 Boundary layers

Boundary layer and wake measurements have been performed at 16 stations, using a small, movable, external traversing mechanism, specially built for the purpose. The mean velocity measurements have been made with pressure probes. Hot-wire measurements to determine the turbulence properties have been carried out at station 8, 12, 13, 14 and 16 (see fig. 1). Typical boundary layer mean velocity profiles are depicted in fig. 4. Fig. 5 and 6 show mean velocities measured in the wing wake above the flap, at a flap gap of 2.6% and 1.3% c respectively. Some turbulence measurement results are plotted in fig. 7. Boundary and wake data accuracy estimate: mean velocities: ± 2%. Turbulence quantities: ± 15%.

4.6 Flow visualization

Surface flow was visualized using the oil flow technique to detect flow separation and attachment lines, and the sublimation technique to determine transition positions.

## 5 TEST MATRICS AND CONDITIONS

5.1 Detailed test matrix

Surface pressure measurements have been carried out at angles of attack between 0 tot 16° at intervals of 1°. Wake traverses and detailed boundary layer measurements have been done at 6.0°, 10.1°, 13.1°. The free-stream Mach number was about 0.185 and the Reynolds number 2.51 * E6.

| | | |
|---|---|---|
| 5.2 | Model/tunnel relations | Tunnel "height/ basic-airfoil chord ratio is 5.26. Tunnel "width"/ chord ratio is about 3.8. |
| 5.3 | Transition details | Tests were made with free transition. Transition positions and position and extent of laminar separation bubbles have been determined at 6.0°, 10.1° and 13.1° angle of attack. |
| 6 | DATA | |
| 6.1 | Availability of data | The data set is freely available. |
| 6.2 | Suitability of data | Data are well suited for CFD validation, and have already been used for this purpose. Tunnel wall interference effects are small and consequently the data can be used for "free air" calculations. Also "in tunnel" calculations can be made, assuming a two-dimensional tunnel test section of infinite length with the tunnel walls at 2.63 chord distance from the model center. |
| 6.3 | Form of data | Data are available in tables and on floppy disk. |
| 6.4 | Corrections applied | Classical tunnel wall interference corrections have been applied. Lift interference correction on lift is less than 1%. Blockage correction on velocity is about 0.5%. |
| 7 | DATA ACCURACY | |
| 7.1 | Accuracy | Angle of attack: ± 0.05°. Free-stream velocity: ± 0.2%. Lift coefficient: ± 0.01. Pitching moment coefficient: ± 0.005. Drag coefficient: ± 2%. Surface pressure coefficients: ± 0.01 or ± 0.5%. Skin friction coefficient: ± 10%. Boundary layer and wake mean velocity data: ± 2%. Wake turbulence data: ± 15%. |
| 7.2 | Repeat measurements | Surface pressure and boundary layer measurements have been done in two different tunnels with good agreement. |

## 8 REFERENCES

B. van den Berg - "Boundary layer measurements on a two-dimensional wing with flap". NLR TR 79009 U (1979).

B. van den Berg, B. Oskam - "Boundary layer measurements on a two-dimensional wing with flap and a comparison with calculations". AGARD Conf. Proc. No. 271 (1979).

B. van den Berg - "Comparison of theory and experiment for a simple two-dimensional airfoil with flap". NLR TR 83034 U (GARTEUR TP-013) (1983).

J.H.M. Gooden, M. van Lent - "Measurements in a two-dimensional turbulent wing wake above a trailing edge flap (data report)". NLR CR 89274 U(?) (1989).

J.H.M. Gooden - "Flow gradient corrections on hot-wire measurements using an X-wire probe". NLR TP 90255 U (1990).

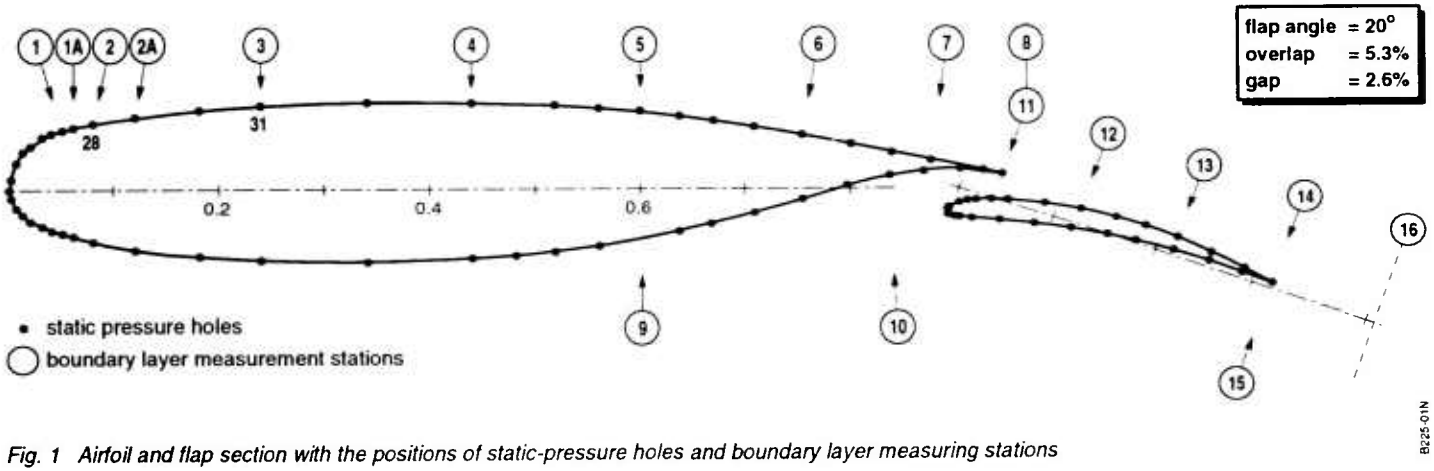



*Fig. 1 Airfoil and flap section with the positions of static-pressure holes and boundary layer measuring stations*

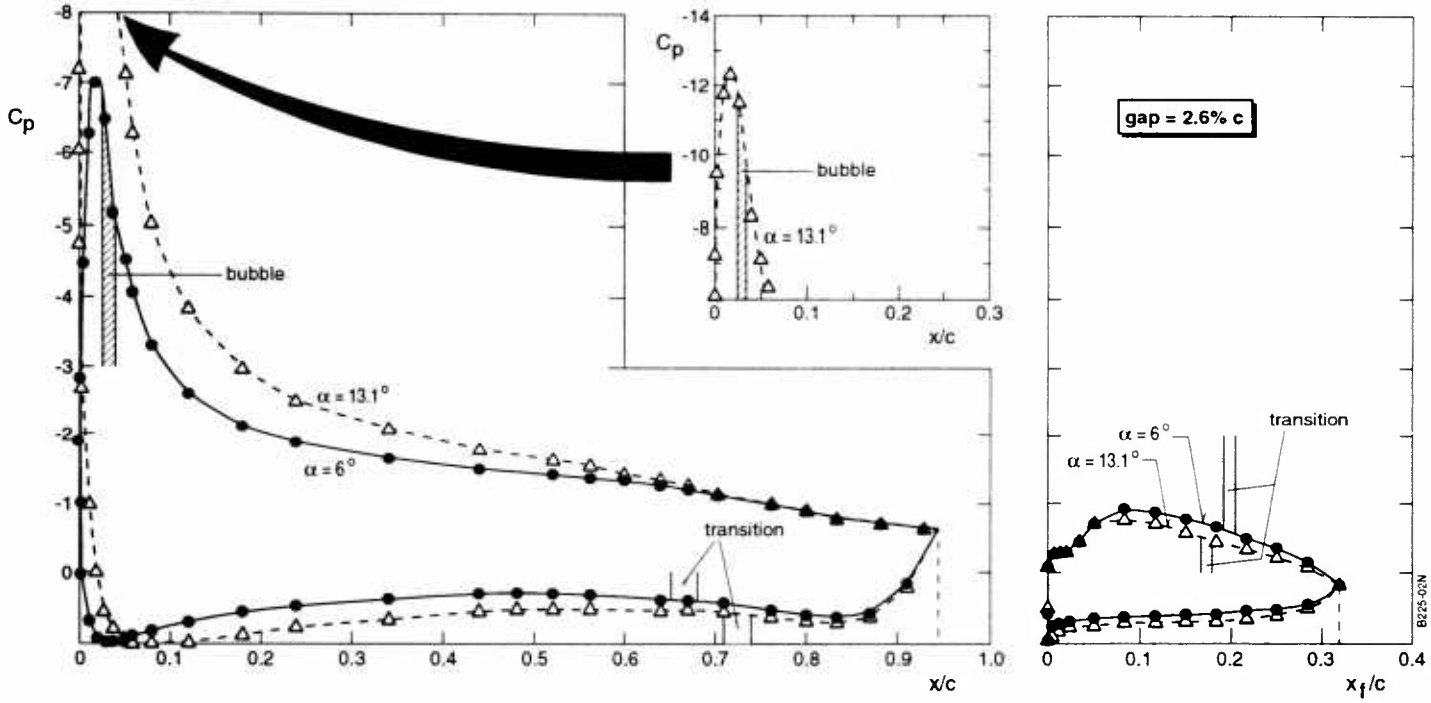



*Fig. 2 Measured surface pressure distribution and position of laminar separation bubbles and transition regions*

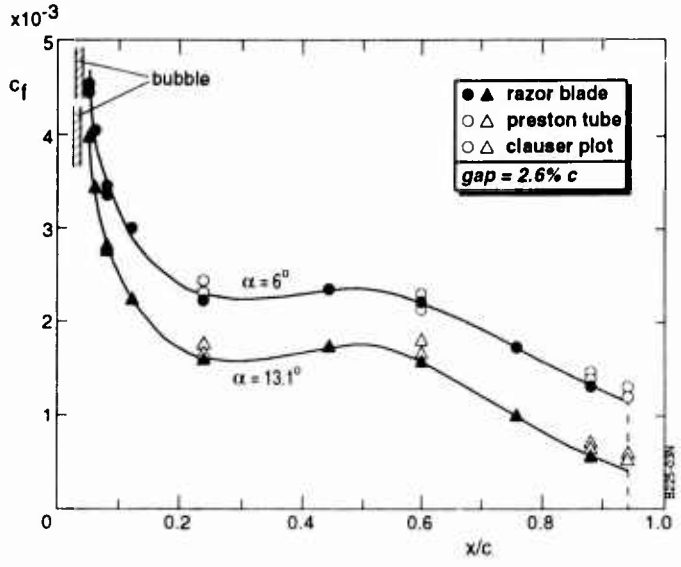



*Fig. 3 Measured wall shear stress variation on wing upper surface*

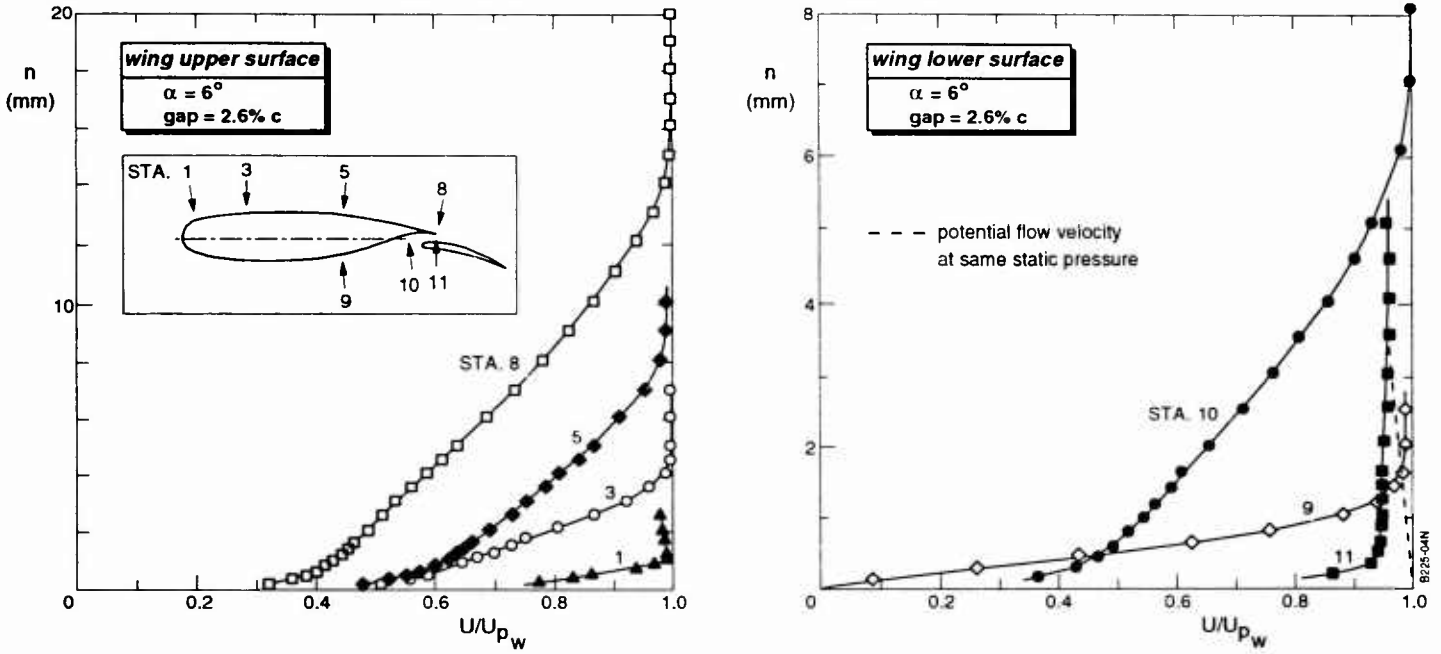



*Fig. 4 Typical measured velocity profiles of boundary layer on wing surface*

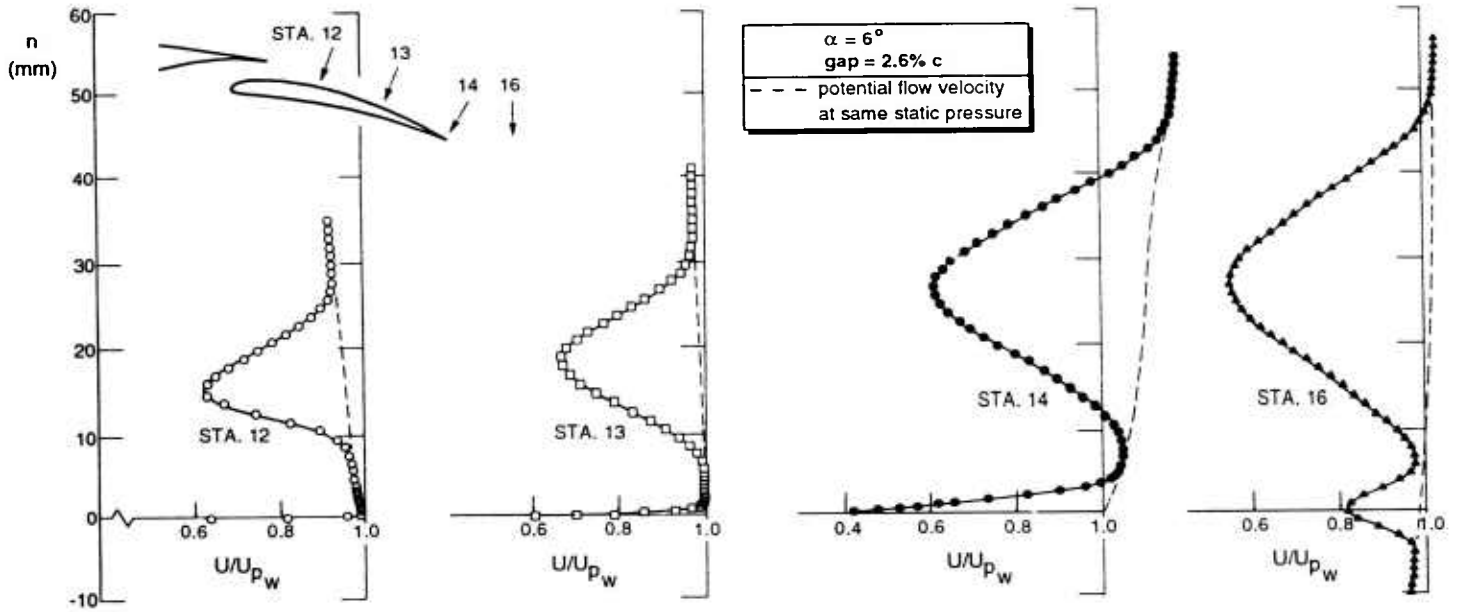



*Fig. 5 Typical measured velocity profiles of shear layer above flap*

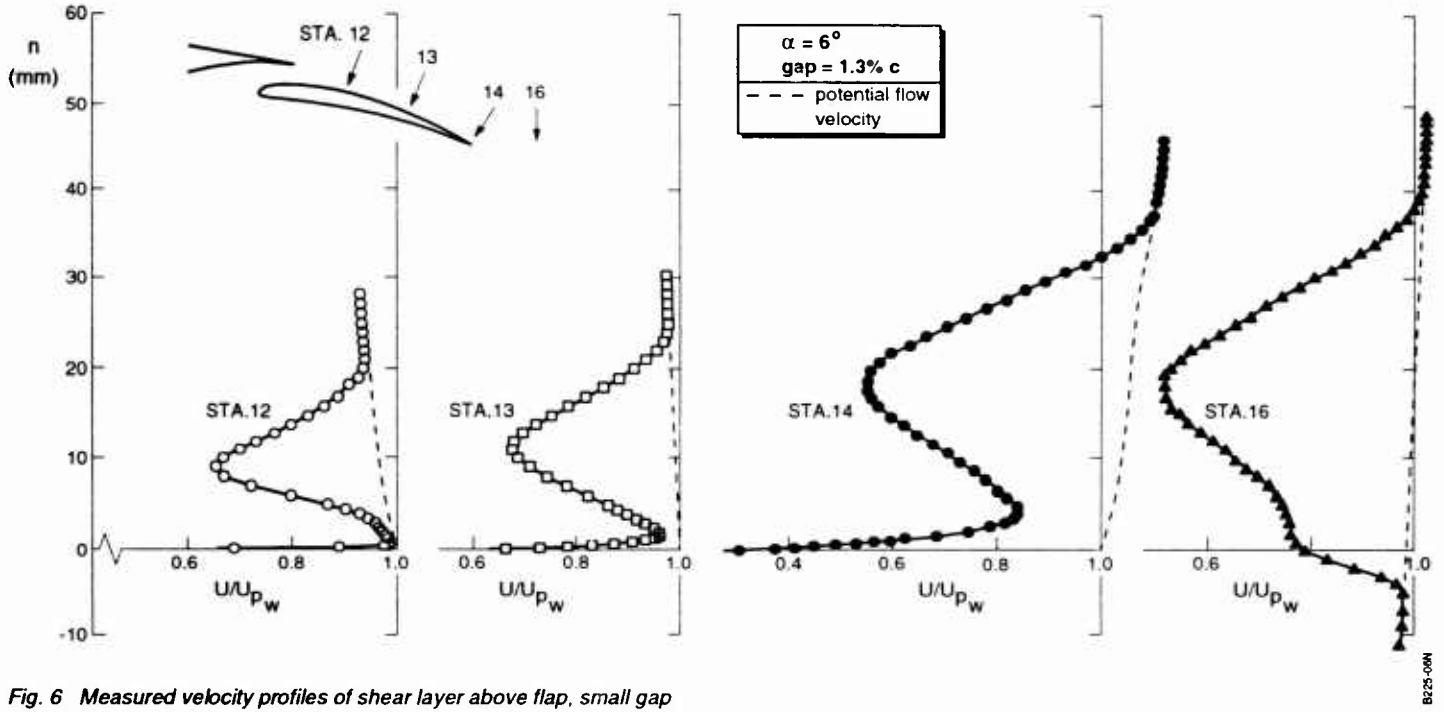



*Fig. 6 Measured velocity profiles of shear layer above flap, small gap*

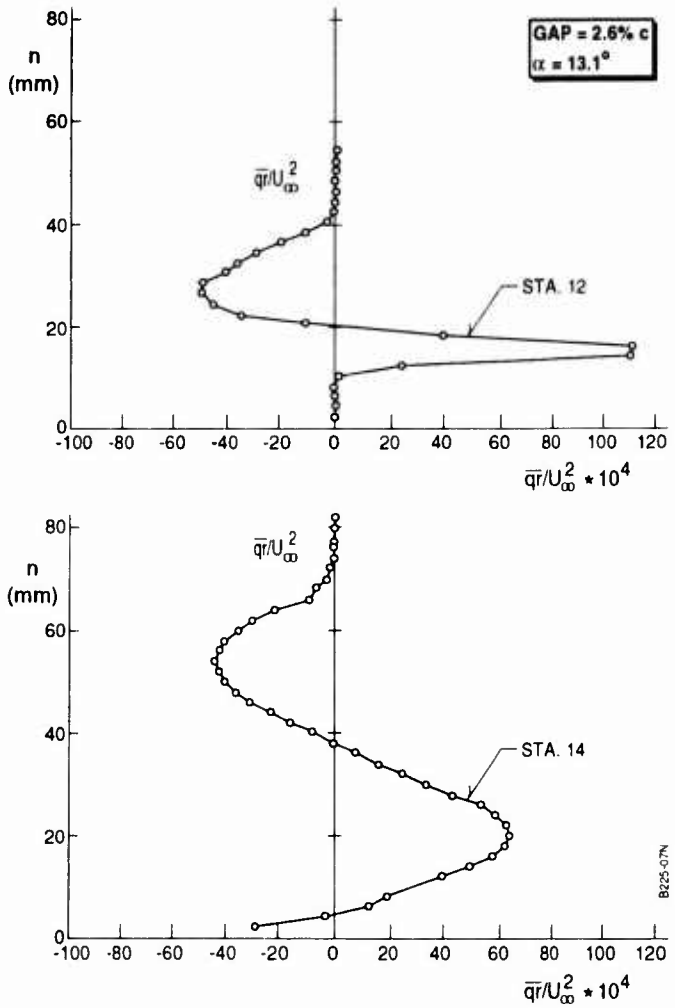



*Fig. 7 Hot-wire results: measured streamwise Reynolds stresses, $\overline{qr}/U_\infty^2$, at two stations*

# Data from the GARTEur (AD) Action Group 02 Airfoil CAST 7/DOA1 Experiments

by
A. Mignosi, J.P. Archambaud and E. Stanewsky

## Introduction

In order to gain a better understanding of the various forms and the magnitude of wind tunnel interferences that may arise in two-dimensional testing and to find improved methods of correction, a GARTEur[1] Action Group was formed in 1979 with the primary objectives of

- comparing test results obtained with one airfoil (CAST 7) in a number of facilities in order to assess wall interference in the individual tunnels and to assess the accuracy of correction methods currently used and
- evaluating three-dimensional interference effects associated with the side wall boundary layer.

The wind tunnels considered consisted of five conventional tunnels with either slotted or perforated test section walls and two adaptive wall wind tunnels, Table I [1]. Based on a comparison of the results from these tunnels, it was concluded that for these two-dimensional airfoil tests the freestream conditions, Mach number and angle of attack, were generally predicted with an accuracy of $\Delta M_\infty = \pm 0.002$ and $\Delta\alpha = \pm 0.1°$ to $\pm 0.05°$, respectively, and the lift and drag coefficients with an accuracy of $\Delta C_L = \pm 0.015$ and $\Delta C_D = \pm 0.0003°$, respectively. For the adaptive wall wind tunnel T2 of ONERA/CERT the accuracy in freestream conditions was determined to be $\Delta M_\infty = \pm 0.001$ and $\Delta\alpha = \pm 0.03°$.

Due to their relatively high accuracy, only the ONERA T2 adaptive wall tests are considered hereafter. The data, obtained with well defined boundary contitions, are believed to be the most suitable for a CFD - assessment. A comparison with results from the other participating facilities is given in Figures 11 through 14. For more information on these facilities, their data and data reports, the user is referred to Ref. 1.

---

**1. GENERAL DESCRIPTION**

1.1 Model name or designation: CAST 7/DOA1

1.2 Model type and flow conditions

2-D airfoil at transonic speeds. The airfoil is of shock-free design with a roof-top pressure distribution and moderate to strong rear loading.

1.3 Design requirements, purpose of test

Shock-free flow at $M_\infty = 0.76$, $\alpha = 0°$.
Tests were carried out in seven wind tunnels to assess wall interference and correction methods(Table I, Ref.1).

1.4 Dominant flow physics

Viscous/inviscid interactions of a turbulent boundary layer with shock waves and moderate to strong rear adverse pressure gradiens with and w/o shock-induced and rear separation.

**2. DETAILS OF MODEL(S)**

2.1 General geometric arrangement
Figure 1 (also see Fig. 4 )

2.2 Configuration
Airfoil of chord - length c = 0.20m, tested on and off tunnel center line

2.3 Airfoil section data

2.3.1 Planform
Model chord = 0.20 m
Model span = 0.40 m
Aspect ratio = 2.00

2.3.2 Basic airfoil section
Airfoil shape: Figure 2
Thickness/chord ratio = 0.1189

2.7 Geometric definition of all components
Design: Figure 2
Tolerances: Figure 2
Measured coordinates are on disk

Surface roughness
Polished to RA 0.2 to 0.4 $\mu m$

2.8 Model support details
Models mounted in rotatable disks inserted into and mounted flush with the side walls, Figure 4

**3. GENERAL TUNNEL INFORMATION**

3.1 Tunnel designation: T2

---

1 Group for Aeronautical Research and Technology in Europe

3.2 Organization running the tunnel
ONERA (CERT)
2, avenue Edouard Belin
B.P. 4025
31055 - Toulouse Cédex

3.3 Tunnel characteristics

Type of tunnel
Injector - driven closed-circuit tunnel with a run time of 30 to 120 sec, Figure 5a

Operating envelope: Figure 5b

3.4 Test section

3.4.1 Test section details
Adaptive wall test section, Figure 4

3.4.2 Test section dimensions (width x height x length)
0.39 m x 0.37 m x 1.5 m
At the time of the CAST 7 tests, the dimensions were 0.40 m x 0.38 m x 1.5 m

3.4.3 Wall geometry details
Type of walls
Flexible adaptive upper and lower walls, solid side walls, Figure 4

Are wall pressures/wall displacements measured? Yes

Boundary layer control on walls

Side wall boundary layer control can be applied but was not utilized in the present CAST 7 tests. However the data selected were corrected for sidewall interference (see Tables III and IV)
Typical wall boundary layer displacement thickness: $\delta_1$ = 2.5 mm

3.5 Freestream conditions

3.5.1 How are reference flow conditions determined?

Total pressure: Measured in settling chamber by pitot probe.

Static pressure: Freestream Mach number is determined from the measured horizontal-wall pressures [1]. The corresponding static pressure is inferred from total pressure and Mach number.

Static temperature: The static temperature is inferred from the total temperature measurement in the settling chamber

3.5.2 Tunnel calibration
Empty tunnel calibration only to determine erroneous wall pressure readings

Date of last calibration:
Wall shape is controlled before each test campaign

3.6 Flow quality (empty tunnel)

3.6.1 Flow uniformity

Static pressure variations over model length: Zero

Mach number variation over model length: The flexible walls are adjusted to compensate the displacement thickness growth, Figure 6

Mach number variation during a run: $\Delta M_\infty < 0.001$

Flow angularity over the model length and span:
Zero due to wall adaptation

3.6.2 Temperature variation

Can the temperature be controlled during a run?
Yes, for operation at cryogenic conditions. At ambient conditions the temperature cannot be controlled.

Variation within the tunnel: $\Delta T < 1K$.

3.6.3 Flow unsteadiness

Overall noise level: Figure 7
Overall turbulence level: Figure 8

## 4. INSTRUMENTATION

4.1 Model position

4.1.1 How is the geometrical incidence measured?
On flat mounting flanches of the airfoil with an inclinometer.

4.1.2 Accuracy of geometrical incidence
± 0.02°; Note that the effective angle of incidence is determined in the wall adaptation process.

4.2 Model pressure measurements

4.2.1 Total number and disposition of pressure holes
The model with c = 0.20 m was equipped with 103 oirfices, Figure 3

4.2.2 Range and accuracy of pressure transducers
Model surface: DRUCK PDCR 22 ± 25 and ± 50 psi; Statham PM 872 ± 35 psi
Accuracy: 0.1 % FS

4.2.3 Are dynamic pressures measured?
No

4.4 Boundary layer and flow field measurements

4.4.1 Measurement technique applied
Total and static probe measurements

4.4.2 Flow regions investigated
Wake: Wake-rake located one chord length downstream of model trailing edge,

Pressure transducer: ENDEVCO 8507 ± 5 psi; Accuracy: 0.1 % FS

4.5 Surface flow visualization

4.5.1 Measurement technique applied
Oil-flow visualization

4.5.2 On which surface is the flow visualized?
Upper and lower airfoil surface

4.5.3 In what form are data available?
Photographs

4.7 Tunnel wall measurements

4.7.1 Type of measurements
Static pressure measurements on upper and lower flexible walls and wall deflection measuremtents

4.7.2 Location and number of pressure holes
Each flexible wall was equipped with 91 pressure orifices, Figure 9
Transducer: DRUCK PDCR 22 ± 25 psi
Accuracy: 0.1 % FS

## 5. TEST MATRIX AND CONDITIONS

5.1 Detailed test matrix
See Table II for the GARTEur AG02 tests

5.1.1 Number of selected test cases: 13

5.1.2 Number of configurations tested: One

5.1.3 Test cases: Table III

5.2 Model/tunnel relations

5.2.4 Height/chord ratio: 1.9

5.2.5 Width/chord ratio: 2.0

5.2.6 Have adiabatic wall temperatures been reached? Yes

5.3 Transition details

5.3.1 Was the test made with free or fixed transition?
For the selected test cases, transition was fixed

5.3.3 Details of fixed transition

Transition location:
Trips of 0.1 c width were located at 7% chord on upper and lower surfaces.

Type and size of trip:
The trip consisted of carborundum grit with an average height of 0.06 mm.

How was effectiveness of trip verified?
The trip effectiveness was verified through integrated drag and lift measurements as function of grit height for the Mach numbers of $M_\infty$ = 0.70 to 0.77 and $Re_c$ = 6 x $10^6$.
Note that tripping will probably somewhat decrease the lift and increase the drag compared to free transition if the beginning of transition is located at the same position as the trip. ($\Delta C_D \approx 0.0004$ at $M_\infty = 0.755$, $\alpha = 0°$, $Re = 6 \times 10^6$).

## 6. DATA

6.1 Availability of data

6.1.1 Organisation owning the data
ONERA/CERT

6.1.2 Who is responsible for the data?
Mr.A. Mignosi / Mr. J.P. Archambaud
c/o CERT - ONERA
2 avenue E. Belin
31055 Toulouse - France
Tel. (33) 61 66 70 44
Fax (33) 61 66 71 72

6.1.3 Are data freely available?
Yes

6.2 Suitability of data for CFD validation

The tests were made in an adaptive wall wind tunnel, i.e., not only are the boundary conditions available so that an "in-tunnel" calculation is possible but the data can also be considered as representing "free - air" conditions.

6.3 Type and form in which data are available

6.3.1 Type and form

a. Freestream: Mach number and angle of attack as determined through the wall adaptation and side wall interference correction process

b. Pressure: Coefficients based on free stream dynamic pressure.

c. Forces: Coefficients based on freestream dynamic pressure. The forces were obtained by integrating surface and wake pressures.

6.3.2 Data carrier
Data are provided on 3.5" compact disk

6.4 Corrections applied to data

6.4.1 Lift interference and blockage corrections
Data are considered basically free of lift and blockage interference.

6.4.2 Side wall interference corrections

Treatment of side wall boundary layer?
No

Correction method used

A correction for side wall effects has been carried out according to the method of Michonneau [2]. Corrected data are given in Tables III and IV, showing the effect on Mach number and global aerodynamic coefficients. A side-wall correction map for CAST 7 is given in Figure 10.

## 7. DATA ACCURACY AND REPEATABILITY ASSESSMENT

7.1 Estimated accuracy of:

7.1.1 Free stream conditions
Mach number: $\Delta M_\infty = \pm 0.001$
Model incidence: $\Delta\alpha = \pm 0.03°$

7.1.2 Measured data
Forces and moments: $\Delta C_L \approx \pm 1\%$;
$\Delta C_m \approx \pm 1\%$, $\Delta C_D \approx \pm 2\%$
Pressure coefficients: $\Delta C_p \approx \pm 1\%$

7.2 Repeat measurements

7.2.1 Type and number of repeat measurements
A sufficient number of repeat measurements were carried out within a test campaign and between campaigns

Repeatability
$\Delta C_L \approx \pm 1\%$; $\Delta C_D \approx \pm 1.6\%$; $\Delta C_m \approx \pm 0.8\%$

7.3 Redundant measurements
No redundant measurements

7.4 Other tests on same (nominal) geometry

The CAST 7/DOA1 airfoil (different models) has been tested in 7 wind tunnels, Table I. Typical comparisons of results at $Re_c = 6 \times 10^6$ are presented in Figures 11 through 14.
Note that the data are not side-wall corrected except for the freestream conditions in Figure 13. It can generally be assumed that side-wall interference is similar in the tunnels compared here.

## 8. REFERENCES

8.1 On the wind tunnel: Ref. 3

8.2 On the model:
Note ONERA N° 103 419
Note ONERA N° 103 452

8.3 On the particular test and test results: Ref. 4 through 6

8.4 On the applied measurement techniques and correction method: Ref. 2, 7 and 8


1. Elsenaar, A.
(Edit.), "Two-dimensional Transonic Testing Methods" Final Report of GARTEur Action Group AD (AG02). GARTEUR/TP-011 / NLR TR 83086L, July 1981

2. Archambaud, J.P., Michonneau, J.F., Mignosi, A.
Analysis of test section side wall effects on 2D aerofoils: Experimental and numerical investigation.
AGARD-FDP Symposium, Brussels, 1993.

3. Archambaud, J.P.
"The Cryogenic Induction Tunnel T2 at Toulouse", AGARD Report No. 774 Special Course on Advances in Cryogenic Wind Tunnel Technology, June 1982

4. Archambaud, J.P., Mignosi, A., Seraudie, A."Rapport d'essais sur profil CAST 7 effectués à la soufflerie T2 en présence de parois auto-adaptables en liaison avec le groupe GARTEur AD (AG02)", Rapport Technique OA No. 24/3075 and (DERAT No. 7/5015 DN) - Juillet 1982

5. Mignosi, A., Seraudie, A., Dor, J.B., Gobert, J.L., Archambaud, J.P., "Premier essais cryogéniques du profil CAST 7 ( c = 150mm) a la soufflerie T2", R.T. 0A No. 57/1685 and (DERAT No. 3/5019DN), Jan. 1984

6. Dor, T.B., Seraudie, A., Plazanet, M., "Essais cryogénique du profil CAST 7 (c = 150mm) à la soufflerie T2," A / Catalogue des essais - R.T. 0A 60/1685 and (DERAT No. 5/5019 DN), April 1985

7. Chevalier, J.P., Mignosi, A., Archambaud, J.P., Seraudie, A.
"T2 Wind Tunnel Adaptive Walls: design construction and some special results", La Recherche Aerospatiale (English Edition), No. 1983 - 4

8. Blanchard, A., "CAST 10-2/DOA 2 Airfoil Studies - 2nd Workshop Results", Rapport Interne DERAT No. 39/5606-23 Mars 1990.


## 9. LIST OF SYMBOLS

| | |
|---|---|
| B | Tunnel width |
| c | Chord |
| $C_D$ | Draft coefficient |
| $C_L$ | Lift coefficient |
| $C_{Dp}$ | Pressure drag coefficient |
| $C_m$ | Pitching moment coefficient |
| H | Tunnel height |
| $M_\infty$, Mo | Freestream Mach number |
| $\Delta M$ | Change in $M_\infty$ due to side wall interference |
| p | Static pressure |
| $p_t$ | Stagnation pressure |
| q | Dynamic pressure |
| Re, $Re_c$ | Reynolds number based on chord |
| $T_t$ | Stagnation temperature |
| $\alpha$ | angle of attack |
| $\delta^*$ | Displacement thickness |
| $\rho$ | Density |
| $\sigma$ | Wall open area ratio |

**TABLE I:** Test section/model characteristics (GARTEur AG02 Participants)

| No. | Tunnel | B(m) × H(m) | Type of walls | σ (%) | NS[1] | c(m) | B/c | H/c | $\delta^*/B$ | Remarks |
|---|---|---|---|---|---|---|---|---|---|---|
| 1a | S3Ma | 0.56 × 0.78 | Perforated | 9.7 | | 0.20 | 2.8 | 3.9 | 0.010 | Straight holes; solid side walls |
| 1b | | | Solid | | | | | | | |
| 2 | TWB | 0.34 × 0.60 | Slotted | 2.35 | 4 | 0.15 | 2.3 | 4.0 | | Solid side walls |
| | | | | | | 0.20 | 1.7 | 3.0 | | |
| 3 | ARA | 0.20 × 0.46 | Slotted | 3.2 | 6 | 0.127 | 1.6 | 3.6 | 0.015 | Solid side walls |
| 4 | TKG | 0.99 × 0.98 | Slotted[2] | 3.4 | 4 | 0.20 | 5 | 4.9 | 0.011 | Solid side walls |
| 5 | T2[3] | 0.40 × 0.38 | Adaptive | | | 0.12 | 3.3 | 3.2 | 0.005 | Parallel side walls, flexible top |
| | | | | | | 0.20 | 2.0 | 1.9 | | and bottom walls |
| 6 | NLR | 0.42 × 0.55 | Slotted | 10 | 7 | 0.18 | 2.3 | 3.1 | 0.007 | Solid side walls |
| 7 | TU-B | 0.15 × 0.15 | Adaptive | | | 0.10 | 1.5 | 1.5 | | Parallel side walls; flexible top and bottom walls |

[1] Number of slots, excluding slots located at intersection of vertical and horizontal walls.
[2] Aluminium bars of 200 mm thickness mounted on perforated walls. Open area is based on slot width only
[3] Models were generally positioned 80 mm below center line.
Tunnel designation/Operator: S3Ma ONERA; TWB, TKG DLR; ARA Aircraft Research Association; T2 ONERA/CERT; TU-B Technical University Berlin

**TABLE II:** Nominal test matrix for the CAST 7 / DOA1 GARTEur exercise
(Nominal Reynolds numbers of $Re_c = 2.5 \times 10^6$ and/or $Re_c = 6 \times 10^6$ were prescribed)

A. Angle of attack sweeps

| $M_\infty$ \ α | -2 | -1 | 0 | 1 | 1.5 | 2 | 2.5 | 3 | 3.5 | 4 | 4.5 | 5 | 5.5 | 6 | 6.5 | 7 | 7.5 | 8 |
|---|---|---|---|---|---|---|---|---|---|---|---|---|---|---|---|---|---|---|
| 0.60 | • | • | • | • | | • | | • | | • | | • | • | • | • | • | • | • |
| 0.70 | • | • | • | • | | • | • | • | • | • | • | • | • | | | | | |
| 0.76 | • | • | • | • | • | • | • | • | • | | | | | | | | | |

B. Mach number sweeps

| $M_\infty$ | 0.60 | 0.65 | 0.70 | 0.72 | 0.74 | 0.75 | 0.76 | 0.77 | 0.78 | 0.79 | 0.80 | 0.82 |
|---|---|---|---|---|---|---|---|---|---|---|---|---|

at angles of attack giving at $M_\infty = 0.76$ lift coefficients of $C_L = 0.52$ and $C_L = 0.73$, respectively.

**Table III:** Selected test cases (ONERA/CERT T2-tests)

| Run N° | $M_\infty$ [1] | $M_{corr}$ [2] | α (°)[1] | $C_L$ [1] | $C_{L\,corr.}$ [2] | $Re_c \times 10^{-6}$ | Remarks |
|---|---|---|---|---|---|---|---|
| 325 | 0.599 | 0.5975 | 0 | 0.414 | 0.4160 | 5.9 | Subcritical with onset of |
| 358 | 0.598 | 0.5960 | 1 | 0.544 | 0.5599 | 5.9 | separation at the highest |
| 369 | 0.594 | 0.5905 | 3 | 0.841 | 0.8554 | 6.0 | incidence (α-sweps) |
| 328 | 0.69 | 0.6935 | 0 | 0.453 | 0.4587 | 6.0 | Sub/Supercritical with |
| 356 | 0.696 | 0.6915 | 1 | 0.623 | 0.6341 | 5.9 | shock waves and moder. |
| 368 | 0.690 | 0.6830 | 3 | 1.014 | 1.0443 | 5.9 | separation (α-sweep) |
| 324 | 0.752 | 0.7495 | -1 | 0.322 | 0.3264 | 5.8 | Sub/Supercritical with |
| 335 | 0.753 | 0.7470 | 0 | 0.522 | 0.5348 | 6.1 | shock waves and massiv |
| 351 | 0.755 | 0.7470 | 1 | 0.736 | 0.7553 | 5.9 | separation (α-sweep) |
| 328 | 0.696 | 0.6935 | 0 | 0.453 | 0.4587 | 5.9 | Mach number sweep |
| 331 | 0.734 | 0.7295 | 0 | 0.484 | 0.4919 | 5.9 | through drag-rise and |
| 335 | 0.753 | 0.7470 | 0 | 0.522 | 0.5348 | 5.9 | into moderate separation |
| 342 | 0.764 | 0.7570 | 0 | 0.525 | 0.5377 | 6.0 | |
| 336 | 0.773 | 0.7650 | 0 | 0.553 | 0.5681 | 5.8 | |
| 341 | 0.783 | 0.7750 | 0 | 0.548 | 0.5641 | 6.0 | |

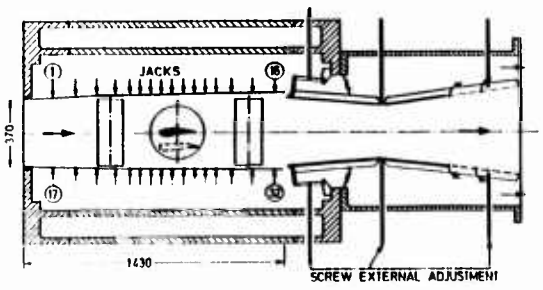
[1] Data are adapted for zero blockage and lift interference
[2] Data are in addition corrected for side-wall interference

**TABLE IV**: The effect of side-wall interference

| Run N° | $M_{corr}$ | $\alpha$ (°) | $C_{Dp}$ | $C_{Dpcorr}$ | $C_M$ | $C_{M\,corr}$ | $C_D$ |
|---|---|---|---|---|---|---|---|
| 325 | 0.5975 | 0 | 0.0043 | 0.00437 | -0.103 | -0.1039 | 0.0090 |
| 358 | 0.5960 | 1 | 0.0053 | 0.00542 | -0.103 | -0.1044 | 0.0095 |
| 369 | 0.5905 | 3 | 0.0096 | 0.00981 | -0.101 | -0.1032 | 0.0117 |
| 328 | 0.6935 | 0 | 0.0060 | 0.00614 | -0.113 | -0.1144 | 0.0095 |
| 356 | 0.6915 | 1 | 0.0072 | 0.00730 | -0.110 | -0.1122 | 0.0107 |
| 368 | 0.6830 | 3 | 0.0248 | 0.02555 | -0.115 | -0.1180 | 0.0285 |
| 324 | 0.7495 | -1 | 0.0059 | 0.00600 | -0.121 | -0.1226 | 0.0097 |
| 335 | 0.7470 | 0 | 0.0066 | 0.00685 | -0.122 | -0.1249 | 0.0102 |
| 351 | 0.7470 | 1 | 0.0154 | 0.01581 | -0.134 | -0.1379 | 0.0205 |
| 328 | 0.6935 | 0 | 0.0060 | 0.00614 | -0.113 | -0.1144 | 0.0095 |
| 331 | 0.7295 | 0 | 0.0061 | 0.00623 | -0.117 | -0.1188 | 0.0098 |
| 335 | 0.7470 | 0 | 0.0066 | 0.00685 | -0.122 | -0.1249 | 0.0098 |
| 342 | 0.7570 | 0 | 0.0070 | 0.00723 | -0.124 | -0.1265 | 0.0103 |
| 336 | 0.7650 | 0 | 0.0097 | 0.01001 | -0.133 | -0.1370 | 0.0120 |
| 341 | 0.7750 | 0 | 0.0129 | 0.01330 | -0.140 | -0.1441 | 0.0153 |

Index "corr": Corrected for side-wall and adapted for zero blockage and lift interference
W/o index "corr": Adapted for zero blockage and lift interference
Note: For $M_\infty$, $Re_c$, $C_L$ and $C_{Lcorr}$ see Table III

ONERA/CERT Test set-up

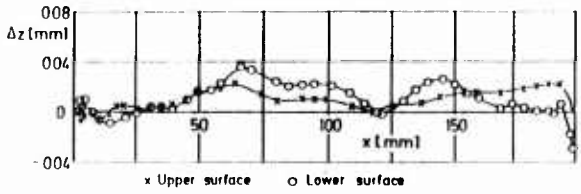



Note that the model was tested in two positions

**Figure 1:** Test section and model arrangement




Maximum thickness: 11.8 % at 35 %c
Base thickness: 0.5 %
Design conditions: $M_\infty = 0.76$ $C_L = 0.573$ $\alpha = 0^o$

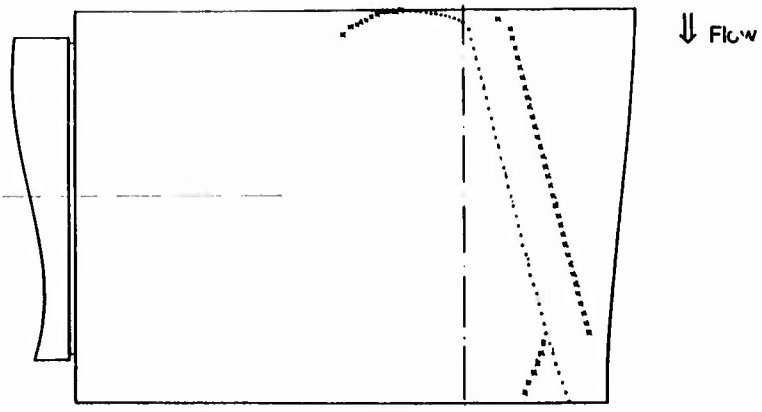



Contour deviations

| SURFACE: | UPPER | LOWER |
|---|---|---|
| x/c | z/c | z/c |
| 0.0000 | 0.000000 | 0.000000 |
| 0.0004 | 0.003365 | -0.003190 |
| 0.0010 | 0.005305 | -0.005060 |
| 0.0020 | 0.007535 | -0.007135 |
| 0.0035 | 0.010125 | -0.009270 |
| 0.0050 | 0.012295 | -0.010820 |
| 0.0075 | 0.015340 | -0.012695 |
| 0.0125 | 0.020110 | -0.015055 |
| 0.0350 | 0.032730 | -0.020850 |
| 0.0475 | 0.037700 | -0.023625 |
| 0.0650 | 0.043075 | -0.027130 |
| 0.0875 | 0.048270 | -0.031020 |
| 0.1150 | 0.053035 | -0.035180 |
| 0.1550 | 0.058090 | -0.040400 |
| 0.2150 | 0.063125 | -0.046320 |
| 0.2750 | 0.066165 | -0.049645 |
| 0.3350 | 0.067865 | -0.050270 |
| 0.3950 | 0.068510 | -0.048365 |
| 0.4550 | 0.068165 | -0.044305 |
| 0.5150 | 0.066765 | -0.038540 |
| 0.5750 | 0.064155 | -0.031525 |
| 0.6350 | 0.060080 | -0.023715 |
| 0.6950 | 0.054230 | -0.015660 |
| 0.7550 | 0.046385 | -0.008095 |
| 0.8150 | 0.036620 | -0.002085 |
| 0.8750 | 0.025410 | 0.001040 |
| 0.9200 | 0.016510 | 0.000785 |
| 0.9500 | 0.010505 | -0.000625 |
| 0.9775 | 0.004950 | -0.002626 |
| 1.0000 | 0.000355 | -0.004655 |

Airfoil CAST 7 section design coordinates

**Figure 2:** Airfoil shape, design coordinates and contour deviations




● Upper surface x Lower surface

**Figure 3:** Pressure orifice locations

ONERA/CERT T2 Wind Tunnel

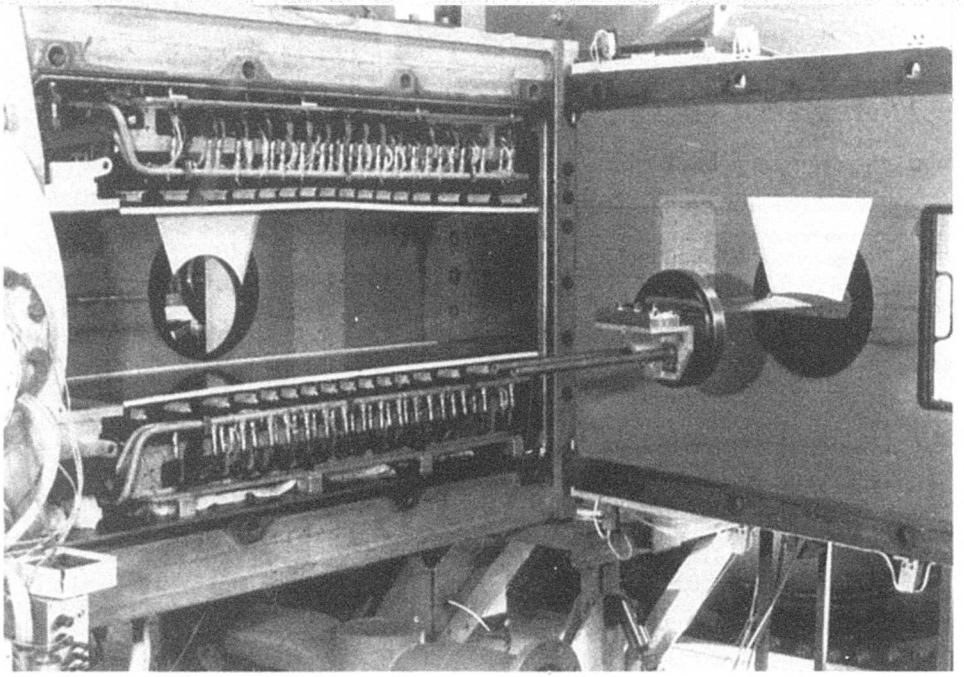
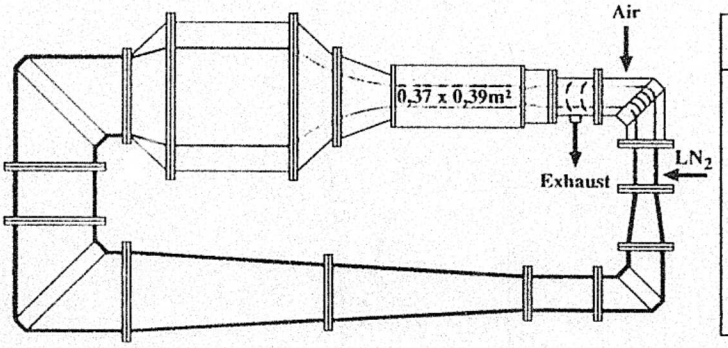


**Figure 4:** Model support and test section details

- **Transonic**
- **Pressurized**
- **Self - Adaptative Walls**
- **Cryogenic**




| Usual range | | |
|---|---|---|
| 0.6 < | $M_0$ | < 0.9 |
| 1.6b < | $P_t$ | < 3b |
| 110K < | $T_t$ | < 290K |
| $3x10^6$ < | $R_c$ | < $30x10^6$ |
| 100mm < | Chord | < 200mm |
| 0.5' < | Run duration | < 2' |

**Figure 5:** T2 Wind tunnel circuit and operating conditions

ONERA/CERT T2 Wind Tunnel

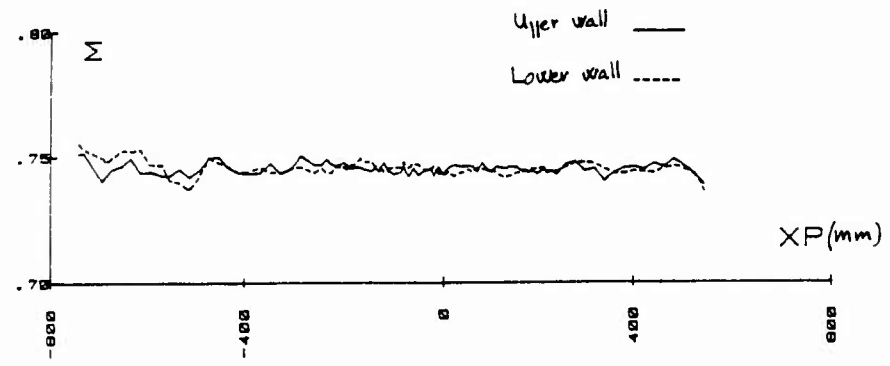



**Figure 6:** Mach number distribution in the adaptive wall test section

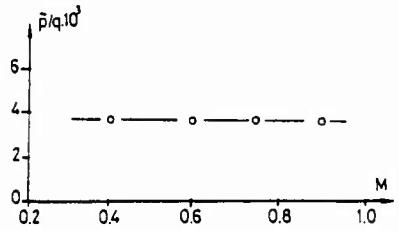



**Figure 7:** Mach number variation of RMS pressure fluctuation on tunnel side wall

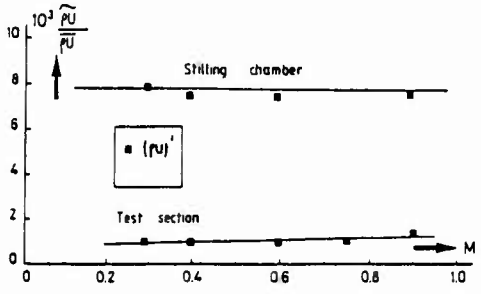



**Figure 8:** Mach number variation of RMS velocity fluctuation on tunnel side wall

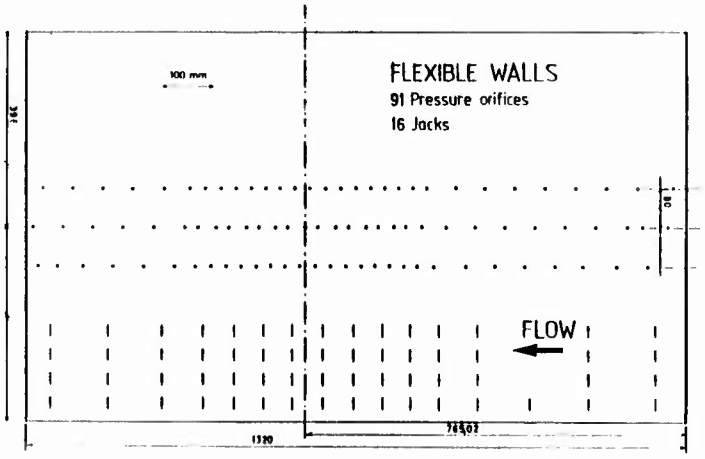



**Figure 9:** Location of wall pressure orifices and jacks

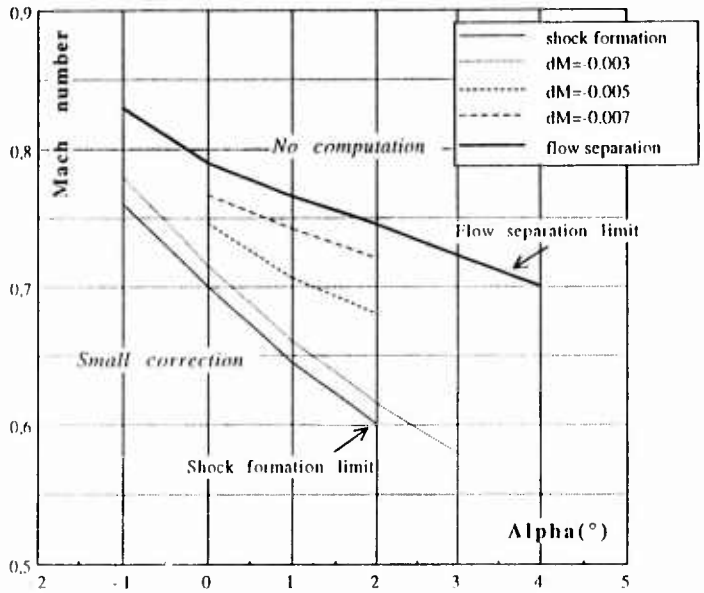



**Figure 10:** Mach number correction due to side-wall effects (CAST 7 tests with b/c=2.67)

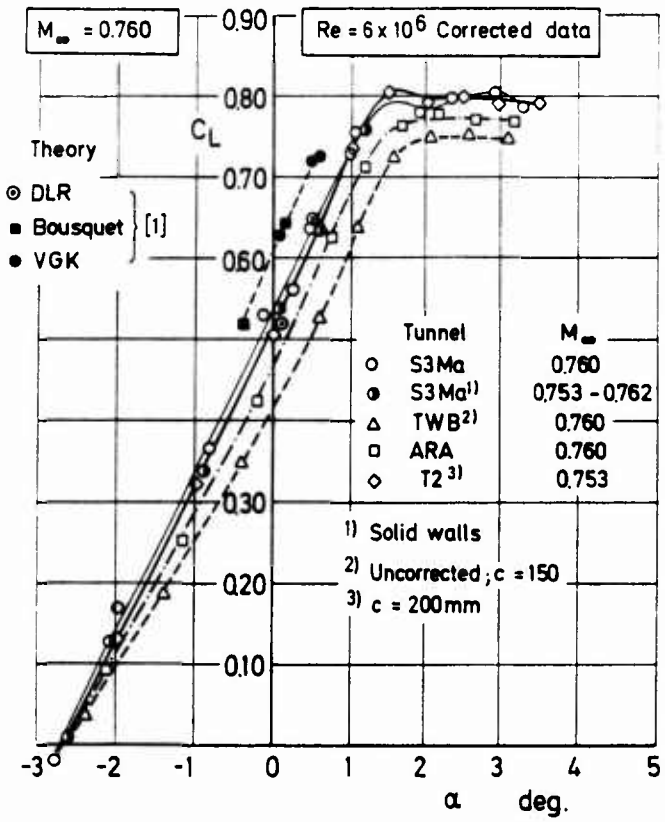



**Figure 11:** Comparison of lift versus angle of attack for various wind tunnels ( also see Note 7.4 )

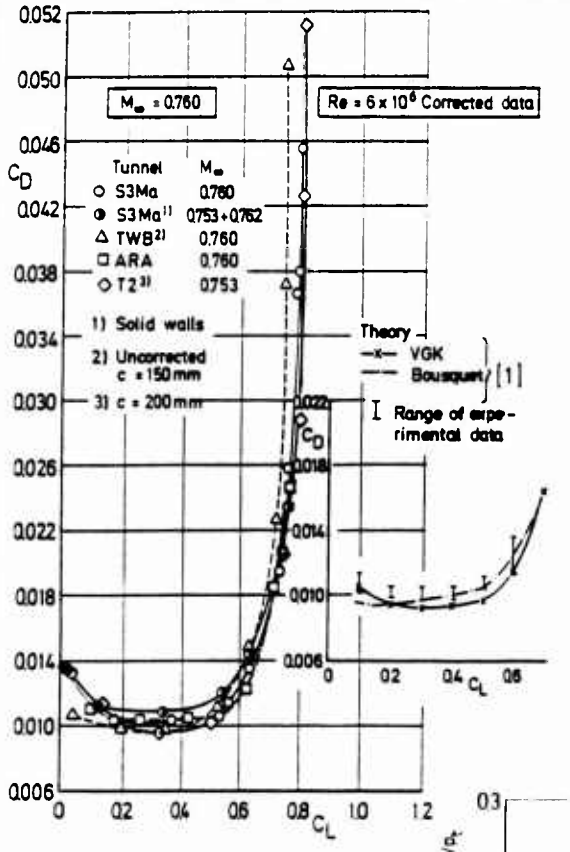



**Figure 12:** Comparison of drag polars from various wind tunnels ( also see Note 7.4 )

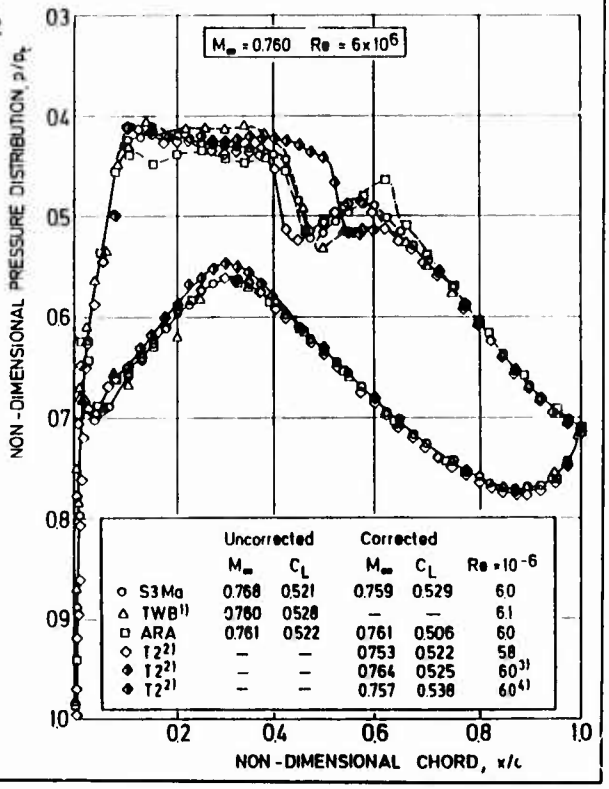



**Figure 13:** Comparison of pressure distributions from various wind tunnels; ( design conditions )

Indices:
1) c=150 mm
2) c=200 mm
3) Top and bottom wall only
4) Top and bottom wall plus side-walls

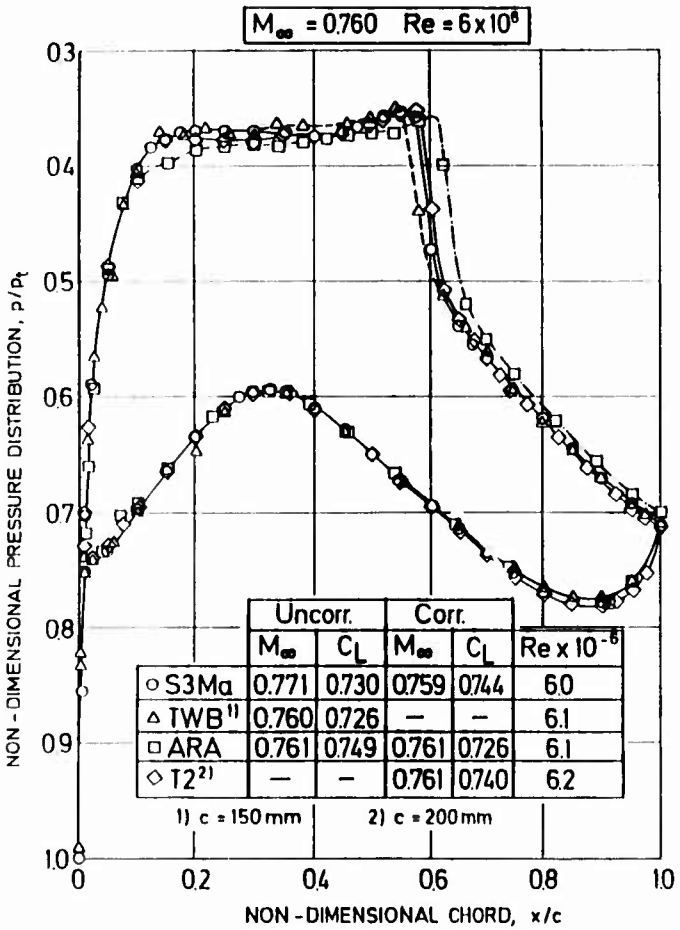



**Figure 14:** Comparison of pressure distributions from various wind tunnels ( high lift conditions )

# OAT15A AIRFOIL DATA

by
A.M. RODDE, J.P. ARCHAMBAUD
ONERA (FRANCE)

## 0 INTRODUCTION

The OAT15A airfoil is a supercritical airfoil for transport aircraft designed a few years ago within the framework of an ONERA/Aerospatiale joint programme devoted to the study of various designs.

The design point is M = 0.73, $C_z$ = 0.65 and the thickness to chord ratio of the airfoil is 12.3 %.

The tests which were performed in the ONERA/CERT T2 wind tunnel were devoted to the Reynolds number effects on the airfoil performance. These effects were investigated within the range 3-20 $10^6$ taking advantage of the cryogenic capability of the tunnel. The adaptative top and bottom walls of the tunnel give quasi free air conditions. However some sidewall effects are present and are taken into account in the correction procedure.

Tests performed on another model in the S3MA wind tunnel with perforated top and bottom walls show good agreement with the T2 tests which give more confidence concerning the quality of the data.

The proposed test cases concern mainly pressure distributions for various Reynolds numbers with fixed transition. However for a selected number of test cases boundary layer measurements with an external probe and LDV flow field data are also given.

The set of data can be used for different purposes :

- Computer code capability for the prediction of Reynolds number effect.
- Detailed 2D computer code assessment.

## 1. General Description

| | | |
|---|---|---|
| 1.1 | Model name or designation | OAT15A |
| 1.2 | Model type and flow conditions | 2-D supercritical airfoil transonic flow |
| 1.3 | Design requirements, purpose of tests | Design point of the airfoil:<br>M = 0.73 $C_z$ = 0.65<br>Reynolds number effect on the airfoil performance |
| 1.4 | Dominant flow physics | Transonic flow with shock B.L. interaction |
| 1.5 | Additionnal remarks | Tests were performed in the T2 wind tunnel with adapted top and bottom walls but without lateral boundary layer control. The lateral wall effect did not appear to be negligible; therefore this effect has been corrected. |

## 2. Details of model

| | | |
|---|---|---|
| 2.1 | General geometric arrangement | 2-D wall to wall model (see figure 1) |
| 2.2 | If various configurations are tested, describe specific features of each configuration | No |
| 2.3 | Wing and/or airfoil data | |
| | 2.3.1 Planform | Rectangular model<br>0.39 m span with 0.15 m chord gives aspect ratio of 2.6. |

| | | |
|---|---|---|
| | 2.3.2 Basic wing section or airfoil | |
| | . airfoil shape | See figure 1 |
| | . thickness/chord ratio | 0.123 maximum thickness/chord |
| | . nose raduis/chord | ~ 0.026 |
| | 2.3.3 Other components on wing | n.a. |
| 2.4 | Body data | n.a. |
| 2.5 | Informations on fins, canard... | n.a. |
| 2.6 | Engine data.. | |
| 2.7 | Geometric definition of all components | |
| | . Is shape analytically or numerically specified? | shape numerically specified |
| | . Design or measured co-ordinates | design co-ordinates |
| | . Tolerances | ±0,02 mm |
| | . Surface roughness | Polished to 0.2 µm |
| 2.8 | Model support details | It is a wall to wall model supported by lateral disks allowing angle of attack variations |

3. General tunnel information

| | | |
|---|---|---|
| 3.1 | Tunnel designation | T2 wind tunnel |
| 3.2 | Organization running the tunnel | ONERA/CEPT |
| 3.3 | Tunnel characteristics | |
| | . type of tunnel | Cryogenic-adaptative walls-induction driven |
| | . indicate operating envelope | Stagnation pressure variation 1.2 to 3.2 bars<br>Stagnation temperature variation 300° K down to 130° K<br>Mach number variation .4 to .9 |
| | . minimum run tire | Blow-down runs between 20 and 60 s |
| 3.4 | Test section | |
| | 3.4.1 Model installation | Rectangular test section (see figure 2) |
| | 3.4.2 Test section dimensions | Width: 390 mm<br>Height: 370 mm<br>Length: 1300 mm |
| | 3.4.3 Wall geometry details | |
| | . type of walls | Solid flexible top and bottom walls<br>Solid side walls |
| | . open area ratio | n.a. |
| | . are wall pressures/wall displacements measured | 91 pressure taps on top and on bottom walls.<br>16 electric actuators for each wall |
| | . typical wall boundary layer displacement thickness | Lateral boundary layer displacement thickness $\delta_1$ = 2.5 mm |

3.5 Freestream conditions

| | |
|---|---|
| 3.5.1 How are reference flow conditions determined for total pressure static pressure, static temperature | Total pressure and total temperature are measured in the settling chamber. The infinite Mach number is computed from the pressure wall measurements (adaptation strategy) |
| 3.5.2 Tunnel calibration | |
| . How was the tunnel calibrated? | The tunnel has been calibrated by empty test section test |

3.6 Flow quality (empty tunnel)

| | |
|---|---|
| 3.6.1 Flow uniformity | |
| . Static pressure/Mach number variations over model length and span | No static pressure/Mach number gradient over the model length<br>The divergent shape of flexible walls compensate the displacement thickness effect of the boundary layers on the four walls (see figure 3) |
| . Mach number variation during a run | The infinite Mach number is computed at each iteration from the Mach number distribution measured quasi-instantaneously at the flexible walls.<br>The test Mach number is known within ±0.002 for usual aerodynamic configurations |
| . How is average flow angularity determined | n.a. |
| 3.6.2 Temperature variation | |
| . Can the temperature be controlled during a run? | No temperature control for tests at ambient condition<br>Control for T < 250° K |
| . Variation within the tunnel | For T < 250° K $\Delta T < 1°$ K |
| . Variation over a run | Not measured |
| 3.6.3 Flow unsteadiness | |
| . Overall turbulence level | $\widetilde{\rho u}/\overline{\rho u} \sim 1\ 10^{-3}$ in the test section<br>$\widetilde{\rho u}$ : RMS value of the fluctuation<br>$\overline{\rho u}$ : mean value<br>(see figure 4) |
| . Overall noise level | $\tilde{p}/q \sim 3{,}6\ 10^{-3}$<br>$\tilde{p}$ : RMS fluctuating pressure<br>q : dynamic pressure<br>(see figure 5) |

4. Instrumentation

4.1 Model position

| | |
|---|---|
| 4.1.1 How is the geometrical incidence measured? | Inclinometer |
| 4.1.2 Accuracy of geometrical incidence | $\Delta\alpha = 0.02°$ |

4.2 Model pressure measurements

| | |
|---|---|
| 4.2.1 Total number and disposition of pressure holes | 56 pressures taps upper side 37<br>lower side 19<br>(see figure 6) |

| | | |
|---|---|---|
| 4.2.2 | Range and accuracy of pressure transducers | Range 15 and 25 psi<br>Accuracy 0.5 mb |
| 4.2.3 | Are dynamic pressures measured? | No |
| 4.3 | Force and moment measurements | No |
| 4.4 | Boundary layer and flow field measurements | |
| 4.4.1 | Measurement technique applied | An external pressure probe has been used for the boundary layer measurements.<br>LDV has been used for the flow field measurements |
| 4.4.2 | Flow regions investigated | Wake survey at half a chord behind the profile<br>Boundary layer behind the shock at 2 stations (X/C = 60% and 95%) (see figure 7)<br>Flow field around the shock (LDV)<br>(see figure 8 and figure 9) |
| 4.4.3 | Details of probe and probe supports | (see figure 10) |
| 4.5 | Surface flow visualization | Oil flow visualization were used to adjust the transition trips (no data available) |
| 4.6 | Flow field visualization | No |
| 4.7 | Tunnel wall measurements | |
| 4.7.1 | Types of measurements | The shape of the top and bottom walls as well as the pressure distributions on these walls are measured |
| 4.7.2 | Location and number of pressure holes | (see figure 11) |
| 4.8 | Other measurements and/or instrumentation used | No |

5. Test matrix and conditions

| | | |
|---|---|---|
| 5.1 | Detailed test matrix | |
| 5.1.1 | Number of selected test cases | 15 test cases |
| 5.1.2 | Number of configuration tested | 1 |
| 5.1.3 | Additional remarks | The model was tested at fixed Mach number 0.73. The proposed cases were made with fixed transition. The Reynolds number variation was from 3 to 20 x $10^6$ and the angle of attack variation was from 0° to 3° (see Table I) |
| 5.2 | Model/tunnel variations | |
| 5.2.1 | Maximum blockage | n.a. |
| 5.2.2 | Model span-tunnel cross section | n.a. |
| 5.2.3 | Wing area/tunnel cross section | n.a. |
| 5.2.4 | Height/chord ratio | 2.47 |

| | |
|---|---|
| 5.2.5 Width/chord ratio | 2.6 |
| 5.2.6 Have adiabatic wall temperatures been reached? | 1 < Tw/Taw < 1,05<br>Tw wall total temperature<br>Taw adiabatic wall total temperature |

5.3 Transition details

| | |
|---|---|
| 5.3.1 Was the test made with free or fixed transition? | The test has been made with fixed transition |
| 5.3.3 Details of fixed transition | |
| . Transition location | X/C = 0.07 at lower and upper surfaces |
| . Type and size of trip | Carborundum of 0.045 mm height |
| . How was effectiveness of trip verified? | The effectiveness of trip was verified by oil visualization |
| . For which flow conditions was effectiveness of trip verified? | The effectiveness of trip was verified at $Re = 3 \times 10^6$<br>See figure 12 the evolution of lift and drag coefficient with the Reynolds number |

6. Data

6.1 Availability of data

| | |
|---|---|
| 6.1.1 Organisation owning the data | O.N.E.R.A. |
| 6.1.2 Who is responsible for the data | Mrs RODDE Anne-Marie<br>Aerodynamics Department<br>O.N.E.R.A. BP N° 72<br>92320 Châtillon Cedex<br>Fax number: 33 46 73 41 46<br>Phone number: 33 46 73 42 14 |
| 6.1.3 Are data freely available? | Yes |

6.2 Suitability of data for CFD validation

| | |
|---|---|
| 6.2.1 Are data suitable for "in-tunnel" calculations | No, data without sidewall correction are not proposed here |
| 6.2.2 Are data corrected to simulate "free air" conditions? | Data are corrected to take into account the sidewall effects; so data are suitable for "free-air" calculations |

6.3 Type and form in which data are available

| | |
|---|---|
| 6.3.1 Type and form | Airfoil<br>pressure coefficient<br>wake drag coefficient<br>Boundary layer<br>static pressure<br>total pressure<br>Flow field<br>mean and fluctuating<br>velocities (u,v,u',v',u'v') |
| 6.3.2 Data carrier | Floppy disk |

| | |
|---|---|
| 5.2.5 Width/chord ratio | 2.6 |
| 5.2.6 Have adiabatic wall temperatures been reached? | 1 < Tw/Taw < 1,05<br>Tw wall total temperature<br>Taw adiabatic wall total temperature |
| 5.3 Transition details | |
| 5.3.1 Was the test made with free or fixed transition? | The test has been made with fixed transition |
| 5.3.3 Details of fixed transition | |
| . Transition location | X/C = 0.07 at lower and upper surfaces |
| . Type and size of trip | Carborundum of 0.045 mm height |
| . How was effectiveness of trip verified? | The effectiveness of trip was verified by oil visualization |
| . For which flow conditions was effectiveness of trip verified? | The effectiveness of trip was verified at $Re = 3 \times 10^6$<br>See figure 12 the evolution of lift and drag coefficient with the Reynolds number |

6. Data

| | |
|---|---|
| 6.1 Availability of data | |
| 6.1.1 Organisation owning the data | O.N.E.R.A. |
| 6.1.2 Who is responsible for the data | Mrs RODDE Anne-Marie<br>Aerodynamics Department<br>O.N.E.R.A. BP N° 72<br>92320 Châtillon Cedex<br>Fax number: 33 46 73 41 46<br>Phone number: 33 46 73 42 14 |
| 6.1.3 Are data freely available? | Yes |
| 6.2 Suitability of data for CFD validation | |
| 6.2.1 Are data suitable for "in-tunnel" calculations | No, data without sidewall correction are not proposed here |
| 6.2.2 Are data corrected to simulate "free air" conditions? | Data are corrected to take into account the sidewall effects; so data are suitable for "free-air" calculations |
| 6.3 Type and form in which data are available | |
| 6.3.1 Type and form | Airfoil<br>pressure coefficient<br>wake drag coefficient<br>Boundary layer<br>static pressure<br>total pressure<br>Flow field<br>mean and fluctuating<br>velocities (u,v,u',v',u'v') |
| 6.3.2 Data carrier | Floppy disk |

| | |
|---|---|
| 6.3.3 Extent of geometry data | ~ 20 000 octets |
| 6.3.4 Extent of aerodynamic test data | ~ 200 000 octets |
| 6.4 Corrections applied to data | |
| 6.4.1 Lift interference and blockage corrections? | No |
| 6.4.2 Side wall interference correction (2-D tests) | Yes |
| . Treatment of side wall boundary layer | No treatment |
| . Correction method used | The side wall effects are taken into account with the MICHONNEAU method (see Ref. 8.4) |
| 6.4.6 Other corrections | No |
| 7. Data accuracy and repeatability assessment | |
| 7.1 Estimate accuracy of | |
| 7.1.1 Free stream conditions | |
| . Mach number | ±0.002 |
| . Model incidence | ±0.02° |
| 7.1.2 Measured data | |
| . Pressure coefficients | ΔCp 1% |
| . Flow field data | Mean velocity 0.2 to 0.4% |
| 7.2 Repeat measurements | |
| 7.2.1 Type and number of repeat measurements within one test compain | Generally only one measurement is made<br>Figure 13 shows a typical example of repeat measurements for the pressure distribution |
| 7.3 Redundant measurements | None |
| 7.4 Other tests on same (nominal) geometry | |
| 7.4.1 Has the same model been measured in another wind tunnel | No |
| 7.4.2 Has a different model been measured in the same or another wind tunnel? | A model of 210 mm chord has been tested in ONERA/S3MA wind tunnel (with the same width/chord ratio)<br>See figure 14 the comparison of the overall forces |
| 8. References | |
| 8.1 On the wind tunnel | Adaptative wind tunnel walls<br>Technology and applications<br>AGARD Advisory Report 269 FDP WG 12<br>(April 1990) |
| 8.4 On the correction methods | J.P. ARCHAMBAUD, J.F. MICHONNEAU, A. MIGNOSI<br>Analysis of test section side wall effects on 2D aerofoils: Experimental and numerical investigation.<br>AGARD-FDP Symposium, Brussels, 1993. |

TABLE I - TEST MATRIX TABLE

| IDENTIFICATION | | FLOW CONDITION | | | POSITION | OTHER INFORMATION | |
|---|---|---|---|---|---|---|---|
| CASE N° | CONF. | MACH | qkPa | Rey x $10^6$ | α° | Type of measure-ments | Remarks |
| 1-5 | TD | 0,724 | 40-80 | 3/6/11 15/20 | 1,15 | a,b | |
| 6-9 | TD | 0,724 | 40-80 | 3/6/11 15 | 3 | a,b | |
| 10-13 | TD | 0,724 | 40 | 3 | 0/1,15 2/3 | a,b,c | B.L. measurements X/C=60 % X/C=95 % |
| 14-15 | TD | 0,724 | 40 | 3 | 1,15/2 | a,d | Flow field measure-ments (x,y,u,v,u', v',u'v') |

Legend : a pressures
b wake drag coefficient
c boundary layer
d flow field

TD Fixed transition

TABLE II - TABLE INDICATING DATA AVAILABILITY

| DATA | ENGIN. UNITS | COEFFICIENTS | NORMALIZED | UNCORRECTED | CORRECTED |
|---|---|---|---|---|---|
| FREESTREAM CONDITIONS | X | | | | X |
| SURFACE PRESSURES | | X | | | X |
| HEATTRANSFER SKINFRICTION | | | | | |
| FORCES | | X | | | X |
| BOUNDARY LAYER DATA | | | X | | X |
| WAKE DATA | | | X | | X |
| FIELD DATA | | | X | | X |
| TEST SECTION WALL POSI-TIONS | | | | | |

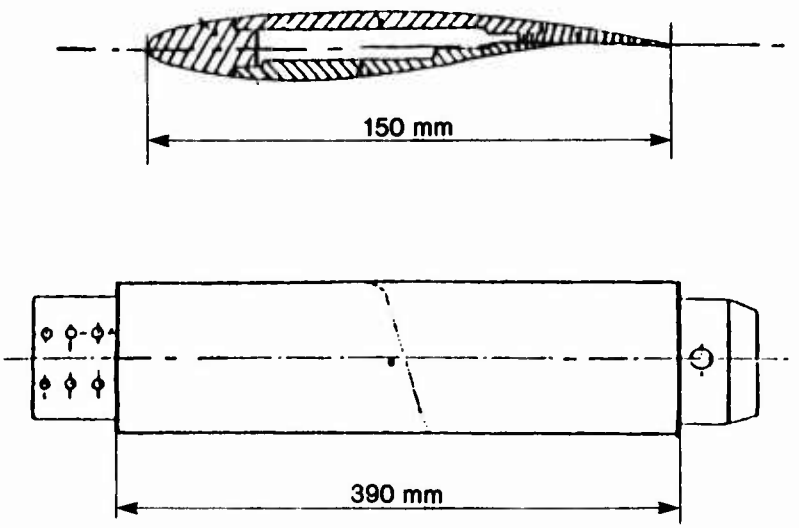



Fig 1 : OAT15A MODEL

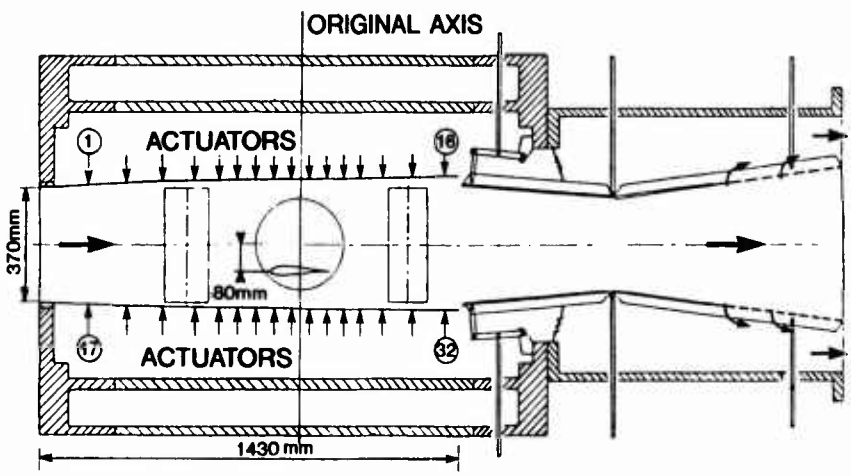



Fig 2 : T2-TEST SECTION

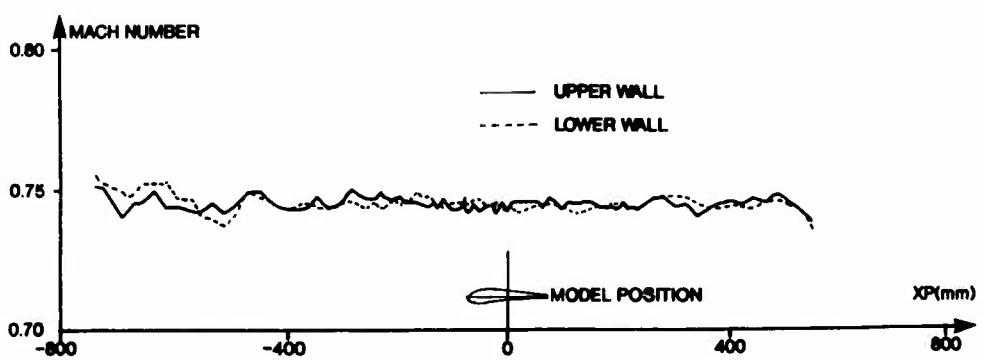



Fig 3 : MACH NUMBER VARIATION IN THE TEST SECTION

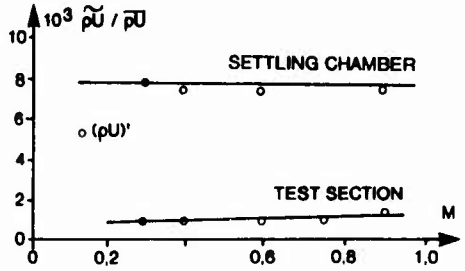



Fig 4 : MACH NUMBER VARIATION OF RMS VELOCITY-FLUCTUATION LEVEL ON A SIDEWALL OF TUNNEL T2 AT ONERA/CERT

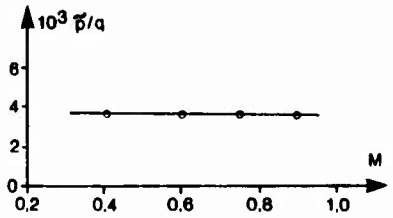



Fig 5 : MACH NUMBER VARIATION OF RMS PRESSURE-FLUCTUATION NOISE LEVEL ON A SIDEWALL OF TUNNEL T2 AT ONERA/CERT



Fig 6 : LOCATION OF PRESSURE HOLES

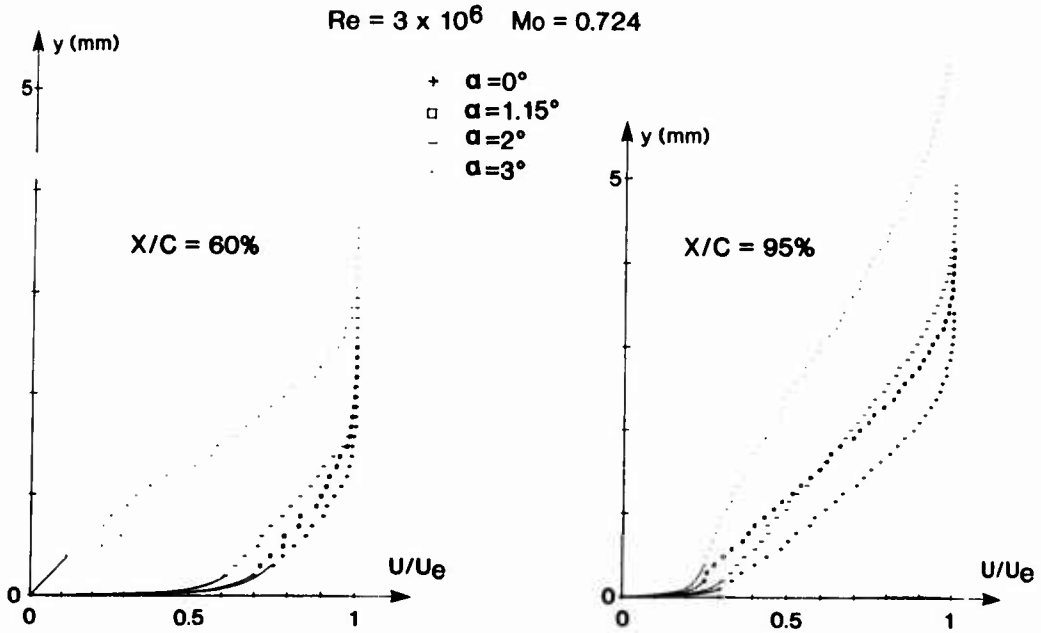
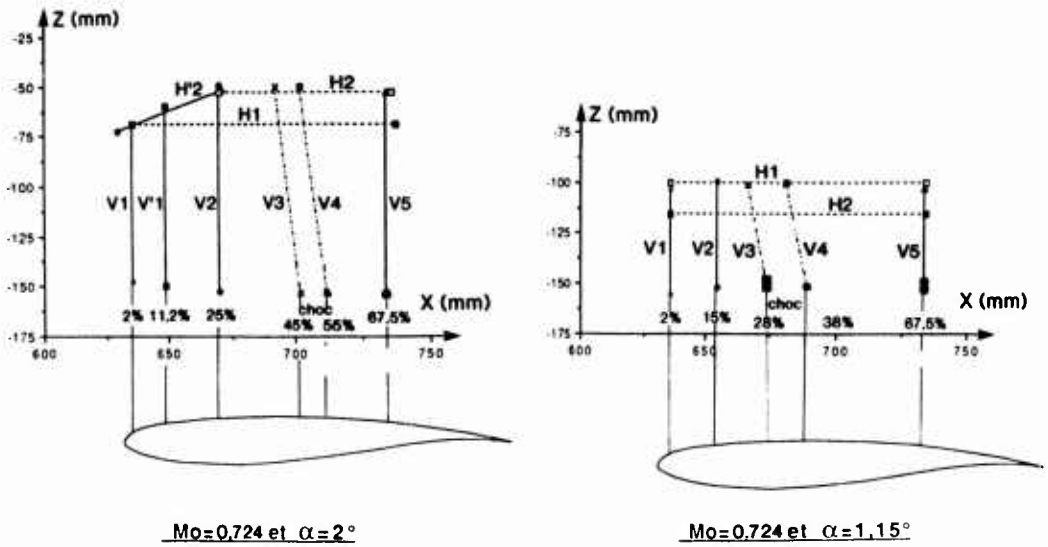
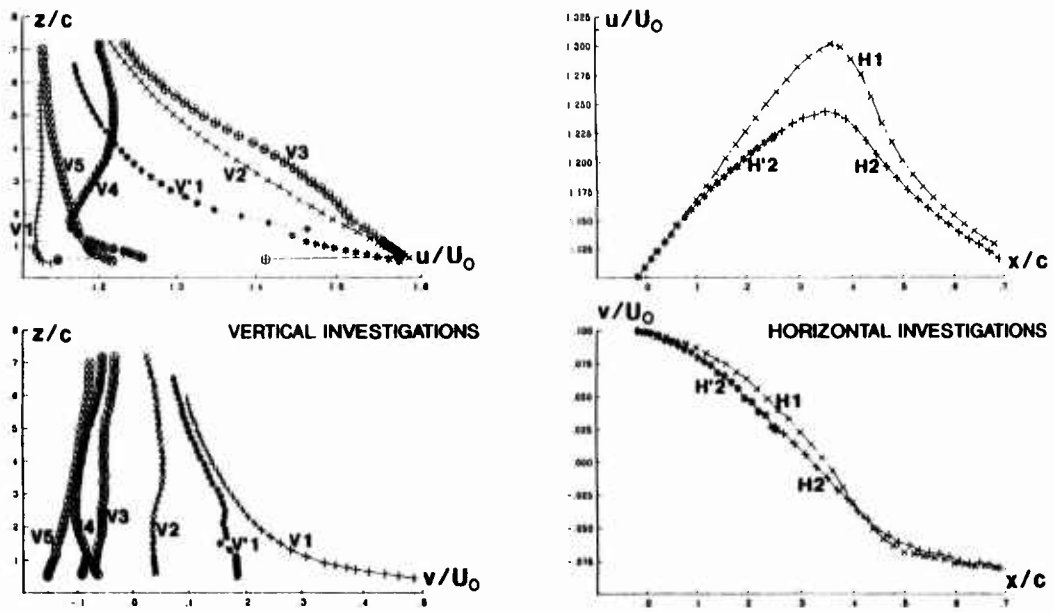



Fig 7 : BOUNDARY LAYER MEASUREMENTS




Mo=0,724 et $\alpha = 2°$ Mo=0,724 et $\alpha = 1,15°$

Fig 8 : DETAILS OF THE FLOW FIELD INVESTIGATIONS




$M_0 = 0.724$ $\alpha = 2°$ $Re = 3 \times 10^6$

Fig 9 : EXAMPLE OF FLOW FIELD MEASUREMENTS (MEAN VELOCITIES)

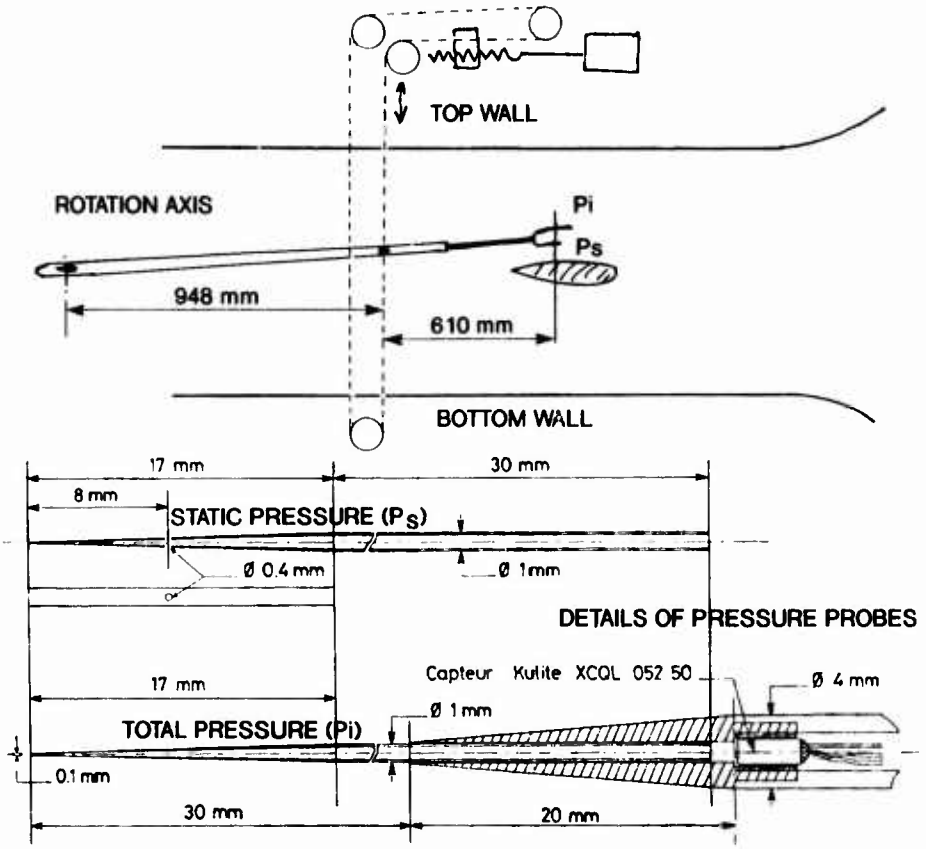



Fig10: BOUNDARY LAYER AND WAKE MEASUREMENT DETAILS

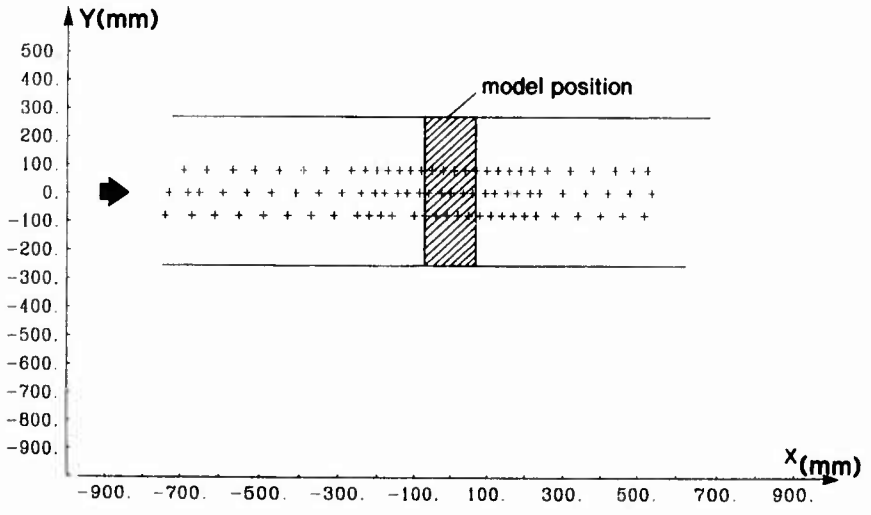



Fig 11 : PRESSURE HOLES ON THE TOP/ BOTTOM WALL

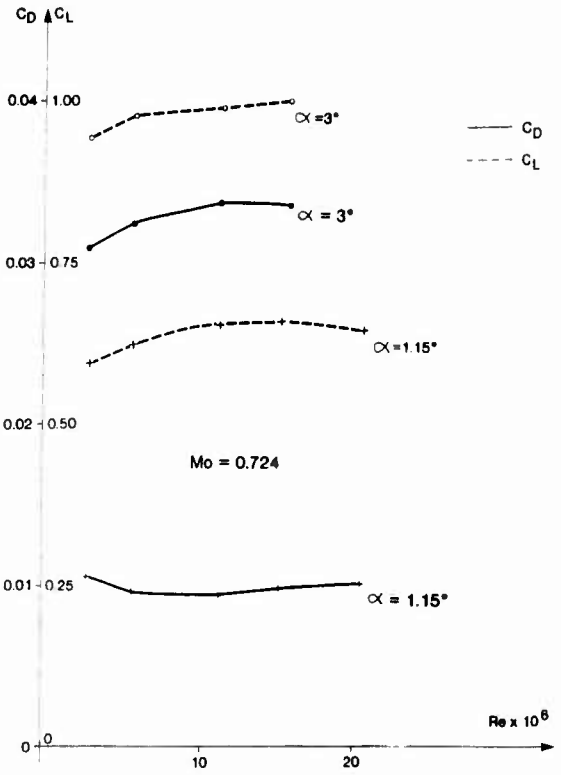



Fig. 12 EVOLUTION OF LIFT AND DRAG COEFFICIENTS WITH REYNOLDS NUMBERS

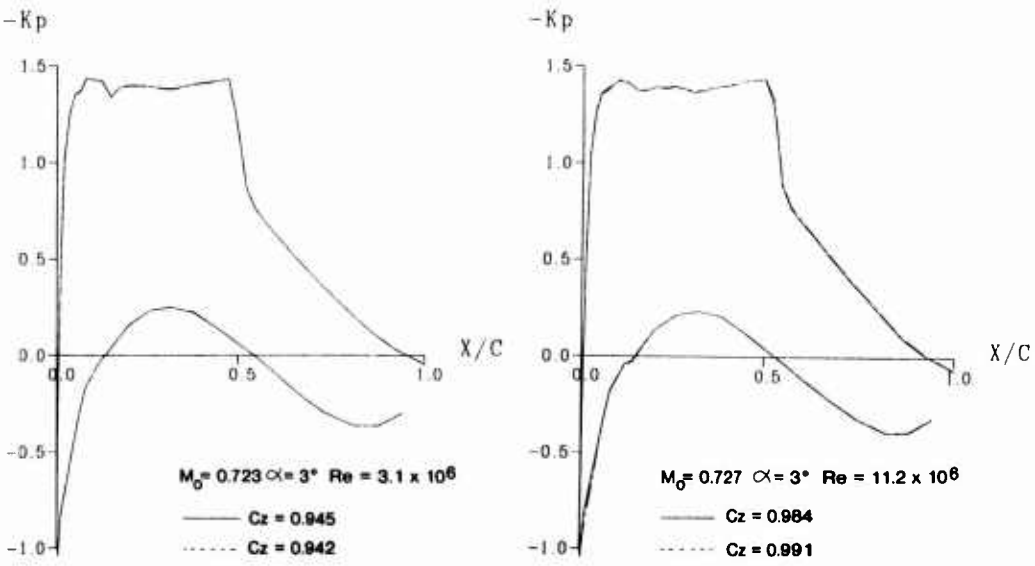



**Fig 13 : TYPICAL EXAMPLES OF REPEAT MEASUREMENTS FOR THE PRESSURE DISTRIBUTIONS**

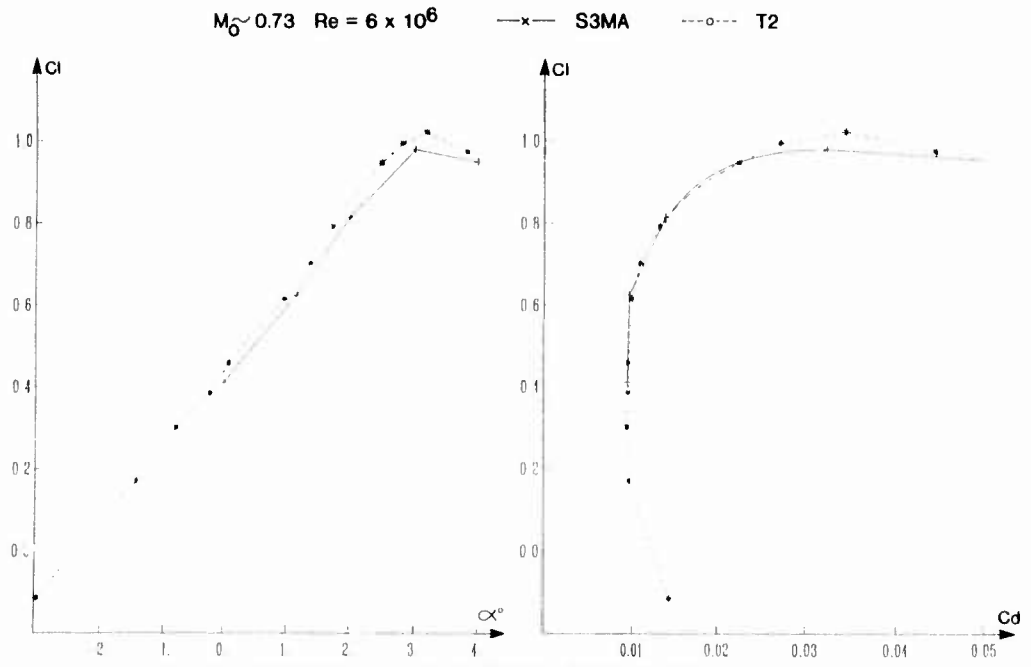



Fig 14 : COMPARISON OF OVERALL FORCES ON THE OAT15A T2 AND S3MA WIND-TUNNELS

# A SUPERCRITICAL AIRFOIL EXPERIMENT

**George G. Mateer**
**H. Lee Seegmiller**
**Lawrence A. Hand**
NASA Ames Research Center, Moffett Field, California
and
**Joachim Szodruch**
MBB Transport-und Verkehreflugzeuge, Bremen, West Germany

## 0. INTRODUCTION

The purpose of this investigation is to provide a comprehensive data base for the validation of numerical simulations. The initial results of the study (single angle of attack) were presented in ref.1, where the effects of various parameters and the adequacies of selected turbulence models were discussed. The objective of the present paper is to provide a tabulation of the experimental data. The data were obtained in the two-dimensional, transonic flowfield surrounding a supercritical airfoil. A variety of flows were studied in which the boundary layer at the trailing edge of the model was either attached or separated. Unsteady flows were avoided by controlling the Mach number and angle of attack. Surface pressures were measured on both the model and wind tunnel walls, and the flowfield surrounding the model was documented using a laser Doppler velocimeter (LDV). Although wall interference could not be completely eliminated, its effect was minimized by employing the following techniques. Sidewall boundary layers were reduced by aspiration, and upper and lower walls were contoured to accommodate the flow around the model and the boundary-layer growth on the tunnel walls. A data base with minimal interference from a tunnel with solid walls provides an ideal basis for evaluating the development of codes for the transonic speed range because the codes can include the wall boundary conditions more precisely than interference corrections can be made to the data sets.

## 1. GENERAL DESCRIPTION

### 1.1 Model name or designation

Messerschmitt-Bolkow-Blohm - VA-2

### 1.2 Model type and flow conditions

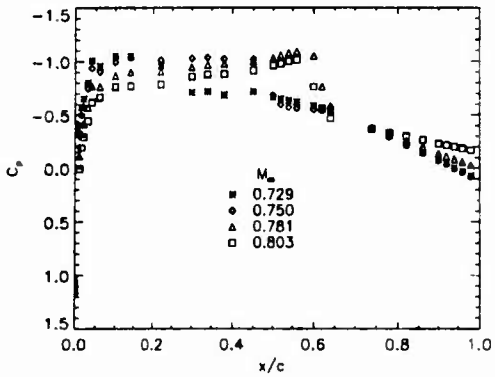
A 2-D, supercritical airfoil that combines high lift and low drag with moderate rear loading, was tested at $0.73 < M_\infty < 0.80$, $0.5° < \alpha < 1.5°$ and at a nominal Reynolds number of $6 \times 10^6$. These conditions were sufficient to produce both separated and attached flows on the upper surface of the model.

### 1.3 Design requirements, purpose of test

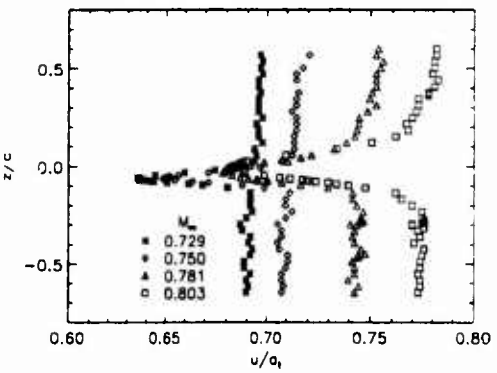
Extensive flowfield and surface pressure measurements in a tunnel with minimal wall interference provides an ideal basis for evaluating codes in the transonic speed range.

### 1.4 Dominant flow physics

Interactions between the shoc wave and turbulent boundary layer on the upper surface produce a variety of separated and attached flows at the trailing edge (see fig. 1).




**(a) wing upper surface pressures.**




**(b) wake velocities; x/c=2.5.**

**Figure 1.- Sample data; $\alpha$=0.9°, Re=6x10$^6$.**

### 1.5 Additional remarks

This data base can be used to validate the ability of codes to describe the development of separation on the surface of the airfoil as well as its influence on the surrounding flowfield.

## 2. DETAILS OF MODEL

### 2.1 General geometric arrangement

Constant chord model that spanned the width of the tunnel (see fig. 2).

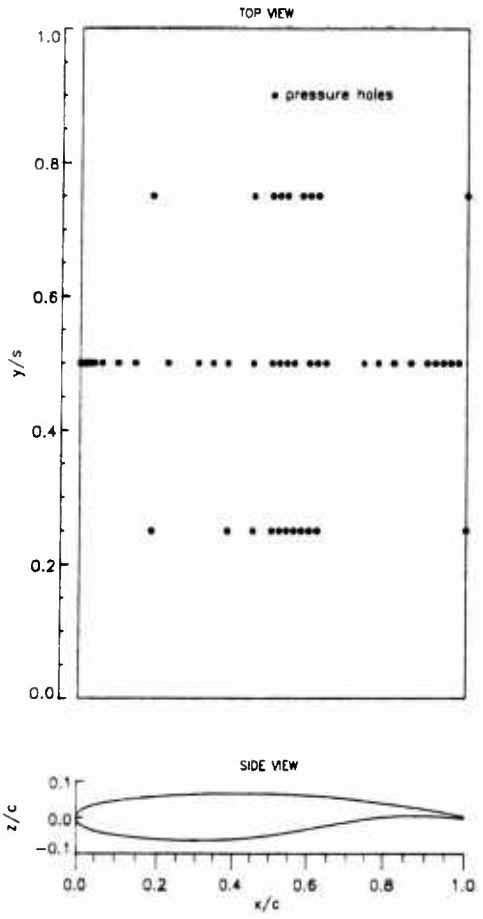



**Figure 2.- Model geometry.**

### 2.2 Configurations

A single model configuration was tested

### 2.3 Wing and/or airfoil data

#### 2.3.1 *Planform*

Aspect ratio = 2.032

Taper ratio = 0

Leading edge sweep = 0

Trailing edge sweep = 0

Twist distribution = no twist

#### 2.3.2 *Basic wing section or airfoil*

The airfoil section is shown in fig. 2 and the coordinates are included with the data. The basic dimensions are:

chord=200mm

max. thickness=13% chord

trailing edge thickness=0.522% chord.

#### 2.3.3 *Other components on wing*

There were no other components on the wing.

### 2.4 Body data

This was a wing-alone experiment.

### 2.5 Information on fins, canard wings and/or vertical/horizontal tail surfaces

There were no fins canards, etc. on the wing

### 2.6 Engine/pylon/nacelle data

No engines, pylons, or nacelles were on the wing.

### 2.7 Geometric definition of all components

The shape of this model was numerically specified and the differences between the design and measured co-ordinates are shown in fig. 3.

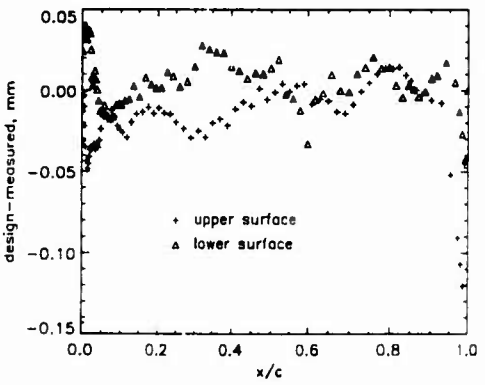



**Figure 3.- Model tolerances.**

### 2.8 Model support details

The model was supported by the tunnel sidewalls with pins as shown in fig. 4.

## 3. GENERAL TUNNEL INFORMATION

### 3.1 Tunnel designation

High Reynolds Number Channel II

### 3.2 Organization running the tunnel

Thermo-Physics Facilities Branch

NASA-Ames Research Center

### 3.3 Tunnel characteristics

This blowdown facility is described in detail in ref. 2. It was designed to operate subsonically using unheated, dry air at ambient temperature. The high Reynolds number capability is achieved by testing at elevated total pressures which provide a unit Reynolds number range of $3x10^6$ to $2x10^8$ per meter, for freestream Mach numbers from 0.6 to 0.8. Run times vary between 1 and 30 minutes depending on the total pressure, however, typical runtimes for this test were 1.5 to 2 minutes.

### 3.4 Test section

#### 3.4.1 *Drawing*

The investigation was conducted in the NASA-Ames High Reynolds Number Channel II (fig. 4).

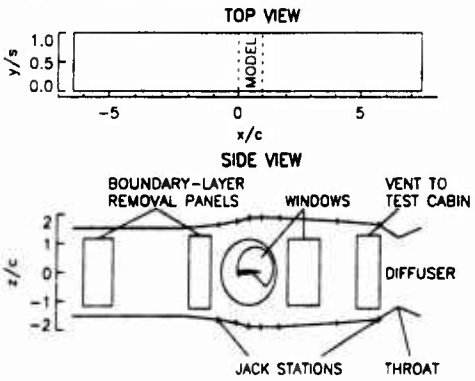



**Figure 4.- Test section.**

The test section is located inside a pressure shell which is maintained at essentially free-stream static pressure by side-wall vent panels located just upstream from the throat. This technique alleviates many of the structural problems associated with high pressure testing by reducing the pressure difference across the test section walls.

#### 3.4.2 *Test section dimensions*

Width = 40.64 cm

Height = 60.96 cm

Length = 279.40 cm

#### 3.4.3 *Wall geometry details*

The influence of the wind tunnel walls on the flow is attenuated by, 1) suction to reduce the sidewall boundary layers and 2) contouring the upper and lower walls to allow for flow expansion. The sidewall suction panels are shown in fig. 4. The upstream panel removed 4.5% of the total mass flow in the tunnel and the downstream panel removed an additional 1%. Contouring accounts for wall boundary-layers, suction, and the model. The magnitude of each of these corrections is shown in table I below. Boundary-layer growth corrections were determined by running the tunnel empty and diverging the top and bottom walls (in their straight configuration), until the Mach number was constant along the tunnel axis. Tunnel sidewall boundary layers were not measured in this test but they are documented in ref. 2. The area-ruling technique described in ref. 2 was used to correct for sidewall mass removal. Airfoil code validation computations that specify upper and lower solid wall shape boundaries with no slip velocity conditions should subtract the boundary layer and suction corrections from the final settings listed in table I. Finally, the flow expansion around the model was accounted for by adding the displacement of the computed (ref. 1,5), free-air streamlines (upper and lower). A single free-air case was used, corresponding to a freestream Mach number of 0.78 and an angle-of-attack of 1 degree. These streamlines were selected by specifying that they must contain the flex-points of the upper and lower walls. The flex-point is defined as the first position on the wall that is no longer rigid. It was determined experimentally from the wall pressures during the boundary layer growth correction study and was the same for both walls.

**Table I: Wall Coordinates**

| Jack Station | x/c | Straight wall setting (z/c) | Boundary layer correction (Δz/c) | Suction correction (Δz/c) | Streamline curvature (Δz/c) | Final setting (sum cols. 3-6) (z/c) |
|---|---|---|---|---|---|---|
| | Upper Wall | | | | | |
| 1 | -0.770 | 1.524 | 0.0081 | -0.0229 | 0.0271 | 1.5363 |
| 2 | -0.008 | 1.524 | 0.0114 | -0.0229 | 0.0530 | 1.5655 |
| 3 | 0.500 | 1.524 | 0.0137 | -0.0229 | 0.0630 | 1.5778 |
| 4 | 1.008 | 1.524 | 0.0160 | -0.0229 | 0.0540 | 1.5711 |
| 5 | 1.770 | 1.524 | 0.0193 | -0.0229 | 0.0320 | 1.5524 |

| Jack Station | x/c | Straight wall setting (z/c) | Boundary layer correction (Δz/c) | Suction correction (Δz/c) | Streamline curvature (Δz/c) | Final setting (sum cols. 3-6) (z/c) |
|---|---|---|---|---|---|---|
| 6 | 4.104 | 1.524 | 0.0295 | -0.0229 | -0.0060 | 1.5246 |
| 7 | 5.739 | 1.524 | 0.0340 | -0.0229 | -0.0170 | 1.5181 |
| | Lower Wall | | | | | |
| 1 | -0.770 | -1.524 | -0.0081 | 0.0229 | 0.0100 | -1.4992 |
| 2 | -0.008 | -1.524 | -0.0114 | 0.0229 | 0.0090 | -1.5035 |
| 3 | 0.500 | -1.524 | -0.0137 | 0.0229 | 0.0080 | -1.5068 |
| 4 | 1.008 | -1.524 | -0.0160 | 0.0229 | 0.0070 | -1.5101 |
| 5 | 1.770 | -1.524 | -0.0193 | 0.0229 | 0.0010 | -1.5194 |
| 6 | 4.104 | -1.524 | -0.0295 | 0.0229 | -0.0240 | -1.5546 |
| 7 | 5.739 | -1.524 | -0.0340 | 0.0229 | -0.0340 | -1.5691 |

Note: dz/dx=0 for x/c ≤ −3.516

### 3.5 Freestream conditions

#### 3.5.1 *Determination of reference flow conditions*

Free-stream Mach number was determined from a sidewall pressure tap located on centerline at x/c=-2.389 and a total pressure probe located at z/c=-0.889 below the static pressure tap. The diameter of the total pressure probe was 1.56 mm and it extended 5 cm into the flow. The cross sectional area of the probe and support was 0.2% of the test section area. The Mach numbers calculated from these measurements were corrected in two ways to arrive at the freestream value. First, the tunnel centerline Mach number was determined by correcting the sidewall value by -0.003 to account for spanwise nonuniformities in the flow (ref. 2). Second, the centerline value was corrected for the presence of the model by using the previous calculations of ref. 1,5. This correction was a linear function of the measured Mach number over the range of 0.73 to 0.80 and is given by the equation:

$$\text{correction}=-0.028507+0.044776*M$$

where M is the Mach number determined from the pressure measurements at x/c=-2.389.

For this blowdown facility the total temperature is a function of the run time. This variation was measured for each run with eight thermocouples located in the stagnation chamber. These data were then used to correct all temperature-dependent quantities (velocities, Reynolds numbers, etc.) to a constant total temperature of 264 °K.

#### 3.5.2 *Tunnel calibration*

The tunnel was last calibrated in 1982 using a pressure rake and the results are presented in ref. 2.

### 3.6 Flow quality (empty tunnel)

#### 3.6.1 *Flow uniformity*

The spanwise variation of Mach number was symmetrical about the tunnel centerline with the minimum value occurring on the centerline. The variation between the wall and centerline was -0.003. The longitudinal variation over the chord of the model was 0.001. Temporal variations of Mach number during a run were -0.002.

#### 3.6.2 *Temperature variation*

Total temperature cannot be controlled in this facility and it decreases with time during a typical run by about 11 °K. Between the stagnation chamber and the test section the total temperature is constant.

#### 3.6.3 *Flow unsteadiness*

Velocity: $\langle u' \rangle / u_\infty = 0.005$

Pressure: $\langle p' \rangle / q_\infty = 0.02$

## 4 INSTRUMENTATION

### 4.1 Model position

#### 4.1.1 *Measurement of geometrical incidence*

The geometrical incidence was measured with a Swiss Precision Instrument Co. Micro Level.

#### 4.1.2 *Accuracy of geometrical incidence*

± 0.03 deg.

### 4.2 Model pressure measurements

#### 4.2.1 *Total number and disposition of pressure holes*

The locations of the pressure orifices are shown on fig. 2. 60 pressures were measured at 50% span, 31 on the upper surface and 29 on the lower. Fewer measurements were made at 25% and 75% span on the upper surface only: 11 @ 25% and 9 @ 75%.

#### 4.2.2 *Range and accuracy of pressure transducers*

The static and total pressures used to determine the freestream Mach numbers were measured with Datametrics Inc., model 570D transducers and model 1015 signal conditioners. These systems were calibrated at intervals during the test with a Consolidated Electrodynamics Corp., type 6-201-001 primary pressure standard. Calibrations were done over 3 separate ranges (0-69, 0-310, and 0-690 kPa) for improved system accuracy. Based on these procedures and the specifications of the manufacturer, the overall system accuracy was estimated to be ±0.06% of reading. This translates to an uncertainty in Mach number of ±0.001. The remaining wall and wing pressures were measured with Pressure Systems Inc., ESP-32 modules having ranges of ±310 kPa. These units were mounted on constant temperature heaters to minimize temperature sensitivity of the calibrations. All modules were calibrated before each run over reduced ranges to minimize the uncertainty in the measurement. As a result of these measures the static error band was reduced to approximately ±0.08% of full scale reading and the corresponding uncertainty in pressure coefficient was ±0.006.

#### 4.2.3 *Dynamic pressures*

Dynamic pressures were not measured in this experiment.

### 4.3 Force and moment measurements

Force and moment balances were not used in this experiment.

### 4.4 Boundary layer and flow field measurements

#### 4.4.1 *Measurement technique*

The flowfield velocity data were obtained with a laser Doppler velocimeter developed exclusively for this facility (ref. 4). This two-component system employs a 4 watt argon laser utilizing the blue 488 nm and green 514.5 nm lines in forward scatter. One of each pair of beams is frequency-shifted 40 mhz to prevent directional ambiguity in the measurement plane. The two, fringe systems are orientated approximately ±45° to the x-direction. The beams are transmitted through a window in the pressure shell to an optical assembly that straddles the test section. This unit consists of a three-dimensional, computer-controlled scanning mechanism with mirrors, focusing lens, and receiving optics. Doppler signal is transmitted from the receiving optics through a 10 m optical fiber to photomultiplier tubes outside the tunnel. Because of large excursions in the traversing mechanism, provision was made to easily change the beam path lengths to place the beam waist at the fringe volume, thereby minimizing variations in fringe spacing. Since both the inner and outer optical assemblies were mounted directly to the pressure vessel, special consideration was given to reducing the transmission of vibration, and thermal or pressure strain to the optical components. In order to provide light-scattering particles of known aerodynamic response, the flow was seeded with polystyrene spheres 0.35 to 0.55 microns in diameter. A special atomizer was developed to insure a uniform distribution of seed in the core flow and to prevent deposition on the windows and side-wall suction panels. For this investigation 1792, simultaneous measurements of the blue and green velocities were made at each point in the flow. The nominal data rate was 500 samples per second although it varied somewhat from run to run and with location in the flowfield.

#### 4.4.2 *Flow regions investigated*

The flow in the wake was documented at two stations, x/c=1.04 & 2.5 (see fig. 7). Also, the flow above the wing including the shockwave was measured at various z/c locations for $0.1204 \le z/c \le 0.6325$. A sample of these data are shown in the following figure.

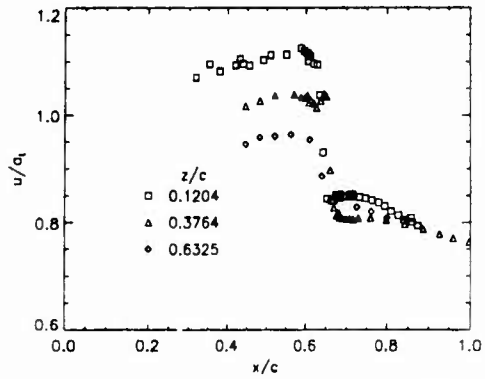



**Figure 5.- Flowfield above wing, α=1°, $M_\infty$=0.780, Re=2x10$^6$.**

### 4.5 Surface flow visualization

#### 4.5.1 *Measurement technique applied*

A mixture of vacuum pump oil and titanium dioxide was used to define the surface flow for a few selected cases to verify the two-dimensionality of the flow.

#### 4.5.2 *Visualization surface*

The area of interest was from the midchord to the trailing edge

of the model, as shown on the following figure.

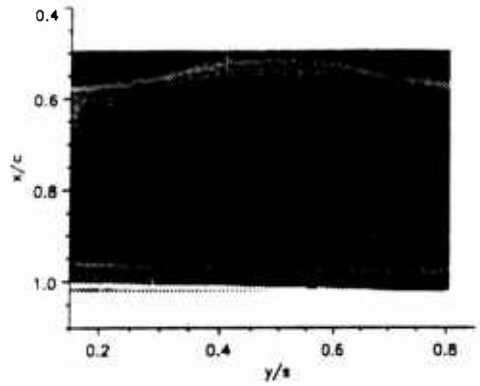



**Figure 6.- Model oilflow; upper surface, α=2°, $M_\infty$=0.782.**

4.5.3 *Data format*

The data are available as photographs or digitized computer images.

**4.6 Flow field visualization**

No flow field visualization techniques were applied.

**4.7 Tunnel wall measurements**

4.7.1 *Type of measurement*

Wall pressure measurements were made on all four walls of the test section.

4.7.2 *Location and number of pressure holes*

Pressure tap locations are shown on the following figure.

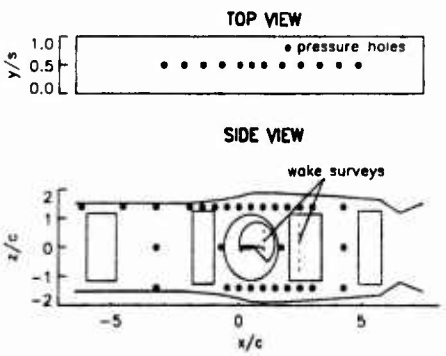



**Figure 7.- Test section pressure hole location.**

## 5 TEST MATRIX AND CONDITIONS

**5.1 Detailed test matrix**

5.1.1 *Number of selected test cases*

6

5.1.2 *Number of configurations tested*

1

5.1.3 *Test matrix table*

Table II below lists the test matrix for this investigation

**Table II: Test Matrix**

| # | $M_\infty$ | $q_\infty$, kPa | Re,x$10^{-6}$ | α, deg | Survey location x/c | type of measurement | remarks |
|---|---|---|---|---|---|---|---|
| 1 | 0.73 | 57 | 6 | 0.5, 0.9, 1.5 | 2.5 | pressure, LDV | |
| 2 | 0.75 | 57 | 6 | 0.5, 0.9, 1.5 | 2.5 | pressure, LDV | |
| 3 | 0.78 | 57 | 6 | 0.5, 0.9, 1.5 | 2.5 | pressure, LDV | |
| 4 | 0.8 | 57 | 6 | 0.5, 0.9, 1.5 | 2.5 | pressure, LDV | |
| 5 | 0.73<br>0.78<br>0.8 | 57 | 6 | 1.0 | 1.04 | LDV | |
| 6 | 0.73<br>0.75<br>0.78<br>0.81 | 19 | 2 | 1.0 | x/c=<br>0-0.65<br>0.4-0.95<br>0.3-0.95<br>0.45-0.95 | LDV (u,v) | z/c=<br>0.12, 0.25, 0.5<br>0.12, 0.25, 0.63<br>0.12, 0.38, 0.63<br>0.25, 0.5 |

### 5.2 Model/tunnel relations

#### 5.2.1 *Maximum blockage*

The blockage in this tunnel is very low since the upper and lower walls have been contoured to account for the presence of the model, boundary layer growth on all four walls, and sidewall suction. An assessment of this technique was given in ref. 3 where it was found that the use of wall contouring reduced wall interference effects on normal force to less than 3%.

#### 5.2.2 *Model span/tunnel width*

1

#### 5.2.3 *Wing area/tunnel cross section*

0.0427

#### 5.2.4 *Height/chord ratio*

3.048

#### 5.2.5 *Width/chord ratio*

2.032

#### 5.2.6 *Adiabatic wall?*

Yes

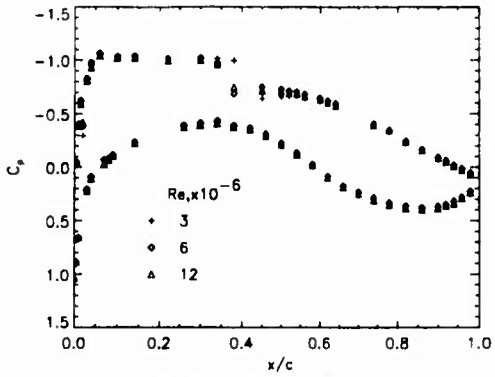
### 5.3 Transition details

#### 5.3.1 *Free or fixed transition?*

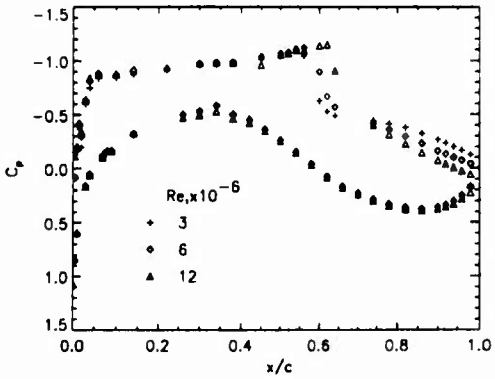
Fixed

#### 5.3.2 *Details of free transition*

Although the investigation was ultimately conducted with transition fixed an assessment of free transition was made during the initial stages of the study. Fig. 8 illustrates Reynolds number effects on wing pressures for Mach numbers of 0.73 and 0.78. These two untripped cases were chosen because of their differences in trailing edge flows. At $M_\infty$=0.73 the flow is attached, and for $M_\infty$=0.78 it is separated. The departure of the trailing edge pressure coefficient from a value of 0.1 was used to define the onset of separation on the upper surface. For the lower Mach number (attached flow) the effects of Reynolds number are confined to the area of the shockwave, whereas, for the separated case, Reynolds number affects the flow from the shock to the trailing edge. The degree of separation is coupled to the position of the shockwave and both effects are a function of the Reynolds number. These changes in the flowfield are due to a combination of boundary layer transition movement and unit Reynolds number variations.




(a) $M_\infty$=0.734, α=1.1°.



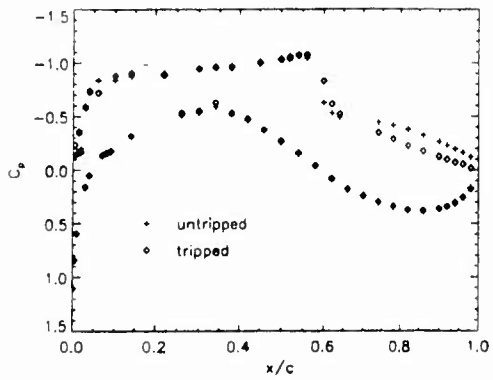

(b) $M_\infty$=0.780, α=1°.

**Figure 8.- Effect of Reynolds number on wing surface pressures.**

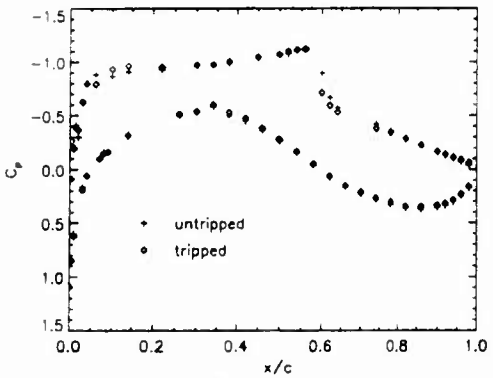
#### 5.3.3 *Details of fixed transition*

Boundary layer trips (230K) were applied at 7% chord to both the upper and lower surfaces of the wing. Oilflow data were used to determine the size of grit necessary to cause transition at the trip location. This was accomplished in preliminary tests by placing patches of various grit sizes at different span locations and finding the minimum grit size that caused transition to occur at the patch. Fixing transition eliminates the possibility that flow-induced roughness would cause transition movement on an otherwise smooth model. The consequences of fixing transition are shown on fig. 9. The effect of trips on the low Reynolds number flow of fig. 9a is significant. The amount of separation is reduced and the pressure distribution is very similar to the higher Reynolds number flow of fig. 9b. The influence of trips is minimal at the higher Reynolds number, indicating that natural transition occurs very close to the trip location (x/c=0.07). Therefore, further changes in the flowfield above 6 million Reynolds number are due to variations in unit Reynolds number. Whereas, below 6 million the

changes are due to the movement of transition.




(a) Re=3x10$^6$, $M_\infty$=0.784, α=1.05°.




(b) Re=6x10$^6$, $M_\infty$=0.778, α=1.0°.

**Figure 9.- Effect of boundary layer trips on wing surface pressures.**

## 6 DATA

### 6.1 Availability of data

*6.1.1 Organization owning the data*

National Aeronautics and Space Administration
USA

*6.1.2 Responsibility for data*

George G. Mateer - Research Engineer
Mail Stop 229-1
NASA-Ames Research Center
Moffett Field, California
USA 94035-1000
phone: (415) 604-6255
fax: (415) 604-4003

*6.1.3 Availability of data*

The data are freely available.

### 6.2 Suitability of data for CFD validation

*6.2.1 Suitability for "in-tunnel" calculation*

Tunnel wall geometry and pressure distributions are defined.

*6.2.2 Corrections to simulate "free-air" conditions*

The data were not corrected, however, the wind tunnel walls were contoured to simulate "free-air" conditions.

### 6.3 Type and form in which data are available

*6.3.1 Type and form*

The type and form of the data are shown on Table III.

*6.3.2 Data carrier*

**Table III: Data Availability**

| DATA | ENGIN. UNITS | COEFFICIENTS | NORMALIZED | UNCORRECTED | CORRECTED |
|---|---|---|---|---|---|
| FREESTREAM CONDITIONS | | X | | | X |
| SURFACE PRESSURES | | X | | X | |
| WAKE DATA | | | X | X | |
| FIELD DATA | | | X | X | |
| TEST SECTION WALL PRESSURES | | X | | X | |

The data is available in ASCII format on 3.5" floppy disk (DOS or Unix) at 720 Kbytes or 1.44 Mbytes density

Electronic mail (E-mail) transfers are also supported.

Printed form is also available.

**6.3.3** *Extent of geometry data*

9 Kbytes

**6.3.4** *Extent of aerodynamic test data*

104 Kbytes

**6.4 Corrections applied to data**

No corrections were applied directly to the data, however, the wind tunnel walls were contoured to accommodate the various "interferences" as discussed below.

**6.4.1** *Lift interference and blockage corrections*

For all of the data the walls were fixed at a single shape corresponding to $M_\infty = 0.78$, and $\alpha = 1°$. As was shown in ref. 1, this shape was sufficient to preserve the major features of the flow field (e.g., shock-wave position and separation) with only a slight alteration in the pressure distributions at the "off-contour" conditions.

**6.4.2** *Side wall interference corrections*

Boundary layer displacement effects on all four walls as well as sidewall suction effects were accounted for by adjusting the upper and lower walls to provide a constant $M_\infty$ at the model location when the tunnel was empty.

**6.4.3** *Half model corrections*

Not applicable.

**6.4.4** *Sting and support corrections*

The model was supported by the tunnel sidewalls.

**6.4.5** *Aero-elastic deformation*

Model deformation under load was insignificant

**6.4.6** *Other corrections*

The flow field was measured by the nonintrusive LDV system so no corrections were needed.

## 7. DATA ACCURACY AND REPEATABILITY ASSESSMENT

**7.1 Estimate accuracy of:**

**7.1.1** *Free stream conditions*

Mach number=$M_\infty$ ±0.001

**7.1.2** *Measured data*

pressure=$C_p$ ±0.006

It is convenient to separate the factors which affect the accuracy of the LDV measurements into three groups. The first group consists of those fixed geometric uncertainties which are invariant during a test run or series of runs. The second group contains the random variations generally introduced by sample size statistics. The more difficult to quantify effects of tunnel flow unsteadiness, particle tracking fidelity, velocity bias, and noise are placed in the third group. The fixed, geometric uncertainties were evaluated from extensive experience with many tests in which the laser beam geometry was measured in a variety of ways. These uncertainties can be as large as ±2% for u, $\langle u'v' \rangle$, and $\langle u'^2+v'^2 \rangle$. When v<<u the geometric uncertainty in v is expressed as 0.027u. Uncertainties due to sample size statistics for these measurements vary between ±0.2% and ±0.6% for the mean velocities and ±3% for the turbulent quantities. Tunnel flow variations (spatial and temporal) are more difficult to quantify. All data are normalized using measured total temperatures to correct for temperature change during each run and for run-to-run variations. Small, unexplained spatial/temporal variations in the mean axial velocity were noted for some conditions in the flow downstream of the airfoil. While small (1-2%) they present difficulties in evaluating the drag. Estimates of the response of the sub-micron polystyrene seed spheres indicate that a 99% velocity adjustment occurs within 0.9 mm of passage through a normal shock. The measurements taken in axial sweeps through the airfoil shock support this estimate of excellent tracking fidelity. Velocity bias corrections were deemed to be inappropriate for these data and were not made. The influence of noise is difficult to evaluate. Care was taken to maintain clean, well aligned optics. The special seeding injector prevented seed deposition on the test-sec-

**Table IV: LDV Uncertainties**

| quantity | group 1 | group 2 | group 3 | worst case | root-sum-square |
|---|---|---|---|---|---|
| u | ±1-2% | ±0.2-0.6% | ±1-2% | ±4.6% | ±1.4-2.9% |
| v | ±0.027u | ±0.2-0.6% | ±1-2% | ±0.027u±0.026v | ±0.027u±0.012-0.026v |
| $\langle u'v' \rangle$ | ±2% | ±3% | ±2-4% | ±9% | ±4.1-5.4% |
| $\langle u'^2+v'^2 \rangle$ | ±2% | ±3% | ±2-4% | ±9% | ±4.1-5.4% |

tion windows and laser flare was largely avoided in the study since near surface measurements were not attempted in the thin airfoil boundary-layer. The small fraction (<<1%) of the data which exceeded three standard deviations was discarded in forming the velocity histograms. The uncertainties (95% confidence limits) assigned to the measured quantities for the three groups are shown in table IV. Also shown are the root-sum-square and worst case combinations.

### 7.2 Repeat measurements

#### 7.2.1 *Type and number of repeat measurements within one test campaign*

A typical LDV wake survey required 5-6 separate tunnel runs to complete. Each segment had data that overlapped neighboring segments. The repeatability of the data in these overlapping regions is shown on fig. 1. The following figure shows the repeatability of the wing pressure data on the upper surface.

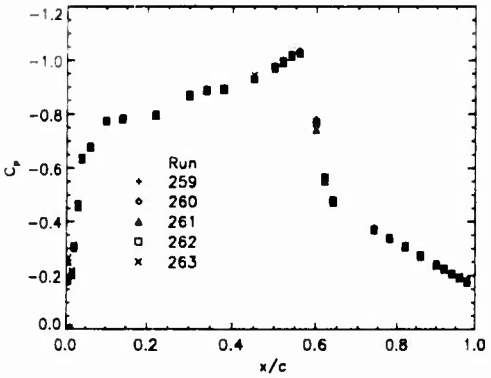



**Figure 10.- Repeatability of wing pressure data for 5 consecutive runs; upper surface, $\alpha$=0.9°, $M_\infty$=0.803, Re=6x10$^6$.**

#### 7.2.2 *Type and number of repeat measurements in successive campaigns*

Although this investigation was conducted within a single tunnel entry, fig. 11 indicates the repeatability of data taken almost 6 months apart.

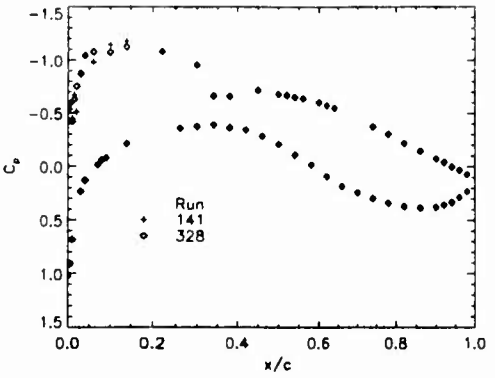



**Figure 11.- Long-term data repeatability; wing upper surface, $\alpha$=1.0°, $M_\infty$=0.730, Re=6x10$^6$.**

### 7.3 Redundant measurements

#### 7.3.1 *Quantities measured independently by different techniques*

At certain locations where the flow had undergone an isentropic expansion from the total conditions Mach numbers were computed from both pressure and LDV data. The agreement was ±0.002.

#### 7.3.2 *Internal consistency of data*

Shockwave locations were verified by comparing wing upper surface pressure data with LDV flowfield data taken above the wing. Wake growth in the z direction correlated with increasing shock strength and separation on the upper surface of the wing. The onset of separation as observed by the trailing edge pressures also coincided with a vertical motion of the minimum in the wake velocity profile.

### 7.4 Other tests on same geometry

#### 7.4.1 *Same model in other tunnels*

This particular model has only been tested in the NASA-Ames High Reynolds Number Channel II.

#### 7.4.2 *Same geometry and/or different scale in other tunnels*

The VA-2 airfoil has also been tested in the DFVLR Transonic Tunnel in Gottingen (refs. 6,7) and in Braunschweig (ref. 8). The data of ref. 6 are uncorrected and are from an aspect ratio=5 model.

### 7.5 Additional remarks

The profile drag of the airfoil was determined from wake velocity and static pressure profiles using the momentum integral method of Jones (ref. 9) extended to high-speed flow (ref. 10 - 12). The technique was modified to calculate the drag

using the non-intrusive LDV and sidewall pressure measurements rather than the traditional pitot and static pressure traverse data. The results are shown in the following table where $\sigma C_D$ is the standard deviation of the drag coefficient.

**Table V: Drag Data.**

| $M_\infty$ | $C_D$ | $\sigma C_D$ |
|---|---|---|
| $\alpha$=0.5 | | |
| 0.728 | 0.01009 | 0.00027 |
| 0.759 | 0.01010 | 0.00059 |
| 0.784 | 0.01537 | 0.00054 |
| 0.802 | 0.03321 | 0.00074 |
| $\alpha$=0.9 | | |
| 0.729 | 0.01078 | 0.00026 |
| 0.750 | 0.01198 | 0.00037 |
| 0.781 | 0.02684 | 0.00142 |
| 0.803 | 0.04585 | 0.00085 |
| $\alpha$=1.5 | | |
| 0.730 | 0.01556 | 0.00054 |
| 0.749 | 0.02075 | 0.00073 |
| 0.781 | 0.04031 | 0.00095 |
| 0.803 | 0.05337 | 0.00131 |

## 8. REFERENCES


1. Mateer, G. G.; Seegmiller, H. L.; Hand, L. A.; and Szodruch, J.: An Experimental Investigation of a Supercritical Airfoil at Transonic Speeds. AIAA Paper 87-1241, June 1987.

2. McDevitt, J. B.; Polek, T. E.; and Hand, L. A.: A New Facility and Technique for Two-Dimensional Aerodynamic Testing. AIAA J. Aircraft, vol. 20, no. 6, June 1983, pp. 543-551.

3. McDevitt, J. B.; and Okuno, A. F.: Static and Dynamic Pressure Measurements on a NACA 0012 Airfoil in the Ames High Reynolds Number Facility. NASA Technical Paper 2485, June 1985.

4. Seegmiller, H. L.; Bader, J. B.; Cooney, J. P.; De Young, A.; Donaldson, R. W., Jr.; Gunter, W. D., Jr.; and Harrison, D. R.: Development of a New Laser Doppler Velocimeter for the Ames High Reynolds Channel No. II. NASA TM-86772, July 1985.

5. Coakley, T. J.: Implicit Upwind Methods for the Compressible Navier-Stokes Equations. AIAA Journal, vol. 23, no. 3, Mar. 1985, p. 374.

6. Boehe, R.D.: Transonic Experiments with the Airfoil VA-2 at the DFVLR Gottingen. (Re=2.5x10$^6$). ZKP-Report 8, LFK 7511, 1976.

7. Krogmann, Paul: Untersuchengen an einem uberkritischen Profil mit Grenzschichtabsaugung im StoBbereich uber einen perforierten Streifen, DFVLR Gottingen, DFVLR-FB 85-15, Feb. 1985.

8. Muller, R.: Experiments with the transonic airfoil VA-2 in the Transonic Windtunnel Brunswick. (Re=6x10$^6$). DFVLR-IB 151-78/13, June 1978.

9. The Cambridge University Aerodynamics Laboratory (Jones, B.M.): The Measurement of Profile Drag by the Pitot-Traverse Method. Reports and Memoranda No. 1688, (British) Aeronautical Research Committee, January 1936.

10. Young, A.D.: Note on the Effect of Compressibility on Jones' Momentum Method of Measuring Profile Drag. Reports and Memoranda No. 1881, (British) Aeronautical Research Committee, February 1939.

11. Young, A.D.: Note on Momentum Methods of Measuring Profile Drags at High Speeds. Reports and Memoranda No. 1963, (British) Aeronautical Research Committee, February 1940.

12. Lock, C.N.H.; Hilton, W.F.; and Goldstein, S.: Determination of Profile Drag at High Speeds by a Pitot Traverse Method. Reports and Memoranda No. 1971, (British) Aeronautical Research Committee, September 1940.


## 9. LIST OF SYMBOLS

| | |
|---|---|
| a | speed of sound |
| c | airfoil chord |
| $C_p$ | pressure coefficient |
| $C_D$ | drag coefficient |
| M | Mach number |
| p | pressure |
| q | dynamic pressure |
| Re | free-stream Reynolds number based on airfoil chord |
| s | airfoil span |

| | |
|---|---|
| u | axial velocity |
| v | vertical velocity |
| x | axial coordinate from the wing leading edge |
| y | spanwise coordinate from the tunnel wall |
| z | vertical coordinate from the tunnel centerline |
| $\alpha$ | angle of attack |
| $\sigma$ | standard deviation |
| < > | ensemble average |

Superscripts

| | |
|---|---|
| ' | fluctuating component |

Subscripts

| | |
|---|---|
| t | value based on total conditions |
| $\infty$ | free stream value |

# TWO-DIMENSIONAL HIGH-LIFT AIRFOIL DATA FOR CFD CODE VALIDATION

BY

G. W. BRUNE

BOEING COMMERCIAL AIRPLANE GROUP
SEATTLE, WASHINGTON / USA, 98124

## 0. INTRODUCTION

The purpose of the experimental investigation summarized below was to provide a complete data set for the validation of two-dimensional multi-element airfoil computer codes. The airfoil model used for this investigation features four elements including a double slotted trailing edge flap and a slotted leading edge device representing a section of a transport wing in high-lift configuration with take-off flap setting. The leading edge flap was tested in a nonoptimum setting in order to produce a thick confluent boundary layer on the upper airfoil surface.

In this wind tunnel experiment, all data were measured on a single high-lift airfoil configuration with a fixed flap setting at one tunnel freestream condition. Emphasis was placed on the acquisition of a few high quality airfoil data with many repeat runs and redundant measurements. Measured data comprise airfoil lift, drag, pitching moment, surface pressures, mean velocity profiles and Reynolds stresses of the confluent boundary layer. The data was obtained in the Boeing Research Wind Tunnel located in Seattle at 0.11 Mach number and 1.55 million Reynolds number based on tunnel freestream velocity and a flaps-up airfoil chord of 0.6096 m (2 ft).

Care was taken to achieve a close approximation to two-dimensional flow by means of turntable and tunnel side wall blowing. Two-dimensional flow was verified by comparing boundary layer mean velocitiy and turbulence profiles at several spanwise stations, and by various surface flow visualizations methods. In addition, lift curves from balance measurements and an integration of surface pressures were compared. Confluent boundary layer measurements were conducted employing a Pitot probe and hot wires. Probes were mounted on a mechanical traverser designed to minimize disturbances of overall airfoil circulation and of the local flow at the measuring station.

Selected test data and a description of the instrumentation have been published previously in the open literature. A document containing further details and tabulated data is available upon request from The Boeing Company.

## 1. GENERAL DESCRIPTION

| | | |
|---|---|---|
| 1.1 | Model designation | BOEING Model TR-1332 |
| 1.2 | Model type | Two-dimensional four-element high-lift airfoil |
| 1.3 | Design requirements/purpose of test | The model represents a section of a transport wing in high-lift configuration with take-off flap settings. The test was conducted to acquire a complete set of CFD validation data for a modern high-lift airfoil. |
| 1.4 | Dominant flow physics | The leading edge flap is in a nonoptimum position to produce a thick confluent boundary layer on the upper airfoil surface (Figs. 1, 2, 3). |

| | | |
|---|---|---|
| 1.5 | Recommended use of data | The data can be used to validate compressible or incompressible two-dimensional high-lift computer codes employing a model for confluent boundary layers. A model for massive flow separation is not required since most boundary layers are attached. |

## 2. MODEL GEOMETRY

| | | |
|---|---|---|
| 2.1 | General | Four-element slotted airfoil (Fig. 1) tested at a fixed setting of flap angles, gaps, and overlaps. |
| 2.2 | Reference chord (flaps-up) | 0.6096 m (2 ft) |
| 2.3 | Thickness ratio of flaps-up reference airfoil | 11.3% |
| 2.4 | Span | 1.524 m (5 ft) |
| 2.5 | Geometric definitions | |
| 2.5.1 | Shape definition | Shape of all 4 airfoil elements is numerically specified. |
| 2.5.2 | Actual airfoil coordinates/ tolerances | Airfoil surface coordinates were checked using templates. Differences between specified and measured coordinates are within $\pm 0.08 \cdot 10^{-3}$ m ($\pm$ 0.003 in). |
| 2.5.3 | Surface condition | Smooth |
| 2.5.4 | Flap sizes and positions | See values in table 1, definitions in figure 4. Flap gaps, heights and overlaps were set using fixed mounting brackets and shims under the pads as required. |

## 3. GENERAL TUNNEL INFORMATION

| | | |
|---|---|---|
| 3.1 | Tunnel designation | Boeing Research Wind Tunnel (BRWT) |
| 3.2 | Organization running the tunnel | Boeing Aerodynamics Laboratory |
| 3.3 | Tunnel characteristics | Closed circuit, single return, continuous flow tunnel with test section vented to the atmosphere.<br>Max. Mach number: 0.18<br>Max. Reynolds number per meter: $3.87 \cdot 10^6$<br>Dynamic pressure range from $0.479 \cdot 10^2$ - $23.938 \cdot 10^2$ N/m$^2$, (1 - 50 psf) |
| 3.4 | Test section | |
| 3.4.1 | Model installation | The model was mounted horizontally at zero sweep angle between two circular turntables installed flush with the tunnel side walls (Figs. 5,6). |
| 3.4.2 | Test section dimensions | 1.524 m wide, 2.438 m high, 6.096 m long (5 ft x 8 ft x 20 ft) |
| 3.4.3 | Wall geometry/boundary layer | Solid walls with 4 blowing slots on each side wall upstream of model. In addition, 4 blowing slots in each turntable (Fig. 6).<br>No measurements of tunnel wall pressures. |

| | | |
|---|---|---|
| 3.5 | Freestream conditions | Reference flow conditions are determined from total pressure and total temperature in the settling chamber, atmospheric pressure, and wall static pressure at the test section entrance 3.048 m (10 ft) upstream of the turntable center. These measurements provide freestream conditions at the test section entrance which are corrected using tunnel calibration data to obtain freestream conditions at the location of the model. |
| 3.6 | Flow quality of empty tunnel | |
| 3.6.1 | Flow uniformity | At turntable center (balance center in Fig. 6), $0.25^0$ upflow angle and cross flow from $0.3^0$ to $-0.5^0$ determined with split film anemometer and hemispherical probe. |
| 3.6.2 | Temperature variation | Tunnel is not equipped with heat exchanger. Temperature changes of up to 14 °C (25 °F) occurred during boundary layer measurements, see section 7.5.3. |
| 3.6.3 | Turbulence level | At tunnel centerline: 0.06 percent at $4.788 \cdot 10^2$ N/m$^2$ (10 psf) dynamic pressure, 0.18 percent at $19.15 \cdot 10^2$ N/m$^2$ (40 psf) |

## 4. INSTRUMENTATION

| | | |
|---|---|---|
| 4.1 | Model position | |
| 4.1.1 | Angle of attack measurement | By mechanical encoder |
| 4.1.2 | Accuracy of angle of attack | $\pm 0.05^0$ |
| 4.2 | Model surface pressure measurements | |
| 4.2.1 | Number of pressure holes | 77 along model centerline including<br>32 on main airfoil element,<br>19 on leading edge flap,<br>15 on main trailing edge flap, and<br>11 on aft trailing edge flap |
| 4.2.2 | Pressure transducers | Range: $3.447 \cdot 10^4$ N/m$^2$ (5 psi),<br>Accuracy: ±0.25% of range |
| 4.2.3 | Dynamic (unsteady) pressures | Not measured |
| 4.3 | Force and moment measurements | |
| 4.3.1 | Balance | External balance located below test section floor |
| 4.3.2 | Range/accuracy of balance data | Lift: $17.792 \cdot 10^3$ N (4,000 lbf)<br>Drag: Not recorded (see 4.3.3)<br>Pitching Moment: $2.260 \cdot 10^3$ mN ($1.667 \cdot 10^3$ ft lbf) |

| | | |
|---|---|---|
| 4.3.3 | Wake rake for drag | Pneumatically integrating wake rake positioned 1 reference chord length (0.6096 m) downstream of trailing edge of aft flap |
| 4.4 | Boundary layer measurements | |
| 4.4.1 | Measurement technique | Pitot probe, double x-hot wires for mean flow velocity profiles and Reynolds stresses. Thermocouple for temperature profiles |
| 4.4.2 | Flow regions investigated | Confluent boundary layer on upper surface of main section (Fig. 7) |
| 4.4.3 | Probes and probe support | See figure 8 |
| 4.5 | Surface flow visualizations | |
| 4.5.1 | Methods applied | Tufts, china clay, sublimation |
| 4.5.2 | Surfaces | Upper airfoil surface |
| 4.5.3 | Form of data | Photos of china clay and sublimation patterns |
| 4.6 | Flow field visualizations | Not performed |
| 4.7 | Tunnel wall measurements | Not performed |

## 5. TEST MATRIX AND CONDITIONS

| | | |
|---|---|---|
| 5.1 | Test matrix | |
| 5.1.1 | Number of test cases | 1 |
| 5.1.2 | Number of configurations | 1 |
| 5.1.3 | Test conditions, test matrix | Freestream Mach number: 0.11<br>Dynamic pressure: $9.575 \cdot 10^2$ N/m$^2$ (20 psf)<br>Chord Reynolds number: $1.55 \cdot 10^6$<br>See test matrix in table 2 |
| 5.2 | Model/tunnel relations | |
| 5.2.1 | Maximum model frontal area/ tunnel cross section | 0.12 |
| 5.2.2 | Model span/tunnel width | 1 (two-dimensional airfoil model) |
| 5.2.3 | Wing area/tunnel cross section | 0.25 |
| 5.2.4 | Height/chord ratio | 4 |
| 5.2.5 | Width/chord ratio | 2.5 |
| 5.3 | Transition details | |
| 5.3.1 | Type of transition | Fixed transition on upper surfaces of leading edge flap and main airfoil element. Free transition on all other surfaces. |
| 5.3.2 | Details of free transition | Laminar separation bubbles observed on upper surface of main flap using china clay (kaolin powder in kerosene). Free transition on lower surface not recorded. |
| 5.3.3 | Details of fixed transition | Upper surface of leading edge flap: $x_{LE}/c_{ref}=0.074$ |

Upper surface of main airfoil element:
$x/c_{ref}$=0.033
Trips consisted of aluminum disks:
Height of disks: $0.2 \cdot 10^{-3}$ m (0.008 in)
Diameter: $1.27 \cdot 10^{-3}$ m (0.05 in)
Spanwise spacing from center to center:
$2.54 \cdot 10^{-3}$ m (0.1 in)
Trip strip effectiveness verified at $15^0$ angle of attack by sublimation using naphthalene with freon as solvent, and also using a stethoscope.

## 6. DATA

### 6.1 Availability of data

| | |
|---|---|
| 6.1.1 Organization owning data | The Boeing Company |
| 6.1.2 Responsible manager | R. L. Bengelink, Chief of Aerodynamics<br>Boeing Commercial Airplane Group<br>P. O. Box 3707, MS 6R-MT<br>Seattle, WA 98124-2207 USA<br>Telephone 206-234-9984<br>Fax 206-237-0849 |
| 6.1.3 Availability | Boeing document containing data plots and tabulated data is available upon request, see references 8.2. |

### 6.2 Suitability for CFD validation

Data are corrected for tunnel wall effects to simulate "free air" conditions.

### 6.3 Type and form of data

| | |
|---|---|
| 6.3.1 Form of data | See table 3 |
| 6.3.2 Data carrier | Boeing document and AIAA technical papers, see references in sections 8.2 and 8.3 |
| 6.3.3 Extent of geometry data | 4 printed document pages (81/2"x11" or A4) |
| 6.3.4 Extent of aerodynamic test data | 16 pages with tabulated data and data plots |

### 6.4 Corrections applied to data

| | |
|---|---|
| 6.4.1 Blockage | Solid and wake blockage, with $\varepsilon = 0.01594$ |
| 6.4.2 Streamline curvature correction | Angle of attack, lift, and pitching moment corrected with $\sigma = 0.012851$ |
| 6.4.3 Reference on wall correction | A. Pope, "Wind Tunnel Testing", John Wiley & Sons, Second Edition, 1954 |

## 7. DATA ACCURACY AND REPEATABILITY ASSESSMENT

### 7.1 Data accuracy

| | |
|---|---|
| 7.1.1 Freestream conditions | Angle of attack: $\pm 0.05^0$<br>Flow velocity accuracy: $\pm$ 0.14% |

| | | |
|---|---|---|
| | 7.1.2 Measured data | See section 3.5 for a description of the measurement of freestream conditions.<br>Lift repeatability: $\Delta c_l = \pm 0.0095$<br>Pitching moment repeatability: $\Delta c_m = \pm 0.0051$<br>Drag: See spanwise variation in figure 9<br>Surface pressure accuracy: $\Delta c_p = \pm 0.09$<br>Error of boundary layer mean velocity: < 1.5 %<br>Error of turbulence data: < 8 to 10 %<br>Probe position accuracy: See figure 10 |
| 7.2 | Repeat measurements | |
| | 7.2.1 Type and number | Balance data: 7 pitch runs<br>Surface pressures: 3 repeat runs<br>Turbulence measurements: See figure 11 |
| | 7.2.2 Other test entries | Not conducted |
| 7.3 | Redundant measurements | |
| | 7.3.1 Airfoil lift | From balance and pressure integration (Fig. 12) |
| | 7.3.2 Boundary layer velocity | From Pitot probe and hot wire (Fig. 13) |
| | 7.3.3 Reynolds stresses | From different hot wires (Fig. 14) |
| 7.4 | Other tests on same geometry | None |
| 7.5 | Additional remarks | |
| | 7.5.1 Flow two-dimensionality | Verified by:<br>a) Surface flow visualization (tufts, china clay).<br>b) Agreement of lift from balance and surface pressures (Fig. 12).<br>c) Boundary layer profiles measured at different spanwise locations (Fig. 15).<br>d) Boundary layer momentum integral balance |
| | 7.5.2 Intrusiveness of mechanical traverser and probes | No effect on surface pressures (Fig. 16) |
| | 7.5.3 Effect of temperature changes | See figure 17 |

## 8. REFERENCES


| | | |
|---|---|---|
| 8.1 | Wind tunnel | Aeronautical Facilities Catalogue, Volume 1, Wind Tunnels, NASA RP 1132, Jan. 1985 |
| 8.2 | Test | Brune, G.W. and Sikavi, D. A., "Experimental Investigation of the Confluent Boundary Layer of a Multielement Low Speed Airfoil", AIAA Paper 83-0566, Jan. 1983<br><br>Brune, G.W. and Sikavi, D. A., "Confluent Boundary Layer Measurements", Boeing Document D6-51453TN, April 1983 |

8.3 Measurement technique — Brune, G.W., Sikavi, D. A., Tran, E.T., and Doerzbacher, R., P., "Boundary Layer Instrumentation for High-Lift Airfoil Models", AIAA Paper 82-0592, March 1982

## 9. LIST OF SYMBOLS

| | |
|---|---|
| $c$ | chord length |
| $c_d$ | drag coefficient |
| $c_l$ | lift coefficient |
| $c_m$ | pitching moment coefficient |
| $c_p$ | surface pressure coefficient |
| $c_{ref}$ | flaps-up reference airfoil chord |
| $G$ | gap |
| $k$ | turbulent kinetic energy |
| $U$ | boundary layer mean flow velocity tangent to airfoil surface |
| $U_e$ | boundary layer edge velocity |
| $U_{ps}$ | inviscid flow velocity at airfoil surface (reference velocity) |
| $x$ | coordinate along chord of main airfoil element |
| $x_{LE}$ | coordinate along chord of leading edge flap |
| $y$ | coordinate normal to airfoil surface |
| $\overline{u'^2}$ | streamwise component of Reynolds normal stress |
| $\overline{-u'v'}$ | turbulent shear stress |
| $\alpha$ | angle of attack |
| $\Delta$ | overlap |
| $\delta$ | flap angle |
| $\Delta c_l$ | repeatability of lift coefficient measurement |
| $\Delta c_m$ | repeatability of pitching moment coefficient measurement |
| $\Delta c_p$ | accuracy of surface pressure coefficient measurement |
| $\varepsilon$ | coefficient of blockage correction |
| $\sigma$ | coefficient of streamline curvature correction |

Subscripts

| | |
|---|---|
| aft | aft trailing edge flap |
| LE | leading edge flap |
| mf | main trailing edge flap |
| ref | reference value |
| $\infty$ | freestream value |

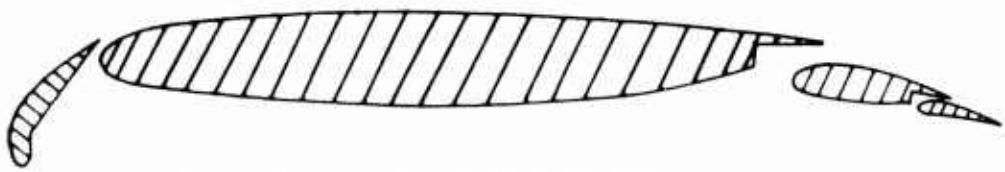


*Fig. 1 Geometry of Boeing Model TR-1332*

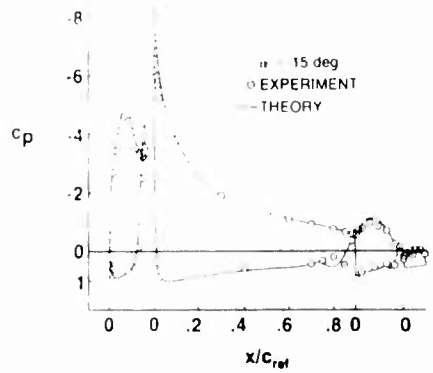



*Fig. 2 Surface Static Pressure of Boeing High-Lift Airfoil TR-1332*

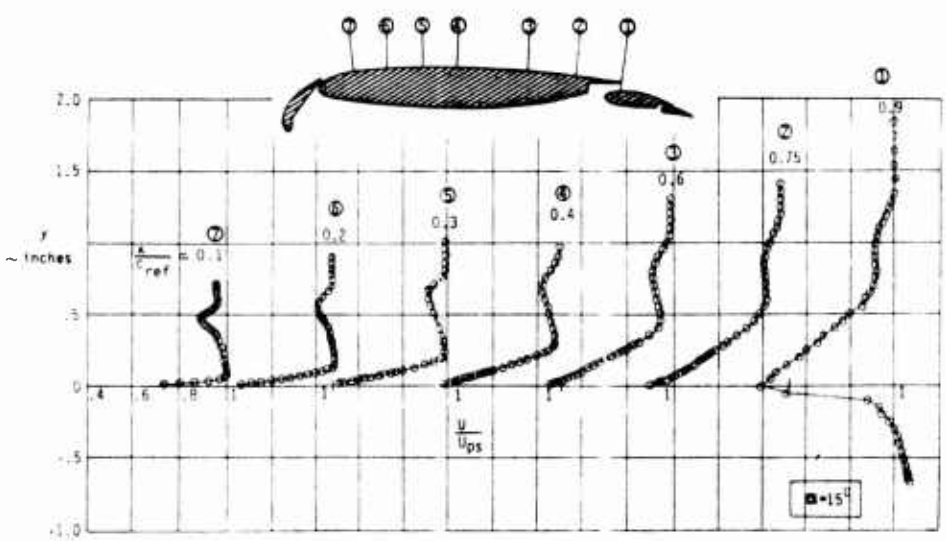



*Fig. 3 Confluent Boundary Layer Mean Velocity Profiles*

| | LE FLAP | MAIN FLAP | AFT FLAP |
|---|---|---|---|
| CHORD LENGTH | $\frac{c_{LE}}{c_{ref}} = 16.5\%$ | $\frac{c_{mf}}{c_{ref}} = 23.8\%$ | $\frac{c_{aft}}{c_{ref}} = 9.9\%$ |
| FLAP ANGLE | $\delta_{LE} = 57.2^{o}$ | $\delta_{mf} = 12.6^{o}$ | $\delta_{aft} = 14.9^{o}$ |
| GAP | $\frac{G_{LE}}{c_{ref}} = 1.68\%$ | $\frac{G_{mf}}{c_{ref}} = 2.55\%$ | $\frac{G_{aft}}{c_{ref}} = 0.6\%$ |
| OVERLAP | $\frac{\Delta x_{LE}}{c_{ref}} = 0.36\%$ | $\frac{\Delta x_{mf}}{c_{ref}} = 4.23\%$ | $\frac{\Delta x_{aft}}{c_{ref}} = 4.18\%$ |

*Table 1 Flap Sizes and Positions*

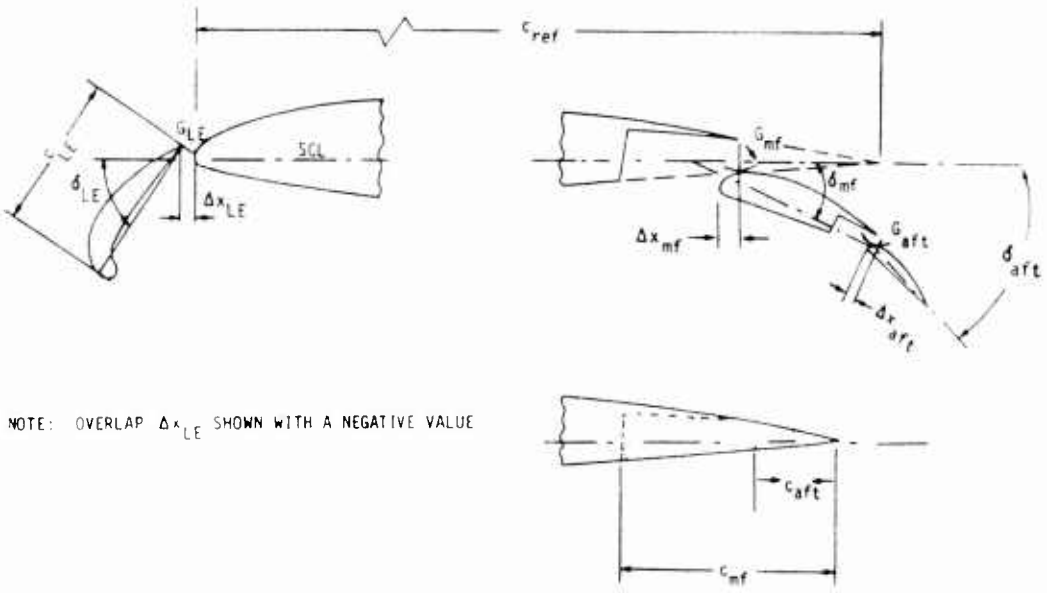



*Fig. 4 Multi-element Airfoil Nomenclature Used in Table 1*

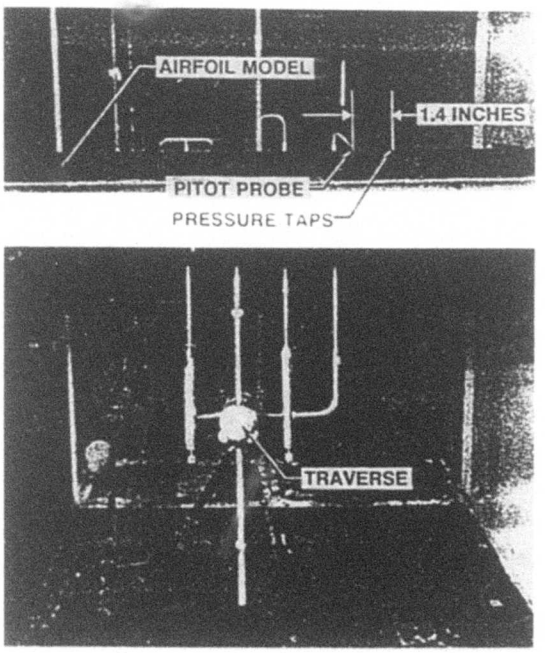



*Fig. 5 Front View of Model and Measuring System in the Boeing Research Wind Tunnel*

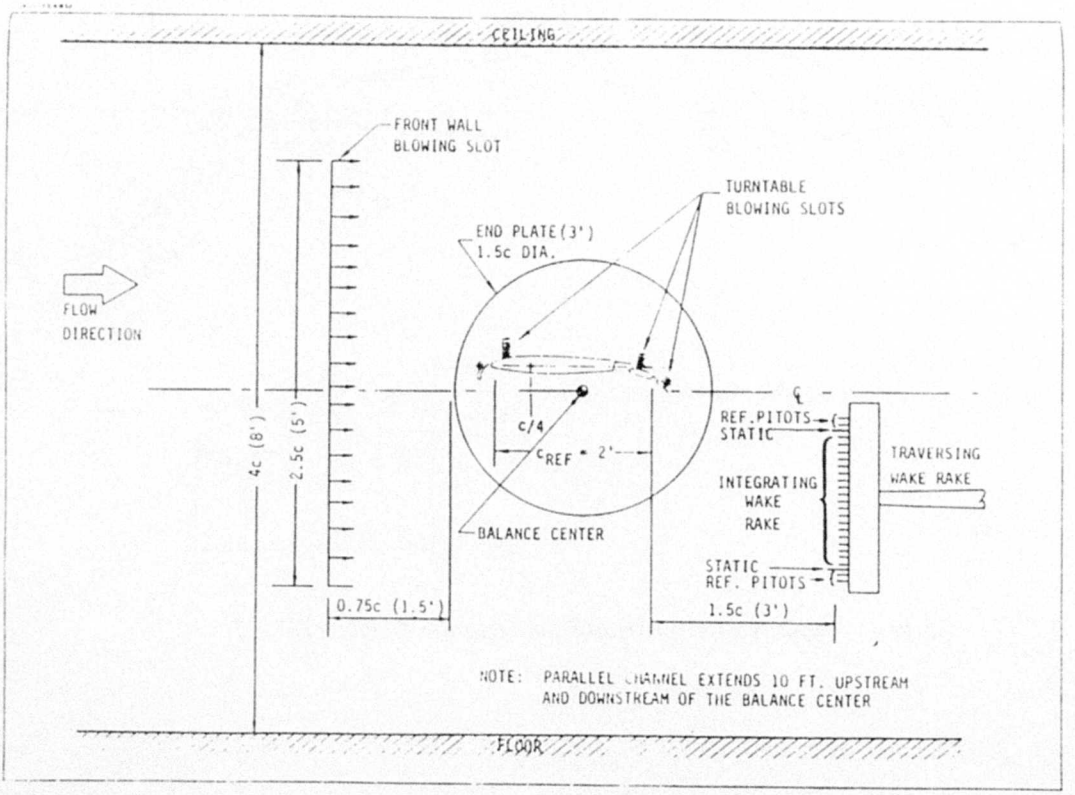
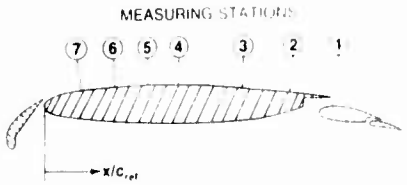



*Fig. 6 Two-dimensional Test Set-up in the Boeing Research Wind Tunnel*




| STATION | 7 | 6 | 5 | 4 | 3 | 2 | 1 |
|---|---|---|---|---|---|---|---|
| $x/C_{ref}$ | 0.1 | 0.2 | 0.3 | 0.4 | 0.6 | 0.75 | 0.9 |

*Fig. 7 Chordwise Confluent Boundary Layer Measuring Stations*

| Angle of Attack (deg) | Airfoil Lift, Drag, Pitching Moment | Surface Pressures | Boundary Layer Mean Flow | Boundary Layer Turbulence |
|---|---|---|---|---|
| 0, 1, 2 (2) 8 | X | X | | |
| 9 | X | X | X | |
| 10 | X | X | | |
| 12 | X | X | X | |
| 14 | X | X | | |
| 15 | X | X | X | X |
| 16, 18, 19 (1) 24 | X | X | | |

*Table 2 Test Matrix*

| Data | Engineering Units | Coefficients | Normalized Data | Uncorrected Data | Corrected Data |
|---|---|---|---|---|---|
| Freestream Conditions | X | | X | | X |
| Lift, Drag, Pitching Moment | | X | | | X |
| Surface Pressures | | X | | | X |
| Boundary Layer Velocity | | | X | | X |
| Reynolds Stresses | | | X | | X |
| Skin Friction | | | X | | X |

*Table 3 Data Availability*

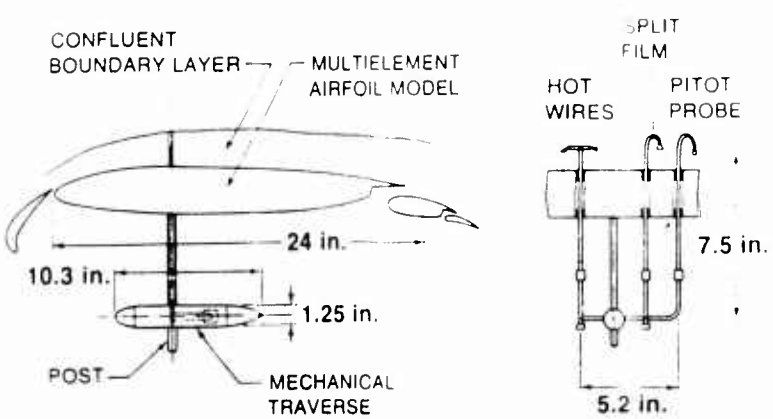



*Fig. 8 Probes and Probe Support*

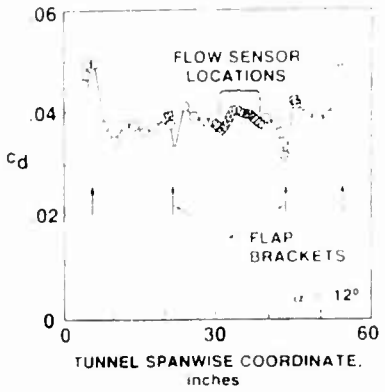



*Fig. 9 Variation of Airfoil Wake Rake Drag Across Tunnel Span*

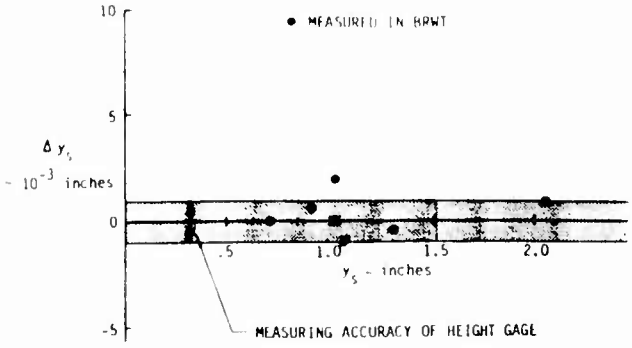



*Fig. 10 Position Accuracy of Mechanical Traverser*

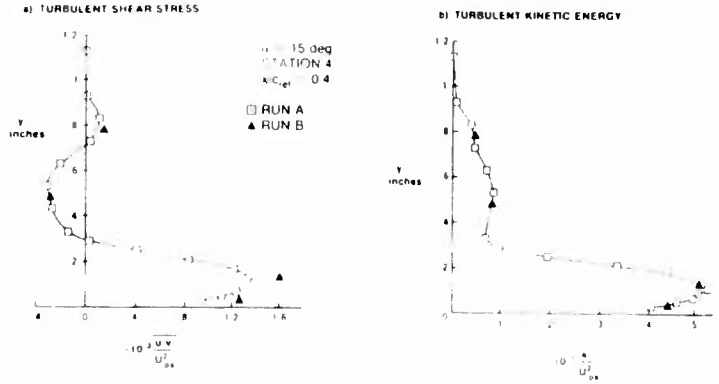



*Fig. 11 Repeatability of Turbulence Measurements*

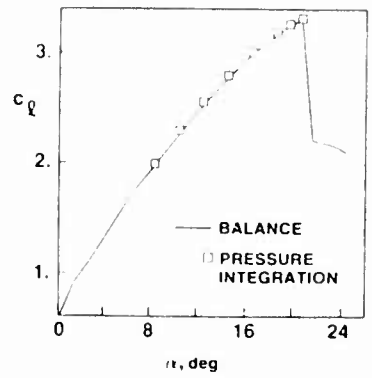



*Fig. 12 Airfoil Lift*

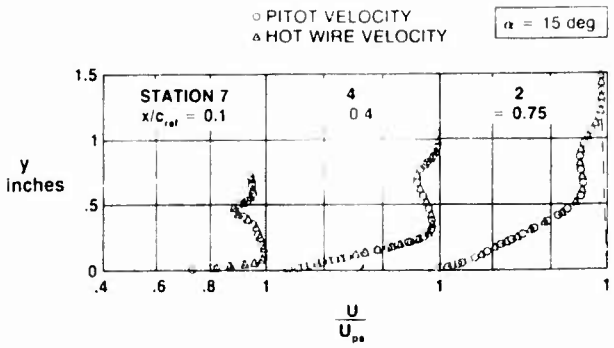



*Fig. 13 Comparison of Velocity Profiles Obtained from Hot Wires and Pitot Probe*

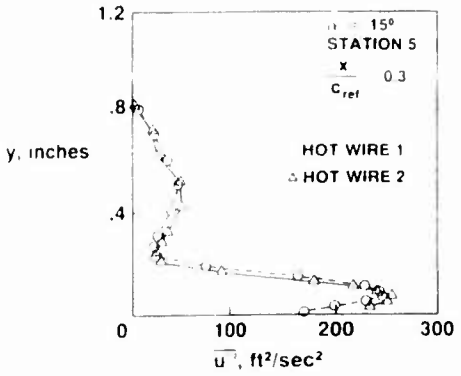



*Fig. 14 Streamwise Component of Reynolds Normal Stresses from Different Hot Wires*

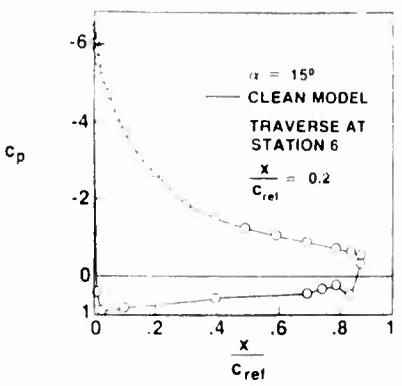



*Fig. 16 Effect of Traverse on Wing Surface Pressures at Model Centerline*

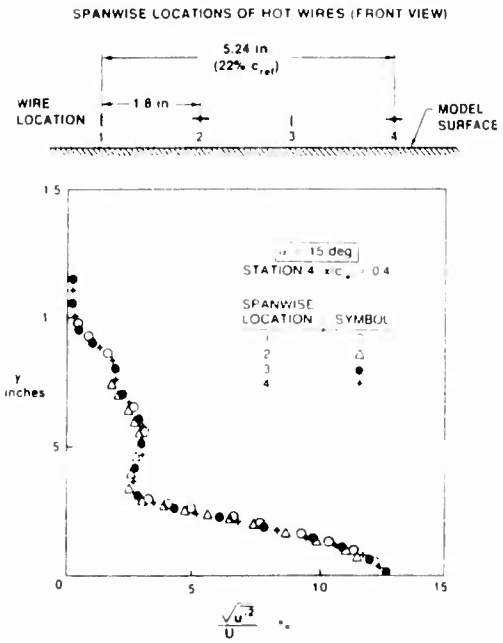
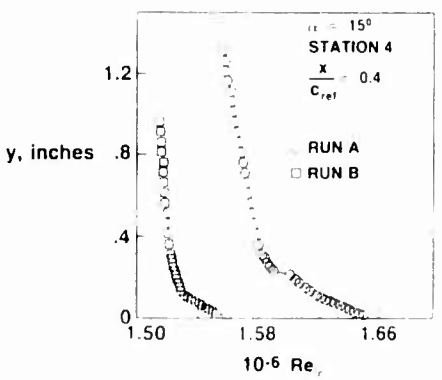
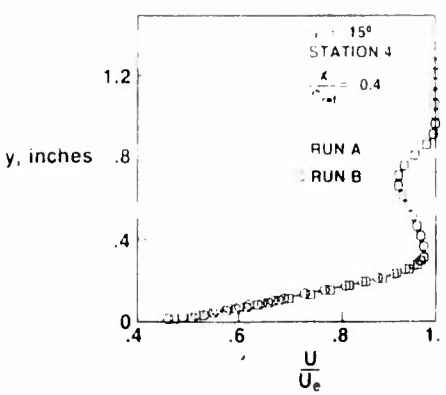



*Fig. 15 Profiles of Streamwise Turbulence at Different Spanwise Measuring Locations*




a) Tunnel Free Stream Reynolds Number




b) Boundary Layer Velocity Profiles

*Fig. 17 Effect of Changes in Reynolds Number on Boundary Layer Profiles*

# MEASUREMENTS OF THE FLOW OVER A LOW ASPECT-RATIO WING IN THE MACH NUMBER RANGE 0.6 TO 0.87 FOR THE PURPOSE OF VALIDATION OF COMPUTATIONAL METHODS.

Part 1: Wing design, Model construction, Surface flow
Part 2: Mean flow in the boundary layer and wake - 4 test cases

by
M C P Firmin
M A McDonald
Aerodynamics & Propulsion Dept.
DRA Farnborough
GU14 6TD, UK

## 1. INTRODUCTION & GENERAL DESCRIPTION

The experiments presented should improve the understanding of the flow over a wing as the speed is increased towards the buffet and separation boundaries. These boundaries limit the flight envelopes of both military and civil aircraft, and the measurements reported will allow Computational Fluid Dynamic (CFD) methods for viscous flow to be validated.

The measurements are reported in two documents (Parts 1 & 2)[2,3] giving detailed measurements of the subsonic free stream flow over a low aspect-ratio wing (RAE Model 2155) at conditions where the boundary layers are subjected to severe adverse pressure gradients. Part 1 provides measurements of pressure distributions on both the wing and on the tunnel walls for a wide range of Mach numbers and lift coefficients, as well as of wing surface skin friction and surface flow direction measurements for four test cases, while Part 2 contains detailed mean flow measurements within the shear layers. For this detailed study, the same four test cases have been used, as presented in Part 1. They were chosen to provide examples of flows with severe adverse pressure gradients, including those with shock waves, and leading in some cases to separation. Two forms of separation are considered, firstly where the flow close to the surface is moving upstream of the wing planform generators in the region of the trailing edge (i.e. trailing edge separation), and secondly where the boundary-layer flow separates in the region of a shock wave, over part of the span, as a result of the sudden pressure rise associated with the shock wave (i.e. shock induced separation). The case with shock-induced separation has reattachment upstream of the trailing edge and, in this respect, is reminiscent of the flow, CASE 10, over the aerofoil RAE 2822[4] which has shown up inadequacies in turbulence modelling. The cases studied also include flows on the upper and lower surfaces where there are severe adverse pressure gradients, on the aft 40 - 50% chord, typical of the flow over the relatively thick wing sections with aft rear loading found on transport aircraft wings. Flows of this type revealed the need for improved boundary-layer methods, including 'higher order' effects, in the methods for aerofoil flows[2].

For the measurements the wing was mounted as a half model in the RAE 8ft x 6ft (2.4m x 1.8m) Transonic Wind Tunnel at Farnborough. The present experiment meets the need for data of comparatively high quality with the initial and boundary conditions of the tunnel flow accurately specified. A boundary-layer trip was used to promote turbulent boundary layers at a known location on both surfaces of the wing using a sparse distribution of particles, and the boundary-layer thicknesses were also measured on the forward part of the wing some distance behind the trip. The wing has been inspected and a set of 'measured' ordinates are available. Solid tunnel walls have been used with pressure measurements having been made on the walls. These wall measurements were also used to calculate the wall interference for the full range of conditions, using the method of Ashill and Weeks[8,9], so indicating the limitations of the data for validating 'free-air' methods. The wall interference can be appreciable for the flows with the higher free stream Mach numbers, and it is recommended that methods to be validated include an adequate representation of the wind-tunnel walls.

Reference 2 presents, in section 2, details about the fluid dynamic design of the wing, details of the ordinates, the model construction, including information about the distribution of the surface pressure points, the traverse mechanisms, and yawmeter probes. In sections 3 and 4 details are given of the tunnel-wall pressure measurements. Details of the analysis of the wall pressure measurements to provide estimates of the magnitude of the wall interference effects are given in section 5. In this section the results from the analysis are also compared with some other methods of predicting the effects. Section 6 is concerned with the surface pressure measurements and surface oil flow. Discussion is included concerned with the mean flow close to the surface of the wing and the regions of flow separation indicated by the pressure measurements. Where results exist these are compared with the separated flow regions shown up by the surface oil flow. Also presented in section 6 are results for the lift coefficients as determined from integration of the pressure measurements. In section 7 results are presented for the boundaries of significant flow separation and flow breakdown, as a function of free stream Mach number and wing incidence (lift coefficient). These boundaries are often used as a guide to the buffet boundary for a wing. The choice of test cases for which boundary-layer measurements are presented in Ref 3 is given in section 7, and full details of the four cases together with the description of the flow for each is given in section 8. In section 9 results are presented from an analysis of the surface oil flow giving flow directions close to the wing surface and measurements of the skin friction of the mean flow as determined using the 'razor blade' technique are also given. In section 10 some comments are included about using the data presented in the report for the validation of computational methods.

The results from the analysis of the yawmeter measurements are given in reference 3, the second report. This includes a wide coverage of mean flow velocity profiles for the four test cases, including some profiles downstream of the trailing edge in the near wake. There are a number of examples where the boundary-layer flow has been measured twice, because of the limited range of calibration of the yawmeter probes. These give a chance to assess the repeatability of the flow and the boundary-layer data where valid information overlaps.

## 2. DETAILS OF MODEL

| | | |
|---|---|---|
| 2.1 | General Geometric arrangement | Half wing mounted in tunnel, See Figure 1. |
| 2.3 | Wing data. | Simple, swept back, tapered with parabolic tip, see Fig 2. |
| 2.3.1 | Planform | |
| | Aspect ratio. | 3.271 |
| | Taper ratio. | 0.3906 |
| | Leading edge sweep. | 39.0 degrees |
| | Trailing edge sweep. | 15.0 degrees |
| | Twist distribution. | See Figure 3 |
| | Semispan. | 1028.7 mm |
| | Details of tip geometry. | Parabolic, see reference 2 |
| 2.3.2 | Basic wing sections. | See Figure 4, a sample of wing sections are given |
| | Thickness/chord ratio. | Variable, about 11.5%, see Figure 3 |
| | Nose radius/chord ratio. | Variable, 0.0215 at the root, reducing to 0.0157 at 35% semi-span. Nearly constant outboard of 35% semi-span |
| 2.4 | Body data. | Wing mounted on wall of test section, with some evidence on the wall boundary-layer thickness available |
| 2.7 | Geometric definition of wing. | |
| 2.7.1 | Shape. | Numerically defined, 131 - 147 ordinates at each section, 33 chordwise sections |
| 2.7.2 | Design or Measured Co-ordinates. | Design at all above locations. Measured at most locations and new co-ordinates generated for all design locations |
| 2.7.3 | Tolerances. | Requested ±0.1 mm with change in error ±0.002 mm per mm. Actual see reference 2 |
| 2.7.4 | Surface roughness. | Requested 0.2 micro-metres |
| 2.8 | Model support details. | |
| 2.8.1 | Mounting. | Mounted on half model balance with gap between wall and model sealed, see Figure 1 |

## 3. GENERAL TUNNEL INFORMATION

| | | |
|---|---|---|
| 3.1 | Tunnel designation. | RAE 8ft x 6ft transonic wind tunnel |
| 3.2 | Organisation running the tunnel. | DRA, Farnborough |

3.3 Tunnel characteristics.

| | | |
|---|---|---|
| 3.3.1 | Type of tunnel. | Continuous, variable pressure, closed circuit plus bypass system for $M_\infty > 0.8$. See Figure 5 |
| 3.3.2 | Operating envelope. | Tests made at constant Reynolds No. based on mean chord ($4.1 \times 10^6$) |
| 3.3.3 | Run time. | Variable: Depends on experiment, usually > 20 mins., < 2 hours. |

3.4 Test section.

| | | |
|---|---|---|
| 3.4.1 | Test section dimensions. | Height = 1.83 m, width = 2.43 m, rectangular with corner fillets 160.5 mm x 45° length = 5.531 m no protruding instrumentation except for centre line support rig. See Figure 1 |
| 3.4.2 | Wall geometry details. | Solid walls for these tests with slots at downstream end, 1.08 m long on roof and floor 0.64 m long on side walls |
| 3.4.3 | Wall measurements. | Pressures at about 80 points on each sidewall and roof. See Figure 6.<br>Boundary layer profiles measured using rake at mid point on each wall including floor at about 0.56 ahead of wing apex for 4 Test Cases (separate tests). |
| 3.4.4 | Boundary layer thickness. | Details given in reference 2, average value for displacement thickness is 5mm, or 0.5% of root chord. (no control). |

3.5 Freestream conditions.

| | | |
|---|---|---|
| 3.5.1 | Total pressure. | Measured on centre line in working section during a calibration and related to wall pressure measured in contraction ahead of working section |
| | Static pressure. | Wall pressure used at upstream part of working section- see reference 2 for details |
| | Total temperature. | Measured in contraction ahead of working section |
| 3.5.2 | Tunnel calibration. | Used centre line static tube and sidewall pressures - adjustment of Mach number gradient using angle of roof |
| | Last calibration. | 1985, just prior to start of tests |

3.6 Flow quality (empty tunnel).

| | | |
|---|---|---|
| 3.6.1 | Flow uniformity. | No detailed measurements made for empty tunnel with solid walls |
| 3.6.2 | Temperature variation. | a) Control - Yes, for general level.<br>b) Variation within tunnel - No measurements made.<br>c) Variation over run - Some variation permitted, Reynolds Number held constant. |
| 3.6.3 | Flow unsteadiness. | See Figure 7 |

## 4. INSTRUMENTATION

4.1 Model position.

| | | |
|---|---|---|
| 4.1.1 | Geometric incidence. | Special rig set with respect to walls of tunnel |
| 4.1.2 | Accuracy. | ±0.01° |

| | | |
|---|---|---|
| 4.2 | Model pressure measurements. | |
| 4.2.1 | Pressure holes. | 469, 308 on upper surface, 161 on lower surface, see Figures 8 & 9 |
| 4.2.2 | Range and accuracy. | Differential-pressure capsule-manometers with stagnation reference pressure. 1 atmosphere range calibrated to give ±0.03% FSD accuracy. Pressure readings frozen when steady and then scanned |
| 4.2.3 | Dynamic pressures. | Not measured |
| 4.3 | Force and moment measurem[illegible] | None measured, deduced from pressures only |
| 4.4 | Boundary layer and flow [illegible] | |
| 4.4.1 | Measurement technique | Pressure probes - mean values only<br>Yawmeters x/c > 0.35<br>Flattened pitots x/c < 0.35 |
| 4.4.2 | Flow region investigated. | Boundary layers & wakes, see Figures 10 & 11 |
| 4.4.3 | Probes. | a) Yawmeters, x/c > 0.6,<br>Support - see Figure 12, Probe - see Figure 13<br>0.35 > x/c > 0.6<br>Support - see Figure 14, Probe - see Figure 15<br>b) Pitots, x/c < 0.35<br>Support - see Figure 14, Probe - see Figure 16 |
| 4.5 | Surface flow visualization. | |
| 4.5.1 | Measurement technique. | Oil flow with a grid for measurements |
| 4.5.2 | Surfaces. | Upper & lower surfaces of wing |
| 4.5.3 | Form of data. | Photographs taken during the tunnel runs. Tables for x/c > 0.45 - same locations as for skin friction also photographs - see reference 2. |
| 4.6 | Flow field visualization. | None |
| 4.7 | Tunnel wall measurements. | |
| 4.7.1 | Type of measurement. | Pressure measurements on walls, excluding wall on which wing is mounted |
| 4.7.2 | Location of pressure holes. | See Figure 6, Pressure differences between empty tunnel and actual runs are presented. |

## 5. TEST MATRIX AND CONDITIONS

| | | |
|---|---|---|
| 5.1 | Detailed test matrix. | |
| 5.1.1 | Number of test cases. | a) Full range of data, including wing surface & wall pressures, boundary layer & wake profiles, skin friction (via 'razor blades'), surface flow direction (via oil flow): 4 cases.<br>b) Wing & wall pressures only: 82 cases.<br>c) Wing & wall pressures + surface oil flow photographs, both surfaces: 12 cases (4 analysed under a) above) |
| 5.1.2 | Number of configurations. | 1 only |

5.1.3 Details of test cases.

a) see 5.1.1 a)
All measurements were made for a Reynolds number based on mean chord = 4.1 x $10^6$

CASE 1.- $M_\infty$ = 0.744, $\alpha_{geo}$ = 2.5°

CASE 2.- $M_\infty$ = 0.806, $\alpha_{geo}$ = 2.5°

CASE 3.- $M_\infty$ = 0.843, $\alpha_{geo}$ = 1.5°

CASE 4.- $M_\infty$ = 0.854, $\alpha_{geo}$ = 1.5°

b) see 5.1.1 b)
The following list, gives the nominal values for the free stream Mach numbers and geometric settings for the incidence of the wing.
For these the CASE is determined by the nominal values of $M_\infty$ & $\alpha_{geo}$:
(i.e. $M_\infty$ = 0.84, $\alpha_{geo}$ = 2.5° is CASE 8425):

$\alpha_{geo}$ = 1.5°, $M_\infty$ = 0.60, 0.70 (0.02) 0.82, 0.83 (0.01) 0.87
$\alpha_{geo}$ = 2.0°, $M_\infty$ = 0.60, 0.70 (0.02) 0.78, 0.79, 0.80, 0.82 (0.01) 0.86
$\alpha_{geo}$ = 2.5°, $M_\infty$ = 0.60, 0.70 (0.02) 0.82, 0.83 (0.01) 0.86
$\alpha_{geo}$ = 3.0°, $M_\infty$ = 0.60, 0.70 (0.02) 0.82, 0.83 (0.01) 0.85
$\alpha_{geo}$ = 3.5°, $M_\infty$ = 0.60, 0.70 (0.02) 0.82, 0.83 (0.01) 0.85
$\alpha_{geo}$ = 4.0°, $M_\infty$ = 0.60, 0.70 (0.02) 0.80, 0.81 (0.01) 0.84
$\alpha_{geo}$ = 4.5°, $M_\infty$ = 0.60, 0.70 (0.02) 0.80, 0.81 (0.01) 0.84

c) see 5.1.1 c)
The following cases from b) above have evidence from oil flow as well:

$\alpha_{geo}$ = 1.5°, $M_\infty$ = 0.84, 0.85, 0.86
$\alpha_{geo}$ = 2.0°, $M_\infty$ = 0.80, 0.82, 0.83, 0.84, 0.85
$\alpha_{geo}$ = 2.5°, $M_\infty$ = 0.74, 0.80, 0.82, 0.84

5.2 Model/tunnel relations.

5.2.1 Maximum blockage. — 1.17%

5.2.2 Maximum span/tunnel height. — 0.53 (mounted vertically)

5.2.3 Wing area/tunnel cross section. — 0.15

5.2.6 Have adiabatic wall temperatures been reached — Yes, minimum run times 20 minutes, usually much longer

5.3 Transition details.

5.3.1 Fixed Transition — Yes

5.3.3 Transition location — Bands centred at 5% local chord on both surfaces, 2.5mm wide, faired into tip, ballotini (glass balls).

5.3.4 Roughness size — Sparse distribution
upper surface 0.21mm to 0.25mm
lower surface 0.15mm to 0.18mm
resin in band < 0.03mm

5.3.5 Effectiveness — Calculated size for highest local Mach number on each surface, for CASES 1 to 4. This may have resulted in "overfixing" at some conditions. Verified by indirect checks. The profiles, at approx 18% chord on both surfaces indicate that the boundary layers are turbulent.

## 6. DATA

### 6.1 Availability of data

| | | |
|---|---|---|
| 6.1.1 | Organisation owning data | Aerodynamics & Propulsion Department<br>DRA Farnborough<br>UK |
| 6.1.2 | Who is responsible for data | Mr. M.C.P. Firmin(c/o Dr. P.D. Smith)<br>Aerodynamics & Propulsion Dept.,<br>R141 Building,<br>DRA Farnborough,<br>Farnborough, Hants. GU14 6TD<br>Tel: 44 252 24461, Extn. 3737<br>Fax: 44 252 375890 |
| 6.1.3 | [illegible] freely available | Yes |
| 6.1.4 | Contact | Head of Aerodynamics & Propulsion Department. |

### 6.2 Suitability of data for CFD validation

| | | |
|---|---|---|
| 6.2.1 | "In-tunnel" calculations. | Yes, see reference 2 for suggested method of use |
| 6.2.2 | "Free-air" calculations. | Not advised, corrections available but variable over wing and large at higher Mach numbers, see reference 2 |

### 6.3 Type and form in which data available

| | | |
|---|---|---|
| 6.3.1 | a) Free Stream | Equivalent empty tunnel Mach number |
| | b) Surface Pressures | Normalized with respect to free stream Total Pressure |
| | c) Skin Friction | Coefficient based upon local flow conditions |
| | d) Forces | Based on appropriate area or chord and Free Stream (i.e. empty tunnel values) |
| | e) Boundary layer | |
| | Integral quantities | Based upon local flow conditions and in terms of root chord. |
| | Profiles | Normalized with respect to velocity determined from Total Pressure at edge of layer and local static pressure for yawmeter measurements. Wall static pressure used for pitot measurements. |
| | f) Wake | |
| | Integral quantities | Based upon local flow conditions and in terms of root chord. |
| | Profiles | Normalized with respect to velocity determined from Total Pressure at edge of layer and local static pressure.<br>(See reference 3 for statement about flow direction at edges of layer) |
| | g) Test section wall pressures | Change in pressure from 'empty tunnel' values given as change in normalized wall pressures. Empty tunnel values interpolated to same free stream values. |
| 6.3.2 | Data carrier. | Floppy disc |
| 6.3.3 | Extent of geometry data. | 370 Kbytes |
| 6.3.4 | Extent of aerodynamic test data. | a)Boundary layers/wake profiles: 500 Kbytes for 4 Cases |

b)Surface pressures: 450 Kbytes for 84 Cases

c)Tunnel wall pressures: 360 Kbytes for 84 Cases

6.4 Corrections applied to data

| | | |
|---|---|---|
| 6.4.1 | Upwash and Blockage. | None applied, because magnitude variable over planform |
| 6.4.2 | Correctable | No, but magnitude available from measured wall pressures, examples:<br>$M_\infty = 0.70$, $\Delta M_\infty < 0.002$, $\Delta\alpha < 0.6°$<br>$M_\infty = 0.80$, $\Delta M_\infty < 0.010$, $\Delta\alpha < 0.8°$<br>$M_\infty = 0.85$, $\Delta M_\infty < 0.020$, $\Delta\alpha < 0.9°$ |
| 6.4.3 | Half model corrections | None applied |
| 6.4.4 | Support corrections | Model mounted on wall of tunnel and thickness of wall boundary layer known |
| 6.4.5 | Aero-elastic deformation | Negligible |

## 7. DATA ACCURACY AND REPEATABILITY ASSESSMENT

7.1 Estimate of accuracy

| | | |
|---|---|---|
| 7.1.1 | Mach number, Model incidence | From calibration $\Delta M_\infty \pm 0.0015$, $\Delta\alpha \pm 0.01°$<br>Datum angle of incidence from measurements on symmetrical aerofoil |
| | Variation of $M_\infty$ during tests: | $M_\infty$ kept within $\pm 0.002$ of required value during tests to obtain wing surface and tunnel wall pressures. In addition, during measurements of boundary-layer profiles, the location of the shock waves on the upper surface of the wing were monitored. $M_\infty$ was adjusted to keep the shock location fixed for each CASE. |
| 7.1.2 | Measured pressure coefficients. | $\Delta p/H$, $\pm 0.0003$ based on calibration of transducer only. |
| 7.1.3 | Boundary layer/wake data. | No assessment made |

7.2 Repeat measurements.

| | | |
|---|---|---|
| 7.2.1 | Wing pressures. | Wing pressures measured many times during measurements of boundary layers, and during skin friction measurements. Some of these measured some 2 years later. - Figure 17a-17d. For 1987 runs 'razor blades' at $x/c = 0.45$ (upper surface) and 0.55 (lower surface) at most $\eta$. There are some inconsistent values at 5% chord, caused by a local effect of the transition trip. |
| 7.2.2 | Boundary layers. | Some repeat checks possible because more than one probe support arm was used for a complete profile, usually where the twist through the layer is large - details in Reference 3. |

7.3 Redundant measurements.

| | | |
|---|---|---|
| 7.3.1 | Skin friction. | Determined by boundary-layer profile, and by 'razor blade' technique |
| | Surface flow direction. | Determined by boundary-layer profile, and by surface-oil flow - Figure 18, also see Reference 3. |

7.4 Other tests on same (nominal) geometry. None, other than on a pilot model of 0.45 scale where surface oil flow showed that the design work had resulted in the required type of flows

## 8. REFERENCES


| | | |
|---|---|---|
| 8.1 On the Wind Tunnel | 1 H F Vessey | Transonic wind tunnel testing techniques: Historical and general introduction. Jour. Royal Aeronautical Society, Vol. 62. (1958) |
| 8.2 On the model and test results | 2 M C P Firmin M A McDonald | Measurements of the flow over a low aspect-ratio wing in the Mach number range 0.6 to 0.87 for the purpose of validation of computational methods. Part 1: Wing design, Model construction, Surface flow. DRA Farnborough TR 92016 (1992) |
| | 3 M C P Firmin M A McDonald | Measurements of the flow over a low aspect-ratio wing in the Mach number range 0.6 to 0.87 for the purpose of validation of computational methods. Part 2: Mean flow in the boundary layer and wake - 4 test cases. DRA Farnborough, TR 930?? (1993), to be published. |
| 8.4 On the applied measurement techniques | 4 P H Cook M A McDonald M C P Firmin | Wind tunnel measurements of the mean flow in the turbulent boundary layer and wake in the region of the trailing edge of a swept wing at subsonic speeds. RAE TR 79062 (1979). |
| | 5 M A McDonald M C P Firmin P H Cook | Measurements and analysis of the mean shear-layer flow over the RAE2822 aerofoil at 28 degrees sweep and at subsonic speeds. RAE TR 89010 (1989) |
| | 6 K G Winter | An outline of the techniques available for the measurement of skin friction in turbulent boundary layers. Prog. A· ospace Sci. Vol 18, pp 1-57, Pergamon Press. (1977) |
| | 7 L F East | Measurement of skin friction at low subsonic speeds by the razor-blade technique. ARC R & M No. 3525 (1968). |
| 8.4 On the Wall Interference method | 8 P R Ashill D J Weeks | A method for determining wall-interference corrections in solid-wall tunnels from measurements of static pressure at the walls. RAE TR 82091 (1982). |
| | 9 P R Ashill D J Weeks | A method for determining wall-interference corrections in solid-wall tunnels from measurements of static pressure at the walls. AGARD CP 335 - paper 1 (1982) |


## 9. LIST OF SYMBOLS

| | |
|---|---|
| A | planform area of wing |
| c | local chord of planform |
| $c_r$ | root chord of planform |
| $\bar{c}$ | geometric mean chord of wing |
| $\bar{\bar{c}}$ | aerodynamic mean chord of wing |
| H | Total pressure |
| M | local Mach number |
| $M_\infty$ | Free stream Mach number, derived from empty tunnel calibration |
| p | local static pressure |
| p | RMS unsteady static pressure |
| q | undisturbed free stream dynamic pressure |
| u | local velocity within a shear layer |
| Up | Velocity obtained from the total velocity at the edge of a shear layer and the local static pressure |
| x | measured from leading edge of section in direction of root chord of planform, or from the wing apex |
| y | spanwise distance measured from the wing apex |
| z | distance normal to the planform |
| $\alpha$ | local incidence |
| $\alpha_{geo}$ | geometric incidence |
| $\beta$ | the total change in the direction of the flow through the shear layer, (degrees) |
| $\beta f$ | the direction of the local flow at the edge of the shear layer in the same axis as for $\beta$ but measured relative to the free stream component of velocity in the plane of the surface, (degrees) |
| $\Delta$ | change in a quantity, usually over planform |
| $\eta$ | spanwise location as a fraction of wing semi-span |

**Figs 1 & 2**

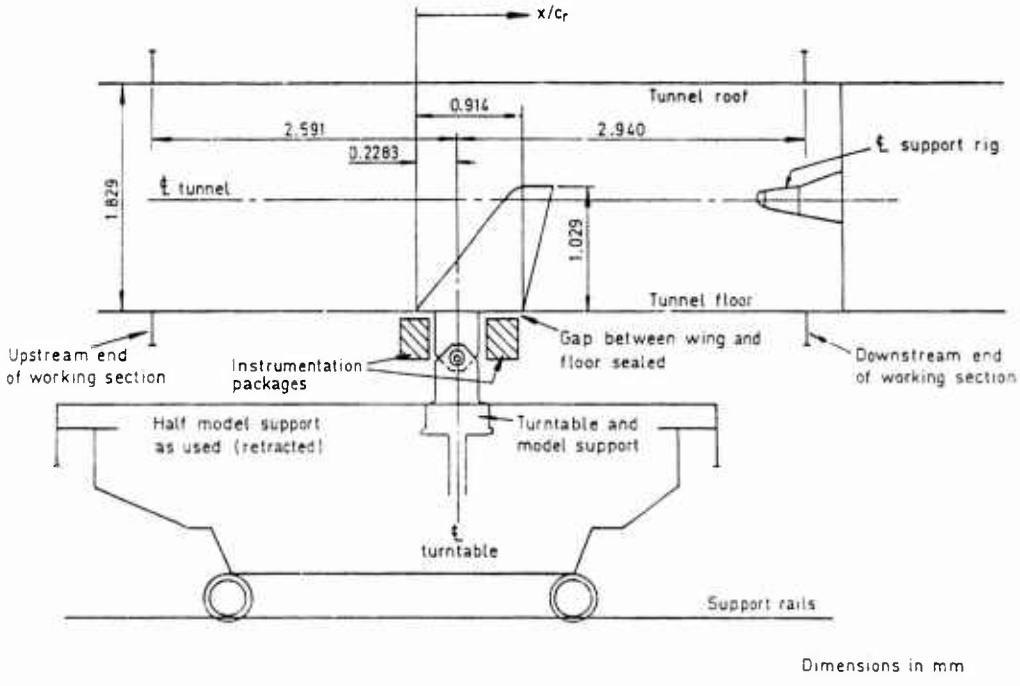



**Fig 1 Model 2155 low aspect-ratio wing mounted in tunnel**

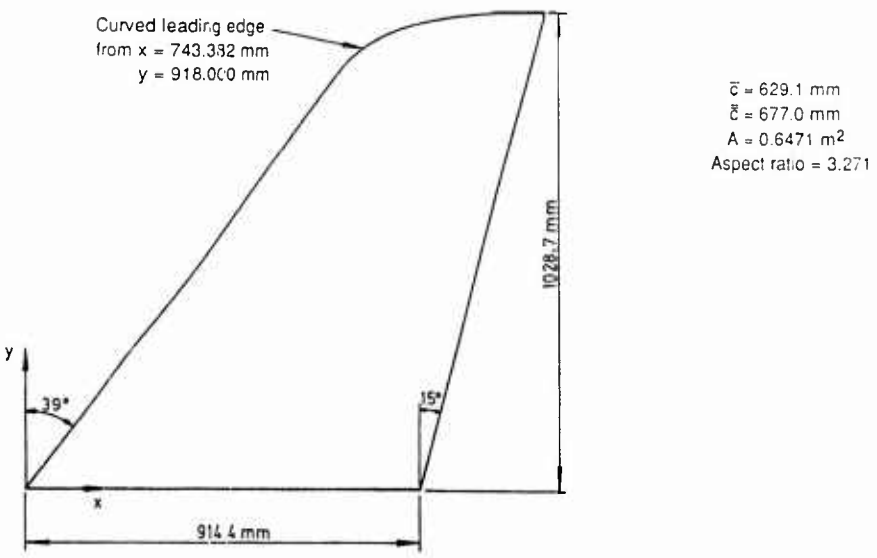



**Fig 2 Main dimension of wing**

**Figs 3 & 4**

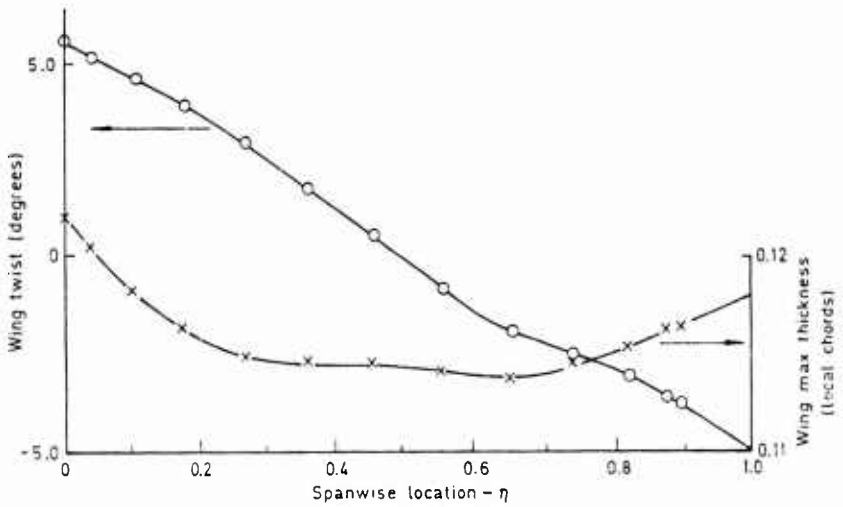



**Fig 3 Spanwise variation of local twist and maximum thickness**

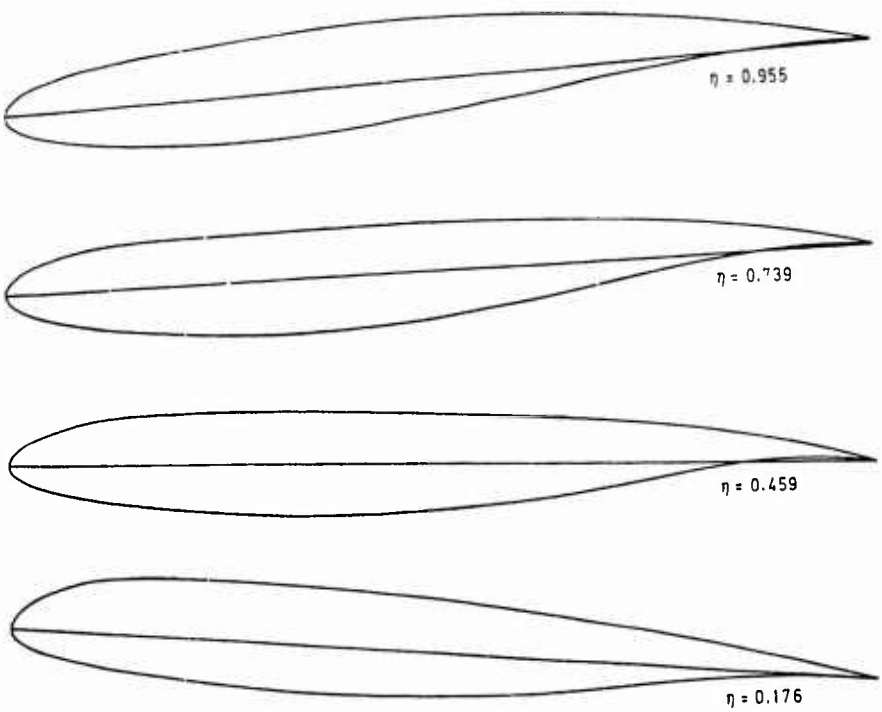



**Fig 4 Wing sections**

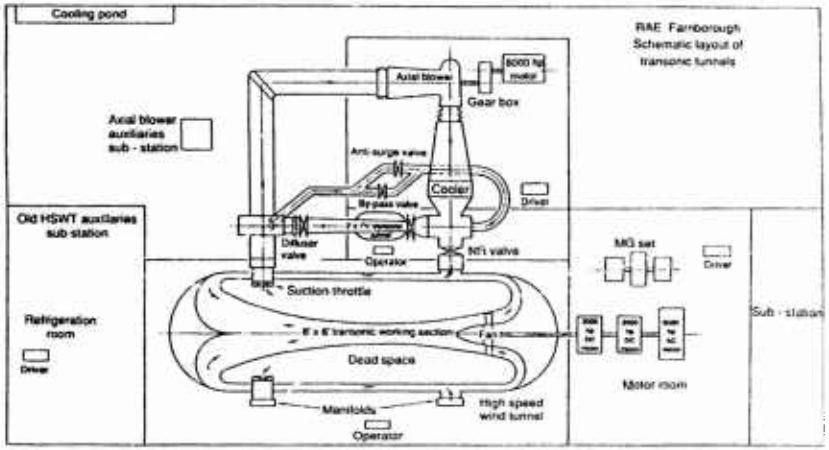



**Fig 5 Schematic layout of RAE 8ft x 6ft transonic tunnel**

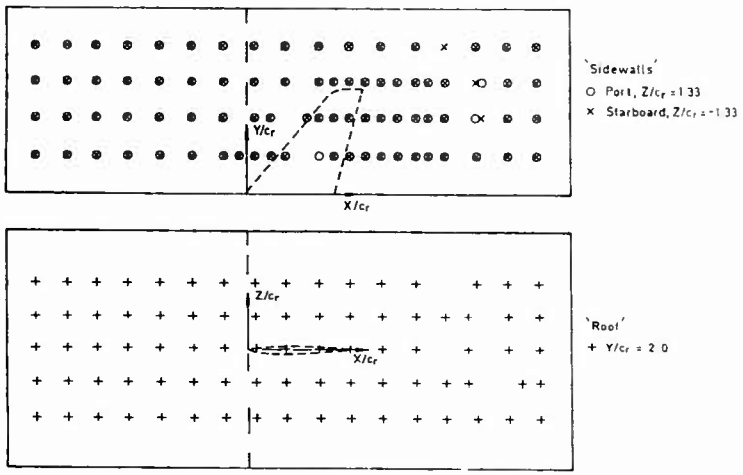



**Fig 6 Location of pressure holes on wind tunnel walls**

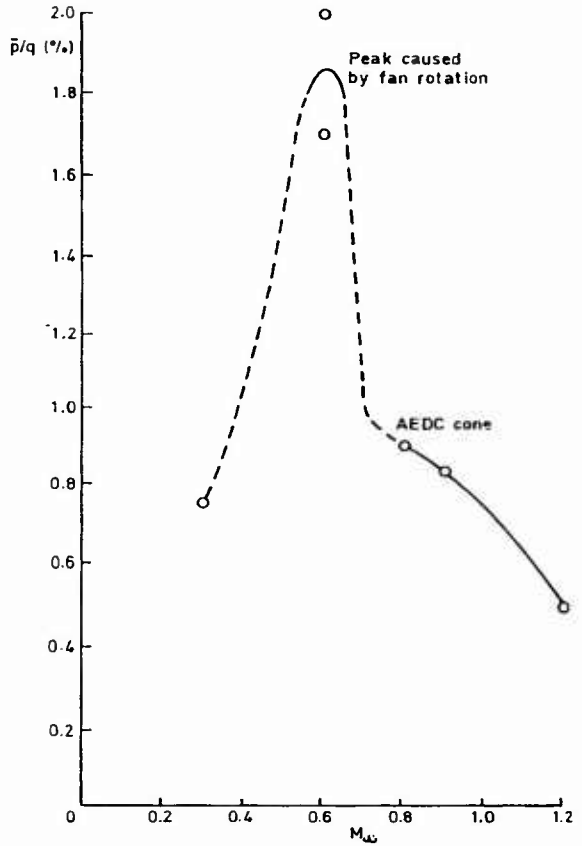



**Fig 7 RAE 8ft x 6ft tunnel - variation of tunnel pressure fluctuations with Mach number**

Figs 5, 6 & 7

B1-11

**Figs 8 & 9**

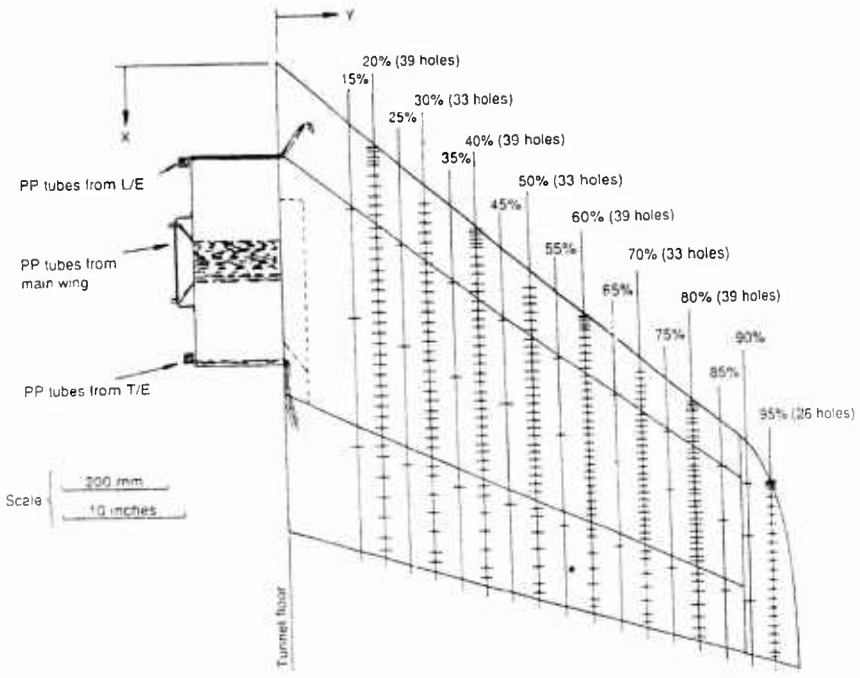



**Fig 8 Plan view of model showing upper surface pressure plotting positions**

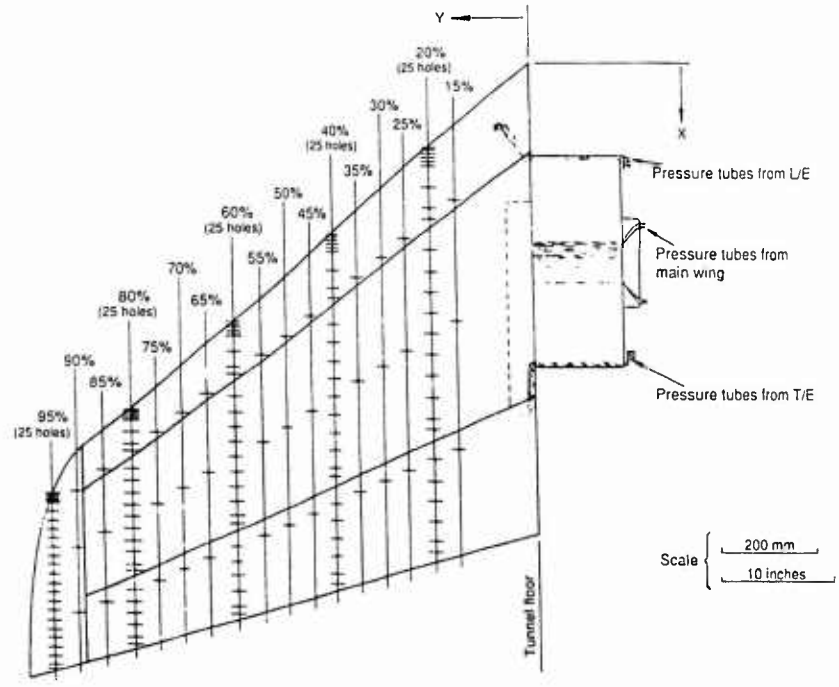



**Fig 9 Plan view of model showing lower surface pressure plotting positions**

**Figs 10 & 11**

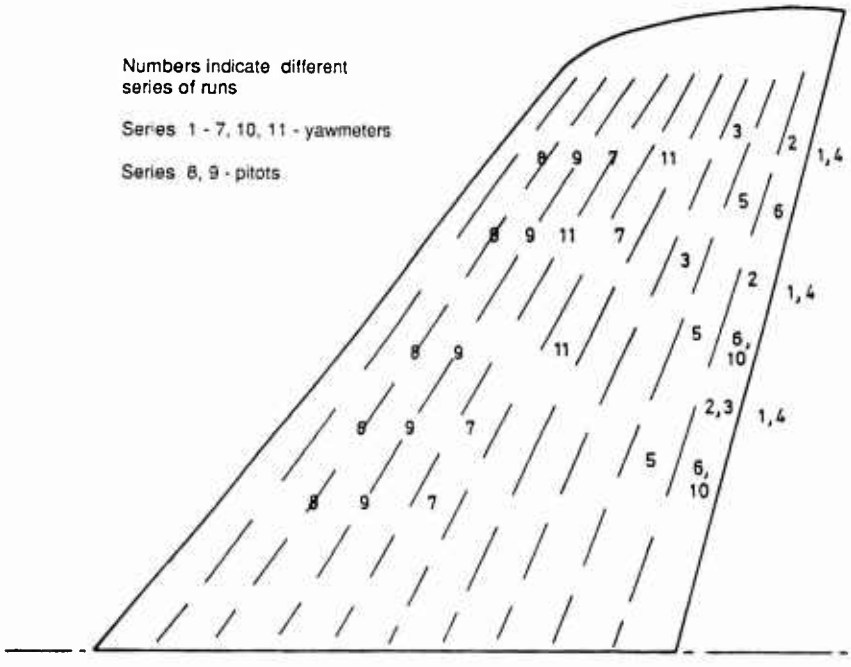



**Fig 10 Locations of measured boundary layer and wake profiles (upper surface)**

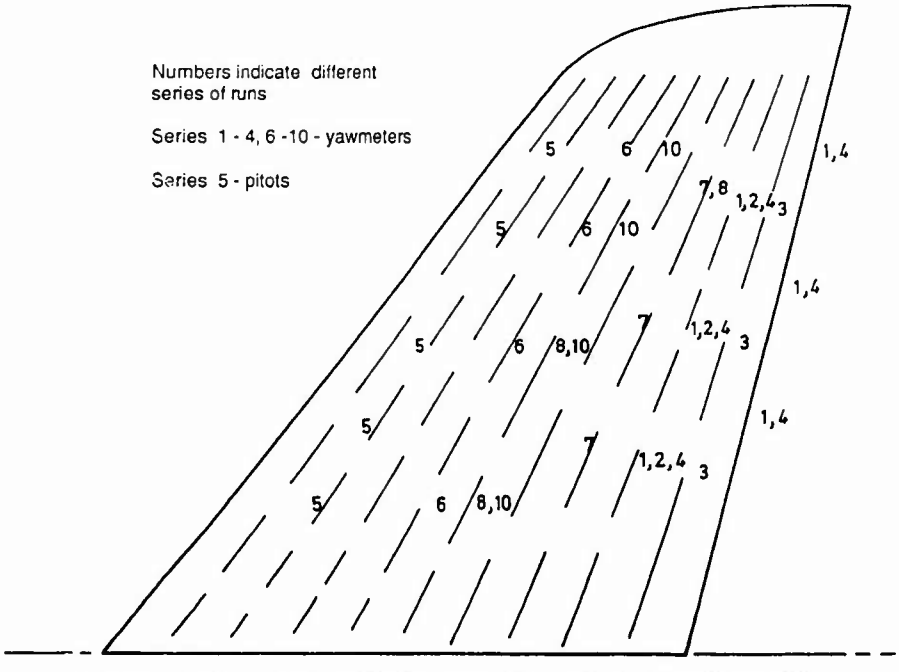



**Fig 11 Locations of measured boundary layer and wake profiles (lower surface)**

**Figs 12 & 13**

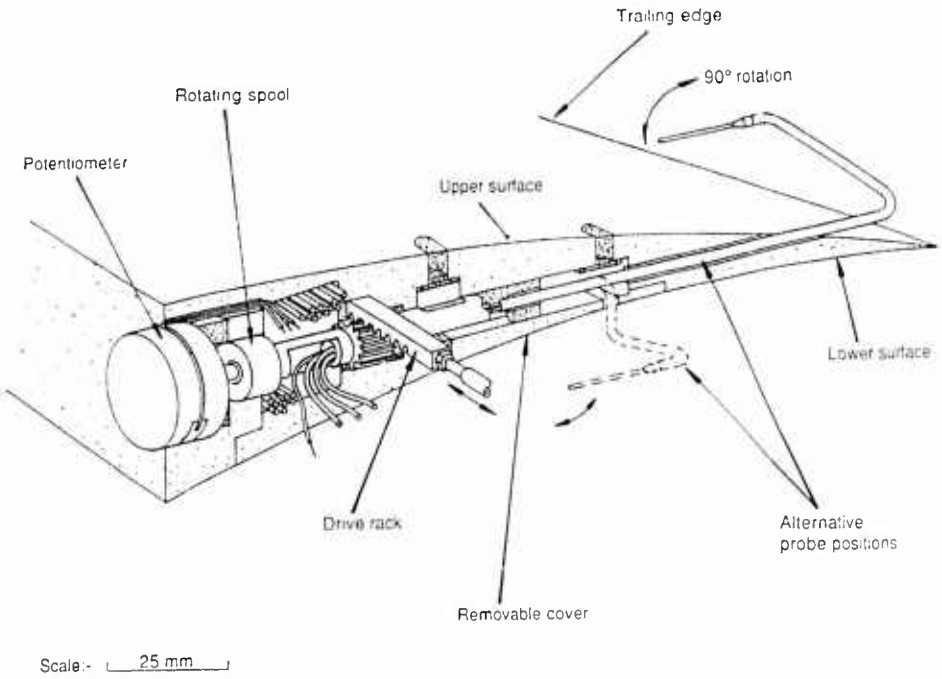



**Fig 12 Wake & boundary layer traverse gear**

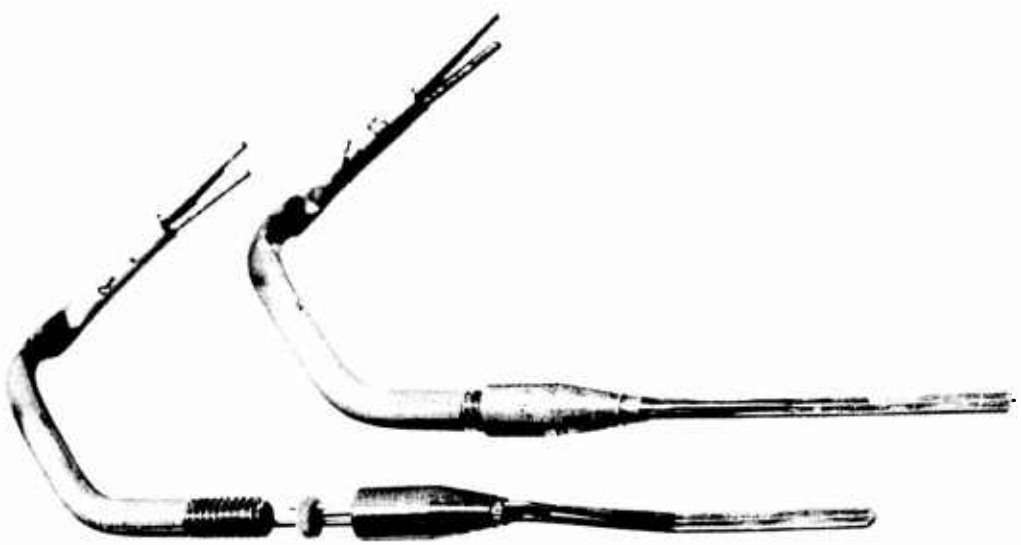


**Fig 13 Assembly of detachable probes for rotary traverses**

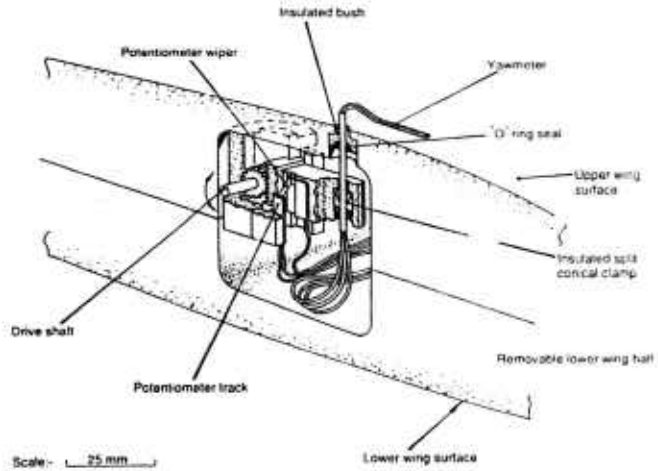



**Fig 14 9.5mm boundary layer traverse gear**

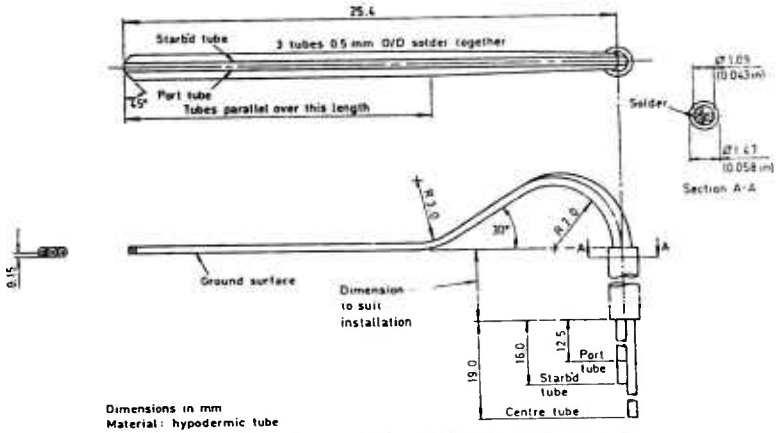



**Fig 15 Yawmeter for linear traverse mechanisms**

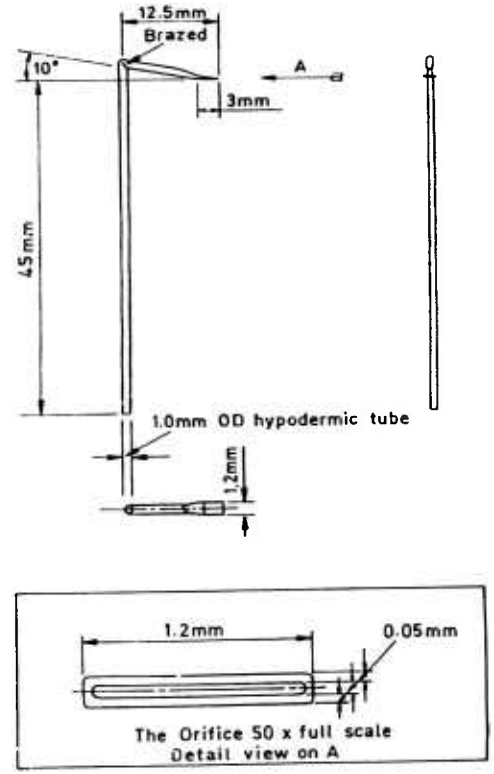



**Fig 16 Flattened pitot probe - 2 x full scale**

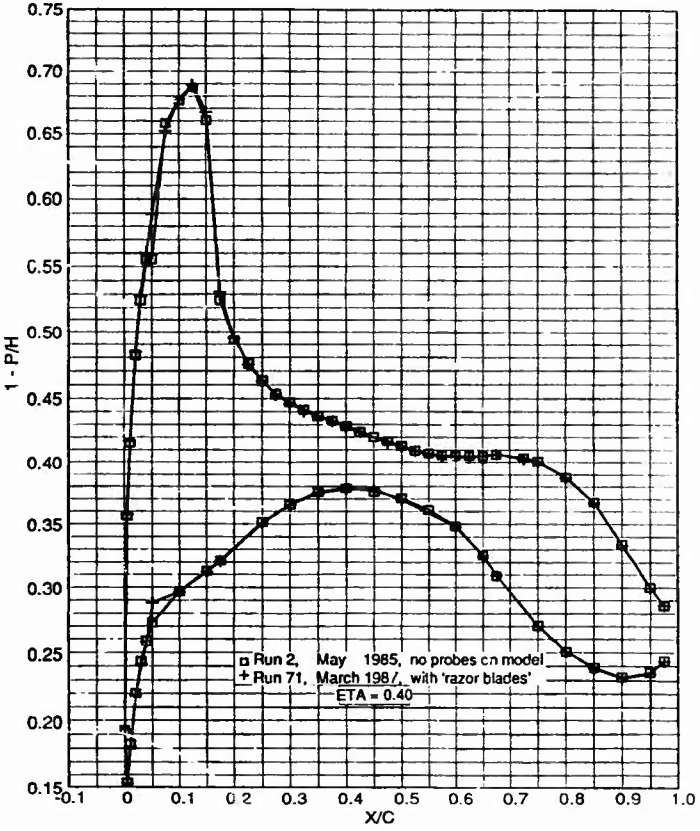



Fig 17a Comparison of pressure distributions measured at the beginning and end of the experimental program
M (inf) = 0.744, Alpha (geo) = 2.5 degs

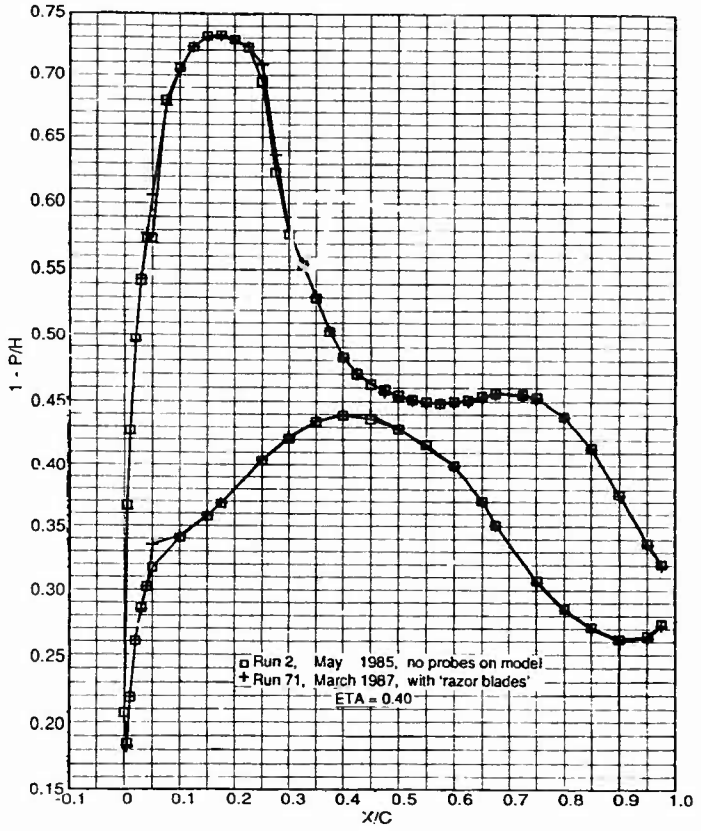



Fig 17b Comparison of pressure distributions measured at the beginning and end of the experimental program
M (inf) = 0.806, Alpha (geo) = 2.5 degs

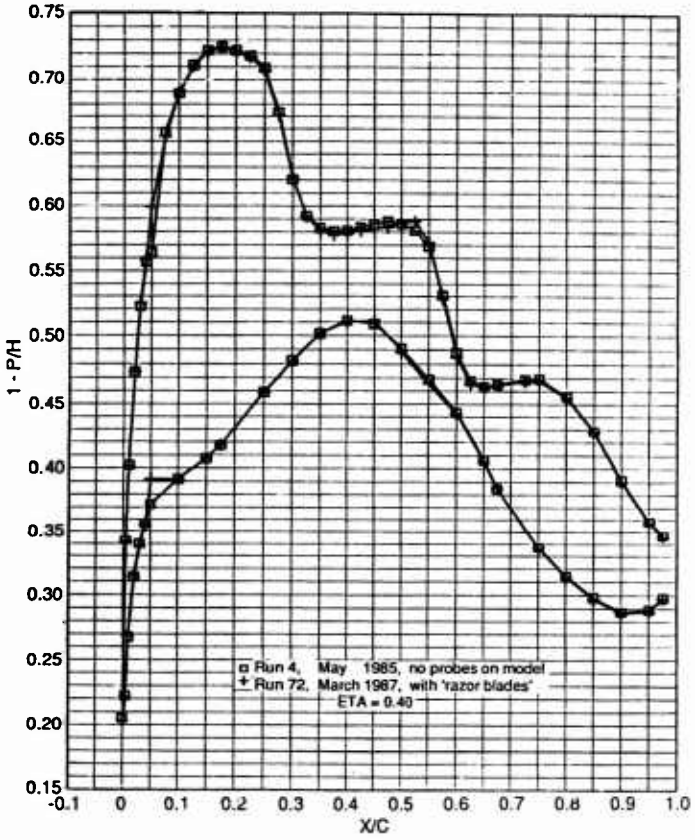



**Fig 17c Comparison of pressure distributions measured at the beginning and end of the experimental program M (inf) = 0.843, Alpha (geo) = 1.5 degs**

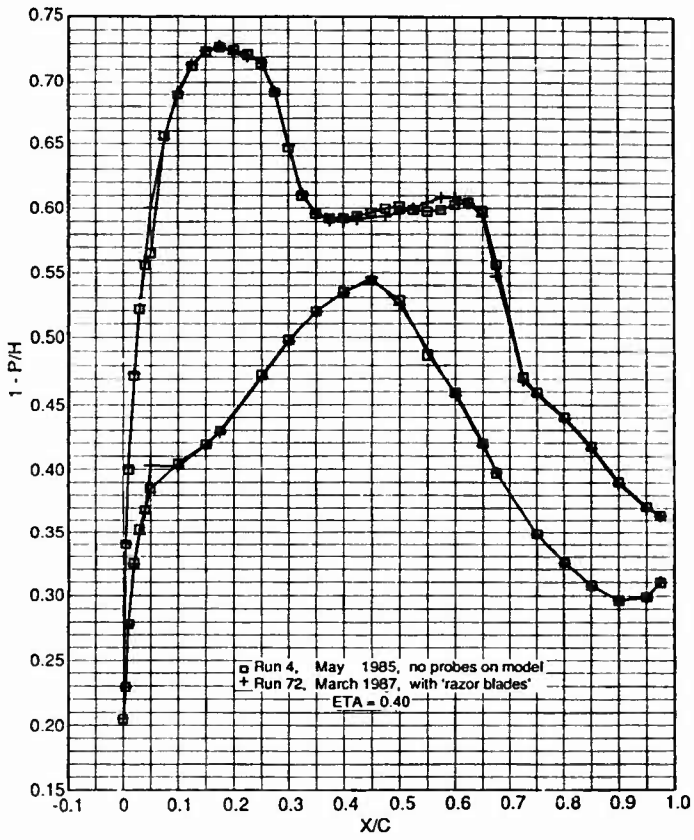



**Fig 17d Comparison of pressure distributions measured at the beginning and end of the experimental program M (inf) = 0.854, Alpha (geo) = 1.5 degs**

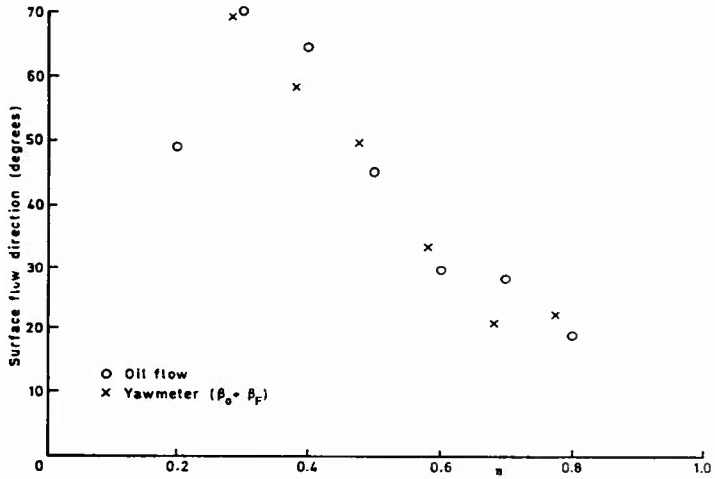



**Fig 18 Upper surface flow direction - x/c = 0.95 - $M_\infty$ = 0.854, $\alpha_{geo}$ = 1.5 degrees Case 4**

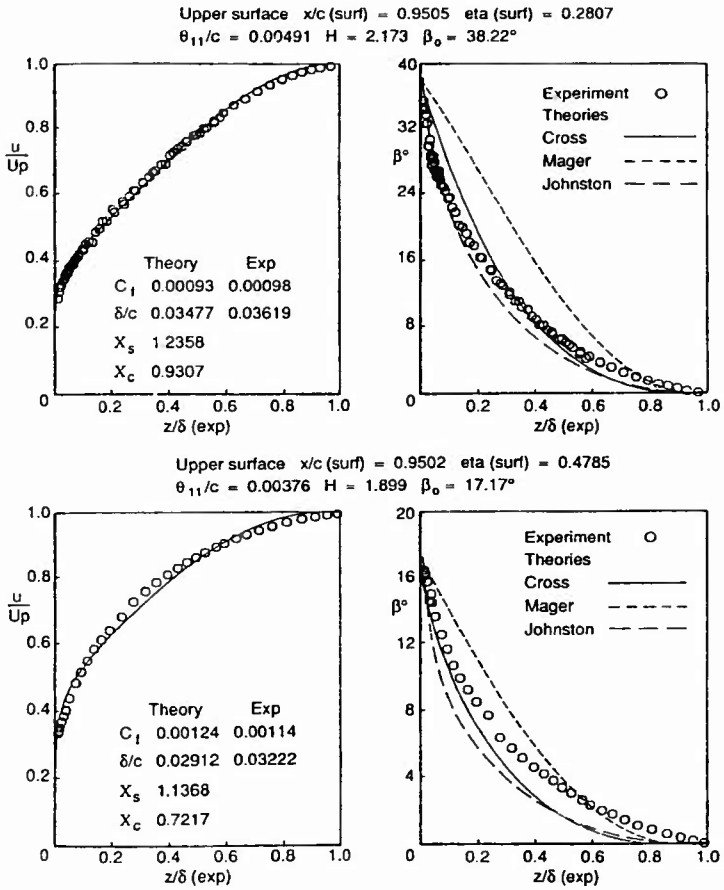



**Fig 19 Example of boundary - layer profiles M (inf) = 0.806, Alpha (geo) = 2.5 degs**

# DETAILED STUDY AT SUPERSONIC SPEEDS OF THE FLOW AROUND DELTA WINGS.

by

M. J. Simmons
DRA, Bedford

## 0 INTRODUCTION

The tests described in this submission were made on two half-models of delta-wing/body configuration suitable for supersonic combat aircraft. The aim of the programme of work was to improve the understanding of supersonic flows over wings with rounded leading edges.

The reasons for choosing the large half-model design were:

a) The attainment of high chordal Reynolds numbers.

b) The facility to make detailed flow measurements.

c) The ability to manufacture the large wing to the desired model accuracy with conventional machine tolerances.

The last requirement is particularly important in the highly-curved region of the leading edge which controls the development of transonic flows on the upper surface.

Both wings are of the same quasi-delta planform of 60° leading edge sweep and thickness form of 4% thickness/chord ratio but with differing camber distributions.

Wing A has a complex camber surface with camber in both spanwise and streamwise planes. Wing C has an uncambered symmetrical section and was used as a datum case for the study.

The only design constraint on model size was the need to ensure that the flow over the wing was not disturbed by shock-wave reflections from the solid walls of the tunnel.

The tests were performed in the 8ft x 8ft Pressurised, Subsonic/Supersonic Wind Tunnel at the Defence Research Agency (DRA Aerospace Division, formerly the Royal Aerospace Establishment) Bedford in July 1985.

The statements in this document apply to both wings unless otherwise stated.

## 1 GENERAL DESCRIPTION

### 1.1 Model name and designation

Model 2205 (Wing A).
Model 2217 (Wing C).

### 1.2 Model type and flow conditions

Delta wing, ½ models, supersonic flow.
($1.4 < M < 2.0$)

### 1.3 Design requirements, purpose of test

Wing A was designed as the first in a series of three models to study in detail the flow over rounded leading edge wings.

The wing was based on an earlier design suitable for a supersonic transport aircraft where the leading edge was the attachment line at a lift coefficient of 0.05 and a Mach number of 2.2.

The spanwise camber distribution of the original wing was retained, but the spanwise ordinates of the original wing were scaled, on the basis of linear theory, so that attached flow at the leading edge occurs at a lift coefficient of 0.10 and a Mach number of 1.5.

The Mach number is typical of supersonic Sustained Turn Rate requirements but the lift coefficient is less than one third of that needed.

In order to increase lift, through increased incidence, to a more representative value while maintaining attached flow at the leading edge, the thickness distribution chosen has a rounded leading edge.
Wing C is an uncambered, symmetrical wing, which was used as a datum for the project.

### 1.4 Dominant flow physics

a) Attached flow at the leading edge.

b) Shock waves above the upper surface with turbulent boundary layer/shock wave interactions.

c) Shock-induced separation in some cases.

## 2 DETAILS OF THE MODEL

### 2.1 General geometric arrangement.

The general arrangement of both models is illustrated in Fig.1. This figure shows the low mounted wing, the position of the surface static pressure measurements, and the body, which is cylindrical and essentially rectangular in cross section at the wing/body junction. Further upstream, the body becomes circular as the nose is approached. (Wing/body data given in Ref.1 and Ref.2 )

### 2.2 Configurations

A. Wing & Body
B. Body alone

### 2.3 Wing data

#### 2.3.1 Planform

Aspect ratio = 1.945

Leading edge sweep = 60°

Trailing edge sweep = 0°

Twist Distribution

Wing A - See Fig.2.
Wing C - No Twist

Semi-span = 3.0988 ft

Tip geometry - Küchemann tip See Fig.1

Details of wing/body junction -Low mounted wing, no fillets or fairings used.

#### 2.3.2 Basic wing section

Thickness/chord = 0.04

Nose radius/chord - See Fig.3
(approximately 0.0013co over most of the span).
co= Root chord = 1.7932m

### 2.4 Body data

#### 2.4.1 Shape

Nose shape - See Fig.1

Body length = 2707.8mm

Cross sectional details - The body is cylindrical and essentially rectangular in cross section at the wing/body junction.
Further upstream the body becomes circular as the nose is approached.

### 2.7 Geometric definition

Wing A is numerically defined in Ref. 1. Both design and actual ordinates are given.

Wing C is numerically defined in Ref. 2. Body ordinates are numerically defined in both Ref.1 and Ref.2

Manufacturing errors are generally small and within a tolerance of 0.05mm in the region of the leading edge, and 0.13mm over the inboard part of the wing. Surface finish is within the range 0.1 - 0.2 μm.

### 2.8 Model support details

The models were mounted on the sidewall of the working section and attached to a five-component strain gauge balance outside the tunnel.

The model plane of symmetry is displaced 25.4mm from the tunnel sidewall. the resulting space is filled by a wooden spacer shaped to the body. The displacement of the model is to minimise the effect of the tunnel sidewall boundary-layer.

## 3 GENERAL TUNNEL INFORMATION

### 3.1 Tunnel designation

8ft × 8ft Subsonic/Supersonic Wind Tunnel.

### 3.2 Organisation running the Tunnel

Defence Research Agency
(formerly Royal Aerospace Establishment),
Aerodynamics and Propulsion Dept.
Bedford, MK41 6AE, England.

### 3.3 Tunnel characteristics

Type of tunnel: continuous flow, closed circuit.
Operating envelope: See Fig. 4

### 3.4 Test section

#### 3.4.1 Test section details

See Fig. 5

### 3.4.2 Test section

2.44m × 2.44m × 14m.

### 3.4.3 Wall geometry details

Type of walls: solid, flexible upper and lower walls for supersonic operation. Typical wall boundary-layer displacement thickness: 19mm.

For further details see Ref.6.

## 3.5 Free-stream conditions

### 3.5.1 Reference conditions

Total pressure: Determined using a pitot in the settling chamber and a 'Midwood' self-balancing capsule manometer of range 120"Hg ≡ 400kPa and accuracy ±0.03% full scale.

Static pressure: The reference static pressure tapping is on the centre-line of the sidewall 1.829m upstream of the tunnel datum (see Fig. 5). The differential 'Midwood' manometer used for this measurement was of range ±100kPa and accuracy ±0.03% full scale.

Static temperature: This is inferred from total temperature measured to an accuracy of ±0.1K by a probe in the settling chamber.

### 3.5.2 Tunnel calibration

Total pressure survey conducted to establish the Mach number distribution in the test section.
The last supersonic calibration was performed in 1981.

## 3.6 Flow quality

### 3.6.1 Flow uniformity

For static pressure variations along the tunnel centre line see Ref.4, but typically $\Delta C_p$ = 0(0.0001).

Mach number variation from the nominal value set during a run is within 0.001.

Flow angularity is determined during the calibration, a typical average downwash has been found to be up to about 0.05°.

### 3.6.2 Temperature variation

The temperature is controlled during the run by altering the flow of water through the cooler in the settling chamber.

Temperature can be controlled to within 0.5K.

Temperature variation within the tunnel is not known.

### 3.6.3 Flow unsteadiness

Overall turbulence level is not known but overall noise level is typically $C_{p_{rms}}$ = 0.004. For further information on the noise characteristics of the wind tunnel see Ref.4.

# 4 INSTRUMENTATION

## 4.1 Model position

Geometrical incidence is measured by a digital encoder attached to the mechanism for rotating the balance. The datum position for the measurements is determined using an electrolevel meter. The estimated accuracy of the setting is ±0.005°.

## 4.2 Model pressure measurement

Wing A has 306 surface static pressure holes arranged in 9 spanwise rows. (See Fig. 1).

Wing C has 312 surface static pressure holes arranged in 9 spanwise rows. (See Fig. 1).

The body has 28 surface static pressure holes along the centre - line. The location of these holes are given in Ref.1.

The differential transducers used for these measurements were of range ±102 kPa with an accuracy of ±0.2% full scale.

No dynamic measurements were made.

## 4.3 Force and moment measurements

### 4.3.1 Type and location of balance

5 component half model balance.

### 4.3.2 Maximum range and accuracy

| | Max. load |
|---|---|
| Normal Force | 44500N |
| Axial Force | 4500N |
| Pitching Moment | 5600Nm |
| Rolling Moment | 56000Nm |
| Yawing Moment | 7000Nm |

All loads
Precision: ±0.05%
Bias: Not determined but believed to be better than

±0.2% .

### 4.5 Surface flow visualisation

On both models, flow visualisations were performed using oil supplied to the upper surface through holes drilled normal to surface in three tubes laid across the span. Photographs were taken through a window in the tunnel roof to the rear of the model.

### 4.6 Field flow visualisation

Laser vapour screens were used, illuminated by a vertical fan of laser light produced by reflecting a beam from a 2W continuous-wave, Argon laser with an oscillating mirror. the arrangement of the equipment in the Wind Tunnel is shown in Fig. 6. The streamwise position of the fan could be changed by rotating the mirror about a vertical axis; thus the fan was normal to the tunnel axis at only one streamwise station. The angle of the beam across the model is shown if Fig. 7 together with drawings made from photographs taken for $C_L$ = 0.2, 0.3 and 0.4. Photographs were taken from:-

a) a pod approximately 2.1m downstream of the trailing edge of the wing.

b) the Schlieren cavity opposite the model.

c) a window in the working section roof.

### 4.7 Tunnel wall measurements

Static pressures were measured along the centre-line of the top and bottom walls of the tunnel. See Fig. 5 for locations.

## 5 TEST MATRIX AND CONDITIONS

### 5.1 Details of test matrix

Results from six test cases for each wing may be available for the wing/body configurations. The corresponding body alone data may also be made available. These data are summarised in Table I.

### 5.2 Model/tunnel relations

Model span/tunnel width = 0.38735

Wing area/tunnel cross sectional area = 0.1543

### 5.2.6 Wall temperatures

Model temperatures were not measured but tunnel temperature was controlled so that excursions of model recovery temperature were minimised.

### 5.3 Transition details

Transition was fixed on both surfaces for the tests by narrow bands of epoxy resin containing sparsely distributed ballotini.

The bands were located 25.4mm normal to the leading edge in plan view and were 5.08mm wide.

On the body the band was located 101.6mm from the nose and was 12.7mm wide. The ballotini used was of diameter 0.21mm - 0.25mm with a density of 155 (±30) beads/cm$^2$.

## 6 DATA

### 6.1 Availability of data

#### 6.1.1 Organization owning data

Defence Research Agency
Bedford
England

#### 6.1.2 Person responsible for data

Mr M J Simmons
Building 17
Defence Research Agency
Bedford, MK41 6AE
England
Tel. 44 234 225836
Fax. 44 234 225848

#### 6.1.3 Availability of data

Data specified in questionnaire are available.

### 6.2 Suitability of data

The data should be suitable for CFD validation validating 'in tunnel' calculation methods. The data are, however, corrected to 'free-air' conditions.

### 6.3 Type and form in which data are available

#### 6.3.1 a) Free stream

Mach number

**b) Pressure**

Coefficients based on free-stream dynamic pressure.

**c) Forces**

Coefficients based on free-stream dynamic pressure, wing area and chord length as appropriate.

### 6.3.2 Data Carrier

Available on floppy disc.

## 6.4 Corrections applied to data

### 6.4.1 Lift interference and blockage correction

Not applicable in supersonic flow.

### 6.4.2 Side wall interference corrections

No corrections have been applied to either Mach number or angle of incidence for this effect.

### 6.4.3 Aeroelastic deformation

No allowance was made for the effect of the variation in aeroelastic deformation across the span.

# 7 DATA ACCURACY AND REPEATABILITY ASSESSMENT

## 7.1 Estimated accuracies

Free stream conditions:

| | |
|---|---|
| Mach number | ±0.001 |
| Incidence | ±0.03° |
| Lift coefficient | ±0.001 |
| Drag coefficient | ±0.0001 |
| Pitching moment coefficient | ±0.001 |
| Pressure coefficient | ±0.002 |

## 7.2 Repeat measurements

Good repeatability has been demonstrated both within and between test campaigns for similar models see Ref. 4. For example, drag coefficient has been shown to repeat to within about ±0.0001 and pressure coefficient to within about ±0.001 between test series performed a number of years apart.

# 8 REFERENCES


1. J.L.Fulker, P.R.Ashill, M.J.Simmons. Pressure and Overall-force data from tests on wing-body configurations at supersonic speeds. Part 1. RAE TM Aero 2092, 1987.

2. M.J.Simmons, J.L.Fulker, P.R.Ashill. Pressure and Overall-force data from tests on wing-body configurations at supersonic speeds. Part 2. RAE TM Aero 2202, 1991.

3. A.Stanbrook, L.C.Squire. Possible types of flow at swept leading edges.

RAE TN Aero 2608, 1951.

4. D. Isaacs — Calibration of the RAE Bedford 8ft × 8ft Wind Tunnel at Subsonic speeds, Including a Discussion of the Corrections to the Measured Pressure Distributions for the Direct and Blockage Effects due to the Calibration Probe. ARC R&M 3583, 1969.

5. A.Elsenaar, L.Hjelmberg, K.Bütefisch, W.J.Bannink — The International Vortex Flow experiment. AGARD-CP-437. Vol.1, Pages 9-1 - 9-23, 1988.

6. K.G.Winter, L.Gaudet — Turbulent boundary-layer studies at high Reynolds number. ARC R&M3712, 1970.

| IDENTIFICATION | | CONDITIONS | | | POSITION | OTHER INFORMATION | |
|---|---|---|---|---|---|---|---|
| CASE NO. | WING/ DP. | Mach No. | q (kPa) | Rc x $10^{-6}$ | $\alpha°$ | Type of measurements | Remarks |
| A | A/905 | 1.605 | 38.906 | 12.722 | 0.81 | a,b | CL=0.0 |
| B | A/910 | 1.605 | 38.835 | 12.693 | 3.31 | a,b | CL=0.1 |
| C | A/914 | 1.605 | 38.849 | 12.692 | 5.32 | a,b,d | CL=0.2 |
| D | A/919 | 1.605 | 38.863 | 12.691 | 7.80 | a,b,c,d | CL=0.3 |
| E | A/924 | 1.605 | 38.892 | 12.695 | 10.32 | a,b,c,d | CL=0.4 |
| F | A/928 | 1.605 | 38.892 | 12.689 | 12.30 | a,b,c | CL=0.5 |
| G | C/64 | 1.605 | 39.077 | 12.704 | 0.24 | a,b | CL=0.0 |
| H | C/68 | 1.605 | 39.234 | 12.726 | 2.25 | a,b | CL=0.1 |
| I | C/73 | 1.605 | 39.334 | 12.724 | 4.76 | a,b | CL=0.2 |
| J | C/77 | 1.605 | 39.263 | 12.728 | 6.76 | a,b,c,d | CL=0.3 |
| K | C/82 | 1.605 | 39.291 | 12.733 | 9.25 | a,b,c,d | CL=0.4 |
| L | C/87 | 1.605 | 39.234 | 12.724 | 11.75 | a,b,c,d | CL=0.5 |

NOTE 1: Types of measurements :

a) Surface static pressures
b) Overall forces
c) Oil filament flow visualisation
d) Laser vapour screens

NOTE 2:

The positions of the test cases in the $\alpha_N$ - $M_N$ plane are shown in Fig.8.

In all cases the leading edge is subsonic $M < 1$.

Some of the cases are to the left of the Stanbrook/Squire[3] boundary where the flow is expected to be separated from the leading edge. However, in all the cases the flow was observed to be attached at the leading edge except possibly close to the tip for case L.

It is interesting to note, however, that cases D, E, F, J, K, L have flows with shock-induced separation on the upper surface between 70% and 80% semi-span at all stations as shown in Figs. 9 and 10. These cases are all in the shaded region shown in Fig.5 where leading edge separation may occur according to Stanbrook and Squire[1]. Some of these cases also lie within the region defined by Elsenaar[5] as 'partial separation'.

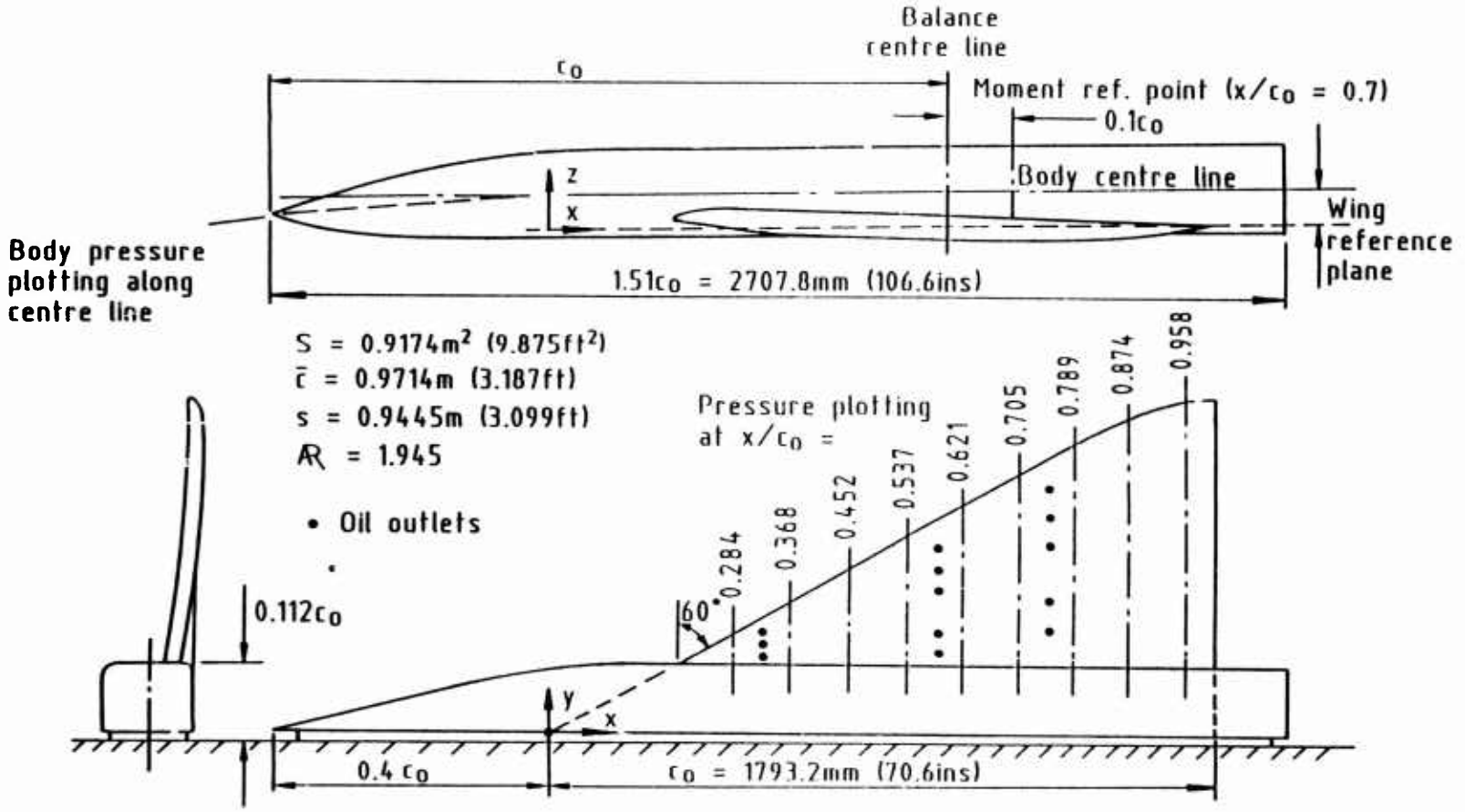



**Fig. 1** **General layout of model.**

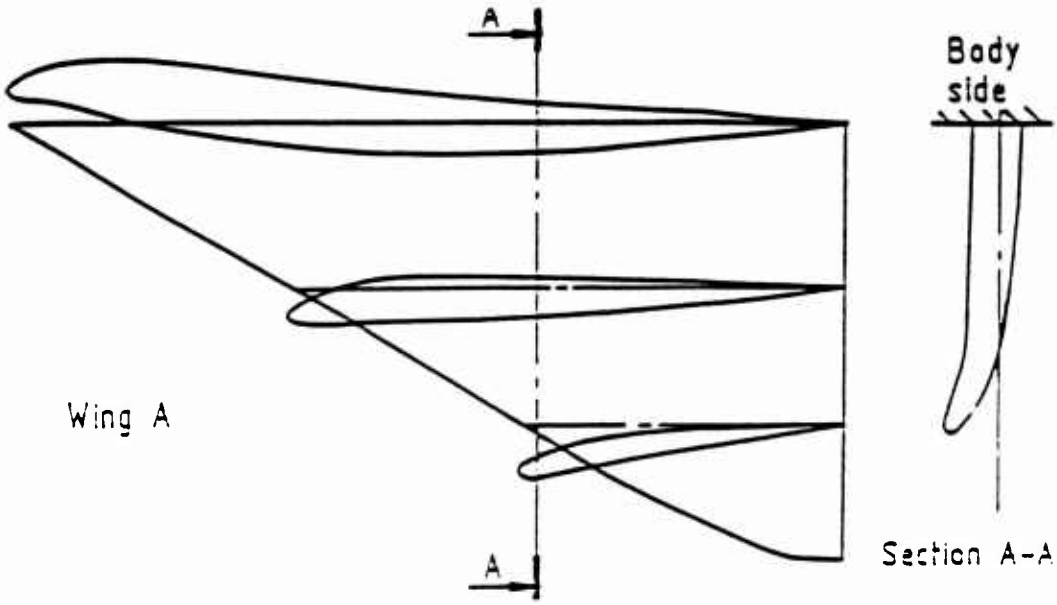



**Fig. 2** **Streamwise and Spanwise wing sections, Wing A.**

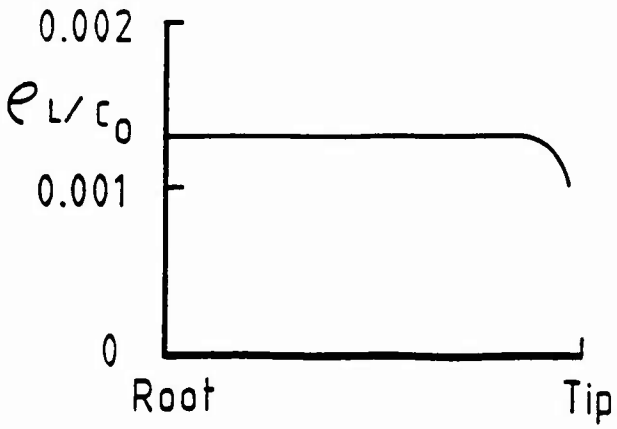



**Fig. 3** **L.E. radius/chord - Spanwise position.**

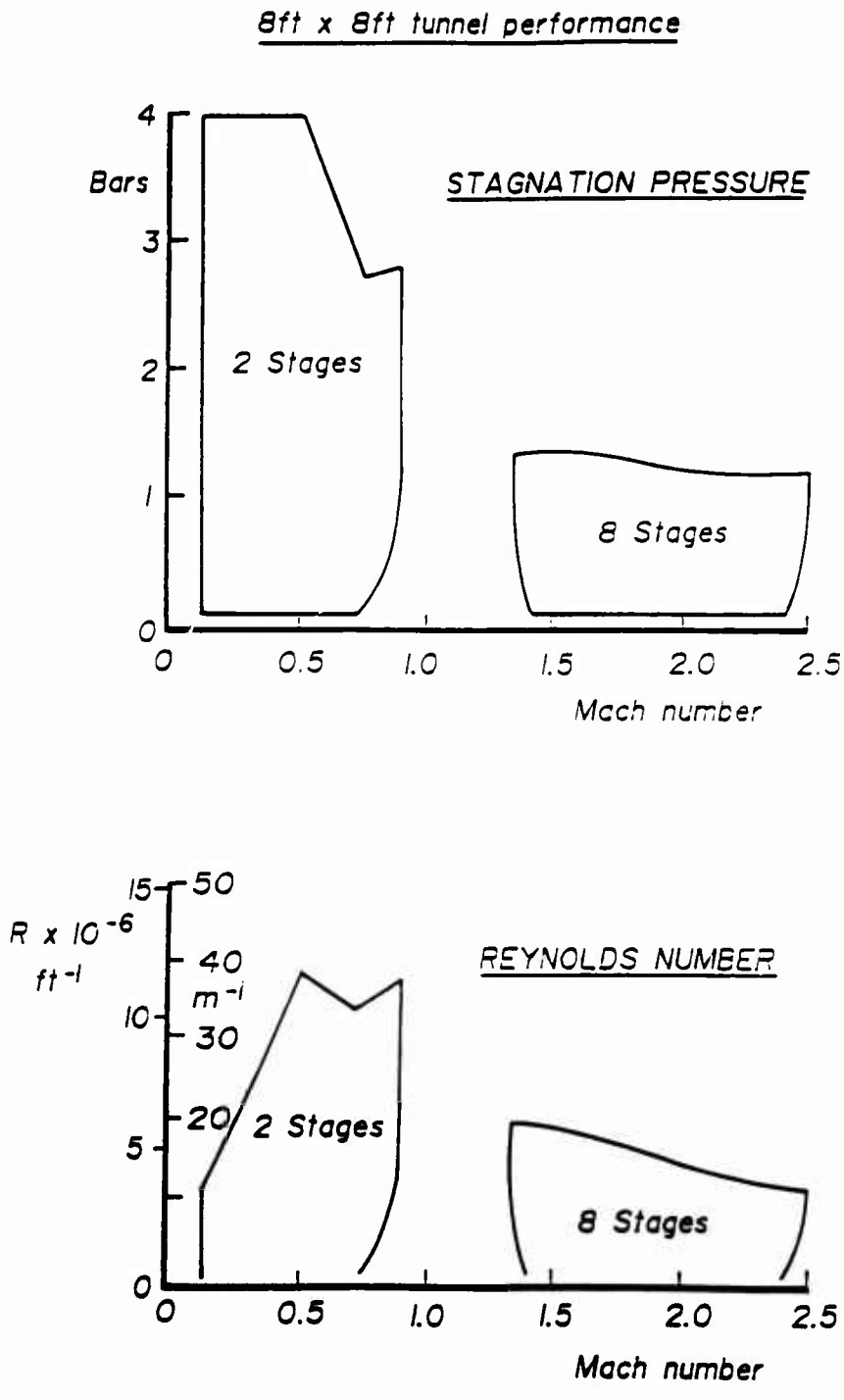



**Fig. 4** **8ft x 8ft Wind Tunnel operating envelope.**

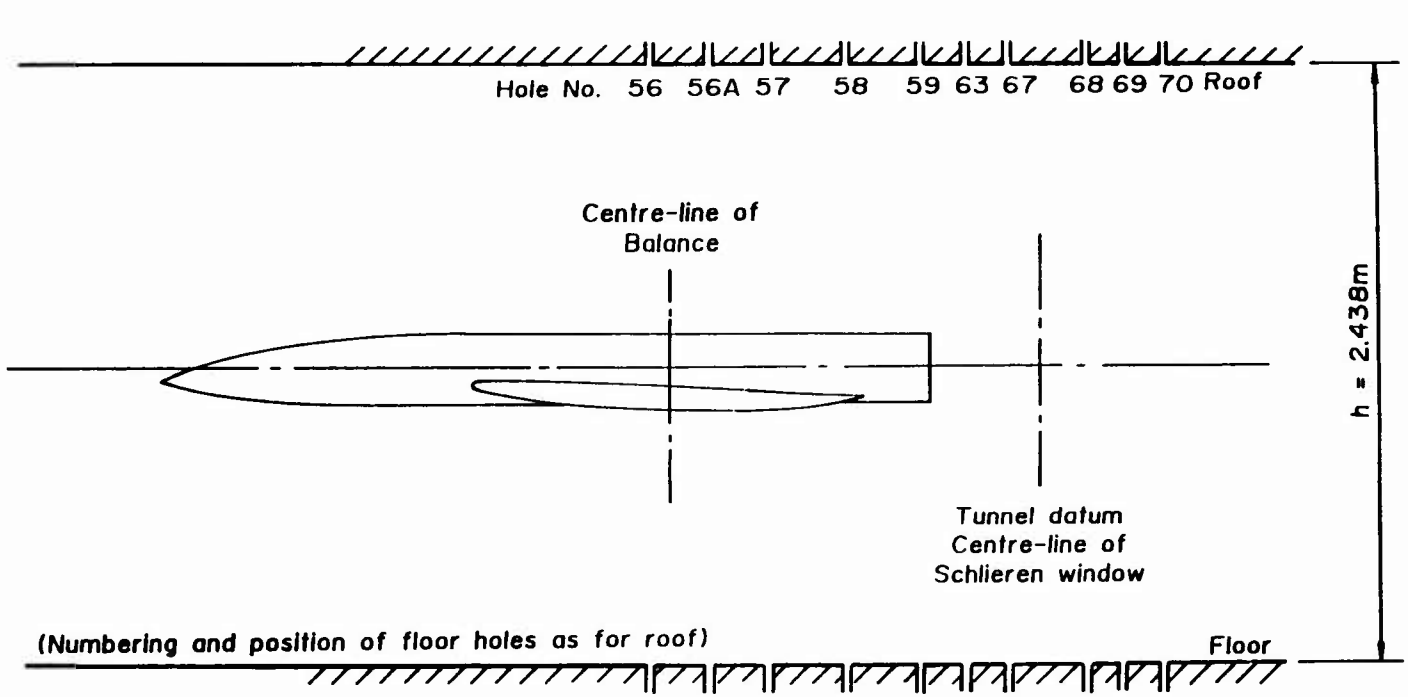



**Fig. 5** **Numbering and position of wall static pressure holes for roof and floor of working section.**

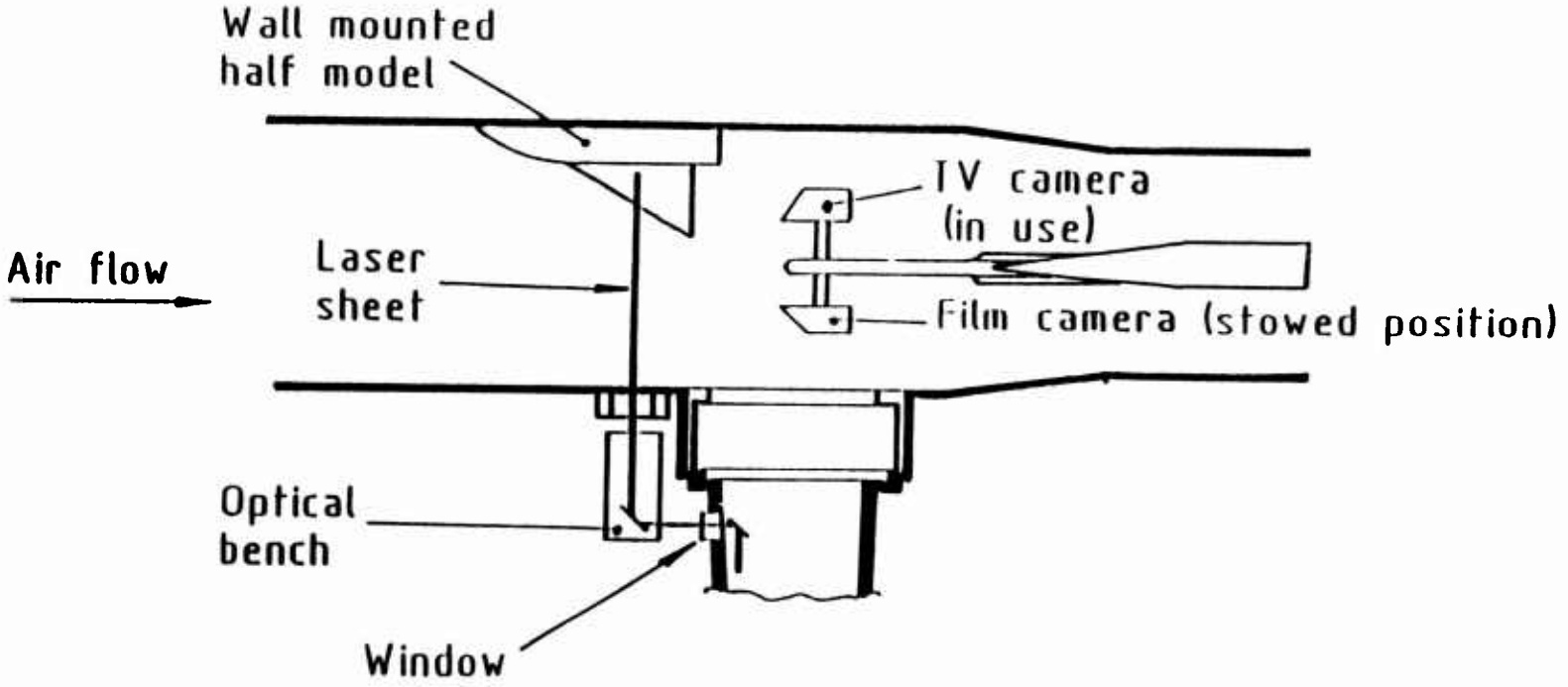



**Fig. 6** **Arrangement of laser vapour screen visualisation system in the RAE 8ft x 8ft Wind Tunnel.**

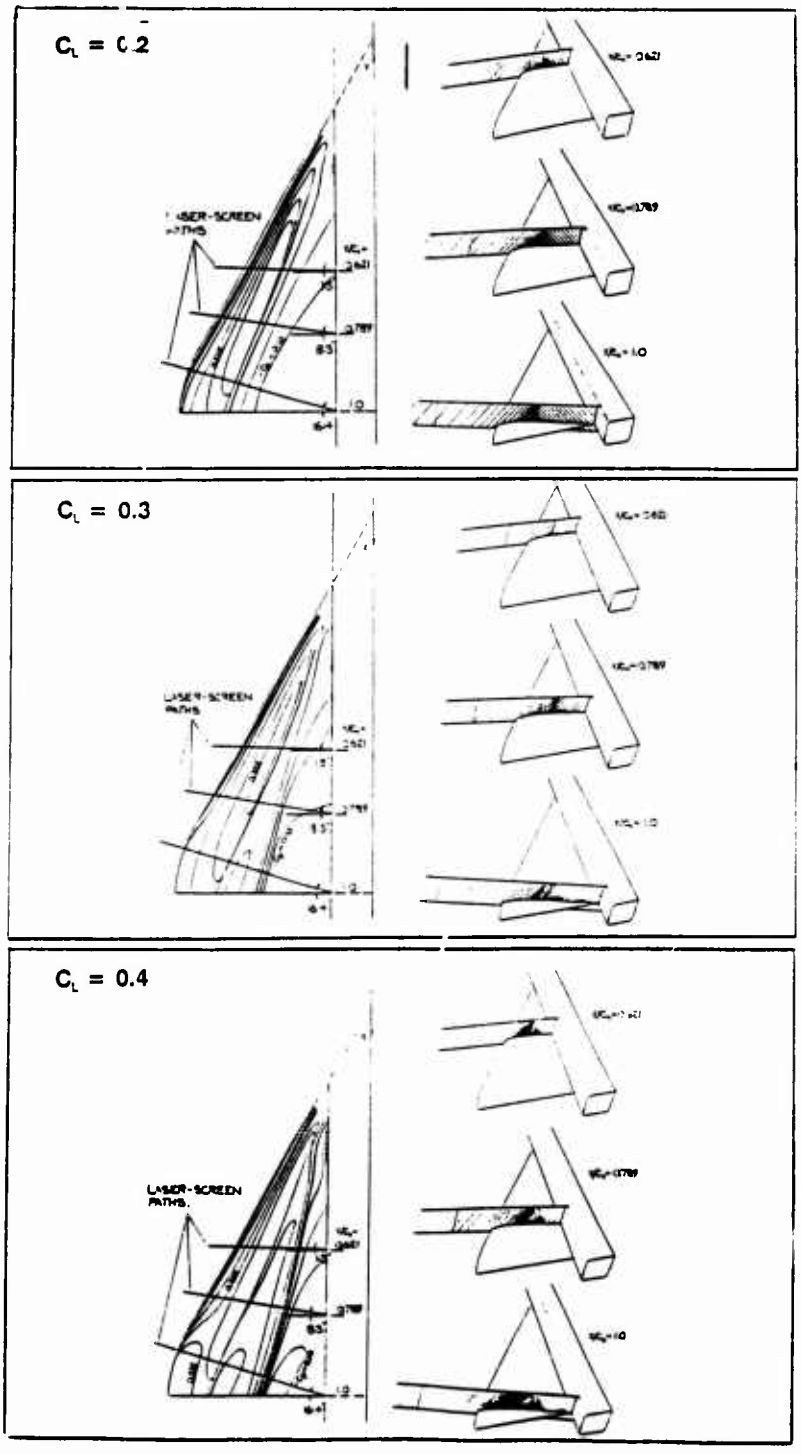



**Fig. 7** **Isobars and flow visualisations, Wing A.**

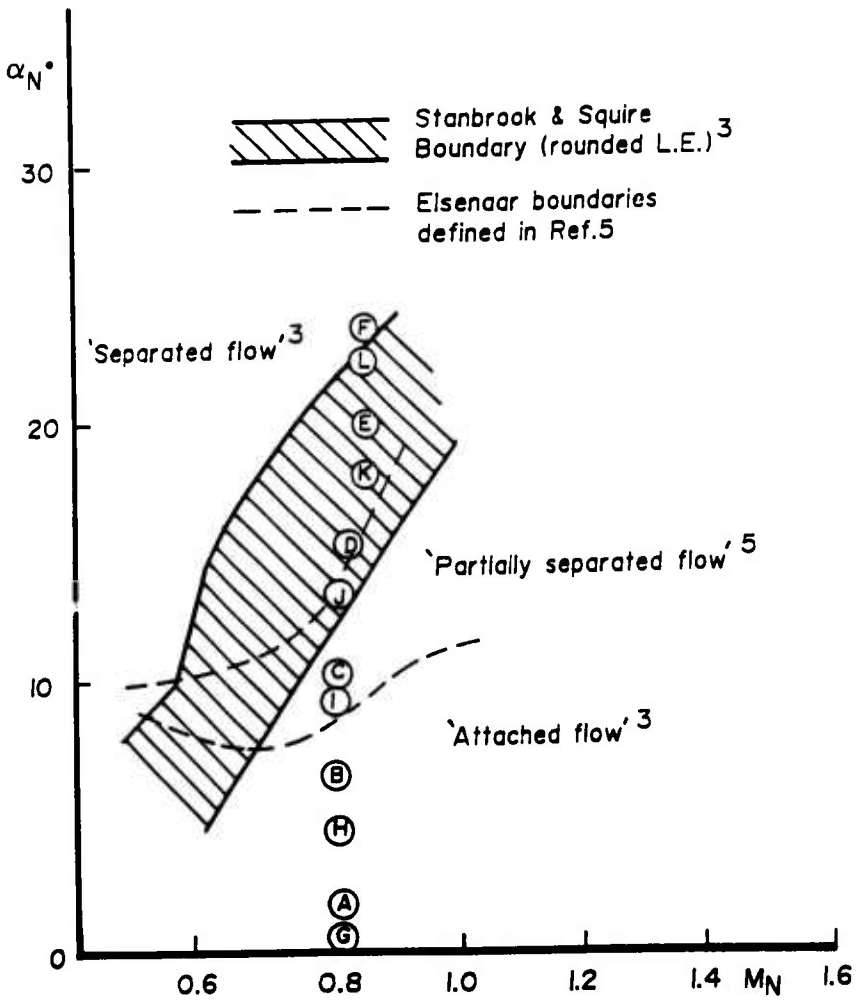



**Fig. 8** **Test case flow classification.**

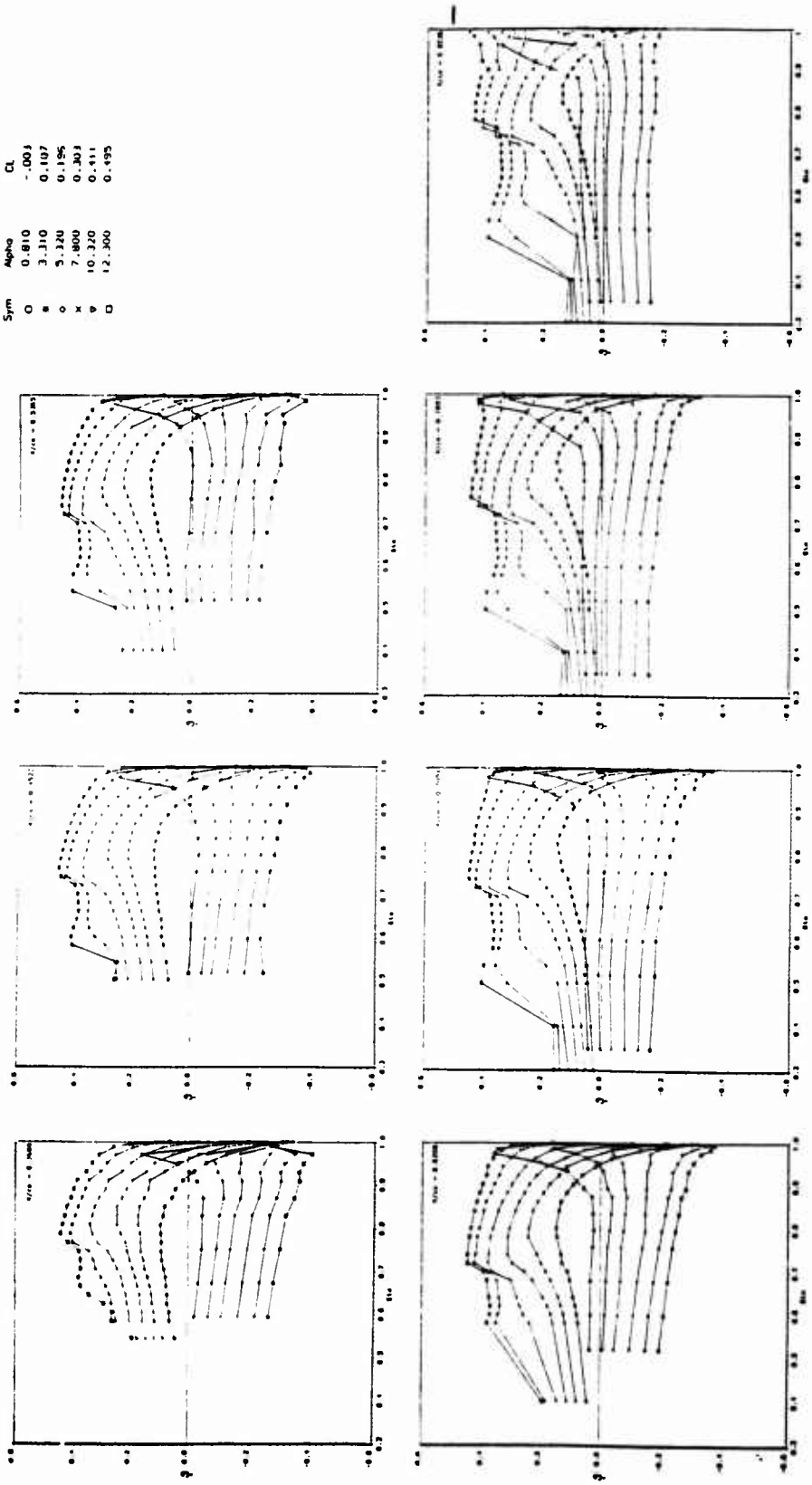



**Fig. 9 Spanwise Pressure Distributions, Wing A.**

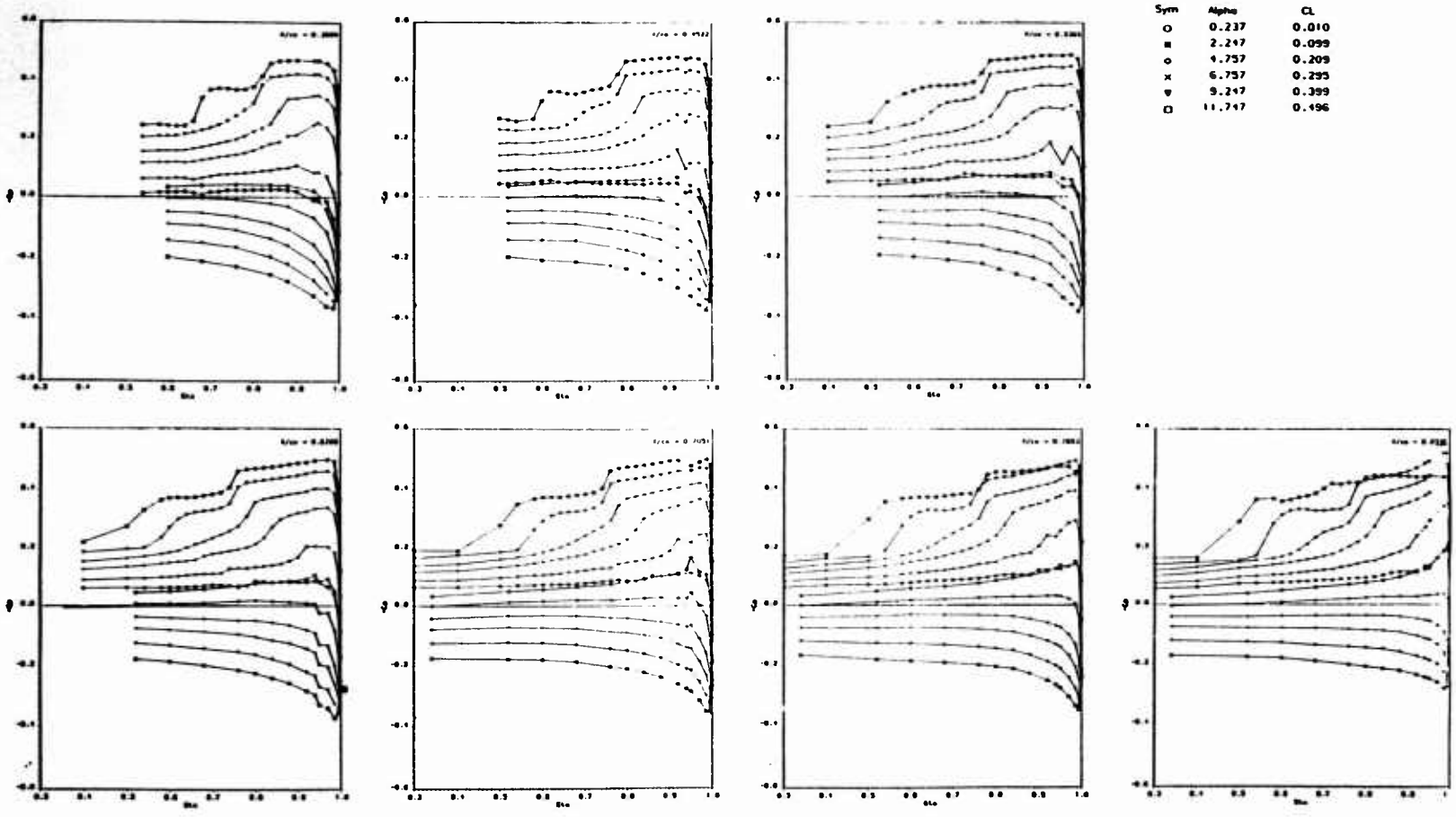



**Fig. 10 Spanwise Pressure Distributions, Wing C.**

# PRESSURE DISTRIBUTIONS ON RESEARCH WING W4 MOUNTED ON AN AXISYMMETRIC BODY

by

J L Fulker
DRA, Bedford

## 0 INTRODUCTION.

The experiments described in this submission were performed on a wing-body configuration suitable for a civil transport aircraft. When the wing was designed (1972) it was recognised that, in order to achieve an advance in technology, a significant increase in rear loading would be required compared to that of earlier designs. As a consequence, the boundary layer conditions close to the trailing edge on the upper surface were expected to be more adverse than in previous designs. This requirement led to the need for a high test Reynolds number, which was achieved by testing a large half model in the Defence Research Agency (DRA) 8ft × 8ft Wind Tunnel at Reynolds numbers, based on geometric mean chord, of up to $15 \times 10^6$. Complementary tests were also performed on a smaller complete model in order to provide an accurate assessment of the drag characteristics of the wing. The wing was designed to have a weak shock wave near mid chord on the upper surface at the cruise condition ( $C_L = 0.32$, $M = 0.78$). This feature, together with the significant rear loading of the wing, is illustrated in Fig. 1. The overall aims of the investigation were to obtain an improved understanding of the behaviour of the flows over wings of this type over a wide range of subsonic Mach numbers and Reynolds numbers.

The tests were performed during 1977 on the complete model and 1978 on the half model. The wind tunnel has solid walls and, since the models are relatively large, the data are strictly not correctable. However, the wall boundary conditions are well defined and so the data may be useful for validating CFD codes which include allowance for the wind-tunnel walls. In addition, measurements were made of the static pressures on the roof and floor of the working section, providing an independent check on the accuracy of the representation of the walls in any CFD method.

## 1 GENERAL DESCRIPTION

**1.1 Model name or designation**

Wing W4, Model 873 -half model
Model 2063 - complete model

**1.2 Model type and flow conditions**

Full span wing-body and semi-span wing-body. Subsonic free-stream speeds ( $0.5 < M < 0.86$ ) The tests include fully attached flow cases and flows with shock-induced separation.

**1.3 Design requirements and purpose of tests**

The model was designed to exploit the benefits of the high chordal Reynolds numbers that can be obtained by testing a large half-model in a pressurised wind tunnel.

**1.4 Dominant flow physics**

The dominant flow physics are:

a) attached turbulent boundary layers with adverse pressure gradients.
b) the interaction between these boundary layers and the inviscid flow.
c) shock waves on the upper surface with, in some cases, shock-induced separation.

## 2. DETAILS OF MODELS

**2.1 General geometric arrangement**

Complete model see Fig. 2. Half model see Fig.3. The linear dimensions of the half model compared to the complete model are in ratio 1 : 0.425.

**2.2 Configurations tested**

All tests on a single configuration.

**2.3 Wing data**

| | |
|---|---|
| **2.3.1 Aspect ratio** | 8.078 |
| **2.3.2 Taper ratio** | 0.20 |
| **2.3.3 Leading edge sweep** | 28.3° |
| **2.3.4 Trailing edge sweep** | 3.5° inboard<br>14.07° outboard |

**2.3.5 Semispan** 0.7324m (complete model)
1.7233m (half model)

**2.3.6 Tip geometry**

Both models have a common parabolic tip.

#### 2.3.7 Wing/fuselage junction

The model wing datum is at a height below the body axis divided by maximum body radius of 0.488. A small flat sided trailing-edge fillet is fitted which extends a relatively short distance downstream of the wing trailing edge.
There is no leading-edge fillet.

### 2.4 Section data

#### 2.4.1 Aerofoil shape

A typical wing section is shown in fig. 1.

#### 2.4.2 Thickness/chord ratio

The variation in thickness/chord (t/c) across the span is shown in Fig. 1.

### 2.5 Body data

Axisymmetric fuselage with tangent ogive nose and rear body. See Fig. 2.

Body length = 3.641m (half model)
= 1.46m (complete model)

The body lengths do not scale as 1 : 0.425 because of the need to shorten the body of the complete model to allow for the entry of the sting in the rear of the model. The half model body is displaced from the wall by a value greater than one side wall boundary-layer displacement thickness (in this case 25mm) so as to minimise the influence of the boundary-layer flow on the wing flow.

### 2.6 Geometric definition of wing

#### 2.6.1 Shape

Numerically defined. 98 ordinates at each section, 11 spanwise sections.

#### 2.6.2 Design or Measured

Design ordinates available at all above locations. Measurements available for some locations.

#### 2.6.3 Tolerances

Requested ±0.1mm with change in error ±0.002mm per mm.

#### 2.6.4 Surface roughness

Requested 0.2 micro-metres.

## 3. GENERAL TUNNEL INFORMATION

### 3.1 Tunnel designation

8ft × 8ft Subsonic/Supersonic Wind Tunnel.

### 3.2 Organisation running the tunnel

Defence Research Agency (formerly Royal Aerospace Establishment), Aerodynamics and Propulsion Department, Bedford, MK41 6AE, England.

### 3.3 Tunnel characteristics

Type of tunnel: continuous flow, closed circuit.
Operating envelope: see Fig. 4.

### 3.4 Test section

#### 3.4.1 Test section

See Fig. 5.

#### 3.4.2 Test section

2.44m × 2.44m × 14m.

#### 3.4.3 Wall geometry details

Type of walls: solid, flexible upper and lower walls for supersonic operation. Shapes of upper and lower walls are set for subsonic tests in such a way as to minimise the pressure gradient on the centre line when the test section is empty (Ref. 1). Typical wall boundary-layer displacement thickness: 19mm. For further details see Ref. 2.

### 3.5 Free-stream conditions

#### 3.5.1 Reference conditions

Total pressure: Determined using a pitot in the settling chamber and a 'Midwood' self-balancing capsule manometer of range 120"Hg ≡ 400kPa and accuracy ±0.03% full scale. Static pressure: The reference static pressure tapping is on the centre-line of the sidewall 6.25m upstream of the tunnel datum (see Fig. 5.).
The differential 'Midwood' manometer used for this measurement was of range ±100kPa and accuracy ±0.03% full scale.
Static temperature: This is inferred from total temperature measured to an accuracy of ±0.1K by a probe in the settling chamber.

#### 3.5.2 Tunnel calibration

Measurements are made of static pressures on the centre-line of the roof and floor of the test section (Ref 1) using differential 'Midwood' manometers of range ±100kPa and accuracy ±0.03% full scale.
The last calibration was performed in October 1991, calibrations being performed annually.

### 3.6 Flow quality

#### 3.6.1 Flow uniformity

For static pressure variations along the tunnel centre line see Ref 1, but typically $\Delta C_p = O(0.0001)$ with the diffuser choked, as in the present tests.
Mach number during a run is within 0.001. Average flow angularity is routinely determined for sting-mounted

models by comparing force measurements made with the model erect and inverted. Some data on flow angularity has also been obtained for typical swept-wing half models on the sidewall as in the present case by testing a model with a horizontal plane of symmetry. In both cases the implied average downwash angle has been found to be up to about 0.03°.

#### 3.6.2 Temperature variation

The temperature is controlled during the run by altering the flow of water through the cooler in the settling chamber.
Temperature can be controlled to within 0.5K.
Temperature variation within the tunnel is not known.

#### 3.6.3 Flow unsteadiness

Overall turbulence level is not known but overall noise level is typically $C_{p_{rms}}$ = 0.004. For further information on the noise characteristics of the wind tunnel see Ref. 1.

## 4 INSTRUMENTATION

### 4.1 Model Position

#### 4.1.1 Geometric incidence

Calculated from a knowledge of the loads on the model and the elastic deflection characteristics of the sting and balance.

#### 4.1.2 Accuracy

±0.005°

### 4.2 Model Pressure Measurements

#### 4.2.1 Pressure holes

252 - 161 on upper surface - 91 on lower surface. See Fig. 6.

#### 4.2.2 Range and Accuracy

Pressures measured using seven differential-pressure transducers, each installed in a 48 way pressure switch and having a working range of ±170 kPa with an accuracy of ±0.05% full scale.
No dynamic pressure measurements were made.

### 4.3 Force and moment measuements

#### 4.3.1 Type and location of balance

RAE 3" 6 component internal balance. RAE 5 component half model balance.

#### 4.3.2 Maximum range and accuracy

Sting balance:

| | Max. load |
|---|---|
| Normal Force | 17800N |
| Axial Force | 2200N |
| Side Force | 4000N |
| Pitching Moment | 2200Nm |
| Rolling Moment | 700Nm |
| Yawing Moment | 700Nm |

All loads Precision: ±0.025%. Bias: Not determined but believed to be better than ±0.2%.

Half Model balance:

| | Max. load |
|---|---|
| Normal Force | 44500N |
| Axial Force | 4500N |
| Pitching Moment | 5600Nm |
| Rolling Moment | 56000Nm |
| Yawing Moment | 7000Nm |

All loads Precision: ±0.05%. Bias: Not determined but believed to be better than ±0.2%.

## 5 TEST MATRIX AND CONDITIONS

### 5.1 Detailed test matrix

Results for a total of 8 test cases may be available. These are given in Table 1 which presents the test matrix.

### 5.2 Model/tunnel relations

#### 5.2.1 Maximum blockage

$\Delta M$ = 0.026 (halfmodel), $\Delta M$ = 0.004 (complete model). This represents an empty tunnel Mach number of M=0.772 for the complete model and M=0.755 for the half model.

#### 5.2.2 Model span/tunnel width

0.707 (half model), 0.60 (complete model).

#### 5.2.3 Wing area/tunnel cross section

0.084 (half model), 0.030 (complete model).

#### 5.2.4 Wall temperatures

Model temperatures were not measured but tunnel temperature was controlled so that excursions of model recovery temperature were minimal.

### 5.3 Transition details

Tests were conducted with fixed transition.
Half model:- transition fixed at 15% of local chord on the upper surface, and 5% of local chord on the lower surface with a width of 2.54mm normal to the leading edge. Ballotini set in a thin film of epoxy adhesive of diameter 0.064 to 0.076mm with a density of 155(±30 ) balls/cm$^2$.
Complete model:- transition fixed on both surfaces at 5% local chord with a width of 2.54mm normal to the leading

edge. Ballotini set in a thin film of epoxy adhesive of diameter 0.076 to 0.089mm with a density of 155(±30) balls/cm$^2$.

The effectiveness of the transition trip for the complete model was checked by measuring the drag at a fixed Mach number over a range of Reynolds number and comparing with theoretical estimates. No checks were carried out for the half model, but it is believed that the trip was effective from comparisons of the data presented here, and that with transition fixed at various positions on the upper surface on the half model together with data from the complete model.

## 6 DATA

### 6.1 Availability of data

**6.1.1 Organization owning data**
Defence Research Agency Bedford England

**6.1.2 Person responsible for data**

Mr J L Fulker
Building 17
Defence Research Agency
Bedford, MK41 6AE
England
Tel. 44 234 225821
Fax. 44 234 225848

**6.1.3 Availability of data**
Data specified in questionnaire are available.

### 6.2 Suitability of data for CFD validation

The data should be suitable for validating 'in tunnel' calculation methods. The data are, however, corrected to 'free-air' conditions. Details will be provided of the corrections made for blockage and wall-induced angle of incidence

### 6.3 Type and form in which data are available

**6.3.1**

**a) Free stream**

Mach number corrected for tunnel wall(roof and floor) interference.

**b) Pressure**

Coefficients based on free-stream dynamic pressure, corrected for tunnel wall (roof and floor) interference.

**c) Forces**

Coefficients based on free-stream dynamic pressure, corrected for tunnel wall (roof and floor) interference, wing area, and mean chord, as appropriate.

**6.3.2 Data Carrier**
Available on floppy disc.

### 6.4 Corrections applied to data

**6.4.1 Lift interference and blockage corrections**

Model incidence has been corrected for the effect of wind-tunnel constraint on lift by the method of Acum Ref. 3.

The effects of wall-induced blockage on freestream dynamic pressure, static pressure and Mach number are allowed for in the way which is standard for subsonic tests in the 8ft × 8ft tunnel. Linear theory was used to calculate the ratio of the blockage velocity-increment on the outer wing of the model to the velocity increment (direct + blockage) at the tunnel wall. This factor was then used to obtain the blockage-velocity increment from the measured change in the wall pressures due to the model. For these calculations the model was represented by a distribution of sources and sinks. An estimate of the model profile drag with attached flow was used to derive the relative strength of the source representing the model wake. Calculations show that, in the case of the half model, the variation of the blockage over the wing was very small despite the fact that the blockage-velocity increments due to the model were high.

**6.4.2 Side wall interference corrections**

No corrections have been applied to either Mach number or angle of incidence for this effect.

**6.4.3 Aeroelastic deformation**

No allowance was made for the effect of the variation in aeroelastic deformation across the span other than the inclusion of a mean aeroelastic twist in the wind-tunnel constraint given in 6.4.1. However, the caculated variation in aeroelastic twist, for both wings, is shown in Fig. 7 for M=0.78, $C_L$=0.39 and a stagnation pressure of 101.4kPa.

## 7 DATA ACCURACY AND REPEATABILITY ASSESSMENT

### 7.1 Estimated accuracies

Free stream conditions:

| | |
|---|---|
| Mach number | ±0.001 |
| Incidence | ±0.01° |
| | ±0.03° (half model) |
| Lift coefficient | ±0.001 |
| Drag coefficient | ±0.0001 |
| Pitching moment coefficient | ±0.001 |
| Pressure | ±0.002 |

coefficient

**7.2 Repeat measurements**

Good repeatibility has been demonstrated both within and between test campaigns for similar models see Ref. 4. For example, drag coefficient has been shown to repeat to within about ±0.0001 and pressure coefficient to within about ±0.001 between campaigns performed a number of years apart.

## 8 REFERENCES


1 Isaacs, D. Calibration of the RAE Bedford 8ft x 8ft Wind Tunnel at subsonic speeds, including a discussion of the corrections to the measured pressure distributions for the direct and blockage effects due to the calibration probe.
ARC R&M 3583, 1969.

2 Winter, K.G.
Gaudet, L. Turbulent boundary-layer studies at high Reynolds numbers at Mach numbers between 0.2 and 2.8.
ARC R&M 3712, 1970.

3 Acum, W.E.A. Corrections for symmetrical swept and tapered wings in rectangular wind tunnels.
ARC R&M 2777, 1950.

4 Wood, M.N.
Capps, D.S. The accurate measurement of drag in the 8ft x 8ft Tunnel.
AGARD-CP-429, pp9.1 - 9.9, 1987.

**TABLE 1: TEST MATRIX**

| IDENTIFICATION | | FLOW CONDITIONS | | | POSITION | OTHER INFORMATION | |
|---|---|---|---|---|---|---|---|
| CASE NO. | CONFIG/ RUN/DP | MACH No. | q (kPa) | $R_c \times 10^{-6}$ | $\alpha°$ | Type of measurement | Remarks |
| A1<br>A2<br>A3<br>A4 | 16/2/934<br>16/2/936<br>16/2/941<br>16/2/943 | 0.780 | 60.8 | 5.12 | -0.500<br>0.060<br>1.523<br>2.049 | a,b | Complete Model |
| B1<br>B2<br>B3<br>B4 | 401/1/289<br>401/1/290<br>401/1/298<br>401/1/301 | 0.781 | 65.6 | 13.30 | -0.815<br>-0.277<br>1.462<br>2.095 | a,b | Half Model |

Notes:

1 Types of measurement: a) Pressure measurements on model b) Measurements of overall forces on the configuration.

Typical pressure distributions for the half model are shown in Fig. 8 and for the complete model in Fig. 9.

2 The flows may be defined as follows:

A1 & B1: A case close to the design condition with essentially subcritical flow and a suction peak on the upper surface near the leading edge.

A2 & B2: A case close to a typical cruise condition for a transport aircraft, with no or weak shock waves on the upper surface.

A3 & B3: A flow close to the onset of shock induced separation on the outer-wing upper surface.

A4 & B4: A flow with shock induced separation on the outer-wing upper surface, which, on the outermost stations extends to the trailing edge, and can therefore be classified as a flow just beyond the buffet onset boundary.

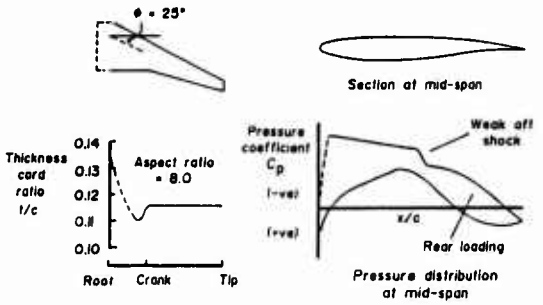



FIG. 1 WING W4 GEOMETRY AND PRESSURES

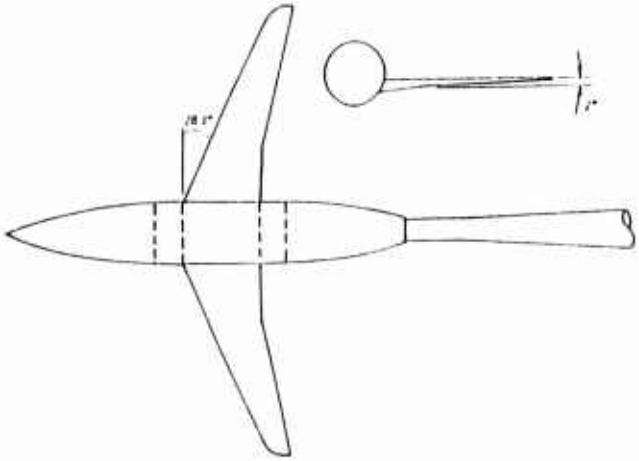


FIG. 2 W4 FULL MODEL

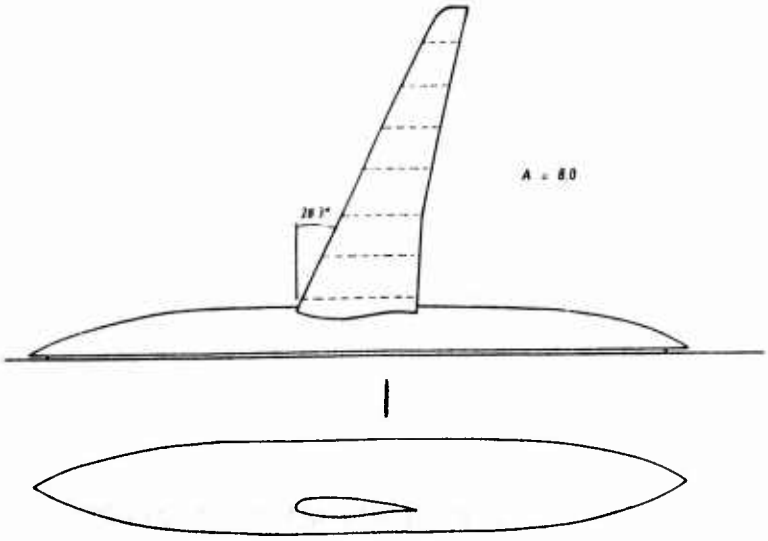



FIG. 3 W4 HALF MODEL

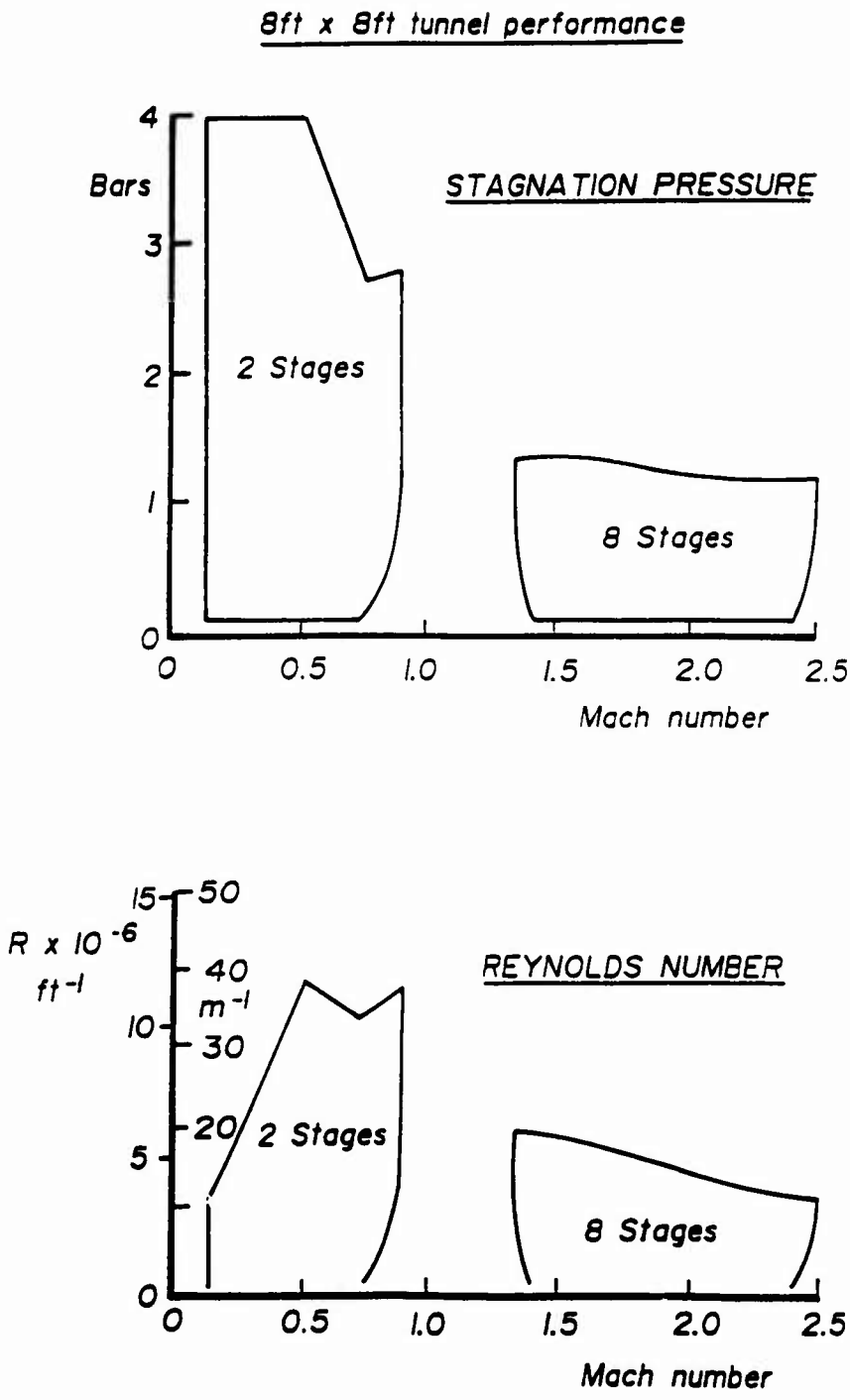



**FIG. 4 TUNNEL OPERATING ENVELOPE**

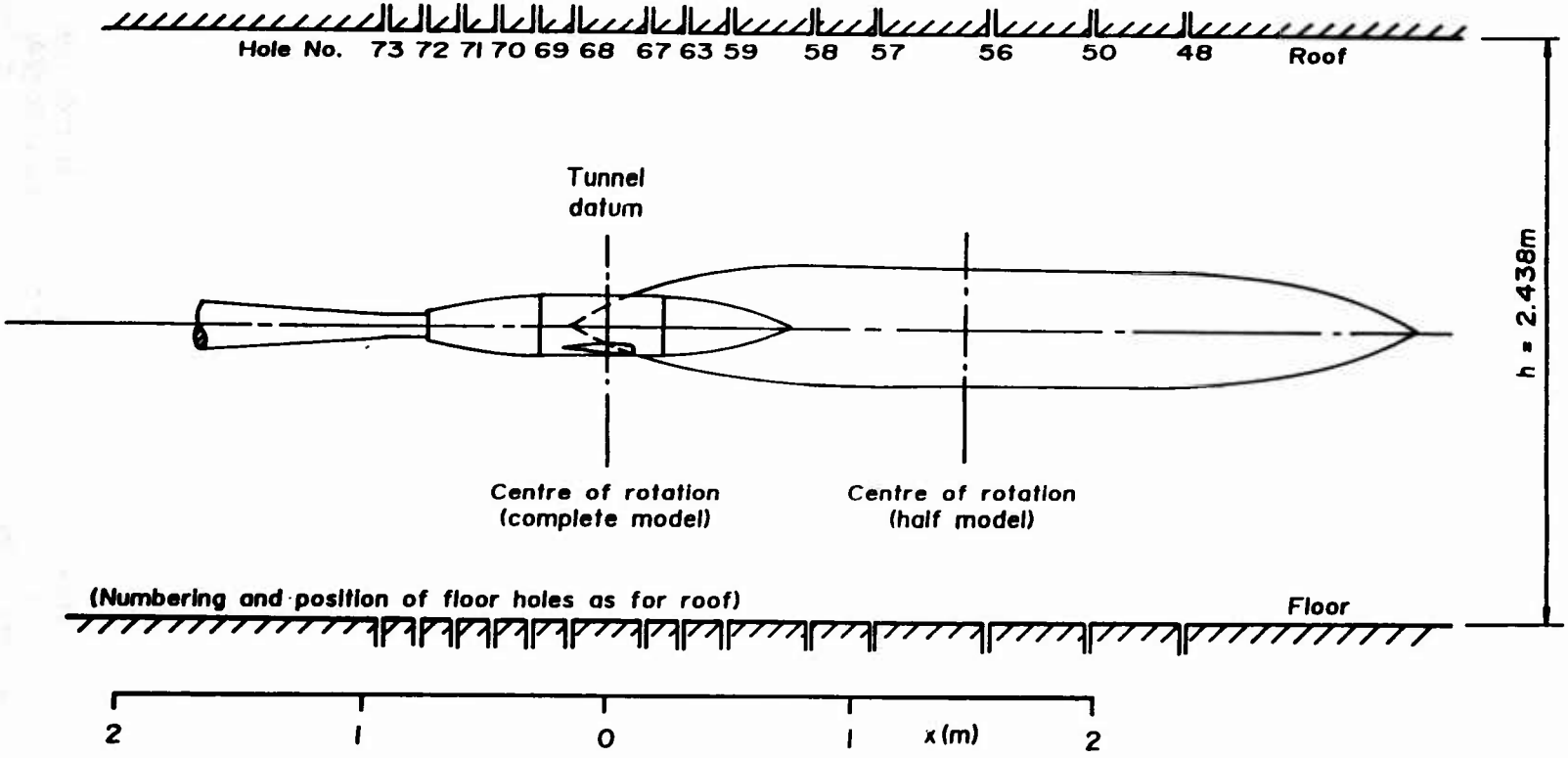



FIG. 5 NUMBERING AND POSITION OF WALL STATIC HOLES FOR ROOF AND FLOOR OF WORKING SECTION

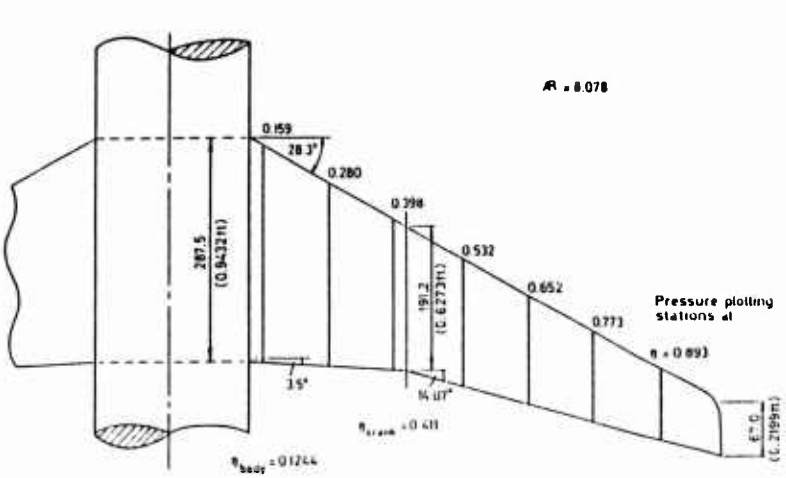



FIG. 6 PLANFORM IF WING W4 SHOWING PRESSURE PLOTTING STATIONS

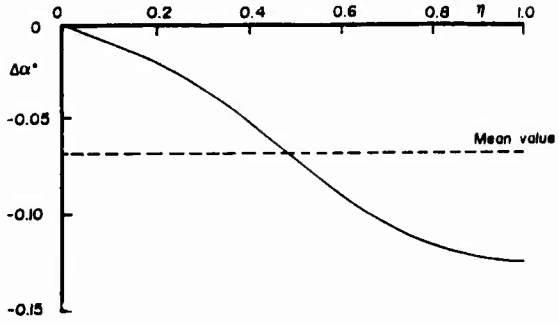



FIG. 7 CALCULATED VARIATION IN AEROELASTIC TWIST ACROSS THE SPAN FOR $M_\infty$ = 0.78, $C_L$ = 0.39 AND 1 ATMOSPHERE STAGNATION PRESSURE

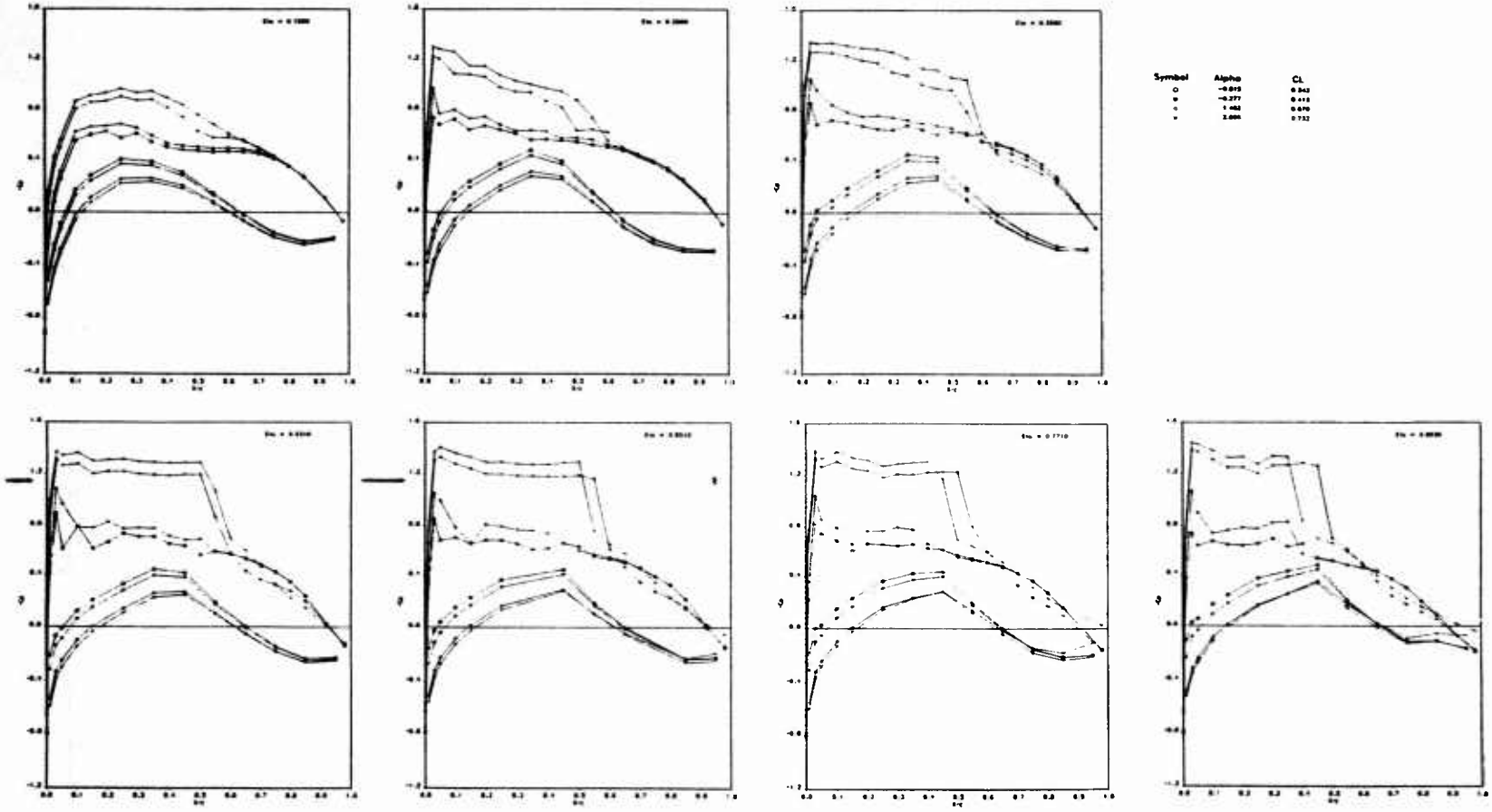


**FIG. 8** **PRESSURE DISTRIBUTIONS - HALF MODEL**
**M=0.781 $R_c$ = 13.3x10$^6$**

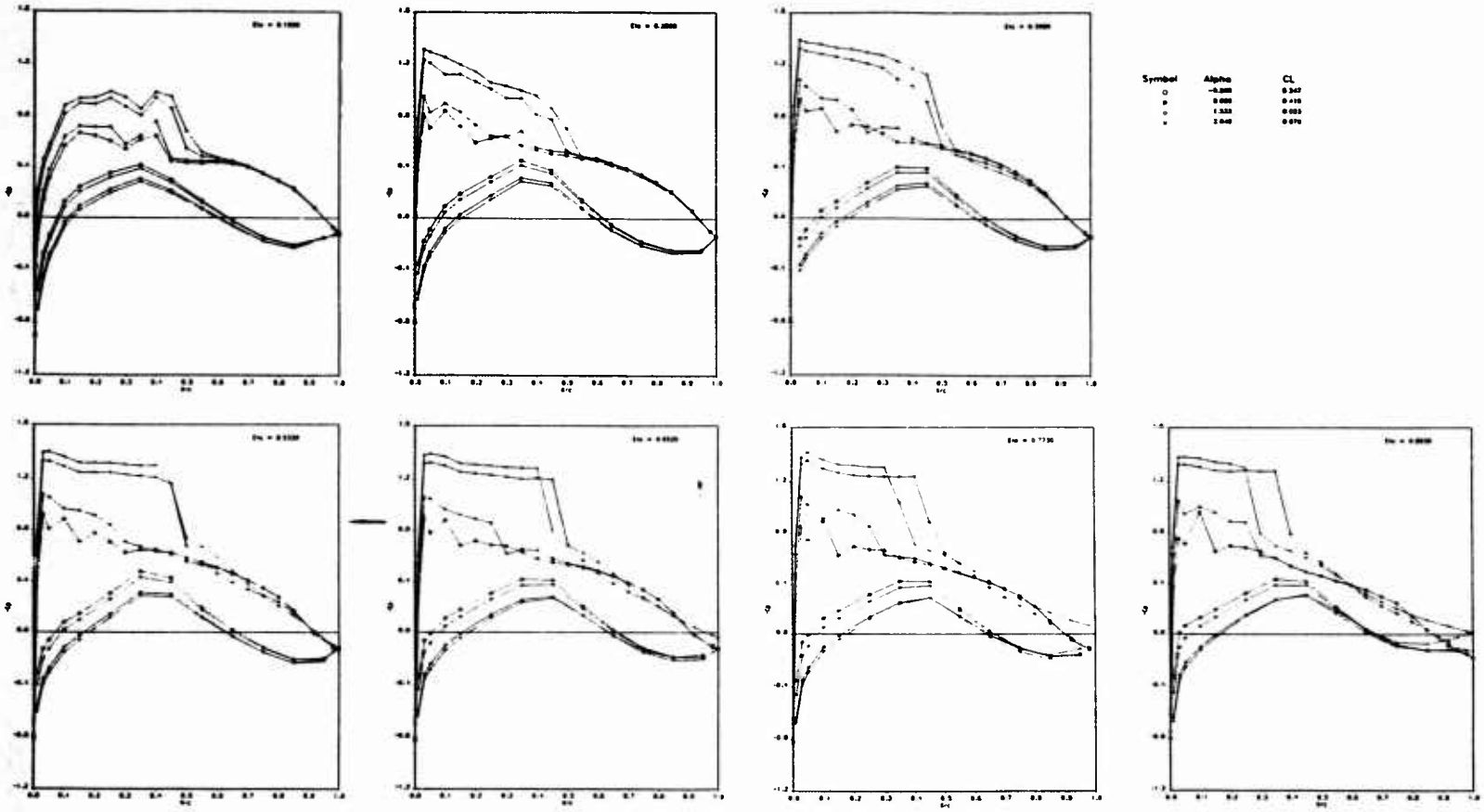



**FIG. 9** **PRESSURE DISTRIBUTIONS - COMPLETE MODEL**
**M = 0.780 $R_c$ = 5.8 x $10^6$**

# DLR-F4 WING BODY CONFIGURATION

by

G. REDEKER

DEUTSCHE FORSCHUNGSANSTALT FÜR LUFT-UND RAUMFAHRT E.V. (DLR)
INSTITUT FÜR ENTWURFSAERODYNAMIK

Lilienthalplatz 7
D-38108 BRAUNSCHWEIG
GERMANY

## 0 INTRODUCTION

These tests have been carried out under the auspices of GARTEUR in order to provide an experimental data base for a modern commercial transport type aircraft against which results of various computational methods may be checked. The tests were carried out in three major European wind tunnels (NLR-HST, ONERA-S2MA, DRA-8ft x 8ft DRA Bedford) in order to compare the results of the same model in different wind tunnels. For the purpose of these tests the available geometry of the DLR-F4 model of a wing body configuration, which was developed as a research configuration of a modern transport type aircraft, was selected by the GARTEUR Action Group AD (AG01) 'Wing body aerodynamics at transonic speeds'.

## 1 GENERAL DESCRIPTION

| | |
|---|---|
| 1.1 Model name | DLR-F4 model [1]. |
| 1.2 Model type and flow conditions | Wing body configuration of a subsonic transport type aircraft. Attached transonic flow on swept back wing of aspect ratio 9.5. |
| 1.3 Design requirements, purpose of tests | Transonic swept wing flow in M-range 0.75-0.8 with supersonic flow regions on upper wing surface terminated by weak shock waves. Data base for validation of 3D transonic codes. Comparison of data for the same model in different wind tunnels. |
| 1.4 Dominant flow physics | Transonic or supercritical flow on sweptback wing with weak shock waves. A small trailing edge separation is present at design condition in the kink region of the trailing edge. |

## 2 DETAILS OF MODEL

| | |
|---|---|
| 2.1 General geometric arrangement | Wing body combination; see Fig. 1. |
| 2.2 Configuration tested | Wing body configuration and body alone tested |
| 2.3 Wing and airfoil data | |
| 2.3.1 Planform | See Fig. 1.; Aspect ratio $\Lambda = 9.5$ ; taper $\lambda = 0.3$<br>L.E. sweep $\varphi_{LE} = 27.1°$ ; 25% sweep $\varphi_{25} = 25°$<br>Twist distribution incorporated in wing sections.<br>Semispan $s = 0.5857$ m<br>Wing ref. area: $S = 0.1454$ m$^2$<br>Aerodynamic mean chord: $\bar{c} = 0.1412$m<br>Tip geometry. half circle of local wing section thickness inside side edge of wing planform.<br>No special wing/body junction; sharp corner. |

| | |
|---|---|
| 2.3.2 Basic wing sections | Wing section shapes see Fig. 2.<br>Wing built up by 4 defining sections as shown in Fig. 2. |
| 2.4 Body data | |
| 2.4.1 Shape | Nose and afterbody shape see Fig. 3.<br>Body length l = 1.1920 m.<br>Cross-sectional details see geometry data disk. |
| 2.7 Geometric definition of c mponents | Wing: Numerically specified by 4 defining sections (Fig. 2). Wing contour is generated by linear lofting between defining sections. Body: Numerically specified by 90 cross-sections x = const. .<br>Data are design coordinates.<br>Tolerances: wing and body ±0.05 mm. |
| 2.8 Model support details (DRA) | The model was mounted on an axisymmetric sting passing through a hole of elliptic cross- section in the rear of the body (Fig. 4). |
| 2.8 Model support details (NLR) | NLR Z-sting Nr. 002 (see Fig.5 and 6);<br>a small unsealed gap is present at the location where the blade enters the model. |
| 2.8 Model support details (ONERA) | ONERA Z-sting see Fig. 7. |

## 3 GENERAL TUNNEL INFORMATION (DRA)

| | |
|---|---|
| 3.1 Tunnel designation | 8ft x 8ft Pressurised, Subsonic/Supersonic Wind Tunnel. |
| 3.2 Organisation running the tunnel | Defense Research Agency (formerly Royal Aerospace Establishment), Aerodynamic and Propulsion Department, Bedford MK41 6AE, England. |
| 3.3 Tunnel characteristics | Type of tunnel: continuous flow, closed circuit. Operating envelope see Fig. 8. |
| 3.4 Test section | |
| 3.4.1 Model mounting | See Fig. 4. |
| 3.4.2 Test section dimensions | 2.44 m x 2.44 m x 14 m (width x height x length). |
| 3.4.3 Wall geometry details | Type of walls: solid, flexible upper and lower walls for supersonic operation. Shapes of upper and lower walls are set for subsonic tests in such a way as to minimise the pressure gradient on the centre line when the test section is empty. Wall pressures are measured along the centre lines of the roof and floor. Typical wall boundary-layer displacement thickness: 19 mm. For further details see [2]. |
| 3.5 Freestream conditions | |
| 3.5.1 Reference conditions | Total pressure: Determined using a pitot probe in the settling chamber and a 'Midwood' self-balancing capsule manometer of range 400 kPa and accuracy ±0.03% full scale. Static pressure: The reference static pressure tapping is on the centre-line of the sidewall 6.25 m upstream of the strain-gauge balance centre-line. The differential 'Midwood' mano-meter used for this measurement was of range 100 kPa and accuracy 0.03% full scale. Static temperature: This is inferred from total temperature measured to an accuracy of ± 0.1K by a probe in the settling chamber. |
| 3.5.2 Tunnel calibration | Measurements were made of static pressures on the test section centre-line and roof and floor [3] using differential 'Midwood' manometers of range ± 100kPa and accuracy ± 0.03% full scale. The last calibration was performed (using electronic scanning of pressure transducers) in October 1991, calibrations being performed annually. |

3.6 Flow quality

3.6.1 Flow uniformity

For static pressure variations along the model axis see [3], but typically $\Delta c_p < 0.001$ with the diffuser choked, as in the present tests.
The variation of (uncorrected) Mach number during a run is within 0.001.
Average flow angularity was determined by comparing force measurements made with the model erect and inverted. The implied average downwash angle was found to be up to about 0.03°.

3.6.2 Temperature variation

The temperature is controlled during the run by altering the flow of water through the cooler in the settling chamber. Temperature can be controlled to within 0.5°C. Temperature variation within the tunnel is not known.

3.6.3 Flow unsteadines

Overall turbulence level is not known but overall noise level is typically $c_{prms} = 0.004$. For further information on the noise characteristics of the wind tunnel see [4].

## 3 GENERAL TUNNEL INFORMATION (NLR)

3.1 Tunnel designation

High Speed Wind Tunnel HST [5].

3.2 Organisation running the tunnel

National Aerospace Laboratory NLR, Amsterdam, The Netherlands.

3.3 Tunnel characteristics

Closed circuit; see Fig. 9 for operating conditions.

3.4 Test section

3.4.1 Model mounting

See Fig.5 and 6.

3.4.2 Test section dimensions

2.00 m x 1.60 m x 2.70 m (width x height x length).

3.4.3 Wall geometry

Slotted top and bottom wall; closed side walls; open area ratio 12% per wall.

3.5 Freestream conditions

3.5.1 Reference flow condition

Total pressure: settling chamber.
Static pressure: from plenum pressure with correction derived from long static pipe calibration.
Static temperature: from total temperature in settling chamber and Mach number.

3.5.2 Tunnel calibration

'Long static pipe' at tunnel center and side wall pressures.
Last 'long static pipe' calibration: 1980; regular checks on possible changes from side wall pressures.

3.6 Flow quality (empty tunnel)

3.6.1 Flow uniformity

Mach number variation over model length: < .001 (at Mach=.75).
Mach number variation during a run :< ± .001.
Flow angularity derived from comparison of model upright and inverted tests at tunnel center; order of magnitude .2°.
Variation of flow angularity over model span:
not measured; estimated to be less than .2°.

3.6.2 Temperature variation

Temperature can be controlled during a run;
variation during a run less than 1°C to 3°C depending on Mach and Reynolds number.

3.6.3 Flow unsteadiness

Turbulence level not measured but assumed to be very low in view of the high contraction ratio ( 1 : 25 ).
Overall noise level: depending on Mach number, .5% $< c_{prms} <$ 1%.

## 3 GENERAL TUNNEL INFORMATION (ONERA)

| | |
|---|---|
| 3.1 Tunnel designation | ONERA-S2MA wind tunnel (ONERA Modane Centre) [10], [11] |
| 3.2 Organization running the tunnel | ONERA |
| 3.3 Tunnel characteristics | |
| Type of tunnel | Continuous with two interchangeable test sections (1 transonic, 1 supersonic). |
| Indicate operating envelope | As far as the transonic test section is concerned:<br>Mach number range: $0.25 \leq M \leq 1.35$<br>Total pressure: $0.3 \leq p_0 \leq 2.5$ bar<br>The maximum total pressure depends on the Mach number.<br>Total temperature: $285 \leq T_0 \leq 320$K |
| 3.4 Test section | |
| 3.4.1 Model installation | See Fig. 10. |
| 3.4.2 Test section dimensions | 1.75 m x 1.77 m x 5.40 m (width x heigth x length). |
| 3.4.3 Wall geometry details | |
| Type of walls | Perforated top and bottom walls; solid side walls. |
| Open area ratio | 6% geometric porosity (maximum). |
| Are wall pressures/wall displacements measured | No |
| Boundary layer control on walls | No |
| Typical wall boundary layer displacement thickness | Side wall boundary layer displacement thickness $\delta_1$ = 14mm. |
| 3.5 Freestream conditions | |
| 3.5.1 Reference conditions | |
| Total pressure | Measured in the settling chamber. |
| Static pressure | Measured on the side wall, at reference pressure tap (PT 629 bis; see Fig. 10). |
| Static temperature | Derived from total temperature measured in the settling chamber. |
| 3.5.2 Tunnel calibration | |
| How was the tunnel calibrated | By static pressure measurements along the tunnel axis using a cylinder probe (length = 6m). |
| Date of the last calibration | The last calibration before the present tests took place in june 1978. |
| 3.6 Flow quality (empty tunnel) | |
| 3.6.1 Flow uniformity | |
| Static pressure variation over model length and span | $\Delta M/m = \pm 3 \times 10^{-3}/m$ in x-direction ($0.7 \leq M \leq 1.2$); unknown in y-direction at the time of the F4 tests. |
| Mach number variation during a run | At fixed angle of attack the Mach number is kept constant at ± 0.001. During a continuous angle of attack variation, the Mach number variation depends on model size and M. |
| How is average flow angularity determination | By tests with model erected and inverted. |

| | |
|---|---|
| Variation of flow angularity over the model length and span | Unknown at the time of the F4 tests. |
| 3.6.2 Temperature variation | |
| Can the temperature be controlled during a run | Partially, depending on the test conditions. |
| Variation within the tunnel | Unknown |
| Variation over a run | Variable, depending on the test conditions. |
| 3.6.3 Flow unsteadiness | |
| Overall turbulence level | Tu ~ 0.002. |
| Overall noise level | $\frac{p'_{rms}}{q}$ = 0.012 at M = 0.75. |

## 4 INSTRUMENTATION

| | |
|---|---|
| 4.1 Model postion (DRA) | |
| 4.1.1 Geometrical angle of incidence | Model incidence derived from support angle corrected for model deflection under load as obtained by calibration. |
| 4.1.2 Accuracy of geometrical incidence | ± 0.005° |
| 4.1 Model position (NLR) | See Fig. 6 for mounting details;<br>model incidence derived from support angle corrected for model deflection under load as obtained by calibration.<br>Accuracy: ± .02°. |
| 4.1 Model postion (ONERA) | |
| 4.1.1 How is the geometrical incidence measured | By both inclinometer in the model and model support angle corrected for model and sting deflection under aerodynamic load. |
| 4.1.2 Accuracy of geometrical incidence | ± 0.02°. |
| 4.2 Model pressure measurements | |
| 4.2.1 Total number and disposition of pressure holes | Wing: 252 at 7 spanwise stations.<br>Fuselage: 44 in upper and lower bottom line (see Fig.11). |
| 4.2.2 Range and accuracy of pressure transducers | Differential transducers were used mainly ranging from 17.5 to 33 kPa and connected groupwise according to the expected pressures.<br>Accuracy: ± .2% full scale. |
| 4.3 Force and moment measurements (DRA) | Forces and moments were measured using a six-component internal strain gauge balance. The position of the balance is shown in Fig. 4. The ranges of the six components are as follows: |

| Component | Range |
|---|---|
| Axial force | 670 N |
| Normal force | 7100 N |
| Side force | 1560 N |
| Pitching moment | 750 Nm |
| Rolling moment | 240 Nm |
| Yawing moment | 240 Nm |

Accuracies: Precision ± 0.05%
Bias: not determined precisely but believed to be better than ± 0.2%.

4.3 Force and moment measurements (NLR)

Task 2" extended range

| Component | kange |
|---|---|
| Normal force | 9220 N |
| Axial force | 930 N |
| Pitching moment | 461 Nm |

Accuracy: ± .3% full scale

4.3 Force and moment measurements (ONERA)

4.3.1 Type and location of balance: Internal 6-component strain gauge balance Φ55 n° 2

4.3.2 Indicate maximum range and accuracy of all components

| | |
|---|---|
| Normal force | N = 20000 N |
| Axial force | A = 1700 N |
| Pitching moment | M = 1700 Nm |

the accuracy being 0.1% full scale.

4.5 Surface flow visualizations (NLR)

Wing upper and lower surface.
Acenaphtene to optimize transition strips.
Oil flow pictures during and after a run.
Data available on photographs.

4.5 Surface flow visualizations(ONERA)

4.5.1 Measurement technique applied: a) Acenapthene for transition location.
b) Oil flow and c) Coloured liquid for wall streamlines.

4.5.2 On which surfaces is the flow visualized: a) Transition location on the right wing.
b) Wall streamlines on the left wing.

4.5.3 In what form are data available: Photographs

4.7 Tunnel wall measurements (DRA)

4.7.1 Types of measurements: Four static pressures were measured close to the peak decrement in pressure on the roof and two on the floor. These holes were, respectively, 152mm upstream and downstream of the balance centre-line which is 11.6mm downstream of the moment reference point of the model.

4.7 Tunnel wall measurements(ONERA)

4.7.1 Type of measurements: None, except static pressure reference measurements

4.7.2 Location and number of pressure holes: See Fig. 10.

## 5 TEST MATRIX AND CONDITIONS

5.1 Detailed test matrix

5.1.1 Number of selected test cases: 10

5.1.2 Number of configurations: 2 ; wing/body (W/B) and body alone (B)

5.1.3 Refer to table: Table 1: Force measurements

| | |
|---|---|
| Test case number | see Table 1 |
| Configuration | wing/body body alone |
| Mach number | 0.6, 0.75, 0.80 |
| Reynolds number | $3.0 \cdot 10^6$ |
| Model attitude | $-4° < \alpha < 10°$, $\beta = 0°$ |
| Type of measurements | force measurements (Fig. 12). |

Refer to table: Table 2:Pressure measurements, M-sweep

| | |
|---|---|
| Test case number | see Table 2 |
| Configuration | wing/body |
| Mach number | M = 0.6, 0.7, 0.75, 0.76, 0.77, 0.78, 0.79, 0.80, 0.81, 0.82 |
| Reynolds number | $3.0 \cdot 10^6$ |
| Model attitude | $c_L = 0.5$ |
| Type of measurements | pressure distribution on wing and body. |

| | |
|---|---|
| Refer to table | Table 3: Pressure measurements, $c_L$-sweep |
| Test case number | see Table 3 |
| Configuration | wing/body |
| Mach number | 0.75 |
| Reynolds number | $3.0 \cdot 10^6$ |
| Model attitude | $c_L$ = 0.3, 0.4, 0.5, 0.6 |
| Type of measurements | pressure distribution on wing and body (Fig. 13). |

5.2 Model/tunnel relations

5.2.1 Maximum blockage

| | |
|---|---|
| DRA-8ft x 8ft | 0.0044 |
| NLR-HST | 0.0081 |
| ONERA-S2MA | 0.0084 |

5.2.2 Model span/tunnel width

| | |
|---|---|
| DRA-8ft x 8ft | 0.480 |
| NLR-HST | 0.586 |
| ONERA-S2MA | 0.662 |

5.2.3 Wing area/tunnel cross-section

| | |
|---|---|
| DRA-8ft x 8ft | 0.0244 |
| NLR-HST | 0.0454 |
| ONERA-S2 MA | 0.0469 |

| | |
|---|---|
| 5.2.6 Adiabatic wall temperatures (DRA) | Reached by ensuring minimal excursion of model temperature between wind on and wind off conditions. |
| 5.2.6 Adiabatic wall temperatures(ONERA) | yes, in principle |

5.3 Transition details

| | |
|---|---|
| 5.3.1 Free or fixed transition | fixed |
| 5.3.3 Details of fixed transition | see Fig. 14.<br>sparsely distributed carborundum grains, strips about 2 mm wide; optimized by each wind tunnel. |
| DRA-8ft x 8ft | upper surface 220 K, lower surface 180 K<br>transition verified by special DRA routine including drag measurements |
| NLR-HST | upper surface 180 K, lower surface 240 K<br>transition verified with acenaphtene |
| ONERA-S2MA | upper surface 220 K, lower surface 240 K<br>transition verified with acenaphtene |

## 6 DATA

6.1 Availability of data

| | |
|---|---|
| 6.1.1 Organisation | Deutsche Forschungsanstalt für Luft- und Raumfahrt (DLR)<br>Institut für Entwurfsaerodynamik |
| 6.1.2 Responsible Person | Dr.-Ing. G. Redeker<br>DLR<br>Postfach 3267<br>38022 Braunschweig<br>Fed. Rep. Germany<br>Tel.: 49 531 295 2430; Fax: 49 531 295 2320 |

| | |
|---|---|
| 6.1.3 Availability | Data are freely available. |
| 6.2 Suitability of data for CFD validation | |
| 6.2.1 Are data suitable for 'in-tunnel' calculations? | No; but uncorrected data of DRA can be used for in-tunnel calculations. |
| 6.2.2 Corrections | Data are corrected to „free-air" conditions. |
| 6.3 Type and form in which data are available | |
| 6.3.1 Type and form | Tables of wing and body geometry<br>Tables of force coefficients and pressure coefficients |
| 6.3.2 Data carrier | 3.5" floppy disk (geometry and aerodynamic data). |
| 6.3.3 Extent of geometry data | 142 kBytes |
| 6.3.4 Extent of aerodynamic test data | 213 kBytes |
| 6.4 Corrections applied to data (DRA) | |
| 6.4.1 Lift interference and blockage corrections | Corrections to angle of incidence and drag coefficient for lift interference obtained using linear theory [7, 8] and the measured lift coefficient. The model is small for the test section and the data are considered to be globally correctable for lift interference.<br>Corrections to Mach number and free-stream static and dynamic pressures were obtained using a method [9] that is standard for the 8ft x 8ft Tunnel. The method is of the model-representation type with the model and wake displacement effects allowed for by an axial distribution of point sources and sinks. The solid walls are represented by a suitable doubly infinite array of images. The ratio of the blockage velocity increment on the tunnel centre line at the moment reference point to the total (direct plus blockage) velocity increment on the tunnel walls at the pressure measuring points is then calculated. The ratio is then used in conjuntion with the measured pressure increments relative to empty-tunnel conditions to give the blockage correction. No corrections have been applied to drag for blockage buoyancy, but see below. |
| 6.4.4 Sting corrections | Apart from correcting base pressure to free-stream static pressure, no corrections have been applied for sting interference. However, tests were made with the body alone as well as with the wing-body. By differencing wing-body and body alone data, it is possible to obtain notional 'wing alone' data largely free of sting interference and blockage buoyancy effects. |
| 6.4.5 Aeroelastic deformation | See 6.4.5 Corrections applied to data (NLR). |
| 6.4 Corrections applied to data (NLR) | |
| 6.4.1 Lift interference and blockage corrections | For the size of the model data are considered to be interference free (this is based on a number of comparisons between the HST and other wind tunnels). |
| 6.4.2 Sting and support corrections | Static pressures are corrected for the upstream support influence using the empty tunnel center line pressure distribution (with the model support present) as measured with a long static pipe. |
| 6.4.4 Other corrections | Buoyancy drag derived from static pressure variation as measured with long static pipe and support present. |
| 6.4.5 Aeroelastic deformation | A theoretical estimate has been made of the wing deformation under load (see Fig. 15) for the 'design' condition at $Re=3 \times 10^6$. This deformation is not included in the geometrical wing data. |

6.4 Corrections applied to data (ONERA)

6.4.1 Lift interference and blockage corrections

| | |
|---|---|
| Are data considered globally correctable | yes |
| Type of correction method applied | analytical [12]. |
| Specify what data are actually corrected and indicate order of magnitude | The following corrections, for example, have been applied at $M = 0.75$, $c_L = 0.5$<br>Mach number: $\Delta M = -0.0001$<br>Drag coefficient: $\Delta c_D = -0.00059$ |

6.4.4 Sting and support corrections

| | |
|---|---|
| Correction method | Computation of the flowfield induced by the support |
| Magnitude and typical variation of support induced pressure field | The magnitude of support induced pressure field results, at $M = 0.75$, $c_L = 0.5$, in a correction of the drag coefficient $\Delta c_{DS} = +0.00192$ |

6.4.5 Aeroelastic deformation

| | |
|---|---|
| How was deformation determined | by NLR computation |
| Typical order of magnitude | wing tip twist angle $\Delta\alpha = -0.43^\circ$ (Fig. 15) |

6.4.6 Other corrections: Empty test section flow buoyancy leading to a correction of the drag coefficient $\Delta c_{Db} = +0.00071$.

## 7 DATA ACCURACY AND REPEATABILITY ASSESSMENT (DRA)

7.1 Accuracy

| | | |
|---|---|---|
| 7.1.1 Freestream conditions | Incidence | $\pm 0.01^\circ$ |
| | Mach number | $\pm 0.001$ |
| 7.1.2 Measured data<br>Forces and Moments | Lift coefficient | $\pm 0.004$ |
| | Drag coefficient | $\pm 0.0004$ |
| | Pitching moment coefficient | $\pm 0.001$ |
| Pressure | Pressure coefficient | $\pm 0.002$ |

7.2 Repeat measurements: Tests of the model in the erect and inverted positions have been made. The discrepancies between the two sets of data for the drag are well within the band $\Delta c_D = \pm 0.0001$.

7.4 Other tests made: The same model was tested in the ONERA-S2MA and NLR-HST wind tunnels.

## 7 DATA ACCURACY AND REPEATABILITY ASSESSMENT (NLR)

7.1 Accuracy estimates

| | |
|---|---|
| 7.1.1 Free stream conditions | $\Delta$ Mach $< \pm 0.002$<br>$\Delta\alpha < \pm 0.02^\circ$ |
| 7.1.2 Measured data | $\Delta c_L < \pm 0.005$<br>$\Delta c_D < \pm 0.0005$<br>$\Delta c_M < \pm 0.002$<br>$\Delta c_p < \pm 0.005$ (0.01 in pressure peaks) |
| 7.2 Repeat measurements | no repeat measurements made |
| 7.3 Redundant measurements | Forces have been measured with and without pressure wiring |

present.
Static load checks ('$\alpha$-sweeps') have been made with model in inverted position showing agreement within measurement accuracy.
Measured wing and body pressures have been integrated to be compared with measured overall forces.

7.4 Other tests made

The same model was tested in the ONERA- S2MA and in the DRA-8ft x 8ft wind tunnels.

## 7 DATA ACCURACY AND REPEATABILITY ASSESSMENT (ONERA)

7.1 Accuracy estimates

7.1.1 Free stream conditions

| | |
|---|---|
| Mach number | $\Delta M = \pm\ 0.001$ |
| Model incidence | $\Delta\alpha = \pm\ 0.02°$ |

7.1.2 Measured data

| | |
|---|---|
| Forces and moments | $\Delta c_L = \pm\ 0.006$<br>$\Delta c_D = \pm\ 0.0004$<br>$\Delta c_M = \pm\ 0.0014$ |
| Pressure coefficients | $\Delta c_p = \pm\ 0.01$ |

7.2 Repeat measurements

7.2.1 Type and number of repeat measurements within one test campaign

Reduced number of total force and moment measurements as well as wing pressure distributions.

7.3 Redundant measurements

7.3.2 Checks made on internal consistency of the data

Shock wave and separation locations by pressure distribution and surface flow visualisations. Buffet onset determination by lift curve, pitching moment curve, tangential force curve, rms-value curve of wing root strain gauge, wing tip accelerometer.

7.4 Other tests on same (nominal) geometry

7.4.1 Has the same (identical) model been measured in another wind tunnel?

The same model was tested in the NLR-HST and in the DRA (former RAE) 8ft x 8ft wind tunnels as a GARTEUR exercise.

## 8 REFERENCES


[1] G. Redeker; R. Müller: A comparison of Experimental Results for the Transonic Flow around the DFVLR-F4 Wing Body Configuration.
GARTEUR/TP-018
DLR-IB 129 - 83/21 (1983).

[2] K.G. Winter; L. Gaudet:
Turbulent boundary-layer studies at high Reynolds number. ARC R&M 3712, 1970

[3] D. Isaacs:
Calibration of the RAE Bedford 8ft x 8ft Wind Tunnel at Subsonic Speeds, Including a Discussion of the Correction to the Measured Pressure Distribution to Allow for the Direct and Blockage Effects due to the Calibration Probe. ARC R&M 2777, 1969.

[4] J. Whitfield; N.S. Dougherty Jr.:
A Survey of Transition Research at AEDC. Paper 25-1, AGARD-CP-224, 'Laminar-Turbulent Transition', Oct. 1971.

[5] User's guide to the 1.60 x 2.00 $m^2$ High Speed Wind Tunnel HST of the National Aerospace Laboratory NLR.

[6] R.H.C.M. Hirdes:
Test results of wind-tunnel measurements on the DFVLR-F4 wing in the NLR high speed wind tunnel HST. NLR TR 83131 L, 1983.

[7] H.C. Garner:
Subsonic wind tunnel wall corrections. AGARDograph 109, 1966.

[8] W.E.A. Acum:
Corrections for symmetrical and tapered wings in rectangular wind tunnels. ARC R&M 2777.

[9] B. Goethert:
Windkanalkorrekturen bei hohen Unterschallgeschwindigkeiten unter besonderer Berücksichtigung des geschlossenen Kreiskanals.
Deutsche Luftfahrtforschung Forschungsbericht 1216, 1940 (translated as NACA Tech Memo 1300).

[10] M. Pierre; G.Fasso:
The aerodynamic test center of Modane-Avrieux. ONERA - TN no 166E, 1972.

[11] M. Pierre, G. Fasso:
Exploitation du centre d'essais aerothermodynamique de Modane-Avrieux. ONERA - TN no 181, 1971.

[12] X. Vaucheret:
Améliorations des calculs des effects de parois dans les souffleries industrielles de l'ONERA. AGARD - CP - 335, 1982.

## 9 LIST OF SYMBOLS

| | |
|---|---|
| Coordinate system of wing/body configuration (see Fig. 1). | x,y,z |
| coordinate system of wing (see Fig. 1) | $x^*,y^*,z^*$ |
| half span in x-y system | $s = b/2$ |
| half span in $x^*$-$y^*$ system | $s^* = b^*/2$ |
| wing ref. area | S |
| leading edge sweep angle | $\varphi_{LE}$ |
| quarter chord line sweep angle | $\varphi_{25}$ |
| local wing chord | c |
| aerodynamic mean chord | $\bar{c}$ |
| spanwise coordinate non-dimensional | $\eta = \frac{y}{s} = \frac{y^*}{s^*}$ |
| aspect ratio of wing | $\Lambda = b^2/S$ |
| taper ratio | $\lambda$ |
| fuselage diameter | D |
| fuselage length | l |
| Mach number | M |
| angle of attack | $\alpha$ |
| lift coefficient | $c_L = L/(q_\infty \times S)$ |
| pitching moment coefficient with ref. to $N_{25}$ (see Fig. 1). | $c_M = M/(q_\infty \times S \times \bar{c})$ |
| drag coefficient | $c_D = D/(q_\infty \times S)$ |
| normal force coefficient | $c_N = N/(q_\infty \times S)$ |
| tangential force coefficient | $c_T = T/(q_\infty \times S)$ |
| freestream dynamic pressure | $q_\infty$ |
| freestream static pressure | $p_\infty$ |
| local surface pressure | p |
| pressure coefficient | $c_p = (p-p_\infty)/q_\infty$ |
| Reynolds number based on aerodynamic mean chord | Re |

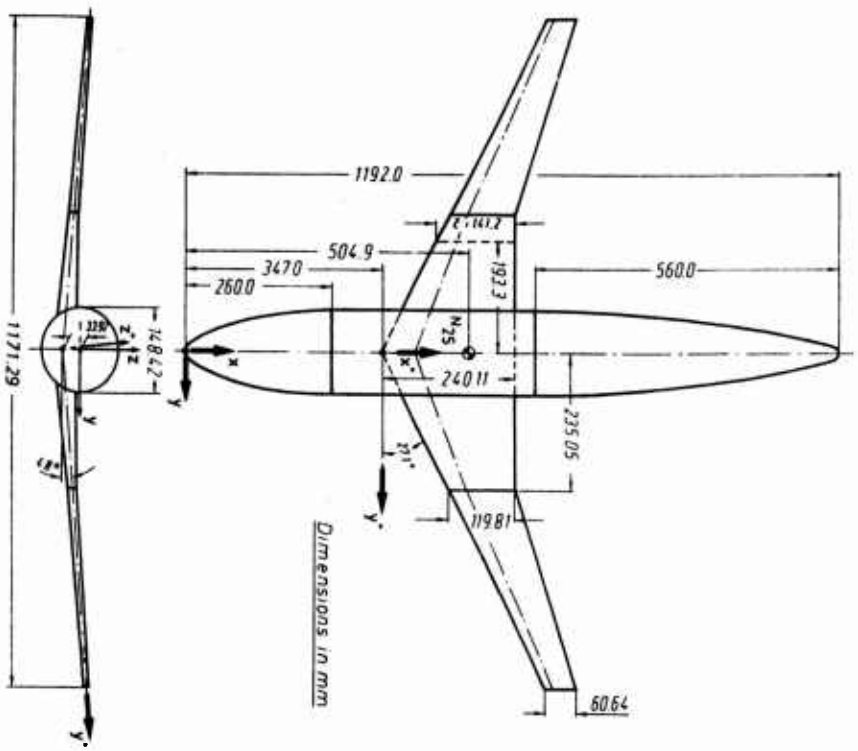



Fig. 1 General arrangement of the DLR-F4 wind tunnel model

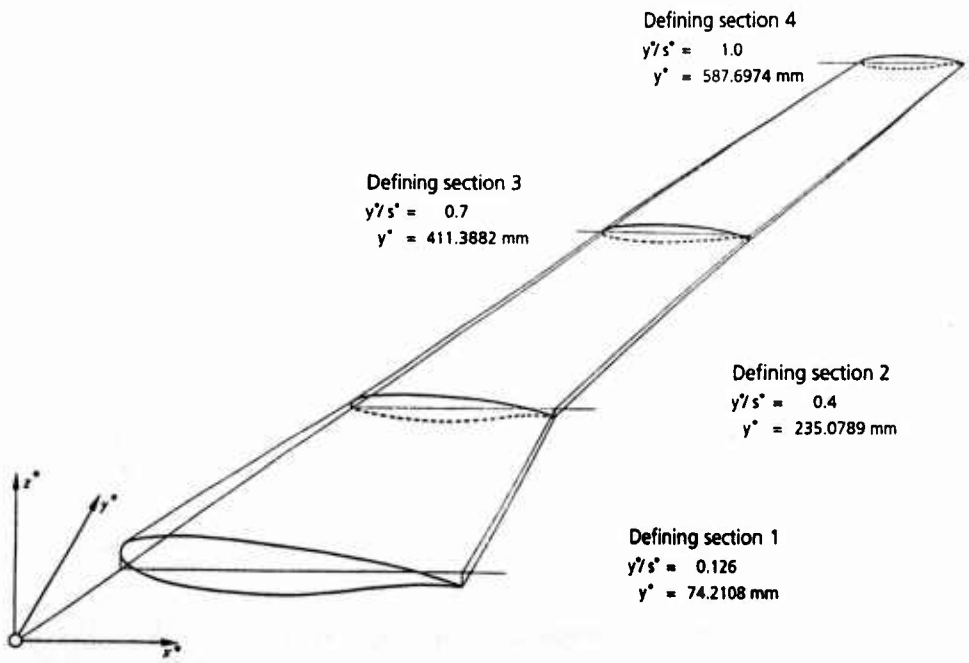



Fig. 2 Definition of the wing

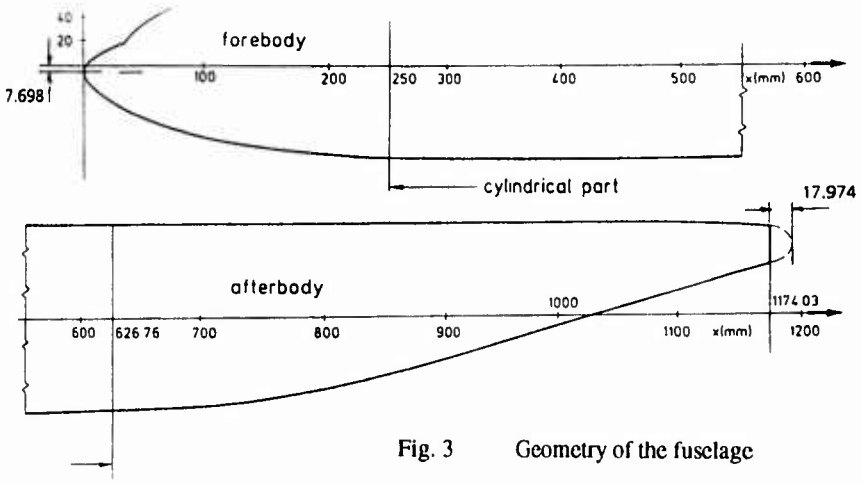



Fig. 3 Geometry of the fuselage

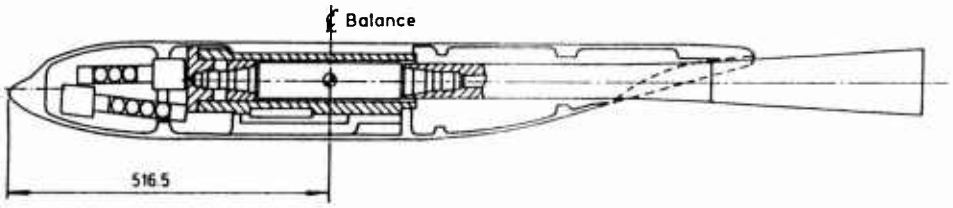



Fig. 4 Arrangement for mounting model in the DRA 8ftx8ft wind tunnel

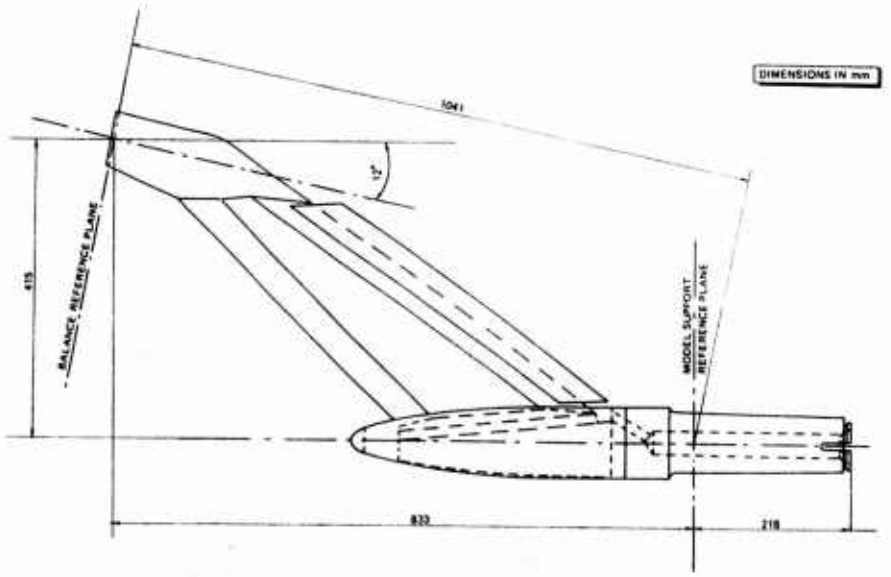



Fig. 5 Dimensions of NLR z-sting Nr. 002

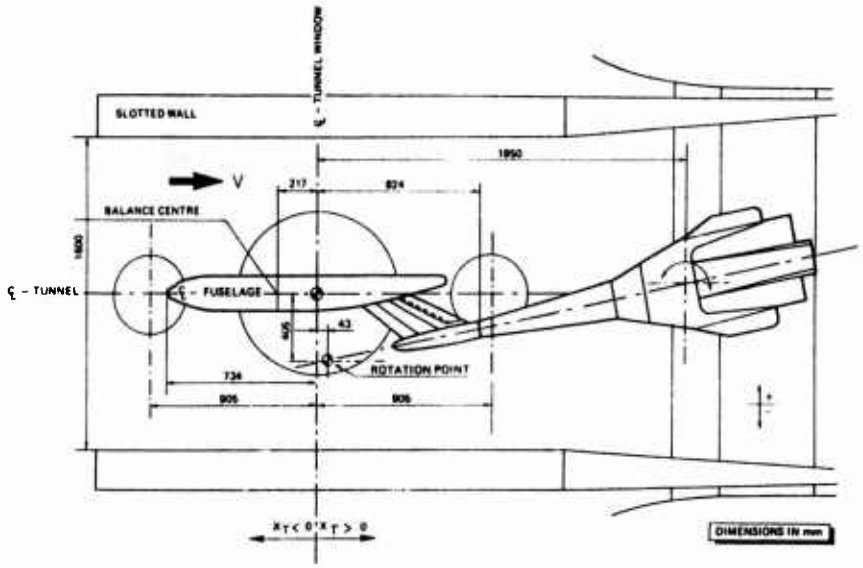



Fig. 6 Position of DLR-F4 model in the HST test-section

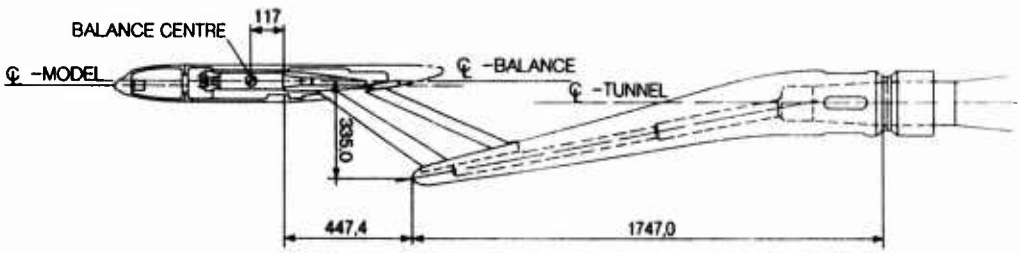



Fig. 7 ONERA z-sting arrangement

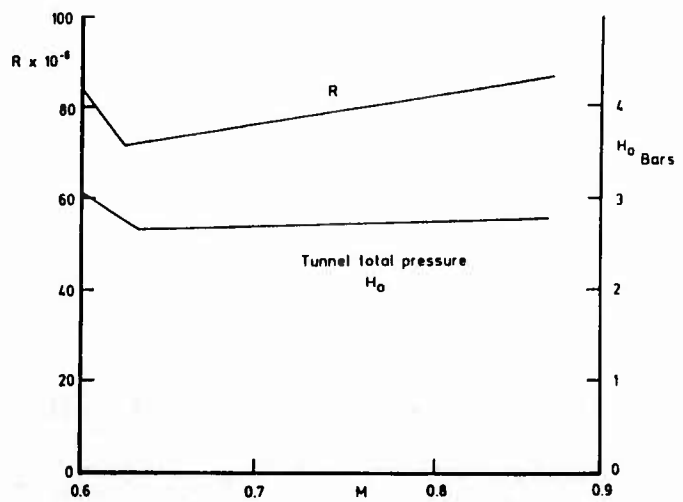



Fig. 8 DRA 8ftx8ft wind tunnel capability at high subsonic speeds

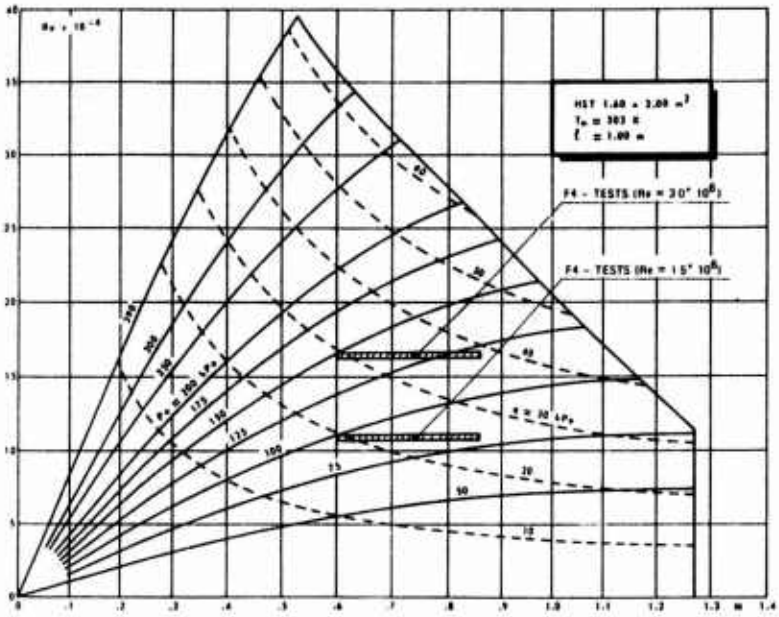



Fig. 9 Reynolds number as function of Mach number in empty test section of NLR-HST

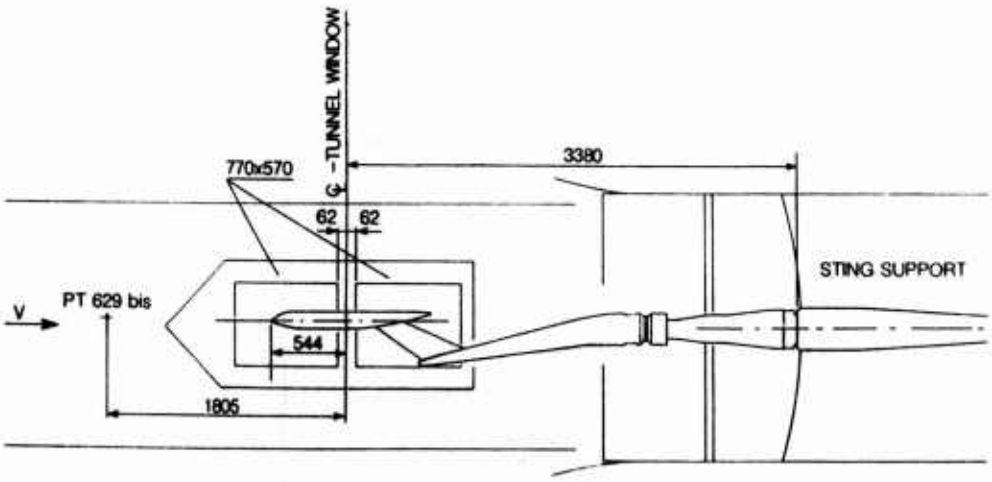



Fig. 10 S2MA-transonic test section with test set-up of DLR-F4 model

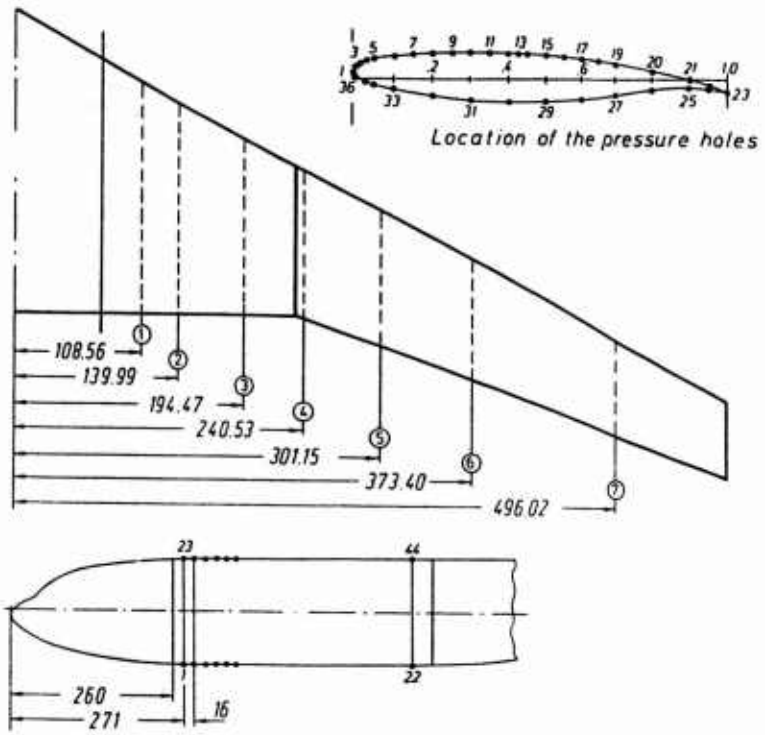



Fig. 11 Positition of pressure holes on wing and fuselage

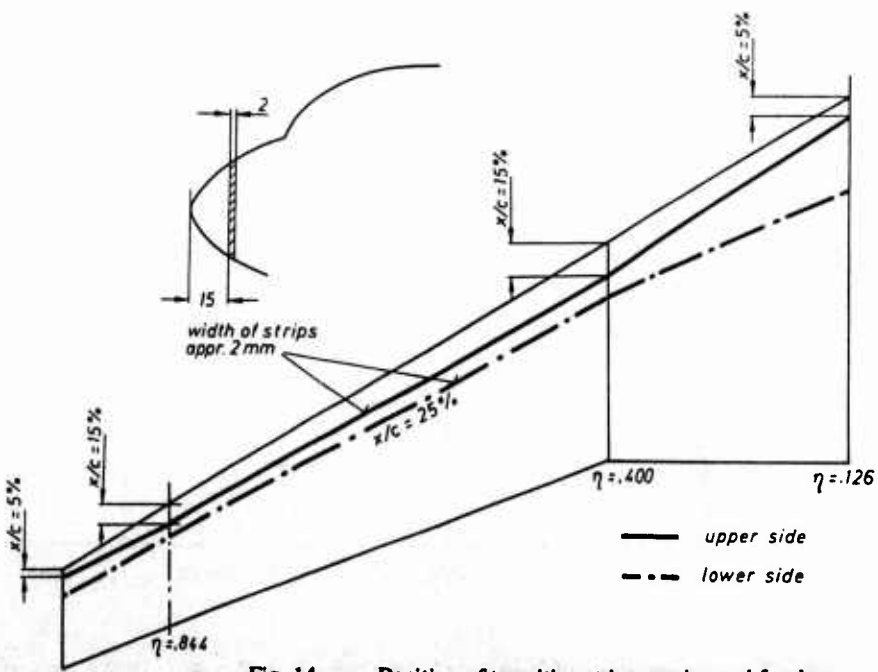
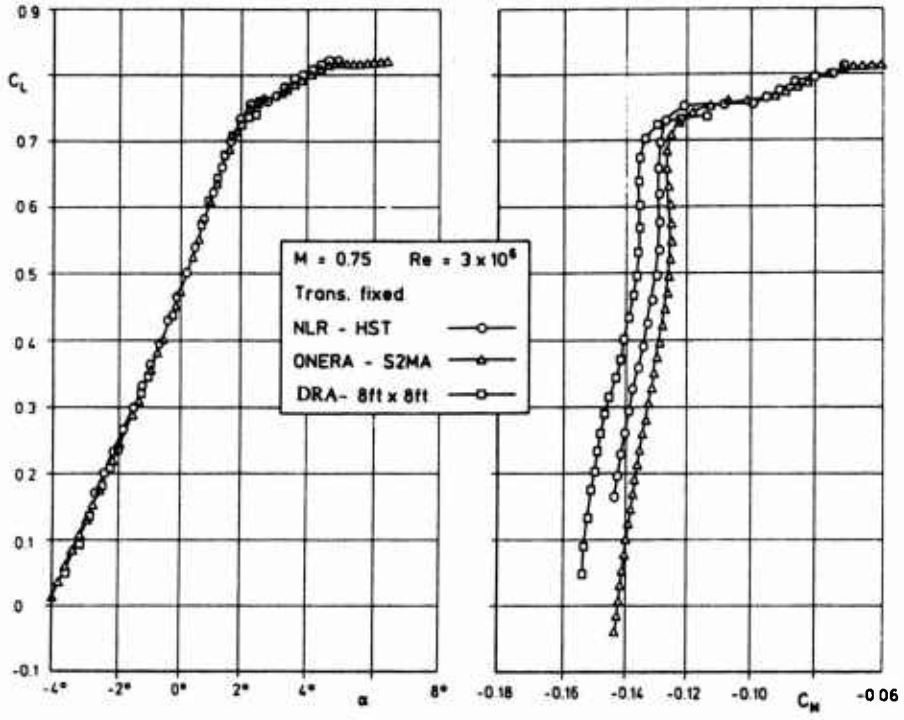



Fig. 14 Position of transition strips on wing and fuselage



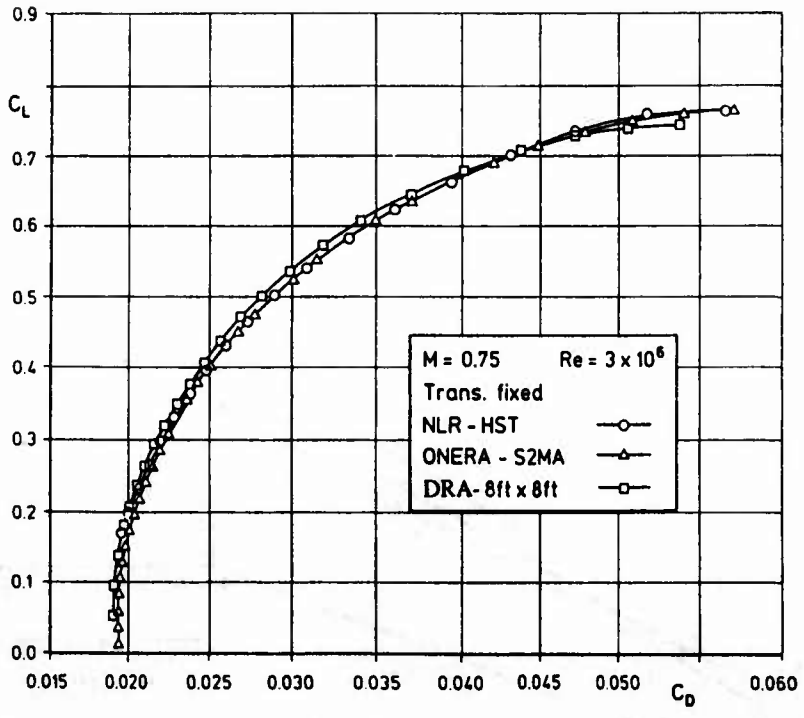




Fig. 12 Comparison of force and pitching moment coefficients of DLR-F4 model

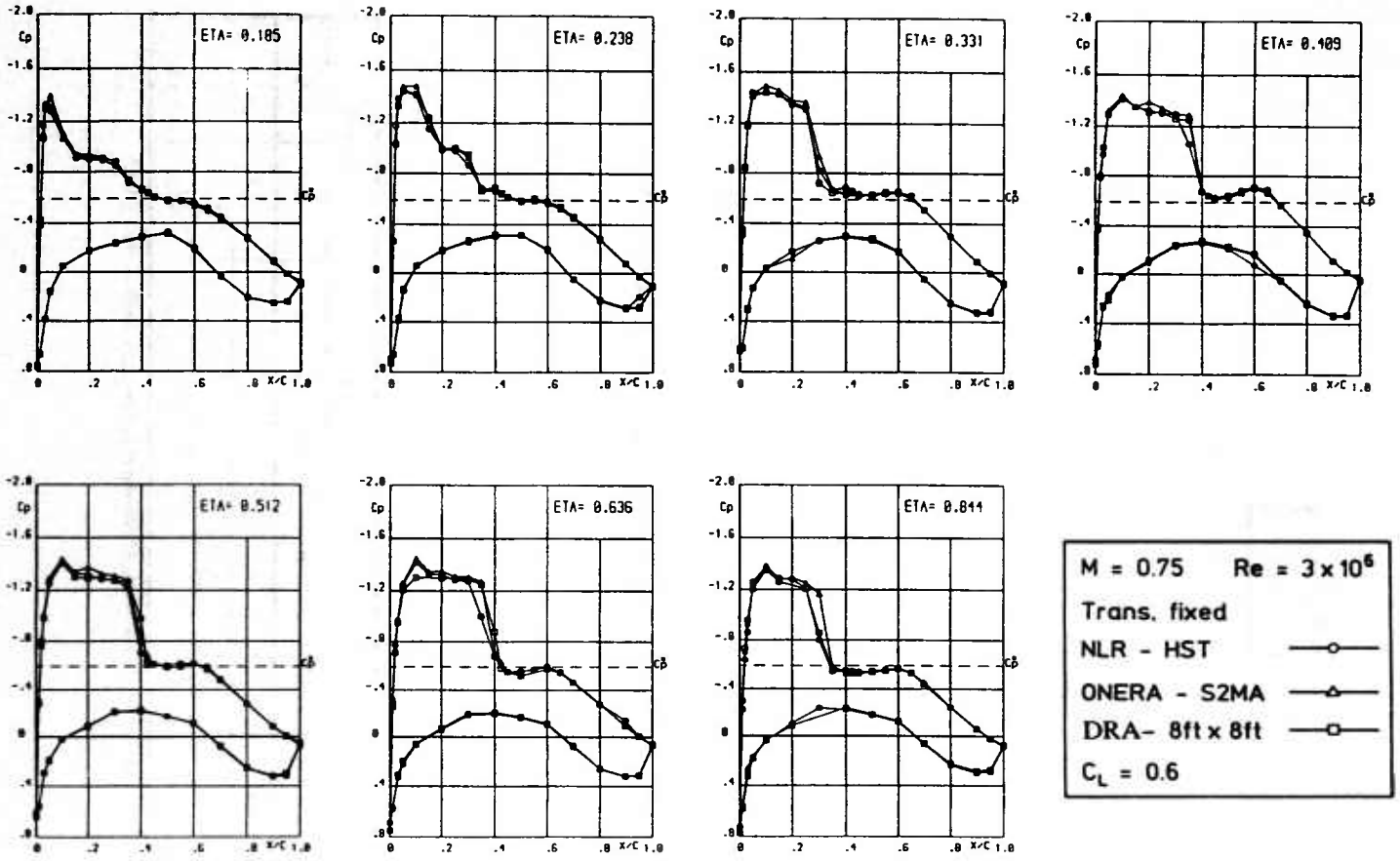



Fig. 13 Comparison of wing pressure distributions of DLR-F4 model

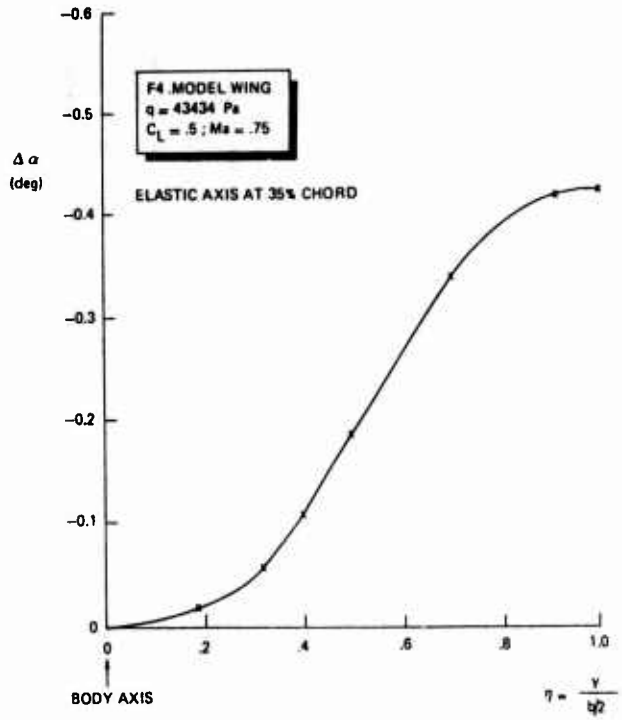



Fig. 15 Calculated wing deformation of DLR-F4 model

| | M = 0.60 | | M = 0.75 | | M = 0.80 | |
|---|---|---|---|---|---|---|
| | W/B | B | W/B | B | W/B | B |
| NLR - HST | 1.1.1.1 | 1.1.2.1 | 1.1.1.2 | 1.1.2.2 | 1.1.1.3 | 1.1.2.3 |
| ONERA-S2MA | 1.2.1.1 | 1.2.2.1 | 1.2.1.2 | 1.2.2.2 | 1.2.1.3 | 1.2.2.3 |
| DRA - 8ft x 8ft | 1.3.1.1 | 1.3.2.1 | 1.3.1.2 | 1.3.2.2 | 1.3.1.3 | 1.3.2.3 |

**Table 1: Force measurements, α-sweep at various Mach numbers, Re = $3.0 \cdot 10^6$**

| | M = 0.60 | M = 0.70 | M = 0.75 | M = 0.76 | M = 0.77 |
|---|---|---|---|---|---|
| | W/B | W/B | W/B | W/B | W/B |
| NLR - HST | 2.1.1.1 | 2.1.1.2 | 2.1.1.3 | ---------- | 2.1.1.5 |
| ONERA-S2MA | 2.2.1.1 | 2.2.1.2 | 2.2.1.3 | 2.2.1.4 | 2.2.1.5 |
| DRA - 8ft x 8ft | 2.3.1.1 | 2.3.1.2 | 2.3.1.3 | ---------- | 2.3.1.5 |

| | M = 0.78 | M = 0.79 | M = 0.80 | M = 0.81 | M = 0.82 |
|---|---|---|---|---|---|
| | W/B | W/B | W/B | W/B | W/B |
| NLR - HST | 2.1.1.6 | 2.1.1.7 | 2.1.1.8 | 2.1.1.9 | 2.1.1.10 |
| ONERA-S2MA | 2.2.1.6 | 2.2.1.7 | 2.2.1.8 | 2.2.1.9 | 2.2.1.10 |
| DRA - 8ft x 8ft | 2.3.1.6 | 2.3.1.7 | 2.3.1.8 | 2.3.1.9 | 2.3.1.10 |

**Table 2: Pressure distribution, Mach number - sweep Re = $3.0 \cdot 10^6$, $c_L = 0.50$**

| | $c_L = 0.3$ | $c_L = 0.4$ | $c_L = 0.5$ | $c_L = 0.6$ |
|---|---|---|---|---|
| | W/B | W/B | W/B | W/B |
| NLR - HST | 3.1.1.1 | 3.1.1.2 | 2.1.1.3 | 3.1.1.3 |
| ONERA-S2MA | 3.2.1.1 | 3.2.1.2 | 2.2.1.3 | 3.2.1.3 |
| DRA - 8ft x 8ft | 3.3.1.1 | 3.3.1.2 | 2.3.1.3 | 3.3.1.3 |

**Table 3: Pressure distribution, $c_L$ - sweep Re = $3.0 \cdot 10^6$, M = 0.75**

**Explanation of the notation of Table 1 to Table 3.**

In order to identify tables with the aerodynamic data, they are numbered with a four digit figure w.x.y.z.
The meaning of the digits w,x,y,z is described below.

1. digit describes the kind of aerodynamica data
   - w = 1 force and moment data
   - w = 2 pressure distribution M-sweep
   - w = 3 pressure distribution $c_L$-sweep

2. digit indicates the wind tunnel, where the data has been achieved
   - x = 1 NLR-HST
   - x = 2 ONERA-S2MA
   - x = 3 DRA-8ft x 8ft

3. digit determines the configuration
   - y = 1 wing/body
   - y = 2 body

4. digit is a running number to identify the various cases in one group.

# DLR - F5:
# Test Wing for CFD and Applied Aerodynamics

**H. Sobieczky**
**DLR Göttingen**

## INTRODUCTION

A swept wing with symmetrical sections was originally created to serve two purposes [1]:

First, the surface generator used for data definition was under development for aerodynamic design and optimization. The wing created was intended therefore to be a selected case of a whole family of configurations obtained by variation of the input parameters. Aerodynamic design and optimization strategies call for such variations.

Second, CFD code development needs both accurate test case geometries as well as experimental results from wind tunnels. The latter usually suffer from corrections which still might suit practical purposes of measuring aerodynamic coefficients but fall short of the requirement to define the flow conditions to the same accuracy as geometrical boundaries are known.

Using the generator software, a compromise was chosen by including the closed wind tunnel wall geometry as a channel boundary surrounding an aerodynamic component. In order to also avoid model support problems, a wing half model mounted on and including a splitter plate was used as "configuration". Geometry of the flow boundaries was completely defined through the simple rectangular channel geometry completed by chosen inlet and exit planes. Flow data were required at these planes to formulate a boundary value problem for CFD.

In a workshop to compare CFD results with the first test case experiment (1986), partners had obtained and used a computer code to generate the wing and the wind tunnel boundary conditions, along with the absolutely necessary parameters to formulate fluid dynamic boundary conditions for the Navier - Stokes equations [2]. This software is a simplified version of the geometry generator for aerospace configurations and CFD grid generation [3] which has since been further developed as an industrial tool for design aerodynamics. The experiment and the refined half - model technique was published [4, 5] and the results of the workshop, comparing numerical results, have been summarised [6]. Based on these results we may conclude that for CFD this test case turns out to be a complicated one basically because of the observed viscous flow phenomena on the wing. On the other hand, the definition of the complete boundary value problem makes the case rather unique and, with the help of generator software and experimental data, easy to implement for CFD validation. The workshop software updated by experimental results for surface pressure distributions [7] is made available in one package.

## 1. GENERAL DESCRIPTION

1.1 Model name: DLR - F5 Test Wing

1.2 Model type and flow conditions
20 deg swept wing (AR = 9.5) in transonic flow.
Supercritical wing flow at Mach ~ 0.82

1.3 Design requirements
Definition of a complete boundary value problem for CFD; analytical description of wing geometry.

1.4 Dominant flow physics
Swept wing flow with large fillet avoiding vortex at wing root leading edge.
Laminar / transitional / turbulent flow
Initially laminar separation bubble at shock - boundary layer interaction.

## 2. DETAILS OF MODEL

2.1 General geometric arrangement: See Fig. 1
Note that the complete geometry is given in form of generator software on the disk.

2.2 Configurations tested
Wing in fixed wind tunnel boundary box

2.3 Wing and airfoil data: See Fig. 2

2.3.1 Planform
Leading edge sweep: 20°
Trailing edge sweep: 12°
Aspect ratio: 9.5; no twist
Wing root: large fillet smoothing corner
Wing tip: rounded
m. a. c.: 170 mm

2.3.2 Wing sections
Defined from analytical blending of an NACA 0036 airfoil at root with a 13% thick, shock- free designed ($M_\infty$ = 0.78) laminar flow - type, symmetrical airfoil.

L. e. radius / chord = 0.005, t. e. thickness / chord = 0.005 over most of the wing.

2.4 Body data
No body; wing mounted to splitter plate (see Fig.3)

2.5 Other components
Vertical splitter plate extends through top and bottom wind tunnel wall to allow for rotation of 5°

2.6 Engine / pylon / nacelle data: None

2.7 Geometric definition of all components
Wing, splitter plate and 3 tunnel walls are solid parts of the geometric boundary.
Inlet and exit plane also define boundary.
Resulting surfaces defined by software, evaluating analytical relations of geometry generator code E88 [3].
Model production with new CAM software based on same code, therefore exceptional section accuracy; max. dihedral deflection $\Delta z = 0.1mm$
Surface finish: < 1 $\mu m$

2.8 Model support details: see Fig. 2, 3.

## 3. GENERAL TUNNEL INFORMATION

3.1 Tunnel designation
Transonic Wind Tunnel Göttingen (TWG) [8]

3.2 Organization running the tunnel
DLR - German Aerospace Research Establishment; Central Wind Tunnel Division
Göttingen Research Center,
D-37073 Göttingen, Germany

3.3 Tunnel Characteristics
Continuous, closed circuit

3.4 Test Section
Cross section 1 x 1m, length 4m;
box length, where measurements were taken, 0.938m
Slotted top and bottom walls. In the present tests, these walls were closed; closed side walls.

3.5 Freestream conditions
Transonic: $0.5 < M < 1.2$

3.5.1 Reference flow conditions
Stagnation pressure: Variation between 0.4 and 1.6 bar, measured in settling chamber.
Stagnation temperature: ~310 K, measured in settling chamber and used to determine static temperature. In the present tests all boundary conditions including static and total pressures in the inflow plane were measured.

3.5.2 Tunnel calibration
Static pipe and side wall static pressures [9]
Last calibration: 1986

3.6 Flow quality

3.6.1 Flow uniformity
$M_\infty \sim 0.8$: $\Delta M_\infty = 0.001$
$\Delta\alpha = \Delta\beta < 0.05°$ ; measurements in the inflow plane by wedge probe (detailed data simulation given by generator code).

3.6.2 Temperature variations: Negligible

3.6.3 Flow unsteadiness
Overall turbulence level: < 0.35%
Overall noise level: $(nF(n))1/2 < 0.001$

## 4. INSTRUMENTATION

4.1 Model position
Angle of attack calibration with Incremental Sensor; accuracy 0.01°

4.2 Model pressure measurements
Scanivalve pressure measurements on wing, splitter plate and three tunnel walls.

4.2.1 Total number and position
Wing: 230 pressure orifices along 10 sections (Figures 2, 6).
Each section: 20 on upper, 3 on lower surface.
Due to symmetry of the sections, the effective number of orifices was 20 on each surface, realised by a corresponding variation in angle of attack. The 3 orifices on the lower surface were used to check data compatibility.

Splitter plate: 87 pressure orifices.
Tunnel walls: 67 pressure orifices.

4.2.2 Range and accuracy of pressure transducers
PSI 780 B Pressure Measurement System with 32 ESP Sensor Modules
Range: 15 PSI;
Static error band: typical 0.07% FS; calibrated on-line

4.3 Force and moment measurements: None

4.4 Boundary layer and flow field measurements
Boundary layer measurements at the location of the inlet and exit planes on the three tunnel walls and the splitter plate; flow field measurements in the inlet and exit planes (Figures 4, 5)

4.4.1 Measurement technique applied

Traversable, calibrated probes (Fig. 4): pressure (static and pitot), temperature and horiz. and vert. flow angularity

Pitot pressure rakes (Fig. 5) for boundary layer and wake profiles.

4.4.2 Flow regions investigated
Inlet flow plane:
Total and static pressure, flow angles, temperature, boundary layer profiles;

Exit flow plane: As inlet, plus wake profiles.

4.4.3 Influence of probe support
All pressure measurements on model were taken for each probe position to control influence on model flow quality.
Final surface pressure data taken without probes

4.5 Surface flow visualization

4.5.1 Measurement technique applied
Acenaphtene method (sublimation technique) for visualizing laminar/turbulent surface flow boundaries (Fig. 7)

4.5.2 On which surfaces is visualization technique applied? On wing upper and lower surface

4.5.3 In what form are data available?
An analytical 'transition ramp function' is modelled from the visualization and added to the data generator code.

4.6 Flow field visualization: None

4.7 Tunnel wall measurements
Surface pressure measurements, see 4.2

4.8 Other measurements
Monitoring unsteady flow onset by tip mounted accelerometer and observing root bending moment measured by strain gages.

## 5. TEST MATRIX AND CONDITIONS

5.1 Detailed test matrix
Mach number (inlet plane) $M_\infty = 0.82$
Angles of attack: 0 and 2 degrees (geometric)
$Re = 2.0 \times 10^6$ (based on mean chord of 170 mm)

5.2 Model / tunnel relations
Configuration consists of whole tunnel boundary box with wing;
- maximum blockage: 0.0091
- model span / tunnel width: 0.77
- adiabatic wall conditions have

5.3 Transition details: Free transition, see 4.5.1

## 6. DATA

6.1 Availability of data

6.1.1 Organization owning data: DLR

6.1.2 Responsibility for data
H. Sobieczky
tel. (49) (551) 709 2287
fax (49) (551) 709 2101
internet e-mail: helmut@ts.go.dlr.de

6.1.3 Are data freely available? Yes

6.2 Suitability of data for CFD validation
Complete formulation of viscous flow boundary value problem, with geometry., analytical inlet and exit flow models.
Data already used for Navier-Stokes workshop computations, Ref.[6].

6.3 Type and form in which data are available
Diskette with analytical geometry generator FORTRAN code and selected surface pressure data [7].

6.4 Corrections applied to data
No corrections to measurements.
Elastic model deformation for lifting flow case ($\alpha = 20$) negligible; determined by bench test.

## 7. DATA ACCURACY AND REPEATABILITY ASSESSMENT

7.1 Accuracy estimates

7.1.1 Freestream conditions
Inlet Mach number (0.82) and flow angularity measured with calibrated probe:
$\Delta M \sim 0.001$; $\Delta\alpha \sim 0.02^\circ$ ; Pressure coefficients: $\Delta cp \sim 0.002$

7.1.2 Acenaphtene visualization
Photographic evaluation and analytical approximation by suitable generator functions (Fig. 8).

7.2 Repeat measurements
Within a few days some of the measurements were repeated several times. Differences of $\Delta cp$ 0.002 were observed.

7.3 Other tests made
A new experiment with DLR - F5 has been made in 1990 with other flow parameters. Further tests in an adaptive wall test section will be carried out in 1994/1995.

## 8. REFERENCES

[1] Sobieczky, H.: A Test Wing for Computational and Experimental Investigations.
U. S. Air Force / BMVg DEA 7425 Meeting paper (1983)

[2] Sobieczky, H.: DFVLR-F5 Test Wing Configuration for Computational and Experimental Aerodynamics, Wing Surface Generator Code, Control Surface and Boundary Conditions.
DFVLR-IB 221 - 85 A 22, - 86 A 18, - 87 A 01, (1985 - 87),
Notes on Num. Fluid Mechanics, Vol. 22, pp. 27 - 37,ed. W. Kordulla, Vieweg Verlag (1988)

[3] Sobieczky, H.: Analytical Surfaces and Grids. in: AGARDograph No. 309, Three Dimensional Grid Generation, H. Yoshihara (Ed.), (1988)

[4] Sobieczky, H., Hefer, G., Tusche, S.: DFVLR-F5 Test Wing Experiment for Computational Aerodynamics.
AIAA 5. Appl. Aerodynamics Conf. Proc., AIAA 87-2485CP, (1987),
Notes on Numerical Fluid Mechanics, Vol. 22, pp.4 - 22,ed. W. Kordulla (1988)

[5] Hefer, G., Sobieczky, H., Tusche, S.: Verbesserung der Halbmodelltechnik im Transsonischen Windkanal Gottingen. Jahrbuch der DGLR, Bd. 2, 87-083 (1987)

[6] Kordulla, W., Schwamborn, D., Sobieczky, H.: The DFVLR-F5 Wing Experiment - Towards the Validation of the Simulation of Transonic Viscous Wing Flow.
AGARD CP 437 "Validation of Computational Fluid Dynamics", (1988)

[7] Sobieczky, H.: DLR - F5 Test Wing for CFD and Applied Aerodynamics; Software and Data for Generating Geometry, Boundary Conditions and Visualizing Wind Tunnel Experiment.
DLR - IB 221 - 90 A 21(1993)

[8] Hottner, Th., Lorenz-Meyer, W.: Der Transsonische Windkanal der Aerodynamischen Versuchsanstalt Gottingen (zweite Ausbaustufe), Jahrbuch 1968 der DGLR, p. 234-244, (1968)

[9] Amecke, J., Pszolla, H.: Machzahlverteilung in der leeren Messtrecke des Transsonischen Windkanals Gottingen, Teil 2: Geschlitzte Messtrecke im Unterschallbereich mit Absaugung und parallelen Seitenwanden.
DFVLR IB 222 - 88 A 10 (1988)

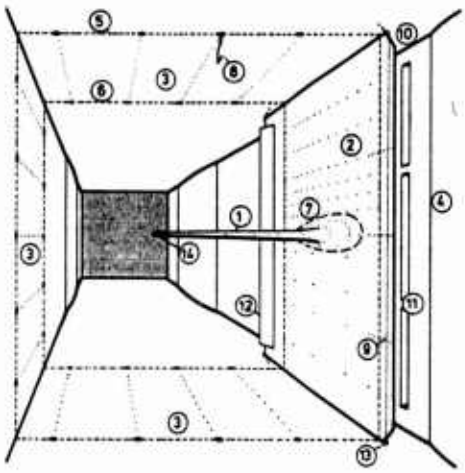


Figure 1: Wind tunnel arrangement: 1 Wing, 2 Splitter plate, 3 Tunnel walls, 4 Fourth wall contoured, 5 Inlet flow control plane, 6 Exit flow control plane, 7 Pressure orifices (total: 416) on wing, plate and walls, 8 Traversable probe or rake in inlet and exit planes, 9 Splitter plate leading edge with transition strip, 10 Bypass channel, 11 Suction devices, 12 Diffusor flap, 13 Rotation device for plate plus wing, 14 Acceleration and strain gages.

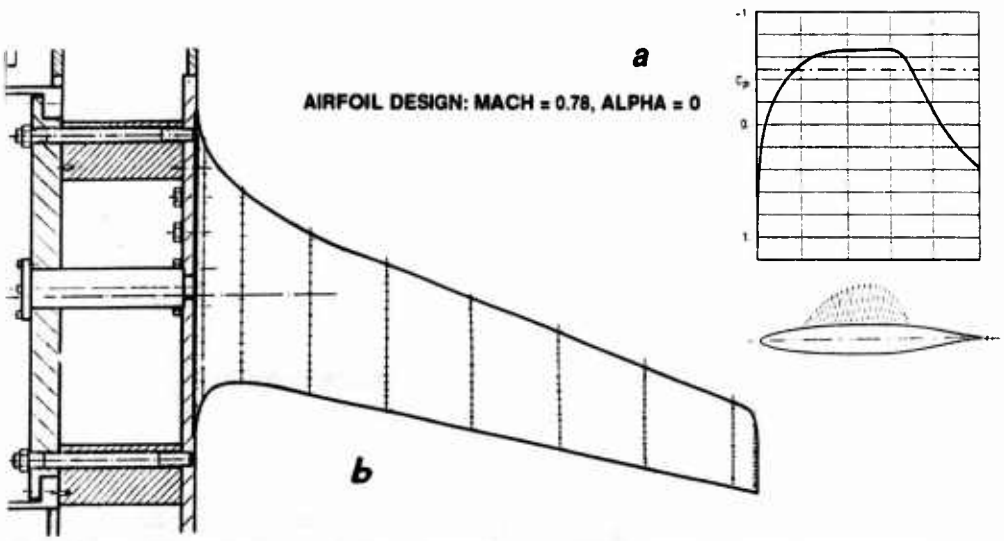
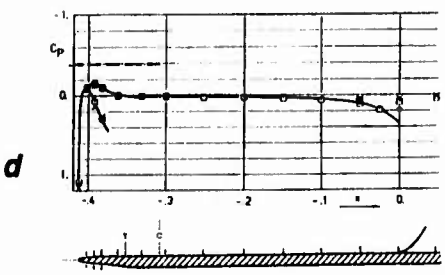



Figure 2: (a) Theoretically shock-free designed symmetrical airfoil as basic wing section,
(b) Wing planform view, mounting to splitter plate and tunnel wall. Pressure orifices on wing.




Flow quality at the splitter plate leading edge is controlled by various devices:

1. The fourth tunnel wall has a fixed added contouring (a).

2. Splitter plate has an adjustable trailing edge flap aft of the exit flow control plane (b).

3. Three suction devices (c) (see also Fig. 2) allow for on-line fine tuning of reaching parallel flow approaching the splitter plate leading edge.

Surface pressure measurements along splitter plate (d) for flow quality control upstream of wing root.

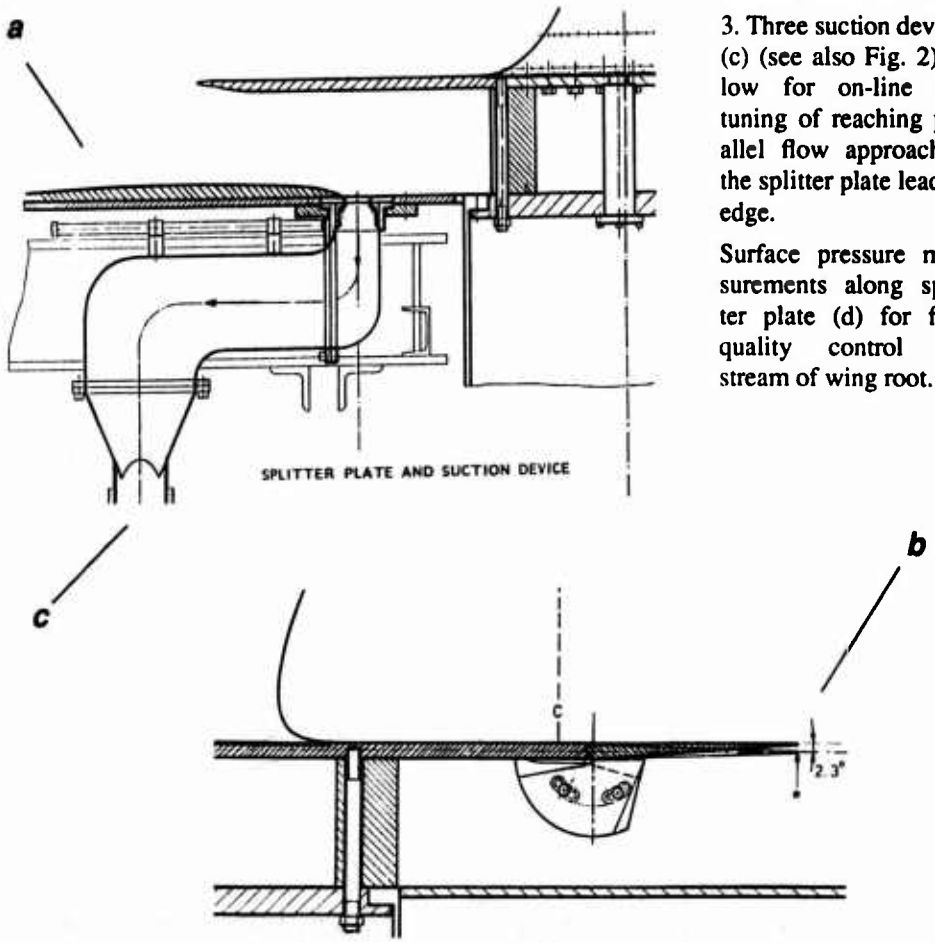



Figure 3: Details of Half-model technology with fine-tuned splitter plate flow quality.

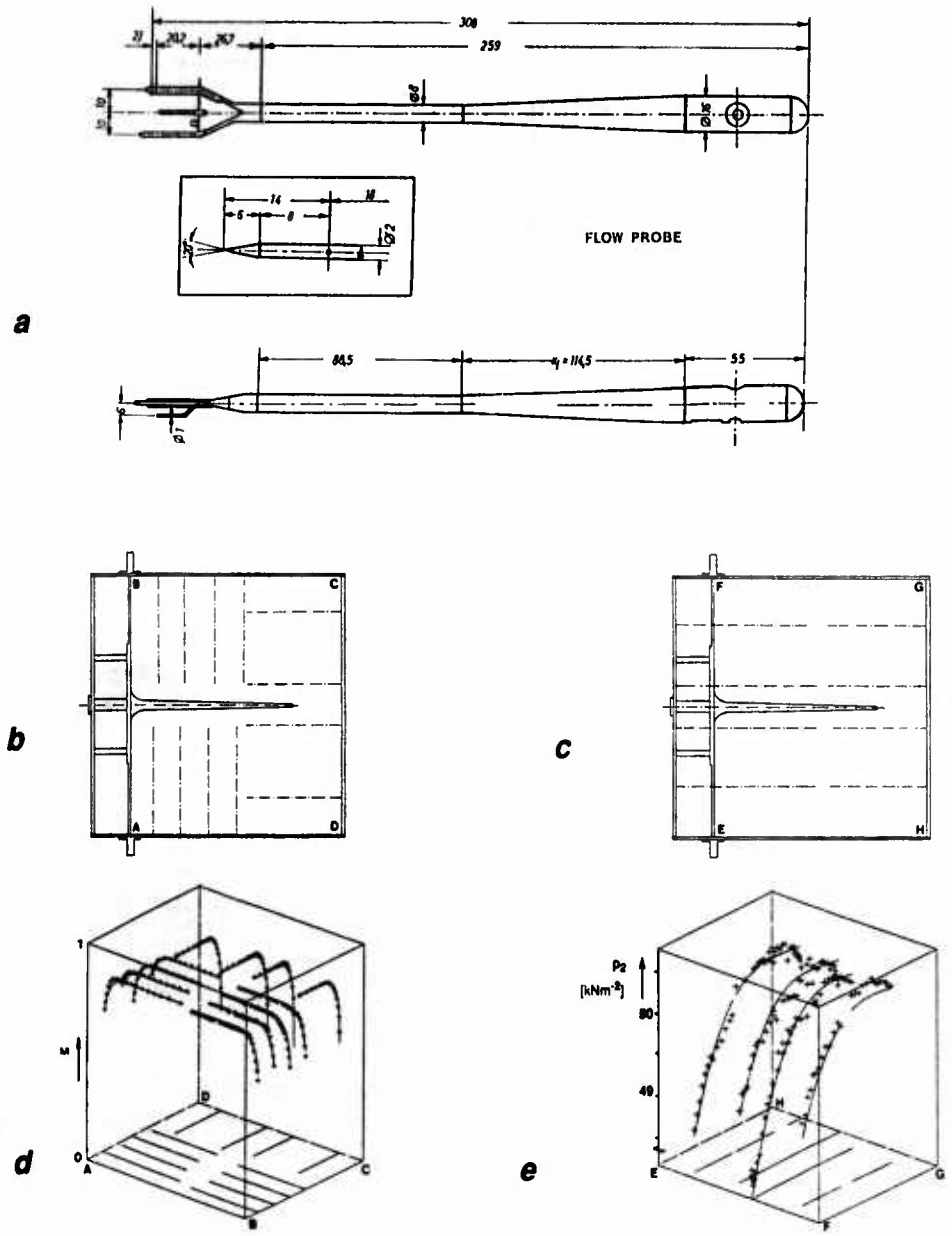
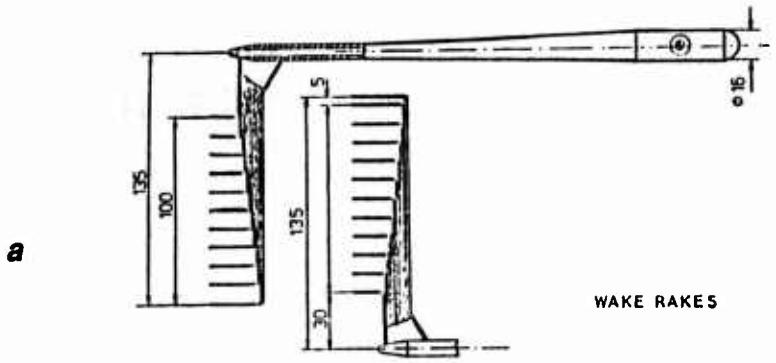
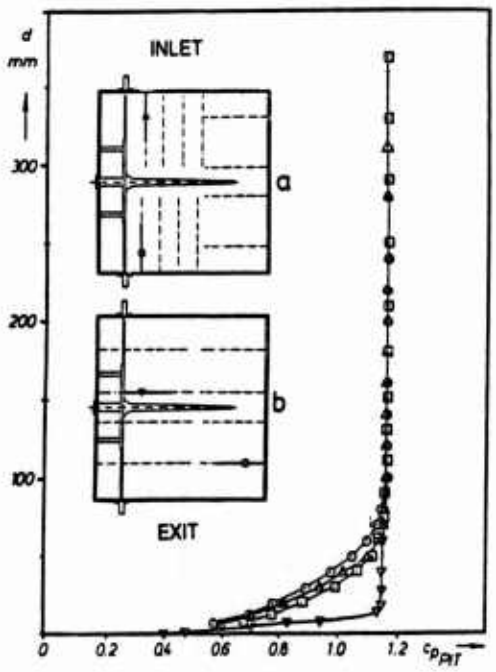



Figure 4: Traversable Probe (a) for static and pitot pressure, horizontal and vertical flow angularity, temperature. Traversing paths of probe in inlet plane (b) and exit plane (c).

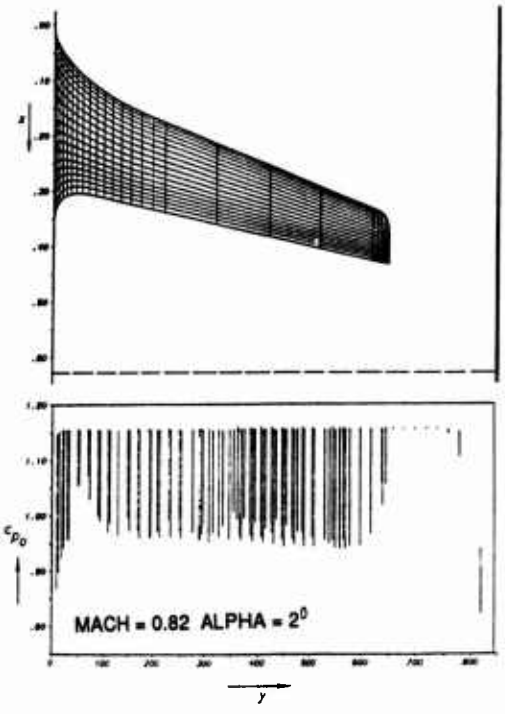
Inlet flow Mach number distribution (d), exit flow static pressure distribution (e); analytic approximation by boundary conditions generator code.




a




b




c

Figure 5: Wake rakes (a), Measured boundary layer profiles in inlet and exit plane (b). Measured wake amplitude distribution behind wing in exit plane (c)

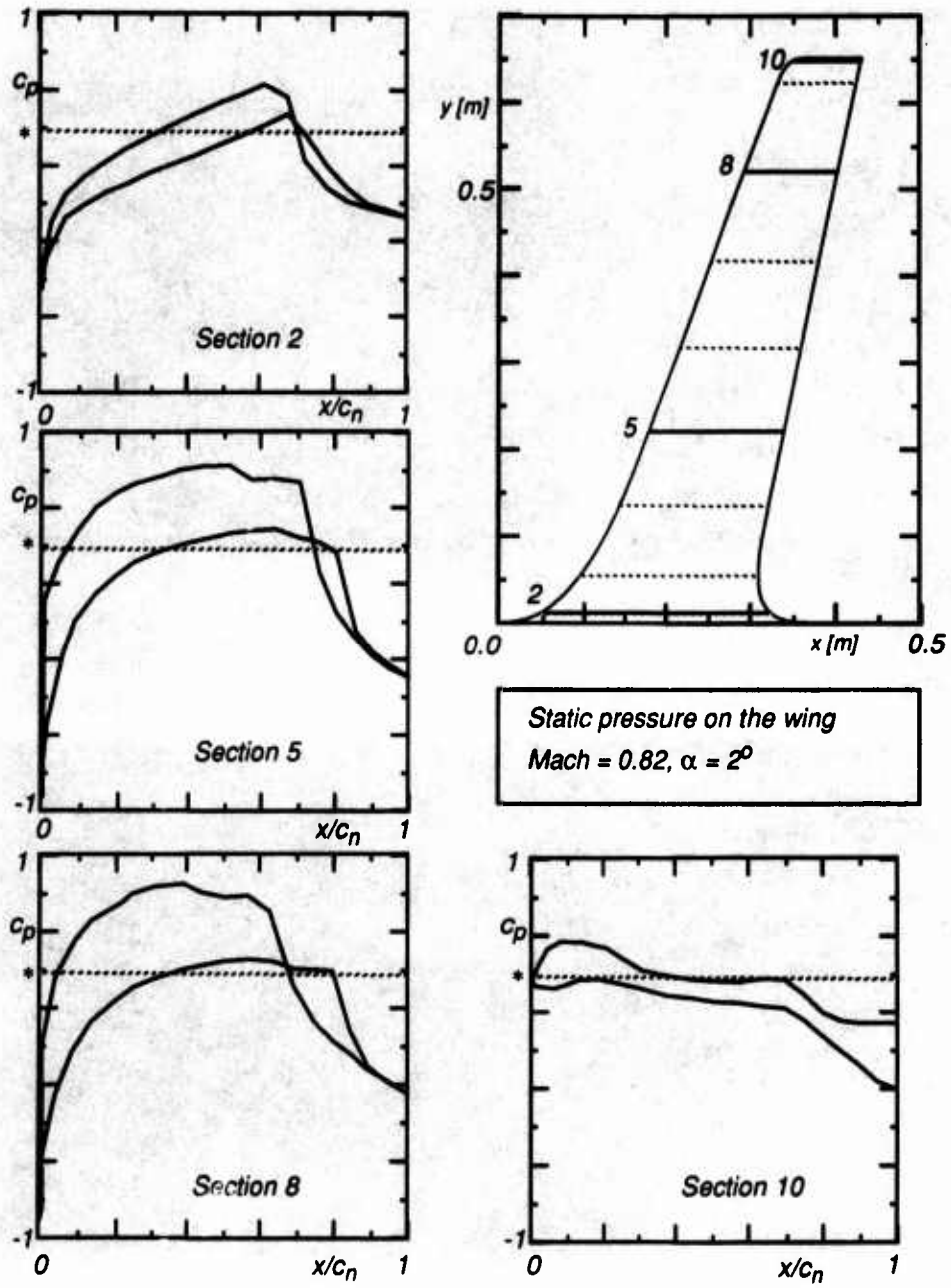



Fig. 6: Selected pressure distributions for Mach = 0.82, $\alpha = 2^{0}$

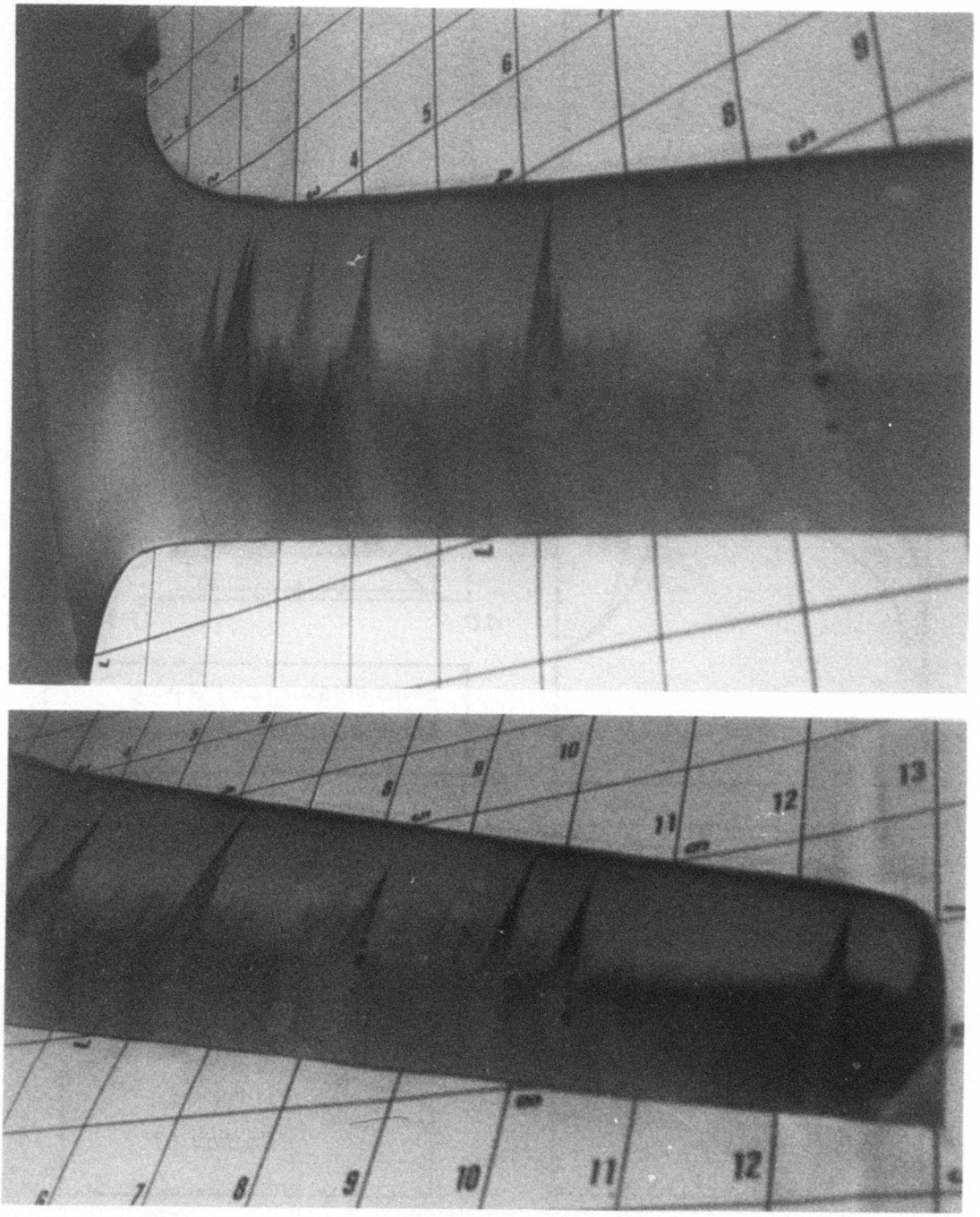


Figure 7: Acenaphtene visualization (Sublimation technique) of laminar / turbulent boundary layer on the wing surface.

(Mach = 0.82, $\alpha = 2^{o}$, upper surface)

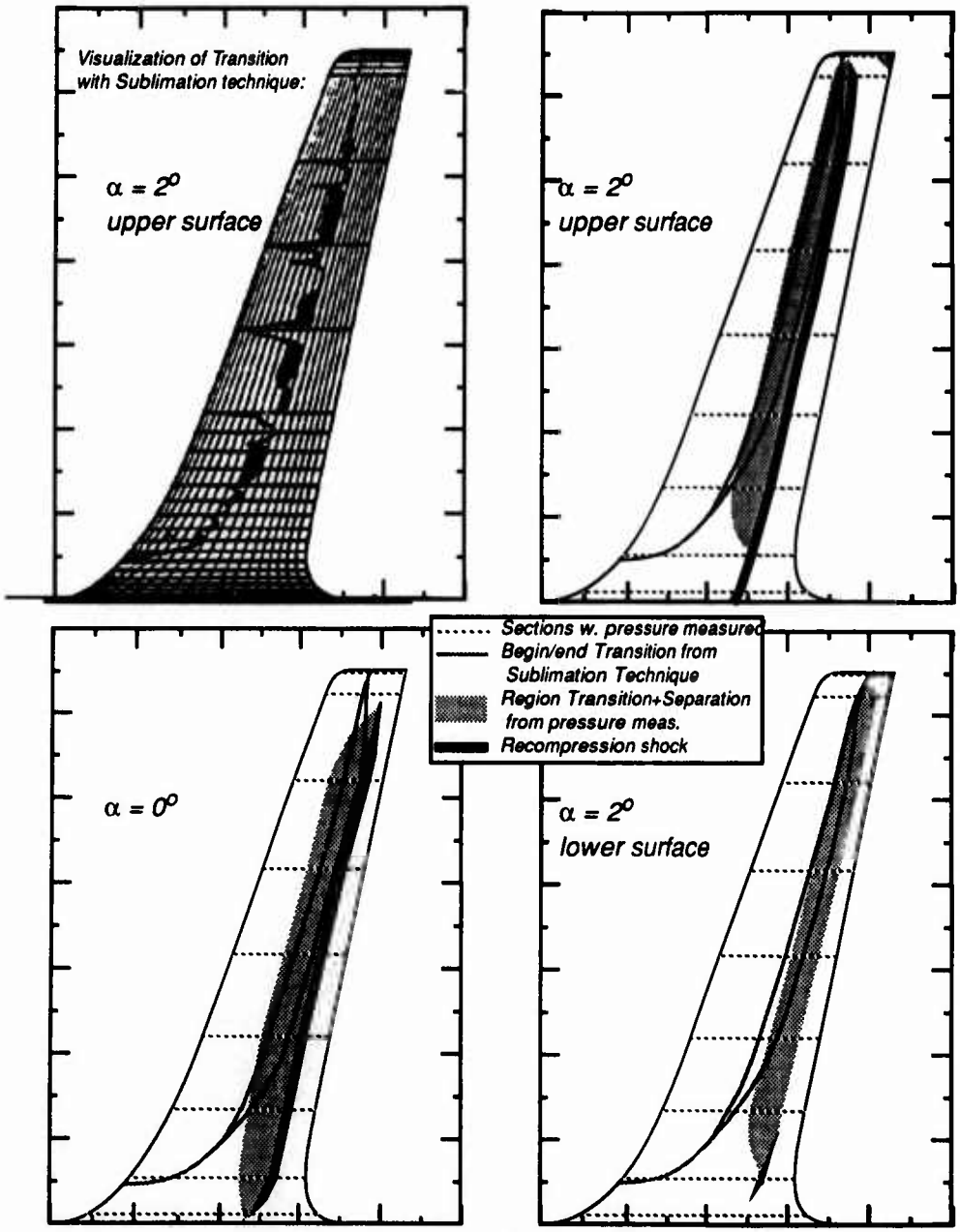



Fig. 8: Evaluation from pressure measurements and sublimation technique: Regions and curves indicating Transition line or laminar separation begin and shock location.

# Low Aspect Ratio Wing Experiment

**Mike Olsen**
**H. Lee Seegmiller**
NASA Ames Research Center, Moffett Field, California

## 0. INTRODUCTION

This test was initiated to provide validation data on low aspect ratio wings at transonic speeds. This is one of the NASA code validation experiments described in references 1 and 2. The test was conducted so that the data obtained would be useful in the validation of codes, and all boundary condition data required would be measured as part of the test. During the conduct of the test, the measured quantities were checked for repeatability, and when the data would not repeat, the cause was tracked down, and either eliminated, or included in the measurement uncertainty. The accuracy of the data was in the end limited by wall imperfections of the wind tunnel in which the test was run.

## 1. GENERAL DESCRIPTION

### 1.1 Model Name

Low Aspect Ratio Wing

### 1.2 Model Type and flow conditions

This is a 3D, semispan model. The flow conditions are transonic at high Reynolds Number, and include conditions with LEV(leading edge vortex) flow.

### 1.3 Design requirements, Purpose of Test

The test was designed to provide a data set which would allow the unambiguous validation of transonic flow codes. As such, any sort of 'wind tunnel corrections' were considered unacceptable in the use of this data. Thus, the test was run with the idea that the computer should be able to accurately model the actual test conditions. This implied then that the focus of the experimental effort was in documenting the actual flow conditions, and test geometries, as opposed to attempting to correct for tunnel walls.

### 1.4 Dominant flow physics

The experiment concentrates on transonic flow. The experimental conditions range from subcritical attached flow to supercritical flow with multiple shock waves and with a detached leading edge vortex. 'Traditional'(i.e. closed) separations are also among the flow physics encountered.

### 1.5 Additional Remarks

The flow conditions were chosen so that, at each angle of attack less than 8°, the lowest $M_\infty$ was subcritical and one $M_\infty$ was close to $M_\infty^{crit}$ when this was possible. (At eight degrees angle of attack, the flow was supercritical near the leading edge even at $M_\infty$= 0.600.) Some of the cases in the experiment are predicted reasonably well with a free-air, transonic full potential(⇒ inviscid), code. By first solving the 'easy case' and then progressing to the more challenging cases at a given angle of attack, the confidence in the numerical modelling of the geometric details can be established before simulation of more demanding flow physics is attempted.

## 2 DETAILS OF MODEL

### 2.1 General geometric arrangement

The model tested is a semispan, low aspect ratio wing. It is mounted in a tunnel 2.4 root chords in height, and 1.6 root chords in width. The model is symmetric about the z(vertical) axis, as is the mounting and the wind tunnel walls (See fig 1.0)

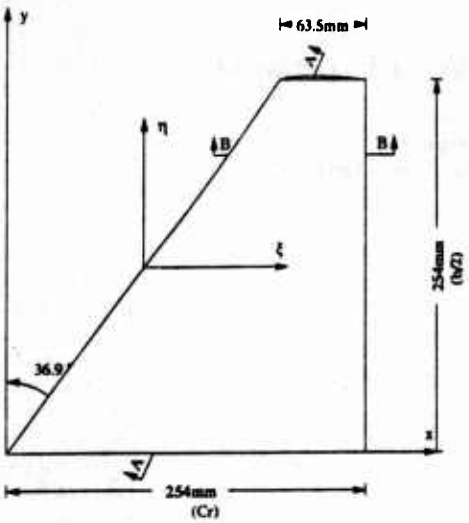
### 2.2 Configuration Features

Single configuration reported in this paper.

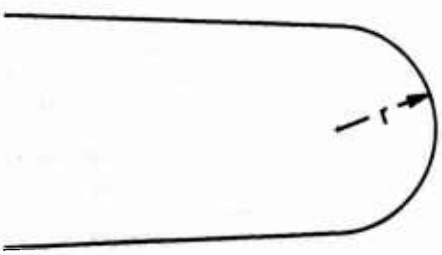
### 2.3 Wing Geometry

*2.3.1 Planform*

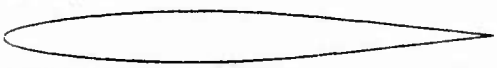
| | |
|---|---|
| Aspect Ratio : | 3.2 |
| Taper Ratio : | 0.25 |
| Leading Edge Sweep : | 36.87° |
| Trailing Edge Sweep : | 0.00° |
| Twist Distribution : | Untwisted |
| Semispan : | 254. mm ($1C_r$) |
| Tip Geometry : | When cut along constant planes of constant x/c, tip is a circular arc section. The arc is tangent to the wing surface at the upper and lower sections of the wing(Fig 1c). |
| Wing Junction : | No fillet or smoothing. |




1a) Wing Planform



1b) Wing Tip Details (Section A—A)



1c) Airfoil (Section B—B)

**FIGURE 1.** Wing Geometry, with section cuts along constant x/c and 2y/b

*2.3.2 Basic wing Section*

The airfoil section used was the NACA 64A010, obtained from a program to calculate 6-series airfoils (reference 3).

- Airfoil Shape:NACA 64A010 (Fig 2)
- Thickness/Chord Ratio: .10 (10% thick)
- Nose Radius/Chord: 0.00687†

*2.3.3 Other wing components*

None

† From Abbot and Von Doenhoff, reference 4

**2.4 Body Data**

No Body

**2.5 Empennage**

No empennage

**2.6 Engine/Pylon/Nacelle**

None

**2.7 Geometric definition of all components**

The airfoil shape was obtained using Ref 3. The actual profile of the airfoil section was checked at the root and tip. Overall tolerance was within 13 $\mu$m at these stations. The surface roughness was called out as $\sqrt{63}$, but the actual surface of the completed model was smoother than this. The surface finish of the model (away from the leading edge) is still mirrorlike, but the leading edge of the wing has been roughened by debris in the airstream. The surface roughness measurements 12mm downstream of the leading edge were less than 0.5 $\mu$m. The roughness measurements of the wing over the portion which still appears mirrorlike were less than .1 $\mu$m, the lower limit of the measurement accuracy.

**2.8 Model Support Details**

Model was semispan, and hence was bolted to the wind tunnel wall at the root. The root of the wing contains alignment pins assuring that the model can not rotate relative to the turntable.

**3. GENERAL TUNNEL INFORMATION**

**3.1 Tunnel Designation**

High Reynolds Number Channel II.

**3.2 Organization operating the tunnel**

Thermo-Physics Facilities Branch
NASA-Ames Research Center

**3.3 Tunnel Characteristics**

This facility is a blowdown wind tunnel, which operates at high total pressures (up to 3.3atm in this test) to acheive high Reynolds number flow. The Reynolds numbers acheived during this test were nominally 8 and 14 million, based on wing root chord. The test section walls are solid, and diverged to account for tunnel empty boundary layer growth. In the current tunnel configuration, the freestream Mach numbers range from .6 to 1.0. As this is a solid wall test section, the actual upper limit on the Mach number depends on the model blockage and the wall configuration.

The wind tunnel's upstream tunnel boundary layer suction system was removed for this test, and the suction panels replaced with windows to allow for optical access and to provide unambiguous upstream boundary conditions.

The run times were sufficiently long to allow at least 45 seconds of steady flow after the wind tunnel came to within .0005 of the desired $M_\infty$. The wind tunnel

is described in detail in reference 6.

### 3.4 Test Section

*3.4.1 Test Section Diagram*

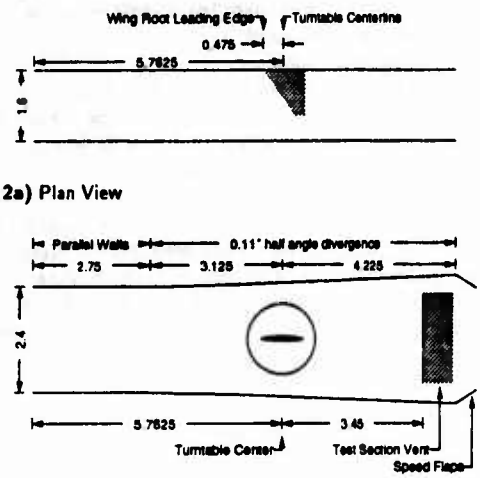



**FIGURE 2.** Diagram of HRC-II test section wall and mounting details. Dimensions are in wing root chords.

A diagram of the test section of the High Reynolds Number Channel II is shown in figure 2.

*3.4.2 Test Section Dimensions*

Width :0.406 m† $(1.6C_r)$
Height :0.610 m† $(2.4C_r)$
Length :2.340 m $(9.2125C_r)$

*3.4.3 Wall Geometry Details*

The test section is rectangular, with a ratio of height to width of 3:2 at the upstream entrance to the test section. The side walls are straight, and the upper and lower walls were diverged slightly to allow for boundary layer growth.

The entrance section of the wind tunnel has straight parallel walls, and extends approximately .7 m from the inlet. At this point, the upper and lower walls begin to thin, and 1.2 m from the inlet, the walls are 1/5 of their original thickness. This is the location of the first wall jacking station which control the upper and lower walls locations. There are a total of 7 wall jacking stations.

For this test, the wall jacking stations were adjusted for tunnel empty boundary layer growth, by diverging the walls at an angle of 0.11° from the tunnel centerline at the jacking stations. The upper and lower walls were then sealed to the sidewalls with a bead of silicone caulk to prevent mass flow between the test section and the surrounding plenum chamber.

† At entrance section

### 3.5 Freestream Conditions

*3.5.1 Determination of reference flow conditions*

The freestream Mach number by which the results are organized and conditions matched were calculated from a static pressure tap located $2.525C_r$ upstream of the wing root leading edge, on the opposite sidewall of the test section. The total pressure was measured by a total pressure probe located $2.25C_r$ upstream of the wing root leading edge, and $.7C_r$ below the centerline of the wing tunnel.

The total temperature of the incoming air was measured in the stagnation chamber upstream of the test section with 3 thermocouples located in the stagnation chamber. The static temperature was then estimated assuming adiabatic flow from the stagnation chamber to the test section.

The freestream Mach number was computed from the ratio of the static and total pressures measured, and was required to match to 0.001 (as a worst case) for checks of repeatability, or to obtain the two pressure distributions (lee and windward) for a single condition from two separate tunnel runs.

*3.5.2 Tunnel Calibration*

The most complete investigation of the flow properties of the wind tunnel was conducted in 1982, at the time of its commissioning. This is reported in reference 6. The tunnel is 'recalibrated' when the model is removed from the test section for any changes. The most recent calibration of this sort was between the pressure and laser Doppler velocimeter sessions of the test, when the model turntable was replaced with a new turntable with windows. This calibration consists of simply measuring the wall pressures and inflow boundary layers for some flow conditions, to verify that the tunnel wall $C_p$ have not changed from those obtained at the start of the test.

### 3.6 Flow Quality (empty tunnel)

*3.6.1 Flow uniformity*

The static pressure variations in the tunnel depend on the Mach number and angle of attack, as the test was performed in a closed wall test section at transonic speeds. The spatial variation in $C_p$ far upstream of the model, and in $C_p$ at symmetric locations for positive and negative angle of attack reveal a nonuniformity in $C_p$ less than .01 for all conditions in the test.

The inflow velocity was measured with a laser Doppler velocimeter with and without the model in the

tunnel. This measurement was obtained $1.775C_r$ upstream of the wing leading edge at 3 span locations, $\eta$ = .4, .8, and 1.2, along the central 1/3 of the tunnels vertical extent. The flow was uniform to within the measurement accuracy ($\pm.01u/a_T$). The flow angularity measured by the two component laser Doppler velocimeter was also uniform and consistent with the inclinometer readings to the accuracy of the LDV (.5°).

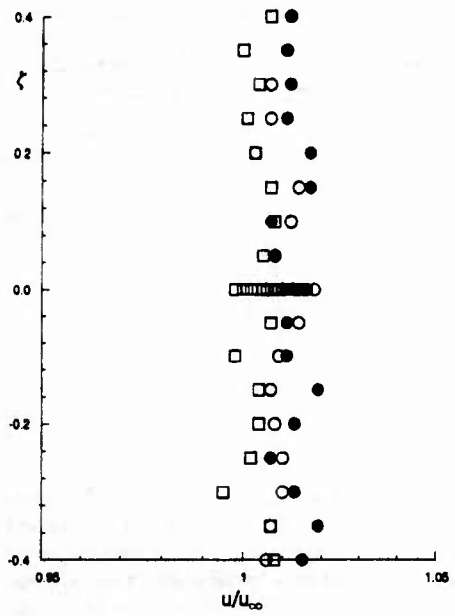



**FIGURE 3.** Inflow Velocity Profile at upstream window

Another means of determining the incoming velocity is by using the $p_\infty$, $p_t$, and $T_t$ measurements. The $p_\infty$ and $p_t$ measurements allow the computation of an isentropic Mach number, $M_\infty$. With this Mach number, $u_\infty/a_t$ can be calculated, $a_t$ can be calculated from the $T_t$ measurements, and thus $u_\infty$ can be computed. The resulting velocity, $u_\infty$, can be used to normalize the laser Doppler velocimeter measurements, and a picture of the uniformity of the incoming flow can be drawn independent of the $M_\infty$, and $Re_{C_R}$ of the flow. A plot of this, with the data for three separate runs, with three different flow conditions overlaid is shown in figure 3.

The total pressure was also measured (although not to compute Mach number) by the exterior portions of two boundary layer rakes on both sides of the wind tunnel, and the pressures measured outside of the wind tunnel boundary layer agreed with the total pressure measured for Mach number determination to within 3 parts per 10,000. Thus it was concluded that the total pressure of the incoming flow was extremely uniform over the 3 upstream location at which it was measured.

*3.6.2 Temperature Variation*

The temperature cannot be controlled during a tunnel run, and can vary by 30°C over the course of a run. During the portion of a run in which the averaged data is obtained however, the variation is generally less than 5°C, and is reported along with the specific data set. No measurement of the spatial variation of temperature is available, but it should be negligible. The laser Doppler velocimeter data, the only data of the set which will drift with the dropping temperature, is normalized by $a_\infty$ or $u_\infty$ compensates for the temperature changes.

*3.6.3 Flow Unsteadiness*

- Overall Turbulence Level- $u'/u_\infty = .005$

## 4 INSTRUMENTATION

### 4.1 Model Position

*4.1.1 Technique for Measurement of Geometrical Incidence*

The geometrical incidence was measured using a mechanical inclinometer to measure the inclination of the turntable on which the model was mounted. As the model was mounted with two (press fit) alignment pins to the turntable this was equivalent to measuring the wing inclination directly. As the model is symmetric, the relative inclination of the flow to the wing was measured by finding the inclination of the wing about which the upper and lower surface taps on the wing would produce equal $C_p$ at negative and positive $\alpha$. This condition determined $\alpha = 0$. This angle was identical (to within measurement accuracy of the inclinometer and $C_p$) for all angles at which the model was run ($0, \pm2, \pm5$ & $\pm8°$). This measurement was also consistent (as noted above under flow uniformity) with the tunnel empty laser Doppler velocimeter measurements, although these were much less precise than the inclinometer and $C_p$ measurements.

*4.1.2 Accuracy of Geometrical Incidence Measurment*

The repeatability of this measurement is to within .03°. The scatter in the $C_p$ measurements used to provide the aerodynamic angle of attack is of the same order. Thus, the accuracy of this measurement can be considered to be ±.03°.

### 4.2 Model Pressure Measurements

*4.2.1 Total Number of Pressure Measurements*

On the wing, there were 128 pressure taps located along 5 span stations on the upper surface of the wing, as shown in figure 4. Four pressure taps were

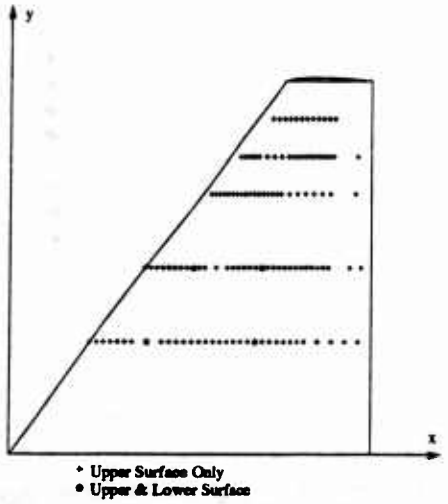



**FIGURE 4.** Planform of wing showing upper and lower surface pressure taps

located on the lower surface of the wing to determine the angle of attack and the symmetry of the flow at the 30% and 50% span stations, also shown in figure 4. The pressure taps were .254mm in diameter, created using EDM machining, and were drilled normal to the wing surface.

*4.2.2 Range and accuracy of the pressure transducers*

The pressure transducers used to measure the pressures on the model were 45 psia (≈ 300KPa) pressure cells. The wall pressure measurements utilizied 15psig (≈ 100KPa) pressure cells. These pressure cells were calibrated at the start of each tunnel run using the Barocel pressure transducers as secondary standards. The barocels in turn were calibrated using a dead weight tester as a primary standard at 3 times during the pressure measurement phase of the test. The accuracy of the calibrations was ± 0.01 psi in terms of the standard deviation of the calibration. The pressures measured during the run were the deviations from the tunnel static pressure, yeilding an overall accuracy of ± 0.02 psia. These imply an accuracy of ±0.0003 in $p/p_t$. This level of accuracy is refered to as the measurement accuracy, and is much higher than the accuracy of the overall data, when tunnel wall and model imperfections are considered as part of the true accuracy of the data set. This level of accuracy was important, however, in maintaining a 'controlled experiment' in the sense of reference 9.

*4.2.3 Are dynamic pressures measured?*

The pressures measured during the run had a sample rate for an individual pressure measurment of 10Hz. The slowest pressure tap had a time response (1/e point) of better than .1 sec based upon a vacuum step response test. Based upon this, and pressure step changes occuring on the model, the data appear to be accurately measured from 10Hz to DC. No anti-aliasing filters were employed. The data compiled for mean $C_p$ measurements had no significant deviations with time, other than random deviations.

**4.3 Force and moment measurements**

No integrated force or moment measurements were conducted.

**4.4 Boundary layer and flow field measurements**

*4.4.1 Measurement technique applied*

A two component laser Doppler velocimeter system was utilized to measure flowfield axial and vertical velocities at one flow condition - $M_\infty = .775$, $\alpha = 5°$, $Re_{C_R} = 14 \times 10^6$. In addition, inflow boundary tunnel boundary layers were measured at all

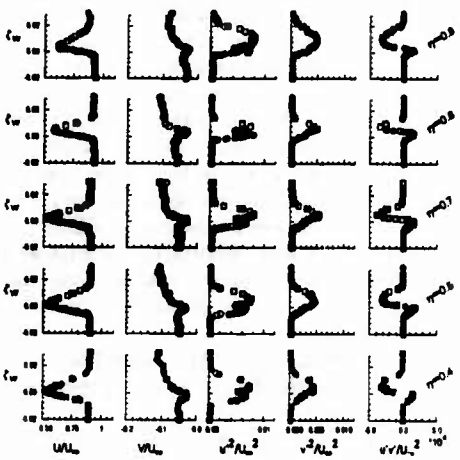


**FIGURE 5.** Wake surveys: $M_\infty$=.775, $\alpha$=7.92°, $Re_{C_R}$=14 × $10^6$ at five span locations. Shown here are mean axial and vertical velocities, and the three Reynolds stress terms measured.

flow conditions documented with two total pressure rakes.

*4.4.2 Flow regions investigated*

The velocities in the wake and over the suction surface of the wing were measured at 5 span stations. The wake surveys extend above and below the trailing edge $0.2C_r$, $0.025C_r$ behind the trailing edge of the wing. The suction side surveys were conducted $0.1, 0.15, 0.25, 0.45 C_r$ above the wing reference plane, and extend ahead of the leading edge and behind the trailing edge of the wing.

Inflow velocities were measured far upstream of the wing with the wing in and out of the tunnel, and with the wing non-lifting and at maximum $C_L$. The flow was uniform to measurement accuracy ($\pm.005a_t$), and the influence of the wing could not be measured at this upstream location in either the lifting or nonlifting condition.

*4.4.3 Probe and probe support details*

The method used, laser Doppler velocimetry, is nonintrusive. The boundary layer rakes were upstream of the wind tunnel model on both sidewalls of the tunnel. The individual tubes of the rake were 2.54mm ($.01C_T$) apart, with the nearest tube touching the tunnel wall. The 15 tubes on each rake thus extended from .005 to .145 root chords into the flow.

**4.5 Surface flow visualization**

*4.5.1 Measurement technique applied*

The measurement technique used to measure the surface flow direction is a variant of the Settles lampblack/kerosene technique. The model was painted with a mixture of flourescent chalk and fuel oil (less volatile than kerosene) and observed with a video camera to verify that conditions captured were those of the steady state conditions and not start-up or shutdown transients. After the run was complete, the data were recorded photographically. The conditions for which the surface flow directions were recorded are at 5° and 7° on the suction surface of the wing.

**4.5.2 On which surfaces is the flow visualized**

The majority of the flow visualization pictures were taken of the suction surface of the wing. Some limited pictures are available of the sidewall on which the model was mounted.

**4.5.3 In what form are the data available**

The data will be available as 8 × 10 photographs or as Postscript files.

**4.6 Flow field visualization**

All flowfield visualization techniques attempted to this date created unacceptable changes in the flowfield over the wing.

**4.7 Tunnel wall measurements**

*4.7.1 Type of measurements*

The wind tunnel is instrumented with 56 taps in the upper and lower walls located in two rows, 25.4 mm from the tunnel centerline. The sidewalls are instrumented with 56 taps arrayed in 3 rows along with two (tunnel) boundary layer rakes each with 15 taps. Boundary layer measurements from these two rakes are shown for 0° and 8° angle of attack, and the extreme insensitivity to the model attitude is apparent (figure 6). Limited surface flow direction measurements are available for the mounting wall at high angle of attack.

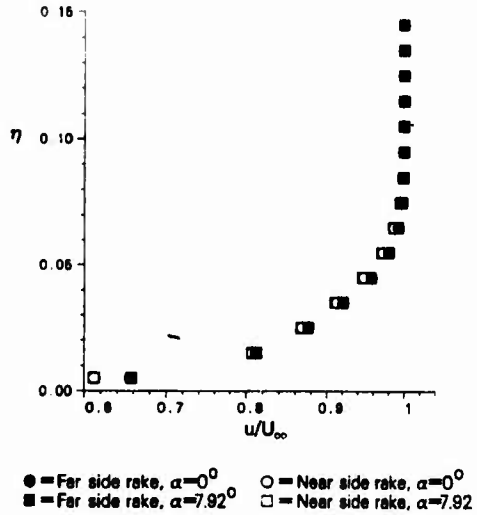



**FIGURE 6.** Tunnel wall boundary layer measurements showing insensitivity to model attitude.

**4.7.2 Location and number of pressure taps**

A diagram of the test section showing the location of the wall pressure taps, as well as other measurement locations is shown in figure 6The pressure taps on the tunnel walls (as opposed to those on the model) are .78 mm in diameter.

**4.8 Other measurements and/or instrumentation**

**5 TEST MATRIX AND CONDITIONS**

**5.1 Detailed test matrix**

This is given in table I, at the end of this paper.

*5.1.1 Number of selected test cases*

22 complete test conditions (with both lee and windward surface pressure measurements) are included. Low Reynolds number data ($Re_{C_R} \approx 7 \times 10^6$) were excluded from the AGARD dataset, but are available in the TM.

*5.1.2 Number of configurations tested*

One configuration, wing alone, is reported here.

*5.1.3 Table of test conditions*

A detailed listing of test conditions is contained in table I, at the end of the report.

**5.2 Model/tunnel relations**

*5.2.1 Maximum Blockage*

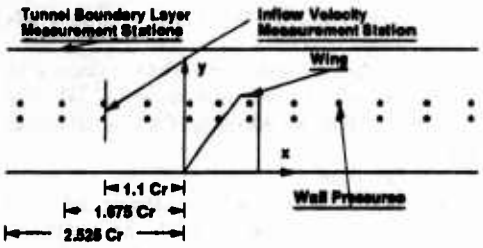
The maximum blockage was less than 1.63%.

*5.2.2 Model span/tunnel width*

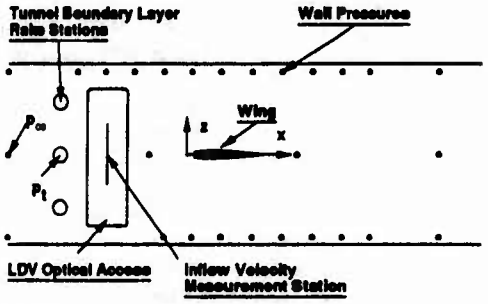
The ratio of the model span to tunnel width is 0.625.

*5.2.3 Planform Area/Tunnel Cross Section*

The ratio of the model planform area to tunnel cross section is 0.163




7a) Plan View




7b) Side View

**FIGURE 7.** Diagram of HRC-II Test Section showing measurement location details

*5.2.4 Height/Chord Ratio*

Inapplicable

*5.2.5 Width/Chord Ratio*

Inapplicable

*5.2.6 Have adiabatic wall temperatures been reached?*

This is unknown, but over the period used to average for mean pressures, the tunnel freestream total temperature is relatively constant. Heat transfer is not deemed an important phenomena in this test.

**5.3 Transition details**

*5.3.1 Was test made with free or fixed transition?*

The test was conducted with free transition.

*5.3.2 Details of free transition*

Fixing transition was attempted with fine grit at less than 10% chord, but the effects of this grit were only a local perturbation of the airflow due to the height of the grit. No measureable variations in the pressures were created outside of the region of the grit.

From the roughness measurements, the leading edge of the wing has a roughness of .5 $\mu$m. Using the freestream conditions of this test, the maximum roughness Reynolds number satisfies

$$Re_k = \frac{U_\infty k_s}{\nu_\infty} \leq 27.$$

Even at the regions of the wing with the highest unit Reynolds number, the roughness Reynolds number is certainly less than 36, which is less than 120, the limit at which the roughness becomes effective.

The location of transition can be fixed by examination of the surface flow visualisation photographs. The method used to visualize the surface flow direction gives a clear indiction of transition, as the chalk is "scrubbed" away just downstream of the transition location. This line is easily identified on the flow vis photographs, such as the one reproduced in figure 8, corresponding to the conditions documented by wake measurements.

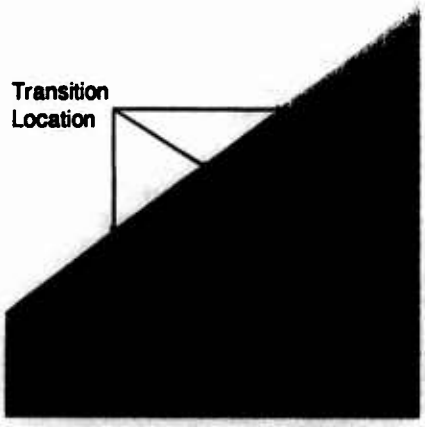



**FIGURE 8.** Flow visualization photograph showing transition location, $M_\infty$=0.775, $\alpha$=5°, $Re_{C_R}$=13 x$10^6$. Transition line is just behind leading edge.



**FIGURE 9.** A comparison of the $C_p$ distribution for the clean wing (open symbol) and with the Settles technique(closed symbol). Outliers caused by plugged taps not removed.

For all of the data at 5°, the transition location is well below ten percent, and the $C_p$ distribution obtained during the flow visualization agrees well with that of the 'clean' wing, except of course for the

pressure taps plugged by the kerosene/chalk mixture. The agreement for the case corresponding to the conditions at which the LDV flowfield measurements were made is shown in figure 9. The transition location is from one to two percent over the first eighty percent of the wing for this case, and increases to approximately six percent by the tip.

The obvious question with this method of determining the transition location is whether the presence of the kerosene/chalk mixture affects the transition location. If the transition location was altered by the presence of the chalk, it did not affect the pressure field. The most serious discrepancy occurs at the wing tip at the condition shown in figure 9. There is a small separation at $\eta = 0.9$, $0.225 \leq \xi \leq 0.275$ on the dirty wing not present on the clean wing. This separation was caused by the accumulation of the kerosene/chalk mixture, and the lack of evaporation of kerosene at this point.

## 6 DATA

### 6.1 Availability of data

*6.1.1 Organization owning the data*

Experimental Fluid Dynamics Branch
NASA Ames Research Center

*6.1.2 Who is responsible for the data*

Mike Olsen
Research Scientist
P.O. Box 1000
NASA Ames Research Center
Moffett Field, Ca. 94035-1000
tel:(415)604-6200
fax:(415)604-5244

*6.1.3 Are the data freely available*

Data will be freely available.

### 6.2 Suitability of data for computational fluid dynamics validation

*6.2.1 Are the data suitable for "in tunnel" calculation*

The data are tailored precisely for this type of validation effort.

*6.2.2 Are the data corrected to simulate "free-air" conditions*

The data are NOT corrected in any manner to simulate free-air conditions. The test was run with solid, straight wall test section. Wall pressure measurements are part and parcel of the $C_p$ data, and can be used (if desired) to produce corrections, or to estimate the extent of wall interference. From comparision with free-air, transonic full potential calculations, and examination of the wall pressures, the data is not heavily influenced by the presence of the tunnel walls for a good portion of the cases in this set (see reference 10).

### 6.3 Type and form in which the data are available

*6.3.1 Type and form*

A listing of the type and form of data available is located at the end of this report, in table II. All measurements include an estimate of the measurement uncertainty.

*6.3.2 Data Carrier*

A TM should be completed by September, 1993. The anonymous ftp (if allowed) should be operational about the same time. Means of distributing the flow images may be as PostScript files, or they may be available only via the TM.

*6.3.3 Extent of geometry data*

The geometry is available as a FORTRAN subroutine, from reference 4, or as output of the program described in reference 3.

*6.3.4 Extent of aerodynamic data*

| | | |
|---|---|---|
| Pressure Data | : | 3000 Kbytes |
| LDV FlowField Data | : | 200 Kbytes |

### 6.4 Corrections applied to data

*6.4.1 Lift interference and blockage corrections*

No corrections were applied to data.

*6.4.2 Side wall interference corrections*

No corrections were applied to data

*6.4.3 Half model corrections*

No corrections were applied to data.

*6.4.4 Sting and support corrections*

No corrections were applied to data.

*6.4.5 Aero-elastic deformation*

The aero-elastic deformation was measured, using the LDV laser beams and positioning system. The amount of deformation (bending) from the root to the tip was 0.5 mm over a semispan of 254.0 mm at $M_\infty$=0.775, $\alpha = 7.92°$, $Re_{C_R} = 14 \times 10^6$. From calculations using a transonic full potential code, this amount of dihedral had an effect orders of magnitude less than the measurment accuracy. The wing twist was less than could be measured with the system used, but from consideration of the magnitude of the aerodynamic moments over the wing, and the relative rigidity of the wing to twist, in comparision to bending, aero-elastic twist was even less significant. As this particular condition is one of the most extreme aerodynamic loads, the aero-elastic deformation of the model is not believed to be significant for this experiment.

*6.4.6 Other corrections*

No corrections were applied to data.

## 7 DATA ACCURACY AND REPEATABILITY ASSESSMENT

### 7.1 Accuracy estimates

*7.1.1 Freestream conditions*

- $M_\infty$: $\pm.0005$

- $u_\infty$ : $\pm.005\, a_t$
- $\alpha$ : $\pm.033^\circ$

*7.1.2 Measured data*

- $C_p$ : $\pm.01$
- $u/a_t$ : $\pm.01$ (LDV data)
- $u/u_\infty$: $\pm.001$ (B.L. rake)

**7.2 Repeat measurements**

*7.2.1 Type and number of repeat measurements within one test campaign*

For the pressure data, at each angle of attack at least two repeat runs were conducted. As a matter of course, the conditions were nearly repeated (within .002 in $M_\infty$) while obtaining the pressure data while attempting to obtain the correct speed flap setting. The differences in the pressure data (which were indeed reliably measureable, i.e. above the measurement accuracy) were consistent with the $M_\infty$ differences. This was monitored throughout the test campaign to ensure that the data aquisition system and the tunnel flow were both operating well. The measurement accuracy of the data aquisition system allowed changes much smaller than .01 in $C_p$ to be measured accurately.

*7.2.2 Type and number of repeat measurements in successive campaigns*

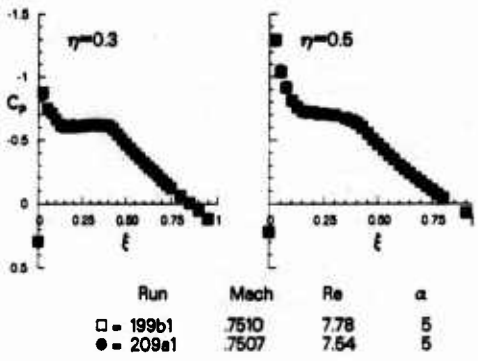



**FIGURE 10.** A representative example of the repeatability of the $C_p$ data for two of the five span locations.

The repeatability of the $C_p$ distributions was excellent, and was generally under the 95% statistical uncertainty margin for the measurements. This level of repeatability exceeded by an order of magnitude the actual accuracy of the $C_p$ measurements, as other factors were dominant in the $C_p$ measurement errors.

**7.3 Redundant measurements**

*7.3.1 Indicate flow quantities that have been measured independently by different techniques.*

One flow quantity measured independently by the laser Doppler velocimeter system and the pressure/temperature data system is the freestream velocity. The inflow velocity was measured at the window $1.775\, C_r$ ahead of the wing leading edge. The velocity obtained from the isentropic Mach number calculated from $p_\infty$ and $p_t$, actually measured $2.525\, C_r$ ahead of the wing root leading edge, and the measurement of $T_t$ (see section 3.6.1, and figure 3) agrees with the laser Doppler velocimeter value to within the accuracy of the measurements and the spatial variation of $M_\infty$ over the tunnel inlet. These two means of measuring inflow velocity are entirely independent.

*7.3.2 Checks make on internal consistency of the data*

As the model is symmetric about the xy plane, $C_p$ measured at positive z at positive angle of attack should correspond with the $C_p$ measured at negative z at negative angle of attack. The wing had 4 pressure taps on the lower surface (used in setting the angle of attack) corresponding to pressure taps on the upper surface. In addition, the wind tunnel walls have pressure taps at which can be compared in this fashion. Comparision of these $C_p$ measurements indicated that the asymmetries of the tunnel geometry (not the wing), were the limiting factor in the accuracy of the data. It should be noted that this level of uncertainty ($\leq \pm.01$ in $C_p$ for all tunnel runs) is very good.

Shock locations inferred from surface flow visualization has been compared with the shock location inferred from pressure measurements and laser Doppler velocimeter flowfield measurements.

**7.4 Other tests on same (nominal) geometry**

No other tests on the same geometry have been conducted, although the geometry of the model was supplied to NASA Langley for possible testing.

**7.5 Additional remarks**

This test was conducted with attention to careful control of the precision and accuracy of the quantities measured. The tabulated pressure data includes individual estimates of the measurement accuracy of each $C_p$. It should be stressed that this is a measurement accuracy and not an overall accuracy. The distinction is that the tabulated data is a measurement of the $C_p$ of this particular wing in this particular wind tunnel accurate to within the measurement accuracy, but if the same wing were tested in a different wind tunnel of nominally the same dimensions, the values could differ by .01 in $C_p$ at some point on the wing for some condition. Of course most of the

measurements would agree to better than .01 in $C_p$.

The geometry of the model has also been measured, and the fidelity of the actual tested wing geometry is also quantified (see section 3.3). The imperfections of the wind tunnel walls were also measured and quantified ($\leq$ 1 mm out of 406 mm deflections from the "true geometry")

## 8 REFERENCES


1 Marvin, J.G.and Holst, T.L. "CFD Validation for Aerodynamic Flows-Challenge for the 90's" AIAA Paper No. 90-2995 AIAA 8th Applied Aerodynamics Conference

2 Marvin, Joseph G. "Accuracy Requirements and Benchmark Experiments for CFD Validation" Paper No. 2, AGARD-CP 437, Vol. 1, Validation of Computational Fluid Dynamics

3 Ladson, Charles L., and Brooks, Cuyler W., Jr. "Development of a Computer Program to Obtain Ordinates for NACA 6- and 6A- Series Airfoils" NASA Technical Memorandum 3069

4 Abbott, Ira H and Von Doenhoff, Albert E. "Theory of Wing Sections" Dover Publications, Inc. 1959

5 Holst, T. "Numerical Solution of Transonic Wing Flow Fields" AIAA Paper No. 82-0105,AIAA 20th Aerospace Sciences Meeting

6 McDevitt, J.B., Polek, T.E., Hand, L.A. "A New Facility and Technique for Two Dimensional Aerodynamic Testing" Journal of Aircraft, Vol 20, Number 6, June 1983, Page 543.

7 Seegmiller, H. Lee, Bader, Jon B., Cooney, John P. De Young, Anemarie, Donaldson, Ralph W. Jr., Gunter, William D. Jr., and Harrison, Dean R. "Development of a New Laser Doppler Velocimeter for the Ames High Reynolds Channel No. II" NASA Technical Memorandum 84367

8 Kaynak, U., Holst, T. Cantwell, B.J., and Sorenson, R.L. "Numerical Simulation of Transonic Separated Flows over Low Aspect Ratio Wings" AIAA Paper 86-0508, Jan. 1986

9 Moffat, Robert J. "Contributions to the Theory of Uncertainty Analysis for Single-Sample Experiments" 1980-91 AFOSR-HTTM-STANFORD Conference on Complex Turbulent Flows – Vol. 1

10 Olsen, M., Seegmiller, H. "Low Aspect Ratio Wing Code Validation Experiment" AIAA Paper 92-0402, Jan. 1992


## 9 SYMBOLS

| | |
|---|---|
| $\xi$ | $(x - x_{le}(\eta))/c(\eta)$ axial distance from leading edge,normalized by local chord. |
| $\xi_0$ | $(x - x_{le}(0))/C_r$; axial distance from root leading edge, normalized by root chord. |
| $\eta$ | $2y/b$; spanwise distance, normalized by $b/2$ |
| $\nu$ | kinematic viscosity |
| $\rho$ | mass density |
| $\zeta$ | $z/C_r$; vertical distance normalized by $C_r$ |
| $a$ | local speed of sound |
| $a^*$ | sound speed at sonic conditions |
| $b/2$ | semispan of wing |
| $c$ | local wing chord (a function of $\eta$) |
| $C_r$ | wing root chord |
| $C_t$ | wing tip chord |
| $C_p$ | coefficient of pressure $\frac{(p-p_\infty)}{q_\infty}$ |
| $M_\infty$ | freestream Mach number |
| $M_\infty^{crit}$ | lowest $M_\infty$ at which sonic flow is attained at some point in the flowfield. |
| $p_\infty$ | static pressure measured at $\xi_0 = 2.525$, $\eta = 1.6$, $\zeta = 0$. |
| $p_t$ | total(pitot) pressure measured at $\xi_0 = 2.25$, $\eta = 0$, $\zeta = -0.7$. |
| $q_\infty$ | freestream dynamic pressure $(\frac{1}{2}\rho_\infty U_\infty^2)$ |
| $Re_{C_R}$ | Reynolds number based on root chord $(\frac{U_\infty C_r}{\nu})$ |
| $T_t$ | freestream total temperature, measured in stagnation chamber |
| $u$ | axial velocity |
| $v$ | spanwise velocity |
| $w$ | vertical velocity |
| $x$ | axial position, origin at wing root leading edge (see fig 3) |
| $y$ | spanwise position, origin at wing root leading edge (see fig 3) |
| $z$ | vertical position(normal to xy plane), origin at wing root leading edge |

Sub/Superscripts

| | |
|---|---|
| $\|^*$ | sonic conditions |
| $\|_\infty$ | static conditions at $\xi_0 = -2.525$ |
| $\|_t$ | total(stagnation) conditions upstream of wing |
| $\|_{le}$ | wing leading edge |
| $\|_{te}$ | wing trailing edge |
| $\|_{c/4}$ | wing quarter chord |

## TABLE I, TEST CONDITIONS

| $\alpha = 0.00°$ | | | |
|---|---|---|---|
| Run(s\|c) | $M_\infty$ | $Re_{C_R} \times 10^{-6}$ | Remarks |
| 163(b1) | 0.6006 | 11.8 | |
| 166(c1) | 0.6999 | 13.2 | |
| 165(b1) | 0.8000 | 14.0 | |

| $\alpha = 2.00°$ | | | |
|---|---|---|---|
| Run(s\|c) | $M_\infty$ | $Re_{C_R} \times 10^{-6}$ | Remarks |
| 171(b1) | 0.5997 | 12.0 | |
| 169(a1) | 0.6999 | 13.1 | |
| 176(b1) | 0.7496 | 14.0 | |
| 178(b1) | 0.7749 | 14.1 | |
| 174(b1) | 0.7998 | 13.8 | |

| $\alpha = -2.00°$ | | | |
|---|---|---|---|
| Run(s\|c) | $M_\infty$ | $Re_{C_R} \times 10^{-6}$ | Remarks |
| 185(b2) | 0.6001 | 12.3 | |
| 187(a1) | 0.7002 | 12.9 | |
| 188(a1) | 0.7500 | 13.3 | |
| 180(a1) | 0.7747 | 13.5 | |
| 186(b1) | 0.8004 | 13.9 | |

| $\alpha = 5.00°$ | | | |
|---|---|---|---|
| Run(s\|c) | $M_\infty$ | $Re_{C_R} \times 10^{-6}$ | Remarks |
| 191(b1) | 0.5996 | 12.1 | |
| 207(c1) | 0.6498 | 12.8 | |
| 194(b1) | 0.6995 | 13.0 | † |
| 206(a1) | 0.7250 | 13.2 | |
| 198(d1) | 0.7496 | 14.0 | † |
| 203(b1) | 0.7747 | 13.5 | †‡ |
| 193(a1) | 0.8001 | 13.8 | † |

| $\alpha = -5.00°$ | | | |
|---|---|---|---|
| Run(s\|c) | $M_\infty$ | $Re_{C_R} \times 10^{-6}$ | Remarks |
| 219(d1) | 0.6008 | 12.1 | |
| 220(c1) | 0.6494 | 12.7 | |
| 213(b1) | 0.6993 | 13.1 | |
| 214(c1) | 0.7251 | 13.7 | |
| 211(c1) | 0.7505 | 13.9 | |
| 227(b1) | 0.7755 | 13.8 | |
| 228(b1) | 0.7998 | 13.8 | |

| $\alpha = 7.92°$ | | | |
|---|---|---|---|
| Run(s\|c) | $M_\infty$ | $Re_{C_R} \times 10^{-6}$ | Remarks |
| 231(b1) | 0.5996 | 11.7 | |
| 238(a1) | 0.6504 | 12.7 | |
| 233(b1) | 0.7002 | 13.0 | † |
| 237(b1) | 0.7250 | 13.5 | |
| 236(a1) | 0.7503 | 13.7 | † |
| 230(b1) | 0.7749 | 13.5 | † |
| 239(b1) | 0.8001 | 14.1 | † |

| $\alpha = -7.92°$ | | | |
|---|---|---|---|
| Run(s\|c) | $M_\infty$ | $Re_{C_R} \times 10^{-6}$ | Remarks |
| 257(a1) | 0.6004 | 12.0 | |
| 267(b1) | 0.6497 | 12.7 | |
| 262(a1) | 0.7005 | 13.1 | |
| 256(a1) | 0.7247 | 13.2 | |
| 263(a2) | 0.7506 | 13.5 | |
| 264(b1) | 0.7757 | 14.2 | |
| 261(b1) | 0.7995 | 14.0 | |

†– Surface flow pattern photos avail for this case.
‡– laser Doppler velocimeter flowfield data available for this case.

## TABLE II, DATA AVAILABILITY

| Data | Engineering Units | Coefficients | Normalized | Uncorrected | Corrected |
|---|---|---|---|---|---|
| Freestream Conditions | | | × | × | |
| Surface Pressures | | × | × | × | |
| Wake Velocities | | | × | × | |
| Field Data | | | × | × | |

# Wind Tunnel Investigations of the Appearance of Shocks in the Windward Region of Bodies with Circular Cross Section at Angle of Attack

BY

H. Esch
DLR, Hauptabteilung Windkanäle
Postfach 906058
D5000 Köln-Porz

## 0 Introduction

Originally the model was designed to investigate differences in the interference of fuselage and control surfaces attached to bodies of circular and rectangular cross sections. During the tests it was found difficult to define the interference since the reference configuration, the isolated body without controls, showed some disturbances in the pressure distribution at certain combinations of Mach number and angle of attack. These disturbances are connected with the appearance of shock waves on the windward side of isolated circular bodies. By checking schlieren pictures made during earlier test series of missiles the range could be defined in which this type of shock occurs. Pressure distribution measurements were made in order to find an explanation for the formation of the shocks and their bending into the windward region. It is believed that three conditions must be fullfilled:

1. Crossflow Mach number must be high enough that a shock forms in front of the wedge-like primary separation.
2. The primary separation line must move towards the windward side of the body. As a result the local Mach number normal to the separation line decreases, and eventually the shock detaches - if the crossflow Mach number is not too high.
3. When the local surface Mach number normal to the body axis is less than one, the disturbance propagates towards the windward region of the body.

In some cases this type of disturbance may lead to confusion especially when there are not enough pressure taps: in the pressure distribution one finds only one or two peaks and from this, one cannot identify the shock trace.

The model is extremely simple and thus the generation of a grid should not be too expensive. The data are considered valuable for CFD validation but on the other hand CFD should be useful to get more information of the outer flow field and further insight into this more fundamental flow phenomenon.

## 1. General Description

| | |
|---|---|
| 1.1 Model name | Kreisrumpf |
| 1.2 Model type | Slender Body, supersonic flow |

| | | |
|---|---|---|
| 1.3 Purpose of test | | Pressure distribution measurements and flow visualization were made to explain the appearance of shocks in the windward region of circular bodies. |
| 1.4 Dominant flow physics | | The shock in front of the primary separation of a circular body at angle of attack detaches and bends towards the windward region, when certain combinations of supersonic flow Mach numbers and incidences are given (see figures 1 ÷ 4). |
| 2. Details of Model | | |
| 2.1 General geometric arrangement | | Isolated body with circular cross section (fig. 5) |
| 2.2 Specific features | | Different noses were tested at different Mach numbers but only one configuration is included in the data set as the nose fineness ratios investigated here do not change the flow phenomenon basically (see figs. 6, 7). The influence is largest at low supersonic Mach numbers (Ma = 1.4 and 1.5 figs. 6, 8). |
| 2.4 Body data | | |
| 2.4.1 Shape | nose shape: | Tangent ogive with a fineness ratio of 3.5 |
| | body length: | Distance from nose tip to instrumented model section $4.4 \leq x/D \leq 7.4$ |
| | cross section: | Circular |
| 2.7 Geometric definition | | The shape is analytically specified (design coordinates). Surface roughness on instrumented section: average roughness: .001 mm single roughness: .005 mm junction between different model sections: .1 mm |
| 2.8 Model support | | Central sting from rear |

## 3. General Tunnel Information

| | |
|---|---|
| 3.1 Tunnel designation | Trisonische Meßstrecke TMK |
| 3.2 Organization running the tunnel | Deutsche Forschungsanstalt für Luft- und Raumfahrt DLR, Hauptabteilung Windkanäle |
| 3.3 Tunnel characteristics | |
| type of tunnel: | Blow down, flexible nozzle |
| operating envelope: | $.5 \leq Ma \leq 4.5$ (5.7)<br>ambient $\leq$ total temperature $\leq$ 550 K<br>$Ma \leq 1.2$: static pressure $\approx 1 \cdot 10^5 N/m^2$<br>$Ma \geq 1.4$: dyn. press. q $\leq 1 \cdot 10^5 N/m^2$ |
| 3.4 Test section | |
| 3.4.1 Model mounting | central sting |
| 3.4.2 Test section dimensions | 60 x 60 x 60 $cm^3$ |
| 3.4.3 Wall geometry (supersonic test section) | |
| type of walls | flexible nozzle, solid walls |
| open area ratio | 0 in supersonic flow, wall pressures and displacement thickness were not measured |
| 3.5 Freestream conditions | |
| 3.5.1 Determination of flow conditions | total pressure in settling chamber, position of nozzle, total temperature |
| 3.5.2 Tunnel calibration | by pitot rake and differential pressure yaw-meters; the last check was made in 1989 |
| 3.6 Flow quality (empty tunnel) | |
| 3.6.1 Flow uniformity | |
| Mach number | Mach number variation over model length is about $\Delta Ma \approx \pm .5\%$ of free stream Mach number. The variation during a run is smaller. |
| Flow angularity | During the calibration local flow angles at the tunnel axis were within $\pm .25°$. Average flow angularity is determined only for force measurements by inverting the model |
| 3.6.2 Temperature variation | In supersonic flow total temperature can be heated from ambient to 550 K. The temperature distribution |

| | |
|---|---|
| | within the test section is not known. During a run total temperature may drop by up to 8K, depending on running time. |
| 3.6.3 Flow unsteadiness | In supersonic flow $C_{p,RMS}$ drops from .9% at Ma = 1.25 to .1% at Ma = 2.5 |
| 4. Instrumentation | |
| 4.1 Model position | |
| 4.1.1 Measurement of incidence | Deflection due to aerodynamic loads was determined from schlieren pictures and added to the nominal angle of attack. |
| 4.1.2 Accuracy of geometrical incidence | $\pm .2°$ |
| 4.2 Model pressure measurements | |
| 4.2.1 Total number of pressure holes | 121 pressure holes, but some could not be used because of leakage (s. fig. 5) |
| 4.2.2 Range of pressure tranducers | $\pm 1 \cdot 10^5 N/m^2$<br>$\pm .1\%$ full scale<br>(according to manufacturer) |
| 4.2.3 Dynamic pressures | Fluctuating pressures were not measured |
| 4.5 Surface flow visualization | |
| 4.5.1 Measurement technique | Oil flow technique |
| 4.5.2 Surface of flow visualization | On the complete body or downstream of the nose when a foil was wrapped around the cylindrical part |
| 4.5.3 Available data | Copies of photographs |
| 4.6 Flow field visualization | |
| 4.6.1 Technique applied | Schlieren pictures |
| 4.6.2 Planes visualized | x-z-plane (side view) |
| 4.6.3 Available data | Copies of photographs |
| 5 Test Matrix and Conditions | |
| 5.1 Detailed test matrix | |
| 5.1.1 Number of selected test cases | 3 |
| 5.1.2 Number of selected configurations | 1 |

| | |
|---|---|
| 5.1.3 Table of test matrix | Table 1 |
| 5.2 Model/tunnel relations | |
| 5.2.1 Maximum blockage | .35% |
| 5.2.6 Adiabatic wall of model | Adiabatic wall temperatures have not been reached. For Ma = 1.5 the ratio $T_{Wall}/T\infty$ at the beginning of the run is 1.4 and drops to a value of about 1.3 when the tunnel stops. |
| 5.3 Transition details | |
| 5.3.1 Free/fixed transition | Most tests were made without fixing transition. In earlier tests it was found that for $Re_D > 5 \cdot 10^5$ there was almost no influence of boundary layer tripping on the normal force of long, slender bodies. During the present series, tests were made with and without a roughness band at the nose - cylinder-junction of the model. There was an influence on the flow in the leeward region (circumferential angles $\varphi > 90°$) but the main flow phenomenon to be investigated, the shock trace in the windward region, remained nearly unaffected (see figs. 6, 9, 12, 13). |

6. Data

| | |
|---|---|
| 6.1 Availability of data | |
| 6.1.1 Organization owning the data | DLR, Hauptabteilung Windkanäle, Köln-Porz |
| 6.1.2 Who is responsible for the data | Klaus Feuerrohr, Dipl.-Ing.<br>Postfach 906058<br>D5000 Köln 90<br>Phone 02203 601 2083<br>Fax 02203 601 2085 |
| 6.1.3 Availability of data | Data are freely available |
| 6.3 Type and form of available data | |
| 6.3.1. Type and form | Table 2 |
| 6.3.2 Data carrier | Floppy disk 3 1/2" |
| 6.3.3 Extent of geometry data | no data necessary (s. fig. 5) |
| 6.3.4 Extent of aerodynamic test data | 45000 words |

| | |
|---|---|
| 6.4 Corrections applied to data | No corrections were applied |
| 6.4.5 Aeroelastic deformation | Angle of attack was taken from schlieren pictures |

7. Data Accuracy and Repeatability Assessment

| | |
|---|---|
| 7.1 Estimated accuracy of: | |
| 7.1.1 Free stream conditions | Ma: $\pm$ .5% |
| | $\alpha$ : $\pm$ .2 ° |
| 7.1.2 Measured data | Cp: $\pm$ .01 |
| 7.2 Repeat measurements | |
| 7.2.1 Within one test campaign | Compare figures 6 and 10 |
| 7.2.2 Within successive campaigns | Compare figures 6, 10, 11. When the flow is attached, e.g. in the windward region, $\Delta Cp$ ist within $\pm$ .01; the flow on the separated leeside is less stable. Sometimes flow details changed considerably in this area. The main objective of the investigations, however, the trace of the shock, remained almost unchanged. |
| 7.4 Different models | Because of the disturbances, introduced by the pressure holes, oil flow - and schlieren pictures were taken using models with a smooth surface. |

8. References


8.1 Windtunnel:
H. Esch
Die 0,6 m x 0.6 m-Trisonische Meßstrecke (TMK) der DFVLR in Köln-Porz (Stand 1986), DFVLR-Mitt.86-21 (1986).

English translation
The 0.6 m x 0.6 m trisonic test section (TMK) of the DFVLR in Köln-Porz (1986 status).
ESA-TT-1052

8.3 Test results:
H. Esch
Windkanaluntersuchungen zum Auftreten von Verdichtungsstößen im Luvgebiet von angestellten kreiszylindrischen Rümpfen.
DLR-FB 90-15 (1990).

English translation:
Wind tunnel investigations of the appearance of shocks in the windward region of bodies with circular cross section at angle of attack.

9. Symbols

| | |
|---|---|
| $C_P$ | Pressure coefficient |
| D | Body diameter |
| l | Distance between the apex of the model and the control surface axis |
| $l_N$ | Length of nose |
| Ma | Mach number |
| $Ma_q$ | Cross-flow Mach number, $Ma_q \cdot \sin \alpha$ |
| q | Dynamic pressure |
| $Re_D$ | Reynolds number referred to the body diameter |
| x | Distance from the apex of the fuselage |
| $\alpha$ | Angle of incidence |
| $\varphi$ | Polar angle windward side: $\varphi = 0°$ |

| Identification | | Flow Condition | | | Position | Other Information | |
|---|---|---|---|---|---|---|---|
| Case No. | Conf. | Mach | q kPa | $Re_D$ | $\alpha$ | type of measurement | remarks |
| 1 | $l_N/D = 3.5$ | 1.5 | 79 | $1.2 \cdot 10^6$ | $9° \div 23°$ (8 angles) | surface pressures | D = 40 mm |
| 2 | $l_N/D = 3.5$ | 1.4 | 70 | $.8 \cdot 10^6$ | 16° | schlieren and oil flow | D = 30 mm |
| 3 | $l_N/D = 3.5$ | 1.5 | 70 | $.8 \cdot 10^6$ | 16° | schlieren and oil flow | D = 30 mm |

**Table 1. Test Matrix Table**

| Data | Engin. Units | Coeffi-cients | Normalized | Uncorrected | Corrected |
|---|---|---|---|---|---|
| Freestream Conditions | × | | | | |
| Surface Pressures | | × | | × | |

**Table 2. Data Availability**

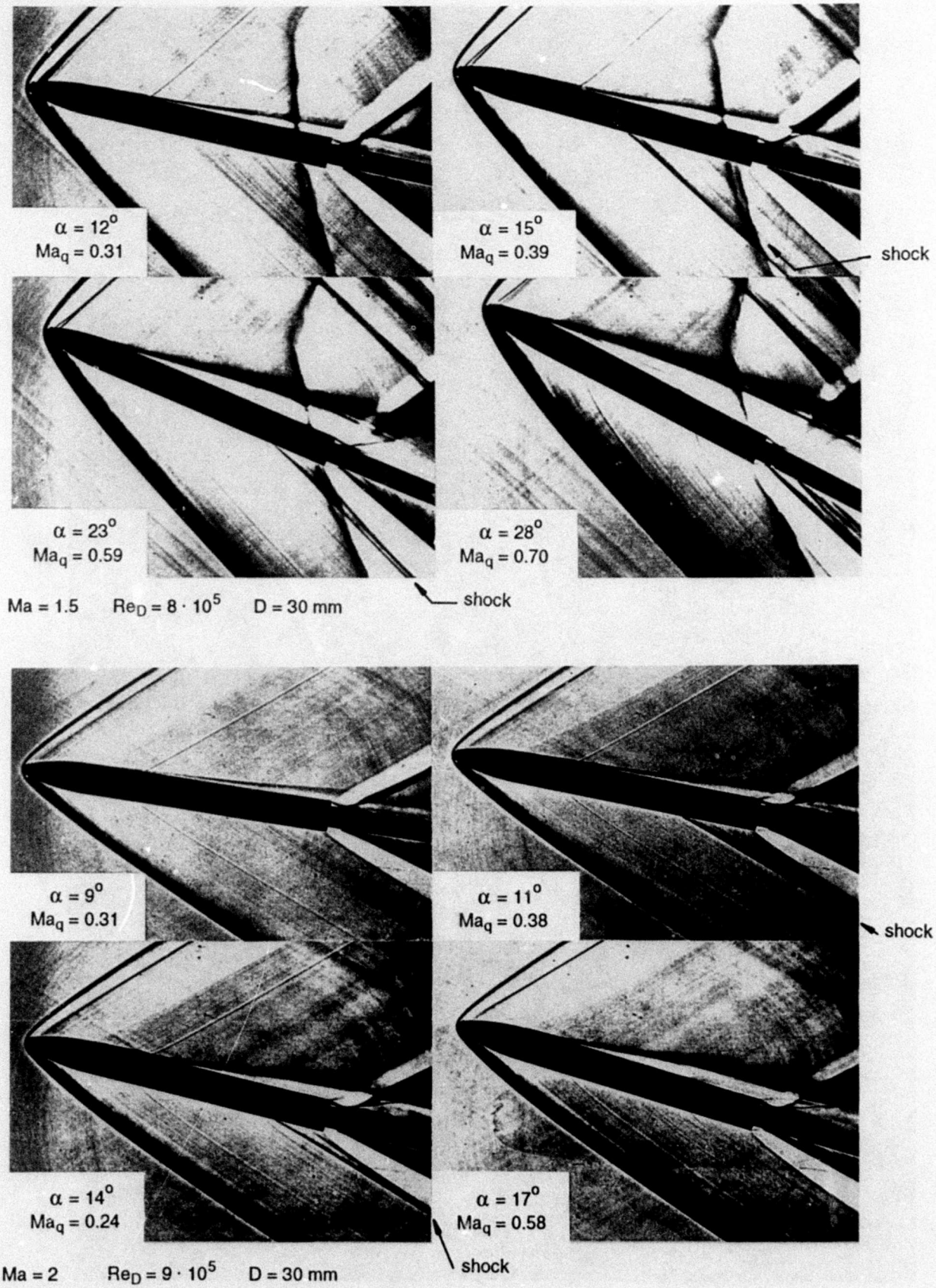



Fig. 1 Schlieren photographs at Ma = 1.5 and 2, showing the appearance of shock waves at the windward side of circular cylinders

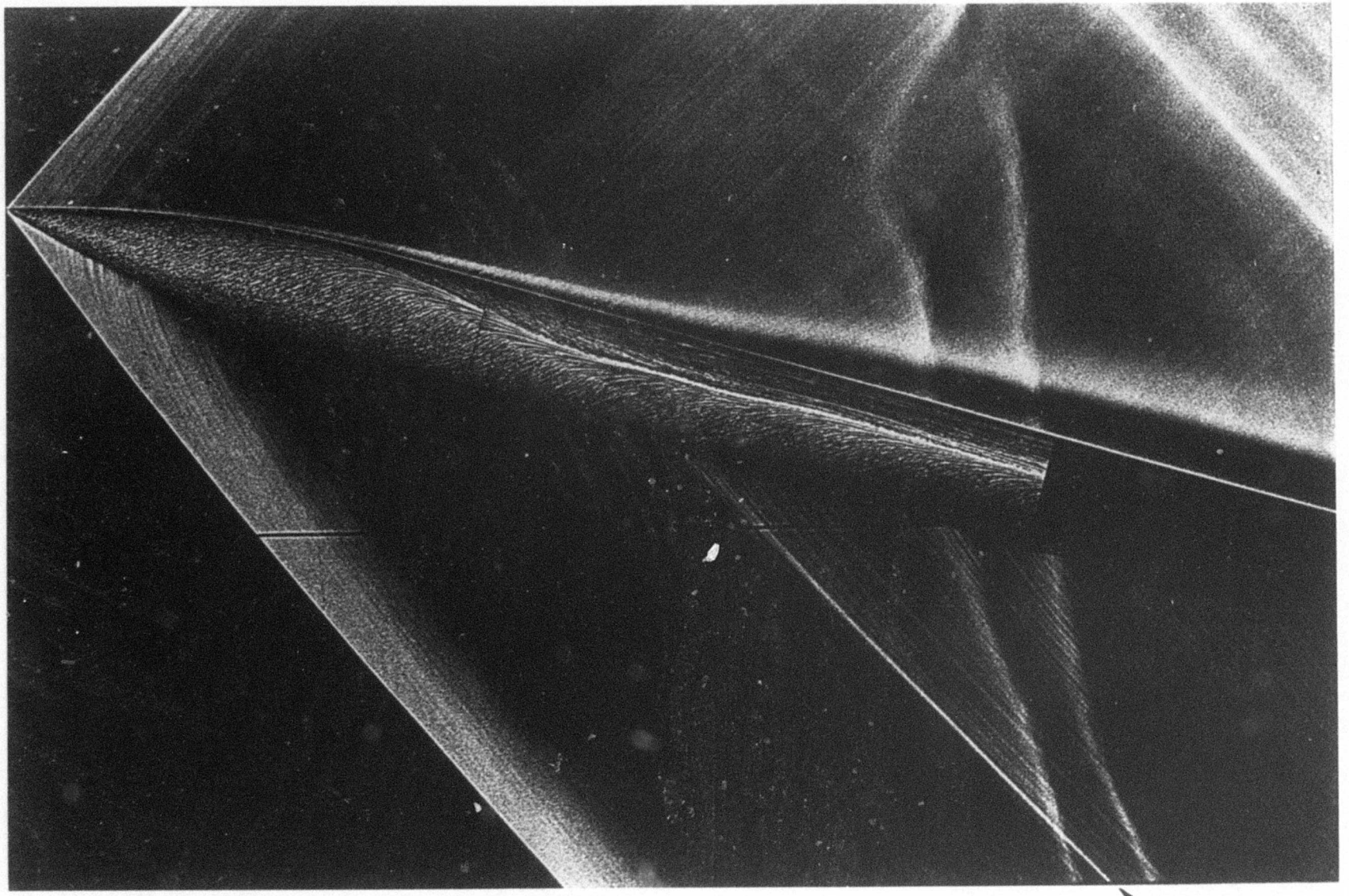



Fig. 2 Appearance of shock at windward side of an isolated circular body, Schlieren/oil flow picture,
Ma = 1.4 ; $Re_D = 8 \cdot 10^6$ ; $\alpha = 16^o$

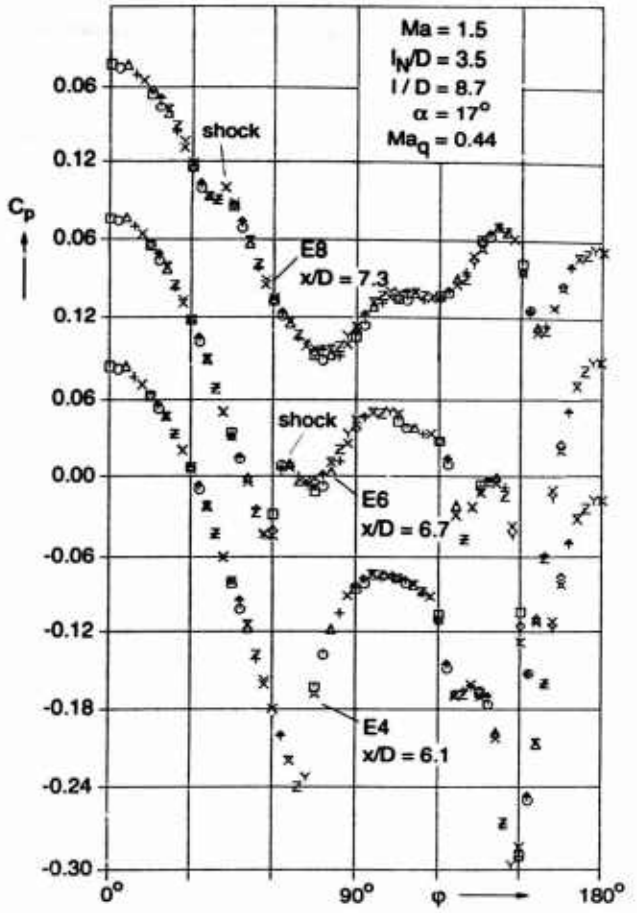



Fig. 3 Pressure distribution on the surface of the cylinder at Ma = 1.5, $C_p$ (φ) in three measurement planes at α = 17°

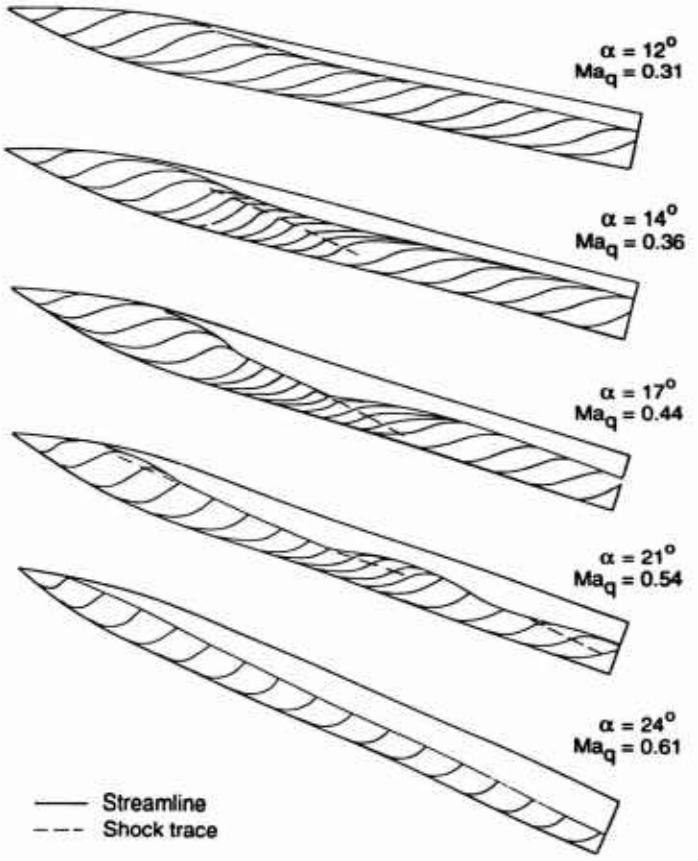
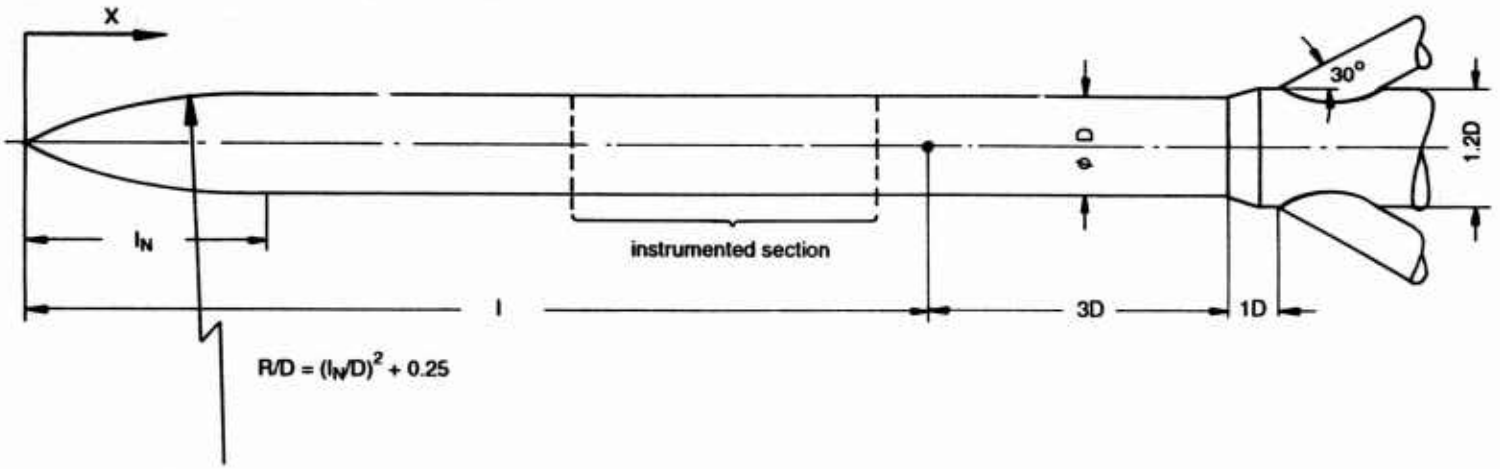
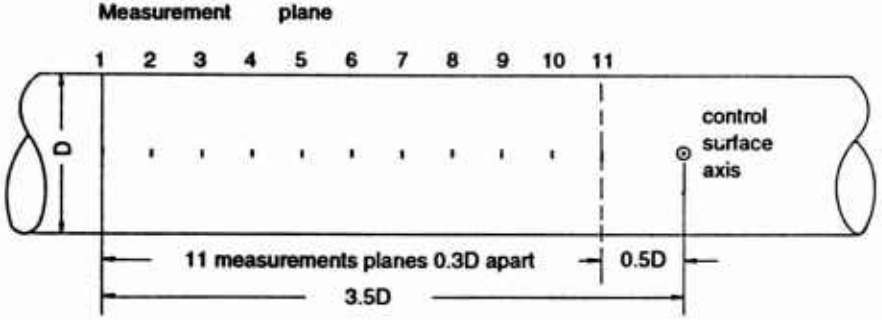



Fig. 4 Flow details in the vicinity of the primary separation line in the critical cross-flow range, Ma = 1.5



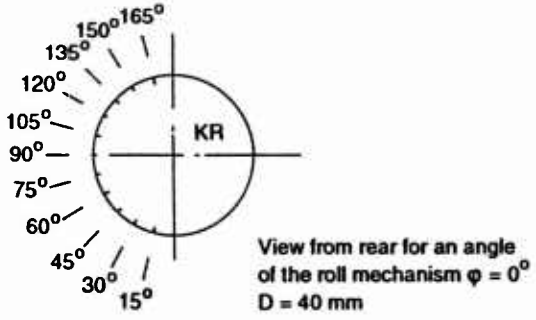




**Fig. 5 Wind tunnel model for pressure distribution measurements**

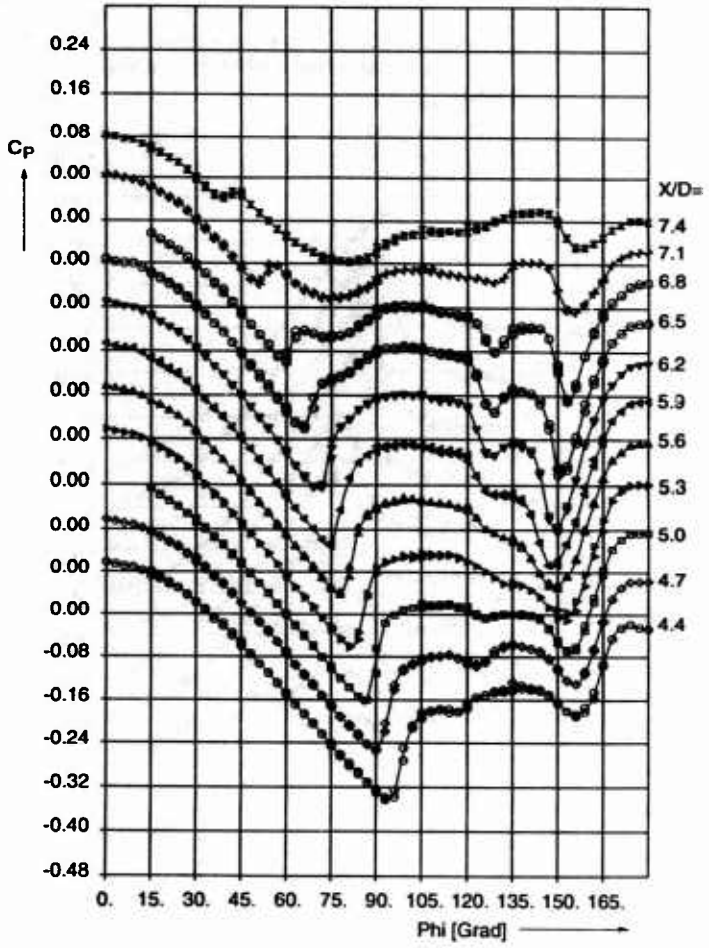



Fig. 6 Kreisrumpf, pressure distribution
$l_N/D = 3.5$ $1/D = 7.9$ Ma = 1.5 $\alpha = 17^o$ no b.l. trip
run 42, March 1990

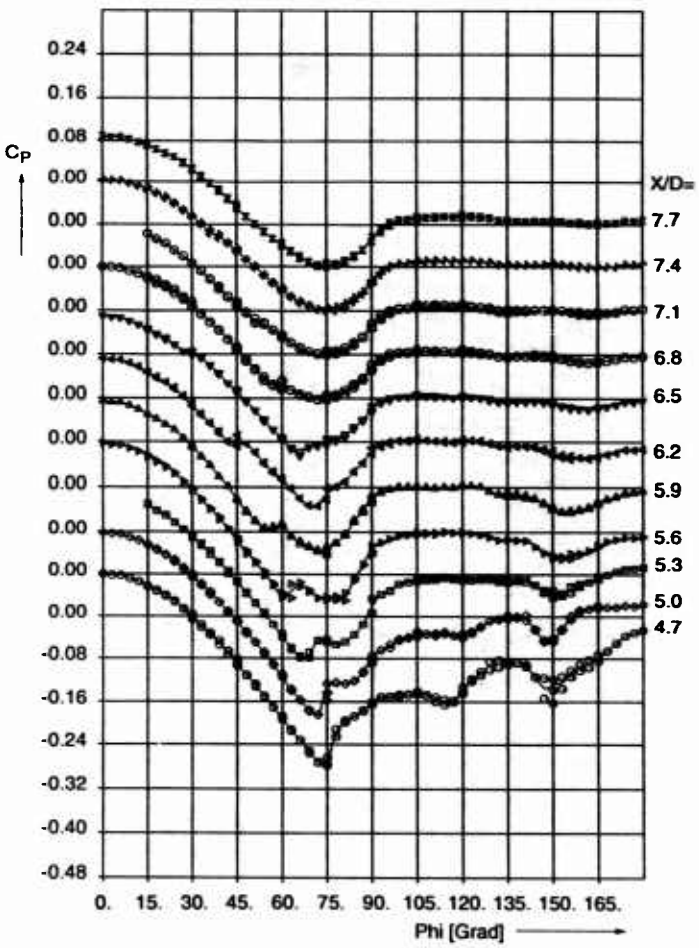



Fig. 7 Kreisrumpf, pressure distribution
$l_N/D = 0.5$ $1/D = 8.2$ Ma = 1.5 $\alpha = 17^o$ no b.l. trip
run 28, March 1990

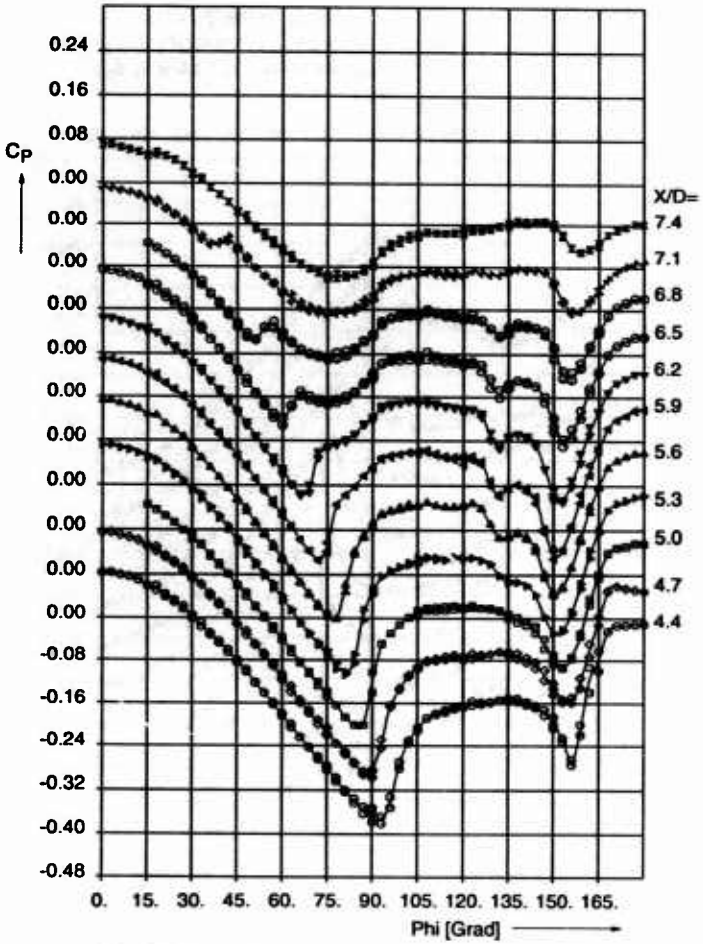



Fig. 8 Kreisrumpf, pressure distribution
$l_N/D = 3.5$ $1/D = 7.9$ Ma = 1.4 $\alpha = 17^o$ no b.l. trip
run 5, March 1990

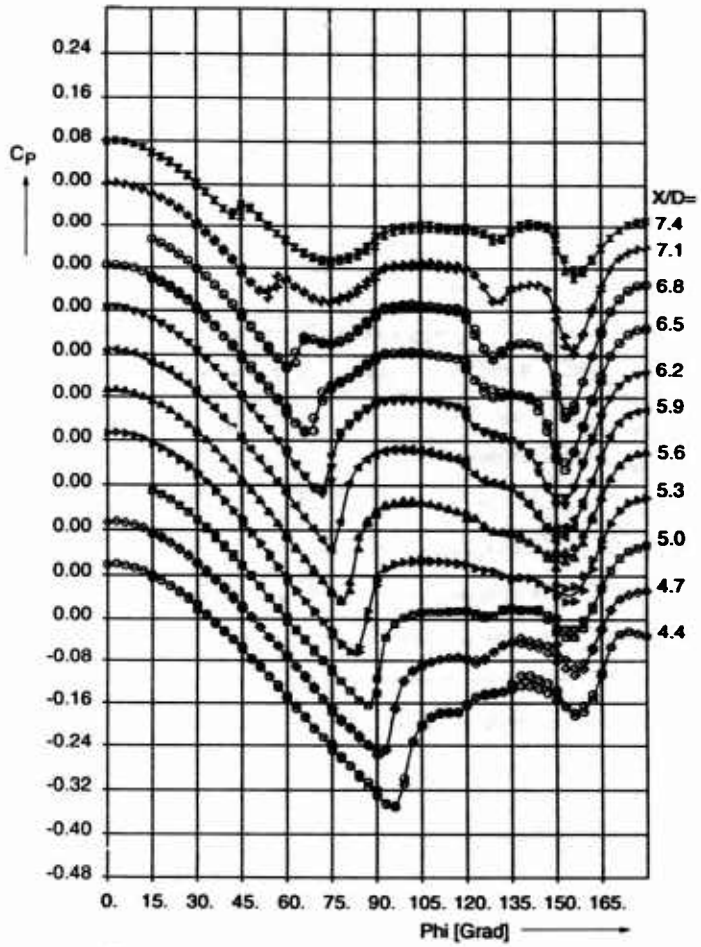



Fig. 9 Kreisrumpf, pressure distribution
$l_N/D = 3.5$ $1/D = 7.9$ Ma = 1.5 $\alpha = 17^o$ no b.l. trip
run 40, March 1990

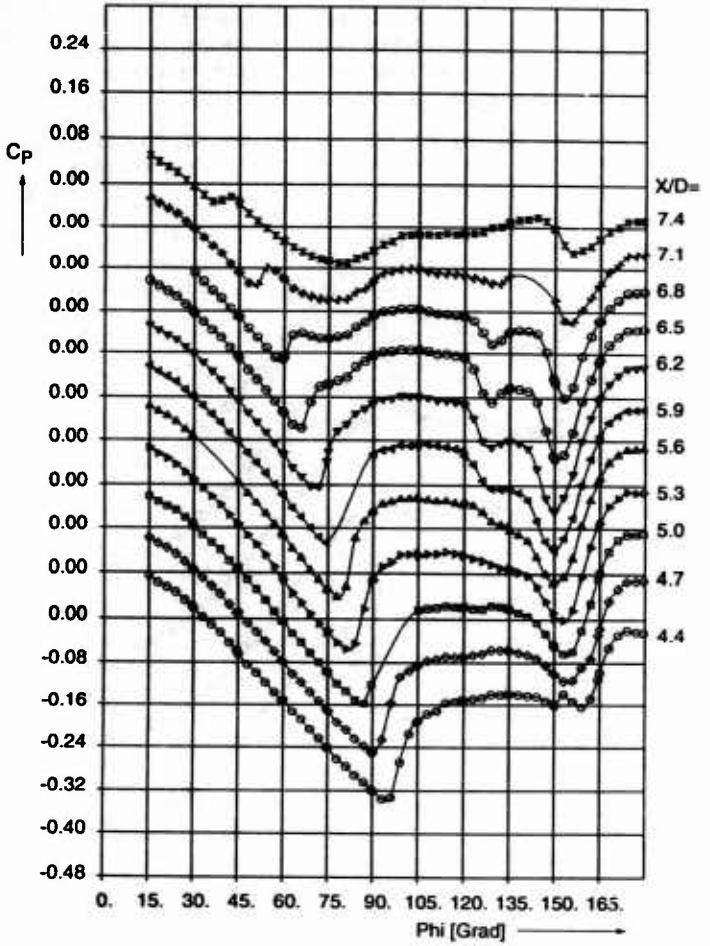



Fig. 10 Kreisrumpf, pressure distribution
$l_N/D = 3.5$ $1/D = 7.9$ Ma = 1.5 $\alpha = 17^o$ no b.l. trip
run 3. March 1990

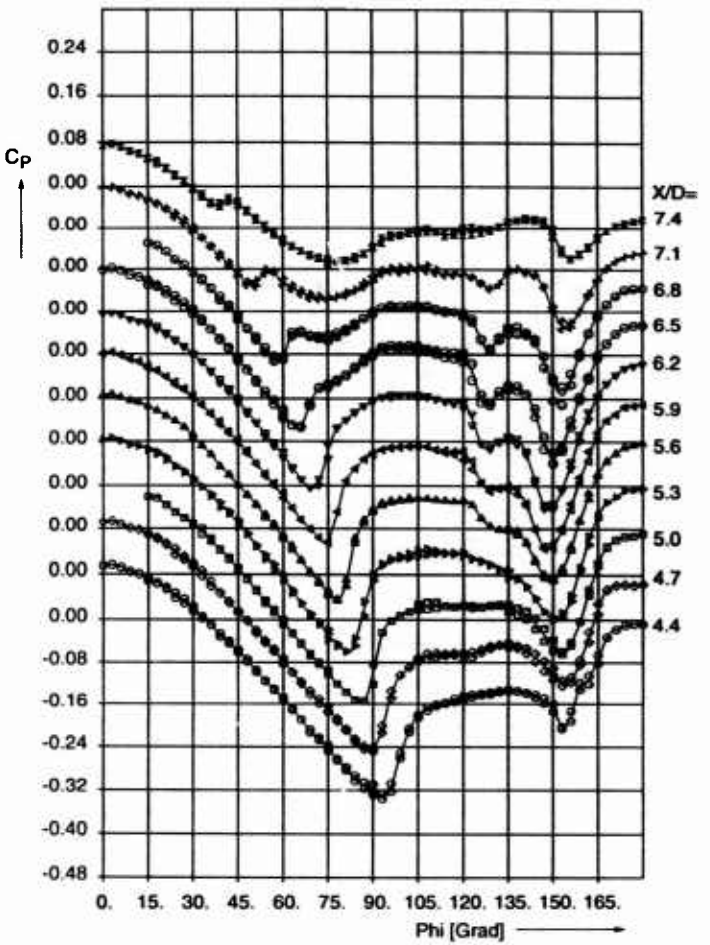



Fig. 11 Kreisrumpf, pressure distribution
$l_N/D = 3.5$ $1/D = 7.9$ Ma = 1.5 $\alpha = 16.8^o$ no b.l. trip
run 15, July 1988

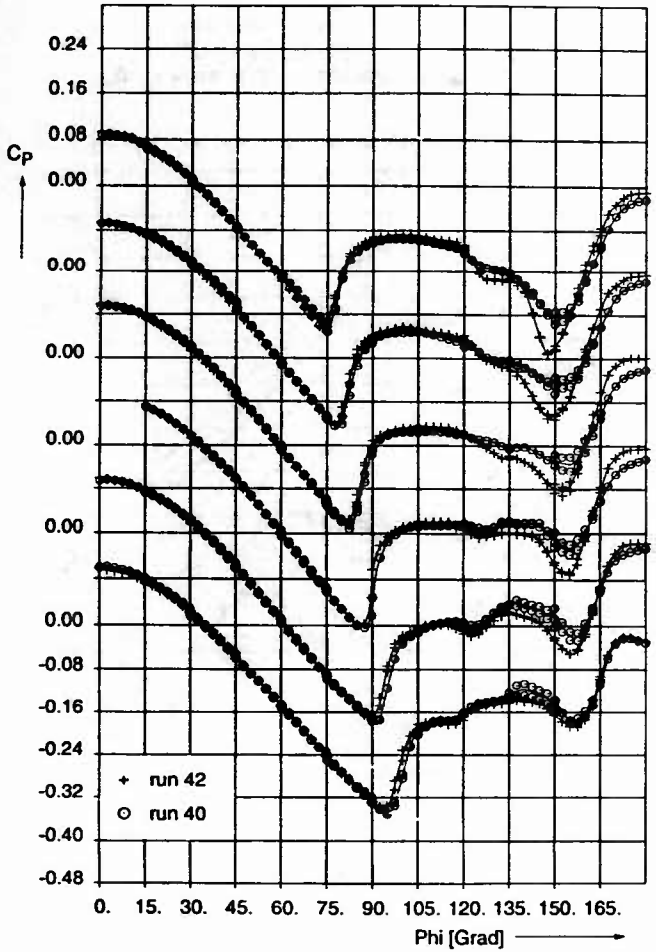



Fig. 12 Kreisrumpf, pressure distribution, comparison of model with (run 40) and without (run 42) b.l. tripping, $4.4 \leqslant x/D \leqslant 5.9$ Ma = 1.5 $\alpha = 17^{o}$

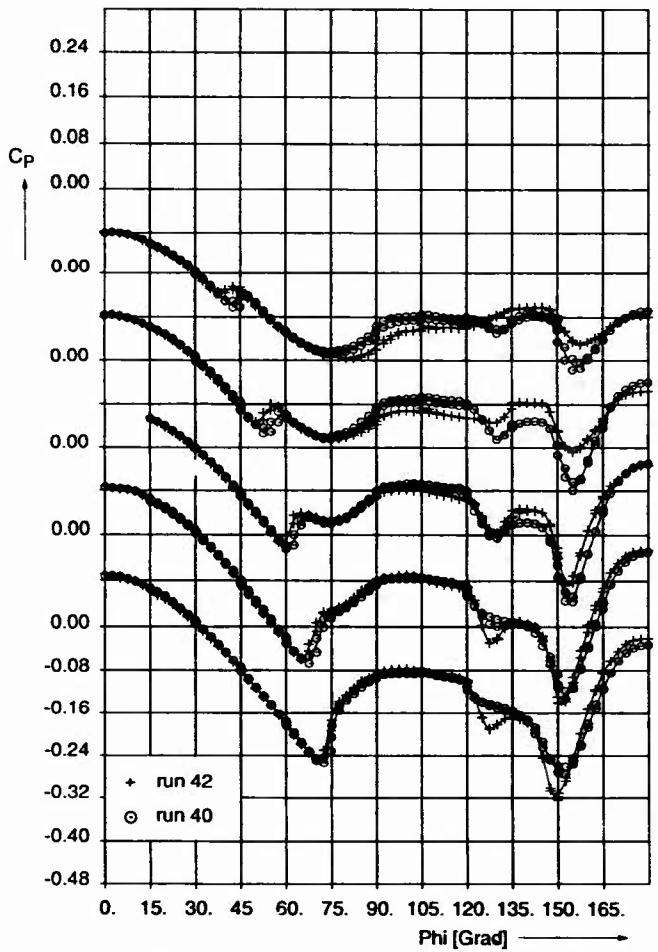



Fig. 13 Kreisrumpf, pressure distribution, comparison of model with (run 40) and without (run 42) b.l. tripping, $6.2 \leqslant x/D \leqslant 7.4$ Ma = 1.5 $\alpha = 17^{o}$

# Three-dimensional boundary layer and flow field data of an inclined prolate spheroid

H.-P. Kreplin

Deutsche Forschungsanstalt für Luft- und Raumfahrt e.V. (DLR)
Institut für Strömungsmechanik
Bunsenstraße 10, D-37073 Göttingen, Germany

## INTRODUCTION

A research project on the investigation of three-dimensional boundary layers on inclined bodies of revolution has been carried out. Experimental data for such flows were provided which can be used for the validation of calculation methods and the testing and development of turbulence models for three-dimensional flows. Problems of laminar-turbulent boundary layer transition as well as laminar and turbulent boundary layer separation have been studied for a range of angles of incidence and Reynolds number.

The wind tunnel model consists of a 6:1 prolate spheroid. This configuration was chosen for the following reasons:

- The flow pattern around the inclined model is characteristic for fuselages and missile shapes.
- The shape and potential pressure distribution are represented by analytic expressions.
- Instrumentation like probe traversing mechanism, hot film anemometers , pressure transducers etc. can be stored inside the model.
- As the model can be turned around its longitudinal axis, the flow can be measured with one probe/sensor in each cross section for arbitrary small steps of the circumferential angle.

Several incidence/Reynolds number combinations have been investigated. Data about transition in the 3d boundary layer, development of the boundary layers, 3d boundary layer separation and the separated flow field have been obtained. Measured data are surface pressures, skin friction, mean velocities in the boundary layer and in the flow field.

After a number of experiments had been performed at DLR Göttingen, a cooperation between ONERA and DLR was established in order to extend the tests to higher Reynolds numbers which can be obtained in the F1 wind tunnel of ONERA.

Three test cases have been selected. These are two angles of incidence, $\alpha$= 10 ° and $\alpha$= 30 ° at a low Reynolds number in the DLR tunnel with fixed and free transition, respectively, and $\alpha$=30 ° at a seven times higher Reynolds number in the ONERA tunnel.

The data of the first test case ($\alpha$= 10 °, fixed transition) has been used a few years ago within the AGARD FDP WG 10 "Calculation of 3d separated turbulent flows in the boundary layer limit for comparison with integral and field type boundary layer calculation methods. Also some data of the third test case ($\alpha$= 30 °, high Reynolds number) was used in this working group.

## 1. GENERAL DESCRIPTION

### 1.1 Model name or designation
DLR Prolate Spheroid

### 1.2 Model type
Slender body (6:1 prolate spheroid)

### 1.3 Purpose of test
The wind tunnel model was designed for the investigation of three-dimensional boundary layers developing on slender bodies of revolution. It has a simple geometry and the potential flow is given by an analytic solution.

### 1.4 Dominant flow physics
Flow around an inclined slender body of revolution. Three-dimensional boundary layers leading to separation depending on model angle of incidence, $\alpha$, and Reynolds number. "Weak" separation at $\alpha$= 10 °, boundary layer thickening, interaction between viscous and inviscid flow regions (Figs. 1.1 - 1.5). Separated flow field with leeside vortices at $\alpha$= 30 ° (Figs. 1.6 - 1.9).

## 2. DETAILS OF MODEL

The experimental investigations on the flow around the inclined prolate spheroid carried out in the 3m Low Speed Wind Tunnel NWG of DLR Göttingen have been extended to higher Reynolds numbers within a cooperation between ONERA and DLR in the pressurized low speed tunnel F1 of ONERA. For this purpose the design and construction of a new model became necessary due to the seven times higher maximum dynamic pressure in the F1 compared to NWG. Both models were made using the same mould, thus shape and size of the models are identical.

### 2.1 General geometric arrangement
Body of revolution

2.4 Body data
6:1 prolate spheroid with a length of L= 2.4 m, major half axes of 1.2 m and 0.2 m.

2.7 Geometric definition
The model shape is described analytically. The coordinates are design values. Contour deviations are less than 0.25% of the maximum diameter.

2.8 Model support
The model is mounted on a central rear sting. The outer diameter of the sting is 110 mm. The model can be turned around its longitudinal axis through $\varphi$= 0° to 360 °. Thus the flow in one cross-section can be measured with one probe/sensor fixed to the model.

3. GENERAL TUNNEL INFORMATION

Measurements with the prolate spheroid models at angle of incidence have been performed in two different wind tunnels. These are the 3m Low Speed Wind Tunnel of DLR,Göttingen (A) and the F1 Wind Tunnel of ONERA, Le Fauga (B)

Tunnel A

3.1.A Tunnel designation
3m Low Speed Wind Tunnel, Göttingen (NWG)

3.2.A Organisation running the tunnel
Deutsche Forschungsanstalt für Luft- und Raumfahrt e.V. (DLR), WT-WK
Bunsenstraße 10, D-37073 Göttingen, Germany

3.3.A Tunnel characteristics
Low speed wind tunnel, Göttingen type with closed return and open test section, nozzle contraction= 5.4, Speed range: 0 - 65 m/s, continously running

3.4.A Test section
Test section dimensions: 3m wide, 3m high and 6m long, open jet. Fig. 3.1 shows a sketch of the prolate spheroid model in the NWG. It also gives an estimate of the dimensions of the model support.

3.5.A Free stream conditions

a) Determination of free stream conditions
The total pressure is determined from the wall pressure in the settling chamber. As the tunnel has an open (free jet) test section the ambient, atmospheric pressure is taken as the static pressure. The dynamic pressure in the test section is calculated from the settling chamber pressure using a correction factor determined from a tunnel calibration. The (total) temperature is measured in the collector and assumed to be constant in the tunnel.

b) Tunnel calibration
The tunnel was calibrated after construction. Spot checks of calibrations have been performed from time to time, [1.1].

3.6.A Flow quality

a) Flow uniformity
Flow uniformity data are given in [1.1]. The deviations of the dynamic pressure are less than ±0.5% at the standard position of the models. At distances from the nozzle exit between 1m and 4m the maximum deviation of the static pressure is ±1.5% of the dynamic pressure. The flow angularity on the test section center line is constant within ±0.25° in the vertical plane, as measured by a multi-hole pressure probe.

b) Temperature variation
As the tunnel has no cooler, the temperature cannot be controlled. This means that the temperature in the tunnel is increasing during each run. The temperature increase with time is depending on the velocity and on the ambient temperature. It was tried to keep the Reynolds number constant by manual control of the fan speed. Temperature variations in the tunnel circuit are assumed to be small and therefore are neclected.
c) Flow unsteadiness
Data about the flow unsteadiness in the NWG are given in [1.2] and [1.3]. The overall turbulence level is rather high compared to other wind tunnels. Values of 0.33% to 0.4% for the streamwise velocity fluctuations and about 0.8% for the vertical and spanwise components have been measured.

Tunnel B

3.1.B Tunnel designation
F1 Wind Tunnel (F1)

3.2.B Organisation running the tunnel
Office National d'Études et de Recherches Aérospatiales (ONERA), Centre du Fauga-Mauzac, F-31410 Noe, France

3.3.B Tunnel characteristics
Pressurized low speed wind tunnel, closed test section, nozzle contraction ratio= 7.2, Maximum pressure : 4 bar, Maximum speed : 125 m/s at 1 bar, 80 m/s at 4 bar, continously running.

3.4.B Test section
Closed test section, Test section dimensions: 4.5m wide, 3.5m high and 10m long. Fig. 3.2 shows a sketch of the test section with the model and the F1 sting support. A slight diver-

gence of the two vertical test section walls compensates the boundary layers along the walls to ensure a flow without longitudinal gradients.

3.5.B Free stream conditions

a) Determination of free stream conditions
Several Prandtl antennas placed in the upstream part of the test section, wall pressure taps at the end of the contraction and a Pitot probe in the settling chamber are used for the determination of the reference static, total and dynamic pressures. The (total) temperature is measured in the settling chamber and assumed to be constant in the tunnel.

b) Tunnel calibration
The tunnel has been calibrated after construction. Sample results are given in [1.4].

3.6.B Flow quality

a) Flow uniformity
Flow uniformity data are given in [1.4]. The longitudinal gradient of static pressure or Mach number is negligble. The flow angularity in the test section is zero, with an inaccuracy of ±0 02°. The stagnation pressure shows almost perfect uniformity. The wind tunnel is supplied with compressed air generated by a centrifugal compressor through a buffer tank. The tank is used in combination with a servo-control for regulating the pressure around an assigned value. The relative deviations of the stagnation pressure are smaller than $\pm 10^{-3}$.

b) Temperature variation
A water cooler is used to stabilize the stagnation temperature around an assigned value between atmospheric temperature and 40°C. A servo-control maintains this temperature around the assigned value within better than 1°C.

a) Flow unsteadiness
Hot wire measurements in the test section showed a low streamwise turbulence level smaller than 0.1%. For Mach numbers above 0.2 the noise level is less than 0.01 in terms of $c_p$-RMS, i.e. if the RMS pressure fluctuations are normalized by the dynamic pressure in the free stream.

4. INSTRUMENTATION

Most of the instrumentation used is described in the report of AGARD FDP-WG 10, [2.2.]

4.1 Model position
In the NWG the model was aerodynamically aligned to the free stream direction. It was adjusted horizontally in the F1 tunnel with a spirit-level on a reference plate which was fixed to the model. The model incidence was measured by an inclinometer located inside the model during the runs. The accuracy of the incidence is estimated to ±0.1°.

4.2 Model pressure measurements
The model is equipped with 42 pressure taps of 0.3 mm diameter positioned on one meridian in non-equidistant distances, cf. Fig. 4.1. Due to the fact that the model could be rotated around its longitudinal axis the wall pressures could be measured in the 42 cross section with high resolution in circumferential direction.
Pressure transducers:
NWG: Hottinger PDI/0.01, 1000 Pa, accuracy= 0.1% of full scale and SETRA 239, 1400 Pa, accuracy= 0.14% of full scale
F1: DRUCK Ltd. PDCR 22, 2.5 psi= 17000 Pa, accuracy= 0.1% of full scale.
Wall pressure fluctuations have not been measured.

4.3 Boundary layer measurements
Mean velocity profiles in the three-dimensional boundary layers have been measured for a model angle of incidence $\alpha$= 10° applying pressure probes, [3.6]. The probe with its traversing mechanism inside the model could be positioned in four cross sections, see Fig. 4.2. The probe was traversed normal to the model surface. A three-hole-direction-probe, Fig. 4.3, was used to determine the longitudinal and spanwise velocity components U and V. The static pressure used in the data reduction was measured at the wall and assumed to be constant through the entire boundary layer thickness. Errors could have been revealed here, if thick boundary layers close to separation were investigated.

4.4 Flow field measurements
Mean velocities in the flow field around the model were measured with pressure probes in both wind tunnels. A 10-hole probe was used in the NWG, [4.2.], [3.8], and a five-hole probe in the F1 tunnel, [4.3]. The NWG probe was mounted to a traversing mechanism outside the test section, Fig. 4.4. The probe was traversed in different cross sections on rays perpendicular to the surface of the model at a given circumferential angle $\varphi$, Fig. 4.5.
The ONERA five-hole probe with a diameter of 3 mm was also traversed on rays perpendicular to the model surface, see Figs. 4.6, 4.7.

4.5 Surface flow visualisations
Surface oil flow visualisations have been performed for several angles of incidence and Reynolds numbers. Photos have been taken.

4.6 Flow field visualisations
Some laser light sheet visualisations have been carried out in the F1 tunnel at low Reynolds numbers.

4.7 Tunnel wall measurements
Pressure distributions on the wind tunnel walls (F1) have not been measured.

4.8 Wall shear stress measurements
Surface hot film sensors were applied for the magnitude and direction of the local wall shear stress. Commercially available V-type sensors, originally designed by McCroskey, [4.4], with two mutually perpendicular films, Fig. 4.8, were flush mounted to the model surface in 12 cross sections, Fig. 4.9. The calibration and data reduction procedures are described in [3.3] and [3.4].

## 5. TEST MATRIX AND CONDITIONS

Only some test cases (incidence and Reynolds number combinations) have been selected.

5.1 Detailed test matrix
Number of selected test cases: 3 , see Table I

5.2 Model/tunnel relations
Maximum blockage:
5% at $\alpha$= 30° in NWG
3% at $\alpha$= 30° in F1
Model span/tunnel width:
0.13 in NWG, 0.09 in F1

5.3 Transition details
Measurements have been carried out with free and/or fixed transition. The position of natural transition depending on the angle of incidence, the circumferential angle and the Reynolds number was determined by means of the surface hot film sensors. Fixed transition was applied for $\alpha$= 10° in the NWG at x/L= 0.2. A 20 mm wide carborundum strip with grains of 0.7 mm average diameter was used, cf. Fig 5.1. The effectiveness of the trip was verified by the surface hot film sensor located some 30 mm downstream of the roughness strip, for details see [3.1].

## 6. DATA

6.1 Availability of data
Organisation owning the data:
DLR, Institute for Fluid Mechanics
Bunsenstr. 10, D-37073 Göttingen, Germany
and
ONERA, OA
BP 72, F-92322 Chatillon Cedex, France

Responsable for the data:
Dr. H.-P. Kreplin, DLR, SM-SM
Bunsenstr. 10, D-37073 Göttingen, Germany
Phone +49-(0)551-709-2259
Fax +49-(0)551-709-2829

Are data freely available?
Yes, the data of the three selected test cases are available in connection with this AGARD working group.

6.2 Suitability of data for CFD validation. No corrections have been applied to the data. Free-air computations are possible after standard corrections have been applied. In-tunnel computations are possible using proper boundary conditions (constant pressure for free jet - NWG, straight wall for closed test section - F1).

6.3 Type and form of data

Uncorrected surface pressure coefficients, wall shear stress vectors and velocity vectors, see Table II
data carrier: tape or floppy
Extent of geometry data:
-- (Model geometry is defined analytically)
Extent of aerodynamic data:
6000 pressure coefficients
3600 wall shear stress vectors
20000 velocity vectors

6.4 Corrections
No corrections were applied to the data. As the boundary conditions are known (free jet in NWG, straight solid wall in F1), conventional corrections are possible. Solid blockage effects are estimated to $\Delta U_\infty/U_\infty$ = -0.003 at $\alpha$= 10° and -0.01 at $\alpha$= 30° for NWG and to $\Delta U_\infty/U_\infty$ = 0.018 at $\alpha$= 30° for F1. Lift interference effects are estimated to $\Delta\alpha$= 0.3° in NWG and 0.2° in F1 at $\alpha$= 30°. They are negligible at $\alpha$= 10°.

## 7. DATA ACCURACY AND REPEATABILITY

7.1 Estimate accuracy of
Free stream conditions:
Flow velocity ±0.25% (NWG)
Dynamic pressure ±0.3% (F1)
Model incidence ±0.1°

Measured data:
Pressure coefficients: $\Delta c_p$= ±0.01 (NWG, $U_\infty$= 55 m/s), $\Delta c_p$= ±0.005 (F1, $U_\infty$= 75 m/s, $p_0$= 4 bar)
Wall shear stress: $\Delta c_f/c_f$= ±0.1, $\Delta\gamma_w/\gamma_w$= ±0.1
Velocity: $\Delta U_r/U_\infty$= ±0.01, $\Delta\gamma$< 1 °

7.2 Repeat measurements
Within one campaign only very few repeat measurements (e.g. velocity profiles) were made. In successive campaigns some spot checks of repeat measurements were performed.

7.3 Redundant measurements
Comparison of wall streamlines integrated from surface hot film data and oil flow visulisations. Surface flow angles with surface hot films and 3-hole probe lying on the wall. Velocities in outer part of the boundary layer by 3-hole boundary layer probe and 10-hole/5-hole flow field probe.

7.4 Other tests on same geometry
The F1 model has also been checked in the NWG. Only some surface pressure and wall shear stress measurements were performed. Checks were made running the same Reynolds number and model incidence in both tunnels, NWG and F1, with the respective models. The overall agreement between these checks is taken to be reasonable.

8. REFERENCES

8.1 On the wind tunnels

[1.1] W. Baumert et al.: Der 3-mx3-m-Niedergeschwindigkeits-Windkanal (NWG) der DFVLR in Göttingen (Stand 1988). DFVLR-Mitt. 89-05, 1989.

[1.2] H.U. Meier, U. Michel, H.-P. Kreplin: The influence of wind tunnel turbulence on the boundary layer transition. Perspectives in Turbulence, Eds. H.U. Meier, P. Bradshaw, pp. 26-46, Springer-Verlag, 1987.

[1.3] U. Michel, E. Froebel: Flow unsteadiness in three low-speed wind tunnels. AGARD-CP 429, pp. 13.1-13.10, 1987.

[1.4] J.M. Carrara, A. Masson: Three years of operation of the ONERA pressurized subsonic wind tunnel. 12th ICAS, Munich, 1980.

8.2 On the model

[2.1] H.-P. Kreplin, H.U. Meier, A Maier: Wind tunnel model and and measuring techniques for the investigation of three-dimensional turbulent boundary layers. Proc. 10th AIAA Aerodyn. Testing Conf., San Diego, CA, AIAA 78-781, 1978.

[2.2] H.U. Meier, H.-P. Kreplin: Description of the DFVLR prolate spheroid and its instrumentation. in: AGARD-AR-255 "Calculation of 3d separated turbulent flows in the boundary layer limit", 1990.

8.3 On test and test results

[3.1] H.U. Meier, H.-P. Kreplin, X. Ming: Problems associated with artificial boundary layer transition. AIAA 16th Fluid and Plasma Dynamics Conf., July 12-14, 1983/Danvers,MA, AIAA-83-1673, 1983.

[3.2] H.U. Meier, H.-P. Kreplin, A. Landhäußer: Wall pressure measurements on a 1:6 prolate spheroid in the DFVLR 3m x 3m Low Speed Wind Tunnel ($\alpha$= 10°, $U_\infty$= 55 m/s, artificial transition) - Data Report. DFVLR IB 222-86 A04, 1986.

[3.3] H.-P. Kreplin, H. Vollmers, H.U. Meier: Measurements of the wall shear stress on an inclined prolate spheroid. Z. Flugwiss. Weltraumforsch. 6, pp. 248-252, 1982.

[3.4] H.-P. Kreplin, H. Vollmers, H.U. Meier: Wall shear stress measurements on an inclined prolate spheroid in the DFVLR 3m x 3m Low Speed Wind Tunnel, Göttingen - Data Report. DFVLR IB 222-84 A33, 1985.

[3.5] H.-P. Kreplin, H. Vollmers, H.U. Meier: Wall shear stress measurements on an inclined prolate spheroid in the ONERA F1 Wind Tunnel - Data Report. DFVLR IB 222-84 A34, 1985.

[3.6] H.U. Meier, H.-P. Kreplin, A. Landhäußer, D. Baumgarten: Mean velocity distributions in three-dimensional boundary layers, developing on a 1:6 prolate spheroid with artificial transition ($\alpha$= 10°, $U_\infty$= 55 m/s, cross sections $x_0/2a$= 0.4[illegible] 0.56, 0.64, 0.73) - Data Report. DF[illegible] IB 222-84 A11, 1984.

[3.7] H. Vollmers, H.-P. Kreplin, H.U. M[illegible] Separation and vortical type flow around a prolate spheroid - evaluation of relevant parameters. AGARD-CP 342, pp. 14.1-14.14, 1983.

[3.8] H. Vollmers, H.-P. Kreplin, H.U. Meier, A. Kühn: Measured mean velocity field around a 1:6 prolate spheroid at various cross sections. DFVLR-IB 221-85 A08, 1985

[3.9] AGARD FDP WG 10: Calculation of 3d separated turbulent flows in the boundary layer limit., AGARD-AR-255, 1990.

8.4 On measurement techniques

[4.1] see [2.1], [2.2], [3.2], [3.3], [3.4], [3.6], [3.8]

[4.2] A. Kühn: Strömungsfeldmessungen im 3-m x 3-m- Niedergeschwindigkeitswindkanal (NWG) der DFVLR in Göttingen. DFVLR-Mitt. 85-14, 1985.

[4.3] Y. Brocard, P. Desplas: Methodes d'exploration des ecoulements tourbillonnaires developpes pour la soufflerie F1 (Vortical flow exploration methods developed for the F1 wind tunnel). AGARD-CP 348, pp. 33.1-33.15, 1987.

[4.4] W.J. McCroskey, E.J. Durbin: Flow angle and shear stress measurements using heated films and wires. ASME J. Basic Eng. 94, pp. 46-52, 1972.

## 9. SYMBOLS

| | |
|---|---|
| a,b | main half axes of the prolate spheroid |
| L=2a | model length |
| x, $x_0$ | longitudinal coordinate, axial distance from model nose |
| $x_0,y_0,z_0$ | model oriented coordinates |
| U | longitudinal velocity component |
| V | circumferential velocity component |
| $U_r$ | resultant velocity |
| $U_{re}$ | $U_r$ at boundary layer edge |
| $\gamma$ | cross flow angle |
| $U_\infty$ | free stream velocity |
| $q_\infty$ | free stream dynamic pressure |
| Re | Reynolds number based on model length |
| Ma | Free stream Mach number |
| $c_f = \tau_w/q_\infty$ | skin friction coefficient |
| $c_p$ | pressure coefficient |
| $\alpha$ | model angle of incidence |
| $\delta_{1r}$ | displacement thickness of resultant velocity |
| $\varphi$, $\Phi$ | circumferential model angle |
| $\tau_w$ | wall shear stress (magnitude) |
| $\gamma_w$ | wall shear stress angle |

Table I: Test matrix and conditions

| IDENTIFICATION | | FLOW CONDITION | | | POSITION | OTHER INFORMATION | | |
|---|---|---|---|---|---|---|---|---|
| CASE NO. | CONF. | Ma | $q_\infty$ kPa | $Re_L$ x $10^{-6}$ | $\alpha$ ° | Type of measurements | Tunnel | Transition |
| 1 | A | 0.16 | 1.75 | 7.7 | 10 | a,b,c | NWG | tripped |
| 2 | A | 0.13 | 1.2 | 6.5 | 30 | a,b,d | NWG | free |
| 3 | B | 0.23 | 12.0 | 43 | 30 | a,b,d | F1 | free |

Legend:

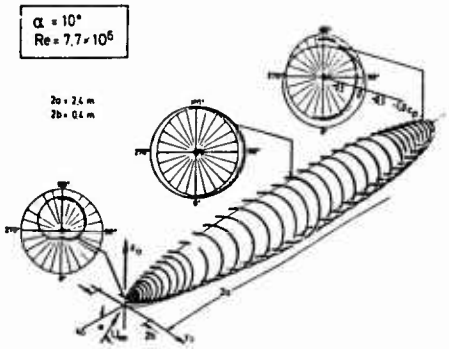
Configuration:
A= NWG-model
B= F1-model

Type of measurement:
a= surface pressures
b= wall shear stress vectors
c= velocity vectors in boundary layer
d= velocity vectors in flow field

Tunnel:
NWG= Low speed tunnel, DLR Göttingen
F1 = F1 pressurized low speed tunnel, ONERA

Table II: Data availability

| Data | Engin. units | Coefficients | Normalized | Uncorrected | Corrected |
|---|---|---|---|---|---|
| Freestream conditions | X | | | X | |
| Surface pressures | | X | | X | |
| Skin friction | | | X | X | |
| Forces | | | | | |
| Boundary layer data | | | X | X | |
| Wake data | | | | | |
| Flow field data | | | X | X | |
| Test section wall pressures | | | | | |



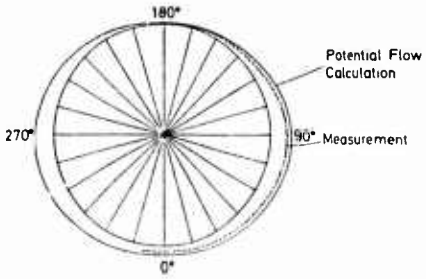




Fig. 1.1: Surface pressure distributions, α= 10 °, fixed transition, NWG

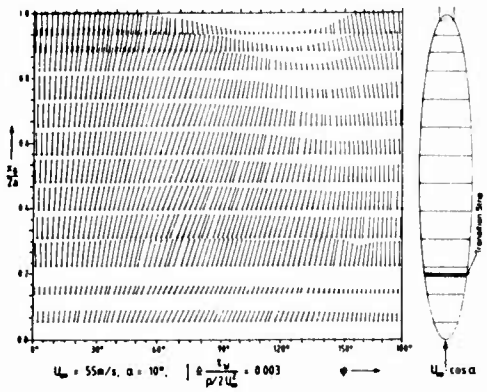



Fig. 1.2: Wall shear stress distributions, α= 10 °, NWG

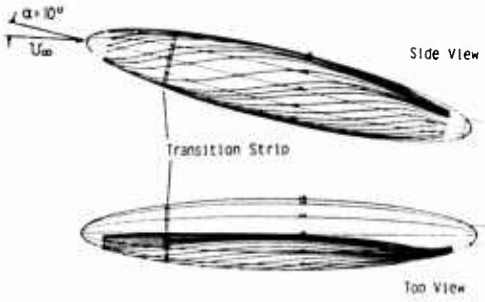



Fig. 1.3: Limiting (wall) streamlines, α= 10 °, U∞= 55 m/s, NWG

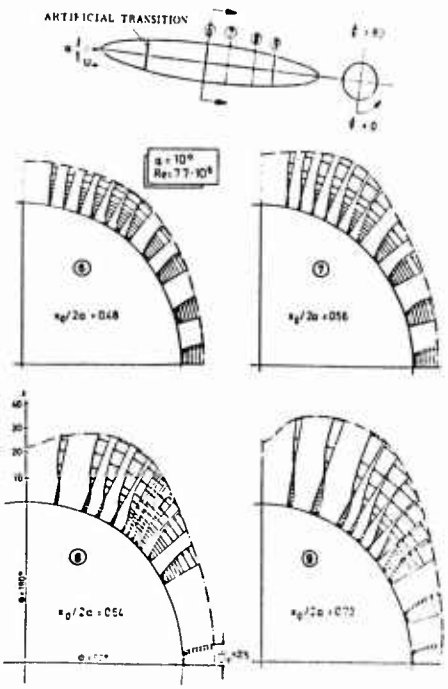



Fig. 1.4: Crossflow profiles of mean velocity in the 3d boundary layer, α= 10 °, NWG

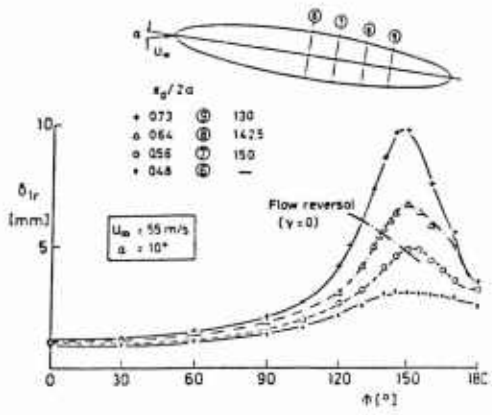



Fig. 1.5: Development of the three-dimensional boundary layer displacement thickness, α= 10 °, artificial transition at $x_0$= 0.2, NWG

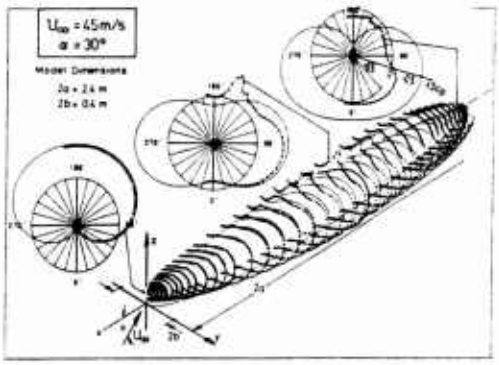



Fig. 1.6: Surface pressure distributions, α= 30 °, NWG

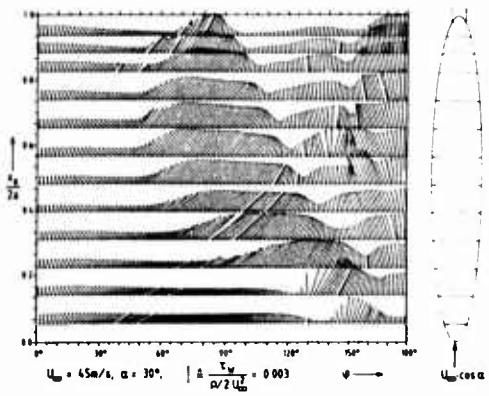


Fig. 1.7: Wall shear stress distributions, α= 30 °, NWG

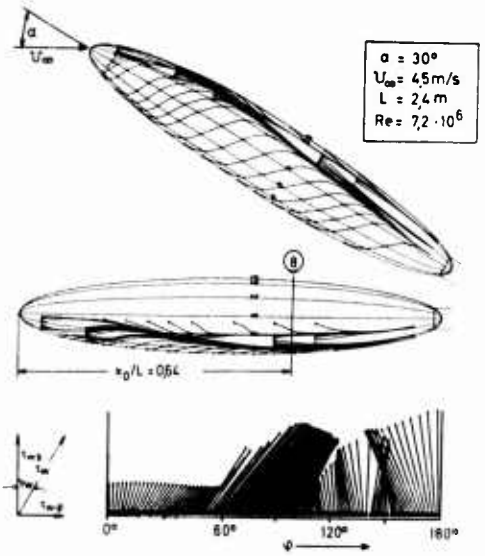



Fig. 1.8: Limiting (wall) streamlines, α= 30 °, NWG

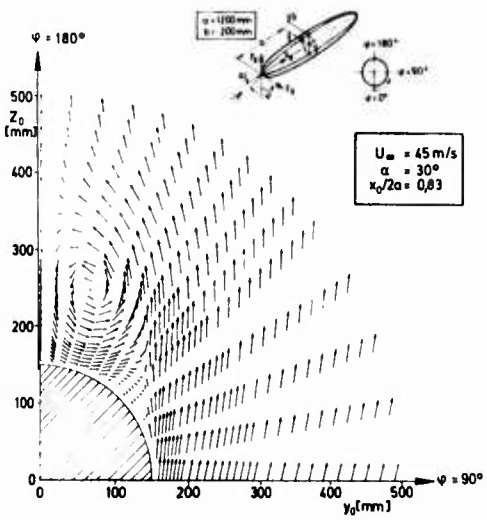



Fig. 1.9: Crossflow velocity vectors showing leeside vortices, α= 30 °, NWG

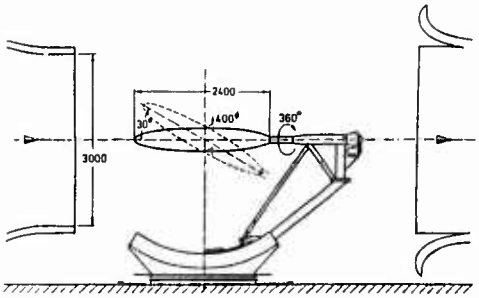



Fig. 3.1: Prolate spheroid model in the DLR 3mx3m Low Speed Wind Tunnel, Göttingen (NWG)

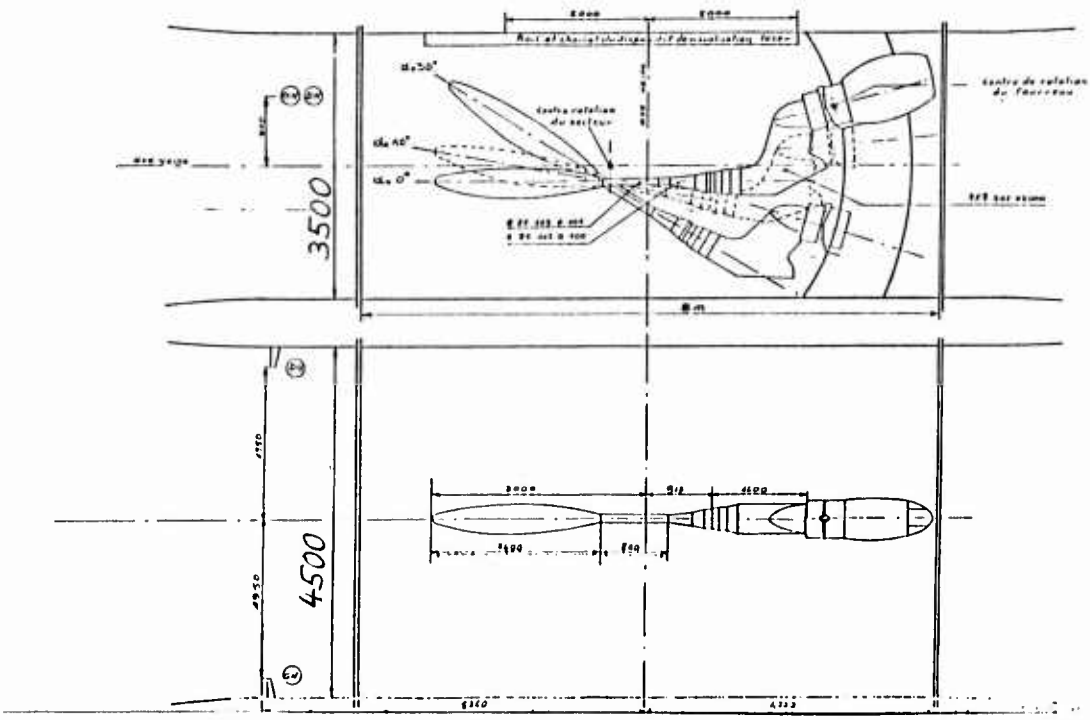



Fig. 3.2: Dimensions of the support of the prolate spheroid model in the ONERA F1 Tunnel

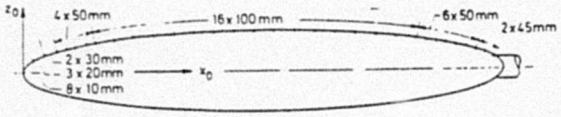



Fig. 4.1: Arrangement of the pressure taps on the prolate spheroid model

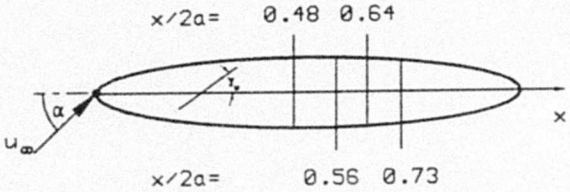



Fig. 4.2: Cross sections of boundary layer measurements

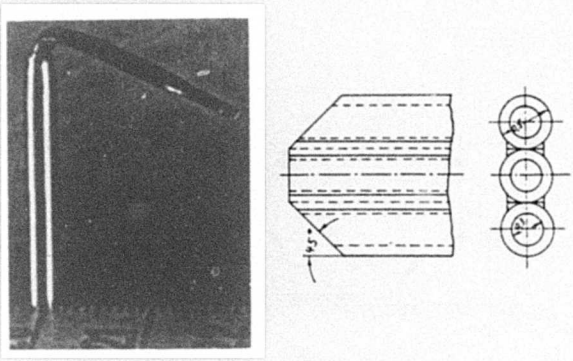
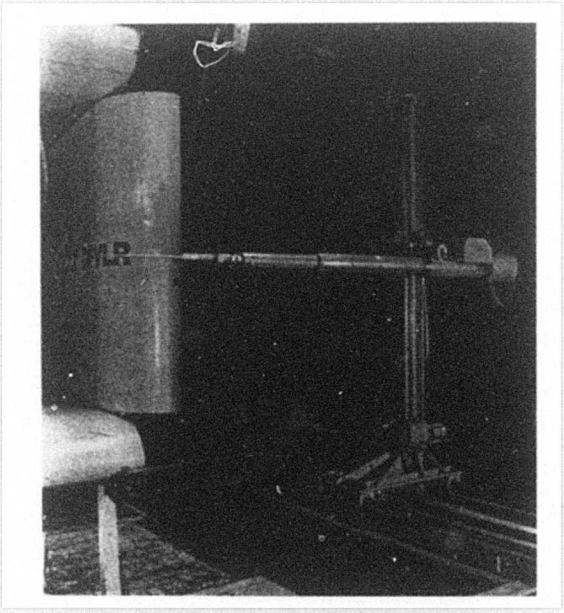


Fig. 4.3: Three-hole direction probe for boundary layer measurements



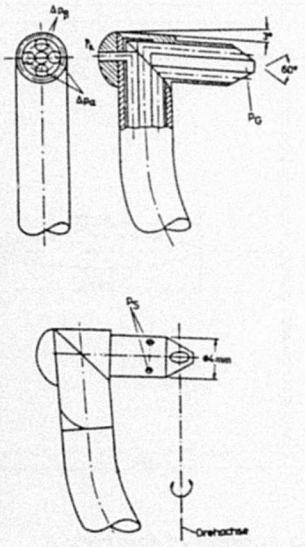



Fig. 4.4: 10-hole direction probe and traversing mechanism (NWG)

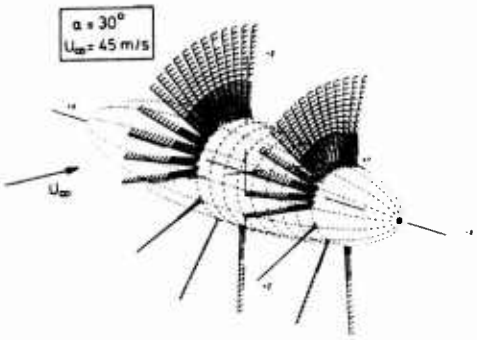



Fig. 4.5: Cross sections of flow field measurements (NWG)

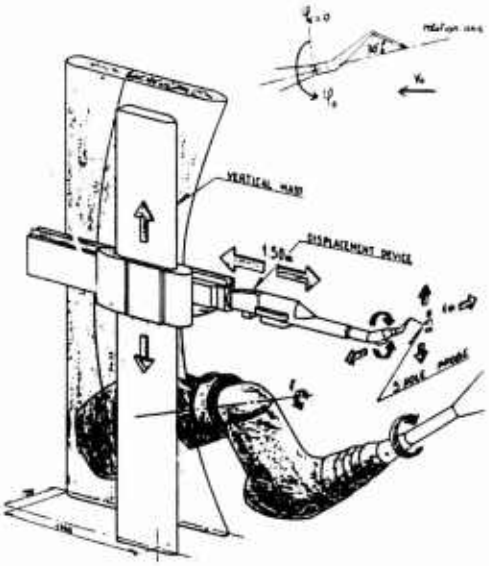
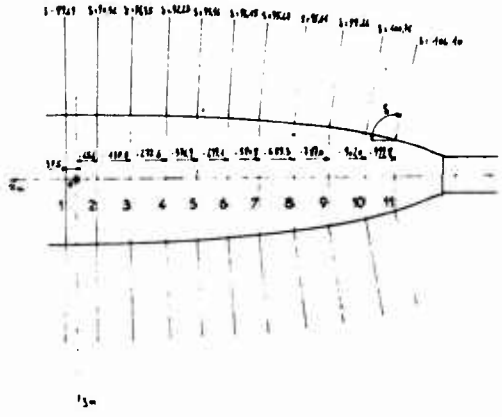



Fig. 4.6: Traversing mechanism of five hole probe mounted on the vertical mast (F1)



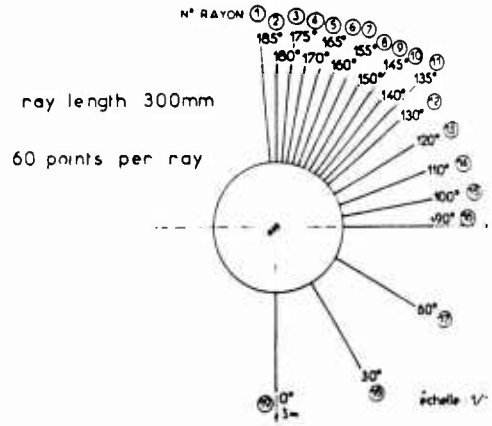




Fig. 4.7: Cross sections and rays for flow field measurements (F1)

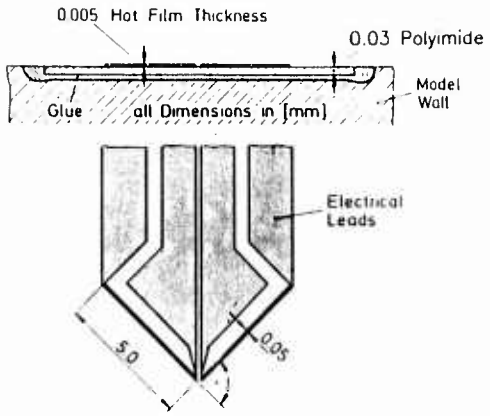



Fig. 4.8: V-type surface hot film sensor

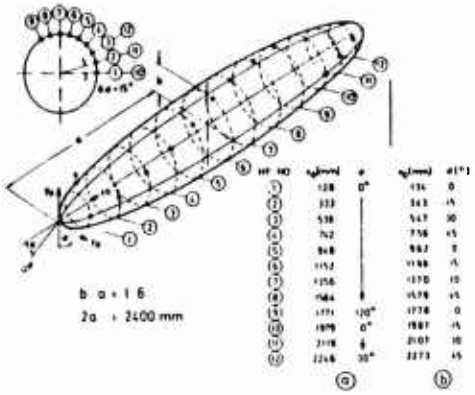
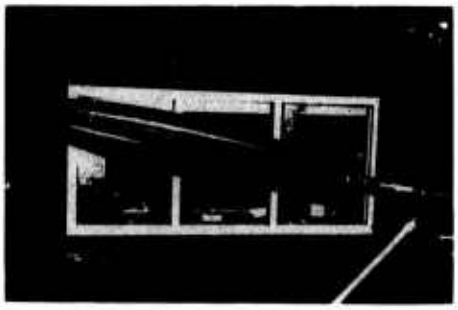



Fig. 4.9: Locations of the surface hot film sensors in different cross sections on the prolate spheroid models used in NWG (a) and F1 (b) tunnels



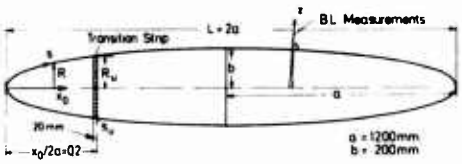



Fig. 5.1: Prolate spheroid model in NWG with transition strip

# Force and pressure data of an ogive-nosed slender body at high angles of attack and different Reynolds numbers

by

K. Hartmann

Deutsche Forschungsanstalt für Luft- und Raumfahrt e.V.
DLR

D-37073 Göttingen, Germany

## Introduction

At high angles of attack the air flows around missile configurations are dominated by the phenomenon of symmetric and asymmetric flow separation on the geometrical components of body-wing-tail combinations. Different kinds of vortex pattern occur. They cause three-dimensional flow fields which are extremely complex. The boundary layers are mainly transitional and/or of the turbulent type. An exclusively theoretical treatment of such flow fields is at present and probably in the near future not possible. From this fact arises the need of systematic experimental investigations in order to contribute to the understanding of the observed fluid mechanic phenomena. In addition, a data base is required for the improvement or development of semiemperical prediction methods and also for the modelling of flows to establish theories. Computer codes, based on solutions of the Euler or Navier-Stokes equations, can be validated by comparison with the experimental data.

For the conceptual design of missile systems fast and inexpensive engineering prediction methods are required which provide highly accurate preliminary estimates of aerodynamic performance, stability and control. The most commonly used type of such methods for this purpose is the so-called component build up method which adds up the forces acting on each individual component of a missile (body, wing, tail) and takes into account interference loads. In this connexion the body of a missile, mostly of a circular cross-section, is the most complicated component because the positions of the separation lines are not known a priori, because of the absence of sharp edges, but evolve from the interaction between the boundary layer and the outer flow. This causes a strong Reynolds number dependence. In certain regions of angles of attack the asymmetric flow separation leads to large lateral forces with random directions.

In order to obtain the required experimental data base, force and moment, flow field and pressure measurements (steady and unsteady) were carried out on an ogive-nosed circular cylinder body with a smooth surface. The tests were performed in the two open jet low speed wind tunnels of the DLR in Göttingen (NWG, test section size 3 m x 3 m) and in Braunschweig (NWB, test section size 2.8 m x 3.25 m). A body diameter of D = 200 mm was chosen to achieve Reynolds numbers as high as possible at the maximum speed in these tunnels. The tests comprise angles of attack from 0° to 90° and Reynolds numbers of $2.5 \times 10^5$, $3.7 \times 10^5$ and $7.7 \times 10^5$ (based on body diameter and free-stream conditions). For six angles of attack between 20° and 70° the dependence on different roll positions of the body was systematically investigated with a complete coverage of 360°. In some cases the turbulence level of the free-stream was varied.

The body vortices were visualized in a water towing tank using hydrogen bubbles and in the wind tunnel with the aid of smoke and a laser light sheet.

## 1. GENERAL DESCRIPTION

### 1.1 Model name

Ogive circular-cylinder body

### 1.2 Model type and flow conditions

Slender ogive-nosed body. Incompressible subsonic flow

### 1.3 Purpose of test

Force and pressure distribution measurements to create a data base and to contribute to the understanding of the flow separation and the very complex 3D-vortex flows

### 1.4 Dominant flow physics

Laminar, transitional and turbulent boundary layers, symmetric and asymmetric flow separation with subsequent formation of lee-side vortices with either symmetric or asymmetric pattern and corresponding lateral forces with random sign at zero yaw. Dependence on Reynolds number and body roll position. Nonlinear characteristic of the forces as function of angle of attack.

## 2. DETAILS OF MODELS

### 2.1 General geometric arrangement

Isolated ogive-nosed slender body with circular cross-section

2.2 Specific features

Configuration A: model for pressure distribution measurements with a length to diameter ratio of 14 (Figure 1)
Configuration B: model for force measurements with a black, smooth surface and a length to diameter ratio of 11 (Figure 2)

2.3 Body data

Nose shape is a tangent ogive with a fineness ratio of 3. Contour equation, Figure 1.
Afterbody of circular cross-section is 8 diameters long (force model) or 11 diameters long (pressure model). Total length is 11 diameters or 14 diameters, respectively.

2.4 Geometric definition

The shape is analytically specified. The surface of the force model is polished, the surface of the pressure model is smooth with an average roughness of .001 mm. Contour deviations are negligible due to the large size of the model

2.5 Model supports

Central rear stings, four different supports; Figures 2 to 4. Support IV not shown in a sketch, because not relevant for the selected test cases. For further detailed geometrical information request drawings No. 12-1-033-00 and 12-1-033-02 from DLR

## 3. GENERAL TUNNEL INFORMATION

3.1 Tunnel designations

a.) 3 m x 3 m low speed wind tunnel NWG at DLR in Göttingen, References 8.1.1
b.) Low speed wind tunnel NWB at DLR in Braunschweig, Reference 8.1.3

3.2 Organization running the tunnels

Deutsche Forschungsanstalt für Luft- und Raumfahrt e.V., DLR, Hauptabteilung Windkanäle

3.3 Tunnel characterstics

a.) NWG, continuously working wind tunnel. Open jet test section with a cross-section size of 3 m x 3 m and a length of 6 m. Maximum speed is 65 m/s
b.) NWB, facility with a closed return circuit comprising an open jet and a closed test section, the cross-section being 3.25 m x 2.80 m. Maximum speed is 90 m/s in the closed tost section and 75 m/s in the open jet. Tests were conducted in the open jet test sections

3.4 Test section

3.4.1 Model mounting

Central stings, Figures 2 to 4

3.4.2 Test section dimensions

Göttingen tunnel NWG 3m x 3m x 6m
Braunschweig tunnel NWB 3.25m x 2.8m x 6m

3.5 Freestream conditions

3.5.1 Reference flow conditions

Total pressure and temperature in settling chamber, ambient (atmospheric) pressure and total temperature

3.5.2 Tunnel calibration

Multi hole probe, long cylindrical probe, thermocouples, hot wires;
Date of last calibration:
1985 for NWG, Göttingen tunnel
1988 for NWB, Braunschweig tunnel

3.6 Flow quality (empty tunnel)

3.6.1 Flow uniformity

NWG: Variation of dyn. pressure ± 0.5% within test section. Variation of static pressure along test section center line is less than ± 1.5% of the dyn. pressure. Flow angularity is less than 0.25° on the test section center line. It was determined by a ten-hole directional probe
NWB: Variation of dyn. pressure ± 0.2%. Variation of static pressure along test section center line is less than 1% of the dyn. pressure. Flow angularity is less than 0.15°

3.6.2 Temperature variation

Temperature cannot be controlled. It increases slightly with running time over a long period.

3.6.3 Flow unsteadines

See Figures 5 and 6

## 4. INSTRUMENTATION

4.1 Model position

4.1.1 Geometrical incidence

Support positions changed by electric step motors. Positions determined by potentiometers.
$\alpha = 0°$ position set by spirit level.
$\beta = 0°$ position set by geometric markings related to nozzle geometry. Sting deflection determined by calibration.

4.1.2 Accuracy of geometrical incidence

$\Delta\alpha$ less than ± 0.1°

4.2 Model pressure measurements

4.2.1 Total number and disposition of pressure holes

A total of 360 pressure holes, 0.5 mm in diameter, are arranged in 15 cross-sections, Figure 1

4.2.2 Range and accuracy of pressure transducers

$\pm$ 7 x $10^3$ N/m$^2$, model PDCR 22 of Druck Ltd. England
$\pm$ 0.06% full scale

4.2.3 Dynamic pressures

Measured with Kulite transducers mounted directly below the model surface at cross-sections x/D = 5 and 11; 16 transducers in each cross-section

4.3 Force and moment measurements

4.3.1 Type and location of balance

6 component internal strain gauge balance 1.5" MK XVI TASK Corporation, USA

4.3.2 Maximum load range and accuracy of components

| | |
|---|---|
| normal force | N = 906 kp |
| side force | Y = 407 kp |
| axial force | A = 59 kp |
| pitching moment | m = 30 mkp, N = 0 |
| yawing moment | n = 10 mkp, Y = 0 |
| rolling moment | l = 14 mkp |

$\pm$1‰ full scale

4.4 Flow field measurements

9-hole pressure probe. Flow field in three crossflow planes at different turbulent levels, the latter varied by a grid.

4.5 Flow field visualization

4.5.1 Techniques applied

Laser light sheet and smoke. Hydrogen bubbles in water

4.5.2 Visualized planes

Planes of cross-section at x/D = 1, 2, 3, 4, 5, 6, 6.5, 7, 8 and 10;
Top view and side view of the 3-D vortices (stereo-photos)

4.5.3 Data availability

Video tape and photos (upon request)

## 5. TEST MATRIX AND CONDITIONS

5.1. Detailed test matrix

5.1.1 Number of selcted test cases

4 (corresponding to Figures 7 to 15), proposed test cases are the cases 2, 3, 5 and 6 of Table I.

5.1.2 Number of configurations tested

3; pressure model, 14 diameters long
force model, 11 diameters long.
plexiglass model for flow visualizations

5.1.3 Table of test matrix

Table I (complete data base)

5.2 Model / tunnel relations

Blockage up to $\alpha$ = 45° is less than 1%.
Blockage increases to 10% if $\alpha$ = 90° and model plan view area is related to cross-section of the undisturbed open jet = cross-section of nozzle exit minus mixing zone area
For the tests at angles of attack $\alpha$ > 45° the support III was positioned at a lower level below the test section so that the pressure instrumented part of the model from the nose tip towards the rear could be kept in the undisturbed region of the open jet

5.3 Transition details

All tests carried out with free transition. Natural transition location can be found approximately from the $c_p$-distributions when compared with the characteristics of the 2-D circular cylinder (also see Figure 8)

## 6. DATA

6.1 Availability of data

6.1.1 Organisation owning the data

DLR, Institute of Experimental
FLuid Mechanics
Bunsenstr. 10
D-37073 Göttingen, Germany

6.1.2 Who is responsible for the data

Dr.-Ing. K. Hartmann
DLR, SM-ES
Bunsenstr. 10
D-37073 Göttingen, Germany
Phone 49 - 551 - 709 - 2255
Fax 49 - 551 - 709 - 2811

6.1.3 Are data freely available

Yes

6.2 Type and form in which data are available

6.2.1 Type and form

Uncorrected force, moment and pressure coefficients

6.2.2 Data carrier

Printed lists, see Ref. 8.3.2
Computer tape, floppy disk 3 1/2"
Video tape, see Ref. 8.3.5

6.2.3 Extent of geometry data

No data are necessary, see Figure 1

6.2.4 Extent of aerodynamic test data

1440 local force coefficients
6480 $c_p$-values
468 overall force coefficients
3444 velocity components

6.3 Corrections applied to data

No corrections were applied:
Conventional corrections are partly possible, because boundary conditions (open jet in both wind tunnels) are known. For standard correction methods see Reference 8.1.8. The maximum solid blockage effect was estimated to $\Delta V_\infty/V_\infty = -0.0343$.

## 7. DATA ACCURACY AND REPEATABILITY ASSESSMENT

7.1 Estimated accuracy of:

7.1.1 Freestream conditions

Flow velocity $V_\infty \pm 0.25\%$

Model incidence $\Delta\alpha < \pm 0.1°$, geometrical

7.1.2 Measured data

Pressure coefficients $\Delta c_p$: 0.01

Force and moment coefficients
More inaccurate than the pressure coefficients, because a very rigid strain gauge balance had to be used. The high load range of this balance was not utilized by the relatively small static aerodynamic forces.
normal force ± 1%
side force ± 4%
axial force ± 3%
pitching moment ± 2%
yawing moment ± 7%
All values mentioned above are related to individual maximum measured steady forces or moments, respectively

Flow field data
Amount of the velocity components: less than ± 0.25 % of $V_\infty$. Flow direction of the vector components in the measuring plane (Fig. 15): $\Delta\alpha$ and $\Delta\beta$ less than 0.1° at velocities greater than 20 m/s, but increasingly higher at smaller velocities.

7.2 Repeat measurements

7.2.1 Type and number within one test campaign

Pressure measurements were repeated for one flow condition at 6 different sampling rates.
Pressure measurements were repeated 5 times at the same sampling rate at nominally the same flow conditions. Between these repeats the tunnel was each time stopped and started again, Figure 8

7.2.2 Type and number in a successive campaign

Pressure measurements with the same model in another tunnel at nominally the same flow conditions. See Figures 9 and 10, showing local force distributions as derived from pressure measuments.

## 8. References

8.1 Wind tunnel, Water towing tank

8.1.1 Werner Baumert et al.

Der 3 m x 3 m - Niedergeschwindigkeits-Windkanal (NWG) der DLR in Göttingen (Stand 1988)
DFVLR-Mitt. 89-05, 1989

8.1.2 Arnulf Kühn

Strömungsfeldmessungen im 3m x 3m Niedergeschwindigkeits-Windkanal (NWG) der DFVLR in Göttingen
DFVLR-Mitt. 85-14, 1985

8.1.3 Gerhard Kausche, Horst Otto, Dietmar Christ und Rüdiger Siebert

Der Niedergeschwindigkeits-Windkanal der DFVLR in Braunschweig
DFVLR-Mitt. 88-25, 1988

8.1.4 Rüdiger Siebert

Druckmeßtechnik in der Hauptabteilung Windkanäle der DFVLR (Stand 1988)
DFVLR-Mitt 88-11, 1989

8.1.5 E. Fröbel

Vergleichende Turbulenzmessungen in Großwindkanälen
DFVLR IB 357 - 75/1

8.1.6 U.Michel and E. Fröbel

Aerodynamic Data Accuracy and Quality: Requirements and Capabilities in Wind Tunnel Testing
AGARD Conference Proceedings No. 348, 1988

8.1.7 Hans Bippes and Pavle Colak-Antic

Der Wasserschleppkanal der DFVLR in Freiburg i.Br., ZFW 21, Heft 4, 1973, S. 113 - 120

8.1.8 H.C.Garner, E.W.E. Rogers, W.E.A. Acum and E.C. Maskell

Subsonic Wind Tunnel Wall Corrections
AGARDograph 109, October 1966

8.2 The models, see Reference 8.3

8.3 Test results

8.3.1 Klaus Hartmann

Einfluß der Reynoldszahl und der Windkanalturbulenz auf die aerodynamischen Beiwerte von Flugkörperrümpfen bei Anstellwinkeln bis zu 90°
DFVLR IB 222 - 84 A 30, 1986

8.3.2 Klaus Hartmann

Pressure and force distributions on an ogive-nosed circular cylinder at high angles of attack in an incompressible airstream
DFVLR IB 222 - 83 A 05, 1983
DFVLR IB 222 - 83 A 05a; data lists, part I, 1983
DFVLR IB 222 - 83 A 05b; data lists, part II, 1983

8.3.3 Hartmut Holst

Strömungsfeldmessungen an einem Flugkörperrumpf bei hohen Anstellwinkeln
- Ergebnisdiagramme -
DFVLR IB 157 - 78 A 11, 1979,

8.3.4 Hartmut Holst

Strömungsfeldmessungen an einem Flugkörperrumpf bei hohen Anstellwinkeln
- Listenbericht -
DFVLR - IB 157 - 78 A 12, 1979

8.3.5 Jürgen Kompenhans und Klaus Hartmann

Strömungssichtbarmachung an einem hochangestellen Ogivkreiszylinderrumpf mit Hilfe der Laser-Lichtschnittmethode
DFLVR - FB 86-45, 1986

8.3.6 Werner Hastreiter

Druckmessungen an einem Kreiszylinder-Rumpf mit Ogivalspitze
DFVLR - IB 19111 - 83 C 19

Teil I: Diagramme für $\alpha$ = 0° bis 35°

Teil II: Diagramme für $\alpha$ = 35° bis 60°

Teil III: Diagramme für $\alpha$ = 65° bis 85°

Teil IV: Diagramme für $\alpha$ = 90°

Teil V: Ergebnistabellen für Versuchsnr. 1 bis 232

Teil VI: Ergebnistabellen für Versuchsnr. 325 bis 565

## 9. Symbols

| | |
|---|---|
| A, B | Designation of configuration |
| CM | Pitching moment coefficient, based on $q_\infty$, body base area and body diameter. Reference point=body nose tip |
| CN | Yawing moment coefficient, based on $q_\infty$, body base area and body diameter. Reference point=body nose tip |
| $C_Y$, CY | Overall side force coefficient, based on $q_\infty$ and body base area. |
| $C_Z$, CZ | Overall normal force coefficient, based on $q_\infty$ and body base area. |
| $(c_Y)_\ell$, CYL3 | Local side force coefficient, based on $q_\infty$ and reference area D × unit length |
| $(c_Z)_\ell$, CZL3 | Local normal force coefficient, based on $q_\infty$ and reference area D × unit length |
| $c_p$ | Pressure coefficient, $(p - p_\infty)/q_\infty$ |
| D | Body diameter |
| L | width of nozzle exit, reference length |
| MR | Number of series |
| MP | Serial number within one series |
| NWB | Designation of low speed tunnel in Braunschweig |

| | |
|---|---|
| NWG | Designation of low speed tunnel in Göttingen |
| p | Pressure on model surface |
| $p_\infty$ | Freestream static pressure |
| $q_\infty$,Q | Freestream dynamic pressure, $\rho_\infty/2V_\infty^2$ |
| R | Maximum body radius |
| $Re_D$, RE, RED | Reynolds number, based on body diameter D |
| r (x) | Local body radius |
| Tu | Turbulence level |
| Tux | Turbulence level in x-direction |
| Tuy | Turbulence level in y-direction |
| Tuz | Turbulence level in z-direction |
| $U_\infty$ | Freestream velocity |
| u', v', w' | Fluctuating part of velocity components in x-, y- and z-direction, respectively |
| $V_{yz}$ | Velocity component in the cross-flow plane yz |
| $V_\infty$, V | Freestream velocity |
| v' | Fluctuating part of velocity component in y-direction |
| w' | Fluctuating part of velocity component in z-direction |
| x, y, z | Cartesian coordinates, see Figures 5, 8 and 9 |
| $\alpha$, ALFA, ALPHA | Angle of attack |
| $\rho_\infty$ | Freestream density |
| $\Phi$, PHI | Roll position of body |
| $\Theta$, THETA | Angle of circumference in body cross-sections, measured from stagnation point (line), independent of roll position. |

Table I: Test Matrix and Conditions

| IDENTIFICATION | | FLOW CONDITION | | | POSITION | | OTHER INFORMATION | |
|---|---|---|---|---|---|---|---|---|
| CASE NO. | CONF. | $V_\infty$ $[\frac{m}{s}]$ | $q_\infty$ [kPa] | $Re_D$ x $10^{-5}$ | $\alpha$ | $\Phi$ | Type of measurements | Remarks |
| 1 | A | 20 | 0.4 | 2.5 | $\alpha_1$ | $\Phi_1$ | a, NWG | Fig 13 |
| 2 | A | 20,60 | 0.4;2.2 | 2.5;7.3 | $\alpha_2$ | $\Phi_2$ | | Fig.14+15 |
| 3 | A | 20,30,60 | 0.4;0.55;2.2 | 2.5;3.8;7.4 | $\alpha_3$ | $\Phi_1$ | a,NWG,NWB | Fig.16 to 21 |
| 4 | A | 30,60 | 0.55;2.2 | 4;7.1 | $\alpha_4$ | $\Phi_1$ | b,NWG | Fig.24 to 31 |
| 5 | B | 20,57 | 0.4;2 | 2.6;7.6 | $\alpha_5$ | $\Phi_1$ | c,NWG | Fig.32 |
| 6 | B | 20 | 0.4 | 2.6 | $\alpha_6$ | $\Phi_1$ | d,NWG | Fig.33 |
| 7 | C | 0.7 | 0.0053 | 0.05 | $\alpha_7$ | $\Phi_1$ | e,WSG | Fig.34 |
| 8 | A | 20 | 0.4 | 2.5 | $\alpha_2$ | $\Phi_1$ | f,NWB | Fig.35 |

Legend:

**1. Configuration:**

A = pressure model, aluminium

B = force model, aluminium, coated with a black paint

C = plexiglass model

**2. $\alpha$ range:**

$\alpha_1$ = 50°, 55°

$\alpha_2$ = 55°

$\alpha_3$ = 30°, 35°, 50°, 55°, 90°

$\alpha_4$ = 35°, 37.5°, 90°

$\alpha_5$ = -5° to 90°, with $\Delta\alpha_5$ = 2.5°

$\alpha_6$ = 30°

$\alpha_7$ = 30°, 50°, 80°

**3. Roll position:**

$\Phi_1$ = 0°

$\Phi_2$ = 0° to 360°, with $\Delta\Phi_2$ = 30°

**4. Type of measurement:**

a = static pressure distribution measurements via pressure taps and PSI pressure modules

b = dynamic pressure measurements via pressure taps and Kulite pressure transducers

c = overall force and moment measurements with a 6-component strain gauge belance

d = flow field meausrements with a 9-hole pressure probe

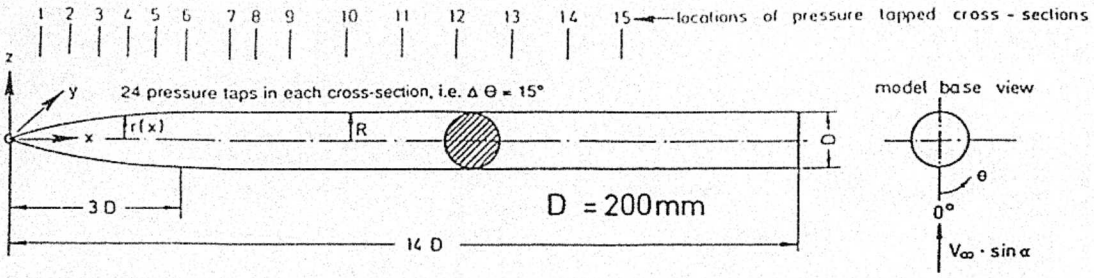
e = flow visualization in a water towing tank by means of hydrogen bubbles

f = flow visualization by smoke and a laser light sheet

NWG = 3 m x 3 m low speed wind tunnel in Göttingen

NWB = 3.25 m x 2.8 m low speed wind tunnel in Braunschweig

WSG = Water towing tank in Göttingen




coordinates of pressure tapped cross-sections:

| cross-section | 1 | 2 | 3 | 4 | 5 | 6 | 7 | 8 | 9 | 10 | 11 | 12 | 13 | 14 | 15 |
|---|---|---|---|---|---|---|---|---|---|---|---|---|---|---|---|
| $\frac{x}{D}$ | 0.525 | 1.025 | 1.525 | 2.025 | 2.525 | 3.025 | 3.775 | 4.225 | 4.825 | 5.825 | 6.825 | 7.825 | 8.825 | 9.825 | 10.825 |

contour of model nose: $\frac{r(x)}{D} = 0.309840 \cdot \left(\frac{x}{D}\right) - 0.039867 \cdot \left(\frac{x}{D}\right)^2 - 0.002615 \cdot \left(\frac{x}{D}\right)^3$

Fig. 1: Model geometry and positions of pressure tapped cross-sections

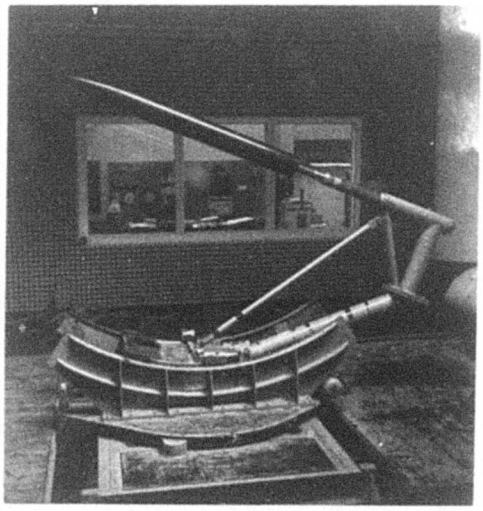
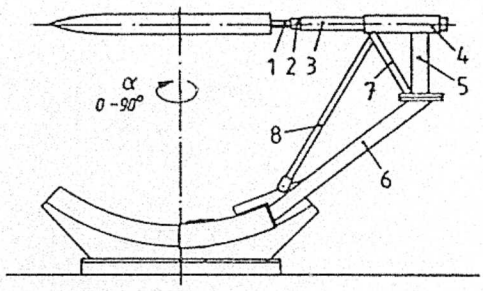


Fig. 2: Model for force measurements on sting support I in the open jet test section of the DLR's 3m x 3m low speed wind tunnel NWG in Göttingen




measures of support I:

| part | 1 | 2 | 3 | 4 | 5 | 6 | 7 | 8 |
|---|---|---|---|---|---|---|---|---|
| lenght [mm] | 175 | 110 | 600 | 750 | 600 | 1500 | 700 | 1750 |
| diameter [mm] | 60 | 85 | 115 | 175 | 175 | 150 | 75 | 60 |

Fig. 3: Geometrical details of model support I

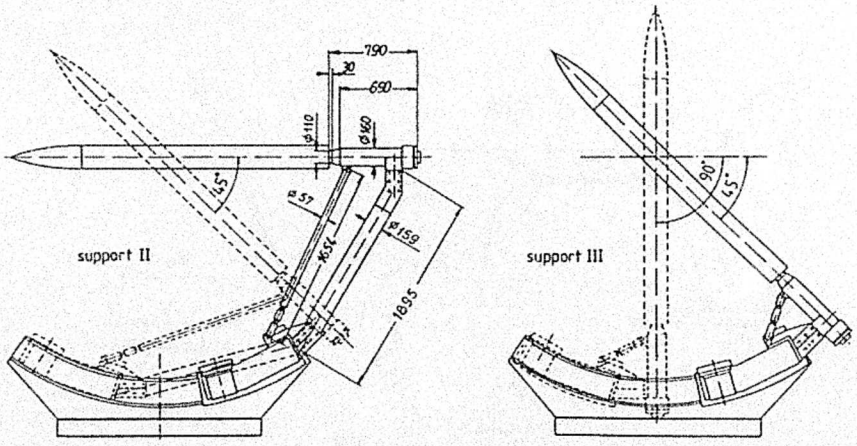



Fig. 4: Model for pressure measurements on sting support II (α-range from 0° to 45°) and sting support III (α-range from 45° to 90°)

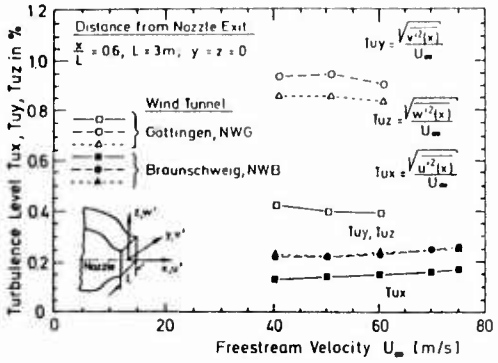



Fig. 5: Turbulence levels of the DLR's low speed wind tunnels in Braunschweig and Göttingen as function of the freestream velocity; according to U. Michel and E. Fröbel, DLR, SM-ES-BE

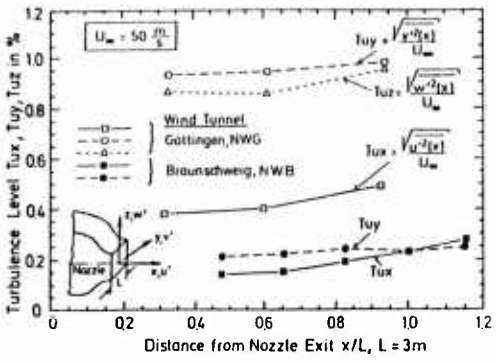



Fig. 6: Turbulence levels of the DLR's low speed wind tunnels in Braunschweig and Göttingen as function of the distance from nozzle exit; according to U. Michel and E. Fröbel, DLR, SM-ES-BE

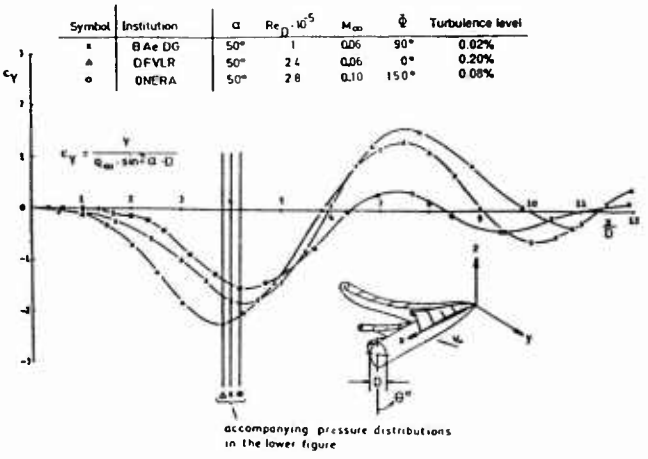



Fig. 7: Comparison of local side force distributions from BAe, DLR and ONERA

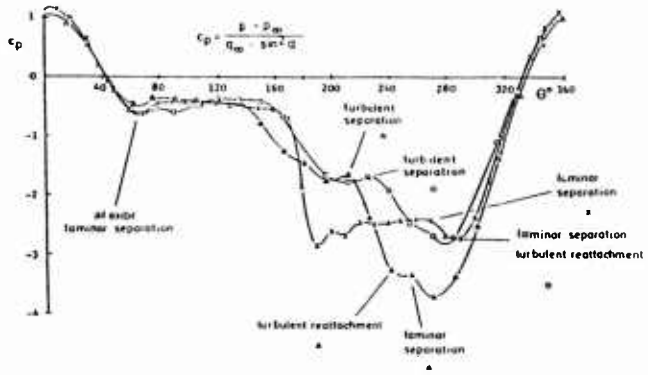



Fig. 8: Pressure coefficient distributions and important features. See indication in Fig. 7

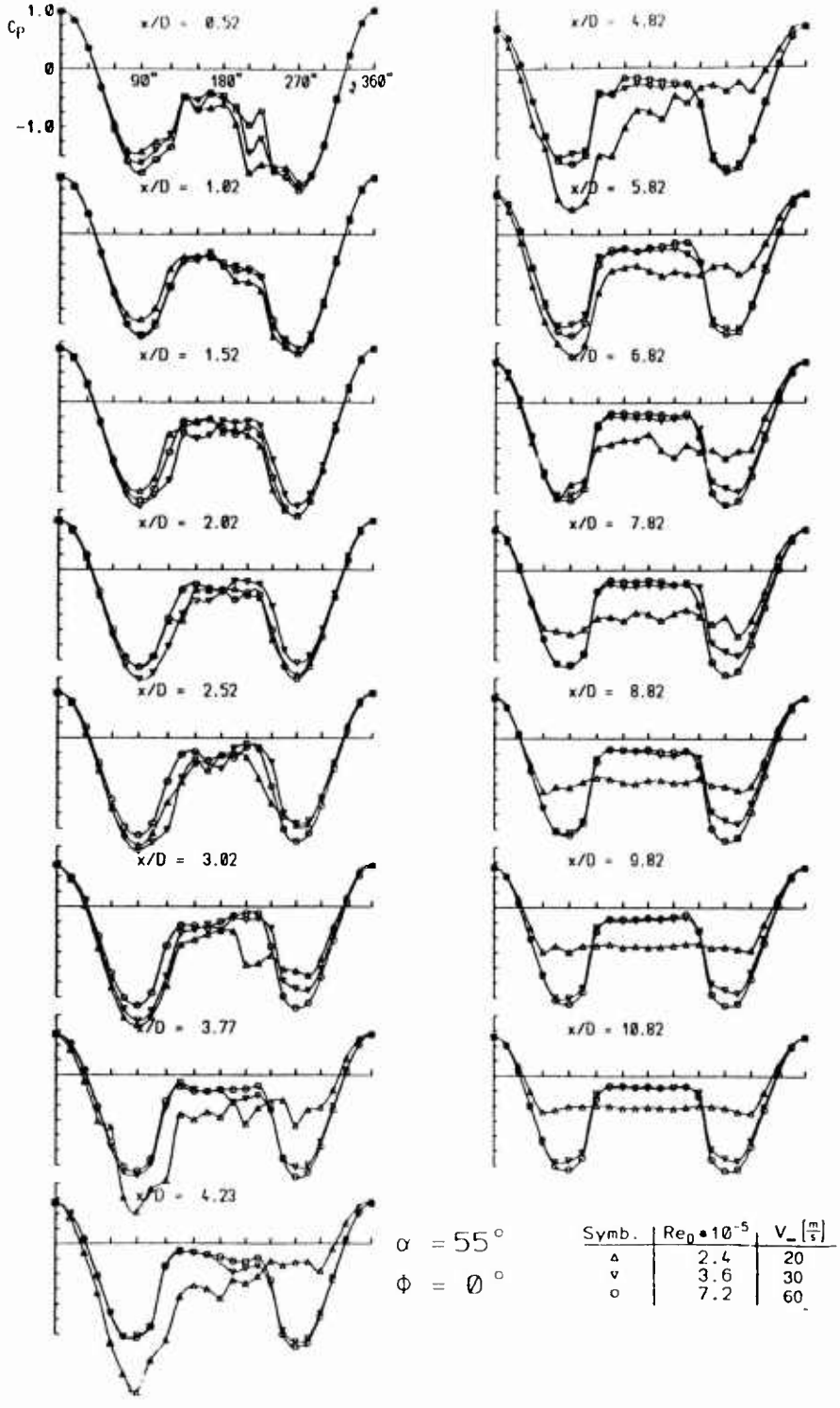



Fig. 9: Pressure distributions in 15 cross sections along the model. Results from the low speed wind tunnel NWG in Göttingen

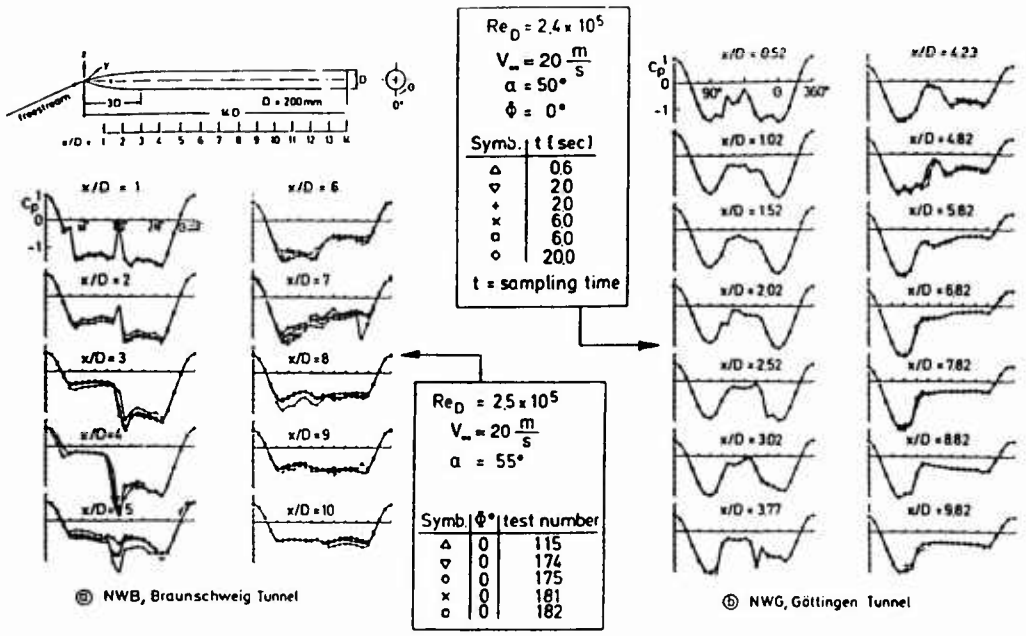



Fig. 10: Demonstration of the repeatability of the static pressure measurements

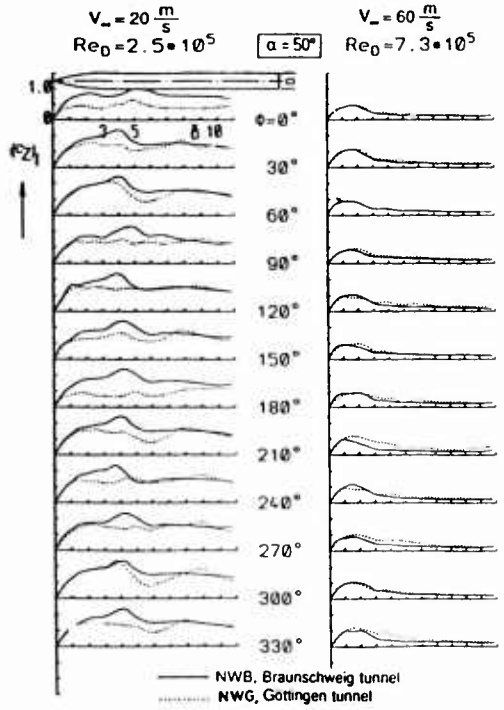



Fig. 11: Comparison of local normal force distributions derived from pressure data obtained for different roll positions Φ at α = 55° and two Reynolds numbers in the DLR's low speed wind tunnels NWB in Braunschweig and NWG in Göttingen

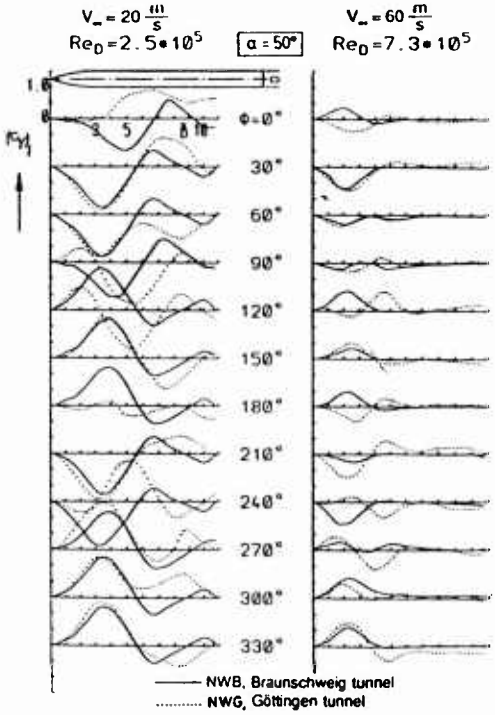



Fig. 12: Comparison of local side force distributions derived from pressure data obtained for different roll positions Φ at α = 55° and two Reynolds numbers in the DLR's low speed wind tunnels NWB in Braunschweig and NWG in Göttingen

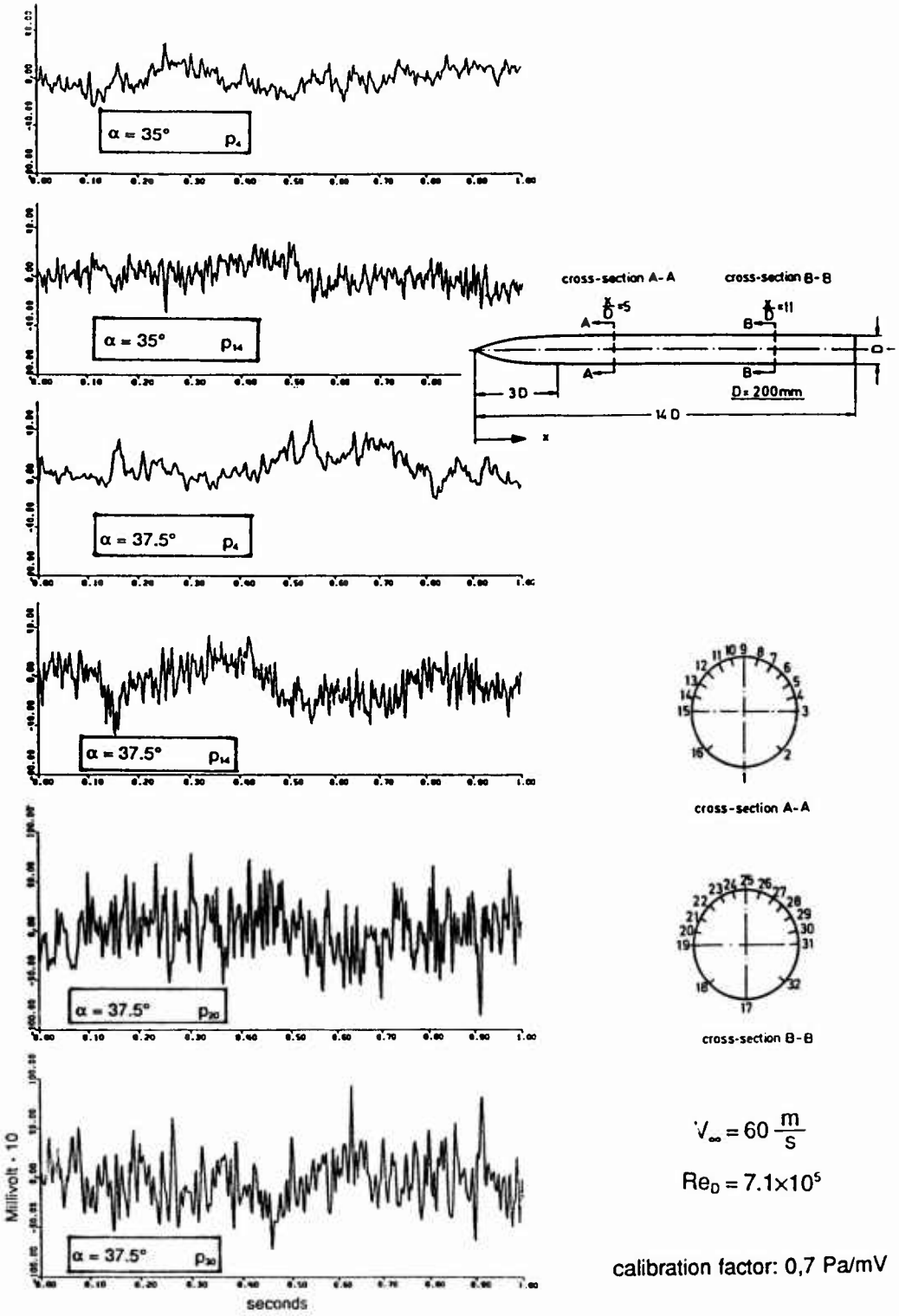



Fig. 13: Time functions of the dynamic part of the surface pressure at several pressure taps

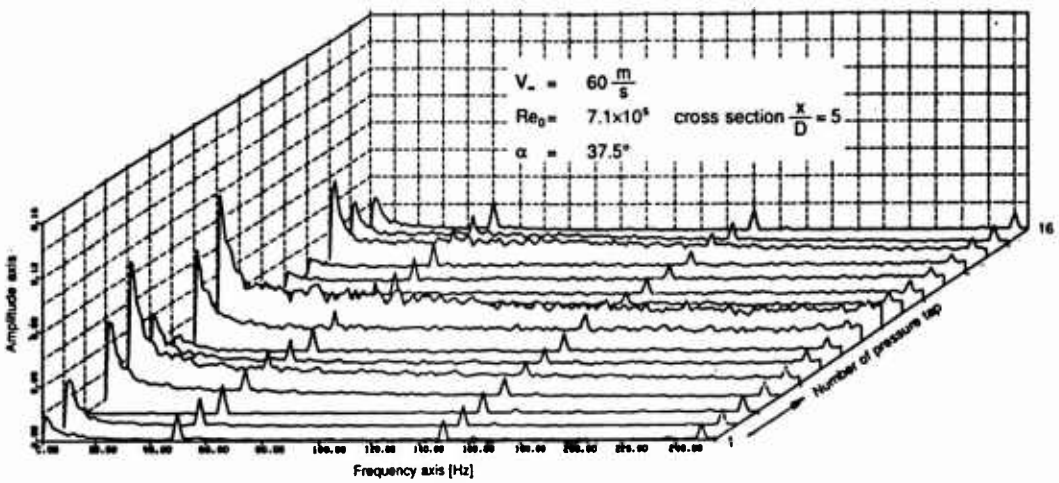



Fig. 14: Amplitude spectra of the dynamic part of the surface pressure of pressure tap 1 to 16 at body cross section $\frac{x}{D} = 5$, related to Fig. 13

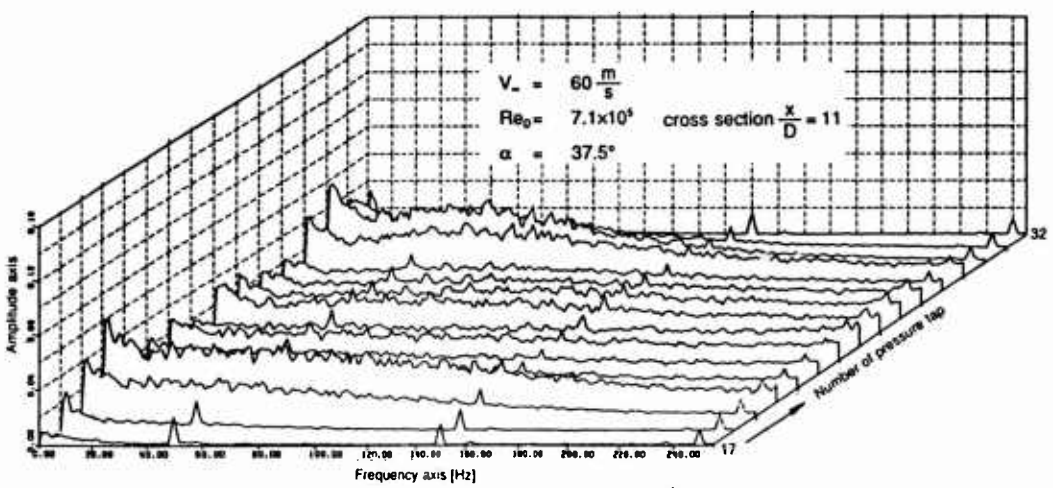



Fig. 15: Amplitude spectra of the dynamic part of the surface pressure of pressure tap 17 to 32 at body cross section $\frac{x}{D} = 11$, related to Fig. 13

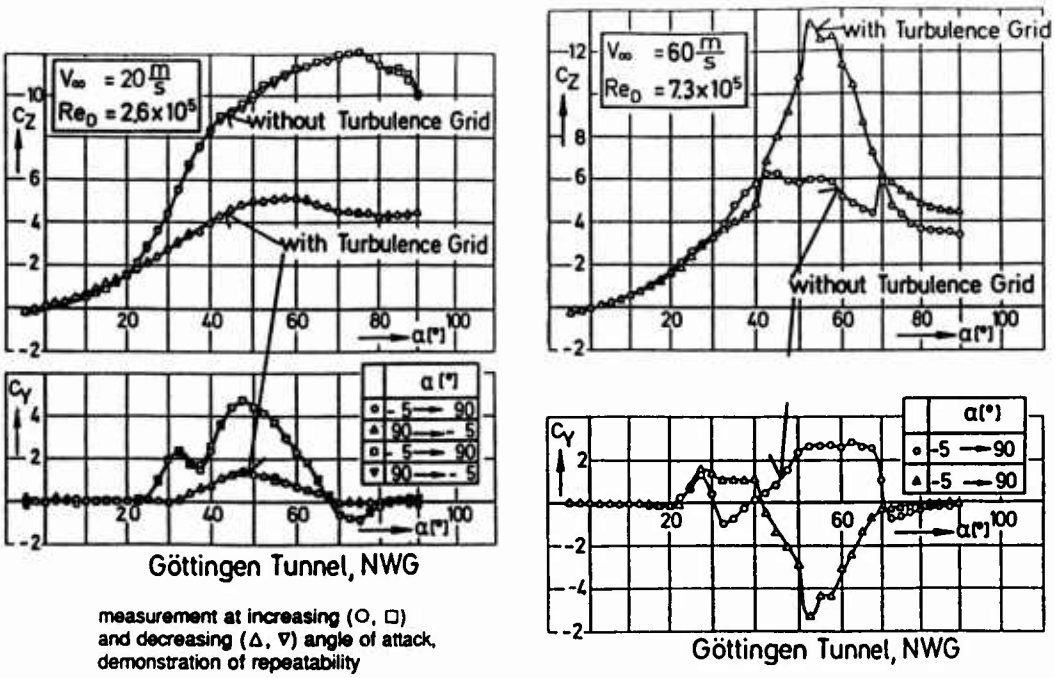



Fig. 16: Total normal and side force coefficients from balance measurements

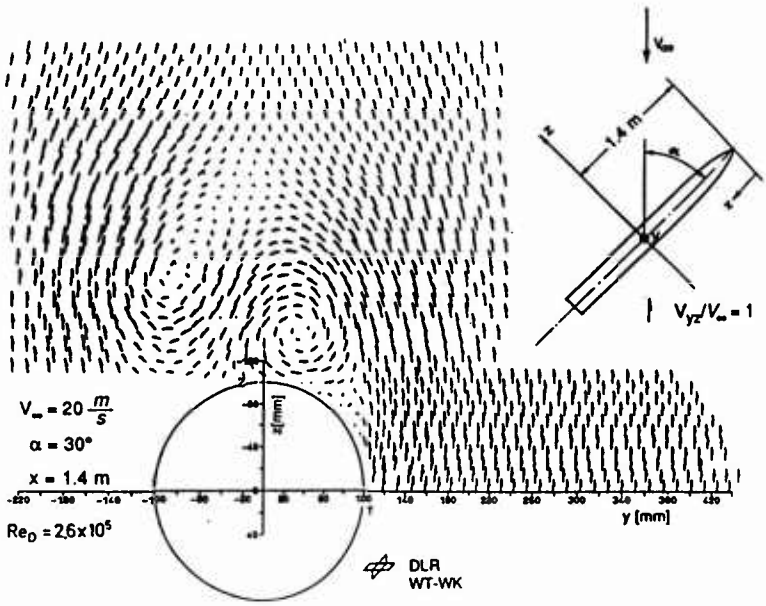



Fig. 17: Velocity vectors of the crossflow in the yz-plane at $\frac{x}{D} = 7$

# ELLIPSOID-CYLINDER MODEL

BY
D. BARBERIS
ONERA - BP72-F92322 CHATILLON CEDEX

## 0 - INTRODUCTION

The data presented in this contribution were obtained in the F2 subsonic wind tunnel of the ONERA Fauga-Mauzac Center. The objective of this work was to obtain detailed experimental data on a separated vortex flow. The model shape has been chosen to be as simple as possible in order to facilitate the mathematical modelling. This model has been defined after preliminary studies in a water tunnel.
The present document reports the results obtained with an axisymmetric model at incidence. For this study, attention has been focused on the boundary layer evolution in the zone of separation and on the mechanism leading to the formation of a well detached primary vortex. The flow has been investigated in great details by using several experimental techniques : surface flow visualizations, surface pressure measurements, field explorations by multi-hole pressure probes and a LDV system.

## 1 - GENERAL DESCRIPTION

1.1 - Model designation: ECR model

1.2 - Model type and flow conditions: Blunt slender body terminated with a slanted flat base. Subsonic flow regime.

1.3 - Design requirements: Large subsonic model with a thick boundary layer which allows very detailed investigations. Fundamental research on 3D turbulent separation in the case where separation occurs on a regular surface with a radius of curvature large compared to the boundary layer thickness.

1.4 - Dominant flow physics: (see Fig. 1). An important feature of the flow on a blunt model is the convergence of the skin friction lines towards a common direction called a 3D separation line.

## 2 - DETAILS OF MODEL

2.1 - General geometric arrangement: (see Fig. 2). The model consists of an half axisymmetric prolate ellipsoid with a cylindrical extension terminated by a flat base, inclined at 45° with respect to the model axis, in order to stabilize the separation on the rear part of the obstacle.

2.2 - Body data

2.2.1- Shape: The length L of the model, comprised between the nose and the middle of the base, is equal to 1600 mm, the ellipsoid major axis is a = 800 mm, its minor axis being b = c = 200 mm. Two models with the same shape have been built : one model was used for surface flow visualizations and LDV measurements, the other for surface pressure measurements and probing with a three-hole pressure probe.

2.3 - Geometric definition of all components

All models have been built in glass fiber and epoxy and covered with black paint.

2.4 - Model support details

(see Fig. 3)

## 3 - GENERAL TUNNEL INFORMATION

3.1 - Tunnel designation

F2 wind tunnel (see Fig. 4).

3.2 - Organization running the tunnel

ONERA - Fauga-Mauzac Centre.

3.3 - Tunnel characteristics

It is a continuous closed circuit wind tunnel driven by a fan with constant blade angle and a variable motor speed with a maximum power of 700 kW.
The air speed is variable from 0 to 100 m/s. The stagnation pressure is the atmospheric pressure. The contraction ratio is equal to 12. Following the wind, the settling chamber is equipped, with a grid in the rapid expansion, an honeycomb and three grids . The cooling section, the fan section, the corner vanes, and the central section (including : contraction, test section and the beginning of the first diffusor) are built of steel. The rest of the tunnel is made of concrete.

3.4 - Test section

3.4.1 - Model mounting in the test section

(see Fig. 3)

3.4.2 - Test section dimensions

The test section is rectangular : height 1.80 m, width 1.40 m, length 5m.

3.4.3 - Wall geometry details

The side walls of the test section are formed by several removable panels, which allows various arrangements of transparent and opaque area. The top and bottom walls are built in ply with a glass window of 0.6 x 2 $m^2$ surface.
The divergence of the wind tunnel can be trimmed by changing inclination of the top and bottom walls.

3.5 - Freestream calibration

3.5.1 - Reference flow conditions

The reference stagnation pressure is measured in the settling chamber. The reference static pressure is obtained from a Prandtl antenna situated at 300 mm from the top wall of the test section and at 786 mm downstream of the beginning of the test section. The static temperature is measured in the settling chamber with a thermocouple ($C_r$ - $A_l$) connected to digital AOIP system with 0.1°C resolution.

3.5.2 - Tunnel calibration

The uniformity of the flow velocity U in various transverse planes of the section was checked successively with laser velocimetry, pressure probe and hot wire. The pressure probe and hot wire were supported by a three degrees of freedom device (X horizontal axial centreline, Y and Z) fastened to the test section inside.
The figure 5 obtained by pressure probe gives the comparison of the local values U, in a vertical plane located 1 meter behind the beginning of the test section, and the reference value $U_0$ measured by a fixed pressure probe located 0.786 m behind the beginning of the test section and 0.3 m under the upper wall ; in this case Z = 0.902 m, Y = 0.798 m

and $U_0$ = 100 m/s.This figure shows a very good uniformity in the plane.
The laser accuracy was estimated to a relative error $\Delta U/U < 1.5\%$, the absolute error on the angle between the velocity vector and the horizontal being 0.5 degree. These measurements show the same uniformity as the pressure measurements and the measured angles were always smaller than the estimated error. The hot wire measurements, although disturbed by small mechanical vibrations of the supporting device, shows the same uniformity of the flow. Dynamic measurements of pressure fluctuations $\sqrt{p^2}$ and speed fluctuations $\sqrt{u^2}$ were made by a microphone and a hot wire in the test section.
A quarter inch Bruel and Kjaer microphone equipped with a cone (16 kHz pass band) was placed 3.6 m from the test section inlet on the horizontal axial centreline. The values of $\sqrt{p^2}$ were obtained without filtering (see Fig. 6).
An horizontal 5 µm hot wire was placed 0.8m from the test section inlet and 0.2 m from the upper wall. The values of $\sqrt{u^2}$ were determined in the 0 to 1000 Hz frequency band (see Fig.7).

## 4 - INSTRUMENTATION

4.1 - Model position

4.1.1 - How is the geometrical incidence measured
By use of a potentiometer.

4.1.2 - Accuracy of geometrical incidence 0.1°

4.2 - Model pressure measurements

4.2.1 - Total number and disposition of pressure holes
(see Fig.8). The forward part of the model, which can rotate along its longitudinal axis, contains a row of 46 surface pressure holes distributed along a meridian line. The possibility of rotating the model around its roll axis allowed to make detailed surface pressure measurements along circumferential directions : thus, the rotation step for these measurements was equal to 1°, with 18 mm axial step length.

4.2.2 - Range and accuracy of pressure transducers
Pressure transducer range ± 1 PSID

4.2.3 - Are dynamic pressures measured No

4.3 - Force and moment measurements No

4.4 - Boudary layer and flow field measurements

4.4.1 - Measurement technique applied
Field explorations by three-hole pressure probes and a three - component LDV system.
The light sources of the LDV system are constituted by two Argon lasers with a maximum power of 15W. The first laser gives the blue and green radiations (respective wave-length, 0.488µm and 0.5145µm); the second laser provides the violet radiation (wave-length 0.4765µm). In order to detect the direction of the measured velocity component, the six beams coming out from the beam splitters traverse Bragg cells inducing a fringe shift at a frequency of 4MHz. Appropriate optics focus the

beams to constitute the probe volume whose diameter is close to 0.35mm. The six beams are contained in a same plane (P) which can be inclined at a chosen angle. The blue and green beams are focused along a common direction making an angle of 38° with respect to the transverse axis Y, the two fringe patterns being respectively inclined at +45° and -45° with respect to (P). The violet beams make an angle of -38° with respect to Y; so that the angle between the blue-green and the violet beams is equal to 76°. The collecting part comprises two Cassegrain telescopes having a diameter of 200mm. The signals coming out from the photomultipliers are then processed by DISA 55L type counters connected to an acquisition system through a simultaneity checking device which checks that the three signals are relative to the same particle having crossed the probe volume. In order to have a sufficiently high data rate, the flow was seeded with particles of incense smoke emitted downstream of the test section, thus avoiding perturbation of the upstream flow by the injection device. At each measurement point, the three instantaneous velocity components were acquired from a sample of 2 000 particles.

4.4.2 - Flow regions investigated

(see Fig. 9). Different means of investigation have been used according to the region of the flow to be studied.

4.4.3 - Probe and probe supports

The two three-hole pressure probes used to investigate the boundary layer are shown in Fig. 10. These probes, of the "cobra" type, are constituted by three tubes welded together and flattened at their extremity to allow the probe to come very close to the surface. Thus, the minimum thickness of these probes is equal to 0.2 mm, their width being 1.6 mm. The traversing mechanism supporting the probe is installed inside the forward part of the model (see Fig. 11). It could be fixed in any longitudinal position in the range 340 mm < $XG'$ < 900 mm ($XG'$ represents the distance along the model longitudinal axis measured from the nose). The traversing mechanism can rotate in such a way that the displacement of the probe remains normal to the surface at the measuring station.

The traversing mechanism can be accessed through a large aperture in the model which is closed during operation (see Fig. 12). The skin of the model is a shell built in glass fiber with reinforcements made of foam and glass fiber. A longitudinal slot in the skin allows the displacement of the probe. During test, this slot is obturated by a steel tinsel fixed to the model by a magnetic track. An electric contact stops the vertical motion of the probe when it touches the model wall.

4.5 - Surface flow visualization

4.5.1 - Technique applied

The surface flow was characterized by using a viscous coating which allows the visualization of the skin friction line pattern (see Fig. 13)

4.5.2 - Results

Results of the surface flow patterns are presented by side and leeward photographs of the model.

4.6 - Flow field visualization

(no flow field visualization were made)

4.7 - Tunnel wall measurements

No tunnel wall measurements were made, because attention has been focused on the boundary layer evolution in the zone of separation and the mechanism leading to the formation of a vortex.

## 5 - TEST MATRIX AND CONDITIONS

5.1 - Detailed test matrix

Mean velocity and turbulent shear stress measurements have been executed in the region of the leeward plane of symmetry of the model set at an incidence $\alpha$ of 20° in a $U_0$ = 50 m/s uniform flow. The description of the flow field has been completed by measurements performed close to the model surface by using three hole pressure probes. Also, surface pressure measurements and surface flow visualizations have been executed.

- All the experiments have been made for the conditions
$U_0$ = 50 m/s and $R_c = 5.6\ 10^6$
- Surface pressure measurements (Model B)
$\alpha$ = 20°; 22°; 24°; 26°; 28°; 30°
- LDV measurements (Model A)
$\alpha$ = 20°
- Three-hole pressure probe measurements (Model B)
$\alpha$ = 20°

5.2 - Transition details

All the tests have been made with natural transition. The technique used to detect the phenomenon of transition is the classical property of acenaphtene sublimation in turbulent zones. The remaining acenaphtene reveals the laminar region. Furthermore, near the model nose, a local separation can be observed which is revealed by an accumulation of product on oil flow visualizations. This separation causes a sudden transition of the flow from laminar to turbulent, the phenomenon being confirmed by visualizations made with acenaphtene.

## 6 - DATA

6.1 - Availability of Data

6.1.1 - Organization owning the data

OFFICE NATIONAL D'ETUDES ET DE RECHERCHES AEROSPATIALES
ONERA -B.P. 72-F92322 CHATILLON CEDEX FRANCE

6.1.2 - Responsible for the data

BARBERIS Didier
Head of Research Group
ONERA-B.P. 72-F92322 CHATILLON CEDEX France
Tel : 33 1 46 23 51 74
Fax : 33 1 46 23 50 61

6.1.3 - Data on ellipsoid-cylinder model are freely available.

6.2 - Suitability of Data for CFD validation

No corrections have been made for simulating free air conditions.

6.3 - Type and form in which data are available

6.3.1 - Type and form

Files are in ASCII form on Floppy Disks. For field measurements, they contain the coordinates of the measuring point and the aerodynamic results at this point (see example, in Figs. 14, 15 and 16).

6.4 - Corrections applied to data

No corrections have been made to take into account the wall, sting and support interference. In the case of boundary layer investigations with three-hole pressure probes, tests have been made to qualify the effects of incidence and Reynolds number on probe calibration curves. These effects have been found to be negligible for the considered range of parameters. A special study has also been executed to elucidate wall effects on the probe indications. It was found that corrections are negligible when the distance to the wall is greater than the probe thickness (0.2 mm in our case).

## 7 - DATA ACCURACY AND REPEATABILITY ASSESSMENT

7.1 - Estimate accuracy of:

7.1.1-Free stream conditions

The upstream flow velocity accuracy is estimated to a relative error $\Delta U_o/U_o = 1\%$.
Accuracy. of the geometrical incidence is equal to 0.02°.

7.1.2 - Measured data

The uncertainty on surface pressure being $\Delta p = \pm$ 7Pa leading to an accuracy $\Delta Kp = \pm$ 1% for Kp = -0.5.
For three-hole pressure probe measurements, the uncertainty on pressure measurement on each hole is ± 7Pa, leading to an uncertainty of ± 0.4° on the measurement of the direction of the velocity vector. The laser accuracy is estimated of ± 1 m/s for the value of the velocity and of ± 1° for the direction of the local velocity vector.

7.2 - Repeat measurements

Several means of investigation have been used according to the region of the flow to be studied. For the first campaign results are relative to the boundary layer in the leeward plane of symmetry. There, the flow was probed by using a three-component LDV system working in the forward scatter mode of operation. Reliable information concerning both the mean and fluctuating flow properties has been obtained. However, with the forward mode of operation it is only possible to make measurements near the model surface in meridian planes close to the symmetry plane. Thus, in order to study the flow in a more extended region, during a second campaign of experiments the LDV system was used in the back scatter mode of operation.
However, in this configuration the quality of the signal tends to degrade significantly, especially in near wall regions. In the last step, the description of the flow field was completed by measurements performed very close to the model surface by using three-hole pressure probes. These measurements gave a precise information on the boundary layer behaviour in the region of formation of the

separation lines. However, this type of probe does not allow turbulence measurements.
Figure 9 shows the domains considered for field measurements. A part of the domain investigated with the three component LDV system in the forward mode and the one investigated with three-hole pressure probes are common. Furthermore, two three-hole pressure probes have been used. At first, explorations were executed with the straight probe. Then, in regions where the angle between the probe axis and the velocity vector becomes too high (>30°), the bent probe is used.

7.3 - Redundant measurements

7.3.2 - Checks made on internal consistency of the data

Will be made in the near future on measurements obtained with three-hole pressure probes and LDV system.

7.4 - Other tests on same geometry

No

## 8 - REFERENCES

8.1 - On the wind tunnel

D. AFCHAIN ; P. BROUSSAUD ; M. FRUGIER G. RANCARANI
"La soufflerie F2 du centre du Fauga-Mauzac ."
20ème Colloque d'Aérodynamique Appliquée AAAF - Toulouse - Novembre 1983.

D. AFCHAIN ; G. RANCARANI "Mise au point et contrôle du fonctionnement de la soufflerie F2".
ONERA - RT 1/3623 GN - Janvier 1984.

D. AFCHAIN ; Ch. GLEYZES "Contrôle aérodynamique de l'écoulement dans la veine d'essais de la soufflerie F2".
ONERA - RT 3/3623 GN - Août 1985.

8.2 - On the model and test results

D. BARBERIS "Etude expérimentale de l'écoulement au voisinage du plan de symétrie extrados d'une maquette d'Ellipsoïde cylindre de révolution".
ONERA - RT N° 22/7252 AN - Octobre 1988.

Ph. LOIRET "Sondage du décollement tridimensionnel sur un Ellipsoïde Cylindrique de Révolution "ECR" en incidence ($\alpha$ = 20°) dans la soufflerie F2".
ONERA - PV n° 23/7252 ANG - Décembre 1988.

Ph. LOIRET ; D. AFCHAIN "Sondage de la couche limite sur un Ellipsoïde - Cylindre de Révolution "ECR" en incidence dans la soufflerie F2".
ONERA - PV n° 26/7252 ANG - Avril 1989.

D. BARBERIS "Etude expérimentale du décollement tridimensionnel sur une maquette de grandes dimensions".

29ème Colloque d'Aérodynamique Appliquée AAAF
Biscarrosse, Septembre 1992.

8.3 - On the applied measurement techniques

D. AFCHAIN. "Mise au point du velocimètre laser tridirectionnel de la soufflerie F2. Etude de la veine vide".
ONERA - RTI n° 4/3623 GN - Novembre 1988.

## 9 - LIST OF SYMBOLS

| | |
|---|---|
| X, Y, Z | wind tunnel referenced and fixed coordinate system |
| $XG^{1'}$, $XG^{2'}$, $XG^{3'}$ | model referenced coordinate system |
| $X^1$, $X^2$, $X^3$ | local coordinate system |
| U | longitudinal component of the velocity in XYZ coordinate system |
| $U_0$ | velocity at upstream infinity |
| $\alpha$ | model angle of incidence |
| $R_c$ | Reynolds number referenced to the length of the model (C = 1.6 m) |

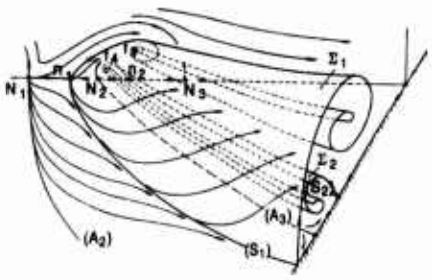



**Fig. 1 - Schematic Representation of Separation Lines and Surfaces**

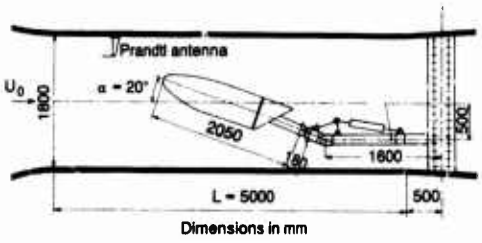



**Fig. 3 - Schematic Representation of the Model in the F2 Wind Tunnel**

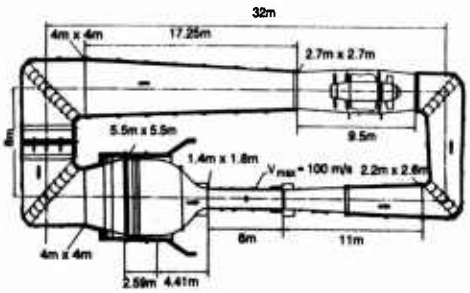



**Fig. 4 - The F2 Wind Tunnel**

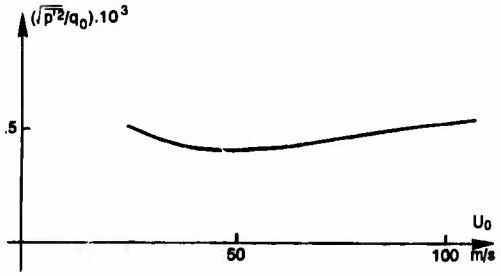
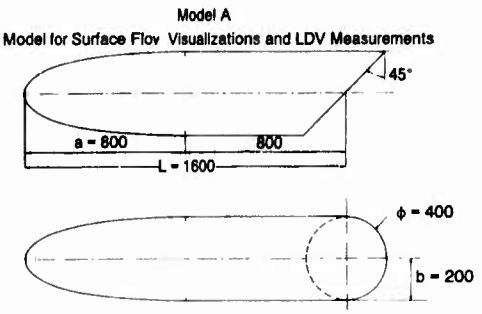



**Fig. 6 - Fluctuation of the Static Pressure**



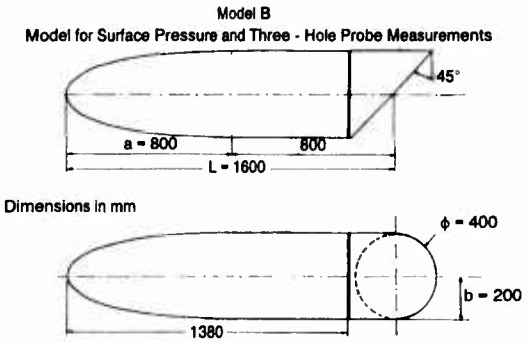




**Fig. 2 - Definition of Ellipsoid - Cylinder Model**

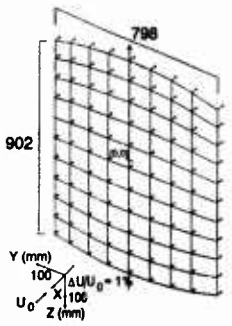



**Fig. 5 - Transversal Survey in the Test Section**

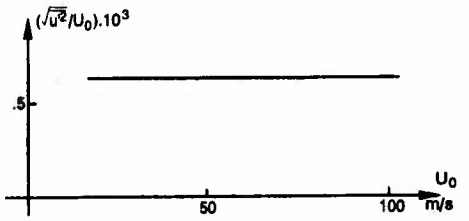



**Fig. 7 - Axial Turbulence**

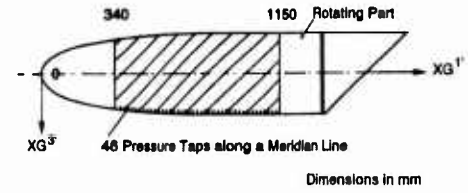



**Fig. 8 - Investigated Domain : Surface Pressure Measurements**

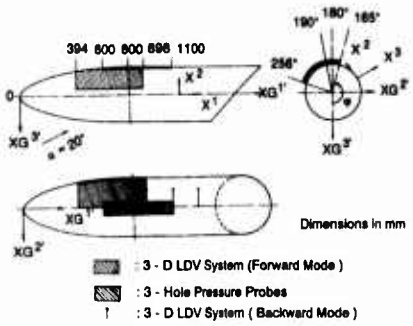



**Fig. 9 - Investigated Domains : Field Measurements**

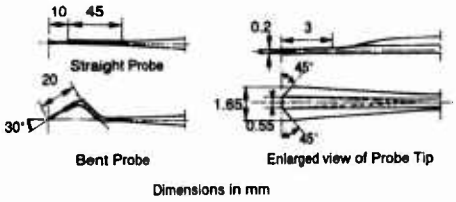



**Fig. 10 - Definition of the Three Hole Pressure Probes**

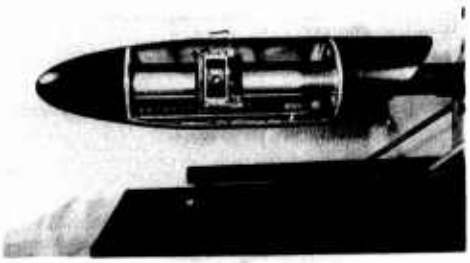


**Fig. 12 - View of the Three Hole Pressure Probe Displacement System Installed Inside the Model**

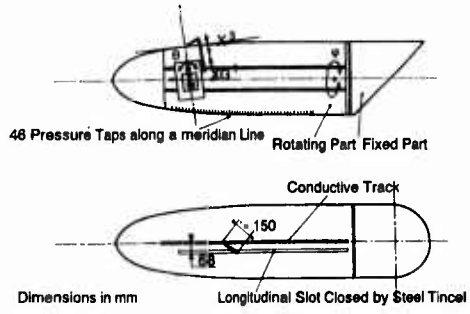



**Fig. 11 - Schematic Representation of the Three Hole Pressure Probe. Displacement System Installed Inside the Model**







**Fig. 13 - Oil Flow Visualization. $\alpha = 20°$, $U_0 = 50$ m/s, $R_c = 5.6\ 10^6$**

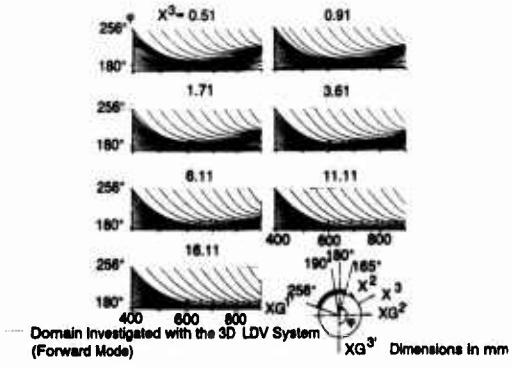



**Fig. 14 - Streamlines Obtained from Three Hole Pressure Probe Measurements. $\alpha = 20°$, $U_0 = 50$ m/s, $R_c = 5.6\ 10^6$**

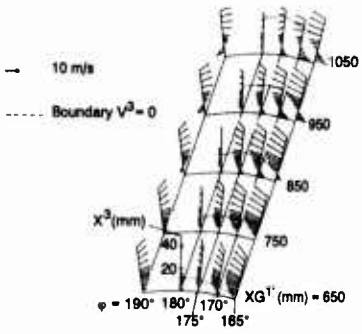



Fig. 15 - Projections of the Mean Velocity Vector in the planes Normal to the Model Longitudinal Axis. $\alpha = 20°$, $U_0 = 50$ m/s. (From 3D LDV Measurements)

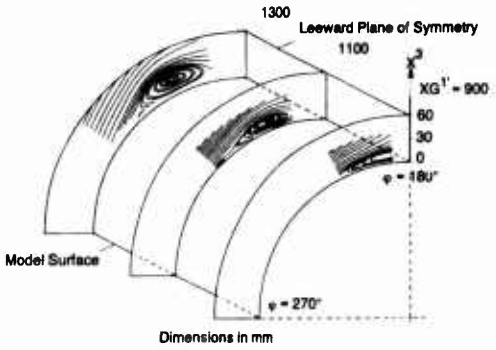



Fig. 16 -Streamlines Projections in the Planes Normal to the Model Longitudinal Axis. $\alpha = 20°$, $U_0 = 50$ m/s, $R_c = 5.6\ 10^6$ (From 3D LDV Measurements)

# SUPERSONIC VORTEX FLOW AROUND A MISSILE BODY

BY
D. BARBERIS
ONERA - BP72 - F92322 CHATILLON CEDEX

## 0 - INTRODUCTION

Boundary-layer separation occurring on a missile body at moderate or high angle of incidence leads to the formation of well organized vortical structures, especially at supersonic flight Mach numbers. Even though a certain number of experimental results are available for this type of flow, none of the published data provide complete information for a supersonic flow.

An experimental study of the flowfield around a 3 calibre tangent ogive-cylinder body in a supersonic flow has been carried out to provide a consistent description of the flow. This experiment includes oil flow visualizations, primary separation line determination, surface pressure measurements and five hole pressure probe surveys for a Mach number of 2 and an angle of incidence varying from 0° to 20°. Results are obtained for a natural and fixed transition.

## 1 - GENERAL DESCRIPTION

1.1 - Model name or designation

ONERA missile body

1.2 - Model type and flow conditions

9 calibre ogive-cylinder body equipped with a 3 calibre circular ogive in a continuous supersonic wind tunnel test facility.

1.3 - Purpose of test

Improvement and validation of the numerical methods require as complete as possible experimental descriptions of the flow around missile-type bodies at incidence. The data base to be constituted should include detailed surface pressure distributions, surface flow visualizations to determine the separation lines, and also accurate external flowfield measurements to define the vortex pattern. Furthermore, the effect of the nature of the boundary layer (laminar or turbulent) on the primary separation line location and on the external flowfield structure has also been studied.

1.4 - Dominant flow physics

An important feature of the flow is the convergence of the skin friction lines towards a common direction called a 3D separation line. From this line, boundary layer separates and induces the development of a vortex. Surface flow visualizations by viscous coating allow the determination of the conjectural skin-friction line pattern (see Fig.1). All the skin-friction lines start at the model apex. An attachment line $A_1$ is present in the windward symmetry plane. Primary separation occurs along line $S_1$. An attachment line $A_2$ is visible in the leeward symmetry plane. A second separation occurs along the secondary separation line $S_2$. Between $S_2$ and $S_1$ a third attachment line $A_3$ exists. The transverse flow organization represented in Fig. 1 is deduced from the skin friction line pattern. It includes one saddle point in the outer flow. Thus, the separation lines $S_1$ and $S_2$ are the traces on the surface of two separation

surfaces which roll up to constitute two vortices.

## 2 - DETAILS OF MODEL

2.1 - General geometric arrangement

The experiments have been performed on a 9 - calibre ogive - cylinder in a continuous supersonic wind tunnel test facility. Models consist of a 6 - calibre cylinder extended by a 3 - calibre circular ogive, whose meridian line is a circle tangent to the cylinder. Ogive extremity is tangent to a cone with an half angle of 18.9°. The area of the test section is 0.3 x 0.3 $m^2$. The characteristics of the incoming freestream have been fixed as follows :
- Mach number $M_0 = 2$
- stagnation pressure $P_{st0} = 0.05$ MPa
- stagnation temperature $T_{st0} = 330$ K

As shown in Fig. 2, the model was sting mounted and its incidence $\alpha$ could be varied from 0° to 20°.

2.2 - Body data

The model has a length L = 270 mm and a diameter D = 30 mm. The Reynolds number calculated with D is $R_{eD} = 0.16\ 10^6$. Two models of identical shape have been manufactured. The first model, equipped with 17 pressure taps equally distributed along a meridian line (see Fig. 2), has been used for surface pressure measurements.
The second model was used to make surface flow visualizations with an oil flow technique. It was equipped with only 3 pressure taps in order to control that the flow was not affected when the model was changed.

2.3 - Geometric definition

All models were manufactured in steel and covered with a black paint.

2.4 - Model support details

(see Fig. 3). The model was sting mounted to a support which can move in a circular path to obtain desired incidence. As the flow was symmetric for the tested conditions ($M_0 = 2$, $0° < \alpha < 20°$), it was possible to determine the surface pressure distribution by rotating the model around its roll axis. This technique allows to be carried out a great quantity of measurements with few pressure taps.

## 3 - GENERAL TUNNEL INFORMATION

3.1 - Tunnel designation

S5Ch wind tunnel (see Fig. 4)

3.2 - Organization running the tunnel

ONERA - Chalais-Meudon Centre.

3.3 - Tunnel characteristics

S5Ch is a continuous supersonic wind tunnel with return circuit. The wind tunnel circuit is shown schematically in figure 4. It includes a twelve-stage axial compressor with 1400 kW motor drive. The stagnation pressure, between 0.4 and 1 bar, is held at the required value by an auxiliary pumping unit. The maximum compression ratio of the compressor is 5.6. This value allows starting of a Mach 3.15 nozzle. A heat exchanger installed downstream of the compressor maintains the stagnation temperature at approximately 300 K. To avoid condensation

phenomena in the test section, the relative humidity is controlled according to the Mach number by injecting dry air into the system.

Different nozzle blocks can be mounted in test section no. 1, to develop transonic flows ($0.8 < M_0 < 1.15$) in a 0.3 x 0.22 $m^2$ test section, or supersonic flows ($1.45 < M_0 < 3.15$) in a 0.3 x 0.3 $m^2$ section. Windows of Schlieren-quality glass with a diameter of 0.35 m are mounted in the side walls of the test section.

The general flow conditions are the following :

- stagnation pressure $P_{sto}$ ranging from $0.4\ 10^5$ to $10^5$ Pa, depending on the Mach number;
- stagnation temperature $T_{sto}$ of about 330 K;
- relative humidity of 1 g of water vapor per kilogram of air, which can be reduced to 0.1 g/kg ;
- maximum unit Reynolds number of $7\ 10^6$/m.

Test section no. 2 consists of a box measuring 0.5 x 1.2 $m^2$. It is used mainly for testing blade cascades (flat or circular) at Mach numbers of about 1.5.

The present tests were conducted in test section no. 1.

3.4 - Test section

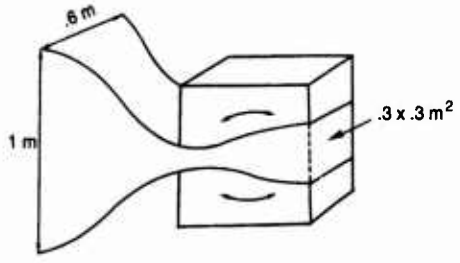
3.4.1-(see Figs. 2 and 3)

3.4.2-Test section dimensions

The cross section of the test section is 0.3 x 0.3 $m^2$. The longitudinal extension of the region where the Mach number is uniform depends on the considered Mach number $M_0$. It varies from 0.3 m, when $M_0$ = 1.6 to 0.58 m, when $M_0$ = 3.

3.4.3 - Wall geometry details

Different nozzle blocks can be mounted in test section n° 1 to produce supersonic flows. Nozzle blocks can rotate slightly which allows to modify the flow Mach number around its nominal value.




| Nominal Mach number | | Mach number variation |
|---|---|---|
| $M_0n$ = | 1.20 | $1.00 < M_0 < 1.30$ |
| | 1.61 | $1.45 < M_0 < 1.71$ |
| | 1.74 | $1.57 < M_0 < 1.85$ |
| | 2.00 | $1.85 < M_0 < 2.12$ |
| | 2.28 | $2.10 < M_0 < 2.42$ |
| | 2.60 | $2.47 < M_0 < 2.78$ |
| | 3.02 | $2.74 < M_0 < 3.15$ |

- Wall pressures and wall displacements are not measured.
- No control of the boundary layer on walls
- The typical wall boundary layer displacement thickness is $\delta_1$ = 1.3 mm and $\delta$ = 6 mm.

3.5 - Freestream conditions

3.5.1 - How are reference flow conditions determined

The reference stagnation pressure $P_{st0}$ and stagnation temperature $T_{st0}$ are measured in the settling chamber. The freestream static pressure $P_0$ is deduced from the measurements of $P_p/P_{st0}$ ratio obtained during tunnel calibration ($P_p$ being the Pitot pressure).

3.5.2 - Tunnel calibration

Determination of $P_p/P_{st0}$ ratio with a Pitot pressure probe and Hg manometer. The last calibration has been performed in 1960.

3.6 - Flow quality

3.6.1 - flow uniformity

The Mach number variation over model length is $\Delta M_0 = \pm 0.01$.
For supersonic flows, the Mach number variation during a test is very small, and less than the accuracy of the measurement apparatus : $\Delta M < \pm 0.002$.
In fact, it is the variation of the stagnation pressure $P_{st0}$ ($\pm$ 5 mb) which induces uncertainty in the determination of the $P_p/P_{st0}$ ratio, thus reducing the accuracy of Mach number determination. The variation of flow angularity will be determined in the near future. Up to now, zero degree aerodynamic angle of incidence is found by inversion of the model in the test section.

3.6.2 - Temperature variation

Temperature cannot be precisely controlled. In the settling chamber, temperature is maintained below 320 K by using the heat exchanger ; in fact $T_{st0}$ can vary between 310 and 320 K (this temperature is function of the atmospheric conditions and the reference stagnation pressure). Anyway, for fixed conditions and after half an hour of running, the variation of $T_{st0}$ during a test is less than 2K.

3.6.3 - Flow unsteadiness

Has not been determined.

## 4 - INSTRUMENTATION

4.1 - Model position

4.1.1 - How is the geometrical incidence measured

The geometrical incidence is measured by an optical method.

4.1.2 - Accuracy of geometrical incidence

0.1°

4.2 - Model pressure measurements

4.2.1 - Total number and disposition of pressure holes

(see Fig. 2)

4.2.2 - Range and accuracy of pressure transducers

15 PSI with $\pm$ 0.3 mb accuracy

4.2.3 - Are dynamic pressures measured

No

4.3 - Flow field measurements

4.3.1 - Measurement technique applied

Measurements have been executed with a five hole pressure probe. The diameter of the probe extremity was 1.5 mm. The probe has been calibrated as function of Mach number $M_0$ and angle of incidence $\theta$ in the range :

$0^\circ < \theta < 40^\circ$

$0 < M_0 < 3$

This probe allows the determination of the local Mach number, stagnation pressure, and velocity vector deduced under the assumption of a constant stagnation temperature, which is a good approximation for this moderate value of the incoming freestream Mach number.

An automated displacement system fixed to the upper wall of the test section moves the probe along the wind tunnel-reference system. This explorer is driven very precisely by a computer (displacement accuracy ± 0.1 mm).

The pressure taps on the model and pressure of the five hole probe are connected by pneumatic tubes to six Scanivalve pressure scanners. The pressures are measured by Statham transducers of 15 PSID range (about $10^5$ Pa). The test procedure and acquisition process is controlled by the S5Ch tunnel SOLAR 16-40 computer.

4.3.2 - Flow regions investigated

The surveys have been carried out in planes perpendicular to the model axis, along radial lines. Points were clustered near the body surface. At each incidence, 4 to 7 planes have been surveyed, each one including 400 to 900 measurement points. Due to flow symmetry and accessibility, only the upper left quadrant has been probed (see fig. 5).

4.4 - Surface flow visualization

4.4.1 - Measurement technique applied

The visualizations were obtained by using Rhône-Poulenc "X" paste as the viscous substance, diluted in Gilotherm. The substance is applied to the model. As this substance is sufficiently fluid when the test begins, it is entrained by the shear forces at the surface, revealing skin friction lines. In the course of the test the substance remaining on the surface becomes thinner and gradually hardens in contact with the surface, which is heated to 60° by the flow (60° C is roughly the adiabatic equilibrium temperature). The surface flow configuration, or surface pattern, is then frozen under stabilized test conditions and undergoes no further change when the flow is stopped at the end of the test. The patterns are then photographed following the dismounting of the model.

4.5 - Flow field visualization

Schlieren visualizations were made using the set up of Fig. 6. This is the device usually used, with the source (S) on the emission side, followed by condenser ($L_0$) and a planar mirror that reflects the source image onto the first knife ($C_1$), placed at the focal point of spherical mirror ($M_1$). The optical axis of $M_1$ is inclined a few degrees so that the various

elements of the optical set up do not partly occult the collimated beam directed at the test section. On the reception side, the optical path is symmetrical about the centre of the test section to the path on the emission side, and includes the following elements :
- spherical mirror $M_2$, which focuses the beam on knife ($C_2$) ;
- planar reflector mirror ($m_2$) ;
- conjugation objective (0) ;
- the collecting device to record the Schlieren image.

The laser tomoscopic method was developed at ONERA by the Physics Department. The principle consists of illuminating part of the flow to be studied with a plane sheet of light. The principle of this method is diagrammed in Fig. 7. It uses three independent devices :
- a tracer injector;
- a means for illuminating the tracer;
- a photo recording device.

The purpose of the injector is to emit a tracer that will be visible in the region of flow to be investigated. In order to visualize and photograph the phenomenon, this area has to be adequately illuminated. A laser having a power of about 15 W is used to do this. A bar of glass placed perpendicular to the laser beam fans it out into a plane. The fanout is broader the smaller the diameter of the glass cylinder. This diameter is therefore chosen so that the illumination is maximum, while completely covering the useful field. The recording device consists of a still or movie camera, arranged as perpendicularly as possible to the plane of illumination.

For the present experiments, the tracer used was hot water (hot to avoid the formation of ice crystals), injected by a 4 mm diameter tube placed in the wind tunnel collector, well upstream of the test section. The laser light enters the test section through one of the side wall windows, along a horizontal line, and fans out in a plane perpendicular to the uniform freestream flow. The camera is placed outside the test section with its optical axis at an angle of 30° to the normal to the laser plane.

## 5 - TEST MATRIX AND CONDITIONS

### 5.1 - Detailed test matrix

For all experiments, the characteristics of the incoming freestream have been fixed as follows :
Mach number $M_0 = 2$
Stagnation pressure $P_{st0} = 0.05$ MPa
Stagnation temperature $T_{sto} = 330$ K
The Reynolds number calculated with D = 30 mm is $Re_D = 0.16 \times 10^6$.
Experiments have been performed for the two following conditions : natural transition and fixed transition (see table 1).
Surveys with the five hole pressure probe have been carried out in planes perpendicular to the body axis, along radial lines. At each incidence, 2 to 7 planes have been surveyed, each one containing 340 to 900 measurement points.

5.2 - Transition details

(see previous section). For natural transition, acenaphtene coating visualization enabled us to verify that the boundary layer remained laminar over the entire body at $\alpha = 0$ degree. Transition was triggered by means of a 5 mm wide carborundum strip located 30 mm downstream of the body apex. It has been verified by using the acenaphtene technique that transition occurred at the location of the carborundum strip for all incidences.

## 6 - DATA

6.1 - Availability of data

6.1.1 - Organization owning the data

OFFICE NATIONAL D'ETUDES ET DE RECHERCHES AEROSPATIALES (ONERA) B.P.72, F92322 CHATILLON CEDEX.

6.1.2 - Responsible for the data

BARBERIS Didier
Head of Research Group
ONERA BP. 72, F92322 CHATILLON CEDEX
Tél : 33 1 46 23 51 74
Fax : 33 1 46 23 50 61

6.1.3 - Data are freely available.

6.2 - Suitability of data for CFD validation

No corrections have been made for simulating free air conditions.

6.3 - Type and form in which data are available

6.3.1 - Type and form

Files are in ASCII form on Floppy Discs. For field measurements they contain the coordinates of the measuring point and the aerodynamic results (see example of results, in Fig. 8).

6.4 - Corrections applied to data

No corrections have been made for taking account of wall interference, sting and support. Aero-elastic deformation of the model and sting has not been determined.

## 7 - DATA ACCURACY AND REPEATABILITY ASSESSMENT

7.1 - Estimate accuracy of :

7.1.1 - Free stream conditions

$\Delta M = \pm 0.01$
$\Delta P = \pm 30$ Pa on the range 2000 - 50000 Pa
$\Delta\alpha = \pm 0.1°$

7.1.2 - Measured data

For the five hole pressure probe, accuracy on calibration results are
$\Delta M = \pm 0.02$
$\Delta P = \pm 30$ Pa on the range 2000 - 50000 Pa
$\Delta X, \Delta Y, \Delta Z = \pm 0.2$ mm
$\Delta\alpha = \pm 0.2°$
$\Delta\theta = \pm 0.3°$ for the range0 - 10°
$\pm 0.5°$ 10° - 20°
$\pm 1°$ 20° - 40°
During experiments, the various quantities given by the five hole pressure probe are determined with an accuracy of a few percent (2-3%) in regions where gradients are moderate. This accuracy can be estimated in the range 5-10% in the core of the more intense vortices due to the existence of very high gradients.

7.2 - Repeat measurements - Redundant measurements - Other Tests

none

7.3 - Additional remarks

- Surface pressure distributions have been obtained by rotating the model around its roll axis. The symmetry of the flow is verified a posteriori from these distributions.
- From the schlieren pictures we have observed that there are no interactions between the reflected shock on wall test section and the rear part of the model.

## 8 - REFERENCES

8.1 - On the wind tunnel

J. PONTEZIERE "Variation continue du nombre de Mach à S5Ch au moyen de tuyères faiblement pivotantes $1.45 < M_0 < 3.15$".
ONERA - NT 18/1865 A (1961).

R. GAILLARD "Etat actuel des systèmes d'acquisition spécifiques de la soufflerie S5Ch."
ONERA - RT 66/1865 AN (Juillet 1982).

8.2 - On the model

P. MOLTON, D. BARBERIS "Etude expérimentale du système tourbillonnaire engendré par un fuselage de missile en incidence. Troisième partie : Mesures par vélocimétrie laser tridirectionnelle".
R.T. N° 47/1147 AY (Mars 1991).

D. PAGAN ; P. MOLTON "Etude expérimentale du système tourbillonnaire engendré par un fuselage de missile en incidence. Première partie : couche limite laminaire"
RT n° 40/1147 AY (Janvier 1990).

D. PAGAN, P. MOLTON "Etude expérimentale du système tourbillonnaire engendré par un fuselage de missile en incidence. Deuxième partie : couche limite turbulente".
R.T. n° 42/1147 AY (Juin 1990).

8.3 - On the applied measurement techniques

R. GAILLARD "Etalonnage et utilisation de sondes cinq trous."
ONERA - TP n° 1984-2.

M. PHILBERT, J.P. FALENI, R. BEAUPOIL "Application d'un dispositif d'éclairage laminaire à la visualisation des écoulements aérodynamiques en soufflerie par émission de fumées".
La Recherche Aérospatiale, N° 1979-3, pp 173-178 (1979).

## 9 - LIST OF SYMBOLS

| | | |
|---|---|---|
| $\alpha$ | : | angle of incidence |
| M | : | Mach number |
| $P_0$ | : | static pressure |
| $P_{st0}$ | : | stagnation pressure |
| $R_{eD}$ | : | Reynolds number referenced to the diameter of the model (D = 30 mm) |
| $T_{st0}$ | : | stagnation temperature |
| X, Y, Z | : | model referenced coordinate system |

**Table 1**

| $\alpha°$ | 5 | 10 | 15 | 20 |
|---|---|---|---|---|
| Natural Transition | a c d e | a c d e | a c d e | a c d e |
| Fixed Transition | a d e | a d e | a d e | a b d e |

a : oil flow visualizations
b : tomoscopic visualizations
c : schlieren
d : surface pressure measurements
e : five - hole pressure probe measurements

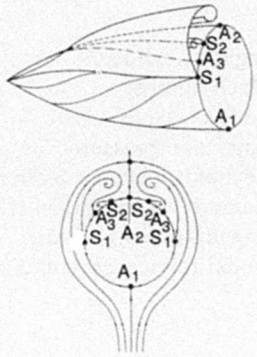



Fig. 1 - Conjectural Pattern of the Flowfield

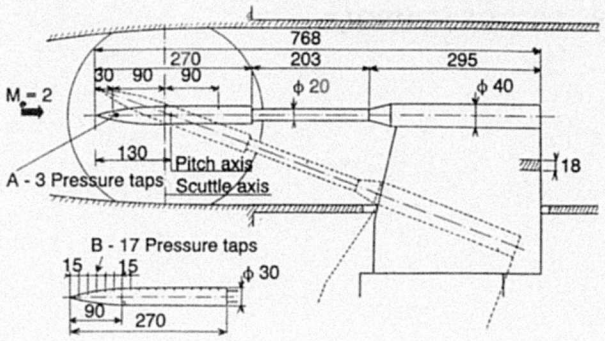



Fig. 2 - Model Definition and Set up Main Dimensions

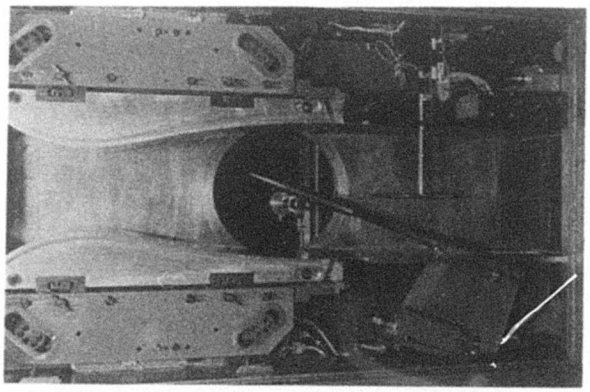


Fig. 3 - Model Installation in the S5Ch Wind Tunnel

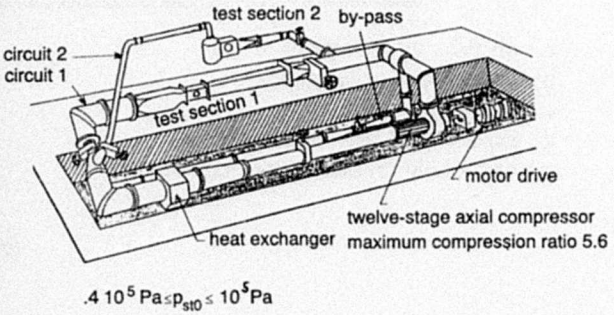



Fig. 4 - The S5Ch Continuous Supersonic Wind Tunnel of the Chalais-Meudon Centre

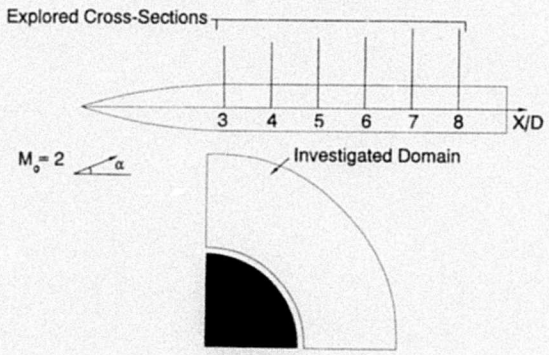



Fig. 5 - Location of the Flow Field Surveys

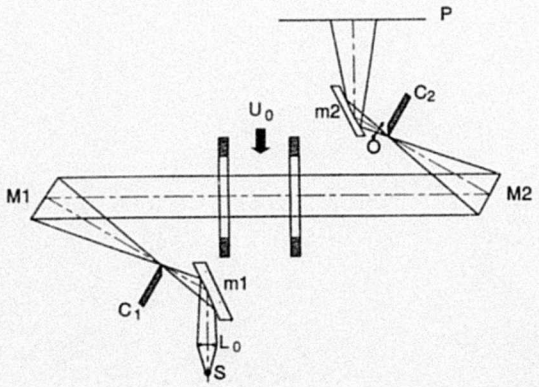



Fig. 6 - Schematic Diagram of the Schlieren Visualization System

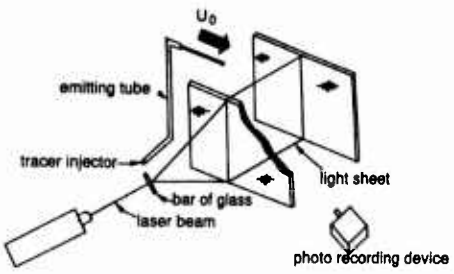



**Fig. 7 - Schematic Diagram of the Laser Tomoscopic System**

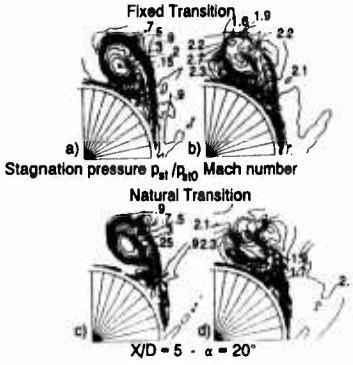



**Fig. 8 - Comparison between Natural and Fixed Transition of the Boundary Layer**

# TEST DATA ON A NON-CIRCULAR BODY FOR SUBSONIC, TRANSONIC AND SUPERSONIC MACH NUMBERS

by
P. CHAMPIGNY
Office National d'Etudes et de Recherches Aérospatiales (ONERA)
BP 72 - 92322 CHATILLON CEDEX - FRANCE

## INTRODUCTION

Measurements on a non-circular body were made in ONERA wind tunnels. This body, representative of non-conventional missile shapes, was studied for Mach numbers from 0.4 to 3.0 (S2MA wind-tunnel) and 4.5 (S3MA wind-tunnel), angles of attack up to 20° and sideslip angles up to 10°, with a free transition. The data base consists of static pressure measurements.

The intent of the experiment was to provide data for evaluation of three-dimensional flow computation methods, as part of a research program sponsored by the "Direction des Recherches, Etudes et Techniques" of the French Ministry of Defense.

The flow exhibits large separation regions and strong vortices, even at low angles of attack, due to the particular shape of the body (lenticular cross-section).

## 1. GENERAL DESCRIPTION

| | |
|---|---|
| 1.1 Model name | ONERA PPF body |
| 1.2 Model type and flow conditions | Slender body ; sub-trans-supersonic speed regime |
| 1.3 Design requirements, purpose of test | This model is representative of non-conventional missile shapes (lenticular cross-section). The test were made for the purpose of providing a data base for CFD validation. |
| 1.4 Dominant flow physics | The flow around this particular body is characterized by large separated zones and strong vortices, even at a relatively low angle of attack. |

## 2. DETAILS OF MODEL

| | |
|---|---|
| 2.1 General geometric arrangement | Body alone (figure 1) |
| 2.2 Various configurations | None |
| 2.3 Wing data | None |
| 2.4 Body data | |
| 2.4.1 Shape | Nose : pointed<br>Body length : 1.2 m<br>Cross section : quasi-lenticular<br>Maximum height : 0.08m<br>Maximum width : 0.24m<br>Boatail : ogival |

| | |
|---|---|
| 2.4.2 Additional details | None |
| 2.5 Fins, canards, tail surfaces | None |
| 2.6 Nacelle | None |
| 2.7 Geometric definition | Shape specified numerically by a CAD system, (see figure 1)<br>Tolerances : ± 50μm<br>Surface roughness : 0.2μm |
| 2.8 Model support | Sting (see figure 2), for which deformations are negligible |

**3. GENERAL TUNNEL INFORMATION**

| | |
|---|---|
| 3.1 Tunnels designation | S2MA and S3MA |
| 3.2 Organisation running the tunnels | CNERA |
| 3.3 Tunnels characteristics | S2MA : continuous<br>0.3≤ M ≤1.3<br>1.5≤ M ≤3.0<br>S3MA : blow down (t≥40s)<br>0.3≤ M ≤1.2-1.5<br>1.7≤ M ≤3.8<br>M = 4.5/5.5 |
| 3.4 Test section | |
| 3.4.1 Model mounted in the test section | Figures 3 and 4 |
| 3.4.2 Dimensions (meters) | S2MA : 1.76 x 1.75 (transonic)<br>1.85 x 1.75) (supersonic)<br>S3MA : 0.78 x 0.56 (transonic)<br>0.80 x 0.76 (supersonic) |
| 3.4.3 Wall geometry details | |
| . Type of wall | Transonic (S2MA) : perforated (2.9%)<br>Supersonic (S2MA and S3MA): closed |
| . Wall pressures | Not measured during the test |
| . Boundary layer control on walls | No |
| . Boundary layer displacement thickness | ≈ 15mm (M=0.4) to 30mm (M=4.5) |

3.5 Freestream conditions

3.5.1 Determinations

| | |
|---|---|
| . Total pressure | Settling chamber |
| . Total temperature | Settling chamber |
| . Static pressure | Transonic : measured on wall, 1500mm upstream of the model |
| | Supersonic : calculated |

3.5.2 Calibration

| | |
|---|---|
| . How ? | Transonic : static probe |
| | Supersonic : pitot probe |
| . Date of the last calibration | S2MA transonic : 1991<br>supersonic : 1985 |
| | S3MA M = 4.5 : 1968 |

3.6 Flow quality

| | |
|---|---|
| 3.6.1 Flow uniformity | Non-provided |
| 3.6.2 Temperature variation | Controlled |
| | ± 1° during a run |

3.6.3 Flow unsteadiness

| | |
|---|---|
| . Overall turbulence level | S2MA transonic :<br>≈ 0.1 to 0.25 % |
| | S2MA Supersonic : unknown |
| | S3MA M = 4.5 : unknown |
| . Overall noise level | S2MA transonic :<br>Cp - RMS ≈ 0.005 to 0.02 |
| | S2MA Supersonic : 0.005 |
| | S3MA M = 4.5 : unknown |

**4. INSTRUMENTATION**

4.1 Model position

| | |
|---|---|
| 4.1.1 Measured incidence | "Q-flex" inclinometer located in the model |
| 4.1.2 Accuracy | ± 0.01° |

**4.2 Model pressure measurements**

| | |
|---|---|
| 4.2.1 Pressure holes | Total number : 207<br>(See figure 5) |
| 4.2.2 Pressure transducers | Range ± $10^5$ Pa<br>Accuracy ± 50Pa |

**5. TEST MATRIX AND CONDITIONS**

5.1 Detailed test matrix

| | |
|---|---|
| 5.1.1 Number of test cases | 15 |
| 5.1.2 Number of configurations | 1 |
| 5.1.3 Test matrix table | See table 1 |

5.2 Model/tunnel relations

| | |
|---|---|
| 5.2.1 Maximum blockage | S2MA : 0.5 %<br>S3MA : 2.5 % |
| 5.2.2 Model span/tunnel width | S2MA : 0.13<br>S3MA : 0.31 |

5.3 Transition details

| | |
|---|---|
| 5.3.1 Transition | The tests were made with a free transition and the natural transition location was not determined during these tests. Nevertheless, from other tests on the same geometry, and from Navier-Stokes calculations, it seems that the transition has only a very little effect on the flow feature and local forces, in supersonic flow. |
| 5.3.2 Natural transition verified | No |

**6. DATA**

6.1 Availability of data

| | |
|---|---|
| 6.1.1 Organisation | ONERA |
| 6.1.2 Responsible of the data | Patrick CHAMPIGNY<br>Deputy Head of Applied Aerodynamic Division<br>B.P. 72<br>92322 CHATILLON CEDEX FRANCE<br>Telephone : 1.46.73.41.88<br>Fax : 1.46.73.41.46 |
| 6.1.3 Data freely available | Yes |

| | |
|---|---|
| 6.2 Suitability of data for CFD validation | |
| 6.2.1 Suitable for "in tunnel" calculation | No, because the boundary conditions are unknown. |
| 6.2.2 Correction to simulate "free air" conditions | Even without correction, the data are considered suitable for "free-air" conditions. |
| 6.3 Type and form in which data are available | |
| 6.3.1 Type and form | See table 2 |
| 6.3.2 Data carrier | Floppy disk |
| 6.4 Corrections applied to data | No corrections have been applied to data |
| 6.4.1 Blockage corrections | The blockage effects evaluated by an analytical method (using distributed singularities) are small (maximum for Mach 0.9 : $\Delta Cp \leq 10^{-2}$) |
| 6.4.2 Sting and support corrections | The sting and support interferences evaluated by an analytical method are more important (up to $\Delta Cp = 5\ 10^{-2}$ at the rear part of the body). |
| 6.5 Test result examples | Figure 8 shows some typical pressure distributions at $\alpha = 10°$, for different Mach numbers. |

## 7. DATA ACCURACY AND REPEATABILITY ASSESSMENT

| | |
|---|---|
| 7.1 Estimate accuracy | $\Delta M = 0.5\ 10^{-3}$ |
| 7.1.1 Free stream conditions | $\Delta\alpha = 0.01°$ |
| 7.1.2 Pressure coefficient | $\Delta Cp = 3.10^{-3}$ |
| 7.2 Repeat measurements | |
| 7.2.1 Within one test campaign | Yes, for each Mach number (example, figure 6) |
| 7.2.2 In successive campaigns | No |
| 7.3 Redundant measurements | No |
| 7.4 Other tests on same geometry | Flow-field measurements on a smaller model (L = 0.36 m) at Mach 2 $\alpha$ = 10°/20° were made in the S5Ch wind tunnel, to complement the pressure measurements. Some examples are given in [1], which shows also typical Navier-Stokes results (figure 7). |

## 8. REFERENCES

[1] C. JOUET, P. D'ESPINEY
3D Laminar and 2D Turbulent computations with the Navier-Stokes solver FLU3M.
8th Int. Conf. on Numerical Methods, July 93, Swansee, U.K.

## 9. LISTE OF SYMBOLS

Cp : pressure coefficient

Mo : freestream Mach number

Pto : freestream total pressure

$Re_L$ : Reynolds number based on total length

To : freestream total temperature

$\alpha$ : incidence angle

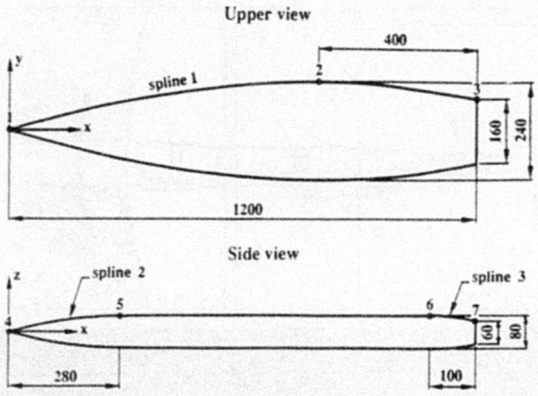
$\beta$ : sideslip angle

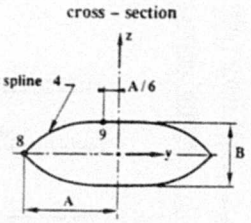
| WIND - TUNNEL | Mo | Pto3 ( $10^5$ Pa ) | To ( K ) | $Re_L$ ( $10^6$ ) | $\alpha$ , $\beta$ |
|---|---|---|---|---|---|
| S2 MA | 0.4 | 1.2 | 287 | 12.5 | $\alpha$ = 0 / 10 / 20 $\beta$ = 10 |
| | 0.9 | 1.2 | 295 | 20.5 | $\alpha$ = 0 / 10 / 20 $\beta$ = 10 |
| | 2.0 | 1.2 | 295 | 17.5 | $\alpha$ = 0 / 10 / 20 $\beta$ = 10 |
| S3 MA | 4.5 | 6.0 | 370 | 18.6 | $\alpha$ = 0 / 10 $\beta$ = 10 |

**Table 1 – Test matrix table**

| DATA | ENGIN. UNITS | COEFFICIENTS | NORMALIZED | UNCORRECTED | CORRECTED |
|---|---|---|---|---|---|
| FREESTREAM CONDITIONS | X | X | | X | |
| SURFACE PRESSURES | | X | | X | |

**Table 2 – Data availability**




| point | spline parameters | | |
|---|---|---|---|
| 1 | y = 0 | dy/dx = 0.3 | |
| 2 | y = 120 | dy/dx = 0 | $d^2y/dx^2 = 0$ |
| 3 | y = 80 | $d^2y/dx^2 = 0$ | |
| 4 | z = 0 | dz/dx = 0.3 | |
| 5 | z = 40 | dz/dx = 0 | $d^2z/dx^2 = 0$ |
| 6 | z = 40 | dz/dx = 0 | $d^2z/dx^2 = 0$ |
| 7 | z = 30 | $d^2z/dx^2 = 0$ | |
| 8 | z = 0 | $dz/dy = \tan \frac{18\,B}{5\,A}$ | |
| 9 | z = B | dz/dy = 0 | $d^2z/dy^2 = 0$ |

figure 1 – "ONERA PPF" body geometry

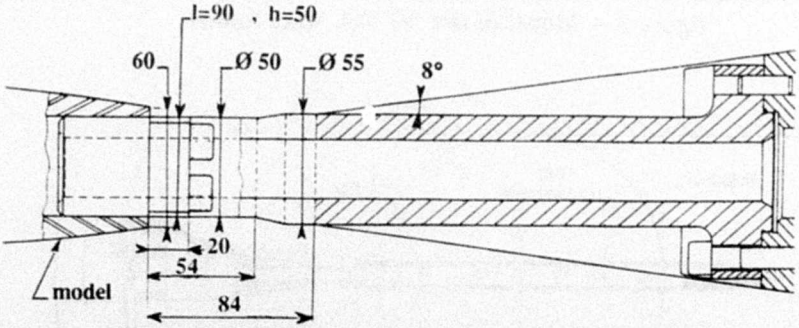
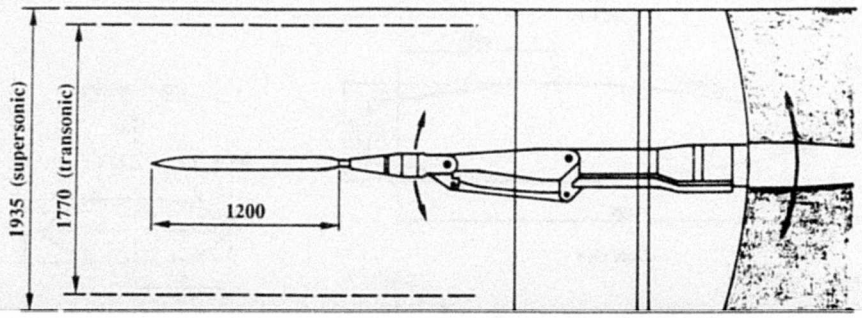





**figure 2 – Model base and sting details**



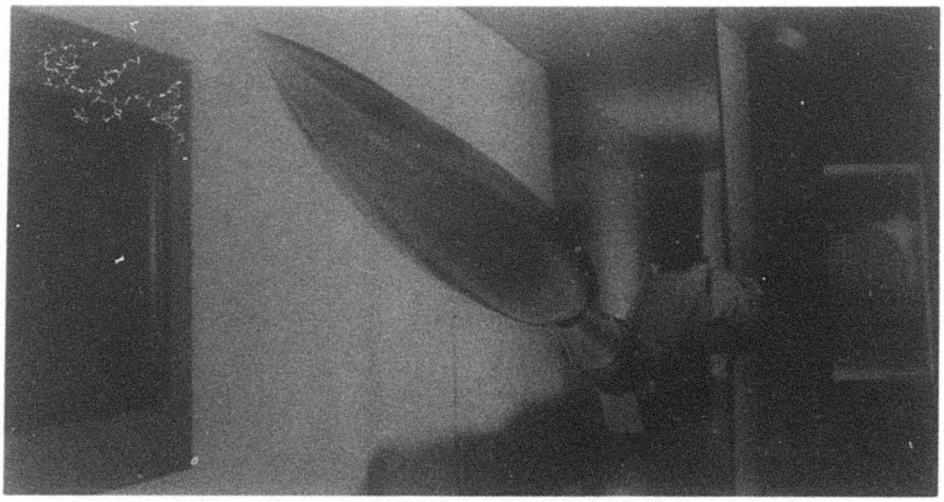
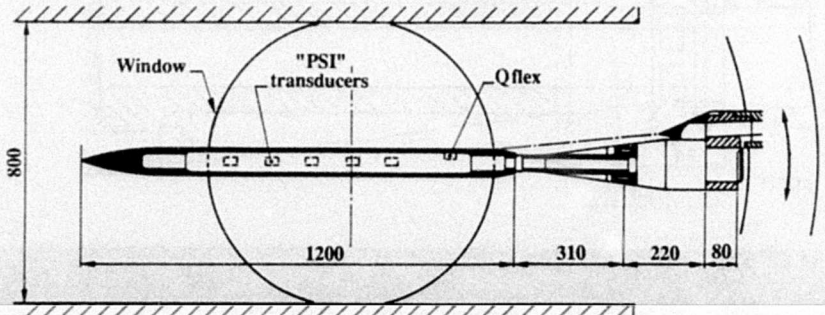



figure 3 – Model in the S2 MA wind tunnel



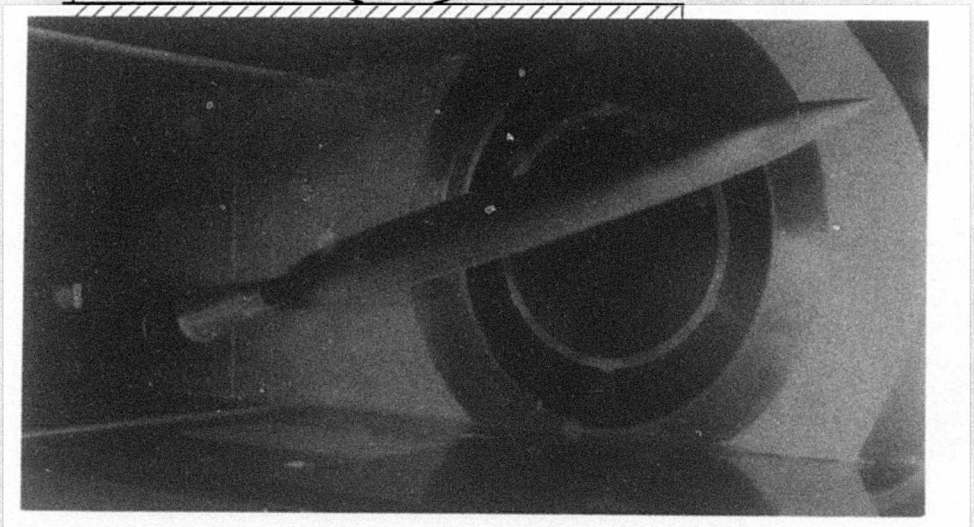



**figure 4 – Model in the S3 MA wind tunnel ( M = 4. 5 )**

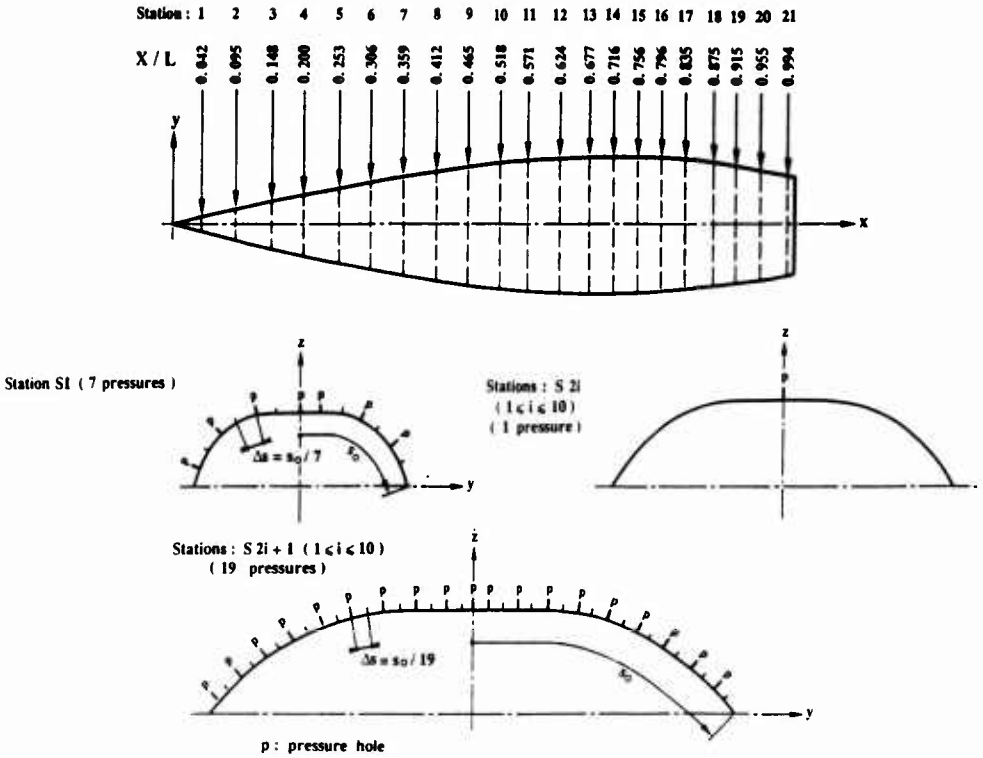



figure 5 – Model instrumentation .
207 pressure taps on upper surface

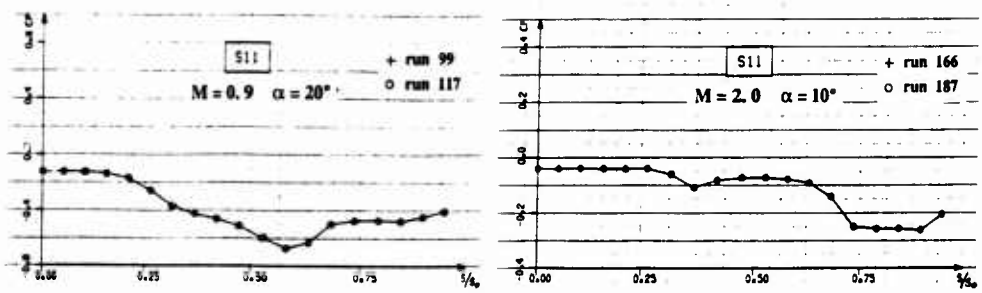



figure 6 – Repeatability of data

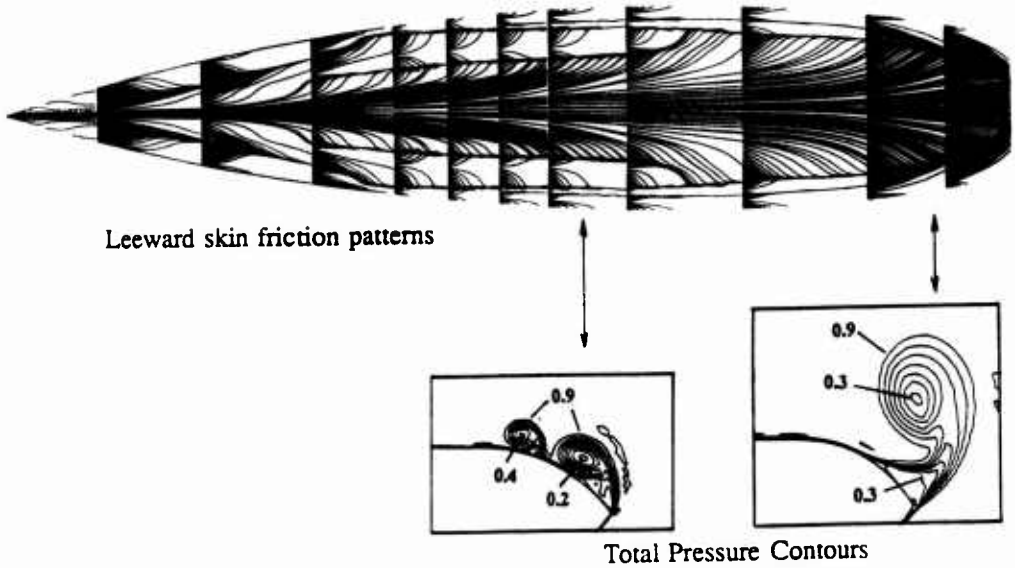



Figure 7 – Navier–Stokes computation – Mach = 2 , $\alpha$ = 10° [ 1 ]

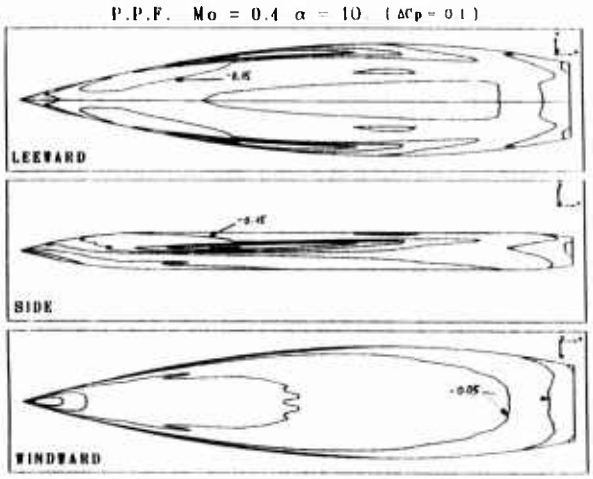
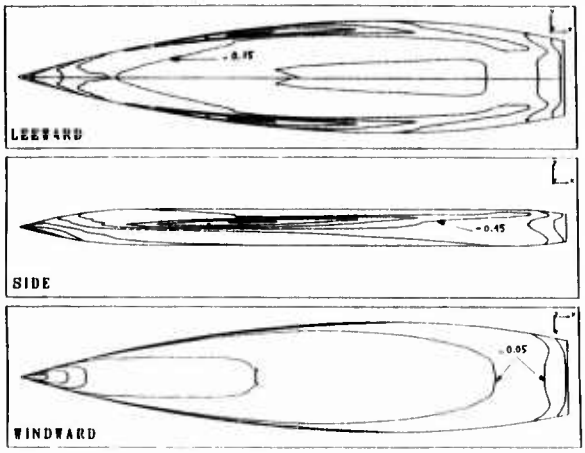
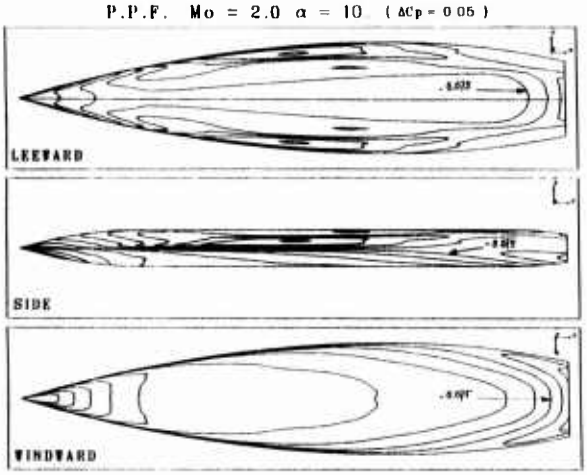



Figure 8 – Typical test results – Effect of the Mach number on the pressure coefficient distributions

P.P.F. Mo = 0.9 α = 10. ( ΔCp = 0.1 )




P.P.F. Mo = 2.0 α = 10 ( ΔCp = 0.05 )




P.P.F. Mo = 4.5 α = 10 ( ΔCp = 0.05 )

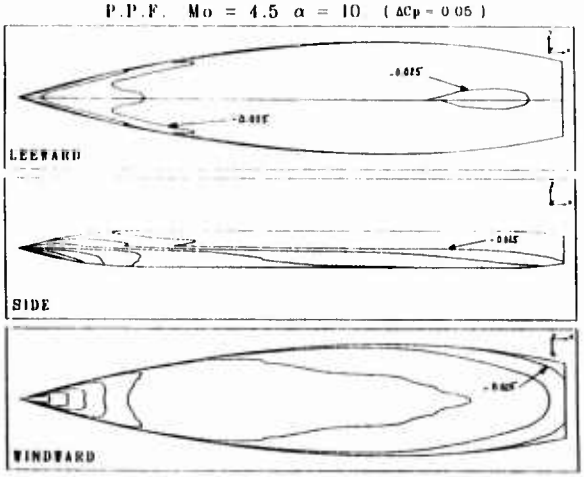



**Figure 8 – concluded**

# WIND TUNNEL TEST ON A 65 DEG DELTA WING WITH A SHARP OR ROUNDED LEADING EDGE - THE INTERNATIONAL VORTEX FLOW EXPERIMENT -

A. Elsenaar
NATIONAL AEROSPACE LABORATORY NLR
ANTHONY FOKKERWEG 2
1059 CM AMSTERDAM
THE NETHERLANDS

## 0. INTRODUCTION

The windtunnel tests carried out on this model resulted from an international co-operation that involved the aeronautical laboratories AFWAL (US), DLR (Germany), FFA (Sweden), NLR (The Netherlands) and the Universities of Braunschweig (Germany) and Delft (The Netherlands). It was the basic aim of these measurements to provide detailed pressure and flow field data on a 65 deg delta wing configuration of a generic shape for the validation of CFD methods, notably Euler methods. For this reason one of the basic configurations had a sharp leading edge. However, there was also considerably interest for configurations with more realistic features and therefore other configurations were added. These featured a wing with a smaller sweep angle (55° instead of 65°), a rounded instead of a sharp leading edge shape, a drooped leading edge and the addition of a canard wing (see fig.1). The windtunnel tests were made in different wind tunnels with different models (see table 1 and 2). They covered a large range of flow conditions and measuring techniques (including force, pressure and flow field measurements) as summarized in the tables 3 to 5 (see also reference 1). The test case to be described here covers only the force and pressure measurements as carried out at NLR in the transonic windtunnel HST and the supersonic windtunnel SST. The measurements executed at DLR, including flow field measurements, can be found in case D-4.

## 1. GENERAL DESCRIPTION

### 1.1 Model name or designation

The International Vortex Flow Experiment

### 1.2 Model type and flow conditions

65 deg delta wing with separated or partly separated flow at the leading edge; tested at subsonic, transonic and supersonic flow conditions

### 1.3 Design requirements

- simple geometry
- minimal influence of supporting body (mounted underneath the delta wing, not protruding in front of the wing)
- constant airfoil shape in streamwise direction
- cropped wing tips

### 1.4 Dominant flow physics

a) Vortex flow at transonic conditions with cross flow shocks and a rear shock (fig.2,3)
b) Classification of vortex flow development from subsonic up to supersonic leading edges for the rounded L.E. case (see fig.4)
c) Well developed vortex flow with separation all along the (sharp) leading edge (fig. 5 to 8)
d) Effect of wing leading edge shape (sharp or rounded) on primary vortex formation (see fig.9,10)
f) Vortex burst and the subsequent break-down of the flow field (see fig.11)
See also ref.1,2 and 3 for a discussion of the flow.

## 2 DETAILS OF MODEL

### 2.1 General geometric arrangement

see fig.12 and Geometry figures G1-G10

### 2.2 Configurations tested

A: sharp leading edge, no canard
B: rounded leading edge, no canard
C: rounded and drooped leading edge, no canard
D: sharp leading edge, with canard

### 2.3 Wing and airfoil data

#### 2.3.1 Planform

- leading edge sweep: 65°
- trailing edge sweep: 0°
- no twist
- cropped wing tip
- body mounted (almost completely) underneath the wing

#### 2.3.2 Basic wing section

- constant airfoil section in streamwise direction
- modified NACA 64A005 profile; straight line aft of 75% chord
- conf.A & D: sharp leading edge (.7 % local chord L.E.radius connected with a simple polynominal curve to the 40% chord position)
- conf.B & C: rounded leading edge as NACA profile

- no camber
- 5% relative thickness

**2.4 Body data**
See fig.12, 15 and G1-G3

**2.5 Canard wings**
Biconvex airfoil with max. t/c=.05
- 60° L.E. sweep; 35° T.E. sweep
- mounted in plane of main wing (see fig.12 and G8-G10)

**2.6 Geometric definition of all components**
- how is shape defined:
  partly numerically, partly analytically
- designed or measured coordinates:
  designed
- tolerances:
  quoted as "close to its prescribed value"

**2.6 Model support details**
I HST tests:
The model was mounted on a rear sting connected to the yaw angle support (see fig.15)
II SST tests:
The model was mounted on the straight sting support (see fig.16)

## 3 GENERAL TUNNEL INFORMATION

**3.1 Tunnel designation**
I High Speed Wind Tunnel HST (see ref.4)
II Supersonic Windtunnel SST (see ref.5)

**3.2 Organisation running the tunnel**
National Aerospace Laboratory NLR,
Amsterdam, The Netherlands

**3.3 Tunnel characteristics**
I closed circuit; see fig. 13 for operating conditions
II blow down; see fig. 14 for operating conditions; typical run time 30 to 60 sec

**3.4 Test section**

**3.4.1 Model mounting and instrumentation**
I see fig.15
II see fig.16

**3.4.2 Test section dimensions**
I 2.00x1.60x2.70 m
(widthxheightxlength)
II 1.2x~1.2 m cross section; uniform flow over ~1.2 m in flow direction (depending on Mach number)

**3.4.3 Wall geometry**
I • slotted top and bottom walls;
closed side walls
• open area ratio 12% per wall
II • all walls closed

**3.5 Freestream conditions**
**3.5.1 Reference flow conditions**
I • total pressure: settling chamber
• static pressure: from plenum pressure with correction derived from calibration
• static temperature: from total temperature in settling chamber and Mach number
II • total pressure in settling chamber
• upstream wall pressure and correction derived from calibration

**3.5.2 Tunnel calibration**
I • "long static pipe" at tunnel center and side wall pressures;
• last "long static pipe" calibration: 1980; regular checks on possible changes from side wall pressures
II • optimization/calibration of the tunnel flow by means of (vertical) traversing rake with static pressures along the tunnel centre line and side wall pressures

**3.6 Flow quality (empty tunnel)**

**3.6.1 Flow uniformity**
I • Mach number variation over model chord: < .001 (at Mach=.75)
• Mach number variation during a run: < ± .001
• average flow angularity: average value of ≈.2° (Mach number dependent) and derived from comparison of model upright and inverted tests at tunnel centre
• variation of flow angularity over model span: not measured; estimated to be less then .2 °
II • Mach number variations < .01 to .02 (Mach number dependent)
• flow angularity determined from model upright and inverted tests,
Mach number dependent
• flow angularity variation < .1°

**3.6.2 Temperature variation**
I • temperature can be controlled during a run;
• variation during a run less then 1° to 3° depending on Mach and Reynolds number
II • temperature variation during a run less then 3° (Mach number dependent)

**3.6.3 Flow unsteadiness**
I • turbulence level not measured but assumed to be very low in view of the high contraction ratio (1:25);

- overall noise level:
  .5% < $C_p$-RMS < 1%

II • overall noise level:
  .5% < $C_p$-RMS < 2%

depending on Mach number and time

## 4 INSTRUMENTATION

### 4.1 Model position

- model incidence derived from support angle corrected for model deflection under load
- accuracy: ± .05°

### 4.2 Model pressure measurements

#### 4.2.1 Number and disposition of pressure holes

- 90 pressure holes (see fig. 12 and G1-G6) (measured by scanivalves)

#### 4.2.2 Type, range and accuracy of pressure transducers

I • model pressures with differential transducers of ±350 and ±100 kPa
  • wall pressures 17 kPa

II • model pressures measured with absolute transducers ranging from 172 kPa (Ma=1.31) up to 1035 kPa (Ma=3.94)

- accuracy: ± .2% Full Scale

### 4.3 Force and moment measurements

- TASK 2" extended range
- range:
  normal force 9220 N
  axial force 930 N
  pitching moment 461 Nm
- accuracy: ± .3% Full Scale

### 4.4 Flow field measurements

Made at FFA (5-hole probe) and DLR (LDV) on a geometrical identical though smaller model

### 4.5 Surface flow visualization

I and II • oil flow during and after a run
data available on photograph's

### 4.6 Flow field visualization

- Schlieren pictures in side view
  available as photograph's

### 4.5 Tunnel wall pressure measurements

I • on centre slat of upper and lower wall; 25 pressures each (see fig.17)

## 5 TEST MATRIX AND CONDITIONS

### 5.1 Detailed test matrix

Out of all NLR data (see fig. 18) a selection has been made for cases of interest provided on floppy disk. These cases are described in the tables 6-10 and relate to the sharp and rounded leading edge configuration tested in the HST and the SST (symetrical conditions only) and a few cases for the sharp leading edge configuration with the canard added, measured in the HST at ijawing conditions.

### 5.2 Model/tunnel relations

- maximum blockage: < .5%
- model span/tunnel width:
  I .24 II .4
- wing area/tunnel cross section:
  I ~.05 II ~.1

### 5.3 Transition details

#### 5.3.1 Free or fixed transition

all data with free transition

#### 5.3.2 Details of free transition

- for Mach=.85, α=10°, 20°, Re=9.10**6 acenaphtene tests have been made that indicated on the upper surface a laminar flow region close to the wing apex (less then .04 m) and an equally small laminar region on the fuselage nose; also, test were made with a carborundum strip wrapped around the model nose (3 mm wide, 65 mm from the apax) that indicated no noticeable effect on the pressure distribution; from these test it was concluded that the boundary layer flow on the model was effectively turbulent for a Reynolds number (based on root chord) of 9 million and beyond. (See ref. 9 for a discussion)

## 6 DATA

### 6.1 Availability of data

#### 6.1.1 Organisation owing data

NLR

#### 6.1.2 Who is responsible for the data


- P.B. Rohne
- tel (020) 5113360
- fax (020) 5113210


#### 6.1.3 Are data freely available

yes

### 6.2 Suitability of data for CFD validation

- data are corrected to "free-air" conditions

### 6.3 Type and form in which data are available

#### 6.3.1 Type and form
- model geometry: numerically (in tables) on floppy disc (canard wing given in figures)
- test data available in tables on floppy disk

#### 6.3.2 Data carrier
floppy disk

#### 6.3.3 Extent of data
460 Kbyte

### 6.4 Corrections applied to data

#### 6.4.1 Lift interference and blockage corrections
for the present model size data are considered to be interference free and hence no correction are applied (this is based on a number of comparisons between the HST and other wind tunnels)

#### 6.4.2 Sting and support corrections
I: static pressures are corrected for the upstream support influence using the empty tunnel center line pressure distribution with the model support present

I and II: drag values are corrected for base drag, using the measured base pressure

#### 6.4.3 Elastic deformation
negligible small; no corrections applied

## 7 DATA ACCURACY AND REPEATABILITY ASSESSMENT

### 7.1 Accuracy estimates

#### 7.1.1 Free stream conditions
$\Delta$ Mach < (I) .003 ; (II) .01
$\Delta \alpha$ < (I&II) .05°

#### 7.1.2 Measured data

| | Mach=.85 | Mach=2.2 |
|---|---|---|
| $\Delta c_L <$ | $\pm$ .005 | .002 |
| $\Delta c_D <$ | $\pm$ .0005 | .0002 |
| $\Delta c_M <$ | $\pm$ .0004 | .00016 |
| $\Delta c_p <$ | $\pm$ .006 | .005 |

### 7.2 Repeat measurements
0 various tunnel entries have been made with the same model indicating no differences within the measurement accuracy

### 7.3 Other tests made
comparisons have been made with results obtained for an identical though smaller scale model measured in the 1x1 $m^2$ transonic windtunnel in Göttingen and in the FFA S-4 blow down tunnel; these comparisons are fair, small differences probably being due to differences in Reynolds number (see fig.19,20)

### 7.4 Additional remarks
more detailed pressure measurements for the sharp leading edge configuration have been obtained on an almost identical configuration; however these results are as yet not freely available; some results, however, have been presented in ref.3

## 8 REFERENCES


1. Elsenaar, A., et al, "The international vortex flow experiment paper", presented at the AGARD FDP Symposium "Validation of Computational Fluid Dynamics", 1987; Lisbon; AGARD CP 437.
2. Elsenaar, A., Bütefisch, K.A., "Experimental study on vortex and shock wave development on a 65° delta wing". Proceedings Symposium Transonicum III, IUTAM, 1988.
3. Hoeijmakers, H.A.M., Elsenaar, A., Symposium Vortex Flow Aerodynamics; Scheveningen, 1990; AGARD CP494, paper 15.
4. Users' guide to the 1.60x2.0 $m^2$ High Speed Wind Tunnel HST of the National Aerospace Laboratory NLR.
5. Users' guide to the 1.2x1.2 $m^2$ windtunnel SST of the National Aerospace Laboratory NLR.
6. Hirdes, R.H.C.M., US/European vortex flow experiment; test report of windtunnel measurements on the 65° wing in the NLR high speed wind tunnel HST, NLR TR 85046 L.
7. Boersen, S.J., US/European vortex flow experiment; test report of windtunnel measurements on a 65°delta wing in the NLR supersonic facility SST, NLR TR 86117 L.
8. Boersen, S.J. Geometry of AFWAL 65°-sweep delta wing configurations, NLR Memorandum AC-87-012.
9. Elsenaar, A., Eriksson, G. Symposium on the international vortes flow experiment on Euler Code Validation (printed by FFA; 1986).

TABLE 1
MODEL CHARACTERISTICS (INTERNATIONAL PROGRAM)

| MODEL | $\Lambda_{LE}$ (°) | b (m) | $C_{ROOT}$ (m) | CANARD MOUNTING POSSIBLE | REMARKS |
|---|---|---|---|---|---|
| AFWAL | 65 | .476 | .500 | YES | Combined Forces & Pressures ($X/C_R$=.3,.6,.8) |
| MBB | 65 | .333 | .420 | YES | Forces or Pressures ($x/c_R$=.3,.6,.8; $y/\frac{1}{2}b$=.55) |
| FFA | 55 | .410 | .345 | YES | Combined Forces & Pressures ($x/c_R$=.3,.6,.8; $y/\frac{1}{2}b$=.20,.50,.85) |
| DELFT | 65 | .095 | .120 | NO | Flat Upper Surface; Nose Protruding in Front of Apex; No Pressure Holes |

TABLE 2
WIND TUNNEL CHARACTERISTICS (INTERNATIONAL PROGRAM)

| TUNNEL | TYPE | TEST SECTION DIMENSIONS ($m^2$) | MACH-RANGE | WALL CONFIGURATION |
|---|---|---|---|---|
| NLR-HST | CONT. | 1.6 x 2 | M<1.3 | Slotted Upper & Lower Wall |
| NLR-SST | BLOW DOWN | 1.2 x 1.2 | 1.3<M<4.0 | Closed |
| DFVLR-TWG | CONT. | 1 x 1 | .4<M<2.2 | Perforated* |
| FFA-S4 | BLOW DOWN | .92 x .90<br>.92 x 1.15 | .5<M<1.2<br>M=1.31/1.42/1.71/1.93 | Slotted Upper & Lower Wall<br>Closed |
| DUT-TST27 | BLOW DOWN | .28 x .255 | 0.55<M<0.85 | Closed |

* At time of tests

TABLE 5
SUMMARY OF FIELD MEASUREMENTS (INTERNATIONAL PROGRAM)

| TEST BY | MODEL | TUNNEL | CONFIGURATION Λ 55° 65° | L.E. SHARP ROUNDED DROOPED | CANARD OFF ON | TEST CONDITIONS MACH | α (°) | β (°) | Re x $10^{-6}$ | TYPE OF MEASUREMENTS/ STATIONS(x/c) |
|---|---|---|---|---|---|---|---|---|---|---|
| DFVLR | MBB | TWG | - X | - X - | X - | | 10 | 0 | 4.5 | LDA(.6/.8) |
| | | | | | | | 20 | 0 | | " (.6/.8/SP) |
| | | | | | | | 25 | 0 | | " (.8) |
| FFA | FFA | S4 | X - | - X - | X X | .85 | 10 | 0 | 4.6 | PP(.3/.6/.8/.95)+ |
| " | MBB | S4 | - X | - X - | X X | | 10 | 0 | 5.6 | PP(.3/.6/.8/.95)+ |
| DELFT | DELFT | TST-27 | - X | FLAT | X - | | 10,20 | 0 | " | PP(.3/.6/1.0/SP) |

NOTE LDA = Laser Doppler Anemometry
PP = Pressure Probe
SP = Plane of Symmetry
\+ = Plus some extra conditions

TABLE 3
SUMMARY OF FORCE AND PRESSURE MEASUREMENTS (INTERNATIONAL PROGRAM)

| TEST BY | MODEL | TUNNEL | CONFIGURATION Λ 55° | Λ 65° | L.E. SHARP | L.E. ROUNDED | L.E. DROOPED | CANARD OFF | CANARD ON | MACH | α (°) | β (°) | Re x $10^{-6}$ | TYPE OF MEASUREMENTS |
|---|---|---|---|---|---|---|---|---|---|---|---|---|---|---|
| NLR | AFWAL | HST | - | X | X | X | X | X | - | .4 | -1(1)25 | 0 | 9 | F&P |
| " | " | " | - | X | X | - | - | X | X | " | 10,16(2)24 | -5(2½)5 | " | " |
| DFVLR | MBB | TWG | - | X | - | X | - | X | X | .5 | 0(2)22 | 0 | 4.5 | F&P |
| FFA | FFA | S4 | X | - | - | X | - | X | X | " | -1(1)24 | 0 | 3.3 | " |
| NLR | AFWAL | HST | - | X | X | X | X | X | - | | -1(1)25 | 0 | 9 | F&P |
| DFVLR | MBB | TWG | - | X | - | X | - | X | X | .7 | 0(2)22 | 0 | 4.5 | " |
| FFA | FFA | S4 | X | - | - | X | - | X | X | | -1(1)24 | 0 | 4.2 | " |
| NLR | AFWAL | HST | - | X | X | X | X | X | - | | -1(1)25 | 0 | 9 | F&P |
| " | " | " | - | X | X | - | - | X | X | | 10,16(2)24 | -5(2½)5 | " | " |
| " | " | " | - | X | - | X | - | X | - | | -1(1)25 | 0 | 13 | F&P |
| DFVLR | MBB | TWG | - | X | - | X | - | X | X | | 0(2)22 | 0 | 4.5 | " |
| " | " | " | - | X | - | X | - | X | - | .85 | 0(2)22 | 0 | 2.4 | " |
| " | " | " | - | X | - | X | - | X | - | | 0(2)12 | 0 | 7 | " |
| " | " | " | - | X | - | X | - | X | - | | 25 | 0 | 4.5 | " |
| FFA | FFA | S4 | X | - | - | X | - | X | X | | 1(1)24 | 0 | 4.6 | F&P |
| " | " | " | X | - | - | X | - | X | X | | 12(2)18 | -5(1)5 | " | F&P |
| NLR | AFWAL | HST | - | X | X | X | X | X | - | | -1(1)10 | 0 | 7 | F&P |
| DFVLR | MBB | TWG | - | X | - | X | - | X | X | 1.2 | 0(2)8+ | 0 | 4.5 | F&P |
| FFA | FFA | S4 | X | - | - | X | - | X | X | | -1(1)12 | 0 | 5.1 | F&P |
| NLR | AFWAL | SST | - | X | X | X | - | X | - | ~1.3 | 0(~2)12 | 0 | ~15 | F&P |
| " | " | " | - | X | X | X | - | X | - | ~1.7 | 0(~2)14 | 0 | ~15 | " |
| " | " | " | - | X | X | X | - | X | - | ~2.2 | 0(~2)10 | 0 | ~18 | " |
| " | " | " | - | X | X | X | - | X | - | ~3.0 | 0(~2)10 | 0 | ~28 | " |
| " | " | " | - | X | X | X | - | X | - | ~3.9 | 0(~2)6 | 0 | ~42 | " |

+ plus some extra conditions

TABLE 4
SUMMARY OF VISUALIZATIONS (INTERNATIONAL PROGRAM)

| TEST BY | MODEL | TUNNEL | CONFIGURATION Λ 55° | Λ 65° | L.E. SHARP | L.E. ROUNDED | L.E. DROOPED | CANARD OFF | CANARD ON | MACH | α (°) | β (°) | Re x $10^{-6}$ | TYPE OF MEASUREMENTS |
|---|---|---|---|---|---|---|---|---|---|---|---|---|---|---|
| FFA | FFA | S4 | X | - | - | X | - | X | X | .5 | 0(5)25+ | 0 | 3.3 | Oil Flow & Schlieren |
| DELFT | DELFT | TST-27 | - | X | FLAT | | | X | - | .55 | 5(5)20 | 0 | 1.5-3.6 | Oil Flow & Schlieren |
| FFA | FFA | S4 | X | - | - | X | - | X | X | .7 | 0(5)25+ | 0 | 4.2 | Oil Flow & Schlieren |
| DELFT | DELFT | TST-27 | - | X | FLAT | | | X | - | .7 | 5(5)20 | 0 | 1.8-4.2 | Oil Flow & Schlieren |
| NLR | AFWAL | HST | - | X | - | X | - | X | - | | 5,10,20 | 0 | 9 | Oil Flow |
| " | " | " | - | X | - | X | - | X | - | | 10,20 | 0 | 9 | Acenaphtene |
| " | " | " | - | X | - | X | - | X | - | | 10(5)25 | 0 | 9 | Schlieren |
| DFVLR | MBB | TWG | - | X | - | X | - | X | - | | 25 | 0 | 4.5 | Oil Flow |
| " | " | " | - | X | - | X | - | - | X | .85 | 15,20,25 | 0 | 4.5 | Oil Flow |
| " | " | " | - | X | - | X | - | X | - | | 20,25 | 0 | 4.5 | Laser Sheet |
| " | " | " | - | X | - | X | - | - | X | | 10,15,20 | 0 | 4.5 | Laser Sheet |
| FFA | FFA | S4 | X | - | - | X | - | X | X | | 0(5)25+ | 0 | 4.6 | Oil Flow & Schlieren |
| DELFT | DELFT | TST-27 | - | X | FLAT | | | X | - | | 5(5)20+ | 0 | 2.0-4.7 | Oil Flow & Schlieren |
| FFA | FFA | S4 | X | - | - | X | - | X | X | 1.2 | 0(5)15+ | 0 | 5.1 | Oil Flow & Schlieren |
| NLR | AFWAL | HST | - | X | - | X | - | X | - | 1.32 | 10 | 0 | 15.2 | Oil Flow & Schlieren |
| | | | - | X | - | X | - | X | - | 1.72 | 4,7.9 | 0 | 15.2 | " " |
| | | | - | X | - | X | X | X | - | 2.18 | 8 | 0 | 18.7 | " " |

| dpn | NPOL | series | Mach | Reynolds * 10^6 | alpha | beta | CL |
|---|---|---|---|---|---|---|---|
| 529 | 1501 | 116 | 1.204 | 7.05 | .04 | -.01 | -.003 |
| 534 | 1501 | 116 | 1.203 | 6.99 | 5.00 | -.01 | .215 |
| 539 | 1501 | 116 | 1.198 | 7.03 | 10.00 | -.01 | .459 |
| 541 | 1502 | 116 | .402 | 9.04 | .00 | .01 | -.013 |
| 546 | 1502 | 116 | .401 | 9.00 | 5.07 | .01 | .177 |
| 551 | 1502 | 116 | .400 | 8.97 | 10.07 | .00 | .411 |
| 556 | 1502 | 116 | .401 | 8.99 | 15.06 | .00 | .660 |
| 562 | 1502 | 116 | .401 | 8.97 | 20.08 | .00 | .912 |
| 563 | 1502 | 116 | .401 | 8.97 | 21.07 | .00 | .961 |
| 564 | 1502 | 116 | .402 | 8.99 | 22.03 | .00 | 1.004 |
| 565 | 1502 | 116 | .400 | 8.99 | 23.08 | .00 | 1.055 |
| 566 | 1502 | 116 | .401 | 9.01 | 24.07 | .01 | 1.083 |
| 567 | 1502 | 116 | .401 | 9.00 | 25.06 | .00 | 1.100 |
| 573 | 1503 | 116 | .701 | 9.00 | -.01 | .00 | -.012 |
| 578 | 1503 | 116 | .701 | 9.02 | 5.02 | .00 | .183 |
| 583 | 1503 | 116 | .701 | 9.04 | 10.02 | .00 | .431 |
| 588 | 1503 | 116 | .703 | 9.06 | 15.05 | -.01 | .682 |
| 593 | 1503 | 116 | .702 | 9.04 | 20.04 | .01 | .924 |
| 594 | 1503 | 116 | .701 | 9.04 | 21.09 | .01 | .969 |
| 595 | 1503 | 116 | .701 | 9.03 | 22.10 | .01 | 1.012 |
| 596 | 1503 | 116 | .702 | 9.01 | 23.09 | .01 | 1.054 |
| 597 | 1503 | 116 | .702 | 9.01 | 24.09 | .01 | 1.093 |
| 598 | 1503 | 116 | .702 | 9.01 | 25.03 | .01 | 1.122 |
| 603 | 1505 | 116 | .851 | 9.01 | .00 | .07 | -.011 |
| 608 | 1505 | 116 | .849 | 9.02 | 5.03 | .06 | .193 |
| 613 | 1505 | 116 | .849 | 9.03 | 10.04 | .06 | .457 |
| 618 | 1505 | 116 | .850 | 9.04 | 15.06 | .06 | .719 |
| 624 | 1505 | 116 | .854 | 9.03 | 20.04 | .06 | .975 |
| 625 | 1505 | 116 | .849 | 9.00 | 21.06 | .06 | 1.022 |
| 626 | 1505 | 116 | .851 | 9.01 | 22.07 | .06 | 1.068 |
| 627 | 1505 | 116 | .850 | 9.00 | 23.07 | .06 | 1.107 |
| 628 | 1505 | 116 | .850 | 9.00 | 24.05 | .06 | .985 |
| 629 | 1505 | 116 | .850 | 9.01 | 25.03 | .06 | 1.000 |
| 630 | 1505 | 116 | .851 | 9.01 | 24.50 | .06 | .993 |

TABLE 6 VORTEX FLOW EXPERIMENT WITH SHARP L.E. IN HST

| dpn | NPOL | series | Mach | Reynolds * 10^6 | alpha | beta | CL |
|---|---|---|---|---|---|---|---|
| 454 | 2001 | 16 | 1.201 | 7.02 | -.03 | .00 | -.004 |
| 459 | 2001 | 16 | 1.202 | 7.01 | 4.99 | .00 | .210 |
| 464 | 2001 | 16 | 1.199 | 7.04 | 9.99 | .00 | .454 |
| 502 | 2003 | 16 | .849 | 9.03 | .03 | .00 | -.011 |
| 507 | 2003 | 16 | .851 | 9.01 | 5.01 | .00 | .177 |
| 515 | 2003 | 16 | .850 | 9.03 | 10.05 | .00 | .439 |
| 520 | 2003 | 16 | .849 | 9.03 | 15.05 | .00 | .704 |
| 527 | 2003 | 16 | .850 | 9.04 | 20.05 | .00 | .953 |
| 528 | 2003 | 16 | .848 | 9.03 | 21.05 | .00 | 1.002 |
| 529 | 2003 | 16 | .848 | 9.04 | 22.04 | .00 | .910 |
| 530 | 2003 | 16 | .850 | 9.05 | 23.04 | .00 | .946 |
| 531 | 2003 | 16 | .849 | 9.04 | 24.06 | .00 | .979 |
| 532 | 2003 | 16 | .848 | 9.04 | 25.03 | .00 | .995 |
| 534 | 2004 | 16 | .700 | 8.99 | .03 | .00 | -.011 |
| 539 | 2004 | 16 | .702 | 9.00 | 5.03 | .00 | .164 |
| 546 | 2004 | 16 | .702 | 9.00 | 10.06 | .00 | .403 |
| 554 | 2004 | 16 | .701 | 8.99 | 15.06 | .00 | .665 |
| 561 | 2004 | 16 | .701 | 8.99 | 20.04 | .00 | .897 |
| 562 | 2004 | 16 | .701 | 8.99 | 21.06 | .00 | .942 |
| 563 | 2004 | 16 | .702 | 9.00 | 22.05 | .03 | .948 |
| 564 | 2004 | 16 | .701 | 8.99 | 23.07 | .04 | .991 |
| 565 | 2004 | 16 | .702 | 9.00 | 24.04 | .00 | .993 |
| 566 | 2004 | 16 | .701 | 8.99 | 25.04 | .00 | 1.025 |
| 568 | 2005 | 16 | .400 | 9.00 | .06 | .00 | -.009 |
| 575 | 2005 | 16 | .400 | 9.00 | 5.07 | .00 | .154 |
| 580 | 2005 | 16 | .400 | 8.97 | 10.05 | .00 | .351 |
| 585 | 2005 | 16 | .399 | 9.00 | 15.08 | .00 | .579 |
| 591 | 2005 | 16 | .400 | 9.00 | 20.06 | .00 | .804 |
| 592 | 2005 | 16 | .399 | 8.99 | 21.08 | .00 | .847 |
| 593 | 2005 | 16 | .400 | 8.98 | 22.07 | .00 | .894 |
| 594 | 2005 | 16 | .399 | 8.97 | 23.03 | .00 | .940 |
| 595 | 2005 | 16 | .400 | 8.97 | 24.06 | .00 | .983 |
| 596 | 2005 | 16 | .400 | 8.95 | 25.05 | .00 | 1.026 |

TABLE 7 VORTEX FLOW EXPERIMENT WITH ROUNDED L.E. IN HST

| dpn | NPOL | series | Mach | Reynolds * 10^6 | alpha | beta | CL |
|---|---|---|---|---|---|---|---|
| 164 | 702 | 172 | .401 | 9.01 | 10.07 | -5.03 | .417 |
| 167 | 702 | 172 | .400 | 8.97 | 20.07 | -4.99 | .946 |
| 729 | 1801 | 172 | .403 | 9.07 | 10.05 | -.01 | .419 |
| 732 | 1801 | 172 | .400 | 8.98 | 20.07 | -.01 | .930 |
| 741 | 1803 | 172 | .400 | 9.01 | 10.05 | 5.00 | .420 |
| 744 | 1803 | 172 | .400 | 8.99 | 20.07 | 5.02 | .943 |
| 182 | 706 | 172 | .850 | 9.04 | 10.07 | -5.01 | .458 |
| 185 | 706 | 172 | .853 | 9.03 | 20.05 | -4.98 | .983 |
| 747 | 1804 | 172 | .851 | 9.03 | 10.07 | .00 | .459 |
| 750 | 1804 | 172 | .852 | 9.09 | 20.06 | .00 | .984 |
| 759 | 1806 | 172 | .850 | 9.03 | 10.05 | 5.03 | .460 |
| 762 | 1806 | 172 | .850 | 9.01 | 20.07 | 4.99 | .989 |

TABLE 8 VORTEX FLOW EXPERIMENT WITH SHARP L.E. AND CANARD IN HST

| dpn | NPOL | series | Mach | Reynolds * 10^6 | alpha | beta | CL |
|---|---|---|---|---|---|---|---|
| 1 | 801 | 111 | 1.313 | 15.41 | 4.39 | .00 | .172 |
| 3 | 901 | 111 | 1.314 | 15.34 | 8.39 | .00 | .357 |
| 2 | 901 | 111 | 1.314 | 15.30 | 10.42 | .00 | .445 |
| 4 | 401 | 121 | 1.716 | 15.75 | 3.79 | .00 | .127 |
| 6 | 501 | 121 | 1.716 | 15.59 | 7.75 | .00 | .270 |
| 5 | 501 | 121 | 1.716 | 15.51 | 9.67 | .00 | .336 |
| 9 | 701 | 131 | 2.184 | 18.76 | 4.02 | .00 | .116 |
| 8 | 601 | 131 | 2.185 | 18.87 | 8.00 | .00 | .229 |
| 7 | 601 | 131 | 2.184 | 18.79 | 9.94 | .00 | .281 |
| 10 | 1101 | 141 | 3.022 | 27.76 | 3.73 | .00 | .088 |
| 12 | 1201 | 141 | 3.020 | 27.97 | 7.73 | .00 | .169 |
| 11 | 1201 | 141 | 3.022 | 27.82 | 9.65 | .00 | .206 |
| 13 | 1501 | 151 | 3.937 | 42.41 | 4.00 | .00 | .082 |

TABLE 9 VORTEX FLOW EXPERIMENT WITH SHARP L.E. IN SST

| dpn | NPOL | series | Mach | Reynolds * 10^6 | alpha | beta | CL |
|---|---|---|---|---|---|---|---|
| 1 | 2601 | 211 | 1.314 | 15.42 | 4.32 | .00 | .169 |
| 2 | 2701 | 211 | 1.314 | 15.65 | 8.41 | .00 | .356 |
| 3 | 2801 | 211 | 1.315 | 15.65 | 10.35 | .00 | .442 |
| 4 | 2001 | 221 | 1.715 | 15.42 | 3.82 | .00 | .134 |
| 6 | 2101 | 221 | 1.715 | 15.36 | 7.75 | .00 | .272 |
| 5 | 2101 | 221 | 1.716 | 15.34 | 9.70 | .00 | .336 |
| 7 | 2401 | 231 | 2.185 | 19.16 | 4.13 | .00 | .123 |
| 9 | 2201 | 231 | 2.185 | 18.71 | 7.98 | .00 | .231 |
| 8 | 2201 | 231 | 2.185 | 18.71 | 9.96 | .00 | .281 |
| 10 | 2901 | 241 | 3.025 | 28.45 | 3.79 | .00 | .094 |
| 12 | 3001 | 241 | 3.026 | 28.30 | 7.70 | .00 | .171 |
| 11 | 3001 | 241 | 3.025 | 28.29 | 9.67 | .00 | .208 |
| 13 | 3201 | 251 | 3.934 | 42.60 | 3.97 | .00 | .077 |

TABLE 10 VORTEX FLOW EXPERIMENT WITH ROUDED L.E. IN SST

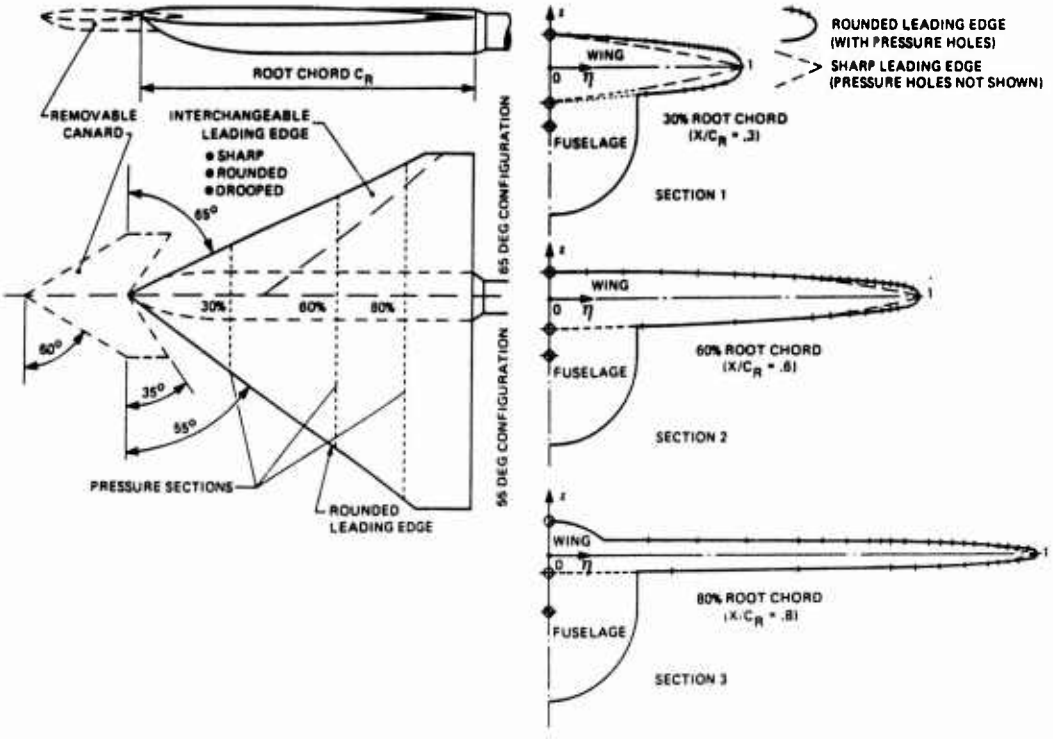



*Fig.1 Summary of model configurations of the international vortex flow* experiment.

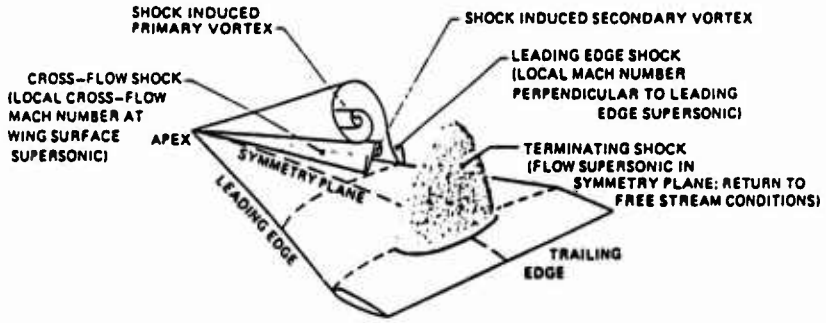



*Fig.2 Shock waves on a delta wing at transonic conditions (tentative).*

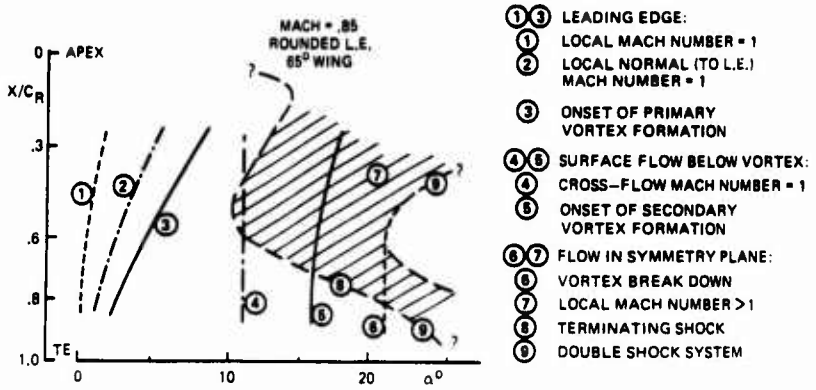



*Fig.3 Flow phenomena on delta wing at Mach = .85.*

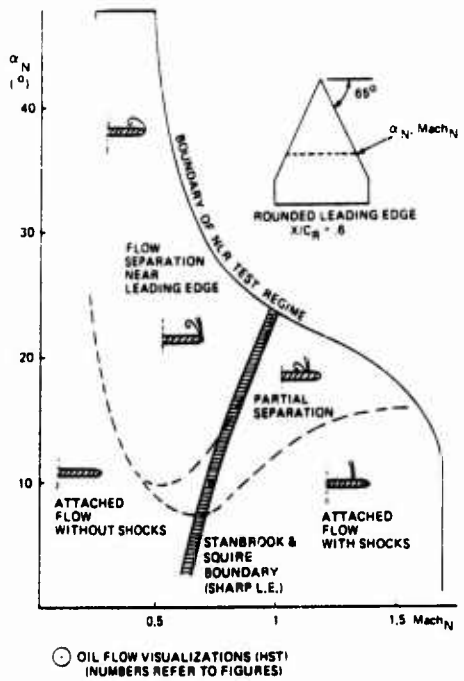



***Fig.4 Tentative flow classification (65 deg delta wing, rounded L.E., $x/c_r = .6$).***

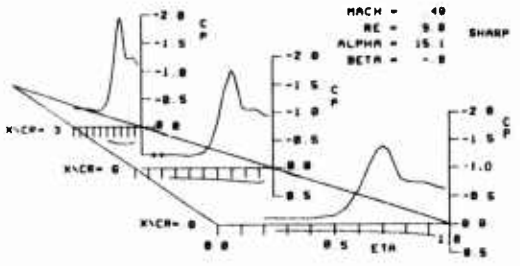



Fig.5 Test case 1 of Ref.1 (sharp leading edge).

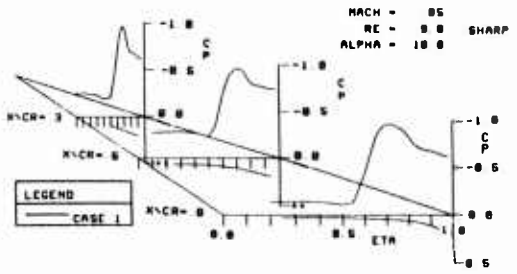



Fig.6 Test case 2 of Ref.1 (sharp leading edge).

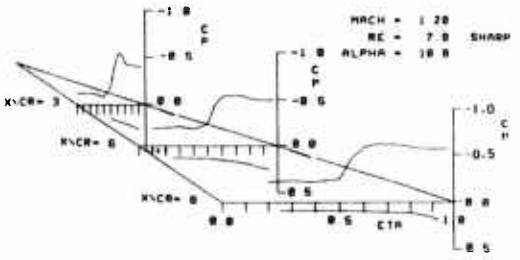



Fig.7 Test case 3 of Ref.1 (sharp leading edge).

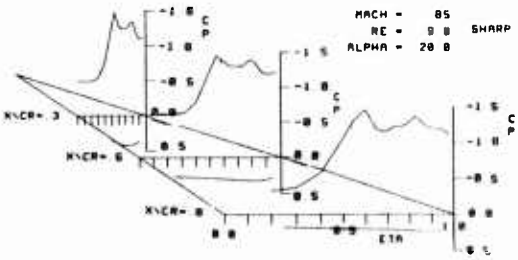



Fig.8 Test case 4 of Ref.1 (sharp leading edge).

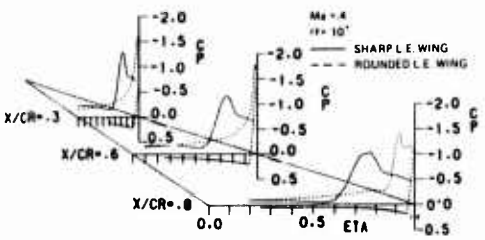



Fig.9 Influence of leading edge shape at subsonic conditions. (Mach = .4, $\alpha = 10^{o}$).

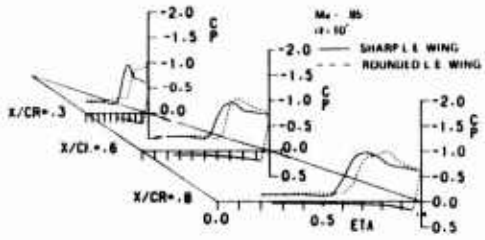



Fig.10 Influence of leading edge shape at transonic conditions. (Mach = .85 and $\alpha = 10^{o}$).

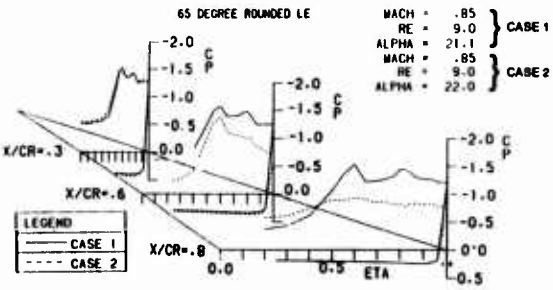



Fig.11 Pressure distributions before and after vortex burst.

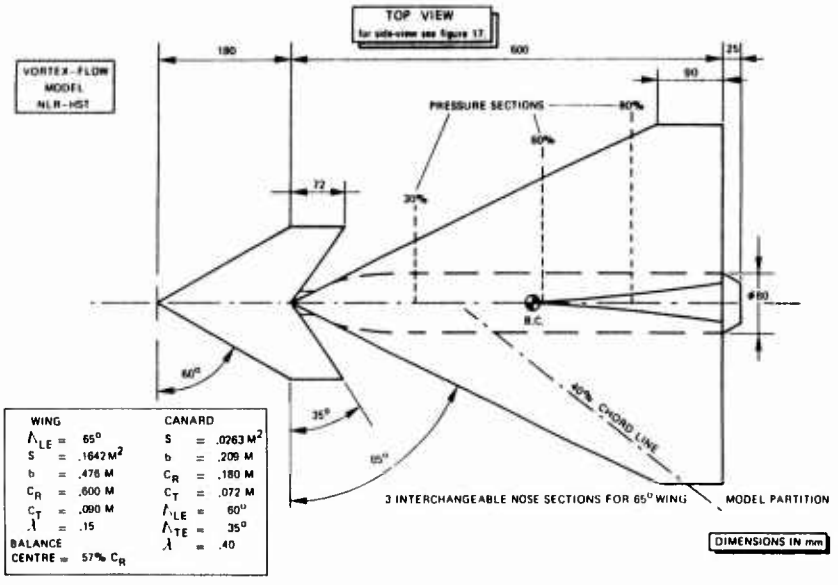



*Fig.12 Main geometric dimensions of 65° vortex flow model.*

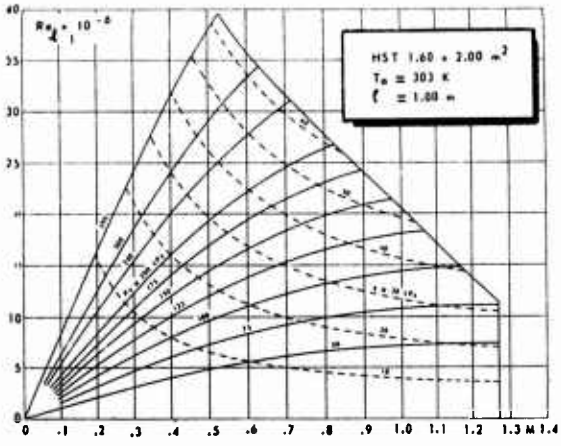



*Fig.13 Performance chart of the high - speed wind tunnel HST.*

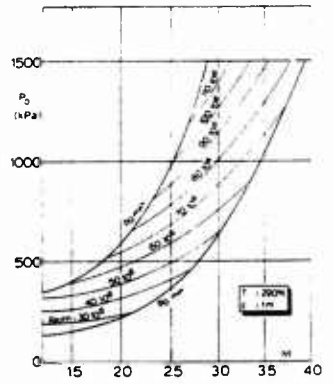


*Fig.14 The stagnation pressure as a function of the Mach number at various constant Reynolds numbers.*

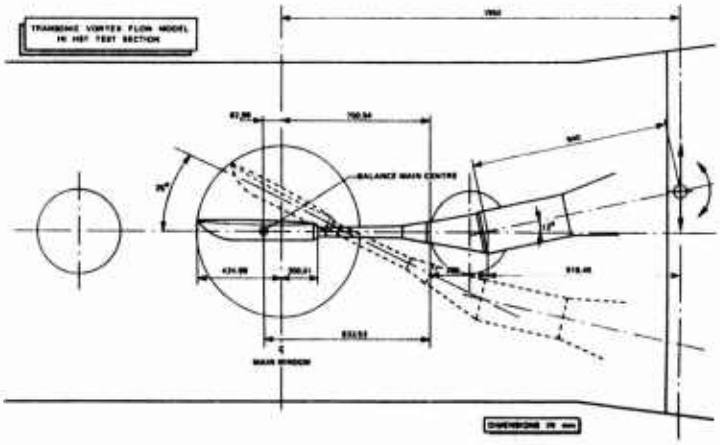



*Fig.15 Position of vortex flow model in HST test section.*

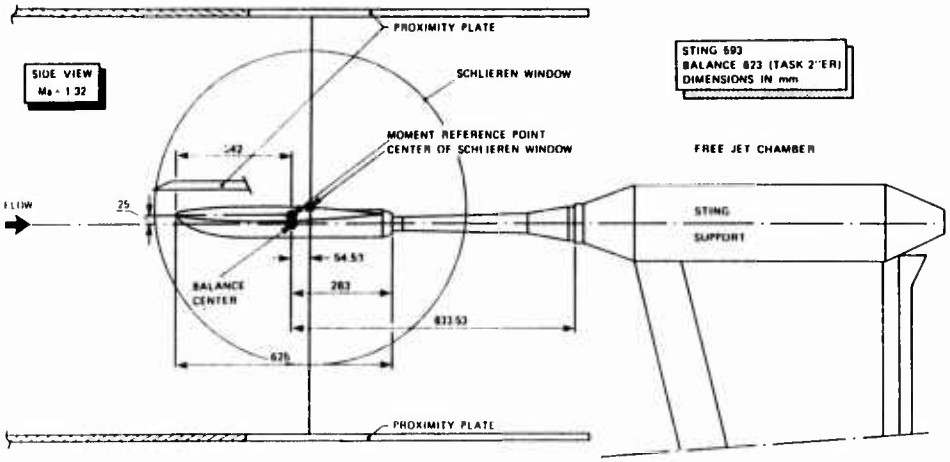



*Fig.16 Position of vortex flow model in SST test section.*

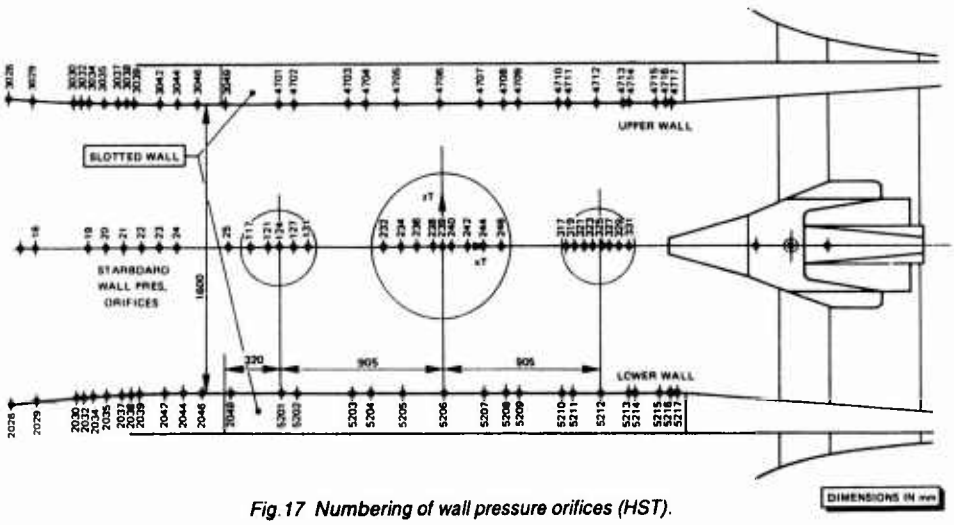



*Fig.17 Numbering of wall pressure orifices (HST).*

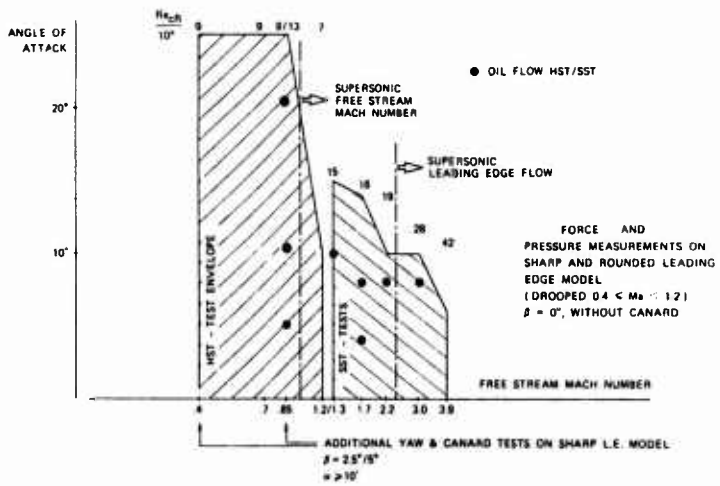



*Fig.18 Summary of 65° delta wing tests at NLR.*

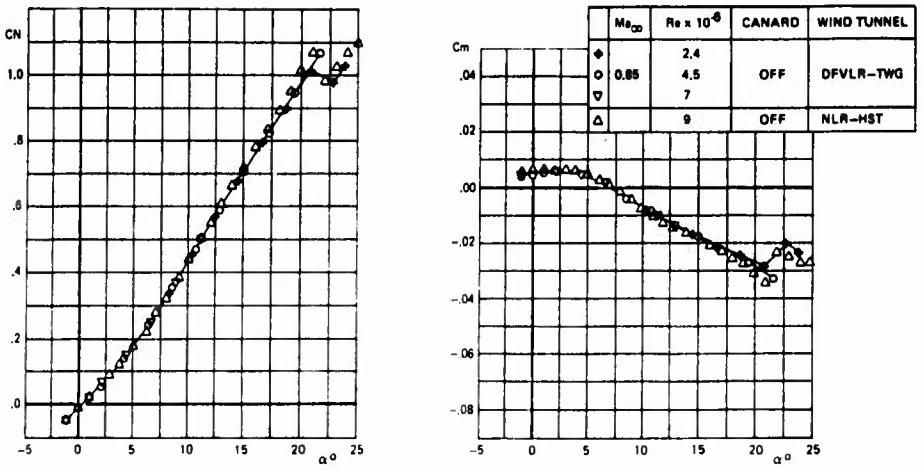



*Fig.19 Comparison of NLR (HST) and DFVLR (TWG) balance measurements (65 deg wing; rounded L.E.).*

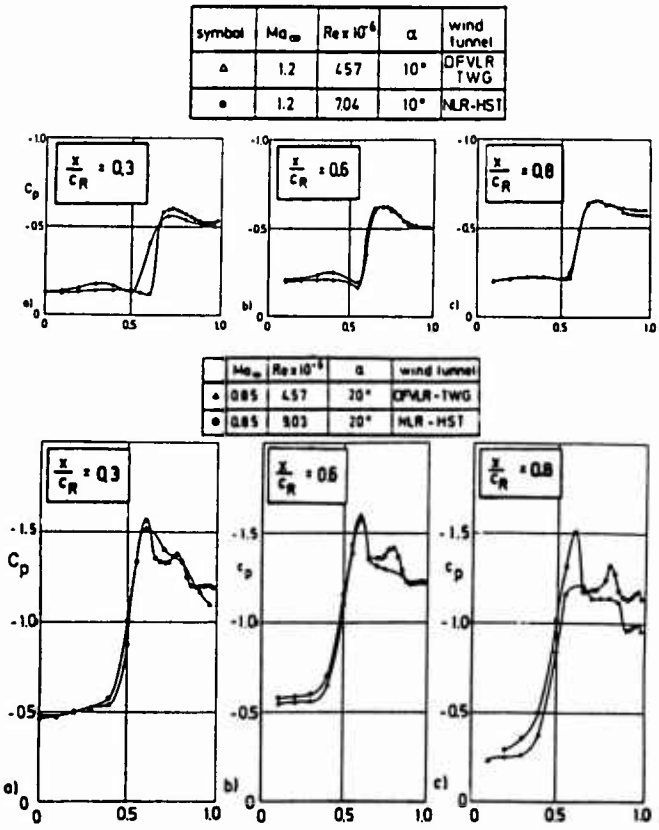



*Fig.20 Comparison of upper surface pressure distributions from NLR (HST) AND DFVLR (TWG) tests (rounded leading edge; 65 deg wing).*

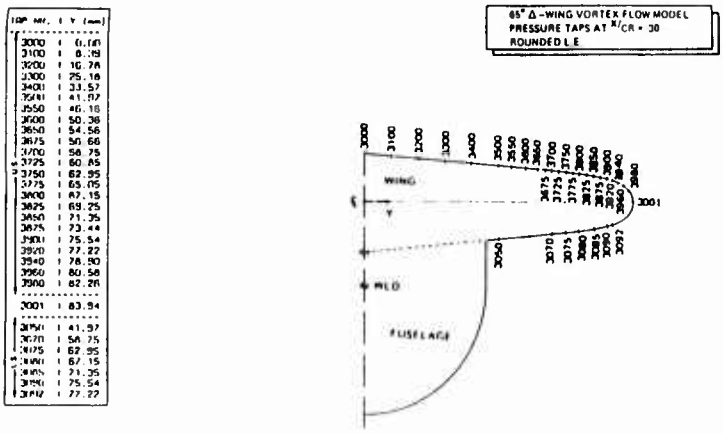



*Fig. geometry 1 Location and number of pressure orifices.*

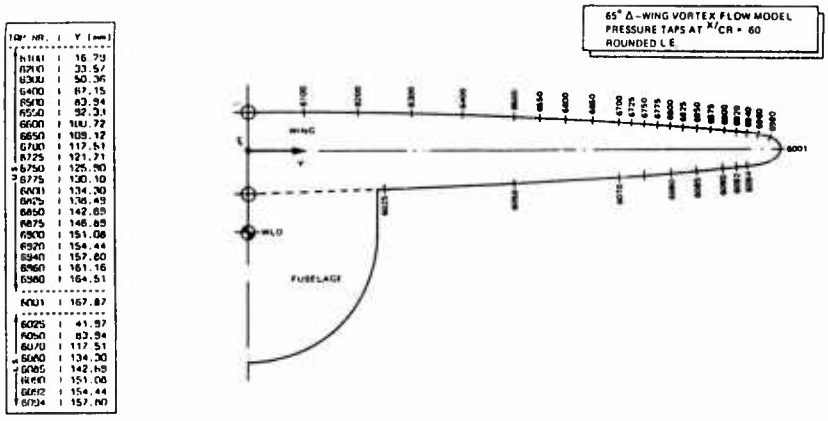



*Fig. geometry 2 Location and number of pressure orifices.*

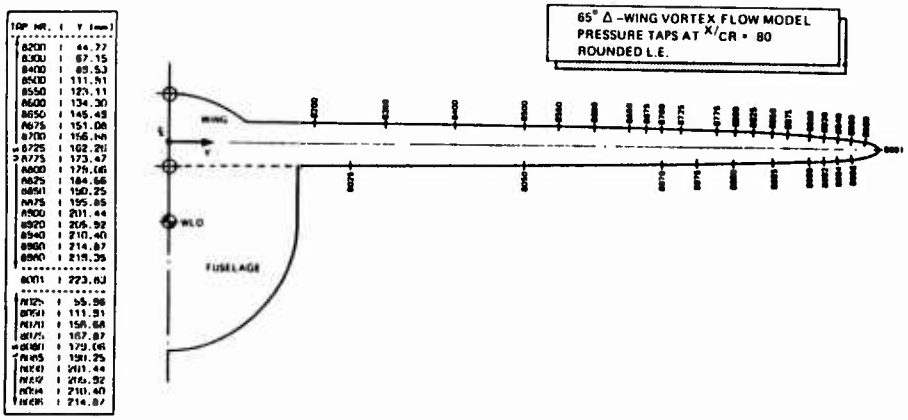



*Fig. geometry 3 Location and number of pressure orifices.*

| TAP NR. | Y (mm) |
|---|---|
| 3000 | 0.00 |
| 3100 | 8.39 |
| 3200 | 16.78 |
| 3300 | 25.18 |
| 3400 | 33.57 |
| 3500 | 41.97 |
| 3550 | 46.16 |
| 3600 | 50.36 |
| 3650 | 54.56 |
| 3675 | 56.66 |
| 3700 | 58.75 |
| 3725 | 60.85 |
| 3750 | 62.95 |
| 3775 | 65.05 |
| 3800 | 67.15 |
| 3825 | 69.25 |
| 3850 | 71.35 |
| 3875 | 73.44 |
| 3900 | 75.54 |
| 3920 | 77.22 |
| 3940 | 78.90 |
| 3960 | 80.58 |
| 3050 | 41.97 |
| 3065 | 54.56 |
| 3070 | 58.75 |
| 3080 | 67.15 |
| 3085 | 71.35 |
| 3090 | 75.54 |

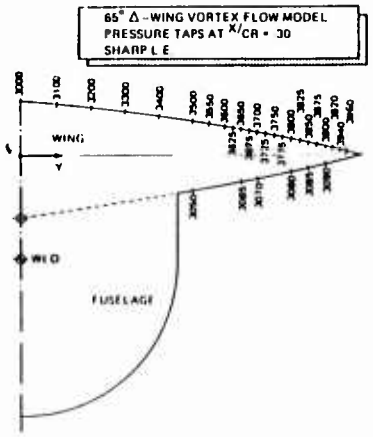



*Fig. geometry 4 Location and number of pressure orifices.*

| TAP NR. | Y (mm) |
|---|---|
| 6100 | 16.79 |
| 6200 | 33.57 |
| 6300 | 50.36 |
| 6400 | 67.15 |
| 6500 | 83.94 |
| 6550 | 92.33 |
| 6600 | 100.72 |
| 6650 | 109.12 |
| 6700 | 117.51 |
| 6725 | 121.71 |
| 6750 | 125.90 |
| 6775 | 130.10 |
| 6800 | 134.30 |
| 6825 | 138.49 |
| 6850 | 142.69 |
| 6875 | 146.89 |
| 6900 | 151.08 |
| 6920 | 154.44 |
| 6940 | 157.80 |
| 6960 | 161.16 |
| 6980 | 164.51 |
| 6025 | 41.97 |
| 6050 | 83.94 |
| 6070 | 117.51 |
| 6080 | 134.30 |
| 6085 | 142.69 |
| 6090 | 151.08 |
| 6092 | 154.44 |
| 6094 | 157.80 |

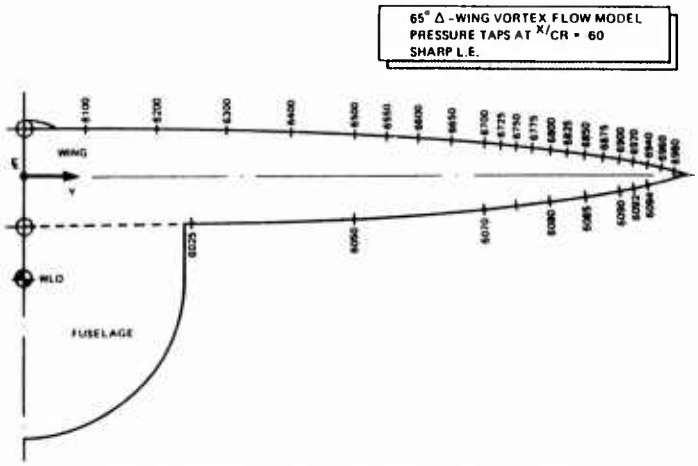



*Fig. geometry 5 Location and number of pressure orifices.*

| TAP NR. | Y (mm) |
|---|---|
| 8200 | 44.77 |
| 8300 | 67.15 |
| 8400 | 89.53 |
| 8500 | 111.91 |
| 8550 | 123.11 |
| 8600 | 134.30 |
| 8650 | 145.49 |
| 8675 | 151.08 |
| 8700 | 156.68 |
| 8725 | 162.26 |
| 8775 | 173.47 |
| 8800 | 179.06 |
| 8825 | 184.66 |
| 8850 | 190.25 |
| 8875 | 195.85 |
| 8900 | 201.44 |
| 8920 | 206.92 |
| 8940 | 210.40 |
| 8960 | 214.87 |
| 8980 | 219.35 |
| 8025 | 55.96 |
| 8050 | 111.91 |
| 8070 | 156.68 |
| 8075 | 167.87 |
| 8080 | 179.06 |
| 8085 | 190.25 |
| 8090 | 201.44 |
| 8092 | 206.92 |
| 8094 | 210.40 |
| 8096 | 214.87 |

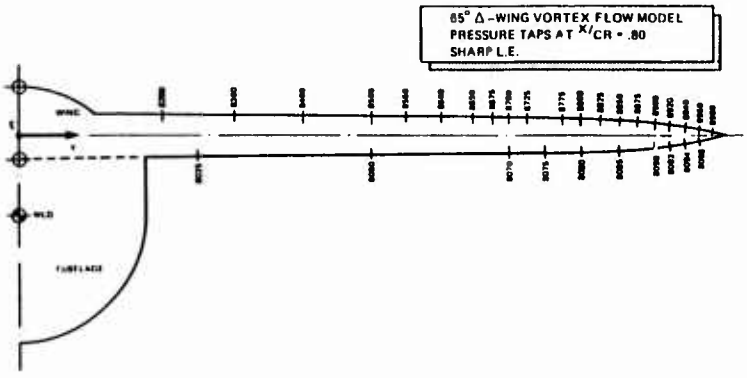



*Fig. geometry 6 Location and number of pressure orifices.*

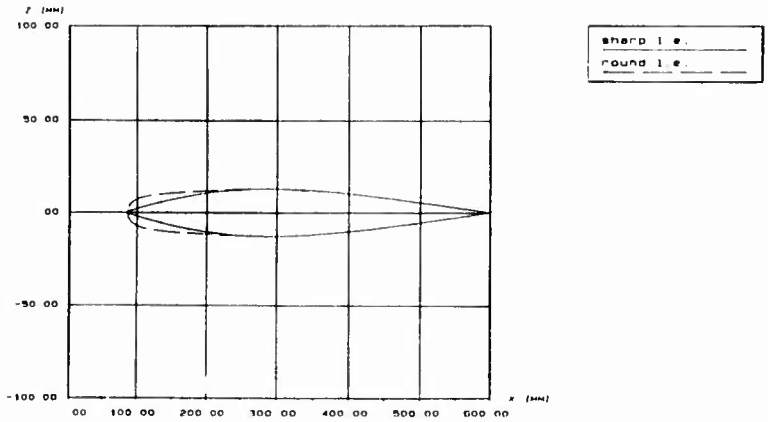
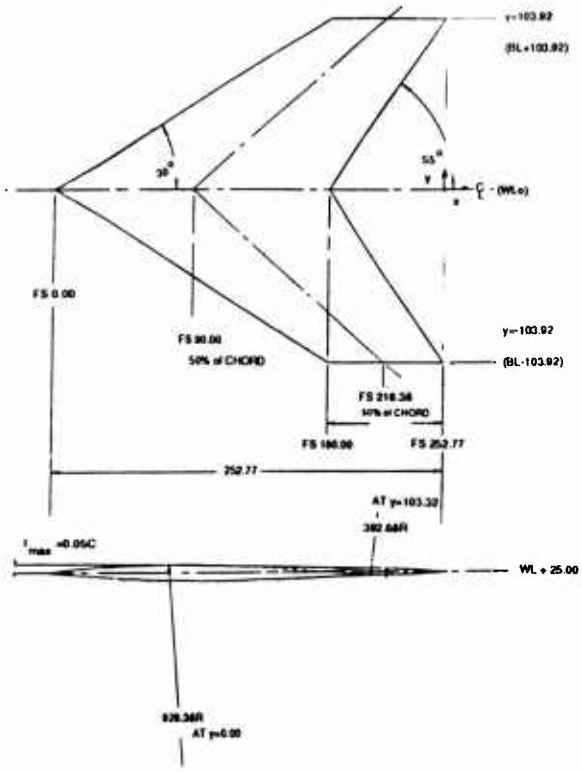



*Fig. geometry 7 Comparison of sharp and round L.E. of VFE - model at y = 40 MM.*




| FS (MM) | | Δy (MM) | C (MM) | R (MM) |
|---|---|---|---|---|
| L.E. | T.E. | | | |
| 0.00 | 180.00 | 0.00 | 180.00 | 928.96 |
| 45.00 | 198.19 | 25.98 | 153.19 | 794.72 |
| 69.28 | 208.01 | 40.00 | 138.73 | 722.31 |
| 90.00 | 216.38 | 51.96 | 126.38 | 660.55 |
| 135.00 | 234.56 | 77.94 | 99.56 | 526.49 |
| 180.00 | 252.77 | 103.92 | 72.77 | 392.68 |

*Fig. geometry 8 Definition of canard geometry.*

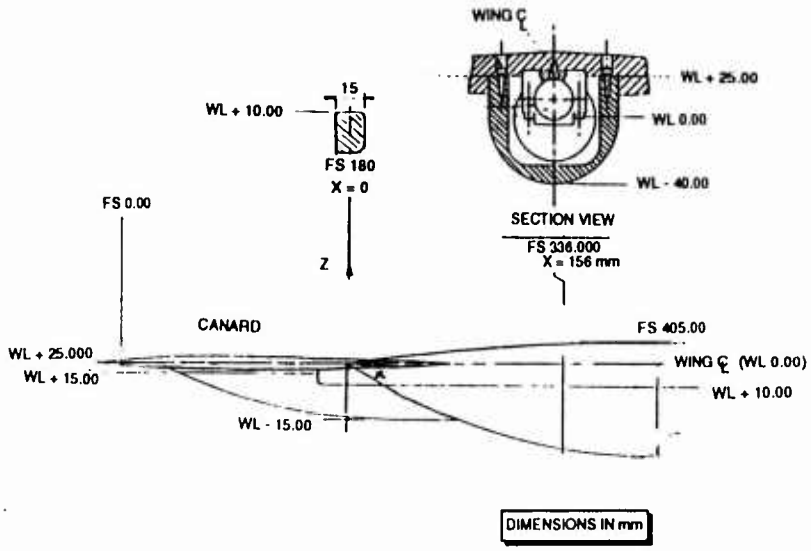



*Fig. geometry 9 Assembly of canard and sharp L.E. wing.*

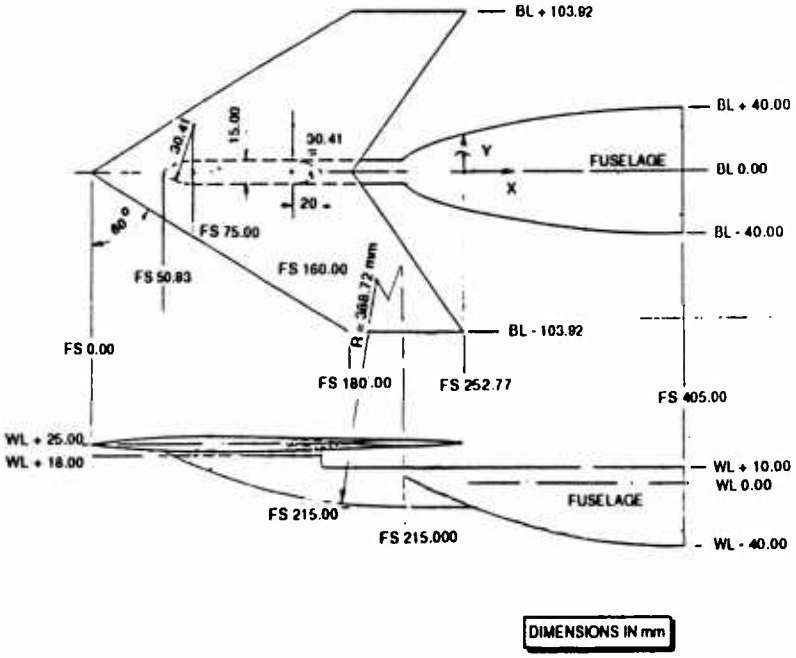



*Fig. geometry 10 Some details of canard support.*

# DELTA-WING MODEL

BY

D. BARBERIS
ONERA-BP 72 - F92322 CHATILLON CEDEX (FRANCE)

## 0 - INTRODUCTION

A detailed study has been made of the flow around a 75° sweep angle delta wing to provide reference material for numerical codes. Experiments were carried out in the F2 wind tunnel of the ONERA Le Fauga - Mauzac Centre. Firstly an examination of the surface flow properties was carried out using surface pressure measurements and surface flow visualizations with a viscous coating. The angle of incidence was varied between 5° and 30° and the upstream velocity between 10 and 75 m/s. Secondly, the aerodynamic field was characterized by means of laser tomography visualizations and surveys with a two component laser Doppler velocimeter system. Mean and fluctuating velocity fields were determined in several vertical planes normal to the wind tunnel longitudinal axis. These measurements were carried out for an angle of incidence of 20° and for two values of the upstream velocity (24 m/s and 40 m/s).

## 1 - GENERAL DESCRIPTION

1.1. Model designation — Delta wing

1.2. Model type and flow conditions — Sweep delta wing with a sharp leading edge. Subsonic flow regime.

1.3. Design requirements — Large subsonic model which allows very detailed investigations. Fundamental research on the rules governing the development of vortex sheets.

1.4. Dominant flow physics — Development of a primary and secondary vortex in the organization of the flow over a delta wing. The vortical system remains stable and organized for moderate values of the incidence of the model.

## 2 - DETAILS OF MODEL

2.1. General geometric arrangement — The model consists of a delta wing with a 75° sweep angle with a chamfer of 15° on the lower side of the leading edge (see Fig.1).

2.2. Body data

2.2.1. Shape — The delta wing has a 1450 mm chord. Two models with the same shape have been built : model A with 252 pressure holes and a 22 mm thickness has been used for surface pressure and LDV measurements; model B with only 9 pressure holes and a 30 mm thickness has been used for surface flow visualizations with a viscous coating.

2.3. Geometric definition of all components — All models have been built in steel and covered with black paint.

2.4. Model support details — A schematic representation of the test set-up is shown in Fig.2. The model was mounted without

yaw to a circular support fixed with a knee cap to the horizontal sting. The model angle of attack is trimmed by a link. The horizontal sting is fixed to a vertical mast traversing the test section. The vertical position of the sting can be adjusted in order to place the model in the centre of the test section for different angles of attack.

## 3 - GENERAL TUNNEL INFORMATION

3.1. Tunnel designation

F2 wind tunnel (see Fig. 3)

3.2. Organization running the tunnel

ONERA - Fauga-Mauzac Centre

3.3. Tunnel characteristics

It is a continuous closed circuit wind tunnel driven by a fan with constant blade angle and a variable motor speed with a maximum power of 700 kW.
The air speed is variable from 0 to 100 m/s. The stagnation pressure is the atmospheric pressure. The contraction ratio is equal to 12. Following the wind, the settling chamber is equipped, with a grid in the rapid contraction, a honeycomb and three grids.
The cooling section, the fan section, the corner vanes, and the central section (including : contraction, test section and the beginning of the first diffusor) are built of steel. The rest of the tunnel is made of concrete.

3.4. Test section

3.4.1. Model mounting in the test section

(see Fig. 2)

3.4.2. Test section dimensions

The test section is rectangular : height 1.80m, width 1.40m, length 5m.

3.4.3. Wall geometry details

The side walls of the test section are formed by several removable panels, which allows various arrangement of transparent and opaque area. The top and bottom walls are built in ply with a glass window of 0.6 x 2m$^2$ surface.
The divergence of the wind tunnel can be trimmed by changing inclination of the top and bottom walls.

3.5. Freestream calibration

3.5.1. Reference flow conditions

The reference stagnation pressure is measured in the settling chamber. The reference static pressure is obtained from a Prandtl antenna situated at 300 mm from the upper wall of the test section and at 786 mm downstream of the beginning of the test section. The static temperature is measured in the settling chamber with a thermocouple (Cr-Al) connected to a digital AOIP system with a resolution of 0.1°C.

3.5.2. Tunnel calibration

The uniformity of the flow velocity U in various transverse planes of the test section was checked successively with laser velocimetry, pressure probe and hot wire. The pressure probe and a hot wire were supported by a three degrees of freedom device ($X_1$ horizontal axial centerline, $Y_1$ and $Z_1$) fastened to the test section inside.
The figure 4, obtained by pressure probe gives the comparison of the local values U, in a vertical plane located 1 meter behind the beginning of the test section, and the reference value $U_0$ measured by a

fixed pressure probe located 0.786 m behind the beginning of the test section and 0.3 m under the upper wall ; in this case $Z_1 = 0.902$ m and $Y_1 = 0.798$ m and $U_0 = 100$ m/s. This figure shows a very good uniformity in the plane.
The laser accuracy was estimated to a relative error $\Delta U/U<1.5\%$ the absolute error on the angle between the velocity vector and the horizontal being 0.5 degree. These measurements show the same uniformity as the pressure measurements and the measured angles were always smaller than the estimated error. The hot wire measurements, although disturbed by small mechanical vibrations of the supporting device, shows the same uniformity of the flow. Dynamic measurements of the pressure fluctuations $\sqrt{\overline{p'^2}}$ and speed fluctuations $\sqrt{\overline{u'^2}}$ were made by a microphone and a hot wire in the test section.
A quarter inch Bruel and Kjaer microphone equipped with a cone (16 k Hz pass band) was placed 3.6 m from the test section inlet on the horizontal axial centreline. The values of $\sqrt{\overline{p'^2}}$ shown in Fig. 5 were obtained without filtering.
An horizontal 5 µm hot wire was placed 0.8 m from the test section inlet and 0.2 m from the upper wall. The values of $\sqrt{\overline{u'^2}}$ were determined in the 0 to 1000 Hz frequency band (see Fig. 6).

## 4 - INSTRUMENTATION

4.1. Model position

4.1.1. How is the geometrical incidence measured — By use of a potentiometer

4.1.2. Accuracy of geometrical incidence — 0.1°

4.2. Model pressure measurements

4.2.1. Total number and disposition of pressure holes

The model (A) is equipped with 252 pressure holes, on the leeward and windward sides, distributed in 9 cross-sections (see Fig.7). The longitudinal positions of the cross-sections are governed by the law $x/C = \sin(k\pi/2)$ where x is the longitudinal position, C the chord length of the model, and k is varied from 0.05 to 0.85 with a 0.1 step. Some pressure holes are distributed on the symmetrical part of the delta wing, in order to verify that the model has a zero degree yaw. The model (B) is equipped with 9 pressure holes distributed in one section located at x = 0.434 m (see Fig. 7).

4.2.2. Range and accuracy of pressure transducers

Pressure transducer range : ± 1 PSID

4.2.3. Are dynamic pressures measured — No

4.3. Force and moment measurements — No

4.4. Boundary layer and flow field measurements

4.4.1. Measurement technique applied — Field explorations by a two-component LDV system. The light sources are constituted by two Argon lasers with a maximum power of 15W. The first laser gives the blue and green radiations (respective wave-length, 0.488µm and 0.5145µm); the second laser

povides the violet radiation (wave-length 0.4765μm). In order to detect the direction of the measured velocity component, the six beams coming out from the beam splitters traverse Bragg cells inducing a fringe shift at a frequency of 4MHz. Appropriate optics focus the beams to constitute the probe volume whose diameter is close to 0.35mm. The six beams are contained in a same plane (P) which can be inclined at a chosen angle. The blue and green beams are focused along a common direction making an angle of 38° with respect to the transverse axis $Y_t$, the two fringe patterns being respectively inclined at +45° and -45° with respect to (P). The violet beams make an angle of -38° with respect to $Y_t$, so that the angle between the blue-green and the violet beams is equal to 76°. The collecting part comprises two Cassegrain telescopes having a diameter of 200 mm. The signals coming out from the photomultipliers are then processed by DISA 55L type counters connected to an acquisition system through a simultaneity checking device which checks that the three signals are relative to the same particle having crossed the probe volume. The forward scattering mode of operation was adopted here to take advantage of a higher signal/noise ratio. In order to have a sufficiently high data rate, the flow was seeded with particles of incense smoke emitted downstream of the test section, thus avoiding perturbation of the upstream flow by the injection device. At each measurement point, the three instantaneous velocity components were acquired from a sample of 2 000 particles.

4.4.2. Flow regions investigated

(see Fig.8)

The wind tunnel reference axis system, $O_1X_1Y_1Z_1$, originates at the wing apex and is such that :

- $X_1$ is the horizontal axis of the test section running in the direction of the wind,
- $Z_1$ is the vertical axis, positive upward,
- The vertical coordinate Z runs vertically upward originating on the wing in each of the measurement planes.
- $Y_1$ is the axis normal to the plane defined by $X_1$ and $Z_1$ directions.
- The abscissa x originating at the apex, runs along the median chord of the wing ($x = X_1/\cos \tilde{\alpha}$)

The velocity components U, V, W, are given in the system $O_1X_1Y_1Z_1$.

LDV data have been obtained in 7 vertical planes for two upstream velocities.

For the velocity $U_0$ = 24 m/s, the planes are located at x = 0.4; 0.55; 0.625; 0.71; 0.116 m

For the velocity $U_0$ = 40 m/s, the planes are located at x = 0.325; 0.375; 0.4; 0.55; 0.116 m.

4.5. Surface flow visualization

4.5.1. Technique applied

Surface flow visualizations were obtained by using a mixing of parafin oil, titanium dioxide and oleic acid. The visualization reveals the surface flow

structure on the leeward side of the model.

4.5.2. Results of the surface flow patterns are presented by photographs.

4.6. Flow field visualization

The laser tomoscopic method was developed at ONERA by the Physics Department. The principe consists of illuminating part of the flow to be studied with a plane of light. The principle of this method is diagrammed in Fig. 9. It uses three independent devices :

- a tracer injector ;
- a means for illuminating the tracer ;
- a photo recording device.

The purpose of the injector is to emit a tracer that will be visible in the region of flow to be investigated. In order to visualize and photograph the phenomenon, this area has to be adequately illuminated. A laser having a power of about 15 W is used. A bar of glass placed perpendicular to the laser beam fans it out into a plane. The fanout is broader the smaller the diameter of the glass cylinder. This diameter is therefore chosen such that the illumination is maximum, while completely covering the useful field. The recording device consists of a still or movie camera, arranged as perpendicular as possible to the plane of illumination.

For the present experiments, the tracer used was smoke produced by hot oil and emitted by a tube placed in the wind tunnel collector, well upstream of the test section. The laser light sheet enters the test section through the top wall window, along a horizontal line and fans out in a plane perpendicular to the uniform freestream flow. The camera is placed inside the test section in a protective box fixed to the vertical mast.

Laser tomoscopic visualizations have been carried out for the following values of the upstream velocity and angle of incidence.

$U_o$ = 10; 24; 40 m/s

$\alpha$ = 10; 15; 20; 25; 30°.

5 - TEST MATRIX AND CONDITIONS

5.1. Detailed test matrix

The selected test cases concern the delta wing tested for several values of the upstream velocity and angle of incidence. All the configurations and types of investigation are given in Table 1.

General test conditions : the stagnation pressure is the atmospheric pressure. The Reynolds numbers based on the chord length C (C = 1.45 m) were :

$U_o$ = 10 m/s, $R_{ec} = 10^6$

$U_o$ = 75 m/s, $R_{ec} = 7.5\ 10^6$

5.2. Transition details

All the tests have been made with natural transition. Transition can be observed on the visualizations using viscous coating by an inflexion of the separation lines occurring where transition takes place. The location of transition depends of Reynolds number and angle of attack of the model (see Figs. 10 and 11).

6 - DATA

6.1. Availability of Data

6.1.1. Organization owning the data: OFFICE NATIONAL D'ETUDES ET DE RECHERCHES AEROSPATIALES (ONERA) B.P. 72, F92322 CHATILLON CEDEX - FRANCE.

6.1.2. Responsible for the data: BARBERIS Didier
Head of Research Group
ONERA-B.P. 72-F92322 CHATILLON CEDEX
Tél : 33.1.46.23.51.74
Fax : 33.1. 46.23.50.61

6.1.3. Data on the present delta wing model are freely available

6.2. Suitability of data for CFD validation: No corrections have been made for simulating free air conditions.

6.3. Type and form in which data are available

6.3.1. Type and form: Files are in ASCII form on Floppy Discs. For field measuments they contain the coordinates of the measuring point and the aerodynamic results at this point (see example of results, in Fig.12).

6.4. Corrections applied to data

6.4.1. Lift interference and blockage corrections: A correction has been made on incidence. It was based on the results of GARNER and ROGERS from AGARDograph n°109 (Oct. 66). The correction is function of the geometrical incidence of the model and can vary from 1.4° for 20° incidence to 3.4° for 42° incidence.

6.4.2. Sting and support corrections: No corrections have been made to take into account the wall, sting and support interference.

7 - **DATA ACCURACY AND REPEATABILITY ASSESSMENT**

7.1. Estimate accuracy of:

7.1.1. Free stream conditions: The upstream flow velocity accuracy is estimated to a relative error $\Delta U_o/U_o = 1\%$.
Accuracy of the geometrical incidence is equal to 0.02°.

7.1.2. Measured data: The uncertainty on surface pressure being $\Delta p = \pm$ 7pa, leading to an accuracy
$\Delta Kp = \pm$ 1% for Kp = -0.5.
The LDV system accuracy can be estimated to $\pm$ 1m/s as far as the flow speed is concerned and to $\pm$ 1° as concerns the direction of the local velocity vector.

7.2. Repeat measurements

7.2.1. Repeat measurements within one test campaign: No

7.2.2. Repeat measurements in successive campaigns: Plane located at x = 1160 mm has been probed twice. The upstream velocity was $U_o$ = 40 m/s and the angle of incidence 20°.

7.3. Redundant Measurements: No

7.4. Other tests on same nominal geometry: Experiments were carried out in three different facilities to generate data for different Reynolds

numbers : the S2L wind tunnel of the Chalais-Meudon Centre and the F1 and F2 wind tunnels of the Fauga-Mauzac Centre. In the first of these tunnels, the flow has a laminar boundary layer, whereas it exhibits a natural transition on the wing in the second and third ones.
Figure 13 gives the diagram and dimensions of the test section and shows how the model was mounted in each case.
The various tests can be broken down as follows :
- experiments in the S2L research tunnel at the Chalais-Meudon Centre on a wing with 0.5 m chord length, placed at a 20° angle of incidence and providing the field characteristics of a laminar boundary layer on the wing.
- experiments on a wing of 1.45 m chord length tested in two wind tunnels (F1 and F2) at the Fauga-Mauzac Centre. The purpose was to determine the effects of the Reynolds number and of the transition from laminar to turbulent flow in the upper surface boundary layer.
The following table specifies the conditions of the tests run in the S2L, F1 and F2 wind tunnels, as well as the main means of investigation used.

| Wind Tunnel | Chords (m) | $U_0$ (m/s) | $Re_c/10^6$ | Wall measurements | | Field measurements | |
|---|---|---|---|---|---|---|---|
| | | | | Pressure | Visual. | Probe | LDA |
| S2L | 0.5 | 20 | 0.7 | X | X | X | 3-D |
| F2 | 1.45 | 24 | 2.3 | X | X | - | 2-D |
| F2 | 1.45 | 40 | 3.9 | X | X | - | 2-D |
| F1 | 1.45 | 20 | 2.5 | X | - | X | - |
| F1 | 1.45 | 40 | 4.1 (*) | X | - | X | - |
| F1 | 1.45 | 80 | 8.3 (*) | X | - | X | - |

(*) Reynolds number obtained with a stagnation pressure of $2 \times 10^5$ Pa.

Comparisons between the various test sections have not been carried out up to now because it was outside the objectives of the research programme.

7.5. Additional Remarks

Recently, tests have been conducted in the F2 wind tunnel with the 1.45 m chord wing, with emphasis being placed on vortex breakdown investigation. The flow above the wing has been probed with a three component LDV system for an angle of incidence equal to 26°.

## 8 - REFERENCES

8.1. On the wind tunnel

D.AFCHAIN, P.BROUSSAUD, M.FRUGIER, G.RANCARANI
"La soufflerie F2 du centre du Fauga-Mauzac". 20ème Colloque d'Aérodynamique Appliquée AAAF - Toulouse - Novembre 1983.

D.AFCHAIN; G.RANCARANI
"Mise au point et contrôle du fonctionnement de la soufflerie F2."
ONERA - RT 1/3623 GN - Janvier 1984

D. AFCHAIN ; Ch. GLEYZES
"Contrôle Aérodynamique de l'écoulement dans la veine d'essais de la soufflerie F2".
ONERA - RT n° 3/3623 GN-Août 1985.

8.2. On the model and test results

P.MOLTON
"Aile delta en écoulement incompressible. Etude expérimentale à F2"
ONERA - RT n° 36/1147 AN - Décembre 1986.

J.L.SOLIGNAC ; D.PAGAN ; P. MOLTON
"Experimental study of incompressible flow on the upper surface of a delta wing".
La Recherche Aérospatiale - N° 1989-6 pp. 47 - 65.

8.3. On the applied measurement techniques

M. PHILBERT ; J.P.FALENI ; R. BEAUPOIL
"Application d'un dispositif d'éclairage laminaire à la visualisation des écoulements aérodynamiques en soufflerie par émission de fumée"
La Recherche Aérospatiale-N° 1979-3 pp. 173-179.

D. AFCHAIN
"Mise au point du vélocimètre laser tridimensionnel de la soufflerie F2 - Etude de la veine vide".
ONERA - RTI n° 4/3623 GN - Novembre 1988.

Table 1

| $\alpha°$ / $U_0$ m/s | 10 | 15 | 20 | 25 | 30 |
|---|---|---|---|---|---|
| 24 | a<br>b<br>c | a<br>b<br>c | a<br>b d<br>c | a<br>b<br>c | a<br>b<br>c |
| 40 | a<br>b<br>c | a<br>b<br>c | a<br>b d<br>c | a<br>b<br>c | a<br>b<br>c |

a : oil flow visualizations
b : tomoscopic visualizations
c : surface pressure measurements
d : LDV measurements

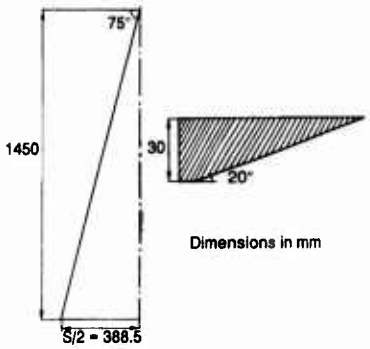



Fig. 1 - Definition of Delta Wing

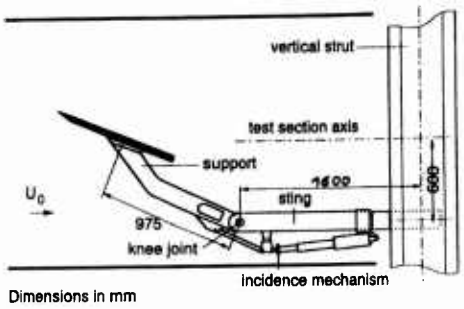



Fig. 2 - Schematic Representation of the Model in the Wind Tunnel

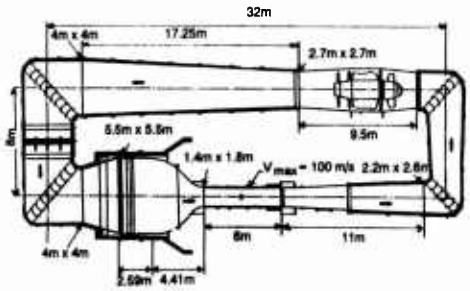



Fig. 3 - The F2 Wind Tunnel

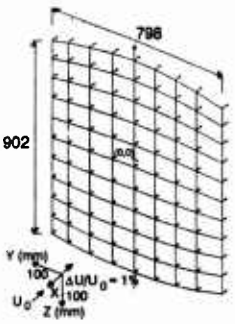



Fig. 4 - Transverse Survey in the Test Section

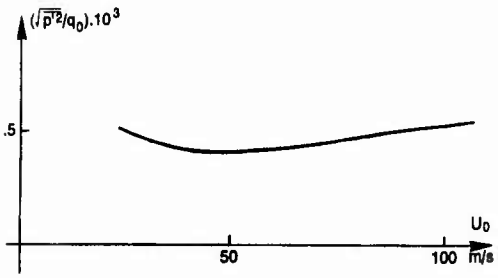



Fig. 5 - Fluctuation of the Static Pressure

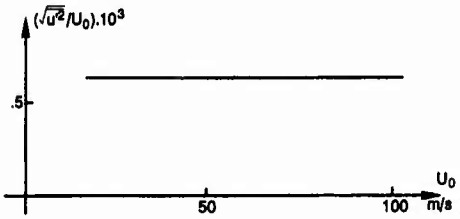



Fig. 6 - Axial Turbulence

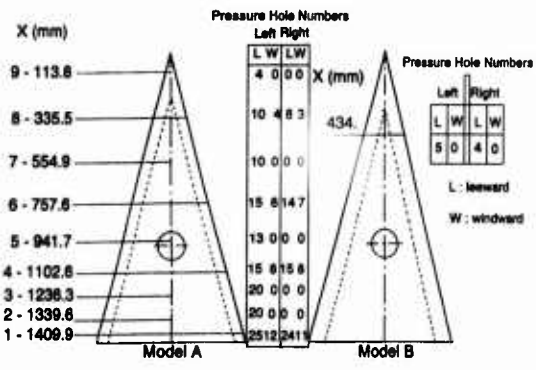



Fig. 7 - Pressure Taps Locations on the Models

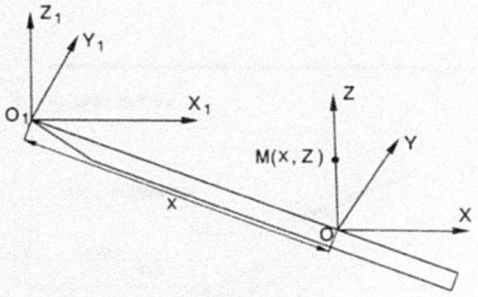



Fig. 8 - Definition of Coordinate Systems

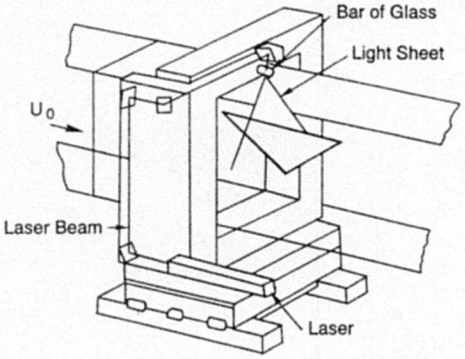



Fig. 9 - Schematic Diagram of the Laser Tomoscopic System

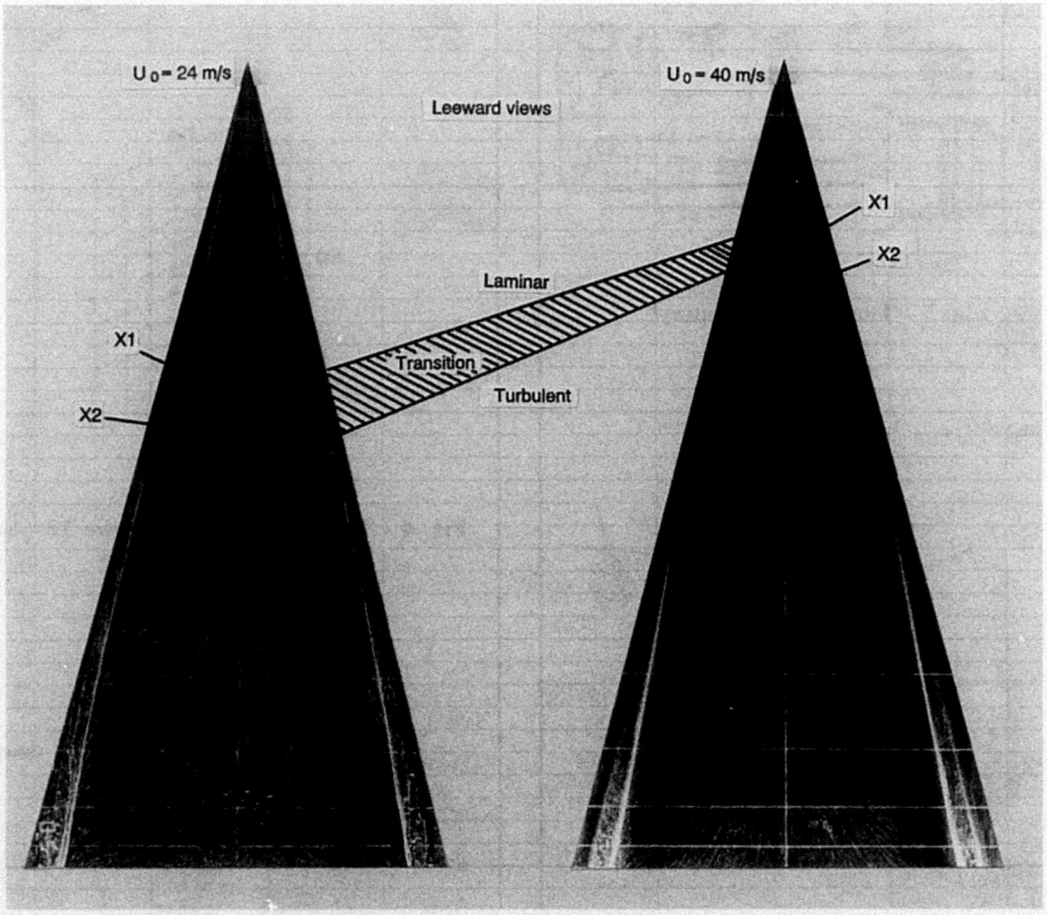



Fig. 10 - Reynolds Number Effect on Transition Location

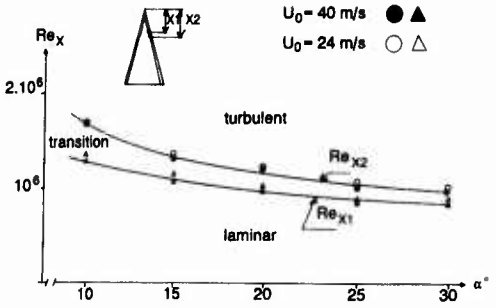



Fig. 11 - Angle of attack Effect on Transition Location

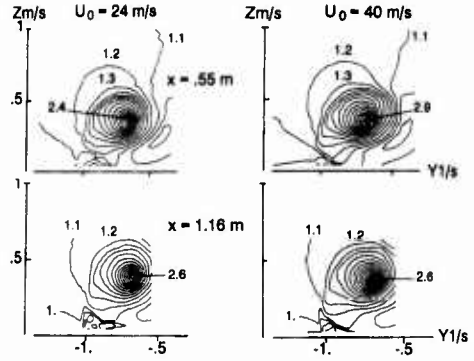



Fig. 12 - $U/U_0$ lines in the planes perpendicular to the wing, with :
s : wing local semi-span
Zm : perpendicular to the wing, origin on the upper surface

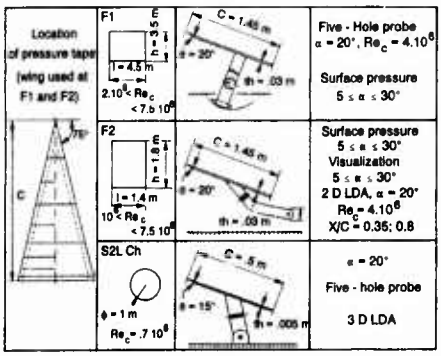



Fig. 13 - Model Setup in the Different Test Sections

# EXPERIMENTAL INVESTIGATION OF THE VORTEX FLOW OVER A 76/60-DEG DOUBLE DELTA WING

BY

N.G. VERHAAGEN AND J.E.J. MASELAND
FACULTY OF AEROSPACE ENGINEERING
DELFT UNIVERSITY OF TECHNOLOGY
P.O. BOX 5058, 2600 GB DELFT
THE NETHERLANDS

## INTRODUCTION

Data was obtained from a low-speed wind-tunnel experiment carried out on a sharp-edged 76/60-deg double-delta wing. The objective of the investigation was to generate data on the vortex interaction downstream of the strake-wing leading-edge kink of a double-delta wing. An oil-flow and laserlight-sheet technique was used to visualize the flow on and off the surface of the wing. Balance measurements were performed to determine the forces and moments acting on the wing. In addition, the pressure on the upper surface of the wing was measured at several wing chordwise stations. Using a thin five-hole probe, the flowfield over the wing panel was surveyed in detail for an incidence of 20 deg. The data provide information on the interaction process of the wing and strake vortex as well as the development of the secondary separation downstream of the leading-edge kink.

## 1. GENERAL DESCRIPTION

| | |
|---|---|
| 1.1. Model Designation | LSW Model 144 |
| 1.2. Model Type | Double-Delta Wing |
| 1.3. Design Requirements | Slender, double-delta wing to study the interaction of vortices over strake/wing configurations. Sharp leading edges to fix boundary layer separation. |

## 2. MODEL DETAILS

2.1. Wing Data

| | |
|---|---|
| 2.1.1. Wing Planform | see Fig. 1. |
| . Aspect ratio | 2.06 |
| . Leading edge sweep | 76 deg (strake)<br>60 deg (main wing) |
| 2.1.2. Wing section | |
| . Cross-sectional shape | flat plate with chamfered edges (Fig. 1) |

| | |
|---|---|
| . Thickness/chord ratio | .03 |
| . Edge thickness | 0.2 mm |
| 2.1.3. Geometric definition wing | |
| . Surface roughness | polished |
| 2.2. Model support details | |
| 2.2.1. Type of support | single strut with fairing (Fig. 2) |
| 2.2.2. Strut/model pivot location | 75% root chord |
| 2.2.3. Fairing details | |
| . cross-sectional shape | symmetric profile |
| . mean chord | 0.15m |
| . taper ratio | 0.5 |
| . mean thickness/chord ratio | 0.22 |

3. TUNNEL INFORMATION

| | |
|---|---|
| 3.1. Designation | low-speed low-turbulence wind tunnel |
| 3.2. Organization | TUD Faculty of Aerospace Engineering |
| 3.3. Tunnel characteristics | |
| . Type | closed circuit |
| 3.4. Test section | |
| 3.4.1. Test setup | see Fig. 2 |
| 3.4.2. Dimensions | 1.80 x 1.25 x 2.60 $m^3$ |
| 3.5. Freestream conditions | |
| 3.5.1. Reference conditions | for Mach number and root-chord-based Reynolds number; see table 1 |
| 3.6. Flow quality (empty tunnel) | |
| 3.6.1. Turbulence level | 0.05% |

## 4. INSTRUMENTATION

| | |
|---|---|
| 4.1. Model position | |
| 4.1.1. Geometrical incidence | measured with inclinometer |
| 4.2. Surface pressure measurements | |
| 4.2.1. Total number | 485 (Fig. 3) |
| 4.3. Force and moment measurements | |
| 4.3.1. Type | six-component balance |
| 4.3.2. Location of balance | overhead test section |
| 4.4. Flowfield measurements | |
| 4.4.1. Technique | five-hole probe (Figs. 4 to 7) |
| 4.4.2. Planes surveyed | 50, 56.25, 62.5, 75 and 87.5% chord; normal to wing surface |
| 4.5. Surface flow visualization | |
| 4.5.1. Technique | oil-flow |
| 4.5.2. Surfaces visualized | upper and lower surface |
| 4.5.3. Data available from | photographs (fig. 8) |
| 4.6. Flowfield visualization | |
| 4.6.1. Technique | laserlight sheet |
| 4.6.2. Planes visualized | 50, 56.25, 62.5, 68.75, 75, 81.25, 87.5, 100 and 112.5% chord; normal to free stream |
| 4.6.3. Data available from | photographs and video movie (Fig. 9) |

## 5. TEST MATRIX AND CONDITIONS

| | |
|---|---|
| 5.1. Detailed test matric | see table 1 |
| 5.2. Model/tunnel relations | |
| 5.2.1. Model span/tunnel width | 0.552/1.800 |
| 5.2.2. Wing area tunnel cross-sectional area | .148/2.070 |

5.3. Transition details

| | |
|---|---|
| 5.3.1. Transition | secondary separation of boundary layer on wing upper surface |
| 5.3.2. Data available in form of | photographs (Fig. 8) |

## 6. DATA

6.1. Availability of data

| | |
|---|---|
| 6.1.1. Organization | Delft University of Technology Faculty of Aerospace Engineering<br>P.O. Box 5058<br>2600 GB Delft, the Netherlands |
| 6.1.2. Originator | |
| . Name | ir. N.G. Verhaagen |
| . telephone | 015-786385 or 781320 |
| . fax | 015-783533 |
| . e-mail adress | vlaangv@dutrex.tudelft.nl |
| 6.1.3. Availability of data | free |
| 6.1.4. Type and form | see table 2 |
| 6.1.5. Data carrier | data reports, disk, videomovie |

6.2. Corrections applied to data

| | |
|---|---|
| 6.2.1. Lift interference and blockage correction | |
| . type of correction method | empirical |
| . corrected data | incidence, dynamic pressure |
| 6.2.2. Strut corrections | |
| . corrections | - strut/model interference determined from dummy strut measurements<br>- strut deflection under aerodynamic load |

## 7. DATA ACCURACY AND REPEATABILITY

### 7.1. Estimated accuracy

| | |
|---|---|
| . incidence | 0.02 deg |

### 7.2. Estimated repeatability

| | |
|---|---|
| . forces and moment coefficients | within 0.1% |
| . surface pressure coefficients | within 0.05% |
| . vortex flow velocities | within 0.03 $U_\infty$ outside subcore<br>within 0.05 $U_\infty$ inside subcore |

## 8. DATA REPORTS

For flow visualization results and balance measurements:

| | |
|---|---|
| . N.G. Verhaagen | An Experimental Investigation of the Vortex Flow over Delta and Double-Delta Wings at Low Speed.<br>TUD Report LR-372, September 1983. |

For flowfield-surveys and surface-pressure measurements:

| | |
|---|---|
| . N.G. Verhaagen<br>J.E.J. Maseland | Investigation of the Vortex Flow over a 76/60-deg Double Delta Wing at 20 deg Incidence.<br>AIAA Paper 91-3208, AIAA 9th Applied Aerodynamics Conference CP918, September 1991. |
| . J.E.J. Maseland<br>N.G. Verhaagen | Experimental and Numerical Investigation of Vortex Flow over a 76/60-deg Double-Delta Wing, Delft University of Technology, Report LR-680, April 1992. |

| AOA | Laserlight sheet viz. | oil-flow viz. | flowfield data | surface pressure data | force balance data |
|---|---|---|---|---|---|
| -2 | | | | x | x |
| 1 | | | | x | x |
| 0 | | | | x | x |
| 1 | | | | x | x |
| 2 | | | | x | x |
| 4 | | | | x | x |
| 5 | | x | | | x |
| 6 | | | | x | x |
| 8 | | | | x | x |
| 10 | x | x | | x | x |
| 12 | | | | x | |
| 14 | | | | x | |
| 15 | x | x | | | x |
| 16 | | | | x | |
| 18 | | | | x | |
| 20 | x | x | x | x | x |
| 22 | | | | x | |
| 24 | | | | x | |
| 25 | x | x | | x | x |
| Machnr. | 0.08 | 0.08 | 0.12 | 0.20 | 0.08 |
| Re nr. | 1.4 M | 1.4 M | 2.0 M | 3.4 M | 1.4 M |

Table 1: Test Matrix

| Data | Coefficient | Normalized | Uncorrected | Corrected |
|---|---|---|---|---|
| Balance data | x | | | x |
| Surface pressures | x | | x | |
| Field data | x | x | | |

Table 2: Availability of data

# Model Geometry

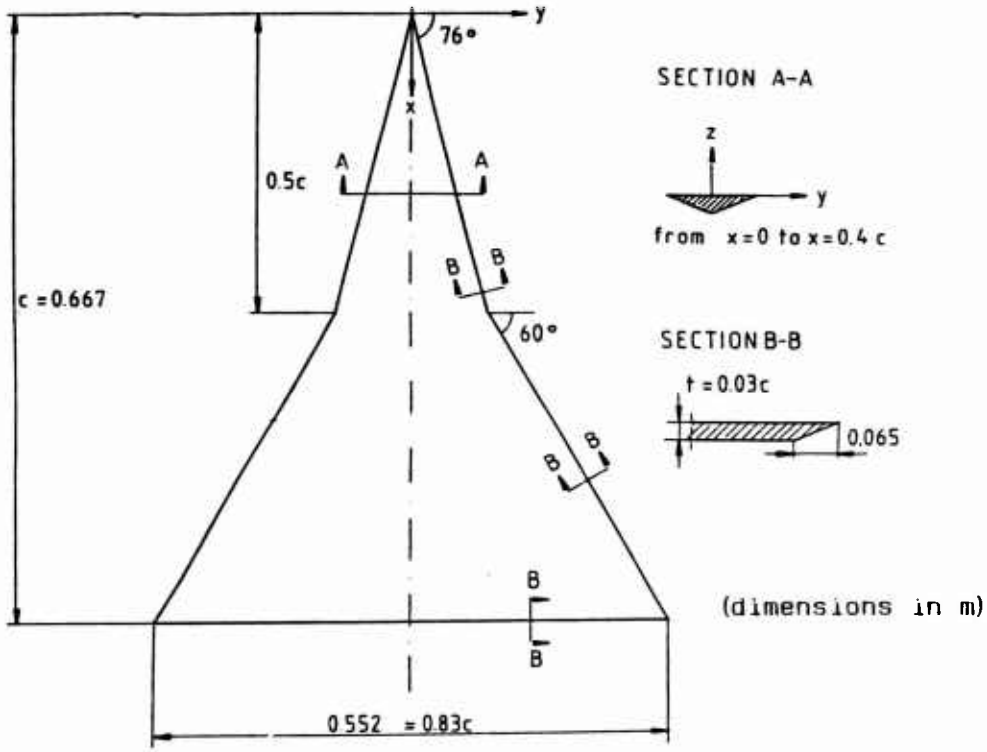



Fig. 1: Wing geometry

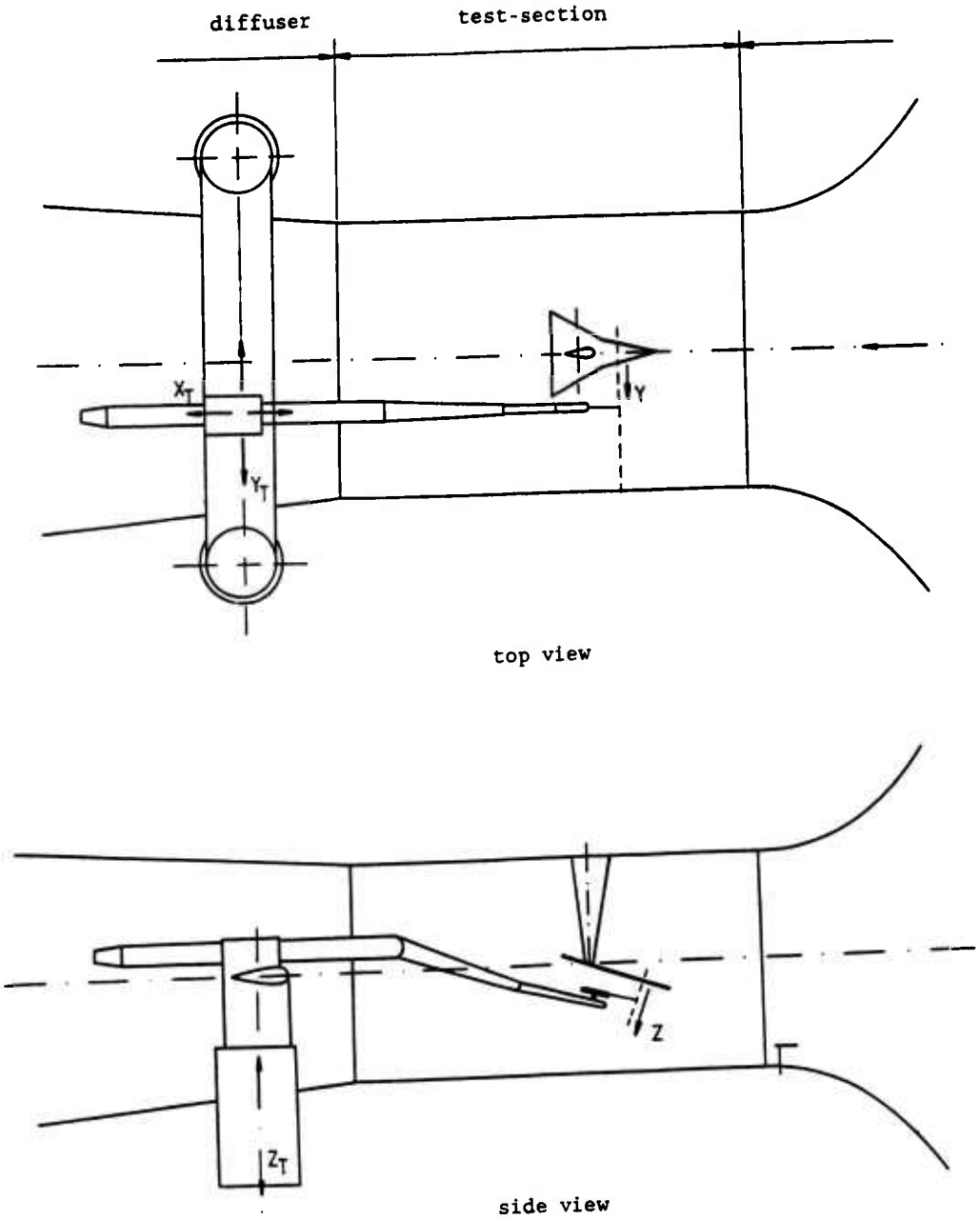



Fig. 2: Setup for flowfield surveys (schematic)

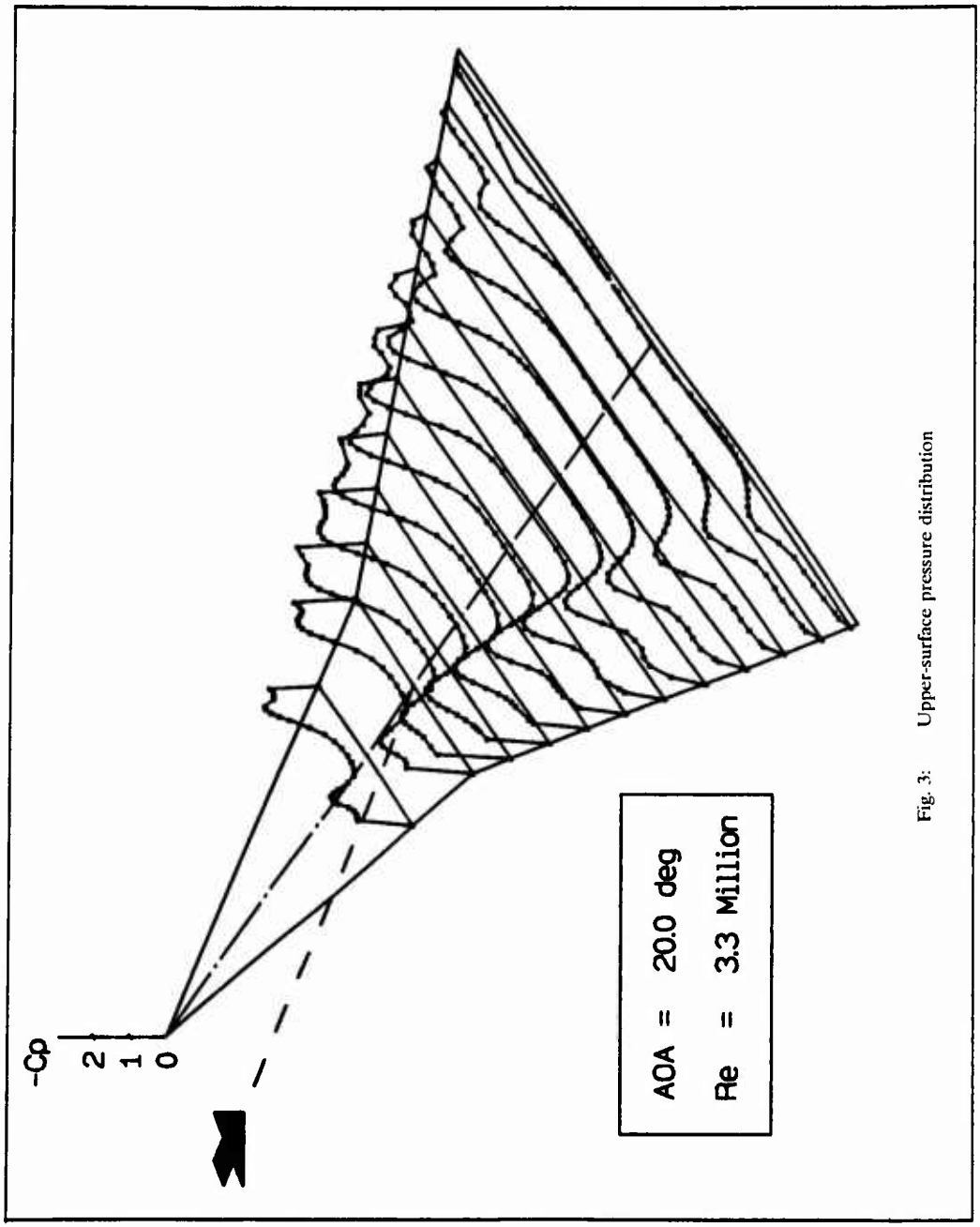



Fig. 3: Upper-surface pressure distribution

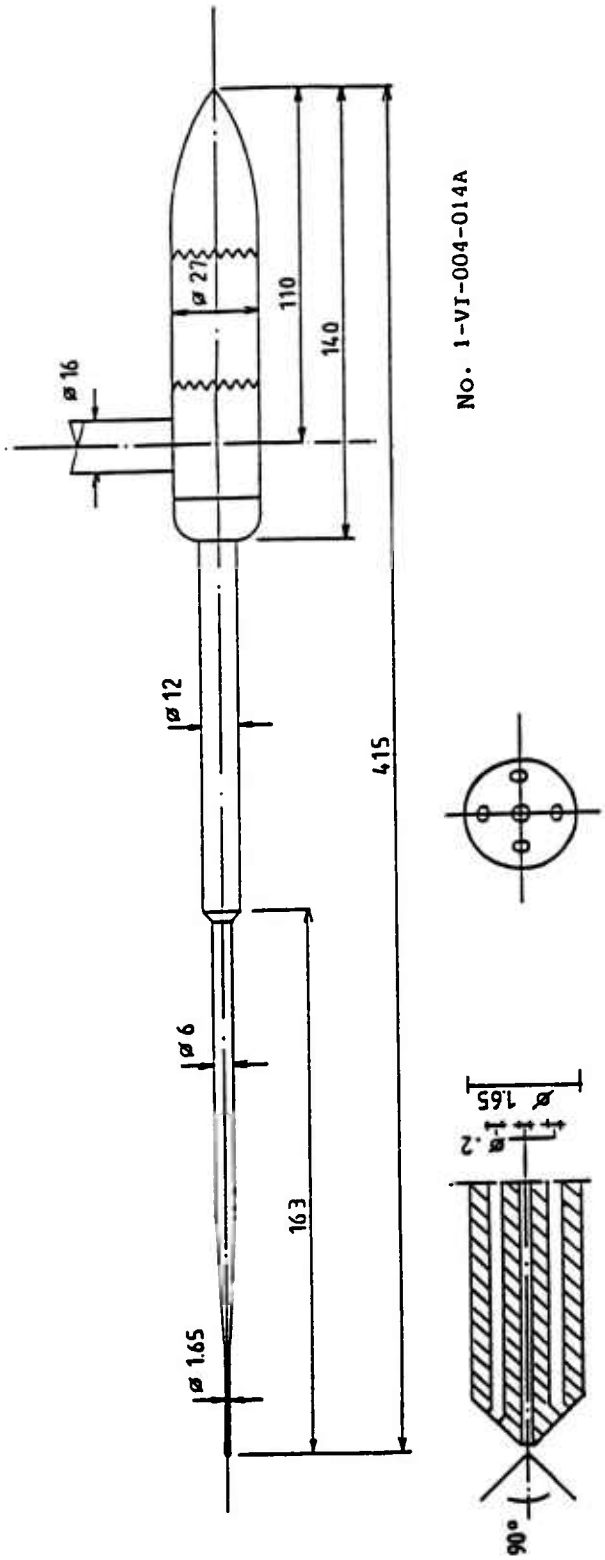



Fig. 4: Five-hole probe (dimensions in mm)

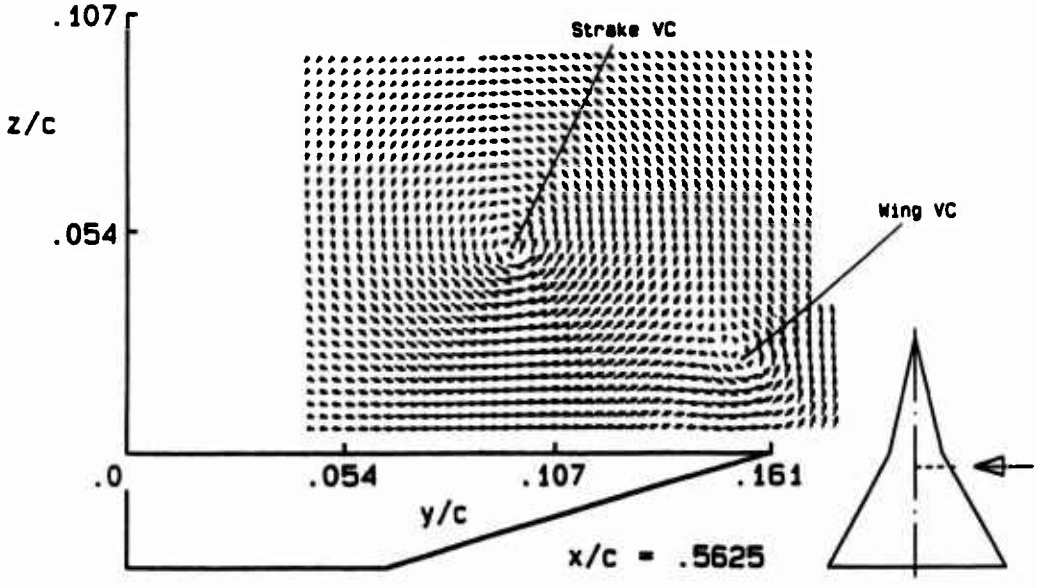



Fig. 5: Crossflow velocity vectors at 56.25% chord

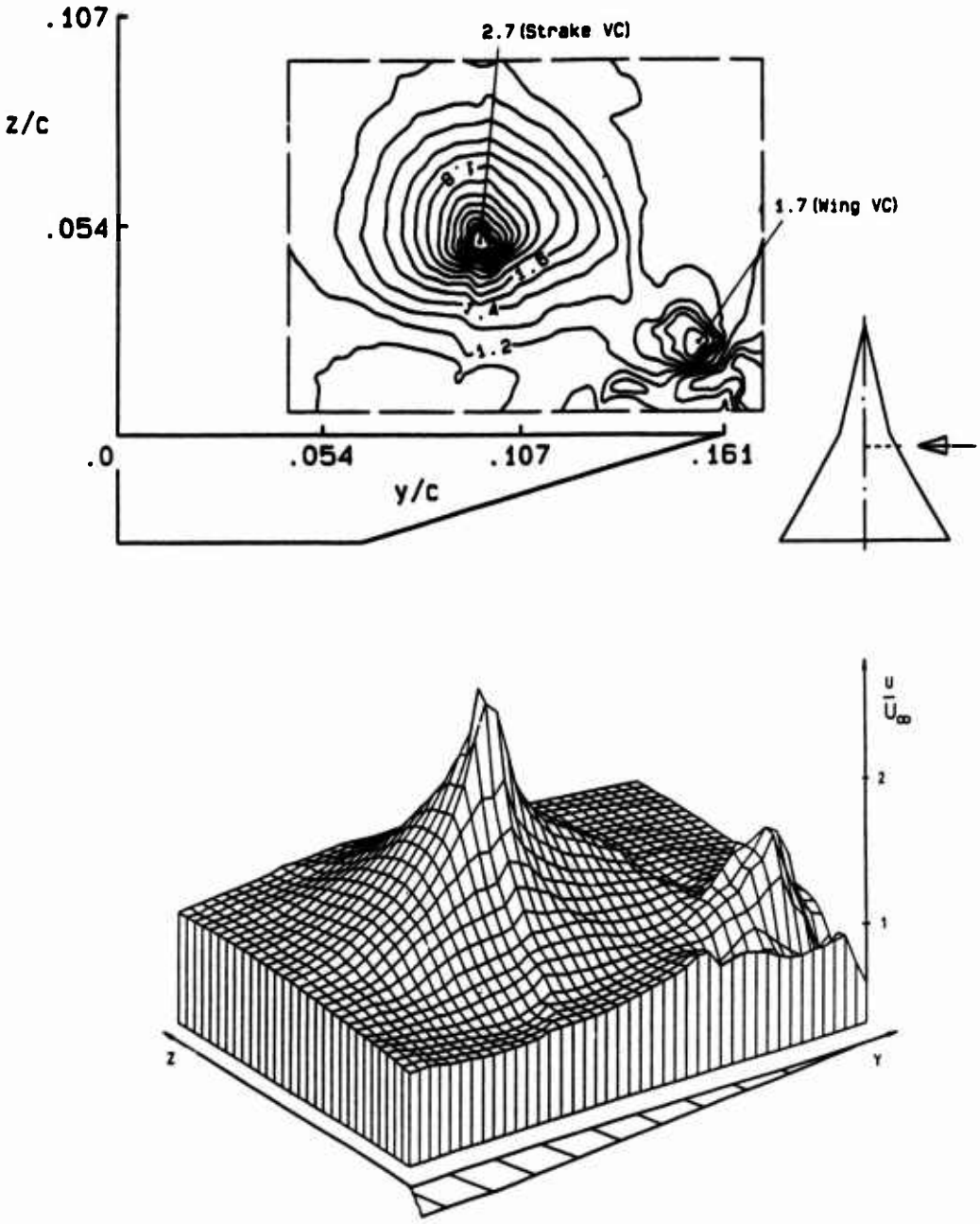



Fig. 6: Chordwise velocity at 56.25% chord

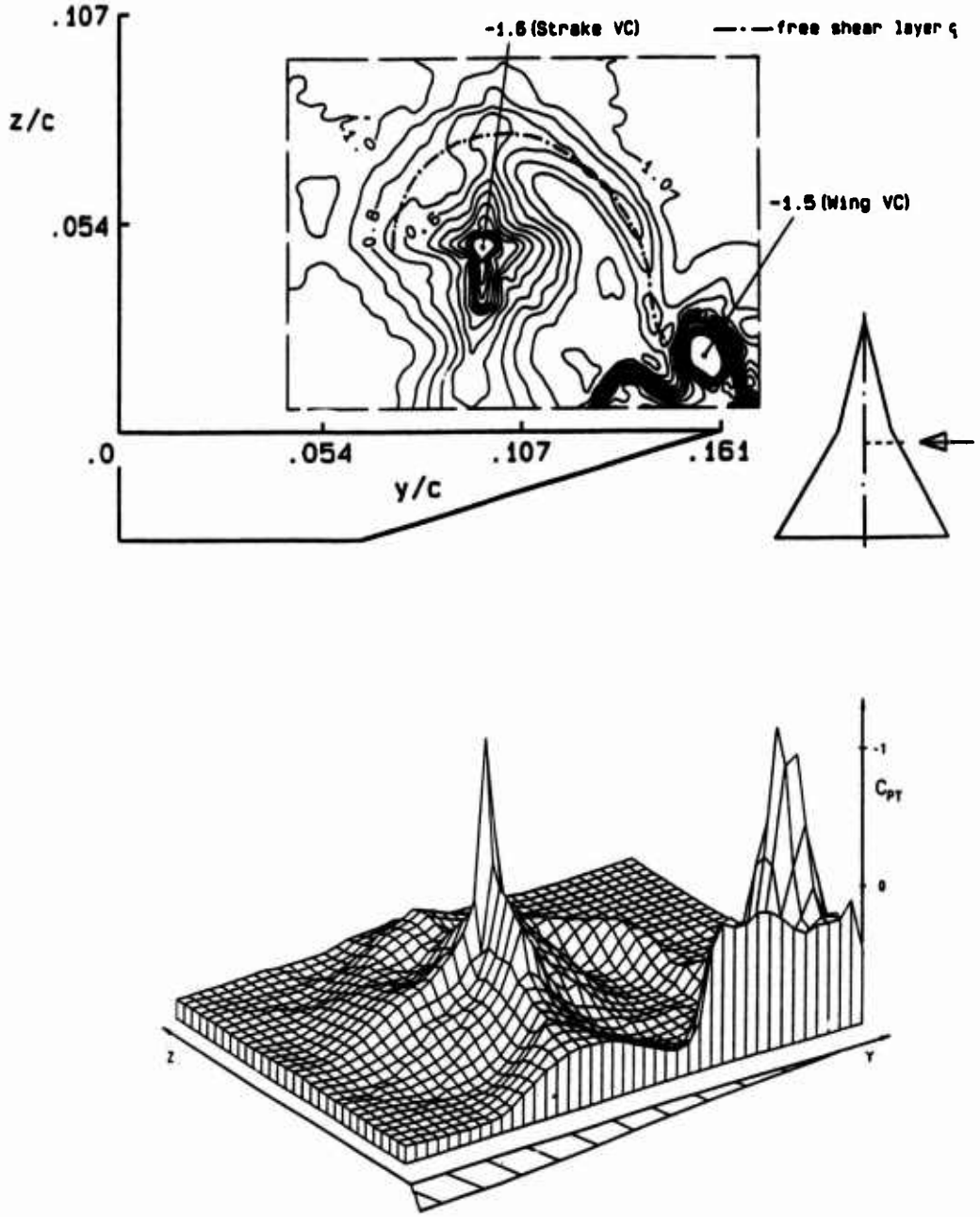



Fig. 7: $C_{pt}$ distribution at 56.25% chord

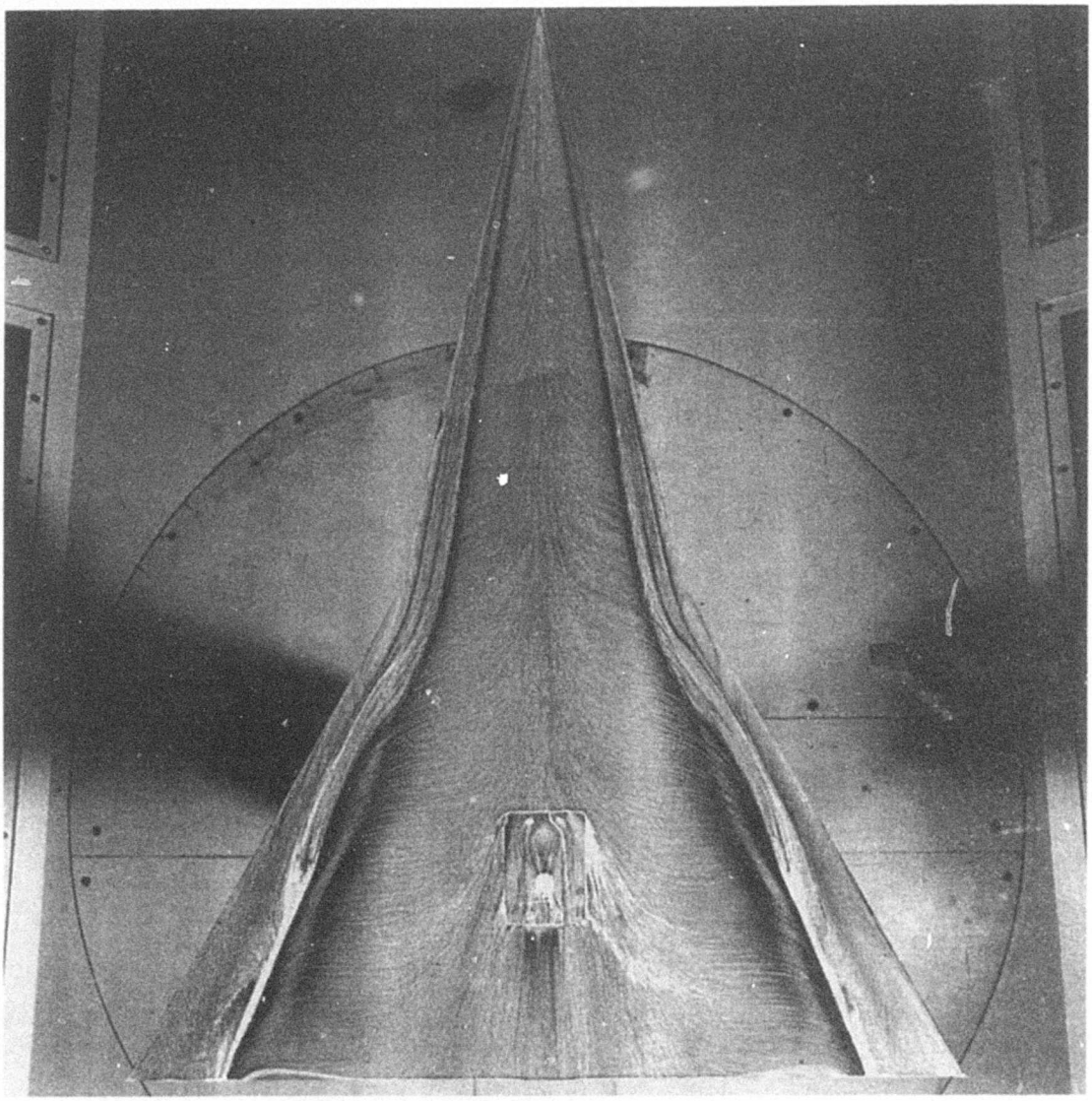
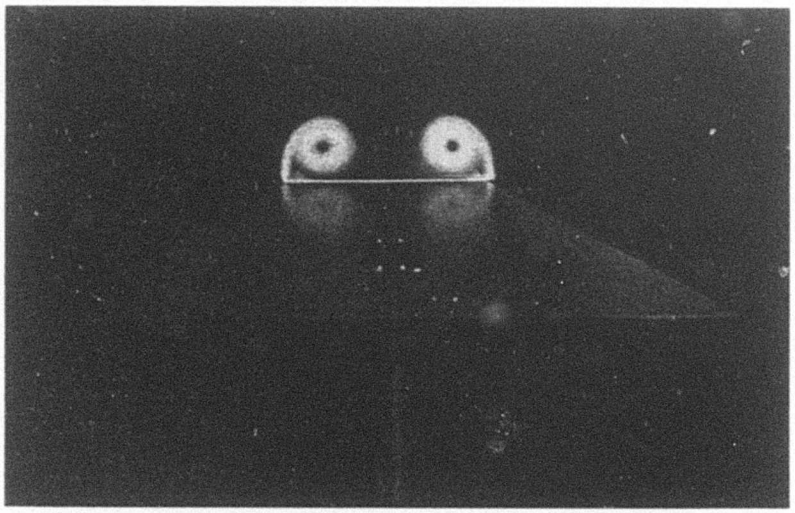
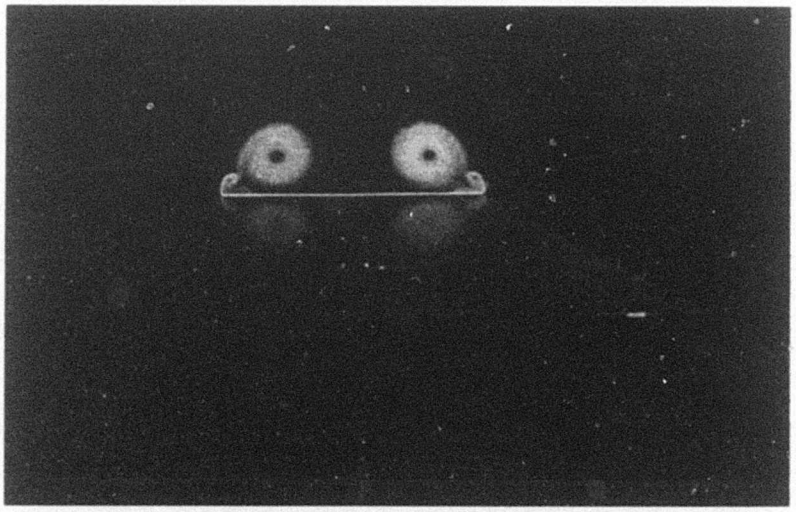


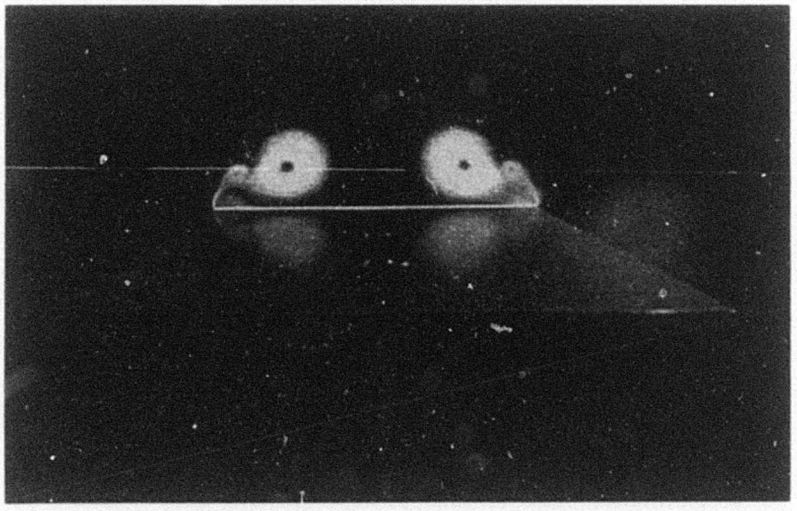
Fig. 8: Surface flow pattern at 20 deg



a. x/c = 0.50



b. x/c = 0.5625



c. x/c = 0.625

Fig. 9: Vortex flow visualized with laserlight-sheet technique

# WIND TUNNEL TEST ON A 65° DELTA WING WITH ROUNDED LEADING EDGES

- THE INTERNATIONAL VORTEX FLOW EXPERIMENT -

BY

K. HARTMANN
K. A. BÜTEFISCH
H. PSZOLLA

DEUTSCHE FORSCHUNGSANSTALT FÜR LUFT- UND RAUMFAHRT, DLR

Bunsenstraße 10
37073 GÖTTINGEN
GERMANY

## INTRODUCTION

The wind tunnel tests carried out on this model resulted from an international cooperation that involved the aeronautical laboratories AFWAL (US), DLR (Germany), FFA (Sweden), NLR (The Netherlands) and the Universities of Braunschweig (Germany) and Delft (The Netherlands). It was the basic aim of these measurements to provide detailed pressure and flow field data on a 65° delta wing configuration of a generic shape for the validation of CFD methods, notably Euler methods. For this reason one of the basic configurations had a sharp leading edge. However, there was also considerable interest for configurations with more realistic features and therefore other configurations were added. These featured a wing with a smaller sweep angle (55° instead of 65°), a rounded instead of a sharp leading edge shape, a drooped leading edge and the addition of a canard wing. The wind tunnel tests were made in different wind tunnels with different models. They covered a large range of flow conditions and measuring techniques including force, pressure and flow field measurements. The test case to be described here covers the force, pressure and flow field measurements and flow visualization as carried out at DLR in the transonic wind tunnel TWG on the smaller scale model with round leading edges. This configuration was designed and manufactured by the MBB company in Germany.

## 1. GENERAL DESCRIPTION

### 1.1 Model name or designation

The International Vortex Flow Model, VOMO, provided by MBB, Germany

### 1.2 Model type and flow conditions

65° delta wing with separated or partly separated flow at the leading edge; tested at subsonic and transonic flow conditions

### 1.3 Design requirements, purpose of test

Generic wing model with rounded leading edges to study the effect of viscosity; sweep angle high to produce strong vortices but not too far from realistic configurations; lee side not disturbed by a supporting fuselage. Supply of a data base including field data for the validation of computer codes (Euler, Navier-Stokes); study of the flow physics.

### 1.4 Dominant flow physics

a. Vortex flow at subsonic and transonic conditions with embedded shocks

b. Vortex burst and the subsequent break- down of the flow field

c. Unsteadiness of vortex burst location

d. There are cases with only partly separated flow, i.e. not extending over the entire length of the leading edge. Leading edge separation boundaries are represented in Figures 1 and 2 in a $M_\infty$, $\alpha$-plane.

## 2. DETAILS OF MODEL

### 2.1 General geometric arrangement

See Figures 3 and 4

### 2.2 Configurations tested

Rounded leading edges with and without canard; only data without canard are included

### 2.3 Wing and airfoil data

#### 2.3.1 Planform

- Aspect ratio: 1.377
- Taper ratio: 0.15
- Leading edge sweep: 65°
- Trailing edge sweep: 0°
- No twist
- Cropped wing tip

- Body mounted (almost completely) underneath the wing

2.3.2 Basic wing section

- Constant airfoil section in streamwise direction, see Figures 3 and 4
- Modified NACA 64A005 airfoil with straight line aft of 75% chord, greater nose radius, greater thickness over the first 40% of the chord
- No camber
- 5% relative thickness

2.4 Body data

See Figure 3

2.5 Geometric definition of all components

- Shape partly numerically, partly analytically defined
- Designed and measured profiles; see Figure 4
- Average of deviation of the actual airfoil contour from the nominal one is less than 0.25 mm. Check carried out for two cross-sections, see Figure 4
- For detailed geometry information see Test Case D1. All linear D1 dimensions have to be multiplied by 0.7 to obtain the geometry of the present model.

2.6 Model support details

The model was mounted on a rear sting in combination with a $15^{o}$ cranked part in order to achieve higher angles of attack than the nominal tunnel sting allows, see Figure 5

## 3. GENERAL TUNNEL INFORMATION

3.1 Tunnel designation

Transonic Wind Tunnel (TWG) in Göttingen

3.2 Organisation running the tunnel

DLR
Central Wind Tunnel Division
Bunsenstr. 10
37073 Göttingen
Germany

3.3 Tunnel characteristics

Continuously operating with closed circuit; perforated test section in tandem with a supersonic test section; operating conditions, see Figure 6

3.4 Test section

3.4.1 Model mounting and instrumentation

See Figures 3 and 5

Model positioned in the downstream position ② for subsonic and transonic tests, Figure 5

3.4.2 Test section dimensions

1m x 1m x 3m

3.4.3 Wall geometry

4 perforated walls with holes of 60° inclination, open area ratio 6%, suction from the plenum is applied at $M_\infty > 0.9$

3.5 Freestream conditions

See Figure 6

3.5.1 Reference flow conditions

- Total pressure: settling chamber
- Static pressure: from plenum pressure with correction derived from calibration
- Static temperature: from total temperature in settling chamber and Mach number

3.5.2 Tunnel calibration

- Static pipe at tunnel center
- Last calibration: 1987

3.6 Flow quality (empty tunnel)

3.6.1 Flow uniformity (model position), see References 8.1.1

- Mach number uniformity:
  $\Delta M_\infty = \pm 0.005$ at $M_\infty = 0.5$
  $\Delta M_\infty = \pm 0.01$ at $M_\infty = 0.9$
  $\Delta M_\infty = \pm 0.015$ at $M_\infty = 1.0$ and 1.5
- Average gradient of Mach number at $M_\infty = 0.70$: $\partial M_\infty / \partial(x/H) \leq 0.002$
- Flow angularity at $M_\infty = 0.70$: 0.1°; Mach number and model dependent, derived from wedge calibrations

3.6.2 Temperature variation

Temperature variation during a run less than 3°C

3.6.3 Flow unsteadiness

Turbulence level determined in settling chamber: see Figure 7 and Reference 8.1.2
Turbulence level estimated for the test section as to be approximately 0.05 %, J.E. Beckwith, J.C. Rotta, see References 8.1.3

## 4. INSTRUMENTATION

4.1 Model position

4.1.1 Determination of geometrical incidence

- Model incidence derived from support angle corrected for sting deflection under load and checked by telescope
- In addition to the incidence the true position of the model (height with respect to the wind tunnel center line) was determined in order to know accurately the model-fixed field coordinates where LDV data were obtained

4.1.2 Accuracy of geometrical incidence

Angle of incidence: ± 0.05°
Position: ± 0.1 mm plus vibration amplitude.The latter was not measured. It is supposed to be less than one millimeter at the wing tip

4.2 Model pressure measurements

4.2.1 Number and disposition of pressure holes

60 pressure holes, see Figure 3

4.2.2 Type, range and accuracy of pressure transducers

- All surface pressures were measured with two ESP-32 pressure sensor modules and the corresponding pressure measurement system 780B of Pressure System Inc. (USA).
- Pressure range of the sensors ± 15 psi, static error band ± 0.15% FS,
- Scanning rate 15 K samples/s.
- Modules installed inside the body

4.3 Force measurements

4.3.1 Type and location of balance

1.25 inch extended range TASK balance, type MIC XIV A, 6 components, installed inside the body

4.3.2 Maximum load range and accuracy of components

| | | |
|---|---|---|
| Normal force: | (pitching moment = 0 ) | 5790 N |
| Side force: | (yawing moment = 0 ) | 2895 N |
| Axial force: | (total) | 400 N |
| Pitching moment: | (normal force = 0 ) | 384 Nm |
| Yawing moment: | (side force = 0 ) | 156 Nm |
| Rolling moment: | (total) | 68 Nm |

Accuracy: ± 0.3 % full scale

4.4 Boundary layer and flow field measurements

4.4.1 Measurement technique applied

3D LDV measurements, see Table I and Fig. 8

4.4.2 Flow regions investigated

The selected cross sections were identical to those of the pressure taps and of the field measurements at FFA by means of a 5-hole probe. In addition, measurements in the plane of symmetry were performed.

4.4.3 Details of the LDV

- 3 components, operated simultaneously in back-scatter mode, Figure 8
- Size of the measurement volume: 0.1 mm x 0.1 mm x 1 mm (reduced length in crosswise direction due to off-axis observation)

4.5 Surface flow visualization

Oil flow pictures, see Table I and paragraph 7.5

4.6 Flow field visualization

4.6.1 Technique applied

Laser light sheet technique with smoke

4.6.2 Planes visualized

- Planes perpendicular to the model axis and roughly normal to the surface
- Planes moved along the model axis from the tip toward the trailing edge (T.E.) and somewhat beyond the T.E.
- Pictures taken by a high sensitivity CCD camera from behind the model, see Figure 9

4.6.3 In what form are data available?

Video tape (U-matic, VHS) PAL

4.7 Tunnel wall pressure measurements

No measurements

## 5. TEST MATRIX AND CONDITIONS

5.1 Detailed test matrix

See Table I

5.1.1 Selected test cases

8; cases 1 to 6 and 9 of Table I

Overall forces and moments, surface pressures, flow field velocity vectors. Examples of results are included in Figures 10 to 18

5.1.2 Number of configurations tested

Two: wing alone
wing-canard combination (not included)

5.2 Model / Tunnel relations

- Maximum blockage: about 0.75 % at $\alpha = 0°$
- Model span / tunnel width: 0.333
- Wing area / tunnel cross section: 0.081

5.3 Transition details

All data with free transition

## 6. DATA

6.1 Availability of data

6.1.1 Organisation owning data

DLR, Institute for
Experimental Fluid Mechanics (SM-ES)
Bunsenstr. 10
D-37073 GÖTTINGEN
GERMANY

6.1.2 Who is responsible for the data

Dr. K. Hartmann
DLR, SM-ES
Tel. (0049) 551 709 2255
Fax (0049) 551 709 2811

Dr. K.A. Bütefisch
DLR, SM-ES
Tel. (0049) 551 709 2660
Fax (0049) 551 709 2830

6.1.3 Are data freely available

Yes

6.2 Suitability of data for CFD validation

Data are considered essentially interference free thus suitable for "free-air" calculations, see also 6.4.1

6.3 Type and form in which data are available

6.3.1 Type and form

- Table II
- Model geometry: Techn. drawings (also see 2.5)
- All test data available in tables, plots and data reports

6.3.2 Data carrier

3.5" disc containing geometry of airfoil and body and aerodynamic data.

6.4 Corrections applied to data

6.4.1 Lift interference and blockage corrections

No corrections applied because blockage ratio is small and a comparison with NLR data, which are considered interference free, suggests that wall interference is negligible

6.4.2 Sting and support corrections

No corrections applied. Pre-tests were carried out in 4 model positions, see Figure 5. It was found that in the upstream positions ① and ② the pressures on the wing suction side are no longer affected by the model support. Therefore all tests were carried out in position ②.

6.4.3 Elastic deformation of the sting

Sting deflection was corrected with regard to the angle of attack $\alpha$ in the usual way by calibrating the deflection with known loads

## 7. DATA ACCURACY AND REPEATABILITY ASSESSMENT

7.1 Accuracy estimates

7.1.1 Freestream conditions

Mach number < 0.005; average value for the Mach number range 0.5 to 1.2

Angle of incidence $\pm$ 0.05° or better

7.1.2 Measured data

Normal force, attached flow $\Delta C_N = \pm 0.006$; $\pm$ 0.5% of max. load. Pitching moment, attached flow $\Delta C_m = \pm 0.0002$; $\pm$ 0,5% of max. moment. Pressure coefficients, attached flow $\Delta c_p = \pm 0.01$; $\pm$ 0.6% of max. $c_p$. Accuracy of velocity data measured by 3 component LDA:
Absolute accuracy: $\pm$ 5%
Relative accuracy: $\pm$ 1%
All depends on wind tunnel conditions; worst case about 5%

7.2 Repeat measurements

Various tunnel entries have been made with the same model indicating no differences within the measurement accuracy

7.4 Other tests made

Comparisons were made with results obtained for an identical though greater scale model measured in the High Speed Wind Tunnel (HST) at NLR, Amsterdam, The Netherlands. These comparisons are fair, small differences probably being due to differences in Reynolds number, see Figures 12 to 14

7.5 Additional remarks

A systematic series of oil flow visualization experiments was carried out later in 1991 in the High Speed Wind Tunnel (HKG) in Göttingen, which is of the blow down type with an open jet test section. See Figures 15 to 17. Results of Figure 18 were derived from pressure measurements. They are comparable with the oil flow pattern of Figures 15 to 17.

7.6 Actual angle of attack

Force measurements:
$\Delta\alpha = \pm 0.05$, less than $\pm$ 0.25% of max. $\alpha$
Pressure and field measurements:
Less than $\pm$ 1% of $\alpha$ = 10° and 20°, respectinely.
See test cases 4 to 6 and 9 of Table I.

## 8. REFERENCES


8.1 Wind tunnel

8.1.1 Amecke J., Pszolla H.
"Machzahlverteilung in der leeren Meßstrecke des Transsonischen Windkanals Göttingen.
Teil 1: Nachmessung in der perforierten Meßstrecke"
DLR-Report IB 222 - 88 A 09, 1988

8.1.2 Pfizenmaier, E., Froebel, E., Michel, U., Pszolla, H.
"Eichmessung am transsonischen Windkanal Göttingen (TWG)
- Turbulenzmessungen in der Beruhigungskammer -"
DLR-Report: IB 22214 - 91 / B1, 1991

8.1.3 Beckwith, J.E.; Rotta, J.C.
Effects of contractions on turbulence in the working section
AGARD-AR-83, pp.113-117, (1975)

8.2 The model, see Reference 8.3

8.3 Test results

8.3.1 Hartmann, K.
"US/European Transonic Vortex Flow Experiment
- Plots of Force Measurements- - Photos of Flow Visualizations-"
DFVLR IB 222-85 A 36, August 1985

8.3.2 Hartmann, K.
"US/European Transonic Vortex Flow Experiment - Data Lists of Force Measurements-"
DFVLR IB 222-86 A 03, Februar 1986

8.3.3 Hartmann, K.
"US/European Transonic Vortex Flow Experiment - Plots of Pressure Measurements - "
DFVLR IB 222-86 A 23, June 1986

8.3.4. Hartmann, K.
"US/European Transonic Vortex Flow Experiment - Data Lists of Pressure Measurements -"
DFVLR IB 222-86 A 26, June 1986

8.3.5. Bütefisch, K.-A.
"Flow Field Study on a 65° Delta Wing"
Paper presented at the FFA Symposium on the US/European Vortex Flow Experiment, held on 1-3 October 1986, Stockholm
Proceedings of the Symposium on the "International Vortex Flow Experiment on Euler Code Validation",
Ed. by A. Elsenaar and G. Eriksson

8.3.6. Hartmann, K.
"Force and Pressure Measurements Including Surface Flow Visualization on a cropped Delta Wing".
Paper presented at the FFA Symposium on the US/European Vortex Flow Experiment, held on 1-3 October 1986, Stockholm
Proceedings of the Symposium on the "International Vortex Flow Experiment on Euler Code Validation",
Ed. by A. Elsenaar and G. Eriksson

8.3.7 Hjelmberg, L.
Personal Transfer of FFA Data to DLR, 1988

8.3.8 Elsenaar, A. et al.
"The International Vortex Flow Experiment"
Paper presented at the AGARD FDP Symposium "Validation of Computational Fluid Dynamics "
Lisbon, AGARD CP 437, 1987

8.3.9 Elsenaar, A., Bütefisch, K.-A.
"Experimental Study on Vortex and Shock Wave Development on a 65° Delta Wing".
Proceedings Symposium Transonicum III, IUTAM,
Göttingen 1988

8.3.10 Narayan, K. Y., Hartmann, K.
"Transonic and Supersonic Flow past a 65° Delta Wing with Rounded Leading Edges
- Analysis of Experimental Data -"
DFVLR FB 88 - 44, 1988

8.3.11 Seshadri, S.N., Bütefisch, K.-A.
"Evaluation of LDA 3-Component Velocity Data on a 65° Delta Wing
at M=0.85 and First Results of an Analysis"
DFVLR FB 89 - 19, 1989

## 9. SYMBOLS

| | |
|---|---|
| a | Distance between screen and turbulence level measuring plane in settling chamber, see Fig. 7 |
| $C_m$, Cm | Pitching moment coefficient |
| $C_N$, CN | Normal force coefficient |
| $c_p = \frac{p - p_\infty}{q_\infty}$ | Surface pressure coefficient |
| $c_R$ | Wing root chord |
| l (y) | Local wing chord |
| $M_\infty$, $Ma_\infty$, MA | Freestream Mach number |
| p | Pressure on model surface |
| $p_\infty$ | Freestream static pressure |
| $q_\infty = \frac{\rho_\infty}{2} U_\infty^2$ | Freestream dynamic pressure |
| R | Radius of the circle on which turbulence data were measured by a hot wire probe, see Fig. 7 |
| Re, RE | Reynolds number based either on $0.1\sqrt{S}$ in case of wind tunnel or on root chord in case of model |
| S | Cross section of test section |
| s | Wing semi-span |
| s (x) | Local wing semi-span |
| $T_u$, $T_v$, $T_w$ | Components of the turbulence level |
| $U_\infty$ | Freestream velocity |
| x, y, z | Cartesian coordinates, see Figure 3 |
| $\bar{x}$ | Coordinate of pressure section 4, origion at leading edge, see Fig.3 |
| $\left.\frac{x}{c}\right]_s$ | Range of attached flow along wing leading edge, measured from wing tip |
| α, ALPHA, ALFA | Angle of attack |
| $\nu_\infty$ | Freestream kinematic viscosity |
| $\rho_\infty$ | Freestream density of air |

Table I: Test cases

| IDENTIFICATION | | FLOW CONDITION | | | POSITION | OTHER INFORMATION | |
|---|---|---|---|---|---|---|---|
| CASE NO | CONF. | Mach | q [kPa] | Re x $10^{-6}$ | α | TYPE OF MEASUREMENTS | REMARKS |
| 1 | A | 0.85 | 13.53 | 2.4 | $\alpha_1$ | a | TWG, sting position ②, Fig. 3 |
| 2 | A | 0.85 | 26.20 | 4.5 | $\alpha_2$ | a | " |
| 3 | A | 0.85 | 42.11 | 7.0 | $\alpha_3$ | a | " |
| 4 | A | 0.85 | 13.53 | 2.38 | $\alpha_4$ | b | " |
| 5 | A | 0.85 | 26.20 | 4.57 | $\alpha_4$ | b | " |
| 6 | A | 0.85 | 42.11 | 7.12 | $\alpha_5$ | b | " |
| 7 | A | 0.85 | 32.32 | 6 | $\alpha_6$ | c | HKG |
| 8 | A | 0.85 | 26.20 | 4.5 | $\alpha_7$ | d | TWG, MP, $\frac{x}{c_R}$ = 0.2 to 1.2 |
| 9 | A | 0.85 | 26.20 | 4.5 | $\alpha_7$ | e | TWG, MP, $\frac{x}{c_R}$ = 0.6 and 0.8 |

Legend:

1. Configuration: A = cropped delta wing, see Fig. 3
2. α-range: $\alpha_1$[°] = 1, 0, 1, 2 to 22, $\Delta\alpha$ = 2
   $\alpha_2$[°] = -1, 0, 1, 2 to 20, $\Delta\alpha$ = 2
   $\alpha_3$[°] = -1, 0, 1, 2 to 10, $\Delta\alpha$ = 2
   $\alpha_4$[°] = 10, 20
   $\alpha_5$[°] = 10
   $\alpha_6$[°] = 10, 15, 20
   $\alpha_7$[°] = 20
3. Type of measurements:
   a = overall forces and moments
   b = pressures on model surface
   c = oil flow pictures
   d = visualization with smoke and laser light sheet
   e = flow field measurements
4. Remarks:
   TWG = transonic wind tunnel of DLR Göttingen
   HKG = high speed wind tunnel of DLR Göttingen
   MP = measuring plane at x/c, see Figures 9 and 10

Table II: Data availability

| DATA | ENGIN UNITS | COEF-FICIENTS | NORMALIZED | UN-CORRECTED | CORRECTED |
|---|---|---|---|---|---|
| FREESTREAM CONDITIONS | X | | | | |
| SURFACE | | X | | X | |
| FORCES | | X | | X | |
| FIELD DATA | uncorrected velocity vectors in planes as indicated in Table I | | | | |

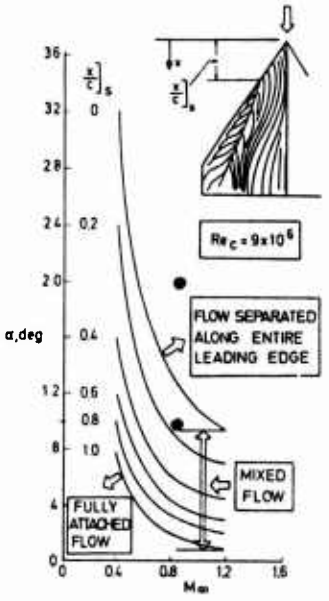



**Figure 1:** Leading edge separation boundary in $M_\infty$, α-plane.
Black points represent selected test cases.

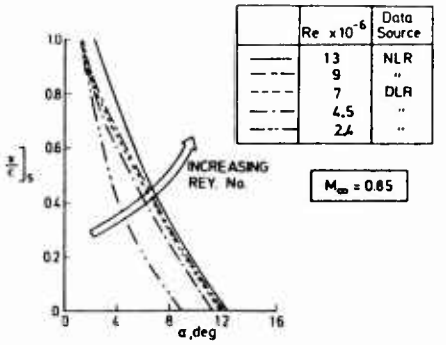



**Figure 2:** Effect of Reynolds number on leading edge separation boundary

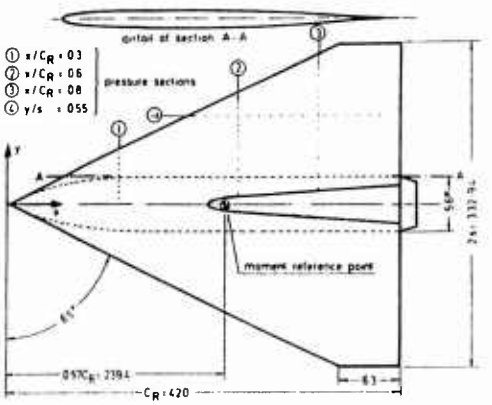



**Figure 3:** Main geometric dimensions of MBB's vortex flow model

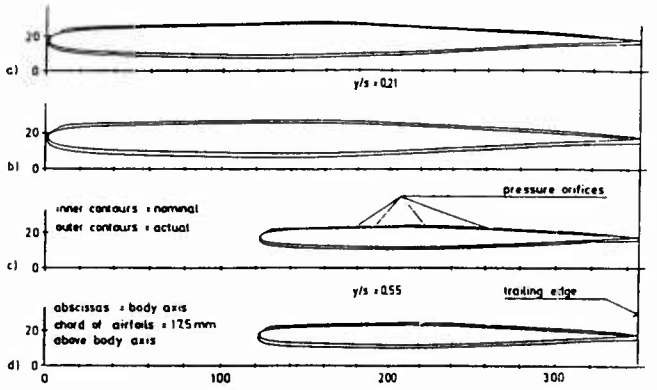



**Figure 4:** Comparison of the nominal and actual airfoil contours of the wing sections at y/s = 0.21 and y/s = 0.55. Differences are depicted five times enlarged.a) and c): without black coating, b) and d) with black coating. Determination of actual contours by G. Eifler,DLR Braunschweig

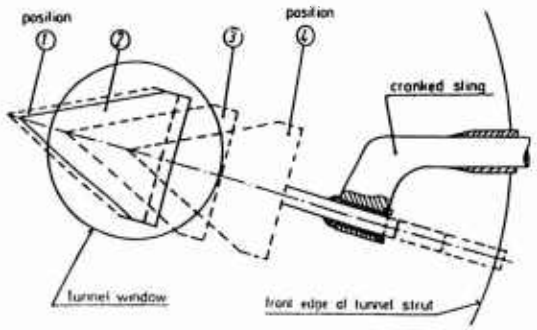



**Figure 5:** Model support arrangement with alternative positions ① to ④ of model relative to tunnel window

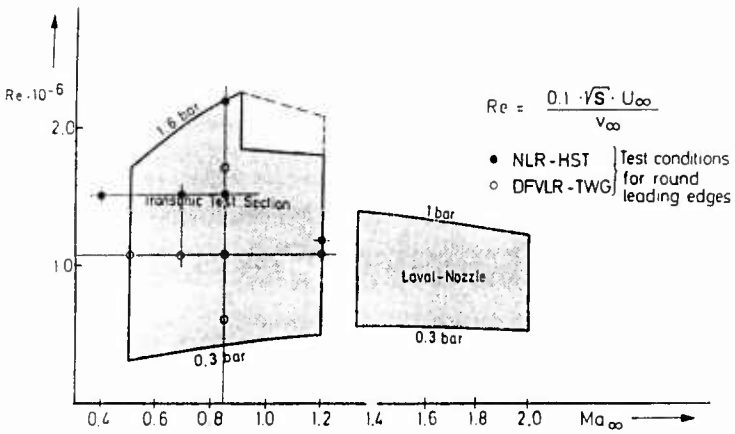



**Figure 6:** Performance envelope of the 1m x 1m Transonic Wind Tunnel (TWG) of the DLR

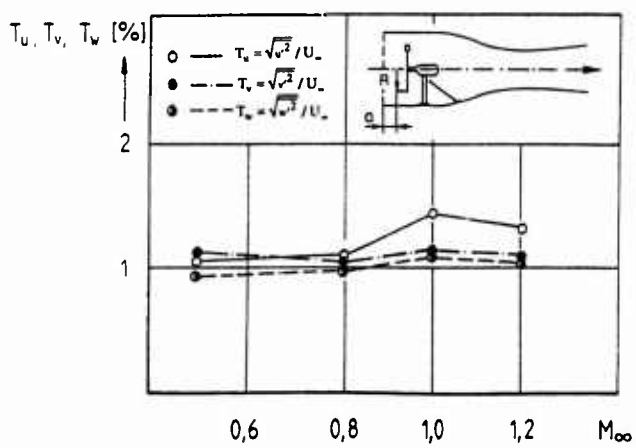



**Figure 7:** Turbulence level in the settling chamber of the Transonic Wind Tunnel (TWG) of the DLR. $T_U$, $T_V$, $T_W$ are averages on a circle with the radius R, data taken at stagnation pressure $p_0$ = 1 bar

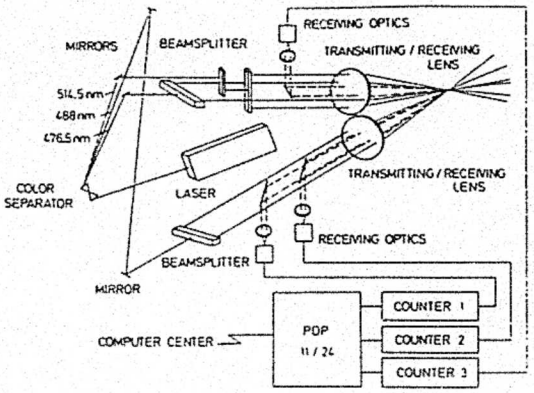



**Figure 8:** Schematical view of the 750 mm three component dual beam Laser Doppler Velocimeter

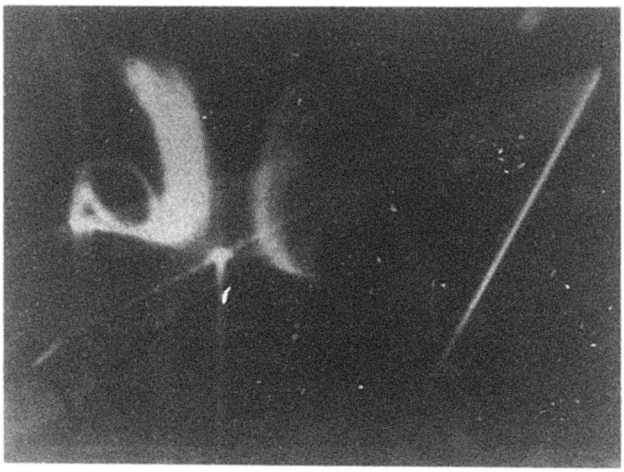
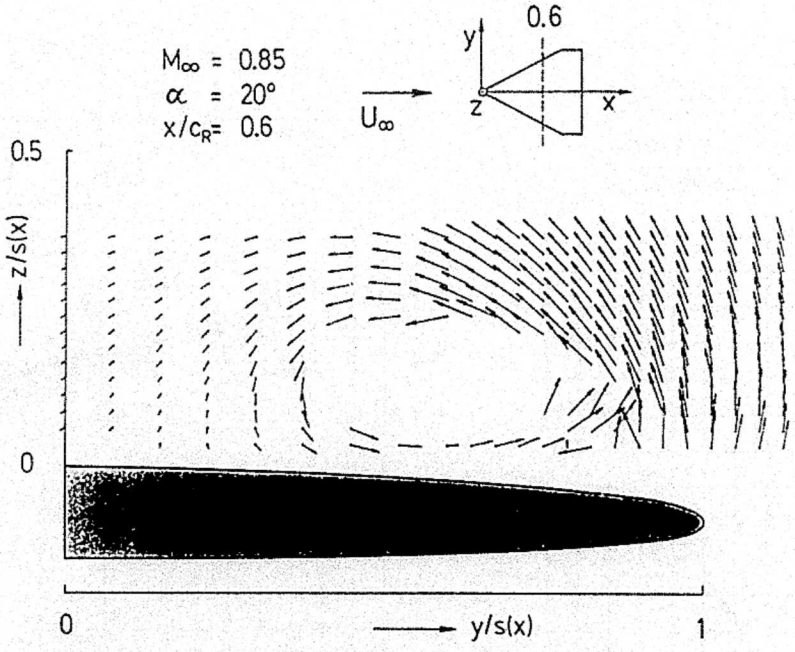


**Figure 9:** Primary and secondary vortices visualized by laser light sheet technique at $M_\infty = 0.85$, $Re = 4.5 \times 10^6$ and $\alpha = 20°$




**Figures 10:** Vector plot in a cross-flow plane at x/c = 0.6. $M_\infty = 0.85$, $Re = 4.5 \times 10^6$, $\alpha = 20°$.

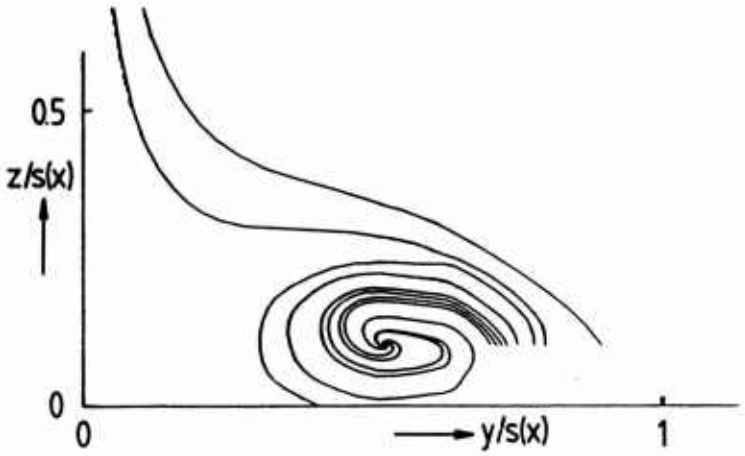



**Figure 11:** Streamlines in a cross-flow plane derived from measured LDA-data.
$M_\infty = 0.85$, $Re = 4.5 \times 10^6$, $\alpha = 20°$.

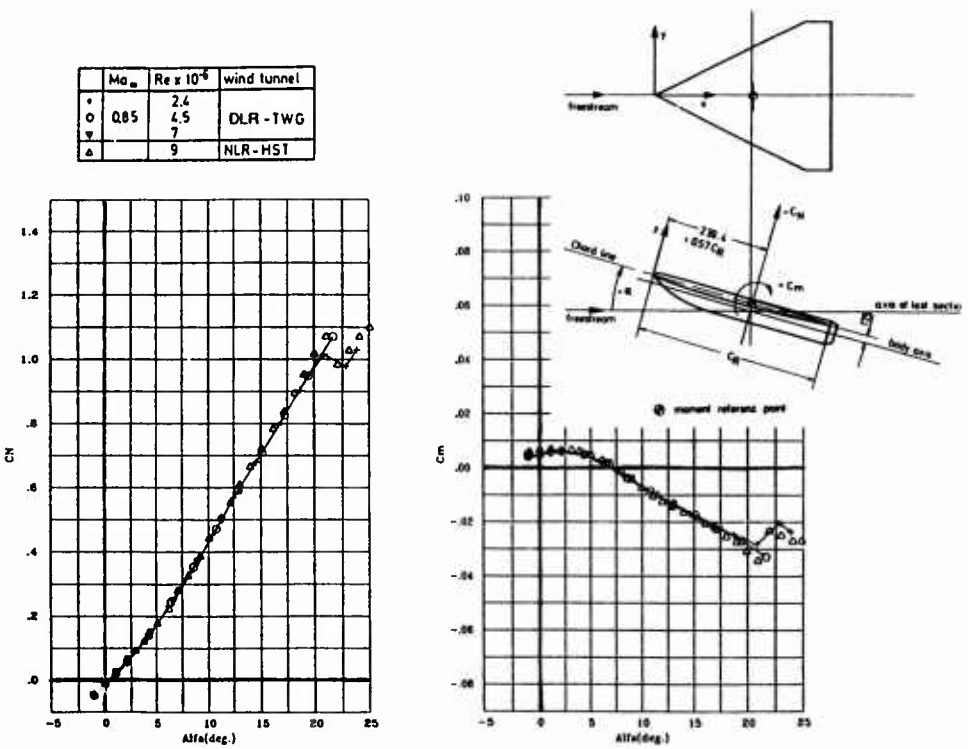



**Figure 12:** Normal force and pitching moment coefficients at different Reynolds numbers. Comparison with NLR data

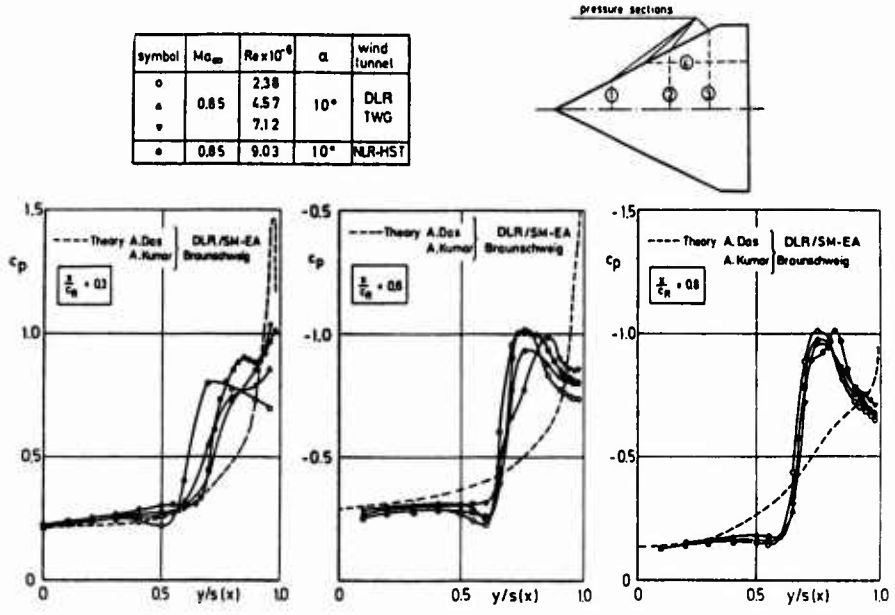



**Figure 13:** Spanwise pressure distribution on the suction side. Comparison with other experimental and theoretical results

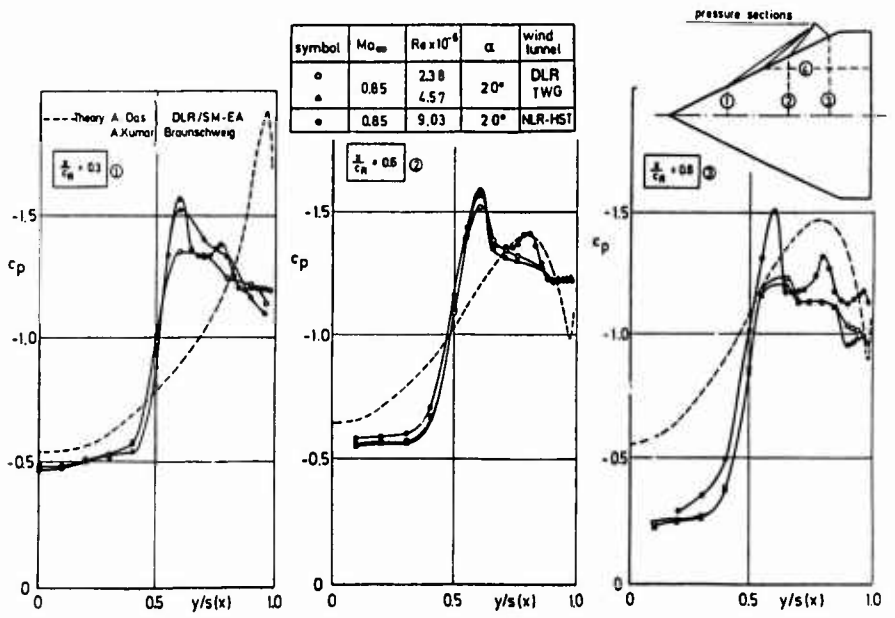



**Figure 14:** Spanwise pressure distribution on the suction side. Comparison with other experimental and theoretical results

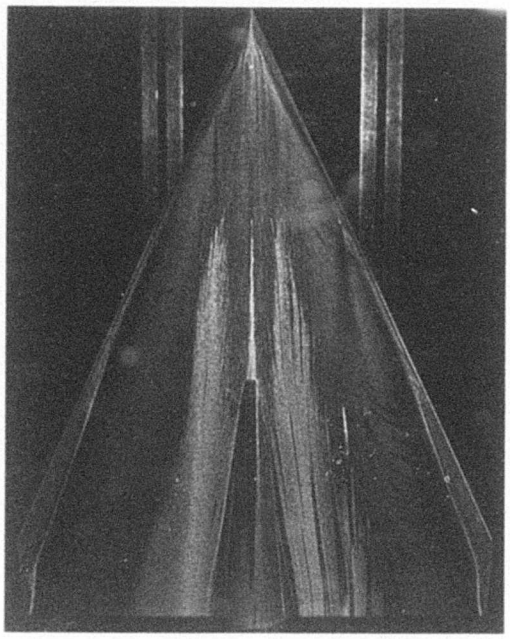


**Figure 15:** Oil flow picture taken in the open jet High Speed Wind Tunnel (HKG) of the DLR at $M_\infty = 0.85$, $\alpha = 10°$, and $Re = 5.9 \times 10^6$, the latter based on a root chord length of 42 cm

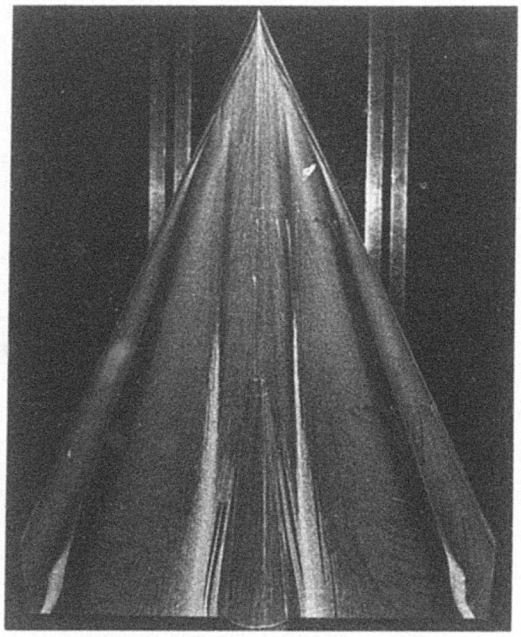


**Figure 16:** Oil flow picture taken in the open jet High Speed Wind Tunnel (HKG) of the DLR at $M_\infty = 0.85$, $\alpha = 15°$, and $Re = 5.9 \times 10^6$, the latter based on a root chord length of 42 cm

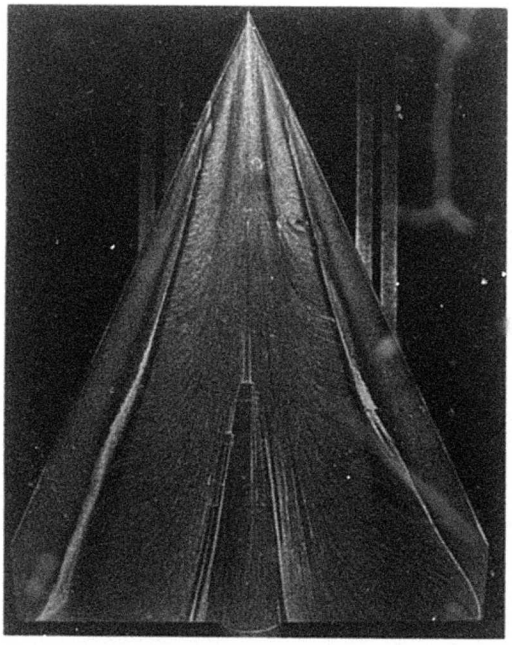


**Figure 17:** Oil flow picture taken in the open jet High Speed Wind Tunnel (HKG) of the DLR at $M_\infty = 0.85$, $\alpha = 20°$, and $Re = 5.9 \times 10^6$, the latter based on a root chord length of 42 cm

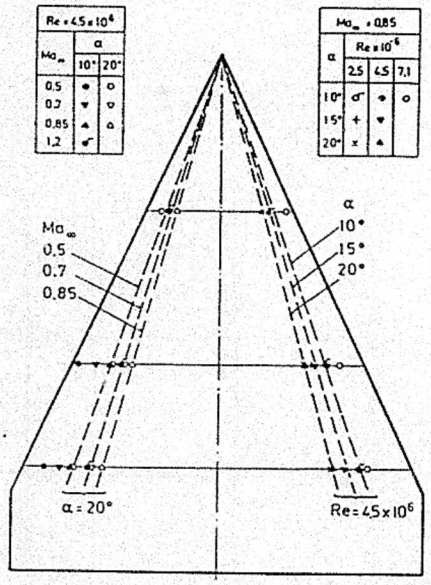



**Figure 18:** Positions of the primary vortices depending on angle of attack, Mach number, and Reynolds number. Dashed lines are footprints of the vortex cores derived from pressure peaks.

# Investigation of the flow development on a highly swept canard/wing research model with segmented leading-and trailing-edge flaps.

*D. Stanniland, ARA, Bedford*

## 0 INTRODUCTION

The results included in this submission are drawn from the extensive testing which has been carried out on a simple canard/wing research model with a low aspect ratio (2.3), highly swept (58°) wing with leading-and trailing-edge flaps. The purpose of these tests was to improve the understanding of the flow development on this class of configuration, to validate the CFD method and philosophy used for the wing design and to provide an extensive data base of pressure data on a precisely specified model geometry for the validation of CFD methods which are capable of handling more complex geometries.

The wing was designed using an FP wing/body code, aiming for attached flow at a high subsonic manoeuvre design point. This results in a highly cambered and twisted wing with a complex flow breakdown on the upper surface. The use of a segmented leading-edge flap means that the vortical flow develops as a series of part-span vortices, even at a constant flap setting with the gaps between the flap segments sealed.

The model has been tested in the ARA 9ft x 8ft Transonic Wind Tunnel over the period 1985 - 1992 to investigate:

1) The effect of a canard, including variation in its position and setting angle.

2) The effect of alternative leading-and trailing-edge flap angles, including both positive and negative settings. Although the model is capable of being tested with graded settings across the span, this option has not been investigated to date.

3) A three surface configuration (canard/wing/tailplane).

4) A blended wing/body derivative of the model, using the existing outer wing and canard designs.

Obviously these tests provide an extensive data base and the results included here comprise the datum wing without flap deflection, both with and without a canard.

# 1 GENERAL DESCRIPTION

## 1.1 Model name and designation

ARA, M165 canard/wing/body research model, based on RAE wing design M2091/6.

## 1.2 Model type and flow conditions

Sting mounted complete Delta wing pressure plotted model with variable camber and close coupled canards ahead of and above the wings. (see Fig. 1) Tested over the range of $0.5 \leq M \leq 1.35$, $-2 \leq \alpha \leq 20$ in the ARA Transonic Wind Tunnel.

### 1.3.1 Design requirements

The datum wing was designed for attached flow with moderate shock strengths on the wing upper surface at the primary manoeuvre design point of $M = 0.90$, $C_L = 0.45$''.
Alternative design points around the flight envelope were to be satisfied by both positive and negative deflections of the leading-and trailing-edge flaps. This was tested on the DRA M2091/6 forces model, which has a representative fuselage, in the DRA (Farnborough) 8ft x 6ft Transonic Tunnel.
The M165 model uses the same wing design mounted on a simple, rectangular fuselage. The net canard, which has 5 alternative positions on the fuselage, each with 5 alternative setting angles, is a 0.3536 scale version of the wing.

### 1.3.2 Purpose of test

The purpose of the tests was to provide overall forces and moments, canard forces and wing pressure distributions for:
a) assessing the basic performance of the datum wing design and validating the theoretical design method.
b) Determining the benefit of leading edge and trailing edge camber variations including graded deflections along the wing span using segmented leading-and trailing-edge flaps. (Data presented relates to LE/TE at 0/0 only).
c) Investigating the aerodynamic coupling between the canards and wings.

## 1.4 Dominant flow physics

Attached flow at the leading edge to moderate incidence with high suctions on forward facing areas of the wing. The flow breakdown depends on Mach number thus:
a) At moderate subsonic Mach numbers a leading edge vortex develops. This breaks down into part span vortices originating from the split lines in the segmented leading edge flaps, even in cases where all the segments have the same angle, and the junction between the flaps is sealed.
b) At high subsonic Mach numbers the vortex development can still be seen at high incidence, but this is preceded by a shock-induced separation on the outer wing at moderate incidences.
c) At supersonic Mach numbers there is a highly swept shock which leads to a shock-induced separation in the cross flow plane.

# 2 DETAILS OF THE MODEL

## 2.1 General geometric arrangement

The general arrangement of the model is illustrated in Fig. 2.
Fore and aft bodies are derived from the ESDU II family of bodies (ESDU 77028). Ref. 8.2.1 (see Fig. 7). Long parallel slab-sided fuselage centre body accommodates a change of canard position with ease. There is extensive pressure plotting on the upper surface of the port wing and the lower surface of the starboard wing.

## 2.2 Configurations

Configuration A:
Datum wing with 0° LE and
TE deflections (W0/0).
Configuration B:
Datum wing with 0° LE and
TE deflections (W0/0) plus canards in position 4 at 0° (C4/0) (see Fig.3).

## 2.3 Wing data

### 2.3.1 Planform

Reference geometry of the wing shown in Fig. 4.

- Reference wing area = 0.4002m²
- Reference wing chord, $\bar{c}$ = 0.4833m
- Reference span = 0.9594m
- Moment reference centre = 0.4163m aft of wing l.e. apex on fuselage axis.
- Aspect ratio = 2.3
- Taper ratio = 0.1833
- Leading edge sweep = 58°
- Trailing edge sweep = 21.8°
- Twist angle of tip relative to root = -5.45° (wing twist is included in the section ordinates).
- Gross semispan = 0.4797m
- Root chord $C_0$ = 0.7050m
- Tip chord = $C_T$ = 0.1292m
- Tip LE point = 0.7676m from wing leading edge apex.
- Details of fuselage/wing junction: low mounted wings on vertical fuselage side. (see Fig. 5)

2.3.2 Basic wing section

- Wing streamwise sections, shown in Fig. 6, were derived from a 3D wing design process.
- Thickness/chord ratio = 5.0% constant across span.

2.3.3 Other components on wing

- Full span leading and trailing-edge flaps were later used to increase wing camber - but are not included in this data set.

## 2.4 Body data

2.4.1 Shape

- Forebody and afterbody are derived from the ESDU II family of bodies (see Fig. 7).
- Body length = 1.7018m
- Maximum cross sectional area = 0.023m²
- Fuselage details are shown in Fig. 8
- Base-rear elevation is shown in Fig. 9
- Typical longitudinal area distribution is shown in Fig. 10

## 2.5 Information on canards

Configuration B only.

- Nett canard planform as wing planform, scaled to be 12.5% gross wing area (see Fig. 11)
- Canard/wing relationship is shown in Fig. 12
- Data presented relates to afterbody without tailplane. Data also exists for tailplane on configurations.

## 2.7 Geometric definition

Wing co-ordinates are specified by 129 points from the lower surface trailing edge, around the leading edge and back to the trailing edge upper surface at 11 equally spaced stations across the span.
Modular wings comprise a main spar with lap joints at front and rear on which are mounted 4 separate LE segments and 2 TE segments for each wing. Each LE segment is 0.25 of exposed semispan, each TE segment is 0.5 of exposed semispan, allowing the fitting of graded deflections along span to produce smooth contours on upper surface of wings at all conditions.
Fuselage co-ordinates given in Fig. 7.

- The wing leading edge shape is manufactured to within 0.03mm. Elsewhere the shape is within a tolerance of 0.08mm.

## 2.8 Model support details

The model was supported in the tunnel by an 83.8mm OD (at base of model) tapered rear sting to the ARA full model cart. Sting, fuselage and strain gauge balance share a common axis. Fuselage base was 121.92mm ahead of sting taper diameter increase. (see Fig. 13)

# 3 GENERAL TUNNEL INFORMATION

## 3.1 Tunnel designation

ARA 2.74m x 2.44m (9ft x 8ft) Transonic Wind Tunnel (see Fig. 14)

## 3.2 Organisation running the tunnel

Aircraft Research Association Ltd
Manton Lane
Bedford MK41 7PF

### 3.3 Tunnel characteristics

The ARA Transonic Tunnel is a rectangular continuous flow, closed circuit tunnel with perforated walls.

- Mach numbers: 0 to 1.4
- Incidence range (straight sting): -10° to 40°
- Roll range: 0 to 360°
- Pressure range: stagnation pressure 0.8 to 1.2 bar.
- Temperature range: stagnation temperature up to 50°C based on Mean Aerodynamic Chord.
- Reynolds number: $4.8 \times 10^6$ at M = 0.55 to $6.6 \times 10^6$ supersonically.
- Run time: continuous.

### 3.4 Test section

3.4.1 Test section details

See Fig 15.

3.4.2 Test section

2.74m x 2.44m. The perforated walls extend 1.33m upstream of the model nose and 1.23m downstream of the model base. The region of uniform onset Mach number extends at least 2.10m upstream of the model nose (the forward limit of pressures measured on the calibration probe).

3.4.3 Wall geometry details

- The perforated tunnel walls have a 22% open area (normal holes), varying over the length of the working section to minimise interference at high subsonic Mach numbers.
- No wall pressures were measured for these test series.
- Wall boundary layer thickness was 13mm at the model centre of rotation, measured for tests with a centreline calibration probe ('empty tunnel').

### 3.5 Free-stream conditions

3.5.1 Reference conditions

Total pressure in the working section is obtained from the static pressure in the settling chamber using calibration data.

Static pressure in the working section is obtained from the static pressure on the wall of the plenum chamber.
The reference pressure used to calibrate pressure transducers is an applied pressure in a large reservoir in the tunnel control room.

Stagnation temperature is measured to an accuracy of ±0.2°K over the operating range of the tunnel, using a probe installed in the settling chamber.

3.5.2 Tunnel calibration

- The tunnel is calibrated using a centreline static probe with wall static pressures.
- Last calibration was performed in October 1986 (complete model testing).

### 3.6 Flow Quality

3.6.1 Flow uniformity

Mach number variation along the length of a model is set to a nominal zero using settings of the wind tunnel walls derived from the tunnel calibration. Typical errors of $\Delta M = 0.0002$ were measured in the last calibration of the tunnel. Mach number is held to within 0.001 of the required value up to moderate incidence, at subsonic Mach numbers. Mean flow angularity is obtained for each model using a small incidence traverse with the model upright and inverted. Flow angles are normally found to lie with ±0.02° of the standard values for most models. For a detailed discussion of the tunnel flow angularity, see Ref. 8.1.2.

3.6.2 Temperature variation

Tunnel temperature is not controlled directly, although the increase in temperature during a run is minimised by a cooler. Stagnation temperature increases by approximately 2°K for a moderate incidence traverse at a given Mach number. Temperature variation across the tunnel is not known.

3.6.3 Flow unsteadiness

Early measurements of the unsteadiness in the ARA TWT indicated a peak at M = 0.7. A more extensive investigation, carried out in 1990 following the installation of a long cell honeycomb, showed that this peak is due to a tone at 2.6 KHz which is not present when a model is present in the working section. See Ref 2 for further details.

## 4 INSTRUMENTATION

### 4.1 Model position

4.1.1 Geometrical incidence measurements

Geometrical incidence is measured by an accelerometer located in the model cart and corrected for deflections of the model support system under load using an accelerometer in the forebody of the model.

4.1.2 Accuracy of geometrical incidence

Model incidence accuracy is $\pm 0.01°$.

### 4.2 Model pressure measurement

4.2.1 Number & locations of pressure holes

Total no. of pressure locations: 344 (see Fig. 16)
6 x 29 Port wing upper surface.
6 x 26 Starboard wing lower surface.
6 Starboard canard upper surface (configuration B)
8 Fuselage base + 2 standard base pressures.
Pressure holes are positioned in 6 streamwise rows along the port wing upper surface and starboard wing lower surface, across the starboard canard upper surface at 0.94 chord (config. B), around the fuselage base (see Fig. 9) and within the model cavity in the region of the main balance.

4.2.2 Range and accuracy of pressure transducers

$\pm$1034mbar range Druck type transducers were used, with a nominal sensitivity of 14.535$\mu$V/mbar scan, calibrated in every scan.

4.2.3 Dynamic pressures

Kulite DDP/N 500/350 semi-conductor strain gauges were used to measure buffet on wings (see Fig. 16) and starboard canard.

### 4.3 Forces and Moment measurements

4.3.1 Type and location of balances

- Overall model loads were measured with ARA No. 4,76.2mm (3") diameter 6 component strain gauge balance, situated on the model centreline (see Fig. 2).
- Overall loads were measured on the port canard (configuration B), using a 3 component canard panel balance.

4.3.2 Maximum range and accuracy

Balance sensitivities are shown in Table 1a for Main Balance and Table 1b for Canard Balance.

### 4.5 Surface flow visualisation

4.5.1 Measurement techniques applied

Oil flow visualisation runs were conducted for both configurations A and B at M = 0.8, $\alpha$ = 6°, 9°, 12°, 15° and 18°.
For configuration B,M = 0.7, 0.9, 0.95 and 1.2 were also visualised at $\alpha$ reducing from maximum.

4.5.2 Recording of visualisation

Video tape recording was made of runs, with flash photographs taken through the plenum shell at each incidence. Still photographs were taken post run of the interesting features.

### 4.6 Field flow visualisation

A survey of the flow field has been carried out using a seven hole probe, but results are not included here.

### 4.7 Tunnel wall measurements

Tunnel wall measurements were not carried out at this time.

### 4.8 Instrumentation used

All measurements were made using the ARA standard data acquisition system.

## 5 TEST MATRIX AND CONDITIONS

### 5.1 Details of test matrix

5.1.1 Number of test cases

Two test cases have been selected.

5.1.2 Number of configurations

One configuration from each test case is presented.

5.1.3 Summary of test cases

For summary of test cases see Table II.

### 5.2 Model/tunnel relations

5.2.1 Blockage effect

Blockage effect caused the Mach number settings to vary over the Transonic region as follows:

$M_{SET}$ = 0.902 : 0.958 : 1.040

$M_{CORRECTED}$ = 0.900 : 0.950 : 1.000

Maximum blockage of the model at zero incidence is 0.5%.

5.2.2 Model span/tunnel width

Ratio of model wing span to tunnel width = 0.35.

5.2.3 Wing area/tunnel cross section

Wing area: tunnel cross sectional area = 0.060.

5.2.6 Wall temperatures

Wall temperatures were not measured.

### 5.3 Transition details

5.3.1 Transition fix

Both test cases were conducted with transition fixed on wings at 0.05C (see Table III).

5.3.3 Details of transition fix

Transition was fixed with a sparse distribution of Ballotini set on a thin film of epoxy resin.
Subsidiary runs to investigate the effect of transition fixing were carried out with transition free wing upper surfaces and with small discrete leading edge strips wrapped around the leading edge at 38mm intervals (~ 20/wing), midway between the pressure holes.

5.3.4 Transition verification

The effectiveness of the transition band was confirmed using the sublimation of acenaphthene at M = 0.9, $C_L$ = 0.35. In fact, natural transition occurs just ahead of 5% chord at moderate incidence, and the only significant difference between transition free and transition fixed is a small difference in the drag level at low $C_L$ (< 0.4).

## 6 DATA

### 6.1 Availability of data

6.1.1 Owners or data

U.K. Ministry of Defence
Technical Authority represented by
Aerodynamics and Propulsion Department
Defence Research Agency
Farnborough
England

6.1.2 Person responsible for data

Mr D Stanniland
Aircraft Research Association Ltd
Manton Lane
Bedford MK41 7PF

Tel: 0234 - 350681
Fax: Groups 2 & 3, 0234 - 328584

6.1.3 Queries about data

Contact ARA in the first instance.

### 6.2 Suitability of data for CFD validation

6.2.1 Suitability for "in tunnel" calculations

The tests were carried out in a perforated tunnel with no measured wall pressures. Hence, the data is unlikely to be appropriate for in-tunnel calculations with a specified boundary condition.

6.2.2 Simulation of 'Free Air' conditions

The data are corrected to 'Free Air' conditions. Extensive calculations have been carried out at ARA and elsewhere, notably using the ARA Multiblock/Euler code, which gives confidence in using the data for attached flow conditions.
However, validation of Navier-Stokes Solvers with some flow breakdown is likely to be complicated by the fact that the model uses a segmented leading edge which is sufficient to create a part-span vortex breakdown, even though the junctions are sealed. Representing this flow in an N-S Solver is likely to require some empirical treatment to create an equivalent numerical effect.

### 6.3 Type and form in which data are available

6.3.1 Type and form of data

For list of available data see Table IV.

6.3.2 Format of data available

Data will be supplied on an IBM compatible floppy disk.

### 6.4 Correction applied to data

6.4.1 Lift interference and blockage

- Mach number is corrected for model blockage.
- Incidence is corrected for small tunnel upwash angle, measured during tests by comparing data for model rolled through 180° with data at 0°.
- Correction to incidence to compensate for tunnel wall constraint in the form $\Delta\alpha$ constraint.
- Base drag.
- Balance axial force drift through the run.

6.4.5 Aero-elastic deformation

Correction has been applied for aeroelastic deformation under load. Calculations suggest that for atmospheric stagnation pressure testing deflections will be small.

## 7 DATA ACCURACY AND REPEATABILITY ASSESSMENT

### 7.1 Estimated accuracies

7.1.1 Free stream conditions

Mach number measured in these tests has a bias of -0.0015 which has been recently identified, with an accuracy of ±0.001. Model incidence is estimated to be accurate to ±0.02° up to $\alpha \simeq 10°$.

7.1.2 Measured data

The RMS errors presented in Table I imply errors at M = 0.8 of typically -

Main balance

| | |
|---|---|
| CY ±0.0002 | based on gross wing reference dimensions. |
| CN ±0.0009 | |
| CA ±0.00006 | |
| Cm ±0.0001 | |
| C$\ell$ ±0.00003 | |
| Cn ±0.00003 | |

Canard balance

| | |
|---|---|
| $CN_c$ ±0.002 | based on nett canard reference dimensions. |
| $Cm_c$ ±0.005 | |
| $C\ell_c$ ±0.002 | |

### 7.4 Other tests on same (nominal) geometry

7.4.2 Similar models in another tunnel

- Further tests have been conducted at ARA with this model, varying configuration. Results are not for general use at this time.
- Companion model has been tested as M2091/6 in the 8' x 6' tunnel at DRA, Farnborough, with forces and oil flow visualisation only. (scale 0.8658 of ARA model M165).

## 8 REFERENCES

### 8.1 On the Wind Tunnel

1. J E Green, C A McHugh, A J Baxendale, D R Stanniland.

The use of a deep honeycomb to achieve high flow quality in the ARA 9' x 8' Transonic Wind Tunnel presented at 18th Congress of ICAS, Beijing, September 1992.

2. D R Stanniland, C A McHugh, J E Green.

Improvement of the flow quality in the ARA Transonic Tunnel by means of a long cell honey-comb. Paper 54, RAes conference on "Wind Tunnels and Wind Tunnel Test Techniques", Southampton 1992.

3. E C Carter, K C Pallister.

Development of testing techniques in a large Transonic Wind Tunnel to achieve a required drag accuracy and flow standards for modern civil transport. AGARD-CP-429, September 1987.

### 8.2 On the Model

1. ESDU 77028
-ESDU II Family of Bodies

2. K Pallister, J Parker, B Probert.

Comparison of recent results from different wind tunnel facilities along with comparisons of measured flight results and wind tunnel based predictions. AIAA Paper 92-3985, July 1992.

3. K H Wilson

Aerodynamic design of a wing with 58° leading edge sweep for a Combat Aircraft Research Model. RAE TM Aero 2074, 1986.

### 8.3 On the Test

1. R Jordan, I Burns, A J Day.

M165 canard/wing/body research model. Details of model design, series 1 test programme and summary of data produced.

Table 1a

M165 MAIN BALANCE SENSITIVITIES

| COMPONENT | | RMS ERROR (N or Nm) | | | MAXIMUM LOAD |
|---|---|---|---|---|---|
| | | AV. | MAX. | % | |
| SIDE FORCE | Y | 2.41 | 5.84 | 0.06 | 4080 N |
| NORMAL FORCE | N | 10.58 | 32.73 | 0.06 | 17792 N |
| AXIAL FORCE | A | 0.72 | 2.44 | 0.03 | 2224 N |
| PITCHING MOMENT | m | 0.82 | 1.84 | 0.04 | 2264 Nm |
| ROLLING MOMENT | $\ell$ | 0.34 | 1.29 | 0.05 | 725 Nm |
| YAWING MOMENT | n | 0.30 | 1.05 | 0.04 | 725 Nm |
| AXIAL FORCE (spare) | As | 0.77 | 2.28 | 0.03 | 2224 N |

RMS ERROR IS EXPRESSED AS A % OF THE MAXIMUM LOAD,
DERIVED FROM THE BALANCE CALIBRATION

Table 1b

M165 CANARD BALANCE SENSITIVITIES

| COMPONENT | | RMS ERROR (N or Nm) | | | MAXIMUM LOAD |
|---|---|---|---|---|---|
| | | AV. | MAX. | % | |
| NORMAL FORCE | Nc | 1.856 | 12.44 | 0.19 | 1000 N |
| PITCHING MOMENT | mc | 0.673 | 12.42 | 1.3 | 50 Nm |
| BENDING MOMENT (about cal.centre) | $\ell$c | 0.297 | 5.72 | 0.46 | 65 Nm |

RMS ERROR IS EXPRESSED AS A % OF THE MAXIMUM LOAD,
DERIVED FROM THE BALANCE CALIBRATION

## TABLE II

## SUMMARY OF TEST CASES

| IDENTIFICATION | | | CONDITIONS | | POSITION | | OTHER INFORMATION | |
|---|---|---|---|---|---|---|---|---|
| CASE NO. | WING/ LE/TE | CANARD POSN/ANGLE | MACH NO. | H | $\alpha°$ | ~ $C_L$ | Type of measurements | Remarks |
| 1 | W0/0 | - | | | | | | Transition on wing U/S at 0.05c |
| | | | 0.7 | 1.0 | 8.0 | 0.424 | a,b | |
| | | | 0.8 | 1.0 | 8.0 | 0.448 | a,b | |
| | | | 0.85 | 1.0 | 8.0 | 0.468 | a,b | |
| | | | 0.9 # | 1.0 | 5,6,8,10,12,15 | - | a,b | # incidence traverse |
| | | | 0.95 | 1.0 | 8.0 | 0.520 | a,b | |
| | | | 1.2 | 1.0 | 8.0 | 0.470 | a,b | |
| | | | 1.35 | 1.0 | 8.0 | 0.429 | a,b | |
| 2 | W0/0 | C4/0 | | | | | | Transition on wing U/S at 0.05c |
| | | | 0.7 | 1.0 | 8.0 | 0.452 | a,b,c | |
| | | | 0.8 | 1.0 | 8.0 | 0.472 | a,b,c | |
| | | | 0.85 | 1.0 | 8.0 | 0.487 | a,b,c | |
| | | | 0.9 # | 1.0 | 5,6,8,10,12,15 | - | a,b,c | # incidence traverse |
| | | | 0.95 | 1.0 | 8.0 | 0.532 | a,b,c | |
| | | | 1.2 | 1.0 | 8.0 | 0.489 | a,b,c | |
| | | | 1.35 | 1.0 | 8.0 | 0.459 | a,b,c | |

(9) SURFACE STATIC PRESSURES
(b) MAIN BALANCE FORCES
(c) CANARD BALANCE FORCES

* For Reynolds numbers see Fig. 17.

## TABLE III

## M165 TRANSITION FIXING

| SURFACE | START OF BAND | WIDTH OF BAND | BALLOTINI SIZE |
|---|---|---|---|
| Fuselage nose | 101.6mm from apex | 5.0mm | 0.13-0.15mm |
| Wing upper surface | 5% local chord from L.E. | 2.5mm | 0.13-0.15mm |
| Wing lower surface | As for wing upper surface | | |
| Canard upper and lower surface | No bands applied | | |

## TABLE IV

## DATA AVAILABILITY

| DATA | ENGIN. UNITS | COEFFICIENTS | NORMALIZED | UN-CORRECTED | CORRECTED |
|---|---|---|---|---|---|
| FREESTREAM CONDITIONS | | | | | X |
| SURFACE PRESSURES | | X | | | X |
| HEATTRANSFER SKINFRICTION | | | | | |
| FORCES | | X | | | X |
| BOUNDARY LAYER DATA | | | | | |
| WAKE DATA | | | | | |
| FIELD DATA | | | | | |
| TEST SECTION WALL PRESSURES | | | | | |

X INDICATES DATA AVAILABLE

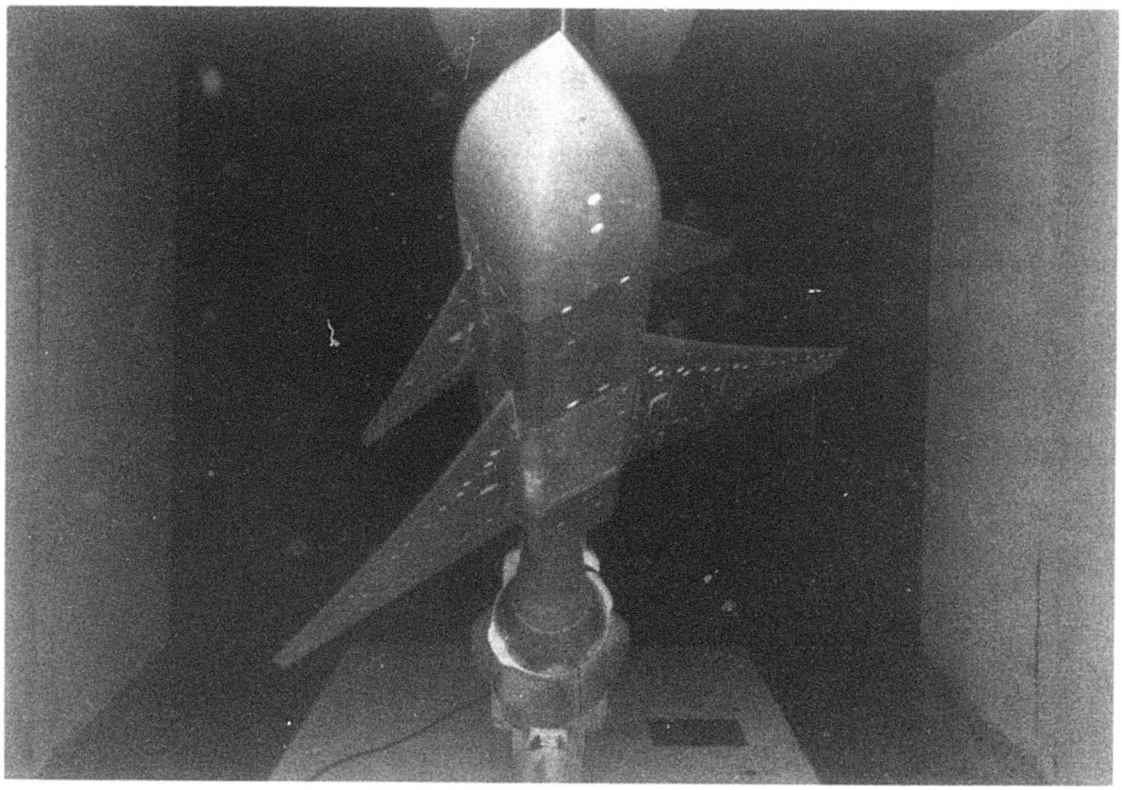


FIG 1 M-165 COMPLETE MODEL IN TUNNEL WORKING SECTION

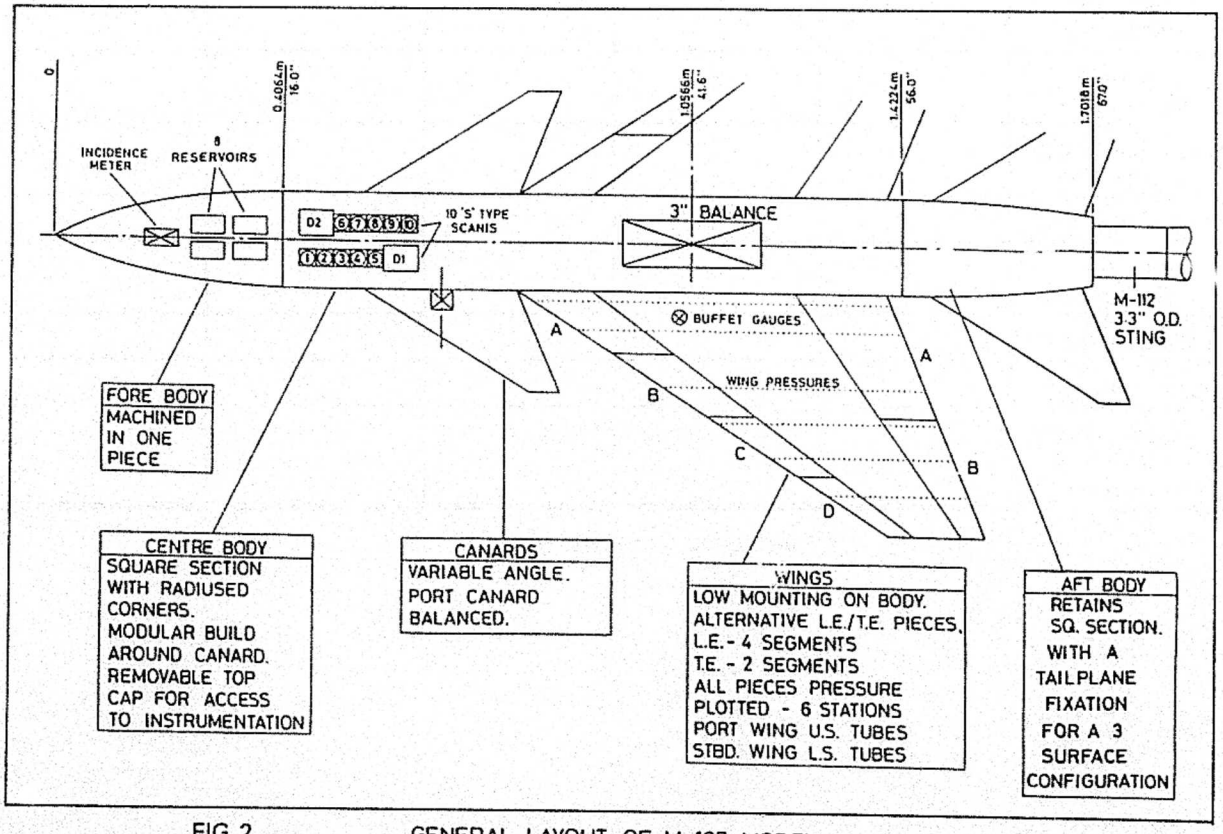



FIG 2 GENERAL LAYOUT OF M-165 MODEL

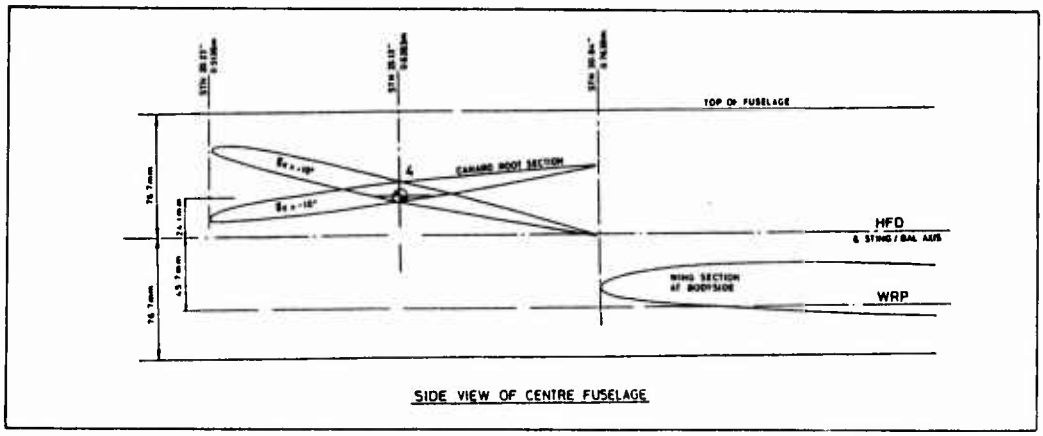
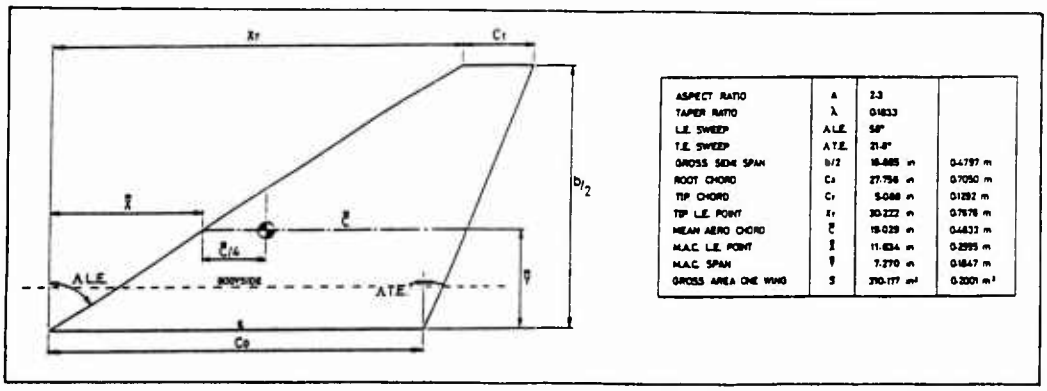



FIG 3 M-165 CANARD LONGITUDINAL POSITION




| | | | |
|---|---|---|---|
| ASPECT RATIO | A | 2.3 | |
| TAPER RATIO | λ | 0.1833 | |
| L.E. SWEEP | A.L.E. | 58° | |
| T.E. SWEEP | A.T.E. | 21.8° | |
| GROSS SIDE SPAN | b/2 | 18.885 in | 0.4797 m |
| ROOT CHORD | $C_R$ | 27.756 in | 0.7050 m |
| TIP CHORD | $C_T$ | 5.088 in | 0.1292 m |
| TIP L.E. POINT | $X_T$ | 30.222 in | 0.7676 m |
| MEAN AERO CHORD | $\bar{C}$ | 18.029 in | 0.4633 m |
| M.A.C. L.E. POINT | $\bar{X}$ | 11.634 in | 0.2955 m |
| M.A.C. SPAN | $\bar{Y}$ | 7.270 in | 0.1847 m |
| GROSS AREA ONE WING | S | 370.177 in² | 0.2001 m² |

FIG 4 M-165 REFERENCE GEOMETRY OF WING

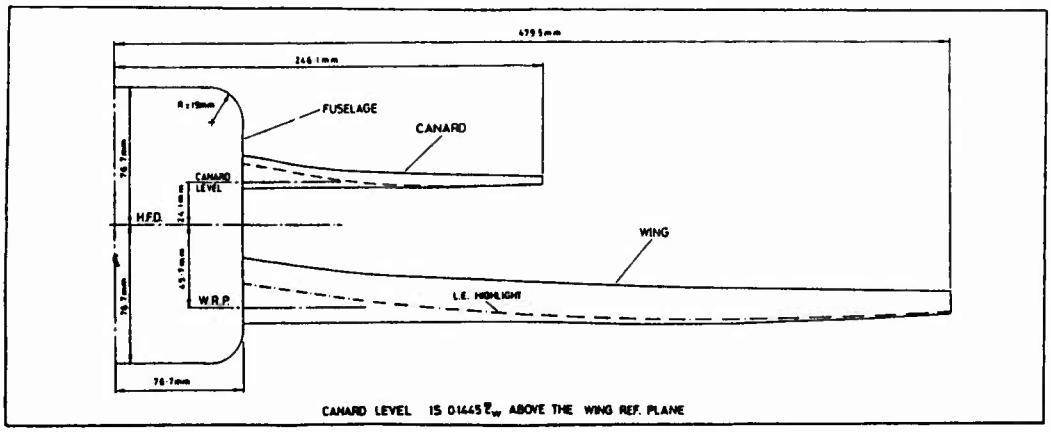



FIG 5 M-165 FUSELAGE SECTION AND CANARD VERTICAL POSITION

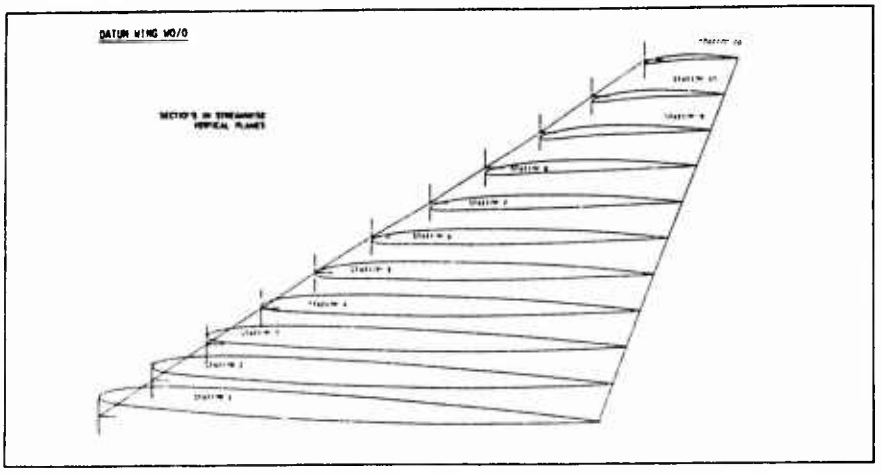



FIG 6 M165 DATUM WING SECTIONS

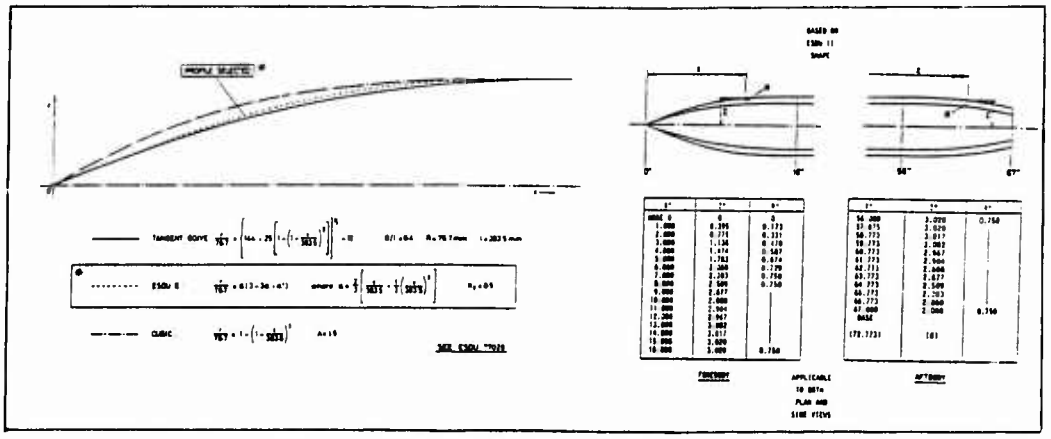


FIG 7 M165 FUSELAGE SPECIFICATION

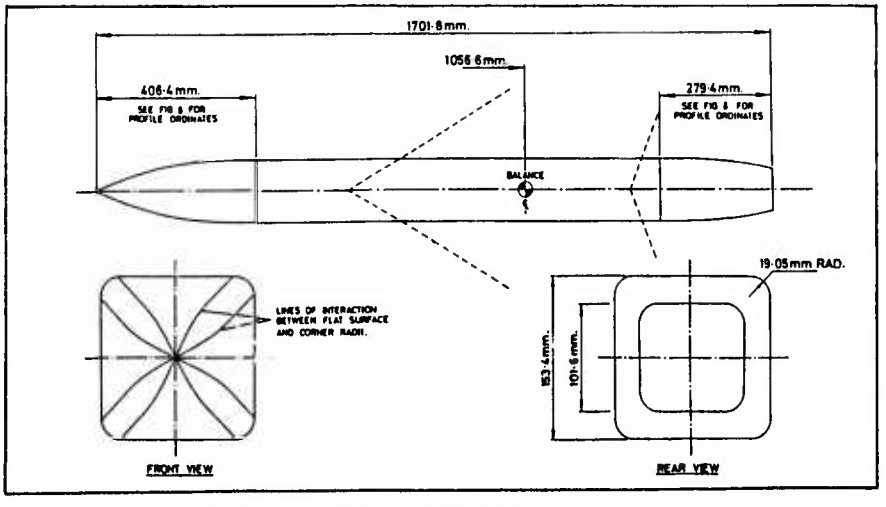



FIG 8 M165 FUSELAGE DETAILS

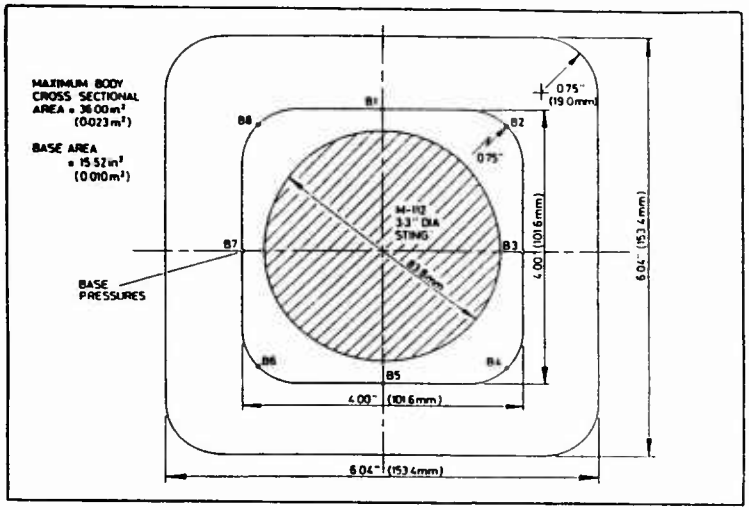



FIG 9 M-165 BASE - REAR ELEVATION

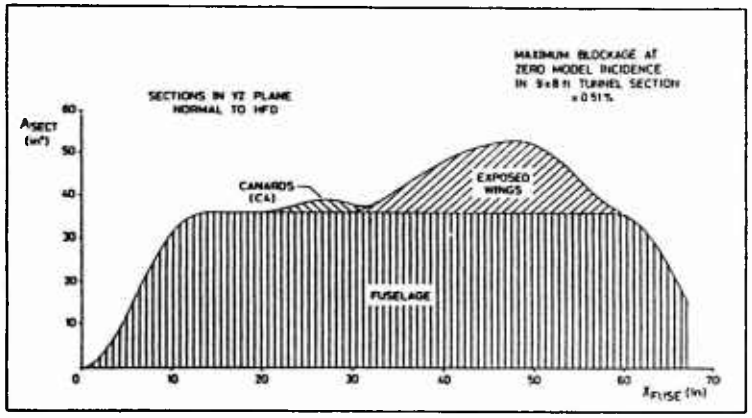
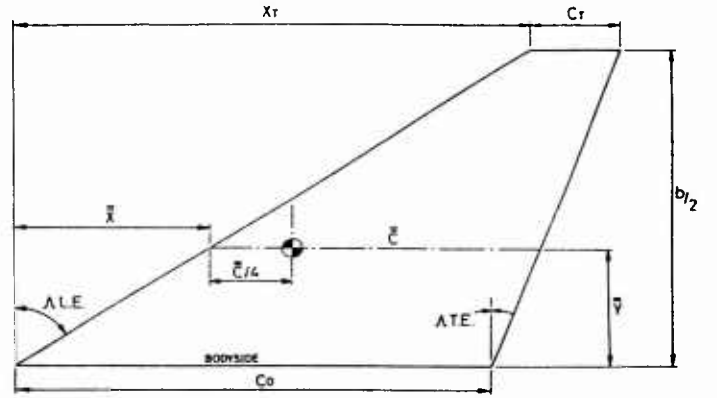



FIG 10 M-165 TYPICAL LONGITUDINAL AREA DISTRIBUTION




CANARD PLANFORM PROJECTED IN HORIZONTAL PLANE

N.B. CANARD SCALED TO BE 12.5% OF GROSS WING AREA

| | | | |
|---|---|---|---|
| ASPECT RATIO | A | 2.3 | |
| TAPER RATIO | λ | 0.1833 | |
| L.E. SWEEP | Λ L.E. | 58° | |
| T.E. SWEEP | Λ T.E. | 21.8° | |
| NETT SEMI SPAN | b/2 | 6.677 in | 0.1696 m |
| ROOT CHORD | Co | 9.813 in | 0.2493 m |
| TIP CHORD | CT | 1.799 in | 0.0457 m |
| TIP L.E. POINT | XT | 10.685 in | 0.2714 m |
| MEAN AERO. CHORD | $\bar{\bar{C}}$ | 6.728 in | 0.1709 m |
| M.A.C. L.E. POINT | $\bar{\bar{X}}$ | 4.113 in | 0.1045 m |
| M.A.C. SPAN | $\bar{\bar{Y}}$ | 2.571 in | 0.0653 m |
| NETT AREA ONE CANARD | S | 38.764 in² | 0.0250 m² |

FIG 11 M-165 REFERENCE GEOMETRY OF CANARD

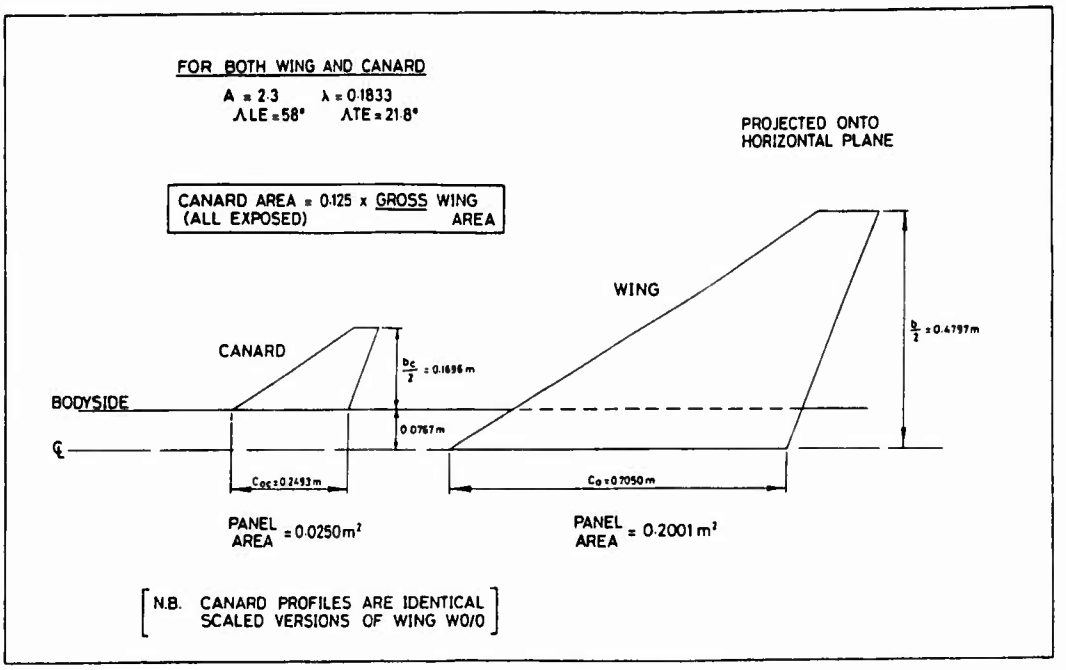



FIG 12 M-165 CANARD / WING RELATIONSHIP

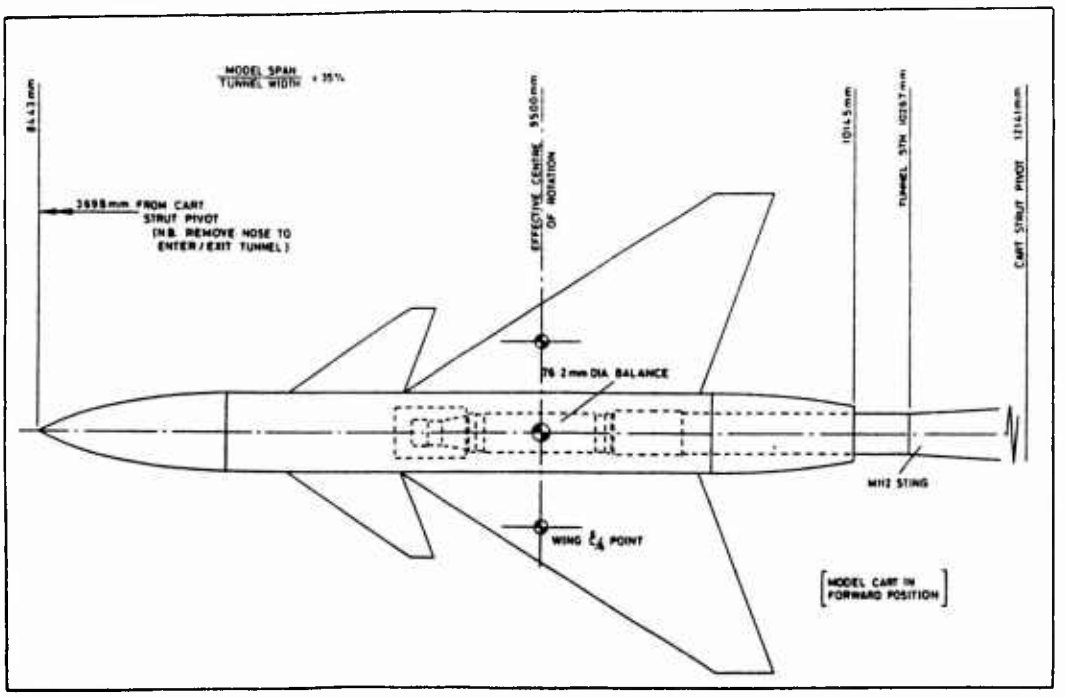



FIG 13 M-165 MODEL POSITION IN WORKING SECTION

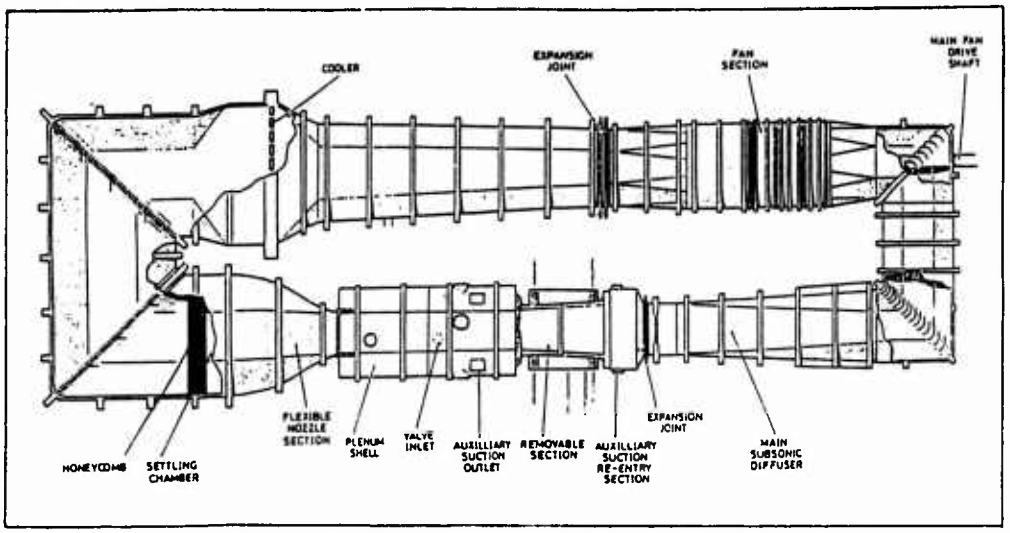



FIG 14 DETAILS OF THE A.R.A. 9'X8' TRANSONIC TUNNEL CIRCUIT

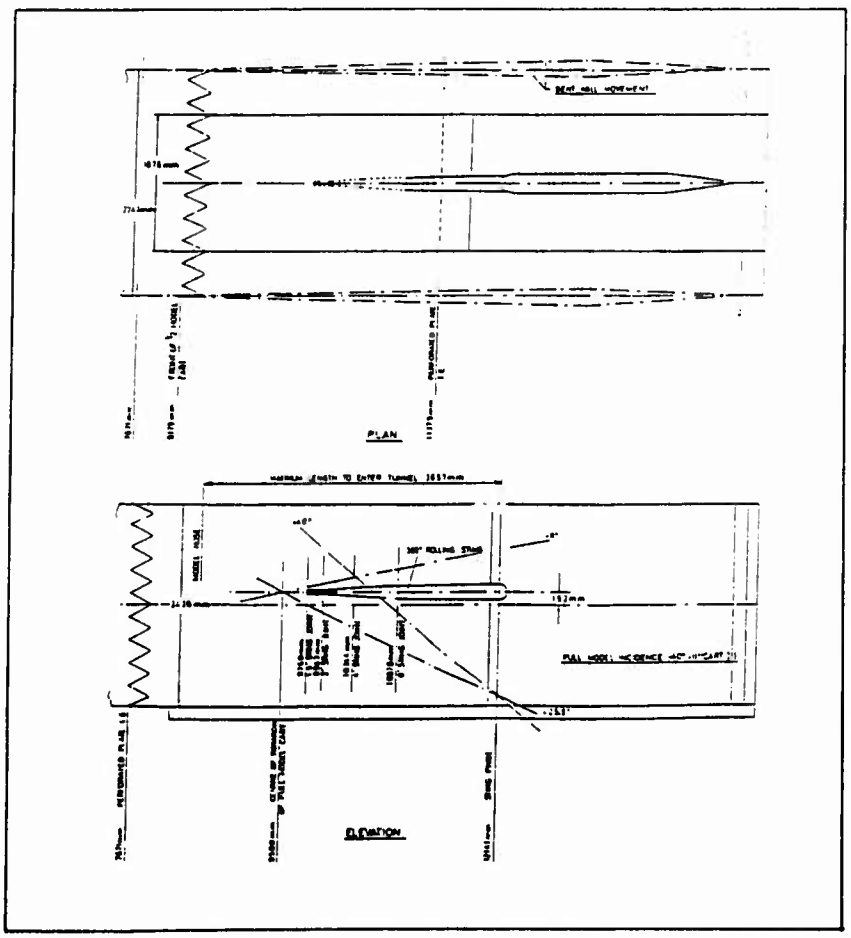



FIG 15 TRANSONIC WIND TUNNEL WORKING SECTION

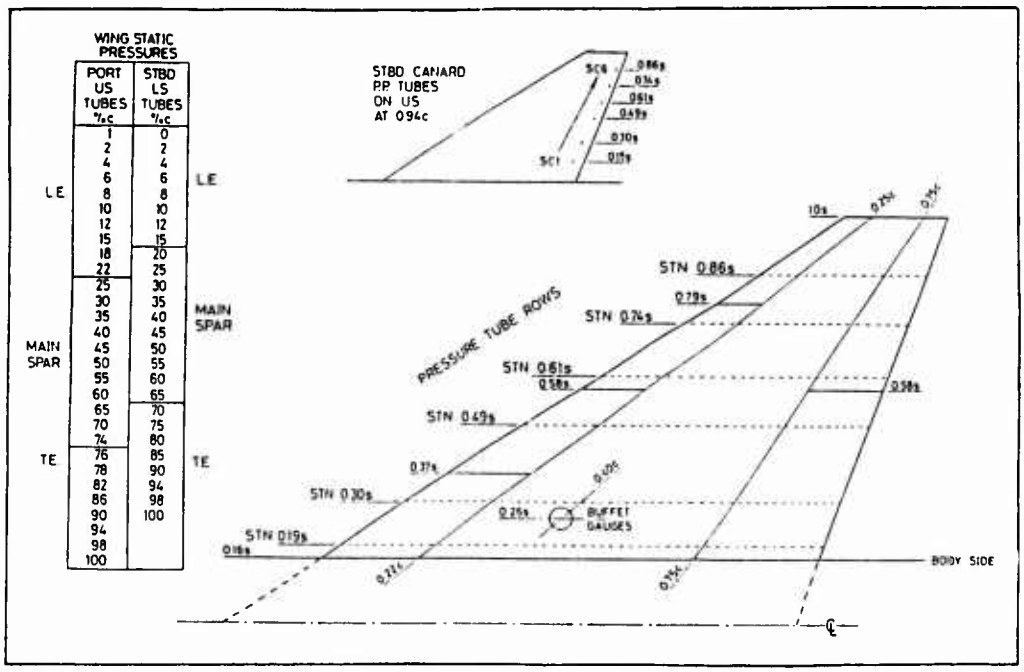



FIG 16 M-165 PRESSURE PLOTTING LAYOUT

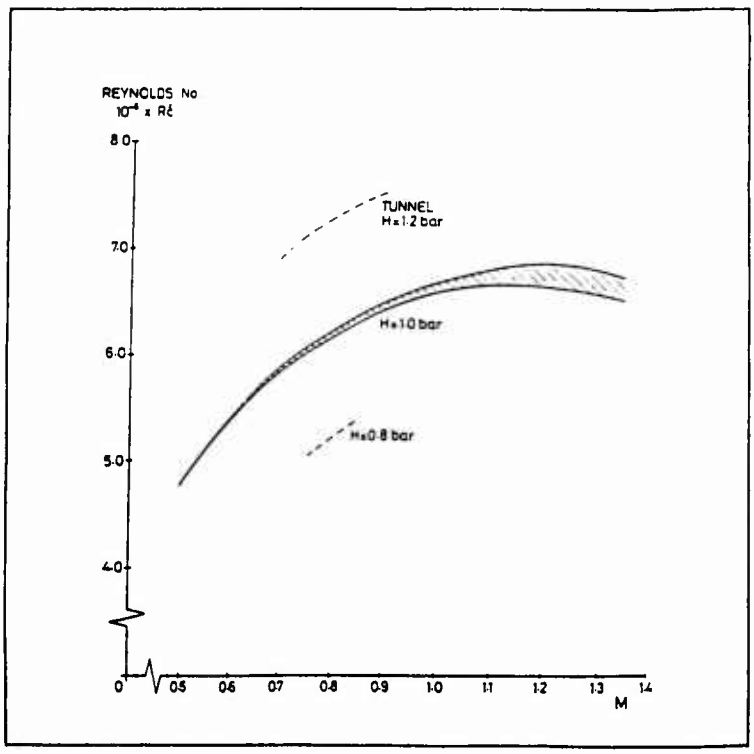



FIG 17 M165 SERIES1 – TYPICAL REYNOLDS NUMBERS

# SUBSONIC FLOW AROUND US-ORBITER MODEL FALKE IN THE DNW

BY

R. RADESPIEL, A. QUAST
DEUTSCHE FORSCHUNGSANSTALT FÜR LUFT- UND RAUMFAHRT E.V. (DLR)
Institut für Entwurfsaerodynamik, Flughafen, 3300 Braunschweig, Germany
D. ECKERT
DNW, P.O. Box 175, 8300 AD Emmeloord, The Netherlands

## 0. INTRODUCTION

The contribution describes wind tunnel measurements of aerodynamic forces, pressure distributions and surface visualization for the FALKE model. FALKE is a model of the US-Orbiter in the scale 1:5.427. The test results taken in the subsonic wind tunnel DNW enable validation of computational methods for reentry vehicles in landing conditions at high Reynolds numbers, where strong vortical flow occurs on the upper side of the configuration.

## 1. GENERAL DESCRIPTION

| | |
|---|---|
| 1.1 Model name or designation | FALKE |
| 1.2 Model type and flow conditions | Blunt body with delta wing and strake in subsonic flow. |
| 1.3 Design requirements, purpose of test | Investigate vortical flow on reentry vehicles at landing conditions with high angle of attack and high Reynolds number. |
| 1.4 Dominant flow physics | Primary and secondary separations on smooth surfaces of wing and fuselage, see Figure 1. |

## 2 DETAILS OF MODEL(S)

| | |
|---|---|
| 2.1 General geometric arrangement | FALKE is a geometrical model of the US-Orbiter in the scale 1:5.427, see Figure 2. It consists of a blunt fuselage, a cropped delta wing with strake, a swept vertical tail, and a body flap. The model is built from composite materials. |
| 2.2 Various configurations | No |
| 2.3 Wing and airfoil data | |
| 2.3.1 Planform | The wing is a combination of a cropped delta wing and a strake. |
| • Aspect ratio | 2.265 |
| • Taper ratio la/li | 0.2 |
| • Leading edge sweep | 45° |
| • Trailing edge sweep | -10° |
| • Semispan b | 2180 mm |
| • Reference chord c | 2222 mm |
| • Details of tip geometry | Tip planform and tip cross section rounded. |
| • Details of fuselage/wing junction | The junction between fuselage and wing is sharp. |
| 2.3.2 Basic wing section(s | |
| • Airfoil shape | Round leading edge |
| • Thickness/chord ratio | 0.1137 → 0.112 (root to tip) |
| • Nose radius/chord | Nose radius varies along the span |
| 2.3.3 Other components on wing | |
| • Control deflection | 0° |
| • Strake leading edge sweep | 80° |
| 2.4 Body data | |
| 2.4.1 Shape | |
| • Nose shape | Blunt nose |
| • Body length | 6000 mm |
| • Cross-sectional details | Vertical side walls with rounded upper and lower contour. |

| | |
|---|---|
| 2.4.2 Additional details | |
| 2.5 Information on vertical/horizontal tail surface | Vertical tail with leading edge sweep 45° and round leading edge, body flap |
| 2.6 Engine/pylon/nacelle data | N.A. |
| 2.7 Geometric definition of all components | |
| • Shape specification | Numerical |
| • Design or measured coordinates? | Design coordinates |
| • Tolerances | ± 1 mm |
| • Surface roughness | 5 µm |
| 2.8 Model support details | |
| 2.8.1 Sting and support geometry | 3 stings on lower surface, see Figure 3. |
| 2.8.2 Special features of mounting | No |

**3. GENERAL TUNNEL INFORMATION**

| | |
|---|---|
| 3.1 Tunnel designation | DNW, Refs. [1,4] |
| 3.2 Organization running the tunnel | DLR and NLR |
| 3.3 Tunnel characteristics | |
| • Type of tunnel | Subsonic, continuous operation |
| • Operating envelope | Max. speed = 116 m/s |
| 3.4 Test section | |
| 3.4.1 Model mounted in the test section | Figure 3 |
| 3.4.2 Test section dimensions | 8 x 6 x 20 $m^3$ |
| 3.4.3 Wall geometry details | |
| • Type of walls | Closed walls |
| • Open area ratio | 0.0 |
| • Wall pressures/wall displacement measurement | No |
| • Boundary layer control on walls | No |
| • Typical wall boundary layer displacement thickness | 20 mm |
| 3.5 Freestream conditions | |
| 3.5.1 Reference flow conditions | |
| • Total pressure<br>• Static pressure<br>• Static temperature | See Figure 4 |
| 3.5.2 Tunnel calibration | |
| • Tunnel calibration | See Figure 4 |
| • Date of last calibration | 14 March 1988 |
| 3.6 Flow quality (empty tunnel) | |
| 3.6.1 Flow uniformity | |
| • Static pressure variations over model length and span | $\lvert\Delta p\rvert < 0.002\ q$ |
| • Mach number variation during a run | $\lvert\Delta M\rvert < 0.004$ |
| • Determination of average flow angularity | 5 hole probe measurement |
| • Variation of flow angularity over the model length and span | $\lvert\Delta\alpha\rvert < 0.2°$ |
| 3.6.2 Temperature variation | |
| • Temperature controlled during a run | Yes |
| • Variation within the tunnel | $\lvert\Delta T\rvert < 0.2°$ |
| • Variation over a run | $\lvert\Delta T\rvert < 0.2°$ |

| | |
|---|---|
| 3.6.3 Flow unsteadiness | |
| • Overall turbulence level | Tu < 0.15% |
| • Overall noise level ($c_p$-RMS) | Lp = 100 dB (0.1-40 kHz) |

**4. INSTRUMENTATION**

| | |
|---|---|
| 4.1 Model position | |
| 4.1.1 Geometrical incidence measurement technique | Inclinometer inside model |
| 4.1.2 Accuracy of geometrical incidence | $\|\Delta\alpha\| < 0.02°$ |
| 4.2 Model pressure measurements | |
| 4.2.1 Total number and disposition of pressure holes | 110 pressure holes, see Figure 2 |
| 4.2.2 Range and accuracy of pressure transducers | Pressure transducers brand DRUCK, 20 kPa, $\|\Delta p\| < 6$ Pa |
| 4.2.3 Dynamic pressures | No |
| 4.3 Force and moment measurements | |
| 4.3.1 Type and location of balance | External balance below test section (Schenk). |
| 4.3.2 Maximum range and accuracy of all components | See Figure 5 |
| 4.4 Boundary layer and flow field measurements | No |
| 4.5 Surface flow visualization | |
| 4.5.1 Measurement technique applied | Oil, infrared pictures |
| 4.5.2 Surfaces with flow visualization | Upper surface of wing and body. |
| 4.5.3 Form of data | Copies of photographs |
| 4.6 Flow field visualization | No |
| 4.7 Tunnel wall measurements | No |
| 4.8 Other measurements and/or instrumentation used | No |

**5. TEST MATRIX AND CONDITIONS**

| | |
|---|---|
| 5.1 Detailed test matrix | |
| 5.1.1 Number of selected test cases | 6 |
| 5.1.2 Number of configurations tested | 1 |
| 5.1.3 Flow conditions | Defined in Table 1 |
| 5.2 Model/tunnel relations | |
| 5.2.1 Maximum blockage factor after Ref. [4] | 0.0175 |
| 5.2.2 Model span/tunnel width | 0.545 |
| 5.2.3 Wing area/tunnel cross section | 0.177 |
| 5.2.6 Adiabatic wall temperature | No, because model structure is made of reinforced epoxy. However, due to the low Mach number, temperature effects on the turbulent boundary layers are assumed to be negligable. |

5.3 Transition details

| | |
|---|---|
| 5.3.1 Free or fixed transition | Fixed transition |
| 5.3.2 Details of free transition | N.A. |
| 5.3.3 Details of fixed transition | |
| • Transition location | 500 mm behind nose of fuselage, 2% of local chord of wing |
| • Type and size of trip | Zick-zack tape of 0.25 mm height |
| • Verification of effectiveness of trip | Infrared pictures |
| • Flow conditions with effectiveness of trip verified | $M_\infty$ = 0.176, $Re_c$ = 9.0 x $10^6$, $\alpha$ = 5° |

## 6. DATA

6.1 Availability of data

| | |
|---|---|
| 6.1.1 Organization owning the data | DLR |
| 6.1.2 Responsible for the data | |
| • Name and title | Dr.-Ing R. Radespiel |
| • Address | DLR, Am Flughafen, D-3300 Braunschweig |
| • Telephone and fax numbers | Phone: ..49-531-3952488<br>FAX: ..49-531-3952320 |
| 6.1.3 Data freely available? | Yes |

6.2 Suitability of data for CFD validation

| | |
|---|---|
| 6.2.1 Data suitable for "in-tunnel" calculation | Yes, if corrections to data are removed according to Refs. [2, 4]. |
| 6.2.2 Data corrected to simulate "free-air" conditions | Yes |

6.3 Type and form in which data are available

| | |
|---|---|
| 6.3.1 Type and form | Table 2 and Figures 6-7 |
| 6.3.2 Data carrier | Printed, and on tape |
| 6.3.3 Extent of geometry data | Geometry defined as sets y=const and x=const (40.000 Records) |
| 6.3.4 Extent of aerodynamic test data | 4000 Records |

6.4 Corrections applied to data

| | |
|---|---|
| 6.4.1 Lift interference and blockage corrections | |
| • Data considered globally correctable | Yes |
| • Type of correction method applied | Classical |
| • Specify what data are actually corrected and indicate order of magnitude | Mach number, incidence, $c_p$, dynamic pressure, forces and moments, order of magnitude is given in Table 3. |
| 6.4.2 Side wall interference corrections (2-D tests) | N.A. |
| 6.4.3 Half model corrections | N.A. |
| 6.4.4 Sting and support corrections | Not applied, the order of magnitude of aerodynamic distortions induced by the 3 stings is estimated for $C_L$=1.0 and $C_D$=0.33 according to [5]: $\Delta q/q_\infty$=0.03, $\Delta\alpha$=0.35°, $\Delta C_L$=-0.0312, $\Delta C_D$=0.003. |
| 6.4.5 Aero-elastic deformation | No |
| 6.4.6 Other corrections | No |

## 7. DATA ACCURACY AND REPEATABILITY ASSESSMENT

7.1 Estimate accuracy of:

7.1.1 Free stream conditions

The accuracy of the free stream conditions may be estimated by adding the errors of flow uniformity, Chapter 3.6, the errors of the measurement system according to Ref. [6], the estimate of the sting interference according to Chapter 6.4.4, and 10% of the classical lift and blockage corrections according to Chapter 6.4.1.

- Mach number
- Dynamic pressure
- Model incidence

} Table 4

7.1.2 Measured data

The accuracy of the measured data is estimated by adding errors of flow uniformity (pressure), measurement system including dynamic pressure for nondimensionalization, estimate of sting interference according to Chapter 6.4.4, and 10% of the classical lift and blockage corrections according to Chapter 6.4.1.

- Forces and moments
- Pressure coefficients

} Table 5

7.2 Repeat measurements

7.2.1 Type and number of repeat measurements within one test campaign

Pressure and force measurements have been repeated for M = 0.172, $\alpha$ = 21.5°. Global force coefficients are reproduced by 0.005, and moments by 0.002. Pressure coefficients differ by 0.05 on the suction side and by 0.01 on the pressure side.

7.2.2 Type and number of repeat measurements in successive campaigns

No

7.3 Redundant measurements

7.3.1 Flow quantities that have been measured independently by different techniques

Separation lines on the surface are measured by oil and infrared pictures, see Figure 8.

7.3.2 Check made on internal consistency of the data

No

7.4 Other tests on same (nominal) geometry

7.4.1 Has the same (identical) model been measured in another wind tunnel?

No

7.4.2 Has a different model (same geometry and/or different scale) been measured in the same or another wind tunnel?

No

7.5 Additional remarks

Data can be compared to aerodynamic data of US-Orbiter.

## 8. REFERENCES

8.1 On the wind tunnel

[1] Eckert, D.: Der Deutsch-Niederländische Windkanal als Hilfsmittel der Flugzeugentwicklung. DGLR Jahrbuch, 1982.

8.2 On the model

[2] Radespiel, R.; Quast, A.: Kraftmessungen, Druckverteilungsmessungen und Strömungssichtbarmachung am Raumgleiter FALKE im Niedergeschwindigkeitsbereich. DLR-IB 129-89/37, 1989.

8.3 On the particular test and test results

Ref. [2] (see above), and [3] Fischenberg, D.: Auswertung von Windkanalmessungen an der FALKE-Space-Shuttle-Konfiguration. DLR-IB 111-89/32, 1989.

8.4 On the applied measurement techniques and correction methods

[4] Eckert, D.: Wall Correction Formulae for On-Line Processing of Measurements With Conventional Aircraft Models at DNW. Report DNW-PA-88.018, 1988.

[5] Eckert, D.: Korrekturen für Flugzeug-Vollmodell-Messungen mit der externen Waage. DNW-PA-83.011, 1983.

[6] Eckert, D.: Kontrolle der Meßstrecken-strömung im DNW. DNW-PA-78.002, 1978.

[7] Quast, A.: Detection of Transition by Infrared Image Technique. International Congress on Instrumentation in Aerospace Simulation Facilities, ICIASF, Williams-burg, June 22-25, 1987.

| IDENTIFICATION | | FLOW CONDITION | | | POSITION | | OTHER INFORMATION | |
|---|---|---|---|---|---|---|---|---|
| CASE NO. | CONF. | Mach | q kPa | $Re_c$ | α | β | type of measurements | remarks |
| 1 | A | 0.176 | 2.204 | $9.0x10^6$ | 5.28 | 0 | a,b,d | |
| 2 | A | 0.175 | 2.193 | $9.0x10^6$ | 10.65 | 0 | a,b,d | |
| 3 | A | 0.174 | 2.156 | $9.0x10^6$ | 16.12 | 0 | a,b,c,d | |
| 4 | A | 0.171 | 2.082 | $9.0x10^6$ | 21.10 | 0 | a,b,c,d | |
| 5 | A | 0.311 | 6.895 | $16.0x10^6$ | 10.60 | 0 | a,b,d | |
| 6 | A | 0.172 | 2.120 | $9.0x10^6$ | 21.54 | -5.01 | a,b | |
| 7 | A | 0.172 | 2.120 | $9.0x10^6$ | 21.54 | +5.01 | a,b,d | |

Legend:
1) type of measurements e.g.: (a) pressures; (b) overall forces; (c) oil flow, (d) infrared

Table 1 Test matrix

| DATA | ENGIN. UNITS | COEFFI-CIENTS | NORMALIZED | UN-CORRECTED | CORRECTED |
|---|---|---|---|---|---|
| FREESTREAM CONDITIONS | X | X | | X | X |
| SURFACE PRESSURES 1) | | X | | | X |
| HEATTRANSFER SKINFRICTION | | | | | |
| FORCES 1) | | X | | | X |

1) corrections can be undone by user

**Table 2 Data availability**

| $M_{\infty_u}$ | $M_\infty$ | $\alpha_u$ | $\alpha$ | $q_u$ | $q$ | $C_{p_u}$ | $C_p$ |
|---|---|---|---|---|---|---|---|
| 0.174 | 0.1775 | 0.01° | -0.10° | 2200P | 2286P | -0.4 | -0.344 |
| 0.167 | 0.1712 | 19.47° | 21.10° | 2200P | 2315P | -4.0 | -3.803 |

Index u denotes uncorrected values

Table 3 Order of magnitude of wind tunnel corrections

| | Flow uniformity | measurement system | sting interference | 10% of blockage and lift interference |
|---|---|---|---|---|
| Mach number | ±0.002 | ±0.0011 | 0.002 | 0.0004 |
| Dynamic Pressure | ±0.001 | ±0.001 | 0.03 | 0.005 |
| Model incidence | ±0.1° | ±0.02° | 0.35° | 0.057° |

Table 4 Estimate of free stream accuracy for $M_\infty = 0.176$, $C_L = 1.0$, $C_D = 0.33$

| | flow uniformity | measurement system | sting interference | 10% of blockage and lift interference |
|---|---|---|---|---|
| $C_L$ | | 0.0017 | 0.03 | 0.005 |
| $C_D$ | | 0.0005 | 0.003 | 0.00003 |
| $C_M$ | | 0.00013 | N.A. | 0.0005 |
| $C_p$ | ±0.001 | ±0.004 | 0.03 | depends strongly on actual value, see Table 3 |

Table 5 Estimate of measured data accuracy for $M_\infty = 0.176$, $C_L = 1.0$ $C_D = 0.33$, $C_M = 0.002$

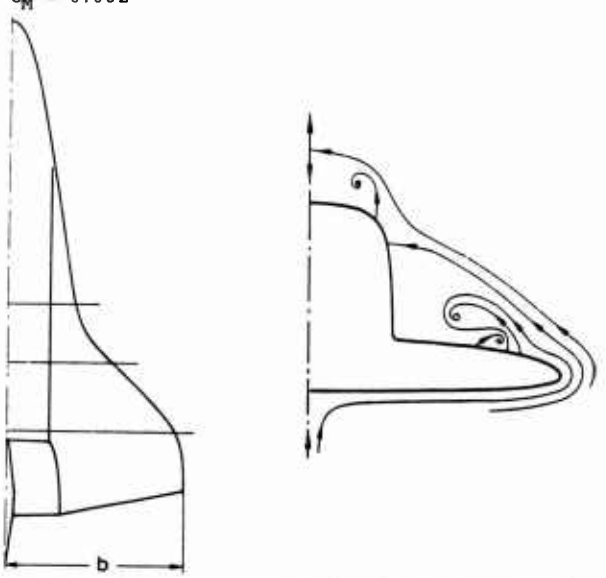



Fig. 1 Vortical flow on reentry configuration at landing conditions

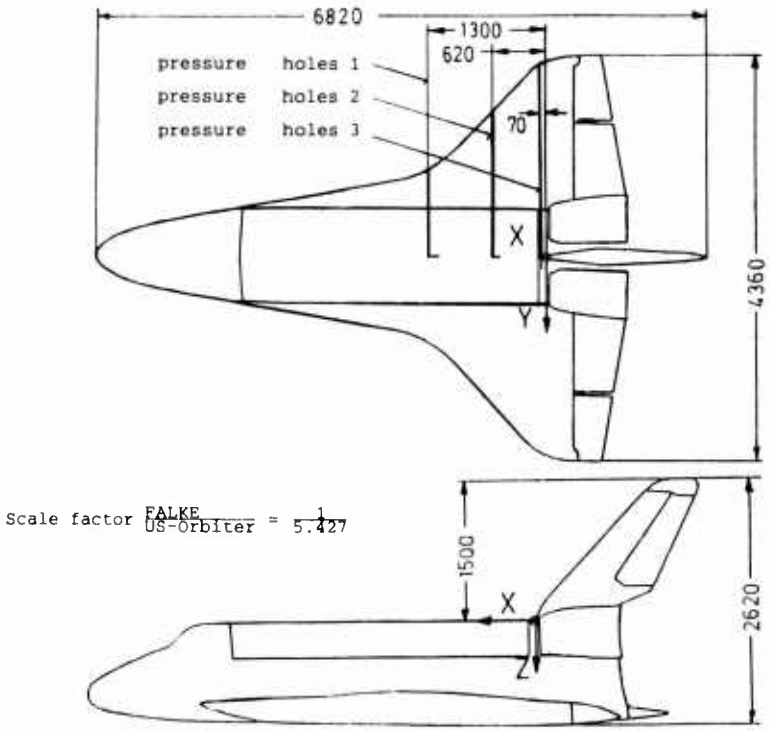



Fig. 2 Geometry of the FALKE model and position of pressure holes

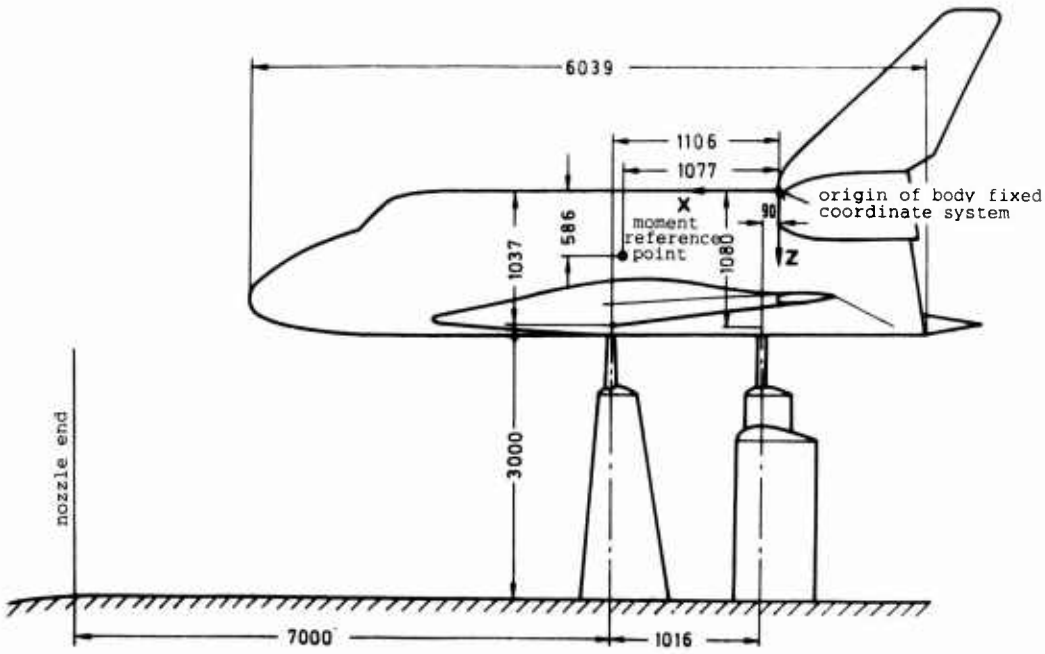
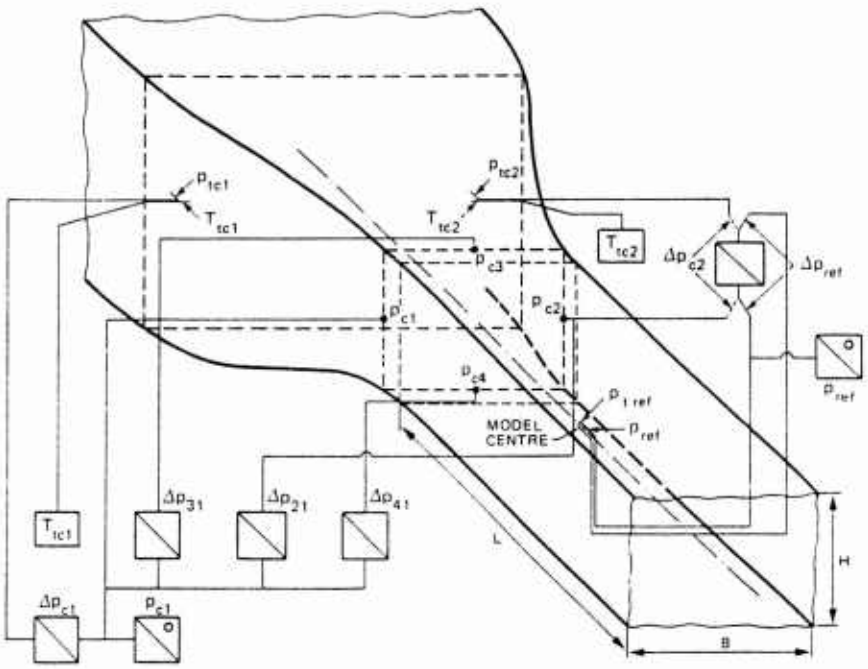



Fig. 3 FALKE mounted in DNW




$$p_c = p_{c1} + (\Delta p_{21} + \Delta p_{31} + \Delta p_{41})/4$$

$$\Delta p_c = (\Delta p_{c1} + \Delta p_{c2})/2 + (\Delta p_{21} - \Delta p_{31} - \Delta p_{41})/4$$

$$q_{ref} = p_c \sum_{i=1}^{3} G_i (\Delta p_c / p_c)^{i-1} \qquad \text{(kinetic pressure)}$$

$$p_{ref} = p_c \sum_{i=1}^{3} H_i (\Delta p_c / p_c)^{i-1} \qquad \text{(static pressure)}$$

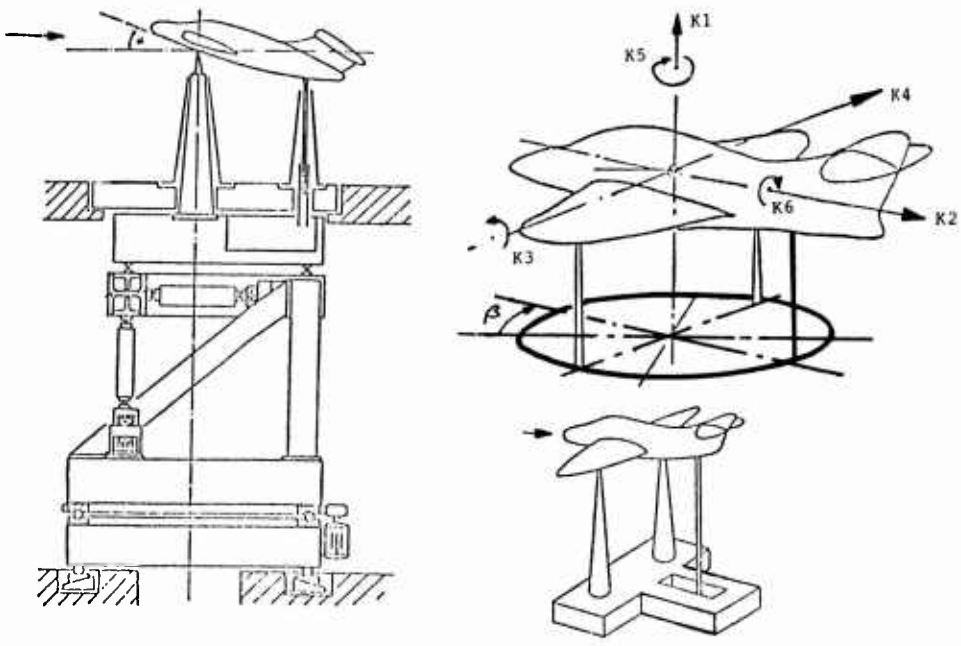
$$T_{t_{ref}} = (T_{tc1} + T_{tc2})/2 \qquad \text{(total pressure)}$$

$$Ma_{ref} = \sqrt{\frac{2}{\kappa} \frac{q_{ref}}{p_{ref}}}$$

$$T_{ref} = T_{t_{ref}} / \left(1 + \frac{\kappa - 1}{2} Ma_{ref}^2\right) \qquad \text{(static temperature)}$$

$$p_{tref} = (p_{tc1} + p_{tc2})/2$$

Fig. 4 Determination of tunnel reference conditions




| Test range and load factor $K_{i\,max}$ | $f_i$ | accuracy |
|---|---|---|
| $K_1$ ± 65.000 N | 1 | $\frac{\delta_i}{\lvert K_{i\,max}\rvert} \le \Delta \cdot f_i + \sum_{n+i}^{6} \Delta \lvert \frac{K_n}{K_{n\,max}} \rvert$ |
| $K_2$ ± 20.000 N | 1 | load ≤ 60% test range: $\Delta = 0.3 \cdot 10^{-3}$ |
| $K_3$ ± 40.000 Nm | 1.5 | repeatability: $\frac{1}{3}\ \delta_i$ |
| $K_4$ ± 20.000 N | 1 | resolution: $\frac{1}{5}\ \delta_i$ |
| $K_5$ ± 35.000 Nm | 1 | natural frequency $\nu_o \ge 2$ Hz |
| $K_6$ ± 20.000 Nm | 2 | measuring times: ≤ 5 s for $0.2 \cdot K_{n\,max}$ load change<br>≤ 3.5 s for $0.05 \cdot K_{n\,max}$ load change |

| setting angle | incidence (α) | yaw (β) |
|---|---|---|
| range | -20°... +45°(-5°... +60°) | 345° |
| rate | 0.1... 1,9°/s | 1°/s |
| accuracy setting | 0.05° | 0.1° |
| measuring | 0.02° | 0.02° |

Fig. 5 Set up of external balance and accuracy

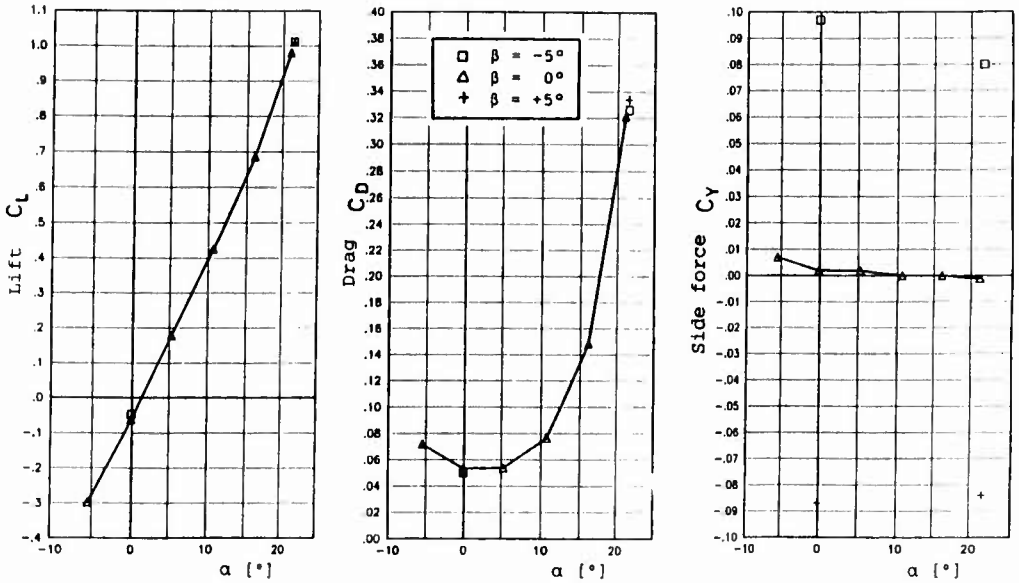



Fig. 6 Influence of angle of attack and yaw angle on total force coefficients, $M_\infty = 0.176$, $Re_c = 9.0 \times 10^6$

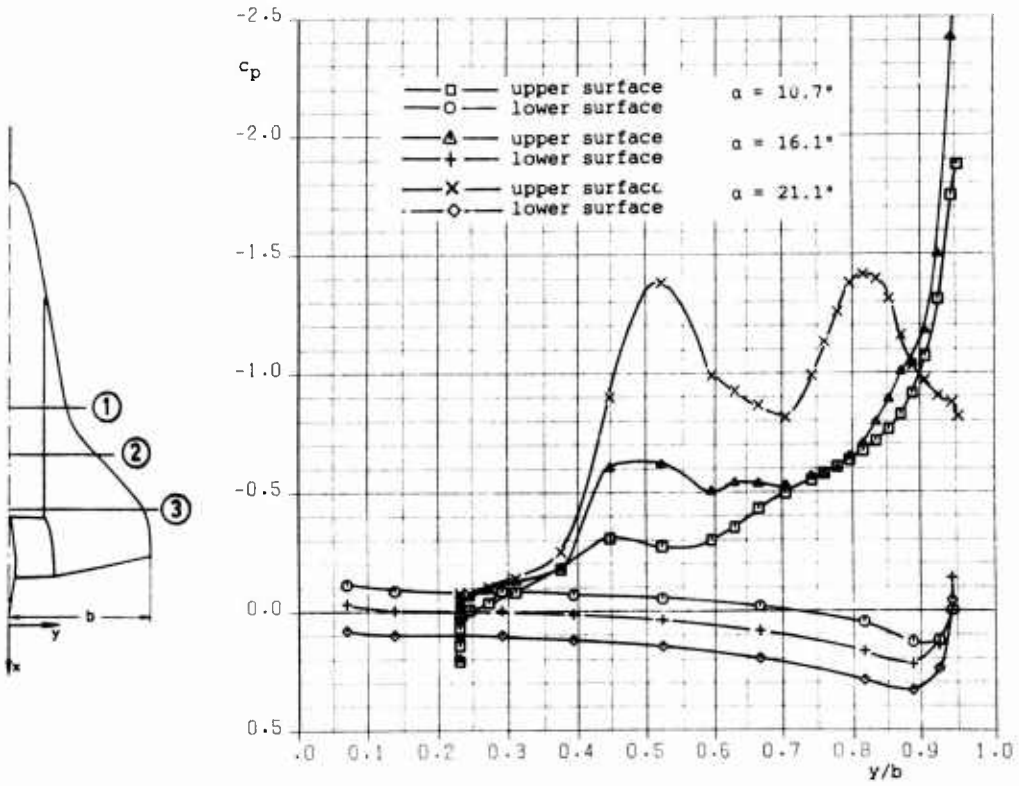
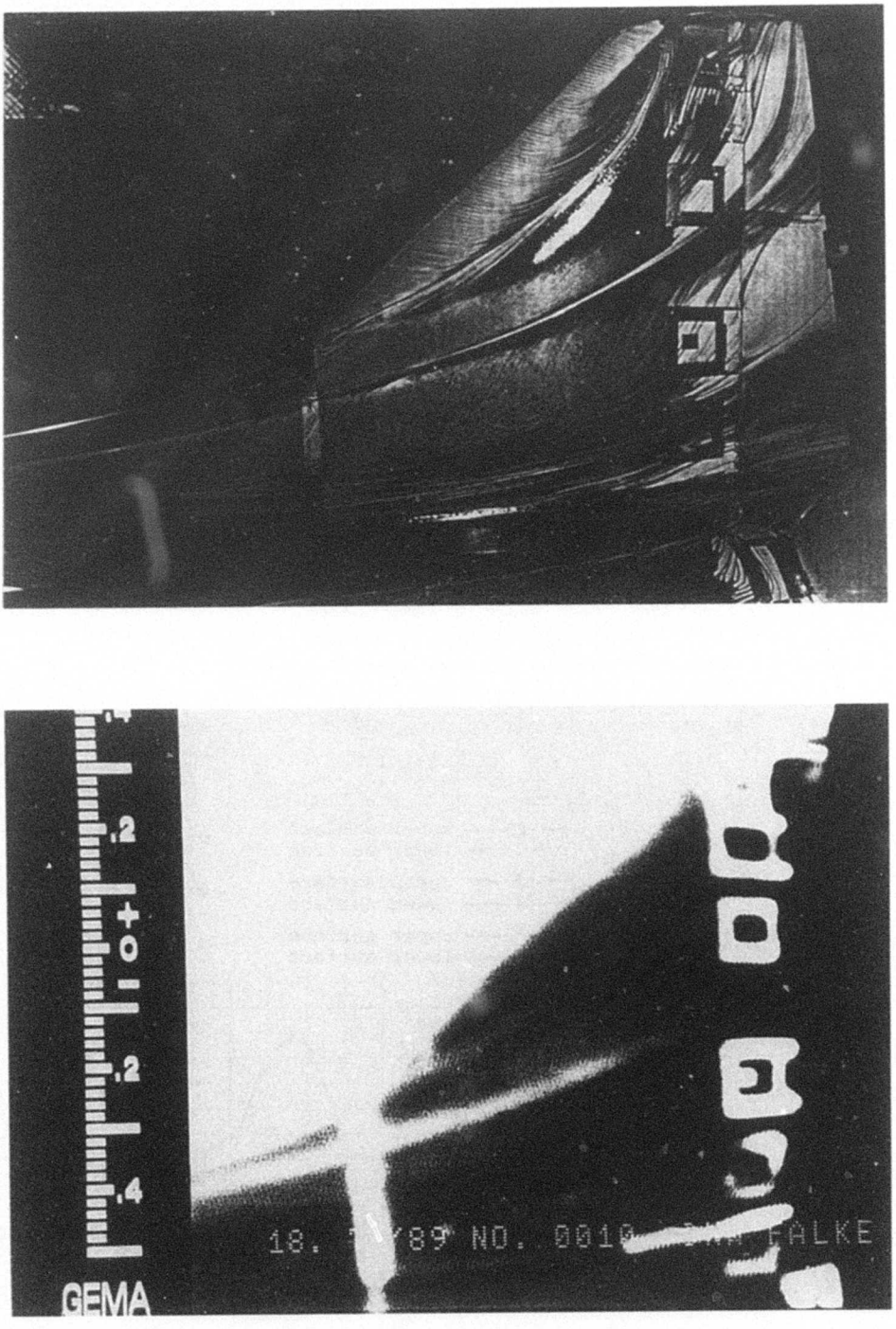
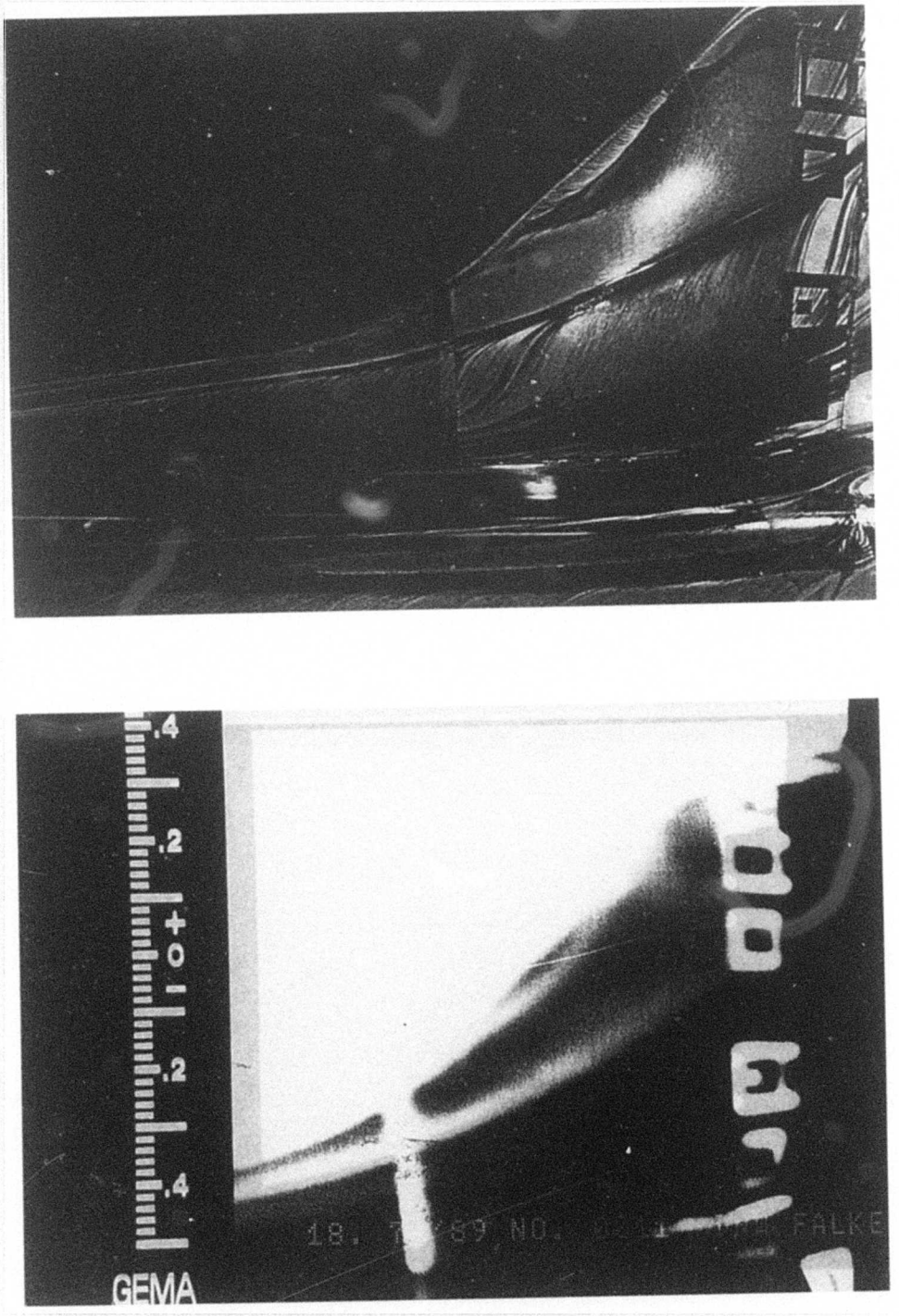



Fig. 7 Influence of angle of attack on pressure distribution of section 3, $M_\infty = 0.176$, $Re_c = 9.0 \times 10^6$




a) $M_\infty = 0.172$, $\alpha = 16.1°$, $\beta = 0°$, $Re = 9.0 \times 10^6$

Fig. 8 Comparison of oil flow and infrared picture




b) $M_\infty = 0.172$, $\alpha = 21.5°$, $\beta = 0°$, $Re = 9.0 \times 10^6$

Fig. 8 continued

# PRESSURE DISTRIBUTION MEASUREMENTS ON AN ISOLATED TPS 441 NACELLE

BY

R. KIOCK* AND W. BAUMERT**
DEUTSCHE FORSCHUNGSANSTALT FÜR LUFT- UND RAUMFAHRT E.V. (DLR)

* Institut für Entwurfsaerodynamik, Flughafen, D-38110 Braunschweig, Germany
** Hauptabteilung Windkanäle, Bunsenstraße 10, D-37073 Göttingen, Germany

## 0. INTRODUCTION

The demand for even more economic jet engines requires extensive experimental investigations of the complete flow field around wing-body-engine-pylon (WBEP) configurations. The engine can be simulated best by pressure-driven devices, so-called Turbine-Powered Simulators (TPS). Though they have been applied for about 20 years, very few nacelle surface pressure measurements were carried out up to now. The reason is seen in the small size of the engine and in the poor theoretical capabilities in the past. Nowadays, WBEP configurations are handled by the Euler code, but experimental validation is required. One prestep is the experimental investigation of the isolated nacelle which is presented here.

## 1. GENERAL DESCRIPTION

**1.1 Model Name:** TPS 441

**1.2 Model Type** Turbine-Powered Simulator of Tech Development Inc. with axisymmetric nacelle based on GE CF6-50C2

Flow condition: low speed

**1.3 Purpose of Test**

- Preliminary testing of wing-body-engine-pylon interference in view of later investigations with Ultra-High-Bypass Engines
- Simulation of fan flow upstream and downstream of the engine
- Validation of the computational methods

**1.4 Dominant Flow Physics**

Parameters at engine simulation

- Mach number $Ma_\infty = V_\infty/a$
- Reynolds number $Re_d = V_\infty d/\nu$
- Degree of turbulence $Tu_\infty = 100\sqrt{\overline{v'^2}}/V_\infty$
- Thrust coefficient $c_T = F_N/(A_W \cdot q_\infty)$
- Stream tube area ratio

$$\epsilon_{HL} = \frac{A_\infty}{A_{HL}} = \frac{\dot{m}_F}{p_\infty Ma_\infty A_{HL}}\sqrt{\frac{RT_\infty}{\kappa}}$$

$$\epsilon_F = A_\infty/A_F$$

- Fan pressure ratio $\pi_F = p_{t2}/p_{t1}$
- Bypass ratio $\mu = \dot{m}_F/\dot{m}_T$

Fig. 1 shows the variation of $c_T$ and $\epsilon_{HL}$ vs. $Ma_\infty$ for maximum number of revolutions.

## 2. DETAILS OF MODEL

**2.6 Engine/Pylon/Nacelle Data**

Details of the simulator are shown in Fig. 2. Pressurized air drives the three-stage turbine which is combined with the two-stage fan of 5" blade tip diameter. The fan area (centre of first fan rotor) amounts to $A_F$ = 9840.3 mm². More data are given in Table 1.

The geometry of intake, fan cowl, core cowl and plug are shown in Fig. 3. The highlight area amounts to $A_{HL}$ = 13710.0 mm², the maximum nacelle diameter is d = 170 mm.

The pylon is symmetric and ranges from x = 235 to 615 mm. It has a maximum width of $b_{max}$ = 29 mm, see Fig. 4.

**2.7 Geometric Definition of all Components**

- Shape is numerically specified. *)
- Coordinates are measured on ZEISS-measuring machine.

**2.8 Model Support Details**

The simulator was supported on a half model balance via a sting as shown in Figs. 5 to 7.

## 3. GENERAL TUNNEL INFORMATION

**3.1 Tunnel Designation**

Low-Speed Wind Tunnel Göttingen (NWG)

**3.2 Organization Running the Tunnel**

DLR

**3.3 Tunnel Characteristics**

- Type of tunnel: closed loop, open test section, running continuously, see also [1].
- Operating range: $V_{max}$ = 65 m/s, $T_{sc}$ = 290 to 310 K.

**3.4 Test Section**

**3.4.1 Test set-up**

was shown in Fig. 5 already. The tube for pressurized air is equipped with three compensators for a force-free connection.

**3.4.2 Test section dimensions**

3m x 3m x 6m

**3.5 Freestream Conditions**

**3.5.1 Reference flow conditions**

- Settling chamber pressure $p_{sc}$ taken by one side wall tapping.
- Ambient pressure $p_a$ measured by digital barometer Bell & Howell (range 105000 Pa, accuracy ± 10 Pa).
- Dynamic pressure from calibration, $q_\infty = 1.035\ (p_{sc} - p_a)$

  pressure difference measured by sensor MKS Baratron 310 (range 10000 Pa, accuracy ± 0.5 Pa via calibration).
- Settling chamber temperature $T_{sc}$ measured by thermocouple (accuracy ± 0.3°).

**3.5.2 Tunnel calibration**

- Rake of pitot probes in 1961, often checked.
- Ten-hole probe.

**3.6 Flow Quality in Model Range**

**3.6.1 Flow uniformity**

- Static pressure 1.5 % of dynamic pressure
- Dynamic pressure ± 0.5 %

*) Basis was a private communication from VEREINIGTE FLUGTECHNISCHE WERKE-FOKKER GmbH, Bremen, of June 11, 1980.

- Flow angularity ± 0.1°
- Flow velocity variation during a run ± 0.2 m/s

**3.6.2 Temperature variation**

- Maximum 10 K/h

**3.6.3 Flow unsteadiness**

- Overall turbulence level 0.8 %.

## 4. INSTRUMENTATION

**4.1 Model Position**

- Geometrical adjustment by spirit level ($\alpha$ = 0° only)

**4.2 Model Pressure Measurements**

**4.2.1 Description of pressure tappings**

see Figs. 3 and 4 as well as Table 2 .

- Intake and fan cowl: 3 rows, 78 tappings (totally)
- Core cowl : 5 rows, 31 tappings (totally)
- Plug : 3 rows, 9 tappings (totally)

Pressure tubes of core cowl, plug and Pitot rakes of fan and turbine were purged in order to prevent blockage by oil and ice.

**4.2.2 Pressure transducers**

Range: 0.07 bar, 0.5 bar, 1 bar
Accuracy: ± 0.06 % full scale

**4.2.3 Reference pressure of scanivalve**

was ambient pressure.

**4.3 Force and Moment Measurements**

See [2].

**4.8 Other Measurements**

Total pressure and temperature downstream of fan and turbine were measured by probes, see Figs. 3 and 4. These data and the results from the simulator calibration in the Calibration Tank Göttingen (ETG) enable the evaluation of mass flows of fan and turbine.

## 5. TEST MATRIX AND CONDITIONS

**5.1 Detailed Test Matrix**

Table 3 shows that 10 test cases were chosen for presentation.

All tests were carried out with zero angle of attack, N = 18000 to 45000 RPM and $V_\infty$ = 20 to 60 m/s.

Surface pressure measurements were taken as described in chapter 4.2.

**5.2 Model/Tunnel Relations**

The blockage of model including support amounts to 1.6 % (maximum width of strut 90 mm).

**5.3 Transition Details**

Tests were made with free transition. Transition was not measured.

## 6. DATA

**6.1 Availability of Data**

**6.1.1 Organization owning the data**

DLR

**6.1.2 Responsible for the data**

Dr.-Ing. R. Kiock
DLR, SM-EA
Flughafen
D-38110 Braunschweig
Tel.: 0531-295-2412
Fax : 0531-295-2320

6.1.3 **Data are freely available**

6.2 **Suitability of Data for CFD Validation**

Data correspond to "free-air" conditions because of low blockage

6.3 **Type and Form in which Data are Available**

6.3.1 **Surface pressures**

were transformed to Mach numbers because of the wide range of internal and external pressures. Isentropic flow is assumed, i.e. total pressure = const. The surface Mach numbers are defined in the following way:

- Intake, fan cowl
  $Ma = f(p/p_{t\infty})$
- Core cowl
  $Ma = f(p/p_{tF})$
- Plug
  $Ma = f(p/p_{tT})$

$p_{tF}$ and $p_{tT}$ are area averaged total pressures taken from pitot rake measurements downstream of fan and turbine.

One example is shown in Fig. 8. Results at x = 261 and 397 mm refer to probe measurements downstream of fan and turbine, respectively. Experimental results were published in [2] to [6].

Due to the large number of pressure tappings it was possible to evaluate the location of the stagnation point directly from the pressure measurements, see Fig. 9.

6.3.2 **Data carrier**

Floppy disc 3 1/2"

6.3.3 **Extent of geometrical data**

189 pairs of coordinates [5]

6.3.4 **Extent of aerodynamic test data**

17 general test data, 120 surface locations, 120 surface Mach numbers.

6.4 **Corrections Applied to Data**

Table 2 contains simulation parameters like thrust coefficient $c_T$ and stream tube area ratios $\epsilon_{HL}$ and $\epsilon_F$ which might be used for computations. Definitions were given in chapter 1.4. The parameters like net thrust

$F_N$, fan mass flow $\dot{m}_F$ and speed N were transformed to standard conditions as following:

$$F = F_m/\delta \; ; \; \dot{m} = \dot{m}_m\sqrt{\theta}/\delta \; , \; N = N_m/\sqrt{\theta}$$

with

$$\delta = \frac{p_{t\infty}\ [Pa]}{101\ 325} \; ; \quad \theta = \frac{T_{t\infty}\ [K]}{288.15}$$

7. DATA ACCURACY AND REPEATABILITY ASSESSMENT

7.1 **Estimated Accuracy**

7.1.1 **Freestream conditions**

- flow velocity: $\Delta V_\infty = \pm 0.25$ %
- model incidence: $\Delta\alpha = \pm 0.1$ %

7.1.2 **Measured data**

- surface Mach number: $\Delta Ma = 0.005$

## 8. REFERENCES

### 8.1 Wind Tunnel

[1] Baumert, W.: Der 3-m x 3-m Niedergeschwindigkeitswindkanal (NWG) der DFVLR in Göttingen (Stand 1988). DFVLR-Mitt. 89-05 (1989), 67 pages, 42 figs., 2 tables, 13 refs.

### 8.2 and 8.3 Model, Test and Test Results

[2] Baumert, W., Binder, B.; Stäger, W.: Engine Simulator Tests: Comparison of Calibration and Wind Tunnel Results. AGARD-CP 429 (1987), paper no. 25, 11 pages, 18 figs., 4 refs.

[3] Kiock, R.; Stäger, W.: Druckverteilungsmessungen an einem Modelltriebwerk bei inkompressibler Windkanalströmung. DFVLR-IB 129-87/39 (1987), 97 pages, 62 figs., 3 tables, 25 refs.

[4] Hoheisel, H.; Kiock, R.; Rossow, C.-C.; Ronzheimer, A.; Baumert, W.; Capdevila, H.: Theoretical and Experimental Investigations on Airframe/Engine Integration Problems. Proceed. 17th ICAS Congress, 9-14 September 1990, Stockholm (1990), Vol. 2, pp. 1277-1289, 21 figs., 23 refs.

[5] Rudnik, R.: Erweiterung eines dreidimensionalen Euler-Verfahrens zur Berechnung des Strömungsfeldes um Nebenstromtriebwerke mit Fan- und Kernstrahl. DLR-FB 91-13 (1991), 110 pages, 58 figs., 4 tables, 17 refs.

[6] Rudnik, R.: Erweiterung eines dreidimensionalen Euler-Verfahrens zur Berechnung des Strömungsfeldes um Nebenstromtriebwerke mit Fan- und Kernstrahl. ZFW, No. 15 (1991), pp. 285-288, 4 figs., 7 refs.

## 9. LIST OF SYMBOLS

| | |
|---|---|
| a | speed of sound |
| A | area |
| $c_T$ | thrust coefficient |
| d | maximum nacelle diameter, d = 0.17 m |
| $F_N$ | net thrust |
| H | altitude |
| $\dot{m}$ | mass flow |
| Ma | Mach number |
| N | number of revolutions |
| p | pressure |
| q | dynamic pressure |
| Re | Reynolds number |
| T | temperature |
| Tu | degree of turbulence |
| V | velocity |
| x | axial coordinate |
| $\alpha$ | angle of attack |
| $\epsilon$ | stream tube area ratio |
| $\kappa$ | ratio of specific heats |
| $\nu$ | kinematic viscosity |
| $\rho$ | density |
| $\varphi$ | angle in circumferential direction, pilot's view |

Subscripts

| | |
|---|---|
| $\infty$ | far upstream condition |
| a | ambient condition |
| F | fan |
| HL | highlight, tangent to nacelle intake |
| m | measured |
| nom | nominal |
| sc | settling chamber |
| t | total conditions |
| T | turbine |
| W | wing |

| | TPS 441, data from TDI | GE CF6-50C2 | | Relation of MBB (Jane's) to TDI data |
|---|---|---|---|---|
| | | DATA from Jane's | Performance data from MBB | |
| Fan | | | | |
| Blade tip diameter, mm | 127 | 2195 | | 17.28 |
| Speed, RPM | 45000 | | 3433 | |
| Total pressure ratio | 1.55 | | 1.70 | 1.10 |
| Mass flow (fan nozzle), kg/s | 2.11 | 533 | 537.6 | $\sqrt{254.8}$ = 16.0 |
| High pressure compressor | | | | |
| Speed, RPM | - | | 9827 | |
| Total pressure ratio | - | 29.11 | 29.10 | |
| Turbine | | | | |
| Inlet pressure, bar | 24.6 | | | |
| Inlet temperature, K | 288.7 | 1600 | | |
| Mass flow, kg/s | 0.95 | 125 | 125.7 | $\sqrt{132.3}$ = 11.5 |
| Overall values | | | | |
| Bypass ratio | 2.22 | 4.3 | 4.33 | 1.95 |
| Net thrust, MTO, kN | 0.753[5] | 206.8 | 223.6 | $\sqrt{295.4}$ = 17.2 |
| Fan net thrust, MTO, kN | 0.593[5] | | 167.6 | $\sqrt{283.1}$ = 16.8 |
| Net thrust, MC, kN | | 50.3[4] | 48.4[2] | |
| Net thrust, FI, kN | 0.060[6] | | 11.0[3] | $\sqrt{182.7}$ = 13.5 |

1) Calculation for take-off (MTO): altitude 0 m, $Ma_\infty$ = 0
2) Calculation for cruise (MC): altitude 10668 m, $Ma_\infty$ = 0.80
3) Calculation for landing (idle FI): altitude 0 m, $Ma_\infty$ = 0.20
4) Cruise (MC): altitude 10670 m, $Ma_\infty$ = 0.85
5) Extrapolation of measurements for $Ma_\infty$ = 0
6) Measurement at $Ma_\infty$ = 0.172, N = 18000 RPM

Table 1 Data of model and real engine

| Part | Section | 1 | 2 | 3 | x |
|---|---|---|---|---|---|
| | φ | 60° | 180° | 300° | mm |
| Intake | Internal | | | | 121.1 |
| | | | | | 111.6 |
| | | | | | 101.6 |
| | | | | | 91.6 |
| | | | | | 81.6 |
| | | | | | 72.1 |
| | | | | | 65.1 |
| | External | | | | 66.1 |
| | | | | | 73.1 |
| | | | | | 80.1 |
| | | | | | 89.1 |
| | | | | | 99.1 |
| | | | | | 109.1 |
| | | | | | 120.1 |
| Fan cowl | External | | | | 198.1 |
| | | | | | 208.1 |
| | | | | | 218.1 |
| | | | | | 228.1 |
| | | | | | 239.1 |
| | | | | | 251.1 |
| | | | | | 263.1 |
| | | | | | 275.1 |
| | | | | | 287.1 |
| | | | | | 299.1 |
| | | | | | 311.1 |
| | | | | | 323.1 |

| Part | Section | 4 | 5 | 6 | x |
|---|---|---|---|---|---|
| | φ | 90° | 180° | 270° | mm |
| Core cowl | External | | | | 345.3 |
| | | | | | 366.3 |
| | | | | | 387.3 |
| | | | | | 408.3 |
| | | | | | 429.3 |
| | | | | | 450.3 |
| | | | | | 471.3 |

| Part | Section | 7 | 8 | x |
|---|---|---|---|---|
| | φ | 30° | 330° | mm |
| Core cowl | External | | | 361.3 |
| | | | | 382.3 |
| | | | | 403.3 |
| | | | | 424.3 |
| | | | | 445.3 |

| Part | Section | 9 | 10 | 11 | x |
|---|---|---|---|---|---|
| | φ | 0° | 120° | 240° | mm |
| Plug | External | | | | 458.9 |
| | | | | | 486.4 |
| | | | | | 513.9 |

Table 2 Location of surface pressure tappings

| Test series | Test no. | α | $N_{nom}$ RPM | $q_\infty$ Pa | $V_\infty$ m/s | $Ma_\infty$ | $Re_d$ $10^{-5}$ | $\frac{N}{N_{max}}$ | $c_T$ | $\epsilon_{HL}$ | $\epsilon_F$ |
|---|---|---|---|---|---|---|---|---|---|---|---|
| 1003 | 2 | 0° | 18000 | 2089 | 59.9 | 0.173 | 6.4 | 0.393 | 0.045 | 0.872 | 1.216 |
| | 3 | | 27000 | 2049 | 59.9 | 0.171 | 6.1 | 0.582 | 0.125 | 1.282 | 1.786 |
| | 4 | | | 900 | 39.8 | 0.113 | 4.1 | 0.581 | 0.314 | 1.924 | 2.680 |
| | 5 | | | 235 | 20.3 | 0.058 | 2.1 | 0.582 | 1.320 | 3.703 | 5.158 |
| 1004 | 2 | | 36000 | 2078 | 60.2 | 0.172 | 6.2 | 0.778 | 0.257 | 1.685 | 2.347 |
| | 3 | | | 922 | 40.3 | 0.115 | 4.1 | 0.775 | 0.619 | 2.527 | 3.520 |
| | 4 | | | 231 | 20.1 | 0.057 | 2.1 | 0.776 | 2.655 | 5.067 | 7.058 |
| 1006 | 3 | | 45000 | 239 | 20.3 | 0.059 | 2.2 | 0.983 | 3.746 | 6.220 | 8.664 |
| | 5 | | | 2056 | 59.6 | 0.171 | 6.3 | 0.977 | 0.491 | 2.153 | 2.999 |
| 1011 | 2 | | | 934 | 40.3 | 0.115 | 4.2 | 0.973 | 1.132 | 3.205 | 4.465 |

Table 3 Test matrix

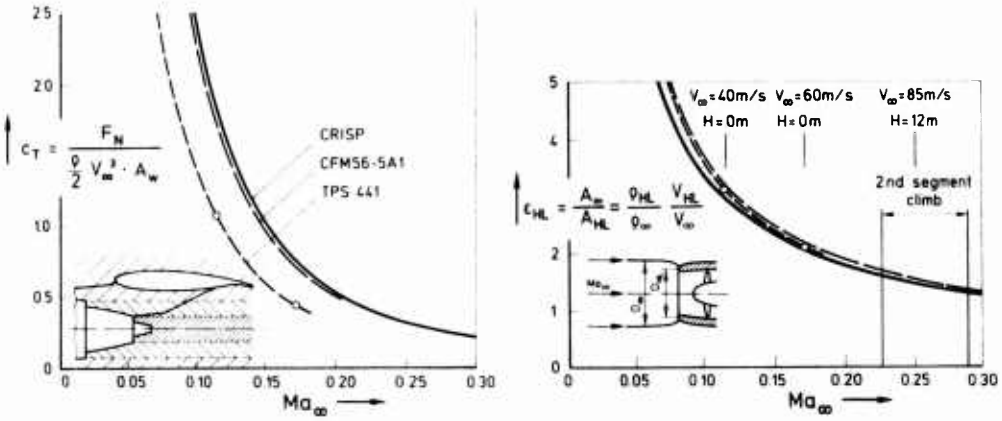



Fig. 1 Thrust coefficient and stream tube area ratio

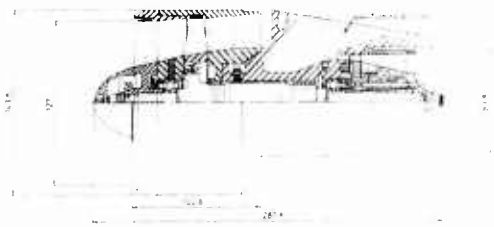


Fig. 2 Geometry of TPS 441

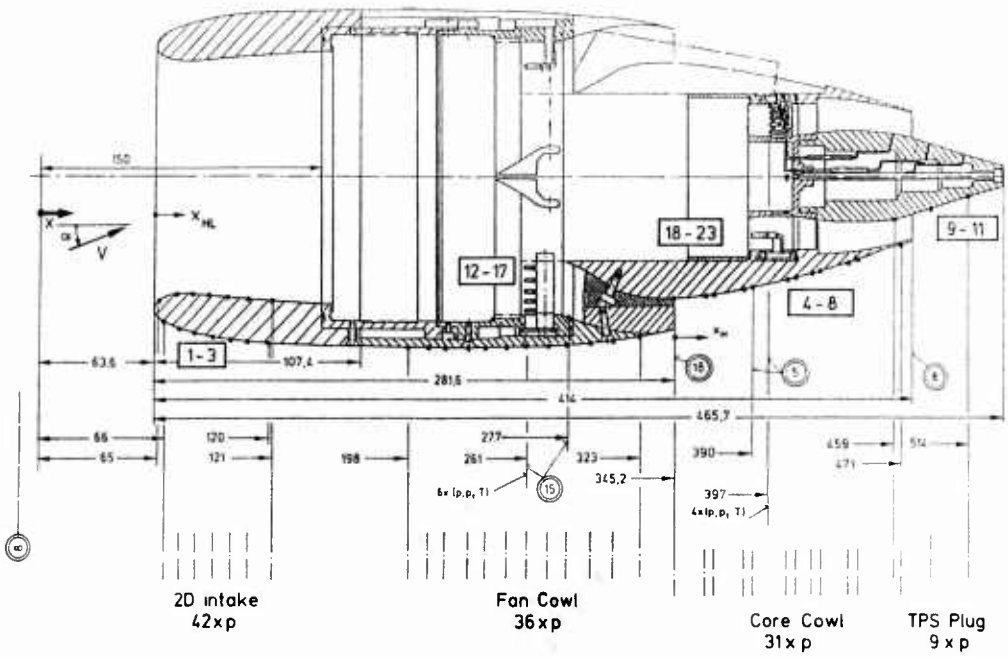



Fig. 3 TPS 441 with cowlings and axial position of measurement places

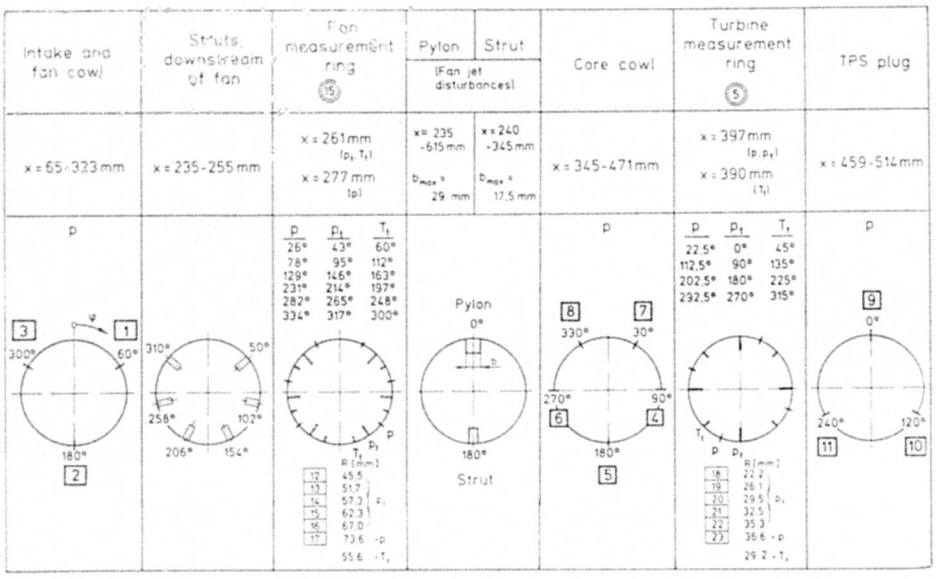



Fig. 4 Locations of measurement places, pilot's view

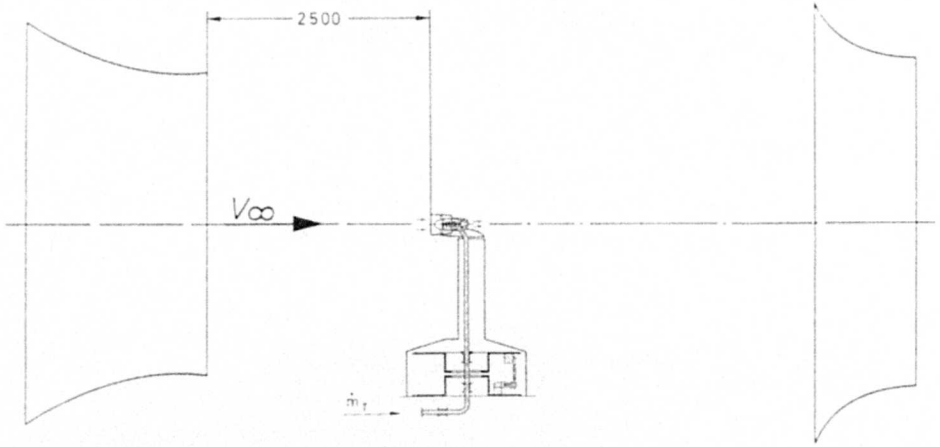



Fig. 5 TPS set-up in NWG test section



Fig. 6 Front view of TPS in test section

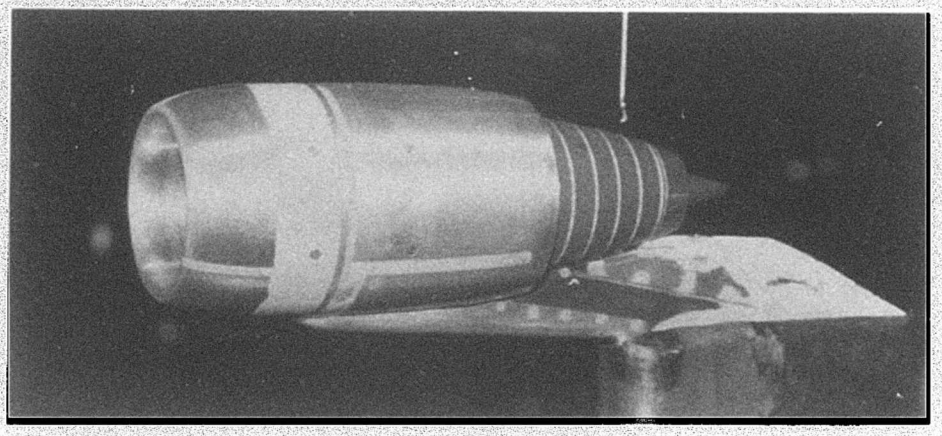


Fig. 7 Side view of TPS on strut

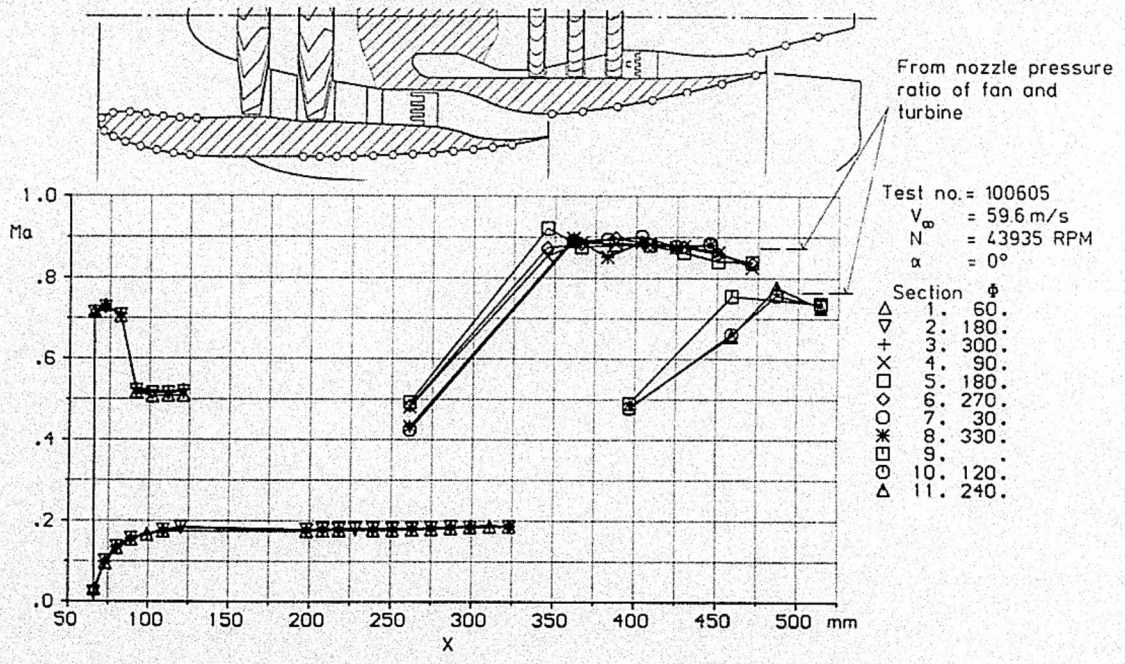



Fig. 8 Surface Mach number distribution

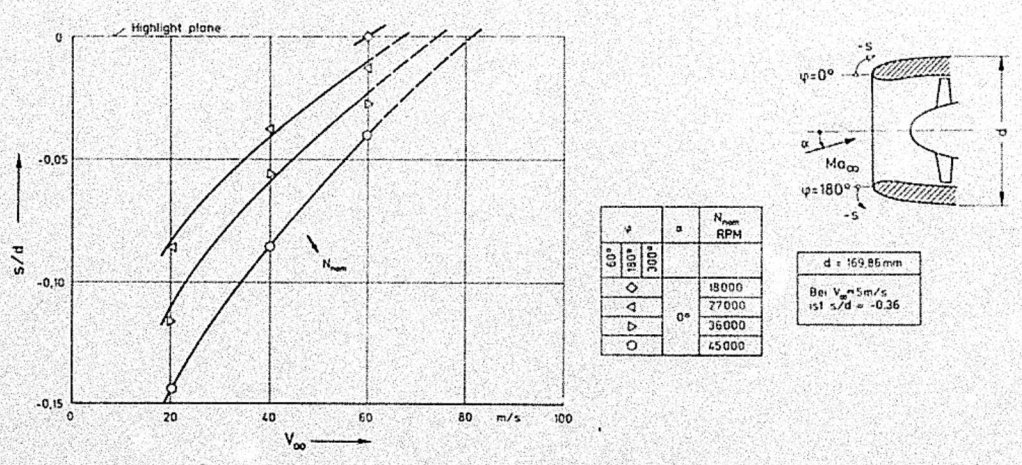



Fig. 9 Location of stagnation point vs. wind tunnel speed

# SINGLE-ENGINE TAIL INTERFERENCE MODEL

BY

BOBBY L. BERRIER
NASA LANGLEY RESEARCH CENTER
MS 280
HAMPTON, VIRGINIA 23665

## 0 INTRODUCTION

The data presented in this contribution were obtained in the NASA Langley 16-Foot Transonic Tunnel. Multiple test entries were completed and the results have been completely reported in five NASA reports. The objective of the initial investigation was to determine the effect of empennage (tail) interference on the drag characteristics of an axisymmetric model with a single engine fighter aft-end with convergent divergent nozzles. Two nozzle power settings, dry and maximum afterburning, were investigated. Several empennage arrangements and afterbody modifications were investigated during the initial investigation.

Subsequent investigations were used to determine the effects of other model variables including tail incidence, tail span, and nozzle shape. For the final investigation, extensive surface pressure instrumentation was added to the model in order to develop an understanding of the flow interactions associated with afterbody/empennage integration and also to provide data for code validation. Extensive computational analysis has been conducted on the staggered empennage configuration at a Mach number of 0.6 utilizing a three-dimensional Navier Stokes code.

Most of the investigations were conducted at Mach numbers from 0.60 to 1.20 and at ratios of jet total pressure to free stream static pressure (nozzle pressure ratio) from 1.0 (jet off) to 8.0. Some angle of attack variation was obtained at jet off conditions.

## 1 GENERAL DESCRIPTION

| | |
|---|---|
| 1.1 Model name or designation | NASA Single-Engine Tail Interference Model |
| 1.2 Model type and flow conditions | Axisymmetric forebody, afterbody and nozzle; with and without tail surfaces; with and without jet exhaust. Subsonic and transonic speed regime (limited data at M = 2.2) |
| 1.3 Design requirements, purpose of test | This model was designed to determine the effect of empennage interference on the drag of a typical (generic) single-engine fighter aft-end and to provide extensive surface pressures for code validation. |
| 1.4 Dominant flow physics | Flow separation on nozzle as illustrated by flow visualization photographs shown in Figure 1 and pressure distributions of Figure 2; afterbody/empennage interactions as illustrated in Figure 3; and exhaust/aft-end interactions as illustrated in Figure 4. |
| 1.5 Additional remarks | Many additional model variables were tested (tail incidence, tail span, nozzle geometry, afterbody contour, etc.) and these data are available in graphical format. However, the remainder of this description will be limited to the model with extensive surface pressure instrumentation. |

## 2 DETAILS OF MODEL

| | |
|---|---|
| 2.1 General geometric arrangement | A sketch of the general model arrangement is shown in Figure 5. Only the afterbody, nozzle and tails were metric (forces and moments measured by strain gage balance). The metric portion of the model extended from Station 40.89 inches to the nozzle exit. Internal nozzle forces were not metric. |

| | |
|---|---|
| 2.2 Configurations tested | The major model geometry varied was empennage arrangement. As illustrated in Figure 6, aft tails, forward tails, staggered tails and body alone configurations were tested. |
| 2.3 Wing/airfoil data | Not applicable. Model did not include wing. |
| 2.4 Body data | |
| 2.4.1 Shape | |
| - Nose shape | Axisymmetric ogive, 24 in. in length with 14 deg. initial angle followed by a constant area cylinder. |
| - Body length | 71.70 inches |
| - Cross-sectional details | Entire body is axisymmetric in cross-section with a maximum diameter of 7.34 inches. |
| 2.4.2 Additional details | |
| - Afterbody | The after body had closure representative of a typical single-engine fighter. |
| - Nozzle | Nozzle expansion ratio was 1.02; length was 6.81 inches; and exit (base) diameter was 2.748 inches. |
| 2.5 Tail surfaces | |
| 2.5.1 Vertical tail | |
| - Tip airfoil | NACA 64-003 |
| - Root airfoil | NACA 64-005 |
| - Height | 13.26 inches |
| - Tip chord | 4.20 inches |
| - Root chord | 16.40 inches |
| - Taper ratio | 0.256 |
| - Exposed aspect ratio | 1.288 |
| - Leading edge sweep | 42.62 deg. |
| 2.5.2 Horizontal tail | |
| - Tip airfoil | NACA 64-003 |
| - Root airfoil | NACA 64-005 |
| - Span (aft location) | 27.26 inches |
| - Tip chord | 2.20 inches |
| - Root chord | 12.70 inches |
| - Taper ratio | 0.173 |
| - Exposed aspect ratio | 2.724 |
| - Leading edge sweep | 45.97 deg. |
| 2.6 Engine/pylon/nacelle data | Not applicable |

2.7 Geometric definition

Shape is numerically specified with design coordinates. (See Section 6.3.3). Afterbody coordinates (x/t from 0.570 to 0.905) were measured from model hardware. Tolerances and surface roughness are unknown but are typical of transonic tunnel models.

2.8 Model support details

2.8.1 Support geometry

As shown in Figure 7, the model was supported in the wind tunnel by a sting-strut ("hockey stick") arrangement. Geometric information on this support system is given in Figure 8.

2.8.2 Special features of mounting

The 5% thick strut attached to the bottom side of the non-metric forebody and carried all instrumentation leads and high pressure air lines (for exhaust simulation) internally.

## 3 GENERAL TUNNEL INFORMATION

3.1 Tunnel designation

16-Foot Transonic Tunnel

3.2 Organization running the tunnel

NASA Langley Research Center
Applied Aerodynamics Division
Propulsion Aerodynamics Branch

3.3 Tunnel characteristics

- Type of tunnel

Continuous-flow, single-return, atmospheric wind tunnel with a slotted octagonal throat and test section and continuous air exchange. Boundary layer air removal (suction) is utilized at Mach numbers above 1.0. Up to 4.5% (depends on desired Mach number) of the tunnel mass flow is removed by this system.

- Operating envelope

Mach 0.2 to 1.3 at atmospheric pressure.

3.4 Test section

3.4.1 General arrangement

The photograph shown in Figure 7 also shows the general arrangement of the tunnel test section. The octagonal test section is surrounded by a 32 foot diameter plenum into which air expands to permit supersonic flow. Air is removed from this plenum by a compressor suction system at Mach numbers above 1.0. No protruding instrumentation exists near or upstream of the model except in the quiescent chamber upstream of the test section.

3.4.2 Test section dimensions

Regular octagon with an approximate distance between flats of 15.5 feet. Wall divergence angle is variable and is set to provide best flow quality at each Mach number. Thus, test section dimensions are slightly dependent on tunnel Mach number. Test section length, as determined from facility calibrations, is also dependent on tunnel Mach number and varies from 40 feet at M = 0.2 to 10 feet at M = 1.3.

3.4.3 Wall geometry details

- Type of walls

Eight solid, flat steel plates(maximum width of 6.66 ft.) separated by slots. Divergence angle of plates is variable.

- Open area ratio

Nominally 4% (depends on divergence angle and thus tunnel Mach number).

- Are wall pressures/wall displacements measured?

Wall pressures not measured for current model but are available when needed. Wall divergence angle is measured.

| | |
|---|---|
| - Boundary layer control on walls | No direct control on walls but some level of boundary layer control results from varying wall divergence angle and, at supersonic speeds, plenum suction through corner slots. |
| **3.5 Free stream conditions** | |
| 3.5.1 How are reference flow conditions determined for: | |
| - Total pressure | Ruska absolute pressure sensor located in quiescent chamber. |
| - Static pressure | Ruska absolute pressure sensor located in plenum tank and calibrated to the tunnel centerline. |
| - Total temperature | Three platinum resistance thermometers located in quiescent chamber. |
| - Dew point | Tunnel wall divergence angle is a function of dew point. Dew point is measured with a condensation mirror-type dew point indicator using continuously sampled air from the wind tunnel. |
| 3.5.2 Tunnel calibration | |
| - How was tunnel calibrated? | The tunnel was calibrated using a centerline probe which reached forward of the tunnel throat. Some flow survey (off centerline) and dynamic data were also obtained. |
| - Date of last calibration | Spring 1991 (not yet published) |
| **3.6 Flow quality (empty tunnel)** | |
| 3.6.1 Flow uniformity | |
| - Mach number/static pressure variations over model length and span | The usable test section length is defined by the extent of constant static pressure down the test section, which decreases with Mach number. For the Mach numbers of the current test, the average Mach number variation per foot (over 6 foot length) was 0.000267. |
| - Mach number variation during a run | Mach number is maintained within approx. +/- 0.003 during a run. Actual Mach number is recorded for each data point. |
| - How is average flow angularity determined? | Flow angularity is determined by running models through angle-of-attack sweeps at upright and inverted conditions. The intersection of the lift vs. angle-of-attack curves yields the upflow angle. Tunnel upflow angle for models without wings is assumed to be the average of this data from many tests. |
| - Variation of angularity over model length and span | Angularity determined by the above method is found at the model center of lift. A flow angularity survey of the test volume was made during the 1991 tunnel calibration. These results are currently being analyzed for future publication. |
| 3.6.2 Temperature variation | |
| - Temperature control during run | Tunnel temperature is not controlled. Jet exhaust temperature is typically controlled at about 70°F. |
| - Variation within the tunnel | With the present system for cooling the tunnel by continuous air exchange in which the cool air is introduced in an annulus adjacent to the wall of the return passage, a radial gradient of temperature in the test section airstream is almost inherent. After passing through the drive fans, the airstream in the return passage is of uniform |

| | |
|---|---|
| | temperature. On the downstream side of the air exchange, the step difference in temperature between the cool incoming air and the recirculated airstream is equal to the difference between stagnation and outside air temperatures. By the time that the airstream has traversed the third and fourth sets of turning vanes, an antiturbulence screen, the quiescent chamber, and the entrance cone, the region of radial gradient of temperature extends inwardly from the test section wall for about one-half of the test section radius. The temperature of the airstream core is very uniform and is identical with stagnation temperature indicated by probes located in the quiescent chamber. The difference between the test section core and wall temperatures is about 0.90 of the difference between stagnation and outside air temperatures. The gradient of temperature in the test section is not a desirable feature but, in general, has no adverse effect on most investigations. The temperature gradient has no effect on Mach number distribution but does result in a velocity gradient directly related to the temperature gradient. Most models are much smaller than the airstream hot core and are therefore not affected. |
| - Variation over a run | Depends on Mach number and length of run. Initial temperature is atmospheric and increases as the run progresses. The tunnel temperature limit is 180°F (normally occurs only at supersonic speeds during summer months) at which time, the tunnel power is reduced for tunnel cooling. |
| 3.6.3 Flow unsteadiness<br>- Overall turbulence level | During the tunnel calibration of 1950-1951 and on several occasions prior to the use of test section air removal and before an antiturbulence screen was installed in the quiescent chamber, attempts were made to measure airstream turbulence. Fluctuating flow angle was measured with a three degree cone meter, but interpretation of the data was uncertain. If isotropic turbulence can be assumed, these results indicated that the stream angle fluctuation expressed in radians ranged from about 0.003 to 0.008. Low turbulence in the tunnel is likely because of the addition of antiturbulence screens in the quiescent chamber and a contraction ratio of 13.31 into the test section. |
| - Overall noise level | For M of current test, $\Delta C_p$ = 0.46% - 1.13%. |

## 4 INSTRUMENTATION

| | |
|---|---|
| 4.1 Model position | |
| 4.1.1 How is geometrical incidence measured? | Inertial accelerometer |
| 4.1.2 Accuracy of geometrical incidence | +/- 0.02° |
| 4.2 Model pressure measurements | |
| 4.2.1 Total number and disposition | As shown in figure 9, 257 static pressure orifices were located in longitudinal rows on the model afterbody and nozzle. In addition, the vertical and horizontal tails contained 20 pressure orifices in 2 longitudinal rows near the root region of each tail. |
| 4.2.2 Range and accuracy of pressure transducers | Electronic scanning pressure transducers with 15psi range and 0.5% accuracy. |
| 4.2.3 Dynamic pressures | None measured. |

| | |
|---|---|
| 4.3 Force and moment measurements | |
| 4.3.1 Type/location of balance | Drag on the external shell of the metric aft end and pressure distributions on the aft end were measured during separate test entries. The model arrangement for the pressure test is shown in figure 5. For the drag test, the dummy balance shown in figure 5 was replaced with a six-component strain-gage balance and the body filler material in the metric break gap removed. Forces on the internal flow system (thrust) were not measured by the balance. |
| 4.3.2 Range/accuracy | Range of balance not known. In general, balance forces are considered to be accurate to 0.5%. |
| 4.4 Boundary layer/flow field measurements | None. |
| 4.5 Surface flow Visualization | |
| 4.5.1 Measurement technique applied | Ink flow |
| 4.5.2 On which surface is flow visualized | Afterbody and nozzle |
| 4.5.3 Data available in what form | Photographs (generally poor quality) |
| 4.6 Flow field visualization | None |
| 4.7 Tunnel wall measurements | None |
| 4.8 Other measurements or instrumentation | Exhaust total pressure (4 probes) and total temperature (1 probe). |

## 5 TEST MATRIX AND CONDITIONS

| | |
|---|---|
| 5.1 Detailed test matrix | |
| 5.1.1 Number of selected test cases | 32 |
| 5.1.2 Number of configurations tested | 4 |
| 5.1.3 Test matrix table | A complete test matrix is provided in TABLE I. |
| 5.2 Model/tunnel relations | |
| 5.2.1 Maximum blockage | 0.00147 (at alpha = 0°) |
| 5.2.2 Model span/tunnel width | N/A |
| 5.2.3 Wing area/tunnel area | N/A |
| 5.2.4 Height/chord ratio(2-D) | N/A |
| 5.2.5 Width/chord ratio(2-D) | N/A |
| 5.2.6 Have adiabatic wall temperatures been reached | Not known |
| 5.3 Transition details | |
| 5.3.1 Free or fixed transition | Fixed. |
| 5.3.2 Details of free transition | N/A |
| 5.3.3 Details of fixed transition | |
| - Transition location | 2.25 in. aft of nose tip. 0.63 in. aft of horizontal tail leading edge. 0.82 in. aft of vertical tail leading edge. |
| - Type and size of trip | 0.15-in.-wide strips of No. 100 corborundum grit, sparsely distributed. |

| | |
|---|---|
| - How was effectiveness of trip verified | Procedure in NASA TN D-3579 followed. |

## 6 DATA

### 6.1 Availability of data

| | |
|---|---|
| 6.1.1 Organization owning data | NASA-Langley Research Center |
| 6.1.2 Who is responsible for the data | Bobby L. Berrier<br>NASA-Langley Research Center<br>MS 280<br>Hampton, Virginia 23665<br>(804) 864-3001/FAX (804) 864-8195 |
| 6.1.3 Are data freely available | Yes. |
| 6.1.4 If not, who should be contacted | N/A |

### 6.2 Suitability of data for CFD validation

| | |
|---|---|
| 6.2.1 Are data suitable for "in-tunnel" calculation | No |
| 6.2.2 Are data corrected to simulate "free-air" conditions | Yes |

### 6.3 Type and form in which data are available

| | |
|---|---|
| 6.3.1 Type and form | Free-stream conditions - Engineering units<br>Surface pressures - Coefficients<br>Drag - Coefficients |
| 6.3.2 Data carrier | Surface pressures - Printed (NASA TP-2753)<br>Drag - Graphical (NASA TN D-8326)<br>Data for selected cases (Case 5: nominal NPR = 2.0 and 5.0; Case 29: nominal NPR = 2.0, 3.0, and 5.0) are available on a 3.5 inch floppy disk. |
| 6.3.3 Extent of geometric data | Model sketches and coordinates provided in references. Electronic transfer of model geometry and grid definition for cases 1-8 and cases 25-32 can be arranged by contacting Bobby L. Berrier (See Section 6.1.2). |
| 6.3.4 Extent of aero. data | N/A |

### 6.4 Corrections applied to data

| | |
|---|---|
| 6.4.1 Lift interference and blockage corrections | No corrections were made for blockage. Blockage effects for the Mach numbers and model blockage tested have been shown to be negligible. |
| 6.4.2 Sidewall interference corrections | None |
| 6.4.3 Half model corrections | N/A |
| 6.4.4 Sting and support corrections | No data correction has been made for the sting/strut support. Past research on the present support system indicated that the major effect was a total pressure defect in the wake downstream of the strut. Effects of the support on static pressure and force measurements were negligible. Similar results were found on the current model as reported in NASA TN D-8326. Because the model was partially metric, the metric break and cavity areas were corrected to free stream static pressure. |

| | |
|---|---|
| 6.4.5 Aeroelastic deformation | N/A |
| 6.4.6 Other corrections | None other than standard wind tunnel corrections for metric break, internal cavity and base pressures if different from free stream. |

## 7 DATA ACCURACY AND REPEATABILITY

| | |
|---|---|
| 7.1 Estimate accuracy of: | |
| 7.1.1 Free stream conditions | |
| - Mach number | +/- 0.002 |
| - Model incidence | +/- 0.02° |
| 7.1.2 Measured data | |
| - Forces and moments | 0.5% |
| - Pressures | The following values are for pressure coefficients:<br>+/- 0.0170 at M = 0.60<br>+/- 0.0100 at M = 0.90<br>+/- 0.0096 at M = 0.95<br>+/- 0.0082 at M = 1.20 |
| 7.2 Repeat measurements | |
| 7.2.1 During same test | Pressure data repeatability was not investigated during pressure test. Some limited repeat data were obtained during force test (usually jet off and one value of NPR). Figure 10 shows the most extensive set of repeat drag data obtained. |
| 7.2.2 During different tests | Some limited repeat pressure data were obtained during pressure and force tests. These pressures were located primarily on the nozzle. |
| 7.3 Redundant measurements | |
| 7.3.1 Flow quantities | None |
| 7.3.2 Checks | None |
| 7.4 Other tests on same (nominal) geometry | |
| 7.4.1 Same model in other facilities | The same (identical) model was tested in the Langley 4-Foot Supersonic Pressure Tunnel but at different flow conditions (M = 2.20). That is, a tunnel to tunnel comparison is not possible. |
| 7.4.2 Different model with same geometry | During the force test, two nozzles having the same geometry were tested. One nozzle had 20 static pressure measurements and the other nozzle had 56 static pressure measurements. Figure 10 compares the integrated (pressure X area) nozzle drag coefficients obtained from these nozzles. |
| 7.5 Additional remarks | None |

## 8 REFERENCES


| | |
|---|---|
| 8.1 On the wind tunnel | Corson, Blake W.; Runckel, Jack F.; and Igoe, William B.: Calibration of the Langley 16-Foot Transonic Tunnel with Test Section Air Removal. NASA TR R-423, August 1974. |

Staff of the Propulsion Aerodynamics Branch: A User's Guide to the Langley 16-Foot Transonic Tunnel Complex. Revision 1. NASA Technical Memorandum 102750, Sept. 1990.

8.2 On the model (other results including CFD)

Burley, James R., II; and Berrier, Bobby L.: Investigation of Installation Effects on Single-Engine Convergent-Divergent Nozzles. NASA TP-2078, 1982.

Burley, James R., II; and Berrier, Bobby L.: Effects of Tail Span and Empennage Arrangement on Drag of a Typical Single-Engine Fighter Aft End. NASA TP-2352, 1984.

Burley, James R., II; Carlson, John R.; and Henderson, William P.: Experimental and Numerical Results for a Generic Axisymmetric Single-Engine Afterbody With Horizontal and Vertical Tails at Transonic Speeds. NASA TM-87755, 1986.

Berrier, Bobby L.: Effect of Empennage Interference on Single-Engine Afterbody/Nozzle Drag. AIAA Paper No. 75-1296, 1975.

Jones, William T.; and Abdol-Hamid, Khaled S.: Computational Analysis of Drag Reduction Techniques for Afterbody/Nozzle/Empennage Configurations. SAE Paper No. 912127, 1991.

8.3 On the particular test and test results

Berrier, Bobby L.: Effect of Nonlifting Empennage Surfaces on Single-Engine Afterbody/Nozzle Drag at Mach Numbers From 0.5 to 2.2. NASA TN D-8326, 1977.

Henderson, William P.; and Burley, James R., II: Effect of Empennage Arrangement on Single-Engine Nozzle/Afterbody Static Pressures at Transonic Speeds. NASA TP-2753, 1987.

8.4 On the applied measurement techniques and correction methods

Mercer, Charles E.; Berrier, Bobby L.; Capone, Francis J.; Grayston, Alan M.; and Sherman, C. D.: Computations for the 16-Foot Transonic Tunnel. NASA, Langley Research Center. Revision 1. NASA Technical Memorandum 86319, 1987.

## 9 LIST OF SYMBOLS

| | |
|---|---|
| b | Tail span (root to tip), in. |
| c | Tail chord, in. |
| $C_D$ | Drag coefficient |
| $C_{D,t}$ | Total (afterbody, nozzle and tails) drag coefficient |
| $C_{D,pn}$ | Nozzle pressure drag coefficient |
| $C_p$ | Pressure coefficient |
| $C_p^*$ | Pressure coefficient for sonic flow (critical) |
| $\Delta C_p$ | Noise (fluctuating pressure), rms, % |
| H.P. | High pressure |

| | |
|---|---|
| $l$ | Model length, in. |
| M | Mach number |
| NPR, $P_{t,j}/p_\infty$ | Nozzle pressure ratio (jet total to freestream static) |
| $P_{t,j}$ | Jet exhaust total pressure, psi |
| $p_\infty$ | Freestream static pressure, psi |
| q | dynamic pressure, psi |
| R | Radius, in. |
| Rey | Reynolds number based on model length of 71.70 inches |
| TS | Tunnel station |
| x | Axial distance downstream from nose tip, in. |
| y | Spanwise distance from tail root, in. |
| $\alpha$, alpha | Angle of attack, deg. |
| $\phi$, phi | Meridian angle about model axis, deg. |

## TABLE I - TEST MATRIX

| IDENTIFICATION | | FLOW CONDITION | | | | POSITION | OTHER INFORMATION |
|---|---|---|---|---|---|---|---|
| CASE | CONF. | Nom. Mach | Nom. q, psi | Nom. Rey x $10^7$ | Nom. NPR | Nom. α, deg. | |
| 1 | Body only | 1.20 | 6.06 | 2.40 | a | 0 | |
| 2 | | 1.20 | 6.06 | 2.40 | 1.0 | A | |
| 3 | | 0.95 | 5.19 | 2.30 | b | 0 | Ink flow at NPR = 1.0 |
| 4 | | 0.95 | 5.19 | 2.30 | 1.0 | A | |
| 5 | | 0.90 | 4.93 | 2.24 | b | 0 | Ink flow at NPR = 1.0 |
| 6 | | 0.90 | 4.93 | 2.24 | 1.0 | B | |
| 7 | | 0.60 | 2.90 | 1.80 | b | 0 | |
| 8 | | 0.60 | 2.90 | 1.80 | 1.0 | C | |
| 9 | Aft tails | 1.20 | 6.06 | 2.40 | a | 0 | |
| 10 | | 1.20 | 6.06 | 2.40 | 1.0 | A | |
| 11 | | 0.95 | 5.19 | 2.30 | b | 0 | Ink flow at NPR = 1.0, 2.0 and 6.0 |
| 12 | | 0.95 | 5.19 | 2.30 | 1.0 | A | |
| 13 | | 0.90 | 4.93 | 2.24 | b | 0 | Ink flow at NPR = 1.0 |
| 14 | | 0.90 | 4.93 | 2.24 | 1.0 | B | |
| 15 | | 0.60 | 2.90 | 1.80 | b | 0 | |
| 16 | | 0.60 | 2.90 | 1.80 | 1.0 | C | |
| 17 | Forward tails | 1.20 | 6.06 | 2.40 | c | 0 | |
| 18 | | 1.20 | 6.06 | 2.40 | 1.0 | A | |
| 19 | | 0.95 | 5.19 | 2.30 | b | 0 | Ink flow at NPR = 1.0 |
| 20 | | 0.95 | 5.19 | 2.30 | 1.0 | A | |
| 21 | | 0.90 | 4.93 | 2.24 | b | 0 | Ink flow at NPR = 1.0 |
| 22 | | 0.90 | 4.93 | 2.24 | 1.0 | B | |
| 23 | | 0.60 | 2.90 | 1.80 | b | 0 | |
| 24 | | 0.60 | 2.90 | 1.80 | 1.0 | C | |
| 25 | Staggered tails | 1.20 | 6.06 | 2.40 | a | 0 | |
| 26 | | 1.20 | 6.06 | 2.40 | 1.0 | A | |
| 27 | | 0.95 | 5.19 | 2.30 | b | 0 | Ink flow at NPR = 1.0 |
| 28 | | 0.95 | 5.19 | 2.30 | 1.0 | A | |
| 29 | | 0.90 | 4.93 | 2.24 | b | 0 | Ink flow at NPR = 1.0 |
| 30 | | 0.90 | 4.93 | 2.24 | 1.0 | B | |
| 31 | | 0.60 | 2.90 | 1.80 | b | 0 | |
| 32 | | 0.60 | 2.90 | 1.80 | 1.0 | C | |

NOTE: Pressures and overall forces available for all cases

a. Nominal NPR = 1.0, 2.0, 4.0, 6.0, 8.0
b. Nominal NPR = 1.0, 2.0, 3.0, 5.0
c. Nominal NPR = 1.0, 2.0, 4.0, 6.0

A. Nominal alpha = -3°, 0°, 3°, 6°
B. Nominal alpha = -3°, 0°, 6°
C. Nominal alpha = -3°, 0°, 3°, 6°, 9°

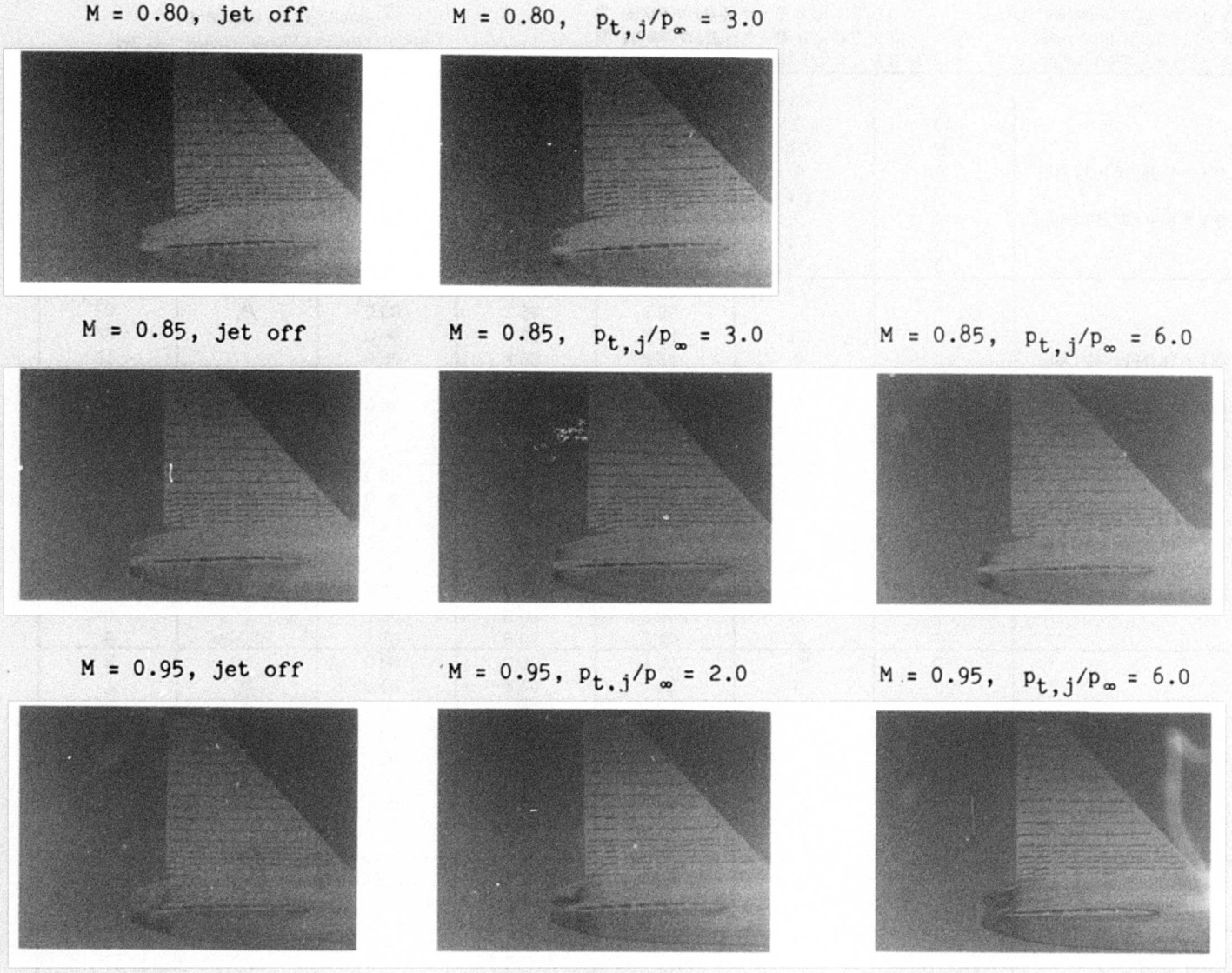



Figure 1.- Ink flow photographs showing effect of jet exhaust flow and Mach number on nozzle separation. Aft tails configuration.

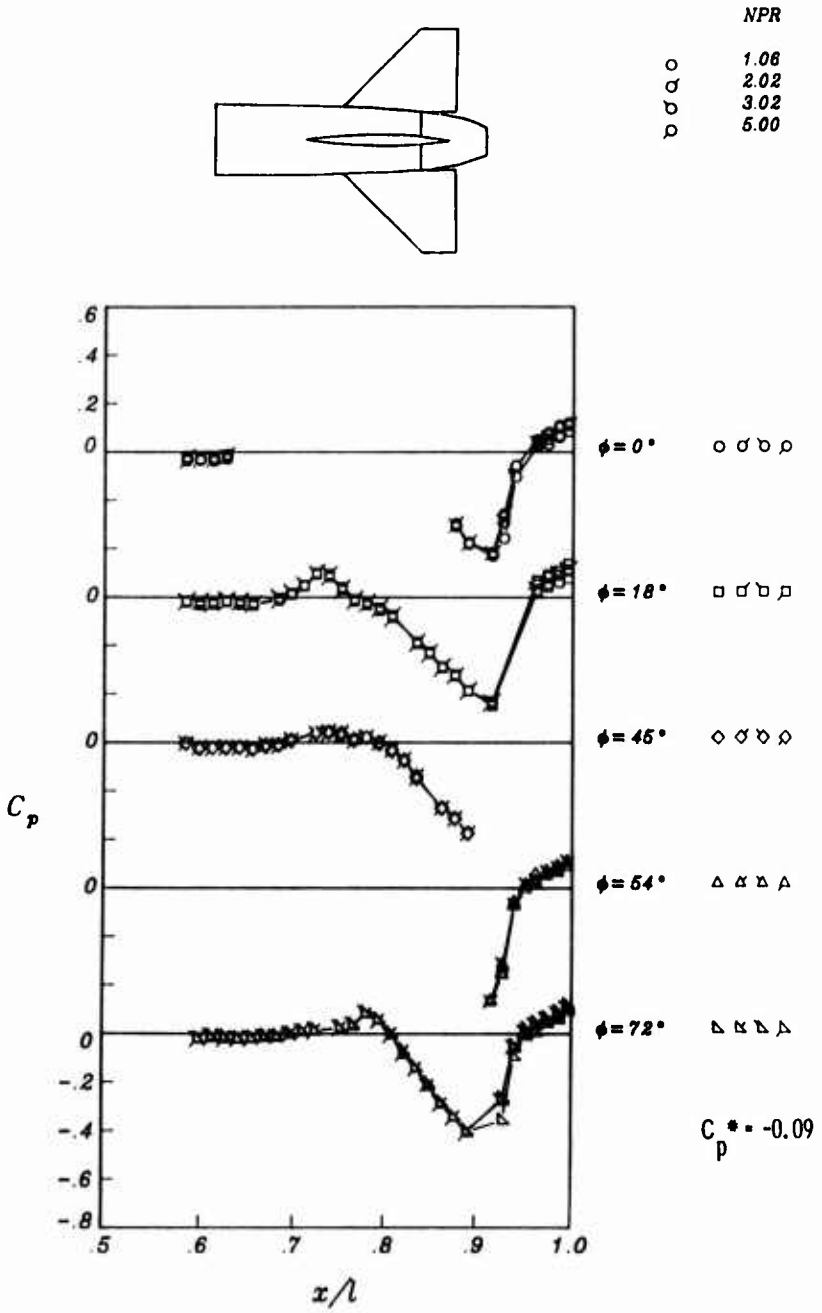



Figure 2.- Pressure distributions on the afterbody/nozzle of the aft tails configuration at Mach = 0.95 and alpha = 0.02 deg.

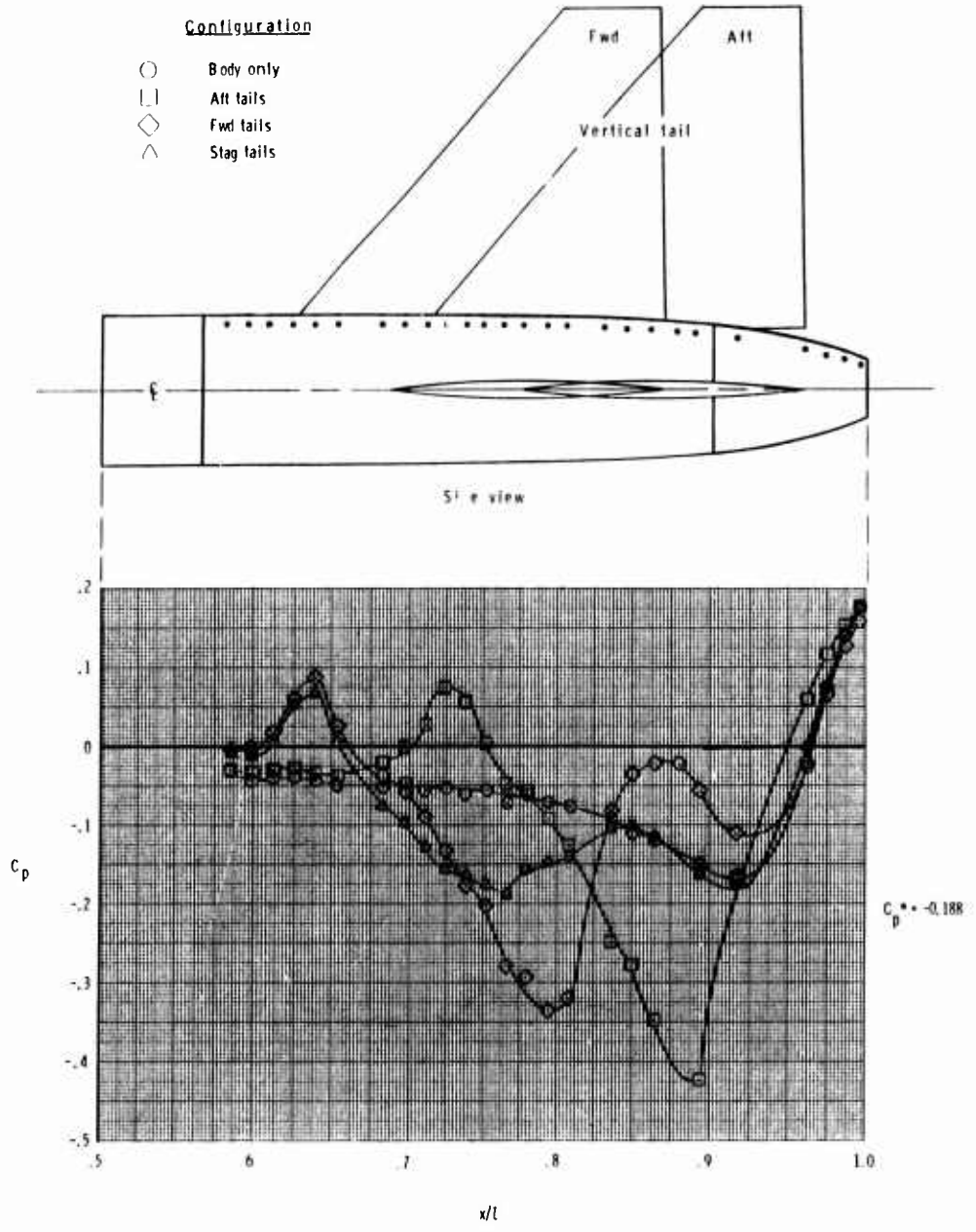



Figure 3.- Effect of empennage arrangement on nozzle/afterbody pressure coefficients at M = 0.90, NPR = 1.0 and alpha = 0 deg. for phi = 18 deg.

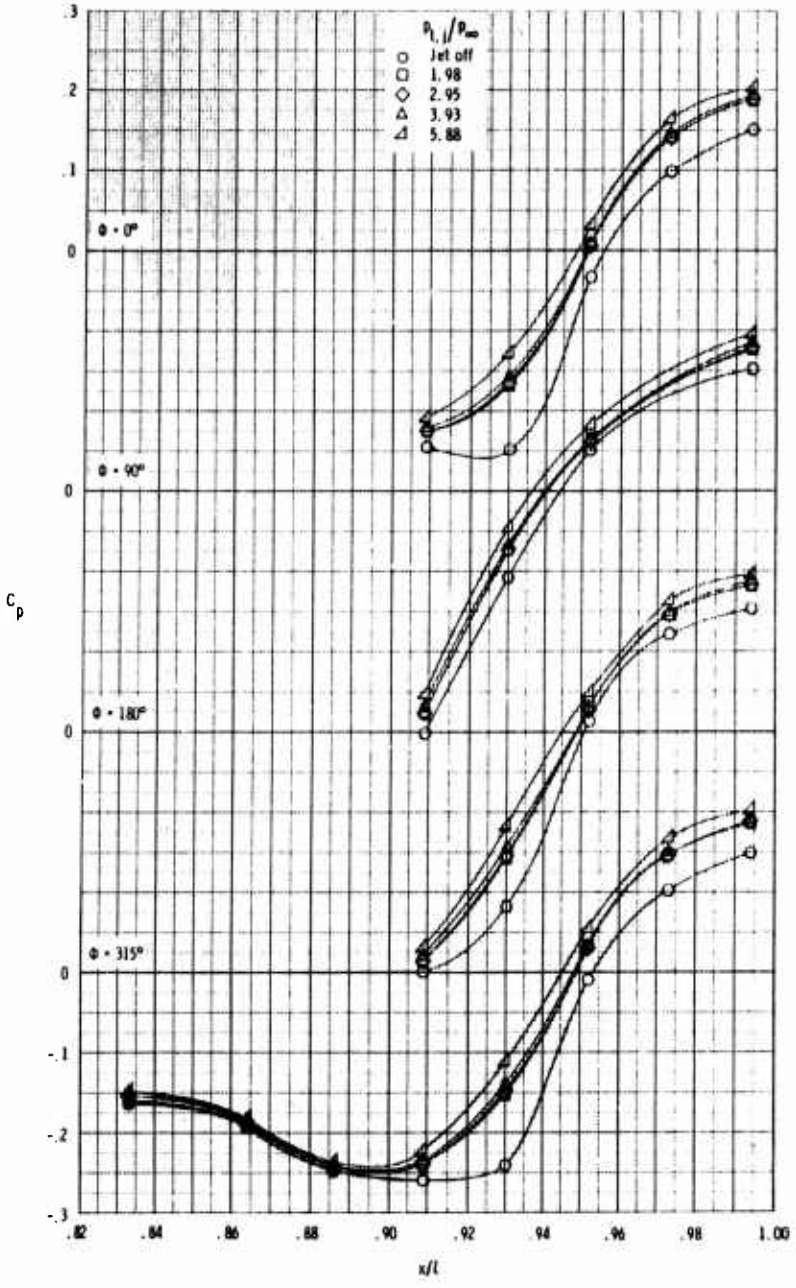



Figure 4.- Effect of jet total pressure ratio on afterbody/nozzle pressure distributions for the staggered tails configuration at M = 0.944.

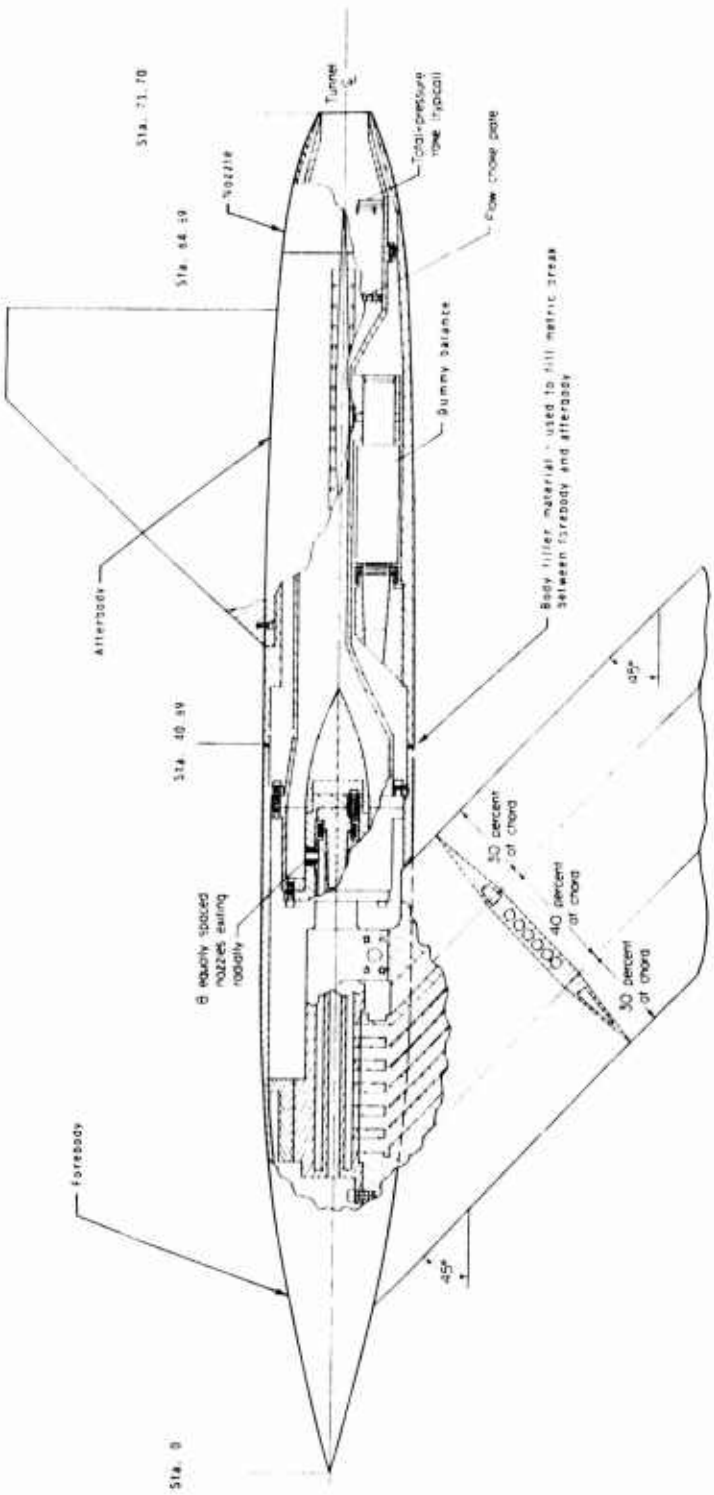



Figure 5.- General model arrangement. Linear dimensions are in inches.

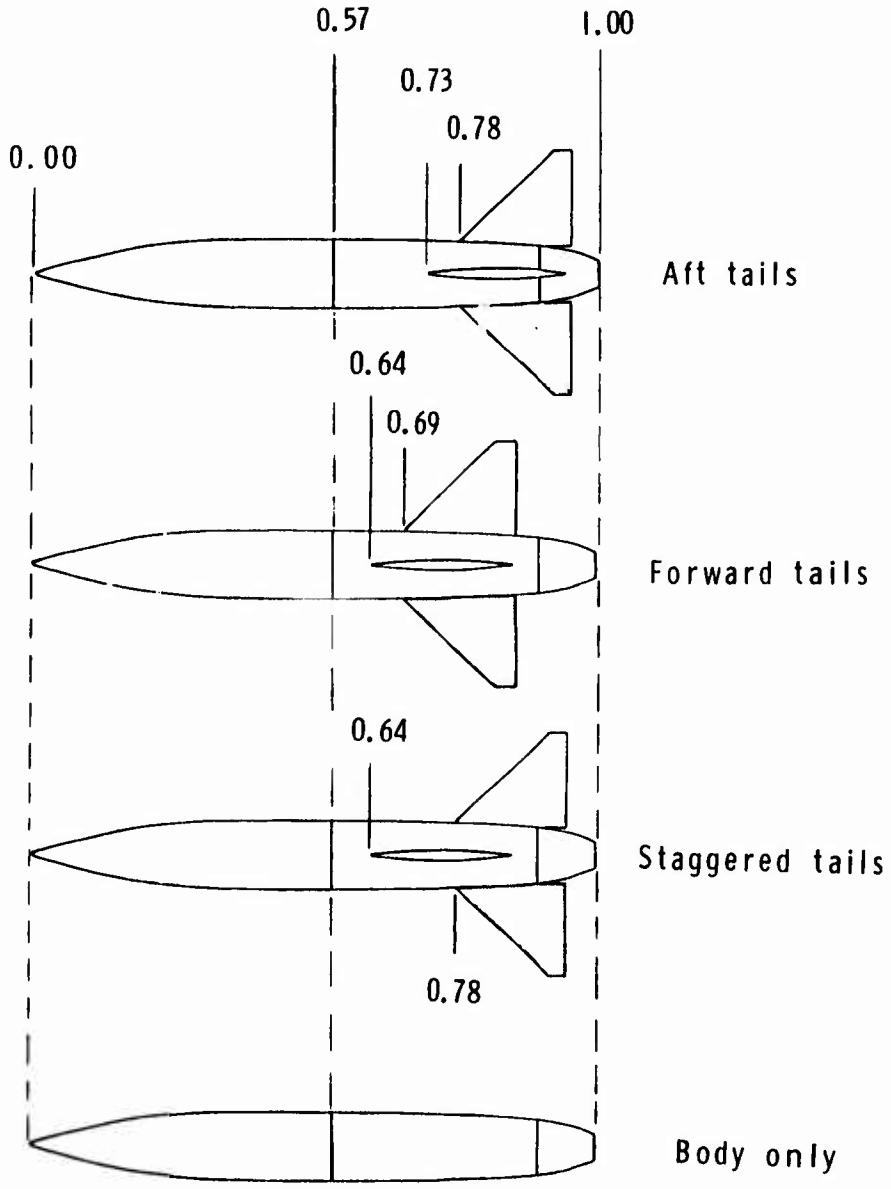



Figure 6.- Planform view of model configurations tested. Dimensions are in fractions of body length.

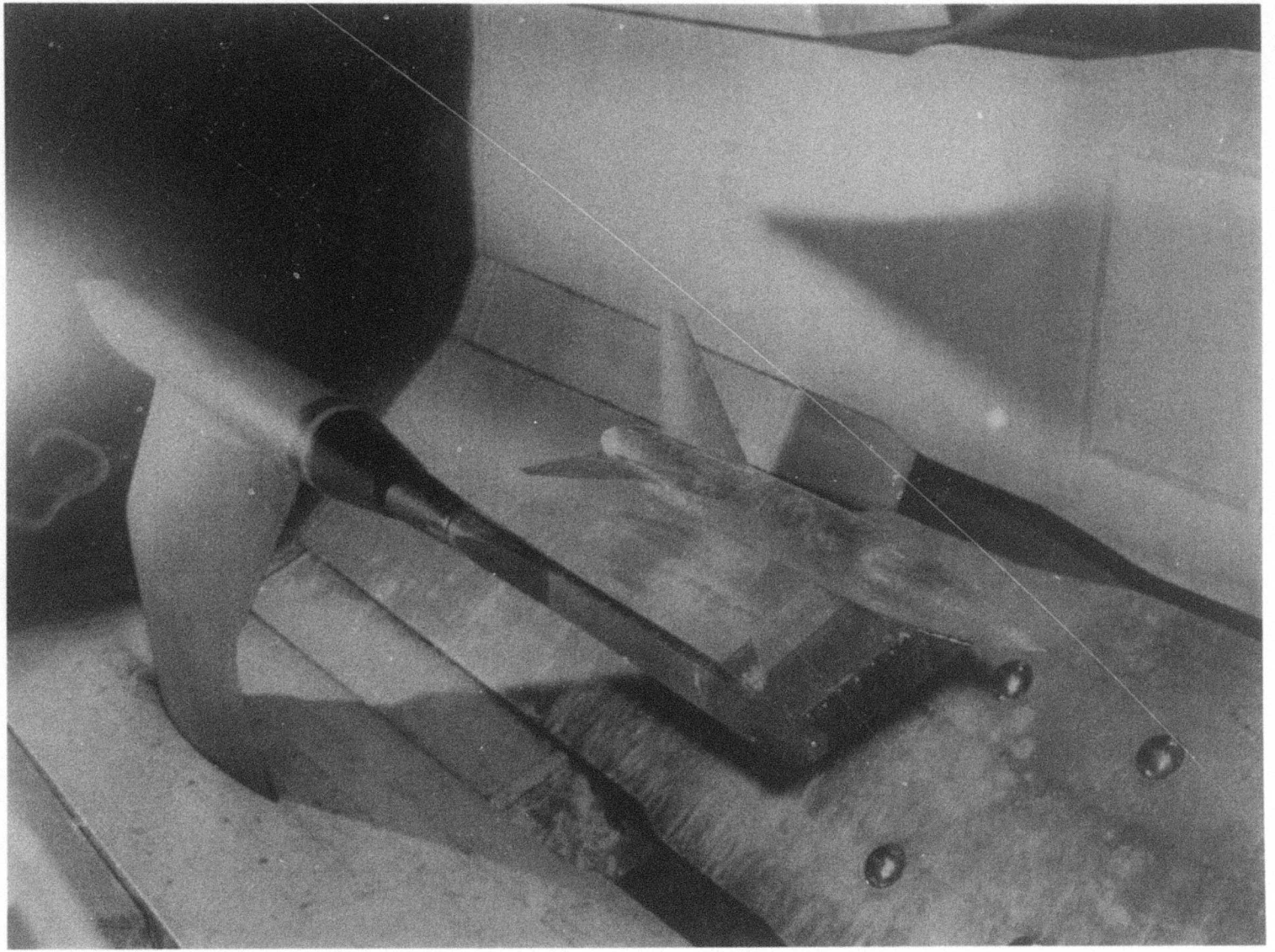


Figure 7.- Photograph showing general arrangement of model, support system and test section.

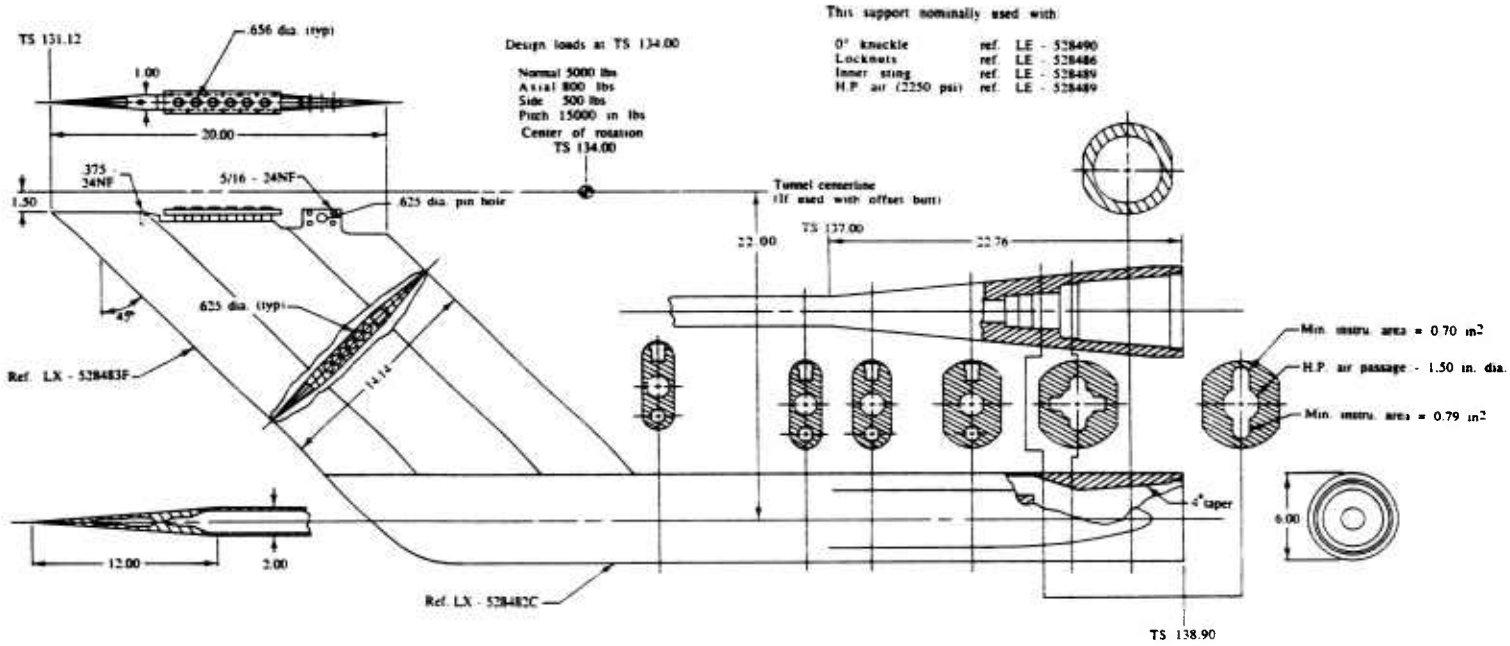
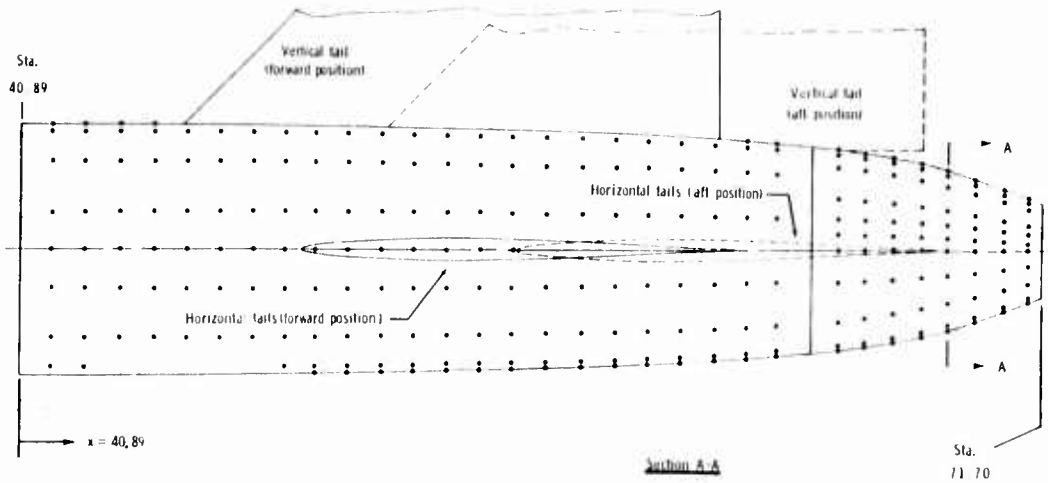
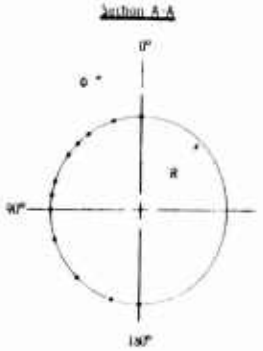



Figure 8.- Sketch of high pressure air sting strut support system. All tunnel stations are in feet.




Nozzle/afterbody external geometry

| | x, in. | r, in. |
|---|---|---|
| 1 | 40.888 | 3.670 |
| 2 | 41.700 | 3.670 |
| 3 | 43.700 | 3.665 |
| 4 | 45.700 | 3.654 |
| 5 | 47.700 | 3.636 |
| 6 | 49.700 | 3.612 |
| 7 | 51.700 | 3.580 |
| 8 | 53.700 | 3.539 |
| 9 | 55.700 | 3.488 |
| 10 | 57.700 | 3.425 |
| 11 | 58.700 | 3.389 |
| 12 | 59.700 | 3.348 |
| 13 | 60.700 | 3.302 |
| 14 | 61.700 | 3.248 |
| 15 | 62.312 | 3.217 |
| 16 | 62.700 | 3.184 |
| 17 | 63.200 | 3.147 |
| 18 | 63.700 | 3.108 |
| 19 | 64.300 | 3.056 |
| 20 | 64.888 | 3.000 |
| 21 | 65.700 | 2.919 |
| 22 | 67.181 | 2.726 |
| 23 | 67.700 | 2.635 |
| 24 | 68.700 | 2.400 |
| 25 | 69.700 | 2.098 |
| 26 | 70.700 | 1.750 |
| 27 | 71.700 | 1.374 |




Pressure taps are on the left side of the afterbody and nozzle when looking upstream.

Pressure orifice locations (see tables A2 through A8)

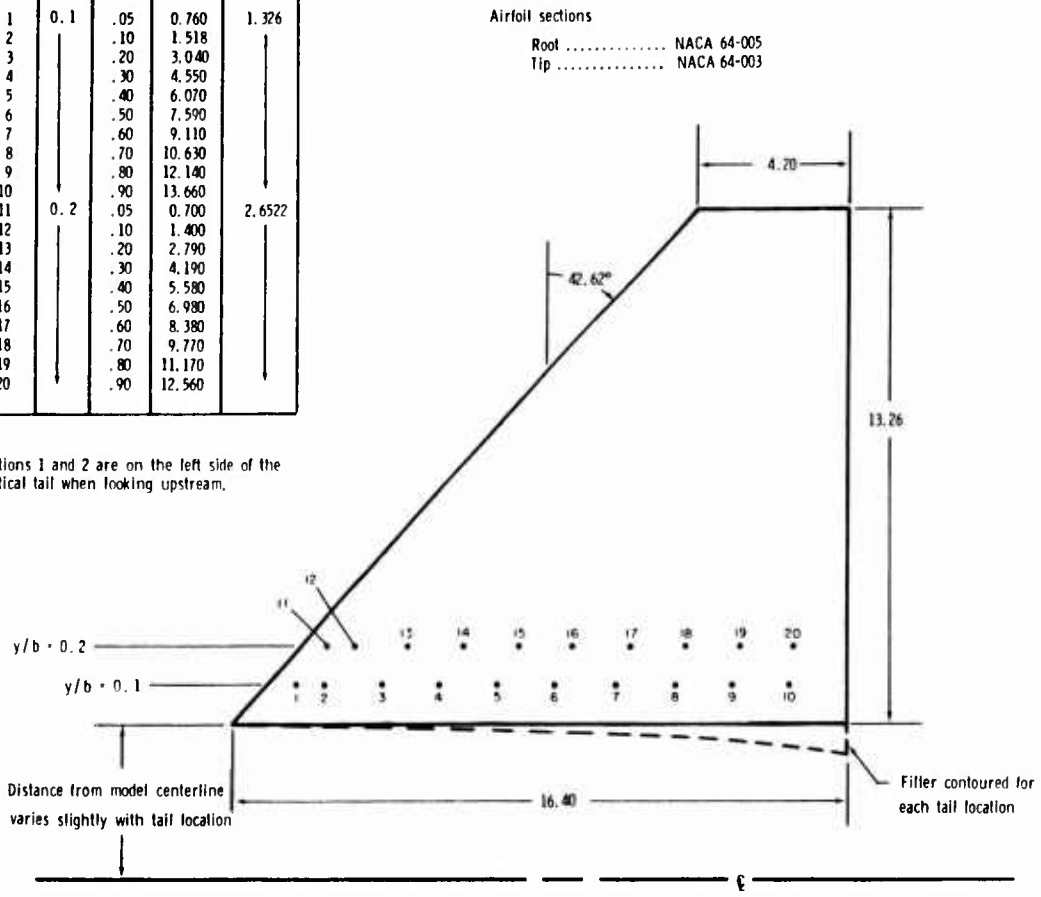
| x, in. | x/L | Φ, deg | | | | | | | | | | |
|---|---|---|---|---|---|---|---|---|---|---|---|---|
| | | 0 | 18 | 36 | 45 | 54 | 72 | 81 | 90 | 108 | 135 | 162 | 180 |

(a) Afterbody/nozzle.

Figure 9.- Pressure instrumentation and external geometry details. Linear dimensions are in inches.

| Orifice | y/b | x/c | x, in. | y, in. |
|---|---|---|---|---|
| 1 | 0.1 | .05 | 0.760 | 1.326 |
| 2 | | .10 | 1.518 | |
| 3 | | .20 | 3.040 | |
| 4 | | .30 | 4.550 | |
| 5 | | .40 | 6.070 | |
| 6 | | .50 | 7.590 | |
| 7 | | .60 | 9.110 | |
| 8 | | .70 | 10.630 | |
| 9 | | .80 | 12.140 | |
| 10 | | .90 | 13.660 | |
| 11 | 0.2 | .05 | 0.700 | 2.6522 |
| 12 | | .10 | 1.400 | |
| 13 | | .20 | 2.790 | |
| 14 | | .30 | 4.190 | |
| 15 | | .40 | 5.580 | |
| 16 | | .50 | 6.980 | |
| 17 | | .60 | 8.380 | |
| 18 | | .70 | 9.770 | |
| 19 | | .80 | 11.170 | |
| 20 | | .90 | 12.560 | |

Stations 1 and 2 are on the left side of the vertical tail when looking upstream.




(b) Vertical tail.

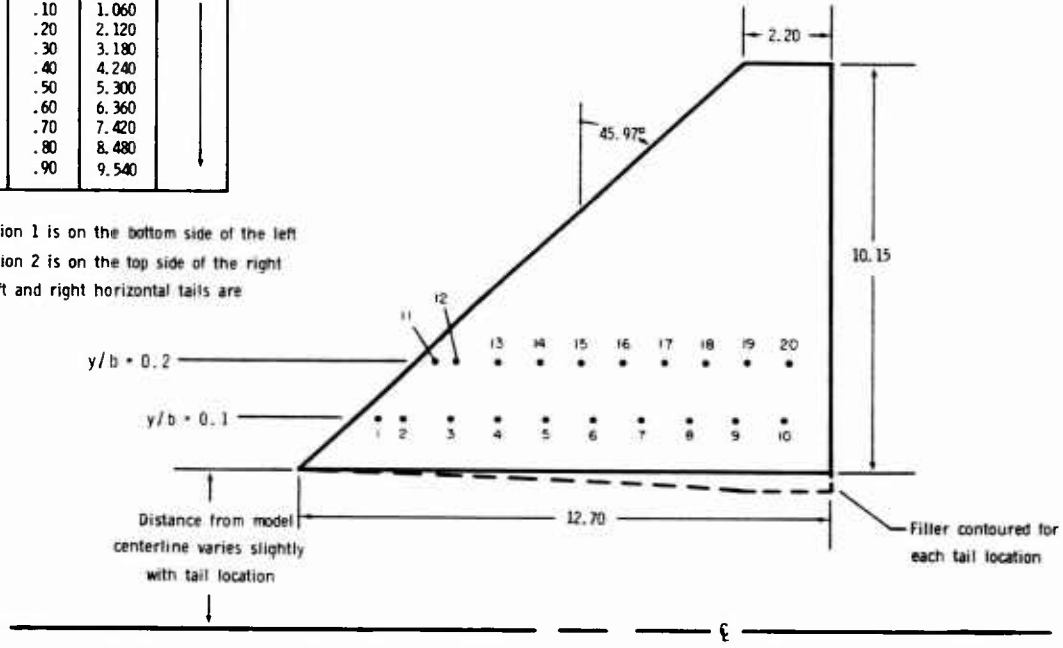
Figure 9.- Continued.

| Orifice | y/b | x/c | x, in. | y, in. |
|---|---|---|---|---|
| 1 | 0.1 | .05 | 0.583 | 1.015 |
| 2 | | .10 | 1.165 | |
| 3 | | .20 | 2.330 | |
| 4 | | .30 | 3.495 | |
| 5 | | .40 | 4.660 | |
| 6 | | .50 | 5.825 | |
| 7 | | .60 | 6.990 | |
| 8 | | .70 | 8.155 | |
| 9 | | .80 | 9.320 | |
| 10 | | .90 | 10.485 | |
| 11 | 0.2 | .05 | 0.530 | 2.030 |
| 12 | | .10 | 1.060 | |
| 13 | | .20 | 2.120 | |
| 14 | | .30 | 3.180 | |
| 15 | | .40 | 4.240 | |
| 16 | | .50 | 5.300 | |
| 17 | | .60 | 6.360 | |
| 18 | | .70 | 7.420 | |
| 19 | | .80 | 8.480 | |
| 20 | | .90 | 9.540 | |

Looking upstream, station 1 is on the bottom side of the left horizontal tail and station 2 is on the top side of the right horizontal tail. The left and right horizontal tails are interchangeable.

Airfoil sections

Root..... NACA 64-005
Tip..... NACA 64-003




(c) Horizontal tails.

Figure 9.- Concluded.

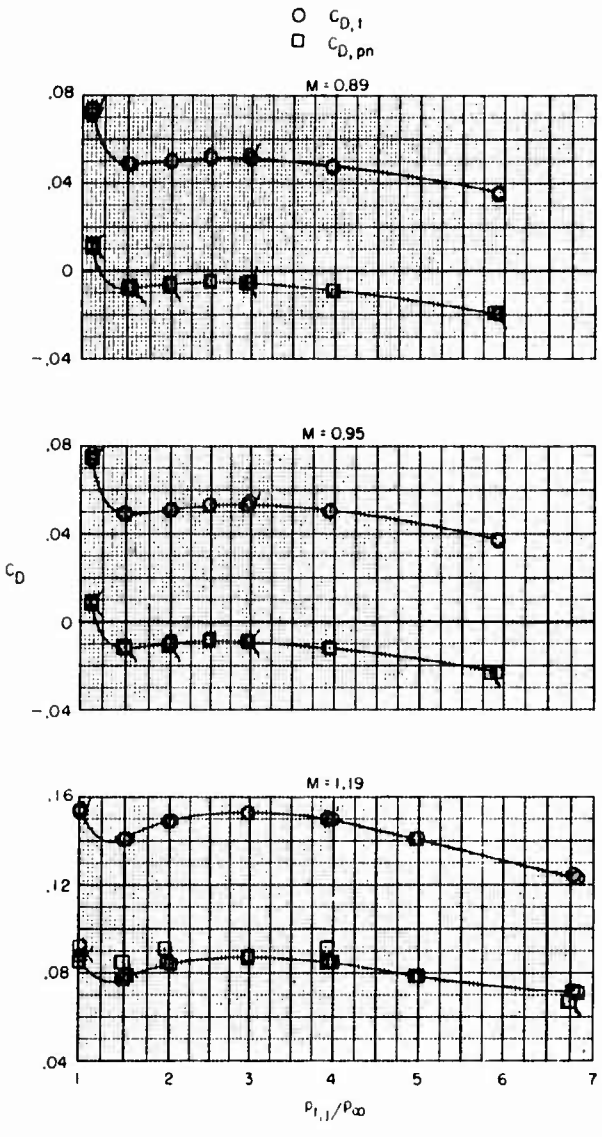



Figure 10.- Comparison of repeat drag force data on tails off confiruration. Flagged symbols indicate repeat data taken during NPR sweep. Tailed symbols indicate data from different nozzle with same geometry. All other repeat points are from different run.

# TWIN ENGINE AFTERBODY MODEL

by

David J. Wing
Propulsion Aerodynamics Branch/M.S. 280
NASA-Langley Research Center
Hampton, VA 23665
USA

## 0 INTRODUCTION

This test was originally conducted to determine the effects of several empennage and afterbody parameters on the aft-end aerodynamic characteristics of a twin-engine fighter-type configuration. Model variables were as follows: horizontal tail axial location and incidence, vertical tail axial location and configuration (twin- vs single-tail arrangements), tail booms, and nozzle power setting. Jet propulsion was simulated by exhausting high-pressure, cold-flow air from the nozzles.

Following a successful test conducted on a single engine nacelle model to validate a CFD code, this model was chosen to be instrumented with pressure taps on the afterbody and nozzles and used as a follow-on test, providing a more complex geometry for the CFD code validation.

A more limited test matrix was run to collect the pressure data, employing only the twin-tail configuration and varying only the horizontal and vertical tail locations. Mach number was varied from 0.6 to 1.2. Nozzle pressure ratio was varied from jet-off to 8. Angle-of-attack was varied from 0° to 8°.

## 1 GENERAL DESCRIPTION

| | | |
|---|---|---|
| 1.1 | Model Designation of Name | Twin-engine afterbody model. |
| 1.2 | Model Type | Generic twin-engine, twin-tail fighter model, 45° swept wing, propulsion simulation. |
| 1.3 | Design Requirements | This model was designed to be tested at transonic speeds with twin-engine propulsion simulation such that pressures and forces only on the afterbody, excluding the thrust, would be measured. |
| 1.4 | Dominant flow physics | Empennage/afterbody interactions (see fig. 1), flow separation (see fig. 2), and exhaust/aft-end interactions (see fig. 3). |
| 1.5 | Additional remarks | Afterbody lift and drag data are presented in NASA TP-2116. The remainder of this description will be devoted to afterbody/nozzle surface pressure measurements made over a more limited test matrix. Approximately 180 static pressure measurements were made on the afterbody, nacelles, and nozzles for the purpose of CFD code validation. Vertical and horizontal tail longitudinal position were varied. |

## 2 DETAILS OF MODEL

**2.1 General geometric arrangement**

The model is a generic, twin-engine, twin-tail, high-wing fighter with a 45° swept wing. See photograph in figure 4 and sketch in figure 5..

**2.2 Describe configurations**

The configurations tested for static pressure distributions include six tail positions (H=horizontal, V=vertical):

Config 1: H(mid), V(fwd)
Config 2: H(mid), V(mid)
Config 3: H(mid), V(aft)
Config 4: H(aft), V(fwd)
Config 5: H(aft), V(mid)
Config 6: H(aft), V(aft)

See NASA TP-2116, fig. 2(f) for definition of tail locations.

**2.3 Wing and/or airfoil data**

**2.3.1 Planform**

- Aspect ratio: 2.4
- Taper ratio: 0.5
- Leading edge sweep: 45°
- Trailing edge sweep: Cranked
- Twist distribution: None
- Semispan: 50.80 cm
- Tip geometry: Thickened for structural support (wingtip support system employed)
- Fuselage/wing junction: Faired junctions

**2.3.2 Basic wing section**

- Airfoil shape: Symmetrical
- T/C ratio: 0.067 at root, increases from 0.077 to 0.10 from BL 27.94 to support booms
- Nose radius/chord: Relatively sharp leading edge, mean chord 44.4 cm

**2.4 Body data**

**2.4.1 Shape**

- Nose shape: Circular cross-section

| | | |
|---|---|---|
| | • Body length | 174.74 cm to nozzle exit plane |
| | • Cross-sectional details | Fuselage has rectangular c/s (25.40 cm x 12.70 cm) with rounded corners (2.54 cm radius), maximum area 317.04 sq. cm. |
| 2.4.2 | Additional details | Faired-over inlets |
| 2.5 | Information on tails | Leading edges of horizontal and vertical tails can be positioned at FS 127.00, FS 136.68, or FS 145.57. |
| 2.5.1 | Vertical tails | |
| | • Airfoil section | Tip: NACA 64-003.5<br>Root: NACA 64-005 |
| | • Chord | Tip: 9.14 cm<br>Root: 24.38 cm |
| | • Taper ratio | 0.375 |
| | • Tail height (root to tip) | 25.4 cm |
| | • Aspect ratio | 1.514 |
| | • Leading edge sweep | 36.52° |
| 2.5.2 | Horizontal tails | |
| | • Airfoil section | Tip: NACA 64-002.5<br>Root: NACA 64-005.5 |
| | • Chord | Tip: 5.08 cm<br>Root: 28.96 cm |
| | • Taper ratio | 0.175 |
| | • Span | Fwd position: 69.09 cm<br>Mid position: 68.58 cm<br>Aft position: 67.51 cm |
| | • Aspect ratio | 2.564 |
| | • Leading edge sweep | 50.0° |
| 2.6 | Nozzle data | |
| | • Nozzle type | Twin-engine, axisymmetric, convergent-divergent |
| | • Attachment station | FS 165.53 |
| | • Maximum diameter | 9.86 cm |
| | • Throat diameter | 4.71 cm |

| | | |
|---|---|---|
| | • Exit diameter (internal) | 5.05 cm |
| | • Exit diameter (external) | 5.67 cm |
| | • Nozzle length | 9.11 cm |
| 2.7 | Geometric definition | |
| | • Is shape analytically or numerically specified? | Numerical specification exists for Config 2: H(mid), V(mid) |
| | • Design or measured co-ordinates? | Model was analytically designed |
| | • Tolerances | |
| | • Surface roughness | Varied due to body filler used in fairing surface |
| 2.8 | Model support details | |
| | • Sting and support geometry | Bifurcated wing-tip support system (see figures 4 and 5) |
| | • Special features of mounting | Structural support requirements resulted in unrealistic wing thickness near tip. |
| 3 | GENERAL TUNNEL INFORMATION | |
| 3.1 | Tunnel designation | 16-Foot Transonic Tunnel |
| 3.2 | Organization running the tunnel | NASA-Langley Research Center<br>Applied Aerodynamics Division<br>Propulsion Aerodynamics Branch |
| 3.3 | Tunnel characteristics | |
| | • Type of tunnel | Continuous-flow, single-return, atmospheric wind tunnel with a slotted octagonal throat and test section and continuous air exchange. Boundary layer air removal (suction) is utilized at Mach numbers above 1.0. Up to 4.5% (depends on desired Mach number) of the tunnel mass flow is removed by this system. |
| | • Operating envelope | Mach 0.2 to Mach 1.3 at atmospheric pressure. |
| 3.4 | Test Section | |
| | 3.4.1 General arrangement | See photograph in figure 4 of model mounted with wing-tip support in the tunnel. The octagonal test section is surrounded by a 32 foot diameter plenum into which air expands to permit supersonic flow. Air is removed from this plenum by a |

compressor suction system at Mach numbers above 1.0. No protruding instrumentation exists near or upstream of the model except in the quiescent chamber upstream of the test section. High pressure air for jet simulation is routed to the model through the sting supports.

3.4.2 Test section dimensions

Regular octagon with an approximate distance between flats of 15.5 feet. Wall divergence angle is variable and is set to provide best flow quality at each Mach number. Thus, test section dimensions are slightly dependent on tunnel Mach number. Test section length, as determined from facility calibrations, is also dependent on tunnel Mach number and varies from 40 feet at M = 0.2 to 10 feet at M = 1.3.

3.4.3 Wall geometry details

- Type of walls: Eight solid, flat, steel plates, 6.66 ft maximum width, separated by slots. Divergence angle of plates is variable.
- Open area ratio: Nominally 4% (depends on divergence angle and thus tunnel Mach number).
- Are wall pressures/wall displacements measured? Wall pressures not measured for current model but are available when needed. Wall divergence angle is measured.
- Boundary layer control on walls: No direct control on walls but some level of boundary layer control results from varying wall divergence angle and, at supersonic speeds, plenum suction through corner slots.

3.5 Free stream conditions

3.5.1 How are reference flow conditions determined for:

- Total pressure: Ruska absolute pressure sensor located in quiescent chamber.
- Static pressure: Ruska absolute pressure sensor located in plenum tank and calibrated to the tunnel centerline.
- Total temperature: Three platinum resistance thermometers located in quiescent chamber.

3.5.2 Tunnel calibration

| | |
|---|---|
| • How was the tunnel calibrated? | The tunnel was calibrated using a centerline probe which reached forward of the tunnel throat. Some flow survey (off centerline) and dynamic data were also obtained. |
| • Date of last calibration | Spring 1991 (not yet published) |

3.6 Flow quality (empty tunnel)

3.6.1 Flow uniformity

| | |
|---|---|
| • Mach number/static pressure variations over model length and span | The usable test section length is defined by the extent of constant static pressure down the test section, which decreases with Mach number. For the Mach numbers of the current test, the average Mach number variation per foot (over 6 foot length) was 0.000267. |
| • Mach number variation during a run | Mach number is maintained within approximately +/- 0.003 during a run. Actual Mach number is recorded for each data point. |
| • How is average flow angularity determined? | Flow angularity is determined by running models through angle-of-attack sweeps at upright and inverted conditions. The intersection of the lift vs angle-of-attack curves yields the upflow angle. Tunnel upflow angle for models without wings is assumed to be the average of this data from many tests. |
| • Variation of angularity over model length and span | Angularity determined by the above method is found at the model center of lift. A flow angularity survey of the test volume was made during the 1991 tunnel calibration. These results are currently being analyzed for future publication. |

3.6.2 Temperature variation

| | |
|---|---|
| • Can temperature be controlled during a run? | Tunnel temperature is not controlled. Jet temperature is typically controlled at about 70°F. |
| • Variation within the tunnel | With the present system for cooling the tunnel by continuous air exchange in which the cool air is introduced in an annulus adjacent to the wall of the return passage, a radial gradient of temperature in the test section airstream is almost inherent. After passing through the drive fans, the airstream in the return passage is of uniform |

| | |
|---|---|
| | temperature. On the downstream side of the air exchange, a radial temperature gradient is created by differences between stagnation and outside air temperatures. By the time that the airstream has traversed the third and fourth sets of turning vanes, an antiturbulence screen, the quiescent chamber, and the entrance cone, the region of radial gradient of temperature extends inwardly from the test section wall for about one-half of the test section radius. The temperature of the airstream core is very uniform and is identical with stagnation temperature indicated by probes located in the quiescent chamber. The difference between the test section core and wall temperatures is about 0.90 of the difference between stagnation and outside air temperatures. The gradient of temperature in the test section is not a desirable feature but, in general, has no adverse effect on most investigations. The temperature gradient has no effect on Mach number distribution but does result in a velocity gradient directly related to the temperature gradient. Most models are much smaller than the airstream hot core and are therefore not affected. |
| • Variation over a run | Depends on Mach number and length of run. Initial temperature is atmospheric and increases as the run progresses. The tunnel temperature limit is 180°F (normally occurs only at supersonic speeds during summer months) at which time, the tunnel power is reduced for tunnel cooling. |
| 3.6.3 Flow unsteadiness | |
| • Overall turbulence level | During the tunnel calibration of 1950-1951 and on several occasions prior to the use of test section air removal and before an antiturbulence screen was installed in the quiescent chamber, attempts were made to measure airstream turbulence. Fluctuating flow angle was measured with a three degree cone meter, but interpretation of the data was uncertain. If isotropic turbulence can be assumed, these results indicated that the stream angle fluctuation expressed in radians ranged from about 0.003 to 0.008. Low turbulence in the tunnel is likely because of anti-turbulence screens in the quiescent chamber and a contraction ratio of 13.31 into the test section. |
| • Overall noise level | For M of current test, $\Delta C_p$ = 0.46% - 1.13%. |

| | | | |
|---|---|---|---|
| 4 | INSTRUMENTATION | | |
| 4.1 | Model position | | |
| | 4.1.1 | How is the geometrical incidence measured? | Inertial accelerometer. |
| | 4.1.2 | Accuracy of geometrical incidence | +/- 0.02° |
| 4.2 | Model pressure measurements | | |
| | 4.2.1 | Total number, disposition | Approximately 120 taps on afterbody and 60 taps on nozzles, arranged in longitudinal rows (see fig. 6). |
| | 4.2.2 | Range and accuracy of pressure transducers | Electronic sensing transducers (ESPs). Range, 15 psi; accuracy 0.5% |
| | 4.2.3 | Dynamic pressures | Not measured. |
| 4.3 | Force and moment measurements | | See NASA TP-2116 for information regarding force and moment data. |
| 4.4 | Boundary layer and flow field measurements | | None. |
| 4.5 | Surface flow visualization | | None. |
| 4.6 | Flow field visualization | | None. |
| 4.7 | Tunnel wall measurements | | None. |
| 4.8 | Other measurements or instrumentation used | | None. |
| 5 | TEST MATRIX AND CONDITIONS | | |
| 5.1 | Detailed test matrix | | |
| | 5.1.1 | Number of selected test cases | Six configurations with surface static pressures |
| | 5.1.2 | Number of configs tested | Six configurations with surface static pressures |
| | 5.1.3 | Test matrix table | Static pressure measurements on the afterbody and nozzles were made for configurations 1 through 6 (see section 2.2) at the following conditions: |

| Mach | Alpha | Nozzle Pressure Ratio |
|---|---|---|
| 0 | 0° | 1.5, 2, 3, 3.46, 4, 6, 8 |
| 0.6, 0.8, 0.9, 1.2 | 0° | 1, 1.5, 2, 3, 3.46, 4, 6, 8 |
| 0.6, 0.8, 0.9, 1.2 | 4° | 1, 3.46 |
| 0.6, 0.8, 0.9, 1.2 | 8° | 1, 3.46 |

Approximate Reynolds Number range: $3 \times 10^6$ to $4.4 \times 10^6$ based on a wing mean aerodynamic chord of 44.4 cm.

Approximate dynamic pressure range: 4200 psf to 8800 psf

5.2 Model/tunnel relations

| | | |
|---|---|---|
| 5.2.1 | Maximum blockage | Less than approx. 0.0025 |
| 5.2.2 | Model span/tunnel dimension | Approx. 0.215 |
| 5.2.3 | Wing area/tunnel x/c | 0.023 |
| 5.2.4 | Height/chord ratio (2-D only) | N/A |
| 5.2.5 | Width/chord ratio (2-D only) | N/A |
| 5.2.6 | Have adiabatic wall temperatures been reached? | Not known. |

5.3 Transition details

| | | |
|---|---|---|
| 5.3.1 | Free or fixed transition | Fixed. |
| 5.3.2 | Details of free transition | N/A |
| 5.3.3 | Details of fixed transition | |
| | • Transition location | 5.08 cm from nose tip.<br>Along wing span at 5% of root chord and 10% of tip chord.<br>1.27 cm from leading edges of vertical and horizontal tails. |
| | • Type and size of trip | 0.254-cm-wide strip of No. 120 corborundum grit, sparcely distributed. |
| | • How was effectiveness of trip verified? | Procedure in NASA TN D-3579 followed. |

6 DATA

6.1 Availability of data

| | | |
|---|---|---|
| 6.1.1 | Organization owning data | NASA-Langley Research Center |

| | | | |
|---|---|---|---|
| | 6.1.2 | Who is responsible for contacted? | Bobby L. Berrier,<br>Head, Propulsion Aerodynamics Branch,<br>NASA Langley Research Center<br>MS 280<br>Hampton, VA 23681-0001<br>(804)864-3001/FAX(804)864-8195 |
| | 6.1.3 | Are data freely available? | Yes |
| 6.2 | Suitability of data for CFD validation | | |
| | 6.2.1 | Are data suitable for "in-tunnel" calculation? | No |
| | 6.2.2 | Are data corrected to simulate "free-air" conditions? | Yes |
| 6.3 | Type and form in which data are available | | |
| | 6.3.1 | Type and form | Free stream conditions - engin. units<br>Surface pressures - coefficients |
| | 6.3.2 | Data carrier | NASA TP<br>Data for selected cases (configuration 1, 2 and 3; see Section 2.2) at a nominal Mach number of 0.90 and a nominal NPR of 3.4 are available on a 3.5 inch floppy disk. |
| | 6.3.3 | Extent of geometry data | Model drawings are available.<br>Electronic transfer of model geometry and grid definition for configurations 1, 2 and 3 (See Section 2.2) can be arranged by contacting Bobby L. Berrier (See Section 6.1.2). |
| | 6.3.4 | Extent of aero. data | N/A |
| 6.4 | Corrections applied to data | | |
| | 6.4.1 | Lift interference and blockage corrections | No corrections were made for blockage. Blockage effects at the Mach numbers tested have been shown to be negligible. |
| | 6.4.2 | Sidewall interference corrections | None. |
| | 6.4.3 | Half model corrections | N/A |
| | 6.4.4 | Sting and support corrections | The wing-tip support system was designed to provide minimum interference, yet provide a more realistic aircraft flow field for the afterbody than that from a blade-mounted support system. By design, the model is supported by wings and not a support strut (See Section 2.8). Interference from the "wings" on the metric afterbody is considered a real effect and not support interference. The twin booms are not |

| | | | |
|---|---|---|---|
| | | | expected to have any interference effects up to Mach numbers of 0.90. Interference tests on a similar wing-tip support system (ref. 21 in NASA TP-2116) indicate low levels of support interference. |
| | 6.4.5 | Aeroelastic deformation | N/A |
| | 6.4.6 | Other corrections | None. |
| 7 | DATA ACCURACY AND REPEATABILITY | | |
| 7.1 | Estimate accuracy of: | | |
| | 7.1.1 | Free stream conditions | |
| | | • Mach number | +/- 0.002 |
| | | • Model incidence | +/- 0.02° |
| | 7.1.2 | Measured data | |
| | | • Pressures | 0.5% full scale of ESP |
| 7.2 | Repeat measurements | | Repeatability was not investigated on this model. |
| 7.3 | Redundant measurements | | The reliability of the ESP static pressure measurements were continuously verified with duplicate transducer measurements of the pressure inside the model and atmospheric pressure outside the test section. |
| 7.4 | Other tests on same geometry | | NASA TP-2116 |
| 7.5 | Additional remarks | | None. |
| 8 | REFERENCES | | |
| 8.1 | On the wind tunnel | | Corson, Blake W.; Runckel, Jack F.; and Igoe, William B.: Calibration of the Langley 16-Foot Transonic Tunnel with Test Section Air Removal. NASA TR R-423, August 1974.<br><br>Staff of the Propulsion Aerodynamics Branch: A User's Guide to the Langley 16-Foot Transonic Tunnel Complex. Revision 1. NASA TM-102750, Sept. 1990. |

| | | |
|---|---|---|
| 8.2 | On the model | Leavitt, Laurence D.: Effect of Empennage Location on Twin-Engine Afterbody/Nozzle Aerodynamic Characteristics at Mach Numbers From 0.6 to 1.2. NASA TP-2116, May 1983.<br><br>Leavitt, Laurence D.; and Bare, E. Ann: Effects of Twin-Vertical-Tail Parameters on Twin-Engine Afterbody/Nozzle Aerodynamic Characteristics. NASA TP-2158, May 1983. |
| 8.3 | On the particular test | See section 8.2 |
| 8.4 | On the applied measurement techniques and correction methods | NASA TM-102750<br><br>Mercer, Charles E.; Berrier, Bobby L.; Capone, Francis J.; Grayston, Alan M.; and Sherman, C.D.: Computations for the 16-Foot Transonic Tunnel. NASA, Langley Research Center. Revision 1. NASA TM-86319, January 1987. |

## 9 LIST OF SYMBOLS

| | |
|---|---|
| $C_p$ | Pressure coefficient |
| $\Delta C_p$ | Noise (fluctuating pressure), rms, % |
| H( ), HTAIL | Horizontal tail position |
| l | Model length, inches. |
| M | Mach number |
| NPR | Nozzle pressure ratio (jet total to freestream static) |
| V( ), VTAIL | Vertical tail position |
| x | Axial distance downstream from nose tip, inches. |
| $\alpha$, alpha | Angle of attack, degrees. |
| $\delta$ | Angular position of pressure tap row on nozzles, degrees. |
| $\theta$ | Angular position of pressure tap row on afterbody, degrees. |
| $\phi$ | Angular position of pressure tap row on interfairing, degrees. |

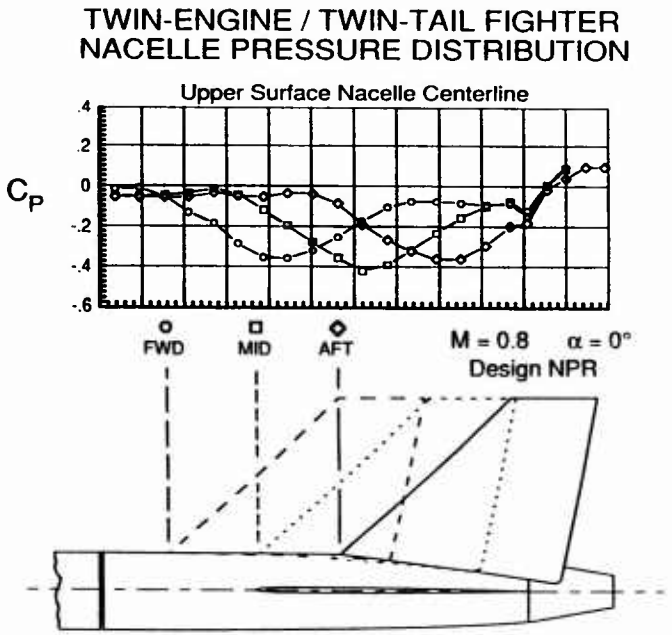



Figure 1. Empennage/afterbody surface pressure interactions on the twin-engine afterbody model.

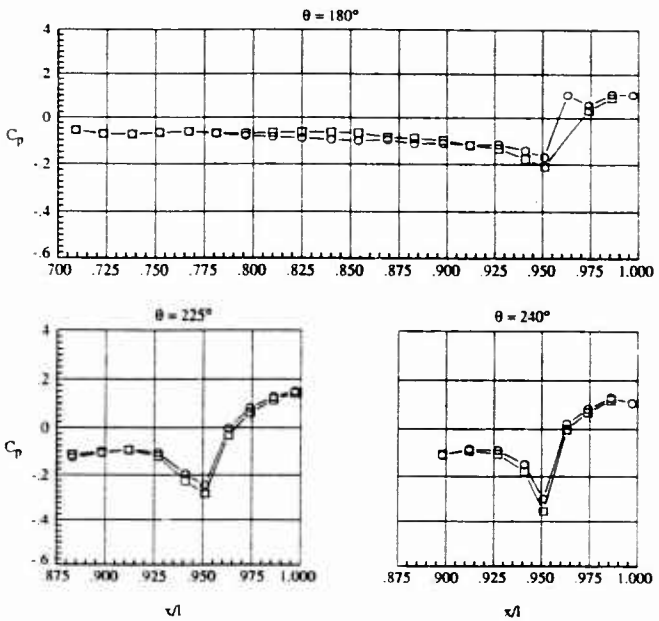



Figure 2. Flow separation on the nozzle boattail of the twin-engine afterbody model.

| | M | α | NPR | HTAIL | VTAIL |
|---|---|---|---|---|---|
| ○ | 0.791 | 0.00 | 1.078 | mid | fwd |
| □ | 0.791 | 0.02 | 1.470 | mid | fwd |
| ◇ | 0.791 | 0.03 | 1.952 | mid | fwd |
| △ | 0.790 | 0.02 | 2.929 | mid | fwd |
| ◺ | 0.793 | 0.02 | 3.365 | mid | fwd |
| ◺ | 0.793 | 0.03 | 3.901 | mid | fwd |
| ∩ | 0.791 | -0.03 | 5.906 | mid | fwd |
| ○ | 0.791 | -0.02 | 7.794 | mid | fwd |

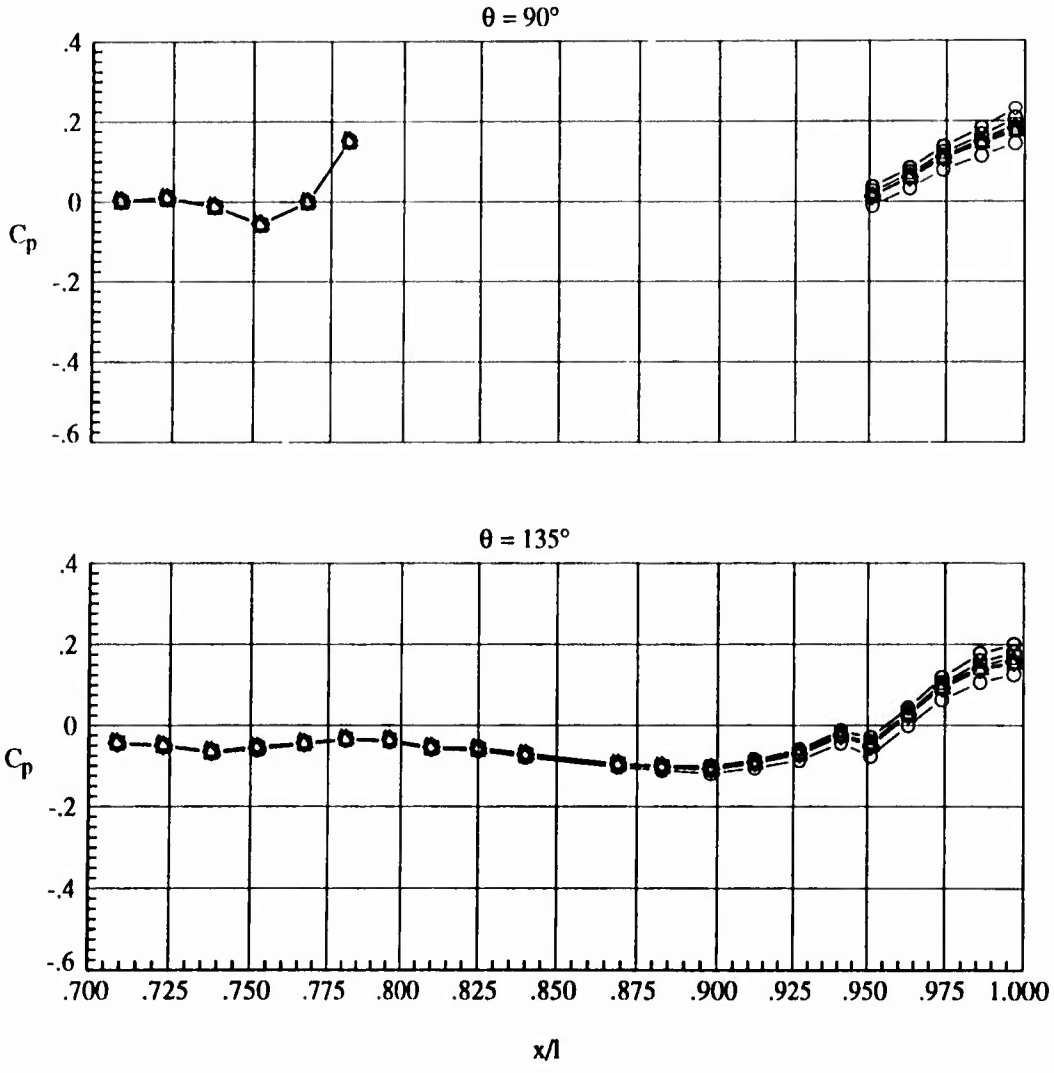



Figure 3. Exhaust/aft-end surface pressure interactions on the twin-engine afterbody model.

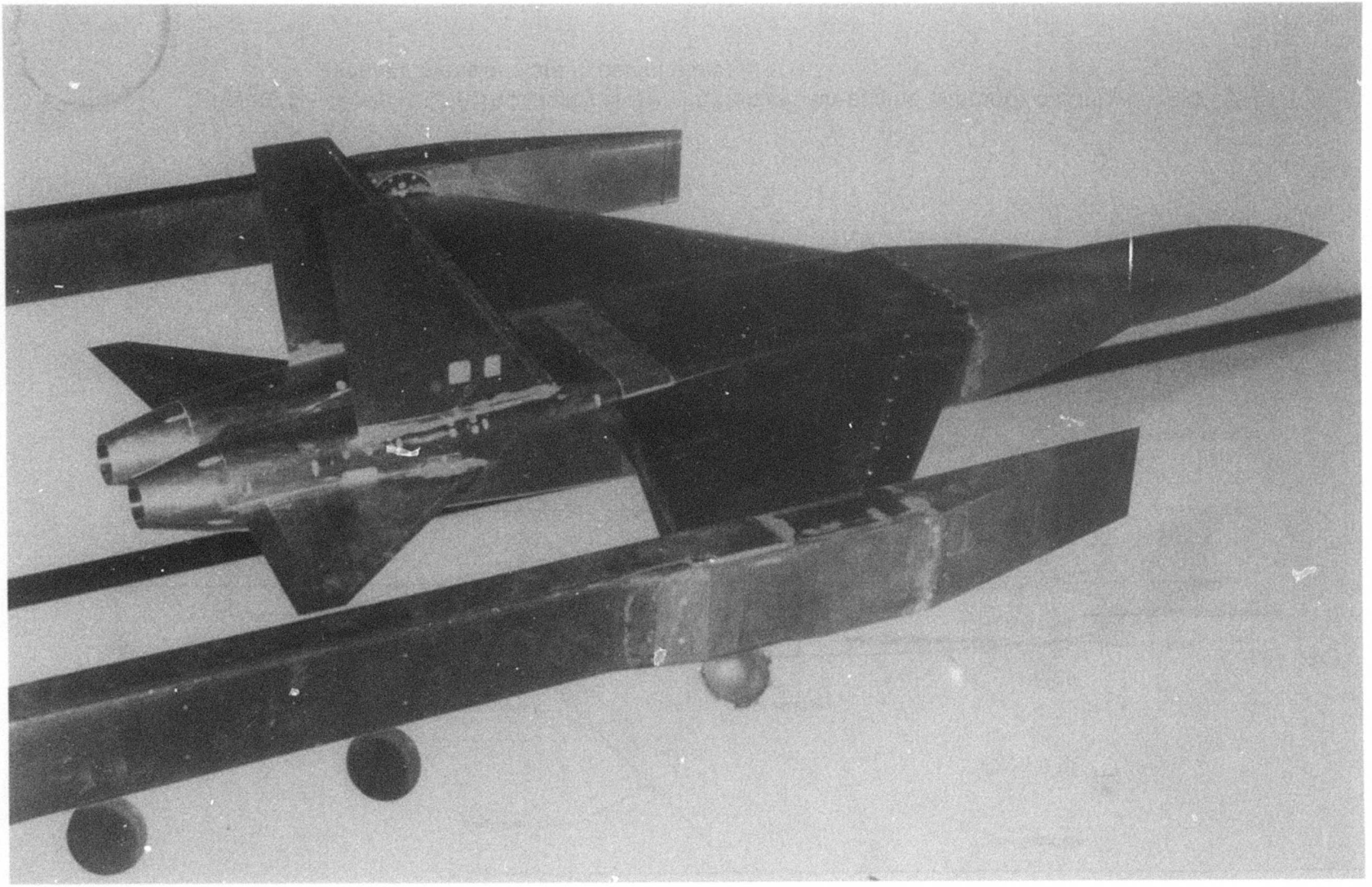


Figure 4.- Photograph of the twin-engine afterbody model installed in the Langley 16-Foot Transonic Tunnel.

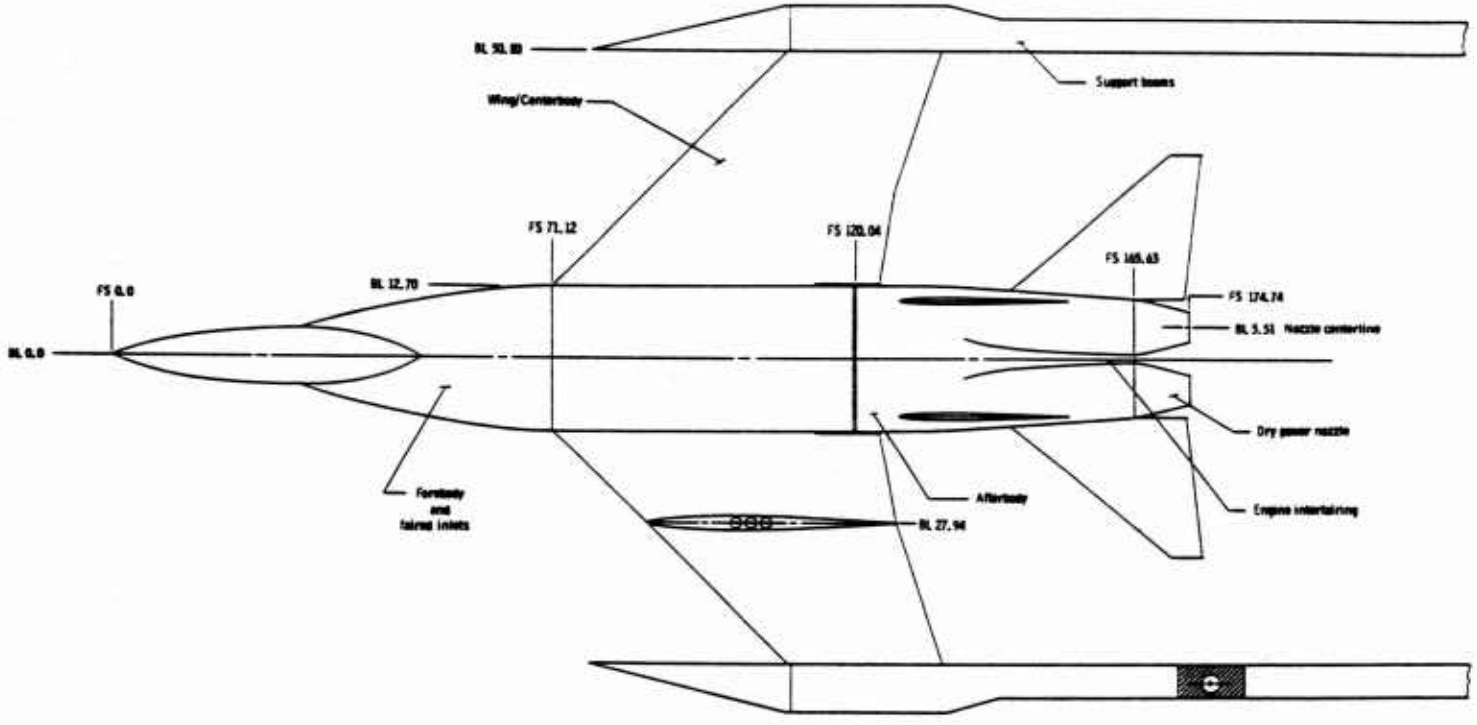
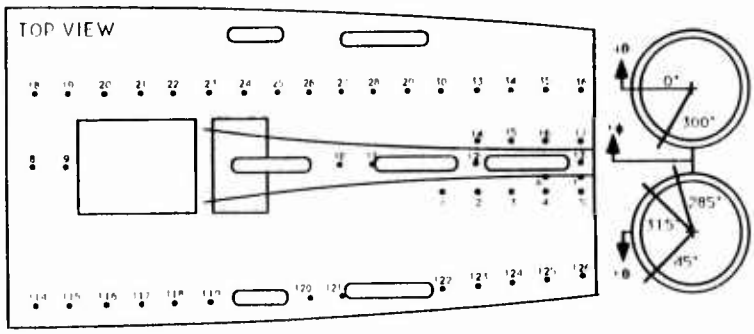
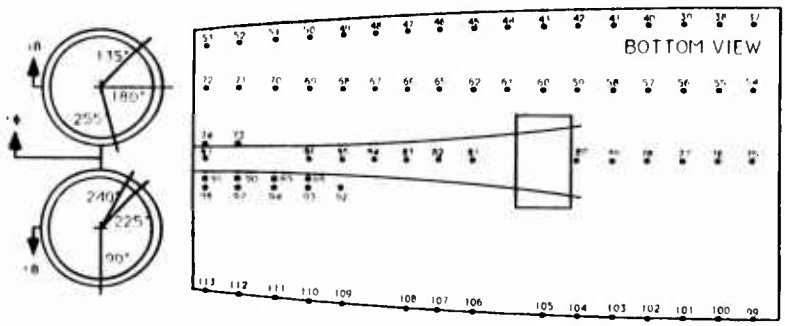


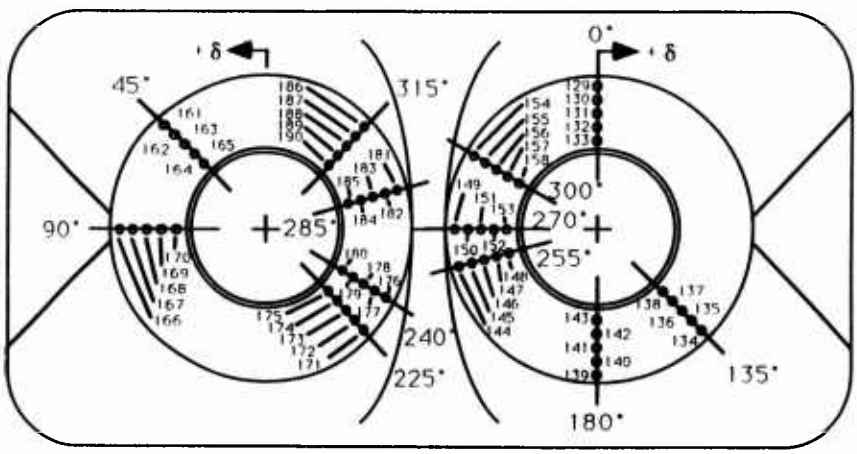

Figure 5.- Sketch of NASA Langley Research Center twin-engine afterbody model with tails. (All linear dimensions are in centimeters)




(a ) Top surface.




(b) Bottom surface.




(c) Nozzles

Figure 6.- Distribution of static pressure orifices on the twin-engine afterbody model.

# STOVL CFD MODEL TEST CASE

KARLIN R. ROTH
NASA AMES RESEARCH CENTER

## 0 INTRODUCTION

The transitional flight characteristics of a geometrically simplified Short Take-Off Vertical Landing (STOVL) aircraft configuration have been measured in the NASA Ames 7- by 10-Foot Wind Tunnel. The experiment is the first in a sequence of tests designed to provide detailed data for evaluating the capability of computational fluid dynamics methods to predict the important flow parameters for powered lift. The model consists of a 60° cropped delta wing planform, a blended fuselage and two circular in-line jets that exit perpendicularly from the flat lower surface. The measured flows have a maximum freestream Mach number of 0.2. Model angle of attack is varied between -10° and +20°. The flow is ambient temperature in both jet exits and the nozzle pressure ratios are varied between 1 and 3. The data presented includes forces and moments, pressures measured at 281 surface pressure ports and the pressures and temperatures of the jets. Measurements of the flow are also made in the tunnel test section upstream and downstream of the model and at the jet exits to guide boundary condition selection for the planned computations. Flow visualization and total pressure measurements in the jet plumes provide a description of the three-dimensional jet efflux flowfield.

## 1 GENERAL DESCRIPTION

| | |
|---|---|
| 1.1 Model name or designation | STOVL CFD Model |
| 1.2 Model type and flow conditions | The STOVL CFD Model consists of a 60° cropped delta wing, a blended fuselage and two circular, in-line jets that exit perpendicularly from the flat lower surface (see Figure 1). Tests were conducted subsonically, with and without lift jets. |
| 1.3 Design requirements, purpose of test | The model was designed and tested for the purpose of validating CFD methods for powered lift applications. The selection of a blended fuselage and a rounded leading edge facilitates computational gridding. Nevertheless, the simplified geometry retains the important aerodynamic and propulsive interactions for powered lift aircraft. |
| 1.4 Dominant flow physics | The dominant flow physics include the interaction of the lift jets with the aerodynamic surface and the wing vortices on the delta wing. The influence of the lift jets and the wing vortices on the surface pressure distribution is illustrated in Figure 2. |
| 1.5 Additional remarks | The data acquired is suitable for CFD validation as well as for limited study of powered lift parameters. |

## 2. DETAILS OF MODEL

| | |
|---|---|
| 2.1 General geometric arrangement | Top and side views of the model are sketched in Figure 1. High pressure air is supplied to the nozzles through the internal plenum. Jet thrust is non-metric. Loads on the aerodynamic shell are metric. |
| 2.2 Configurations tested | Only one set of hardware was tested. However, measurements were made with two model orientations and with and without lift jets.<br>(1) wing mounted vertically without lift jets<br>(2) wing mounted vertically with lift jets<br>(3) wing inverted without lift jets<br>(4) wing inverted with lift jets exhausting vertically<br>A sketch of the wing vertical installation is shown in Figure 3. |

| | |
|---|---|
| 2.3 Wing/airfoil data | |
| 2.3.1 Planform | |
| -Aspect ratio | 1.59 |
| -Taper ratio | 0.13 |
| -Leading edge sweep | 60.00° |
| -Trailing edge sweep | -10.98° |
| -Twist distribution | No twist. |
| -Semispan | 34.290 cm (13.500 in) |
| -Mean aerodynamic chord | 51.592 cm (20.312 in) |
| -Details of tip geometry | Cropped wing with numerically rounded tip |
| -Details of fuselage/wing junction | Blended fuselage wing junction |
| 2.3.2 Basic wing sections | |
| -Airfoil shape | Numerically defined, flat-bottomed airfoil |
| -Thickness/chord ratio | 0.05 |
| -Nose radius/chord | 0.0033 |
| -Leading edge radius | 2.54 mm (0.100 in) at the nose tip and varies smoothly to 0.36 mm (0.014 in) at the wing tips. |
| 2.4 Body data | |
| 2.4.1 Shape | |
| -Nose shape | N/A |
| -Body Length | 76.200 cm (30.000 in) |
| -Cross-sectional details | A typical cross-section, taken at x/c = 0.800, is sketched in Figure 4. The canopy transitions from a 4.445 cm (1.750 in) radius at x = 20.320 cm (8.000 in) to a constant 4.001 cm (1.575 in) fuselage radius for x > 27.986 cm (11.018 in). The fuselage/wing junction is blended with a 3.810 cm (1.500 in) radius fillet. |
| 2.4.2 Additional remarks | None. |
| 2.5 Nozzle Details | The circular jet nozzles have a 3.048 cm (1.200 in) exit diameter. Nozzle length is 4.666 cm (1.837 in) and the contraction ratio is 1.417:1 A perforated plate is placed between the plenum and the nozzle to provide uniform flow distribution at the nozzle exit (see Figure 5). |
| 2.6 Engine/pylon/nacelle data | N/A |
| 2.7 Geometric definition | |
| -Is shape analytically or numerically specified? | The model geometry is numerically specified. Cross-sections from the CAD database are available. |
| -Design or measured coordinates? | Design coordinates are specified. |
| -Tolerances | The CAD database is accurate to ±0.003 cm (±0.001 in) The as-built tolerance is unknown. |
| -Surface roughness | The upper surface of the model is a fiberglass shell and the lower surface is aluminum. Both surfaces are painted and lightly sanded. No additional surface roughness is applied. |

2.8 Model support details

2.8.1 Support geometry

The model support system consists of a vertical support approximately 1.067 m (42.0 in) in total height and a horizontal sting approximately 1.016 m (40.0 in) in length which attaches to the internal plenum at the rear of the STOVL CFD Model. A sketch of the model and its support system installed in the test section is shown in Figure 3. The model support geometry is specified in the design drawings. A numerical database containing the model support geometry also exists.

2.8.2 Special features of mounting

High pressure air is delivered through the sting support system to a 2.540 cm (1.000 in) flow distribution tube located on the centerline of the internal plenum. A series of small holes drilled on either side of the tube create a high pressure drop and help to distribute the flow uniformly along the length of the plenum, equalizing flow in the front and rear nozzles. Instrumentation leads are attached to the outside of the sting.

## 3. GENERAL TUNNEL INFORMATION

3.1 Tunnel designation

NASA Ames 7- by 10-Foot Wind Tunnel, Number 1

3.2 Organization running the tunnel

Full Scale Aerodynamics Division
NASA Ames Research Center

3.3 Tunnel characteristics

-Type of tunnel

Subsonic, closed throat, single return, atmospheric tunnel with approximately 10% air exchange.

-Operating envelope

Maximum operating speed is 483 km/hr (300 mi/hr) or $M < 0.4$

3.4 Test section

3.4.1 General arrangement

See the installation sketch in Figure 3 which is drawn to scale. A humidity sensor is mounted on the tunnel ceiling, near the upstream edge of the test section, approximately 30 cm (1 ft) from the side-wall. No other protruding instrumentation exists upstream of the model except in the quiescient chamber upstream of the test section. A streamlined trapeze, which is used for test section surveys, is retracted to the ceiling at its most downstream position when not in use.

3.4.2 Test section dimensions

The rectangular test section has a constant height of 2.134 m (7.0000 ft) and the width increases linearly from 3.048 m (10.0000 ft) to 3.089 m (10.1335 ft) over the test section length of 4.572 m (15.0000 ft) The turn-table axis is 1.524 m (5.0000 ft) from the start of the test section.

3.4.3 Wall geometry details

-Type of walls

Solid, removable side-walls and roof panels, each containing laser access windows, were used for this test.

-Contraction ratio

14.14:1

-Are wall pressures/wall displacements measured?

Wall pressures were not obtained during this test entry.

-Boundary layer control on walls

No direct boundary layer control is applied on the walls. However, the variation of tunnel width over the length of the test-section provides some allowance for boundary layer growth.

| | |
|---|---|
| -Wall boundary displacement thickness | Based on empty test section data, the wall boundary layer thickness is approximately 15.2 cm (6.0 in) and the displacement thickness is approximately 1.3 cm (0.5 in) in the test section at u = 71.9 m/s (236 ft/s). |
| 3.5 Freestream conditions | |
| 3.5.1 How are reference flow conditions determined for: | |
| -Total pressure | Reservoir static pressure, measured using a 6.985 kPa (1.000 psi) Barocel transducer in the quiescient chamber upstream of the test section, is a reasonable estimate of tunnel total pressure. |
| -Static pressure | Static pressure was measured at the static ring, a series of wall pressure taps located in the contraction cone 31.45 cm (12.38 in) upstream of the test section, using a 6.895 kPa (1.000 psi) Barocel transducer. The difference between the reservoir static pressure and the static pressure is the tunnel dynamic pressure, $q_\infty$. Measured $q_\infty$ is corrected in the test section using the wind-tunnel calibration data. |
| -Total temperature | Temperature is measured in the quiescient chamber upstream of the test section. |
| -Relative humidity | A humidity sensor is located near the upstream edge of the test section. |
| 3.5.2 Tunnel calibration | |
| -How was tunnel calibrated? | Pressure probe and hot wire surveys made on the tunnel centerline as well as some limited off-centerline flow surveys were reported. Some unsteady measurements were also reported. See Ref. 1. |
| -Date of last calibration | Tunnel calibration data was acquired in 1987 and is reported in Ref. 1. A new calibration of the test section dynamic pressure was made in August 1992. |
| 3.6 Empty tunnel flow quality | |
| 3.6.1 Flow uniformity | |
| -Static pressure variations over model length and span | A small favorable pressure gradient, $\Delta C_p$ = -0.005, exists over the first 3.048 m (10.000 ft) of the test section. $\Delta p_s/q_\infty$ is less than ±0.2% over the model span. |
| -Velocity variation in the test section | $\Delta q/q_\infty$ is less than 0.30% or $\Delta u/u_\infty$ is less than 0.15% across the test section. |
| -Flow meander during a run | Low frequency unsteadiness in the tunnel dynamic pressure at constant fan rpm, $\Delta q/q_\infty$, is less than ±1%. |
| -Variation of angularity across the test section | Flow angularity was measured using a 5-hole pressure probe to make vertical and lateral surveys at the test section centerline. $\Delta\alpha$ = ±0.1° and $\Delta\beta$ = ±0.5° |
| 3.6.2 Temperature variation | |
| -Temperature control during run | Tunnel temperature is not controlled. Jets are maintained at ambient temperature which is approximately 21°C (70°F). |
| -Variation within the tunnel | Not known. |

| | |
|---|---|
| -Variation over a run | Tunnel temperature variation depends on the air exchange, jet temperature and run length. For a typical run lasting 1 to 2 hours during the STOVL CFD Model test, temperature increased approximately 3 to 6°C (5 to 10°F) |
| 3.6.3 Flow unsteadiness | |
| -Overall turbulence level | $e'/u_x$ = .77% at 30 m/s (100 ft/s)<br>$e'/u_x$ = .94% at 91 m/s (300 ft/s) |
| -Overall noise level ($C_p$-RMS) | Not known. |

## 4. INSTRUMENTATION

| | |
|---|---|
| 4.1 Model position | |
| 4.1.1 How is geometrical incidence measured? | For the wing vertical installation, angle of attack is varied by rotating the turntable; a resolver is used to obtain the incidence.<br><br>For the wing horizontal installation, the model remained in a fixed position for all measurements. This position was measured with a digital protractor and with a hand held bubble protractor. |
| 4.1.2 Accuracy of geometrical incidence | The accuracy of the yaw resolver is 0.05°.<br><br>Model incidence accuracy is 0.1° for the inverted wing. |
| 4.2 Model pressure measurements | |
| 4.2.1 Total number and disposition | 281 pressure ports are located on the model surface with 88 taps on the upper surface, 63 taps clustered radially near the front jet, 62 taps clustered radially near the rear jet and the remaining taps distributed on the lower surface. See Figure 6 for the pressure tap layout. |
| 4.2.2 Range and accuracy of pressure transducers | All pressure tubing and six, 48 port electronically scanned pressure modules were internal to the STOVL CFD Model. Transducer ranges were chosen by estimating the expected pressures to be acquired on the model. Pressures were measured with better than 0.1% full scale accuracy using transducers ranging from 2.491 kPa (10 inches of water) in the expected low pressure regions to 17.24 kPa (2.50 psi) transducers in the regions near the jet exits. Specifically, the selected range of modules included one module at 2.491 kPa (10 inches of water), two modules at 4.982 kPa (20 inches of water), two 6.895 kPa (1.000 psi) modules and one 17.24 kPa (2.50 psi) module. |
| 4.2.3 Unsteady pressures | Unsteady pressures were measured at 16 pressure port locations. Most of these ports were located near the jet exits (7 symmetry plane locations and 6 off-symmetry plane locations) to gather information on jet-induced unsteadiness. |

4.3 Force and moment measurements

4.3.1 Type and location of balance

-Aerodynamic loads

A 2.54 cm (1.00 in), six-component force balance was installed in the STOVL CFD Model to measure aerodynamic loads on the model surface. The balance center is located 37.465 cm (14.750 in) from the model nose tip.

-Jet thrust

The jets were calibrated in an independent test by mounting the internal plenum and nozzles on a calibration rig instrumented with a 3.81 cm (1.50 in) , six-component force balance.

4.3.2 Range/accuracy

-Aerodynamic loads

For the 2.54 cm (1.00 in) balance installed in the model, gauge limits are 890 N (200 lb) for the normal, axial and side forces and 271 N-m (200 ft-lb) for the rolling moment. An accuracy of 0.5% full scale gauge limit was attained during the tests.

-Jet Thrust

For the 3.81 cm (1.50 in) balance used for nozzle calibration, the gauge limits are 2224 N (500 lb) for the normal, 1334 N (300 lb) for the axial (thrust direction) and 1112 N (250 lb) for the side gauges and 91 N-m (67 ft-lb) for the rolling moment. An accuracy of 0.5% full scale gauge limits was attained.

4.4 Boundary layer and flowfield measurements

4.4.1 Measurement technique applied

-Nozzle instrumentation

Each of the jet nozzles contains a total temperature probe and a reference pressure port. All nozzle pressure measurements were made using 690 kPa (100 psia) pressure transducers.

-Pressure probe measurements

A micropitot probe instrumented with a 690 kPa (100 psia) transducer was used to survey the jets in the exit plane and at selected locations above the jet exits to determine the jet exit profile and decay of the jet core for static tunnel conditions.

A 5-hole pressure probe instrumented with 6.895 kPa (1.000 psid) pressure transducers was used for flowfield surveys.

4.4.2 Flow regions investigated

-Jet plumes

Jet plume measurements were made with $q_\infty$ = 0.0 kPa. Micropitot surveys were made in the jet exit plane with a spacing of $\Delta x = \Delta y$ = 2.54 mm (0.10 in). Vertical surveys were made at the center of the nozzle. Symmetry plane surveys were made at locations 1, 2, 4 and 8 jet diameters above the nozzle exit.

-Farfield

Measurements were made using a five-hole probe in the symmetry plane and in several planes perpendicular to the freestream. Measurement planes were located at 0.96, 0.98 and 1.00 chords and at 1.46, 1.48, 1.50 chords downstream of the model. Some surveys were also made upstream and to the side of the model. These measurements are expected to guide the selection of appropriate computational boundary conditions.

4.4.3 Details of probe and probe supports

All probes were mounted on the wind tunnel survey rig using probe mounts to extend the probe tip approximately 79 cm (31 in) ahead of the rig to eliminate rig interference on the probe measurement. Positioning accuracy for the probes positioned using the facility survey rig was determined by a survey rig calibration immediately preceding the STOVL CFD Model tests. Positioning accuracy for the probes was 0.3 mm (0.01 in) for the nozzle surveys and 1.3 mm (0.05 in) for surveys across the test section.

4.5 Surface flow visualization

Not used

4.6 Flowfield visualization

4.6.1 Measurement technique applied

Schlieren and laser light sheet were used.

4.6.2 Visualized planes in the flow

Schlieren photos were taken in the symmetry plane while the laser light sheet was used in the cross plane.

4.6.3 Data available in what form

Photographs of the visualization are available.

## 5 TEST MATRIX AND CONDITIONS

5.1 Detailed test matrix

5.1.1 Number of selected test cases

One test case includes force and pressure measurements as well as detailed flow surveys and is suitable for CFD validation. This "detailed case" is representative of decelerating transition or short landing conditions. In addition, force and pressure measurements for the model through a range of angles of attack are presented for 30 combinations of freestream Mach number and jet nozzle pressure ratio. Table 1 summarizes the range of test parameters and defines the detailed case.

5.1.2 Number of configurations tested

Tests were conducted with and without lift jets. Also, two installations of the same hardware were tested. Configurations are defined in Section 2.2

5.1.3 Test matrix table

A summary of the measured conditions without lift jets is presented in Table 2. Table 3 presents the test matrix for configuration (2).

5.2 Model / tunnel relations

5.2.1 Maximum blockage

Maximum test section blockage for the model and its support system is approximately 2% at $\alpha$=20°.

5.2.2 Model span/tunnel width

Model span / tunnel width = 0.23
Model span / tunnel height = 0.32

5.2.3 Wing area/tunnel cross section

Wing area / tunnel cross section = 0.05

5.2.6 Have adiabatic wall temperatures been reached?

Not known.

5.3 Transition Details

5.3.1 Free or fixed transition

Free transition.

5.3.2 Details of free transition

Transition was not verified

5.3.3 Details of fixed transition

N/A

## 6 DATA

| | |
|---|---|
| 6.1 Data Availability | |
| 6.1.1 Organization owning data | U.S. Government / NASA Ames Research Center |
| 6.1.2 Person responsible for the data | Name / title: Dr. Karlin R. Roth<br>Aerospace Engineer<br>Fixed Wing Aerodynamics Branch<br><br>Address: Mail Stop 247-2<br>NASA Ames Research Center<br>Moffett Field, CA 94035-1000<br><br>Telephone: (415) 604-6678<br>FAX: (415) 604-3489 |
| 6.1.3 Are data freely available | Yes. |
| 6.1.4 If no, who should be contacted | N/A |
| 6.2 Suitability of data for CFD validation. | |
| 6.2.1 Are data suitable for "in-tunnel"calculation? | Yes. |
| 6.2.2 Are data corrected to simulate "free-air" conditions? | No. |
| 6.3 Type and form in which data are available. | |
| 6.3.1 Type and form | Freestream conditions - Engineering Units<br>Jet exit conditions - Engineering Units<br>Forces and moments - Coefficients<br>Surface pressures - Coefficients<br>Flow survey data - Engineering Units |
| 6.3.2 Data carrier | Data will generally be available in printed or graphical form. Some force and pressure data is available on 8.9 cm (3.5 in) floppy disk from a Macintosh computer. |
| 6.3.3 Extent of geometric data | Geometric data for 177 cross-sections has been extracted from the design database and requires 2500 blocks of storage on a Microvax computer. A subset of this database containing less than 50 cross-sections resides on a Macintosh computer and is suitable for computational gridding. |
| 6.3.4 Extent of aerodynamic data | Full database requires 45000 blocks of storage on a VAX computer. However, only a subset of this database will be available. |
| 6.4 Corrections applied to data | The data is currently uncorrected. |

## 7 DATA ACCURACY AND REPEATABILITY ASSESSMENT

| | |
|---|---|
| 7.1 Accuracy Estimates | |
| 7.1.1 Freestream conditions | |
| -Dynamic pressure | ±14 Pa (±0.3 psf) |
| -Model incidence | Wing vertical: 0.05°<br>Wing inverted: 0.1° |
| 7.1.2 Measured data | |
| -Forces and moments | 0.5% full scale gauge limit |
| -Pressures | 0.1% full scale |

| | |
|---|---|
| 7.2 Repeat Measurements | |
| 7.2.1 Type and number of repeat measurements within one test campaign | Approximately 3 repeat points were taken during each run sequence with the wing mounted vertically. Repeat runs were made and are noted in Table 2. Multiple force and pressure measurements were repeated while flow surveys were made with the model inverted. Selected pressure probe measurements, flow visualization and unsteady surface pressure measurements were also repeated during this phase of the test. |
| 7.2.2 Type and number of repeat measurements in successive campaigns | Only one test entry has been completed. |
| 7.3 Redundant measurements | |
| 7.3.1 Flow quantities | Compared force measurements with integrated pressure distribution<br>Compared nozzle instrumentation readings with schlieren photos and jet exit surveys |
| 7.3.2 Checks on data consistency | The repeat runs described above were used. |
| 7.4 Other tests on same geometry | |
| 7.4.1 Same model (in other facilities) | To date, only one test entry has been made using this model. |
| 7.4.2 Similar models tested in other facilities. | (1) Tests were conducted in the NASA Langley 14- by 22-Foot Wind Tunnel (Ref. 3) to investigate the jet-induced effects on a planform identical to the STOVL CFD Model using the same jet nozzles and internal plenum. Only the upper surface differed from the present STOVL CFD Model geometry. Data from both tests follow similar trends.<br><br>(2) A water tunnel test of a similar configuration at roughly 1/3 scale is reported in Ref. 4. |

## 8 REFERENCES


| | |
|---|---|
| 8.1 On the wind tunnel | [1]Wadcock, A., "The NASA Ames 7-Foot by 10-Foot Wind Tunnel-- Present Flow Quality and Recommendations for Improvement," Analytical Methods Report 8705, July 1987. |
| 8.2 On the model | [2]Roth, K. R., "A Powered Lift Experiment for CFD Validation," AIAA Paper 91-1731, June 1991. |
| 8.3 On similar models | [3]Kuhn, R. E. and Stewart, V. R., "Effect of Forward Speed and Jet Arrangement on Jet Induced Suckdown and Fountain Effects,", KSA Report 92-2, Apr. 1992.<br><br>[4]Miller, L. S., Papadakis, M. and Klausmeyer, S., "Flow Visualization fro a STOVL Aircraft in Ground Proximity," AIAA Paper 91-0769, Jan. 1991. |

## 9 LIST OF SYMBOLS

| | |
|---|---|
| b | Wing span, 68.580 cm (27.000 in) |
| c | Chord length, 76.200 cm (30.000 in) |
| e' | Turbulence intensity, $\left[\frac{1}{3}\left(\overline{u}'^2 + \overline{v}'^2 + \overline{w}'^2\right)\right]^{0.5}$ |
| NPR | Nozzle pressure ratio, $p_{t,j} / p_a$ |
| $p_t$ | Total pressure, kPa (psf) |
| p | Pressure, kPa (psf) |
| q | Dynamic pressure, kPa (psf) |
| u,v,w | Cartesian velocity components, m/s (ft/s) |
| x,y,z | Cartesian design coordinate system with origin at model nose tip, x is streamwise and y is spanwise coordinate, cm (in) |
| $V_e$ | Effective velocity ratio, $(q_\infty/q_j)^{0.5}$ |
| $\alpha$ | Angle of attack, degrees |
| $\beta$ | Yaw angle, degrees |
| Subscripts | |
| j | Jet |
| $\infty$ | Freestream |

Table 1. Test Parameters.

| VARIABLE | RANGE | DETAILED CASE |
|---|---|---|
| Number of jets | 0, 1 or 2 | 2 |
| Angle of attack, $\alpha$ | -10° to +20° | +10° |
| Yaw, $\beta$ | 0° to 5° | 0° |
| Freestream dynamic pressure, $q_\infty$ | 0.48 kPa to 2.39 kPa | 1.44 kPa |
| Freestream Mach number, $M_\infty$ | 0.08 to 0.18 | 0.14 |
| Nozzle pressure ratio, NPR | 1.0 to 3.3 | 1.9 (Front nozzle)<br>2.0 (Rear nozzle) |
| Effective velocity ratio, Ve | 0, 0.05 to 0.32, $\infty$ | 0.15 (Front nozzle)<br>0.14 (Rear nozzle) |

Table 2. Test Matrix for Configuration (1)

| $q_\infty$ (kPa) | $\alpha$ (degrees) | Remarks |
|---|---|---|
| 0.72 | -10 to +20 | (R), (a) |
| 0.96 | -10 to +20 | |
| 1.20 | -10 to +20 | |
| 1.44 | -10 to +20 | |
| 1.68 | -10 to +20 | |
| 1.92 | -10 to +18 | (b) |
| 2.15 | -10 to +10 | |
| 2.39 | -10 to +12.5 | |

Remarks: (R) denotes repeat runs.
(a) $\alpha$ varies from -10° to +20° with a 2.5° increment.
(b) $\alpha$ range is limited by model forces for $q_\infty \geq 1.92$

Table 3. Test Matrix for Configuration (2)

| $q_\infty$ (kPa) | α (degrees) | NPR Front Nozzle | NPR Rear Nozzle | Ve Front Nozzle | Ve Rear Nozzle | Remarks |
|---|---|---|---|---|---|---|
| 0.00 | 0 | 1.3 to 3.1 | 1.4 to 3.3 | 0.00 | 0.00 | |
| 0.00 | 0 | 2.1 | 2.3 | 0.00 | 0.00 | (R), (a), (b) |
| 0.00 | 0 | 1.4 to 3.1 | 1.4 to 3.3 | 0.00 | 0.00 | (R), (c) |
| 0.72 | 0 to 10 | 1.3 | 1.4 | 0.17 | 0.14 | |
| 0.72 | 0 to 10 | 1.6 | 1.7 | 0.13 | 0.11 | |
| 0.72 | -10 to +20 | 1.8 | 2.0 | 0.11 | 0.10 | |
| 0.72 | -10 to +20 | 2.2 | 2.3 | 0.10 | 0.09 | |
| 0.72 | -10 to +20 | 2.5 | 2.6 | 0.09 | 0.08 | |
| 0.96 | -10 to +20 | 1.5 | 1.6 | 0.16 | 0.13 | |
| 0.96 | -10 to +20 | 2.1 | 2.3 | 0.11 | 0.10 | |
| 1.20 | -10 to +20 | 1.8 | 2.0 | 0.15 | 0.13 | |
| 1.20 | -10 to +20 | 2.1 | 2.3 | 0.13 | 0.11 | |
| 1.20 | -10 to +20 | 2.4 | 2.6 | 0.11 | 0.10 | |
| 1.44 | -10 to +20 | 1.9 | 2.0 | 0.16 | 0.14 | (d) |
| 1.44 | -10 to +20 | 2.2 | 2.3 | 0.14 | 0.12 | |
| 1.44 | 0 | 1.3 to 3.0 | 1.4 to 3.3 | 0.24 to 0.11 | 0.20 to 0.09 | (e) |
| 1.68 | -10 to +20 | 2.4 | 2.7 | 0.13 | 0.12 | (R) |
| 1.92 | -10 to +15 | 2.1 | 2.3 | 0.16 | 0.14 | (R) |
| 2.15 | -10 to 15 | 2.4 | 2.6 | 0.15 | 0.13 | |
| 2.15 | 0 to 10 | 2.8 | 2.9 | 0.14 | 0.13 | |
| 2.39 | -10 to +15 | 1.8 | 2.0 | 0.20 | 0.18 | |
| 2.39 | -10 to +10 | 2.1 | 2.3 | 0.18 | 0.16 | (R) |
| 2.39 | -10 to +10 | 3.1 | 3.3 | 0.13 | 0.12 | |
| 2.39 | 0 | 1.3 to 3.1 | 1.4 to 3.3 | 0.32 to 0.14 | 0.26 to 0.12 | (e) |
| 1.44 to 2.39 | 0 | 2.1 | 2.3 | 0.14 to 0.18 | 0.12 to 0.16 | (f) |

Remarks: (R) denotes repeat runs.

(a) α is varied between -10° and +20° with a 5° increment. $\Delta\alpha = 2.5°$ for some sequences.

(b) probe surveys in the symmetry plane at the nozzle exit plane

(c) pressure probe measurement in the nozzle exit plane at the center of the nozzle

(d) conditions selected for detailed measurement in configuration (4)

(e) NPR increased in increments of approximately 0.3, Ve decreases due to change in NPR

(f) $q_\infty$ increased in increments of 0.12 kPa, Ve increases due to change in $q_\infty$

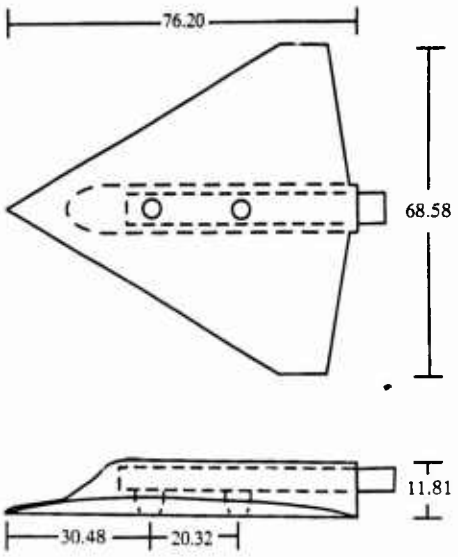
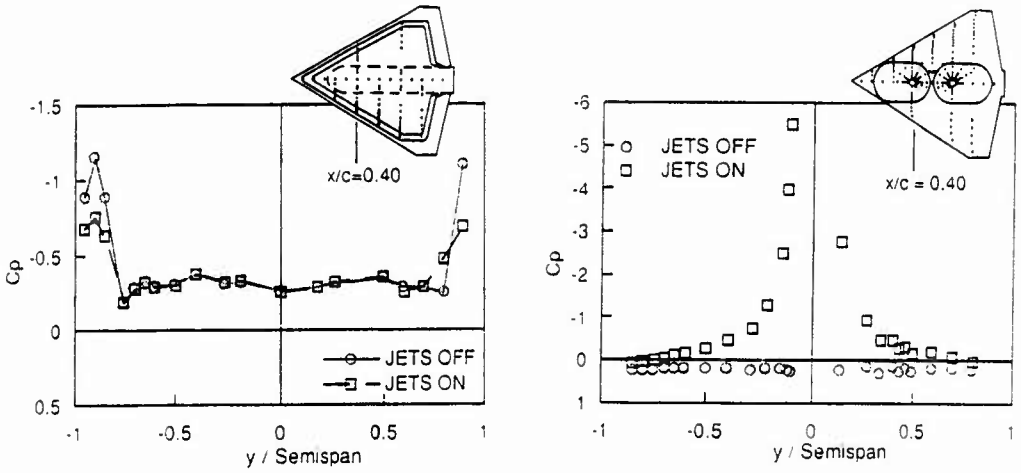



Fig. 1 Sketch of the STOVL CFD Model. Top and side views.
Dimensions are in centimeters.




a) Upper surface pressures.

b) Lower surface pressures.

Fig. 2 Measured surface pressure distribution at x/c = 0.40
$M_\infty$ = 0.14, $\alpha$ = 10°, NPR (Front jet) = 1.85, NPR (Rear jet) = 2.00

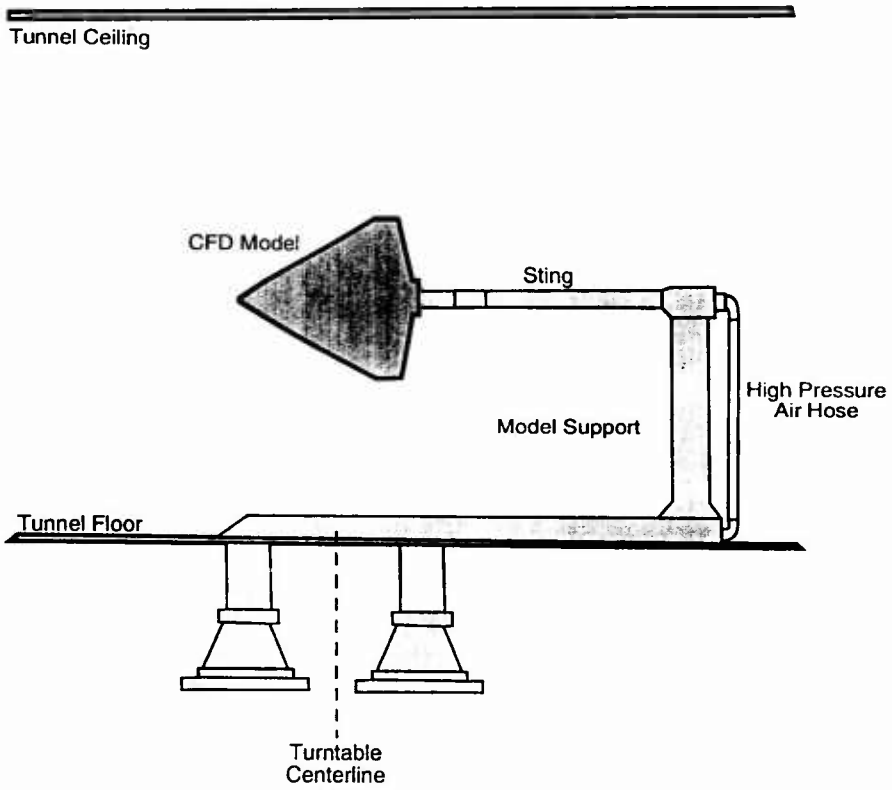



Fig. 3 STOVL CFD Model installed in the NASA 7-by 10-Foot Wind Tunnel. Wing mounted vertically.

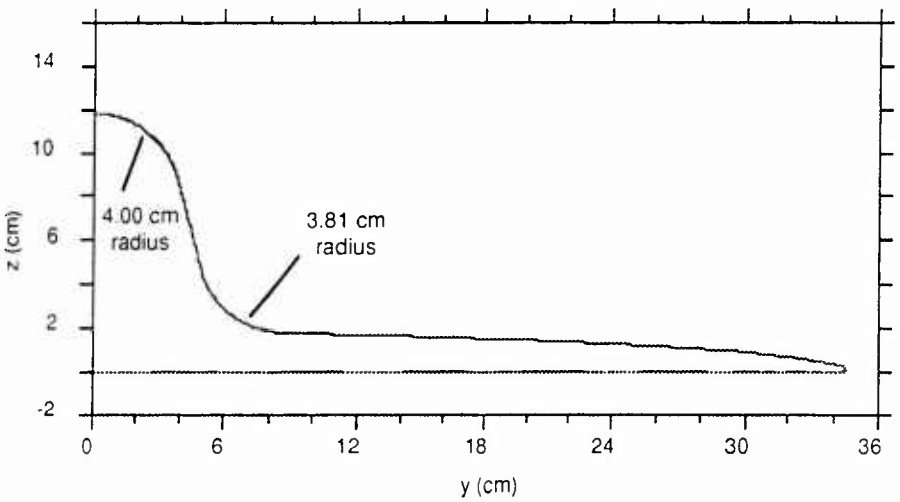



Fig. 4 Typical cross-section taken at x/c = 0.80. The positive half-plane is sketched for the symmetric model.

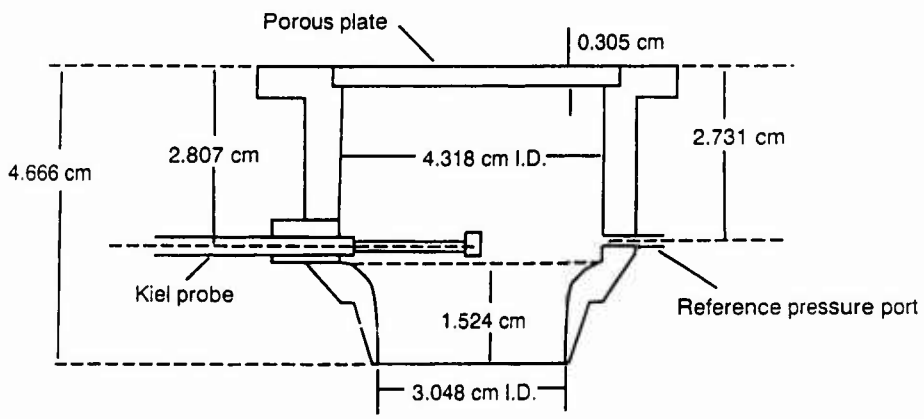



**Fig. 5 Details of instrumented nozzle.**

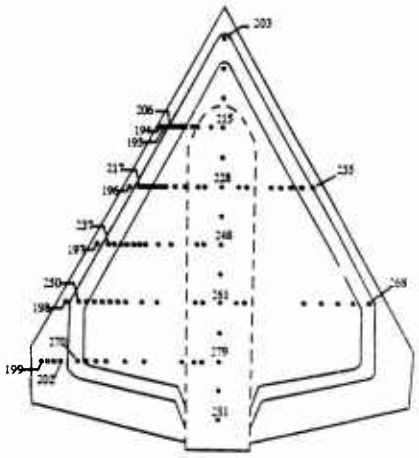


Fig. 6a Instrumented top surface.

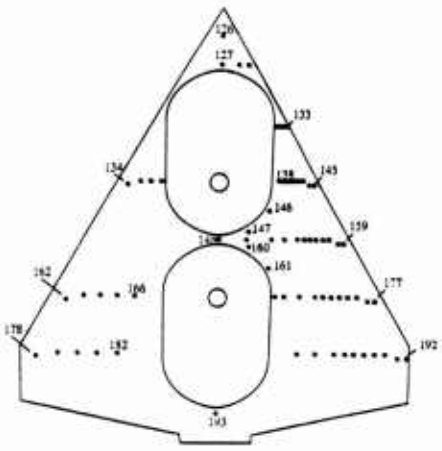
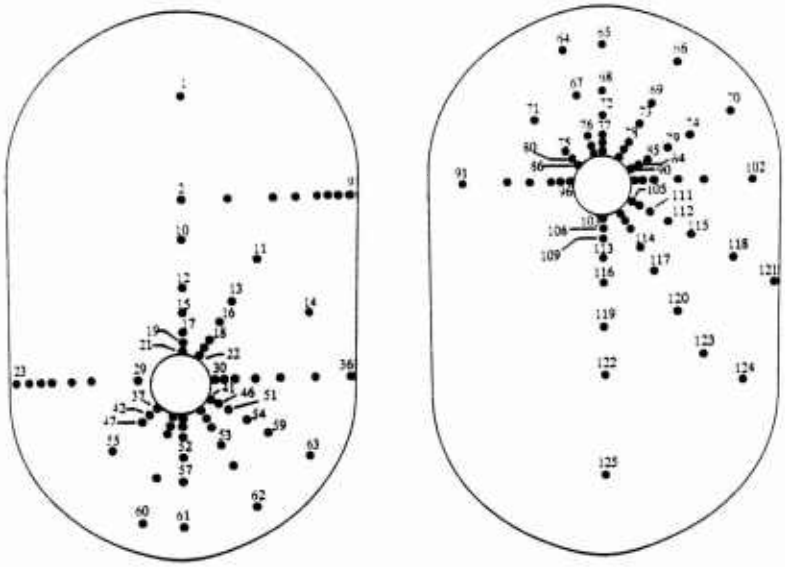


Fig. 6b Instrumented lower surface.



Forward plate

Aft Plate

Fig. 6c Instrumented nozzle plates.

# LOW SPEED PROPELLER SLIPSTREAM AERODYNAMIC EFFECTS

I. Samuelsson
FFA, The Aeronautical Research Institute of Sweden
P.O. Box 11021, S-16111 Bromma
SWEDEN

## SUMMARY

The data presented in this contribution to AGARD WG-14: "EXPERIMENTAL TEST CASES FOR CFD VALIDATION" were obtained at tests in the FFA Low Speed Wind Tunnel LT1 (diameter 3.6 m) as part of an aeronautical research programme sponsored by the Swedish Board for Technical Development (STU). The intent of the experiment was twofold: a) to gain some physical insight to the complex aerodynamic interference phenomena occuring when the slipstream from a highly loaded propeller washes downstream located surfaces (nacelle and wing); b) to provide surface pressures and flow field data for evaluation of three-dimensional flow computation methods.

The performed wind tunnel tests show that in high power conditions at low speeds large asymmetrical loads can develop on the nacelle and on the wing. For e.g. an aircraft with two propellers having the same sense of rotation these loads do not cancel out but combine to a net increase in asymmetrical loads (in particular side force and yawing moment). These effects, if not known or accounted for in advance, could lead to a resizing of the aircraft control surfaces and/or necessary trim changes with subsequent increased trim drag.

## INTRODUCTION

The test setups represented propeller, nacelle and a schematic wing layout with a wing span of about 3.2 propeller diameters, that is, only the aerodynamic surfaces closest to the propeller slipstream were set up in the tests (no tail). The 1:5 scale propeller (diameter = 0.64 m) is considered to be typical of modern medium speed turboprop commuter aircraft. Four different configurations were tested:

1) propeller + axisymmetrical nacelle (no wing);
2) propeller + axisymmetrical nacelle + symmetrical mid-wing;
3) propeller + 'high' nacelle (no wing);
4) propeller + 'high' nacelle + symmetrical low wing.

Each of these configurations represents a selected test case at one and the same power condition:

thrust coefficient $C_T = 0.23$
power coefficient $C_P = 0.23$
advance ratio $J = 0.7$
angle of attack $\alpha = 0°$ (no sideslip).

The wind tunnel measurements included wing and nacelle surface static pressures, propeller thrust and shaft torque (by means of a rotating two-component balance) and flow field velocities and pressures (by means of a traversing five-hole probe).

During the tests there were some concern about the consistency of the rotating two-component (thrust and torque) balance used. In order to check this, the slipstrean flow field immediately downstream of the propeller disk, as measured by means of the radially traversing five-hole probe, was integrated for both thrust and torque and good agreement was found between the balance values and the integrated probe data. For more details of the comparisons between the balance and probe measurements, see Ref [4] and [5].

The data set included in this report (on diskettes) comprises distributions of static pressures (on nacelle and wing) and slipstream flow field data (three velocity components, total and dynamic pressures) in at least three axial planes (perpendicular to the propeller axis) obtained by means of radially traversing five-hole pressure probe. Also some limited prop/off data (surface pressure and flow field data) are included in the data set.

The original test programme also included variation of angles of attack and sideslip and variation of the propeller power setting (thrust, power and advance ratio), but no results from this are included in the data set. These data can however be made available from FFA upon request.

## CONTENTS

1 GENERAL DESCRIPTION

2 DETAILS OF MODELS

3 GENERAL TUNNEL INFORMATION

4 INSTRUMENTATION

5 TEST MATRIX AND CONDITIONS

6 DATA

7 DATA ACCURACY AND REPEATABILITY ASSESSMENT

8 REFERENCES

9 LIST OF SYMBOLS

FIGURE CAPTIONS
TABLES
FIGURES
4 DATA DISKS:

No. 1: AGARD WG-14, TEST CASE: SW-4 (1)
No. 2: AGARD WG-14, TEST CASE: SW-4 (2)
No. 3: AGARD WG-14, TEST CASE: SW-4 (3)
No. 4: AGARD WG-14, TEST CASE: SW-4 (4)

DISK DATA DESCRIPTION

## 1 GENERAL DESCRIPTION

| | | |
|---|---|---|
| 1.1 | Model name or designation | LOW SPEED PROPELLER SLIPSTREAM AERODYNAMIC EFFECTS |
| 1.2 | Model type, flow conditions | Isolated nacelles (axisymmetrical, high)<br>Nacelle/wing (symmetrical) combinations<br>Propeller (scale 1:5) (model propeller diameter =0.64 m)<br>Subsonic freestream: 50 m/s<br>Propeller power setting: $N$ = 6650 RPM, $C_T$ = 0.23, $C_P$ = =0.23, $J$ = 0.7 |
| 1.3 | Design requirements, purpose of test | Investigation of high power slipstream induced aerodynamic effects (asymmetrical loads) on nacelle and wing. |
| 1.4 | Dominant flow physics (see Figures 1a,b) | Complex interaction of the swirling propeller slipstream (with increased total pressures and velocities) with downstream located aerodynamic surfaces. |
| 1.5 | Additional remarks | Propeller thrust and torque measured by means a rotating 2-component balance.<br>Surface static pressure measurements (nacelle and wing).<br>Some prop/off measurements exist ( static pressures and flow field surveys). |

## 2 DETAILS OF MODELS

| | | |
|---|---|---|
| 2.1 | General geometric arrangement | See Figure 2 |
| 2.2 | Various configurations | Four different nacelle/wing combinations, see Figure 3:<br>CONF1: isolated axisymmetrical nacelle<br>CONF2: axisymmetrical nacelle with symmetrical mid-wing<br>CONF3: isolated high nacelle<br>CONF4: high nacelle with symmetrical low wing |
| 2.3 | Wing and airfoil data | See Figure 4 |
| 2.3.1 | Planform | Rectangular |
| | • Aspect ratio | 4.12 |
| | • Taper ratio | 1.0 |
| | • Leading edge sweep | 0° |
| | • Trailing edge sweep | 0° |
| | • Twist distribution | No twist |
| | • Semispan | 1.03 m (span=2.06 m) |
| | • Details of wing tip geometry | Hoerner tip |
| | • Details of nacelle/wing junction | No blending (only tape fairing) |
| 2.3.2 | Basic wing section | NACA $63_{(10)}$A-012 (scaled up NACA 63A-010) |
| | • Airfoil shape | See Figure 4 |
| | • Thickness chord ratio | 12 % |
| | • Nose radius/chord | 1.068 % |
| 2.3.3 | Other components on wing | None |
| 2.4 | Body data | -(not applicable) |
| 2.5 | Information on fins, canard wings and/or vertical/horizontal tal surfaces | -(not applicable) |
| 2.6 | Engine/pylon/nacelle data | |
| 2.6.1 | Engine | Hydraulic propeller drive motor (located inside nacelle) |
| 2.6.2 | Pylon | None |
| 2.6.3 | Nacelle | See Figure 5a for geometry, Figure 5b for nacelle coordinates. Note: the middle part of the high nacelle (CONF3 and CONF4) is composed by plane sides (completely faired-off air inlet) |
| 2.7 | Geometric definition of all components | |
| | • Is shape analytically or numerically specified? | Numerically |
| | • Design or measured coordinates | Design (nominal coordinates) |

| | | |
|---|---|---|
| | • Tolerances | Estimated: Nacelle ±1 mm (shape), ±3 mm (position); wing: ±0.5 mm (shape), ±1° (sweep and dihedral) |
| | • Surface roughness | Estimated: Nacelle and wing: ±0.1 mm |
| 2.8 | Model support details | |
| | 2.8.1 Sting and support geometry | See Figures 6a,b |
| | 2.8.2 Special features of mounting | Steel tubes for hydraulic oil inside the aft sting. Hydraulic hoses connected to the sting steel tubes at rearmost end of the sting frame. The hydraulic hoses were drawn vertically from the rear end of the sting frame down through the wind tunnel floor to a hydraulic pump. |
| **3** | **GENERAL TUNNEL INFORMATION** | |
| 3.1 | Tunnel designation | FFA Low Speed Wind Tunnel LT1 |
| 3.2 | Organisation running the tunnel | FFA (Flygtekniska Försöksanstalten), The Aeronautical Research Institute of Sweden |
| 3.3 | Tunnel characteristics | |
| | • Type of tunnel | Low speed closed circuit wind tunnel with drive fan (electrical motor) |
| | • Indicate operating envelope | Maximum speed ≈ 85 m/s |
| | • Minimum run time | No time limits |
| 3.4 | Test section | |
| | 3.4.1 Model mounted in the test section | See Figure 7 |
| | 3.4.2 Test section dimensions | Circular, diameter 3.6 m, length 8 m |
| | 3.4.3 Wall geometry details | |
| | • Type of walls | Solid |
| | • Open area ratio | ≈ Zero |
| | • Are wall pressures/wall displacements measured? | No |
| | • Boundary layer control on walls | None |
| | • Typical wall boundary layer displacement thickness | 0.01-0.02 m (estimated) |
| 3.5 | Freestream conditions | |
| | 3.5.1 How are reference flow conditions determined for: | |
| | • Total pressure | Total pressure = static pressure + dynamic pressure |
| | • Static pressure | Test section static pressure is equal to atmospheric (ambient) pressure; the test section is ventilated to atmosphere |
| | • Static temperature | By means of measured total temperature (temperature probe) |
| | 3.5.2 Tunnel calibration | |
| | • How was the tunnel calibrated? | By means of flow field surveys in the test section (flow angles and dynamic pressures) |
| | • Date of latest calibration | 1982 |
| 3.6 | Flow quality (empty tunnel) | |
| | 3.6.1 Flow uniformity | |
| | • Static pressure variations over model length and span | Propeller disk: ≈±0.25 % of free stream dynamic pressure<br>Nacelle length: ≈ 0.5 % of free stream dynamic pressure<br>Wing span: ≈ 0.9 % of free stream dynamic pressure |
| | • Velocity varition during a run | ≈ 0.5 % |
| | • How is average flow angularity determined? | Average of flow angles over model span and length |
| | • Variation of flow angularity over the model length and span | Propeller, nacelle length: $\lvert\Delta\alpha\rvert,\lvert\Delta\beta\rvert \leq 0.3°$<br>wing span: $\lvert\Delta\alpha\rvert,\lvert\Delta\beta\rvert \leq 0.5°$ |
| | 3.6.2 Temperature variation | |
| | • Can the temperature be controlled during a run? | No |
| | • Variation within the tunnel | Not known |
| | • Variation over a run | Dependent on run time, typical increase: less than 5°C |

| | | |
|---|---|---|
| 3.6.3 | Flow unsteadiness | |
| | •Overall turbulence level | ≈0.25% |
| | •Overall noise level ($C_p$-RMS) | Not known |
| **4** | **INSTRUMENTATION** | |
| 4.1 | Model position | |
| 4.1.1 | How is geometrical incidence measured? | By means of a potentiometer mounted on the model support link system |
| 4.1.2 | Accuracy of geometrical incidence | 0.1° (approximately) |
| 4.2 | Model pressure measurements | |
| 4.2.1 | Total number and disposition of pressure holes | CONF1: 96 taps on nacelle (Fig 8a)<br>CONF2: 94 taps on nacelle and 96 taps on wing (Fig 8b,10)<br>CONF3: 144 taps on nacelle (Fig 9a)<br>CONF4: 144 taps on nacelle and 96 taps on wing (Fig 9b,10) |
| 4.2.2 | Range and accuracy of pressure transducers | Range: ±17.5 kPa, accuracy: ≈0.1 % FS |
| 4.2.3 | Are dynamic pressures measured? | No |
| 4.3 | Force and moment measurements | |
| 4.3.1 | Type and locations of balance(s) | Propeller balance (2 components: thrust and torque) located inside the spinner. The balance is rotating with the propeller and the balance signals are transmitted by means of slip rings. |
| 4.3.2 | Indicate maximum range and accuracy of all components | Thrust: maximum : 1000 N<br>accuracy: ± 20 N<br>Torque: maximum: 100 Nm<br>accuracy: ±2 Nm |
| 4.4 | Boundary layer and flow field measurement | |
| 4.4.1 | Measurement technique | 5-hole pressure probe |
| 4.4.2 | Flow regions investigated | Three axial planes downstream the propeller disk (10, 525 and 925 mm axial distances from the disk), see test matrix. |
| 4.4.3 | Probe details and probe support | See Figures 11a,b,c,d,e (including calibration details) |
| 4.5 | Surface flow visualization | None carried out |
| 4.6 | Flow field visualization | None carried out |
| 4.7 | Tunnel wall measurements | None carried out |
| 4.8 | Other measurements and/or instrumentation used | Tachometer for propeller RPM; accuracy of propeller RPM control system : ± 15 RPM |
| **5** | **TEST MATRIX AND CONDITIONS** | |
| 5.1 | Detailed test matrix | |
| 5.1.1 | Number of selected test cases | 4 |
| 5.1.2 | Number of configurations tested (selected cases only) | 4 |
| 5.1.3 | Test case information<br>• test case number<br>• configuration<br>• velocity<br>• dynamic pressure q<br>• Reynolds number<br>• model attitude (α, β, etc.)<br>• type of measurement<br>• additional remarks | } See Table I<br>surface pressures<br>flow field data<br>limited amount of prop/off data |
| 5.2 | Model/tunnel relations | |
| 5.2.1 | Maximum blockage | A/C = 0.10 % (CONF1)<br>0.38 % (CONF2)<br>0.95 % (CONF3) |

| | | |
|---|---|---|
| | | 1.65 % (CONF4)<br>$A_{prop}/C$= 3.16 %<br>(A: cross-sectional area of configuration at $\alpha = 0°$)<br>C: wind tunnel cross section area;<br>$A_{prop}$: propeller disk area = 0.322 $m^2$) |
| 5.2.2 | Model span/tunnel diameter | 0.57 (CONF2, CONF4) |
| 5.2.2.1 | Propeller diameter/tunnel diameter | 0.178 |
| 5.2.3 | Wing area/tunnel cross section | 0.10 (CONF2, CONF4) |
| 5.2.4 | Height/chord ratio (2-D only) | - |
| 5.2.5 | Width/chord ratio (2-D only) | - |
| 5.2.6 | Have adiabatic wall temperatures | - |
| 5.3 | Transition details | |
| 5.3.1 | Was the test made with free or fixed transition? | Free (not known whether this fact had any particular significance for results obtained) |
| 5.3.2 | Details of free transition<br>• where did natural transition take place? | Not known |
| 5.3.3 | Details of fixed transition | Not applicable |
| **6** | **DATA** | |
| 6.1 | Availability of data | |
| 6.1.1 | Organization owning the data | FFA, The Aeronautical Research Institute of Sweden |
| 6.1.2 | Who is responsible for the data<br>• name and title<br>• address<br>• telephone and fax numbers | Ingemar Samuelsson, Senior Research Scientist<br>Flygtekniska Försöksanstalten (FFA)<br>Aerodynamics Department<br>P.O. Box 11021<br>S-161 11 Bromma<br>SWEDEN<br>phone: +46 8 634 1000 (ext. 1132)<br>fax: +46 8 253481 |
| 6.1.3 | Are data freely available? | No |
| 6.1.4 | If not, who should be contacted? | See 6.1.2 |
| 6.2 | Suitability of data for CFD validation | |
| 6.2.1 | Are data suitable for "in-tunnel" calculation? | No |
| 6.2.2 | Are data corrected to simulate "free-air"-condition? | Yes |
| 6.3 | Type and form in which data are available | |
| 6.3.1 | Type and form (refer to table II) | See table II |
| 6.3.2 | Data carrier (printed, tape, floppy disk) | Floppy disks (4 of them) |
| 6.3.3 | Extent of geometry data | 20 kB |
| 6.3.4 | Extent of aerodynamic test data | 4.35 MB |
| 6.4 | Corrections applied to data | |
| 6.4.1 | Lift interference and blockage corrections<br>• are data considered globally correctable?<br>• type of correction method applied<br>• specify what data are actually corrected and indicate order of magnitude | Yes<br>Classical (Prandtl-Glauert compressibility correction, Glauerts' wind tunnel/propeller interference correction)<br>Free stream velocity: -2 %<br>advance ratio: -2 %<br>flow field velocities: -2 % |
| 6.4.2 | Side wall interference corrections | - |
| 6.4.3 | Half model corrections | - |
| 6.4.4 | Sting and support interference | Not known |
| 6.4.5 | Aero-elastic deformation | Not known |
| 6.4.6 | Other corrections (e.g. flow unsteadiness, empty test section flow, intrusive effects of measuring equipment, etc.) | None applied |

## 7 DATA ACCURACY AND REPEATABILITY ASSESSMENT

| | | |
|---|---|---|
| 7.1 | Estimate accuracy of: | |
| 7.1.1 | Free stream conditions | |
| | • Mach number | - |
| | • flow velocity | ± 0.5 % |
| | • model incidence | ± 0.5 ° |
| 7.1.2 | Measured data | |
| | • forces and moments | ± 3 % |
| | • pressure coefficients | ± 0.06(within the slipstream)<br>± 0.03 (outside the slipstream) |
| | • flow field data | velocity: ± 3 %<br>flow angles: ± 1.5 °<br>pressure coefficients: ± 0.06 |
| 7.2 | Repeat measurements | |
| 7.2.1 | Type and number of repeat measurements within one test campaign | None |
| 7.2.2 | Type and number of repaet measurements in successive test campaigns | 1 repeat measurement (flow field survey along a particular radius, see Figure 12 for example) |
| 7.3 | Redundant measurements | None carried out |
| 7.4 | Other tests on the same (nominal) model | None carried out |
| 7.5 | Additional remarks | Test of flow axisymmetry, see Figure 13 |

## 8 REFERENCES

8.1 On the wind tunnel

8.2 On the model

8.3 On the particular test and test results

8.4 On the applied measurement techniques and correction methods


1. Anon.,
"FFA Wind Tunnel Facilities"
FFA Memorandum 93,
Stockholm, 1974.

2. Skoglund, K.E.,
"Kalibrering av FFA låghastighetsvindtunnel LT1" ("Calibration of FFA Low Speed Wind Tunnel LT1")
In Swedish, to be published.

3. Samuelsson, I.,
"Low Speed wind Tunnel Investigation of Propeller Slipstream Aerodynamic Effects on Different Nacelle/Wing Combinations"
Part 1: "Total Forces and Moments and Pressure Distributions on Nacelle/Wing at Different Angles of Attack and Yaw and at Different Thrust Coefficients"
FFA, TN 1987-22,
Stockholm, 1987.

4. Samuelsson, I.,
(Same title as Ref. 3)
Part 2: "Propeller Slipstream Flow Field Surveys (Velocity components, Dynamic, Total and Static Pressure Distributions) at Zero Angle of Attack and High Power"
FFA TN 1990-24,
Stockholm, 1990.

5. Samuelsson, I.,
"Experimental Investigation of Low Speed Model Propeller Slipstream Aerodynamic Characteristics Including Flow Field Surveys and Nacelle/Wing Static Pressure Measurements"
ICAS-90-3.13,
Stockholm, 1990.

## 9 LIST OF SYMBOLS

| | |
|---|---|
| A | area, [$m^2$] |
| c | wing chord = 0.500 m |
| $c_{ref}$ | reference chord =1.672 m |
| C | wind tunnel cross-sectional area = 10.18 $m^2$ |
| $C_p$ | pressure coefficient = $(p-p_\infty)/q_\infty$, [-] |
| $C_P$ | power coefficient = (propeller power)/($\rho n^3 D^5$), [-] |
| $C_T$ | thrust coefficient = (propeller thrust)/($\rho n^2 D^4$), [-] |
| D | propeller diameter = 0.64 m |
| $F_A$, $F_H$, $F_P$, $F_Q$ | 5-hole probe calibration pressure coefficients, [-] |
| IHOLE | pressure tap number, [-] |
| J | advance ratio = $U_\infty/(nD)$, [-] |
| Mach | Mach number = $U_\infty$/(speed of sound), [-] |
| n | propeller rotational speed, RPS, [1/s] |
| $n_x$,$n_y$, $n_z$ | components of unit normal vector (pointing outwards, [-] |
| N | propeller rotational speed, RPM, [1/min] |
| p | pressure, [Pa] |
| P | propeller power =$Q\omega$, [W] |
| $q_\infty$ | free stream dynamic pressure = $0.5\rho_\infty U_\infty^2$, [Pa] |
| Q | propeller shaft torque, [Nm] |
| Re | Reynolds number = $\rho_\infty U_\infty c_{ref}/\mu_\infty$, [-] |
| $R_p$ | propeller radius =D/2 = 0.32 m |
| r | radius, [m] |
| swirl | swirl angle = - arctan($u_t/u_x$), [radians] |
| T | propeller thrust, [N] |
| $u_x$,$u_r$, $u_t$ | flow velocity components in cylindrical coordinates, [m/s] |
| $U_\infty$ | free stream velocity, [m/s] |
| x,r,φ | cylindrical coordinates, [m,m , radians] |
| x,y,z | Cartesian coordinates, [m] |
| X,Y,Z | force components in (x,y,z) coordinate system (positive force direction in resp. axis positive direction), [N] |
| α | angle of attack, [° or radians] |
| α,ψ | 5-hole calibration angles, [°] |
| β | angle of sideslip, [° or radians] |
| $\beta_{.75}$ | propeller pitch at 75 %-radius (0.75 $R_p$), [°] |
| $\mu_\infty$ | free stream dynamic viscosity, [kg/(ms)] |
| $\rho_\infty$ | free stream density, [$kg/m^3$] |
| ω | propeller angular velocity, [radians/s] |

Subscripts

| | |
|---|---|
| 1,2,3,4 | pertaining to nacelle geometry definition |
| aver | average (aritmetic mean) |
| min | minimum |
| x,r,t | axial, radial and tangential, respectively |
| t,tot | pertaining to total (stagnation )conditions |
| prop | pertaining to propeller |
| ∞ | free stream conditions |

## FIGURE CAPTIONS

| | |
|---|---|
| **Figure 1a** | **Dominant flow physics: complex interaction of the swirling propeller slipstream (with increased total pressures and velocities ) with downstream aerodynamic surfaces** |
| **Figure 1b** | **Dominant flow physics: complex interaction of the swirling propeller slipstream (with increased total pressures and velocities ) with downstream aerodynamic surfaces** |
| **Figure 2** | **General geometric arrangement Propeller+spinner, nacelle and wing** |
| **Figure 3** | **Tested model nacelle/wing configurations** |
| **Figure 4** | **Wing and aerofoil data** |
| **Figure 5a** | **Nacelle/spinner geometry (CONF4). Coordinates are given in Figure 5b** |
| **Figure 5b** | **Nacelle geometry definition (including propeller spinner)** |
| **Figure 6a** | **Sting and support geometry** |
| **Figure 6b** | **Sting and support geometry** |
| **Figure 7** | **Model mounted in the wind tunnel LT1** |
| **Figure 8a** | **Nacelle pressure tap location and numbering (CONF1)** |
| **Figure 8b** | **Nacelle pressure tap location and numbering (CONF2)** |
| **Figure 9a** | **Nacelle pressure tap location and numbering (CONF3)** |
| **Figure 9b** | **Nacelle pressure tap location and numbering (CONF4)** |
| **Figure 10** | **Wing pressure tap locations (on both sides of wing)** |
| **Figure 11a** | **Five-hole probe layout** |
| **Figure 11b** | **Five-hole probe cranked sting** |
| **Figure 11c** | **Five-hole probe calibration set-up** |
| **Figure 11d** | **Five-hole probe calibration scheme and α'-ψ map** |
| **Figure 11e** | **Five-hole probe traversing mechanism** |
| **Figure 12** | **Examples of test repeatability (CONF1)** |
| **Figure 13** | **Slipstream characteristics (CONF1). Test of axisymmetry (nominal axisymmetrical geometry and onset flow)** |

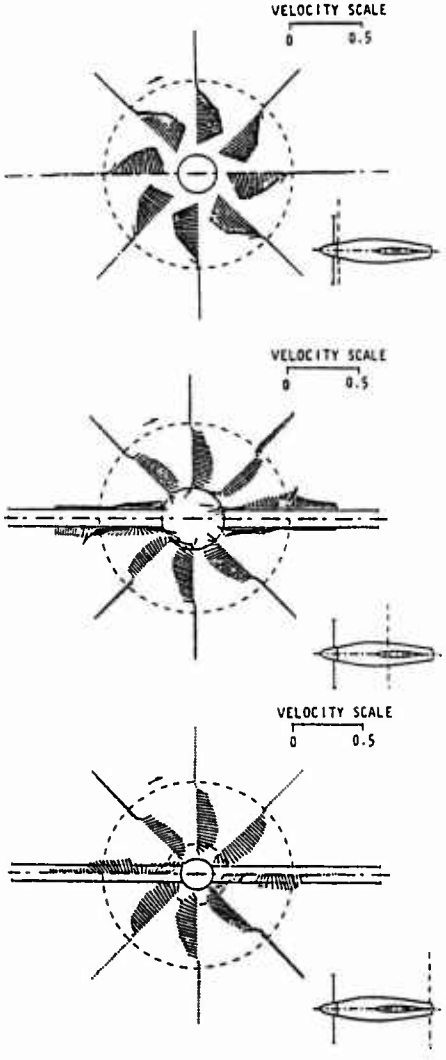
| IDENTIFICATION | | FLOW CONDITIONS | | | | PROPELLER WORKING CONDITIONS | | | | | POSITION | | OTHER INFORMATION | |
|---|---|---|---|---|---|---|---|---|---|---|---|---|---|---|
| CASE NO. | CONF. | $U_\infty$ (m/s) | Mach | $q_\infty$ (kPa) | Re ($10^6$) | N (RPM) | $\beta_{.75}$ (°) | J | $C_T$ | $C_P$ | $\alpha$ (°) | $x_{probe}$ (mm) | type of measurement | Remarks |
| 1 | 1 | 50 | 0.15 | 1.5 | 1.7 | 6650 | 29 | 0.7 | 0.23 | 0.23 | 0 | 10<br>115<br>525<br>925 | surface pressures, flow field survey | Prop/on/off (prop/off: no flow field data) |
| 2 | 2 | 50 | 0.15 | 1.5 | 1.7 | 6650 | 29 | 0.7 | 0.23 | 0.23 | 0 | 10<br>525<br>925 | surface pressures, flow field survey | Prop/on/off (prop/off: no flow field data) |
| 3 | 3 | 50 | 0.15 | 1.5 | 1.7 | 6650 | 29 | 0.7 | 0.23 | 0.23 | 0 | 10<br>525<br>925 | surface pressures, flow field survey | Prop/on/off (prop/off: no flow field data) |
| 4 | 4 | 50 | 0.15 | 1.5 | 1.7 | 6650 | 29 | 0.7 | 0.23 | 0.23 | 0 | 10<br>525<br>925 | surface pressures, flow field survey | Prop/on/off (prop/off: no flow field data) |

**TABLE I TEST MATRIX AND CONDITIONS**

| DATA | ENGINEERING UNITS | COEFFICIENTS | NORMALIZED | UNCORRECTED | CORRECTED |
|---|---|---|---|---|---|
| FREESTREAM CONDITIONS | X | | | | X |
| SURFACE PRESSURES | | X | | X | |
| HEAT TRANSFER SKIN FRICTION | | | | | |
| PROPELLER LOADS | | X | | X | |
| BOUNDARY LAYER DATA | | | | | |
| WAKE DATA | | | | | |
| FIELD DATA | | X | | | X |
| TEST SECTION WALL PRESSURES | | | | | |

**TABLE II DATA AVAILABILITY (TYPE AND FORM)**

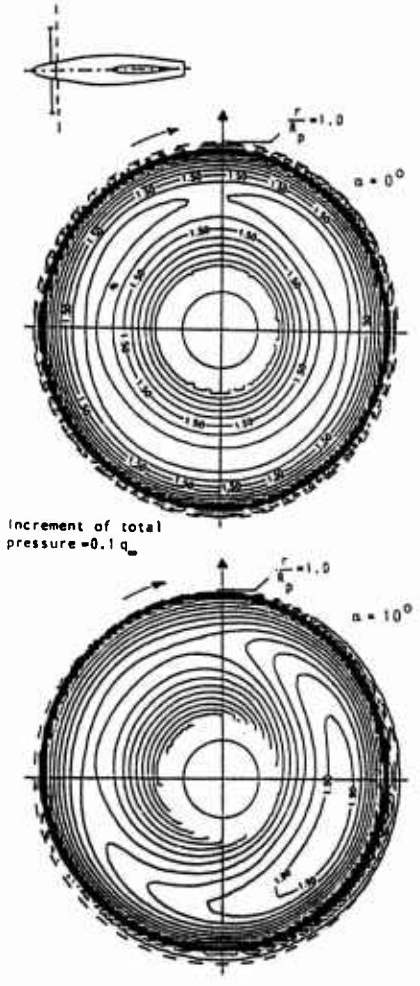
**Axial development of propeller slipstream cross-flow**




**CONF2**

**$U_\infty$ =49.3 m/s, $\alpha = \beta = 0°$**
**$\beta_{.75}$ = 29°, N = 6650 RPM**
**J = 0.696, $C_T$ = 0.232, Cp = 0.242**

**Total pressure distribution (isobar map) Effect of angle of attack**



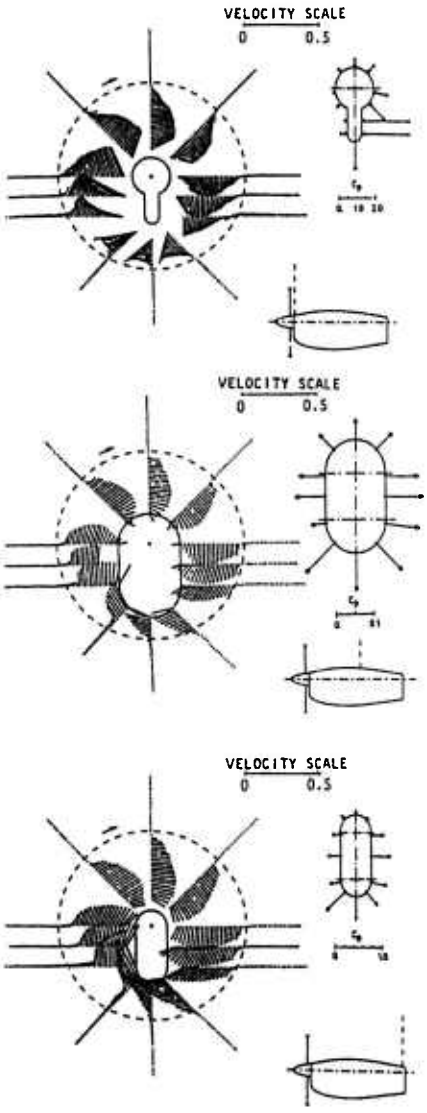

**Flow field survey at 0.14 propeller radius downstream distance from propeller disk**

**CONF2**

**$U_\infty$ =49.6 m/s, $\alpha$ = 0° and 10°, $\beta$ = 0°**
**$\beta_{.75}$ = 29°, N = 6650 RPM**
**J = 0.699, $C_T$ = 0.235, Cp = 0.242**

**Figure 1a** **Dominant flow physics: complex interaction of the swirling propeller slipstream (with increased total pressures and velocities) with downstream located aerodynamic surfaces**

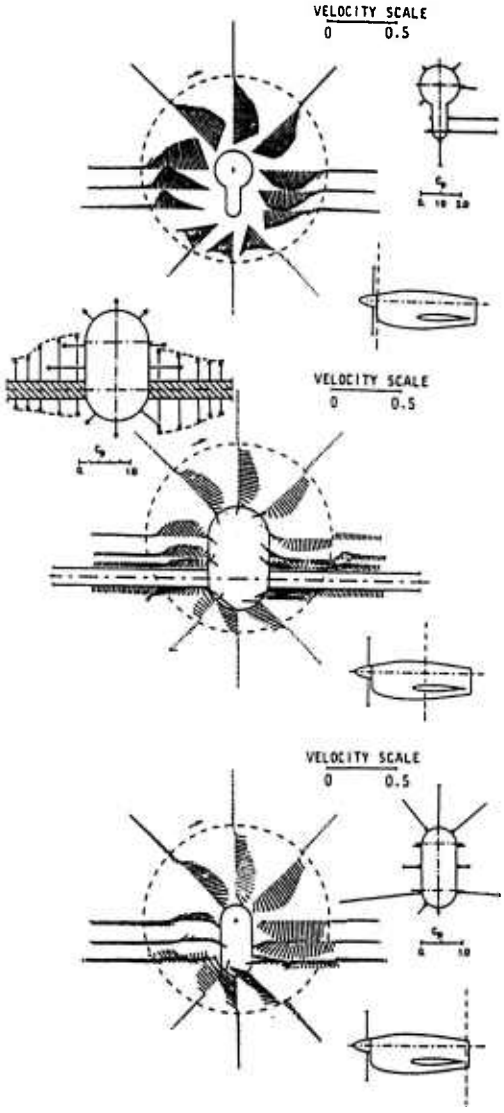
**Axial development of propeller slipstream cross-flow**




**CONF3**

$U_\infty$ =50.0 m/s, $\alpha = \beta = 0°$
$\beta_{.75}$ = 29°, N = 6650 RPM
J = 0.705, $C_T$ = 0.231, Cp = 0.225

**Axial development of propeller slipstream cross-flow**




**CONF4**

$U_\infty$ =49.8 m/s, $\alpha = \beta = 0°$
$\beta_{.75}$ = 29°, N = 6650 RPM
J = 0.705, $C_T$ = 0.229, Cp = 0.232

**Figure 1b** Dominant flow physics: complex interaction of the swirling propeller slipstream (with increased total pressures and velocities) with downstream located aerodynamic surfaces

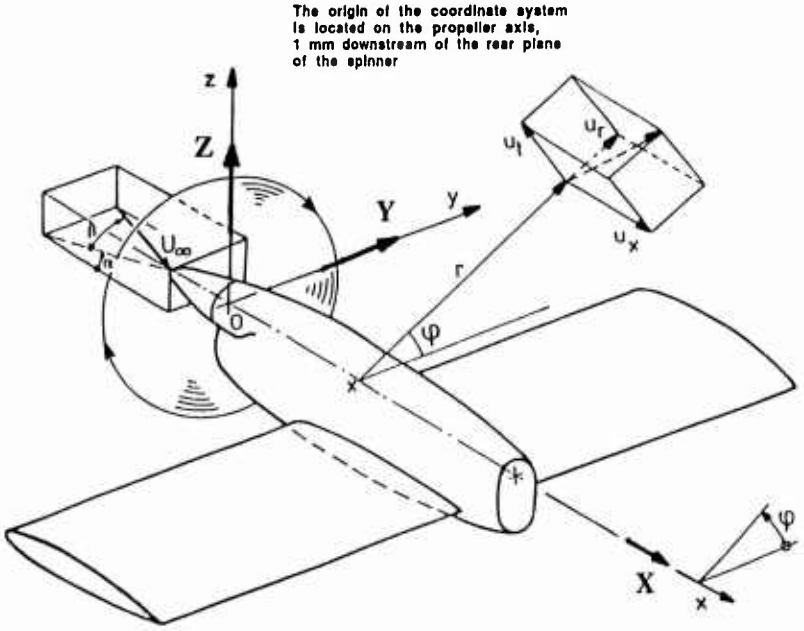



Figure 2 General geometric arrangement
Propeller+spinner, nacelle and wing

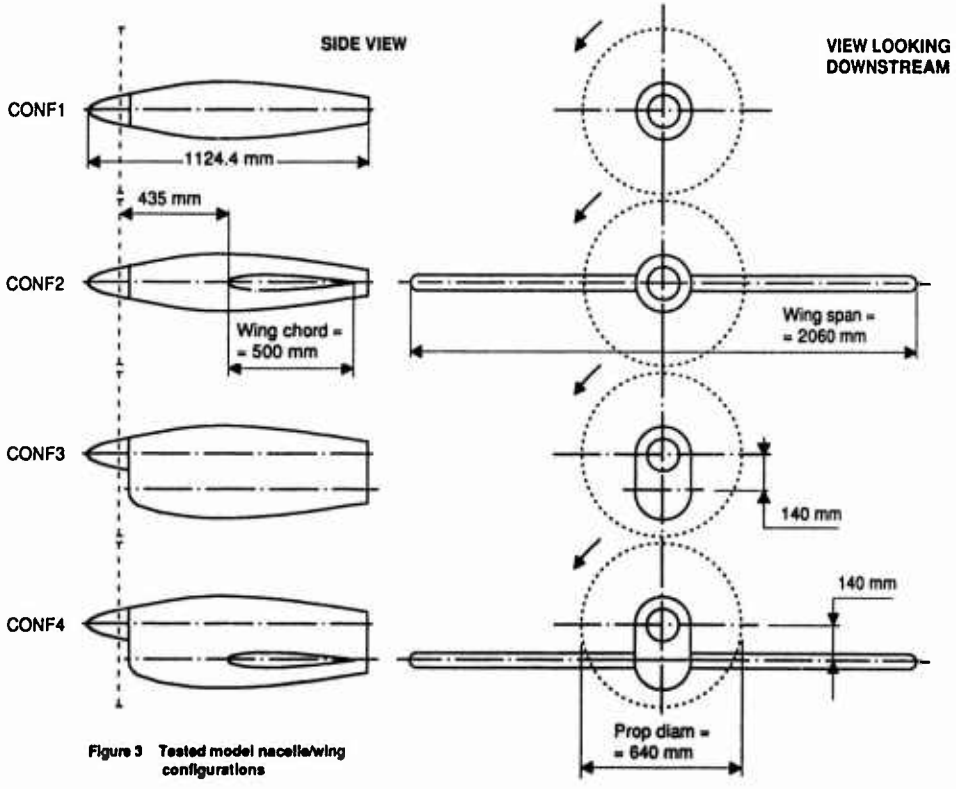
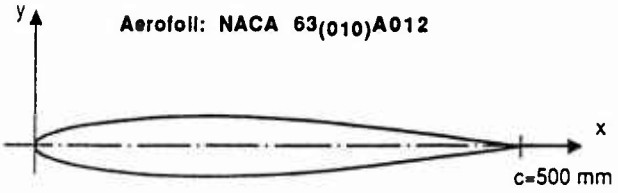
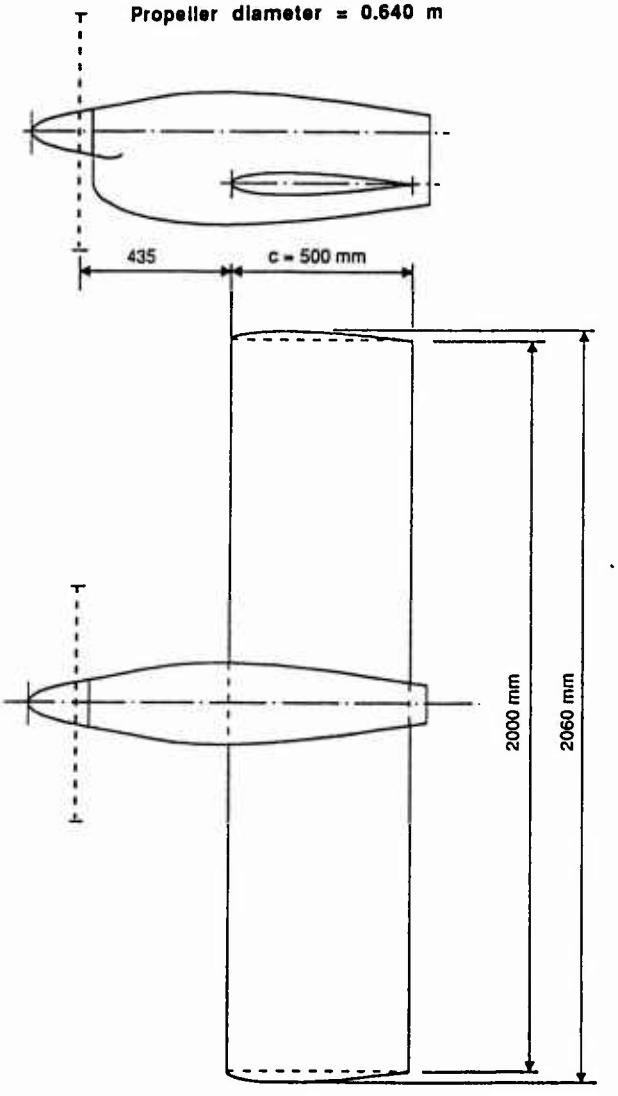



Figure 3 Tested model nacelle/wing
configurations




**Aerofoil coordinates**

| x/c (%) | ±y/c (%) |
|---|---|
| 0.00 | 0.000 |
| 0.50 | 0.979 |
| 0.75 | 1.180 |
| 1.25 | 1.500 |
| 2.50 | 2.084 |
| 5.00 | 2.894 |
| 7.50 | 3.500 |
| 10.00 | 3.989 |
| 15.00 | 4.740 |
| 20.00 | 5.280 |
| 25.00 | 5.657 |
| 30.00 | 5.896 |
| 35.00 | 5.994 |
| 40.00 | 5.962 |
| 45.00 | 5.804 |
| 50.00 | 5.536 |
| 55.00 | 5.173 |
| 60.00 | 4.732 |
| 65.00 | 4.220 |
| 70.00 | 3.653 |
| 75.00 | 3.054 |
| 80.00 | 2.448 |
| 85.00 | 1.842 |
| 90.00 | 1.236 |
| 95.00 | 0.630 |
| 100.00 | 0.025 |

**Figure 4 Wing and aerofoil data**

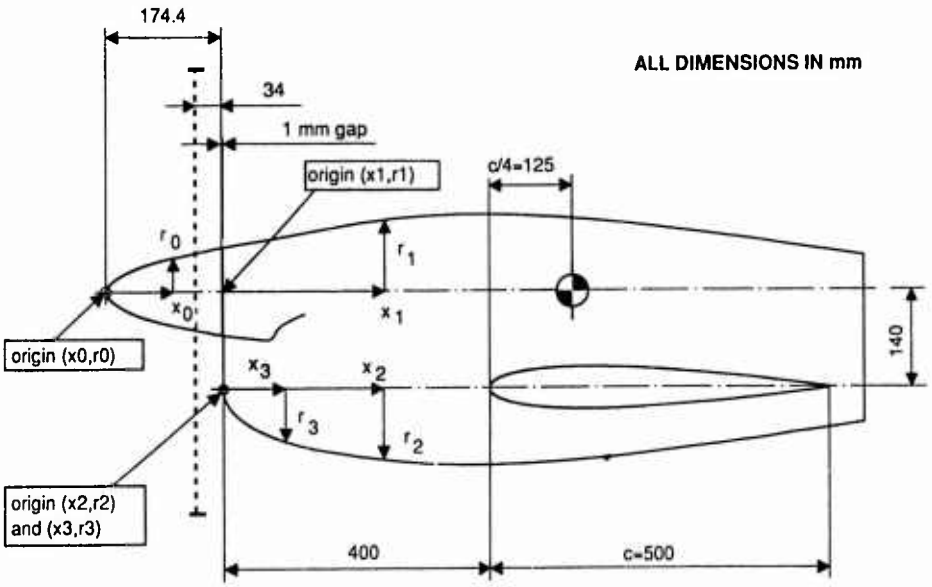



Figure 5a Nacelle/spinner geometry (CONF4)
Coordinates are given in tables in Fig 5b

Nacelle coordinates ($x_1$,$r_1$)

All dimensions in mm

| $x_1$ | $r_1$ | $x_1$ | $r_1$ | $x_1$ | $r_1$ | $x_1$ | $r_1$ | $x_1$ | $r_1$ |
|---|---|---|---|---|---|---|---|---|---|
| 0. | 63.500 | 190. | 97.290 | 380. | 110.737 | 570. | 100.474 | 760. | 77.312 |
| 5. | 64.362 | 195. | 98.062 | 385. | 110.687 | 575. | 99.989 | 765. | 76.598 |
| 10. | 65.224 | 200. | 98.813 | 390. | 110.623 | 580. | 99.495 | 770. | 75.881 |
| 15. | 66.088 | 205. | 99.542 | 395. | 110.545 | 585. | 98.992 | 775. | 75.162 |
| 20. | 66.954 | 210. | 100.249 | 400. | 110.453 | 590. | 98.480 | 780. | 74.439 |
| 25. | 67.821 | 215. | 100.935 | 405. | 110.348 | 595. | 97.960 | 785. | 74.714 |
| 30. | 68.690 | 220. | 101.596 | 410. | 110.230 | 600. | 97.432 | 790. | 72.987 |
| 35. | 69.561 | 225. | 102.239 | 415. | 110.099 | 605. | 96.896 | 795. | 72.259 |
| 40. | 70.434 | 230. | 102.857 | 420. | 109.956 | 610. | 96.352 | 800. | 71.530 |
| 45. | 71.309 | 235. | 103.453 | 425. | 109.801 | 615. | 95.801 | 805. | 70.800 |
| 50. | 72.187 | 240. | 104.025 | 430. | 109.635 | 620. | 95.244 | 810. | 70.070 |
| 55. | 73.068 | 245. | 104.575 | 435. | 109.457 | 625. | 94.679 | 815. | 69.340 |
| 60. | 73.952 | 250. | 105.102 | 440. | 109.267 | 630. | 94.109 | 820. | 68.611 |
| 65. | 74.838 | 255. | 105.605 | 445. | 109.066 | 635. | 93.531 | 825. | 67.882 |
| 70. | 75.728 | 260. | 106.085 | 450. | 108.855 | 640. | 92.948 | 830. | 67.115 |
| 75. | 76.622 | 265. | 106.542 | 455. | 108.633 | 645. | 92.359 | 835. | 66.429 |
| 80. | 77.519 | 270. | 106.975 | 460. | 108.400 | 650. | 91.763 | 840. | 65.704 |
| 85. | 78.421 | 275. | 107.384 | 465. | 108.157 | 655. | 91.162 | 845. | 64.981 |
| 90. | 79.327 | 280. | 107.770 | 470. | 107.903 | 660. | 90.555 | 850. | 64.260 |
| 95. | 80.239 | 285. | 108.132 | 475. | 107.638 | 665. | 89.943 | 855. | 63.539 |
| 100. | 81.156 | 290. | 108.471 | 480. | 107.363 | 670. | 89.325 | 860. | 62.820 |
| 105. | 82.080 | 295. | 108.785 | 485. | 107.076 | 675. | 88.702 | 865. | 62.102 |
| 110. | 83.009 | 300. | 109.076 | 490. | 106.778 | 680. | 88.074 | 870. | 61.384 |
| 115. | 83.941 | 305. | 109.343 | 495. | 106.469 | 685. | 87.440 | 875. | 60.668 |
| 120. | 84.877 | 310. | 109.586 | 500. | 106.149 | 690. | 86.801 | 880. | 59.953 |
| 125. | 85.814 | 315. | 109.805 | 505. | 105.816 | 695. | 86.156 | 885. | 59.238 |
| 130. | 86.750 | 320. | 110.000 | 510. | 105.473 | 700. | 85.507 | 890. | 58.524 |
| 135. | 87.685 | 325. | 110.171 | 515. | 105.118 | 705. | 84.852 | 895. | 57.811 |
| 140. | 88.615 | 330. | 110.319 | 520. | 104.751 | 710. | 84.193 | 900. | 57.098 |
| 145. | 89.539 | 335. | 110.466 | 525. | 104.373 | 715. | 83.527 | 905. | 56.386 |
| 150. | 90.455 | 340. | 110.551 | 530. | 103.983 | 720. | 82.857 | 910. | 55.675 |
| 155. | 91.362 | 345. | 110.637 | 535. | 103.583 | 725. | 82.181 | 915. | 54.964 |
| 160. | 92.256 | 350. | 110.703 | 540. | 103.171 | 730. | 81.501 | 920. | 54.253 |
| 165. | 93.138 | 355. | 110.751 | 545. | 102.748 | 735. | 80.814 | 925. | 53.544 |
| 170. | 94.004 | 360. | 110.781 | 550. | 102.314 | 740. | 80.123 | 930. | 52.834 |
| 175. | 94.853 | 365. | 110.794 | 555. | 101.869 | 745. | 79.427 | 935. | 52.125 |
| 180. | 95.685 | 370. | 110.791 | 560. | 101.414 | 750. | 78.726 | 940. | 51.417 |
| 185. | 96.497 | 375. | 110.772 | 565. | 100.949 | 755. | 78.021 | 945. | 50.708 |
| | | | | | | | | 950. | 50.000 |

Propeller spinner coordinates ($x_0$,$r_0$)

| $x_0$ | $r_0$ |
|---|---|
| 0. | 0. |
| 1. | 3. |
| 2. | 5 |
| 3. | 6.7 |
| 4. | 7.9 |
| 5. | 9.1 |
| 10. | 14.1 |
| 20. | 21.2 |
| 30. | 26.7 |
| 40. | 31.2 |
| 50. | 35.0 |
| 60. | 38.4 |
| 70. | 41.4 |
| 80. | 44.1 |
| 90. | 46.4 |
| 100. | 48.6 |
| 110. | 50.5 |
| 120. | 52.5 |
| 130. | 54.5 |
| 140. | 56.5 |
| 150. | 58.5 |
| 160. | 60.5 |
| 170. | 62.5 |
| 174.4 | 63.5 |

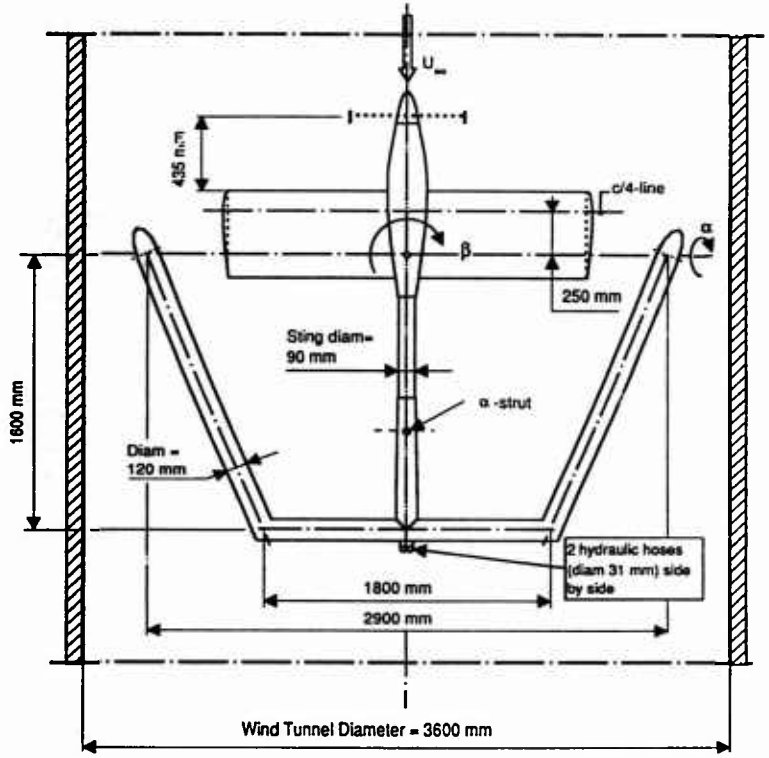
1 mm clearance between spinner and nacelle

($x_2$,$r_2$)- coordinates for lower half of the nacelle for CONF3 and CONF4 are identical to ($x_1$,$r_1$)-coordinates from $x_1$=140

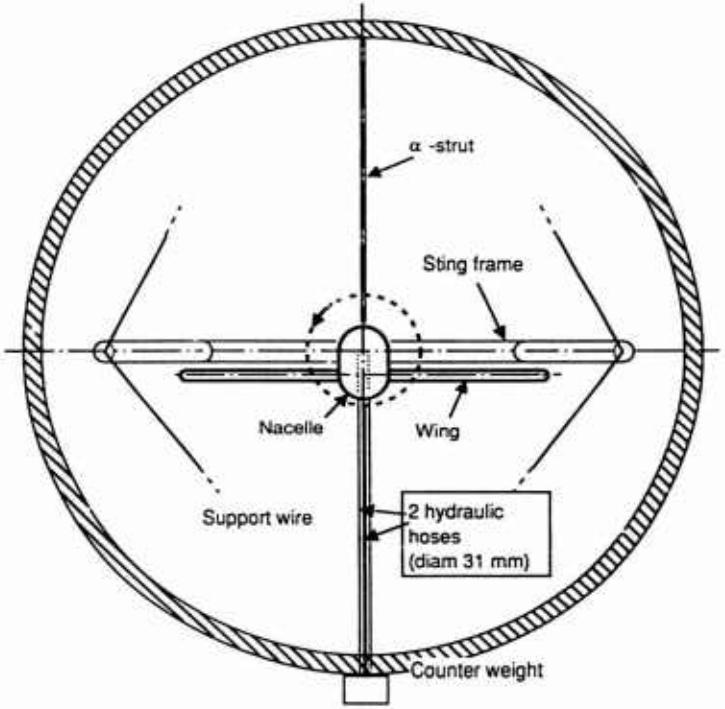
Air inlet fairing coordinates ($x_3$,$r_3$)

| $x_3$ | $r_3$ |
|---|---|
| 0. | 0. |
| 5. | 16.0 |
| 10. | 24.8 |
| 15. | 31.4 |
| 20. | 36.5 |
| 25. | 41.3 |
| 30. | 46.1 |
| 50. | 57.6 |
| 75. | 69.2 |
| 100. | 78.3 |
| 125. | 85.1 |
| 140. | 88.7 |

Figure 5b Nacelle geometry definition (including propeller spinner)



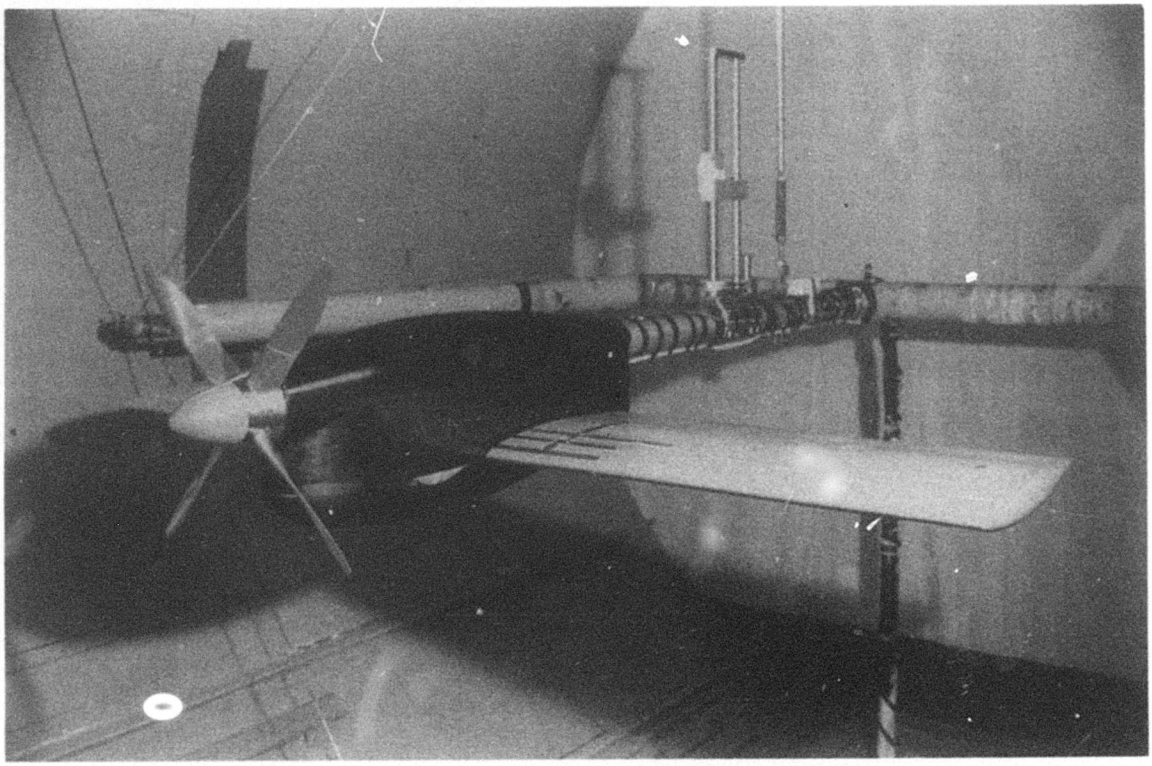

View from above




View looking downstream

Figure 6a Sting and support geometry

Figure 6b Sting and support geometry



## Wind Tunnel Model Installation (CONF4)

Figure 7 Model mounted in the wind tunnel LT1

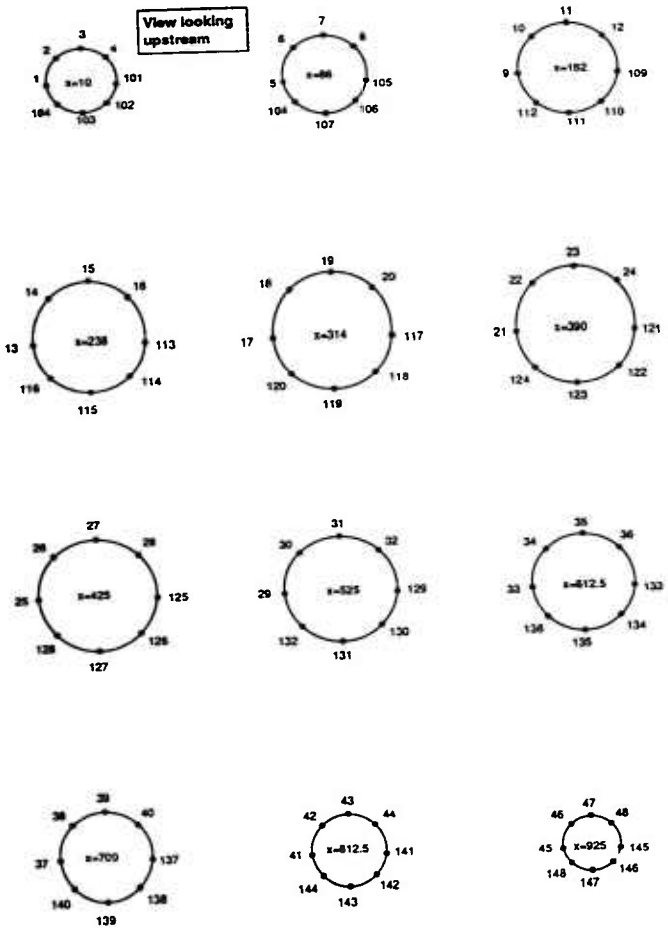



Figure 8a Nacelle pressure tap location and numbering (CONF1)

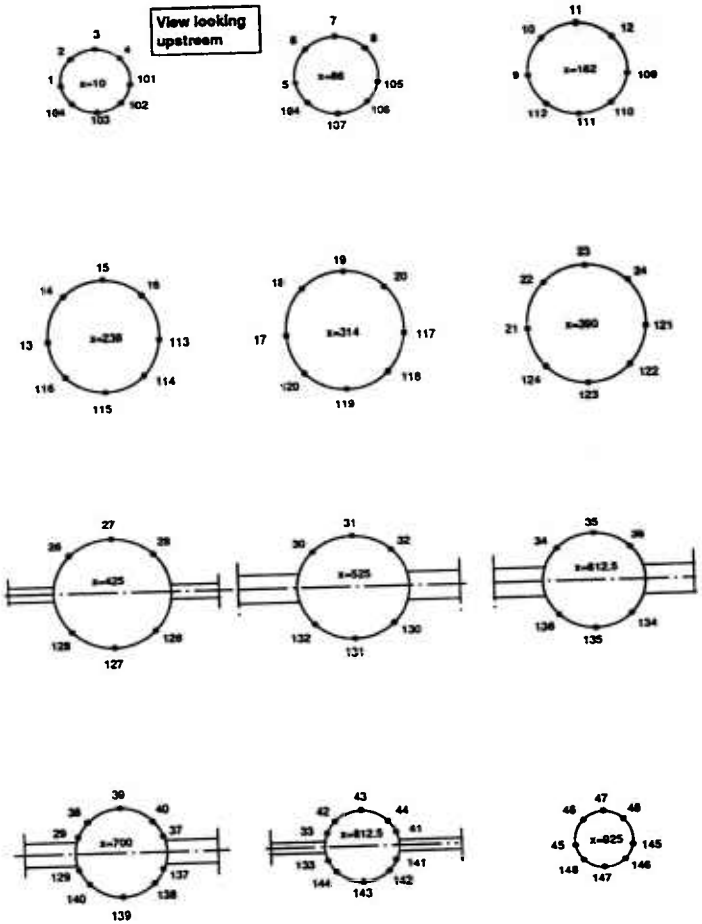



Figure 8b Nacelle pressure tap location and numbering (CONF2)

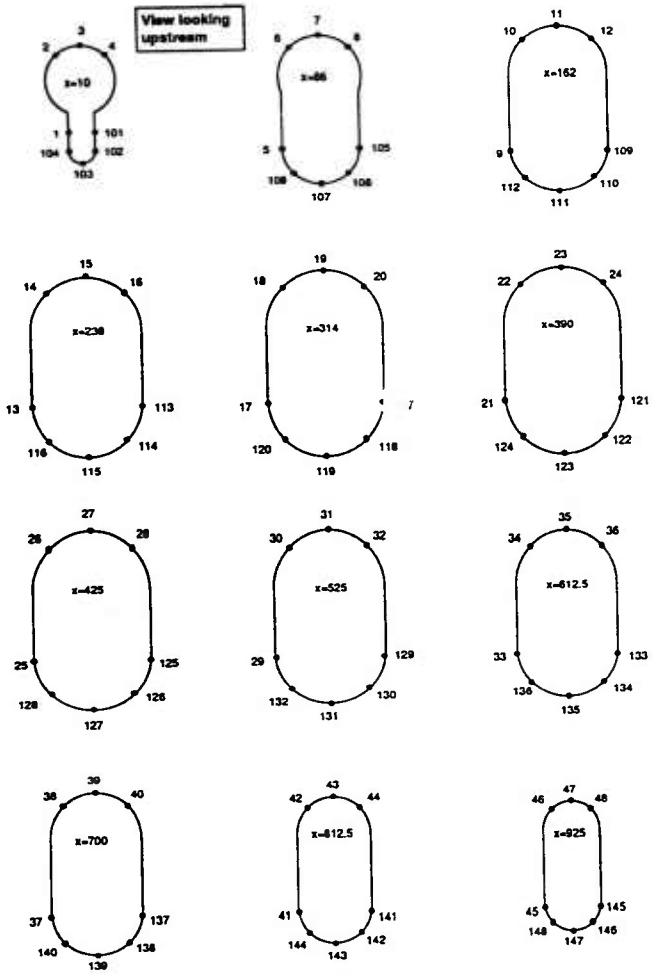



Figure 9a Nacelle pressure tap location and numbering (CONF3)

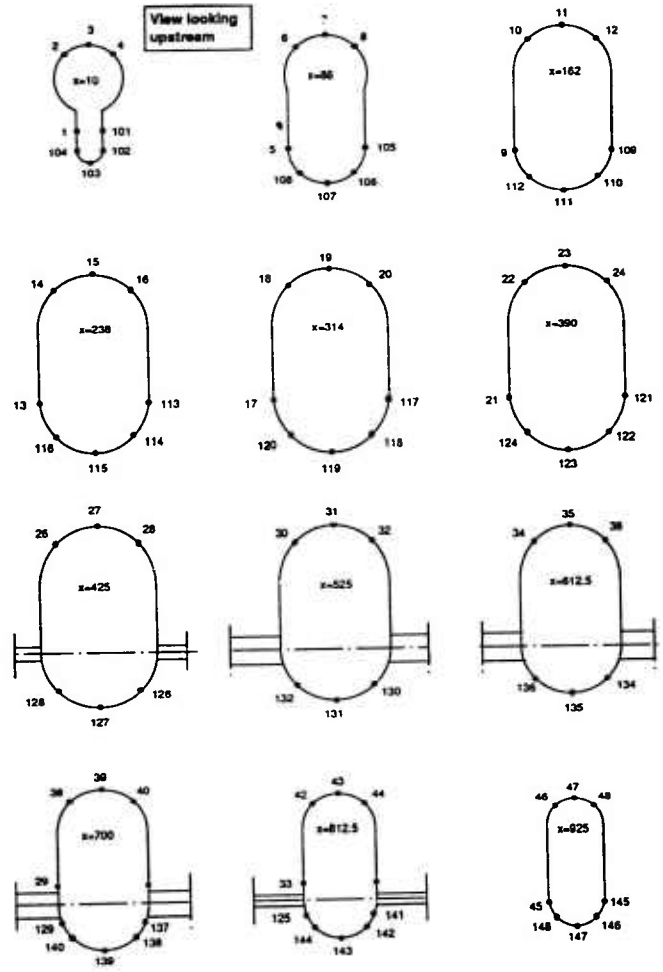



Figure 9b Nacelle pressure tap location and numbering (CONF4)

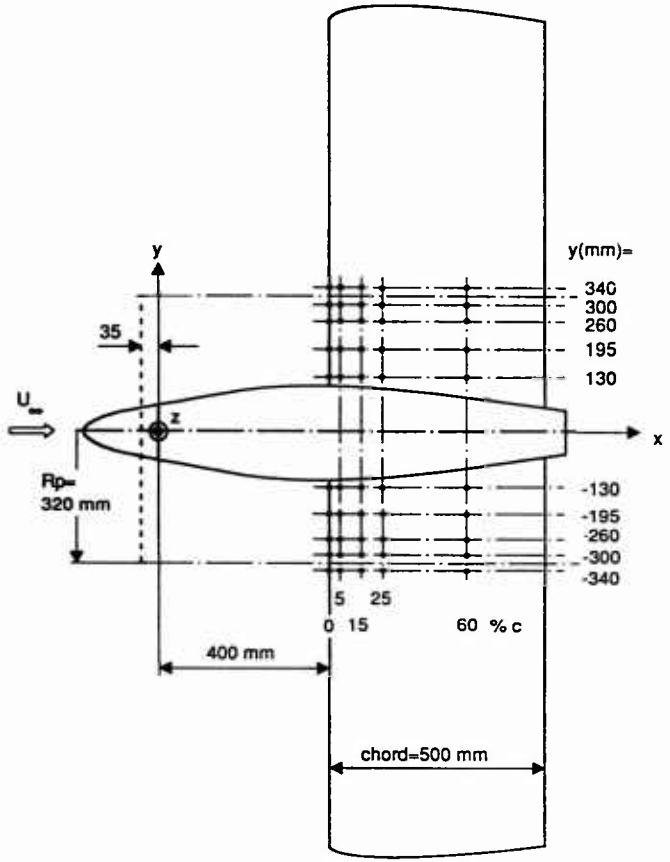



Figure 10 Wing pressure tap locations (on both sides of wing)

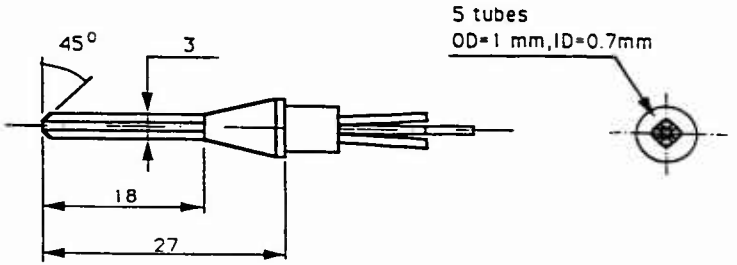



Figure 11a Five-hole probe layout

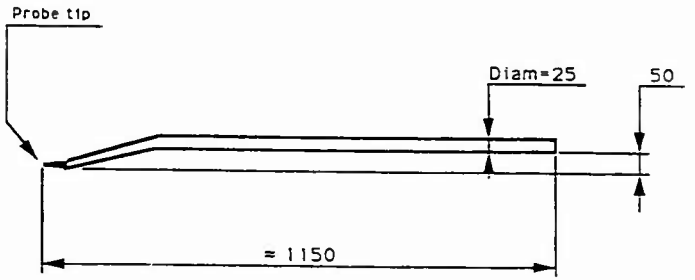



Figure 11b Five-hole probe cranked sting

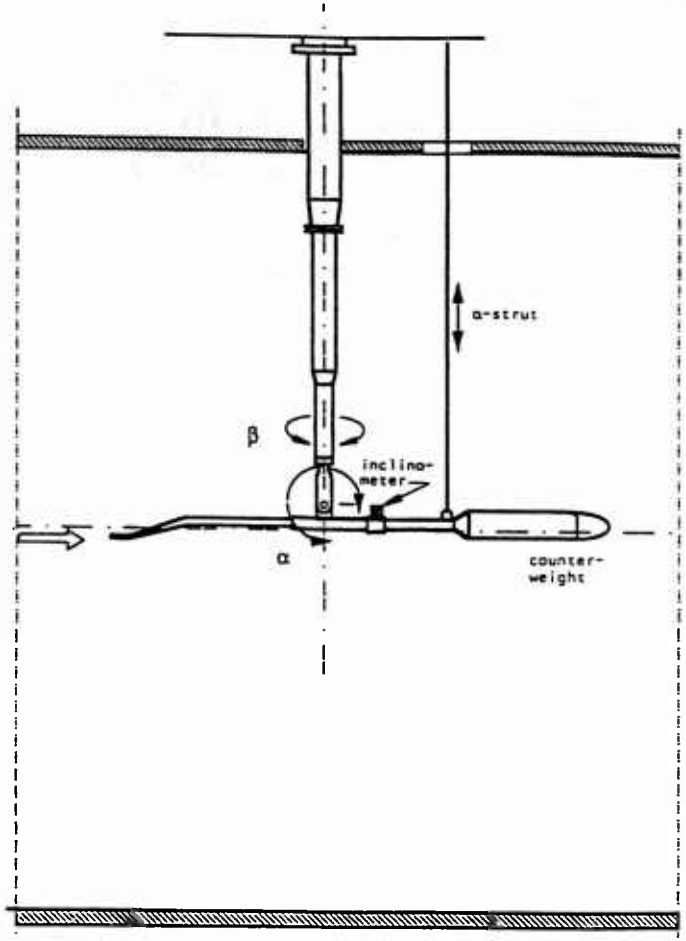



Figure 11c Five-hole probe calibration set-up

Five - hole probe
(looking downstream)




Measure $p_1$ through $p_5$

Determine minimum and average pressures:

$p_{min} = \min(p_1, p_2, p_3, p_4)$

$p_{aver} = \frac{1}{4}(p_1 + p_2 + p_3 + p_4)$

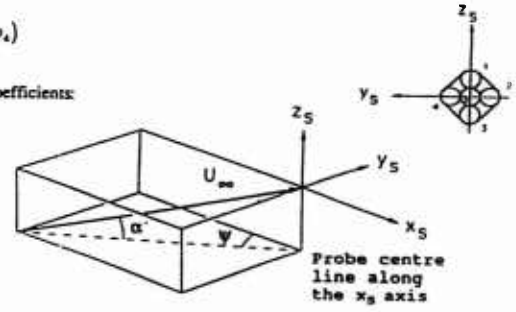
Define probe pressure coefficients:

$F_A = \frac{p_2 - p_1}{p_5 - p_{min}}$

$F_P = \frac{p_2 - p_4}{p_5 - p_{min}}$

$F_Q = \frac{p_5 - p_{aver}}{q_\infty}$

$F_H = \frac{H_\infty - p_5}{p_5 - p_{min}}$




Alpha'-Psi Map

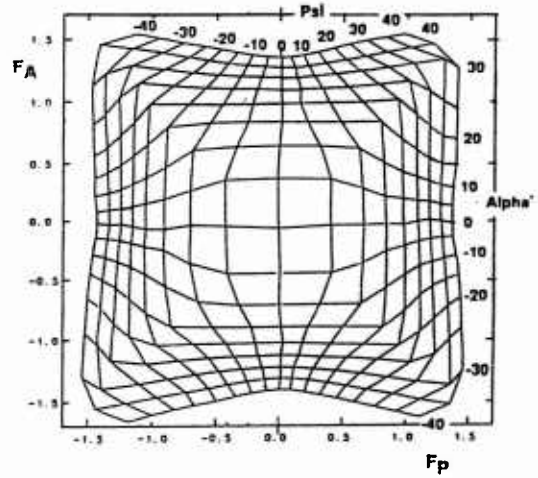



Figure 11d Five-hole probe calibration scheme and α'- ψ map

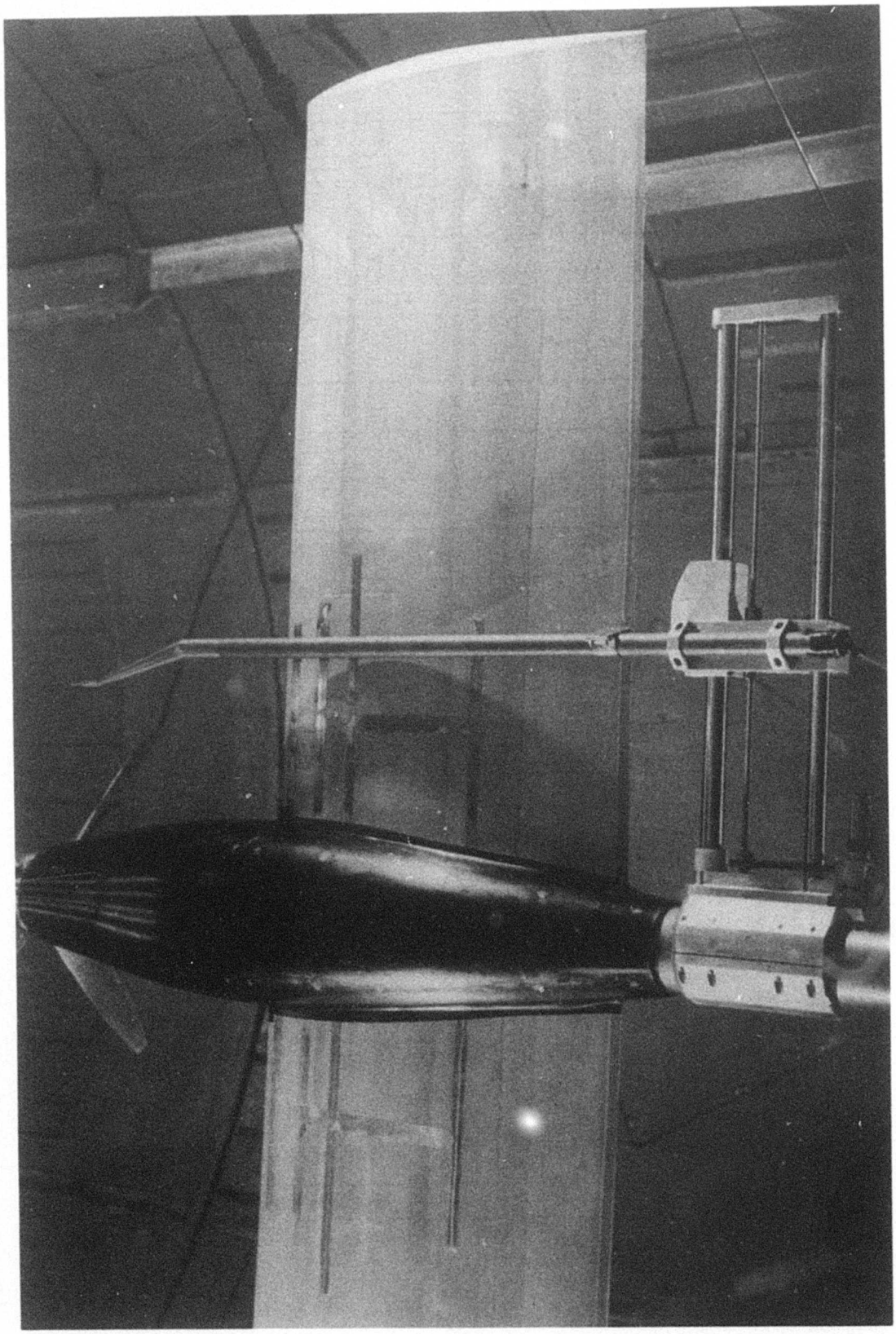


**Figure 11e** Five-hole probe traversing mechanism

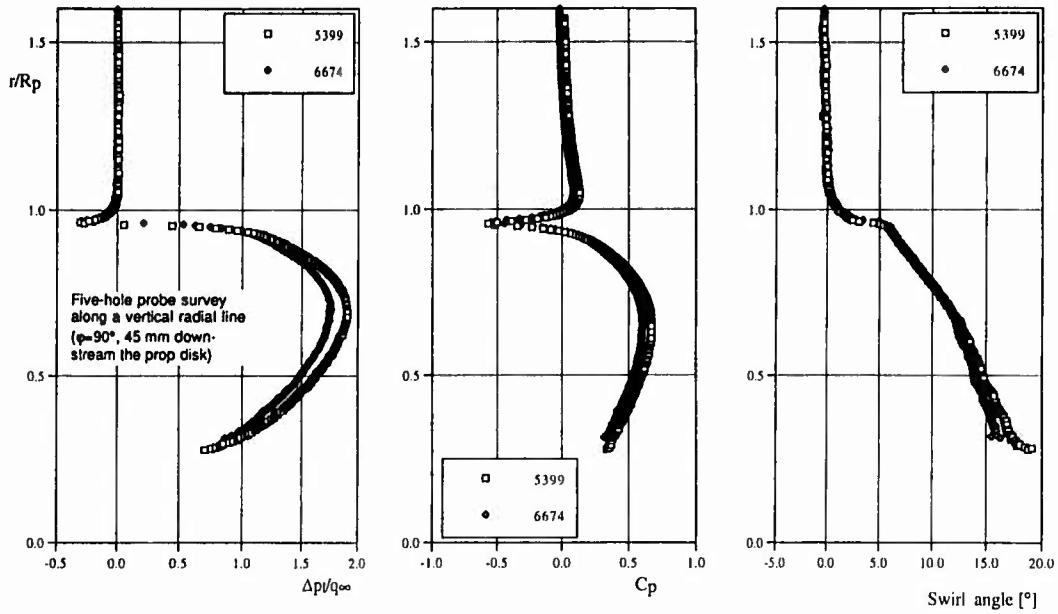



**Figure 12** **Examples of test repeatability (CONF1)**

| Run no. | $U_\infty$ (m/s) | α [°] | β [°] | N [RPM] | J | $C_F$ | $C_T$ | $C_P$ | η |
|---|---|---|---|---|---|---|---|---|---|
| 5399 | 48.56 | 0.1 | 0.0 | 6641.1 | 0.686 | 0.242 | 0.232 | 0.248 | 0.642 |
| 6674 | 49.41 | 0.0 | 0.0 | 6643.1 | 0.697 | 0.236 | 0.234 | 0.242 | 0.674 |

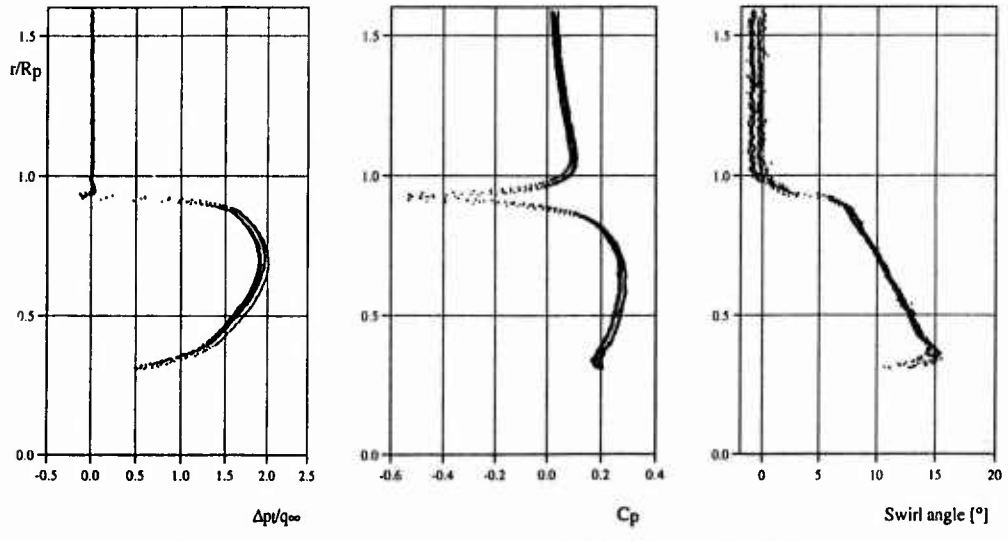
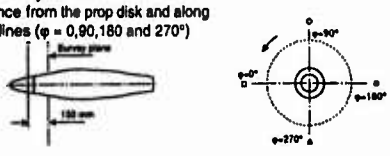



**Figure 13** **Slipstream characteristics (CONF1)**
**Test of axisymmetry (nominal axi-symmetrical geometry and onset flow)**

**$U_\infty$=48.4 m/s, N=6645 RPM, $\beta_{.75}$=29°**
**$C_F$=0.247, J=0.685, $C_T$=0.236, $C_P$=0.255**

Flow field survey at 150 mm downstream axial distance from the prop disk and along four radial lines (φ = 0,90,180 and 270°)



# Experimental Data on the Aerodynamic Interactions Between a Helicopter Rotor and an Airframe

by

J.G. Leishman
Associate Professor

Nai-pei Bi
Research Associate

**Center for Rotorcraft Education and Research,**
Department of Aerospace Engineering,
University of Maryland at College Park,
College Park, Maryland 20742, USA

## Summary

The data presented in this contribution were obtained at the Center for Rotorcraft Education and Research at the University of Maryland under part of a research program sponsored by the United States Army Research Office. The experiments were performed in several wind-tunnel entries during the period from June 1988 through to June 1990. The purpose of the experiments was to provide a better understanding into the origin of rotor/airframe interactional aerodynamic effects that are present on helicopters and other rotary wing aircraft. The measured results provide several unique and challenging engineering test cases for computational fluid dynamic methods used to model helicopter rotor wakes and rotor/airframe interaction phenomena.

## Introduction

Interactional aerodynamic problems suffered by rotorcraft arise from rotor effects on airframe loads, and airframe effects on the rotor loads and performance. These interactional effects are accentuated on conventional helicopters by design trends toward the use of higher rotor disk loadings (higher thrust carried by less rotor area) and smaller clearances between the rotor and the fuselage. The higher disk loading of smaller rotors allows lighter blades and hub designs, with increased payload capability. The correspondingly lower moments of inertia also allow greater aircraft agility/maneuverability. The benefits of smaller rotor/airframe clearances are reduced hub drag in forward flight, and a more compact aircraft for storage or transportation. However, these gains from higher disk loadings and smaller rotor/airframe clearances must be balanced against their effects on the aerodynamic interactions between the rotor and the airframe.

One obvious effect of higher rotor disk loadings is increased slipstream velocities, which increases the loads on parts of the airframe within the rotor wake boundary. In addition, individual wake filaments impinging directly on the airframe will be stronger, causing greater local loading. A reciprocal effect of the airframe on rotor loads and performance arises because the airframe alters the rotor inflow and wake geometry. The fluid dynamic mechanisms contributing to these aerodynamic interactions are very complex, especially since several contributing phenomena are often present at once. Until 1988, the mechanisms responsible had not been extensively studied or isolated from an experimental perspective, and today many aspects of the problem still remain beyond the state-of-the art in theoretical modeling.

The specific data presented in this contribution were obtained from a study to investigate the mutual aerodynamic interactions between a four-bladed fully articulated rotor and a helicopter like fuselage (body), and between the rotor and a fixed lifting surface (wing). A relatively simple body was chosen for the study to provide a good geometric definition for computational studies, and to minimize the possibilities of complex flow separations/reattachments that would normally be associated with an actual helicopter airframe. The lifting wing installed in the flow field near the rotor provided a greater challenge for these computational methods. This wing can represent the tailplane present on most helicopters, or the wing or empennage of a tilt rotor aircraft. The overall objective of these tests was to provide a further insight into the possible rotor/airframe interactional mechanisms, and to attempt to isolate some of the mechanisms for comparison with CFD methods.

Data were measured for several different configurations including: the isolated rotor, the isolated body, the body with hub rotating but without rotor blades attached, and the rotor/body/wing combination. A first objective was to obtain results for the isolated components to provide a solid basis for comparison with mathematical models of the isolated component flow fields. Another objective was to try to isolate some of the important interaction mechanisms. To this end, comprehensive measurements were made of the forces and moments on the body, thrust and power on the rotor, and time-averaged and dynamic pressures on the body and lifting surface. Measurements were also made of the induced velocities below and behind the rotor in forward flight. These quantitative measurements were supported by flow visualization of the rotor wake and the behavior of the wake near the airframe by using wide-field shadowgraphy. Tests were conducted in hover (on a hover tower) and in forward flight (in a wind tunnel) at various combinations of rotor thrust, advance ratio and tip path plane angle of attack.

A large part of this data base is suitable for CFD validation, and a summary of the measured data are included in this report. The data are available on request through the Department of Aerospace Engineering, University of Maryland.

## 1. General Description

| | |
|---|---|
| 1.1 Model Name or Designation | University of Maryland Rotor/Airframe Interaction Model |
| 1.2 Model Type(s) | Small scale (close to 1/6th scale), four-bladed articulated helicopter rotor. Body of revolution. Isolated low aspect ratio lifting surface (wing). |
| 1.3 Purpose of Test(s) | To examine the aerodynamic interactions between a rotor and an airframe (body and 3-D wing) in hover and forward flight. |

| | |
|---|---|
| 1.4 Dominant Flow Physics | Strong rotor tip vortices, highly energetic vortical wake that envelopes the body and/or wing. Vortex/surface impingement phenomena. |

## 2. Details of Model(s)

| | |
|---|---|
| 2.1 General Geometric Arrangement | See Figure 1. |
| 2.2 Specific Configurations Tested | 1. Isolated body.<br>2. Isolated rotor.<br>3. Rotor/body combination.<br>4. Rotor/body combination without blades.<br>5. Rotor and isolated lifting surface.<br>6. Rotor/body and lifting surface. |

2.3 Rotor Data

A four-bladed, fully articulated rotor system was used in the tests. Rotor diameter was 1.65 meters (65 inches). The rotor consisted of a fully articulated hub with swashplate, driveshaft and transmission. The rotor blades were attached to the hub through coincident flap and lead-lag hinges. The pitch assembly of each blade was connected to the swashplate by a pitch link. Collective and cyclic pitch angles were set via remote-control by positioning the swashplate by means of three electro-mechanical actuators. The basic geometric characteristics of the rotor and body are summarized in Table 1.

| | |
|---|---|
| 2.3.1 Blade Planform | The blades were rectangular planform with a chord of 6.35 cm (2.5 in.). The blades were made of composite materials with a balsa wood core, and were structurally very stiff relative to a full scale rotor to help minimize aeroelastic effects. |
| 2.3.2 Blade Taper | The blades were of rectangular planform, with no taper. However, tests have also been performed using blades with a 3:1 taper over the outboard 94% of span and of the same thrust weighted solidity as the untapered blades. |
| 2.3.3 Twist Distribution | The blades incorporated $12^{o}$ of linear nose down twist. |
| 2.3.4 Rotor Airfoils | A distribution of NASA RC(4)-10 and NACA RC(3)-10 series airfoil sections were used on the rotor blades. The RC(3)-10 airfoil has high drag-divergence Mach number and a low pitching moment for the tip sections. The RC(4)-10 airfoils provided good high lift capability for inboard parts of the blade. |
| 2.3.5 Distribution of Airfoils | The distribution of rotor blade airfoils is specified on an engineering drawing. If specifically requested, this information can be released as part of the data package. |
| 2.3.6 Hub Components | The flap and lead/lag hinge were coincident at a 6.53% radius hinge offset. The hub had a nominal diameter of 8% (excluding blade attachments) relative to the rotor diameter, and about 50% relative to the body diameter. |
| 2.3.7 Drive Fairing | For the isolated rotor tests, the rotor transmission was covered with a minimum body fairing (see Figure 2). The effects of this fairing have been shown to provide only a minimal influence on the rotor performance and the resulting wake geometry. |

2.4 Body Data

To keep the body relatively simple, but still provide some challenge for CFD modeling of the flow field, the particular body shape selected for the current studies was a body of revolution with a long tail boom, as shown in Figure 1. The possibility of flow separation on the tail boom and other parts of the airframe was considered in the design of the body shape. The rotor wake was expected to impinge on the tail boom at low advance ratios, producing locally high adverse pressure gradients and a strong possibility of flow separation. Nevertheless, to provide a baseline case, the isolated body was designed to have mild adverse pressure gradients. The body is one of a family that can be defined theoretically as the zero streamline that exists when superimposing the potential functions of a point 3-D source and two point 3-D sinks of appropriate strengths in a uniform flow. While the body was designed to be relatively simple, emphasis was also placed on keeping this body shape, and its location relative to the rotor, reasonably representative of a real helicopter.

| | |
|---|---|
| 2.4.1 Body Length | The total length of the body was 1.94 m (76.5 in.) |
| 2.4.2 Cross-sectional Details | Body maximum diameter was 0.254 m (10.0 in.). Body taper ratio was 2.5:1, making the diameter of the tailboom 0.102 m (4.0 in.) - see Figure 1. |
| 2.4.3 Rotor/Body Spacing | The spacing between the rotor hub plane and the longitudinal centerline of body was 29% of rotor radius. |

2.5 Lifting Surface (Wing) Data

A lifting surface (wing) was mounted horizontally in the flow field to model the interactional effects between the rotor and a horizontal stabilizer on a helicopter or wing or empennage of a tilt rotor - see Figure 3. The tests were performed with the wing in four different positions relative to the rotor.

| | |
|---|---|
| 2.5.1 Planform | Wing was rectangular, with an aspect ratio of 2, square cut tips. |
| 2.5.2 Twist Distribution | Untwisted. |
| 2.5.3 Airfoil | NACA 0014 |

2.6 Geometric Definition of all Components

| | |
|---|---|
| 2.6.1 Rotor Geometry | See Section 2.3 |
| 2.6.2 Body Geometry | The body geometry is prescribed numerically. Coordinates for the body revolution are given in the data package. |
| 2.6.3 Lifting Surface (Wing) | The geometry of the lifting surface is numerically prescribed from the NACA 0014 airfoil shape. |
| 2.6.4 Tolerances | The body had a surface tolerance of ± 0.5 mm. The wing geometry had a surface tolerance of ± 0.25 mm. |
| 2.6.5 Surface Roughness | The model surfaces were aerodynamically smooth with no artificial roughness. |

2.7 Model Support Details

The complete rotor and/or body assembly was mounted on a single tubular support that was hinged under the wind tunnel floor - see Figure 4. This arrangement allowed the whole rotor and body assembly to be tilted in unison to simulate forward flight conditions. The shaft angle was varied remotely using a hydraulic actuator connected to the support, which enabled shaft angles of ± 10 degrees to be obtained, if required. The wing was mounted separately on a single tubular support, and was set to an incidence of zero degrees relative to the free-stream flow.

## 3. General Tunnel Information

| | |
|---|---|
| 3.1 Tunnel Designation | Glenn L. Martin Wind Tunnel (GLMWT) of the University of Maryland. |
| 3.2 Organization Running Tunnel | Department of Aerospace Engineering, University of Maryland. |
| 3.3 Tunnel Characteristics | |
| 3.3.1 Type of Tunnel | Subsonic. Closed-return. |
| 3.3.2 Operating Envelope | The speed range in the test section is 2 m/s (6 ft/s) to 100 m/s (320 ft/s). |
| 3.3.4 Maximum Run Time | Continuous operation is possible up to the maximum speed. |
| 3.4 Test Section | |
| 3.4.1 Arrangement | The general arrangement of the rotor/body model in the wind tunnel test section is shown in Figure 4. |
| 3.4.2 Test Section Dimensions | Test section dimensions are 3.36 m (11.04 ft) wide by 2.36 m (7.75 ft) high by 3.96 m (13 ft) long with 25.4 cm (10 in.) fillets in the four corners. |
| 3.4.3 Wall Geometry Details | The test section has non porous walls. The external walls have steel plates installed for rotor testing. Glass windows and rectangular slots provide for optical access for laser or shadowgraph equipment. The complete ceiling and a large part of the floor of the test section can be removed for hover or low advance ratio testing, if required. There are rows of pressure taps on the ceiling and both side walls to measure the wall pressure signatures. |
| 3.5 Freestream Conditions | |
| 3.5.1 Reference Flow Conditions | Reference flow conditions were determined from the pressure difference between an orifice ring in the settling chamber and an orifice ring at the leading edge of the test section. Static pressure was very close to atmospheric. Temperature was measured in the settling chamber. |

3.5.2 Tunnel Calibration

The tunnel was calibrated against a standard pitot tube that has a known calibration factor. The flow uniformity was measured with a rake of static probes spaced 30.5 cm (12 in.) apart, located at 30.5 cm intervals in the vertical dimension. The static pressure variation in the streamwise direction was measured with a static pipe and by comparison with the ceiling pressures.

3.5.3 Date of Last Calibration

The tunnel was last calibrated in 1980 for full flow uniformity. It has been checked against a standard pitot tube for dynamic pressure calibration at least once each year.

3.6 Flow Quality

Overall turbulence level: 0.21 % (turb. factor 1.05). Overall noise level: 88 dB measured in the flow at test section speed of 30.5m/s (100 ft/s). No boundary layer control for these experiments. Typical floor boundary layer displacement thickness: 1 cm.

3.6.1 Uniformity

Static pressure variation over model length and span: less than ±0.5% free-stream dynamic pressure ($q_\infty$). Dynamic pressure variation over model length and span: less than ±0.3%$q_\infty$. Dynamic pressure variation less than 1%, measured simultaneously with force and/or pressure measurements. Flow angularity measured by 7 hole probes and by calibration wing. Flow angularity less than ±0.25 degrees over model span.

3.6.2 Temperature Variation

Temperature is not controlled, and varies during a run depending on the heating rate. For these tests it varied less than 1 degree Celsius as measured in the settling chamber.

## 4. Instrumentation

4.1 Model Position

The support post for the rotor/body model was installed at the geometric center of the test section. The distance from the body centerline to the tunnel floor was 1.18 m (3.87 ft) and the distance from the rotor hub center to the floor was 1.424 m (4.67 ft) - see Figure 4.

4.1.1 Geometrical Incidence

Model geometric incidence angle (shaft tilt) was measured using a calibrated potentiometer mounted at the support post hinge.

4.1.2 Accuracy of Incidence

The accuracy of the shaft tilt was ±0.01 degrees.

4.2 Body Pressure Measurements

4.2.1 Number and Disposition of Static Pressure Taps

Body: A total of 142 static pressures were measured on the body. These pressure taps were distributed in three longitudinal rows and at two circumferential rings, as shown schematically by Figure 5. One row was located on the top centerline, with other rows on each side. All 41 taps along each row were uniformly spaced based on surface arc length. At the two circumferential locations, 31 pressure taps were used (one forward ring with 15 taps and one aft ring with 16 taps). The actual tap locations are available as part of the data package.

Wing: A total of 30 static pressures were measured on the lifting surface (wing). These pressure taps were located at 30%, 60% and 80% of span. The actual tap locations on the wing are available as part of the data package.

4.2.2 Number and Disposition of Pressure Transducers

Body: Unsteady (dynamic) pressures were measured on the body surface using dynamic pressure transducers. Two bodies were used for these tests. On the first body, 21 pressure transducers were distributed over the body. The transducer locations are shown schematically in Figure 6. On the second body, 32 transducers were used, which were concentrated over the tail region, as shown in Figure 7. In each case, the actual transducer locations are available as part of the data package.

Wing: Unsteady pressures were measured on the lifting surface at 30 locations and at 25%, 65% and 85% of span. The actual transducer locations on the wing are available as part of the data package.

4.2.3 Range and Accuracy of Pressure Transducers

Electromechanical scani-valves were used for static pressure measurements on the body. Typically, the scani-valves had pressure sensors with a range of

0.3626 kPa (2.5 lb/in$^2$) and with a net measuring accuracy of $\pm 7.25.10^{-4}$ kPa ($\pm 0.005$ lb/in$^2$). Tunnel total pressure and dynamic pressure were measured by each valve and used as reference pressures. Static pressure measurements on the wing were made using a multi-channel modular pressure transducer system. These modules contained miniature quartz pressure transducers, analog multiplexers and analog to digital converters. A miniature pneumatic valving system in each module permitted rapid on-line calibration and re-zeroing of the pressure sensors. This capability was essential to maintain measurement accuracy over considerable tunnel run times. Frequent on-line calibrations enabled measurements of the static and dynamic pressures to be made to less than 7.5 Pa (0.001 lb/in$^2$) with high repeatability. The dynamic pressure transducers used for unsteady pressure measurements had a range of $\pm$ 0.145 kPa ($\pm$1 lb/in$^2$), and a combined linearity and hysteresis of $\pm$ 0.1% of full-scale.

4.3 Force and Moment Measurements

4.3.1 Balances

Two independent strain-gage balances were used to measure the rotor and body loads. The rotor balance was a six-component strain-gage balance, which measured rotor lift, side-force, axial-force, pitching moment, rolling moment and yawing moment. The body balance was a three-component strain-gage balance, which was used to measure the body lift, drag and pitching moment. Both rotor and body balances were mounted independently. Rotor torque was measured using a torque disc instrumented with a strain-gage bridge and attached to the rotor shaft. The rotor balance was isolated from the transmission by means of a flexible diaphragm coupling.

4.3.2 Range and Accuracy

The maximum range and accuracy of each component of the rotor and body balances are given in Table 3.

4.4 Flow Field Measurement Technique

An array of four miniature seven-hole pneumatic probes were used to measure total pressure, static pressure and flow angularities in the rotor wake. The probes were mounted on a computer controlled traverse system.

4.4.1 Flow Regions Investigated

The flow field was measured over a 28 by 16 point grid on both the left and right hand sides of the rotor, giving a total of 896 points in one horizontal measurement plane. Three planes were surveyed at heights of 1.03 m, 1.16 m and 1.29 m relative to the wind tunnel floor, or heights of z/R = -0.14, -0.29 and -0.45 relative to the rotor hub center. The actual measurement coordinates are available as part of the data package.

4.4.2 Probes

The seven-hole probes were manufactured from seven stainless steel hypodermic tubes inserted into a larger stainless tube. The inner tubes had an inside diameter of 0.07 mm with a wall thickness of 0.13 mm. The tubes were silver soldered together and machined to provide a 25 degree half angle at the tip. The resulting probes had a diameter of about 3 mm. The probes were then calibrated to angularities of $\pm$ 70 degrees in three mutually perpendicular directions.

4.4.3 Probe Supports

Four probes, spaced 15.24 cm (6 in) apart, were mounted on a traversing system which was secured to the wind tunnel floor. To insure that the probes were kept well within the calibrated angularity limits (conservatively $\pm$ 50 degrees) when traversing the rotor flow field, they were pitched to an angle of 30 degrees relative to the free-stream flow. The probes were traversed in the tunnel horizontal reference plane in increments of 7.62 cm (3 in). Three horizontal planes below the rotor were surveyed.

4.4.4 Pressure Measurements

The probe pressure measurements were made using the multi-channel modular pressure transducer system described in Section 4.2.3.

4.5 Surface Flow Visualization

Due to the highly unsteady nature of the flow field in this experiment, no surface flow visualization was performed.

4.6 Flow Field Visualization

4.6.1 Technique Applied

The wide-field shadowgraph technique was used for rotor wake visualization. Components of the system include a still or video camera, a short duration high intensity point-source strobe, and a retroreflective screen. A schematic of the shadowgraph setup is shown in Figure 8.

| | |
|---|---|
| 4.6.2 Planes Visualized | The rotor wake was visualized below and above the rotor. Special attention was paid to views from the side. Rotor tip vortices and tip vortex/body surface interactions were observed. |
| 4.6.3 Data Format | Flow visualization results were recorded on 35mm black and white film, 35mm Polaroid, and on video tapes. Approximately 600 shadowgraph images were acquired, and about 6 hrs. of video. Shadowgraphs are available to data users only by special arrangement. |
| 4.7 Tunnel Wall Measurements | |
| 4.7.1 Types of Measurement | Wall pressure signatures were obtained along the length of the tunnel working section. Signatures were measured on the ceiling and on both sidewalls. |
| 4.7.2 Number and Location of Wall Pressure Taps | A total of 72 pressure taps were located in three rows of 24 each The taps were placed 15.24 cm (6 in) apart, with the No.12 tap being located at the center-line of the test section directly above the rotor support post. The taps extended a distance of about two rotor radii (2.03 R) forward and 2.22 R aft of the working section centerline. The actual tap locations are available as part of the data package. |
| 4.7.3 Instrumentation | The wall pressure measurements were made using a modular multi-channel pressure transducer module (described previously in Section 4.2.3). Accuracy was typically less than 7.5 Pa (0.001 $lb/in^2$). |
| 4.8 Other Instrumentation | Other instrumentation on the rotor was provided for trimming purposes and safety of flight. Hall-effect sensors were placed at the rotor flap and lead/lag hinges to monitor the blade response. Strain gauges on a reference blade monitored blade bending, lag and torsion loads. |

## 5. Test matrix and Conditions

| | |
|---|---|
| 5.1 Test Matrix | See Table 4. |
| 5.1.1 Number of Test Cases | Over 200 test points performed - see Table 4. Sub-set is available to users. |
| 5.1.2 Number of Configurations Tested | Six different configurations were tested - see Section 2.2. |
| 5.2 Model/Tunnel Relations | |
| 5.2.1 Maximum Blockage | 3% |
| 5.2.2 Rotor Diameter/ Tunnel Width | 48.2% |
| 5.2.3 Rotor Disk Area/ Tunnel Cross Section | 27% |

## 6. Data

| | |
|---|---|
| 6.1 Availability of Data | |
| 6.1.1 Organization Owning Data | All test data belong to the US Army Research Office and the Department of Aerospace Engineering, University of Maryland. |
| 6.1.2 Person Responsible | Most of the test data are readily available and can be obtained by request from: |
| | Dr. J. Gordon Leishman, Associate Professor<br>Department of Aerospace Engineering<br>University of Maryland<br>College Park, Maryland 20742<br>USA<br>Tel: (301) 405-1126<br>Fax: (301) 314-9001 |
| 6.2 Suitability for CFD Validation | Most of the test data are suitable for CFD validation. |

| | |
|---|---|
| 6.3 Type and Form in Which Data Are Available | |
| 6.3.1 Type and Form | Data are mostly in the form of aerodynamic coefficients. |
| 6.3.2 Data Carrier | By arrangement. Data can be given out in a variety of formats, including magnetic tape or floppy disk. Apple Macintosh files are the preferable format. User must supply data carrier. |
| 6.3.2 Extent of Geometry Data | 500K Bytes. |
| 6.3.3 Extent of Aerodynamic Test Data | Raw data is over 50 M Bytes. Processed sub-set data available to users varies up to 10 M Bytes. |
| 6.4 Corrections Applied to Data | None, unless specifically stated. |
| 6.4.1 Interference and Blockage Corrections | None directly applied to measured data. |
| 6.4.2 Sting and Support Corrections | None applied. |
| 6.4.3 Aeroelastic Deformation | There were no significant aeroelastic deformations. |

## 7. Data Accuracy and Repeatability Assessment

| | |
|---|---|
| 7.1 Estimated Accuracy of: | |
| 7.1 1 Free Stream Conditions | See Table 5. |
| 7.1.2 Measured Data | See Table 5. |
| 7.2 Repeat Measurements | Selected repeat measurements were made of rotor performance, body loads, and pressure distributions. |

## 8. References


Leishman, J.G., and Bi, Nai-pei, "Aerodynamic Interactions Between a Rotor and a Body in Forward Flight," *Journal of the American Helicopter Society*, Vol. 35, No. 3, pp. 22-31, July 1990.

Bi, Nai-pei and Leishman, J.G., "Experimental Study of Aerodynamic Interactions Between a Rotor and a Body," *Journal of Aircraft*, Vol. 27, No. 9, pp. 779-788, September 1990.

Leishman, J.G., and Bi, Nai-pei, "Measurements of Rotor Flow Field and the Effects on a Body in Forward Flight," *Vertica*, Vol. 14, No. 3, pp. 401-415, 1990.

Bi, Nai-pei and Leishman, J.G., "Analysis of Unsteady Pressures Induced on a Body by a Rotor," *Journal of Aircraft*, Vol. 28, No. 11, pp. 756-767, November, 1991.

Bi, Nai-pei, Leishman, J.G. and Crouse, G.L., "Investigation of Rotor Wake Interactions with a Body in Low Speed Forward Flight," AIAA paper 91-3228, *AIAA 9th Applied Aerodynamics Conference*, Sept. 23-26, 1991, Baltimore, MD To appear in J. of Aircraft, 1994.

Bi, Nai-pei, "*Contributions to the Experimental Investigation of Rotor/Body Aerodynamic Interactions*," Ph.D. Thesis, Dept. of Aerospace Engineering, University of Maryland, College Park, Maryland, USA, May 1991.

Crouse, G.L., Leishman, J.G., and Bi, Nai-pei, "Theoretical and Experimental Study of Unsteady Rotor/Body Aerodynamic Interactions," *Journal of the American Helicopter Society*, Vol. 37, No. 1, pp. 55-65, January 1992.

Bagai, A., and Leishman, J.G., "A Study of Rotor Wake Development and Wake/Body Interactions in Hover," *Journal of the American Helicopter Society*, Vol. 37, No. 2, April 1992.

Leishman, J.G., and Bagai, A., "Fundamental Studies of Rotor Wakes in Low Speed Forward Flight using Wide-field Shadowgraphy," AIAA paper 91-3232, *AIAA 9th Applied Aerodynamics Conference*, Sept. 23-26, 1991, Baltimore, MD.

Leishman, J.G., Bi Nai-pei, "A Study of Rotor/Lifting Surface Interactions," AIAA Paper 93-0871, *21st AIAA Aerospace Sciences meeting and Exhibit*, Reno, NV, Jan. 11-14, 1993. To appear in J. of Aircraft, 1994.

Crouse, G.L., "An Analytical Study of Unsteady Rotor/Fuselage Interaction in Hover and Forward Flight," Ph.D. Thesis, Dept. of Aerospace Engineering, University of Maryland, College Park, Maryland, USA, December 1992.

## 9. Typical Results

### 9.1 Isolated Body

The aerodynamic force and moment characteristics of the isolated body are shown in coefficient form in Figure 9 as a function of angle of attack (shaft pitch angle). The forces and moments were resolved to a fictitious point coincident with the body longitudinal centerline and the rotor shaft axis. The particular results shown here are for a wind-speed of 24 m/s (79 ft/s), which corresponded to a Reynolds number of 3.24 million based on body diameter, or to an advance ratio of 0.15 if the rotor were present.

The results shown in Figure 9 are a consequence of the changing distribution of pressure over the body with angle of attack. The static pressure distribution along the top center-line of the isolated body is shown in Figure 10 for three angles of attack. From a stagnation point at the nose, the flow accelerates to approximately the free-stream value over the region with the uniform cross-section. At the body taper, the flow is briefly accelerated again, and this is followed by a gradual pressure recovery over the tail region. A comparison of a 3-D source panel model with the test data was satisfactory, confirming that the isolated body is free of complicated flow separations. These data are also useful for the purposes of making comparisons of the body loads in the presence of the rotor.

### 9.2 Isolated Body and Hub

Since the rotor had an unscaled hub relative to an actual helicopter, a series of tests were conducted to assess the significance of the hub alone on the body loads. When the bladeless hub was spun at the normal rotor speed, this simulated high speed forward flight with the rotor since under these conditions the rotor wake will be swept above the body and the rotor will have a minimal influence on the body loads apart from the hub wake. While the body lift was found to be relatively unaffected by the presence of hub, see Figure 9, there was some hub influence on the pitching moment, albeit quite small. As shown in Figure 11, this is due to the modified pressure distribution on the body dorsal due to the hub wake. A region of increased total pressure was created immediately upstream of the hub, and downstream, a region of decreased total pressure indicated the formation of a wake. These results show that the possibility of a rotor hub wake should be taken into account in CFD studies at high rotor advance ratios.

### 9.3 Rotor Trim Procedure and Data Presentation

For all forward flight tests, the rotor speed was established at the normal operating rpm, $N_R$, and the wind turned-on. Once the desired advance ratio was obtained, the collective pitch angle was gradually increased to give the required value of thrust while maintaining $N_R$, and the rotor trimmed by means of longitudinal and lateral cyclic to remove the first harmonic of blade flapping. The blade flapping response was measured by means of Hall-effect sensors mounted in the blade flapping hinges. This is a standard trim procedure for articulated rotors in a wind-tunnel situation, and ensures that the rotor tip-path-plane (TPP) is perpendicular to the rotor shaft axis and, therefore, parallel to the longitudinal axis of the body.

With the rotor present there were significant changes to the mean and unsteady pressure loads on the body, and the wing. The pressure data were reduced to pressure coefficients (denoted by $C_p'$). Since the airframe components may operate partly inside the boundaries of the rotor wake, there is a non-uniform increase in total pressure due to energy addition to the flow by the rotor. Consequently, the airframe pressures depend on the combined effects of the free-stream dynamic pressure and the (non-uniform) increase in local dynamic pressure produced by the rotor. Non-dimensionalization of the pressures by a constant parameter, therefore, avoids any ambiguity when interpreting the results, and gives a better overall measure of the magnitude of interactional effects on the body pressures.

### 9.4 Effects of Rotor on Fuselage

The effects of the rotor on the body loads are shown in Figure 12 as a function of rotor thrust and advance ratio. At low advance ratios the rotor provides a download on the body that increases in magnitude with increasing rotor thrust. This download significantly diminished with increasing advance ratio, and became an upload at the highest advance ratios tested. At the same time, the rotor caused a fairly complex variation in the body pitching moment.

The overall trends exhibited in Figure 12 are a direct consequence of changes in strength and position of the rotor wake relative to the body. At the lower advance ratios, the wake almost completely envelopes the body producing stagnation pressure along the top and a suction pressure along the sides. A typical static pressure distribution along the top and sides of the body in the presence of the rotor is shown in Figure 13. The high stagnation pressures along the top of the body are responsible for the down force and a nose-up pitching moment at low advance ratios. Since the rotor downwash is a maximum near the edges of the rotor disk, the boundary of the rotor wake becomes quite clearly defined by the peaks in the body pressures. Also note in Figure 13 that significant reductions in pressure were obtained on the sides of the body. Again, this was particularly pronounced where the leading and trailing-edge boundaries of the rotor wake impinged the body. Different pressure distributions were obtained on each side of the body, which indicated that the body may experience a yawing moment (not measured). The source of this dissymmetry is related to the presence of a swirl velocity component in the rotor wake as well as the asymmetric flow separation characteristics on the lower part of the body.

Changes in rotor thrust and advance ratio were found to dramatically alter the body pressure distribution. The effects of increasing advance ratio on the static pressure on the retreating (left) side of the body at the same blade loading is shown in Figure 14. (The other pressure distributions are not shown to preserve clarity.) Increasing the advance ratio moves the suction peaks further aft along the body. This is because the rotor wake skew angle increases with advance ratio, and so the rotor wake boundary intersects the body further back on the tailboom. It should also be noted that the maximum suction and stagnation pressures are significantly reduced with increasing advance ratio since the induced velocities in the wake become increasingly streamwise. At the highest advance ratios, the wake is swept back well above the top of the body, and the body exhibits a positive lift force. This is due to a Coanda effect that exists between the body flow and the higher speed rotor wake. The

corresponding trend toward a nose-down pitching moment confirms that most of this Coanda lift is being generated on the body tailboom.

### 9.5 Effects of the Body on the Rotor

The body has a complicated mutual effect on the rotor loads and performance, and due to limitations of both time and instrumentation it has not yet been possible to fully document all these effects. However, the general effects of the body on the net rotor performance in forward flight are shown in Figure 15. The data are presented as curves of blade loading (or rotor thrust) versus collective pitch angle, shown with and without the body. At low advance ratios, the presence of the body was found to provide a significant positive increment to the rotor thrust, which was about 10% of the isolated rotor thrust. As the advance ratio was increased, the rotor thrust increment quickly reduced such that at an advance ratio of 0.15 there was only a very small effect of the body. Measurements of the corresponding rotor torque coefficient have also shown that at low advance ratios (as well as hover) there is a significant reduction in power required for a given thrust due to the influence of the body.

### 9.6 Unsteady Pressure Measurements

Unsteady pressure measurements were made at many points over the body. Overall, the unsteady pressure fluctuations were found to be the greatest in regions immediately below and downstream of the rotor. A typical illustration of the magnitude of the unsteady pressure loads on the body is shown in Figure 16, where the peak to peak values of the unsteady pressure at various points along the top of the body are superimposed on the time-averaged (mean) values. Note that the unsteady pressure fluctuations are very large in comparison to the time averaged values, and often exceed the mean pressure values. These results reinforce the requirement that any CFD modeling of the rotor/airframe aerodynamic interaction process must be fully unsteady, and a quasi-steady assumption will not be sufficient. Also note that in the case of the time-averaged measurements previously discussed, these results are a time-average of unsteady loads. Therefore, CFD comparisons with these data also require an unsteady analysis to be performed. The time-histories of unsteady pressure data were event-averaged, i.e., the data were first ensemble averaged over ten rotor revolutions, and since a four-bladed rotor was used, the results were further ensemble averaged over 90 degrees of blade azimuth angle. All the unsteady pressure data represent the fluctuations of the measured pressures about the mean value, and were synchronized in a phase-locked loop sense relative to the rotor position.

From the analysis of results from many tests, four characteristic unsteady pressure signatures on the body surface were identified. These signatures were classified into four categories: 1. Blade passage, 2. Close tip vortex/surface interactions, 3. Tip vortex/surface impingement, and 4. Post vortex/surface impingement. The first characteristic signature is due to rotor blade passage over the airframe. Blade passage effects are felt on parts of the airframe immediately below the rotor, and the magnitude of these loads are primarily a function of rotor blade loading. The other three characteristic signatures are related to the influence of the rotor wake and the individual tip vortices. Wake effects are felt at many different points on the airframe, and are primarily functions of the wake skew angle (which depends on rotor thrust and advance ratio). However, the strength, location and velocity of the wake vortices relative to the body, and also the distortion of the wake induced by the body, determines the magnitude and phasing of the unsteady pressure response.

Figure 17(a) shows a typical unsteady pressure signature caused by blade passage effects. This type of loading is characterized by regular pressure pulsations, with the peak pressure occurring in-phase with the blade passage over the body, i.e., at integer multiples of 90 degrees for a 4-bladed rotor. The unsteady loads induced by blade passage effects are approximately proportional to rotor thrust (blade lift or average bound circulation on the blade), and were found largely independent of the advance ratio, i.e., independent of the position of the rotor wake and blade tip vortices. The features of blade passage induced loads have been shown to be predictable by means of unsteady potential flow theory and, in principle, should be predictable by any inviscid methodology so long as the appropriate unsteady terms are retained in the governing equations.

The remainder of the characteristic unsteady pressure signatures are related to the rotor wake, and the wake/airframe interaction process. Figure 17(b) shows a type of signature that has been classified as a close tip vortex/surface interaction. These interactions occur when the rotor tip vortices pass close to the measurement point, but do not impinge on the body surface until downstream of that point. These loads have also been shown to predictable by means of an inviscid analysis. Figure 17(c) shows a typical pressure signature that results from tip vortex impingement on the body surface near the measurement point. It is characterized by a transient loading with a high suction pressure (and associated pressure gradient) due to the proximity of the vortex core. When the measurement point was just downstream of the vortex impingement, regular multiple pressure peaks were produced - see Figure 17(d). This is likely to be indicative of boundary layer separation the body surface due to the high adverse pressure gradients associated with the impingement, and possibly the creation of coherent secondary vortex structures. The prediction of this type of loading clearly requires a CFD model with all the necessary viscous terms retained in the governing equations.

### 9.7 Wake Surveys

The wake surveys permitted the quantification of the time-averaged total pressure and local velocities in the rotor wake, and were a useful indicator of the location of the rotor wake relative to the rotor and airframe. A global picture of the wake structure was obtained by plotting the total pressure distribution in the rotor wake in the form of contour plots for each of the measurement planes. An example of these data are shown in Figure 18. The highest total pressures occurred toward the rear of the disk. Specifically, the loadings were higher in the fourth quadrant where the lift on the blade is concentrated more toward the tip. The highest pressure gradients occurred at the boundaries of the rotor wake. There was considerable wake contraction in the longitudinal direction, this being about 78% of the rotor diameter at 0.45R below the rotor. However, there was a slight expansion of the wake in the lateral direction, this being about 105% of the rotor diameter.

It was noted that regions of both very high and very low total pressure also occurred downstream in the wake further behind rotor. The contours were closely spaced, indicating that the downstream wake had a very definite boundary. A very concentrated region of high dynamic pressure was formed on the advancing side of the wake. This was due to the relatively large induced velocities created by the tip vortices from each of the rotor blades as they interacted and produced a self distorting bundle of vortices just downstream of the disk. Regions of very low dynamic pressure also occurred downstream of the

retreating side of the disk, however, the distribution in the wake was found to be notably different from the advancing side. This is because of the fundamental differences in blade loading, wake geometry and induced velocity field between the advancing and retreating sides of the disk.

Away from the immediate vicinity of the body, both the total pressures and flow angularities were almost identical to those measured for the isolated rotor. Some differences in the flow field velocities were found to occur near the nose of the body for low advance ratios, however, as the advance ratio was increased these differences significantly diminished. An example of the longitudinal variation in the vertical component of induced velocity is shown in Figure 19. Note that the highest induced velocities were biased toward the rear of the disk. This trend is consistent with other experimental measurements and also mathematical models of the rotor wake induced velocity field, where the skewness of the wake is the source of this biased velocity field. Note that at the highest advance ratio tested here the longitudinal variation in velocity is very close to the linear form assumed by simple inflow models. Near the rotor hub region, the rotor does little useful work, so there is little change in the inflow in the immediate vicinity of the hub.

The lateral variation of vertical velocity also conveys some useful information about the rotor wake structure. The wake velocities were consistently higher on the advancing side of the disk because of the distribution of blade loading over this region and the subsequent evolution of the far wake. The wake surveys showed that downstream of the rotor disk, the wake rolled up very quickly to form into two major vortex "bundles" which are the rolled-up remnants of the individual tip vortices trailed from each blade. The wake roll-up process behind a rotor was observed by Heyson at NASA Langley in the 1950's, and is in fact very similar to the trailed wake obtained from a low aspect ratio wing. This can be readily seen in Figure 20 where the vertical component of induced velocity is plotted, and is very similar to that obtained between two rectilinear vortices of approximately equal strength.

### 9.8 Flow Visualization

All of the above results were supplemented by flow visualization. Although both laser sheet and shadowgraph methods were used, wide-field shadowgraphy was found to be the most useful in helping to understand the details of the rotor wake mechanisms responsible for the airframe loads. Shadowgraphs of the entire rotor wake were not obtained because of the relatively short distance between the recording camera, the rotor and the screen in the wind-tunnel environment. Therefore, separate images were obtained of the front and rear of the rotor wake - see Figure 8. However, the field of view in each case was still much greater than could practically be obtained with a conventional schlieren system. Furthermore, the closeness of the camera to the screen in these experiments meant that finer details of the wake could be observed. A zoom lens on both the still and video camera was used to provide fine details of the tip vortex formation from the rotor blade, as well as the interactions of the wake vortices with the body.

One important goal of the flow visualization work was to help quantify the positions of the rotor tip vortices relative to the rotor and to the airframe. For this quantification process, the strobe/camera positions were adjusted so that the optical axis was in the rotor tip path plane (TPP). Key reference points in the form of cross-hairs were marked directly onto the shadowgraph projection screen to establish the optical scaling factors. The system was set up such that at zero degrees of blade azimuth, the reference blade was parallel to the body centerline and, therefore, parallel to the screen. The quantitative measurements of the rotor wake geometry were made from the video recordings by digitizing and processing from shadowgraph screen coordinates into the rotor coordinate system using the appropriate optical scaling factors. Plots were then be made of the wake geometry versus wake age, with and without the airframe present in the flow field.

At the front of the disk, the presence of the body was found to make little difference to the wake geometry over the range of advance ratios tested. It was found that the wake vortices were normally convected above, and subsequently through, the TPP at the leading-edge of the disk (even at negative TPP angles of attack). This resulted in several dynamic blade/tip vortex interactions, which have been visualized and documented on video tape. These blade/vortex interactions involve strong viscous effects and clearly complicate the mathematical modeling of the blade loads and rotor wake. At the rear of the disk, very significant wake distortions occurred due to the body, both near the rotor and as the vortex filaments came in proximity to the body surface. Figure 21 shows results for the tip vortex displacements versus wake age in the presence of the body. This figure shows that the initial vertical wake displacements are slightly larger when the body is present, implying an increase in local downwash near the rotor plane. The body affects the rotor thrust, producing an increase in mean thrust and a decrease in power for a given collective pitch. This is partly because the body decreases the induced angle of attack on the blades as they pass over the body. The consequence of this increase in lift on the blade is to cause an increase in downwash below the rotor. The effect on the wake displacements was particularly pronounced in hover, although in forward flight the vortices were convected downstream away from the rotor and the effects were somewhat weaker.

Figure 21 also shows that the corresponding streamwise displacements are significantly different from the isolated rotor case, both near the rotor disk and near the body surface, especially at the lower advance ratio of 0.05. Near the rotor disk the presence of the body retards the initial streamwise convection of the tip vortices. Note that the effects of subsequent blade passages also causes sudden changes in the streamwise velocities. The tip vortices approached the body surface when they were about 180 degrees old, and at this point their vertical displacements were progressively retarded. The wake could not be easily observed for wake ages greater than 220 degrees since the wake/surface impingement process caused vortex bursting, resulting in a loss of wake visibility. Prior to this, near the body surface there was a progressive increase in the streamwise convection of the tip vortices. As the tip vortex filaments approached very close to the surface, they were convected quickly downstream and the wake trajectory became almost parallel to the body surface.

### 9.9 Rotor/Lifting Surface Interactions

Experiments were also conducted to study the aerodynamic interactions between the rotor and a fixed lifting surface. An instrumented low aspect ratio rectangular wing was positioned at different locations in the rotor flow field to simulate the aerodynamic environment encountered by the wings of tilt-rotors, or by the empennage of helicopters. Steady and unsteady pressure measurements were made on the wing at various chordwise and spanwise stations for various rotor thrusts and advance ratios. These results were complemented by flow visualization using the wide-field shadowgraph method, which helped identify the locations of the rotor wake relative to the wing. The results have shown that compared to the body, a lifting surface operates

in an even more complex unsteady three-dimensional flow environment, with regions of partial or complete flow separation. In addition, large unsteady loads are produced due to rotor blade passage effects and/or close passage or impingement of the rotor tip vortices on the wing surface. This particular situation creates several unique challenges for CFD prediction methodologies.

Time-averaged pressure distributions on the lifting surface were measured on both the upper and lower surfaces at the three spanwise stations. These measurements were mainly used to help interpret the state of the flow on the wing, i.e., whether the flow was attached, partially separated or fully separated. Typical chordwise pressure coefficient distributions measured on the lifting surface when positioned at the aft position (tailplane location) are shown in Figure 22. In this case, the 80% span station is further inboard and closer to the longitudinal centerline of the rotor. It can be seen that only the inboard section of the lifting surface exhibits a chordwise pressure distribution indicative of attached flow, with high suction pressures on the lower surface near the leading edge. At the outboard sections, the uniform pressure distribution on the lower surface suggests that the flow was completely separated. From these measurements, it can be inferred that for these conditions all three sections of the wing were operating at large negative effective angles of attack, but with the highest angles of attack biased toward the outboard parts of the wing. These large negative angles of attack are a result of the high local downwash created by the rotor at this low advance ratio.

As the advance ratio was increased from 0.075 to 0.10, the flow conditions on the lifting surface were found to change progressively. At $\mu$=0.10 all three spanwise stations showed chordwise pressure distributions that were symptomatic of either fully or partially attached flow. Much larger suction pressures were created at the leading edge on the lower surface at all three spanwise stations. Therefore, it was clear that the flow had begun to reattach to the surface as the advance ratio was increased over this range. This was mainly due to the decrease in the induced flow angle at the wing location (or increase in wake skew angle) as the advance ratio was increased. However, there was still a highly non-uniform flow over the lifting surface, with the inboard section producing the largest amount of negative lift. At the outboard spanwise stations, only partially attached flow occurred on the surface. This was especially the case at the 60% span locations, where there was evidence of significant trailing edge separation. As the advance ratio was further increased from 0.10 to 0.125 and higher, it was found that the whole lifting surface operated with nominally attached flow. At this advance ratio the rotor wake skew angle is much larger with lower downwash velocities and higher streamwise velocities, and so the induced flow angles of attack at the wing were correspondingly much lower.

Time-dependent pressures on the lifting surface were measured at 32 points. As for the body loads, all the results were nondimensionalized and converted to coefficient form, and are presented in terms of the alternating component only. All data was measured in a phase-locked sense and synchronized with the rotor position. A spectral analysis of the unsteady pressure measurements showed that the dominant frequency at nearly every location was at 4 per rotor revolution (4P), although many locations showed significant responses at 8P, 12P and 16P. The fundamental source of these loads is the rotor, but there are several possible constituent sources of unsteady loading that may be produced on a lifting surface located near a rotor. For locations near the rotor, blade passage effects produce a strong impulsive type of noncirculatory loading on the surface. At other locations, the rotor tip vortices will induce rapid changes in angle of attack as they are convected near the wing and, therefore, time-dependent aerodynamic loads will be produced. There may also be time-dependent aerodynamic effects due to the wake generated by the wing itself. Clearly, the relative magnitude of all these effects will depend on several interrelated parameters, and one purpose of this part of the experiment was to gain some insight into this problem.

At the forward wing locations (below the rotor), the loads were primarily of a blade passage type (see Figure 17). However, downstream of the rotor disk, the pressure signatures measured on the lifting surface at the rear positions showed many more complex variations. At the aft wing locations, the unsteady loads are closely related to the proximity of the rotor wake vortices. Figure 23 shows the time-dependent pressures measured at the aft wing position for five chordwise locations on the upper surface at the 85% span station - that is, the station closest to the longitudinal centerline of the rotor. Note that the pressure responses varied from fairly large near the leading edge to quite benign at the trailing edge.

From an examination of results at several different test conditions, it has been found that these complex pressure loads are related to the rotor thrust (and hence to the strengths and convection speeds of the rotor tip vortices). Furthermore, by means of flow visualization, the relative distance between the wake vortices and the measurement location were also found to be very important. The unsteady pressures measured on the upper surface of the lifting surface were found to vary significantly with advance ratio. As the advance ratio was increased from 0.1 to 0.125, the pressure signatures exhibited only relatively small changes. However, as the advance ratio was changed from 0.125 to 0.15 and then to 0.20, the magnitude of unsteady pressure response first decreased and then increased again. When the advance ratio was increased to 0.125, it was confirmed by flow visualization that the rotor wake skew angle was such that the most of the tip vortex filaments passed just above the top surface of the lifting surface (glancing impingement). At an advance ratio of 0.15, the wake was skewed back to an angle such that there was less likelihood of close tip vortex/surface interactions, and the pressure responses were benign. However, at an advance ratio of 0.20, the unsteady pressures were noted to increase again, even though the wake filaments were further away from the lifting surface than at $\mu$=0.15. This is due to the unsteady loads induced by the higher rotor wake convection velocities, and is consistent with the observations made on the body. In general, the observed sensitivity of the pressure loads at different points on the wing will make the theoretical prediction of these effects a significant challenge to the analyst.

In addition, note that the time-varying downwash field induced by the convecting wake vortices must also result in local time-varying angles of attack and time-dependent circulatory loads on the wing. Thus, there will be an unsteady wake system trailed from the wing. Besides the complexity inherent to any unsteady flow, the reduced frequencies of the rotor wake induced gust field at the lifting surface may be quite high, since for a four-bladed rotor operating the reduced frequency of the flow at the lifting surface (based on wing chord) would be of order 2. This requires the wing flow field to be considered as an unsteady CFD problem. Also, if and when stall occurs locally on the wing, the high effective reduced frequency of the flow means that separation and stall will be more dynamic in nature. This adds an additional level of complexity to the mathematical modeling of the interaction problem.

## 10. List of Symbols

| | |
|---|---|
| $b$ | Number of blades |
| $c$ | Blade chord, *m* |
| $C_p$ | Pressure coefficient = $100\,(p - p_\infty) / (0.5\rho V_\infty^2)$ |
| $C_p^u$ | Unsteady press. coeff.= $100\,(p^u - p_\infty) / (0.5\rho\Omega^2 R^2)$ |
| $C_p'$ | Pressure coefficient = $100\,(p - p_\infty) / (0.5\rho\Omega^2 R^2)$ |
| $C_{p0}$ | Total pressure coefficient = $(p_0 - p_\infty) / q_\infty$ |
| $C_T$ | Rotor thrust coefficient = $T / (\pi\rho\Omega^2 R^4)$ |
| $N_R$ | Normal rotor operating rpm |
| $p$ | Time-averaged static pressure, *Pa* |
| $p_\infty$ | Free-stream static pressure, *Pa* |
| $p^u$ | Unsteady component of pressure, *Pa* |
| $p_0$ | Measured local total pressure, *Pa* |
| $q_\infty$ | Free-stream dynamic pressure = $0.5\,\rho\,V_\infty^2$, *Pa* |
| $R$ | Rotor radius, *m* |
| $T$ | Rotor thrust, *N* |
| $V$ | Local flow velocity, *m / s* |
| $V_\infty$ | Tunnel free-stream velocity, *m / s* |
| $x$ | Longitudinal coordinate, *m* |
| $y$ | Lateral coordinate, *m* |
| $z$ | Vertical coordinate, *m* |
| $\alpha_s$ | Shaft tilt angle (positive aft), *deg.* |
| $\rho$ | Air density, $kg / m^3$ |
| $\sigma$ | Rotor solidity, $b\,c / \pi / R$ |
| $\mu$ | Advance ratio, $V_\infty / (\Omega R)$ |
| $\phi$ | Circumferential angle, *deg.* |
| $\psi$ | Blade azimuth angle, *deg.* |
| $\Omega$ | Rotor rotational frequency, *rad / s* |

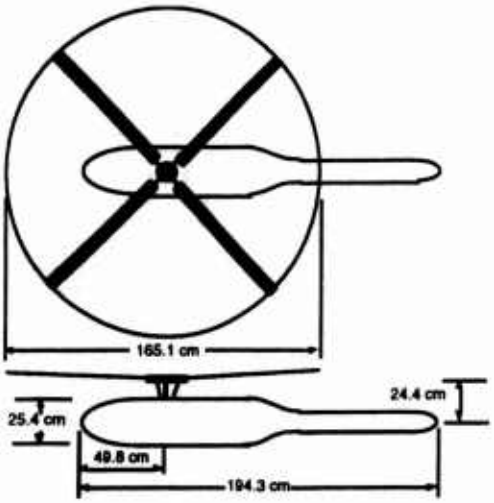



**Figure 1: General geometry of rotor and body (Not to scale)**

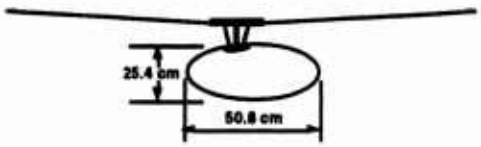



**Figure 2: General geometry of rotor with minimum body aerodynamic fairing (Not to scale)**

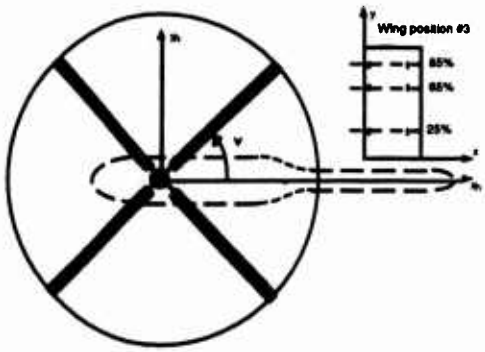



**Figure 3: Schematic of rotor/lifting surface (wing) interaction geometry. (Not to scale). See Table 2 for location of wing relative to rotor.**

| Item | Quantity |
|---|---|
| Number of blades, b | 4 |
| Rotor radius, R | 0.8255 m (32.5 inches) |
| Blade chord, c | 0.0635 m (2.5 inches) |
| Rotor solidity, b c/π R | 0.098 |
| Blade twist (linear) | -12 degrees |
| Blade taper ratio | 1.0 (most cases) |
| Airfoils | NASA RC(3)10/(4)10 |
| Body length, L | 1.94 m (76.5 inches) |
| Body max. diameter. | 0.254 m (10 inches) |
| Body taper ratio | 2.5:1 |

**Table 1: Geometric characteristics of rotor and body.**

| Wing Position | Location of Port Leading Edge |
|---|---|
| 1 | $x_h/R = -0.102$, $y_h/R = 0.215$ |
| 2 | $x_h/R = -0.102$, $y_h/R = -0.954$ |
| 3 | $x_h/R = 1.237$, $y_h/R = 0.215$ |
| 4 | $x_h/R = 1.237$, $y_h/R = -0.954$ |

**Table 2: Location of wing relative to rotor shaft axis (see also see Figure 3)**

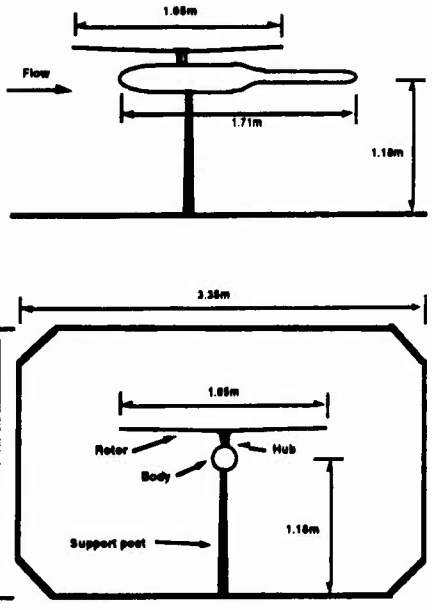



Figure 4: General geometric arrangement of rotor/body model in GLM wind tunnel (Not to scale)

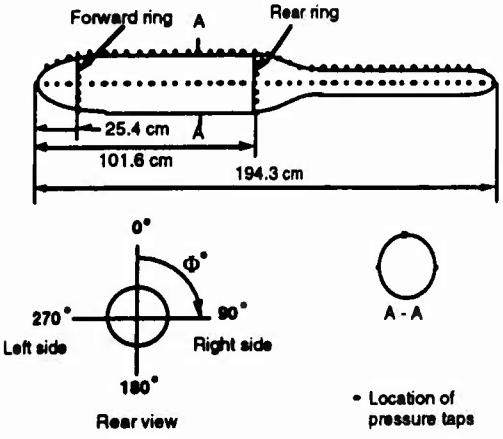
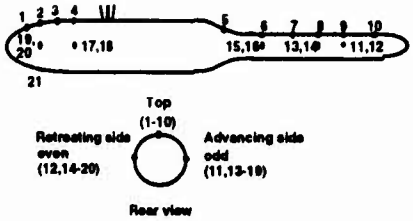



Figure 5: Schematic showing locations of static pressure taps on body (Not to scale)



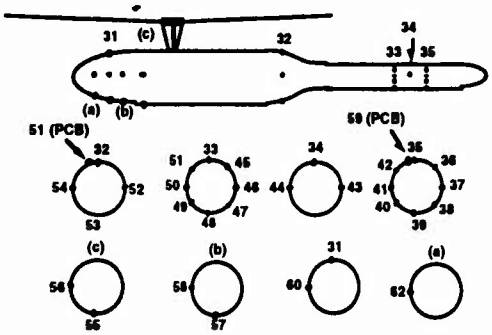

• Location of pressure sensor

Location of sensor from nose:

#1 – 3.25", #2 – 5.12", #3 – 8.06", #4 – 10.94", #5 – 41",

#6 – 48.75", #7 – 54.90", #8 – 58.75", #9 – 62.90", #10 – 68.9"

Figure 6: Schematic showing locations of dynamic pressure transducers - Body 1. (Not to scale)




• Location of pressure sensor

Distance of section from nose

#a – 3", #1 – 5", #b – 7", #c – 10",

#2 – 41", #3 – 59", #4 – 61", #5 – 63"

Figure 7: Schematic showing locations of dynamic pressure transducers - Body 2. (Not to scale)

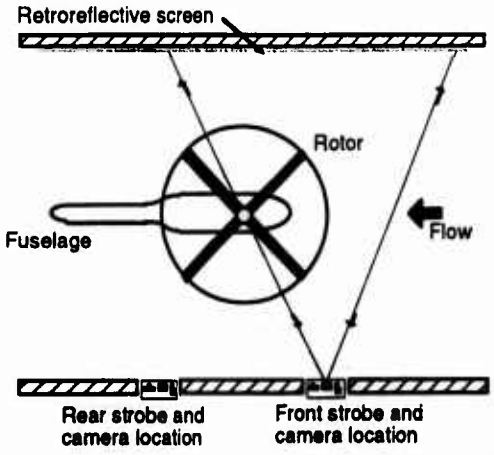



Figure 8: Schematic of shadowgraph set-up (Not to scale)

| Component | Maximum range | Accuracy |
|---|---|---|
| | | |
| ***Rotor balance:*** | | |
| Normal force | 2224N (500 lb.) | ±4.448N (±1 lb.) |
| Side force | 890N (200 lb.) | ±2.224N (±0.5 lb.) |
| Axial force | 890N (200 lb.) | ±2.224N (±0.5 lb.) |
| Pitching moment | 542.4 Nm (400 in-lb) | ±1.355 Nm (±1 in-lb) |
| Rolling moment | 542.4 Nm (400 in-lb) | ±1.355 Nm (±1 in-lb) |
| Yaw moment | 542.4 Nm (400 in-lb) | ±1.355 Nm (±1 in-lb) |
| | | |
| ***Body balance:*** | | |
| Normal force: | 445N (100 lb.) | ±1.11N (±0.25 lb.) |
| Axial force: | 223N (50 lb.) | ±0.56N (±0.125 lb.) |
| Pitching moment: | 407 Nm (300 in-lb) | ±0.68 Nm (±0.5 in-lb) |

**Table 3: Force balance range and accuracy**

| Parameter | Test Values |
|---|---|
| Advance ratio | 0.05, 0.06, 0.065, 0.07, 0.075, 0.08, 0.10, 0.125, 0.15, 0.2, 0.25 |
| Wind speeds (m/s) | 8, 9.6,10.4, 11.2, 12, 12.8, 16, 20, 24, 32, 40 |
| Shaft angles (deg.) | -8, -6, -4, -2 |
| Collective pitch angles (deg.) | 4, 6, 8, 10, 11, 12 |
| Rotor rotation speed | 1860 rpm (31 Hz) |
| Hover tip Mach. No. | 0.5 |

**Table 4: Test matrix**

| Parameter | Estimated error |
|---|---|
| Wind speeds | ±1% |
| Advance ratio | ±2% |
| Shaft angles | ±0.05 deg. |
| Collective pitch angles | ±0.1 deg. |
| Cyclic pitch angles | ±0.1 deg. |
| Rotor forces | ±0.5% |
| Rotor moment | ±0.5% |
| Mean pressures | ±1.5% |
| Unsteady pressures | ±1.5% |

**Table 5: Estimated measurement errors**

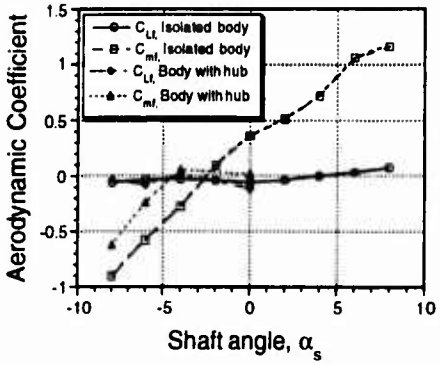



**Figure 9: Aerodynamic force and pitching moment characteristics of isolated body**

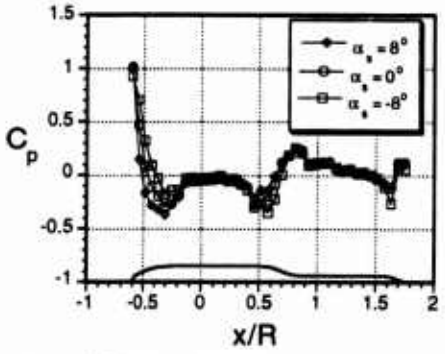



**Figure 10: Pressure distribution over isolated body at three angles of attack**

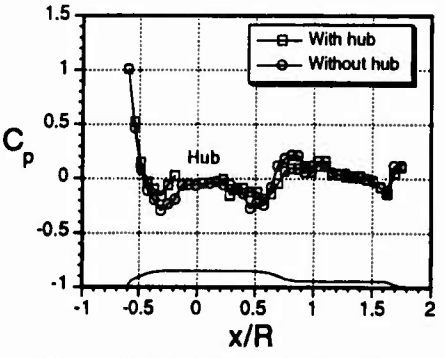



**Figure 11: Effects of rotor hub on body pressure distribution (top centerline)**

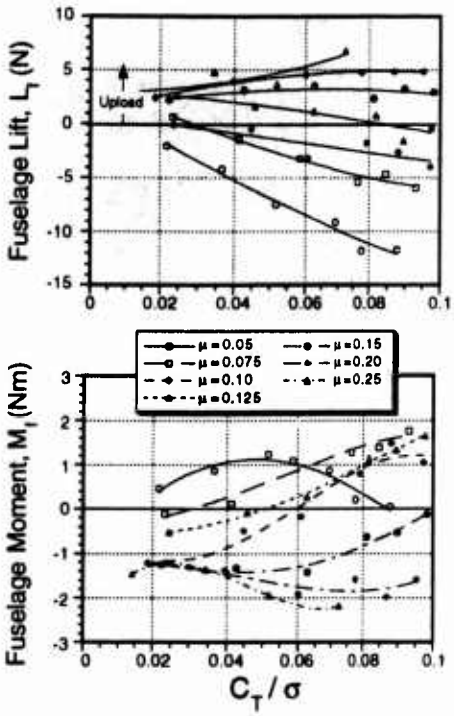



**Figure 12: Aerodynamic force and moment characteristics of body as affected by the rotor**

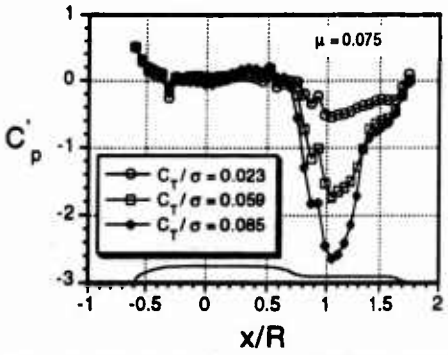



**Figure 13: Time-averaged pressure distribution on body due to rotor at low advance ratio**

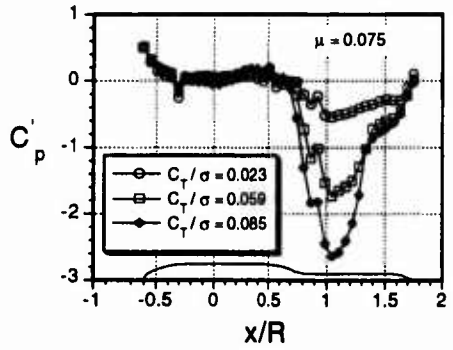



**Figure 14: The effects of increasing advance ratio on body pressure distribution (left side)**

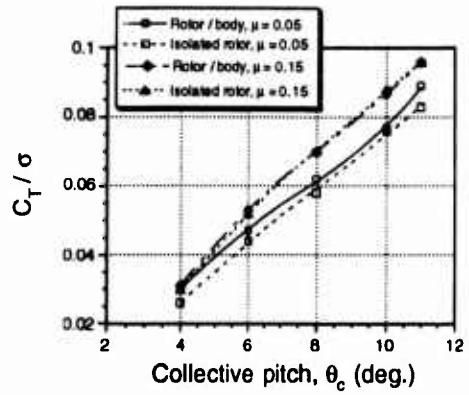



**Figure 15: Effects of the body on rotor thrust performance**

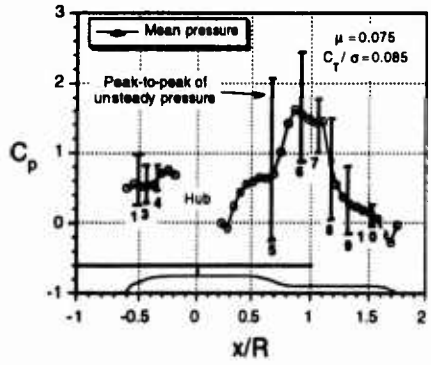



**Figure 16: Significance of unsteady pressures on body in comparison to time-averaged pressures**

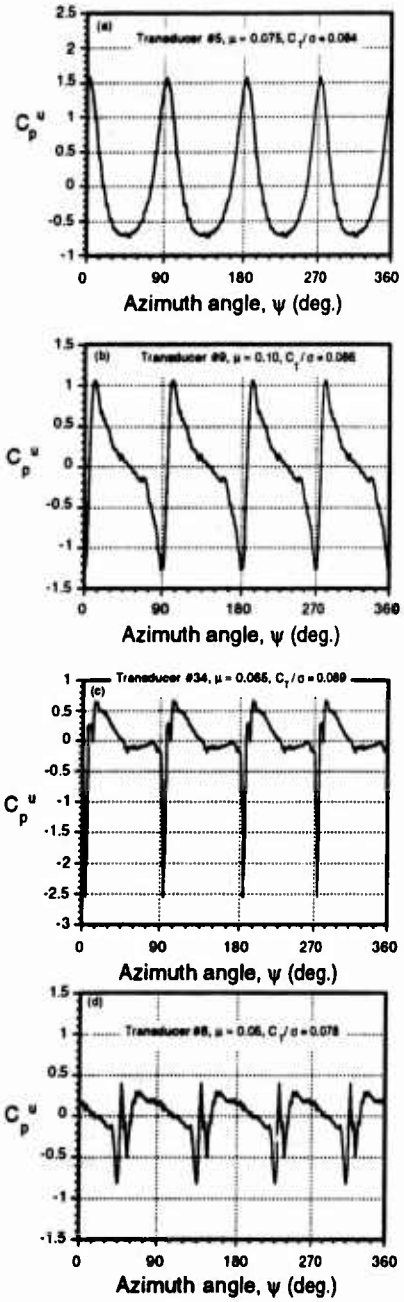



**Figure 17: Typical unsteady pressures measured on body. (a) Blade passage, (b) Close vortex/surface interactions, (c) Tip vortex impingement, (d) Post-wake impingement**

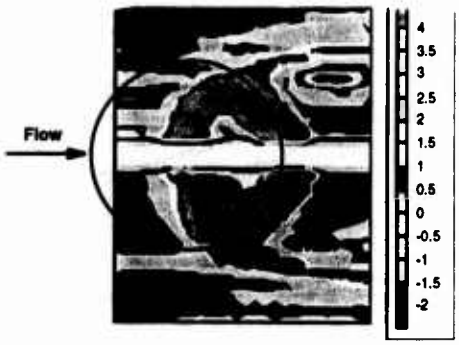



**Figure 18: Contour map of total pressure below and behind the rotor showing wake roll-up**

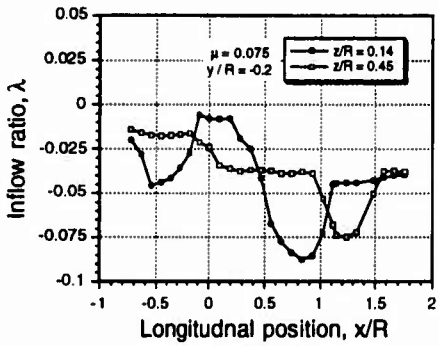



**Figure 19: Longitudinal variation of time-averaged downwash below rotor**

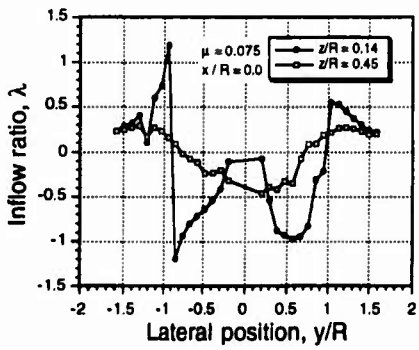



**Figure 20: Lateral variation of downwash below the rotor disk**

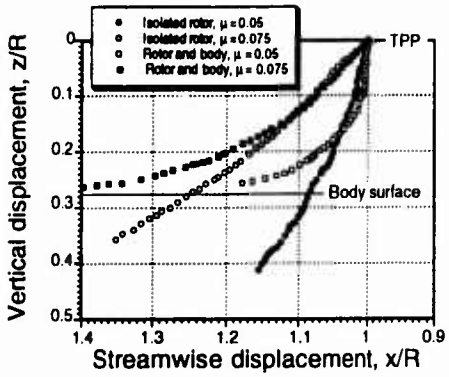



**Figure 21: Comparison of tip vortex displacements at rear of rotor disk due to presence of body**

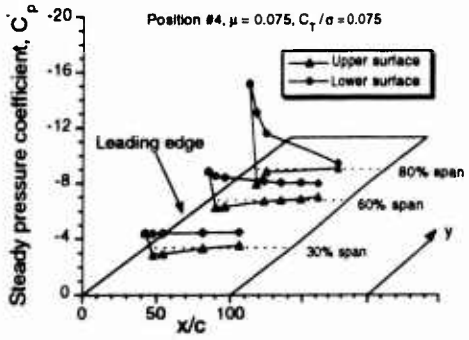



**Figure 22: Representative chordwise pressure distributions on lifting surface operating in rotor wake**

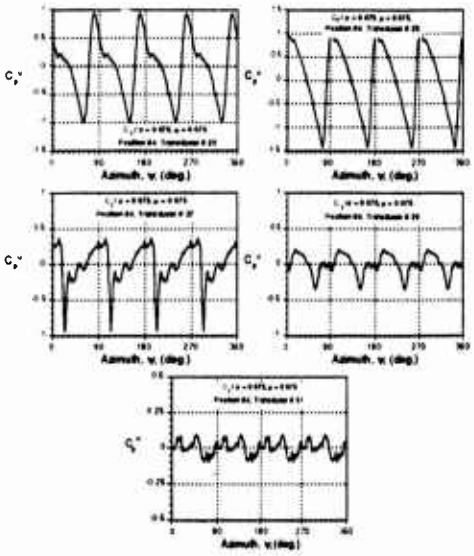


**Figure 23: Representative unsteady pressure measurements on lifting surface due to rotor**

# Investigation into the aerodynamic characteristics of a combat aircraft research model fitted with a forward swept wing.

*D. Stanniland, ARA, Bedford*

## 0 INTRODUCTION

This submission covers a series of tests on a combat aircraft research model fitted with a forward swept wing. The purpose of the tests was to investigate the flow development of the upper surface of the wing and to establish a level of confidence in the CFD methods used for the wing design. The fuselage was specified algebraically in order to permit a precise definition of the geometry both for CFD calculations and model manufacture, and the model was fitted with pressure tappings on the wing, fuselage and canard.

The tests were performed in the ARA 9ft x 8ft Transonic Wind Tunnel in February 1985.

# 1 GENERAL DESCRIPTION

## 1.1 Model name and designation

ARA M151/1 forward swept wing research model based on BAe (Warton) model R63. See Fig 1.

## 1.2 Model type and flow conditions

The Layout of the model comprises a sting mounted, simple pressure plotted fuselage/wing/canard configuration. Tested over the range $0.5 \leq M \leq 1.35$, $-2° \leq \alpha \leq 10°$, (Upper limit being increased to 20° (or maximum safe angle) at selected subsonic M).

## 1.3 Design requirements, purpose of test

The performance characteristics of a combat aircraft can be interpreted in aerodynamic terms by a flight envelope such as shown in Fig 2. This exercise takes design point 1 as the primary design point with secondary consideration of points 2 and 3. The only concession to supersonic flight is to maintain a thin section ($\approx$ 5% t/c) with superficial consideration of the cross sectional area distribution to minimise wave drag.

The purpose of the tests was to establish whether the theoretical methods used for the design are adequate for forward sweep. It was also intended to use the data to provide some guidance on the suitability of forward sweep for future combat aircraft projects and to obtain a definitive data base for this class of aircraft.

## 1.4 Dominant flow physics

M=0.7 can be taken as representative of a typical subcritical flow on a 30° swept wing in which supercritical regions are confined to the vicinity of the wing leading edge.

At M=0.85 the flow has developed into rather more complex shock patterns. On the inner wing there is a strong, unswept shock with a separation bubble downstream. Further outboard there is a weak highly swept shock which originates from the wing tip leading edge, with a weak lower sweep shock further aft. There is a trailing edge separation which develops slowly with increasing incidence.

By M=0.9 there is a more clearly defined flow pattern in which the supercritical flow is terminated by a single shock on the inner wing. This is a strong unswept shock with a separation bubble downstream. On the outer wing the shock is well swept and relatively weak, with the inboard drift of the surface boundary layer downstream of the shock and a more extensive area of trailing edge separation.

# 2 DETAILS OF THE MODEL

## 2.1 General geometric arrangement

The general geometric arrangement of the model is shown in Fig. 3.

## 2.2 Configurations

02419 Fuselage expanding, canard off

02519 Fuselage parallel, canard off

02119 Fuselage expanding, canard angle -3°

## 2.3 Wing data

### 2.3.1 Planform

- Reference wing area = 0.3600m²
- Reference wing chord, $\bar{c}$ = 0.3000m
- Reference wing span = 1.2000m
- Moment reference centre = 0.9000m aft of the model nose on the horizontal fuselage datum.
- Aspect ratio = 4.0
- Taper ratio = 0.4
- Leading edge sweep = -30°
- Twist distribution = See Table 1 for twist definition
- Gross semi-span = 0.600m
- Root chord $C_o$ = 0.4286m
- Tip chord $C_T$ = 0.17143m
- Tip L.E. point = 0.6225m
- Details of fuselage/wing junction: Low mounted with a negative wing/fuselage setting angle.

2.3.2 Basic wing section

The basic trapezoidal wing is positioned longitudinally with the mean aerodynamic quarter chord at X = 90.00cm and the wing leading edge apex at Z = -7.575cm. It is defined by three control stations as specified in Table 2, with linear generation between these stations. The inner wing leading edge is unswept near the body side giving a structurally sounder means of carrying the wing loads into the fuselage than the V junction which the trapezoidal wing would imply. The unswept inner wing is obtained by stretching the trapezoidal wing in the X direction.

## 2.4 Body data

2.4.1 Shape

The fuselage is based on a simple rectangular section (13cm wide) with rounded corners (2cm away from the nose). There is a faired chin intake (rectangular section with 2cm corner radii), providing an upswept rear fuselage which permits a low mounted wing with a negative wing/fuselage setting angle. A simple canopy is also included. This has an elliptic section forward of X = 48.00cm and blends back into the rectangular fuselage at X = 90.00cm. Two alternative bodysides are used in the vicinity of the wing root. The basic fuselage has a constant width of 13cm, reducing to 12cm over the final 10cm of the body length. The expanding fuselage has a maximum width of 20.119cm, occurring near the wing trailing edge. The fuselage of an FSW aircraft would normally end just downstream of the wing trailing edge, but the length has been extended significantly in order to close the expanding fuselage down to a reasonable base area. This will have the additional advantage of increasing the distance between the critical inner wing flow and the model base which could ease the interpretation of the base drag of the FSW model.

## 2.5 Information on Canards

The canard is a conventional aft swept surface with a leading edge sweep of 45°, unswept trailing edge and nett taper ratio = 0.2. The nett canard mean aerodynamic chord is positioned at X = 54.083cm, Z = -0.5cm and the canard rotates about this point. The normal canard setting is -3°. The canard is specified by modified NACA 64206 sections at the bodyside and the tip with 4° of washout (ie the tip is set 4° nose down to the bodyside chord).

## 2.7 Geometric definition

The wing leading and trailing edges are defined mathematically see Table 2. The wing section and twist definition is defined geometrically in Table 1.

The fuselage is defined mathematically see Table 3.

The canard is defined geometrically in Table 4.

## 2.8 Model support details

The complete model was mounted on a single rear sting of 83.8mm diameter, via the ARA No 4 76.2mm diameter balance.

# 3 GENERAL TUNNEL INFORMATION

## 3.1 Tunnel designation

ARA 2.74m x 2.44m (9ft x 8ft) Transonic Wind Tunnel (see Fig. 4)

## 3.2 Organisation running the tunnel

Aircraft Research Association Ltd
Manton Lane
Bedford MK41 7PF

## 3.3 Tunnel characteristics

The ARA Transonic Wind Tunnel is a rectangular, continuous flow, closed circuit tunnel, with perforated walls.

- Mach numbers: 0 to 1.4
- Incidence range (straight sting) -10° to 40°
- Roll range 0 to 360°.
- Pressure range; stagnation pressure 0.8 to 1.2 bar.

- Temperature range: stagnation temperature up to 50°C.
- Reynolds number: (based on reference chord length) from 3.2 x $10^6$ at M=0.55, to 4.4 x $10^6$ at supersonic speeds.
- Run time: continuous.

### 3.4 Test section

#### 3.4.1 Test section details

See Fig. 5.

#### 3.4.2 Test section size

2.74m x 2.44m. The perforated walls extend 1.49m upstream of the model nose and 1.07m downstream of the model base. The region of uniform Mach number extends at least 2.26m upstream of the model (the forward limit of the calibration probe).

#### 3.4.3 Wall geometry details

- The perforated tunnel walls have a 22% open area (normal holes), varying over the length of the working section to minimise interference at high subsonic Mach numbers.
- No wall pressures were measured for this test series.
- Wall boundary layer thickness was 13mm at the model centre of rotation, measured for tests with a centre-line calibration probe ('empty tunnel').

### 3.5 Free-stream conditions

#### 3.5.1 Reference conditions

- Total pressure in the working section is obtained from the static pressure in the settling chamber using calibration data.
- Static pressure in the working section is obtained from the static pressure on the wall of the plenum chamber.
- The reference pressure used to calibrate pressure transducers is an applied pressure in a large reservoir in the tunnel control room.
- Stagnation temperature is measured to an accuracy of ± 0.2K over the operating range of the tunnel using a probe installed in the settling chamber.

#### 3.5.2 Tunnel calibration

- The tunnel is calibrated using a centre-line static probe with wall static pressures.
- The last calibration was performed in October 1986 (complete model testing).

### 3.6 Flow Quality

#### 3.6.1 Flow uniformity

Mach number variation along the length of a model is set to a nominal zero using settings of the wind tunnel walls derived from the tunnel calibration. Typical errors of $\Delta M = 0.0002$ were measured in the last calibration of the tunnel. Mach number is held to within 0.001 of the required value up to moderate incidence, at subsonic Mach numbers.

Mean flow angularity is obtained for each model using a small incidence traverse with model upright and inverted. Flow angles are normally found to lie within ± 0.02° of the standard values for most models. For a detailed discussion of the tunnel flow angularity see ref. 2.

#### 3.6.2 Temperature variation

Tunnel temperature is not controlled directly, although the increase in temperature during a run is minimised by a cooler. Stagnation temperature increases by approximately 2°K for a moderate incidence traverse at a given Mach number. Temperature variation across the tunnel is not known.

#### 3.6.3 Flow unsteadiness

Early measurements of the unsteadiness in the ARA TWT indicated a peak at M=0.7. A more extensive investigation, carried out in 1990 following the installation of a long cell honeycomb, showed that this peak is due to a tone at 2.6KHz which is not present when a model is present in the working section. See Ref 2 for further details.

## 4 INSTRUMENTATION

### 4.1 Model position

See Fig 5

4.1.1 Geometrical incidence measurements

Geometrical incidence is measured by an accelerometer located in the model cart, corrected for deflections of the model support system under load using an accelerometer in the forebody of the model.

4.1.2 Accuracy of geometrical incidence

Model incidence accuracy ± 0.01°.

## 4.2 Model pressure measurement

4.2.1 Number and locations of pressure holes

Total number of pressure holes = 329

5 x 22 port wing upper surface
5 x 16 starboard wing lower surface.
See Table 5 and Figs 6 and 7 for locations.
3 x 12 port canard upper surface
3 x 8 starboard canard lower surface.
See Table 6 and Fig 8 for locations.
The fuselage had pressure measurements in the vicinity of the wing root (see Table 5) and over the afterbody. See Table 7 and Fig 9 for locations.

4.2.2 Range and accuracy of pressure transducers

± 1034 mbar range Druck type transducers used, nominal sensitivity 14.535 $\mu$V/mbar scan, calibrated in every scan.

## 4.3 Forces and Moment measurements

4.3.1 Type and location of balance

Overall model loads were measured with ARA No. 4 76.2mm (3") diameter 6 component strain gauge balance.

Buffet measurements were made using semi-conductor strain gauges set in pockets on the wing upper surface near the fuselage junction to measure the oscillatory wing root bending moment.

4.3.2 Maximum range and accuracy

Balance sensitivities are shown in Table 8.

## 4.5 Surface flow visualisation

4.5.1 Measurement techniques applied

Oil flow visualisation runs were carried out, comparing the expanding fuselage on the starboard side, with the parallel fuselage on the port side. The canards were omitted from this configuration and a forward transition band was used in order to show as much of the wing flow as possible. Tests were carried out over a range of incidence at M = 0.7, 0.85 and 0.9.

4.5.2 Recording of visualisation

Photographs of selected incidences from these runs were taken.

## 4.6 Field flow visualisation

None.

## 4.7 Tunnel wall measurements

None.

## 4.8 Instrumentation used

All measurements were made using the ARA standard data acquisition system.

# 5 TEST MATRIX AND CONDITIONS

## 5.1 Details of test matrix

5.1.1 Number of test cases

Three tests cases have been selected.

5.1.2 Number of configurations

One configuration for each test case.

5.1.3 Summary of test cases

For summary of test cases see Table 9.

## 5.2 Model/tunnel relations

5.2.1 Blockage effect

Zero lift blockage = 0.5%

5.2.2 Model span/tunnel width

Ratio of model wing span to tunnel width = 0.438.

5.2.3 Wing area/tunnel cross section

Wing area: tunnel cross sectional area = 0.0538.

5.2.6 Wall temperatures

Wall temperatures were not measured.

### 5.3 Transition details

5.3.1 Transition fix

For the test cases selected transition was fixed as shown in Table 10.

5.3.3 Details of transition fix

Transition was fixed by narrow bands of Ballotini set in a thin film of Araldite.

5.3.4 Transition verification

The effectiveness of the transition band was checked using the sublimation of Acenaphthene at M = 0.5, $C_L$ = 0.2. Experience has shown that this condition requires the maximum Ballotini size for successful transition over the range of conditions tested, including low supersonic Mach numbers.

## 6 DATA

### 6.1 Availability of data

6.1.1 Organisation owning data

U.K. Ministry of Defence
Technical Authority represented by
Aerodynamics and Propulsion Department
Defence Research Agency
Farnborough
England

6.1.2 Person responsible for data

Mr D Stanniland
Aircraft Research Association Ltd
Manton Lane
Bedford MK41 7PF

Tel: 0234 - 350681
Fax: Groups 2 & 3, 0234 - 328584

6.1.3 Queries about data

Contact ARA in the first instance.

### 6.2 Suitability of data for CFD validation

6.2.1 Suitability for "in tunnel" calculations

The tests were carried out in a perforated tunnel with no measured wall pressures. Hence, the data is unlikely to be appropriate for in-tunnel calculations with a specified boundary condition.

6.2.2 Simulation of 'Free Air' conditions

The data are corrected to simulate "Free Air" conditions. The fuselage geometry is precisely defined and the model can readily be represented in CFD methods. The availability of pressure tappings on the wing fuselage and canard means that the results are appropriate for CFD calculations on this class of complex configuration.

### 6.3 Type and form in which data available

6.3.1 Type and form of data

For list of available data see Table 9.

6.3.2 Format of data available

Data will be supplied on an IBM compatible floppy disk.

### 6.4 Correction applied to data

6.4.1 Lift interference and blockage

Corrections were made to the measured data to account for the following:

- Sting and balance deflection under load
- Model cart deflection under load
- Tunnel constraint
- Tunnel flow pitch angularity and curvature

- Model blockage
- Model blockage buoyancy
- Base drag. The model axial force was corrected to allow for model base drag which is obtained as the sum of several components thus.

i) The cavity pressure acting over the cavity cross section at the base of the model.

ii) The pressures measured in the model base, acting over their areas of influence. (See Table 12 and Fig 10).

iii) The pressures measured on the fuselage downstream of X=1.500m acting over the rearward facing areas. (See Table 12 and Fig 10).

6.4.5 Aero-elastic deformation

No correction has been applied for aeroelastic deformation under load. Calculations suggest that for atmospheric stagnation pressure testing deflections will be small.

## 7 DATA ACCURACY AND REPEATABILITY ASSESSMENT

### 7.1 Estimated accuracies

7.1.1 Free stream conditions

Mach number measured in these tests has a bias of -0.0015 which has been recently identified, with an accuracy of $\pm 0.001$. Model incidence is estimated to be accurate $\pm 0.02°$ up to $\alpha \simeq 10°$.

7.1.2 Measured data

The RMS errors presented in Table 1 imply errors at M = 0.8 of typically.

$C_y$ $\pm 0.0002$
$C_N$ $\pm 0.0010$
$C_A$ $\pm 0.00007$
$C_m$ $\pm 0.00015$
$C_\ell$ $\pm 0.00003$
$C_n$ $\pm 0.00003$

## 8 REFERENCES

### 8.1 On the Wind Tunnel

1. J E Green/C A McHugh
A J Baxendale/D R Stanniland

The use of a deep honeycomb to achieve high flow quality in the ARA 9' x 8' Transonic Wind Tunnel presented at 18th Congress of ICAS, Beijing, September 1992.

2. D R Stanniland/C A McHugh
J E Green

Improvement of the flow quality in the ARA Transonic Tunnel by means of a long cell honey-comb. Paper 54, RAes conference on "Wind Tunnels and Wind Tunnel Test Techniques", Southampton 1992.

3. E C Carter/K C Pallister

Development of testing techniques in a large Transonic Wind Tunnel to achieve a required drag accuracy and flow standards for modern civil transport. AGARD-CP-429, September 1987

### 8.2 On the Model

4. D R Stanniland/P J Johnson

The aerodynamic design of a supercritical forward swept wing for a combat aircraft. ARA MTN M151/1 September 1984

### 8.3 On the Test

5. D R Stanniland/P J Johnson

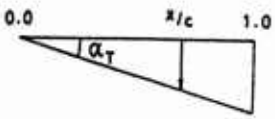
Results and analysis of tests on the M151/1 forward swept wing research model.
ARA MTN M151/3 January 1986

## TABLE 1

## M151 WING SECTION AND TWIST DEFINITION

| | | | |
|---|---|---|---|
| | Y = 0.000 | 21.429 | 60.000 cm |
| | $\alpha_T$ = -2.800 | -3.000 | 2.000 |
| x/c = 0.000000 | Z/c = 0.000000 | 0.000000 | 0.000000 |
| 0.002408 | 0.005839 | 0.006068 | 0.005492 |
| 0.009607 | 0.011572 | 0.012115 | 0.011091 |
| 0.021530 | 0.017091 | 0.018051 | 0.016800 |
| 0.038060 | 0.022290 | 0.023616 | 0.022500 |
| 0.059040 | 0.027103 | 0.028560 | 0.028069 |
| 0.084265 | 0.031550 | 0.032954 | 0.033481 |
| 0.113495 | 0.035734 | 0.036958 | 0.038736 |
| 0.146447 | 0.039742 | 0.040586 | 0.043713 |
| 0.182804 | 0.043576 | 0.043759 | 0.048216 |
| 0.222215 | 0.047167 | 0.046465 | 0.052153 |
| 0.264302 | 0.050405 | 0.048719 | 0.055462 |
| 0.308659 | 0.053172 | 0.050493 | 0.058036 |
| 0.354858 | 0.055387 | 0.051730 | 0.059837 |
| 0.402455 | 0.057000 | 0.052393 | 0.060941 |
| 0.450992 | 0.057921 | 0.052489 | 0.061414 |
| 0.500000 | 0.057986 | 0.052056 | 0.061190 |
| 0.549009 | 0.057062 | 0.051103 | 0.060106 |
| 0.597545 | 0.055214 | 0.049566 | 0.058012 |
| 0.645142 | 0.052627 | 0.047347 | 0.054892 |
| 0.691342 | 0.049402 | 0.044393 | 0.050899 |
| 0.735699 | 0.045579 | 0.040725 | 0.046259 |
| 0.777785 | 0.041221 | 0.036451 | 0.041145 |
| 0.817197 | 0.036428 | 0.031750 | 0.035685 |
| 0.853553 | 0.031339 | 0.026837 | 0.030044 |
| 0.886505 | 0.026116 | 0.021947 | 0.024452 |
| 0.915735 | 0.020940 | 0.017294 | 0.019153 |
| 0.940961 | 0.016002 | 0.013052 | 0.014348 |
| 0.961940 | 0.011505 | 0.009348 | 0.010180 |
| 0.978470 | 0.007654 | 0.006291 | 0.006760 |
| 0.990393 | 0.004655 | 0.003981 | 0.004190 |
| 0.997592 | 0.002707 | 0.002518 | 0.002571 |
| 1.000000 | 0.002000 | 0.002000 | 0.002000 |

$\alpha_T$ is positive nose up and is applied as a shear relative to the wing leading edge




Z/c is positive normal to the wing datum plane and is applied as a shear relative to the wing twist line

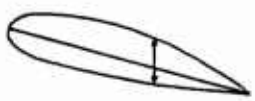


**TABLE 1 (contd)**

| | | | |
|---|---|---|---|
| | Y = 0.000 | 21.429 | 60.000 cm |
| | $\alpha_T$° = -2.800 | -3.000 | +2.000 |
| x/c = 0.000000 | Z/c = 0.000000 | 0.000000 | 0.000000 |
| 0.002408 | -0.002970 | -0.003150 | -0.002500 |
| 0.009607 | -0.005553 | -0.005500 | -0.004451 |
| 0.021530 | -0.007532 | -0.007250 | -0.005773 |
| 0.038060 | -0.008898 | -0.008350 | -0.006310 |
| 0.059040 | -0.009720 | -0.008750 | -0.006112 |
| 0.084265 | -0.010037 | -0.008600 | -0.005069 |
| 0.113495 | -0.009858 | -0.007720 | -0.003135 |
| 0.146447 | -0.009184 | -0.006000 | -0.000884 |
| 0.182804 | -0.008013 | -0.004850 | 0.000898 |
| 0.222215 | -0.006313 | -0.003861 | 0.002175 |
| 0.264302 | -0.004013 | -0.002909 | 0.003356 |
| 0.308659 | -0.001058 | -0.001737 | 0.004695 |
| 0.354858 | 0.002481 | -0.000405 | 0.006285 |
| 0.402455 | 0.006364 | 0.001005 | 0.008144 |
| 0.450992 | 0.010278 | 0.002501 | 0.010115 |
| 0.500000 | 0.013964 | 0.004188 | 0.011896 |
| 0.549009 | 0.017283 | 0.006196 | 0.013418 |
| 0.597545 | 0.020118 | 0.008494 | 0.014949 |
| 0.645142 | 0.022108 | 0.010638 | 0.016432 |
| 0.691342 | 0.022596 | 0.011782 | 0.017024 |
| 0.735699 | 0.021177 | 0.011317 | 0.015898 |
| 0.777785 | 0.018268 | 0.009510 | 0.013262 |
| 0.817197 | 0.014824 | 0.007235 | 0.010133 |
| 0.853553 | 0.011588 | 0.005190 | 0.007357 |
| 0.886505 | 0.008780 | 0.003566 | 0.005164 |
| 0.915735 | 0.006319 | 0.002253 | 0.003411 |
| 0.940961 | 0.004106 | 0.001117 | 0.001922 |
| 0.961940 | 0.002130 | 0.000110 | 0.000630 |
| 0.978470 | 0.000449 | -0.000747 | -0.000453 |
| 0.990393 | -0.000853 | -0.001413 | -0.001282 |
| 0.997592 | -0.001695 | -0.001844 | -0.001811 |
| 1.000000 | -0.002000 | -0.002000 | -0.002000 |

## TABLE 2

## MATHEMATICAL DEFINITION OF WING

DIMENSIONS IN CENTIMETRES, MODEL SCALE

LEADING EDGE

$0 \leq y \leq 6.50$ $\quad x = 88.2700$

$6.50 \leq y \leq 16.00$ $\quad x = [(21.429 - y)(-0.000015848y^4 + 0.001339156y^2 + 88.24171)$

$+(y - 6.500)(-0.021824598y^2 + 0.358008616y + 86.86503]/14.929$

$16.00 \leq y \leq 21.429$ $\quad x = [(21.429 - y)(-0.030102543y^2 + 0.63168139y + 84.80175)$

$+ (y - 16.00)(-0.01516362y^2 + 0.07253242y + 89.92377)]/5.429$

$21.429 \leq y \leq 60.00$ $\quad x = 96.8769 - 0.57735y$

TRAILING EDGE

$x = 139.745 - 1.00592y$

## TABLE 3

## MATHEMATICAL DEFINITION OF THE FUSELAGE

DIMENSIONS IN CENTIMETRES, MODEL SCALE

Fuselage upper surface

$0.00 \le x \le 50.00$ $\quad z = [15449.898 - (x - 50.000)^2\ ]^{1/2} - 117.7976$
$50.00 \le x \le 160.00$ $\quad z = 6.5000$
$160.00 \le x \le 170.00$ $\quad z = 6.5000 - 0.0050\ (x - 160.000)^2$

Fuselage lower surface

$0.00 \le x \le 35.00$ $\quad z = 198.6667 - [42298.778 - (x - 35.000)^2\ ]^{1/2}$
$35.00 \le x \le 55.00$ $\quad z = -7.0000$

Fuselage plan view - parallel bodyside

$0.00 \le x \le 40.00$ $\quad y = [15958.492 - (x - 40.000)^2\ ]^{1/2} - 119.8269$
$40.00 \le x \le 160.00$ $\quad y = 6.5000$
$160.00 \le x \le 170.00$ $\quad y = 6.5000 - 0.0050\ (x - 160.000)^2$

Fuselage plan view - expanding bodyside

$88.2745 \le x \le 133.00$ $\quad y = -0.000079548x^3 + 0.026403042x^2 - 2.801815x + 102.8050$
$133.00 \le x \le 170.00$ $\quad y = 0.000087201x^3 - 0.040984257x^2 + 6.274314x - 304.6070$

Fuselage corner radius

$0.00 \le x \le 15.00$ $\quad r = 4(x/15) - 2(x/15)^2$
$15.00 \le x \le 170.00$ $\quad r = 2.00$

Canopy upper surface

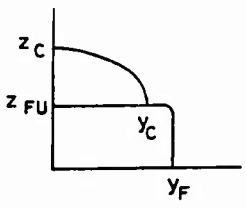
$23.75 \le x \le 34.00$ $\quad z = 0.50953x - 8.4039$
$34.00 \le x \le 48.00$ $\quad z = 0.00035234x^3 - 0.0615350x^2 + 3.472015x - 51.8454$
$48.00 \le x \le 90.00$ $\quad z = 0.000148472x^3 - 0.03073372x^2 + 1.924198x - 25.97085$

Canopy plan view

$23.75 \le x \le 45.00$ $\quad y = 6.500\ [1 - (x - 45.000)^2/21.25^2\ ]^{1/2}$

Canopy section

$23.75 \le x \le 48.00$ ellipse with semi-axes $(y_c, (z_c - z_{FU})$




$48.00 \le x \le 90.00$ elliptic shoulder with semi-axes $(r_y, r_z)$ with flat top

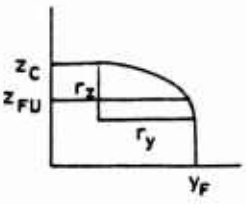


**TABLE 3 (contd)**

$$r_y = \left[\frac{90.000 - x}{42.000}\right](-0.002551020x^2 + 0.244897959x + 0.622448979)$$

$$+ \left[\frac{x - 48.000}{42.000}\right](0.002551020x^2 - 0.459183673x + 22.66326530)$$

$$r_z = \left[\frac{90.000 - x}{42.000}\right](0.001993254x^2 + 0.191352381x + 0.923642857)$$

$$+ \left[\frac{x - 48.000}{42.000}\right](0.001993254x^2 - 0.358785714x + 18.14535714)$$

Intake lower surface

| | |
|---|---|
| $26.77 \le x \le 40.00$ | $z = -0.36397x + 2.9088$ |
| $40.00 \le x \le 55.00$ | $z = -0.00022330x^3 + 0.04395311x^2 - 2.80836111x + 44.6539$ |
| $55.00 \le x \le 100.00$ | $z = -0.00000835x^3 + 0.00310815x^2 - 0.2661593x - 7.3749$ |
| $100.00 \le x \le 160.00$ | $z = -0.000005572x^3 + 0.001297561x^2 + 0.012709937x - 19.9305$ |
| $160.00 \le x \le 170.00$ | $z = -7.5000 + 0.0050\,(x - 160.000)^2$ |

Intake plan view

$26.77 \le x \le 55.00$ $\quad y = [4167.029 - (x - 55.000)^2\,]^{1/2} - 58.0525$

Intake corner radius

$26.77 \le x \le 40.00$ $\quad r = 4((x - 26.77)/13.23) - 2((x - 26.77)/13.23)^2$

## TABLE 4

## M151 CANARD SECTION AND TWIST DEFINITION

The canard has a constant NACA 64-206 section:

| NACA 64-206 (Stations and ordinates given in per cent of airfoil chord) | | | |
|---|---|---|---|
| Upper Surface | | Lower Surface | |
| Station | Ordinate | Station | Ordinate |
| 0 | 0 | 0 | 0 |
| 0.459 | 0.542 | 0.541 | -0.442 |
| 0.704 | 0.664 | 0.796 | -0.524 |
| 1.198 | 0.859 | 1.302 | -0.645 |
| 2.440 | 1.208 | 2.560 | -0.836 |
| 4.934 | 1.719 | 5.066 | -1.087 |
| 7.432 | 2.115 | 7.568 | -1.267 |
| 9.933 | 2.444 | 10.067 | -1.410 |
| 14.937 | 2.970 | 15.063 | -1.624 |
| 19.943 | 3.367 | 20.057 | -1.775 |
| 24.952 | 3.667 | 25.048 | -1.877 |
| 29.961 | 3.897 | 30.039 | -1.935 |
| 34.971 | 4.011 | 35.029 | -1.951 |
| 39.981 | 4.066 | 40.019 | -1.924 |
| 44.991 | 4.014 | 45.009 | -1.824 |
| 50.000 | 3.878 | 50.000 | -1.672 |
| 55.008 | 3.670 | 54.992 | -1.480 |
| 60.015 | 3.402 | 59.985 | -1.260 |
| 65.020 | 3.080 | 64.980 | -1.028 |
| 70.023 | 2.712 | 69.977 | -0.799 |
| 75.025 | 2.307 | 74.975 | -0.587 |
| 80.024 | 1.868 | 79.976 | -0.401 |
| 85.020 | 1.410 | 84.980 | -0.259 |
| 90.015 | 0.940 | 89.985 | -0.187 |
| 95.007 | 0.473 | 94.993 | -0.224 |
| 100.000 | 0 | 100.000 | -0.500 |
| LE radius : 0.256<br>Slope of radius through LE : 0.084 | | | |

The section has been modified aft of x/c = 0.600 on the canard lower surface to introduce a trailing edge thickness of 0.005.

The twist is 0° at the model bodyside and -4° at the canard tip, applied as a shear relative to the canard half chord, with linear generators between the bodyside and the tip.

## TABLE 5

## M151 WING PRESSURE TAPPINGS

Pressures are measured on the wings and the adjacent fuselage at the following x/c positions.

| Fuselage z=0 | Wing/body junction | η=0.200 Y=120.0mm | 0.350 210.0 | 0.500 300.0 | 0.700 420.0 | 0.900 540.0 |
|---|---|---|---|---|---|---|
| Port side of fuselage | | Upper surface: port wing | | | | |
| | 0.01 | 0.01 | 0.01 | 0.01 | 0.01 | 0.01 |
| | 0.02 | 0.02 | 0.02 | 0.02 | 0.02 | 0.02 |
| | 0.05 | 0.05 | 0.05 | 0.05 | 0.05 | 0.05 |
| 0.10 | 0.10 | 0.10 | 0.10 | 0.10 | 0.10 | 0.10 |
| | 0.15 | 0.15 | 0.15 | 0.15 | 0.15 | 0.15 |
| 0.20 | 0.20 | 0.20 | 0.20 | 0.20 | 0.20 | 0.20 |
| | 0.25 | 0.25 | 0.25 | 0.25 | 0.25 | 0.25 |
| 0.30 | 0.30 | 0.30 | 0.30 | 0.30 | 0.30 | 0.30 |
| | 0.35 | 0.35 | 0.35 | 0.35 | 0.35 | 0.35 |
| 0.40 | 0.40 | 0.40 | 0.40 | 0.40 | 0.40 | 0.40 |
| | 0.45 | 0.45 | 0.45 | 0.45 | 0.45 | 0.45 |
| 0.50 | 0.50 | 0.50 | 0.50 | 0.50 | 0.50 | 0.50 |
| | 0.55 | 0.55 | 0.55 | 0.55 | 0.55 | 0.55 |
| 0.60 | 0.60 | 0.60 | 0.60 | 0.60 | 0.60 | 0.60 |
| | 0.65 | 0.65 | 0.65 | 0.65 | 0.65 | 0.65 |
| 0.70 | 0.70 | 0.70 | 0.70 | 0.70 | 0.70 | 0.70 |
| | 0.75 | 0.75 | 0.75 | 0.75 | 0.75 | 0.75 |
| 0.80 | 0.80 | 0.80 | 0.80 | 0.80 | 0.80 | 0.80 |
| | 0.85 | 0.85 | 0.85 | 0.85 | 0.85 | 0.85 |
| 0.90 | | 0.90 | 0.90 | 0.90 | 0.90 | 0.90 |
| | 0.95 | 0.95 | 0.95 | 0.95 | 0.95 | 0.95 |
| | 0.98 | 0.98 | 0.98 | 0.98 | 0.98 | 0.98 |
| | | Lower surface: starboard wing | | | | |
| 0.00 | 0.00 | 0.00 | 0.00 | 0.00 | 0.00 | 0.00 |
| | | 0.02 | 0.02 | 0.02 | 0.02 | 0.02 |
| | | 0.05 | 0.05 | 0.05 | 0.05 | 0.05 |
| | | 0.10 | 0.10 | 0.10 | 0.10 | 0.10 |
| | | 0.15 | 0.15 | 0.15 | 0.15 | 0.15 |
| | | 0.20 | 0.20 | 0.20 | 0.20 | 0.20 |
| | | 0.25 | 0.25 | 0.25 | 0.25 | 0.25 |
| | | 0.30 | 0.30 | 0.30 | 0.30 | 0.30 |
| | | 0.40 | 0.40 | 0.40 | 0.40 | 0.40 |
| | | 0.50 | 0.50 | 0.50 | 0.50 | 0.50 |
| | | 0.60 | | 0.60 | 0.60 | 0.60 |
| | | | 0.70 | 0.70 | 0.70 | 0.70 |
| | | 0.80 | 0.80 | 0.80 | 0.80 | 0.80 |
| | | 0.90 | 0.90 | 0.90 | 0.90 | 0.90 |
| | | 0.98 | 0.98 | 0.98 | 0.98 | |
| 1.00 | | 1.00 | 1.00 | 1.00 | 1.00 | 1.0 |

## TABLE 6

## M151 CANARD PRESSURE TAPPINGS

Pressures are measured on the canard at the following x/c positions:

| | Upper surface: port canard | | | Lower surface: starboard canard | | |
|---|---|---|---|---|---|---|
| $\eta_{Nat}$ | 0.100 | 0.500 | 0.900 | 0.100 | 0.500 | 0.900 |
| Ymm | 85.0 | 165.0 | 245.0 | 85.0 | 165.0 | 245.0 |
| x/c | 0.02 | 0.02 | 0.02 | 0.00 | 0.00 | 0.00 |
| | 0.05 | 0.05 | 0.05 | | | |
| | 0.10 | 0.10 | 0.10 | 0.10 | 0.10 | 0.10 |
| | 0.20 | 0.20 | 0.20 | 0.20 | 0.20 | 0.20 |
| | 0.30 | 0.30 | 0.30 | | | |
| | 0.40 | 0.40 | 0.40 | 0.40 | 0.40 | 0.40 |
| | 0.50 | 0.50 | 0.50 | | | |
| | 0.60 | 0.60 | 0.60 | 0.60 | 0.60 | 0.60 |
| | 0.70 | 0.70 | 0.70 | | | |
| | 0.80 | 0.80 | | 0.80 | 0.80 | 0.80 |
| | 0.90 | 0.90 | | 0.90 | 0.90 | |
| | | | | 0.98 | | |

## TABLE 7

## DETAILS OF REAR FUSELAGE PRESSURE POINTS

Pressures are measured on the port side of the rear fuselage at the following positions:

### Parallel Fuselage

| Xmm | Tube | 1 | 2 | 3 | 4 | 5 | 6 | 7 | 8 | 9 |
|---|---|---|---|---|---|---|---|---|---|---|
| 1300.0 | Ymm | 0.0 | -39.6 | | -65.0 | -65.0 | -65.0 | | -39.6 | 0.0 |
| | Zmm | 65.0 | 65.0 | | 39.6 | 0.0 | -60.5 | | -85.9 | -85.9 |
| 1400.0 | Ymm | 0.0 | -39.6 | | -65.0 | -65.0 | -65.0 | | -39.6 | 0.0 |
| | Zmm | 65.0 | 65.0 | | -39.6 | 0.0 | -54.7 | | -80.9 | -80.9 |
| 1500.0 | Ymm | 0.0 | -39.6 | | -65.0 | -65.0 | -65.0 | | -39.6 | 0.0 |
| | Zmm | 65.0 | 65.0 | | 39.6 | 0.0 | -50.9 | | -76.3 | -76.3 |
| 1600.0 | Ymm | 0.0 | -39.6 | | -65.0 | -65.0 | -65.0 | | -39.6 | 0.0 |
| | Zmm | 65.0 | 65.0 | | 39.6 | 0.0 | -49.6 | | -75.0 | -75.0 |
| 1690.0 | Ymm | 0.0 | -35.6 | | -61.0 | -61.0 | -61.0 | | -35.6 | 0.0 |
| | Zmm | 61.0 | 61.0 | | 35.6 | 0.0 | -45.6 | | -71.0 | -71.0 |
| 1700.0 | Ymm | 0.0 | -34.6 | -39.6 | -54.2 | -51.4 | -54.2 | -39.6 | -34.6 | 0.0 |
| | Zmm | 54.2 | 54.2 | 39.6 | 33.6 | 0.0 | -43.6 | -49.6 | -64.2 | -64.2 |

### Expanding Fuselage

| Xmm | Tube | 1 | 2 | 3 | 4 | 5 | 6 | 7 | 8 | 9 |
|---|---|---|---|---|---|---|---|---|---|---|
| 1300.0 | Ymm | 0.0 | -74.7 | | -100.1 | -100.1 | -100.1 | | -74.7 | 0.0 |
| | Zmm | 65.0 | 65.0 | | 39.6 | 0.0 | -60.5 | | -85.9 | -85.9 |
| 1400.0 | Ymm | 0.0 | -72.5 | | -97.9 | -97.9 | -97.9 | | -72.5 | 0.0 |
| | Zmm | 65.0 | 65.0 | | 39.6 | 0.0 | -54.7 | | -80.1 | -80.1 |
| 1500.0 | Ymm | 0.0 | -61.6 | | -87.0 | -87.0 | -87.0 | | -61.6 | 0.0 |
| | Zmm | 65.0 | 65.0 | | 39.6 | 0.0 | -50.9 | | -76.3 | -76.3 |
| 1600.0 | Ymm | 0.0 | -47.2 | | -72.6 | -72.6 | -72.6 | | -47.2 | 0.0 |
| | Zmm | 65.0 | 65.0 | | 39.6 | 0.0 | -49.6 | | -75.0 | -75.0 |
| 1690.0 | Ymm | 0.0 | -35.6 | | -61.0 | -61.0 | -61.0 | | -35.6 | 0.0 |
| | Zmm | 61.0 | 61.0 | | 35.6 | 0.0 | -45.6 | | -71.0 | -71.0 |
| 1700.0 | Ymm | 0.0 | -34.6 | -39.6 | -54.2 | -51.4 | -54.2 | -39.6 | -34.6 | 0.0 |
| | Zmm | 54.2 | 54.2 | 39.6 | 33.6 | 0.0 | -43.6 | -49.6 | -64.2 | -64.2 |

## TABLE 8

## M151 MAIN BALANCE SENSITIVITIES

| COMPONENT | | RMS ERROR (N or Nm) | | | MAXIMUM LOAD |
|---|---|---|---|---|---|
| | | AV. | MAX | % | |
| SIDE FORCE | Y | 2.41 | 5.84 | 0.06 | 4180 N |
| NORMAL FORCE | N | 10.58 | 32.73 | 0.06 | 17792 N |
| AXIAL FORCE | A | 0.72 | 2.44 | 0.03 | 2224 N |
| PITCHING MOMENT | m | 0.82 | 1.84 | 0.04 | 2264 Nm |
| ROLLING MOMENT | l | 0.34 | 1.29 | 0.05 | 725 Nm |
| YAWING MOMENT | n | 0.30 | 1.05 | 0.04 | 725 Nm |
| AXIAL FORCE (spare) | As | 0.77 | 2.28 | 0.03 | 2224 Nm |

RMS ERROR IS EXPRESSED AS A % OF THE MAXIMUM LOAD,
DERIVED FROM THE BALANCE CALIBRATION

## TABLE 9

## SUMMARY OF TEST CASES

| IDENTIFICATION | | CONDITIONS | | POSITION | OTHER INFORMATION | |
|---|---|---|---|---|---|---|
| CASE NO | CONFIGURATION | MACH NO | H | ALPHA/DEG | TYPE OF MEASUREMENTS | ADDITIONAL REMARKS |
| 1 | 02419 FUSELAGE EXPANDING | | | | | |
| | CANARD OFF | 0.7 | 1.0 | 5.5 | a,b | |
| | | 0.8 | 1.0 | 5.5 | a,b | |
| | | 0.85 | 1.0 | 5.5 | a,b | |
| | | 0.9 | 1.0 | 0, 2, 3.5, 5.5, 7, 8 | a,b | |
| | | 0.95 | 1.0 | 5.5 | a,b | |
| | | 1.10 | 1.0 | 5.5 | a,b | |
| | | 1.19 | 1.0 | 5.5 | a,b | |
| | | 1.35 | 1.0 | 5.5 | a,b | |
| 2 | 02519 FUSELAGE PARALLEL | | | | | |
| | CANARD OFF | 0.7 | 1.0 | 5.5 | a,b | |
| | | 0.8 | 1.0 | 5.5 | a,b | |
| | | 0.85 | 1.0 | 5.5 | a,b | |
| | | 0.9 | 1.0 | 0, 2, 3.5, 5.5, 7, 8 | a,b | |
| | | 0.95 | 1.0 | 5.5 | a,b | |
| | | 1.10 | 1.0 | 5.5 | a,b | |
| | | 1.19 | 1.0 | 5.5 | a,b | |
| | | 1.35 | 1.0 | 5.5 | a,b | |

## TABLE 9

CONTINUED

| IDENTIFICATION | | CONDITIONS | | POSITION | OTHER INFORMATION | |
|---|---|---|---|---|---|---|
| CASE NO | CONFIGURATION | MACH NO | H | ALPHA/DEG | TYPE OF MEASUREMENTS | ADDITIONAL REMARKS |
| 3 | 02119 FUSELAGE EXPANDING | | | | | |
| | CANARD ANGLE -3° | 0.7 | 1.0 | 5.5 | a,b | |
| | | 0.8 | 1.0 | 5.5 | a,b | |
| | | 0.85 | 1.0 | 5.5 | a,b | |
| | | 0.9 | 1.0 | 0, 2, 3.5, 5.5, 7.0, 8.0 | a,b | |
| | | 0.95 | 1.0 | 5.5 | a,b | |
| | | 1.10 | 1.0 | 5.5 | a,b | |
| | | 1.19 | 1.0 | 5.5 | a,b | |
| | | 1.35 | 1.0 | 5.5 | a,b | |

(a) Surface static pressures (b) Main balance Forces

**TABLE 10**

**DETAILS OF TRANSITION FIXING**

| Component | Position of leading edge band | Streamwise band width/mm | Ballotini diameter/mm |
|---|---|---|---|
| Fuselage nose | 50 mm from nose | 5.0 | 0.100-0.125 |
| Canard upper surface | 5%c | 2.0 | 0.100-0.125 |
| Canard lower surface | 5%c | 2.0 | 0.100-0.125 |
| Wing upper surface | 5%c | 2.0 | 0.100-0.125 |
| Wing lower surface | 5%c | 2.0 | 0.100-0.125 |

**TABLE 11**

**DATA AVAILABILITY**

| DATA | ENGIN. UNITS | COEFFICIENTS | NORMALIZED | UN-CORRECTED | CORRECTED |
|---|---|---|---|---|---|
| FREESTREAM CONDITIONS | | | | | X |
| SURFACE PRESSURES | | X | | | X |
| HEAT TRANSFER SKIN FRICTION | | | | | |
| FORCES | | X | | | X |
| BOUNDARY LAYER DATA | | | | | |
| WAKE DATA | | | | | |
| FIELD DATA | | | | | |
| TEST SECTION WALL PRESSURES | | | | | |

X INDICATES DATA AVAILABLE

## TABLE 12

## BASE AND REAR FUSELAGE PRESSURE DRAG CORRECTIONS

The model axial force and pitching moment has been corrected to allow for the pressures acting on the base of the model and the rear fuselage aft of x = 1.500m. The areas associated with the tubes indicated in Table 7, which are shown in Fig 9, are:

Table of areas ($mm^2$) for the parallel fuselage:

| Xmm | Tube 1 | 2 | 3 | 4 | 5 | 6 | 7 | 8 | 9 |
|---|---|---|---|---|---|---|---|---|---|
| 1500.0 | 0 | 0 | | 0 | 0 | 0 | | 89 | 39 |
| 1600.0 | 50 | 120 | | 120 | 112 | 130 | | 120 | 64 |
| 1690.0 | 133 | 331 | | 331 | 304 | 368 | | 331 | 133 |
| 1700.0 | 496 | 688 | 968 | 624 | 736 | 728 | 1016 | 648 | 496 |

Table of areas ($mm^2$) for the expanding fuselage:

| Xmm | Tube 1 | 2 | 3 | 4 | 5 | 6 | 7 | 8 | 9 |
|---|---|---|---|---|---|---|---|---|---|
| 1500.0 | 0 | 107 | | 575 | 640 | 655 | | 119 | 61 |
| 1600.0 | 59 | 277 | | 1102 | 1262 | 1261 | | 309 | |
| 1690.0 | 134 | 347 | | 500 | 467 | 558 | | 347 | 134 |
| 1700.0 | 496 | 688 | 968 | 624 | 736 | 728 | 1016 | 648 | 496 |

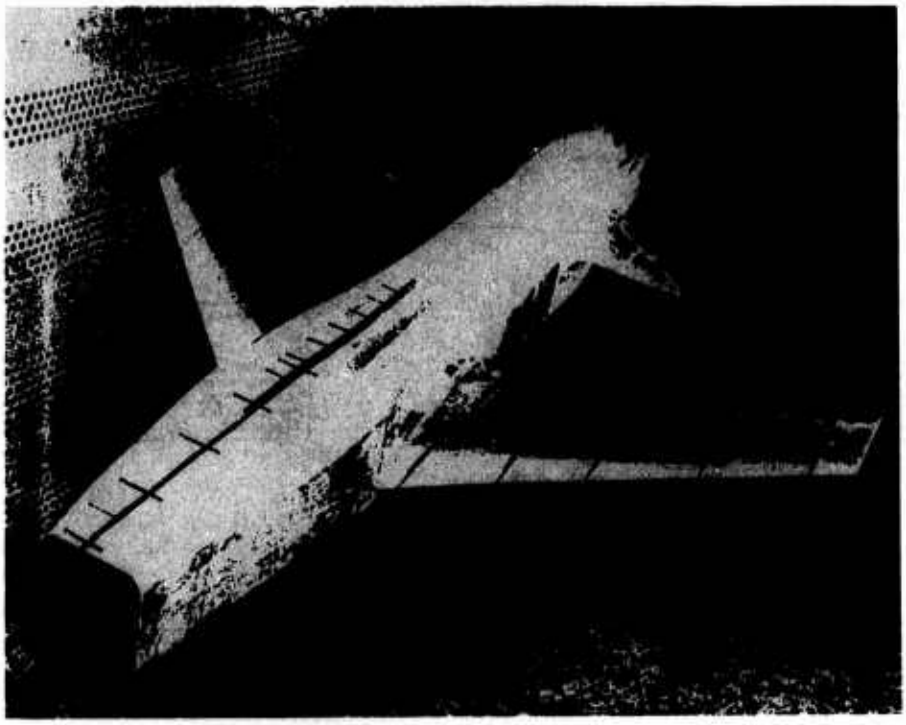
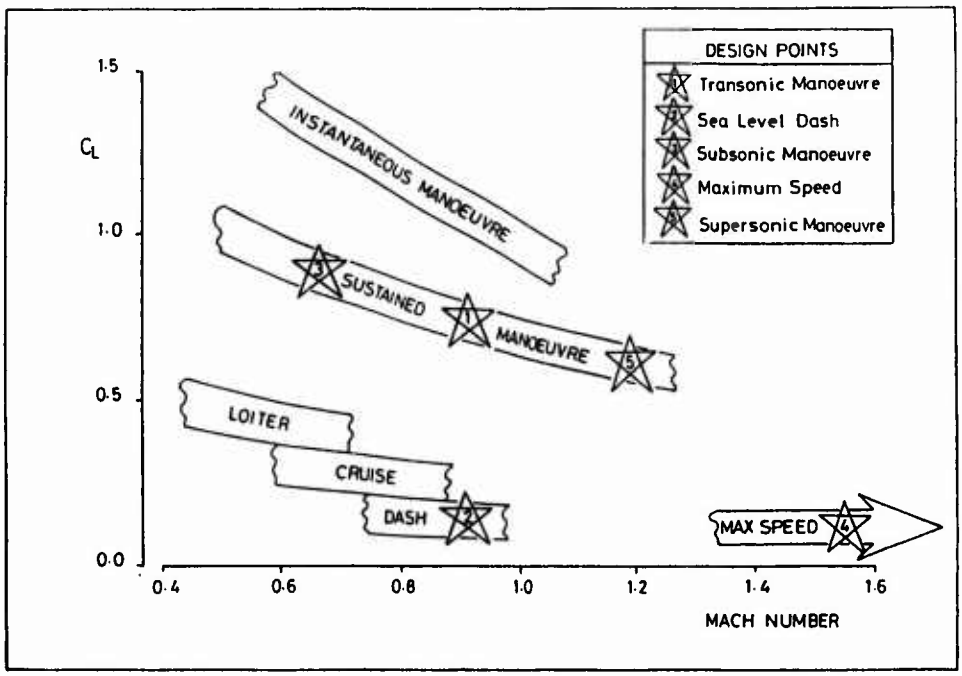


FIG 1 PHOTOGRAPH OF THE M151/1 FSW MODEL INSTALLED IN THE ARA 2.7m X 2.4m TRANSONIC WIND TUNNEL




WING DESIGN REQUIREMENTS

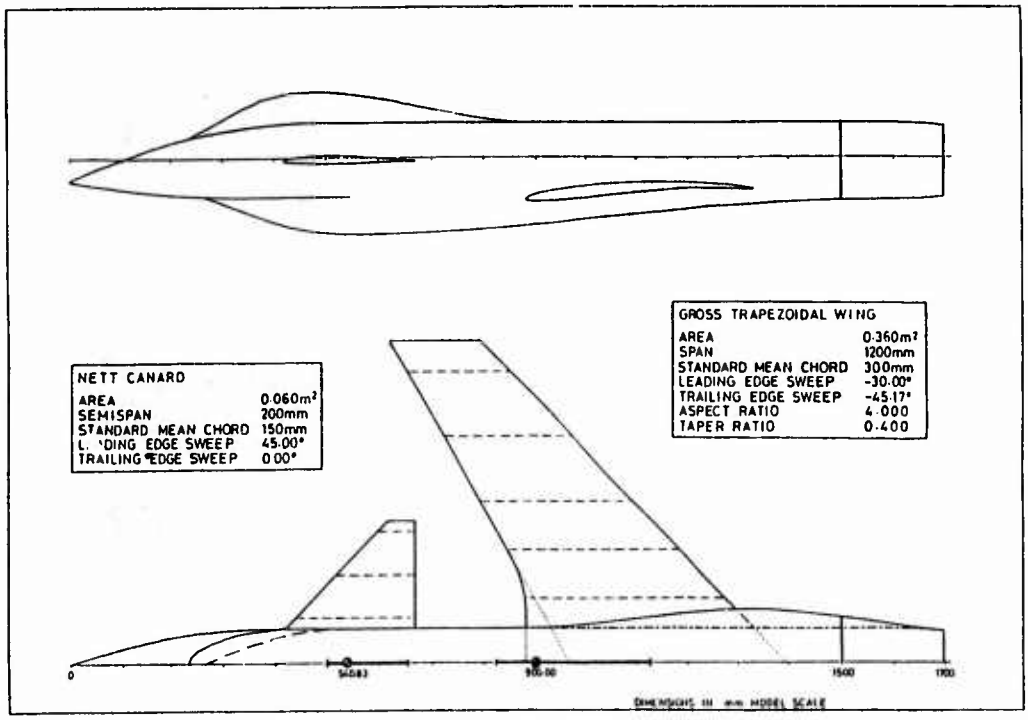



FIG 3 LAYOUT OF THE M151 FORWARD SWEPT WING MODEL

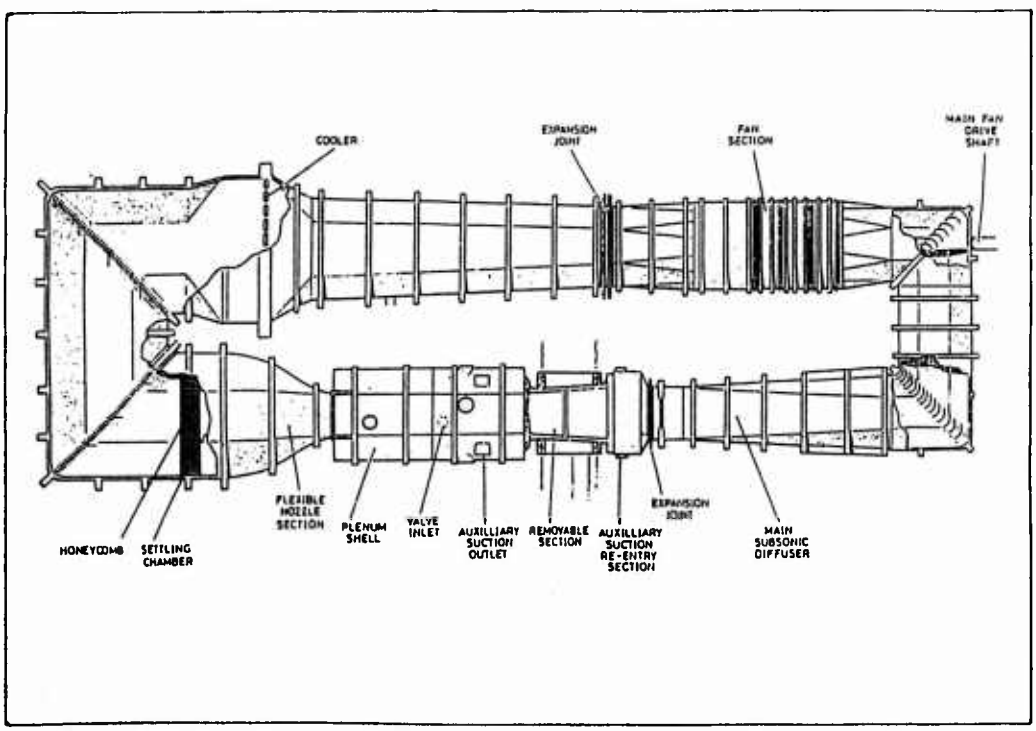



FIG 4 DETAILS OF THE A.R.A. 9'X8' TRANSONIC TUNNEL CIRCUIT

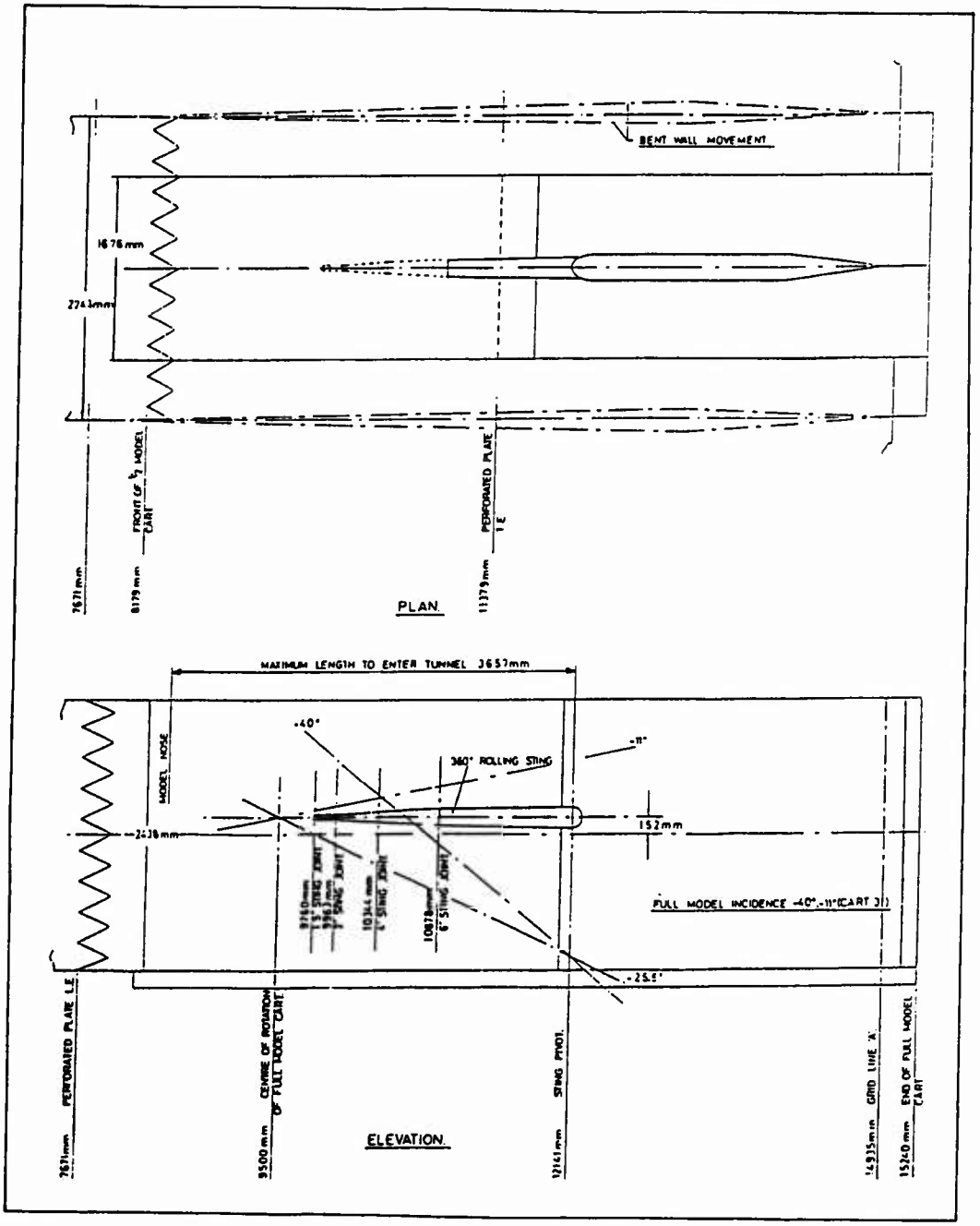



FIG 5 TRANSONIC WIND TUNNEL.

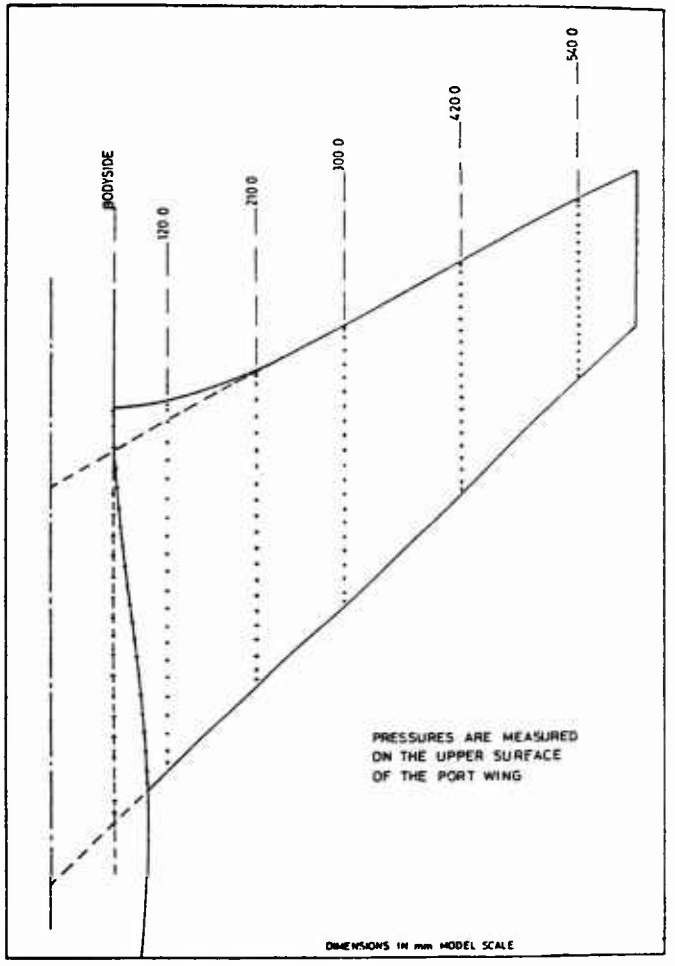



FIG 6 SPECIFICATION OF M151/1 PRESSURE PLOTTING: WING UPPER SURFACE

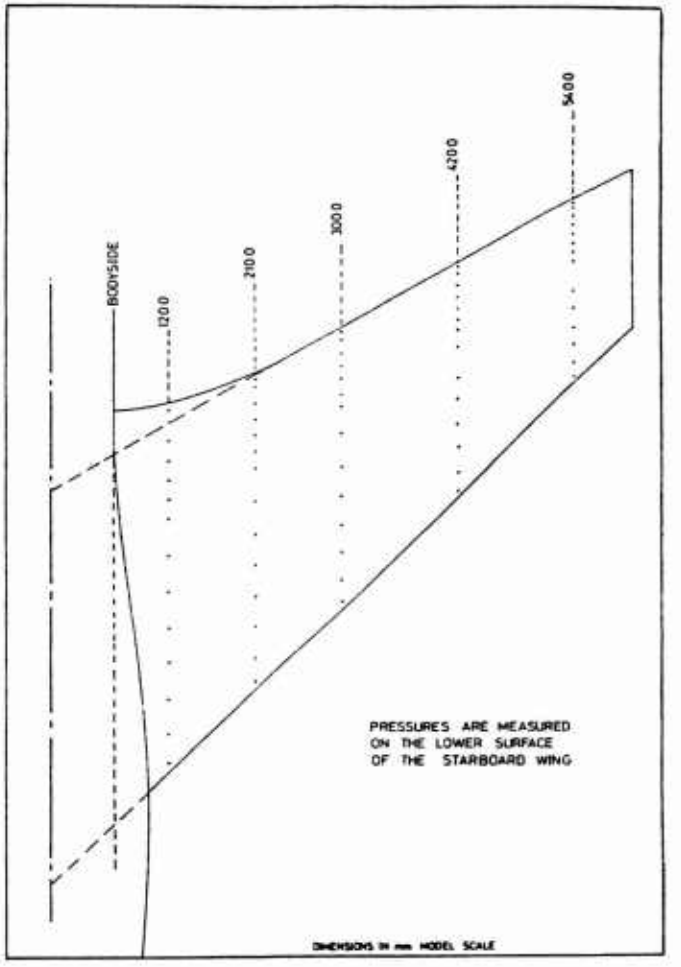



FIG 7 SPECIFICATION OF M151/1 PRESSURE PLOTTING: WING LOWER SURFACE

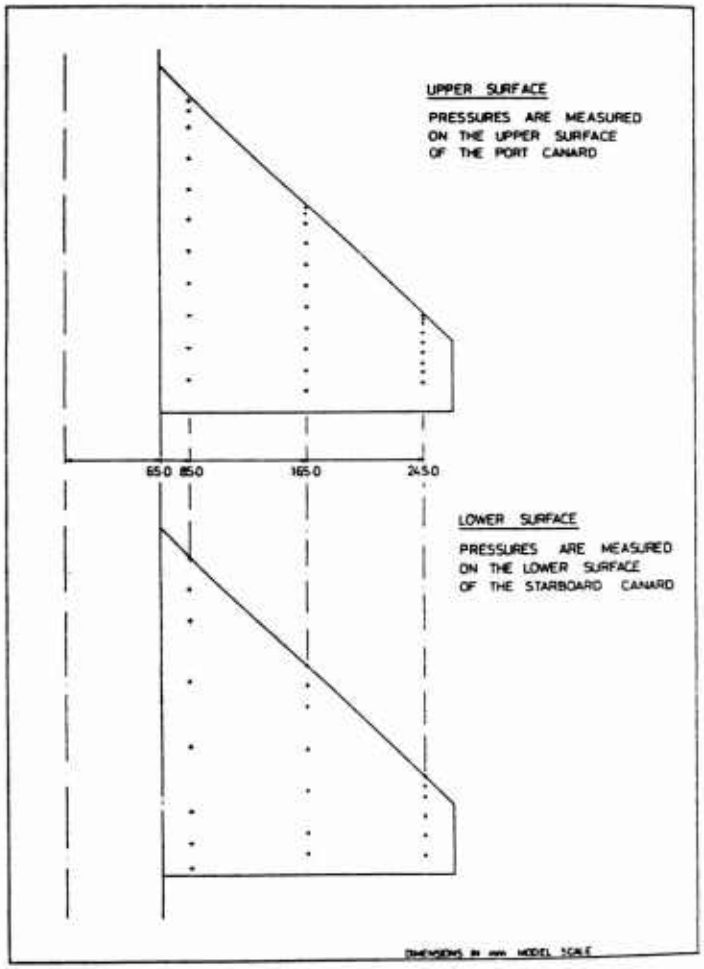



FIG 8 SPECIFICATION OF M151/1 PRESSURE PLOTTING: CANARD UPPER AND LOWER SURFACES

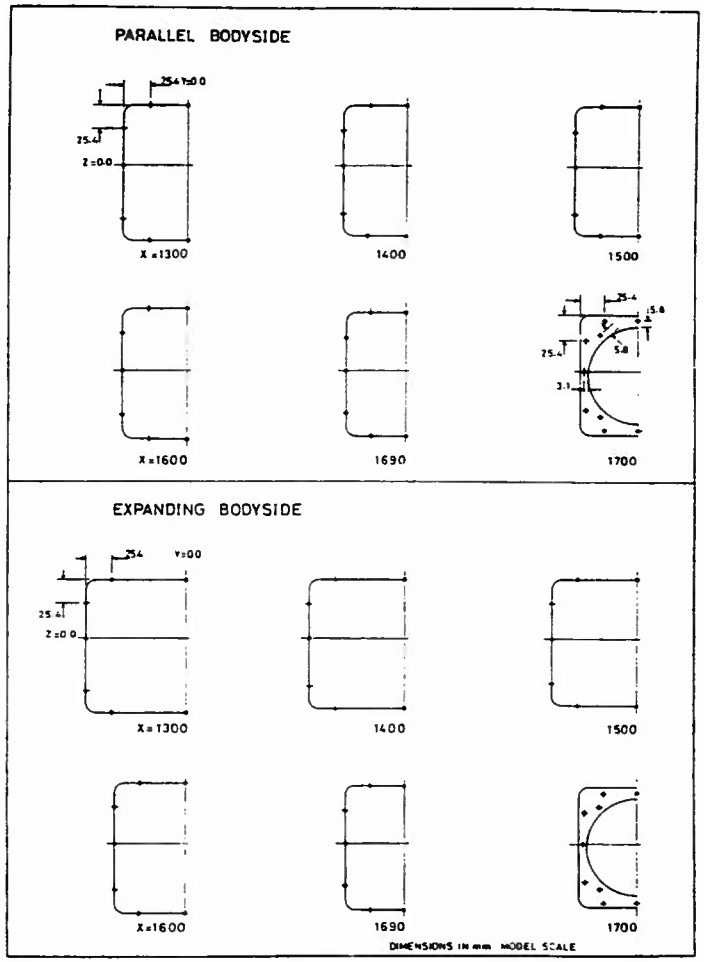



FIG 9 SPECIFICATION OF M151/1 PRESSURE PLOTTING: REAR FUSELAGE

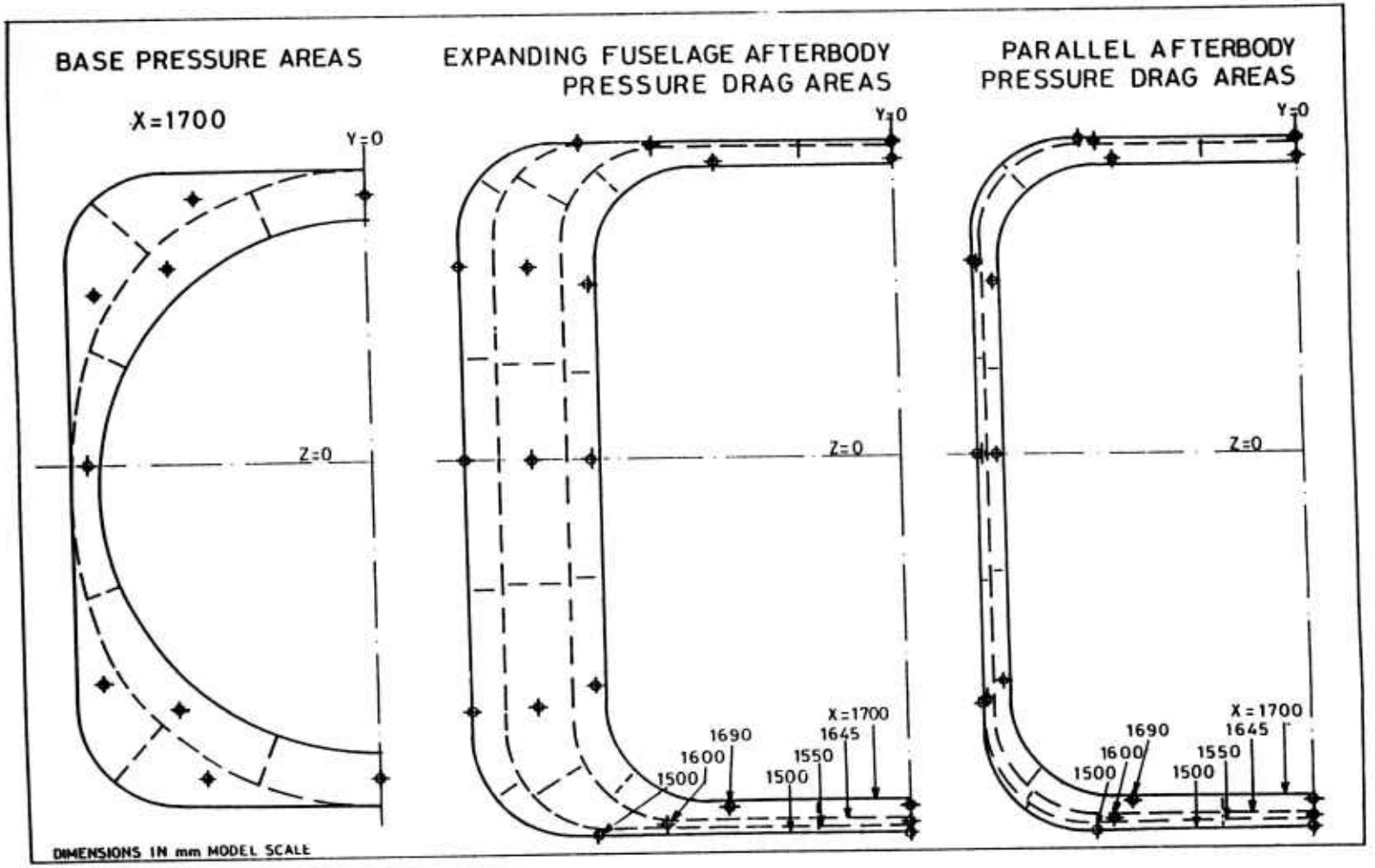



FIG 10 BASE AND REAR FUSELAGE PRESSURE DRAG CORRECTIONS

# Investigation of the influence of Pylons and Stores on the Wing Lower Surface Flow

*D. Stanniland, ARA, Bedford*

## 0 INTRODUCTION

This submission describes a series of tests on a large half model with a constant chord, untwisted, constant section wing with 25° sweep. The aim of these tests was to investigate the influence of pylons and stores on the wing lower surface flow, particularly the development of shocks and separations around the pylons with an associated increase in drag. To this end a large number of surface pressure tappings were provided on the wing lower surface (17 stations), on the inboard and outboard sides of each of the pylons and around the mid-pylon store. Since these data were to be used primarily for the validation of CFD codes, for this class of configuration, the fuselage and store are precisely defined bodies of revolution which can be modelled easily by the CFD geometry packages.

The tests were performed in the ARA 9ft x 8ft Transonic Wind Tunnel in February 1986.

# 1 GENERAL DESCRIPTION

## 1.1 Model name and designation

ARA M180/1 Half Model. See Fig. 1.

## 1.2 Model type and flow conditions

A large half model with a simple fuselage and a constant section, untwisted, untapered wing panel. Clean wing, with various pylon installations and a mid-pylon mounted store.

Tests were carried out over a range of Mach numbers from 0.55 to 0.86, primarily investigating the flow on the wing lower surface at low $C_L$.

## 1.3 Purpose of test

- To establish a level of confidence in the theoretical methods used to design the pylons.
- To provide an indication of the potential drag benefits which can be obtained from designing pylons.
- To provide a data base of increasing complexity against which future theoretical methods can be judged.

## 1.4 Dominant flow physics

Development of shocks and flow breakdown around the pylons and store on the wing lower surface, particularly in the open channels between the pylons.

# 2 DETAILS OF THE MODEL

## 2.1 General geometric arrangement

The general arrangement of the model is illustrated in Fig. 2(a).

## 2.2 Configurations

See Table 1.

81101 Clean wing.

81021 Three favourable interference pylons.

81014 Three favourable interference pylons, mid-pylon store.

## 2.3 Wing data

2.3.1 Planform See Fig. 2(a).

- Reference half-wing area = 0.7742m²
- Reference half-wing span = 1.5240m
- Reference chord = 0.5080m
- Moment reference centre = 0.4315m aft of wing l.e. apex on fuselage axis.
- Aspect ratio = 6.0
- Taper ratio = 1.0
- Leading edge sweep = 25°
- Trailing edge sweep = 25°
- Twist distribution - the section ordinates in Table 2 imply a wing/body setting angle of -0.79°. No additional twist is applied across the span.
- Semi-span = 1.5240m
- Tip chord = 0.508m
- Tip geometry - untapered.
- Details of fuselage/wing junction: wing mounted centrally on the fuselage.

2.3.2 Basic wing section

The wing has a constant chord, 8.5% thick RAE 5220 section applied normal to the wing leading edge (see Table 2).

## 2.4 Body data

2.4.1 Shape

The fuselage has a simple forebody and a parallel centrebody and afterbody, with a circular cross section offset from the tunnel floor by a plinth. Details of the forebody are shown in figure 2(b).

2.4.2 Additional details

Base cavity at rear of fuselage model to take accurate account of base drag values.

2.6 **Pylon data**

See Fig. 3 for geometry of pylons.

2.7 **Geometric definition**

- The fuselage forebody is defined numerically in Fig. 2(b).
- The wing has a constant section defined numerically in Table 2.
- The pylons are defined by 11 sections varying over the depth of the pylon, available separately (see also Fig. 3).
- The store is a simple body of revolution defined numerically in Fig. 4.
- Manufacturing errors are generally small, particularly relative to the large scale of the present model. The precise values for this model are no longer available.

2.8 **Model support details**

Floor mounted half model. The fuselage is offset from the floor of the tunnel by a 74mm parallel section and 2.5mm gap, to ensure clearance between the live parts of the model and the tunnel floor.

## 3 GENERAL TUNNEL INFORMATION

3.1 **Tunnel designation**

ARA 2.74m x 2.44m (9ft x 8ft) Transonic Wind Tunnel (see Fig. 5)

3.2 **Organisation running the tunnel**

Aircraft Research Association Ltd
Manton Lane
Bedford MK41 7PF

3.3 **Tunnel characteristics**

Rectangular continuous flow, closed circuit tunnel with perforated walls.

- Mach numbers: 0 to 1.4
- Half model incidence range from -10° to +30°
- Pressure range: stagnation pressure 0.8 to 1.2 bar.
- Temperature range: stagnation temperature up to 50°C.
- Reynolds number: Based on wing chord $5.5 \times 10^6$ at $M = 0.55$, increasing to $7.0 \times 10^6$ at $M = 0.86$.
- Run time: continuous.

3.4 **Test section**

3.4.1 Test section details. See Fig 6.

3.4.2 Test section size. 2.74m x 2.44m.

3.4.3 Wall geometry details

- Perforated walls.
- Variable increasing to a maximum of 22% open area (normal holes).
- Bent wall movement to optimise the Mach number distribution for higher Mach numbers.
- No wall pressures measured for this test series.
- Wall boundary layer displacement thickness 14mm at half model centre of rotation.

3.5 **Free-stream conditions**

3.5.1 Reference conditions

- Total pressure in the working section is obtained from the static pressure in the settling chamber using calibration data.
- Static pressure in the working section is obtained from the static pressure inside the plenum chamber.
- The reference pressure used to calibrate pressure transducers is an applied pressure in a large reservoir in the tunnel control room.

- Stagnation temperature is measured to an accuracy of ±0.2°K over the operating range of the tunnel, using a probe installed in the settling chamber.

3.5.2 Tunnel calibration

- Tunnel is calibrated using a centreline probe located in the vicinity of a half model fuselage.
- Last calibration specific to half model test requirements in August 1991.

## 3.6 Flow Quality

3.6.1 Flow uniformity

Mach number variation along the length of a model is set to a nominal zero using settings of the wind tunnel walls derived from the tunnel calibration. Typical errors of $\Delta M$ = 0.0002 were measured in the last calibration of the tunnel. Mach number is held to within 0.001 of the required value up to moderate incidence, at subsonic Mach numbers. No flow angle correction is applied for half model testing.

3.6.2 Temperature variation

Tunnel temperature is not controlled directly, although the increase in temperature during a run is minimised by a cooler. Stagnation temperature increases by approximately 2°K for a moderate incidence traverse at a given Mach number. Temperature variation across the tunnel is not known.

3.6.3 Flow unsteadiness

Early measurements of the unsteadiness in the ARA TWT indicated a peak at M = 0.7. A more extensive investigation, carried out in 1990 following the installation of a long cell honeycomb, showed that this peak is due to a tone at 2.6 KHz which is not present when a model is present in the working section. See Ref 2 for further details.

# 4 INSTRUMENTATION

## 4.1 Model position See Fig. 6

4.1.1 Geometrical incidence measurements

Half model zero incidence is set by measurement from the model to a reference bar fixed to the tunnel floor. Model incidence is obtained relative to this zero using a 'synchro' measurement/control device.

4.1.2 Accuracy of geometrical incidence

Zero incidence is set to an accuracy of approximately 0.02°. Measurement of the angle of incidence relative to the defined zero is accurate to 0.01°.

## 4.2 Model pressure measurement

4.2.1 Number of pressure holes

| | |
|---|---|
| wing upper surface | = 164 |
| lower surface | = 256 |
| Pylon | = 74/pyl. |
| Store | = 63 |

Pressures are measured close to the intersection of the three pylon stations with the wing lower surface. The location of pressure tappings and arrangement of pylons is shown in Fig. 7(a). Pressures were measured along two rows parallel to the pylon foot and at three constant x/c positions over the depth of the pylon, and at various positions around the store. (see Fig. 7(b)).

## 4.3 Forces and Moment measurements

4.3.1 Type and location of balance

Underfloor mounted high range half model balance, with the forces and moments obtained from the average of two independent 5 component balances.

4.3.2 Maximum range and accuracy

Balance sensitivities are shown in Table 3.

4.5 **Surface flow visualisation**

None.

4.6 **Field flow visualisation**

None.

4.7 **Tunnel wall measurements**

None.

## 5 TEST MATRIX AND CONDITIONS

5.1 **Details of test matrix**

5.1.1 Number of test cases

Three tests cases have been selected.

5.1.2 Number of configurations

Three configurations.

5.1.3 Summary of test cases

For summary of test cases see Table 4.

5.2 **Model/tunnel relations**

5.2.1 Blockage effect

Maximum blockage (clean wing) = 1.65%.

5.2.2 Model span/tunnel width ratio

Gross model semi-span/tunnel height = 0.625.

5.2.3 Wing area/tunnel cross section

Gross half wing area/tunnel cross sectional area = 0.116.

5.2.6 Wall temperatures

Wall temperatures were not measured.

5.3 **Transition details**

5.3.1 Transition was fixed for all components

5.3.3 Details of transition fix

- See Table 5.
- Transition was fixed on the model using narrow bands of Ballotini set in a thin film of Araldite.
- The effectiveness of the chosen transition bands was confirmed using an Acenaphthene sublimation test at M = 0.66, $\alpha$ = -0.1°.

## 6 DATA

6.1 **Availability of data**

6.1.1 Owners of data

U.K. Ministry of Defence
Technical Authority represented by
Aerodynamics and Propulsion Department
Defence Research Agency
Farnborough
England

6.1.2 Person responsible for data

Mr D Stanniland
Aircraft Research Association Ltd
Manton Lane
Bedford MK41 7PF

Tel: 0234 - 350681
Fax: Groups 2 & 3, 0234 - 328584

6.1.3 Queries about data

Contact ARA in the first instance.

6.2 **Suitability of data for CFD validation**

6.2.1 Suitability for "in tunnel" calculations

The tests were carried out in a perforated tunnel with no measured wall pressures. Hence, the data are unlikely to be appropriate for in-tunnel calculations with a specified boundary condition.

6.2.2 Simulation of 'Free Air' conditions

Data are corrected to simulate "Free Air" conditions. Although the model is large relative to the tunnel, the relatively low test Mach numbers and low incidences under consideration mean that the results do not exhibit significant wall interference. The model is complex from the point of view of multiple component interference, but each of the components can be easily and precisely defined in a CFD calculation. The large number of pressure tappings on the wing adjacent to the pylons, on the pylons themselves and on the store on the mid-pylon mean that the results are particularly appropriate for this purpose. The data has been used extensively for CFD code validation, notably for the ARA Multi-block suite of programs (Refs. 4 and 5).

## 6.3 Type and form in which data available

6.3.1 Type and form of data

For list of available data see Table 6.

6.3.2 Format of data available

Data will be supplied on an IBM compatible floppy disk.

## 6.4 Correction applied to data

6.4.3 Half model correction

Tunnel constant. A correction has been applied to the model incidence based on a comparison between full model and half model tests in the ARA TWT.

6.4.6 Other corrections

Base drag. 25 pressure measured in the fuselage base were used to correct the model axial force to free stream static base pressure. This is a large correction. ($C_{XB} \approx 0.01$ compared with a corrected axial force at zero incidence = 0.014).

# 7 DATA ACCURACY AND REPEATABILITY ASSESSMENT

## 7.1 Estimated accuracies

7.1.1 Free stream conditions

Mach number measured in these tests has a bias of -0.0015 which has been recently identified, with an accuracy of $\pm 0.001$.
Model incidence is estimated to be accurate to $\pm 0.02°$ up to $\alpha \simeq 10°$.

7.1.2 Measured data

The RMS errors presented in Table 3 imply errors at M = 0.8 of typically.

$C_N$ $\pm 0.0003$
$C_A$ $\pm 0.0003$*
$C_m$ $\pm 0.0004$
$C_\ell$ $\pm 0.0008$
$C_n$ $\pm 0.0007$

* Incremental drag differences between configurations have been analysed separately and are believed to be accurate to $\pm$ 0.00005.

# 8 REFERENCES

## 8.1 On the Wind Tunnel

1. J E Green, C A McHugh, A J Baxendale, D R Stanniland

The use of a deep honeycomb to achieve high flow quality in the ARA 9' x 8' Transonic Wind Tunnel presented at 18th Congress of ICAS, Beijing, September 1992.

2. D R Stanniland, C A McHugh, J E Green

Improvement of the flow quality in the ARA Transonic Tunnel by means of a long cell honey-comb. Paper 54, RAes conference on "Wind Tunnels and Wind Tunnel Test Techniques", Southampton 1992.

3. E C Carter, K C Pallister

Development of testing techniques in a large Transonic Wind Tunnel to achieve a required drag accuracy and flow standards for modern civil transport.
AGARD-CP-429, September 1987.

## 8.3 On the Test

4. A J Baxendale

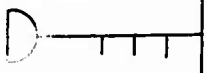
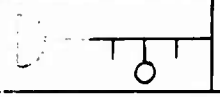
Application of a Multiblock CFD system to obtaining flowfield predictions about wing/body/pylon/store configurations.
17th ICAS Congress, Stockholm, 1990.

5. D R Stanniland, A J Baxendale, K G Carr

The use of CFD methods to aid the Aerodynamic design and analysis of wing/pylon/store installations. RAE's Store Carriage Symposium, 1990.

## TABLE 1

## M180/1 CONFIGURATION LIST

| CONFIGURATION | INBOARD | MID | OUTBOARD |
|---|---|---|---|
| 81101  | - | - | - |
| 81021  | PYLON | PYLON | PYLON |
| 81014  | PYLON | PYLON + TANK | PYLON |

## TABLE 2

## RAE 5220 SECTION ORDINATES APPLIED NORMAL TO THE WING LEADING EDGE

| x/c | z/c upper | z/c lower | x/c contd. | z/c upper cntd | z/c lower cntd |
|---|---|---|---|---|---|
| 0.000000 | 0.001560 | 0.001560 | 0.443660 | 0.047290 | -0.035527 |
| 0.002981 | 0.009172 | -0.006151 | 0.466596 | 0.047400 | -0.034024 |
| 0.008679 | 0.013717 | -0.010951 | 0.489449 | 0.047444 | -0.032224 |
| 0.014039 | 0.016445 | -0.013975 | 0.512244 | 0.047423 | -0.030077 |
| 0.019292 | 0.018575 | -0.016392 | 0.535006 | 0.047340 | -0.027582 |
| 0.024707 | 0.020448 | -0.018536 | 0.557751 | 0.047193 | -0.024774 |
| 0.030523 | 0.022214 | -0.020528 | 0.580492 | 0.046983 | -0.021659 |
| 0.037083 | 0.023984 | -0.022447 | 0.603241 | 0.046713 | -0.018270 |
| 0.044772 | 0.025850 | -0.024365 | 0.626004 | 0.046377 | -0.014644 |
| 0.054190 | 0.027766 | -0.026339 | 0.648790 | 0.045967 | -0.010742 |
| 0.066066 | 0.029627 | -0.028392 | 0.671609 | 0.045482 | -0.006595 |
| 0.081200 | 0.031513 | -0.030492 | 0.694469 | 0.044937 | -0.002289 |
| 0.100083 | 0.033545 | -0.032516 | 0.717388 | 0.044353 | 0.002096 |
| 0.122447 | 0.035634 | -0.034317 | 0.740383 | 0.043749 | 0.006413 |
| 0.147263 | 0.037623 | -0.035930 | 0.763482 | 0.043000 | 0.010534 |
| 0.173324 | 0.039396 | -0.037239 | 0.786719 | 0.042050 | 0.014341 |
| 0.199722 | 0.040924 | -0.038214 | 0.810138 | 0.040887 | 0.017722 |
| 0.255942 | 0.042215 | -0.038912 | 0.833793 | 0.039369 | 0.020562 |
| 0.251746 | 0.043301 | -0.039375 | 0.857753 | 0.037650 | 0.022690 |
| 0.277060 | 0.044209 | -0.039604 | 0.882101 | 0.035581 | 0.023972 |
| 0.301888 | 0.044966 | -0.039619 | 0.906941 | 0.033200 | 0.024233 |
| 0.326276 | 0.045595 | -0.039430 | 0.932402 | 0.030300 | 0.023282 |
| 0.350281 | 0.046112 | -0.039057 | 0.958646 | 0.026700 | 0.020500 |
| 0.373966 | 0.046529 | -0.038498 | 0.985879 | 0.021600 | 0.015905 |
| 0.397389 | 0.046859 | -0.037736 | 1.000000 | 0.018250 | 0.012500 |
| 0.420605 | 0.047111 | -0.036758 | | | |

**TABLE 3**

**TWT 1/2 CART HIGH RANGE BALANCE SENSITIVITY**

| COMPONENT | | RMS ERROR | | MAXIMUM LOAD |
|---|---|---|---|---|
| | | Balance 1 | Balance 2 | |
| NORMAL FORCE | N | 5.3 N | 5.1 N | 27600 N |
| AXIAL FORCE | A | 7.9 N | 7.9 N | 3780 N |
| PITCHING MOMENT | m | 4.4 Nm | 4.3 Nm | 2700 Nm |
| ROLLING MOMENT | l | 7.6 Nm | 7.4 Nm | 20300 Nm |
| YAWING MOMENT | n | 7.6 Nm | 7.6 Nm | 2800 Nm |

**TABLE 4**

**SUMMARY OF TEST CASES**

| IDENTIFICATION | | CONDITIONS | | POSITION | OTHER INFORMATION |
|---|---|---|---|---|---|
| CASE NO | CONFIGURATION | MACH NO | H | ALPHA/DEG | TYPE OF MEASUREMENTS |
| 1 | 81101 CLEAN WING | | | | |
| | | 0.72 | 1.0 | 0 | a,b |
| | | 0.77 | 1.0 | 0 | a,b |
| | | 0.80 | 1.0 | 0 | a,b |
| | | 0.82 | 1.0 | -1, 0,1,2,3,4 | a,b |
| | | 0.84 | 1.0 | 0 | a,b |
| | | 0.86 | 1.0 | 0 | a,b |
| 2 | 81021 WING WITH THREE PYLONS | | | | |
| | | 0.72 | 1.0 | 0 | a,b |
| | | 0.77 | 1.0 | 0 | a,b |
| | | 0.80 | 1.0 | 0 | a,b |
| | | 0.82 | 1.0 | -1, 0,1,2,3,4 | a,b |
| | | 0.84 | 1.0 | 0 | a,b |
| | | 0.86 | 1.0 | 0 | a,b |

TABLE 4

CONTINUED

| IDENTIFICATION | | CONDITIONS | | POSITION | OTHER INFORMATION |
|---|---|---|---|---|---|
| CASE NO | CONFIGURATION | MACH NO | H | ALPHA/DEG | TYPE OF MEASUREMENTS |
| 3 | 81014 WING WITH THREE PYLONS + STORE | | | | |
| | | 0.72 | 1.0 | 0 | a,b |
| | | 0.77 | 1.0 | 0 | a,b |
| | | 0.80 | 1.0 | 0 | a,b |
| | | 0.82 | 1.0 | -1, 0,1,2,3,4 | a,b |
| | | 0.84 | 1.0 | 0 | a,b |
| | | 0.86 | 1.0 | 0 | a,b |

(a) Surface static pressures

(b) Main balance Forces

TABLE 5

DETAILS OF TRANSITION FIXING

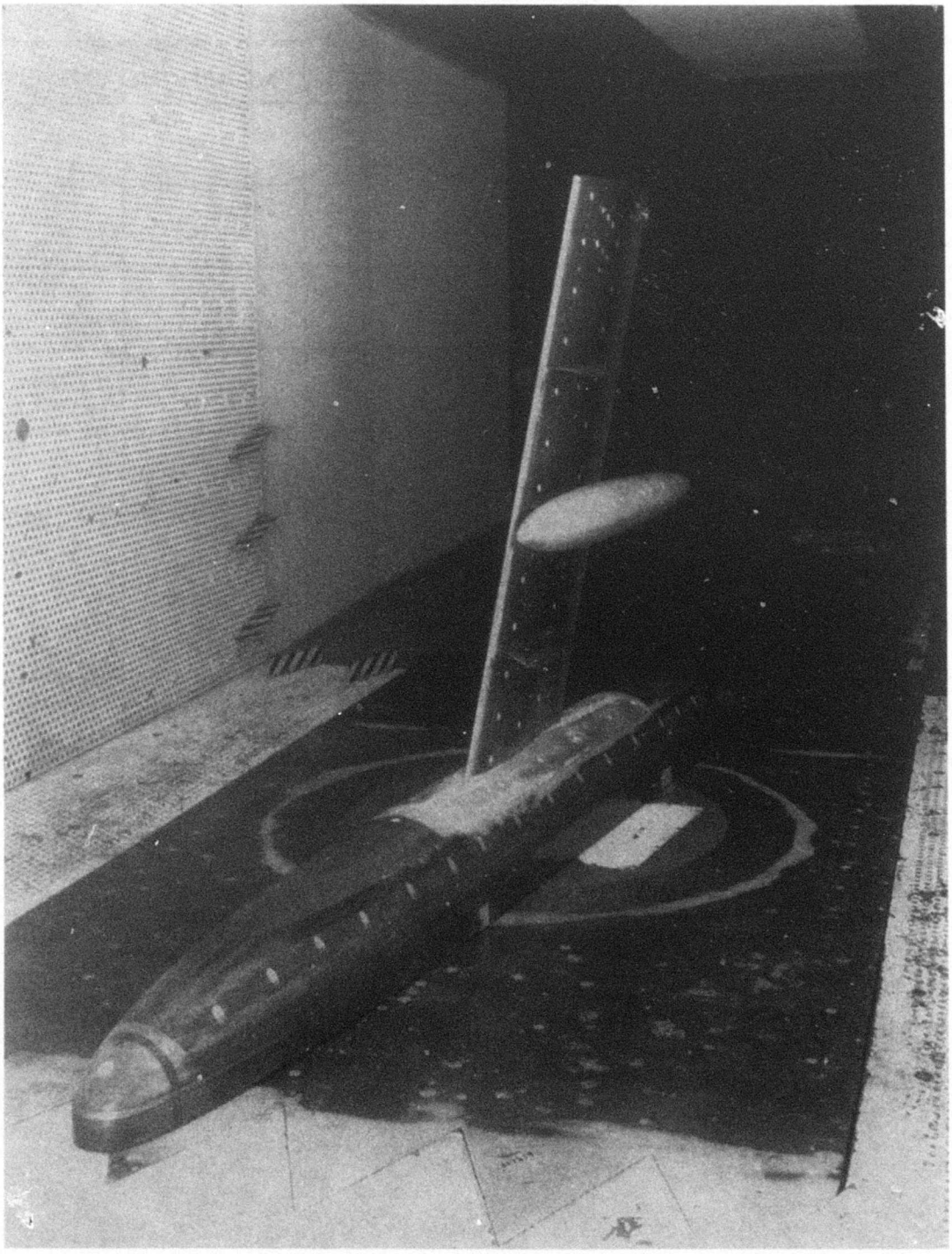
| Component | Position of leading edge band | Streamwise band width/mm | Ballotini diameter/mm |
|---|---|---|---|
| Fuselage nose | 100mm from nose | 15.0 | 0.125 - 0.150 |
| Wing upper surface | 8%c | 3.8 | 0.125 - 0.150 |
| Wing lower surface | 8%c | 3.8 | 0.125 - 0.150 |
| Pylons | 5%c | 2.0 | 0.100 - 0.125 |
| Tank | 5%l | 2.0 | 0.125 - 0.150 |

TABLE 6

DATA AVAILABILITY

| DATA | ENGIN. UNITS | COEFFICIENTS | NORMALIZED | UN-CORRECTED | CORRECTED |
|---|---|---|---|---|---|
| FREESTREAM CONDITIONS | | | | | X |
| SURFACE PRESSURES | | X | | | X |
| HEAT TRANSFER SKIN FRICTION | | | | | |
| FORCES | | X | | | X |
| BOUNDARY LAYER DATA | | | | | |
| WAKE DATA | | | | | |
| FIELD DATA | | | | | |
| TEST SECTION WALL PRESSURES | | | | | |

X INDICATES DATA AVAILABLE



PHOTOGRAPH OF THE M180/1 MODEL INSTALLED IN THE A.R.A 9 FT X 8 FT TRANSONIC WIND TUNNEL

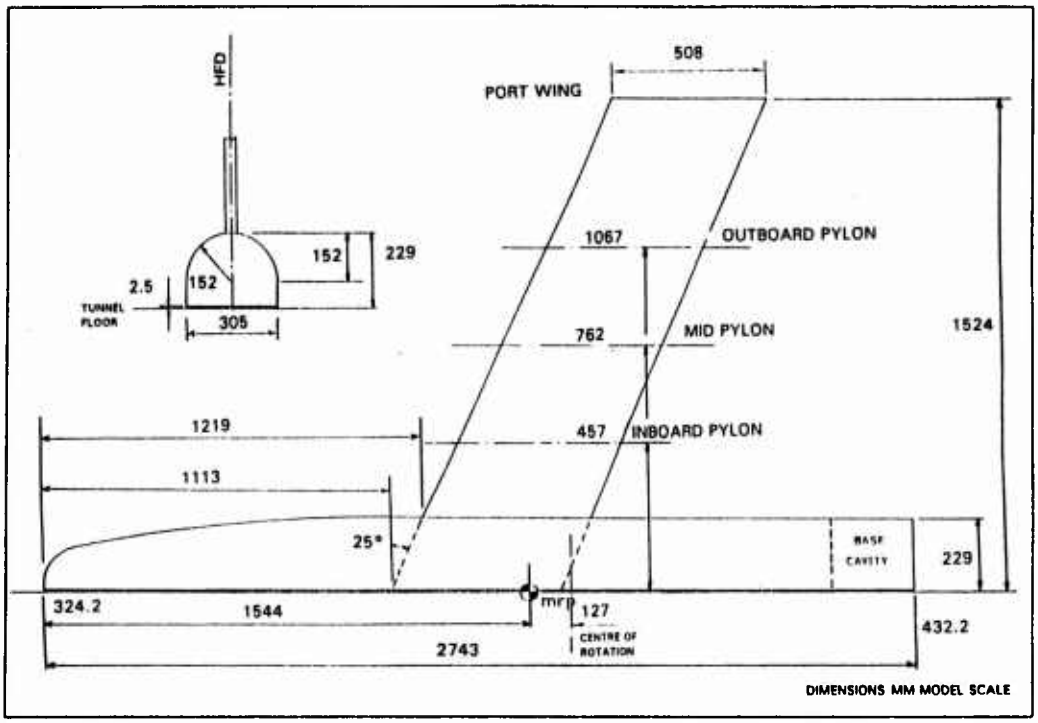



FiG 2(a) GENERAL ARRANGEMENT OF MODEL M180/1

| X | Y |
|---|---|
| 0.000 | 0.000 |
| 1.575 | 15.951 |
| 8.3058 | 37.617 |
| 20.320 | 56.744 |
| 37.490 | 72.847 |
| 59.665 | 86.487 |
| 86.589 | 98.933 |
| 117.983 | 110.515 |
| 153.490 | 121.387 |
| 192.786 | 131.547 |
| 235.407 | 141.021 |
| 280.090 | 149.758 |
| 328.828 | 157.810 |
| 378.638 | 165.125 |
| 429.844 | 171.679 |
| 481.863 | 177.521 |
| 534.137 | 182.651 |
| 586.156 | 187.071 |
| 637.362 | 187.710 |
| 687.170 | 190.830 |
| 735.101 | 193.954 |
| 780.618 | 196.520 |
| 823.239 | 198.526 |
| 862.508 | 200.076 |
| 898.042 | 201.219 |
| 929.411 | 202.032 |
| 956.335 | 202.590 |
| 978.510 | 202.895 |
| 995.705 | 203.175 |
| 1006.704 | 203.200 |
| 1016.000 | 203.200 |
| 2743.20 | 203.200 |

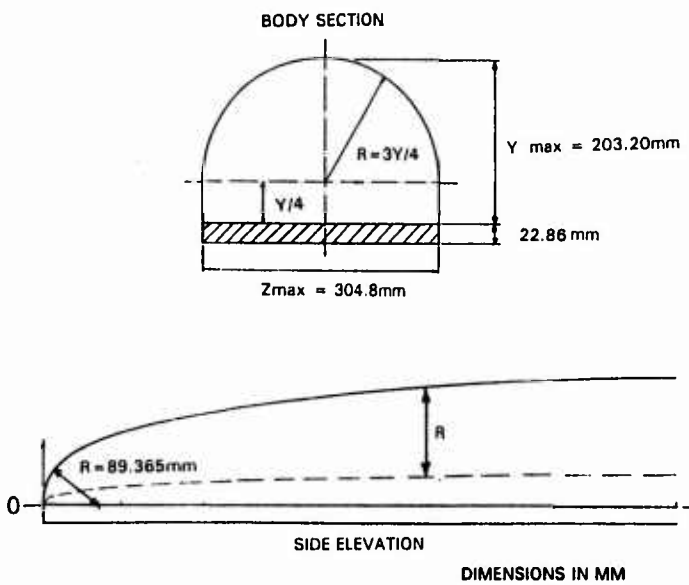



FIG 2(b) M180/1 - BODY CONTOURS

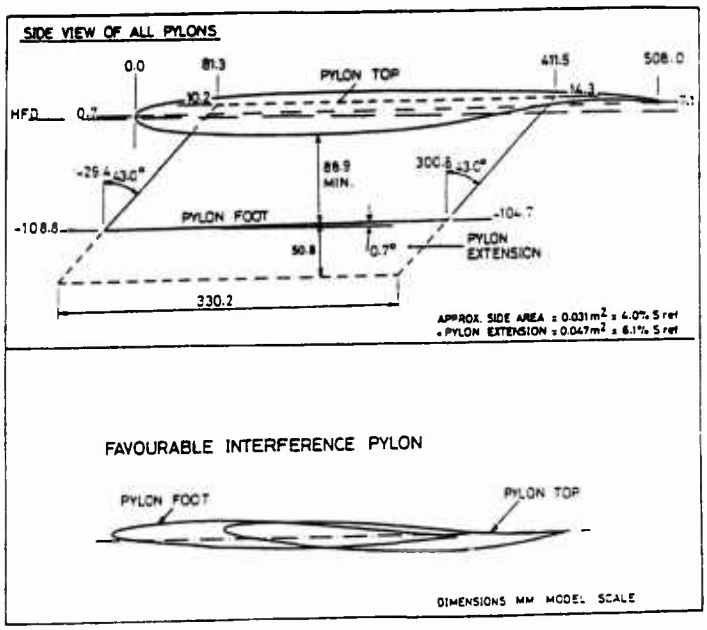
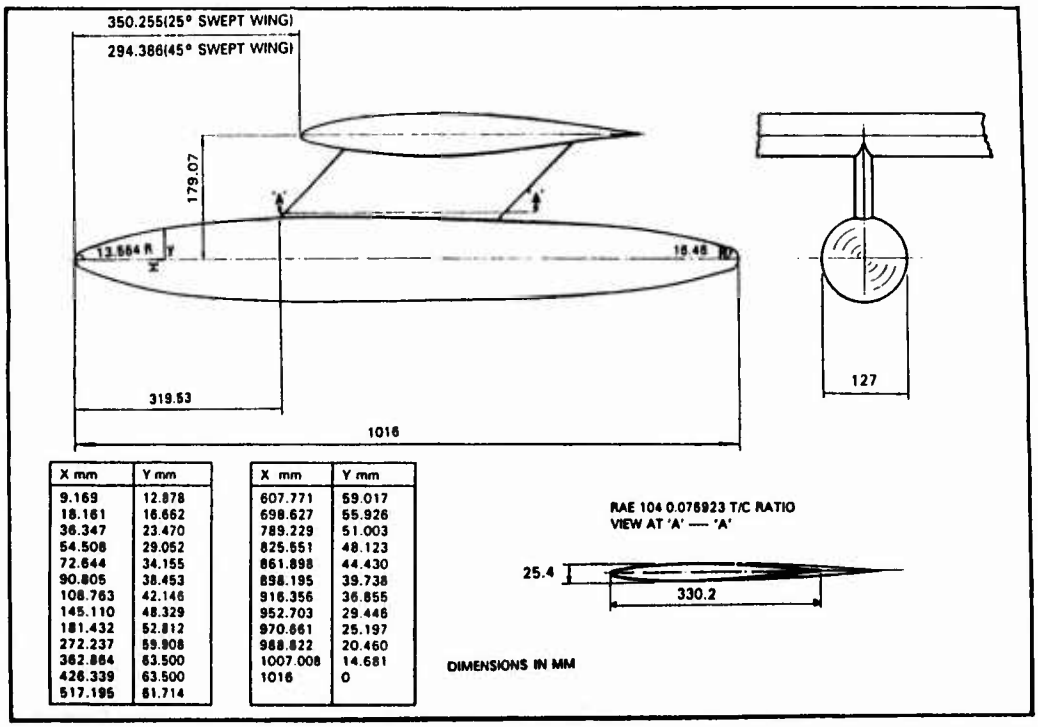



FIG 3 GEOMETRY OF PYLON




| X mm | Y mm |
|---|---|
| 9.169 | 12.878 |
| 18.161 | 16.662 |
| 36.347 | 23.470 |
| 54.508 | 29.052 |
| 72.644 | 34.155 |
| 90.805 | 38.453 |
| 108.763 | 42.146 |
| 145.110 | 48.329 |
| 181.432 | 52.812 |
| 272.237 | 59.908 |
| 362.864 | 63.500 |
| 426.339 | 63.500 |
| 517.195 | 61.714 |

| X mm | Y mm |
|---|---|
| 607.771 | 59.017 |
| 698.627 | 55.926 |
| 789.229 | 51.003 |
| 825.551 | 48.123 |
| 861.898 | 44.430 |
| 898.195 | 39.738 |
| 916.356 | 36.855 |
| 952.703 | 29.446 |
| 970.661 | 25.197 |
| 988.822 | 20.460 |
| 1007.008 | 14.681 |
| 1016 | 0 |

FIG 4 GEOMETRY OF STORE

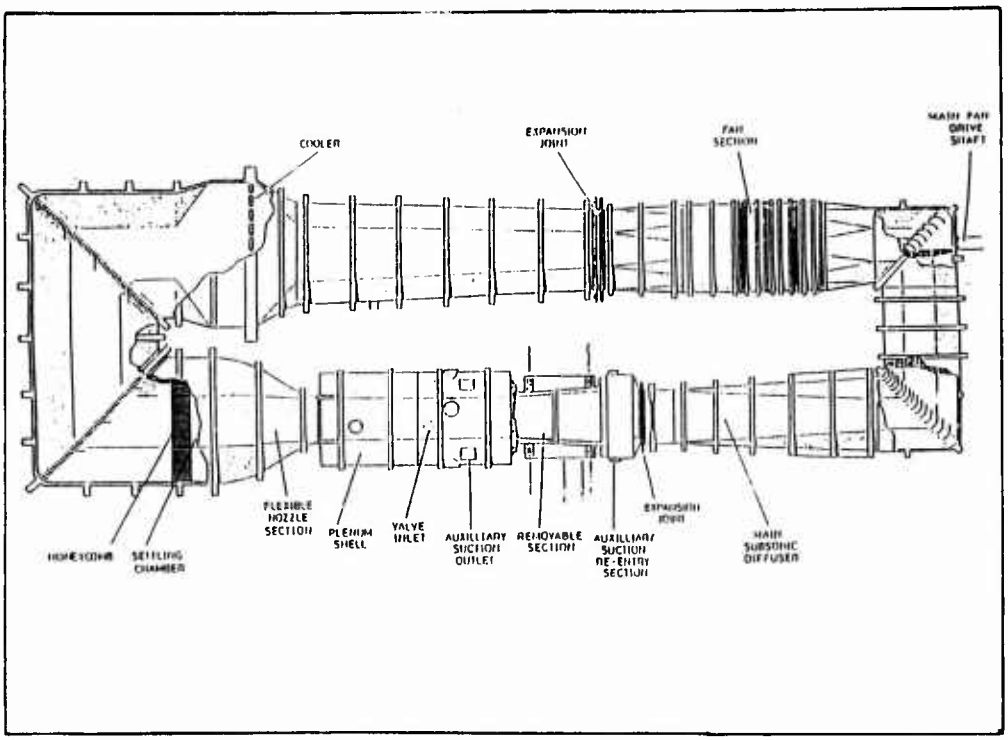



FIG 5 DETAILS OF THE A.R.A. 9'X8' TRANSONIC TUNNEL CIRCUIT

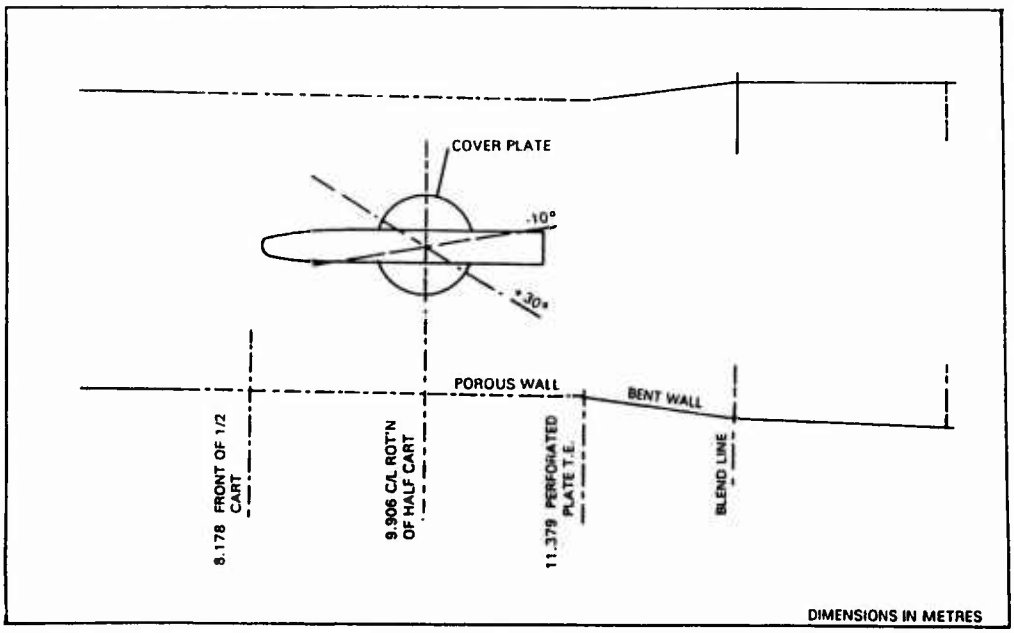



FIG 6 ARRANGEMENT OF HALF MODEL IN WORKING SECTION OF ARA 9 FT X 8 FT TRANSONIC WIND TUNNEL

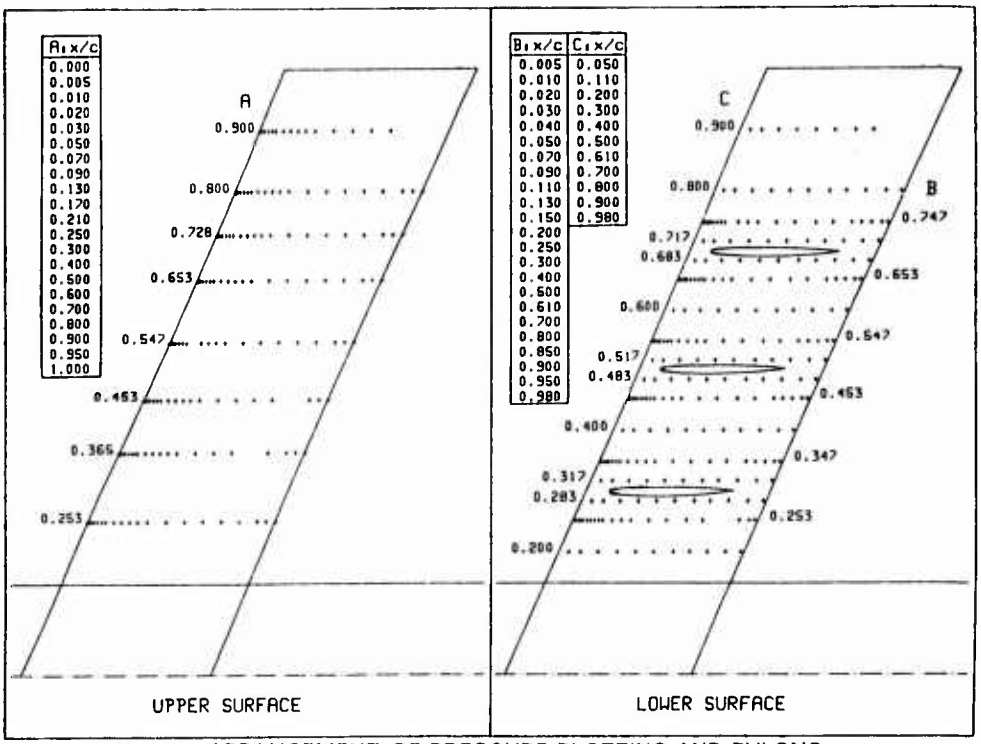



FIG 7(a) ARRANGEMENT OF PRESSURE PLOTTING AND PYLONS ON M180/1 WING

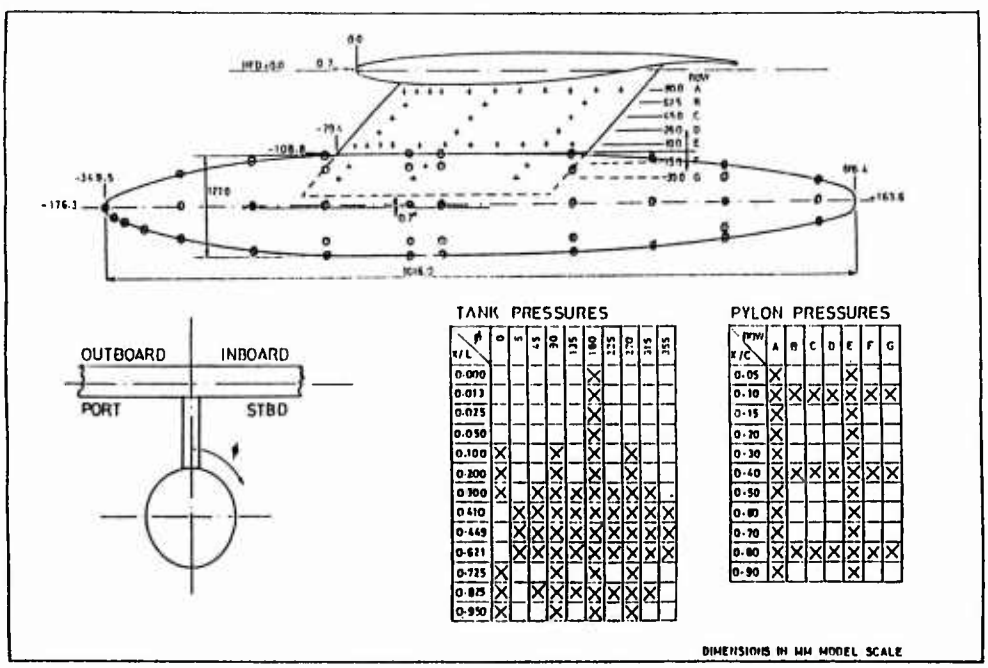



FIG 7(b) ARRANGEMENT OF PYLON AND TANK PRESSURE PLOTTING

# ANNEX A

## PROCEDURE FOR OBTAINING AND USING FLOPPY DISKS

A complete set of data is available on a set of nine 3.5 inch floppy disks. These disks are on file at the various National Centers listed below. Specific details, costs, and procedures for obtaining a copy of the floppy disks varies from one center to the other. Therefore, interested parties must contact the appropriate location within their country or the center that is most geographically convenient.

Information regarding procedures to be followed in using the data is provided on the disks. In addition, on the following page, information regarding the contents of the disks, procedures to extract the data from an archive file, and the hard disk size needed for the various uncompressed datasets is provided.

Etat-Major de la Force Aérienne
(VSL/AGARD)
rue d'Evere
B-1140 Bruxelles
BELGIUM
Person to contact: Major J.J. Lecluyse
Tel:32(2)701-4955
Fax:32(2)701-3723

Directorate of Scientific Information Services
National Defence Headquarters
MGeneral George R. Pearkes Building
Ottawa, Ontario K1A OK2
CANADA
Person to contact: Ms. Robin Leckie
Tel:1(613)992 7237
Fax:1(613)996 0392

Dept. of Fluid Mechanics
Technical University of Denmark
Building 404
DK 2800 Lyngby
DENMARK
Person to contact: Dr. P. S. Larsen
Tel:45 4593 1222 - Ext: 4332
Fax:45 4288 2421

Fachinformationszentrum Karlsruhe
Gesellschaft fur wissenchaftlich-technische Information mbh
D-76344 Eggenstein-Leopoldshafen
GERMANY
Person to contact: Dr. Claus von Consbruch
Tel:(49)7247/808-400
Fax:(49)7247/808-133

ONERA - DED
B.P. 72
92322 Châtillon Cedex
France
Person to contact: Mme F. Lhullier
Tel:33(1)4673 3799
Fax:33(1)4673 4141

Aeronautica Militare
Ufficio del Delegato Nazionale all AGARD
Aeroporto Militare Pratica di Mare
00040 - Pomezia (RM)
ITALY
Person to contact: Colonel F. Celegato
Tel:39 6 91092683
Fax:39 6 9105887

National Aerospace Laboratory
Attn: Library
P.O. Box 153
8300 AD Emmeloord
NETHERLANDS
Person to contact: Mr. C.W. de Jong
Tel:31 5274 8444
Fax:31 5274 8210

Norwegian Defence Research Establishment
(NDRE) Library
P.O. Box 25
N.2007 Kjeller
Norway
Person to contact: Per Ekern
Tel:4763 807105
Fax:4763 807115

Aeronautical Engineering Department
Middle East Technical University
P.K. 06531
Ankara
TURKEY
Person to contact: Prof. Dr. Ing. C. Ciray
Tel:90(312)210 1000 - Ext: 2471
Fax:90(312)210 1272 or 1110

Defence Research Information Centre
Kentigern House
65 Brown Street
Glasgow, G2 8EX
UNITED KINGDOM
Contact: Document Supply Section
Tel:44(0)41 224 2456
Fax:44(0)41 224 2470

NASA Center for Aerospace Information
800 Elkridge Landing Road
Linthicum Heights
MD 21090-2934
U.S.A.
Contact: NASA Access Help Desk
Tel:1(301) 621 0390
Fax:1(301)621 0134

# PROCEDURE TO USE THE SET OF FLOPPY DISKS

To reduce the amount of diskspace needed for distribution of the data all datasets are compressed in self-extracting archive files.
For most of the datasets this means that all data are available in one file, the name of these archive files is SET_nr.EXE where nr is the set number (e.g. SET_A1.EXE contains all data of dataset A1). For two larger datasets (sets C4 and E6) the data have been split over more than one archive file to avoid very large files. In that case the file names are SET_nr_i.EXE where nr is again the dataset number and i is the sequence number of the file (e.g. SET_C4_2.EXE is the 2nd file of dataset C4).

To extract the data from an archive file, copy that archive file to an appropriate directory on a harddisk of your (IBM compatible, DOS operating system) personal computer. Move to that directory and give the DOS-command

```
SET_nr -x
```

or

```
SET_nr_i -x
```

which will extract all datafiles from the archive file SET_nr.EXE. In all cases the user will be asked to confirm that data should be extracted from the archive, in some cases confirmation will be asked that new subdirectories may be created which is necessary to avoid duplicate filename problems. After the extraction process has completed, the dataset is available in the same form as provided by the author(s) of the dataset (in addition, the archive file remains available unchanged).
The complete database is available on nine 3.5" DOS-format floppy disks with 1.44Mbytes capacity. The contents of the disks is as follows:

datasets A disk 1 contains sets A1, A2, A3, A4, A5, A7, A8, A9, A10, A11, A12 and A13
datasets A disk 2 contains set A6
datasets B contains sets B1, B2, B3, B4, B5 and B6
datasets C disk 1 contains sets C1, C2, C3, C5 and C6
datasets C disk 2 contains the first half of set C4 (archive files C4_1, C4_2 and C4_3)
datasets C disk 3 contains archive files C4_4, C4_5 and C4_6
datasets D contains sets D1, D2, D3, D4 and D5
datasets E disk 1 contains sets E1, E2, E3, E4, E5, E7, E8 and E9
datasets E disk 2 contains set E6 in the archive files E6_1, E6_2, E6_3 and E6_4

The following table gives an overview of the harddisk size needed for the various uncompressed datasets.

| dataset | authors | organisation | extent of data (Kbytes uncompressed) |
|---|---|---|---|
| A1 | W. Bartelsheimer<br>K.H. Horstman<br>W. Puffert-Meissner | DLR Braunschweig | 128 |
| A2 | I.R.M. Moir | DRA Farnborough | 121 |
| A3 | P.R. Ashill | DRA Bedford | 39 |
| A4 | D.J. Jones<br>Y. Nishimura | IAR/NRC Ottawa | 772 |
| A5 | V.D. Chin<br>C.J. Dominic<br>F.T.Lynch<br>D.L. Rodrigruez | McDonnel Douglas | 2558 |
| A6 | P. Guntermann<br>G.Dietz | RWTH Aachen | 2700* |
| A7 | L.H.J. Absil<br>D.M. Passchier | Delft Univ. of Technology | 133 |
| A8 | S.O.T.H. Han | NLR | 341 |
| A9 | B van den Berg<br>J.H.M. Gooden | NLR | 107 |

| dataset | authors | organisation | extent of data (KBytes uncompressed) |
|---|---|---|---|
| A10 | A. Mignosi | ONERA | 137 |
| | J.P. Archambaud | | |
| | E. Stanewsky | DLR Goettingen | |
| A11 | A.M. Rodde | ONERA | 123 |
| | J.P. Archambaud | | |
| A12 | G.G. Mateer | NASA-Ames | 146 |
| | H.L. Seegmiller | | |
| | J. Szodruch | | |
| A13 | G.W. Brune | Boeing | 76 |
| B1 | M.C.P. Firmin | DRA Farnborough | 1719 |
| | M.A. McDonnald | | |
| B2 | M.J. Simmons | DRA Bedford | 158 |
| B3 | J.L. Fulker | DRA Bedford | 133 |
| B4 | G. Redeker | DLR/DRA/ONERA/NLR | 335 |
| B5 | H.Sobieczy | DLR Goettingen | 157 |
| B6 | M. Olsen | NASA Ames | 677 |
| | H.L. Seegmiller | | |
| C1 | H. Esch | DLR Cologne | 167 |
| C2 | H.P. Kreplin | DLR Goettingen | 2575 |
| C3 | K. Hartmann | DLR Goettingen | 402 |
| C4 | D. Barberis | ONERA | 7094 |
| C5 | D. Barberis | ONERA | 3345 |
| C6 | P. Champigny | ONERA | 201 |
| D1 | A. Elsenaar | NLR | 449 |
| D2 | D. Barberis | ONERA | 760 |
| D3 | N.G. Verhaagen | Delft Univ. | 561 |
| | J.E.J. Maseland | of Technology | |
| D4 | K. Hartmann | DLR Goettingen | 200 |
| | K.A. Butefisch | | |
| | H. Pszolla | | |
| D5 | D. Staniland | ARA | 662 |
| E1 | R. Radespiel | DLR Braunschweig | 757 |
| | A. Quast | | |
| | D. Eckert | DNW | |
| E2 | R. Kiock | DLR Braunschweig | 63 |
| | W. Baumert | DLR Goettingen | |
| E3 | B.L. Berrier | NASA Langley | 11 |
| E4 | D.J. Wing | NASA Langley | 6 |
| E5 | K.R. Roth | NASA Ames | 328 |
| E6 | I. Samuelsson | FFA | 4273 |
| E7 | J.G. Leishman | Univ. of Maryland | 148* |
| | Nai-pei Bi | | |
| E8 | D. Staniland | ARA | 638 |
| E9 | D. Staniland | ARA | 560 |

Datasets marked with an * are presented by their authors as subsets of the total available data. Please contact their authors if more details are required.

## AGARD FDP AR-303 TEST CASES FOR CFD VALIDATION

**– TEST CASE COMMENT FORM –**

TEST CASE NUMBER: .....

☐ This test case was very useful for the validation of my CFD code

☐ The test case was not very useful:

- ☐ information in the test case description insufficient
- ☐ the data on the floppy disk was not complete
- ☐ I suspect that the experimental data are seriously in error

Please specify below:

Name: _____ Date: _____

Address: _____

_____


## AGARD FDP AR-303 TEST CASES FOR CFD VALIDATION

**– TEST CASE COMMENT FORM –**

TEST CASE NUMBER: .....

☐ This test case was very useful for the validation of my CFD code

☐ The test case was not very useful:

- ☐ information in the test case description insufficient
- ☐ the data on the floppy disk was not complete
- ☐ I suspect that the experimental data are seriously in error

Please specify below:

Name: _____ Date: _____

Address: _____

_____

## AGARD FDP AR-303 TEST CASES FOR CFD VALIDATION

**– TEST CASE COMMENT FORM –**

TEST CASE NUMBER: .....

☐ This test case was very useful for the validation of my CFD code

☐ The test case was not very useful:

- ☐ information in the test case description insufficient
- ☐ the data on the floppy disk was not complete
- ☐ I suspect that the experimental data are seriously in error

Please specify below:

Name: _____ Date: _____

Address: _____

_____

## AGARD FDP AR-303 TEST CASES FOR CFD VALIDATION

**– TEST CASE COMMENT FORM –**

TEST CASE NUMBER: .....

☐ This test case was very useful for the validation of my CFD code

☐ The test case was not very useful:

- ☐ information in the test case description insufficient
- ☐ the data on the floppy disk was not complete
- ☐ I suspect that the experimental data are seriously in error

Please specify below:

Name: _____ Date: _____

Address: _____

_____

AGARD
FLUID DYNAMICS PANEL
Chairman TES Committee
Attn: Executive Fluid Dynamics Panel
7, rue Ancelle
92200 Neuilly-sur-Seine
FRANCE

AGARD
FLUID DYNAMICS PANEL
Chairman TES Committee
Attn: Executive Fluid Dynamics Panel
7, rue Ancelle
92200 Neuilly-sur-Seine
FRANCE

AGARD
FLUID DYNAMICS PANEL
Chairman TES Committee
Attn: Executive Fluid Dynamics Panel
7, rue Ancelle
92200 Neuilly-sur-Seine
FRANCE

AGARD
FLUID DYNAMICS PANEL
Chairman TES Committee
Attn: Executive Fluid Dynamics Panel
7, rue Ancelle
92200 Neuilly-sur-Seine
FRANCE

## REPORT DOCUMENTATION PAGE

| 1. Recipient's Reference | 2. Originator's Reference | 3. Further Reference | 4. Security Classification of Document |
|---|---|---|---|
| | AGARD-AR-303 Volume II | ISBN 92-836-1003-2 | UNCLASSIFIED |

**5. Originator** Advisory Group for Aerospace Research and Development
North Atlantic Treaty Organization
7 rue Ancelle, 92200 Neuilly-sur-Seine, France

**6. Title**
A Selection of Experimental Test Cases for the Validation of CFD Codes

**7. Presented at**

| 8. Author(s)/Editor(s) | 9. Date |
|---|---|
| Multiple | August 1994 |
| **10. Author's/Editor's Address** | **11. Pages** |
| Multiple | 596 |

**12. Distribution Statement** There are no restrictions on the distribution of this document. Information about the availability of this and other AGARD unclassified publications is given on the back cover.

**13. Keywords/Descriptors**

Computational fluid dynamics
Aerodynamic configurations
Aircraft
Missiles
Wind tunnel tests
Data bases
Validity

**14. Abstract**

This report presents the results of a study by Working Group 14 of the AGARD Fluid Dynamics Panel. This group was formed to establish an accessible, detailed experimental data base for the validation of Computational Fluid Dynamics (CFD) codes.

The thirty nine test cases that are documented cover the subsonic, transonic, and supersonic flow regimes and five classes of geometries. Included in the five classes of geometries are: Two Dimensional Airfoils; Three Dimensional Wings, designed for predominantly attached flow conditions; Slender Bodies, typical of missile type configurations; Delta Wings, characterized by a conical type of vortex flow; and Complex Configurations, either in a geometrical sense or because of complicated flow interactions.

The report is presented in two volumes. Volume I provides a review of the theoretical and experimental requirements, a general introduction and summary of the test cases, and recommendations for the future. Volume II contains detailed information on the test cases. The relevant data of all test cases has been compiled on floppy disks, which can be obtained through National Centers.

AGARD Advisory Report No 303
Advisory Group for Aerospace Research and Development, NATO
A SELECTION OF EXPERIMENTAL TEST CASES FOR THE VALIDATION OF CFD CODES
Published August 1994
596 pages

This report presents the results of a study by Working Group 14 of the AGARD Fluid Dynamics Panel. This group was formed to establish an accessible, detailed experimental data base for the validation of Computational Fluid Dynamics (CFD) codes.

The thirty nine test cases that are documented cover the subsonic, transonic, and supersonic flow regimes and five classes of geometries. Included in the five classes of geometries are: Two Dimensional Airfoils; Three Dimensional Wings, designed for predominantly attached

AGARD-AR-303
Volume II

Computational fluid dynamics
Aerodynamic configurations
Aircraft
Missiles
Wind tunnel tests
Data bases
Validity

AGARD Advisory Report No 303
Advisory Group for Aerospace Research and Development, NATO
A SELECTION OF EXPERIMENTAL TEST CASES FOR THE VALIDATION OF CFD CODES
Published August 1994
596 pages

This report presents the results of a study by Working Group 14 of the AGARD Fluid Dynamics Panel. This group was formed to establish an accessible, detailed experimental data base for the validation of Computational Fluid Dynamics (CFD) codes.

The thirty nine test cases that are documented cover the subsonic, transonic, and supersonic flow regimes and five classes of geometries. Included in the five classes of geometries are: Two Dimensional Airfoils; Three Dimensional Wings, designed for predominantly attached

AGARD-AR-303
Volume II

Computational fluid dynamics
Aerodynamic configurations
Aircraft
Missiles
Wind tunnel tests
Data bases
Validity

AGARD Advisory Report No 303
Advisory Group for Aerospace Research and Development, NATO
A SELECTION OF EXPERIMENTAL TEST CASES FOR THE VALIDATION OF CFD CODES
Published August 1994
596 pages

This report presents the results of a study by Working Group 14 of the AGARD Fluid Dynamics Panel. This group was formed to establish an accessible, detailed experimental data base for the validation of Computational Fluid Dynamics (CFD) codes.

The thirty nine test cases that are documented cover the subsonic, transonic, and supersonic flow regimes and five classes of geometries. Included in the five classes of geometries are: Two Dimensional Airfoils; Three Dimensional Wings, designed for predominantly attached

AGARD-AR-303
Volume II

Computational fluid dynamics
Aerodynamic configurations
Aircraft
Missiles
Wind tunnel tests
Data bases
Validity

AGARD Advisory Report No 303
Advisory Group for Aerospace Research and Development, NATO
A SELECTION OF EXPERIMENTAL TEST CASES FOR THE VALIDATION OF CFD CODES
Published August 1994
596 pages

This report presents the results of a study by Working Group 14 of the AGARD Fluid Dynamics Panel. This group was formed to establish an accessible, detailed experimental data base for the validation of Computational Fluid Dynamics (CFD) codes.

The thirty nine test cases that are documented cover the subsonic, transonic, and supersonic flow regimes and five classes of geometries. Included in the five classes of geometries are: Two Dimensional Airfoils; Three Dimensional Wings, designed for predominantly attached

AGARD-AR-303
Volume II

Computational fluid dynamics
Aerodynamic configurations
Aircraft
Missiles
Wind tunnel tests
Data bases
Validity

| | |
|---|---|
| flow conditions; Slender Bodies, typical of missile type configurations; Delta Wings, characterized by a conical type of vortex flow; and Complex Configurations, either in a geometrical sense or because of complicated flow interactions.<br><br>The report is presented in two volumes. Volume I provides a review of the theoretical and experimental requirements, a general introduction and summary of the test cases, and recommendations for the future. Volume II contains detailed information on the test cases. The relevant data of all test cases has been compiled on floppy disks, which can be obtained through National Centers.<br><br>ISBN 92-836-1003-2 | flow conditions; Slender Bodies, typical of missile type configurations; Delta Wings, characterized by a conical type of vortex flow; and Complex Configurations, either in a geometrical sense or because of complicated flow interactions.<br><br>The report is presented in two volumes. Volume I provides a review of the theoretical and experimental requirements, a general introduction and summary of the test cases, and recommendations for the future. Volume II contains detailed information on the test cases. The relevant data of all test cases has been compiled on floppy disks, which can be obtained through National Centers.<br><br>ISBN 92-836-1003-2 |
| flow conditions; Slender Bodies, typical of missile type configurations; Delta Wings, characterized by a conical type of vortex flow; and Complex Configurations, either in a geometrical sense or because of complicated flow interactions.<br><br>The report is presented in two volumes. Volume I provides a review of the theoretical and experimental requirements, a general introduction and summary of the test cases, and recommendations for the future. Volume II contains detailed information on the test cases. The relevant data of all test cases has been compiled on floppy disks, which can be obtained through National Centers.<br><br>ISBN 92-836-1003-2 | flow conditions; Slender Bodies, typical of missile type configurations; Delta Wings, characterized by a conical type of vortex flow; and Complex Configurations, either in a geometrical sense or because of complicated flow interactions.<br><br>The report is presented in two volumes. Volume I provides a review of the theoretical and experimental requirements, a general introduction and summary of the test cases, and recommendations for the future. Volume II contains detailed information on the test cases. The relevant data of all test cases has been compiled on floppy disks, which can be obtained through National Centers.<br><br>ISBN 92-836-1003-2 |